

Biosystems & Biorobotics

Diego Torricelli
Metin Akay
Jose L. Pons *Editors*

Converging Clinical and Engineering Research on Neurorehabilitation IV

Proceedings of the 5th International
Conference on Neurorehabilitation
(ICNR2020), October 13–16, 2020

 Springer

Biosystems & Biorobotics

Volume 28

Series Editor

Eugenio Guglielmelli, Laboratory of Biomedical Robotics, Campus Bio-Medico
University of Rome, Rome, Italy

The BIOSYSTEMS & BIOROBOTICS (BioSysRob) series publishes the latest research developments in three main areas: 1) understanding biological systems from a bioengineering point of view, i.e. the study of biosystems by exploiting engineering methods and tools to unveil their functioning principles and unrivalled performance; 2) design and development of biologically inspired machines and systems to be used for different purposes and in a variety of application contexts. In particular, the series welcomes contributions on novel design approaches, methods and tools as well as case studies on specific bio-inspired systems; 3) design and developments of nano-, micro-, macro- devices and systems for biomedical applications, i.e. technologies that can improve modern healthcare and welfare by enabling novel solutions for prevention, diagnosis, surgery, prosthetics, rehabilitation and independent living. On one side, the series focuses on recent methods and technologies which allow multi-scale, multi-physics, high-resolution analysis and modeling of biological systems. A special emphasis on this side is given to the use of mechatronic and robotic systems as a tool for basic research in biology. On the other side, the series authoritatively reports on current theoretical and experimental challenges and developments related to the “biomechatronic” design of novel biorobotic machines. A special emphasis on this side is given to human-machine interaction and interfacing, and also to the ethical and social implications of this emerging research area, as key challenges for the acceptability and sustainability of biorobotics technology. The main target of the series are engineers interested in biology and medicine, and specifically bioengineers and bioroboticists. Volume published in the series comprise monographs, edited volumes, lecture notes, as well as selected conference proceedings and PhD theses. The series also publishes books purposely devoted to support education in bioengineering, biomedical engineering, biomechatronics and biorobotics at graduate and post-graduate levels.

Indexed by SCOPUS, WTI Frankfurt eG, SCImago

More information about this series at <http://www.springer.com/series/10421>

Diego Torricelli · Metin Akay · Jose L. Pons
Editors

Converging Clinical and Engineering Research on Neurorehabilitation IV

Proceedings of the 5th International
Conference on Neurorehabilitation
(ICNR2020), October 13–16, 2020

 Springer

Editors

Diego Torricelli
Neural Rehabilitation Group
Cajal Institute
Madrid, Spain

Metin Akay
Department of Biomedical Engineering
University of Houston
Houston, TX, USA

Jose L. Pons
Department of Biomedical Engineering
Shirley Ryan AbilityLab
Chicago, IL, USA

ISSN 2195-3562

Biosystems & Biorobotics

ISBN 978-3-030-70315-8

<https://doi.org/10.1007/978-3-030-70316-5>

ISSN 2195-3570 (electronic)

ISBN 978-3-030-70316-5 (eBook)

© The Editor(s) (if applicable) and The Author(s), under exclusive license to Springer Nature Switzerland AG 2022

This work is subject to copyright. All rights are solely and exclusively licensed by the Publisher, whether the whole or part of the material is concerned, specifically the rights of translation, reprinting, reuse of illustrations, recitation, broadcasting, reproduction on microfilms or in any other physical way, and transmission or information storage and retrieval, electronic adaptation, computer software, or by similar or dissimilar methodology now known or hereafter developed.

The use of general descriptive names, registered names, trademarks, service marks, etc. in this publication does not imply, even in the absence of a specific statement, that such names are exempt from the relevant protective laws and regulations and therefore free for general use.

The publisher, the authors and the editors are safe to assume that the advice and information in this book are believed to be true and accurate at the date of publication. Neither the publisher nor the authors or the editors give a warranty, expressed or implied, with respect to the material contained herein or for any errors or omissions that may have been made. The publisher remains neutral with regard to jurisdictional claims in published maps and institutional affiliations.

This Springer imprint is published by the registered company Springer Nature Switzerland AG
The registered company address is: Gewerbestrasse 11, 6330 Cham, Switzerland

Contents

SS1: How To Challenge Patients During Robot-Assisted Gait Training: From Technical Aspects to Clinical Evidence	
How to Challenge Patients During Gait Training: The Effect of Immersive Virtual Reality on the Gait Pattern in People Post-stroke	3
E. De Keersmaecker, D. Rodriguez-Cianca, B. Serrien, B. Jansen, C. Rodriguez-Guerrero, E. Kerckhofs, and E. Swinnen	
Automatic Versus Manual Tuning of Robot-Assisted Gait Training	9
C. Bayón, S. S. Fricke, H. van der Kooij, and E. H. F. van Asseldonk	
Six weeks Use of a Wearable Soft-robotic Glove During ADL: Preliminary Results of Ongoing Clinical Study	15
Anke I. R. Kottink, Corien D. M. Nikamp, Jaap H. Buurke, Foskea Bos, Corry K. van der Sluis, Marieke van den Broek, Bram Onneweer, Janneke M. Stolwijk-Swüste, Sander M. Brink, Johan S. Rietman, and Gerdienke B. Prange-Lasonder	
Proof-of-Concept of POF-Based Pressure Sensors Embedded in a Smart Garment for Impact Detection in Perturbation Assessment	21
Leticia Avellar, Arnaldo Leal-Junior, Carlos Marques, E. Rocon, and Anselmo Frizera	
Influence of Innovative Rehabilitation Technology on Intensity of Training: Preliminary Results	27
Anke I. R. Kottink, Gerdienke B. Prange-Lasonder, Lars Dijk, Chris T. M. Baten, Judith F. M. Fleuren, and Jaap H. Buurke	
Wearable Vibrotactile Biofeedback to Improve Human-Exoskeleton Compliance During Assisted Gait Training	33
Cristiana Pinheiro, Joana Figueiredo, and Cristina P. Santos	

Challenges in Adaptive Robot-Assisted Gait Training: The Balancing Act of Minimizing Assistance While Preserving Safety	39
Alejandro Melendez-Calderon and Serena Maggioni	
SS2: Commanding Lower-Limb Exoskeletons by Means of Brain-Machine Interfaces: Achievements and Challenges	
Detection of Attempted Stroke Hand Motions from Surface EMG	47
Mads Jochumsen, Asim Waris, and Imran K. Niazi	
Comparison of Different Brain-Computer Interfaces to Assess Motor Imagery Using a Lower-Limb Exoskeleton	53
L. Ferrero, V. Quiles, M. Ortiz, E. Iáñez, A. Navarro-Arcas, J. A. Flores-Yepes, J. L. Contreras-Vidal, and J. M. Azorín	
Optimal Calibration Time for Lower-Limb Brain-Machine Interfaces	59
L. Ferrero, V. Quiles, M. Ortiz, E. Iáñez, J. L. Contreras-Vidal, and J. M. Azorín	
Comparison Between Methods to Create the Leg Length Discrepancy (LLD) Patient-Specific Model: Musculoskeletal Modeling	65
Hamidreza Barnamehei, Farhad Tabatabai Ghomsheh, Afsaneh Safar Cherati, Majid Pouladian, Arghavan Aminishahsavarani, and Neda Golfeshan	
Shoulder Kinematics and Kinetics Comparison Between Amateur and Professional Athletics During High-Speed Overhead Tasks: Computer Simulation Study	71
Hamidreza Barnamehei, Farhad Tabatabai Ghomsheh, Afsaneh Safar Cherati, Majid Pouladian, Arghavan Aminishahsavarani, and Neda Golfeshan	
Subject-Independent Detection of Movement-Related Cortical Potentials and Classifier Adaptation from Single-Channel EEG	77
Mads Jochumsen	
SS3: Towards Patient-Specific Robotic and Neuroprosthetic Technologies and Therapies for Walking Rehabilitation and Assistance	
A Random Forest Based Methodology for the Development of an Intelligent Classifier of Physical Activities	85
Asier Brull, Sergio Lucas, A. Zubizarreta, Eva Portillo, and Itziar Cabanes	

Human-Centered Approaches for Patient-Specific Wearable Robots 91
 Philipp Beckerle

Effect of Gel Type and Anode Selection in Ankle Movements Elicited by a Multi-field FES Device 97
 Aitor Martín-Odriozola, Cristina Rodríguez-de-Pablo, Haritz Zabaleta-Rekondo, Eukene Imatz-Ojanguren, and Thierry Keller

In Vitro Evaluation of a Protocol and an Architecture for Bidirectional Communications in Networks of Wireless Implants Powered by Volume Conduction 103
 Laura Becerra-Fajardo, Jesus Minguillon, Camila Rodrigues, Filipe O. Barroso, José L. Pons, and Antoni Ivorra

A Study on Reference Range of Healthy Subjects for Detection and Evaluation of Abnormal Foot Movement During Walking in Hemiplegic Subject Using Inertial Sensors 109
 Taihei Noro, Takashi Watanabe, Katsunori Murakami, and Naomi Kuge

A Preliminary Study on Prediction of Initial Contact Timing During Gait Using LSTM for FES Control 115
 Yuto Uwaseki and Takashi Watanabe

Smart Wearable Garment and Rapid Musculoskeletal Modelling for Accurate Neuromechanical Analysis 121
 D. Simonetti, B. F. J. M. Koopman, and M. Sartori

Effect of Rollator Assistance on Sit-to-Stand Balance in Older Adults 127
 Lizeth H. Slood, Matthew Millard, Christian Werner, and Katja Mombaur

A ROS2-Based Approach to Enable Simultaneous and Real-Time Tracking of Humans and Exoskeleton Motion 133
 Guillermo Asín-Prieto, Francisco Martín Rico, and Diego Torricelli

Neural Coherence of Homologous Muscle Pairs During Direct EMG Control of Standing Posture in Transtibial Amputees 139
 Aaron Fleming, Wentao Liu, and He (Helen) Huang

Exoskeleton Design Using Subject-Specific Synergy-Driven Neuromusculoskeletal Models 145
 Marleny M. Arones, Josep M. Font-Llagunes, and Benjamin J. Fregly

SS4: User Experience in Robot-Aided Rehabilitation and Assistance

Usability Evaluation of SMA Based Exoskeleton: Pilot Testing in Post-stroke Patients	153
D. Copaci, D. Serrano del Cerro, I. Alguacil-Diego, D. Fernández Vázquez, F. Molina-Rueda, J. C. Miangolarra-Page, L. Moreno, and D. Blanco	
Wireless Eye-Tracking Technology Application and Self-report Measures to Explore Users' Approach to Smart Home Systems (SHS)	159
Laura Angioletti, Federico Cassioli, and Michela Balconi	
Learning Teleoperation of an Assistive Humanoid Platform by Intact and Upper-Limb Disabled Users	165
Mathilde Connan, Marek Sierotowicz, Bernd Henze, Oliver Porges, Alin Albu-Schäffer, Máximo A. Roa, and Claudio Castellini	
Assessment of Clinical Requirements for a Novel Robotic Device for Upper-Limb Sensorimotor Rehabilitation After Stroke	171
Raphael Rätz, René M. Müri, and Laura Marchal-Crespo	
TestEd Information System: Automatic Evaluation of Exoskeletons Subjective Performance and User Experience	177
Angel Dacal-Nieto, Jawad Masood, Daniel Vergara, and Mariana Alves	
sEMG-Based Classification Strategy of Hand Gestures for Wearable Robotics in Clinical Practice	183
Nicola Secciani, Alberto Topini, Alessandro Ridolfi, and Benedetto Allotta	
Perceived Exertion During Robot-Assisted Gait After Stroke	189
Nina Lefeber, Emma De Keersmaecker, E. Kerckhofs, and E. Swinnen	
Pilot Testing of a New Questionnaire for the Assessment of User Experience During Exoskeleton-Assisted Walking	195
I. Pisotta, N. L. Tagliamonte, A. Bigioni, F. Tamburella, M. Lorusso, F. Bentivoglio, I. Pecoraro, P. Argentieri, F. Marri, L. Zollo, and M. Molinari	
Psychophysiological Assessment of Exoskeleton-Assisted Treadmill Walking	201
I. Pecoraro, N. L. Tagliamonte, C. Tamantini, F. Cordella, F. Bentivoglio, I. Pisotta, A. Bigioni, F. Tamburella, M. Lorusso, P. Argentieri, M. Molinari, and L. Zollo	
Kinematic and Functional Evaluation of a 3D Printed Robotic Hand ...	207
V. Bueyes-Roiz, I. Quiñones-Uriostegui, L. Anaya-Campos, J.L. Zavaleta-Ruiz, G. Rodríguez-Reyes, and Y. Quijano	

Evaluation of Balance Abilities in Expert Paralympic Athletes with Lower Limb Amputation 213
 G. Marchesi, A. Bellitto, E. Ricaldone, A. De Luca, C. Sanfilippo, K. Torre, E. Quinland, J. Saglia, V. Squeri, A. Massone, M. Casadio, and A. Canessa

SS5: Boosting Neurorehabilitation in a Sustainable Way

Frequency Domain Analysis of EMG and HRV in Self-Support Exercise 221
 S. Shimoda, Alvaro Costa Garcia, Hiroshi Yamasaki, F. Alnajjar, M. Sonoo, Shotaro Okajima, Sayako Ueda, Ken-ichi Ozaki, and Izumi Kondo

Translation from Functional Training to Independent Living: The Importance of a Real-Time Feedforward-Feedback Approach 227
 Subhasis Banerji, John Heng, Daphne Menezes, Shirish Hastak, Manasi Bane, Sharon Gerken, and Dorothy Wi

Ankle-Foot Orthoses in the Rehabilitation After Stroke: Results of a Randomized Controlled Trial 233
 Corien D. M. Nikamp, Johan S. Rietman, Erik C. Prinsen, Hermie J. Hermens, and Jaap H. Buurke

An Integrated Rehabilitation Platform Based on Action Observation Therapy, Mixed Reality and Wearable Technologies 239
 Paolo Mosna, Stefano E. Lenzi, Stefano Lazzarini, Massimiliano Gobbo, Monica Angelini, Riccardo Buraschi, Stefano Negrini, Maddalena Fabbri Destro, Pietro Avanzini, Giacomo Rizzolatti, and Nicola F. Lopomo

A Novel Tool for Quantitative Assessment of Lower Limb Proprioception with Healthy Adults, Elderly, and Stroke Survivors 245
 Asya Mikhaylov, Yogev Koren, Simona Bar-Haim, and Ilana Nisky

Accuracy of Single RGBD Camera-Based Upper-Limb Movement Tracking Using OpenPose 251
 Timothy Dev, Reetajanetsureka, Samuelkamaleshkumar Selvaraj, Henry Prakash Magimairaj, and Sivakumar Balasubramanian

Designing a Music-Based Game for Training Pattern Recognition Control of a Myoelectric Prosthesis 257
 D. Bessa, N. F. Rodrigues, E. Oliveira, J. Kolbensschlag, and C. Prahm

Correlation Between EEG Band Power Parameters and Functional Scale in Stroke Patients 263
 Marc Sebastián-Romagosa, Rupert Ortner, Josep Dinarès-Ferran, and Christoph Guger

SS6: Simulation and Prediction of Human Motion

Adaptive Oscillators as Template for Modeling and Assisting Rhythmic Movements	271
Renaud Ronsse	
Converting Biomechanical Models from OpenSim to MuJoCo	277
Aleksi Ikkala and Perttu Hämäläinen	
Quaternions-Based Normal Gait Kinematics Model	283
Juan C. Gonzalez-Islas, Omar A. Dominguez-Ramirez, Omar Lopez-Ortega, Ma. de los Angeles Alonso-Lavernia, and Felix A. Castro-Espinoza	
Estimation of Ground Reaction Forces from Lower Limb Joint Kinematics During Walking	293
Shui Kan Lam and I. Vujaklija	
Effect of Muscle Modeling in the Efficiency and Accuracy of the Forward-Dynamics Simulation of Human Gait	299
Francisco Mouzo, Florian Michaud, Mario Lamas, Urbano Lugris, and Javier Cuadrado	
Sitting Posture Monitoring Device for People with Low Degree of Autonomy	305
Nerea Perez, Patrick Vermander, Elena Lara, Aitziber Mancisidor, and Itziar Cabanes	
Effects of Parkinson’s Disease and a Secondary Cognitive Task on Standing Postural Stability	311
Vu Phan, Daniel S. Peterson, Sutton B. Richmond, and Hyunglae Lee	
Gait Analysis for Normal and Crouch Gaits Applying No-Common Metrics in the Cartesian Space	317
Juan C. Gonzalez-Islas, Omar A. Dominguez-Ramirez, Omar Lopez-Ortega, Felix A. Castro-Espinoza, and Ma. de los Angeles Alonso-Lavernia	
Rapid Predictive Simulations to Study the Interaction Between Motor Control and Musculoskeletal Dynamics in Healthy and Pathological Human Movement	327
Friedl De Groote and Antoine Falisse	
Sit-to-Stand Models of Older Adults Should Include Muscle Nonlinearities and Arms	333
Matthew Millard and Katja Mombaur	

Functional Analysis of Upper-Limb Movements in the Cartesian Domain 339
 Marco Baracca, Paolo Bonifati, Ylenia Nisticò, Vincenzo Catrambone, Gaetano Valenza, A. Bicchi, Giuseppe Averta, and Matteo Bianchi

A Machine Learning Approach for Near-Fall Detection Based on Inertial and Force Data While Using a Conventional Rollator 345
 Nuno Ferrete Ribeiro, Ana Pereira, Joana Figueiredo, José A. Afonso, and Cristina P. Santos

Clustering of Data that Quantify the Degree of Impairment of the Upper Limb in Patients with Alterations of the Central Nervous System 351
 Anaya-Campos L., Quiñones-Uriostegui I., Quijano Y., and Bueyes-Roiz V.

Artificial Neural Networks to Quantify Motor Skills in Children with Cerebral Hemiparesis 357
 L. Anaya-Campos, I. Quiñones-Uriostegui, Y. Quijano, and V. Bueyes-Roiz

Analysis of a Predictive Forward Simulator of Human Gaits 363
 T. Bonis, N. Pronost, and S. Bouakaz

SS7: Development of Novel Neural Interfaces to Improve Neurorehabilitation

Effects of Decomposition Parameters and Estimator Type on Pseudo-online Motor Unit Based Wrist Joint Angle Prediction 371
 Dennis Yeung, Francesco Negro, and I. Vujaklija

Highly Intuitive 3-DOF Simultaneous and Proportional Myocontrol of Wrist and Hand 377
 Markus Nowak, I. Vujaklija, Claudio Castellini, and Dario Farina

A Portable P300-Based Brain–Computer Interface as an Alternative Communication Device 383
 Víctor Martínez-Cagigal, Eduardo Santamaría-Vázquez, and Roberto Hornero

On the Crosstalk in Motor Unit Spike Train Identification from High-Density Surface Electromyograms 389
 Matjaž Divjak, Lukas G. Wiedemann, Andrew J. McDavid, and A. Holobar

Altered Motor Unit Territories After Intramuscular Botulinum Toxin Injection in Spastic Biceps Brachii Muscle 395
 Sourav Chandra, A. Holobar, Babak Afsharipour, William Zev Rymer, and Nina L. Suresh

Motor Unit Tracking Across Low Contraction Levels of Biceps Brachii Muscle 401
A. Frančič and A. Holobar

Preventing Cognitive Decline in Elderly Population Through Neurofeedback Training: A Pilot Study 407
Eduardo Santamaría-Vázquez, Víctor Martínez-Cagigal, Daniel Rodríguez, Jaime Finat, and Roberto Hornero

Wearable Sensor for Multi-wavelength Near-Infrared Spectroscopy of Skin Hemodynamics Along with Underlying Muscle Electromyography 413
Radhika Mujumdar, Mancheung Cheung, Shweta Pramod Kadam, and Anirban Dutta

SS8: “One Size Does Not Fit All”: New Approaches for a Patient-Tailored Rehabilitation Process

Closed-Loop Acquisition of Training Data Improves Myocontrol of a Prosthetic Hand 421
Donato Brusamento, Andrea Gigli, Roberto Meattini, Claudio Melchiorri, and Claudio Castellini

Allied Rehabilitation Using Web-Based Caregiver MEDIated Exercises for STROKE: The ARMED4STROKE Trial Design 427
Corien D. M. Nikamp, Gert Kwakkel, Erik C. Prinsen, Rinske H. M. Nijland, Marijn Mulder, Erwin E. H. van Wegen, Hermie J. Hermens, and Jaap H. Burke

Augmented Reality for Rehabilitation Tuning and Assessment 433
M. Pezzera, E. Chitti, and N. A. Borghese

Towards the Use of Neuromusculoskeletal Modeling in Clinical Practice: A Feasibility Study in Parkinson Disease Patients 439
M. Romanato, D. Volpe, A. Guiotto, F. Spolaor, M. Sartori, and Z. Sawacha

The Effect of Visual, Auditory, Tactile and Cognitive Feedback in Motor Skill Training: A Pilot Study Based on VR Gaming 445
F. Alnajjar, Qi An, Mohit Saravanan, Khaled Khalil, Munkhjargal Gochoo, and S. Shimoda

Comparison of Wearable Sensor Based Algorithms for Upper Limb Activity Detection 451
Tanya Subash, Ann David, Varadhan SKM, and Sivakumar Balasubramanian

Targeted Muscle Training with a Hybrid Body-Machine Interface 457
Dalia De Santis and Ferdinando A. Mussa-Ivaldi

Towards Objective Assessment of Upper Limb Spasticity by Means of Collaborative Robots 463
 Edwin Daniel Oña, Ana Casanova, Anaëlle Gordillo, Carlos Balaguer, and Alberto Jardón

Source Localization of Simulated Electroencephalogram of Virtual Epileptic Patient to Investigate Clinically Feasible Montages 469
 Zoe Herrick, Ping Li, and Anirban Dutta

An Open-Source, Wheelchair Accessible and Immersive Driving Simulator for Training People with Spinal Cord Injury 475
 Filippo Gandolfi, A. Bellitto, Angelo Basteris, A. Canessa, A. Massone, Serena Ricci, and M. Casadio

SS9: Joint Stiffness: The Sleeping Giant of Neuromechanics

A Powered Ankle Foot Orthosis Based on Shaft Twisted String Actuation to Assist Persons with Foot-Drop: A Feasibility Study 483
 Pedrin Denoth, Pascal Geitner, Lukas Krähenbühl, Konrad S. Stadler, and Eveline S. Graf

Towards a Myoelectric Prosthetic Wrist with Rigid and Compliant Behaviour 489
 P. Capsi-Morales, C. Piazza, G. Grioli, A. Bicchi, and M. G. Catalano

Identification of Time-Varying Ankle Joint Impedance During Periodic Torque Experiments Using Kernel-Based Regression 495
 Gaia Cavallo, Christopher P. Cop, M. Sartori, Alfred C. Schouten, and John Lataire

Robotic Approach to Characterize Ankle Stiffness in Multiple Sclerosis Patients During Standing and Walking 501
 Varun Nalam, Ermytrude Adjei, Joshua Russell, Megan C. Eikenberry, Dean Wingerchuk, and Hyunglae Lee

A Muscle Model Incorporating Fiber Architecture Features for the Estimation of Joint Stiffness During Dynamic Movement 507
 Christopher P. Cop, Alfred C. Schouten, Bart F. J. M. Koopman, and M. Sartori

Quantifying Joint Stiffness During Movement: A Quantitative Comparison of Time-Varying System Identification Methods 513
 Mark van de Ruit, Winfred Mugge, and Alfred C. Schouten

Inhibition of Knee Sensory Receptors Alters Quadriceps Muscle Coordination in the Rat 519
 Cristiano Alessandro and Matthew C Tresch

A Transparent Lower Limb Perturbator to Investigate Joint Impedance During Gait 525
 Ronald C. van 't Veld, S. S. Fricke, Ander Vallinas Prieto, Arvid Q. L. Keemink, Alfred C. Schouten, H. van der Kooij, and E. H. F. van Asseldonk

Apparent Stiffness and Damping as a Metric for Fall Risk 531
 Jordan Smith, Robert Felmlee, Jozsef Laczko, Mary Crowe, Scott Steinbrink, and Davide Piovesan

SS10: Neural Correlates of Cognitive-Motor Robotic Neurorehabilitation

Feature Consistency Criterion for Motor Imagery-Based Neuromodulation 539
 Carlos A. Stefano Filho, J. Ignacio Serrano, Romis Attux, Gabriela Castellano, M. Dolores del Castillo, and Eduardo Rocon

Real-Time Access to Attention and Attention-Based Brain-Machine Interfaces 545
 C. Gaillard, C. De Sousa, J. Amengual, and S. Ben Hamed

Explicitness of Task Instructions Supports Motor Learning and Modulates Engagement of Attentional Brain Networks 551
 Joaquin Penalver-Andres, Karin A. Buetler, Thomas König, René M. Müri, and Laura Marchal-Crespo

Agency and Responsibility While Controlling Movement Through Brain-Computer Interfaces for Neurorehabilitation 557
 Maria V. Sanchez-Vives, Mel Slater, and Birgit Nierula

Adaptation to Virtual Surgeries Across Multiple Practice Sessions 563
 Daniele Borzelli, Sergio Gurgone, Maura Mezzetti, Paolo De Pasquale, Denise J. Berger, Demetrio Milardi, Giuseppe Aciri, and Andrea D'Avella

Brain-Computer Interface-Based Neurorehabilitation: From the Lab to the Users' Home 569
 C. Escolano, E. López-Larraz, J. Minguez, and L. Montesano

Healing the Virtualizing Brain Using Virtual Reality: How Goal-Oriented, Embodied, Immersive VR Training Works 575
 Paul F. M. J. Verschure

The Application of Sensory Error Manipulations to Motor Rehabilitation and Diagnostics After Brain Damage 579
 Ballester R. Belén and Verschure F. M. J. Paul

SS11: Advances and Challenges on Artificial Sensory Feedback Techniques in Manipulation and Locomotion

Investigation of Vibrotactile Transducers for a Bone Conduction Sensory Feedback System 587
 Raphael M. Mayer, Siyuan Chen, Zhuo Li, Alireza Mohammadi, Ying Tan, Gursel Alici, Peter Choong, and Denny Oetomo

Multi-frequency Stimulation: Spatial Differentiation of Bone-Conducted Tactile Stimulation on the Elbow Bony Landmarks 593
 Raphael M. Mayer, Alireza Mohammadi, Ying Tan, Gursel Alici, Peter Choong, and Denny Oetomo

A User-Centered Approach to Artificial Sensory Substitution for Blind People Assistance 599
 Federica Barontini, Gemma Carolina Bettelani, Barbara Leporini, Giuseppe Averta, and Matteo Bianchi

Post-stroke Voluntary Movements Improve When Combined with Vibration-Induced Illusion of Movement 605
 Francesca Ferrari, Courtney E. Shell, Zachary C. Thumser, Francesco Clemente, Ela B. Plow, Christian Cipriani, and Paul D. Marasco

Effects of Non-in Situ Vibrations on Hand Sensations: A Pilot Study ... 611
 Anke Fischer, Leonardo Cappello, Leonard F. Engels, and Christian Cipriani

HaptiTrack: A Novel Device for the Evaluation of Tactile Sensitivity in Active and in Passive Tasks 617
 Simone Ciotti, Matteo Bianchi, Davide Doria, Francesco Lacquaniti, and Alessandro Moscatelli

A Parallel Actuated Haptic Device for De-localized Tactile Feedback in Prosthetics 623
 Daniele Leonardis, Leonardo Cappello, Christian Cipriani, and Antonio Frisoli

A Compact Soft Exoskeleton for Haptic Feedback in Rehabilitation and for Hand Closing Assistance 629
 Tommaso Bagneschi, Daniele Leonardis, Domenico Chiaradia, and Antonio Frisoli

Human Neuromarkers of Tactile Perception: State of the Art in Methods and Findings 635
 Gianna Adalia Cannestro, Moaed A. Abd, Erik D. Engeberg, and Emmanuelle Tognoli

SS12: Human-Machine Interface for Real-Time Wearable Robots Control

Wearable Neurofeedback Training for Boosting Attention Regulation at the Wheel 643

Davide Crivelli, Laura Angioletti, and Michela Balconi

Wearable Neurotechnologies for Neurocognitive Empowerment in Applied Contexts 649

Davide Crivelli, Giulia Fronda, Laura Angioletti, Claudia Spinosa, and Michela Balconi

Simultaneous and Proportional Myocontrol of a Hand Exoskeleton for Spinal Muscular Atrophy: A Preliminary Evaluation 655

Marco Ricciardi, Alberto Topini, Nicola Secciani, Alessandro Ridolfi, and Claudio Castellini

Study of the ERD Induced by Different Motor Tasks Through Non-invasive EEG Analysis to Improve Stroke Rehabilitation Outcomes 661

S. Ezquerro, A. Bertomeu-Motos, J. Barios, J. M. Catalan, J. Diez, and N. Garcia-Aracil

Real-Time Cycling Cadence Estimation Using an Inertial Sensor for Gamified Pedaling Therapy 667

Ana Rojo, Rafael Raya, and J. C. Moreno

Development of an Interface for the Control of Robotic Exoskeletons Based on Stroke Rehabilitation Techniques 673

P. Barría, R. Aguilar, D. Unquen, A. Moris, A. Andrade, A. Biskupovic, and J. M. Azorín

KNN Learning Techniques for Proportional Myocontrol in Prosthetics 679

Tim Sziburis, Markus Nowak, and Davide Brunelli

Controlling an Assistive Robotic Manipulator via a Non-linear Body-Machine Interface 685

Marco Giordano, Fabio Rizzoglio, G. Ballardini, Ferdinando A. Mussa-Ivaldi, and M. Casadio

Offline Repeatability Correlates with Real-Time Performance of Pattern Recognition Controllers 691

Yuni Teh and Levi J. Hargrove

Understanding Human-Prosthesis Interaction via Reinforcement Learning-Based Echo Control: A Case Study 697

Ruofan Wu, Minhan Li, Jennie Si, and He (Helen) Huang

SS13: Novel Developments of Non-Invasive Brain and Peripheral Stimulation in Neurorehabilitation

Comparison of Configuration Postures for a Foot Drop Multi-field FES Device 705
 Aitor Martín, Cristina Rodriguez-de-Pablo, Haritz Zabaleta, Eukene Imatz-Ojanguren, and Thierry Keller

Pathways of Hemodynamic Response During Anodal Transcranial Direct Current Stimulation: A Computational Approach 711
 Yashika Arora, Anirban Dutta, and Shubhajit Roy Chowdhury

Effect of Transcutaneous High-Frequency Alternating Current Over Handgrip Muscle Strength 717
 D. Serrano-Muñoz, J. Gómez-Soriano, D. Martín-Caro, R. López-Peco, J. Taylor, and J. Avendaño-Coy

A Music Therapy Serious Game with Dynamic Difficulty Adjustment for Stimulating Short-Term Memory 723
 María A. Gutiérrez, Juan J. Rosero, Diego E. Guzmán, and Carlos F. Rengifo

Feasibility of Transcutaneous Spinal Cord Stimulation Combined with Robotic-Assisted Gait Training (Lokomat) for Gait Rehabilitation of an Incomplete Spinal Cord Injury Subject 735
 N. Comino-Suárez, J. Gómez-Soriano, D. Serrano-Muñoz, A. Megía-García, A. J. del Ama, A. Gil-Agudo, and J. C. Moreno

On Spatial Whitening of High-Density Surface Electromyograms in Compound Muscle Action Potential Decomposition by Differential Evolution 741
 Matej Kramberger and A. Holobar

A Phenomenon of Self-support Exercise in Severe Stroke Patients 747
 F. Alnajjar, S. Shimoda, and Alistair A. Vogan

Human Brain Organoid Platform for Neuroengineering Optical Theranostics in Neonatal Sepsis 753
 Sneha S. Karanth, Radhika Mujumdar, Jagdish P. Sahoo, Abhijit Das, Michal K. Stachowiak, and Anirban Dutta

Grey-Box Model-Based Analysis of the Effects of Anodal Transcranial Direct Current Stimulation on the Reaction Time in Healthy Human 759
 Namrata Sridhar Kadambi, Shilpa Ramanarayanan, Filip Stefanovic, and Anirban Dutta

Different Stimuli Configuration in Paired Associative Stimulation Protocol: A Pilot Study 765
 A. San Agustín, José L. Pons, A. Oliviero, and J. C. Moreno

Intensity Dependent Long-Term Potentiation and Inhibition in Paired Associated Stimulation by Transcranial Magnetic Stimulation: A Pilot Study 771
A. San Agustín, D. Crevillén, A. Oliviero, José L. Pons, and J. C. Moreno

Bilateral and Multi-joint Surface Electrical Stimulation for Tremor Reduction. An Essential Tremor Pilot Study 777
Alejandro Pascual-Valdunciel, Beatriz Adán-Barrientos, Alejandra García-Álvarez, Miguel González-Sánchez, Javier Ricardo Pérez-Sánchez, J. C. Moreno, Francisco Grandas, Filipe O. Barroso, and José L. Pons

SS14: Protocols and Software for the Standardization of sEMG Processing and Analysis for Muscle Synergy Extraction

Feasibility Assessment of Muscle Force Estimation Using the Myo Armband During Arm Curl Training 785
Maialen Zelaia Amilibia, Gabriel Hadjadje, Camilo Cortés, A. de los Reyes-Guzmán, A. Gil-Agudo, and Álvaro Bertelsen

The Influence of Harmonics Filtering for Weak EMG Analysis 791
R. Aydın, F. Alnajjar, M. Sonoo, A. Costa Garcia, K. Takatsune, and S. Shimoda

Online Continuous Detection of Time-Varying Muscle Synergies 797
Simone Ranaldi, Claudio Castellini, Andrea D’Avella, and Silvia Conforto

Approximate Credibility Intervals for Independent Component Analysis 803
Olivier Thill and Luca Citi

Muscle Tension Analysis in Stroke Patient Sit-to-Stand Motion by Joint Torque-Based Normalization 809
Ruoxi Wang, Qi An, Ningjia Yang, Hiroki Kogami, Kazunori Yoshida, Hiroyuki Hamada, S. Shimoda, Hiroshi Yamasaki, M. Sonoo, F. Alnajjar, Noriaki Hattori, Kouji Takahashi, Takanori Fujii, Hironori Otomune, Ichiro Miyai, Atsushi Yamashita, and Hajime Asama

SS15: Technologies for Daily Robotic Assistance and Rehabilitation

An Embedded Implementation of EMG-Driven Control for Assisted Bilateral Therapy 817
A. Císnal, V. Moreno-SanJuan, D. Sierra, J. P. Turiel, and J. C. Fraile

MERLIN: Upper-Limb Rehabilitation Robot System for Home Environment 823
Ainara Garzo, Javier Arcas-Ruiz-Ruano, Iñigo Dorronsoro, Gabriel Gaminde, Je Hyung Jung, Javier Téllez, and Thierry Keller

A Wearable Sensorised Thimble for Assessment and Rehabilitation of Grasping 829
 P. Maiolino, L. Ottoveggio, E. Montalesi, S. Denei, F. Mastrogiovanni, M. Casadio, and G. Cannata

Isometric Force Pillow: Using Air Pressure to Quantify Involuntary Finger Flexion in the Presence of Hypertonia 835
 Caitlyn E. Seim, Chuzhang Han, Alexis J. Lowber, Claire Brooks, Marie Payne, Maarten G. Lansberg, Kara E. Flavin, Julius P. A. Dewald, and Allison M. Okamura

Feasibility of Using Visual Cues for Evoking Self-induced Perturbations for Assessing Dynamic Balance During Walking 841
 Andrej Olenšek, Matjaž Zadavec, and Zlatko Matjačić

Development of Impact Absorber Mechanism for Wearable Exoskeleton Using Shape Memory Alloy Spring 845
 Hyunho Kim, Hyerim Jeon, Yongho Jeong, and Yeongjin Kim

A Robot-Aided Rehabilitation Platform for Occupational Therapy with Real Objects 851
 C. Tamantini, M. Lapresa, F. Cordella, F. Scotto di Luzio, C. Lauretti, and L. Zollo

Effects of an Overground Robotic Based Gait Training Intervention on Parameters Provided by a Smart-Tip: An Exploratory Study in People with Multiple Sclerosis 857
 L. Santisteban, E. Otxoa, A. Zubizarreta, and A. Rodriguez-Larrad

Simultaneous Control of Natural and Extra Degrees-of-Freedom by Isometric Force and EMG Null Space Activation 863
 Sergio Gurgone, Daniele Borzelli, Paolo De Pasquale, Denise J. Berger, Tommaso Lisini Baldi, Nicole D’Aurizio, Domenico Prattichizzo, and Andrea D’Avella

Preliminary Clinical Evaluation of the X-Limb Hand: A 3D Printed Soft Robotic Hand Prosthesis 869
 Alireza Mohammadi, Jim Lavranos, Ying Tan, Peter Choong, and Denny Oetomo

Surface EMG Based Guidance Force Feedback System for Muscle-Specific Upper Limb Training in Stroke Patients 875
 Sojung Lee and Suncheol Kwon

Hybrid Actuation Mechanism for an Ultra Low-Cost Transhumeral Prosthesis: Preliminary Study 883
 T. Reboli, S. Meloni, G. Ballardini, G. Carlini, M. Casadio, F. Sante, M. Serafica, G. Vigo, and L. Schiatti

SS16: Neuromechanical Biomarkers in Robot-Assisted Motor Rehabilitation

Empirical Evidence Connecting the Neural Mechanism Behind Motor Coordination and Force Generation on Healthy Humans 891

Álvaro Costa-García, Á. Úbeda, E. Iáñez, and S. Shimoda

Synergistic Parameters of Motor Adaptation in Variable Resistance Cycling Activities 897

A. M. Pertusa, I. Vujaklija, R. M. Sánchez-Pérez, E. Iáñez, A. Costa, and A. Úbeda

Muscle Synergies as a Tool to Unveil Specific Features in the Muscle Patterns After Cerebellar Damage 903

Denise J. Berger, Marcella Masciullo, M. Molinari, Francesco Lacquaniti, and Andrea D'Avella

On Repeatability of MU Fatiguing in Low-Level Sustained Isometric Contractions of Tibialis Anterior Muscle 909

Giovanni Corvini, A. Holobar, and J. C. Moreno

Kinematic Features Analysis from Active and Active-Assistive Upper Arm Robotic Rehabilitation 915

Donghwan Hwang, Joon-Ho Shin, and Suncheol Kwon

SS17: AITADIS Session

Subscription Video on Demand (SVOD) Platform Accessibility Verification Method 923

Gema López-Sanchez and Francisco Utray

Application of Capabilities of Upper Extremity Questionnaire During a Robotic Therapy Based on Armeo[®] Spring Exoskeleton 929

V. Lozano-Berrio, A. de los Reyes-Guzmán, M. Alcobendas-Maestro, B. Polonio-López, and A. Gil-Agudo

Safety, Feasibility and Acceptance with HANK Ambulatory Robotic Exoskeleton in Incomplete Spinal Cord Injury Patients 935

A. Megía-García, A. J. del-Ama, V. Lozano-Berrio, I. Sinovas-Alonso, N. Comino-Suárez, and A. Gil-Agudo

Towards Functional Description of Gait Impairments After Neurological Diseases for the Development of Personalized Robotic and Neuroprosthetic Wearable Systems for Walking Assistance 941

I. Sinovas-Alonso, A. Gil-Agudo, N. Comino-Suárez, A. Megía-García, N. Murillo-Licea, E. Opiiso-Salleras, J. Vidal-Samsó, and A. J. del-Ama

Implementation of an Exoskeleton for Neuromuscular Hand Rehabilitation 947
B. Troncoso, P. Alberti, P. Maldonado-Cárdenas, E. Peña, and P. Barría

Design and Implementation of a “Wireless-Hand” Mechatronic Prototype for the Control of a Robotic Hand 953
E. Peña, P. Alberti, S. Bustamante, P. Maldonado-Cárdenas, and P. Barría

Analysis of Frequency Bands and Channels Configuration for Detecting Intention of Change Direction Through EEG 959
V. Quiles, L. Ferrero, E. Iáñez, M. Ortiz, and J. M. Azorín

Gait Analysis as an Objective Tool Previous to Botulinum Toxin Injection in Spinal Cord Injured Patients: A Case Study 965
C. Redondo-Galán, S. Ceruelo-Abajo, I. Sinovas-Alonso, A. de los Reyes-Guzmán, J. Madrid-Sánchez, and A. Gil-Agudo

Ewe: A Computational Tool to Assist People in Emergencies 971
Luz Ariel and Fehine Joseana

SS1: How To Challenge Patients During Robot-Assisted Gait Training: From Technical Aspects to Clinical Evidence

How to Challenge Patients During Gait Training: The Effect of Immersive Virtual Reality on the Gait Pattern in People Post-stroke



E. De Keersmaecker, D. Rodriguez-Cianca, B. Serrien, B. Jansen, C. Rodriguez-Guerrero, E. Kerckhofs, and E. Swinnen

Abstract Virtual reality (VR) during gait training in people post-stroke can offer added value by providing a task-specific training in more interactive and motivating environments. Nevertheless, scarce research has been presented concerning more detailed information about the influence immersive VR has on the gait pattern of stroke survivors. This exploratory study was conducted to examine the effect of walking with immersive VR on the gait pattern while walking on a self-paced treadmill in people post-stroke. Spatiotemporal gait parameters (i.e. walking speed, stride time, step width, step length) and gait variability measures of stride time, ankle, knee and hip range of motion were analyzed. Our preliminary results suggest that walking with immersive VR can positively influence spatiotemporal gait parameters. The addition of VR introduced less step-by-step variability in joint kinematics in both patients. More research with a larger sample size is necessary.

E. De Keersmaecker (✉) · E. Kerckhofs · E. Swinnen
Rehabilitation Research Group, Faculty of Physical Education and Physiotherapy, Vrije
Universiteit Brussel, Brussels, Belgium
e-mail: emma.de.keersmaecker@vub.be

D. Rodriguez-Cianca · C. Rodriguez-Guerrero
Robotics and Multibody Mechanics Research Group, Department of Mechanics, Vrije
Universiteit Brussel, Brussels, Belgium

Flanders Make, Lommel, Belgium

B. Serrien
Department of Movement and Sport Sciences, Vrije Universiteit Brussel, Brussels, Belgium

B. Jansen
Department of Electronics and Informatics, Vrije Universiteit Brussel, Brussels, Belgium

IMEC, Leuven, Belgium

1 Introduction

Post-stroke gait rehabilitation remains a major clinical challenge. Two-thirds of all stroke survivors suffer from walking impairments, causing them to experience a decrease in activities of daily living, level of participation and quality of life [1]. In order to improve these walking impairments, patients need to be provided with a high-intensive, repetitive and task-specific rehabilitation [2]. Treadmill training is an example of a repetitive and task-specific gait training and has the potential to enhance neural plasticity—the ability to create permanent structural and functional changes of the brain and spinal cord—which is vital to trigger the learning process of the sensorimotor system [3].

The downside of treadmill training is that it can quickly become monotonous. Due to the repetitive movements associated with treadmill training and the monotonous practice environments, patients can lose their interest and become demotivated for their gait training [4]. Virtual reality (VR) has been proposed as a new tool to increase relevant concepts of neural plasticity by providing gait training in more interactive and motivating environments [3]. Up to now only limited trials focused on the use of VR to improve the walking ability of people post-stroke and enhance their gait training. Nevertheless, positive results have been reported when combining VR and gait training [5]. However, despite these positive effects, a more detailed picture of how VR influences the gait pattern in people post-stroke is still lacking. Knowing specifically how VR influences the gait pattern, could potentially enlarge its effect.

In this exploratory study, we investigated the effect of immersive VR on spatiotemporal gait parameters and gait variability while walking on a self-paced treadmill in people post-stroke.

Table 1 Patients characteristics

	Patient 1	Patient 2
Gender	Male	Male
Age (years)	60	55
Stroke onset (months)	115	33
Paretic side	Left	Right
FAC (/5)	4	4
Body mass (kg)	100	85
Body height (cm)	166	191

2 Materials and Methods

2.1 Participants

Two chronic stroke survivors participated in the study. Inclusion criteria were stroke onset ≥ 6 months, ambulatory with an impaired gait pattern (Functional Ambulation Categories (FAC) 2, 3 or 4), able to walk on a treadmill for at least 20 min without bodyweight support, a body height between 155 and 200 cm (limitation is due to the design of the treadmill system) and able to signal pain, fear and discomfort. The protocol was approved by the Ethics Committee of the University of Brussels (B.U.N. 143201939043) and written consent was obtained prior to participation. Patients characteristics are presented in Table 1.

2.2 Materials and Procedure

The experimental setup contained a head-mounted display ‘Oculus Rift’ (Oculus Rift, USA) to provide a fully immersive VR, a 10-camera motion capture system by Vicon (Vicon Motion Systems, USA) and a self-paced treadmill. The treadmill has a total of two 6 axis force sensors connected to each side of the human user’s pelvis through a ball joint that support a harness. The treadmill’s speed is controlled in real time based on the measured interaction forces between the patient and the harness caused by the natural dynamic displacement of the user’s center of mass during walking.

Both patients had to walk two times on the self-paced treadmill for 22 min under 2 conditions: without the VR and while being immersed in a virtual environment (a park outside). Both conditions were carried out on separate days.

Twenty-one minutes of continuous kinematic marker data of the lower limbs were acquired by Vicon Nexus software (Vicon Motion Systems, USA) and used for analysis (the first minute of each trial was not used). Spatiotemporal gait parameters (walking speed, stride time, step width, step length) and sagittal angular range of motion (ROM) of ankle, knee and hip joints were calculated in Python 3.7 (Anaconda Inc., USA). For each outcome, we additionally calculated step-by-step variability by the coefficient of variation (CV) and Sample Entropy (SampEn). CV is a linear measure that quantifies the amount of step-by-step variability, whereas SampEn is a non-linear measure and quantifies the structure of the variability. Lower levels of SampEn would indicate that the data is more predictable, more regular, less complex and less adaptive [6].

Table 2 Mean (SD) values for walking speed, stride time, step width, step length and variability in stride time, ankle, knee and hip ROM

Gait parameter	Patient 1		Patient 2	
	Non-VR	VR	Non-VR	VR
Walking speed (m/sec)	0.42 (0.10)	0.45 (0.11)	0.36 (0.08)	0.46 (0.11)
Stride time (sec)	1.8 (0.04)	1.7 (0.1)	2.0 (0.1)	1.8 (0.1)
Step width (cm)	29.8 (1.2)	26.4 (0.9)	18.2 (1.1)	18.6 (1.3)
Step length (cm) (paretic/nonparetic)	34.5 (1.6)/35.2 (2.4)	35.7 (1.9)/36.0 (2.2)	43.6 (2.5)/22.5 (3.1)	49.3 (3.3)/31.3 (2.8)
Stride time variability (paretic/nonparetic)				
%CV	3.2/3.1	4.1/3.9	5.0/5.0	3.7/4.0
SampEn	1.8/1.8	1.7/1.6	2.2/2.2	2.0/2.2
Gait variability—ankle (paretic/nonparetic)				
%CV	10.2/7.3	10.3/6.4	10.1/14.5	8.4/8.0
SampEn	1.9/2.0	1.8/2.0	2.0/2.0	2.1/1.9
Gait variability—knee (paretic/nonparetic)				
%CV	6.9/3.2	6.9/3.3	15.5/5.6	11.2/3.3
SampEn	1.9/2.1	1.7/2.0	2.1/1.9	2.1/2.0
Gait variability—hip (paretic/nonparetic)				
%CV	9.1/6.9	6.9/4.4	14.4/8.0	13.4/5.7
SampEn	1.7/1.8	1.8/2.0	2.0/1.5	1.9/1.5

3 Results

Mean (SD) values for walking speed, stride time, step width, step length and variability in stride time, ankle, knee and hip ROM can be found in Table 2. Both patients walked faster with longer step lengths in both the paretic and nonparetic leg and with shorter stride times in the VR condition. Patient 1 took more narrow steps, while patient 2 slightly broadened his step width when being immersed in the virtual environment. For gait variability, differences between the non-VR and VR condition were also obtained. The VR condition elicited lower CV values for the ankle, knee and hip ROM than the non-VR condition in both patients. For stride time variability, the VR condition exhibited higher CV values in patient 1 and lower CV values in patient 2. Minor to no changes were observed in SampEn values between the non-VR and VR condition in both patients.

4 Discussion and Conclusion

It can be concluded that walking with immersive VR led to positive changes in walking speed and spatiotemporal gait parameters of both patients. However, the addition of immersive VR introduced less step-by-step variability in joint kinematics in both patients. The amount of variability was decreased in magnitude (freezing the degrees of freedom), but the structure of the variability did not change. Literature regarding the effect of VR on spatiotemporal gait parameters and gait variability is scarce, especially within the neurological population. Our preliminary data of the two patients suggest that VR can influence the gait pattern and gait variability in people post-stroke. The results should be further investigated with a larger sample size.

Acknowledgements E. De Keersmaecker and D. Rodriguez-Cianca are both Strategic Basic Research fellows funded by the Research Foundation Flanders (FWO).

References

1. E.J. Benjamin et al., Heart disease and stroke statistics-2017 update: a report from the American Heart Association. *Circulation* **135**(10), e146–e603 (2017)
2. J. Mehrholz, S. Thomas, B. Elsner, Treadmill training and body weight support for walking after stroke. *Cochrane Database Syst. Rev.* **8**, Cd002840 (2017)
3. D. Cano Porrás, P. Siemonsma, R. Inzelberg, G. Zeilig, M. Plotnik, Advantages of virtual reality in the rehabilitation of balance and gait: systematic review. *Neurology* **90**(22), 1017–1025 (2018)
4. M.C. Howard, A meta-analysis and systematic literature review of virtual reality rehabilitation programs. *Comput. Hum. Behav.* **70**, 317–327 (2017)
5. E. De Keersmaecker, N. Lefeber, M. Geys, E. Jespers, E. Kerckhofs, E. Swinnen, Virtual reality during gait training: does it improve gait function in persons with central nervous system movement disorders? A systematic review and meta-analysis. *NeuroRehabilitation* **44**(1), 43–66 (2019)
6. D. Katsavelis, L. Decker, N. Kochi, N. Stergiou, Effect of optic flow produced by virtual reality on gait variability. *J. Sport Exerc. Psychol.* **30**, S97–S98 (2008)

Automatic Versus Manual Tuning of Robot-Assisted Gait Training



C. Bayón, S. S. Fricke, H. van der Kooij, and E. H. F. van Asseldonk

Abstract Robot-assisted gait training (RAGT) is a promising rehabilitation technique that is increasingly used in the clinic to improve walking ability after a neurological disorder. The effectiveness of RAGT might depend on the customization of the robotic therapy, which in most of the cases is done either manually by the clinical practitioner (MT) or by adaptive controllers developed to automatically adjust the assistance (AT). In this contribution we present a comparison of automatic versus manual tuning of RAGT, where we assessed the differences in the adjustment of the therapy for ten participants with neurological disorders (six stroke, four spinal cord injury). The AT approach reached stable assistance levels quicker than the MT approach. Moreover, the AT ensured a good performance for all subtasks of walking with lower assistance levels than the MT. Future clinical trials need to be performed to show whether these apparent advantages result in better clinical outcomes.

1 Introduction

In clinical practice, robot-assisted gait training (RAGT) is used to provide intensive, repetitive and task-specific training, while it also contributes to reduce physical load for therapists [1]. The amount of robotic assistance provided during RAGT is frequently manually chosen by the practitioner (MT). This leads to outcomes that can be influenced by subjective decisions, and assistance tuning may become a time-consuming task. In the last years, automatic algorithms have been developed with the aim to objectively and quickly tune the assistance (AT) and properly tailor the therapy to patient's capabilities [2, 3]. In this contribution we present the main results

C. Bayón and S. S. Fricke are contributed equally to the presented work. First author is shared between C. Bayón and S. S. Fricke.

C. Bayón (✉) · S. S. Fricke · H. van der Kooij · E. H. F. van Asseldonk
Department of Biomechanical Engineering, University of Twente, Enschede, The Netherlands
e-mail: c.bayoncalderon@utwente.nl

of an exploratory study [4] where we compare the MT and AT approaches by using the LOPES II gait trainer.

2 Materials and Methods

2.1 Robotic Device

The LOPES II gait trainer is a treadmill-based rehabilitation device with eight actuated degrees of freedom for the hips, knees and pelvis to guide the lower limbs following prescribed gait patterns. The robotic assistance provided by the device can be classified into seven subtasks of walking (i.e. weight shift, lateral foot placement, leading limb angle, trailing limb angle, prepositioning, stability during stance and foot clearance). For each of those subtasks, the assistance can be tuned from 0 to 100%.

2.2 Tuning of the Robotic Assistance

In both approaches (MT and AT) the subtask-based assistance could be adjusted individually and separately for each leg in steps of 10%.

For the MT, an intuitive user interface was used by an experienced therapist. The subtasks could be coupled or decoupled for the adjustments, allowing simultaneous changes in assistance for the coupled subtasks. Visual feedback about the user's performance with respect to the reference gait pattern was provided for each subtask to the physical therapist.

For the AT, the algorithm described in [2] was used. It tuned the assistance by evaluating deviations of the measured joint angles from the reference pattern at specific key points of the gait cycle (e.g. max. knee flexion). Each key point corresponded to one particular subtask of walking.

2.3 Experimental Protocol

Six stroke survivors (STR) and four persons with incomplete spinal cord injury (SCI), all in chronic phase (>6 months after injury), took part in this study. Experiments were approved by the local ethical committee (METC Twente), and participants gave written informed consent prior participation.

The experiment consisted of two sessions: familiarization and experimental session. The familiarization session was used to practice walking in the LOPES II and to set the preferred walking speed and partial body weight support (PBWS)

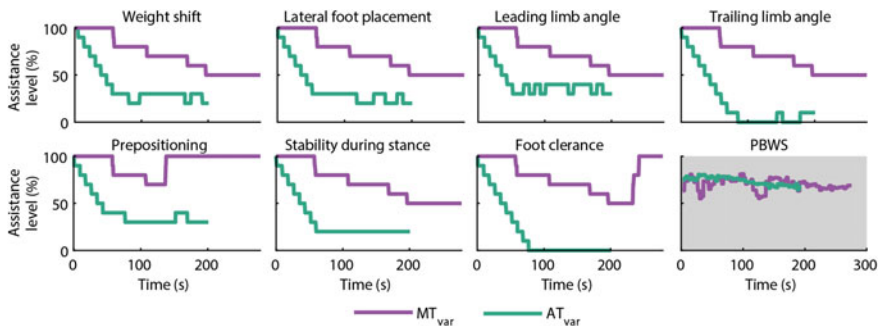


Fig. 1 Subtask-based assistance tuning for the most impaired leg of one of the SCI subjects in MT_{var} and AT_{var} trials. PBWS was not tuned, but measured, and it varied due to the use of handrails

for each participant. In the experimental session, these parameters were used while assessing the MT and AT approaches in four trials: MT_{var} , MT_{const} , AT_{var} and AT_{const} . For the “var” trials, the assistances were tuned for each subtask, either by the physical therapist (MT_{var}) or by the automatic algorithm (AT_{var}). For the “const” trials, the robotic assistances were kept constant at the levels found during the tuning, and the participants walked for 3 min with these levels.

2.4 Assessment

To analyze differences between the MT and AT approach, we focused on several aspects: time to reach stable assistance levels (difference to final level $<10\%$ for all subtasks), final amount of assistance, errors with respect to the reference pattern at final amount of assistance, and participants’ preferences.

3 Results

On average, a stable assistance level was reached more quickly for AT_{var} (110 ± 54 s) than for MT_{var} (279 ± 120 s). Figure 1 shows as an example how the robotic assistance was tuned for the different subtasks in AT_{var} and MT_{var} , for one of the SCI participants.

The amount of final robotic assistance was higher for the MT approach than for the AT approach in 53 of 70 cases (70 cases = 7 subtasks · 10 participants), see Fig. 2 as an example. Remarkably, although often less assistance was applied for AT_{const} than for MT_{const} , the largest errors of up to 20° of deviation from the reference trajectory were found for MT_{const} (Fig. 2).

Participants did not report any clear preference of one approach over the other regarding safety, comfort, effect and amount of assistance.

4 Discussion and Conclusion

The AT approach had several advantages compared to the MT approach, from which we highlight: (1) quicker tuning to stable assistance levels, (2) lower assistance levels reached, (3) good performance for all subtasks with respect to reference patterns. This AT algorithm [2] may be easily transferred to other robotic trainers that use kinematic references in their control.

The therapist often provided higher assistances than the AT algorithm, which could mean that the MT approach is not that good in enhancing the active participation of the patient. One of the reasons for that might be that the therapist acted on the safe side, by trying to prevent possible problems as stumbling or exhaustion. Although he could use the user interface to see the participant's performance respect to the reference trajectories for all subtasks, he mainly relied on visual assessment of the gait pattern when tuning the assistance. This could be an indication that the therapist tried to reach an acceptable walking pattern rather than to decrease deviations from reference trajectories.

Although it is not known which combination would work best, we believe that a combination of AT and MT subtask-based assistance could be beneficial for future RAGT as it would take into account therapist's knowledge but also the advantages of the AT algorithm.

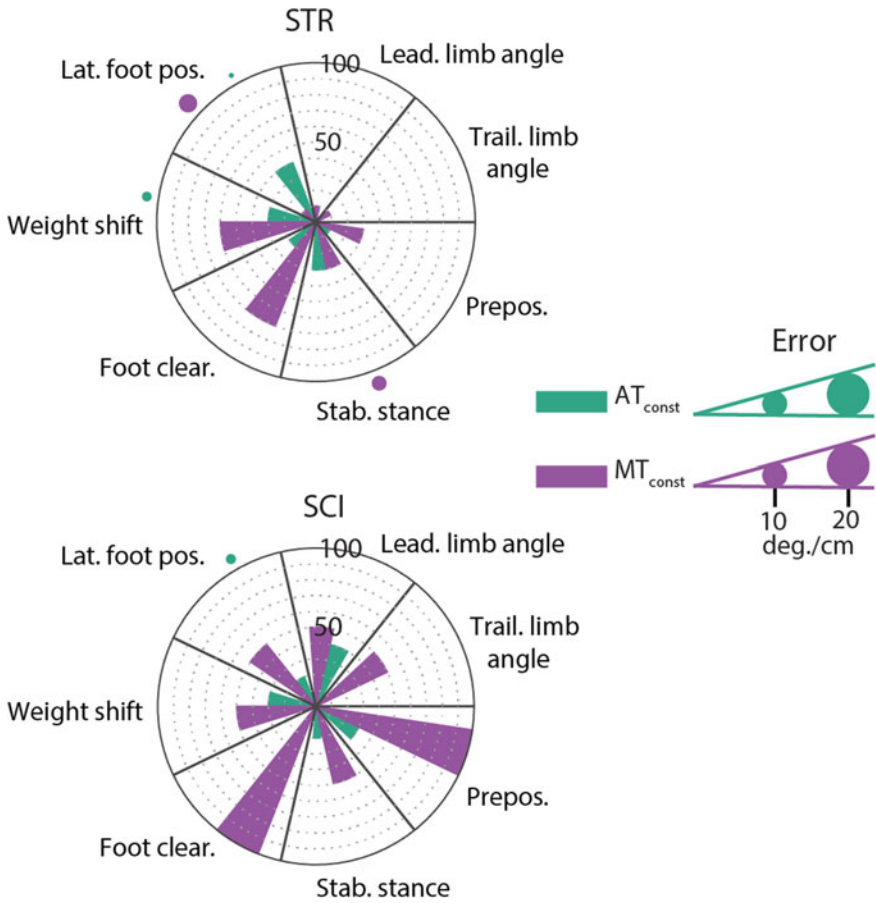


Fig. 2 Assistances (bars) and errors (circles) for all subtasks with respect to the reference pattern in the more impaired leg for one STR and one SCI subjects, in MT_{const} and AT_{const}

Acknowledgements This work was supported by the Dutch NWO Domain Applied and Engineering Sciences, project number 12850 (AWARD project).

References

1. M.R. Spiess, F. Steenbrink, A. Esquenazi, Getting the best out of advanced rehabilitation technology for the lower limbs: minding motor learning principles. *PM R* **10**(9), S165–S173 (2018)
2. C. Bayón, S. Fricke, E. Rocon, H. van der Kooij, E. van Asseldonk, Performance-based adaptive assistance for diverse subtasks of walking in a robotic gait trainer: description of a new

controller and preliminary results, in IEEE International Conference on Biomedical Robotics and Biomechatronics (BioRob) (2018)

3. S. Maggioni, N. Reinert, L. Lünenburger, A. Melendez-Calderon, An adaptive and hybrid end-point/joint impedance controller for lower limb exoskeletons. *Front. Robot. AI* **5** (2018)
4. S.S. Fricke, C. Bayón, H. Van Der Kooij, E.H. Edwin, Automatic versus manual tuning of robot-assisted gait training in people with neurological disorders. *J. Neuroeng. Rehabil.* **17**(1), 1–15 (2020)

Six weeks Use of a Wearable Soft-robotic Glove During ADL: Preliminary Results of Ongoing Clinical Study



Anke I. R. Kottink, Corien D. M. Nikamp, Jaap H. Buurke, Foskea Bos, Corry K. van der Sluis, Marieke van den Broek, Bram Onneweer, Janneke M. Stolwijk-Swüste, Sander M. Brink, Johan S. Rietman, and Gerdienke B. Prange-Lasonder

Abstract In this ongoing study, an assistive wearable soft-robotic glove, named Carbonhand, is tested at home for 6 weeks by subjects with decreased handgrip strength to receive a first insight in the therapeutic effect of using this assistive grip-supporting glove during ADLs. Preliminary results of the first 13 participants showed that participants appreciated use of the glove to assist them with daily life activities. Even more, grip strength without glove improved and functional performance showed increases as well. These preliminary findings hold promise for observing a clinical effect of using the soft-robotic glove as assistance in ADLs upon completion of data collection.

A. I. R. Kottink (✉) · C. D. M. Nikamp · J. H. Buurke · J. S. Rietman · G. B. Prange-Lasonder
Roessingh Research and Development, University of Twente, Enschede, The Netherlands
e-mail: a.kottink@rrd.nl

J. S. Rietman
Roessingh Center for Rehabilitation, Enschede, The Netherlands

F. Bos
Reade, Amsterdam, The Netherlands

C. K. van der Sluis
University Medical Center Groningen, Groningen, The Netherlands

M. van den Broek
Sint Maartenskliniek, Nijmegen, The Netherlands

B. Onneweer
Rijndam Rehabilitation, Rotterdam, The Netherlands

J. M. Stolwijk-Swüste
De Hoogstraat Rehabilitation, Utrecht, The Netherlands

S. M. Brink
Isala, Zwolle, The Netherlands

1 Introduction

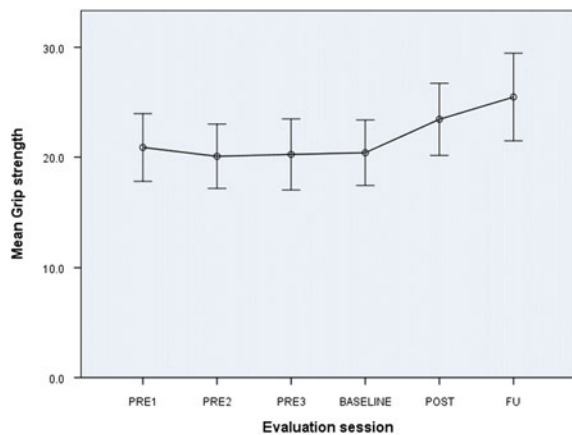
Hand function is very important to perform activities of daily living (ADLs). One of the most common problems concerning hand function is a decrease in hand strength, which occurs across a wide range of disorders. Specifically, people with reduced hand function often have difficulties with holding and manipulating objects, subsequently leading to difficulties with independently performing ADLs [1]. These limitations can have a negative effect on their participation in society or on quality of life [2]. Wearable robotics seem a promising approach to enable direct support of motor function for prolonged periods in the home environment of patients. With a wearable assistive device, performance of functional activities are supported directly, while it is hypothesized that using the affected arm and hand repeatedly during ADLs provides intensive and task-specific training at the same time. This might result in improved unsupported arm and hand function after prolonged use. In the present study, the aim was to investigate if six weeks home-use of an assistive soft-robotic glove during ADLs resulted in a therapeutic (i.e. clinical) effect on hand strength and hand function.

2 Methods

2.1 Study Design

This ongoing study consists of a multicenter uncontrolled intervention study and takes place in seven centers in the Netherlands. All participants will be assessed five times, consisting of three pre-evaluations, a post- and follow-up evaluation.

Fig. 1 Carbonhand system



2.2 Participants

The aim is to include 63 chronic patients with decreased handgrip strength. Subjects with a wide variety of disorders are included, such as traumatic brain injury, spinal cord injury, orthopaedic problems or a stroke, but all in a chronic and stable phase of disease. Main inclusion criteria are: at least 10° active extension of wrist/fingers and 10° active flexion of fingers. Main exclusion criteria are: severe acute pain of the most-affected hand, severe contractures limiting passive range of motion, severe spasticity of the hand and receiving arm-/hand function therapy during the course of the study. The study is approved by the Medical Ethical Committee of Twente and the Dutch Health Inspectorate. All participants signed an informed consent prior to study start.

2.3 Intervention

The soft-robotic glove was manually adjusted to each individual participant. All participants used the soft-robotic glove during ADLs at home for six weeks. Participants were free to choose for which activities, when and for how long they used the system. However, it was recommended to use the glove at least 180 min a week during the most common ADLs, such eating/drinking, functional transfers and personal hygiene.

2.4 Soft-robotic Glove

The Carbonhand system (Fig. 1) is based on the concept of a wearable soft-robotic glove that can provide extra grip strength to the thumb, middle and ring finger. A tendon-driven mechanism in the system is used to provide assistance in flexion of the fingers. The amount of assistance is modulated by pressure sensors in the fingertips and movement sensors along the fingers. The extra grip strength is always activated in a natural and intuitive way and in proportion to the force applied by the user due to an intention-detection mechanism. Glove settings (e.g. maximum force, sensitivity level) can be tuned for each individual.

2.5 Study Procedure

All involved therapists received an extensive training prior to the study in order to adapt the soft-robotic glove and its settings to each individual participant and to standardize the execution of the measurements across centers. Three pre-evaluations

Fig. 2 Change in grip strength (kg) over time



(T0, T1 and T2) were scheduled in three weeks for each participant. After the third assessment, the intervention period started, in which the participant used the soft-robotic glove at home for a period of six weeks. After ending the intervention period, a post-evaluation (T3) took place. Four weeks after the intervention period a follow-up evaluation (T4) was scheduled.

2.6 Outcome Measures

To examine the therapeutic effect of the soft-robotic glove, all tests were performed without using the glove. The primary outcome measure of the study was grip strength of the (most) affected hand, measured with the Jamar dynamometer (Patterson medical, Warrenville, IL, USA). A selection of secondary outcome measures is presented here: Jebson-Taylor Hand Function Test (JTHFT) and user experience, measured by self-reported grading (1–10) of ease of donning, ease of use and support from glove.

2.7 Data Analysis

Data was analysed using IBM SPSS Statistics (v23.0). A baseline value was calculated as the mean of the three pre-evaluation values, to average out day-to-day changes. Data was inspected for normality using normal probability plots and Kolmogorov-Smirnov tests. In order to assess the effect of the intervention over time, and because of the preliminary character of the study, paired-samples t-tests were performed between evaluation sessions. Descriptive analysis were performed

for participant characteristics and user experience ratings. The significance level was set at 0.05.

3 Results

3.1 Participants

Of the 13 participants included so far, nine (69%) were female. Mean age was 53 years (range 36–75 years; SD 12 years). Mean time after injury was 5.8 years (range 9 months–24 years; SD 7.8 years). The most prevalent causes of hand function limitations were trauma (46%) and rheumatoid arthritis (23%), followed by osteoarthritis, juvenile idiopathic arthritis, neuropathy and amyloidosis (each 8%). All but one participant had their right hand affected (most), which was their dominant hand. Data were missing for grip strength (T4) from two and for user experience (T3) from one participant.

3.2 Outcome Measures

Grip strength improved significantly from baseline (mean 20.4 kg; SD 10.8; indicating stable phase pre-intervention, see Fig. 2) to post-intervention (mean 23.4 kg; SD 11.8) with 3 kg (SD 4.7; $p = 0.038$). JTHFT did not change significantly, but showed a trend of improved performance after intervention. Performance was faster by 5.0 s (SD 8.7) from baseline to post intervention ($p = 0.074$) and 6.1 s (SD 10.7) from baseline to follow-up ($p = 0.087$). User experience grades were positive, with a mean grade of 8.3 for ease of donning (SD 1.1) and 7.3 for both ease of use and support from glove (SD 1.5 and 2.0, resp.).

4 Discussion

The goal of the present study was to explore first outcomes of a therapeutic effect of a soft-robotic glove on grip strength in patients with hand function problems, after using the glove for six weeks during ADLs. Findings of the first 13 participants showed that grip strength improved and hand function also tended to increase. The improvement in JTHFT performance from baseline to follow-up reached the level of its minimal clinically important difference (6 s faster execution of total test), indicating that at least a portion of the participants achieved a more functional task performance.

In addition, a high grade for donning the glove was found, which is often considered a bottleneck in use of hand devices. This implies that use of this soft-robotic glove at home is feasible, without users requiring help from a spouse or family member to start using the glove in their daily life.

However, the current statistics should be interpreted with caution, due to the underpowered sample and the lack of correction for multiple testing in this ongoing study.

5 Conclusion

The findings at the current stage of this ongoing study, with 21% of needed participants, hold promise for observing a therapeutic effect of using the soft-robotic glove during ADLs, upon completion of data collection: unsupported hand strength and hand function improve after 6-week assistive glove use.

Acknowledgements We would like to thank all participating centers for their contribution to this study, and Bioservo Technologies AB for the provided systems and their technical support during the study.

This study was funded by the European Union's Horizon 2020 research and innovation programme.

References

1. P. Langhorne, J. Bernhardt, G. Kwakkel, Stroke rehabilitation. *Lancet* **377**(9778), 1693–1702 (2011)
2. N.E. Mayo, S. Wood-Dauphinee, R. Rôte, L. Durcan, J. Carlton, Activity, participation, and quality of life 6 months poststroke. *Arch. Phys. Med. Rehabil.* **83**(8), 1035–1042 (2002)

Proof-of-Concept of POF-Based Pressure Sensors Embedded in a Smart Garment for Impact Detection in Perturbation Assessment



Leticia Avellar, Arnaldo Leal-Junior, Carlos Marques, E. Rocon, and Anselmo Frizera

Abstract This paper presents the proposal of intensity variation-based POF pressure sensors embedded in a smart garment for impact detection in perturbation assessment. The proposed system presents low cost and is based on multiplexing technique using side-coupling light source. In addition, it is able to acquire the optical power variation when the pressure on the sensor is applied and to detect the region where the

This research is financed by FAPES (84336650), CNPq (304049/2019-0) and Petrobras (2017/00702-6). C. Marques acknowledges Fundação para a Ciência e a Tecnologia (FCT) through the CEECIND/00034/2018 (iFish project) and this work was developed within the scope of the project i3N, UIDB/50025/2020 & UIDP/50025/2020, financed by national funds through the FCT/MEC. This work is also funded by national funds (OE), through FCT, I.P., in the scope of the framework contract foreseen in the numbers 4, 5 and 6 of the article 23, of the Decree-Law 57/2016, of August 29, changed by Law 57/2017, of July 19. This work was partially funded by BenchBalance EU project (EU-H2020-779963-FSTP1-BenchBalance).

L. Avellar (✉) · A. Leal-Junior · A. Frizera
Graduate Program of Electrical Engineering, Federal University of Espírito Santo, 29075-910
Vitoria, Brazil
e-mail: leticia.avellar@aluno.ufes.br

A. Leal-Junior
e-mail: leal-junior.arnaldo@ieee.org

A. Frizera
e-mail: frizera@ieee.org

C. Marques
I3N & Physics Department, Universidade de Aveiro, Campus Universitário de Santiago, 3810-193
Aveiro, Portugal
e-mail: carlos.marques@ua.pt

L. Avellar · E. Rocon
Centro de Automática y Robótica, CSIC-UPM, Arganda del Rey, Madrid, Spain
e-mail: e.rocon@csic.es

perturbation occurred. Then, a proof-of-concept test was performed with application of pressure on different sensors which show the ability of the system to identify the impact region in a wearable device during a perturbation protocol.

1 Introduction

THE use of wearable sensors is progressively growing for monitoring information about motion activities in real time [1]. Textile sensors have been an interesting solution in recent years, since clothing has large portable surfaces in which sensors and electronics can be integrated [2].

However, textile are usually not optimized for sensing purposes, and electrical sensors embedded in textile can present some disadvantages, such as hysteresis provoked by compressed material, which lead to measurement errors [3]. In addition, electrical sensors may be dangerous some under conditions, since they conduct electrical energy and may provoke short circuit.

Optical fiber sensors (OFS) has been widely used as an alternative in order to overcome these drawbacks for it good accuracy and good sensitivity, besides offering the possibility to implement distributed sensors, and to be electrically passive (and hence safer to use), bio-compatible and immune to electromagnetic interference [4–6].

Among the optical fiber materials, polymer optical fibers (POFs) present some advantages such as low cost, lightweight, flexibility and robustness, and they are able to measure high strain values without damage [7]. In addition, POF sensors combined with intensity variation-based interrogation technique comprise a simple and low cost solution for smart textile [4, 8].

This paper present a proof-of-concept of intensity variation based POF pressure sensors embedded in a garment for impact area detection for assessment of perturbation protocol.

2 Materials and Methods

Figure 1a shows the Smart Garment structure, which consists of two POFs made of polymethyl methacrylate, PMMA (HFBR-EUS100Z, Broadcom Limited) with a core diameter of 980 μm , a cladding of fluorinated polymer with 20 μm thickness and a polyethylene coating that results on a total diameter of 2.2mm for the fiber considering its coating. The light source used is a light-emitting diode (LED) flexible lamp belt, and to enable the side-coupling of the LED and, at the same time, increase the sensor sensitivity, a lateral section is made on the fiber, where the cladding and part of the core are removed through abrasive removal of material following the guidelines presented in [9]. This creates the sensitive zones that act as sensors in

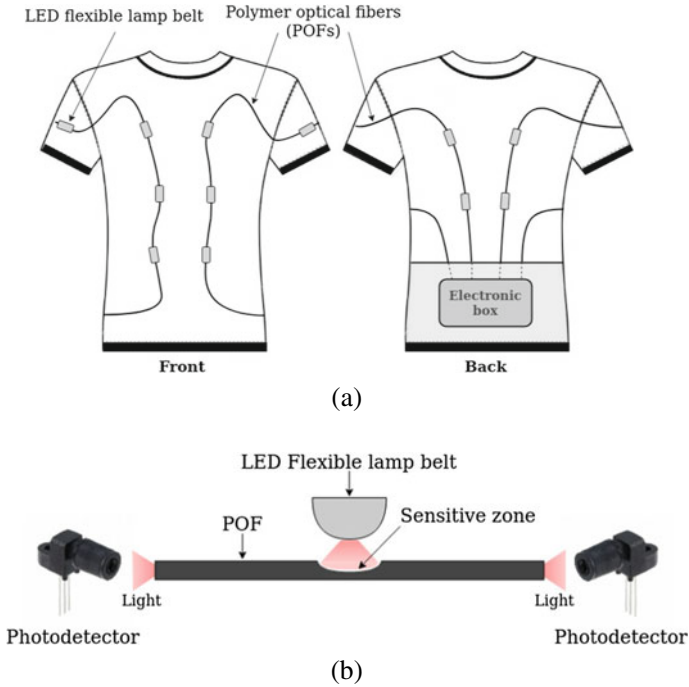


Fig. 1 System setup. **a** Smart garment overview. **b** System operating principle

this work (see Fig. 1b). In this case, 6 lateral sections were produced on each fiber, resulting in 12 pressure sensors.

The sensors' responses, i.e., the optical power variation, were acquired by four photodetectors IF-D92 (Industrial Fiber Optics, Tempe, AZ, USA), one at each fiber end. The signal acquisition and the LEDs control are performed by the microcontroller FRMD-KL25Z (NXP Semiconductors, Netherlands) and all the data were analyzed and processed in MATLAB (MathWorks Inc., Natick, MA, USA). The proposed system was based on multiplexing technique proposed by [10], which comprises of a sequential activation of each LED with a predefined frequency and activation sequence. The microcontroller is responsible for the acquisition of the optical power measured by each photodetector when each LED is active.

For a proof-of-concept of the proposed sensor system, a test was performed by pressing eight different sensors sequentially, while a volunteer was wearing the smart garment, in order to evaluate the multiplexing capacity and, hence the ability of impact area detection.

3 Results and Discussion

The results of the proof-of-concept test are presented in Fig. 2. Eight perturbations were applied on different sensors while a volunteer was wearing the smart garment. Figure 2a shows the perturbation area of each applied pressure and Fig. 2b shows the normalized sensor responses to pressures applied on each sensor with respective colors representing each perturbation over time. The sensors responses were normalized since in this preliminary assessment the optical power variation of each sensor was used to identify whether there is or not the perturbation, and not to measure the applied force.

The results show that the sensor system is multiplexed and the crosstalk between the sensors is negligible. This makes it possible to identify which sensor was pressed, and hence identify which region of human body the perturbation occurred. The number of sensors was defined to prove the concept, however it can be increased according to requirement of spatial resolution. In addition, this setup can be employed

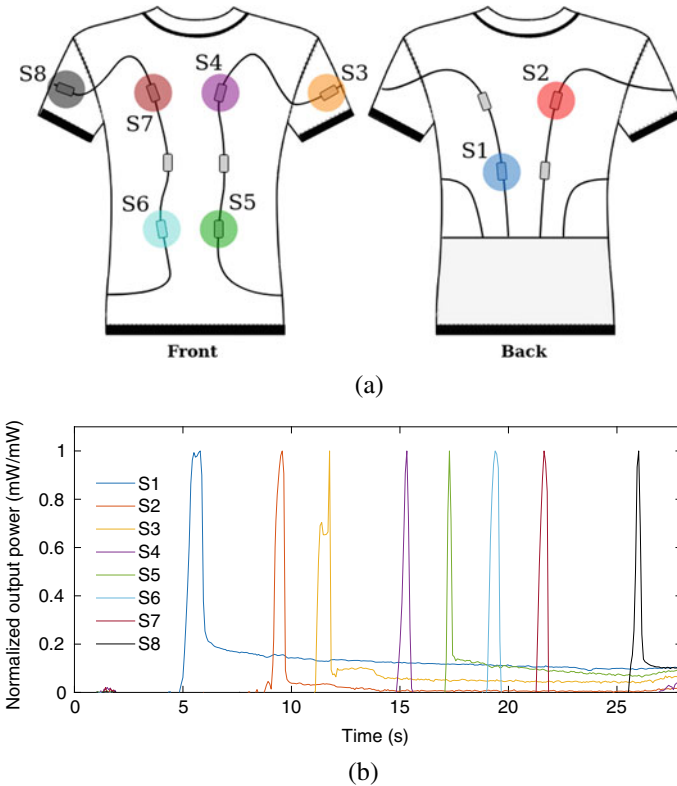


Fig. 2 Results of the proof-of-concept test. **a** Impact area of smart garment. **b** Sensor responses to pressures applied on the smart garment

in other textile applications which involve impact detection, such as a textile to identify the interaction between exoskeleton and a lower limb or smart gloves.

4 Conclusion

This paper presented a proof-of-concept of intensity variation-based POF pressure sensors embedded in a smart garment for impact detection in perturbation assessment. The proposed smart garment is comprised of two POFs with twelve sensors which were fabricated by lateral sections made in the fibers and the light coupling of LED flexible lamp belt laterally arranged. A simple pressure test was performed with application of a perturbation on eight different sensors and results showed that the system is capable to detect impact region and the crosstalk between sensors is negligible. The system shows a good alternative to the current electrical textile sensors since this system present low cost and fabrication simplicity, besides allowing the increase of the number of sensors in the same fiber. Future works involve the system application in the real time impact detection, the study of the response latency and the use of the proposed smart garment in perturbation protocol with patients.

References

1. S. Majumder, T. Mondal, M.J. Deen, Wearable sensors for remote health monitoring. *Sensors (Switzerland)*, **17**(1) (2017)
2. F. Pizarro, P. Villavicencio, D. Yunge, M. Rodríguez, G. Hermosilla, A. Leiva, Easy-to-build textile pressure sensor. *Sensors (Switzerland)* **18**, 4 (2018)
3. J. Meyer, B. Arnrich, J. Schumm, G. Troster, Design and modeling of a textile pressure sensor for sitting posture classification. *IEEE Sens. J.* **10**(8), 1391–1398 (2010)
4. C. Massaroni, P. Saccomandi, E. Schena, Medical smart textiles based on fiber Optic technology: an overview. *J. Funct. Biomat.* **6**(2), 204–221 (2015)
5. L.S.M. Alwis, K. Bremer, F. Weigand, M. Kuhne, R. Helbig, B. Roth, Textile carbon reinforcement structures with integrated optical fibre sensors designed for SHM applications, in *25th International Conference on Optical Fiber Sensors*, vol. 10323 (2017), p. 1032376
6. Z. Gong, Z. Xiang, X. OuYang, J. Zhang, N. Lau, J. Zhou, C.C. Chan, Wearable fiber optic technology based on smart textile: a review. *Materials* **12**(20), (2019)
7. K. Peters, Polymer optical fiber sensors—a review. *Smart Mater. Struct.* **10**, (2011)
8. L.M. Avellar, A.G. Leal-Junior, C.A.R. Diaz, C. Marques, A. Frizzera, POF smart carpet: a multiplexed polymer optical fiber-embedded smart carpet for gait analysis. *Sensors* **19**(15), 3356 (2019). [Online]. Available: <https://www.mdpi.com/1424-8220/19/15/3356>
9. A.G. Leal-junior, A. Frizzera, M.J. Pontes, Sensitive zone parameters and curvature radius evaluation for polymer optical fiber curvature sensors. *Opt. Laser Technol.* **100**, 272–281 (2018)
10. A.G. Leal-junior, C.R. Díaz, C. Marques, M.J. Pontes, A. Frizzera, Multiplexing technique for quasi-distributed sensors arrays in polymer optical fiber intensity variation-based sensors. *Opt. Laser Technol.* **111**, 81–88 (2018). [Online]. Available: <https://doi.org/10.1016/j.optlastec.2018.09.044>

Influence of Innovative Rehabilitation Technology on Intensity of Training: Preliminary Results



Anke I. R. Kottink, Gerdienke B. Prange-Lasonder, Lars Dijk, Chris T. M. Baten, Judith F. M. Fleuren, and Jaap H. Buurke

Abstract The present study compared intensity of training between technology-supported and conventional exercises during a regular therapy session in three brain injured patients with arm/hand limitations. Results showed that intensity was higher during technology-supported exercises. Further research with a larger sample is needed to confirm these outcomes and assess its potential relation to treatment effect.

1 Introduction

Upper limb motor impairment is one of the most common deficits after stroke, which has substantial impact on a person's quality of life. To stimulate upper limb motor function, therapy should consist of several key elements: repetitive, high-intensive, task-specific and functional exercises with active contribution of the patient [1]. A proposed solution to achieve a high intensity of training is the use of rehabilitation technology, such as robotics, which has shown to be as effective as conventional therapy for improving arm/hand function [2].

A common, and compelling, assumption is that using technology for motivation and repetition increases the intensity of training. When expressed as number of movements, intensity of functional upper extremity exercise in clinical practice was reported to be only an average 32 per session, which is much lower than commonly used in studies aiming for (animal and human) motor learning [3]. One could question whether the number of movements is a good representation of intensity of practice,

A. I. R. Kottink (✉) · G. B. Prange-Lasonder · C. T. M. Baten · J. H. Buurke
Roessingh Research and Development and University of Twente, Enschede, The Netherlands
e-mail: a.kottink@rtd.nl

L. Dijk
University of Groningen, Groningen, The Netherlands

J. F. M. Fleuren
Roessingh Center for Rehabilitation, Enschede, The Netherlands

as this is not applicable to functional non-repetitive movements, and doesn't take into account the effort of the movement.

A direct comparison of intensity between conventional and technology-supported exercises is yet to be examined. Therefore, the aim of the present study was to get a first insight into intensity of arm/hand movement during gaming exercises of the upper extremity with respect to conventional exercises.

2 Methods

2.1 Study Design and Procedure

A pilot observational study was conducted at Roessingh Centre for Rehabilitation, Enschede, the Netherlands. All participants followed their regular arm-/hand function therapy sessions, consisting of a circuit mixing conventional and technology-supported exercises during 1-h group sessions. During one of those sessions, recordings were made during a set of conventional exercises (CON set) and exercises supported by rehabilitation technology (RT set). The order was determined by randomization.

The therapist chose the most appropriate exercises within each set matching individual treatment goals, as usual, and instructed the participants to perform the exercises as usual. Ten minutes of both sets were recorded, of which five minutes were used for analysis. No approval of the Medical Ethical Committee was needed for this observational study. All participants signed an informed consent prior to the start of the study.

2.2 Participants

Participants of the study involved a small sample of sub-acute stroke or acquired brain injury (ABI) patients with some functional ability of their upper extremity (ARAT > 9).

2.3 Interventions

Technology-supported exercises (RT set)

Therapists could choose from two systems (Fig. 1):

- ArmeoBoom: Participants with minimal arm function were trained with the ArmeoBoom (Hocoma AG, Switzerland), a passive device providing weight support of the arm in a 3D work space. It has a webcam and a laptop, on which

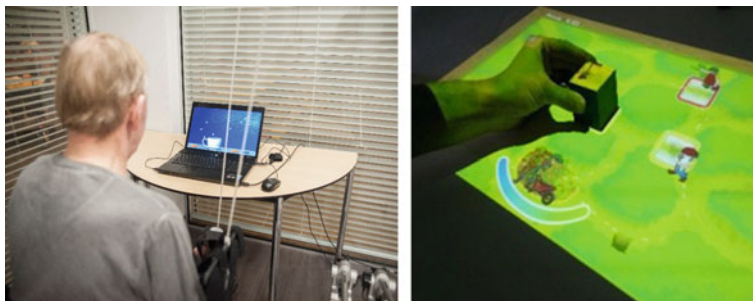


Fig. 1 Devices in RT set: ArmeoBoom (left) and HandsOn game (right)

interactive exercises are played by moving the affected arm in an individually adjusted virtual environment, practicing reaching.

- HandsOn game: Participants who had at least moderate arm function and minimal hand function were trained with the HandsOn game, an applied game, designed inhouse, to train functional movements. The virtual environment is projected on a table by a beamer and the game is controlled by moving physical objects, detected by Kinect camera. The choice of the objects, a variety of different shapes and sizes, determines the grasp, hand and/or wrist movement to be practiced, integrating reaching and grasping/releasing.

Conventional exercises (CON set)

Exercises in CON set were ‘analog’, without mechanical supports or computerized training environments.

2.4 Equipment

Hand movements were recorded with 5 inertial measurement units (IMUs, Xsens Technologies, NL) at a frequency of 40 Hz. IMUs were positioned on the hand, lower arm and upper arm of the affected limb, on the sternum and pelvis. All sensors were fixated by straps, except the sternum marker, which was attached by a small unobtrusive harness. Custom-made software was used for calibration protocols, performed each time sensors were (re-) applied, collection of all movement data and estimation of horizontal hand position relative to the center of intervertebral body L5/S1.

2.5 Data Analysis

Of the 10-min recordings, 5 min were used for analysis. The cumulative length of the 3D trajectories of the hand (distance travelled) represented dosage. Movement

Table 1 Participant characteristics

Participant	Gender	Age (years)	Diagnosis	Affected side
1	Male	74	Stroke	Left
2	Female	42	Stroke	Left
3	Male	49	Cerebral toxoplasmosis	Left

effort was assessed by measuring the maximal work area of the hand covered during exercises, considering that effort is increasing with increasing RoM due to reduced independent joint control [4]. Data was analysed using IBM SPSS Statistics (v23.0). Descriptive statistics were used to compare the 3D hand trajectories between sets. No statistical tests were done due to the small sample size.

3 Results

3.1 Participants

Table 1 shows the characteristics of the three included participants. The mean time after injury was 14.3 weeks (SD = 4.2). Participants one only had minimal arm function, while participant two and three already had some hand function.

3.2 Intensity of Practice

Figure 2 shows typical hand position data for two participants (P2 and P3) in a transverse plane. The maximal area covered by the affected hand was larger during RT set compared to CON. Remarkably, the work area during the RT set covered a different section than during CON set; movements were performed further away from the body in RT exercises. The mean distance traveled by the hand was substantially larger during RT exercises (31 m) compared to CON (21.1 m).

4 Discussion

The present findings showed that three patients with neurological motor impairments performed larger hand trajectories during 5 min of technology-supported exercises compared to conventional exercises. In addition, the difference in work area suggests that technology-supported exercises might stimulate making movements towards the edges of the reachable workspace, more so than conventional exercises.

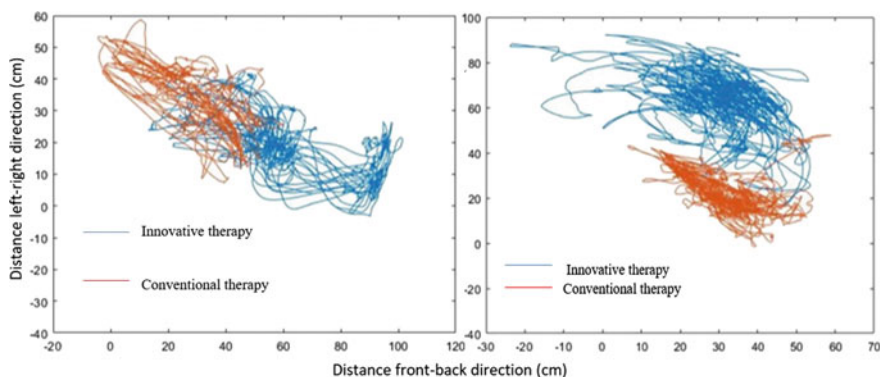


Fig. 2 Hand position traces of affected hand with respect to pelvis in transverse plane (left figure: P2; right figure: P3)

Increased intensity of practice is often used to convey potential benefit of a technology-supported approach, such as robotic training, but this is usually defined as number of repetitions (dosage). When considering number of movements, post-stroke patients receiving different doses of functional exercises didn't show differences in treatment effects [3]. In this study, regarding intensity as a concept that represents both the dosage and effort during movement, we observed a positive influence of technology-supported approaches (gaming and/or arm support) on intensity in a single session. This underlines the importance for defining intensity of treatment explicitly and considering other aspects of intensity, beyond simply dose. Whether differences in intensity of practice as represented in this study would contribute to different treatment effects has yet to be investigated.

Although seemingly confirming the hypothesis, these initial results need to be interpreted with utmost care due to the small sample size and descriptive nature of the analysis, and further research is needed to support current findings and relate them to clinical relevance.

Acknowledgements This study was funded by foundation “Hulpfonds Roessingh”.

We would like to thank the therapists of Roessingh Center for Rehabilitation (Enschede, the Netherlands) involved in NovaLab treatment for their contribution to this study.

References

1. P. Langhorne, J. Bernhardt, G. Kwakkel, Stroke rehabilitation. *Lancet* **377**(9778), 1693–1702 (2011)
2. J.M. Veerbeek, A.C. Langbroek-Amersfoort, E.E. van Wegen, C.G. Meskers, G. Kwakkel, Effects of robot-assisted therapy for the upper limb after stroke. *Neurorehabil. Neural Repair* **31**, 107–121 (2017)

3. C.E. Lang et al., Dose response of task-specific upper limb training in people at least 6 months poststroke: a phase II, single-blind, randomized, controlled trial. *Ann. Neurol.* **80**, 342–354 (2016)
4. M.D. Ellis, A.I.R. Kottink, G.B. Prange, J.S. Rietman, J.H. Buurke, J.P. Dewald, Quantifying loss of independent joint control in acute stroke with a robotic evaluation of reaching workspace, in *33rd Annual International Conference of the IEEE EMBS*, Aug 30–Sept 3, 2011.

Wearable Vibrotactile Biofeedback to Improve Human-Exoskeleton Compliance During Assisted Gait Training



Cristiana Pinheiro, Joana Figueiredo, and Cristina P. Santos

Abstract Biofeedback may accelerate post-stroke motor recovery during exoskeleton-assisted gait training. A wearable vibrotactile human-robot interaction (HRI)-based biofeedback is proposed to improve human-exoskeleton compliance during gait training assisted by an ankle-foot exoskeleton (AFE). A pre-post study with four healthy subjects was conducted to evaluate biofeedback training's efficacy. Results show statistically significant improvements (p -value: $4.56e-4-0.03$) in HRI torque outcomes and the participants felt motivated about training. Findings suggest that the proposed biofeedback can enhance human-robot compliance.

1 Introduction

Biofeedback systems (BSs) can potentiate post-stroke neuroplasticity during exoskeleton-assisted gait training by encouraging the patient's active motor relearning and preventing dependence on the exoskeleton [1]. Most of the studies report the use of BSs with assistive hip and knee exoskeletons during functional gait training [2, 3]. In [2], electromyography (EMG) feedback is provided through a non-wearable display of colored stripes representing levels of muscle contraction. In [3], HRI feedback is given by a non-wearable display of a smiley character with mouth's length/shape modulated according to averaged/threshold HRI torque. Only the study [4] reported the use of a BS with an assistive AFE. A character that moves according to ankle angle is displayed on a non-wearable screen during non-functional gait training (ankle movements while sitting) [4]. It is still needed to develop fully

C. Pinheiro (✉) · J. Figueiredo · C. P. Santos
Center for MicroElectroMechanical Systems (CMEMS), University of Minho, Braga, Portugal
e-mail: a73727@alunos.uminho.pt

J. Figueiredo
e-mail: id6003@alunos.uminho.pt

C. P. Santos
e-mail: cristina@dei.uminho.pt

wearable biofeedback solutions, in line with the use of wearable assistive devices in gait rehabilitation, to enable ambulatory use and biofeedback strategies for functional gait training assisted by AFE to foster recovery of post-stroke ankle-foot deformities.

This work innovatively proposes a biofeedback control strategy held by a fully wearable BS that enables vibrotactile cues according to the HRI torque. This BS may encourage post-stroke patients to actively control their compliance with an assistive unilateral AFE during functional gait training, potentiating neuroplasticity. A pre-post study was conducted with healthy subjects to evaluate the biofeedback training's efficacy regarding participant-exoskeleton compliance.

2 Methods

2.1 HRI-Based Biofeedback Control Strategy

The HRI-based biofeedback control strategy enables a vibrotactile cue when the user interacts with a trajectory tracking controlled wearable AFE (the exoskeleton's actuator is controlled so that the user's ankle follows a reference joint angle, *Ref*) [5] and HRI torque's direction is equal to AFE's direction of movement. The cue encourages users to actively control the magnitude of their interaction and, thus, their compliance with the robot. The cue is provided at 200 Hz 1.8 G through eccentric rotating mass motors held by a vibrotactile elastic shank band (Fig. 1) [5]. The strategy is configured according to the user's imminent needs assessed from pre-training walking trials, as follows: (i) the cues are enabled during the gait phase in which the user achieves the lowest mean performance P , as computed in (1) (one of GPs1-4 from Fig. 1—training gait phase); (ii) a user-adaptive module threshold $|Thr|$ is defined using (2) according to pre-training data for training gait phase so the users are encouraged to actively control their interaction with the AFE within an interval ranging from Bas and Thr . This personalization allows a low cognitive effort and user-oriented gait training.

$$P(\%) = \frac{\sum_{i=1}^n \begin{cases} 1 & \text{if } Int(i) \in Bas \\ 0 & \text{otherwise} \end{cases}}{n} \times 100 \quad (1)$$

$$|Thr| = \frac{\max(|Int(1 : n)|)}{2} \quad (2)$$

where $Int(i)$ is the HRI torque (measured by strain gauges connected in a full Wheatstone bridge embedded in the AFE and filtered through a 2nd order Butterworth low-pass filter at 5 Hz) at sample i (100 Hz sample frequency) of the gait phase, Bas was empirically defined as baseline HRI torque range (from 2 to -2 N m) when

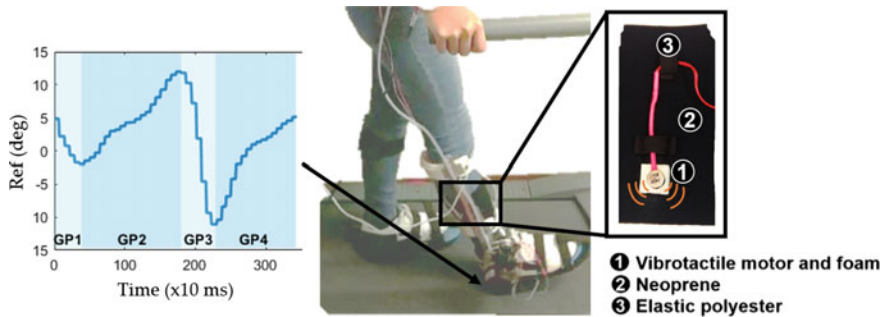


Fig. 1 Picture of one participant during biofeedback training and a detailed representation of the Ref segmented in four gait phases (GP1-4) and vibrotactile elastic shank band

considering the trajectory tracking controlled AFE suspended in the air without a user, and n is the gait phase's total number of samples.

2.2 Experimental Validation

1. Participants

Four healthy subjects (two male, 25 ± 1 years, 65 ± 12 kg, 1.69 ± 0.13 m) were recruited and gave their informed consent to participate in a pre-post study to evaluate the efficacy of the biofeedback training regarding participant-exoskeleton compliance. The protocol was approved by the Ethics Committee CEICVS 006/2020. All the participants are familiarized with the AFE.

2. Experimental protocol

The protocol included three procedures: (i) pre-training (PRTR) involved three walking trials on a treadmill at 1 km/h for 1 min with the trajectory tracking controlled AFE; (ii) training (TR) (Fig. 1) was similar to pre-training with the addition of the BS and one familiarization trial; (iii) post-training (PSTR) challenged the participants to replicate the trained gait pattern with AFE but without BS for 1 min.

3. Data collection and processing

The HRI torque was acquired during all procedures. The following metrics were computed per procedure: mean and standard deviation (std) of the Root-Mean-Square (RMS) HRI torque, P , and performance according to Thr , $P Thr$, determined using (3a, 3b) (all for training gait phase).

$$P Thr(\%) = \frac{\sum_{i=2}^n z}{n} \times 100 \quad (3a)$$

$$z(i) = \begin{cases} 1 & \text{if } [Ref(i) - Ref(i-1) > 0 \text{ and } Bas \geq Int(i) \geq -Thr] \\ & \text{or } [Ref(i) - Ref(i-1) < 0 \text{ and } Bas \leq Int(i) \leq Thr] \\ 0 & \text{otherwise} \end{cases} \quad (3b)$$

The first and last three gait cycles were discarded from processing. There were no withdrawals nor dropouts. Two paired two-sided *t*-tests and Wilcoxon Signed Rank tests were performed per parametric and non-parametric metrics, respectively, considering a level of significance of 0.05 between PRTR and TR, and PRTR and PSTR procedures. The comments of the participants regarding their experience with the biofeedback were annotated.

3 Results

The modal training gait phase was the GP3 (from AFE's heel-off to toe-off events) and $|Thr|$ varied between 3 and 5 N m. Table 1 shows the mean \pm std of the *t*-tests and the resulted *p*-values. It was verified statistically significant improvements (*p*-value: $4.56e-4-0.03$) regarding *P* between PRTR and PSTR and for *P Thr*. Additional improvements were verified (*p*-value = $5.57e-2-0.07$) for *P* between PRTR and TR and for RMS HRI. Further, the participants reported that the biofeedback motivated them to be involved in the trials and they felt more compliant with the exoskeleton after training.

4 Discussion

This work proposes HRI-based biofeedback aiming to improve human-robot compliance during AFE-assisted gait training. This hypothesis is reinforced by [2] concluding that HRI feedback is more effective than EMG feedback to improve human-robot compliance. The pre-post study was performed to evaluate the efficacy of biofeedback training on healthy participants as in [4]. The minimum $|Thr|$ of 3 N m (above baseline) found in PRTR proves that all the healthy participants had difficulties to be compliant with the exoskeleton prior BS use. Thus, the biofeedback may foster their compliance with the AFE as with post-stroke patients.

The statistical results show that the biofeedback training significantly improved the participant-exoskeleton compliance, as mentioned by the participants, enhancing *P Thr* outcomes. These improvements in HRI torque outcomes were also verified between PRTR and PSTR suggesting that occurred motor learning regarding HRI. Findings from [2, 4] also suggest improved motor learning upon biofeedback training, contrarily to [3]. However, the proposed biofeedback strategy presents advantageous features when compared to [2–4]: (i) does not require time-consuming preparation and expertise as EMG feedback; (ii) is fully wearable and personalized according to the user's needs.

Table 1 Mean \pm std and p -values of the t -tests

	RMS HRI	P	P Thr
PRTR	5.74 \pm 1.74 N m	20.87 \pm 13.28%	39.26 \pm 16.03%
TR	3.39 \pm 1.51 N m	39.27 \pm 19.79%	64.97 \pm 24.32%
PSTR	3.13 \pm 1.09 N m	39.12 \pm 15.01%	67.06 \pm 22.53%
PRTR versus TR	0.07	5.57e -2	0.03
PRTR versus PSTR	0.07	4.56e-4	8.59e-3

5 Conclusion

The 3-min HRI-based biofeedback training was able to improve significantly participant-exoskeleton compliance through HRI torque. Future work will address an experimental validation with further participants, including post-stroke patients, and the design of a novel biofeedback strategy to encourage users to improve HRI torque's direction, complementing the presented strategy.

Acknowledgements This work has been supported by the FEDER Funds through the Programa Operacional Regional do Norte and national funds from Fundação para a Ciência e Tecnologia with the SmartOs project under Grant NORTE-01-0145-FEDER-030386, and under the national support to R&D units grant, through the reference project UIDB/04436/2020 and UIDP/04436/2020.

References

1. G. Morone et al., Rehabilitative devices for a top-down approach. *Expert Rev. Med. Devices* **16**(3), 187–195 (2019)
2. F. Tamburella et al., Influences of the biofeedback content on robotic post-stroke gait rehabilitation: electromyographic vs joint torque biofeedback. *J. Neuroeng. Rehabil.* **16**(1), 95 (2019)
3. O. Stoller, M. Waser, L. Stammler, C. Schuster, Evaluation of robot-assisted gait training using integrated biofeedback in neurologic disorders. *Gait Posture* **35**(4), 595–600 (2012)
4. G. Asín-Prieto et al., Haptic adaptive feedback to promote motor learning with a robotic ankle exoskeleton integrated with a video game. *Front. Bioeng. Biotechnol.* **8**(February), 1–5 (2020)
5. C. Pinheiro, J.M. Lopes, J. Figueiredo, L.M. Gonçalves, C.P. Santos, Design and technical validation of a wearable biofeedback system for robotic-based gait rehabilitation, in 20th IEEE International Conference on Autonomous Robot Systems and Competitions (2020)

Challenges in Adaptive Robot-Assisted Gait Training: The Balancing Act of Minimizing Assistance While Preserving Safety



Alejandro Melendez-Calderon and Serena Maggioni

Abstract To maximize functional outcomes, rehabilitation strategies must provide challenging environments that encourage active participation of the users. Robotic gait trainers can provide adaptive and personalized environments that guide the patient as needed and encourage the patient to be active during the whole therapy session. However, even though research in neurological recovery may favor such approaches, they may be highly difficult to implement in practice. Here, we share some challenges in implementing adaptive robot-assisted gait training in practice.

1 Introduction

Multiple evidence, from animal models to clinical studies in humans, has demonstrated that functional improvements after neurological injury are better achieved when the patient is encouraged to produce voluntary neuromuscular activity (active participation) and receives early and intensive therapy, i.e. high amount of movement repetitions, but without repetition, or in other words “repetitive attempts at the same task accompanied by variable trajectories of elemental variables” [1].

Robotic gait trainers (e.g. Lokomat, Walkbot, G-EO, Lexo, Gait Trainer GT II) are valuable tools for gait therapy after neurological injury. Such devices can provide intensive training with a high amount of repetitions, and encourage active participation and challenging training conditions by, for example, providing increased walking speed or decreased robotic assistance, and exer-games.

While commercially-available devices offer opportunities for personalization of these challenging environments, such parameters are typically adapted by the therapist via a user interface. This implies that the robotic assistance is left at the

A. Melendez-Calderon (✉)

Biomedical Engineering, School of ITEE, The University of Queensland, Brisbane, Australia
e-mail: alej.melendez@uq.edu.au

S. Maggioni

Hocoma AG, Volketswil, Switzerland
e-mail: serena.maggioni@hocoma.com

discretion of the therapist, and it is typically ‘fixed’ for the duration of the therapy session—missing opportunities for challenging the patient at an optimal level.

To address the limitation of ‘fixed’ robotic assistance (which can be high, or low), several research groups have proposed the concept of “Assist-As-Needed” (AAN) control for robot-assisted training, e.g. [2–4]. In this case, the robotic assistance is no longer set by a therapist but adapts constantly, and automatically, based on the user’s performance. As a training approach, AAN is believed to be more effective than traditional assistive controllers, because it encourages the patient to be active during the whole therapy session.

In recent work, we implemented an ANN algorithm in the Lokomat (Hocoma AG, Switzerland), a commercially-available robotic gait trainer widely used in clinical practice [2]. The objective of this implementation is to investigate opportunities for using ANN control as a valid, reliable and sensitive assessment method of walking activity in a robotic gait trainer. While several aspects still need to be addressed to be able to reach this goal, preparation for and the conduction of a clinical study on 15 SCI patients with this algorithm has given us insights into the challenges of implementing adaptive robot-assistance that can be used for training in clinical settings. This paper summarizes those challenges with the aim of fostering transdisciplinary activities across multiple stakeholders (industry, research, healthcare provides, etc.) to find solutions to those.

2 Challenge I: Risk of Injury and Liability

In conventional locomotor training, a therapist (or more) is in direct contact with the legs of the patient; he/she can feel whether the patient needs more or less assistance to provide adequate foot clearance and prevent scuffing. If, for any reason, the patient is injured because of inadequate foot clearance, liability lies on the healthcare provider.

In the case of robotic locomotor training, the device guides the legs of the patient. When decreasing the amount of robotic support, potential hazards can come from unwanted interactions between the foot and the treadmill. For example, if there is no sufficient support to provide foot clearance or lift the body, but the robot continues to force movement on the legs, the device can seriously injure the patient. This situation can result because of improper implementation, or due to human error in selecting parameters and setting up a patient in the device. Liability in this case is not white or black and is typically shared between the medical device manufacturer and the healthcare provider. The medical device manufacturer is responsible for evaluating any possible risk of injury when operating the device in all possible configurations, and to provide necessary safety mechanisms to make sure that such risky situations are extremely unlikely. The healthcare provider is responsible for operating the device with trained personnel and according to the intended use and user manual.

The big responsibility for medical device manufacturers creates a very conservative approach for implementing novel robot-assistance techniques in commercial

devices. Therefore, even though research in neurological recovery may favor challenging environments for training (e.g. more transparent, less guided movements), such approaches may be highly difficult to implement in practice. What works on a well-controlled, research trial, may result in injury to a patient when implemented in real clinical settings. For example, a therapist needs to take care of many more variables in a busy clinical setting which may result in insufficient supervision, or due to the heterogeneity of the patients' characteristics, unstable circumstances may arise which may never have been encountered during testing.

3 Challenge II: Testing and Validation

Adaptive controllers pose challenges in guaranteeing stability and safety in human applications. A conservative approach for safety is usually adopted, because testing for certification of a medical device does not necessarily include all possible neuromechanical impairments that would make the device safety mechanisms fail (Fig. 1). This conservative approach to safety restricts opportunities for implementing novel training techniques that are more likely to result in better functional outcomes.

In [5], we propose the use of bio-inspired robotic testbenches, rendering biomechanical properties of human motion, as platforms for testing algorithms in a systematic way (Fig. 1). Although such testbenches may be a simplistic representation of

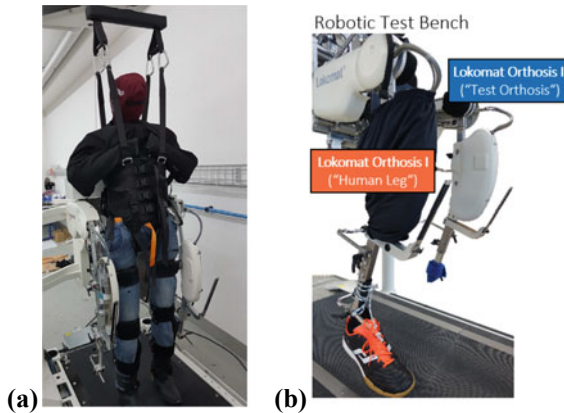


Fig. 1 **a** Manikins are typically used in life-cycle testing of medical robots. The figure shows a passive manikin on the Lokomat. Such manikins are passive and do not allow the testing of realistic conditions, e.g. spastic or voluntary activity, which may cause unsafe interaction with adaptive controllers. **b** Bio-inspired robotic testbenches [5] allow the testing of more realistic conditions. The figure shows one of the Lokomat orthosis acting as a 'human' leg as a possible configuration; but one could also envision full robotic manikins replacing passive manikins as in (a). This provides opportunities in testing the safety of adaptive robot-assistive training strategies and benchmarking across different devices

the complex biomechanics and control exhibit by patients, they provide a powerful method for simulating repeatable and controlled input, and identifying situations in which safety mechanisms can be ‘relaxed’ or need to be improved. Simulating known impairments reduces the causes of uncertainty and allows to perform tests in controlled conditions, and study the behavior of adaptive robot-assistive training strategies.

4 Challenge II: Intuitive Task Instructions

Assist-as-needed approaches vary robotic guidance based on a measure of user’s performance on a given task. For instance, in our ANN implementation, subjects were instructed to follow the movements of a walking avatar while trying to remain inside two shaded rectangles around the thigh and the shank that indicate the reference position (Fig. 2a), or to follow the blue trajectory in space and in time (the blue dot indicated the desired position at every instant) (Fig. 2b). In both cases, the adaptation of robotic assistance (knee and hip stiffness, and body weight support) was driven by the kinematic error between the actual and ‘desired’ joint angle trajectories. However, feedback on leg segments was more difficult to follow by patients than feedback on endpoint positions. Moreover, the desired endpoint trajectory was based on a reference gait trajectory that may have been different from the patient’s own trajectory, increasing thereby the difficulty of the task.

While such cognitive load may not be an issue in some patient population, e.g. SCI patients, the increased cognitive difficulty of the task might create undesired movement patterns in other patient population, e.g. stroke. When it comes to commercial implementation, the challenge here is in creating motivating environments that are suitable for the majority of users, which can include multiple populations.

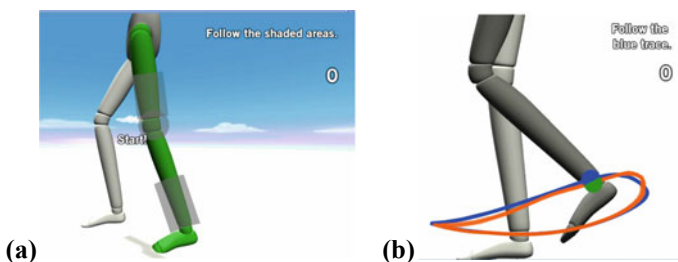


Fig. 2 **a** Visual feedback and instructions provided to the subjects in our RAGA implementation of ANN control [1]: **a** follow independent leg segments; or **b** follow an ankle trajectory

5 Conclusion

The concept of robot-aided neurorehabilitation has been around for more than 30 years, but first commercial robots for gait rehabilitation only became available until year 2000 (e.g. Lokomat, Hocoma AG, Switzerland). In these past 20 years, we have seen the flourishing of several commercial robotic gait trainers. While there have been enormous advances in research using these devices, the requirements needed for promoting recovery, e.g. active participation and challenging environments, may be extremely difficult to implement in commercial products. We see the need for gaining a better understanding on acceptable risks, and for dialogue between different stakeholders to determine legislation, liability and ethics around adaptive robot-assisted approaches to therapy.

Acknowledgements We thank Lars Lünenburger, Robert Riener, Marc Bolliger and Armin Curt for their contributions and support to the RAGA (Robot-Aided Gait Assessment) project.

References

1. M.L. Latash, Movements that are both variable and optimal. *J. Hum. Kinet.* **34**(1), 5–13 (2012)
2. S. Maggioni et al., Robot-aided assessment of walking function based on an adaptive algorithm, in *IEEE International Conference on Rehabilitation Robotics (ICORR)* (2015)
3. J.L. Emken et al., Robotic movement training as an optimization problem: designing a controller that assists only as needed, in *IEEE International Conference on Rehabilitation Robotics (ICORR)* (2005)
4. S.S. Fricke et al., Automatic versus manual tuning of robot-assisted gait training in people with neurological disorders. *J. Neuroeng. Rehabil.* (2020)
5. S. Maggioni et al., A bio-inspired robotic test bench for repeatable and safe testing of rehabilitation robots, in *IEEE International Conference on Biomedical Robotics and Biomechanics (BioRob)* (2016)

SS2: Commanding Lower-Limb Exoskeletons by Means of Brain-Machine Interfaces: Achievements and Challenges

Detection of Attempted Stroke Hand Motions from Surface EMG



Mads Jochumsen, Asim Waris, and Imran K. Niazi

Abstract Brain-Computer Interfaces have been proposed for stroke rehabilitation, but a potential problem with this technology is the dependence of high-quality brain signals. The aim of this study was to investigate if attempted hand open motions can be detected from the muscle activity instead. Ten stroke patients performed 63 ± 7 attempted movements while three channels of EMG were recorded. Hudgins time-domain features and linear discriminant analysis were used, and $92 \pm 3\%$ of the movement activity was correctly classified. The Spearman correlation between the upper limb Fugl-Meyer score and the classification accuracies was 0.58 ($P = 0.08$). In conclusion, attempted movements from stroke patients can be detected using EMG.

1 Introduction

Brain-Computer Interfaces have been proposed as a means for stroke rehabilitation. Several studies have reported clinical improvements and induction of neural plasticity after training with a Brain-Computer Interface (BCI) [1] where movement-related brain activity has been detected and used for triggering electrical stimulation or rehabilitation robots. To be able to drive the external devices, the movement-related brain activity such as movement-related cortical potentials or event-related desynchronization must be detected from single-trial EEG. Movement detection through EEG in stroke patients has been reported to be in the range of roughly 70–80% [2].

M. Jochumsen (✉)

Department of Health Science and Technology, Aalborg University, Aalborg, Denmark
e-mail: mj@hst.aau.dk

A. Waris

Department of Biomedical Engineering and Sciences, School of Mechanical and Manufacturing Engineering, National University of Sciences and Technology (NUST), Islamabad, Pakistan
e-mail: asim.waris@smme.nust.edu.pk

I. K. Niazi

Centre for Chiropractic Research, New Zealand College of Chiropractic, Auckland, New Zealand
e-mail: imran.niazi@nzchiro.co.nz

It is a challenging task to detect attempted movements from single-trial EEG due to several factors such as non-stationarity of the signals, artifacts and shifts in attention. Moreover, the signal quality must be good, which requires that the EEG cap is mounted correctly, and the impedance of the electrodes is low. This will often require the help of an extra person (therapists or relatives) to mount the cap and prepare the electrodes [3]. Thus, it would be ideal if another control signal than EEG could be used, which would be more accessible such as surface EMG. It has been shown that there was no difference between the induction of neural plasticity using EEG- and EMG-triggered electrical stimulation [4]. Moreover, many stroke patients have or quickly regain residual EMG activity that may be used to drive an external rehabilitation device. Several studies have reported that EMG of different arm motions can be decoded in stroke patients with various levels of impairment [5–8]. The aim of this study is to detect attempted hand open motions of the affected hand in stroke patients using a simple electrode setup with three surface bipolar EMG channels. The motions will be detected using simple signal processing techniques. The contribution of the features to the motion classification will be investigated, and it will be tested if the motion classification is correlated with the upper limb Fugl-Meyer score.

2 Methods

2.1 Subjects

Ten chronic stroke subjects participated in this study (see Table 1). All subjects provided their informed consent before participation; the local ethical committee (Riphah/RCRS/REC/00651) approved the procedures.

Table 1 Patient information

Subject	Upper limb Fugl-Meyer score (max 66)	Affected side	Lesion type
1	55	Left	Ischemic
2	36	Right	Ischemic
3	23	Right	Ischemic
4	46	Left	Ischemic
5	26	Left	Ischemic
6	65	Right	Ischemic
7	17	Right	Ischemic
8	59	Left	Ischemic
9	55	Right	Ischemic
10	28	Right	Hemorrhagic

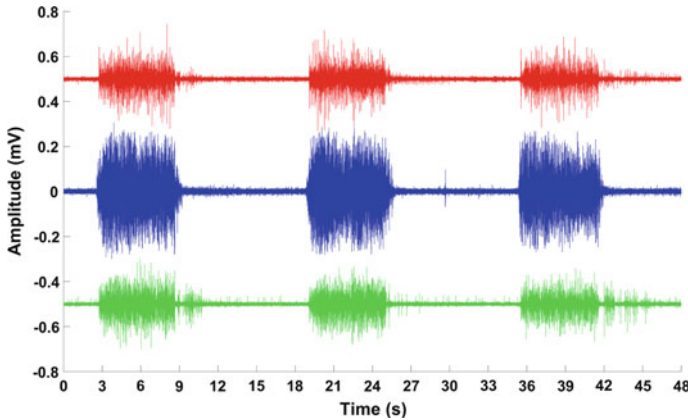


Fig. 1 EMG of three hand open motions (subject 4). Red: Flexor Carpi Radialis. Blue: Extensor Carpi Radialis. Green: Flexor Carpi Ulnaris

2.2 Recordings

Six surface EMG electrodes were placed on Flexor Carpi Radialis, Extensor Carpi Radialis, and Flexor Carpi Ulnaris forming one bipolar derivation from each muscle. The signals were referenced to a moist wristband. The signals were amplified with a gain of 10,000 and sampled with 2048 Hz.

2.3 Experimental Setup

The subjects were seated in a comfortable chair, and electrodes were placed on the most affected forearm. The signal quality was checked, and the subjects were instructed in how to perform the movements. The movements were hand open, which they had to maintain for six seconds. Between the movements, the subjects were given a break of ~ 12 s (see Fig. 1). The movements were visually cued and synchronized with the amplifier. The EMG onsets were visually inspected before further processing. On average 63 ± 7 movements were performed.

2.4 Pre-processing, Feature Extraction and Classification

The EMG was bandpass filtered from 20 to 500 Hz and notch filtered from 48 to 52 Hz using a 2nd order Butterworth filter. Movement epochs were extracted from the movement onset and two seconds after this point. Idle epochs were extracted during the rest period from one to three seconds prior the movement onset. Four feature types

were extracted from 200-ms windows in the 2-s epoch without overlap. The features were: (1) mean absolute value (MAV), (2) waveform length (WL), (3) zero crossings (ZC), and (4) slope sign changes (SSC). The features of the movement and idle class were classified using linear discriminant analysis in five different scenarios using all feature types and each feature type individually. The classification was performed using 5-fold cross-validation using all epochs movement and idle epochs.

2.5 Statistics

A Friedman test with “Feature Type” as factor (five levels: All, MAV, WL, ZC, and SSC) was performed on the classification accuracies obtained using the different feature types. This was followed up with posthoc analysis using a Bonferroni correction. The Spearman correlation was calculated between the classification accuracies obtained using all feature types and the upper limb Fugl-Meyer score.

3 Results

The results are summarized in Fig. 2. The following classification accuracies were obtained (mean \pm standard): $92 \pm 3\%$ (all features), $90 \pm 5\%$ (MAV), $89 \pm 5\%$ (WL), $87 \pm 5\%$ (ZC), and $89 \pm 3\%$ (SSC). A significant effect of “Feature Type” ($\chi^2_{(4)} = 20.8$; $P < 0.001$) was found. The posthoc analysis revealed higher classification accuracies when using all features compared to WL, ZC, and SSC. The Spearman correlation between the classification accuracies and the upper limb Fugl-Meyer score was 0.58, the correlation between the two variables was not significant ($P = 0.08$).

4 Conclusion

It is possible to discriminate between attempted hand open motions and resting EMG using a simple EMG setup and processing methods. Thus, EEG may not be needed for movement detection. This could be important for motor rehabilitation applications of the hand where patients need to activate a rehabilitation device. However, the patients would need to have some residual EMG. The limitation of this work is that only a small sample of stroke patients were included, and stroke is a very heterogeneous condition.

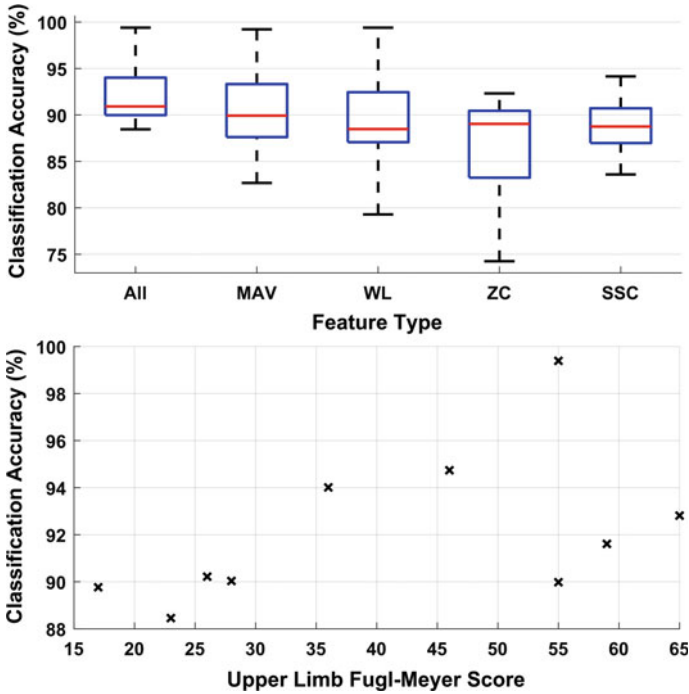


Fig. 2 Top: boxplot of the classification accuracies across subjects when using the different feature types. Bottom: scatter plot of the upper limb Fugl-Meyer score and the classification accuracies obtained using all feature types

Acknowledgements This work was funded by VELUX FONDEN (project no. 22357).

References

1. M.A. Cervera et al., Brain-computer interfaces for post-stroke motor rehabilitation: a meta-analysis. *Ann. Clin. Transl. Neurol.* **5**(5), 651–663 (2018)
2. M. Jochumsen et al., Detecting and classifying movement-related cortical potentials associated with hand movements in healthy subjects and stroke patients from single-electrode, single-trial EEG. *J. Neural Eng.* **12**(5), 056013 (2005)
3. M. Jochumsen et al., Evaluation of EEG headset mounting for brain-computer interface-based stroke rehabilitation by patients, therapists, and relatives. *Front. Hum. Neurosci.* **14**, 13 (2020)
4. M. Jochumsen et al., EMG-versus EEG-triggered electrical stimulation for inducing corticospinal plasticity. *IEEE TNSRE* **27**(9), 1901–1908 (2019)
5. S.W. Lee et al., Subject-specific myoelectric pattern classification of functional hand movements for stroke survivors. *IEEE TNSRE* **19**(5), 558–566 (2010)
6. A. Ramos-Murguialday et al., Decoding upper limb residual muscle activity in severe chronic stroke. *Ann. Clin. Transl. Neurol.* **2**(1), 1–11 (2015)

7. S. Balasubramanian et al., Is EMG a viable alternative to BCI for detecting movement intention in severe stroke? *IEEE Trans. Biomed. Eng.* **65**(12), 2790–2797 (2018)
8. X. Zhang, P. Zhou, High-density myoelectric pattern recognition toward improved stroke rehabilitation. *IEEE Trans. Biomed. Eng.* **59**(6), 1649–1657 (2012)

Comparison of Different Brain–Computer Interfaces to Assess Motor Imagery Using a Lower-Limb Exoskeleton



L. Ferrero, V. Quiles, M. Ortiz, E. Iáñez, A. Navarro-Arcas, J. A. Flores-Yepes, J. L. Contreras-Vidal, and J. M. Azorín

Abstract The combination of a lower-limb exoskeleton with brain computer interfaces (BCI) can assist patients with motor impairment to walk again. In addition, it can promote the neural plasticity of the affected brain region. The present paper shows a research performed on seven able-bodied subjects that walked with an assistive exoskeleton controlled by external commands. The main objective was to identify in which frequency band the differences between periods of motor imagery and rest were more evident. The comparison was done with different classifiers and the results reveal that for the majority of them, the frequency band of 14–19 Hz provided the highest accuracy.

L. Ferrero (✉) · V. Quiles · M. Ortiz · E. Iáñez · J. M. Azorín
Brain–Machine Interface System Lab, Miguel Hernández University of Elche, Elche, Spain
e-mail: lferrero@umh.es

V. Quiles
e-mail: vquiles@umh.es

M. Ortiz
e-mail: mortiz@umh.es

E. Iáñez
e-mail: ianez@umh.es

J. M. Azorín
e-mail: jm.azorin@umh.es

M. Ortiz · J. L. Contreras-Vidal
Noninvasive Brain–Machine Interface Systems Laboratory, Department of Electrical and Computer Engineering, University of Houston, Houston, TX 77204, USA
e-mail: jlcontreras-vidal@uh.edu

A. Navarro-Arcas · J. A. Flores-Yepes
Miguel Hernández University of Elche, Elche, Spain
e-mail: abel.navarro@umh.es

J. A. Flores-Yepes
e-mail: ja.flores@umh.es

1 Introduction

Motor impairments may be described as functional limitations that affect the movement of body structures, usually the limbs.

Brain Computer Interfaces (BCIs) are systems that use brain activity patterns and translate them to provide a communication with an external device. The combination of limb exoskeletons with BCI can contribute not only as assistive devices but also from the rehabilitation point of view [1]. Electroencephalography (EEG) is the most used methodology to get information about brain activity and the most common BCI approach is based on the detection of motor imagery (MI). MI is mostly related to changes in alpha (8–14 Hz) and beta (14–32 Hz) [2, 3].

In this research, a non-invasive BCI based on MI is presented. Three frequency bands are analyzed: alpha [3], beta [3] and low gamma [4]. The objective is to find in which frequency band the periods of motor imagery and rest could be better discriminated.

2 Material and Methods

2.1 *Experimental Setup*

Seven able-bodied subjects (S1–S7) participated voluntarily in the experiments. They did not report any known disease and signed an informed consent. The procedures were approved by the Institutional Review Board of the University of Houston, TX (USA). They were fitted to the REX exoskeleton (Rex Bionics, New Zealand) and it was controlled by commands sent from the computer.

EEG signals were acquired with 64 electrode system actiCap (Brain Products GmbH, Germany), amplified by 2 BrainVision BrainAmp amplifiers and transmitted to the BrainVision recorder software (Brain Products GmbH, Germany).

The experiment consisted of 8–12 trials per subject. The experimental setup can be seen in Fig. 1. Only periods of Normal Step and Standing were considered for the analysis.

2.2 *Brain Computer Interface*

EEG signals were sampled at a frequency of 100Hz. Concerning the signal-to-noise ratio, H^∞ framework presented by Kilicarslan et al. [5] was applied to the signals to mitigate artifacts associated with eye movements. In order to prevent motion artifacts, electrode wires were fixed with clamps and a medical mesh. Afterwards, the recordings from each electrode were standardized as in [6]. The signals were processed following a pseudo-online approach. It was defined a processing window

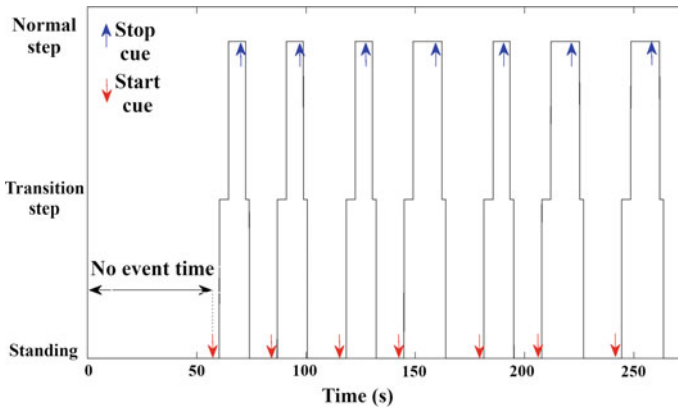


Fig. 1 Experimental setup. During periods of transition and normal step (after start cue) subjects had to perform motor imagery of gait while they were being moved by the exoskeleton. During periods of standing (after stop cue) they had to relax and the exoskeleton was not moving. The exoskeleton needs a transition step in order to start and to stop and that time was labeled as transition step

of 1 s that was shifted 0.5 s for each new epoch. Then, the epochs were analyzed with the Stockwell Transform [7]. For each channel, the instantaneous power of the considered frequencies were added and averaged through the epoch. Only 10 electrodes associated with MI tasks were considered: Fz, FC1, FCz, FC2, C1, Cz, C2, CP1, CPz and CP2. This process was repeated for 8–14, 14–19 and 30–45 Hz.

Concerning the discrimination between periods of motor imagination and rest, three classifiers were employed: Linear Discriminant Analysis (LDA), Support Vector Machine (SVM) and k-nearest neighbors (KNN) with $k = 3$ and 5. Results were obtained using leave-one-out cross-validation. For each subject, all trials except one were used for training and the model was tested with the other one. This process was repeated using every trial once as test. For the evaluation, the percentage of epochs correctly classified is calculated.

3 Results

The results of the classification are summarized in Table 1. The differences among methodologies were tested using the repeated measures analysis of variance (rANOVA). The analysis was designed with the accuracy as the independent variable and the classifier, frequency band, subject and their interactions as factors. The rANOVA revealed that the performance of the classifiers was significantly different ($p < 0.05$), the interaction between the classifier and the frequency band was significantly different ($p < 0.05$) and the differences among subjects were relevant ($p < 0.05$).

Table 1 Average % accuracy of the methods by subject

Methods	Subjects										Average
	S1	S2	S3	S4	S5	S6	S7				
SVM (8–14 Hz)	72.3 ± 5.5	60.0 ± 2.3	81.0 ± 6.1*	66.8 ± 10.1	58.9 ± 1.2	57.6 ± 2.1	73.2 ± 8.3	67.1 ± 8.8			
LDA (8–14 Hz)	72.3 ± 5.7	53.5 ± 8.9	81.3 ± 11.5*	65.3 ± 11.5	70.6 ± 4.7	60.4 ± 8.8	77.2 ± 6.8	68.7 ± 9.7			
KNN-3(8–14 Hz)	67.2 ± 5.7	53.6 ± 7.3	81.1 ± 7.2*	65.7 ± 8.4	74.1 ± 11.7	60.0 ± 4.7	74.2 ± 6.7	68.0 ± 9.4			
KNN-5(8–14 Hz)	68.5 ± 5.3	56.0 ± 7.2	82.6 ± 6.1*	65 ± 6.7	73.4 ± 10.3	59.5 ± 4.3	75.5 ± 7.4	68.6 ± 9.3			
SVM (14–19 Hz)	58.7 ± 1.1	63 ± 5.6	74.3 ± 5.5	60.6 ± 6.5	73.8 ± 7.3	56.1 ± 6.2	82.4 ± 10*	67.0 ± 9.9			
LDA (14–19 Hz)	64.7 ± 9.5	55.6 ± 11.6	86.3 ± 7.3*	72.7 ± 12.5	75.5 ± 9.1	67.3 ± 12.8	81.6 ± 11.7	72.0 ± 10.4			
KNN-3(14–19 Hz)	59.3 ± 4.1	57.2 ± 4.1	76.5 ± 6.7	66.5 ± 10.7	78.6 ± 8.3*	61.4 ± 8.8	77.8 ± 12.2	68.2 ± 9.3			
KNN-5(14–19 Hz)	62.2 ± 4	57.9 ± 5.7	76.5 ± 7.3	68.0 ± 10.5	79.0 ± 6.9*	60.0 ± 8.5	79.2 ± 12.1	69.0 ± 9.2			
SVM (30–45 Hz)	58.7 ± 1.1	65.0 ± 4.7	58.1 ± 1.3	58.4 ± 1.3	64.8 ± 4.1	66.3 ± 5.7	89.4 ± 8.9*	65.8 ± 11.0			
LDA (30–45 Hz)	55.0 ± 11.6	68.4 ± 4.9	83.6 ± 10.2	62.9 ± 9.1	76.6 ± 10.4	59.6 ± 12.5	89.2 ± 9.2*	70.8 ± 12.8			
KNN-3(30–45 Hz)	52.1 ± 7.6	64.2 ± 7.7	66.3 ± 20.6	56.8 ± 7.3	74.7 ± 13.4	59.3 ± 6.1	85.2 ± 13*	65.5 ± 11.3			
KNN-5(30–45 Hz)	52.5 ± 8.1	64.9 ± 8	67.7 ± 19.2	55.8 ± 7.5	73.4 ± 13.3	60.4 ± 6.2	86.7 ± 13.8*	65.9 ± 11.6			
Average	62.0 ± 7.1	59.9 ± 5.0	76.3 ± 8.4	63.7 ± 5.0	72.8 ± 5.4	60.7 ± 3.2	81.0 ± 5.7				

The highest accuracies by subject are in bold and the highest accuracies by method have an asterisk. KNN-3 and KNN-5 are the KNN method that uses 3 and 5 close samples

4 Discussion

The accuracy of the different methods was not equal for all the subjects that participated in the research. This could be explained by the fact that some subjects find it more difficult to perform MI and change to rest state.

The effect of the frequency band employed with the different classifiers was statistically significant and all classifiers except SVM showed better results in the 14–19 Hz band. Similar results were obtained in [3] and in [8], in which the most relevant features were obtained in 7–22 and 7–27 Hz. Regarding the classifier, LDA outperformed the rest.

5 Conclusion

Different frequency bands have been compared to identify MI and rest periods from EEG signals in an open-loop scenario while individuals are fitted to a lower-limb exoskeleton. The results show that the performance differs in a great extent depending on the subject. Overall, the best accuracy was obtained in the 14–19 Hz frequency band.

Acknowledgements This research was funded by the Spanish Ministry of Science, Innovation and Universities through grant CAS18/00048 ‘José Castillejo’; by the Spanish Ministry of Science, Innovation and Universities, the Spanish State Agency of Research, and the European Union through the European Regional Development Fund in the framework of the project Walk—Controlling lower-limb exoskeletons by means of brain-machine interfaces to assist people with walking disabilities (RTI2018-096677-B-I00); and by the Consellería de Innovación, Universidades, Ciencia y Sociedad Digital (Generalitat Valenciana) and the European Social Fund in the framework of the project ‘Desarrollo de nuevas interfaces cerebro-máquina para la rehabilitación de miembro inferior’ (GV/2019/009).

References

1. T. Nierhaus, C. Vidaurre, A. Villringer, Immediate brain plasticity after one hour of brain-computer interface (BCI). *J. Physiol.* 17 (2020)
2. P. Wierzgała, D. Zapała, G.M. Wojcik, J. Masiak, Most popular signal processing methods in motor-imagery BCI: a review and meta-analysis. *Front. Neuroinform.* 12(November), 1–10 (2018)
3. G. Pfurtscheller, C. Brunner, A. Schlo, F.H. Lopes, Mu rhythm (de)synchronization and EEG single-trial classification of different motor imagery tasks. *Neuroimage* 31, 153–159 (2006)
4. M. Ortiz, E. Iáñez, J. Gaxiola, A. Kilicarslan, J.M. Azorín, S. Member, Assessment of motor imagery in gamma band using a lower limb exoskeleton, in *IEEE International Conference on Systems, Man and Cybernetics (SMC)* (2019), pp. 2773–2778
5. A. Kilicarslan, R.G. Grossman, J.L. Contreras-vidal, A robust adaptive denoising framework for real-time artifact removal in scalp EEG measurements. *J. Neural Eng.* 13(2), 26013 (2016)

6. Á. Costa et al., Decoding the attentional demands of gait through EEG gamma band features. *PLoS One* (2016)
7. R.G. Stockwell, R.P. Lowe, L. Mansinha, Localization of the complex spectrum: the S transform. *IEEE Trans. Signal Process.* (1996)
8. J.S. Kirar, R.K. Agrawal, Relevant frequency band selection using sequential forward feature selection for motor imagery brain computer interfaces, in *2018 IEEE Symposium Series on Computational Intelligence (SSCI)* (2018), pp 52–59

Optimal Calibration Time for Lower-Limb Brain–Machine Interfaces



L. Ferrero, V. Quiles, M. Ortiz, E. Iáñez, J. L. Contreras-Vidal,
and J. M. Azorín

Abstract Brain Machine Interfaces (BMI) combined with lower-limb exoskeletons can assist patients that have difficulties in walking. However, BMI need some calibration to adjust their parameters to each user. This process is time-consuming and can be fatiguing for the users. In this work, the optimal number of recordings needed to adjust a EEG-based BMI to distinguish between MI of gait and rest state has been studied based on three subjects. The results show that the BMI reaches its highest accuracy with 5 recordings.

1 Introduction

Lower-limb functionality can be affected by injuries in the neural system, resulting in pathological gait. Therapies have the objective to restore the motor function by promoting the neuroplasticity of the neural system [1].

L. Ferrero (✉) · V. Quiles · M. Ortiz · E. Iáñez · J. M. Azorín
Brain–Machine Interface System Lab, Miguel Hernández University of Elche, Elche, Spain
e-mail: lferrero@umh.es

V. Quiles
e-mail: vquiles@umh.es

M. Ortiz
e-mail: mortiz@umh.es

E. Iáñez
e-mail: eianez@umh.es

J. M. Azorín
e-mail: jm.azorin@umh.es

M. Ortiz · J. L. Contreras-Vidal
Noninvasive Brain–Machine Interface Systems Laboratory, Department of Electrical and
Computer Engineering, University of Houston, Houston, TX 77204, USA
e-mail: jlcontreras-vidal@uh.edu

Brain Machine Interfaces (BMI) are systems that use brain activity patterns and translate them into commands or messages. This brain activity is usually measured using electroencephalography (EEG). BMI allow to establish a communication between the brain and external devices. Their combination with lower-limb exoskeletons offers a new paradigm for the assistance of people with motor disabilities related to the gait. Furthermore, since the movements of the exoskeleton depend on user's brain activity, the device can provide real-time feedback [2].

One of the main challenges that BMI have to face is the amount of information needed to train the BMI before its usage. The adjustment consists of training the BMI classifier to differentiate between distinct brain activity patterns. It is done for each user independently and generally the calibration time is long due to the number of recordings needed. The performance of repeated mental tasks may be fatiguing for the users and additionally, it can limit its usage in practice. Previous studies have tried to reduce or suppress the calibration time without affecting the performance of the system by using the data from other users or by designing user-independent approaches but they showed poor performance on the long-term [3, 4].

In this paper, it is assessed the calibration time that is needed to achieve an acceptable level of performance for a EEG-based BMI that aims to differentiate between periods of motor imagery (MI) of gait and rest while the users are fitted to a lower-limb exoskeleton.

2 Material and Methods

2.1 *Experimental Setup*

Data were acquired using 64 electrodes over an easyCap unit (Brain Products GmbH, Germany). 4 electrodes were positioned next to the eyes for the removal of the eye artifacts and reference and bound electrodes were located in the ears.

Three healthy subjects participated in the experiment, they did not report any known disease. They participated voluntarily and signed an informed consent. The procedures were approved by the Institutional Review Board of the University of Houston, TX (USA). Users were attached to the Rex exoskeleton (Rex Bionics, New Zealand) that avoids any free lower-limb movement. The exoskeleton was in open-loop control which means that the actions of the device were controlled by predefined commands and not by the user.

Each subject performed 10 trials following the protocol defined in Fig. 1. The trial alternates periods of rest and MI of gait. The last trial of subject S01 was not considered for the experiment due to movement artifacts.

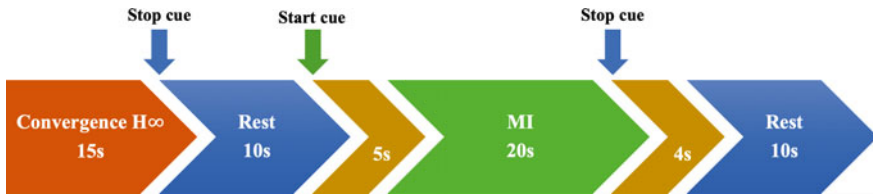


Fig. 1 Protocol of the trial. First, EEG signal is recorded during 15 s for the convergence of the algorithm to remove ocular artifacts. Then, an acoustic cue indicates the start of the rest event and the user must keep relaxed in a standing position. The second cue indicates the start of the MI event and during this time, the user is being moved by the exoskeleton while he is performing MI of gait. The last cue indicates the change to rest event and the exoskeleton stops the movement. For the first and last step of the exoskeleton there are two windows of 5 and 4 s respectively because the steps had variable time

2.2 Signal Processing

All the analysis was done after recording the signals. However, since the future goal is the implementation of the system in a real-time scenario, the signal was divided in windows of 1 s that were shifted every 0.5 s. Data was recorded at 200 Hz. For each windows of data, it was preprocessed with the following methodologies: H_{∞} algorithm [5] to remove the contribution of eye movements; Common Average Reference (CAR); notch filter at 60 Hz in order to reduce the power line noise and standardization of each channel using the method defined in [6].

Afterwards, Welch’s method was employed to estimate the spectral density of the data and only the features of the frequency band between 14 and 19 Hz were considered [7].

Once the features of all the windows were obtained, the performance of the BMI was assessed using cross-validation. Linear Discriminant Analysis (LDA) classifier was used to distinguish between two classes: MI of gait and rest. Cross-validation technique over the whole signal was repeated changing the number of trials that are used for training from 1 to 9 (8 for subject S01). In order to evaluate the performance of the model, four different metrics were computed: global accuracy (%), % of MI events correctly classified and % of rest events correctly classified.

3 Results and Discussion

Figure 2 shows the average global accuracy for all the subjects when the model is trained with different number of trials. It can be seen that the performance increases as the number of training trials does but the improvement is minor after the fifth recording.

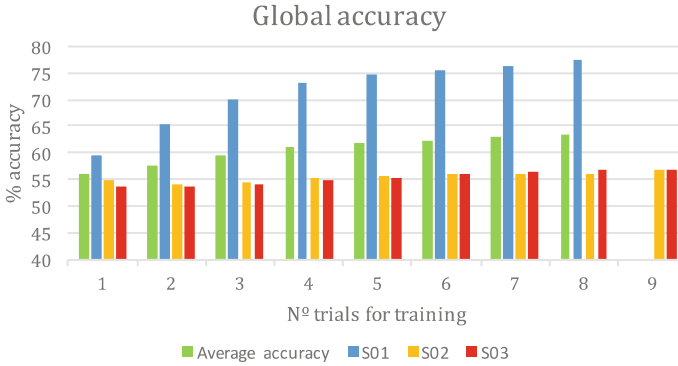


Fig. 2 Average global accuracy

Focusing on the performance related to the single detection of MI and rest (Figs. 3 and 4.), while the accuracy of the detection of one type of event increases, the detection of the other event decreases. Therefore, after a certain number of recordings, the model cannot further improve. Indeed, the model can lose the ability to generalize. In [4], it was proved that with 10 trials, the algorithm could reach a similar performance than another algorithm with 30. Therefore, future work should focus on the design of algorithms and features with low variability among subjects that could provide a better generalization. In addition, invariant features/models could facilitate inter-subject calibration that may result in lower calibration time for each individual.

4 Conclusion

Different calibration time has been employed to adjust a lower-limb BMI. The algorithm has been tested in a pseudo-online scenario for its future implementation in real-time. Results showed that the highest accuracy was obtained when the model was trained with the five previous recordings.

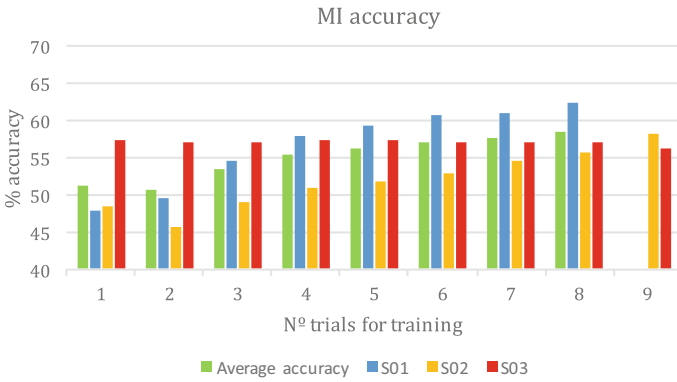


Fig. 3 MI accuracy

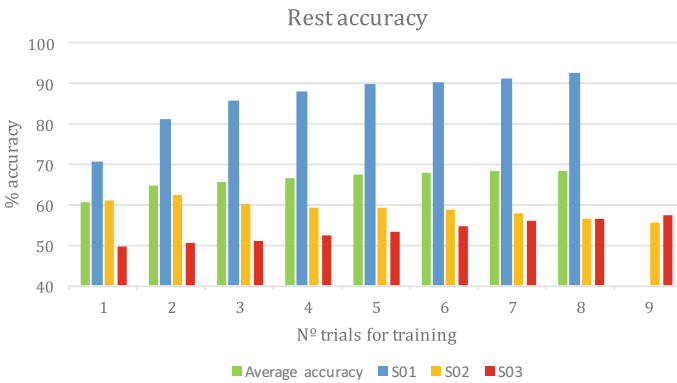


Fig. 4 Rest accuracy

Acknowledgements This research was funded by the Spanish Ministry of Science, Innovation and Universities through grant CAS18/00048 ‘José Castillejo’; by the Spanish Ministry of Science, Innovation and Universities, the Spanish State Agency of Research, and the European Union through the European Regional Development Fund in the framework of the project Walk—Controlling lower-limb exoskeletons by means of brain-machine interfaces to assist people with walking disabilities (RTI2018-096677-B-I00); and by the Consellería de Innovación, Universidades, Ciencia y Sociedad Digital (Generalitat Valenciana) and the European Social Fund in the framework of the project ‘Desarrollo de nuevas interfaces cerebro-máquina para la rehabilitación de miembro inferior’ (GV/2019/009).

References

1. S.C. Cramer, Repairing the human brain after stroke. II. Restorative therapies. *Ann. Neurol.* **63**(5), 549–560 (2008)
2. R.P.N. Rao, *Brain Computer Interfacing: An Introduction* (2013)
3. M. Krauledat, B. Schröder, B. Blankertz, K.R. Müller, Reducing calibration time for brain-computer interfaces: a clustering approach, in *Advances in Neural Information Processing Systems* (2007), pp. 753–760
4. F. Lotte, Signal processing approaches to minimize or suppress calibration time in oscillatory activity-based brain-computer interfaces. *Proc. IEEE* **103**(6), 871–890 (2015)
5. A. Kilicarslan, R.G. Grossman, J.L. Contreras-Vidal, A robust adaptive denoising framework for real-time artifact removal in scalp EEG measurements. *J. Neural Eng.* **13**(2) (2016)
6. Á. Costa et al., Decoding the attentional demands of gait through EEG gamma band features. *PLoS ONE* **11**(4), e0154136–e0154136 (2016)
7. G. Pfurtscheller, C. Brunner, A. Schlo, F.H. Lopes, Mu rhythm (de)synchronization and EEG single-trial classification of different motor imagery tasks. *Neuroimage* **31**, 153–159 (2006)

Comparison Between Methods to Create the Leg Length Discrepancy (LLD) Patient-Specific Model: Musculoskeletal Modeling



Hamidreza Barnamehei, Farhad Tabatabai Ghomsheh,
Afsaneh Safar Cherati, Majid Pouladian, Arghavan Aminishahsavarani,
and Neda Golfeshan

Abstract The purpose of this study was to compare the image-based and marker-based scaling methods to create subject-specific models for LLD children. One of the important applications of subject-specific models is gait analysis of the leg length discrepancy (LLD) patients. The LLD is defined as a situation in which the paired lower body segments have a noticeably unequal length. Twenty-two children were categorized to normal and LLD (average more than 1 cm) groups (Normal: 11 and LLD: 11) who participated in this study. The Gait2354_Simbody model of OpenSim consists of joints with 23 degrees of freedom and 92 muscle-tendon actuators to represent 76 muscles in the lower extremities and torso was used to simulate the gait. Significant differences were found between normal and LLD children in total square error and RMS of marker error ($p < 0.05$). This study demonstrates the feasibility of using musculoskeletal modelling to compare methods to create patient-specific model in patients with knee height asymmetry.

Keywords Musculoskeletal · LLD · Modeling · Patient-specific · Simulation

1 Introduction

Musculoskeletal modeling is a computational method to estimate biomechanical variables of humans or animals [1]. One of the challenging parts of musculoskeletal modeling is to create subject-specific models [2]. There are various methods to create subject-specific models [3]. One of the important applications of subject-specific models is gait analysis of the leg length discrepancy (LLD) patients [4]. The LLD

H. Barnamehei · F. T. Ghomsheh · A. S. Cherati · M. Pouladian · N. Golfeshan
Department of Integrative Physiology and Neuroscience, Washington State University, Pullman,
WA 99164, USA
e-mail: h.barnamehei@wsu.edu

A. Aminishahsavarani (✉)
Biomedical Engineering Department, Central Tehran Branch, Islamic Azad University, Tehran,
Iran

is defined as a situation in which the paired lower body segments have a noticeably unequal length. Therefore, the aim of the current study was to compare the image-based and marker-based scaling methods to create subject-specific models for LLD children.

2 Methods and Materials

Twenty-two children were categorized to normal and LLD (average more than 1 cm) groups (Normal: 11 and LLD: 11) who participated in this study (23.4 ± 5.7 kg, 98 ± 8.5 cm, 6.5 ± 2.5 years). Twelve Vicon motion captures (Vicon MX, Oxford, UK, 200 Hz) and two force plate (Kistler, 2000 Hz) were used to record the reflective marker trajectories and ground reactions, respectively [5-7]. Children walked the length of a 10-m walkway barefoot at a self-selected speed. Marker data were calculated from a minimum of 20 gait cycles. Gait cycle defined according our previous study [4]. The Gait2354_Simbody model of OpenSim consists of joints with 23 degrees of freedom and 92 muscle-tendon actuators to represent 76 muscles in the lower extremities and torso was used to simulate the gait [9]. The generic model was scaled by two different methods: images based (CT and MRI) and marker based [9]. The inverse kinematics was used to examine the best methods for scaling. The quality of methods was examined by comparison with marker errors during inverse kinematics analysis. Statistical analysis for comparison of gait parameters between groups included a Kolmogorov-Smirnov test for testing normal distribution, an independent—t-test (normal distributed) and Mann–Whitney U test (not normal distributed) [10]. The significance level was set at $p < 0.05$ in order to find the differences among methods. All statistical analyses were conducted using MATLAB (MathWorks, USA, 2019b) [11].

3 Results

Figure 1 presents the schematic of creating the subject-specific model for normal and LLD children from the generic model. The image and marker-based subject-specific models compared with the experimental results of total square of marker error from inverse kinematics to examine the methods for creating the subject-specific model. Figure 2 presents the mean of total square of marker error during walking. Significant differences were found between normal and LLD children in total square of marker error ($p < 0.05$). The mean and peak values of marker errors for marker-based was higher than imaged-based. The maximum differences were observed at the end of gait cycle (after 80%).

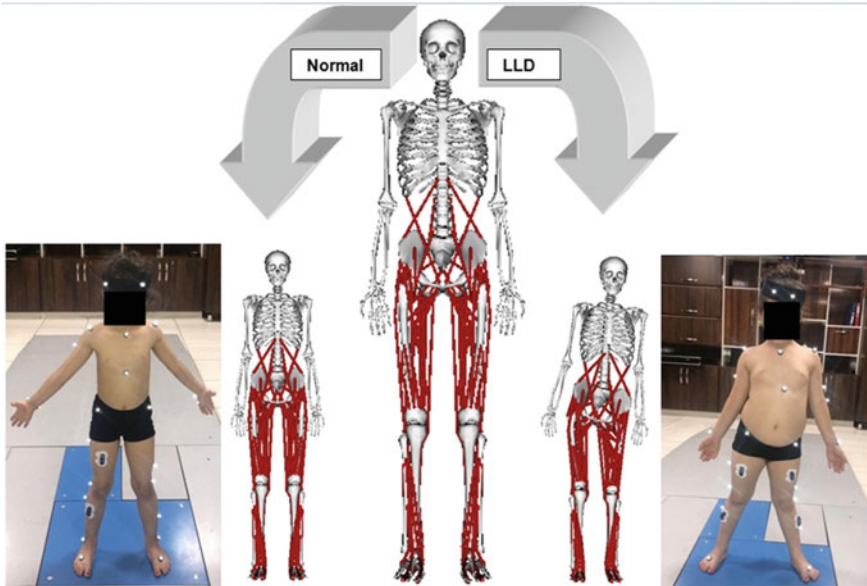


Fig. 1 The schematic of creating the subject-specific musculoskeletal model for normal and LLD children from the generic model

4 Discussion

This study demonstrates the feasibility of using musculoskeletal modelling to compare methods to create patient-specific model in patients with knee height asymmetry [12]. The results show different patterns of lower limb kinematics between the right and left sides compared to the more symmetrical patterns shown by the health subject. This study demonstrates a technique which can be used to compare methods to create patient-specific model in patients with knee height asymmetry for a variety of activities of daily living. According to results, the differences between methods before the 80% of gait cycle were not significant, while the marker errors differences between methods were significant at the end of gait cycle (80–100%) [4].

5 Conclusion

Create the subject-specific model is one of the challenging parts of musculoskeletal simulation especially in the LLD patient studies. Therefore, this study examined the two methods of creating the LLD patient-specific models. According to results, the quality of OpenSim scaling tools depends on experimental marker placement quality, although our results present significant differences between this method and scaling with images, and both methods have weak points. Therefore, the authors suggest

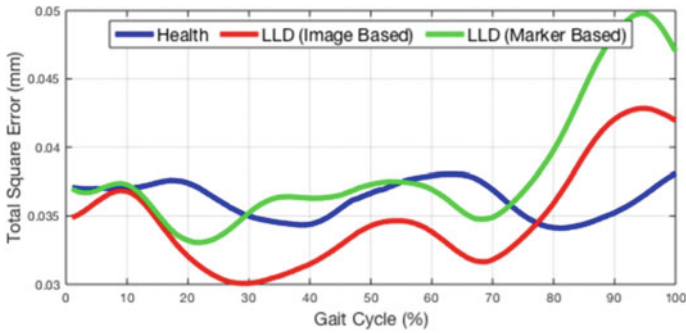


Fig. 2. The mean of total square of marker error

future studies use both methods to create patient-specific models. Future studies will look at kinetics for patients with knee height asymmetry to determine any atypical loading which could indicate a need to adjust the surgical management of children with LLD.

References

1. H. Barnamehei, M. Karimidastjerdi, M. Torabigoudarzi, M.R. Kharazi, M. Barnamehei, Simulation of flat-foot gait with and without running shoes by evaluation of hip kinematics and balance control variations via OpenSim. *Gait Posture* **81**, 32–33 (2020). <https://doi.org/10.1016/j.gaitpost.2020.07.039>
2. H. Barnamehei, F.T. Ghomsheh, A.S. Cherati, M. Pouladian, Muscle and joint force dependence of scaling and skill level of athletes in high-speed overhead task: musculoskeletal simulation study. *Inf. Med. Unlocked* (August), 100415 (2020). <https://doi.org/10.1016/j.imu.2020.100415>
3. H. Barnamehei, M. Kharazi, M. Barnamehei, P83: heel height affects lower extremity joint moments during walking with OpenSim software. *Gait Posture* **57**, 319–320 (2017). <https://doi.org/10.1016/j.gaitpost.2017.06.441>
4. H. Barnamehei, A.B. Derakhshan, A. Zomorrodi, M.M. Ali, Hip kinetics, kinematics, and motor control differences between normal and leg length discrepancy (LLD) children during gait: simulation and experimental. *Gait Posture* **81**, 30–31 (2020). <https://doi.org/10.1016/j.gaitpost.2020.07.038>
5. H. Barnamehei, M. Alimadad, S. Alizadeh, S.Z. Mofrad, F. Bagheri, Electromyographic activity of selective lower extremity muscles comparison between ankle-foot orthosis and barefoot gait (2018). <https://doi.org/10.1109/ICBME.2018.8703569>
6. H. Barnamehei et al., Identification and quantification of modular control during Roundhouse kick executed by elite Taekwondo players (2018). <https://doi.org/10.1109/ICBME.2018.8703602>
7. N. Golfeshan, H. Barnamehei, M. Torabigoudarzi, M. Karimidastjerdi, A. Panahi, Upper body postures effect on neuromuscular activities of the lower limb during a squat : musculoskeletal modeling. *Gait Posture* **81**, 107–108 (2020). <https://doi.org/10.1016/j.gaitpost.2020.07.087>
8. A. Aminishahsavarani, H. Barnamehei, F. Khazae, E. Karimi, M. Beigi, B. Valiollahi, Effect of ankle sprain brostrom surgery on the lower extremity kinematics chain during sit-to-stand task. *Gait Posture* **81**, 11–12 (2020). <https://doi.org/10.1016/j.gaitpost.2020.07.028>

9. H. Barnamehei, Y. Zhou, X. Zhang, A. Vasavada, Cervical spine intervertebral kinematics estimated from inverse kinematics and compared to dynamic X-ray data. *Gait Posture* **81**, 36–37 (2020). <https://doi.org/10.1016/j.gaitpost.2020.07.041>
10. N. Golfeshan, M. Barnamehei, A. Rezaei, H. Barnamehei, M.R. Kharazi, M.A. Safaei, Muscles kinetics effect on the generation of proximal to distal tasks: simulation of the knife hand block movement via OpenSim. *Gait Posture* **81**, 109–110 (2020). <https://doi.org/10.1016/j.gaitpost.2020.07.088>
11. F. Bagheri, H. Barnamehei, M.R. Kharazi, A. Panahi, N. Golfeshan, M. Razaghi, Comparison of biarticular muscles effects on balance variation between bare-foot and wearing high-heel shoe conditions: experimental and simulation by OpenSim. *Gait Posture* **81**, 20–21 (2020). <https://doi.org/10.1016/j.gaitpost.2020.07.033>

Shoulder Kinematics and Kinetics Comparison Between Amateur and Professional Athletics During High-Speed Overhead Tasks: Computer Simulation Study



Hamidreza Barnamehei, Farhad Tabatabai Ghomsheh, Afsaneh Safar Cherati, Majid Pouladian, Arghavan Aminishahsavarani, and Neda Golfeshan

Abstract The purpose of this study was to compare the amateur and professional badminton player by generic and scaled models during execution of the Badminton Forehand Smash (BFS). The BFS is high-speed overhead stroke and is sample of proximal to distal motion. The injuries rate and stroke style depend on skill level of athletics. Twenty-four athletics categorized to the amateur and professional groups. Vicon motion captures were used to record the marker trajectories attached on bony land markers. The shoulder model was used as a base model in the OpenSim to estimate kinetics and kinematics. The generic model was scaled by mass, height, and markers data in the static position. The inverse kinematics and dynamics were used to estimate kinetics and kinematics relationships during the BFS. Significant differences were found in shoulder angles, angular velocities, and moments between groups ($p < 0.05$). In addition, large differences were observed in shoulder angular velocity between groups while shoulder angular position patterns of both groups seems similar. Knowledge of shoulder kinetics and kinematics during overhead tasks performed at high velocity could improve the understanding of various sport-specific adaptations and pathologies.

Keywords Musculoskeletal · Badminton · Modeling · Shoulder · Simulation

H. Barnamehei · F. T. Ghomsheh · A. S. Cherati · M. Pouladian
Department of Integrative Physiology and Neuroscience, Washington State University, Pullman, WA 99164, USA
e-mail: h.barnamehei@wsu.edu

A. Aminishahsavarani (✉)
Biomedical Engineering Department, Central Tehran Branch, Islamic Azad University, Tehran, Iran

N. Golfeshan
Science and Research branch, Islamic Azad University, Tehran, Iran

1 Introduction

Badminton forehand smash (BFS) is high-speed overhead stroke and is sample of proximal to distal motion [1]. The injuries rate and stroke style depend on skill level of athletics [2]. In addition, computer simulation provides basic horizon to estimate biomechanical variables during motions [3]. On the other sides, creating subject-specific model is important and in some cases is difficult [4, 5]. Although, scaling by marker data prepare easy way to making subject-specific model, there are no certain agreements to reliability of this method [6]. Thus, the question remain is what is the shoulder kinetics and kinematics differences between amateur and professional players during the BFS? Therefore, the aim of current study was to compare the amateur and professional groups by generic and scaled models during the BFS.

2 Methods and Materials

Twenty-four athletics (65.3 ± 6.5 kg, 173 ± 8.1 cm, 28.5 ± 5.5 years) categorized to the amateur ($n = 12$) and professional ($n = 12$) groups. Ten Vicon motion captures (Vicon MX, Oxford, UK, 200 Hz) were used to record the surface marker trajectories attached on bony land markers [7, 8]. The shoulder model consists of 5 segments, and 10 degrees of freedom was used as a base model in the OpenSim to estimate kinetics and kinematics [9, 10]. The generic model was scaled by mass, height, and markers data in the static position [11]. The inverse kinematics and dynamics were used to estimate kinetics and kinematics variables during the BFS (Fig. 1) [12].

3 Results

Figure 2 presents the average of angles, angular velocities, and moments of shoulder over a BFS cycle across all the trials. The red and blue lines indicate the professional and amateur groups. Significant differences were found in shoulder angles, angular velocities, and moments between groups ($p < 0.05$). In addition, large differences were observed in shoulder angular velocity between groups while shoulder angular position patterns of both groups seems similar. Professional group presents sudden angular velocity at contact point while amateur group represents steady angular velocity.

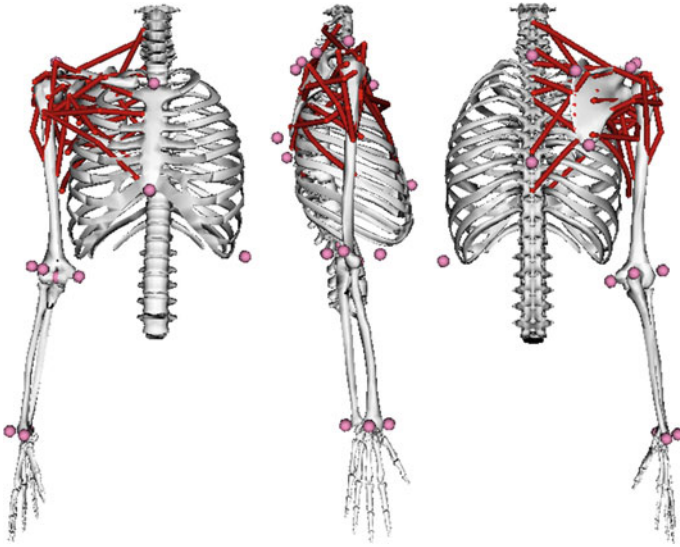


Fig. 1 The anterior view (left), lateral view (middle), and posterior view sides of the musculoskeletal model used in the current study

4 Discussion

Based on our results, amateur and professional athletics use different motor control strategy to execute the BFS. The kinematics and kinetics variables before, after, and at contact point are depend on level of athletics. Therefore, this suggests that the amateur athletics in order to improve their abilities not only should focus in the kinetics and kinematics variables but also execute the suitable motion at inappropriate time of movement. Knowledge of shoulder kinetics and kinematics during overhead tasks performed at high velocity could improve the understanding of various sport-specific adaptations and pathologies. The previous study verified results such as peak of kinetics and kinematics variables [13].

5 Conclusion

Majority of differences were related to timing. Our results represent many differences between skilled and non-skilled athletes are due to lack of timing control during BFS. Most effects of training are coordination between muscle activity, kinetics, and kinematics variables. Long time training may help to athletes to find best relationships among these variables. This study discovered pattern and differences between two different skill levels.

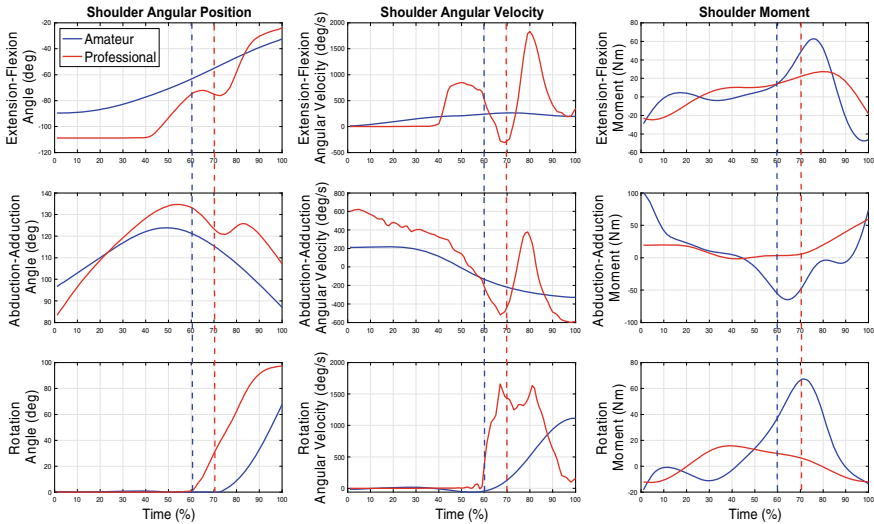


Fig. 2 The average of angles, angular velocities, and moments of shoulder over a BFS cycle across all the trials. The red and blue lines indicate the professional and amateur groups. The red and blue dash lines show the contact point for the professional and amateur players

References

1. H. Barnamehei, F. Tabatabai Ghomsheh, A. Safar Cherati, M. Pouladian, Upper Limb neuromuscular activities and synergies comparison between elite and nonelite athletics in badminton overhead forehand smash. *Appl. Bionics Biomech.* **2018**, 6067807 (2018). <https://doi.org/10.1155/2018/6067807>
2. H. Barnamehei, F.T. Ghomsheh, A.S. Cherati, M. Pouladian, Muscle and joint force dependence of scaling and skill level of athletes in high-speed overhead task: musculoskeletal simulation study. *Inf. Med. Unlocked* (August), 100415 (2020). <https://doi.org/10.1016/j.imu.2020.100415>
3. F. Bagheri, H. Barnamehei, M.R. Kharazi, A. Panahi, N. Golfeshan, M. Razaghi, Comparison of biarticular muscles effects on balance variation between bare-foot and wearing high-heel shoe conditions: experimental and simulation by OpenSim. *Gait Posture* **81**, 20–21 (2020). <https://doi.org/10.1016/j.gaitpost.2020.07.033>
4. A. Aminishahsavarani, H. Barnamehei, F. Khazae, E. Karimi, M. Beigi, B. Valiollahi, Effect of ankle sprain brostrom surgery on the lower extremity kinematics chain during sit-to-stand task. *Gait Posture* **81**, 11–12 (2020). <https://doi.org/10.1016/j.gaitpost.2020.07.028>
5. H. Barnamehei, A.B. Derakhshan, A. Zomorodi, M.M. Ali, Hip kinetics, kinematics, and motor control differences between normal and leg length discrepancy (LLD) children during gait: simulation and experimental. *Gait Posture* **81**, 30–31 (2020). <https://doi.org/10.1016/j.gaitpost.2020.07.038>
6. H. Barnamehei, Y. Zhou, X. Zhang, A. Vasavada, Cervical spine intervertebral kinematics estimated from inverse kinematics and compared to dynamic X-ray data. *Gait Posture* **81**, 36–37 (2020). <https://doi.org/10.1016/j.gaitpost.2020.07.041>
7. H. Barnamehei, Effect of motor nerve on lower limb coordination variability during high-heel and barefoot gait, vol. 21 (2019)
8. N. Golfeshan, M. Barnamehei, A. Rezaei, H. Barnamehei, M.R. Kharazi, M.A. Safaei, Muscles kinetics effect on the generation of proximal to distal tasks: simulation of the knife hand block

- movement via OpenSim. *Gait Posture* **81**, 109–110 (2020). <https://doi.org/10.1016/j.gaitpost.2020.07.088>
9. W. Wu, P.V.S. Lee, A.L. Bryant, M. Galea, D.C. Ackland, Subject-specific musculoskeletal modeling in the evaluation of shoulder muscle and joint function. *J. Biomech.* **49**(15), 3626–3634 (2016). <https://doi.org/10.1016/j.jbiomech.2016.09.025>
 10. A. Kian et al., Static optimization underestimates antagonist muscle activity at the glenohumeral joint: a musculoskeletal modeling study. *J. Biomech.* **97**, 109348 (2019). <https://doi.org/10.1016/J.JBIOMECH.2019.109348>
 11. H. Barnamehei, P. Shamloo, N. Golfeshan, N. Naghavi, M. Barnamehei, M.R. Kharazi, Effect of design of assisting devices on the lower body muscular activities during gait with crutch executed by amputees. *Gait Posture* **81**, 34–35 (2020). <https://doi.org/10.1016/j.gaitpost.2020.07.040>
 12. N. Golfeshan, S. Fatemigarakani, F. Aflatounian, A. Fattahzadeh, A. Maboudmanesh, Effect of medial-lateral hand positions on glenohumeral and acromioclavicular joint kinematics during push-up exercise. *Gait Posture* **81**, 111–112 (2020). <https://doi.org/10.1016/j.gaitpost.2020.07.089>
 13. C.-L.T. Wei-Cheng Liao, K.-M. Pan, Y.-C. Hsueh, Kinematical analysis of two different forehand badminton drop shots techniques, pp. 272–275

Subject-Independent Detection of Movement-Related Cortical Potentials and Classifier Adaptation from Single-Channel EEG



Mads Jochumsen

Abstract Brain-computer interfaces have been proposed for stroke rehabilitation, but there are some impeding factors for them to be translated into clinical practice. One of them is the need for calibration. In this study it was investigated if subject-independent calibration is possible for detecting movement-related potentials associated with hand movements, and what the optimal number of movement epochs is to maximize the detection performance. Twelve healthy subjects performed 100 palmar grasps while continuous EEG was recorded. Template matching was performed between movement and idle epochs. $72 \pm 10\%$ of all epochs were correctly classified using the subject-independent approach while $78 \pm 9\%$ of the epochs were correctly classified using the individualized approach. The highest classification accuracies were obtained when using 54 ± 23 movement epochs for calibration. In conclusion, it is possible to use a subject-independent approach for detecting movement-related cortical potentials, but the performance is slightly lower compared to individualized calibration.

1 Introduction

Brain-Computer Interfaces have been proposed for stroke rehabilitation over the past years. It has been shown in several studies that neural plasticity, the underlying factor of motor recovery, can be induced [1] and gains in functional scores have been reported in stroke patients [2]. A Brain-Computer Interface (BCI) can induce neural plasticity by pairing movement-related brain activity with temporally correlated somatosensory feedback from e.g. electrical stimulation of nerves and muscles or passive movement from rehabilitation robots and exoskeletons [3]. It is not known how strict the temporal association between movement-related activity and inflow of somatosensory feedback has to be. It has been suggested that there should be a very strict timing where the intended movement is predicted [4], while other findings have

M. Jochumsen (✉)

Department of Health Science and Technology, Aalborg University, Aalborg, Denmark
e-mail: mj@hst.aau.dk

suggested that such a strict temporal association may not be needed [5]. However, if a strict temporal association is needed, the movement-related activity has to be predicted from single-trial EEG. This is possible through detection of movement-related brain activity that precedes a movement, which can be done from either movement-related cortical potentials (MRCPs) or event-related desynchronization (ERD) [6]. It has been shown in several studies that these two phenomena can be detected from single-trial EEG with accuracies in the range of 70–80% in stroke patients [7]. To be able to utilize this in a BCI, a number of movements (roughly 30–50 movements) needs to be performed such that a classifier can be trained to discriminate between movement and idle activity. This takes time, especially in a potential rehabilitation scenario where the therapist needs to mount the EEG cap and perform the system calibration. It is likely that this will take too much time for the therapist, and this wasted time may be deducted from the actual training with the patient. To increase the acceptance of a BCI-approach for stroke rehabilitation, it would be ideal if the patient could mount the cap him/herself [8], and that the BCI would not require any calibration, or at least a very low number of movement trials for calibration. It has been shown previously in a couple of studies that ERD [9, 10] and MRCPs [11, 12] can be detected using a global approach where previously recorded data from multiple subjects can be used for calibration hence removing the calibration time. For the MRCP, it has been reported for foot movements. In this study, it will be investigated if similar findings are obtained for hand movements. The aims of this study are to: (1) compare the detection of MRCPs associated with hand movements from single-trial EEG using a global and individualized detector approach, and (2) determine the relationship between detection performance and number of movements used for calibration.

2 Methods

2.1 Subjects

Twelve healthy subjects participated (28 ± 3 , two females). The subjects gave their written informed consent prior to participation. The local ethical committee (N-20130081) approved all procedures.

2.2 Recordings

Nine channels of EEG were recorded from F3, Fz, F4, C3, Cz, C4, P3, Pz and P4 (EEG amplifiers, Nuamps Express, Neuroscan). The channels were referenced to the right mastoid bone and a ground electrode was placed on the forehead. The signals were sampled with 500 Hz. The impedance of the electrodes was below 5 k Ω .

Table 1 Global versus individualized classification

Subject	Global [%]	Individual [%]	No. epochs for best performance
1	82	86	67
2	79	76	43
3	65	81	65
4	60	71	79
5	69	73	75
6	84	88	64
7	78	76	38
8	69	78	74
9	76	80	59
10	86	91	6
11	61	74	62
12	56	59	18
Mean \pm std	72 \pm 10%	78 \pm 9%	54 \pm 23

2.3 Experimental Setup

The subjects were seated in a comfortable chair. They performed 100 visually cued ballistic palmar grasps of the right hand. A digital trigger was used to synchronize the visual movement cues with the EEG. The subjects were instructed to sit as still as possible and minimize blinking and activity of the facial muscles during the recordings. Each movement was separated by a 10-s rest period.

2.4 Data Analysis

Only Cz was used for the data analysis. The raw EEG was bandpass filtered from 0.05 to 5 Hz using a 4th order Butterworth filter with zero phase shift and downsampled to 25 Hz to reduce the processing time. The processed continuous signal was divided into two types of trials/epochs (1) movement epochs (from -1.5 to 0.5 s with respect to the task onset), and (2) idle epochs (from -5 to -3 s with respect to the task onset). 100 movement and idle epochs were extracted in total. The mean value of each epoch was subtracted from the respective epoch. To investigate the global approach, a linear discriminant analysis (LDA) classifier was trained on all movement and idle epochs from the subjects that were available except for the test subject (all the epochs from the test subject was used for testing). A template was obtained from all movement epochs (average across epochs), and the autocorrelation was calculated between the template and each epoch, movement and idle. To investigate the effect of the number of movement epochs for the individualized calibration, the first five movement epochs were used to extract a template and to calibrate the LDA, and the remaining epochs

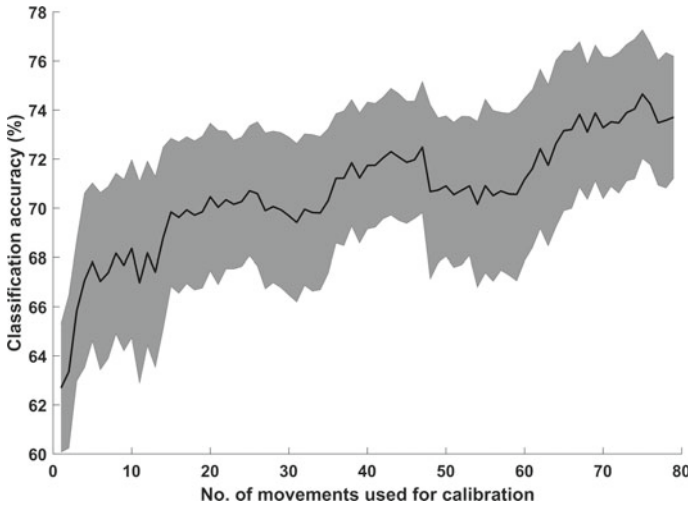


Fig. 1 Average and standard error of the classification across subjects for the individualized calibration

were used for testing. The number of epochs was increased by one hence increasing the number of movement epochs for calibration until 20 epochs remained for testing. A paired t-test was performed between the classification accuracies obtained for the global approach and for the highest classification accuracy in the individualized approach.

3 Results

The results are summarized in Table 1 and Fig. 1. $72 \pm 10\%$ (across subjects) of the epochs were correctly classified for the global approach while $78 \pm 9\%$ of the epochs were correctly classified in the individualized approach. The accuracies were significantly higher for the individualized approach ($t_{(11)} = -3.5$; $P = 0.005$). The highest accuracies in the individualized approach were obtained when 54 ± 23 movements were performed; however, there is a large standard deviation.

4 Conclusion

It was possible to use a subject-independent approach for detecting MRCPs associated with hand movements, although the performance was slightly lower compared to the individualized approach. This may have implications for the calibration strategies of MRCP-based BCIs.

Acknowledgements This work was funded by VELUX FONDEN (project no. 22357).

References

1. R. Xu et al., A closed-loop brain-computer interface triggering an active ankle-foot orthosis for inducing cortical neural plasticity. *IEEE Trans. Biomed. Eng.* **20**(4), 2092–2101 (2014)
2. M.A. Cervera et al., Brain-computer interfaces for post-stroke motor rehabilitation: a meta-analysis. *Ann. Clin. Transl. Neurol.* **5**(5), 651–663 (2018)
3. M. Jochumsen et al., Investigation of optimal afferent feedback modality for inducing neural plasticity with a self-paced brain-computer interface. *Sensors* **18**(11), 3761 (2018)
4. N. Mrachacz-Kersting et al., Precise temporal association between cortical potentials evoked by motor imagination and afference induces cortical plasticity. *J. Physiol. (Lond.)* **590**(7), 1669–1682 (2012)
5. M. Jochumsen et al., EMG-versus EEG-triggered electrical stimulation for inducing corticospinal plasticity. *IEEE Trans. Neural Syst. Rehabil. Eng.* **27**(9), 1901–1908 (2019)
6. J. Ibáñez et al., Detection of the onset of upper-limb movements based on the combined analysis of changes in the sensorimotor rhythms and slow cortical potentials. *J. Neural Eng.* **11**(5), 056009 (2014)
7. M. Jochumsen et al., Detecting and classifying movement-related cortical potentials associated with hand movements in healthy subjects and stroke patients from single-electrode, single-trial EEG. *J. Neural Eng.* **12**(5), 056013 (2015)
8. M. Jochumsen et al., Evaluation of EEG headset mounting for brain-computer interface-based stroke rehabilitation by patients, therapists, and relatives. *Frontiers Hum. Neurosci.* **14** (2020)
9. S. Fazli et al., Subject independent EEG-based BCI decoding. *Adv. Neural Inf. Process. Syst.* **22**, 513–521 (2009)
10. M. Krauledat et al., Towards zero training for brain-computer interfacing. *PLoS ONE* **3**(8) (2008)
11. I.K. Niazi et al., Detection of movement-related cortical potentials based on subject-independent training. *Med. Biol. Eng. Comput.* **51**(5), 507–512 (2013)
12. M. Jochumsen et al., Effect of subject training on a movement-related cortical potential-based brain-computer interface. *Biomed. Signal Process. Control* **41**, 63–68 (2018)

**SS3: Towards Patient-Specific Robotic
and Neuroprosthetic Technologies
and Therapies for Walking Rehabilitation
and Assistance**

A Random Forest Based Methodology for the Development of an Intelligent Classifier of Physical Activities



Asier Brull, Sergio Lucas, A. Zubizarreta, Eva Portillo, and Itziar Cabanes

Abstract An appropriate amount of Physical Activity (PA) has been demonstrated to be positive for health. However, most of the developed approaches to monitor PA do not consider people that require assistive devices for walking (ADW), in which gait patterns differ significantly from normal gait. In this work, a methodology is proposed to define a neural-network based classifier that uses the data from a sensorized crutch tip to detect the different PA. To achieve this, a series of features are obtained from the sensorized tip's sensors, and a proper selection is carried out using a Random Forest approach. Based on the relative influence of each feature, a set of them are selected to define a Multi-Layer Perceptron neural network to classify four types of PA. Results show that using this procedure leads to appropriate classifiers.

1 Introduction

In recent years, interest on Physical Activity (PA) monitoring has increased significantly due to its direct impact on health. In rehabilitation processes associated to recovering the mobility of the lower-limb, monitoring PA can provide important information for the functional assessment of the patient [1]. In particular, the therapist can give feedback on the intensity and type of PA to perform in order to aid in the recovery process.

In order to monitor the different PA, different technological solutions have been proposed. Wearable devices are currently one of the most popular approaches [2]. However, attaching sensors to different parts of the body can be invasive for patients,

This research was supported by the University of the Basque Country under grant number PIF18/067 and project number GIU19/045 (GV/EJ IT1381-19) and by the Ministerio de Ciencia e Innovación (MCI) under grant number DPI2017-82694-R (AEI/FEDER, UE).

A. Brull · S. Lucas · A. Zubizarreta (✉) · E. Portillo · I. Cabanes
University of the Basque Country UPV/EHU, Leioa, Spain
e-mail: asier.zubizarreta@ehu.es

A. Brull
e-mail: asier.brull@ehu.es

© The Author(s), under exclusive license to Springer Nature Switzerland AG 2022
D. Torricelli et al. (eds.), *Converging Clinical and Engineering Research on Neurorehabilitation IV*, Biosystems & Biorobotics 28,
https://doi.org/10.1007/978-3-030-70316-5_14

difficulting their motion. Hence, some less invasive approaches have been proposed, such as the use of the internal sensors of mobile phones [3] or the use of sensorized assistive device systems such as crutches or canes [4]. The latter approaches are less invasive and offer great monitoring potential.

The data provided by these devices, however, needs to be processed so that the PA that the patient is executing can be identified. In order to perform this task, methods such as Artificial Neural Networks (ANN) can be used [5]. However, multiple features can be defined considering the raw sensor data. Moreover, currently there are no works that analyze the particular case of patients that use assistive devices for walking, whose gait presents different parameters in comparison with normal gait.

Hence, there is a lack of studies regarding the detection of PA on people that use assistive devices, and a methodology to define a classifier for that purpose. Hence, in this work a methodology based on a Random Forest [6] approach is proposed to design a PA classifier that uses the data from a sensorized crutch tip. Four types of PA are selected: (A) walking straight, (B) going up stairs, (C) going down stairs and (D) standing still.

2 Design Methodology

A set of tests to emulate each PA with 6 healthy people. In these trials, the data provided by a Sensorized Tip [7] was captured (Fig. 1). The device contains a series of sensors: a force sensor to measure the applied load; a barometer to measure the height; and an Inertial Measurement Unit (IMU), which contains a triaxial accelerometer and a triaxial gyroscope.

The raw data from these sensors are first segmented in windows considering the crutch cycle composed by the swing and stance phases. A balanced distribution (528 samples) for each PA is carried out as shown in Table 1.

In a second step, a series of features based on statistical operations are obtained for each cycle. For each measured variable their mean, standard deviation, percentile, kurtosis, variance, correlation coefficient, interquartile range, area under the curve, slope, cycle time and tip usage percentage are calculated, making a total of 90 different features.

In order to determine which of these features are more significant to perform the required PA classification, a Random Forest [6] approach is used (1500 trees, sample with replacement, node size 1, $mtry = \sqrt{M}$ and the *interaction-curvature* predictor). This approach allows to detect the relative weight of each feature in the classification. Due to space constraints, only the 20 most significant features and their relative weight are shown in Fig. 2. As it can be seen, variables related to the gyroscope and the barometer are among the most relevant features to be considered.

Once the most relevant features are defined, an ANN is designed to implement the classifier based on the selected features. In order to evaluate the effectiveness of the approach, five different ANNs are trained considering: (1) the most; (2) the 10 most; (3) the 20 most; (4) all; and (5) the 10 less relevant features. All ANNs have a

Fig. 1 Sensorized Tip and its elements, and local axes of the Tip

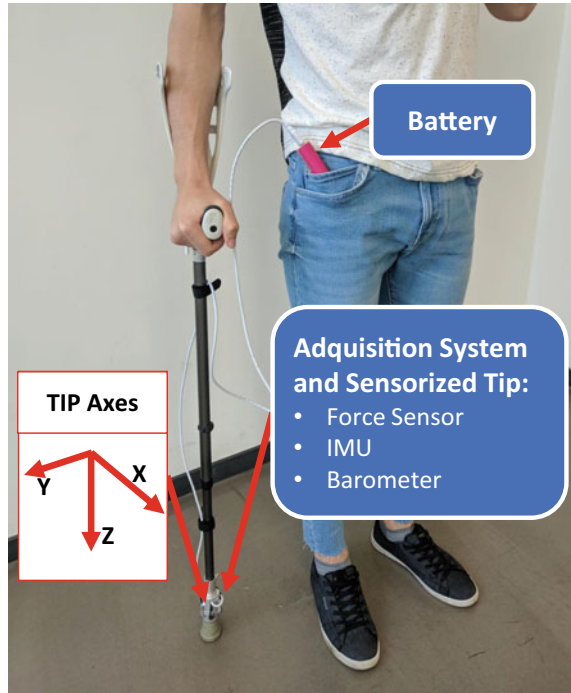


Table 1 Number of windows per physical activity (PA)

Type of PA	Number of windows	Balanced set
(A) Walk normal	389	145
(B) Go up Stairs	142	142
(C) Go down stairs	144	144
(D) Standing still	97	97

single hidden layer with 20 neurons and 4 outputs (one for each PA). The outputs are codified in binary. The ANNs have hyperbolic tangent transfer function and random initialization of thresholds and weights. They are trained using the Training Set and a K-fold Cross Validation procedure with $K = 5$. For each fold, each ANN is trained 10 times with random weight initializations and the Bayesian Regularization method, and the best network is selected as representative for the fold.

3 Results

Figure 3 shows the success rates statistical distribution for the K-fold training procedure for the proposed ANNs. It can be seen that with even only the best feature the

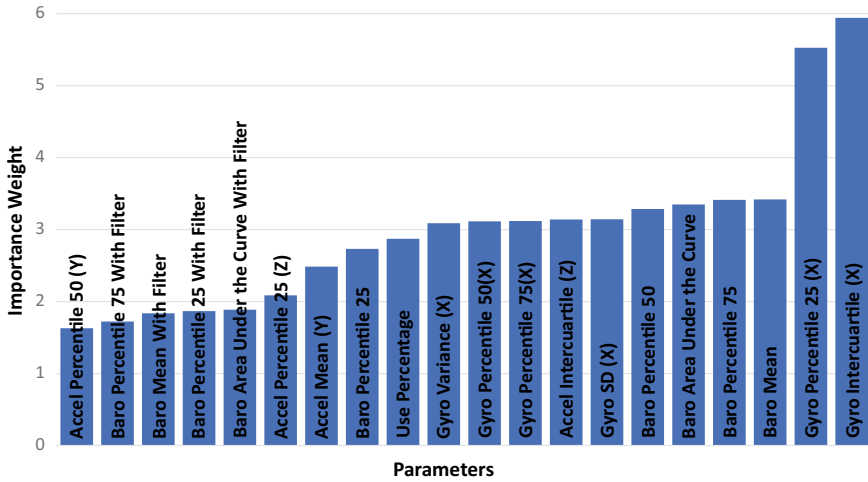


Fig. 2 Indicator weight according to Random Forest, ordered from least to greatest (Accel = Accelerometer, Gyro = Gyroscope and Baro = Barometer)

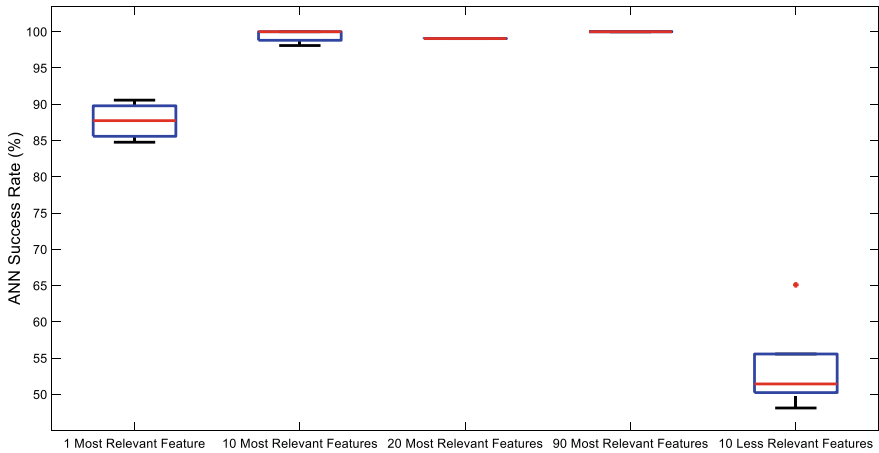


Fig. 3 Success rate (cross validation data)

success rates are high (minimum of 85% and mean of 87%). In creasing the number of relevant features increases the success rate even up to 99% with 20 neurons, with very small deviation in the results, demonstrating the generalization capability of the approach. Table 2 shows the confusion matrix of two of the cases.

Moreover, the last column in Fig. 3 represents the ANN trained with the 10 less relevant features. It can be seen that the rates oscillate between (47–65 %, with no clear normal distribution due to the number of samples), which are much lower than the relevant features cases. This validates the approach.

Table 2 Confusion matrices for ANN-based classifiers

	10 features					All features			
	A	B	C	D		A	B	C	D
A	144	1	0	0	A	145	0	0	0
B	0	141	1	0	B	0	142	0	0
C	0	0	144	0	C	0	0	144	0
D	0	0	0	97	D	0	0	0	97

4 Conclusion

Monitoring PA allows to provide feedback to enhance recovery of patients whose lower-limb mobility is affected. However, there is a lack of works in this area.

This work focuses on proposing the development of an ANN based algorithm that classifies PA. The selection of the input features for the ANN is carried out based on a Random Forest approach.

High success rates are achieved in the classification, using those indicators that the Random Forest marks as most relevant for this task as input.

References

1. F. Tokucoglu, Monitoring physical activity with wearable technologies. *Arch. Neuropsychiatry* **55**(Suppl 1), S63 (2018)
2. P.B. Shull, W. Jirattigalachote, M.A. Hunt, M.R. Cutkosky, S.L. Delp, Quantified self and human movement: a review on the clinical impact of wearable sensing and feedback for gait analysis and intervention (2014)
3. M. Shoaib, S. Bosch, O.D. Incel, H. Scholten, P.J.M. Havinga, Fusion of smartphone motion sensors for physical activity recognition. *Sensors (Switzerland)* **14**(6), 10146–10176 (2014)
4. A. Souza, A. Kelleher, R. Cooper, R.A. Cooper, L.I. Iezzoni, D.M. Collins, Multiple sclerosis and mobility-related assistive technology: systematic review of literature. *J. Rehabil. Res. Dev.* **47**(3), 213 (2010)
5. I.C. Gyllensten, A.G. Bonomi, Identifying types of physical activity with a single accelerometer: evaluating laboratory-trained algorithms in daily life. *IEEE Trans. Biomed. Eng.* **58**(9), 2656–2663 (2011)
6. L. Toloşi, T. Lengauer, Classification with correlated features: unreliability of feature ranking and solutions. *Bioinformatics* **27**(14), 1986–1994 (2011)
7. A. Brull, A. Zubizarreta, I. Cabanes, A. Rodríguez-Larrad, Sensorized tip for monitoring people with multiple sclerosis that require assistive devices for walking. *Sensors* **20**(15), 4329 (2020)

Human-Centered Approaches for Patient-Specific Wearable Robots



Philipp Beckerle

Abstract To support human motions, wearable robots tightly interact with their human users. Besides demanding for functional assistance, user experience is of paramount importance. Remarkably, both aspects are subject to inter-individual differences and, hence, call for personalized solutions. This paper outlines how to address this challenge combining appropriate design methods, human-in-the-loop experiments, and cognitive modeling. Emphasis is put on the capabilities of the methods towards patient-specific solutions offline during design and online during operation.

1 Introduction

While wearable robotics, e.g., prostheses or exoskeletons, receive a lot of scientific interest [1–3], considering individual factors still bears various potentials: patient-specific design and control might provide individually optimized assistance [4] and tailored human-robot interaction [5, 6]. In cognitive and physical interaction, individual demands directly influence users' satisfaction and experiences, which can be approached by personalizing human-centered design approaches [7].

Human factors shape users' experiences and comprise design-related, but also individual aspects, e.g., predispositions towards/against technical aids [8], which can be considered by human-centered design [7]. Although human factor analysis often remains on a population level, it is possible to individually assess subjective experience of wearable robots through questionnaires or interviews, e.g., overall [9,

P. Beckerle (✉)

Chair of Autonomous Systems and Mechatronics, Department of Electrical Engineering & Department of Artificial Intelligence in Biomedical Engineering, Friedrich-Alexander Universität Erlangen-Nürnberg, Erlangen, Germany
e-mail: philipp.beckerle@fau.de

Institute for Mechatronic Systems, Department of Mechanical Engineering, TU Darmstadt, Darmstadt, Germany

10] or body experience [6, 11]. To consider the acquired knowledge, human-in-the-loop techniques [4, 6] and cognitive models [12] appear to be promising tools.

Human-in-the-loop approaches allow involving users during design, e.g., in testing and assessing early component performance and experience [6]. Using a subsystem in an emulated environment, participants can explore the system and its control when interacting with it. Recent research shows that human-in-the-loop approaches can foster personalization of wearable robots and their interaction capabilities. To this end, not only functional and performance outcomes [13, 14], but also user experience need to be considered [5, 6].

Moreover, cognitive models such as Bayesian or connectionist models facilitate predicting human sensorimotor behavior and support our understanding of human cognition [15]. They might be used to personalize wearable robots by shaping their interaction behavior considering their users' individual experience [12].

This contribution presents design methods using human-in-the-loop experiments to personalize wearable robots and shows how cognitive models might enable online adaptation.

2 Design Methods

During human-centered design, individual preferences can already be fused in during requirement analysis as shown in Fig. 1. Taking the systems engineering perspective of V model design [7, 16], those requirements will be defined on system level and might rely on individual user surveys.

To improve the consideration of human factors in design, understanding the interrelations of particular user demands and technical requirements, e.g., specific components, would be important [7, 8]. Expert opinions can augment personalization by revealing such interrelations [7]. However, since assessing individual demands is hardly achievable by statistically interpreting population data, human-in-the-loop experiments and personalized cognitive models are proposed to accompany human-centered design (see Fig. 1).

3 Human-in-the-Loop Experiments

Through human-in-the-loop experiments, two aspects of personalization can be considered (see Fig. 2). On the one hand, users can give individual feedback about their experience of a particular component realization, e.g., how haptic interfaces influence prosthetic device embodiment [6]. On the other hand, already developed components might be tuned during such experiments by parameterizing with respect to individual preferences. To this end, method of adjustment tasks where users vary and select system parameters, e.g., control parameters determining apparent prosthesis stiffness, during interaction could be a valid approach [17].

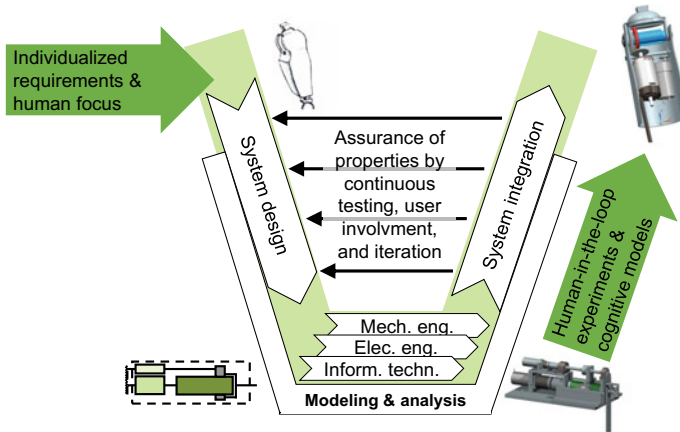


Fig. 1 Individualization possibilities during human-centered systems engineering, e.g., in the V model [7, 16]. Besides individualized requirements (upper left), human-in-the-loop experiments (right) support considering user-specific demands during system integration, e.g., control parameters can be tuned to individualize the apparent stiffness of a prosthesis. Cognitive models enable online user adaptation (right), e.g., comprehending multisensory integration to tailor haptic feedback patterns and intensity

As for survey studies, human-in-the-loop techniques are currently mostly applied to investigate population-wide effects. To improve their capabilities for personalization, individual sensorimotor programs might be identified in the laboratory and in the field through wearable robots [18]. Turning the wearable robot into a measurement system and surveying user experience in addition would help to tailor robotic assistance and augmentation.

4 Cognitive Modeling

As outlined in Fig. 2, cognitive models can help for three purposes in human-robot systems: (1) predicting the users’ intention and behavior, (2) generating robot behavior, and (3) adapting human-robot interaction [19]. Especially in the latter two aspects, users’ preferences might be considered to personalize cognitive and physical interaction.

In predicting and generating behavior, cognitive models might provide for realistic imitation of human behavior [12, 20]. A straightforward approach to individualize behavior and, spatially as well as temporally, align interaction would be fitting free parameters to inter-individual differences [19]. Moreover, robots could be taught to anticipate the human users’ intentions in the long-term, i.e., going beyond (immediate) intention recognition aiming for a joint task awareness [21]. Yet, the issue of overfitting individual data should be treated with care [19].

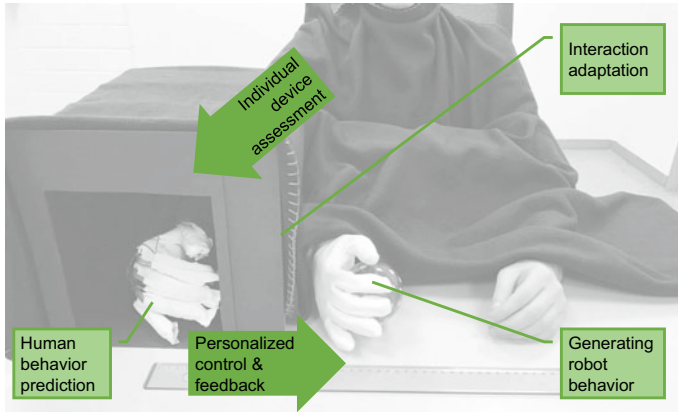


Fig. 2 A robotic embodiment as an exemplary human-in-the-loop experiment: the user assesses whether the robotic hand is perceived as the own one. Based on the individual assessment, developers can tailor personalized control and feedback. Cognitive models can be applied to predict human behavior, generate robot behavior, and align their interaction, e.g., embodiment might improve if triggered by appropriate haptic stimulation

5 Conclusions

Personalization of wearable robots is a challenging, but also very promising endeavor. It emphasizes the relevance of user experience, which is even harder to comprehend and consider on an individual level. Fortunately, existing human-centered methods supported by human-in-the-loop experiments and cognitive models can foster designing individualized wearable robots that adapt to their users online.

References

1. A.M. Dollar, H. Herr, Lower extremity exoskeletons and active orthoses: challenges and state-of-the-art. *IEEE Trans. Rob.* **24**(1), 144–158 (2008)
2. C. Castellini, P.K. Artemiadis, M. Wininger, A. Ajoudani, M. Alimusaj, A. Bicchi, B. Caputo, W. Craelius, S. Došen, K.B. Englehart, D. Farina, S. Gijsberts, S.B. Godfrey, L.J. Hargrove, M. Ison, T.A. Kuiken, M. Markovic, P.M. Pilarski, R. Rupp, E. Scheme, Proceedings of the first workshop on peripheral machine interfaces: going beyond traditional surface electromyography. *Frontiers Neurobotics* **5**(22), 1–17 (2014)
3. M. Windrich, M. Grimmer, O. Christ, S. Rinderknecht, P. Beckerle, Active lower limb prosthetics: a systematic review of design issues and solutions. *BioMed Eng. OnLine* **15**(3), 5–19 (2016)
4. C. Walsh, Human-in-the-loop development of soft wearable robots. *Nat. Rev. Mater.* **3**(6), 78–80 (2018)
5. P. Beckerle, G. Salvietti, R. Unal, D. Prattichizzo, S. Rossi, C. Castellini, S. Hirche, S. Endo, H. Ben Amor, M. Ciocarlie, F. Mastrogiovanni, B. D. Argall, M. Bianchi, A human-robot

- interaction perspective on assistive and rehabilitation robotics. *Front. Neurobotics* **11**(24) (2017)
6. P. Beckerle, C. Castellini, B. Lenggenhager, Robotic interfaces for cognitive psychology and embodiment research: a research roadmap. *Wiley Interdisc. Rev. Cogn. Sci.* **10**(2), (2019)
 7. P. Beckerle, O. Christ, T. Schürmann, J. Vogt, O. von Stryk, S. Rinderknecht, A human-machine-centered design method for (powered) lower limb prosthetics. *Rob. Auton. Syst.* **95**, 1–12 (2017)
 8. C. Gauthier-Gagnon, M.C. Grisé, P.D. Enabling factors related to prosthetic use by people with transtibial and transfemoral amputation. *Arch. Phys. Med. Rehabil.* **80**(6), 706–713 (1999)
 9. F. Cordella, A.L. Ciancio, R. Sacchetti, A. Davalli, A.G. Cutti, E. Guglielmelli, L. Zollo, Literature review on needs of upper limb prosthesis users. *Front. Neuroscience* **10**, 209 (2016)
 10. E.C. Baars, E. Schrier, P.U. Dijkstra, J.H.B. Geertzen, Prosthesis satisfaction in lower limb amputees: a systematic review of associated factors and questionnaires. *Medicine* **97**(39), (2018)
 11. J.W. Breakey, Body image: the lower-limb amputee. *J. Prosthet. Orthot.* **9**(2), 58–66 (1997)
 12. T. Schürmann, B.J. Mohler, J. Peters, P. Beckerle, How cognitive models of human body experience might push robotics. *Front. Neurobotics* **13**, 14 (2019)
 13. J.G.W. Wildenbeest, D.A. Abbink, C.J.M. Heemskerk, F.C.T. van der Helm, H. Boessenkool, The impact of haptic feedback quality on the performance of teleoperated assembly tasks. *IEEE Trans. Hapt.* **6**(2), 242–252 (2013)
 14. J. Zhang, P. Fiers, K.A. Witte, R.W. Jackson, K.L. Poggensee, C.G. Atkeson, S.H. Collins, Human-in-the-loop optimization of exoskeleton assistance during walking. *Science* **356**(6344), 1280–1284 (2017)
 15. M. Berniker, K. Körding, Bayesian approaches to sensory integration for motor control. *Wiley Interdisc. Rev.: Cogn. Sci.* **2**(4), 419–428 (2011)
 16. Verein Deutscher Ingenieure, VDI 2206, Design methodology for mechatronic systems (2004)
 17. I.V. Piryankova, J.K. Stefanucci, J. Romero, S. De La Rosa, M.J. Black, B.J. Mohler, Can i recognize my body’s weight? the influence of shape and texture on the perception of self. *ACM Trans. Appl. Percep.* **11**(3) (2014)
 18. C. Schumacher, A. Seyfarth, Sensor-motor maps for describing linear reflex composition in hopping. *Front. Comput. Neurosci.* **11**(108) (2017)
 19. T. Schürmann, P. Beckerle, Personalizing human-agent interaction through cognitive models. *Front. Psychol.* **11**, 2299 (2020)
 20. M. Hoffmann, H. Marques, A. Hernandez Arieta, H. Sumioka, M. Lungarella, R. Pfeifer, Body schema in robotics: a review. *Autonom. Mental Dev.* **2**(4), 304–324 (2010)
 21. T.J. Prescott, D. Camilleri, U. Martinez-Hernandez, A. Damianou, N.D. Lawrence, Memory and mental time travel in humans and social robots. *Philosoph. Trans. Royal Soc. B* **374**(1771), 20180025 (2019)

Effect of Gel Type and Anode Selection in Ankle Movements Elicited by a Multi-field FES Device



Aitor Martín-Odriozola, Cristina Rodríguez-de-Pablo,
Haritz Zabaleta-Rekondo, Eukene Imatz-Ojanguren, and Thierry Keller

Abstract Functional electrical stimulation (FES) is an evidence-based technique for treating foot drop, the inability to lift the foot due to weak or absent ankle dorsiflexors. Surface multi-field electrodes have brought some advantages such as improved selectivity or possibility of performing automatic motor-search configurations. In fact, they provide new stimulation paradigms that should be tested. This pilot study analyses the movements created using different anode combinations and gel types with the Fesia Walk system, a commercial multi-field technology-based FES device for foot drop compensation. 8 different anode combinations and 2 gel types were tested in 4 healthy subjects. Results show that the most lateral anodes located on the shank produce predominantly ankle plantarflexion and eversion, while the ones located most medially produce more dorsiflexion and inversion. No significant effect was observed between both gel types. This study suggests that anode selection has an influence on the elicited ankle movements and therefore it should be taken into account in the configuration process.

A. Martín-Odriozola (✉) · C. Rodríguez-de-Pablo · H. Zabaleta-Rekondo
Fesia Technology, Donostia-San Sebastián, Spain
e-mail: amartin@fesia.net

C. Rodríguez-de-Pablo
e-mail: crodriguez@fesia.net

H. Zabaleta-Rekondo
e-mail: hzabaleta@fesia.net

E. Imatz-Ojanguren · T. Keller
Tecnalia, Derio, Spain
e-mail: eukene.imatz@tecnalia.com

T. Keller
e-mail: thierry.keller@tecnalia.com

1 Introduction

Foot drop is a gait impairment consisting in the inability to lift the foot due to weak or absent ankle dorsiflexors [1]. This condition appears in up to 20% of the stroke patients, who usually adopt a steppage or equine gait [2].

Functional electrical stimulation (FES) is an evidence-based technique for treating foot drop, which consists in providing short bursts of electrical pulses to induce an action potential in the motor neurons that innervate a muscle, producing a contraction. Most commercial FES-based devices stimulate the common peroneal nerve, producing an ankle dorsiflexion during gait [3].

Surface multi-field electrodes have emerged in the last years, showing great potential on improving activation selectivity and delaying muscle fatigue. This technology also increases exponentially the number of possible stimulation patterns, allowing a more personalized therapy [4]. Another remarkable feature relies on the possibility of doing the configuration automatically [5], avoiding the time-consuming manual motor-point search.

In this pilot study we present an analysis that compares the movements created using different anode combinations and gel types with a commercial multi-field technology-based FES device.

2 Material and Methods

2.1 *Material*

The Fesia Walk system (Fesia Technology, Donostia-San Sebastián, Spain), a commercial multi-field technology-based FES device, was used in this study. It consists of a stimulator, a garment, a multi-field electrode (comprises 16 cathodes and 4 anodes), a wireless inertial sensor and a tablet PC with a software application.

The system includes an automatic configuration process, in which the 16 electrode-fields are activated sequentially while the sensor measures the generated ankle movements. The sensor includes a classification algorithm that classifies the movements as dorsiflexion, plantarflexion, inversion or eversion [5].

2.2 *Experimental Protocol*

Four healthy volunteers (age 39 ± 5) who signed the informed consent, were included in the study.

Eight different anode combinations (Anode 1; Anode 2; Anode 3; Anode 4; Anode 1 and 2; Anode 2 and 3; Anode 3 and 4; Anode 1, 2, 3 and 4) and two different

gels (Gel 1: Axelgaard, stimulating gel AG735, 1500 Ω -cm max; Gel 2: Axelgaard, stimulating gel AG835, 15,000 Ω -cm min, 30,000 Ω -cm max) were tested.

The multi-field electrode was placed on the shank taking as a reference the midline between anodes 2 and 3, which was aligned with the tibia, right under the patella. Like this, anodes 1 and 2 were located on the anterior-medial side of the shank, whereas anodes 3 and 4 were located on the anterior-lateral side.

The stimulation waveform was biphasic compensated, and parameters were set to frequency 25 Hz and pulse width 250 μ s. The amplitude was set for each gel at 10 mA above motor threshold if tolerated by the subject, otherwise above motor threshold at subject's tolerance. Motor threshold was defined as the minimum amplitude at which foot movement was visually appreciated with at least one of the fields and the anode combination "Anode 1, 2, 3 and 4". The configuration posture consisted in sitting on top of a stretcher with the knee extended and the ankle and foot hanging freely.

First, one of the gels was tested with each of the eight anode combinations (in random order). The automatic configuration process was launched 3 times for each anode combination and 1 min of rest was applied between different anode combinations. Then, a minimum resting time of 10 min was applied to avoid fatigue and the process was repeated with the other type of gel. This process was repeated in five different days with each subject.

2.3 Analysis

A qualitative analysis was carried out, in which for each combination the percentage of times that each movement was achieved was represented by means of pie charts.

3 Results

In Fig. 1, the ankle movement classification results obtained with different anode combinations and gels are shown. Each of the pies group the classification results from configurations carried out with different subjects and during different days.

If we focus on gel 1, the dorsiflexion was the predominant movement with almost all anode combinations (35–58%). Anode combinations involving anodes 1 and 2 produced an ankle inversion more often (16–31%) than anodes 3 or 4 (2–5%). On the other hand, anodes 3 and 4 showed the capacity of inducing an eversion more often (12–20%) than anodes 1 and 2 (7–8%). Regarding ankle plantarflexion, it seemed that the capacity of inducing it was reduced as the anode was located more medially. Anode 1 and its combinations did not elicit ankle plantarflexion so often (16%) as Anode 4 and its combinations did (40–43%). In the case of gel 2 a similar trend is appreciated, but the main difference resides in the anode combinations involving anodes 3 and 4. In these cases, a more balanced generation of four movements was

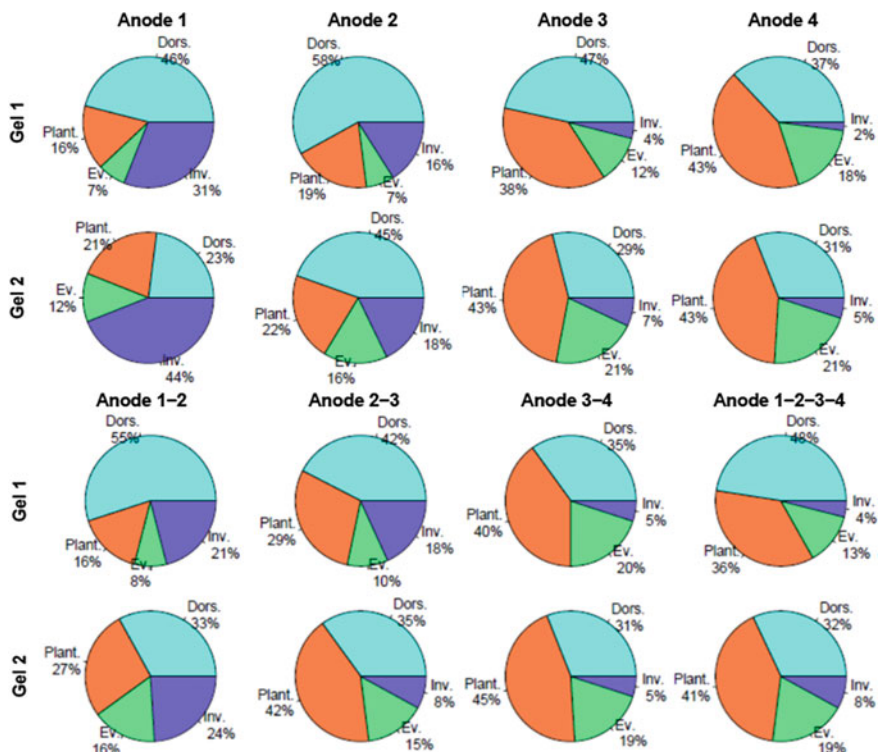


Fig. 1 Ankle movements obtained with different gels and different anode combinations

found with gel 2, resulting in less fields causing dorsiflexion (23–45%), and more fields causing inversion, plantarflexion, or eversion (18–44%, 21–27% and 12–16% respectively).

4 Discussion

The aim of the analysis was to find how the anodes and the gels affected the generation of movements during the configuration of the FES system.

This analysis proved that when anodes located more medially were selected, the capacity of the system to produce eversion and plantarflexion was reduced, probably due to the increased presence of ankle inversion generated with these anodes. On the other hand, the activation of the most lateral anodes showed the capacity to induce ankle eversion and plantarflexion but big limitations to generate ankle inversion.

These differences on the movements generated by the different anode combinations could be due to their location, as lateral anodes are closer to the peroneal nerve and thus, may promote the ankle eversion, whereas the medial anodes are located on

top of the tibialis anterior and may promote inversion and dorsiflexion. However, if the anodes are combined the current spreads through a bigger area and this effect is diminished, resulting in a more balanced distribution of ankle movements.

Regarding the gel effect on the movement, we found a slightly more balanced generation of the four movements with gel 2 when compared with gel 1, but no significant differences were appreciated.

5 Conclusions

We conclude that the anode combination of the Fesia Walk has an important influence in the generated ankle movements. This fact allows a better adaptation of the stimulation to the specific needs of the patient and it should be taken into account during the configuration process. No significant difference was perceived in term of gel resistivity, so the one with the lowest impedance (Gel 1) seems to be a better option to reduce the energy consumption from the stimulator side. Although the study was carried out with healthy people, these results can be extrapolated to patients with neurological pathology, since it has been studied a characteristic that does not vary if there is a neurological disorder. Further research with people with neurological disorders and a larger sample is necessary to confirm these conclusions.

Acknowledgements This work has been supported in part by FIK.

References

1. J. Perry, J. Burnfield, *Gait Analysis: Normal and Pathological Function*, 2nd edn. (SLACK Incorporated, New Jersey, 2010).
2. J. Graham, Foot drop: explaining the causes, characteristics and treatment. *Br. J. Neurosci. Nurs.* **6**, 168–172 (2013)
3. L.R. Sheffler, J. Chae, Neuromuscular electrical stimulation in neurorehabilitation. *Muscle Nerve* **35**, 562–590 (2007)
4. E. Imatz-Ojanguren, G. Sánchez-Márquez, J.R. Asiain-Aristu, J. Cueto-Mendo, E. Jaunarena-Goicoechea, H. Zabaleta et al., A foot drop compensation device based on surface multi-field functional electrical stimulation-usability study in a clinical environment. *J. Rehabil. Assist. Technol. Eng.* **6** (2019)
5. J. Malešević, S.D. Dujović, A.M. Savić, L. Konstantinović, A. Vidaković, G. Bijelić et al., A decision support system for electrode shaping in multi-pad FES foot drop coorection. *J. Neuroeng. Rehabil.* **14**, 1–4 (2017)

In Vitro Evaluation of a Protocol and an Architecture for Bidirectional Communications in Networks of Wireless Implants Powered by Volume Conduction



Laura Becerra-Fajardo, Jesus Minguillon, Camila Rodrigues, Filipe O. Barroso, José L. Pons, and Antoni Ivorra

Abstract Wireless active implantable medical devices (AIMDs) can be an alternative for overcoming the drawbacks faced with superficial and percutaneous technologies. However, current AIMDs require bulky and rigid components for powering, hampering their miniaturization. AIMDs based on power transfer by volume conduction do not need these voluminous parts, allowing the development of thread-like devices that could be used for distributed stimulation and sensing of the neuromuscular system. In this paper, we present an in vitro evaluation of a protocol and an architecture for bidirectional communications in networks of injectable wireless implants powered and controlled by volume conduction. The wireless prototypes were successfully addressed from the external systems, and end-to-end bidirectional communication was performed at 256 kbps with a success rate of 87%.

1 Introduction

Musculoskeletal modelling and robotics are currently used to aid in the management of tremor suppression and spinal cord injury rehabilitation. However, both fields rely

L. Becerra-Fajardo (✉) · J. Minguillon
Department of Information and Communications Technologies, Universitat Pompeu Fabra,
Barcelona, Spain
e-mail: laura.becerra@upf.edu

C. Rodrigues · F. O. Barroso
Neural Rehabilitation Group, Cajal Institute, Spanish National Research Council (CSIC), Madrid,
Spain

J. L. Pons
Legs and Walking AbilityLab, Shirley Ryan AbilityLab, Chicago, IL, USA

Department of Biomedical Engineering and Department of Mechanical Engineering, McCormick
School of Engineering, Northwestern University, Chicago, IL, USA

A. Ivorra
Serra Hünter Fellow Programme, Dept. of Information and Communications Technologies,
Universitat Pompeu Fabra, Barcelona, Spain

on superficial or percutaneous methods for electromyography (EMG) acquisition and electrical stimulation, which present several drawbacks including lack of selectivity in the former, and creation of infection pathways in the latter.

Wireless active implantable medical devices (AIMDs) are an alternative for overcoming these drawbacks. Yet their development has been hampered by the methods used to power them, as those usually require bulky and rigid components that result in devices that are too thick and stiff to be easily implanted through injection [1].

To overcome these limitations, we have proposed an implantable technology based on wireless power transfer by volume conduction: an external system delivers to the tissues high-frequency (HF) currents in the form of bursts, and these currents are picked up by thread-like injectable implants to power their electronics, and perform tasks such as electrical stimulation and EMG acquisition. This implantable technology will be used to develop minimally invasive “Bidirectional Hyper-connected Neural Systems” (BHNS) for distributed stimulation and sensing of neuromuscular activity, which could be used for tremor suppression management and spinal cord injury rehabilitation.

The BHNS will be composed of external systems and wireless implants (hereinafter “functional units” (FUs)). The external systems will consist of (1) one top-level control device (hereinafter “Brain”) that will communicate with the FUs through (2) several low-level control units (CUs) that act as bidirectional gateways (i.e. protocol translators) between the Brain and the FUs. These CUs will apply bursts of HF currents through external electrodes. The FUs will pick up these currents and rectify them to obtain power and information, and to perform the task defined by the Brain.

In this paper we will present a first in vitro evaluation of a protocol and an architecture for bidirectional communications in networks of wireless FUs powered by volume conduction.

2 Materials and Methods

2.1 External Systems

The Brain consists of a PC/104 board computer with a PCIe/104 stackable bus structure (CMA34CRQ2100HR, by RTD) and a 2.1 GHz Quad-Core processor. The CUs consist of: (1) a HF sinusoidal generator and modulator (4064 by BK Precision); (2) a digital control to manage the communication interfaces with the Brain, the FUs and controlling the whole CU; (3) a custom-made demodulator that decodes the modulation performed by the FUs for the uplink communication (i.e. from the FUs to the Brain); and (4) a custom-made high-power amplifier that applies the HF current bursts to the tissues through the external electrodes. The currents are delivered in the form of bursts to avoid tissue heating, and they are in HF to avoid unwanted electrostimulation [2].

The information between the external systems and the FUs is modulated in the HF current bursts. To avoid tissue heating, an *ad hoc* communication protocol stack was implemented. It consists of a four-layers architecture based on the Open System Interconnection (OSI) model. With the current protocol stack, thirteen different tasks can be performed.

2.2 Functional Units—Wireless Devices

The proof-of-concept FUs used in this evaluation are based on the architecture described in [3]. They are made only of off-the-shelf components soldered on a printed circuit board (PCB), which can be easily connected to wire electrodes, or to thin-film electrodes that can be injected using a needle [4]. For the uplink, the FUs digitally modulate the HF current bursts according to the protocol stack.

2.3 In Vitro Evaluation

The in vitro setup, including Brain, CUs and FUs (Fig. 1a) is based on two 6.5 cm diameter agar cylinders made from a NaCl solution with a conductivity of 0.57 S/m, equivalent to that of muscle tissue at 3 MHz. Two aluminum external electrodes were strapped around the cylinders, at a distance of 10 cm, and each pair of electrodes were connected to one CU. The electrode pads of the FUs' PCBs were soldered to two silver plated copper wire electrodes with an exposed length of 3.65 mm and a diameter of 0.25 mm, and the ends of these wires were inserted into the cylinders, at a distance of 3 cm.

One Brain controlled the two CUs, each one delivering sinusoidal signals in the form of bursts, with an amplitude of 37 V, a duty cycle of 8% and a frequency of 3 MHz. The signals delivered by the FUs and those obtained by the CUs were recorded using an oscilloscope with isolated channels (TPS2014 by Tektronix).

Three sets of experiments were done: (1) downlink communication (i.e. request from the Brain to the FUs) to two FUs in a single agar cylinder (i.e. one CU); (2) downlink communication to two FUs, each one in one agar cylinder (i.e. two CUs); and (3) downlink and uplink communication (i.e. request from the Brain to the FUs and reply from the FUs to the Brain) using one FU in a single agar cylinder.

3 Results

For experiments 1 and 2, as a visual demonstration, two LEDs were added to the FUs to show if the Brain was able to address each one of them independently. In both experiments, all the FUs were successfully addressed with no error. A video of

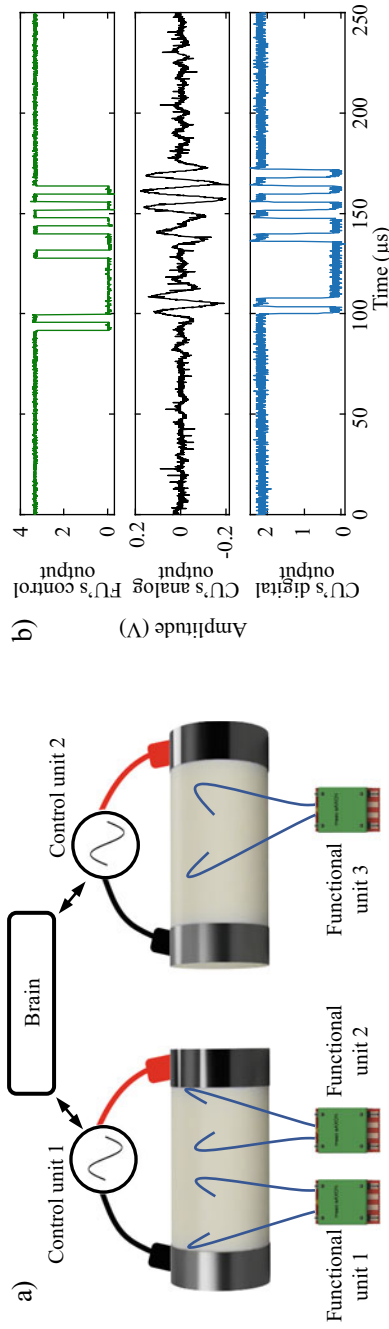


Fig. 1 In vitro evaluation of a protocol and an architecture for bidirectional communications in networks of wireless implants (FUs) powered by volume conduction. **a** Setup used. **b** Results obtained during an uplink sequence, including (1) control signal of the FU for its modulator; an acknowledge (ACK) message is sent to the CU according to the protocol stack, (2) filtered signal obtained by CU's demodulator, and (3) digital output of comparator circuit in CU's demodulator

experiment 2 is available in this link (<https://drive.google.com/file/d/1sH8ypgcTDe9ZvZrk3TRvfz26g8MzYcSo/view?usp=sharing>). In experiment 3, the whole system was able to perform end-to-end bidirectional communication between the Brain and one FU at 256 kbps with a success rate of 87%.

Figure 1b shows how the CU demodulates the uplink information coming from the FU. The modulation made by the FU is seen by the CU as variations on the current applied to the tissues. These fluctuations are filtered, amplified and passed through a Schmitt trigger, to obtain a digital signal that can be processed by the CU. The delay between the FU and the CU is only tens of microseconds.

4 Discussion

Here we in vitro evaluated a protocol and an architecture for bidirectional communications in networks of wireless implants powered by volume conduction. The communication speed is high enough for controlled electrical stimulation and EMG acquisition. The circuit architecture of the FUs used is the basis of a fully injectable device based on an application specific integrated circuit (ASIC). The resulting wireless device will have an unprecedented level of minimal invasiveness, which will be paramount for the viability of the BHNS for distributed stimulation and sensing of neuromuscular activity.

Acknowledgements This work was funded by the European Union's Horizon 2020 Research and Innovation Programme (Project EXTEND—Bidirectional HyperConnected Neural System) under grant agreement No 779982. Antoni Ivorra gratefully acknowledges the financial support by ICREA under the ICREA Academia programme.

References

1. A. Kim, M. Ochoa, R. Rahimi, B. Ziaie, New and emerging energy sources for implantable wireless microdevices. *IEEE Access* **3**, 8998 (2015)
2. M. Tudela-Pi, L. Becerra-Fajardo, A. García-Moreno, J. Minguillon, A. Ivorra, Power transfer by volume conduction: in vitro validated analytical models predict DC powers above 1 mW in injectable implants. *IEEE Access* **1** (2020)
3. L. Becerra Fajardo, M. Schmidbauer, A. Ivorra, Demonstration of 2-mm-thick microcontrolled injectable stimulators based on rectification of high frequency current bursts. *IEEE Trans. Neural Syst. Rehabil. Eng.* **25**(8), 1343–1352 (2017)
4. S. Muceli et al., A thin-film multichannel electrode for muscle recording and stimulation in neuroprosthetics applications. *J. Neural Eng.* **16**(2) (2019)

A Study on Reference Range of Healthy Subjects for Detection and Evaluation of Abnormal Foot Movement During Walking in Hemiplegic Subject Using Inertial Sensors



Taihei Noro, Takashi Watanabe, Katsunori Murakami, and Naomi Kuge

Abstract Abnormal foot movements seen in hemiplegic patients include drop foot and clubfoot. This study aimed to detect and evaluate abnormal foot movements during early stance phase of hemiplegic patients using inertial sensors. Two inclination angles associated with abnormal foot movement were calculated from acceleration and angular velocity obtained from inertial sensors, and reference range of healthy subjects was created by defining a two-dimensional plane with these two angles. In addition, the angle distribution was divided into 3 groups based on the stride length, and the reference range was created for each group. Measured data of paralyzed side of a hemiplegic subject was suggested to be abnormal foot movements by comparing to the reference range. Therefore, the reference ranges of healthy subject for different stride lengths are expected to be useful for the detection and evaluation of abnormal movements of hemiplegic subjects.

1 Introduction

When stroke develops, mortality rate is low [1], but hemiplegia often occurs, affecting the patient's quality of life. Especially when motor dysfunction occurs in the lower limbs, the patient's walking function deteriorates, causing a significant decrease in ADL. On the other hand, stroke is a disease that can be expected to return to society through appropriate rehabilitation, and early rehabilitation is important [1].

Most of the current rehabilitation sites evaluate the entire body movement, and detailed abnormal movement of each segment of the body such as the foot is not

T. Noro

Graduate School of Engineering, Tohoku University, Sendai, Japan
e-mail: taihei.noro.q3@dc.tohoku.ac.jp

T. Watanabe (✉)

Graduate School of Biomedical Engineering, Tohoku University, Sendai, Japan
e-mail: t.watanabe@tohoku.ac.jp

K. Murakami · N. Kuge

Kurokawa Hospital, Taiwa Town, Miyagi, Japan

detected and evaluated. It is thought that optimized rehabilitation can be performed by objectively and quantitatively evaluating the walking function of the patient. This study focused on gait rehabilitation, and therefore detection and evaluation of abnormal movement during gait for the objective assessment. In this paper, reference range of healthy subject was created and tested to detect abnormal foot movement during gait.

2 Methods

2.1 Calculation Method of Inclination Angle

Inclination angle of the foot was calculated from measured data with an inertial sensor attached on the foot [2]. First, the angular velocity measured by the inertial sensor was converted into quaternion. In the integration process to calculate the quaternion, the integration error was accumulated. In order to compensate for the error, Kalman filter was applied with the acceleration vector measured by the inertial sensor as the observed value. Then, the rotation matrix was calculated from the corrected quaternion and applied to the unit vector defined for the foot segment to obtain the posture vector. The angle was calculated from the posture vector.

2.2 Creation Method of Reference Range for Healthy Subjects

The foot inclination angle in the sagittal plane at the initial contact (IC) and that in the frontal plane at the foot flat (FF) calculated from the acceleration and angular velocity measured with the inertial sensor were used to detect abnormal movements. The two-dimensional plane was defined by the two inclination angles, and reference range for healthy subject was created. Regarding the inclination angle in the frontal plane at FF, the negative value means the inversion and the positive value is the eversion. Regarding the inclination angle in the sagittal plane at IC, negative value is the planter flexion and positive value is the dorsiflexion. If angle plot of hemiplegic subject falls outside the range, it is detected as abnormal movement. The reference range was created using Mahalanobis distance in this study. Furthermore, we calculated the stride length for each stride [3] and tried to divide the reference range according to the stride length.

2.3 Experimental Method

Gait data were measured with 30 healthy subjects in their 20s (15 males and 15 females) and a hemiplegic subject with wireless inertial sensors. The hemiplegic subject (Brunnstrom stage II) was 75 years old and about 9 years had passed since the onset. The sensor signals were sampled at 100 Hz and recorded by a personal computer. In gait measurement, inertial sensors were fixed to subject's feet, shanks, thighs, and lumbar region using elastic band. The number of measurement trials was 6, and the first 2 trials were excluded from the analysis as practice walking. The healthy subjects walked 15 m at self-selection speed. The hemiplegic subject walked 10 m at self-selection speed and use the cane that the subject used daily.

3 Results

Measured inclination angles with 30 healthy subjects were shown in Fig. 1. The number of analyzed stride was 1669. As seen in Fig. 1, angles were widely distributed on the angle plane. Therefore, in this study, stride length was calculated and normalized by the height of subject. The calculated angle data was divided into 6 groups based on the normalized stride length (NSL), and a reference range was created for each group. After that, groups with nearly overlapping reference ranges and/or small sample sizes were integrated. Finally, the reference ranges were created for 3 groups based on the NSL. Here, the NSL for the three groups were $NSL \leq 0.70$ as Short, $0.70 < NSL \leq 0.80$ as Middle, and $0.80 < NSL$ as Long, respectively. For each group, reference range for healthy subject was created using Mahalanobis distance. The number of strides classified into each group was 143 strides for Short, 557 strides for Middle, and 969 strides for Long.

Figure 2 shows created reference ranges for 3 groups and reference range for all the data. The reference range created using all data included 94.3% of measured data with healthy subjects. The average values of inclination angle in the frontal plane at the FF and in the sagittal plane at the IC for 3 groups were 2.10° and 17.2° for Short, 0.488° and 22.4° for Middle, and -0.356° and 26.8° for Long, respectively. Angle data of a hemiplegic subject was also shown in Fig. 2. The angles of the non-paralyzed side was almost in the Short group, and those of paralyzed side was outside the reference range.

4 Discussion

As the stride length became shorter, inclination angle in the frontal plane at the FF tended to be larger and that in the sagittal plane tended to be smaller. These angle changes are considered to be natural for walking of healthy subject. Therefore,

Fig. 1 Measured angles under self-selected walking speed with 30 healthy subjects

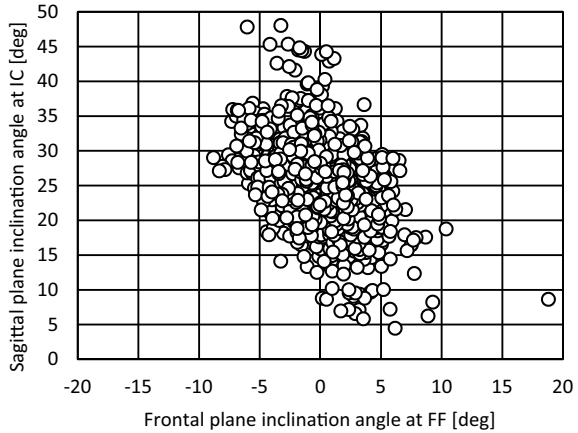
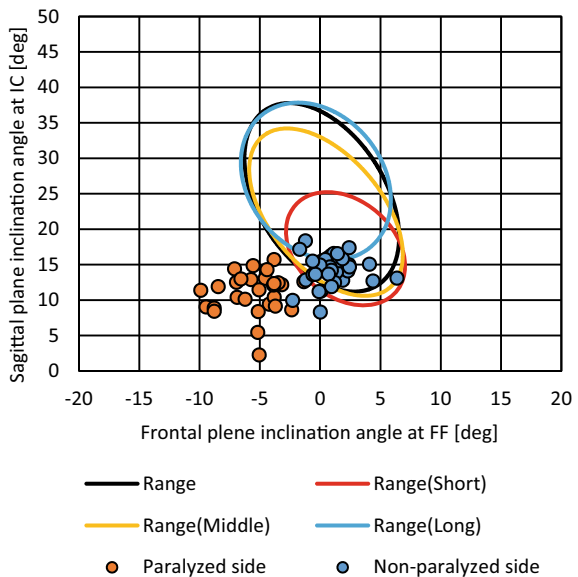


Fig. 2 Reference ranges for all data and 3 groups (short, middle and long). Angle data of a hemiplegic subject are also shown



reference range for healthy subject was divided into 3 groups based on the stride length in this study. Since the number of strides for the Short group was small, it is desirable to increase the number of data and to re-create the reference range.

Stride length of hemiplegic subject was considered to belong to the Short group. As seen in Fig. 2, the angles of the non-paralyzed side of the hemiplegic subject were almost within the reference range of Short group. On the other hand, although the angles of the paralyzed side were near the reference range of Short group, they were outside of the range, which suggested the movements were abnormal.

5 Conclusion

In this study, in order to detect and evaluate foot abnormal movements of hemiplegic gait, reference range for healthy subject was created using inclination angles in the sagittal plane at the IC and in the frontal plane at the FF. The reference range was divided into three groups based on the stride length. Measured data of a hemiplegic subject suggested that abnormal movement could be detected by comparing to the reference range. In the future, increasing the number of Short data and that of hemiplegic subject's data will be an issue. In addition, quantitative evaluation using the reference range is also an issue.

Acknowledgements This work was partly supported by JSPS KAKENHI Grant Number JP19K22735.

References

1. W.H. Hou, C.H. Ni, C.Y. Li, P.S. Tsai, L.F. Lin, H.N. Shen, Stroke rehabilitation and risk of mortality: a population-based cohort study stratified by age and gender. *J. Stroke Cerebrovasc. Dis.* **24**(6), 1414–1422 (2015)
2. T. Watanabe, Y. Teruyama, K. Ohashi, Comparison of angle measurements between integral-based and quaternion-based methods using inertial sensors for gait evaluation. *Commun. Comput. Inf. Sci.* **511**, 274–288 (2016)
3. Y. Nozaki, T. Watanabe, Development of artificial neural network based automatic stride length estimation method using IMU: validation test with healthy subjects. *IEICE Trans. Inf. Syst.* **E103-D**(9), 2027–2031 (2020)

A Preliminary Study on Prediction of Initial Contact Timing During Gait Using LSTM for FES Control



Yuto Uwaseki and Takashi Watanabe

Abstract This study focused on feedback FES control of foot movements of hemiplegic gait. In order to create target movement trajectory, prediction of initial contact (IC) timing would be useful. In this paper, a method for predicting the IC timing using LSTM network was tested. The prediction was based on short-term historical signal data of an inertial sensor mounted on the foot. The prediction test were performed for measured data with 2 healthy individuals. The results showed that the mean and standard deviation of the errors tended to decrease as the percentage of the gait cycle increased, with a significant decrease after heel-off. The proposed method was suggested to be applicable in IC timing prediction.

1 Introduction

Foot drop correction using functional electrical stimulation (FES) has been shown to be an effective method to improve gait of hemiplegic subjects [1]. Since FES has therapeutic effects in restoring function of ankle dorsiflexion, FES can be used as an effective tool for gait rehabilitation for hemiplegic patients [2].

In our previous study [3], stimulation timing was determined by detecting the toe off (TO) and foot flat (FF) timings using a single inertial measurement unit (IMU). In this system, the foot inclination angle during gait was not controlled. Since healthy subjects walk with more complex joint angle trajectories, feedback FES control of foot movements may lead to better rehabilitation. Therefore, this study aimed to develop feedback FES control system of foot drop correction. In order to realize feedback FES control, target angle trajectory is required. However, gait movements of a hemiplegic subject varies between steps. Therefore, it is desirable to determine

Y. Uwaseki

Graduate School of Engineering, Tohoku University, Sendai, Japan

e-mail: yuto.uwaseki.p7@dc.tohoku.ac.jp

T. Watanabe (✉)

Graduate School of Biomedical Engineering, Tohoku University, Sendai, Japan

e-mail: t.watanabe@tohoku.ac.jp

the angle trajectory for each step. To determine the angle trajectory, this study focused on prediction of initial contact (IC) timing.

In this paper, a method to predict the upcoming IC timing using single IMU after detecting the IC timing of the previous step was studied. The IC timing was predicted using the long short-term memory (LSTM) network, which has shown great success in many problems with time series information [4].

2 Methods

2.1 Outline of IC Timing Prediction

IC timing is predicted based on output values of the LSTM model. Figure 1 shows the flow of the IC timing prediction. The LSTM model outputs 100 values based on the historical data of IMU attached to the foot. The output values are predicted values of probability of the IC at each time after the input time. The time with the highest value among the outputs of the model was determined as the predicted IC timing.

2.2 IC Prediction Model

The IC prediction model consists of single LSTM layer and fully connected layer. The LSTM layer had 1200 units with dropout rates of 20% to prevent overfitting, and the fully connected layer had 100 units. Activation function of the output layer was sigmoid function. Adam was used as optimizer and the loss function was mean squared error.

The inputs were tri-axis signals of angular velocity and tri-axis acceleration measured with IMU attached on the left dorsum foot for last 20 times. The label signal was “1” for the IC time step and “0” for all other times.

2.3 Experimental Method

Gait data were wirelessly measured with 2 healthy subjects with IMU (MPU-9150, InvenSense) wrapped around the dorsum of the left foot with an elastic band. The subjects walked 16 m straight at 3 self-selected speeds (slow, moderate and fast). 40 trials were performed for each self-selected speed. The sensor signals were sampled at 100 Hz. Gait speed of each trial was calculated by dividing the walking distance, which was the distance from the 3rd step to the step that the distance from the 3rd step becomes longer than 10 m, by the elapsed time for the distance. Gait event timings

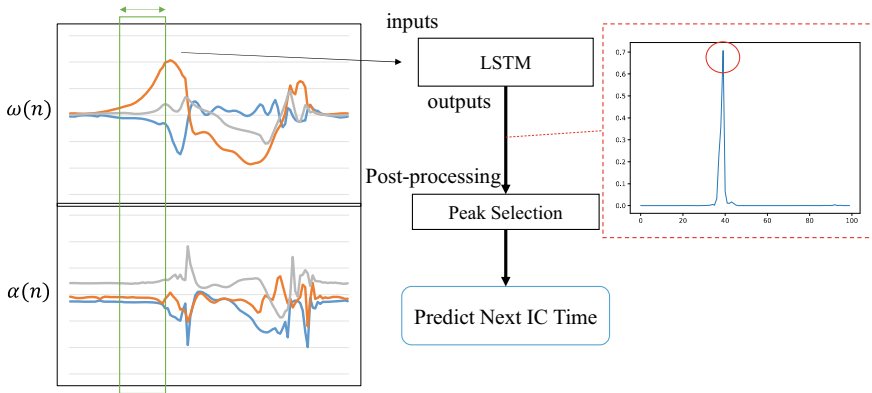


Fig. 1 Flow of IC timing prediction using LSTM

were detected using a single IMU attached on the dorsum of the foot, based on the method proposed in a previous study [3].

Model training and off-line IC timing prediction of the left foot were performed for each subject. Since the gait pattern is dependent on its speed [5], a total of 120 trials for each subject were sorted in order of speed, and 15 trials for training were selected at equal intervals including the maximum and minimum speed. Another one trial from each speed was randomly chosen and used for model validation.

IC timing prediction was tested for 5 trials for each self-selected speed of each subject. Prediction errors in milliseconds were calculated for each stride. The first and last strides for each trial were excluded before error calculation. Since the sampling frequency of the IMU was 100 Hz, the model predicted the IC timing in the next 1 s after the input time. Therefore, we excluded the prediction results when the IC was out of the predictable range for the calculation of the mean and standard deviation.

3 Results

Figure 2 shows the mean and standard deviation of the errors for one subject in each 2% interval of the normalized gait cycle. Shown in blue area is the range of the mean and standard deviation of HO timing for the subject. One outlier of the predicted IC timing was found at around 98% of the gait cycle for this subject. Table 1 shows the calculated results of the mean and standard deviation of the prediction error at 10% intervals for each speed of the subject of Fig. 2, excluding the outlier after 90% of the gait cycle.

Table 1 The mean and standard deviation of the errors of the normalized gait cycle at 10% intervals

	0-9%	10-19%	20-29%	30-39%	40-49%	50-59%	60-69%	70-79%	80-89%	90-99%
Slow [ms]	-	-	-29.78 ± 48.26	-8.46 ± 46.41	6.19 ± 32.96	-2.84 ± 15.93	-2.53 ± 13.74	-7.21 ± 12.80	-3.76 ± 12.49	-3.50 ± 8.56
Moderate [ms]	-	-4.65 ± 26.26	3.96 ± 42.06	-6.08 ± 42.28	1.86 ± 21.33	-3.23 ± 11.58	-4.13 ± 10.74	-3.88 ± 10.42	-0.83 ± 12.76	-6.01 ± 7.86
Fast [ms]	-4.17 ± 50.25	7.17 ± 58.73	3.46 ± 80.44	15.67 ± 39.78	8.62 ± 22.35	3.15 ± 14.18	0.43 ± 12.90	3.49 ± 11.01	3.52 ± 16.05	1.29 ± 11.99

4 Discussion

The results showed that the mean and standard deviation of the errors tend to be decreased as the percentage of the gait cycle increased, with a significant decrease after HO timing. Since feedback FES control of the foot drop correction can be started at just before the HO timing, the decrease of error shows that the proposed method would be applicable.

As shown in Fig. 2, one outlier was found near the end of the gait cycle under the fast speed. Outliers in similar cases were found in the other subject. These outliers were considered to be due to its fast gait speed. In the case of fast gait speed, the gait cycle tend to be shorter than any other speed. In the prediction for the gait with a short gait cycle, there would be multiple IC events within 1 s, which is the predictable range of the present model. In this case, the model output shows multiple peaks in one prediction, which correspond to different IC timings, respectively. Since the method of this paper determines the time with the maximum value as the predicted IC timing, misprediction may occur by the amplitude of the peaks when there are multiple peaks. However, since the most hemiplegic patients tend to walk slower than healthy people, this problem may not occur in actual foot drop correction. In addition, since no cases of continuous outliers were found, and the numerical values of outliers were greatly deviated compared to predicted values of previous times, it is considered that this problem can be solved by implementing an algorithm that exclude outliers based on the previous prediction results.

The hemiplegic patients may have greater individual difference in gait pattern due to compensatory movements. For this reason, it is preferable to train the model to be applied for actual use based on user’s individual measurement signals. Therefore, in this study, the training of ANN and its evaluation was performed for each subject.

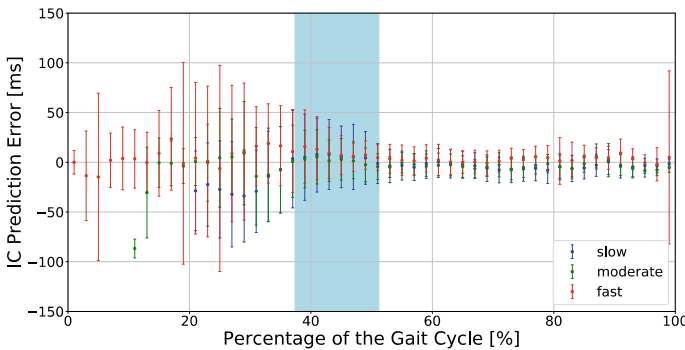


Fig. 2 The mean and standard deviation of the prediction errors at 2% intervals of the normalized gait cycle

5 Conclusion

In this paper, a method of IC timing prediction with single IMU using LSTM was tested. The proposed prediction method was suggested to be applicable for IC timing prediction with IMU. For future works, improvement of the prediction accuracy and evaluation of the predictions using measurement data from hemiplegic individuals are expected to be conducted.

References

1. J.H. Burridge, Does the drop-foot stimulator improve walking in hemiplegia? *Neuromodulation* **4**(2), 77–83 (2001)
2. G. Morone, A. Fusco, P. Di Capua, P. Coiro, L. Pratesi, Walking training with foot drop stimulator controlled by a tilt sensor to improve walking outcomes: a randomized controlled pilot study in patients with stroke in subacute phase. *Stroke Res. Treat.* **2012**, 523564 (2012)
3. T. Watanabe, S. Endo, R. Morita, Development of a prototype of portable FES rehabilitation system for re-learning of gait for hemiplegic subjects. *Healthc. Technol. Lett.* **3**(4), 284–289 (2016)
4. F.A. Gers, J. Schmidhuber, F. Cummins, Learning to forget: continual prediction with LSTM, in *1999 Ninth International Conference on Artificial Neural Networks ICANN 99* (2007), pp. 850–855
5. C.A. Fukuchi, R.K. Fukuchi, M. Duarte, Effects of walking speed on gait biomechanics in healthy participants: a systematic review and meta-analysis. *Syst. Rev.* **8**, 153 (2019)

Smart Wearable Garment and Rapid Musculoskeletal Modelling for Accurate Neuromechanical Analysis



D. Simonetti, B. F. J. M. Koopman, and M. Sartori

Abstract Current clinical diagnostic tools for post-stroke motor deficits are based on rapid but subjective evaluation. Greater accuracy could be provided in well-equipped biomechanical laboratories. However, this involves lengthy set-up, data acquisition, and offline data analysis available only days, or weeks, after the initial assessment, no longer reflecting the patient's actual state. The ability to capture the patient's muscle activity as well as joint kinematics is key for neuromechanical assessment, but the process of muscle localization for electrode placement and joint angle measurement is not always viable in clinical environments. Here, we propose a new wearable technology with an integrated high-density electromyography and kinematics sensors able to provide simultaneously a rapid and accurate diagnosis. The soft sensorized garment in conjunction with automatic clustering of the HD-EMG channels into muscle groups and real-time modeling of the neuromusculoskeletal system allows estimation of internal mechanical forces in a rapid, quantitative, and clinically viable way.

1 Introduction

Currently, the clinical assessment of post-stroke gait is based on rapid but non-objective metrics; the functional ambulation categories (FACs) [1], i.e. self-paced 10-m walking speed and fastest 10-m walking speed. To provide a successful motor assessment, clinicians need to rapidly and objectively evaluate patient-specific neuro-physical conditions over time. Electromyography (EMG)-driven musculoskeletal modeling and simulation [2] could potentially provide quantitative assessment but requires lengthy procedures, i.e. capturing the patient's myoelectrical activity as well as joint kinematics. This is already possible in biomechanical laboratories. Nevertheless, the high cost, the lengthy set up such as the process of manual muscle localization for electrode placement, joint angle measurements, and the time-consuming

D. Simonetti (✉) · B. F. J. M. Koopman · M. Sartori
Department of Biomechanical Engineering, University of Twente, Enschede, The Netherlands
e-mail: d.simonetti@utwente.nl

processing of the data are not viable in the clinical environment on a large group of patients.

The present work proposes an advanced technology that combines (1) a fully wearable soft sensorized garment, (2) an automatic algorithm for muscle localization from HD-EMG, and (3) a framework for patient-specific neuro-mechanical modeling (as shown in Fig. 1). The sensorized garment, in combination with automated muscle localization, allows reducing the set-up time and preventing human error to manually identify the muscles and place the electrodes. To automatize the process of clustering the HD channel space into muscles' specific activation, we apply non-negative matrix factorization (NNMF) [3] to extract muscle synergies during locomotion. We applied the NNMF-based extraction of muscle synergies to segment the HD-EMG grid capturing the spatial distribution of lower leg muscles without any prior knowledge on the electrodes' position. The NNMF is applied to HD-EMG to extract 4 main clusters related to the Tibialis Anterior (TA), Soleus (SOL), Gastrocnemius Lateralis (GL), and Medialis (GM), and Peroneus (PR). The average activation profile of each electrodes' cluster drive, thereafter, the framework for neuromuscular simulation of the patient-specific internal neuro-mechanical system.

In the following paragraphs, we show two preliminary studies assessing (1) extraction of 5 mean activation profiles from NNMF-muscle synergies using the soft HD-EMG garment placed on the lower leg and (2) torque estimation at ankle joint during different locomotion tasks using EMG-driven musculoskeletal model.

2 Material and Methods

Both experiments were performed on healthy male subjects performing locomotor tasks at three different speeds (slow, comfortable, and fast). Ground reaction forces (GRF), trajectories of 35 retro-reflective markers on the subject's body, and electromyography were recorded. In Test 1 the muscle activity was recorded on the right lower leg using a garment equipped with 64 monopolar electrodes equally distributed. Whereas, in Test 2, bipolar electrodes were used to record 9 muscles on the leg.

Test 1 focuses on the automatic extraction of muscle activation profiles from HD-EMG grid. The channel-space of 64 electrodes is reduced in 4 signals, one for each main muscle in the lower leg. This reduction is the output of the NNMF algorithm. To automatically identify the 5 lower leg muscles, the NNMF is performed two times. The first application of NNMF extracts conventional synergies describing the recruitment of two main muscle groups, calf, and TA, as a function of the gait cycle. The TA activation is computed as an average of the active channels that exceed a 70% threshold. However, the calf can still be dimensionally reduced in the remaining ankle muscles, Gastrocnemius Medialis and Lateralis, Peroneus, and Soleus. Therefore, the NNMF is applied a second time on the calf primitive active channels to identify 4 different groups of electrodes that activate together because part of the same muscle group. The synergies combined with the prior knowledge of muscle location in the leg allows associating each extracted sub-region to each muscle and extract and

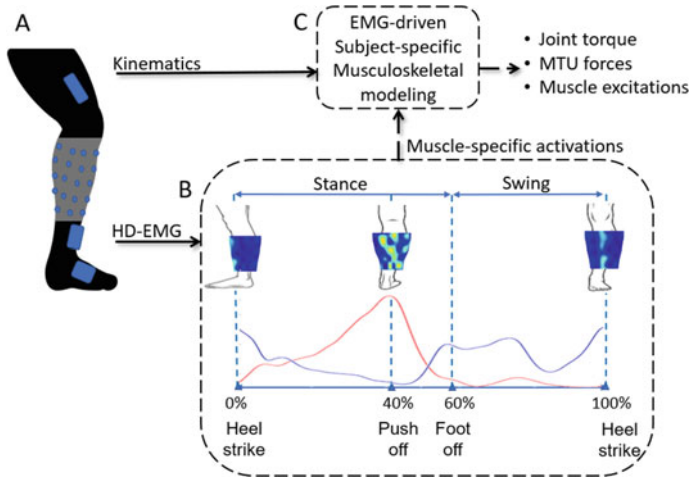


Fig. 1 Schematics of the proposed technology. **a** Fully wearable soft sensorized garment, **b** the automatic algorithm for the segmentation of HD-EMG. The two curves represent the conventional synergies during the push-off (red curve) and the swing (blue curve) phase. **c** Framework for patient-specific neuro-mechanical modeling

average activation. The computed mean activation profiles are then compared with the linear envelope of electrodes manually selected from the HD electrode grid that were located on each muscle belly.

Test 2 output is a subject-specific representation of the underlying neuromechanical processes obtained performing two steps: (1) modeling and simulation of the recorded movements and (2) simulation of musculoskeletal properties of the lower leg. Initially, the markers trajectories are input to the OpenSim software [4] to scale the musculoskeletal geometry and match the subject-specific anthropometry. Secondly the scaled model with the GRFs and the markers trajectories are processed in OpenSim to retrieve joint angles, joint torques, and musculotendon units (MTUs) lengths, and moment arms. The step (2) allows estimating subject-specific neuromechanical properties during dynamic motor tasks. First, the subject-specific model is calibrated to match the subject-specific internal parameters describing MTUs activation and contraction. Then the EMG-driven estimation of ankle torque is computed and compared with the experimental torque using the square of the Pearson coefficient of correlation (R^2).

3 Results

The 64 EMG channels are reduced by NMF in 2 non-negative factors with 64 weightings each. The heatmaps of the weights showed two main active clusters: a big area that is supposed to be the calf and related to the push-off primitive, and

a reduced cluster highlighting the TA active area related to the swing primitive. The second NNMF applied to the calf results in 4 synergies that cluster the grid in 4 different active regions. The extracted averaged activation profiles from these clusters resemble the ones from the manual selected channels with greater accuracy for 1 km/h ($R^2 = 0.97 \pm 0.03$) and 3 km/h ($R^2 = 0.95 \pm 0.06$) speeds respect to the faster locomotion velocity ($R^2 = 0.78 \pm 0.21$).

Test 2 instead assessed the ability to estimate joint torque from experimental EMG and inverse kinematics (IK) angles. Ankle torque estimation curves fit the relative inverse dynamics (ID)-moment with greater accuracy, for slow ($R^2 = 0.87 \pm 0.13$) and comfortable ($R^2 = 0.91 \pm 0.07$) walking speeds than the faster velocity ($R^2 = 0.63 \pm 2.6$).

4 Discussions

This work proposed a new technology that integrates advanced signal processing and musculoskeletal modelling techniques within wearable technology. We showed positive preliminary results of a new approach for lower leg muscle localization using NNMF-based muscle synergies extraction during locomotion and ankle joint torque estimation using bipolar EMG-driven musculoskeletal modeling offline. Merging these two steps in the future would lead to a new pipeline for fast and advanced clinical assessment.

With Test 1 we proved that (1) the NNMF can be used to localize active regions of the lower leg during locomotion and (2) we can associate them to specific muscles. The extracted activation profiles show to resemble the activation of all the lower leg muscles suggesting that the NNMF-based extraction of muscle synergies can be a suitable approach for the HD-EMG muscle localization.

The calibrated EMG-driven model can predict with good accuracy muscle-generated torque at the ankle joint in motor tasks not used for the subject model calibration. Using bipolar electrodes on muscles we can provide insights on subject-specific internal mechanical properties. Can we use HD-EMG to drive the estimation of internal mechanical properties with the same accuracy?

Future works will merge both experiments resulting in a framework for HD-EMG extraction of muscle-specific activation driving subject-specific neuromuscular modeling for rapid neuromechanical analysis.

5 Conclusion

The combination of flexible sensorized garment, the automatic procedure of muscle activity extraction added to the framework for neuromuscular modeling has a good potential to become a resource for clinicians. It will give them rapidity and a new

and enhanced perspective on the patient's musculoskeletal system helping to tailor the rehabilitation treatment on the patient-specific needs for optimal recovery.

References

1. J. Mehrholz, K. Wagner, K. Rutte, D. Meißner, M. Pohl, Predictive validity and responsiveness of the functional ambulation category in hemiparetic patients after stroke. *Arch. Phys. Med. Rehabil.* **88**(10), 1314–1319 (2007)
2. M. Sartori, M. Reggiani, D. Farina, D.G. Lloyd, EMG-driven forward-dynamic estimation of muscle force and joint moment about multiple degrees of freedom in the human lower extremity. *PLoS ONE* **7**(12), e52618 (2012)
3. J. Kim, H. Park, Toward faster nonnegative matrix factorization: a new algorithm and comparisons, in *Proceedings of the 8th IEEE International Conference on Data Mining*, 2008
4. S.L. Delp et al., OpenSim: open-source software to create and analyze dynamic simulations of movement. *IEEE Trans. Biomed. Eng.* **54**(11), 1940–1950 (2007)

Effect of Rollator Assistance on Sit-to-Stand Balance in Older Adults



Lizeth H. Sloot, Matthew Millard, Christian Werner, and Katja Mombaur

Abstract Although rollators are often given to older adults, the quality of support has yet to be quantified. This paper evaluates static and dynamic balance during STS in older and younger adults during 3 conditions: unassisted, with a normal rollator, and with a low-handled rollator. We found that older adults get up faster while maintaining both static and dynamic balance less conservatively with the support of a rollator. As such, the assistance reduced the difference in balance that was previously noted between older and younger adults during unassisted STS, and even slightly more so with the low-handled rollator. These results seem to indicate that rollator assistance compensated for reduced physical ability or confidence rather than impaired balance control in these participants. Such insight into the effect of rollator support is necessary to further development of individualized smart robotic rollators.

1 Introduction

Many older adults suffer injuries due to falls as the ability to move safely degrades. Assistive devices such as rollators are often provided to fall-prone older adults to support balance and weakened leg muscles. However, the effectiveness of such assistance has received little attention.

L. H. Sloot (✉) · M. Millard

Optimization, Robotics and Biomechanics Lab, Institute of Computer Engineering (ZITI), Heidelberg University, Heidelberg, Germany
e-mail: lizeth.sloot@ziti.uni-heidelberg.de

C. Werner

Center for Geriatric Medicine, AGAPLESION Bethanien Hospital Heidelberg, Heidelberg, Germany

K. Mombaur

Canada Excellence Chair in Human-Centred Robotics and Machine Intelligence, Department of Systems Design Engineering and Department of Mechanical and Mechatronics Engineering, University of Waterloo, Waterloo, Canada

The ability to get up from a chair is a prerequisite to independent living. Surprisingly, more falls occur getting into or out of a chair than during walking [1]. Only a few studies have evaluated assistance during sit-to-stand (STS), but none have quantified the conditions for balance [2, 3]. We recently presented a new approach to analyze both static and dynamic balance by incorporating the person's base-of-support and a model-based dynamic balance metric called the foot-placement-estimator [4]. Our analysis has shown that older adults stay closer to being statically stable than younger adults during unassisted STS, while both groups are effective at dynamic balance control [4].

Here we use the same approach to evaluate how STS duration as well as static and dynamic balance are affected by rollator assistance in older compared to younger adults. We also studied support strategies by comparing the effect of a low-handled to a normal rollator.

2 Methods

Eight older (79 ± 8 yr) and nine younger adults (28 ± 5 yr) participated.¹ Older adults did not normally use assistance, but had an increased risk of falling with a measured score on the Short Physical Performance Battery of 9.8 ± 1.9 (range: 7–12) [5, 6]. The SPPB was not assessed in younger participants.

2.1 Protocol

STS was performed 5 consecutive times at comfortable speed in 3 different conditions (Fig. 1a): unassisted (U); with a normal rollator (N) and with a low-handled rollator (L). Upper handles were adjusted to standing wrist height. Participants sat at a stool (adjusted to knee height) placed on one force plate, with their feet on a second force plate.

We collected ground reaction force (Bertec, 900 Hz) and motion capture (Qualisys, 150 Hz) data. Seat-off was defined as the time the stool's force-plate registered a value of within 1N of the stool's weight. STS start and end were defined using a k-means++ algorithm [4]. The body center of mass position and velocity were calculated in Visual3D (IOR full-body model with 2 trunk segments). All other quantities were evaluated using Matlab.

¹ The protocol was approved by the IRB of the medical faculty of Heidelberg University. Participants signed written informed consent.

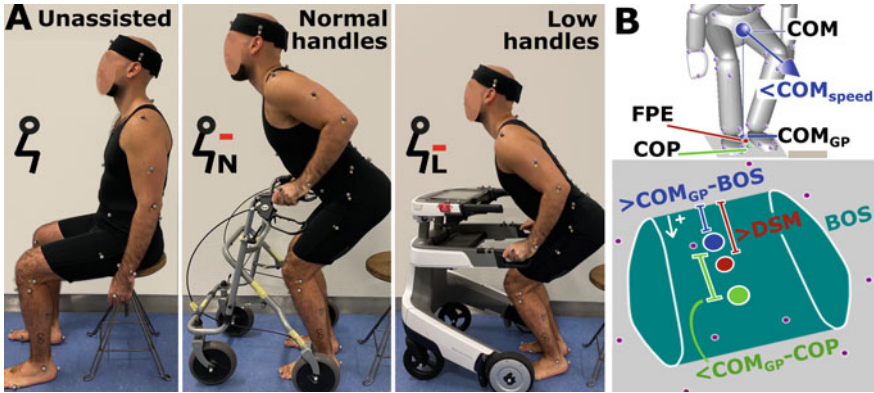


Fig. 1 a STS conditions: unassisted (U), with a conventional rollator with normal handles (N) and with a rollator with low handles (L), located at seated height to support seat-off, after which participants were instructed to transfer to the standing height handles. b More conservative balance means that COM_{GP} and FPE are further from BOS, COP is closer to COM_{GP} and COM_{speed} is small

2.2 Balance Metrics

Participants were considered statically balanced at seat-off if they were only in contact with the ground through their feet and their velocities were comparable to quiet standing. We defined being more conservatively statically balanced as a larger distance between the center-of-mass-ground-projection (COM_{GP}) and the nearest edge of the base-of-support (BOS); a smaller distance between the COM_{GP} and the center-of-pressure (COP); and a lower COM speed (Fig. 1b). The BOS was defined as the convex hull that enclosed the area participants were able to move the COP around in during flat foot standing.

We defined being more conservatively dynamically balanced as a larger dynamic balance margin: more distance between the foot-placement-estimator (FPE) and the nearest BOS edge. When this margin is positive (inside the BOS), the motion can continue without a compensatory step. We used the FPE as it takes the large amounts of linear and angular momentum present during STS into account.

2.3 Statistics

Static and dynamic balance metrics were sampled at the instant of seat-off, which is the moment with typically the highest velocities. These metrics, as well as duration from seat-off to stance, were averaged across STS repetitions. A 2-factor mixed-model ANOVA (fixed = group; variable = assistance) was performed with Helmert

contrast to compare: (1) unassisted U versus assisted (mean effect N and L), and (2) support strategies (N vs. L) using SPSS.

3 Results

Rollator assistance affected static balance and duration differently between groups. With assistance older adults stood up 0.7 times faster with considerably lower variation between individuals compared to without assistance, while younger adults became 3.2 times slower ($p_{\text{interaction}} = 0.001$; Fig. 2d).

Static balance was maintained less conservatively with assistance by the older adults, with COM_{GP} closer to the BOS heel-side edge ($p_{\text{interaction}} = 0.009$; Fig. 2a) and COM_{GP} tended to be further from the COP ($p_{\text{interaction}} = 0.06$; Fig. 2c), compared with younger adults who became closer to being statically balanced. COM speed did reduce in both groups compared with without assistance ($p_{\text{assistance}} = 0.007$; Fig. 2e). Although both groups maintained the FPE well within the BOS, the dynamic balance margin to the (heel-side) edge was reduced ($p_{\text{assistance}} = 0.03$; Fig. 2b).

The effect of handle height also differed between groups. While older adults were less affected, younger adults were slower with lower handles ($p_{\text{interaction}} = 0.008$; Fig. 2d) and further from statically balanced—with COM_{GP} more outside the BOS ($p_{\text{interaction}} = 0.005$; Fig. 2a) and more distance between COM_{GP} and COP ($p_{\text{interaction}} < 0.001$; Fig. 2c). Both groups had smaller dynamic balance margins with lower handles; which tended to be more in younger adults ($p_{\text{interaction}} = 0.06$; Fig. 2b).

4 Discussion

While smart assistive technology is becoming increasingly popular in rehabilitation medicine, enhancement of rollators seems to be lagging. More insight into the impact of rollator assistance is warranted, and through the presented approach we not only showed that the effect was different between age groups but also between handle height.

We found that the assistance reduced the need for a slow and conservative balance strategy, which we recently noticed in older adults during unassisted STS [4]. In contrast, younger adults slowed down, probably as the handle interaction forms an extra task without any benefits. These results indicate that the assistance might be compensating for reduced physical ability or confidence rather than impaired balance control in older adults.

The low-handled rollator was designed to offer better grasp and thus improved weight and balance support during the first phase of STS. It also provided more counterweight, which could have triggered more of a pulling technique. Regardless of the cause, the low-handled rollator normalized static and dynamic balance in older adults towards those of unassisted younger adults, and slightly more so than the normal

rollator. Interestingly, bar-support—the closest type of support to rollator assistance studied during STS—has been shown to not improve static balance (in terms of COM and COP to foot position) [3]. These results demonstrate the importance of tailoring the design of rollators towards different tasks and needs.

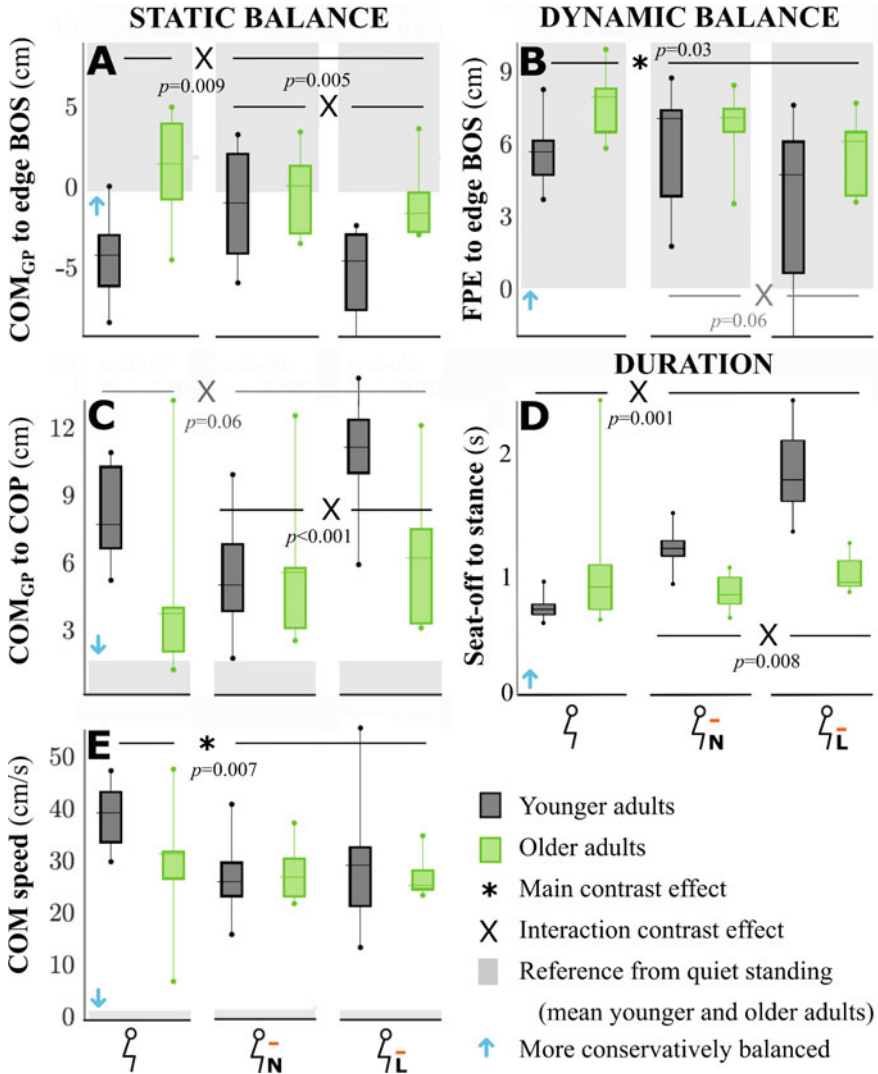


Fig. 2 Effect of assistance on balance metrics. The bar graph represents median values and 25th and 75th percentiles for unassisted, normal rollator N and low-handled rollator L. Upper result line indicate the contrast results between unassisted and assisted (mean effect N and L) and the second line the contrast results between N and L

This study is our first step in quantifying the effect of rollator assistance on STS balance. Next, we aim to include the handles in a human-rollator model to assess joint loading, evaluate a rollator's effect on the BOS and measure older adults who struggle with STS and are prone to falling.

Acknowledgements Financial support from Carl Zeiss-Foundation is gratefully acknowledged.

References

1. K. Rapp et al., Epidemiology of falls in residential aged care. *J. Am. Med. Dir. Assoc.* **13** (2012)
2. N. Millor et al., Kinematic parameters to evaluate STS [...]: a review. *IEEE Trans. Neural Syst. Rehabil. Eng.* **22**, 926–936 (2014)
3. J. Jeyasurya et al., Comparison of seat, waist and arm sit-to-stance as-sistance modalities in elderly population. *J. Rehab. Res. Dev.* (50) (2013)
4. L.H. Sloot et al., Slow but steady: similar sit-to-stand balance at seat-off in older versus younger adults. *Frontiers Sports Act. Living* **2**, 144 (2020)
5. J.C. Kim et al., Associated between fall history and physical performance tests in elderly [...]. *Ann. Rehabil. Med.* **41**, 239–247 (2017)
6. J.M. Guralnik et al., A short physical performance [...]. *J. Gerontol.* **49**, 85–94 (1994)

A ROS2-Based Approach to Enable Simultaneous and Real-Time Tracking of Humans and Exoskeleton Motion



Guillermo Asín-Prieto, Francisco Martín Rico, and Diego Torricelli

Abstract Commercially available motion capture systems (MOCAPs) were initially developed for human motion analysis. Nowadays, they are a fundamental chain in robotics, when the motion of different agents (humans or not) should be tracked in real-time. In robotics, ROS is rapidly gaining relevance as a standard for managing, synchronizing and integrating wide range of sensor modalities in the control structure of a robotic system. Nevertheless, there is clear lack of standardized support from ROS and/or ROS2 for most of existing MOCAP systems in the market, which prevent their full (and community-driven) integration in the available robotic systems. In this paper we propose a full implementation of an official package for ROS2 able to manage optoelectronic and inertial MOCAPs, with special focus on wearable robotics applications.

1 Introduction

In robotics, there is an exponential growth of applications in which robots are in close interaction with humans. Examples are humanoids for assistance, intelligent prostheses, and wearable robots for clinical rehabilitation or support in the manufacturing industry (see Fig. 1, dotted red box). In these application domains, the real time monitoring of both human and robot motion is crucial to ensure safety and improved functionality. Motion Capture (MOCAP) systems provide reliable information on the

The work presented in this paper was supported by MOCAP4ROS2 project, funded as a Focused Technical Project by ROSIN (European Union's Horizon 2020 research and innovation program under grant agreement No 732287).

G. Asín-Prieto (✉) · D. Torricelli
Neural Rehabilitation Group, Spanish National Research Council, Madrid, Spain
e-mail: diego.torricelli@csic.es

G. Asín-Prieto
Gogo Mobility Robots S.L., Abadiño, Spain

F. M. Rico
Intelligent Robotics Lab, Rey Juan Carlos University, Fuenlabrada, Spain
e-mail: francisco.rico@urjc.es

© The Author(s), under exclusive license to Springer Nature Switzerland AG 2022
D. Torricelli et al. (eds.), *Converging Clinical and Engineering Research on Neurorehabilitation IV*, Biosystems & Biorobotics 28,
https://doi.org/10.1007/978-3-030-70316-5_22



Fig. 1 Overview of the main relevant application domains of robotics. In the blue-dotted box are those domains with typically no physical interaction between humans and robots. In the red-dotted box are domains related to collaborative robots, most of them not ROS2 supported

position of elements in an environment, by using visual markers and/or inertial sensors. These systems have been successfully used during decades to obtain the ground truth of robots in an environment and to evaluate human performance in clinical, sport, and film industry. Unfortunately, none of the commercially available MOCAP systems are currently supported by ROS2, preventing a reliable real-time tracking of collaborative tasks between humans and robots. The project MOCAP4ROS wants to fill this gap by providing a framework, as other ROS2 projects do [4, 5], where different MOCAP systems can be integrated. Due to its layered design, applications using the MOCAP systems' output can be independent of the particular MOCAP system. Last, the output of the available MOCAP systems is fused at runtime, providing more complete information.

2 Proposed Solution

The solution to integrate all these elements needs to be easily expandable, allow for a reliable source of synchronization, and, if possible, be something that could be eventually standard.

In the development of software for robots, ROS [2] is a de facto standard used for the innards of these humanoids; but this is not the case of biomedical devices, exoskeleton and prostheses in our interest case. Nonetheless, ROS provides a reliable interface between systems, common clock signal and thus synchronization, and is easily expandable with new nodes in the network.

2.1 MOCAP4ROS2 Project

MOCAP4ROS2 (motion capture for ROS2) is a project that aims to standardize the use of MoCaps in ROS2. This project begins to support EURO BENCH but to

transcend it and become a standard in this type of system in ROS. In this way, manufacturers of MoCaps will be able to integrate their drivers and applications within MOCAP4ROS2.

The proposed architecture is shown in Fig. 2. It is an architecture composed of three layers:

- **Drivers layer** deals with each MoCap's particular drivers, providing a standard interface with the upper layer. For each category of MoCap (vision-based, inertial sensors, ...) a standard interface is defined. For each different driver there will be a ROS2 node that adapts the information to the format of this standard interface.
- **Composer layer** collects standardized information from MoCaps and combines it to obtain spatial geometric information in real-time (RT). ROS/ROS2 has successfully used the geometric transform system (TFs) in recent years, using a publication/subscription system for high-frequency geometric relationships. This layer will offer the upper layer spatial information obtained by MoCaps, such as a tree of geometric relationships between joints, each on its reference axis. Some categories, such as inertial sensor-based systems, will need information such as the distance between sensors. This information can be loaded from configuration files.
- **Application layer** is where the applications exploit the information obtained from the MoCap, once standardized and with spatial significance. These applications can save this information, represent it, or analyze it.

The main idea of this project is that the layers can be independent so that the application layer is independent to the used MoCap. Furthermore, several additional layers can be combined to improve the reliability of the information.

2.2 Real-Time Experiments

These preliminary experiments seek to characterize the RT characteristics of communications by sending the information collected by MoCaps. ROS2 uses DDS as a network layer, which is a RT communications standard. Several DDS vendors can be used in ROS. We have designed these experiments to measure the performance of each of them, with real data. We have compared the two main DDS implementations in ROS2: FastRTPS and Cyclone. We will do it based on these three characteristics: bandwidth (BW), offered frequency and latency.

Figure 3 (up) shows the evolution of the BW transmitted by each one of them. Both versions of DDS offer similar data in a wired and wireless scenario (FastRTPS unstable with wireless). In the same way, FastRTPS fails to keep the frequency (Fig. 3 -down-) constant on a wireless scenario, while it has no problem with a wired scenario. Cyclone is reliable and stable.

As for latencies (Fig. 4, Cyclone is significantly better in both scenarios, guaranteeing latencies of 50 ns on wired and 40 ns on wireless.

Fig. 2 MOCAP4ROS2 software architecture

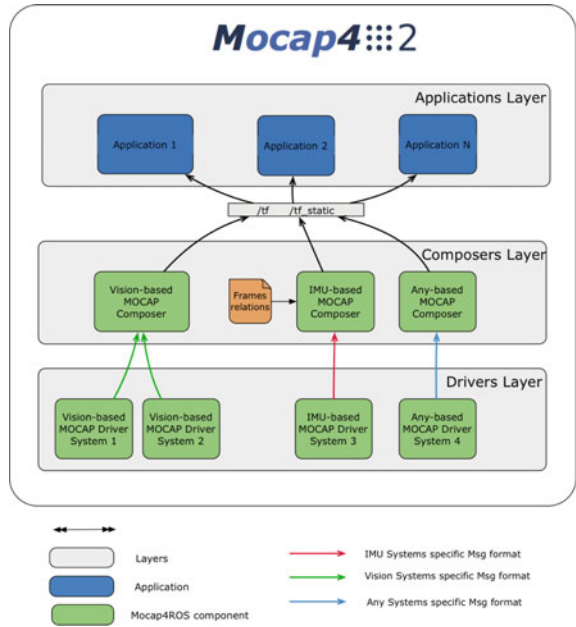
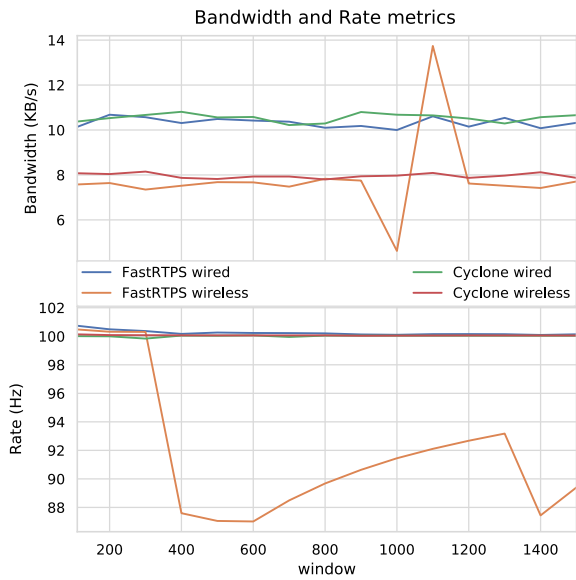


Fig. 3 Up: bandwidth rate; down: frequency



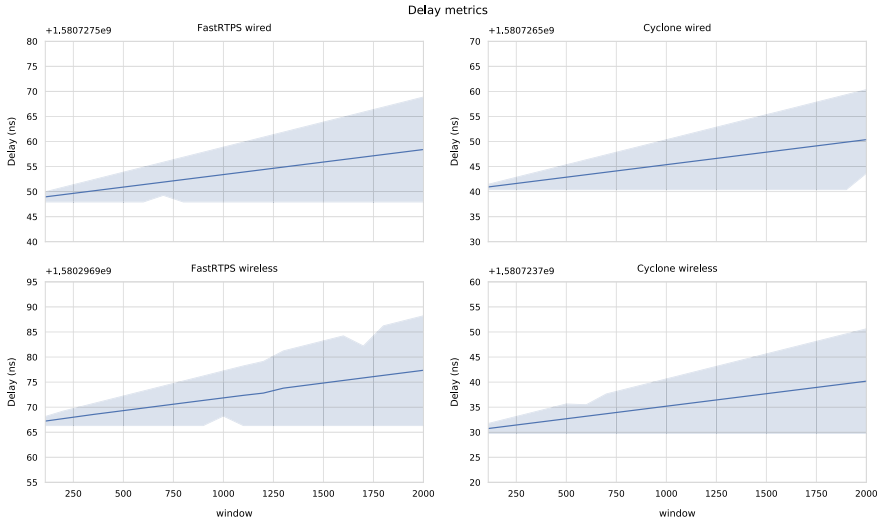


Fig. 4 Latency for FastRTPS (LEFT) and CycloneDDS (RIGHT), for wired (UPPER) and wireless (LOWER) conditions

3 Conclusion

This paper proposed a solution to enable the use of current MOCAP systems under ROS2, to be used in applications in which human and robot are physically interacting. The use of ROS2 will permit to monitor in real-time the movement of the human subject and wearable robotic devices and integrate these feedback signals into the control of the machine.

This project aims to be a reference in ROS2, developing it in public repositories and creating packages that are incorporated into the official ROS2 distributions. Continuous Integration techniques will be applied to guarantee the quality of the software in the future.

References

1. EUROBENCH project Webpage. <http://eurobench2020.eu>. Last visited 14 July 2020
2. ROS Webpage. <https://www.ros.org/>. Last visited 14 July 2020
3. ROS vs ROS2. <https://blog.generationrobots.com/en/ros-vs-ros2/>. Last visited 14 July 2020
4. S. Macenski, F. Martín, R. White and J. Ginés, The Marathon 2: a navigation system, in *2020 IEEE/RSJ International Conference on Intelligent Robots and Systems (IROS)* (2020)
5. D. Coleman, I.A. Şucan, S. Chitta, N. Correll, Reducing the barrier to entry of complex robotic software: a MoveIt! case study. *J. Softw. Eng. Rob.* **5**(1), 3–16 (2014)

Neural Coherence of Homologous Muscle Pairs During Direct EMG Control of Standing Posture in Transtibial Amputees



Aaron Fleming, Wentao Liu, and He (Helen) Huang

Abstract The objective of this preliminary study was to investigate the feasibility of a transtibial amputee to improve interlimb muscle coordination while using direct, continuous control of a powered ankle prosthesis combined with physical therapist guided training, for improved standing postural control. A participant with transtibial amputation received an extended PT-guided training on posture while using the dEMG control of powered ankle with his residual Tibialis Anterior and Lateral Gastrocnemius. We quantified cross-correlation of Center of Pressure excursions and coherence in EMG signals from the bilateral shank muscles. Between-limb coordination was observed as synchronized activation of homologous muscles in the shank. We observed increased coherence in the TA muscle pair after training in 0–5 Hz and 10–20 Hz frequency ranges. These results demonstrate the potential for amputees to closely coordinate residual muscle activations with intact muscles given sufficient training. It is further possible amputees adapt sources of descending neural commands between homologous muscle pairs after guided training. Future study requires more participants to validate these results.

1 Introduction

Recent studies have started to show increased promise for the use of descending neural signals for the control of powered lower-limb prostheses. One common neural control paradigm, direct electromyographic (dEMG) control, modulates prosthetic joint parameters proportional to the magnitude of residual muscle activity. This control paradigm is particularly attractive since it affords amputees the ability to continuously and volitionally control their prosthetic joint and takes advantage of the decision-making capabilities of the human user. This has the potential to improve

A. Fleming · W. Liu · H. (Helen) Huang (✉)

Joint Department of Biomedical Engineering, NC State University, Raleigh, North Carolina, USA
e-mail: hhuang11@ncsu.edu

University of North Carolina at Chapel Hill, Chapel Hill, North Carolina, USA

prosthetic limb function in tasks that would be otherwise difficult for autonomous control paradigms to assist (picking up a child, dribbling a soccer ball, etc.).

Amputees retain the ability to activate their residual muscles, however the structure and function of these muscles are significantly altered. Several studies have shown the potential for amputees to adapt residual muscle activity for control of a prosthetic ankle during locomotion [1, 2]. However, it is unclear whether amputees are capable of coordinating *both* antagonistic residual muscles for non-cyclic tasks like squatting, or whether amputees can coordinate homologous (inter-limb) muscle pairs during this type of bi-lateral control task. To test this, we asked a transtibial amputee to use dEMG control of a prosthetic ankle during a physical therapist (PT) guided training program using common daily-life postural control tasks. We tested neural synchrony between limb using coherence analysis [3].

2 Methods

2.1 Participants and Measurements

We recruited one person with a unilateral transtibial amputation to participate in this extended training study. This participant provided written, informed consent (approved by Institutional Review Board at the University of North Carolina at Chapel Hill). The participant was an active community ambulator (K3), male, 131 kg, 58 years old, and 3 years post-amputation (septic shock).

To study neural connectivity between homologous intact and residual muscle pairs we placed electrodes on the sound limb (Motion Lab System, MA-420, Gain x20) and residual limb (Neuroline 715, 1 mm thickness) over the Lateral Gastrocnemius (GAS) and Tibialis Anterior (TA) muscles. Electrode leads for the residual limb were routed away from bony landmarks and connected to a pre-amplifier (Motion Lab Systems, MA-412, Gain x20) outside of the prosthetic socket. We used alternative EMG sensors for residual muscles due to the limited space and the sensitivity of the residual limb within the limb-socket interface. We connected all sensors to an amplifier (MLS, MA300-XVI, Gain x1000). We determined electrode placements based on anatomical locations and palpation [1].

We captured full-body kinematics using 3D motion capture (100 Hz, 53 Markers, Vicon). We measured ground reaction forces using a split-belt treadmill (1000 Hz, Bertec).

2.2 Device and Control Signal

In this study we provided proportional myoelectric control of a powered prosthetic ankle actuated with pneumatic artificial muscles. The details of this device can be

found in [1]. In this setup we controlled the inflation pressure via two proportional pressure valves (MAC Valves, Wixom) for plantar and dorsiflexor artificial muscles. The input signal for these valves was 0–10 V and the output pressure was 0–90 psi. We processed inputs from surface EMG from the residual TA (rTA) and residual GAS (rGAS) muscles using a real-time control setup (dSPACE, CLP-1103, 0–10 V output) and sent the output to the pressure regulators in real-time. We established a set-stiffness based on previous study protocol [1], resulting in ~3 V baseline control signal for each muscle. Surface EMG signals were processed in real time to generate a smooth control signal (1) High-pass filter 2nd Order Butterworth (100 Hz Cutoff) (2) Rectification (3) Low-pass filter, 2nd Order Butterworth. We applied a gain to each control signal such that a maximum contraction would generate a control signal of ~9–10 V.

2.3 Training

This study consisted of 5 physical therapist-guided training sessions with the direct EMG controlled prosthesis. In these sessions the participant practiced several tasks relevant to daily-life: Load Transfer, Sit-to-stand, Forward Reach, and Arm Raise. During training, the PT observed repetitions from the participant and provided feedback about the relative contribution of each limb toward task completion. The participant received cues to shift his weight onto his prosthetic side and to recruit muscles in ‘toes up’ or ‘toes down’ direction when learning tasks.

2.4 Data Analysis and Statistics

For this initial evaluation we selected the load transfer task from the beginning and end of training (Day 1 and 5) for ± 2 s on either side of the moment of object pickup (as determined by vertical ground reaction force). For each windowed repetition we calculated the coherence between homologous muscles EMG activity (TA-rTA) and (GAS-rGAS). We processed EMG and calculated coherence between muscle EMG similar to previously described methods [3] (Welch’s periodogram, hamming window of 512 samples, 256 sample overlap). 95% Confidence interval was calculated as described in [3] based on the average window size of all trials. Coherence arrays were averaged across all trials for each condition (pre vs. Post-training). We selected representative trials from initial and final days of training for qualitative comparison of EMG activity. We calculated the cross-correlation (CC_0) of CoP excursion between limbs and averaged across all trials for each condition.

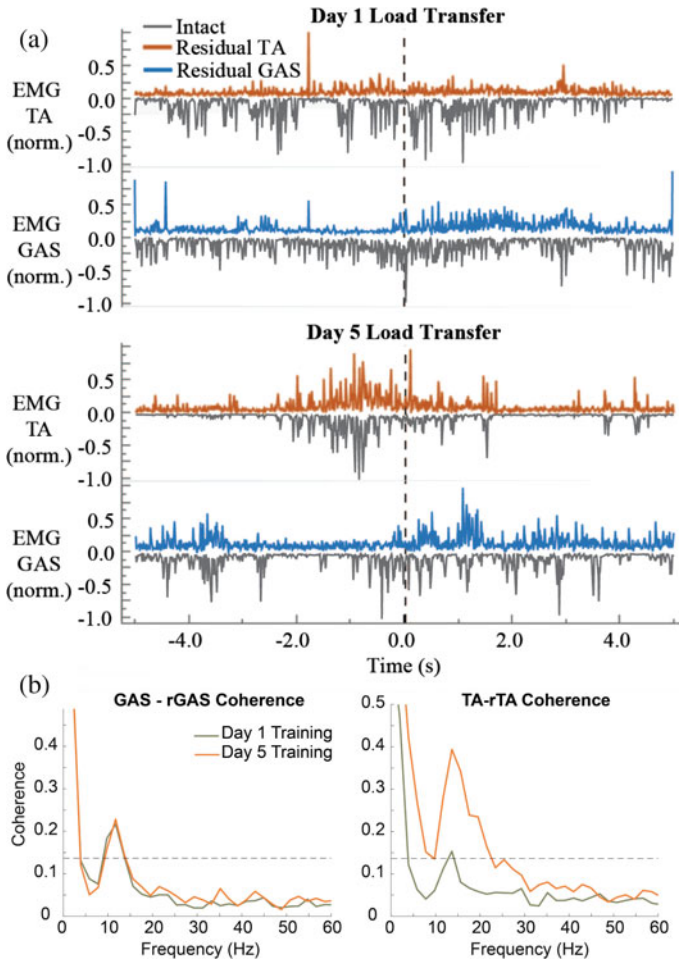


Fig. 1 Pre versus post training EMG comparison. **a** Rectified EMG from homologous muscle pairs (negative of EMG for intact muscles) from representative trials. (*Vertical Dashed line*) moment of peak squat during load transfer. **b** Average coherence from homologous muscles pairs compared from pre- and post-training. (*Horizontal dashed line*) 95% CI for coherence

3 Results

After training, we observed significant changes in EMG synchronization between limbs. Visual inspection of EMG and control signals during load transfer trials (Fig. 1a) demonstrated lack of synchronization in the TA-rTA pair pre-training and limited rTA activation. Post-training, we observed synchronization between the muscle pairs (Fig. 1a), specifically the TA-rTA pair. We observed that CoP excursions between feet were more closely synchronized post-training (CC_0 pre: $0.39(\pm 0.29)$ CC_0 post: $0.83(\pm 0.07)$).

Alongside visual observation of the load transfer trials, we observed noticeable increases in coherence post-training (Fig. 1b). In the GAS-rGAS pair the synchronization at low (0–5 Hz) and higher (10–20 Hz) frequency bands was significant for pre-and post-training, however the average coherence did not change. The TA-rTA pair coherence noticeably increased (Fig. 1b), post-training, for both low and higher frequency bands.

4 Discussion and Conclusion

This preliminary study is the first study to demonstrate the ability for a transtibial amputee to use antagonistic residual muscles for the control of standing posture (i.e. load transfer) after guided training. Improved co-modulation of muscle pairs (as evidenced by increased Coherence in the 0–5 Hz range) demonstrated the promise for amputees to coordinate a dEMG controlled prosthetic ankle joint with their intact limb. Surprisingly, we observed increase coherence in the 10–15 Hz range (Fig. 1a) suggesting the increased recruitment of common neural sources for the intact and residual ankle muscles. It would be interesting for future study to attempt to determine the potential neural sources recruited during dEMG of a prosthetic ankle.

In this preliminary study we have demonstrated the potential for transtibial amputees to improve synchronization and potentially recruit alternative neural control sources for dEMG of a prosthetic limb during daily-life tasks.

Acknowledgements Funding for this study is provided by NIH NICHD F31HD101285, NIH EB024570, and NSF 1954587.

References

1. S. Huang, J.P. Wensman, D.P. Ferris, An experimental powered lower limb prosthesis using proportional myoelectric control. *J. Med. Dev.* **8**(2) (2014)
2. J.A. Dawley, K.B. Fite, G.D. Fulk, EMG control of a bionic knee prosthesis: exploiting muscle co-contractions for improved locomotor function, in *2013 IEEE 13th International Conference on Rehabilitation Robotics (ICORR)* (IEEE, 2013), pp. 1–6
3. T.W. Boonstra, M. Roerdink, A. Daffertshofer, B. van Vugt, G. van Werven, P.J. Beek, Low-alcohol doses reduce common 10-to 15-Hz input to bilateral leg muscles during quiet standing. *J. Neurophysiol.* **100**(4), 2158–2164 (2008)

Exoskeleton Design Using Subject-Specific Synergy-Driven Neuromusculoskeletal Models



Marleny M. Arones, Josep M. Font-Llagunes, and Benjamin J. Fregly

Abstract Most assistive devices available today are unable to improve gait asymmetries due to the lack of knowledge on how to directly enforce kinematic symmetry in the formulation of cost functions. We designed a cost function to potentially target kinematic symmetry, and observed improvements in gait asymmetries specifically at the hip and ankle.

1 Introduction

Walking asymmetry is generally a main concern in gait impairments experienced by amputees, post-stroke patients, and the elderly [1]. Therefore, many rehabilitation programs measure gait asymmetry to evaluate the effectiveness of rehabilitation treatments [2]. While many assistive devices have been proposed to improve gait symmetry, the devices currently available are geared towards reducing metabolic cost, gait training and performance enhancement [3]. This discrepancy may be due to a lack of knowledge on how to directly target kinematic symmetry in design formulation and optimization.

This study predicted the assistive joint moments needed to improve walking asymmetry and thus walking function. An improvement in walking function was quantified by calculating changes in metabolic cost and spatiotemporal symmetry measures.

M. M. Arones · B. J. Fregly (✉)
Mechanical Engineering Department, Rice University, Houston, TX, USA
e-mail: fregly@rice.edu

M. M. Arones
e-mail: ma86@rice.edu

J. M. Font-Llagunes
Mechanical Engineering Department, Polytechnic University of Catalonia, Barcelona, Spain
e-mail: josep.m.font@upc.edu

2 Methods

This study analyzed data from previously collected walking trials from a high functioning male subject suffering from stroke walking dysfunctions. All experimental procedures were approved by the University of Florida Health Science Center Institutional Review Board (IRB-01), and the subject provided written informed consent prior to participation. Motion capture (Vicon Corp), ground reaction (Bertec Corp), and electromyography (EMG) data (Motion Lab Systems) were collected simultaneously from the subject as he walked on a split-belt instrumented treadmill (Bertec Corp) at his self-selected speed. The subject’s neuromusculoskeletal components were represented using four modeling elements: a kinematic model, an EMG-driven model, a foot-ground contact model, and a motion prediction model using the concept of muscle synergies; see [4] for more details. Originally, the subject-specific neuromusculoskeletal model was calibrated using five muscle synergies per leg. However, this study used the subject-specific neuromusculoskeletal model with two muscle synergies controlling the paretic leg and five muscle synergies controlling the non-paretic leg, which produced a deteriorated walking motion [5].

An optimization was developed within Matlab and GPOPS-II, a direct collocation optimal control software [6], to find ideal joint moment loads that would allow the walking function of the model to improve. The cost function was designed to target kinematic symmetry while allowing minimal changes in the neural commands. To impose kinematic symmetry, the joint angles of the paretic leg were added to the corresponding joint angles of the non-paretic leg, where the goal is to minimize the integral of the continuous summed curves for all six joints (Fig. 1). The six joints of interest include: hip flexion, hip adduction, hip rotation, knee flexion, ankle plantarflexion, and ankle inversion.

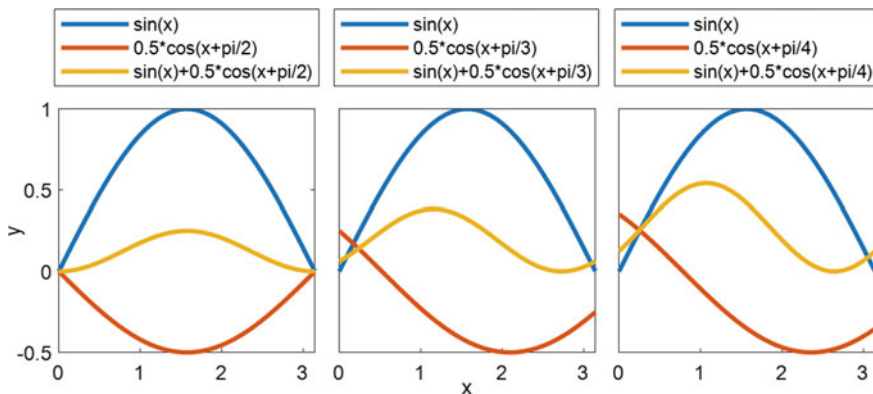


Fig. 1 An example to help visualize the minimization of asymmetry between the red and blue curves occurs when the integral of the summation curve (yellow) is minimized

Table 1 Cost of transport, and spatiotemporal symmetry measures

	CoT	Spatial	Temporal
Original	7.49	0.18	0.44
Assisted	5.67	0.51	0.59

The cost of transport (CoT) was calculated using Bhargava's model [7] along with ratios describing spatial and temporal symmetry to determine if the assistive moments resulted in an improved walking motion.

3 Results

The ideal joint moment loads found by the optimizer to minimize kinematic asymmetry improved walking function by decreasing cost of transport and increasing spatial symmetry (Table 1). The predicted walking motion showed a decrease in hip hiking, increase in symmetry between paretic and non-paretic hip flexion, decrease in leg circumduction, and correction of the foot drop (Fig. 2). Additionally, although the range of motion at the knee did not increase, the timing of the peak knee flexion improved. Despite improvements to most joints of interest, the new walking motion resulted in excessive ankle eversion along with over correction of temporal symmetry.

4 Discussion

This study predicted ideal assistive joint moments needed to improve gait asymmetries along with the cost of transport and spatiotemporal asymmetries. We found that kinematic symmetry may be enforced in the cost function by minimizing the integral of the summed curved between paretic and non-paretic joint angles. The joints of interest for this study included: hip flexion, hip adduction, hip rotation, knee flexion, ankle plantarflexion, and ankle inversion.

The predicted walking motion showed improvements in the common clinical features in hemiparesis walking observed in the two-synergy walking motion. However, it was observed that the temporal symmetry did not improve in the same manner as the cost of transport and spatial symmetry. This finding is consistent with [8] which reported that spatial and temporal symmetry can be targeted independently.

It is important to note that a key limitation of our study is the lack of experimental data as our starting point. Additionally, although the symmetry between the non-paretic and paretic legs was improved for the hip flexion, hip adduction, ankle plantarflexion, future development is needed to improve symmetries in hip rotation, knee flexion and ankle inversion.

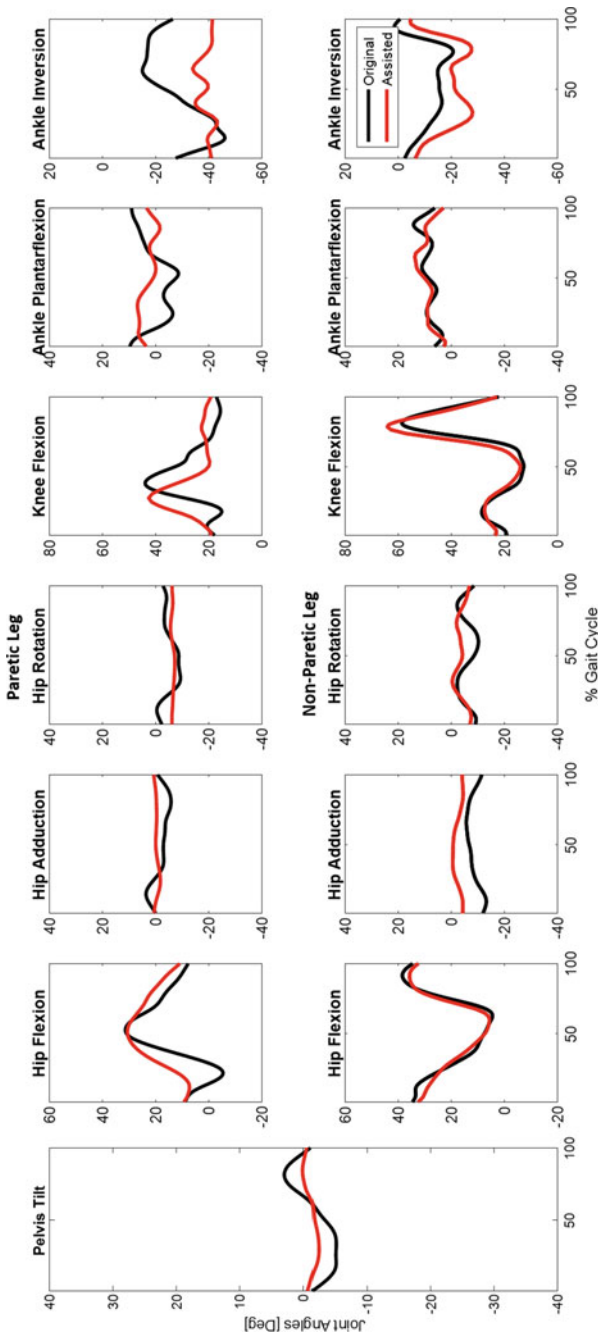


Fig. 2 Comparison between the original (black) and assisted (red) walking motions

5 Conclusion

In conclusion, our preliminary findings may shed light on the formulation of a cost function to implement kinematic symmetry to improve the cost of transport and spatial asymmetry measures. Our findings could potentially lead to a paradigm shift in the design of assistive devices for neurologically-influenced walking impairments.

Acknowledgments Funding provided by the Cancer Prevention and Research Institute of Texas Grant RR170026, and NSF Graduate Research Fellowship.

References

1. E.T. Hsiao-Weckler, J.D. Polk, K.S. Rosengren, J.J. Sosnoff, S. Hong, A review of new analytic techniques for quantifying symmetry in locomotion. *Symmetry (Basel)* **2**(2), 1135–1155 (2010)
2. S. Hesse, C. Werner, A. Bardeleben, H. Barbeau, Body weight-supported treadmill training after stroke. *Curr. Atheroscler. Rep.* **3**(4), 287–294 (2001)
3. P. Malcolm, S. Galle, P. Van den Berghe, D. De Clercq, Exoskeleton assistance symmetry matters: unilateral assistance reduces metabolic cost, but relatively less than bilateral assistance. *J. Neuroeng. Rehabil.* **15**(1), 74 (2018)
4. A.J. Meyer, I. Eskinazi, J.N. Jackson, A.V. Rao, C. Patten, B.J. Fregly, Muscle synergies facilitate computational prediction of subject-specific walking motions. *Front. Bioeng. Biotechnol.* **4** (2016)
5. M. Arones, C. Patten, B.J. Fregly, Does a unilateral reduction in muscle synergies lead to alterations in gait post stroke?, in *XVII International Symposium on Computer Simulation in Biomechanics*, July 28th–30th 2019, Alberta, Canada
6. A.V. Patterson, M.A. Rao, GPOPS-II: a MATLAB software for solving multiple-phase optimal control problems using hp-adaptive gaussian quadrature collocation methods and sparse nonlinear programming. *ACM Trans. Math. Softw.* **1**(41), 1–37 (2014)
7. L.J. Bhargava, M.G. Pandy, F.C. Anderson, A phenomenological model for estimating metabolic energy consumption in muscle contraction. *J. Biomech.* **37**(1), 81–88 (2004)
8. L.A. Malone, A.J. Bastian, Thinking about walking: effects of conscious correction versus distraction on locomotor adaptation. *J. Neurophysiol.* **103**(4), 1954–1962 (2010)

SS4: User Experience in Robot-Aided Rehabilitation and Assistance

Usability Evaluation of SMA Based Exoskeleton: Pilot Testing in Post-stroke Patients



D. Copaci, D. Serrano del Cerro, I. Alguacil-Diego, D. Fernández Vázquez, F. Molina-Rueda, J. C. Miangolarra-Page, L. Moreno, and D. Blanco

Abstract Rehabilitation robotic devices are currently used with success as a complement to the physiotherapist task. However, this technology is still attracting the research interest because aspects such as the effectiveness of rehabilitation therapy, the cost of the device, the weight and ergonomic are only a few of aspects which can continuously be improved. This work presents the analysis and usability evaluation for elbow joint Shape Memory Alloy (SMA) based exoskeleton. This was tested and evaluated in flexion-extension movement with 10 patients with stroke and 6 physiotherapists. Firstly, the robotic device was used for data acquisition, which permitted an evaluation of the patient to define the elbow range of movement, and after, it was used in the passive mode where the patients relax the articulation and the exoskeleton executes the forearm movement in flexion-extension. After the test with the exoskeleton, the patients were asked to complete the QUEST 2.0, which permits to evaluate the usability (effectiveness, efficiency and user satisfaction with the exoskeleton).

The work presented in this paper has been carried out with the financial support from the RoboHealth (DPI2013-47944-C4-3-R) and the EDAM (DPI2016-75346-R) Spanish research projects.

D. Copaci (✉) · D. Serrano del Cerro · L. Moreno · D. Blanco
Systems Engineering and Automation, Carlos III University of Madrid, Madrid, Spain
e-mail: dcopaci@ing.uc3m.es

I. Alguacil-Diego · D. Fernández Vázquez · F. Molina-Rueda · J. C. Miangolarra-Page
Department of Physiotherapy, Occupational therapy, Rehabilitation and Physical Medicine,
Faculty of Health Sciences, Laboratory of Movement Analysis, University Rey Juan Carlos,
Móstoles, Spain

Biomechanics, Ergonomics and Motor Control, Faculty of Health Sciences, University Rey Juan Carlos, Móstoles, Spain

1 Introduction

Eighty per cent of the subjects who suffer a stroke survive the acute phase; 6 months later, 85% of them still present motor disorders as well as neurological deficits, communication, cognitive and visuospatial perception disorders [1]. The stroke normally results in series of motor impairments contralateral to the brain lesion, such as muscle weakness, coordination disorders, somatosensory deficits, motor control disorders and hemiparesis [2], which limits the patient's level of activity and both physical and social interactions. Upper-limb training is important for stroke subjects, since it directly addresses the restoration of functional motion for activities of daily-living (ADL) [3].

The inclusion of robotic devices in motor rehabilitation therapies has been increasing over the last decade. The robot-assisted therapies complement conventional rehabilitation by providing intensive, repetitive, task-specific, and interactive treatment. All these factors contribute to a more effective rehabilitation [4] in subjects with stroke. However, the clinical applicability of robot-assisted arm training is debatable, due to the high costs of the equipment [5].

A Cochrane review [6] assessed the effectiveness of electromechanical and robot-assisted arm training for improving ADLs, arm function, arm muscle strength in people post-stroke and the acceptability and safety of the therapy. The authors identified 34 trials (involving 1160 participants). Electromechanical and the robot-assisted arm training was compared with other interventions (task-specific practice of functional activities, occupational therapy, standard arm and hand exercises, mirror therapy, Botox or repetitive goals-based arm therapy) placebo interventions or no treatment. The review concluded that electromechanical and robot-assisted arm and hand training improved ADLs in people post-stroke function and muscle strength of the affected arm.

This study analyses and evaluate the SMA based exoskeleton developed in our research group [7], in terms of usability. With this rehabilitation device we propose an improvement in the area of the upper limb exoskeletons in aspects such: dimensions, weight, cost of fabrication, set-up time and noise during the rehabilitation therapy. Results will be applied to the following phases of device development.

2 Methods

2.1 Patients and Physiotherapist

Ten post-stroke subjects, age 61.8 ± 12.98 years, 9 males and one female, with a predominance of brachial hemiparesis, and 6 physiotherapists were recruited for this study. Patients met the following inclusion criteria: (1) age between 18 and 85 years; (2) ability to understand instructions and actively participate in tasks; (3) spasticity less than or equal to two in the Modified Ashworth Scales [8]; (4) right affected

upper limb (the exoskeleton was designed for this side). The experimental protocol for this study was approved by the Ethical Committee of the “Universidad Rey Juan Carlos” (Spain) and warranted to be in accordance with the Declaration of Helsinki. All patients signed a written informed consent.

2.2 *Satisfaction Assessment*

The patients and physiotherapists evaluated the exoskeleton using the Quebec User Evaluation of Satisfaction with assistive Technology (QUEST 2.0) [9]. This consists of 12 satisfaction items where the users rate their satisfaction with the assistive device and the related services they experienced by using the scale of 1–5. In addition, the participants select the three items that they consider to be the most important to them. In this study, we evaluated only the items related with the assistive device (items 1–8).

2.3 *SMA Based Exoskeleton*

SMA based exoskeleton is a robotic device which helps the patients with cerebrovascular accident (CVA) to recover the motor functions in the upper limbs, through the passive rehabilitation therapy. This is a portable device actuated by SMA based actuators, with a low-cost of fabrication and low weight, which will be placed over the patient arm and forearm and adjusted according to its dimensions, using belts and hook and loop fasteners. The device was presented previously in “SMA based exoskeleton for rehabilitation therapy and patient evaluation” [7].

2.4 *Test Setup*

All patients were informed beforehand and provided consent. The therapies were individually adapted according to each patient choosing between the operation mode of the exoskeleton: data acquisition mode and in passive mode assisting in flexion or flexion-extension [7]. Firstly, the physiotherapist evaluated the patient and the engineer explained the rehabilitation device to the patient: how it works and in what the test consists. After that, the exoskeleton was adjusted over the patient (Fig. 1) where the exoskeleton elbow axis was aligned with the elbow joint axis and the pronosupination piece was adjusted in function of the forearm dimensions. The average time to set-up the exoskeleton over the human body was approximately 2 min, and the patient performed the tests for 15 min (one cycle every 25 s with rest every 5 cycles).

Fig. 1 SMA based exoskeleton over patients



3 Results

The average score of the QUEST 2.0 evaluation by the patients was 33 ± 6.90 . The most appreciated items were the *weight* and *dimensions* of the rehabilitation device, the both evaluated with 4.3 ± 0.674 . The less appreciated was the item *effectiveness* scored with only 3.8 ± 1.03 points, followed by the *comfort* and *simplicity* scored with 4 ± 1.2 and 4 ± 1.33 respectively. In the Sect. 3 of the QUEST 2.0, where the patients need to select between the 8 items, 3 of which are considered the most important, the *safety* was the most selected by 6 from 10 patients followed by the *effectiveness* 5 from 10 patients. The less important items selected were the *dimensions*, *adjustment* and *weight* with only 2 from 10 patients for the firstly 2 and only 1 from 10 patients for the weight.

The average score obtained in the QUEST 2.0 evaluation by the physiotherapists was 27.33 ± 3.77 , slightly less than obtained from the patients. The item which was better evaluated was the *safety* with a score of 4 ± 0.82 and the least being the items *dimensions* with 3.17 ± 1.1 , *simplicity* with 3.17 ± 1.07 and *effectiveness* with 3.17 ± 0.37 . For the physiotherapists the item most important selected in the section three of the QUEST 2.0 was the *weight* chosen by 5 from 6 physiotherapists, followed by the *comfort* 4 from 6 physiotherapists. The less selected items were the *dimensions*, *durability* and *safety* each of them with selected only one time.

4 Conclusions

The results of QUEST 2.0 were considered satisfactory with an average score of 33 ± 6.9 over 40, obtained with the patient's evaluation and 27.33 ± 3.77 obtained with the physiotherapists evaluation. The best scored aspects were the weight, dimen-

sions and safety and the less scored was the effectiveness of the device in the rehabilitation therapy, but with a score above 3. These results have been influenced that the exoskeleton is in improvement stage and only was tested in passive mode where the patients with the activity in the motor function do not consider it useful for their rehabilitation therapy. Future research will be focused in the development of active mode of operation proposed in [10].

References

1. E. Monge-Pereira, J. Ibañez-Pereda, I.M. Alguacil-Diego, J.I. Serrano, M.P. Spottorno-Rubio, F. Molina-Rueda, Use of electroencephalography brain-computer interface systems as a rehabilitative approach for upper limb function after a stroke: a systematic review. *PM&R* **9**(9), 918–932 (2017)
2. F. O. Barroso, D. Torricelli, F. Molina-Rueda, I. M. Alguacil-Diego, R. Cano-de-la Cuerda, C. Santos, J. C. Moreno, J. C. Miangolarra-Page, J. L. Pons, Combining muscle synergies and biomechanical analysis to assess gait in stroke patients, *Journal of biomechanics* 63 98
3. M. Cempini, F. Giovacchini, N. Vitiello, M. Cortese, M. Moisé, F. Posteraro, M. C. Carrozza, Neuroexos: A powered elbow orthosis for post-stroke early neurorehabilitation, in: *Engineering in Medicine and Biology Society (EMBC), 2013 35th Annual International Conference of the IEEE, IEEE, 2013*, pp. 342–345
4. C. Cortés, A. Ardanza, F. Molina-Rueda, A. Cuesta-Gómez, L. Unzueta, G. Epelde, O.E. Ruiz, A. De Mauro, J. Florez, Upper limb posture estimation in robotic and virtual reality-based rehabilitation. *BioMed research international* **2014**, (2014)
5. J.M. Veerbeek, E. van Wegen, R. van Peppen, P.J. van der Wees, E. Hendriks, M. Rietberg, G. Kwakkel, What is the evidence for physical therapy poststroke? a systematic review and meta-analysis. *PloS one* **9**(2), e87987 (2014)
6. J. Mehrholz, M. Pohl, T. Platz, J. Kugler, B. Elsner, Electromechanical and robot-assisted arm training for improving activities of daily living, arm function, and arm muscle strength after stroke (2015)
7. D. Copaci, F. Martín, L. Moreno, D. Blanco, Sma based elbow exoskeleton for rehabilitation therapy and patient evaluation, *IEEE Access* **7**, 31473–31484 (2019). <https://doi.org/10.1109/ACCESS.2019.2902939>
8. N.N. Ansari, S. Naghdi, T.K. Arab, S. Jalaie, The interrater and intrateer reliability of the modified ashworth scale in the assessment of muscle spasticity: limb and muscle group effect. *NeuroRehabilitation* **23**(3), 231–237 (2008)
9. C.A. Mora Barrera, Validación de la versión en español de la evaluación de quebec de usuarios con tecnología de asistencia (quest 2.0)/validity of the spanish version of quebec user evaluation of satisfaction with assistive technology (quest 2.0), Ph.D. thesis, Universidad Nacional de Colombia
10. D. Copaci, D. Serrano, L. Moreno, D. Blanco, A high-level control algorithm based on semg signalling for an elbow joint sma exoskeleton. *Sensors* **18**(8), 2522 (2018)

Wireless Eye-Tracking Technology Application and Self-report Measures to Explore Users' Approach to Smart Home Systems (SHS)



Laura Angioletti, Federico Cassioli, and Michela Balconi

Abstract The relation between individual differences in some psychological traits and eye-gaze behavior in participants exploring a Smart Home System (SHS) was considered. Real-time eye-gaze metrics were recorded while subjects were engaged with 5 tech-interaction (TI) areas with different levels of complexity in the SHS. Results suggested easiness to visually process a simpler TI compared to complex ones, in terms of higher number of fixations and of slower Time To First Fixation (TTFF). In two of the TIs (Living Room and Bathroom) we found a negative correlation: between the external Locus of Control (LoC) and the number of fixations, which might indicate a possible tendency for individuals with low external LoC to explore more actively complex TIs. A negative correlation was found between Behavioural Activation System Reward Responsiveness (BAS-RR) and fixation duration, suggesting a tendency for subjects with high BAS-RR to scan the TIs with more quick and dynamic visual patterns.

1 Introduction

Human-Computer Interaction (HCI) is a multidisciplinary field of study focusing on the relation between users and computers. Nowadays, advanced technologies are considered those which are less visible and weave themselves in everyday life,

L. Angioletti (✉) · F. Cassioli · M. Balconi

International Research Center for Cognitive Applied Neuroscience (IrcCAN), Catholic University of the Sacred Heart, Milan, Italy

e-mail: laura.angioletti1@unicatt.it

Research Unit in Affective and Social Neuroscience, Department of Psychology, Catholic University of the Sacred Heart, Milan, Italy

F. Cassioli

e-mail: federico.cassioli@unicatt.it

M. Balconi

e-mail: michela.balconi@unicatt.it

© The Author(s), under exclusive license to Springer Nature Switzerland AG 2022

D. Torricelli et al. (eds.), *Converging Clinical and Engineering Research*

on *Neurorehabilitation IV*, Biosystems & Biorobotics 28,

https://doi.org/10.1007/978-3-030-70316-5_26

factories, and home environment. Smart Home Systems (SHS) aims at improving the user's quality of life through the habitation. In previous works, the relation between personality-cognitive factors on interface interaction was studied [1] and the role of Locus of Control (LoC) was highlighted as an important trait for an interface interaction and technology attitude [2]. Furthermore, Behavioural Inhibition System (BIS) and Behavioural Activation System (BAS) might be useful indicators for individual differences regarding motivational significance [3]. Specifically, higher BIS is connected to avoidance of risk situations, high control of an inhibitory attitude, and BAS, especially the subscale BAS Reward Responsiveness (BAS-RR) is sensitive to signals of reward and potential benefits [4]. Also, the use of eye-tracking with behavioral metrics, is a reliable method for HCI [5] and the adoption of it with questionnaires might provide deeper insights. The relation between LoC, BIS/BAS traits and eye-tracking metrics while subjects were engaged with gradually complex and different tech-interactions (TIs) was analyzed.

2 Material and Methods

2.1 Sample

19 healthy adults ($M_{\text{age}} = 25.05$, $SD_{\text{age}} = 3.05$, Age Range: 18–27, $n_{\text{male}} = 7$) participated in the study. Exclusion criteria were the presence of sensory/cognitive deficits, an history of psychiatric or neurological diseases.

Experimental setting was the home automation showroom owned by Duemmegi S.r.l. domotics company based in Milan (Italy). This study was approved by the ethics committee of the Department of Psychology of the Catholic University of the Sacred Heart of Milan in Italy and followed the principles of the Declaration of Helsinki.

2.2 Locus of Control Measure

The Locus of Control Behavior Questionnaire (LCBQ) [6] was administered to evaluate the LoC in different situations. Seven of the 17 items are referred to internal control, the other 10 to the external one. For this study, we used the Italian LCBQ [7], scoring internal and external LoC, corresponding respectively to an individual's tendency to believe that he/she can control events in his/her life, the future, and their outcomes by his own efforts, and, for external LoC, the propensity to attribute importance to outside forces.

2.3 *BIS/BAS Scales*

To understand the subject's propensity to experience new situations, the Italian version of BIS/BAS scales was adopted [8]. BIS is sensitive to signals of punishment and its activation may cause a state of inhibition of movement toward goals. Instead, BAS has been linked to approach tendency and positive feeling. BAS items compose 3 subscales: BAS Drive, the motivation to achieve a goal; BAS-RR, that measures the impact of environmental rewards; BAS Fun Seeking, corresponding to the personal motivation to engage with new rewards.

2.4 *Eye-Tracking Metrics Collection*

A wireless Tobii Pro Glasses 2 eye-tracking technology (Version 1.95, 07/2018. Tobii Pro AB, Stockholm, Sweden) was adopted to collect fixations and saccades which were then analyzed (Tobii Pro Glasses Analyzer) to derive viewer's attention patterns. Areas of Interest (AOI) were created for each TI, considering the number of fixations, Time To First Fixation (TTFF) and fixations duration. All the data are referred to a standard time frame after the TIs activation.

2.5 *Procedure*

The experiment took place in SHS. Participants were asked to fill in pre-experiment questionnaires, as BIS/BAS scales and the LCBQ. After the eye tracker montage, subjects were asked to interact and activate TIs, using an app, and observe the environmental effects of their action. The points of interaction were 5, with a certain amount of complexity, based on the SHS response, which during the experiment became more and more sophisticated: hall, kitchen, living room, bathroom, and bedroom. In the hall, the interaction consisted of activating a light. In the kitchen condition, the activation of the command provoked the transformation of an apparently normal set of desks in an accessorized kitchen. The living room interaction consisted of activating a projector on the wall. The fourth one (bathroom) involved the presentation of some features like lights for make-up or chromotherapy. Lastly, the bedroom area consisted of home bedtime mode activation: blinds were closed, the home was secured by locking external doors and gas and lights were turned off. Users were asked to pay attention to the experience provoked by the activation focusing on the SHS interactions.

3 Results

A set of 3 repeated measures ANOVA was applied to eye-tracking data. About number of fixations, ANOVA revealed a main effect for TI ($F[4,72] = 4.740, p = 0.004, \eta^2 = 0.345$). Pairwise comparisons showed significant higher number of fixations in the hall compared to the living room TI ($p = 0.002$).

For TTFF, a main effect for TI was detected ($F[4,72] = 5.36, p = 0.002, \eta^2 = 0.437$). Significant higher TTFF in the bathroom compared to the kitchen TI ($p = 0.005$) and a significant difference ($p = 0.005$) between bathroom and living room were found in pairwise comparisons. No significant differences were found for fixations duration.

Pearson's coefficients were performed between eye-tracking metrics and questionnaires score. Firstly, a significant correlation was found between the number of fixations in the living room TI and external LCBQ [$r(17) = -0.613, p = 0.045$]. Secondly, a significant correlation was found between the number of fixations and external LCBQ for the bathroom TI [$r(17) = -0.688, p = 0.019$]. Thirdly, a significant correlation was found between BAS-RR and fixation duration for both bathroom [$r(17) = -0.658, p = 0.028$] and living room [$r(17) = -0.681, p = 0.021$]. No other significant correlations were observed.

4 Discussion and Conclusion

For TIs, a sign of easiness to process and visually elaborate a simpler TI (hall), compared to a more sophisticated one (living room) was identified, in fact number of fixations can be seen as a direct function of visual exploration behavior [9]. Similar results were found for TTFF, where a more complex TI (bathroom) required more time to be fixated for the first time compared to simple ones (kitchen and living room), which is an indicator of motivational and engagement levels and might indicate increased general interest in the users [10].

Regarding personal traits, in two conditions (living room and bathroom) we found two negative correlations between the number of fixations and external LCBQ. These results can be interpreted as tendency for low external LoC individuals, so those who attribute small importance to unpredictable factors, to explore more actively complex TIs and showing interest in them. Results partially confirmed past evidence on the impact of LoC on the interface interaction suggesting that internally controlled individuals were more curious and less anxious towards technology artefact [2].

The correlation between BAS-RR scores and fixation duration found in two TIs (living room, bathroom), indicate a tendency for subjects with higher BAS-RR scores to explore more the point of interaction, with a reduced fixation duration average. This exploratory pattern might be more impulsive and fluid with reduced average time per fixation.

Despite its high ecological validity, this study did not take into consideration variables such as gender and age in extensive analyses, which are known to be impactful in HCI. Current evidence confirms the need for an always more human centered interface, which considers the individual features and psychological traits of users navigating and living SHS and using home technologies for daily assistance.

Acknowledgements Authors kindly thank the tech company Duemmegi S.r.l. (Milan, Italy) as project partner.

References

1. T.M. Green, B. Fisher, The impact of personality factors on interface interaction and the development of user profiles. *Inf. Vis.* **11**, 205–221 (2012)
2. S. Arndt, J. Feltes, J. Hanak, Secretarial attitudes towards word processors as a function of familiarity and locus of control. *Behav. Inf. Technol.* **2**, 17–22 (1983)
3. M. Balconi, G. Mazza, Brain oscillations and BIS/BAS (behavioral inhibition/activation system) effects on processing masked emotional cues: ERS/ERD and coherence measures of alpha band. *Int. J. Psychophysiol.* **74**, 158–165 (2009)
4. J.A. Gray, Personality dimensions and emotion systems, in *The Nature of Emotion: Fundamental Questions*, 2nd edn., ed. by P. Ekman, R.J. Davidson (Oxford University Press, New York, 1994), pp. 329–331
5. P. Majoranta, A. Bulling, Eye tracking and eye-based human-computer interaction. *Adv. Physiol. Comput.* **3**, 39–65 (2014)
6. A.R. Craig, J.A. Franklin, G. Andrews, A scale to measure locus of control of behavior. *Br. J. Med. Psychol.* **57**, 173–180 (1984)
7. T. Farma, I. Cortinovis, Un questionario sul “locus of control”. Suo utilizzo nel contesto italiano. *Ric. Psicoterapia* **2**, 1–8 (2000)
8. L. Leone, A. Pierro, L. Mannetti, Validità della versione italiana delle scale BIS/BAS di Carver e White (1994). *Ital. J. Psychol.* **29**, 413–436 (2002)
9. A. Glockner, A.K. Herbold, An eye-tracking study on information processing in risky decisions: evidence for compensatory strategies based on automatic processes. *Behav. Decis. Making* **24**, 71–98 (2011)
10. G. Buscher, E. Cutrell, M.R. Morris, What do you see when you’re surfing ? Using eye tracking to predict salient regions of web pages, in *Proceedings of the SIGCHI Conference on Human Factors in Computing Systems*, vol. 2, July 2009, pp. 21–30

Learning Teleoperation of an Assistive Humanoid Platform by Intact and Upper-Limb Disabled Users



Mathilde Connan, Marek Sierotowicz, Bernd Henze, Oliver Porges, Alin Albu-Schäffer, Máximo A. Roa, and Claudio Castellini

Abstract With the advent of highly dexterous robotic arms, assistive platforms for home healthcare are gaining increasing attention from the research community. Control of the many degrees of freedom of such platforms, however, must be ensured uniformly, both for non-disabled and disabled users, in order to give them as much autonomy as possible. Nine users, including two upper-limb disabled, were asked to complete highly complex bimanual tasks by teleoperating a humanoid robot with biosignals. The users were equipped with a light and wearable interface consisting of a body tracking device for guiding the torso and arms and two electromyography armbands for controlling the hands by means of interactive machine learning. All users were able to complete the required tasks, and learning curves are visible in completion time metric.

1 Introduction

The world around us is shaped to be operated by arms and hands, and the loss or impairment of the upper limb leads therefore to a dramatic degradation in the quality of living. A person with upper-limb amputation is prevented from swiftly acting in the world for the rest of her/his life, since state-of-the-art prosthetic or assistive solutions cannot usually operate more than one degree of motion, or if they can operate more than one, this can only happen sequentially, one motion at a time. Extensive application of statistical techniques to surface electromyography (sEMG) has revealed that, in controlled conditions, users can produce several discernible signal patterns corresponding to the intended actions to be performed by the absent limb. Unfortunately such techniques have so far shown little generalization power across users and when used online in daily-living environments, while, e.g., lifting

M. Connan (✉) · M. Sierotowicz · B. Henze · O. Porges · A. Albu-Schäffer · M. A. Roa · C. Castellini

Institute of Robotics and Mechatronics, DLR—German Aerospace Center, 82234 Wessling, Germany

e-mail: mathilde.connan@dlr.de

weights and unpredictably changing one's body posture [1]. Attempts at solving this problem can be found, e.g., in [2], where unreliability is tackled using incremental machine learning (iML), i.e., an algorithm that can accommodate for new knowledge on the fly, in order to mend the instability of the intent detection system online. Degris et al. [3] as well as Nowak et al. [4] have explored the usage of reinforcement learning in the context of user/prosthesis interaction. Whether this idea works in practice, however, is still controversial [5].

In order to verify its effectiveness, we have designed an experiment in which both non-disabled and upper-limb disabled users were challenged to teleoperate a dexterous assistive humanoid platform using sEMG bracelets and a custom-made body posture detection device [6]. iML was employed to account for and correct instabilities of the intent detection system, whose model was updated whenever the user deemed the task to be unattainable. We hypothesized that such a setup and protocol would enable human users to complete all tasks, and that a learning effect would appear over time, leading, in the end, to uniform results across users, irrespective of their disability.

2 Materials and Methods

2.1 Experimental Setup

Seven non-disabled users (28.4 ± 7.1 yo) and two upper-limb disabled users (34 yo, congenital absence of the right hand; 48 yo, trans-radial bilateral traumatic amputation) were involved in this experiment. All subjects signed an informed consent form prior to the experiment.

The users were equipped with a wearable upper-body tracking device (Fig. 1) based on inertial measurement units (IMUs) [6] placed on their forearms, upper-arms, and torso for controlling the position and orientation of the robot's hands, as well as, indirectly, its torso and arms thanks to the controller detailed in [7]. Additionally, a Myo armband from Thalmic Labs was placed on each of their forearms in order to record sEMG activity. From the sEMG signals, the desired hand poses of the robotic hands were predicted thanks to a ridge regressor with random Fourier features [8]. In the case of the impaired users, this regressor also predicted the wrist movements. For intact users, this was determined by the IMU-based tracking device with an IMU placed on the dorsal part of each hand. Due to the high instability resulting from the high number of hand and wrist poses to predict for the amputees, a slightly different training protocol was implemented for them in which only the task-specific poses were trained by the machine learning algorithm. The humanoid platform TORO controlled by the users was developed at the German Aerospace Center (DLR) [7, 9].

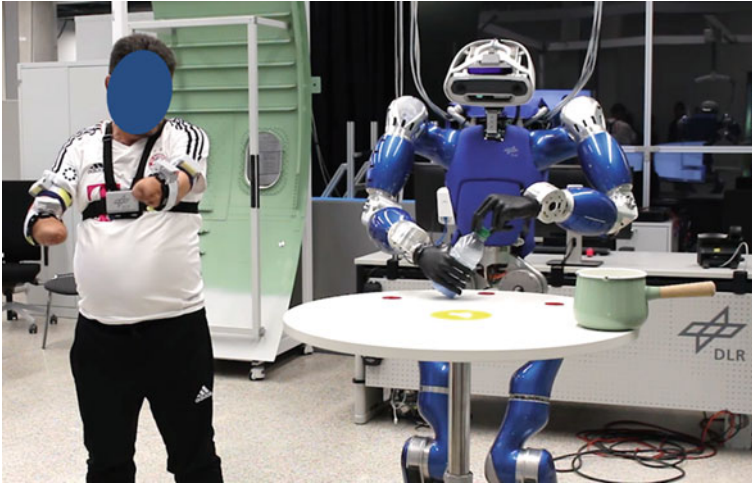


Fig. 1 A bilateral amputee performing highly complex bimanual tasks by teleoperating a humanoid robotic platform

2.2 User Study Protocol

The users were asked to achieve highly complex tasks inspired from daily living activities and requiring a high level of bimanual coordination. The experiment consisted of three tasks, the first two being divided in two subtasks. The users had an unlimited number of trials and were free to stop or pause the experiment at any moment. Each task was performed four times. If an object dropped on the floor or if the experimenter judged that the user would not be able to recover a correct objects' setting, the task was reset to the initial setting of the subtask. The list of the tasks is visible in Table 1. The subject performance was evaluated in terms of the time it took them to complete each task (Time to Complete Task, TCT).

3 Results

The summary results on the TCTs are given in Fig. 2. A decrease in the TCTs is visible when considering each task and repetition. The one-sided amputee (D1) achieved better results than the pool of subjects for the first three tasks. For the last two tasks his TCTs are higher but still comparable. The double-sided amputee (D2) also presents TCTs in line with the non-disabled users. The improvement ratio of the TCTs, between repetition 1 and 4, ranges from 3.6 times (Task 1a) to 1.7 times (Task 3), with an average over all tasks of 2.2 times (1.5 for D1 and 2.2 for D2).

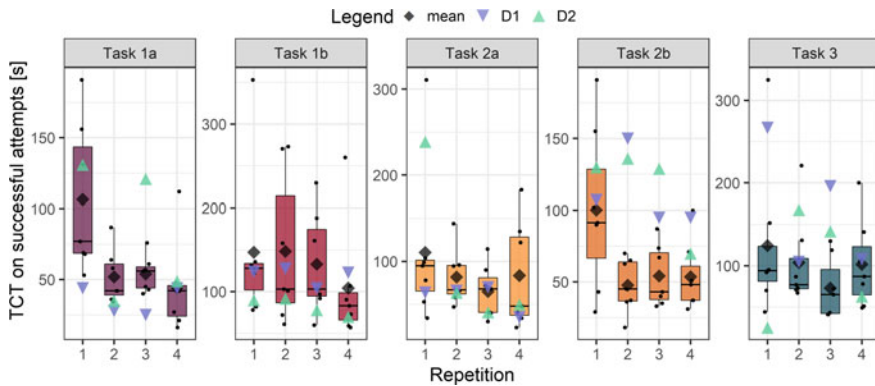


Fig. 2 Results of the user study on successful attempts

Table 1 Description of the tasks

Task ID	Summary of the task
1a	Take the lid off the pot and place it on the table
1b	Take the ball, put it in the pot, place back the lid
2a	Unscrew the cap of the bottle
2b	Pour the bottle's content into the pot
3	Press a sequence of buttons on the fixed telephone

4 Discussion

We have presented here an assistive platform for daily-living activities and put it to the test by asking non-disabled users as well as users with different upper-limb disabilities to perform complex tasks requiring a high level of bimanual coordination. The experimental results confirm that, with the use of iML, all users were able to quickly and efficiently learn to teleoperate the platform and successfully complete all tasks, and that a learning effect was apparent, speeding up the execution of the tasks over time. This was confirmed by a significant difference between repetition 1 and 4 but as well between 1 and 2 when performing a Wilcoxon Signed-Rank test on the TCTs of all participants. Learning was uniform across seven non-disabled users and two upper-limb disabled persons, namely a person born with right-hand trans-radial congenital deficiency and a bilateral trans-radial traumatic amputated user. Previous research has also studied the use of accelerometry data in prosthetic control [10]. In future work, we intend to develop a machine learning algorithm fusing IMU and sEMG data in order to further improve the hand control without the necessity to train in several positions.

Acknowledgements This work was partially supported by the German Research Society projects Tact-Hand (DFG Sachbeihilfe CA-1389/1-1) and Deep-Hand (DFG Sachbeihilfe CA-1389/1-2).

References

1. A. Fougner, E. Scheme, A.D.C. Chan, K. Englehart, Ø. Stavdahl, O. Stavdahl, Resolving the limb position effect in myoelectric pattern recognition. *IEEE Trans. Neural Syst. Rehabil. Eng.* **19**, pp. 644–651 (2011)
2. J.M. Hahne, S. Dähne, H.-J. Hwang, K.-R. Müller, L.C. Parra, Concurrent adaptation of human and machine improves simultaneous and proportional myoelectric control. *IEEE Trans. Neural Syst. Rehabil. Eng.* **23**, pp. 618–627 (2015)
3. T. Degris, P.M. Pilarski, R.S. Sutton, Model-free reinforcement learning with continuous action in practice, in *IEEE American Control Conference (ACC)*, Montreal, QC, Canada (2012)
4. M. Nowak, C. Castellini, C. Massironi, Applying radical constructivism to machine learning: a pilot study in assistive robotics. *Constructivist Found.* **13** (2018)
5. C. Castellini, Upper limb active prosthetic systems—overview, in *Wearable Robotics* (Elsevier, Amsterdam, 2020), pp. 365–376
6. M. Sierotowicz, M. Connan, C. Castellini, Human-in-the-loop assessment of an ultralight, low-cost body posture tracking device. *Sensors* **20**, 890 (2020)
7. B. Henze, M.A. Roa, C. Ott, Passivity-based whole-body balancing for torque-controlled humanoid robots in multi-contact scenarios. *Int. J. Robot. Res.* **35**, pp. 1522–1543 (2016)
8. A. Gijssberts, R. Bohra, D. Sierra González, A. Werner, M. Nowak, B. Caputo, M.A. Roa, C. Castellini, Stable myoelectric control of a hand prosthesis using non-linear incremental learning. *Frontiers Neurorobotics* **8**, 15 (2014)
9. C. Ott, M.A. Roa, F. Schmidt, W. Friedl, J. Engelsberger, R. Burger, A. Werner, A. Dietrich, D. Leidner, B. Henze, O. Eiberger, A. Beyer, B. Bäuml, C. Borst, A. Albu-Schäffer, Mechanisms and design of DLR humanoid robots, in *Humanoid Robotics: A Reference*, ed. by A. Goswami, P. Vadakkepat (2016), pp. 1–26
10. A. Radmand, E. Scheme, K. Englehart, On the suitability of integrating accelerometry data with electromyography signals for resolving the effect of changes in limb position during dynamic limb movement. *JPO: J. Prosthet. Orthot.* **26**, pp. 185–193 (2014)

Assessment of Clinical Requirements for a Novel Robotic Device for Upper-Limb Sensorimotor Rehabilitation After Stroke



Raphael Rätz, René M. Müri, and Laura Marchal-Crespo

Abstract In order to identify the clinical requirements for a novel upper-limb robotic device for sensorimotor neurorehabilitation, a survey with 33 participants (including physiotherapists, occupational therapists, speech therapists, nurses and physicians) was conducted. The results show that grasping, eating and personal hygiene are amongst the most important activities of daily living to be exercised. Hand/finger extension were reported as crucial movements. In serious games for neurorehabilitation, adjustable quantity of virtual objects as well as adjustable game difficulty are highly demanded features. The majority of the participants would like to spend less than 10 min for the setup of a robotic device.

1 Introduction

Although researchers and clinicians agree that a clinical-driven design approach is crucial for the successful development and acceptance of novel robotic devices, there is a deficiency of literature on clinical requirements for robotic devices in neurorehabilitation [1]. Even though reporting of identified requirements for novel devices would be critical for the general advancement of robotic neurorehabilitation, often, only user feedback on the final device is published.

This work was supported by the Innosuisse grant 32213.1 IP-CT “Novel Clinical-Driven Robot-Assisted Sensorimotor Therapy”.

R. Rätz (✉) · L. Marchal-Crespo
Motor Learning and Neurorehabilitation Laboratory, ARTORG Center for Biomedical Engineering Research, University of Bern, Bern, Switzerland
e-mail: raphael.raetz@artorg.unibe.ch

L. Marchal-Crespo
Department of Cognitive Robotics, Delft University of Technology, Delft, The Netherlands

R. M. Müri
Department of Neurology, University Neurorehabilitation, University Hospital Bern (Inselspital), University of Bern, Bern, Switzerland

Preferred body positions for exercising upper and lower-limb movements in robotic systems, as well as preferences about adjustability of device parameters were identified in [2]. In [3], a large survey with 85 questions and 233 participants on design requirements for a robotic device for upper-limb rehabilitation was conducted. Requirements for the successful implementation of technology in stroke rehabilitation were established in [4] through literature research and interviews with therapists, while in [5], requirements for stroke rehabilitation technology were determined in interviews with patients.

Here, we present results from a survey conducted prior to the development of a novel robotic device for upper-limb sensorimotor rehabilitation with focus on forearm and hand functions. The goal was to analyse project-specific clinical needs to complement existing research.

2 Methods

A total of 33 participants (4 physicians, 1 nurse, 2 speech therapists, 1 neuropsychologist, 6 occupational therapists and 19 physiotherapists) from the University Hospital (Inselspital) Bern (26 respondents), and Reha Rheinfelden (Switzerland) answered 35 questions in an online survey.

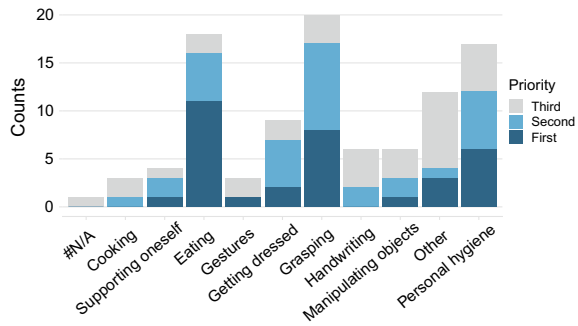
After initial questions related to their professional experience, participants were instructed to list 3 activities of daily living (ADL) which they consider crucial to be exercised during stroke rehabilitation and sort them based on priority. Following, they had to judge the importance of practising various lower-arm and hand movements using five-point Likert-items. Potential elements to be employed in serious games were also evaluated. Participants were then asked to estimate the maximum time they would be willing to spend for the patient setup in a robotic device. Finally, they had to judge if they prefer a compact device with a low number of functionalities or a large device with more functionalities. They also had the possibility to express concerns about robotic-assisted neurorehabilitation and to leave a comment. The survey was anonymous, and all participants gave their consent to the usage of the data in scientific publications.

3 Results

The professional experience was found to be 5 years or less for 30.3%, between 5 and 20 years for 33.3% and more than 25 years for 36.4% of the participants.

Answers regarding the most important ADL were categorized according to a prior defined classification. The majority of the listed ADL could be attributed to the pre-defined categories, which confirmed the validity of the chosen classification (Fig. 1). Responses that did not fit this classification were grouped in the category “Other”. Out of the 33 respondents, 25 participants specified those activities categorized as

Fig. 1 Activities of daily living that should be trained in stroke rehabilitation and their given priority



“Eating”, “Grasping” or “Personal hygiene” as first priority, whereof “Eating” was mentioned the most frequent with 11 responses. Including all three priorities (total of 99 answers), activities related to “Grasping” were mentioned at the highest count with with 20, followed by “Eating” with 18 and “Personal hygiene” with 17.

The training of extension movements (finger and elbow extension, dorsiflexion) was found to be of higher importance compared to practicing flexion movements (finger and elbow flexion, palmarflexion), as shown in Fig. 2. A Wilcoxon signed-rank test of the accumulated Likert-items showed a significant difference ($p = 0.0007$) between flexion and extension movements. Likewise, the training of wrist supination appears to be of higher priority compared to pronation ($p = 0.005$). Furthermore, based on the responses, exercising of independent thumb and index finger movements is more essential than independent movements of the middle, ring and little finger. Also, radial and ulnar abduction tend to be the least important movements to be practised.

When it comes to potential tasks in serious games for neurorehabilitation after stroke, adjustability of virtual object quantity and training difficulty are desired features (Fig. 3). A small number of objects by default as well as a colorful virtual environment were less appreciated by the respondents.

A setup time over 30 min was classified as outlier (4 subjects) because it was assumed that the question was misunderstood and confounded with the initial setup time after delivery of the device. Out of the remaining 29 participants, 25 specified a maximum setup time of 10 min or less. The median was found to be 5 min.

In regard to the size-functionality trade-off, no apparent tendency could be found as 14 subjects preferred a larger device with more functionalities and 18 subjects preferred a compact device with fewer functionalities while 1 respondent did not have an opinion.

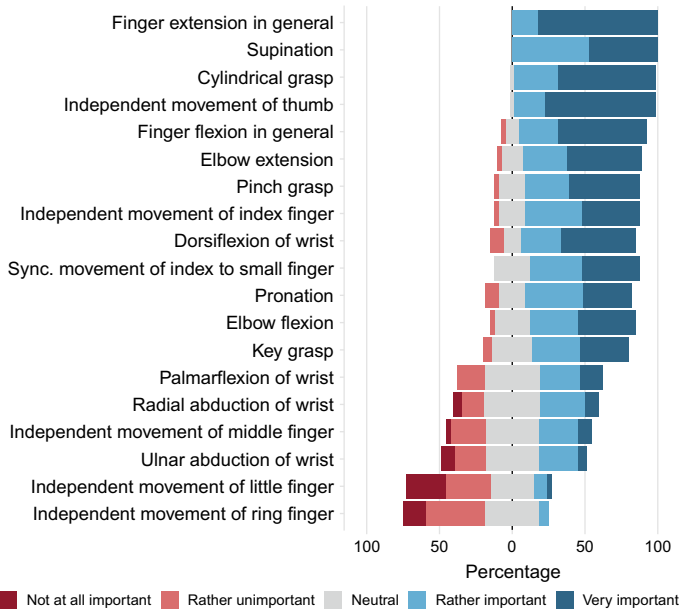


Fig. 2 Importance of different upper-limb movements in stroke rehabilitation

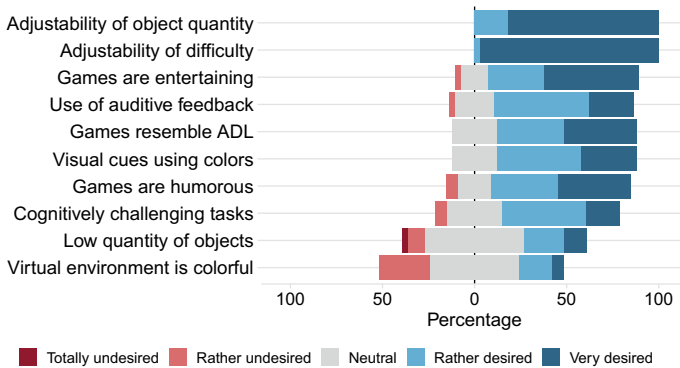


Fig. 3 Desired features for serious games in robotic stroke rehabilitation

4 Conclusion

The presented work complements precedent research by investigating the importance of practising specific upper-limb and hand movements as well as ADL in stroke rehabilitation from a point of view of clinical personnel. It was found that grasping is amongst the most important ADL to be exercised. Extension movements appear to be particularly important. Moreover, adjustability of difficulty and the quantity of virtual objects were identified as highly demanded features of serious games. The

maximum setup time specified by the participants for a robotic device indicates that a user-friendly design is a key factor for successful clinical integration. The results of this survey contribute to the formalization of clinical requirements for robotic upper-limb rehabilitation devices and serious games in virtual training environments.

Acknowledgements Many thanks go to the personnel of the Department of Neurorehabilitation, University Hospital Bern, specifically Colette Carroz, Irène Thaler, Isabelle Lehmann, Sandra Briner and Claudia Kuster for their participation. The authors would also like to thank Dr. Corina Schuster for including therapists from the Reha Rheinfelden. The authors are grateful for the support of Force Dimension (Switzerland).

References

1. R. Holt, S. Makower, A. Jackson, P. Culmer, M. Levesley, R. Richardson, A. Cozens, M. Williams, B. Bhakta, User involvement in developing rehabilitation robotic devices: An essential requirement, in *2007 IEEE 10th International Conference on Rehabilitation Robotics, ICORR'07*, vol. 00, no. c, pp. 196–204 (2007)
2. M. Lee, M. Rittenhouse, H.A. Abdullah, Design issues for therapeutic robot systems: results from a survey of physiotherapists. *J. Intell. Rob. Sys.: Theo. Appl.* **42**(3), 239–252 (2005)
3. E.C. Lu, R.H. Wang, D. Hebert, J. Boger, M.P. Galea, A. Mihailidis, The development of an upper limb stroke rehabilitation robot: identification of clinical practices and design requirements through a survey of therapists. *Disability Rehabilitation: Assistive Tech.* **6**, 420–431 (2011)
4. A. Hochstenbach-Waelen, H.A. Seelen, Embracing change: practical and theoretical considerations for successful implementation of technology assisting upper limb training in stroke. *J. Neuro-Eng. Rehabil.* **9**(1), 52 (2012)
5. N. Nasr, B. Leon, G. Mountain, S. M. Nijenhuis, G. Prange, P. Sale, F. Amirabdollahian, The experience of living with stroke and using technology: opportunities to engage and co-design with end users. *Disability Rehabil.: Assistive Technol.* (2015) pp. 1–8

TestEd Information System: Automatic Evaluation of Exoskeletons Subjective Performance and User Experience



Angel Dacal-Nieto, Jawad Masood, Daniel Vergara, and Mariana Alves

Abstract Uncertainty still remains about the suitability of a given exoskeleton or exosuit to a specific workstation. This is currently done by complex and controlled test experiences either in simulated or real environments. Thus, benchmarking seems a proper solution to minimize this uncertainty. The European H2020 project EUROBENCH aims to create the first benchmarking framework for exoskeletons in Europe. The subproject TestEd is one of the testbeds developed under EUROBENCH, focusing on the use case of moving in narrow spaces. TestEd information system aims to automate the exoskeleton performance evaluation in both objective and subjective sense while using the testbed, providing automatic quantitative results from each test session. In this paper we focused on the subjective methods where we share our experience in digitalization of the questionnaire survey and the Borg Scale 10. This approach can improve the exoskeleton subjective evaluation time, providing a new evaluation tool in this field.

1 Introduction

Workers at manufacturing industry with standing work schedule for extend length of time, often have knee and back problems, that limit their job and life quality. Examples are assembly of seats in aeronautics, and working inside a cabin in truck/car manufacturing. Minimizing of standing posture is one of the main goals for the industry, both for users and managers. Although job rotation is a common practice, this problem has still no universal solution. Recently, the emergence of industrial

A. Dacal-Nieto · J. Masood (✉) · D. Vergara
Processes and Factory of the Future Department, CTAG—Centro Tecnológico de Automoción de Galicia, O Porriño, Spain
e-mail: jawad.masood@ctag.com

A. Dacal-Nieto
e-mail: angel.dacal@ctag.com

M. Alves
LD&T—Local Design and Technology, As Neves, Spain

© The Author(s), under exclusive license to Springer Nature Switzerland AG 2022
D. Torricelli et al. (eds.), *Converging Clinical and Engineering Research on Neurorehabilitation IV*, Biosystems & Birobotics 28,
https://doi.org/10.1007/978-3-030-70316-5_29

exoskeleton technology [1, 2] for both health and industrial domains meant a new approach for helping the workers, by reducing musculoskeletal diseases. Exoskeletons have been tested and introduced in the last years, proving themselves as a good option in some applications.

However, in these first experiences of exoskeleton implementation in industry, it has been assessed that there is no clear path from the user needs to the final usage of the device. Thus, a deep testing stage is required, and although some protocols have been proposed [3], no standard or regulations are defined for that purpose. This evaluation consumes time and costs, but is fundamental to allow a successful integration of the exoskeleton in the field.

Benchmarking is a proper solution, since it can describe a list of atomic sub-operations (use cases), allowing to express any workstation as a combination of these use cases. This would permit to treat the evaluation process from a global perspective, and re-use experiences from apparently different fields.

This is the trigger of the European H2020 project EUROBENCH (EB) [4], which aims to create the first benchmarking framework for lower-limbs exoskeletons in Europe. The final picture of EB is having a grid of 16 testbeds, each one designed for a specific use case.

The subproject TestEd is one of the testbeds developed under EB, focusing in the use case of moving in narrow spaces. In this paper, we will present the information system (IS) of TestEd, as a tool to perform automatic evaluation of the exoskeleton performance. TestEd software controls and configures the physical components, and its results can be connected as an input to the EB general software.

In literature, we can find some initiatives to look for the performance metrics of wearable robotics [5], especially in rehabilitation area [6]. Pons et al. [7] present an in-depth review of literature and highlight the major performance metrics based on the Goals Level, Kinematics and Kinetics and Human-Robot Interaction.

TestEd aims to reduce the testing time from the selection to the implementation of an industrial exoskeleton by using both a testbed and software routines. The paper is organized as follows: Sect. 2 will be devoted to the description of the testbed, the IS will be presented in Sect. 3, and finally Sect. 4 will discuss results and conclusions.

2 Description of the Testbed

Our test design consists of a subject walking straight through narrow spaces and performing a work simulated task. The test operator or evaluator is able to run the same test a predefined number of times during a test session, with different exoskeletons and with different assistance levels.

To reproduce this scenario, the TestEd system is physically composed of a testbed (shown in Fig. 1), mainly formed by two sensorized walls and a set of telescopic hurdles. One of the walls can be moved by motors, so custom distances between walls, and hurdles configurations, can be set up. The predefined distances simulate a narrow space for various industrial necessities, like automotive, construction or aeronautical.

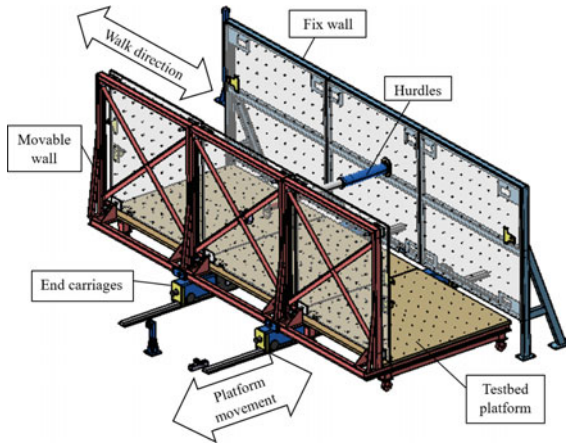


Fig. 1 The physical testbed developed in TestEd, which is complemented by an information system to automate the evaluation

Additionally, the hurdles simulate industry equipment interaction during the work task.

These physical components are controlled by an automation layer and an IS, which are able to interact with actuators and sensors, through technologies such as ROS and Node-RED. One of the sensorized walls can detect the force and point of force application. The other sensorized walls and telescopic hurdles can detect collisions, that are interpreted as the lack of ability of the person using the testbed while using a specific configuration of narrow space.

3 Information System (IS)

The IS is a stack of components from the communication with the physical elements, to the application domain. It is composed by an Angular front-end (HMI), a Java/Seedstack back-end, and a MongoDB database. The main analysis algorithms, which calculate the performance metrics, are developed using Octave.

For these algorithms, we follow our assessment process of testing [3] as baseline. A proposed workflow is shown in Fig. 2. The basic concept is the “test session”, which refers to a specific test under a set of input parameters (subject data, testbed configuration, and evaluation devices-methods). All data generated during the evaluation session are automatically acquired and stored in the database. At the end of the session, subjective data are also obtained via questionnaires and Borg charts.

As an output, the system provides a set of performance metrics, so that objective and subjective results are presented, automatically calculated from the testbed and subject data.

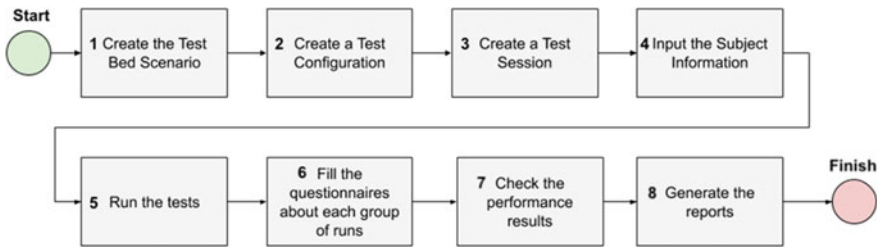


Fig. 2 Information system architecture

It is important to note that these metrics calculate local and global performances. The local performance metrics address only one evaluation criterion at a time, meanwhile the global performance metric addresses the overall performance of the exoskeleton. Currently, the global performance provides a result from six points of view: Impact, Utility, Safety, Usability, Familiarity and Training, but other aspects could be included in the future.

These quantitative results help to quickly evaluate the performance, so long term studies can be executed and compared, as well as different exoskeletons or different subjects, potentially with different configurations. Summaries of running tests can be seen in the EB website.

Regarding the subjective evaluation, it is based on questionnaires survey¹ and Borg Scale 10² that are presented to the subject in order to obtain user experience assessment during a specific session, from Usability, Impact and Utility perspectives. The values provided by the user are analyzed using an Octave algorithm, that eventually creates a local performance metric. This procedure is GDPR compliant.

The information system serves not only as a stand-alone application that can collect the information from the subjects and process it, but also to generate a series of output files which are consumed as an input by the EB general software.

4 Results and Conclusion

TestEd is an innovative benchmarking approach for evaluating industrial exoskeletons, focused on the case of moving in narrow spaces. Besides a mechanical structure, TestEd provides a novel GDPR complaint IS and specific algorithms which can automatically assess the subjective performance of a specific exoskeleton. It can improve time, tracking and monitoring, as well as minimizing human error and paperwork. The EB interface ensures the benchmarking of the software i.e. one more step towards the boosting of exoskeleton technology into the factories with confidence.

¹ https://github.com/jamatics/pi_ctag/tree/master/questionnaire.

² https://github.com/jamatics/pi_ctag/tree/master/borgScale10.

Acknowledgements The authors want to thank the project EUROBENCH (European Robotic Framework for Bipedal Locomotion Benchmarking), which has received funding from the European Union's Horizon 2020 research and innovation programme under grant agreement No 779963, and supports this work.

References

1. A.J. Young, D.P. Ferris, State of the art and future directions for lower limb robotic exoskeletons. *IEEE Trans. Neural Syst. Rehabil. Eng.* **25**(2), 171–182 (2017)
2. S. Viteckova et al., Empowering lower limbs exoskeletons: state-of-the-art. *Robotica* 14
3. J. Masood, A. Dacal-Nieto, V. Alonso-Ramos, M.I. Fontano, A. Voilqué, J. Bou, *Industrial Wearable Exoskeletons and Exosuits Assessment Process* (Springer, Cham, 2019), pp. 234–238
4. Eurobench, Available: <https://eurobench2020.eu>. Accessed 23 April 2020
5. A. Schiele, *Fundamentals of ergonomic exoskeleton robots* (2008)
6. S. Tyson, L. Connell, The psychometric properties and clinical utility of measures of walking and mobility in neurological conditions: a systematic review. *Clin. Rehabil.* **23**(11), 1018–1033 (2009)
7. D. Torricelli, D. Pinto-Fernandez, R. Conti, N. Vitiello, J.L. Pons, *A Review of Performance Metrics for Lower Limb Wearable Robots: Preliminary Results* (Springer, Cham, 2019), pp. 147–151

sEMG-Based Classification Strategy of Hand Gestures for Wearable Robotics in Clinical Practice



Nicola Secciani, Alberto Topini, Alessandro Ridolfi, and Benedetto Allotta

Abstract Every day more and more robotic aids, of different shapes, sizes, and functions, enter the clinics to take part in the rehabilitative and assistive paths for patients with reduced mobility. Accompanying discharged patients with robotics-based remote rehabilitation and home assistance seems to be one of the most promising avenues to follow to increase the success rate of these practices and lighten the overall burden on national health systems. However, to get out of clinics effectively, robotics must become wearable and, therefore, based on the use of embedded low-power electronics, both for practicality and safety reasons. The point is further complicated when it comes to assisting or rehabilitating lost hand functionalities due to the small size and complex mobility of such a limb; moreover, ensuring the real-time execution of gesture classification algorithms for controlling these devices hence becomes a vital engineering challenge. A hand gesture classification solution, specifically designed for the implementation of embedded electronics, based on surface electromyography, and ensuring real-time action, will be presented in this paper.

1 Introduction

Robotic devices, in addition to the mechanical hardware, generally incorporate internal memory, communication channels, and an automatic control system to provide monitoring capabilities, as well as intuitive and safe utilization. These characteristics have made them particularly attractive to the clinical practice for which remote rehabilitation sessions or home assistance exploiting low-cost robotic devices can

The authors would like to thank RING@LAB (joint laboratory between the University of Florence and the Don Carlo Gnocchi Foundation) for logistic and clinical support to the research, and the University of Florence that funded this work through the HOLD project.

N. Secciani (✉) · A. Topini · A. Ridolfi · B. Allotta
Department of Industrial Engineering (DIEF), University of Florence, Via di Santa Marta 3,
50139 Florence, Italy
e-mail: nicola.secciani@unifi.it

© The Author(s), under exclusive license to Springer Nature Switzerland AG 2022
D. Torricelli et al. (eds.), *Converging Clinical and Engineering Research*
on *Neurorehabilitation IV*, Biosystems & Biorobotics 28,
https://doi.org/10.1007/978-3-030-70316-5_30

be indeed an effective solution to democratize services otherwise not accessible to everyone. Indeed, people with disabilities do not always have the opportunity to do rehabilitation in the clinic or can afford someone to assist them at home.

It is important to note that when moving from clinical to home, these devices shall guarantee some additional features such as: ensuring the greatest possible freedom of movement of the user while being worn for a long time and being easily and intuitively usable by people with reduced mobility.

In this article, the attention will be focused on a hand gesture classification strategy based on the analysis of electromyographic signals, which will be first introduced and then quantitatively analyzed. Such a procedure is in charge of providing the high-level command signals for a Hand Exoskeleton System developed by the Department of Industrial Engineering of the University of Florence (DIEF) [1].

2 Background

Control strategies for assistive or rehabilitative devices, as exoskeletons, shall be as intuitive as possible to best simulate a condition of pseudo-normality. When it comes to that, the literature suggests using techniques based on the recognition of the user's motor intentions and their subsequent reproduction using external devices, as HESs. The most accredited methods are based on the classification of surface ElectroMyoGraphic (sEMG) signals [2].

These signals, despite very convenient to use—their collection is indeed completely non-invasive—are particularly tricky to process, primarily because of their noisy nature. Many are the strategies that have been developed for their classification, but only a few are suitable for being implemented on wearable robotic devices. A compromise should be reached on the number of intentions discriminated against to simplify these approaches and make them runnable on low-power embedded electronics. For the proposed method, according to what reported in [3]—where it is highlighted that the simultaneous use of fingers is sufficient to carry out most of the Activities of Daily Living (ADLs)—the number of classifiable gestures has been limited to three, i.e., hand opening, closing, and resting.

In a previous pilot study [4], this technique has been implemented on a low-powered micro-controller to run at the operative frequency 50 Hz (the same setup used in this work). Then, this strategy's performance has been qualitatively evaluated by enrolling a patient with Spinal Muscular Atrophy (SMA) and showed noteworthy results. Conversely, a quantitative analysis of the results, which may be used as a term of comparison with other classification techniques, does arise as the novel major contribution of the presented research work.

3 Classifier Evaluation

The classification process exploited in this work involves the use of a particular algorithm, the so-called “Point-In-Polygon (PIP)”, which allows for the classification of a general two-dimensional input. The PIP functionality relies on checking whether or not a point belongs to a specified polygonal area. In this case, its application primarily involves the sampling of a pair of sEMG signals collected in the form of an Integrated EMG (IEMG) value by two MyoWare™ Muscle Sensors placed on the *extensor digitorum* and *flexor digitorum* muscle bands. These are the muscles naturally involved in the hand opening and closing movement. The IEMG value is calculated by the sensors themselves as follows:

$$IEMG = \sum_{i=1}^M |y_i| \quad (1)$$

where y_i is the i -th sample of an arbitrary time window, and M is the total number of samples of the same time window. For the nature of the sensors, it is not possible to directly manipulate the inner parameters of the calculation (e.g., M), but it is possible to define the sampling frequency of the IEMG values by means of an external micro-controller. A Pro Trinket (3 V, 12 MHz) has been used to read IEMG measurements at a frequency 50 Hz. The pair of measurements is then considered as a point on a Cartesian plane (see Fig. 1) whose axes report the IEMG values coming from the above mentioned muscles—the axes range goes from 0 to 255 since the IEMG is collected as an 8-bit integer.

A proper dataset has been collected to train, validate and test the classifier. A real patient suffering from SMA voluntarily enrolled in this study. He has been asked to reproduce for about 60 s the muscle contractions he would have liked to associate to each of the three possible exoskeleton’s behaviors (hand opening, closing, and resting). This dataset—roughly 3000 samples for each gesture, for a total of about 9000 samples—has been labelled on the go by an operator (supervised learning), and has hence been split into the training set (equal to the 80% of the data, randomly chosen), and the testing set (the remaining 20%).

The training of the PIP classifier consisted in the drawing, by external intervention, of the polygonal areas that circumscribed the IEMG samples corresponding to the hand opening and closing intention (see Fig. 1). The coordinates of the polygon vertices are then stored in the EEPROM memory of the Pro Trinket micro-controller which use them to real-time classify each new sEMG sample.

4 Results and Conclusions

From the confusion matrix shown in Fig. 2, it can be seen that the resulting metrics have achieved values ranging from 93.2 to 93.4%, confirming valuable performance.

Fig. 1 The figure shows a sample of the acquired sEMG dataset, in particular the training and validation set is reported here; in green, blue and red, the opening, the closing and the resting samples respectively. Besides, the decision boundaries after the training and validation phase are shown

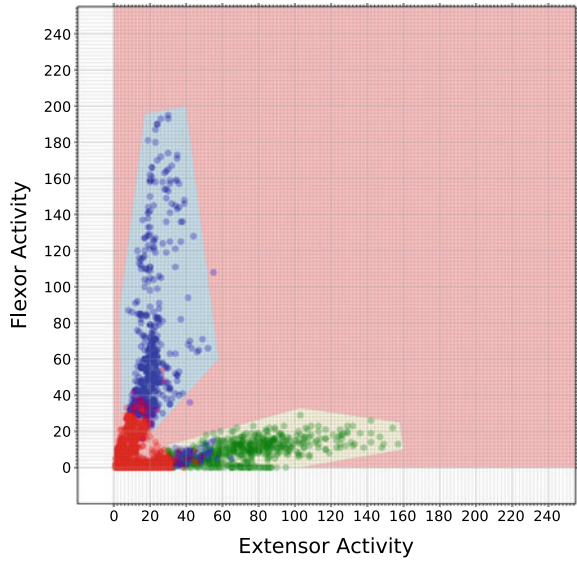


Fig. 2 The confusion matrix of the proposed Point-in-Polygon-based classifier (Accuracy: 0.934, Precision: 0.932, Recall: 0.932)

True label	opening	0.958	0.000	0.042
	closing	0.096	0.860	0.044
	resting	0.023	0.029	0.947
		opening	closing	resting
		Predicted label		

Furthermore, the confusion matrix highlights a tiny number of misclassifications in which the movement that is opposite to the desired one is predicted (i.e., hand opening intentions classified as hand closing ones, and vice versa). This result is especially important since such errors can be annoying for the user and harmful both for the user and the device due to the sudden motion inversion. Besides, circumscribing only hand opening and closing intentions makes the algorithm implicitly classifying the remaining part of the plan as “resting”. These misclassification are indeed harmless since such errors are not associated with any exoskeleton movement.

This study has presented an analytical and quantitative analysis of the classification performance of a PIP-based sEMG classifier. In this research activity, the examined scenario concerned the classification of three possible hand gestures to accordingly control a wearable hand exoskeleton in assisting people with hand dis-

abilities. The evaluation metrics outline the algorithm's correct functioning. Finally, the qualitative analysis of the nature and structure of the decision boundaries shows remarkable robustness against motion artifacts disturbances.

References

1. N. Secciani, M. Bianchi, A. Meschini, A. Ridolfi, Y. Volpe, L. Governi, B. Allotta, Assistive hand exoskeletons: the prototypes evolution at the University of Florence, in *The International Conference of IFToMM ITALY* (2019), pp. 307–315
2. N. Nazmi, M. Abdul Rahman, S.-I. Yamamoto, S. Ahmad, H. Zamzuri, S. Mazlan, A review of classification techniques of EMG signals during isotonic and isometric contractions. *Sensors*, **16**(8), 1304 (2016)
3. F. Montagnani, M. Controzzi, C. Cipriani, Independent long fingers are not essential for a grasping hand. *Sci. Rep.* **6**, 35545 (2016)
4. N. Secciani, M. Bianchi, A. Ridolfi, F. Vannetti, B. Allotta, Assessment of a hand exoskeleton control strategy based on user's intentions classification starting from surface EMG signals, in *International Symposium on Wearable Robotics* (2019), pp. 440–444

Perceived Exertion During Robot-Assisted Gait After Stroke



Nina Lefeber, Emma De Keersmaecker, E. Kerckhofs, and E. Swinnen

Abstract The present study investigated the level of perceived exertion during robot-assisted walking in non-ambulatory stroke survivors. In addition, we studied the relationship between the user's subjective level of perceived exertion and objective measures of exertion (i.e. oxygen consumption and heart rate). Our results suggest that stroke survivors perceive fully assisted Lokomat walking as extremely light to very light and fully assisted Ekso GT walking as very light to somewhat hard. Weak positive correlations were found between subjective and objective measures of exertion.

1 Introduction

Worldwide, stroke is a prevalent health issue. Each year, roughly 15 million people experience a stroke. Initially after stroke, half of the stroke survivors is unable to walk and around 12% needs assistance of a person to walk [1]. As a result, stroke survivors spend the majority of their rehabilitation time on practicing walking (25–45%) [2].

To induce neuroplasticity, gait rehabilitation requires sufficient training intensity. To increase the intensity and volume of gait rehabilitation, two types of lower limb

The work of N. Lefeber and E. De Keersmaecker was supported by the Research Foundation Flanders (FWO).

N. Lefeber (✉) · E. De Keersmaecker · E. Kerckhofs · E. Swinnen
Rehabilitation Research Group, Vrije Universiteit Brussel, Brussels, Belgium
e-mail: nina.lefeber@vub.be

E. De Keersmaecker
e-mail: Emma.De.Keersmaecker@vub.be

E. Kerckhofs
e-mail: Eric.Kerckhofs@vub.be

E. Swinnen
e-mail: Eva.Swinnen@vub.be

robotic exoskeletons have been introduced: (1) static (or treadmill-based) exoskeletons, such as the Lokomat (Hocoma), and (2) dynamic (or wearable) exoskeletons, such as the Ekso GT (Ekso Bionics) [3]. However, few studies have evaluated the training intensity of robot-assisted gait rehabilitation after stroke [4].

The aims of this study were: (1) to investigate how physically exerting stroke survivors perceive static and dynamic exoskeleton training and (2) to investigate if the user's subjective level of exertion correlates with objective physiological measures of exertion.

2 Methods

2.1 Study Protocol

In this manuscript, we present a secondary analysis of the data collected as part of two clinical trials investigating the physiological responses during robot-assisted gait after stroke. Detailed descriptions of the protocols can be found elsewhere [5, 6]. The studies were approved by the medical ethics committees of the University Hospital Brussels (B.U.N. 143201526040 and 143201734424), the Jessa Hospital Hasselt (16.124/reva16.15), the IRCCS Fondazione Santa Lucia Rome (CE/PROG.630) and the GasthuisZusters Antwerp Hospitals (HD/vv/2018/07.19). All participants signed consent prior to participation in this trial.

2.2 Participants

We included 20 adult non-ambulatory stroke survivors (functional ambulation category ≤ 2) in the subacute stage after stroke (1 week to 6 months) and excluded persons with unstable cardiovascular conditions, lower limb musculoskeletal problems (unrelated to stroke), concurrent pulmonary diseases, concurrent neurological diseases, communicative or cognitive problems constraining the ability to comprehend and follow instructions, and other contra-indications for exoskeleton training (Table 1).

2.3 Experimental Procedure

One group ($n = 10$) walked 20 minutes on a treadmill wearing a static lower limb exoskeleton (Lokomat, Hocoma; Fig. 1). Robotic assistance was set to the maximum (100%). The level of bodyweight was decreased as much as tolerable and the walking speed was increased as much as tolerable (Table 1).

Table 1 Participant characteristics

Outcome	Lokomat group (n = 10)	EksoGT group (n = 10)
Age (years)	66 (11)	71 (9)
Sex (male/female)	6/4	5/5
BMI (km/m ²)	25 (3)	23 (3)
Time since stroke (days)	89 (40)	50 (42)
FAC (0/1/2)	1/2/7	0/7/3
β-blockers (yes/no)	4/6	4/6
Bodyweight support (%)	44 (7)	–
Walking speed (m/s)	0.61 (0.03)	0.21 (0.02)

Continuous variables are reported as mean (standard deviation) and categorical variables as numbers

BMI body mass index; *FAC* functional ambulation category

A second group (n = 10) walked 20 minutes overground wearing a mobile lower limb exoskeleton (Ekso GT™, Ekso Bionics; Fig. 1). Robotic assistance was set to the maximum (100%). Participants walked at a self-selected walking speed and did not use any walking aid. A certified and experienced physiotherapist guided the exoskeleton in the back.

At the start of each session, a flexible mouth mask, portable respiratory gas analysis system (MetaMax3B, Cortex, Germany) and heart rate belt (Polar H7, Polar, Finland) were fitted. Participants rested in their wheelchair for 5 minutes wearing the equipment. Thereafter, participants were accommodated in the exoskeleton. Gas exchange and heart rate were monitored from the beginning of rest to the end of walking. At the end of seated rest and every 3 or 5 minutes during walking (resp. Lokomat and EksoGT group), participants were asked to rate their rating of perceived exertion (RPE) by pointing on a 6–20 Borg Scale (6 meaning “no exertion at all” and 20 meaning “maximum exertion”). Gas and volume calibrations were performed in accordance with manufacturer’s instructions. Participants were asked not to consume food, alcohol, caffeine, or nicotine at least 3 h prior to the sessions, nor to perform additional strenuous activities (apart from their regular therapy) at least 12 h prior to the sessions.

2.4 Outcomes

Outcomes of interest were RPE (6–20 Borg scale), heart rate (beats/min) and oxygen consumption (mL/kg/min). The first 4 minutes (EksoGT group) and 5 minutes

Fig. 1 Illustration of a person in the static Lokomat (left) and dynamic Ekso GT™ (right) exoskeleton (© Johan Swinnen)



(Lokomat group) of walking were used to reach a steady-state condition and were omitted from the analyses.

2.5 Statistical Analysis

Repeated measures ANOVAs were conducted to investigate changes in RPE over time. Pearson correlation coefficients were calculated to measure the relationship between RPE, oxygen consumption and heart rate (SPSS version 25).

3 Results

In both groups, RPE significantly increased over time (Lokomat: $F(4.906, 1.236)$, $p = 0.043$; Ekso GT: $F(8.791, 3)$, $p = 0.0004$; Fig. 2) and RPE was weakly correlated with objective measures of exercise intensity (Table 2).

Fig. 2 Mean (95% CI) rating of perceived exertion during 20-minute Lokomat and EksoGT walking

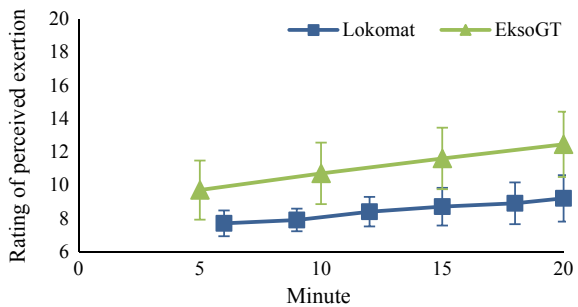


Table 2 Pearson correlation coefficients between subjective and objective measures of exertion

	Group	Minute	VO ₂	HR
RPE	Lokomat	6	0.30	0.50
		9	0.08	0.45
		12	0.26	0.18
		15	0.01	0.52
		18	0.08	0.43
		20	0.06	0.44
	Ekso GT	5	0.21	0.11
		10	0.01	0.05
		15	0.03	0.15
		20	0.42	0.45

* $p < 0.05$ *HR* heart rate; *VO₂* oxygen consumption; *RPE* rating of perceived exertion

4 Discussion and Conclusion

Our results suggest that non-ambulatory stroke survivors perceive fully assisted Lokomat walking as extremely light to very light and fully assisted Ekso GT walking as very light to somewhat hard. However, since patient characteristics were not matched between both groups, no between-group comparisons could be made. Weak correlations between the subjective and objective measures of exercise intensity in both groups suggest that subjective measures alone may be insufficient to monitor exercise intensity during robot-assisted gait rehabilitation. A more extensive set of subjective and objective measures (including e.g. motivation and discomfort) should be studied in future large-scale trials.

Acknowledgements The authors would like to thank the patients and therapists of the neurorehabilitation units of the IRCCS Fondazione Santa Lucia, the Jessa Hospital campus St-Ursula and the Rehabilitation Hospital RevArte for participating in this trial.

References

1. H.S. Jorgensen, H. Nakayama, H.O. Raaschou, T.S. Olsen, Recovery of walking function in stroke patients: the Copenhagen stroke study. *Arch. Phys. Med. Rehabil.* **76**(1), 27–32 (1995)
2. N.K. Latham et al., Physical therapy during stroke rehabilitation for people with different walking abilities. *Arch. Phys. Med. Rehabil.* **86**(12 Suppl 2), S41–S50 (2005)
3. G. Morone et al., Robot-assisted gait training for stroke patients: current state of the art and perspectives of robotics. *Neuropsychiatr. Dis. Treat* **13**, 1303–1311 (2017)
4. N. Lefeber, S. De Buyzer, N. Dassen, E. De Keersmaecker, E. Kerckhofs, E. Swinnen, Energy consumption and cost during walking with different modalities of assistance after stroke: a systematic review and meta-analysis. *Disabil. Rehabil.* **17** (2019)

5. N. Lefeber, et al., Physiological responses and perceived exertion during robot-assisted treadmill walking in non-ambulatory stroke survivors. *Disabil. Rehabil.* 1–9 (2019)
6. N. Lefeber, et al., Robot-assisted overground walking: physiological responses and perceived exertion in nonambulatory stroke survivors. *IEEE Robot. Autom. Mag.* (2019)

Pilot Testing of a New Questionnaire for the Assessment of User Experience During Exoskeleton-Assisted Walking



I. Pisotta, N. L. Tagliamonte, A. Bigioni, F. Tamburella, M. Lorusso, F. Bentivoglio, I. Pecoraro, P. Argentieri, F. Marri, L. Zollo, and M. Molinari

Abstract Scientific literature provides weak attempts in analyzing user experience during the use of rehabilitation and assistive wearable robotic devices. The objective of this study is to develop and preliminary test a new questionnaire evaluating the subjective perspective of people using lower limb exoskeletons. A literature search was conducted to investigate acceptance and usability/quality models, theories and questionnaires with the aim of extracting relevant factors to be considered. A four-factor questionnaire was developed and its feasibility was tested on four participants with central nervous system lesions walking with overground and treadmill-based exoskeletons in rehabilitation scenarios.

1 Introduction

User Experience (UX) is defined by ISO 9241-210 as “*user’s perceptions and responses that result from the use or anticipated use of a product, system or service*” [1]. UX has been recognized to be central in the development and evaluation of assistive and rehabilitation robotic technologies even if current scientific literature does not provide systematic and validated methods for its assessment, especially in the field of wearable robotics. The most successful development results can be potentially achieved when users are involved in every step of the design process through either direct feedback, testing, observation or informed evaluation or by

Partial financial support was provided by: (i) EXPERIENCE, funded by the FSTP-1 cascade funding program H2020 EU project EURO BENCH (ICT-2017-1-779963); (ii) the Italian Ministry of Health under *Ricerca Corrente* program; (iii) Italian Ministry of Health *Ricerca Finalizzata* program 2018 (GR-2018-12367485).

I. Pisotta (✉) · A. Bigioni · F. Tamburella · M. Lorusso · P. Argentieri · F. Marri · M. Molinari
Spinal Rehabilitation Laboratory (SPIRE Lab) and Laboratory of Robotic Neurorehabilitation
(NeuroRobot Lab), Neurorehabilitation 1 Department, Fondazione Santa Lucia, Rome, Italy
e-mail: i.pisotta@hsantalucia.it

N. L. Tagliamonte · F. Bentivoglio · I. Pecoraro · L. Zollo
Research Unit of Advanced Robotics and Human-Centred Technologies (CREO Lab), Università
Campus Bio-medico di Roma, Rome, Italy

using previously gathered information on user needs and perspective. If this process is not pursued, the well-known phenomenon of technology abandonment and a high dropout rate during prototypes testing, may occur. Exoskeleton technology has evolved substantially over the past decade as an adjunctive therapy to enhance neurorehabilitation or as an aid to improve the quality of life of people with disabilities [2]. Anyhow, there are few examples of a substantial users' involvement in the process of development of new devices and minimal evidence, nor even consensus, on the assessment of UX, as shown by the heterogeneity of studies surveyed in [2].

In this framework, we developed a novel multi-factor questionnaire for the assessment of UX during the use of lower limb exoskeletons. In this paper we present our new tool and the preliminary tests carried out with an overground exoskeleton and a treadmill-based exoskeleton, including in the study stroke and incomplete Spinal Cord Injury (iSCI) participants.

2 Materials and Methods

2.1 Questionnaire Development

We identified the relevant factors for the development of the new questionnaire by reviewing the literature and by identifying psychological theories on technology acceptance and usability/quality models suitable to assess UX during the use of rehabilitation and assistive robotic systems. These models and theories have been applied in a wide variety of domains to understand and predict users' behavior and adoption of new technologies [3, 4]. Moreover, they have been demonstrated to be the theoretical ground needed to build evaluation processes by taking into account the totality of aspects involved in the UX. In the revision process, we also included questionnaires available in the fields of robotic neurorehabilitation [2, 5]. We finally selected the factors that affect (or could be influenced by) UX during exoskeletons usage. In particular, we identified 16 Sub-Factors grouped in 4 Factors: Usability, Acceptability, Perceptibility and Functionality (Fig. 1).

Each of the Sub-Factors includes a variable number of items to be rated on a 7-point Likert-type scale (from 1 “*I strongly disagree*” to 7 “*I strongly agree*”). The total score for each Sub-Factor is obtained averaging its related item scores. Each

Usability	Perceptibility	Acceptability	Functionality
Effectiveness ES	Embodiment and Ownership EO	Attitude toward Technology AT	Learnability LY
Efficiency EY	Agency AG	Self-Efficacy SE	Flexibility FY
Satisfaction SN	Emotion and Attachment EA	Motivation MN	Robustness and Reliability RR
	Health and Quality of life HQ	Comfort CT	Workload WD
		Safety SY	

Fig. 1 Factors and sub-factors of the developed questionnaire

Factor score is calculated as the weighted average among the related Sub-Factor scores. The weights are derived from the pairwise comparison between Sub-Factors administered to the subject under testing. In particular, Sub-Factors are sorted based on the number of expressed preferences and the weights are consequently assigned.

The questionnaire was developed to assess exoskeleton-aided walking during overground rehabilitation (Overground Rehabilitation Exoskeleton, ORE) and treadmill rehabilitation (Treadmill Rehabilitation Exoskeleton, TRE). 115 general purpose items, shared between the two applications, are merged to application-specific (TRE or ORE) items. Overall, ORE questionnaire consists of 132 items, while TRE questionnaire consists of 124 items.

2.2 Questionnaire Testing

We tested the questionnaire in Italian on 4 participants: P1 (stroke, 35 y.o.) and P2 (iSCI, 57 y.o.) used the Ekso GT (Ekso Bionics) while P3 (iSCI, 35 y.o.) and P4 (iSCI, 64 y.o.) used the Lokomat Pro (Hocoma). The protocol was approved by Fondazione Santa Lucia Ethics Committee. Participants underwent at least 4 preliminary walking sessions to become familiar with the devices. During these familiarization sessions, a physiotherapist performed the mechanical adjustment of the systems based on the anthropometric assessment of the participants, and the regulation of the parameters related to the robotic support, according to the participant's needs and residual motor functions. After the familiarization, a measurement session was carried out for data collection. Before questionnaire administration, performed by an expert psychologist, participants received instructions on the questionnaire in order to know in advance aspects needing specific focus during the exoskeleton experience. The measurement session was supervised by the same physiotherapist and with the same walking conditions as in the familiarization phase. After the assessment, the participants were also asked to score the questionnaire itself in terms of clarity of definitions and methodology of administration.

3 Results

In the ORE application (Fig. 2), participants P1 and P2 showed a very similar behavior in evaluating Usability and Acceptability. The difference in the evaluation of AT was probably affected by age-related perception. In assessing Perceptibility, P1 provided higher scores in HQ, AG and EO. The difference in the assessments of P1 and P2 were likely due to the different clinical conditions affecting the analyzed Sub-Factors. In the Functionality assessment P2 rated the WD as very high. Also this Sub-Factor could be influenced by age.

Results of P3 and P4 are reported in Fig. 3. In assessing Usability P4 rated as low the SN and both participants rated as low the EY. In the Acceptability factor both

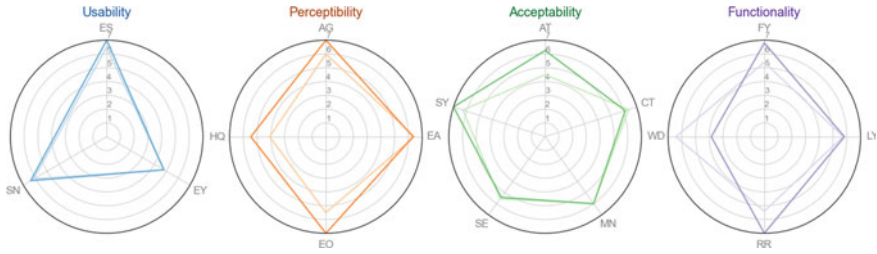


Fig. 2 Results of the Sub-Factors for the ORE application. P1 in dark color and P2 in light color

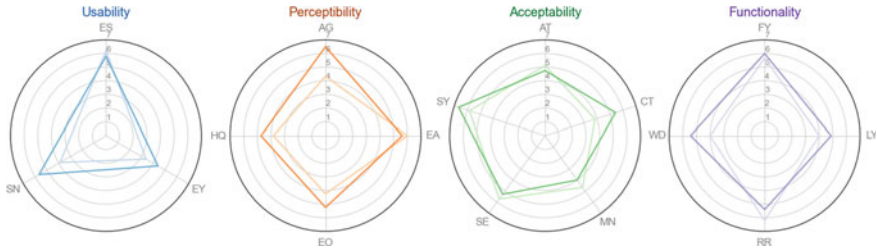


Fig. 3 Results of the sub-factors for TRE application. P3 in dark color and P4 in light color

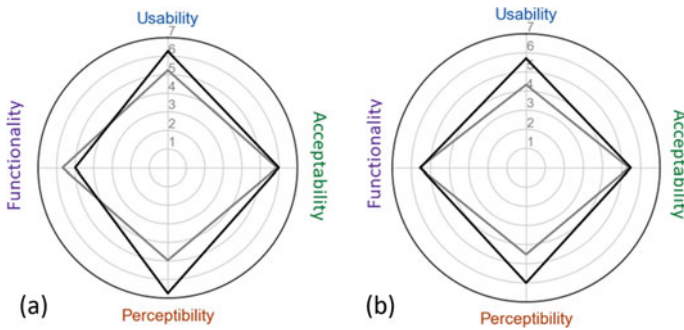


Fig. 4 Results of the factors for the ORE (a) and TRE (b) applications

participants rated MN and AT as low and P4 rated the CT as very low. In Perceptibility assessment, P3 and P4 provided the same evaluation except for AG (rated as very low by P4). Moreover, there are similarities in the Functionality Sub-Factor ratings, except for WD that was evaluated as very high by P4. The overall results of the Factors had a similar trend among the 4 participants: for both applications (Fig. 4), participants rated as equal Acceptability and Functionality, while they disagreed on Usability and Perceptibility. It is also worth to highlight the importance of external determinants as age and clinical conditions, that could affect specific Sub-Factors, providing a theoretical justification for the differences in the evaluation. Moreover, the participants positively evaluated the whole questionnaire, the assessment method-

ology, the clarity of items and the definitions of Factors and Sub-Factors. Even if participants considered a bit long the administration time, none of them withdrew from the study.

4 Conclusion

We designed a new four-factor questionnaire for the assessment of UX during exoskeleton-assisted walking. In our pilot study we confirmed the feasibility and applicability of our tool for the assessment of Factors involved in the targeted application and its adaptability in different scenarios (overground and treadmill-based walking). We are confident that this new tool will contribute to the improvement of rehabilitation technologies by including the results of user subjective perspective in the design process. Future activities will be devoted to enlarge the cohort of participants to possibly achieve statistical validation of the questionnaire.

References

1. ISO DIS 9241-210. *Ergonomics of Human System Interaction-Part 210: Human-Centered Design for Interactive System. Technical Report* (ISO, Switzerland, 2010)
2. D. Hill, et al., What are user perspectives of exoskeleton technology? *Int. J. Tech. Assess. Health Care* **33**(2), 160–167 (2017)
3. V. Venkatesh et al., User acceptance of information technology: toward a unified view. *MIS Q.* **27**(3) (2003)
4. K. Sagar et al., A systematic review of software usability studies. *Int. J. Inf. Tech.* **11**, (2017). <https://doi.org/10.1007/s41870-017-0048-1>
5. Y. Koumpouros, A systematic review on existing measures for the subjective assessment of rehab and assistive robot devices. *J. Health Eng.* 1048964 (2016)

Psychophysiological Assessment of Exoskeleton-Assisted Treadmill Walking



I. Pecoraro, N. L. Tagliamonte, C. Tamantini, F. Cordella, F. Bentivoglio, I. Pisotta, A. Bigioni, F. Tamburella, M. Lorusso, P. Argentieri, M. Molinari, and L. Zollo

Abstract Despite being able to derive quantitative data on motor performance, rehabilitation robots typically do not provide information on users' subjective experience, and in particular on their psychophysiological state. The aim of this work was the development of a method for the psychophysiological assessment of users whose treadmill walking is assisted by a lower limb exoskeleton. Four indicators were estimated based on physiological data by using a Fuzzy logic approach. The assessment of human-exoskeleton interaction was performed on a group of four healthy participants and the correlation between different pairs of indicators was evaluated.

1 Introduction

Neurological diseases often lead to motor disorders and gait alterations. Neurorehabilitation allows patients to recover independent walking in daily life activities and may involve the use of robotic systems, such as exoskeletons, to enhance conventional physical therapy. Among several benefits, rehabilitation robots offer the possibility of collecting data on the subjects' motor performance based on embedded sensors (joint angles and torques, interaction forces, etc.). Anyhow, these systems typically do not provide information on the subjective experience of users and, in particular, on their PsychoPhysiological (PP) state. In many applications of robot-aided therapy it is useful to identify the PP state of the patient to monitor motivation and active participation since these factors can improve motor recovery and therefore

Partial financial support was provided by: (i) the sub-projects EXPERIENCE and BenchBalance, funded by the FSTP-1 cascade funding program of the H2020 EU project EUROBENCH (ICT-2017-1-779963); (ii) the Italian Ministry of Health under *Ricerca Corrente* program.

I. Pecoraro · N. L. Tagliamonte (✉) · C. Tamantini · F. Cordella · F. Bentivoglio · L. Zollo
Research Unit of Advanced Robotics and Human-Centred Technologies (CREO Lab), Università Campus Bio-Medico di Roma, Rome, Italy
e-mail: n.tagliamonte@unicampus.it

I. Pisotta · A. Bigioni · F. Tamburella · M. Lorusso · P. Argentieri · M. Molinari
Spinal Rehabilitation Laboratory (SPIRE Lab) and Laboratory of Robotic Neurorehabilitation (NeuroRobot Lab), Neurorehabilitation 1 Department, Fondazione Santa Lucia, Rome, Italy

© The Author(s), under exclusive license to Springer Nature Switzerland AG 2022

201

D. Torricelli et al. (eds.), *Converging Clinical and Engineering Research on Neurorehabilitation IV*, Biosystems & Biorobotics 28,
https://doi.org/10.1007/978-3-030-70316-5_33

the outcome of neurorehabilitation [1]. In the last decade, many attempts have been made to develop a reliable methodology for the automatic identification of the PP state of a subject, starting from the analysis of facial expressions and posture [2]. Anyhow, the most effective solutions are based on the detection and evaluation of specific physiological signals and on the extraction of relevant indicators [3]. Indeed, autonomous physiological responses can be detected as a function of certain stimuli, during the use of video games or the interaction with robotic systems [3]. The analysis of the literature highlighted the lack of studies investigating physiological measures to determine the PP state during walking aided by lower limb assistive and rehabilitation exoskeletons. The objective of this work was to develop a method for the PP assessment during exoskeleton-assisted treadmill walking and to test it with healthy participants.

2 Materials and Methods

2.1 Experimental Setup

Physiological signals of interest, i.e. the Galvanic Skin Response (GSR), the Heart Rate (HR), the Heart Rate Variability (HRV) and the Respiration Rate (RR), were measured by means of two commercial devices: the ZephyrBioModule 3 sensor (Medtronic), a chest belt measuring the RR and the electrocardiogram (ECG), and the Shimmer sensor (Shimmer), acquiring GSR by using two electrodes positioned on the index and middle fingers.

Data from the two sensors were sent to a host PC via Bluetooth Low Energy protocol (ECG signal was sampled 250 Hz while the other signals were sampled 25 Hz) and were synchronized through a C# interface. The treadmill-based exoskeleton Lokomat Pro (Hocoma), available at Neurorehabilitation 1 Department of Fondazione Santa Lucia (FSL) in Rome, was employed.

2.2 Experimental Protocol

Four healthy participants (1 male and 3 female, 34.0 ± 15.7 y.o.) were involved in the study. Each one performed at least 2 preliminary walking sessions with the Lokomat to become familiar with it. After the familiarisation sessions, a measurement session was carried out for data collection. Each (familiarisation or measurement) session lasted about 60 min including preparation time. The measurement session was divided in two phases: *i*) participants were seated in a comfortable position for 4 min, with their eyes closed and acoustically isolated to promote relaxation (*Resting Baseline*, RB); *ii*) participants underwent exoskeleton-assisted walking for 20 min with the assistance level set to walk comfortably, similarly to the setting achieved

during the familiarization session (*Exoskeleton Training*, ET). The protocol was approved by the FSL Ethics Committee (no: CE/PROG 746).

2.3 Data Analysis

Three features were extracted from the ECG data: the HR and two HRV metrics, i.e. the RMS of successive heart beats (rMSSD) and the power distribution in the Low-Frequency (LF) band (0.04–0.15 Hz). Two components were extracted from the GSR signal: Skin Conductance Level (SCL), i.e. the tonic level in the absence of any particular environmental event, and the Skin Conductance Response (SCR), i.e. an event-dependent, phasic and highly responsive parameter. Among different possible methods, a Fuzzy logic approach was selected and implemented for the extraction of four PP indicators of interest: *stress level* (measure of perceived safety), *fatigue level* (measure of prolonged physical engagement), *energy expenditure* (measure of comfort), *attention level* (measure of involvement). The physiological signals of the ET phase were considered only for the last 15-min recording and were normalized with respect to the data collected during the RB phase. The employed Fuzzy logic method included 6 inputs (HR, RMSSD, RR, SCR, SCL and LF) and 4 outputs (PP indicators). For each physiological signal, the membership functions were constructed by considering the total number of occurrences in all the collected data [7]. Low, medium and high levels for the model inputs and outputs were introduced. IF/THEN rules were defined based on trends of variation of physiological signals retrieved from a careful analysis of the scientific literature [4–6]. These rules combine all the input physiological data to estimate the four PP indicators in time intervals of 1 min, considered suitable for reasonable changes within the present application. A participant-specific and a global statistical analysis were performed to find correlations among PP indicators. In particular, the Spearman's correlation coefficient ρ was calculated in pairwise comparisons.

3 Results and Discussion

In Fig. 1 the time-series of the four PP indicators along 15 min of recordings (first row) and their pairwise correlations (second row) are reported. For the four participants, we found a high correlation ($|\rho| \geq 0.5$) in two cases: positive correlation between stress level and energy expenditure $\rho = 0.84 \pm 0.21$ and $p = 0.01 \pm 0.03$ (mean \pm SD) and negative correlation between energy expenditure and fatigue level $\rho = -0.56 \pm 0.47$ and $p = 0.17 \pm 0.34$ (mean \pm SD). Hence, as energy expenditure increases, stress level increases and fatigue decreases. Other correlations for pairs of PP indicators were heterogeneous among participants. Negative correlation between fatigue and stress levels was common for P1 and P2 ($\rho = -0.72$ and $\rho = -0.84$, respectively). Different results were found for the attention-stress ($\rho = 0.91$ and

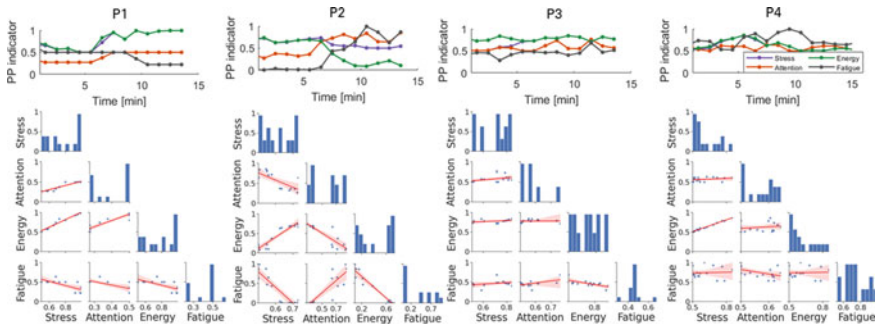


Fig. 1 First row: Time-series of the PP indicators along 15 min of the ET recording; a common trend among all the participants was not clearly evidenced. Second row: Pairwise correlations of the PP indicators (on the diagonal the univariate distribution of the data is shown; in the other cells the linear regression models fitted on the scatter plots are reported); positive stress-energy correlation and negative energy-fatigue correlation were found

$\rho = -0.66$ for P1 and P2, respectively), the energy-attention ($\rho = 0.89$ and $\rho = -0.85$ for P1 and P2, respectively) and the fatigue-attention ($\rho = -0.62$ and $\rho = 0.89$ for P1 and P2, respectively) correlations. A common trend for all participants was not clearly evidenced in PP time-varying patterns (Fig. 1).

4 Conclusions

The present work was devoted to estimate PP indicators for the assessment of human-exoskeleton interaction during treadmill walking. Due to the limited number of participants the method was demonstrated to be effective only in highlighting a correlation between energy expenditure and both stress and fatigue levels. Additional correlations in pairwise comparisons were heterogeneous and also no trends of variation in the time-series of the PP indicators were evidenced. More clear explanations for these preliminary findings (fatigue-energy-stress correlations) will deserve further investigations in a wider group of participants, possibly also including subjects with lesions of the central nervous system. Moreover, a correlation with subjective evaluations, assessed by means of dedicated questionnaires, will be performed.

References

1. R. Riener et al., Bio-cooperative robotics: controlling mechanical, physiological and mental patient states, in *2009 IEEE International Conference on Rehabilitation Robotics ICORR 2009*(July), 407–412 (2009)
2. F. T. Sun et al., Activity-aware mental stress detection using physiological sensors, in *Lecture Notes of the Institute for Computer Sciences, Social Informatics and Telecommunications*

Engineering LNICST, vol. 76 LNICST, no. April 2015 (2012) pp. 282–301

3. F. Cavallo et al., Emotion modelling for social robotics applications: a review. *J. Bionic Eng.* **15**(2), 185–203 (2018)
4. D. Novak et al., Psychophysiological responses to robotic rehabilitation tasks in stroke. *IEEE Trans. Neural Syst. Rehabil. Eng.* **18**(4), 351–361 (2010)
5. Y. (David) Shi, Galvanic skin response (GSR) as an index of cognitive load Conference on Human Factors in Computing systems, ed. by Chi, et al., *San Jose* (California, USA, 2007)
6. S. Miller, *Workload Measures Literature Review*
7. R.L. Mandryk et al., A fuzzy physiological approach for continuously modeling emotion during interaction with play technologies. *Int. J. Hum. Comput. Stud.* **65**(4), 329–347 (2007)

Kinematic and Functional Evaluation of a 3D Printed Robotic Hand



V. Bueyes-Roiz, I. Quiñones-Uriostegui, L. Anaya-Campos, J.L. Zavaleta-Ruiz, G. Rodríguez-Reyes, and Y. Quijano

Abstract The hand has a complex structure that allows us to perform daily living activities. When the hand is lost, hand prosthesis is used to restore the lost functions, usually, a hook is used and, in some cases, a mechanical hand. In the last few years, there has been a growth in 3D prosthetic designs since it has many benefits. We propose a method to test both the functionality and kinematic performance of a prosthesis and his/her user respectively. All types of activities performed with the hook were above 4 points on average, while depending on the type of activity the average score for the mechanical and 3D printed hand varied. The overall performance was 100% for the hook, while for the mechanical 69% and 3D printed hand was below 60%.

1 Introduction

The hand is a body segment that allows us to interact with the environment, through object manipulation in such a way that we can perform daily living activities that give us independence, this by making eight different types of hand grasp. When the hand is lost, hand prosthesis have been placed on upper limb amputees to replace the lost segment, and its objective is to restore the lost functions usually they are body-powered meaning that the body needs to move in a certain way to operate the terminal device (hand prosthesis) habitually this device is a hook, even though it is not anatomically correct, it is low maintenance and their dexterity allows to perform most of the daily living activities [1].

On the other hand, 3D printing is a process that creates solid, three-dimensional objects with the use of digital files [2], in the last years there has been a growth in 3D prosthetic designs since their benefits include lower cost (usually between \$50 to \$300 USD compared to robotic prosthetics \$5000 to \$100,000 USD), speed (their

V. Bueyes-Roiz (✉) · I. Quiñones-Uriostegui · L. Anaya-Campos · Y. Quijano
Movement Analysis Laboratory, National Institute of Rehabilitation, Mexico City, Mexico

J.L. Zavaleta-Ruiz · G. Rodríguez-Reyes
Prosthetics and Orthotics Laboratory, National Institute of Rehabilitation, Mexico City, Mexico

© The Author(s), under exclusive license to Springer Nature Switzerland AG 2022

207

D. Torricelli et al. (eds.), *Converging Clinical and Engineering Research on Neurorehabilitation IV*, Biosystems & Biorobotics 28,

https://doi.org/10.1007/978-3-030-70316-5_34

fabrication can be in one day), versatility (different terminal devices can be made with specific needs) and all of them can be customizable [3]. Anyone that wants to create a 3D printed hand can use a search engine to find several options of printable hands such as “The Open Hand Project” [4] or “National Institutes of Health 3D Print Exchange” [5] between others, each option include files and tutorials on how to make and assemble a 3D printed hand [6, 7].

To our knowledge, there does not exist a 3D printed prosthetic hand that can replace all the functions the human hand, and we think that there is a necessity of showing the advantages and disadvantages of this kind of devices to the end-user to make an informed choice of what kind of hand the user is going to have. The aim of this project was to design a functionality test and a kinematic test to evaluate the user performance when using the 3D printed prosthetic hand and determine if there are abnormal movements that could prone the user to an injury.

2 Materials and Methods

A third-party 3D printed hand that claimed to replace the human hand and have great functionality was used. This hand consisted of five fingers that could move as follows, thumb included a rotation and flexion movement, an index finger with independent flexion while the middle, ring, and little fingers move together and only can flex. All of the hand movements were enabled by independent motors and were activated by an electrical switch input the patient could push in their shoe sole. The protocol was reviewed and approved by the Research and Ethics Committee of the National Institute of Rehabilitation in Mexico City. A 60-year-old male patient with 17 years using a mechanically powered prosthesis with a hook to perform its daily living activities, participated in this experiment. The subject was trained for five sessions of one hour over five days to be familiarized with the device and not measure its learning curve.

The functionality test consisted of 35 daily living activities divided into four groups: only grasping (G), grasping with weight (G & W), and grasping, weight, and ability (G,W & A), each item or task was based on completion, and on the time required to complete each one, if it took more than one minute to complete it was considered not functional. Each item was graded from 1 to 5, 5 being an item completed without difficulty and in less than 20s and 1 a task that could not be completed or it took over a minute, in the end, all items score were added, the functionality test was carried out using the subjects choice terminal device (hook 5X-R), an ottobock mechanical hand (8K23) and the 3D printed hand previously described, we defined an item as functional if the score was over 3 points. Finally, a kinematic test was carried out, in which we selected one activity of each group, intending to find movement differences regarding trajectories and range of motion, for this test the subject was instrumented with reflective markers on the prosthetic

arm, terminal device, and trunk and measured with a 12 flex13 Optitrack System (Natural Point, Corvallis Oregon, USA).

3 Results

The average score of each type of activity obtained with the terminal devices is shown in Fig. 1. All types of activities performed with the hook were above 4 points on average, while depending on the type of activity the average score for the mechanical and 3D printed hand varied. For both hands, the activity with the lowest scores were the ones of grasp and ability such as picking up coins, opening and closing a zipper.

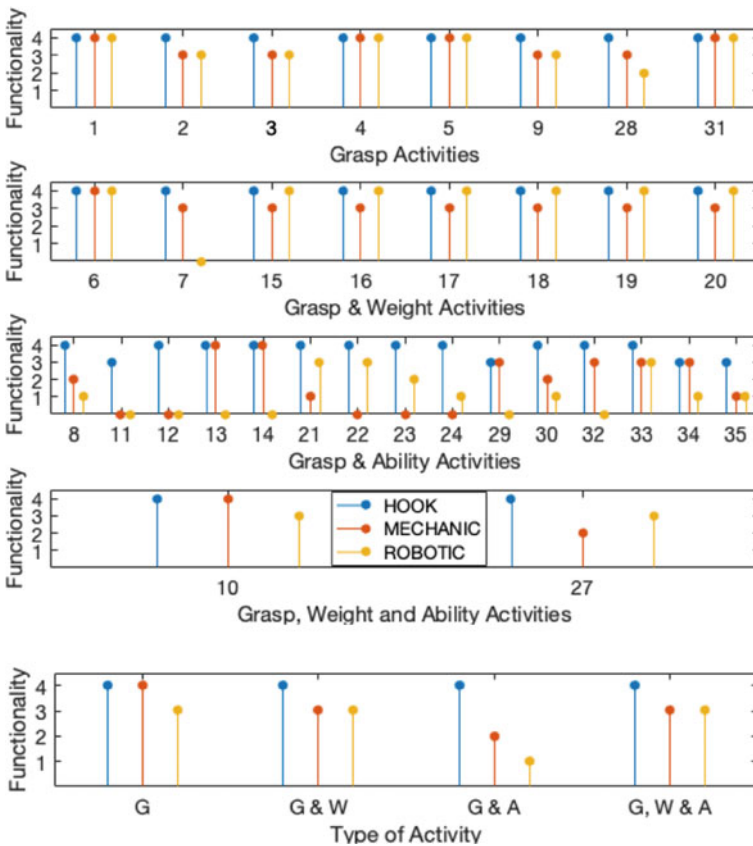


Fig. 1 (Top 1:4) Representations of each of the 35 activities scores. (Bottom) Average of activitie’s scores performed with each terminal device blue hook, orange mechanical hand and yellow 3D printed hand; abbreviations: G, grasp; G & W, grasp and weight; G & A, Grasp and ability; G, W & A, Grasp, Weight and ability

Table 1 Kinematic values for the different type of tasks

		S. max abd	S. max flex	E. ROM
G	Hook	70	47	9
	Mechanical	160	153	20
	3D Printed	47	30	13
G & W	Hook	120	90	30
	Mechanical	160	140	22
	3D Printed	100	80	24
G & A	Hook	23	20	14
	Mechanical	40	70	18
	3D Printed	30	15	14

The overall functionality of each terminal device was 100% for the hook, 69% for the mechanical hand and 57% for the 3D printed hand.

For the kinematic analysis we obtained the maximum shoulder abduction and flexion, and elbow's range of motion for each type of task as seen on Table 1.

4 Discussion

Our main goal for this study besides determining the functional and kinematic differences when using different kinds of prosthetic hands was of determining the feasibility of the procedure with the aims of applying it to a bigger population and evaluating different 3D printed hands. With the subject selected for this study, the results showed that the most effective prosthetic terminal device to perform daily living activities was the hook, with 100% of the functionality, which was expected. On the other hand, the mechanical hand and 3D printed hand have 69 and 57% of functionality respectively, the most difficult task to perform with these devices was the ones of G & A, in which the subject needed to handle small objects and put them on specific places, in these activities the 3D printed hand has a lower score than the mechanical, but for the G& W and G,W & A both hands have similar values. Regarding the kinematic evaluation, we found differences in how the patient moves the shoulder and elbow with each device. We believe that even though the 3D printed hand has more possibilities of movement, the design is not optimal for performing daily living activities and the materials selected does not give traction to create a good grasping of the objects and in case of object manipulation, the grasp loses its traction, which explains the low functionality that is presented.

5 Conclusion

In recent years 3D printed hands have had an increased interest since it has become easier and cheaper to produce one, even though there exist different models, with different option to move the hand and fingers, we do think that it is important to develop functionality test specialized for 3D printed hands and determine their functionality, these with the objective of the developer let know the interested person on acquiring one of their capabilities with each hand.

Acknowledgements Funding support for this project was provided by the Secretaria de Educación, Ciencia, Tecnología e Innovación of Mexico City (SECITI/101/2016 and SECTEI/183/2019). The authors wish to thank Mr. Hernando Ortega from IIMAS-UNAM for providing us the 3D printed hand.

References

1. J. Ferreira, Alves, N., Bartolo, P., Rapid manufacturing of medical prostheses. *IJMTM*. **6**, 567–583 (2004). <https://doi.org/10.1504/IJMTM.2004.005940>
2. J. Ten Kate, G. Smit, P. Breedveld, 3D-printed upper limb prostheses: a review. *Disabil Rehabil Assist Technol*. **12**(3), 300–314 (2017). <https://doi.org/10.1080/17483107.2016.1253117>
3. J. Fajardo, V. Ferman, A. Lemus, E. Rohmer, An Affordable open-source multifunctional upper-limb prosthesis with intrinsic actuation. *IEEE Workshop on Advanced Robotics and its Social Impacts (ARSO)*. Austin, TX **2017**, 1–6 (2017). <https://doi.org/10.1109/ARSO.2017.8025206>
4. Openhandproject.org Retrieved from <http://www.openhandproject.org/?LMCL=MbWcGU>
5. NIH 3D Print Exchange | A collection of biomedical 3D printable files and 3D printing resources supported by the National Institutes of Health (NIH). Retrieved from <https://3dprint.nih.gov/>
6. A. Arjun, L. Saharan, Y. Tadesse, *Design of a 3D Printed Hand Prosthesis Actuated by Nylon 6-6 Polymer Based Artificial Muscles* (2016), pp. 910–915. <https://doi.org/10.1109/COASE.2016.7743499>
7. J. Cuellar, G. Smit, A. Zadpoor, P. Breedveld, Ten guidelines for the design of non-assembly mechanisms: the case of 3D-printed prosthetic hands. *Proc. Inst. Mech. Eng., Part H: J. Eng. Med.* **232**, 095441191879473 (2018). <https://doi.org/10.1177/0954411918794734>
8. T. Campos, UNAM y el gobierno de la CDMX unen esfuerzos para desarrollar esta mano robótica [News post]. Retrieved from <https://www.xataka.com/investigacion/unam-y-el-gobierno-de-lass-cdmx-unen-esfuerzos-para-desarrollar-esta-mano-robotica> (2016)

Evaluation of Balance Abilities in Expert Paralympic Athletes with Lower Limb Amputation



G. Marchesi, A. Bellitto, E. Ricaldone, A. De Luca, C. Sanfilippo, K. Torre, E. Quinland, J. Saglia, V. Squeri, A. Massone, M. Casadio, and A. Canessa

Abstract Amputation of the lower limb affects balance abilities and leads subjects to learn how to balance relying on a single leg. Challenging evaluations for expert athletes, who have greater performance level than those of able-body subjects, are missing. Here, we propose a comprehensive protocol created ad-hoc for expert

G. Marchesi (✉) · A. Bellitto · M. Casadio · A. Canessa
University of Genoa, DIBRIS, Genoa, Italy
e-mail: giorgia.marchesi@edu.unige.it

Spinal Cord Italian Lab (SCIL), Santa Corona Hospital, Pietra Ligure, Italy

A. Bellitto
e-mail: amy.bellitto@edu.unige.it

M. Casadio
e-mail: maura.casadio@unige.it

A. Canessa
e-mail: andrea.canessa@unige.it

E. Ricaldone
University of Genoa, Genoa, Italy
e-mail: ricaldone.elena@virgilio.it

K. Torre · E. Quinland · A. Massone
Santa Corona Hospital, Pietra Ligure, Italy
e-mail: k.torre@asl2.liguria.it

E. Quinland
e-mail: e.quinland@asl2.liguria.it

A. Massone
e-mail: a.massone@asl2.liguria.it

A. De Luca · C. Sanfilippo · J. Saglia · V. Squeri
Movendo Technology srl, Genoa, Italy
e-mail: alice.deluca@movendo.technology

C. Sanfilippo
e-mail: carlo.sanfilippo@movendo.technology

J. Saglia
e-mail: jody.saglia@movendo.technology

© The Author(s), under exclusive license to Springer Nature Switzerland AG 2022
D. Torricelli et al. (eds.), *Converging Clinical and Engineering Research on Neurorehabilitation IV*, Biosystems & Biorobotics 28,
https://doi.org/10.1007/978-3-030-70316-5_35

athletes with lower limb amputation to test their balance abilities in challenging conditions. In our evaluation, we tested the feasibility of this protocol that included dynamic exercises assessing both the active and proactive balance components while standing and sitting. Two Paralympic athletes, both with amputation level above the knee, are included in this pilot study. We evaluated their performance mainly assessing the trunk motion throughout an inertial measurement unit placed over the sternum. The protocol included three different exercises repeated in different conditions (i.e. eyes open vs. eyes closed). All subjects completed the protocol and the exercises and the measure we propose allow us to evaluate changes in subjects' strategies, confirming the feasibility of this protocol to quantitatively evaluate balance performance.

1 Introduction

Sudden accidents change the perception we have of our self and capabilities. Being engaging in sports, or adapted sports for people with disabilities, has many advantages both physically and psychologically [1]. Nordic ski has been adapted to match the needs of different categories of people with disabilities, including amputees. Amputees' abilities to balance on a single leg, and hence of expert athletes with lower limb amputation, are greater than those of an able-bodied person [2]. In fact, when testing experts, we need to consider their greater performance level. Here, we propose a protocol created ad-hoc for expert athletes with lower limb amputation. Our protocol aims to comprehensively evaluate balance abilities in single-leg challenging tasks targeting the postural response after both auto-induced and externally induced perturbations while standing and sitting.

2 Materials and Methods

2.1 Subjects

We tested two unilateral lower limb amputees that are also expert Paralympic ski athletes (S1 25 yo man and S2 24 yo woman). Athletes matched the criteria of amputation of a single lower limb above the knee; they had normal or corrected-to-normal vision and absence of any cognitive impairment. All subjects were naïve to the motor tasks proposed in this study.

The study conforms to the ethical principles of the 1964 Declaration of Helsinki, and all subjects signed an informed consent to the analysis and publication of their data for research purposes.

2.2 Robotic Device and Motor Tasks

We used hunova[®], a medical robotic device with two independently controlled platforms, one under the chair and one under the feet, that guarantee well defined interaction either while sitting or standing. In our study, we evaluated tasks in both conditions:

1. Standing reaching task: here, subjects, standing on the platform with arms free to move, were requested to move a cursor from a central starting point toward one of eight equidistant radially arranged targets that appeared on the screen (placed 1-m far from the subject) by tilting the feet platform in the direction of the targets. The platform was maintained in unstable equilibrium and it tilted in response to the subjects' weight shift providing, throughout an impedance control, an elastic force field tending to restore the platform parallel to the floor (see [3] for details).
2. Unstable sitting with perturbation at the foot level: here subjects were sitting on the tilting chair with crossed arm by the chest. The chair was maintained in unstable equilibrium (i.e. tilting in response to the subjects' weight shift) while the foot platform moved in a pre-programmed and repeatable way. Subjects were requested to maintain the trunk, and hence the sitting chair, the more stable they could.
3. Standing with continuous perturbation: subjects were requested to maintain the standing position while the foot platform tilted in a pre-programmed and repeatable way.

2.3 Protocol

The protocol we propose includes 17 exercises, each lasting 60 s. From ex. 1 to ex. 6, the standing reaching task is repeated alternating two target distances: 5° and 7° of platform inclination, respectively T5 and T7. From ex. 7 to ex. 12, the unstable sitting was repeated alternating one with eyes open (EO) and one with eyes closed (EC). From ex. 13 to ex. 16, the standing task with continuous perturbation was repeated alternating one repetition with EO and one with EC. Between all those exercises, subjects were resting 30 s. Lastly, without any break from the previous exercise, subjects performed the standing reaching task with 7° target distance, where we tested the effect of the fatigue due to both the absence of break and the whole protocol.

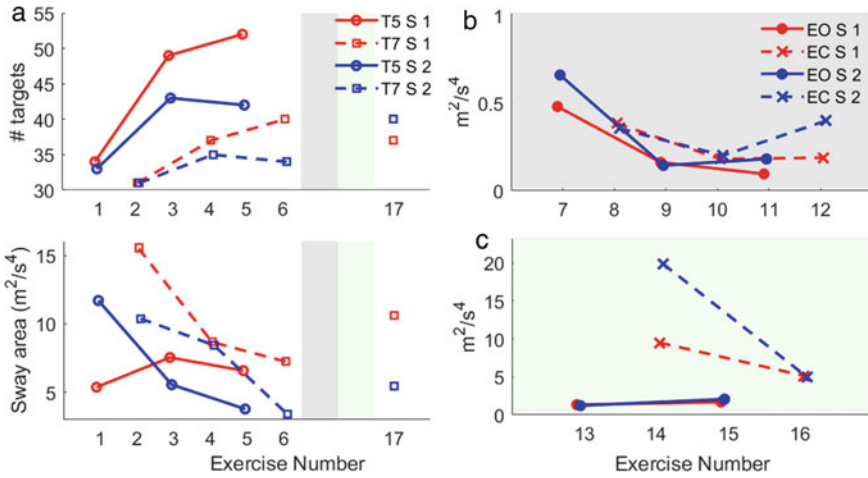


Fig. 1 Subject performance; red lines refer to subject S1 and blue lines to S2. **a** (top) Number of correct reached targets and (bottom) the sway area during the standing reaching task repetitions (from ex. 1 to 6) and the under strain standing reaching exercise (ex. 17). Circles refer to T5 and squares to T7. **b** Sway area for the unstable sitting repetitions (from ex. 7 to 12). Dots refer to EO and crosses to EC. **c** same as **b** for the standing exercises with continuous perturbation (from ex. 13 to 16)

2.4 Data Acquisition and Data Analysis

We collected data from the inertial measurement unit positioned on the subjects’ sternum to record the movement of the trunk. Data were sampled at a frequency of 30 Hz. We filtered the data with a low-pass Butterworth filter (4th order, cutoff frequency of 12 Hz). For all exercises we quantified trunk movements computing the sway area from the acceleration measures, expressed as m²/s⁴ [3], as quantitative evaluation of trunk motion, with small values as signs of good trunk control. In addition, for the reaching task, we also computed the number of reached targets.

3 Results and Discussion

Both S1 and S2 could complete the whole protocol, which highlighted changes in performance due to the repetition of the same exercises or to the different modalities requested to perform the exercises. More precisely, in the standing reaching exercises, independently on the target distance, both subjects improved their performance across repetitions increasing the number of reached targets (Fig. 1a, top) and lowering the trunk motion (Fig. 1a, bottom), more evident for further targets (T7). Lastly, in the 17th exercise, where we tested subjects under strain, the number of reached targets

was not affected but, to reach the same performance level, both subjects moved their trunk more than in the last repetition of the same exercise (6th).

Concerning the unstable sitting task, except for the first repetition of the task, as expected, subjects controlled the trunk better when they performed the exercises with EO. Despite a familiarization phase before the beginning of the test, the first repetition of this task has the worst performance as subjects adapted to the exercises with the repetitions, improving their performance.

During the standing task with continuous perturbation, subjects had a greater dependency on the visual feedback than in the other tasks.

4 Conclusion

This pilot study aims at assessing the feasibility of a protocol to evaluate balance performance of expert athletes with lower limb amputation in challenging conditions. The protocol includes only dynamic tasks, allowing to test the responses to both auto and externally induced perturbations. Here, we evaluated two expert athletes that confirmed this protocol is feasible and might be used in future studies with a greater number of athletes to assess to what extent different sporting levels affect performance. Also, this protocol may be used to assess deficits of single athletes for tailoring specific trainings.

Acknowledgements This work was supported by Ministry of Science and Technology, Israel (Joint Israel-Italy lab in Biorobotics “Artificial somatosensation for humans and humanoids”) and GM is supported by the ‘regione liguria’ Ph.D. scholarship.

References

1. B. Blumenstein, I. Orbach, Psychological preparation for Paralympic athletes: a preliminary study. *Adapt. Phys. Act. Q.* **32**(3), 241–255 (2015)
2. A.H. Vrieling et al., Balance control on a moving platform in unilateral lower limb amputees. *Gait Posture* **28**(2), 222–228 (2008)
3. G. Marchesi, et al., Robot-based assessment of sitting and standing balance: preliminary results in Parkinson’s disease, in *2019 IEEE 16th International Conference on Rehabilitation Robotics (ICORR)*, 2019, pp. 570–576

SS5: Boosting Neurorehabilitation in a Sustainable Way

Frequency Domain Analysis of EMG and HRV in Self-Support Exercise



S. Shimoda, Alvaro Costa Garcia, Hiroshi Yamasaki, F. Alnajjar, M. Sonoo, Shotaro Okajima, Sayako Ueda, Ken-ichi Ozaki, and Izumi Kondo

Abstract We have observed that the self-support exercises triggered electromyographic activities on the dormant muscles of the post-stroke patients. Self-support exercise here implies that the patients move their paretic arms with the supports of their non-paretic arms. The similarity of the muscle activities between the paretic and the non-paretic arms show that the motor paralysis is improved during the self-support exercises. We have showed through the clinical tests that biofeedback rehabilitation using this self-support exercises can improve the recovery speed from the motion paralysis. In this paper, we report that EMG frequency and heart rate variability during self-support exercises became smaller than those during bimanual exercises, suggesting that parasympathetic nerve system in the self-support exercise became more active than in bimanual exercise. Instead the causality between the motor paralysis improvement and the changes of the autonomous nerve states is unclear, these results is the evidence that the neural pathways that was used before stroke are used in the self-support exercise though abnormal pathways are used in the bimanual exercises.

1 Introduction

Stroke is one of the leading causes of serious motor paralysis, which appears in many cases on the one side of the body. Rehabilitation from the motor paralysis aims to help the patients the best possible quality of life. We have so far observed that the self-guided motion support by the non-paretic arm triggers electromyographic (EMG) activities of the paretic arm with normal muscle synergies [1]. The self-guided motion support implies that the paretic arm movements are supported by their non-paretic arm movements. The clinical tests with 54 patients and 25 age-matched healthy elderly showed that the similarities of the muscle synergies between paretic and non-paretic arms were drastically improved in the self-support exercises to be

S. Shimoda (✉) · A. C. Garcia · H. Yamasaki · F. Alnajjar · M. Sonoo · S. Okajima · S. Ueda · K. Ozaki · I. Kondo

RIKEN Center of Brain Science, TOYOTA Collaboration Center, Nagoya, Japan
e-mail: shingo.shimoda@riken.jp

the similar level with the healthy elderly. The brain imaging by fMRI and fNIRS in the self-support exercises suggested that the self-support exercises activated the local neural pathways that was used before stroke [1]. The effect by the self-support exercise can be explained, therefore, that the external stimulation activates the local neural pathways that was not damaged but cannot be activated by the motion intention.

We have applied the self-support effect to the bio-feedback training that activate simultaneously the local neural pathways and the motion intentions, expecting Hebbian-type conditioning of the broken connection between them by stroke. The controlled tests in the two groups of with/without the proposed training showed the fast recovery from the motor paralysis by the proposed training [1].

One of the most interesting phenomena of the self-support effect is unexpected activation of dormant muscles with the very simple behavior. Instead we have shown the source of the self-support effect by brain imaging as the stimulation of normal neural pathways for arm movement control, the details of the immediate muscle activity changes are still unclear. In this paper, we will discuss the details of the self-support effect based on EMG frequency and the heart rate variability (HRV).

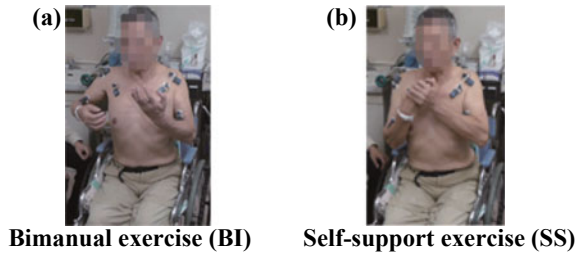
It is well known that EMG frequency changes represent the muscle fatigue level. Piper first detected a reduction of frequency as a consequence of muscle fatigue [2]. Following this finding, many researches showed this fact introducing the several indices such as central frequency and median frequency. In addition to the muscle fatigue quantification, EMG frequency can quantify the number of required motor unit. HRV is a variability in the time interval of successive heartbeats. It is commonly accepted that HRV is a non-invasive indicator of automatic nerve system that comprises the sympathetic and parasympathetic nerve systems [3]. HRV is used, nowadays, as biomarkers related with the autonomous nerve system activities such as sleep problem [4], difficulty of emotion regulation [5] and chronic pains [6].

The purpose of this paper is to clarify the state of autonomous nerve system in the self-support exercise through the analysis of HRV, and find the source of EMG frequency changes. We asked 10 patients the elbow bending motions measuring the bicep muscles EMG and the heart beat, and analyze these bio-signals in the frequency domain. Based on the analysis results, we will derive the state of the autonomous nerve system and discuss the source of EMG frequency changes in self-support exercise.

2 Method

We asked the elbow-bending exercises in the two ways with 10 moderate paralysis post-stroke patients who can move his/her paretic arm with the strong efforts. One of the elbow-bending exercises is the bimanual exercise (BI) where the patients bend both arms at the elbows in the same timing (See in Fig. 1a). The other is the self-support exercise (SS) where the elbow-bending motion of the paretic arm is supported by the same motion of non-paretic arm as described in Fig. 1b.

Fig. 1 Overview of bimanual and self-support exercises



The patients moved in three sets with enough interval from muscle fatigue. One set includes ten times movements of BI and SS in the randomized order. We measure EMG of biceps muscles and heart beat during these motions. EMG signals are analyzed in the frequency domain in this paper. The results in amplitude and muscle synergy domain were summarized in the previous paper [1]. We use the median frequency to compare the difference of the frequency features between BI and SS as described in Fig. 2. The heart beat is used for computing HRV. The cubic spline interpolation was used to re-sample R-R interval 10Hz. We use FFT analysis of the re-sampled data to discuss the features of HRV (See in Fig. 3).

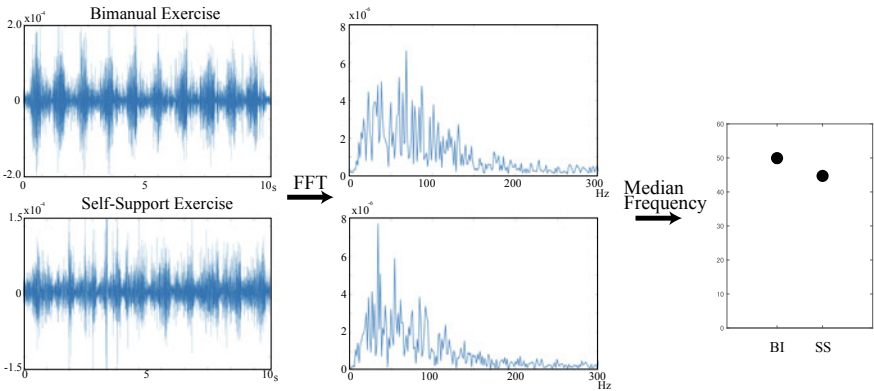


Fig. 2 Process to analyze EMG frequency

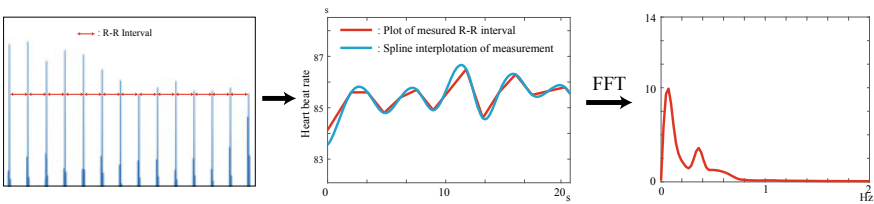


Fig. 3 Process to analyze HRV

3 Result

Figure 4 describes the median frequencies and the maximum amplitude of EMG of 10 patients in Fig. 4. As you can see in Fig. 4a, the median frequencies in BI are higher than the median frequency in SS for all patients though the values are depending on the individuals. For the statistical analysis, we have normalized the median frequencies and the maximum amplitude by the value in SS for each patient. The statistical analysis results are illustrated in Fig. 4b, c. The results show that the median frequency is significantly decreased in SS comparing with BI though the amplitude of EMG did not show the significant changes.

Figure 5 describes HRV analysis results. Figure 5a, b illustrate the typical result of R-R interval and its FFT analysis for one patient. R-R interval became smoother in SS comparing with R-R interval in BI, and the median frequency in SS was smaller than that in BI. The normalized median frequency was significantly decreased in SS from BI.

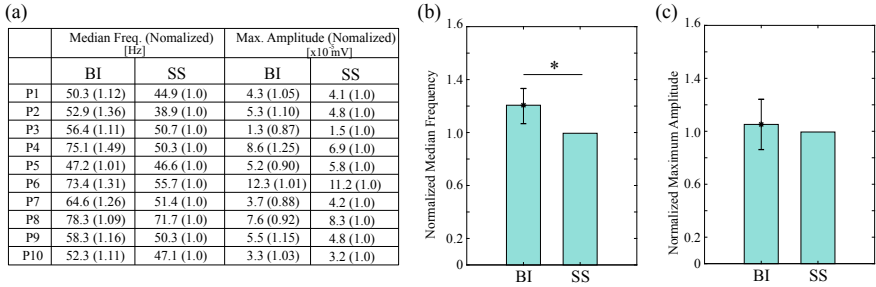


Fig. 4 Results of EMG analysis in frequency domain

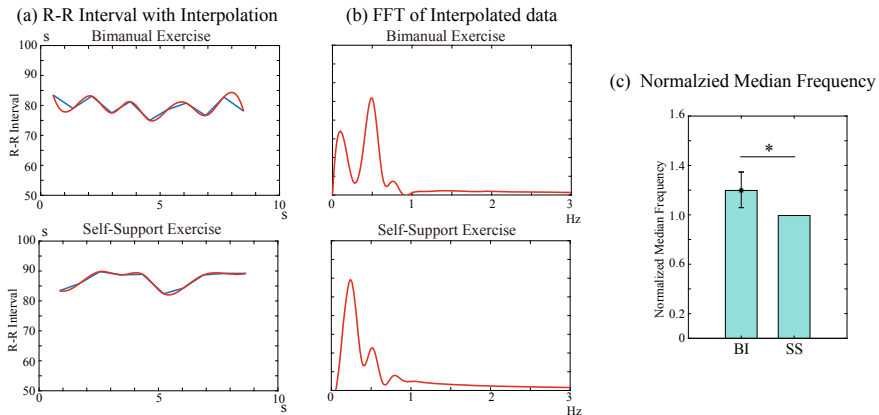


Fig. 5 Results of HRV analysis

4 Discussion and Conclusion

The reduction of HRV in SS suggest that parasympathetic nerve system became more active in SS rather than in BI. All patients in this experiment need the effort motion in BI, where abnormal muscle synergies using the abnormal neural pathways were frequently appeared. This result, therefore, is another evidence for verifying the hypothesis of self-support effect in which the neural pathways in SS were the normal control loops that was used before stroke for controlling the arm movement.

On the other hand, EMG frequency reduction in SS cannot be explained by the scientific knowledge so far because the muscle fatigue and the number of recruited motor units in BI and SS seems not to be different from frequency and amplitude changes. Instead of differences of these factors, the neural pathways in SS and BI seem to be different as we showed above. It is anatomically known that 6 spinal tracts exists to activate motor neurons in the spinal cord. Even though the role of each spinal tract is well studied, there are many uncertainties such as the connections with intermediate neurons in the spinal cord. We need the further analysis to understand the EMG frequency changes in SS, expecting EMG signals to be the window of neural system activities in our daily motions.

References

1. F.S. Alnajjar, K. Ozaki, M. Itkonen, H. Yamasaki, M. Tanimoto, I. Ueda, M. Kamiya, M. Tournier, C. Nagai, A.C. Garcia, K. Ohno, A. Osawa, I. Kondo, S. Shimoda, Self-support biofeedback training for recovery from motor impairment after stroke. IEEE Access
2. R. Merletti, D. Farina, *Surface Electromyography Physiology, Engineering and Applications* (Wiley-IEEE Press, 2016)
3. G.G. Berntson, J.T. Bigger Jr., D.L. Eckberg, P. Grossman, P.G. Kaufmann, M. Malik, H.N. Nagaraja, S.W. Porges, J.P. Saul, P.H. Stone, M.W. van der Molen, Heart rate variability: origins, methods, and interpretive caveats. *Psychophysiology* **34**, 623–648 (1997)
4. D. Ziegler, D. Laude, F. Akila, J.L. Elghozi, Time- and frequency domain estimation of early diabetic cardiovascular autonomic neuropathy. *Clin. Auton. Res.* **11**, 369–376 (2001)
5. N. Mazurak, N. Seredyuk, H. Sauer, M. Teufel, P. Enck, Heart rate variability in the irritable bowel syndrome: a review of the literature. *Neurogastroenterol Motil* **24**, 206–216 (2012)
6. L. Tracy, L. Ioannou, K. Baker, S. Gibson, N. Georgiou-Karistianis, M. Giummarra, Meta-analytic evidence for decreased heart rate variability in chronic pain implicating parasympathetic nervous system dysregulation. *Pain* **157**, 7–29 (2016)

Translation from Functional Training to Independent Living: The Importance of a Real-Time Feedforward-Feedback Approach



Subhasis Banerji, John Heng, Daphne Menezes, Shirish Hastak, Manasi Bane, Sharon Gerken, and Dorothy Wi

Abstract With the reducing median age of stroke sufferers and large numbers of survivors below the age of 45 years, patient needs have shifted significantly from functional training to regaining independence. Similarly, children with learning difficulties struggle to be independent of adult assistance in reading and writing tasks in spite of remedial classes. This paper describes the importance of real-time, multi-modal feedback in rehabilitation with an added component, namely, feedforward. It reports the effect of this approach to facilitate exploratory, sensory, and goal-directed learning for neurorehabilitation needs. Research outcomes from two studies with two diverse neurorehabilitation patient groups—adult stroke and children with learning difficulties—are presented to highlight the importance of this approach in the translation from functional training to independent living.

S. Banerji (✉) · D. Menezes · D. Wi
Synphne Pte. Ltd., Singapore, Singapore
e-mail: subhasis@synphne.com

D. Menezes
e-mail: daphne@synphne.com

D. Wi
e-mail: dorothy@synphne.com

J. Heng
Nanyang Technological University, Singapore, Singapore
e-mail: johnheng@synphne.com

S. Hastak
Wockhardt Hospitals, Mumbai, India
e-mail: shirish.hastak@globalhospitalsindia.com

M. Bane
Synphne Care Centre, Synphne India Pvt. Ltd., Mumbai, India
e-mail: manasi@synphne.com

S. Gerken
Dyslexic Association of South Africa (DASA), Ballito, South Africa
e-mail: sharon@synphne.com

1 Introduction

Learning in infancy, when the brain is at its most neuroplastic, happens in two broad categories [1–3]:

1. Exploratory, sensory, and non-instructional learning—largely feedback oriented
2. Goal oriented, imitative, and instructional learning—feedforward and feedback oriented.

In exploratory learning, association between sensory inputs and its movement or task correlates are embedded into the neuro-muscular system in a Hebbian manner and reinforced by iterative repetitions [2]. Such learning usually involves brain and body together, to explore which combinations of cognitive, physical, and environmental strategies optimally result in successful task completion. More complex goals are then led by a parent or sibling (a mature social partner) whom the infant tries to imitate (feedforward) and emulate [3]. The child then starts to understand how to leverage both types of learning and move towards independence. Independent living demands proficiency in several cognitive and physical abilities which are used individually or in combination. These include strength regulation, decompensation, relaxation, attention, sequential planning, executive control, eye-hand co-ordination, among others [4, 5]. The unpredictable external world demands the self-regulation of these elements in real-time, which conventional functional training does not always directly address or measure in an integrated manner, perhaps due to a lack of sensitive tools and technologies [6].

This paper presents the outcomes on subjects using SynPhNe (www.synphne.com); a connected, wearable system which trains brain and muscle together, using a feedforward-feedback modality.

2 Materials and Methods

2.1 Technology Description

SynPhNe captures electroencephalography (EEG) and electromyography (EMG) signals and helps subjects self-correct movements in real-time (Fig. 1).

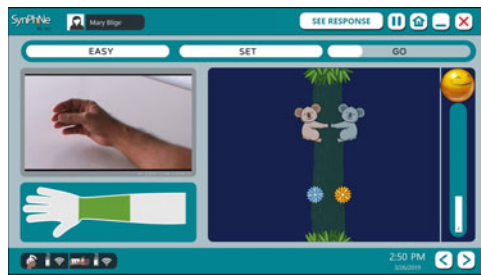
The multi-modal SynPhNe user interface trains upper limb muscle use while maintaining relaxed focus (Fig. 2).

Subjects try to imitate movements and tasks watching a series of videos (feedforward), while self-regulating brain (attention/relaxation) and muscle (agonist-antagonist balance, agonist contraction) response using real-time EEG and EMG feedback respectively. Subjects train in activities such as grasping, eating, reading, writing, amongst others. Subjects combine tasks to train in specific independence goals. Feedforward-feedback training introduces an iterative, synergistic, neuro-physio learning process instead of mechanical repetitions alone [3].



Fig. 1 The SynPhNe device with electroencephalography (EEG) and electromyography (EMG) sensors and software user interface

Fig. 2 Users imitate various movements and tasks watching the exercise video, (feedforward) while responding to real-time EEG (smiley emoji) and EMG (koalas on a tree) feedback



2.2 Study Methods

Two studies of adult, chronic stroke patients ($n = 5$) and teenage children diagnosed with attention deficit and dyslexia ($n = 6$) in a pre-post design are presented. Both groups were undergoing standard care—outpatient therapy for the stroke group and remedial lessons in school for the dyslexia group—but were plateaued. Thus, they acted as their own controls. Independence goals for the adult stroke group was activities of daily living and returning to work while for the children, it was better reading and comprehension. The stroke group underwent 18 sessions, thrice a week over 6 weeks at a Training Centre, while the dyslexia group underwent 10 sessions (45–60 min each) over 4 weeks in between regular classroom sessions in school. The training activities suited each subject’s pre-selected goals.

Fugl Meyer Assessment (FMA) and Action Research Arm Test (ARAT) were used as standardized scales for stroke. Test of Word Reading Efficiency-Sight Word Efficiency (TOWRE-2 SWE) and Phonemic Decoding Efficiency (TOWRE-2 PDE), J. C. Daniels and H. Diack Reading Test (JCDHD) and Visual Aural Digit Span (VADS) test were used for the children.

Table 1 Pre-post outcome measures of stroke group study

User	Age (years)	Fugl-Meyer score (FMA)			Action Research Arm Test (ARAT)		
		Week 0	Week 6	Diff	Week 0	Week 6	Diff
AM	60	66	66	0	57	57	0
SS	46	54	59	5	46	54	8
LK	45	53	61	8	53	57	4
AM	81	24	30	6	0	22	22
SM	39	17	24	7	0	9	9
Mean	54.2	42.8	48	5.2	31.2	39.8	8.6
Std.	15.06	18.9	17.4	2.79	25.72	20.29	7.42

3 Results

4 Discussion

Table 1 illustrates that mean pre-post changes were close to or exceeded MCID in FMA [7] and ARAT [8]. The stroke subjects showed improved agonist-antagonist management and self-regulation of attention, relaxation, and execution of movement. Subjects AM and LK returned to work. Others reported improvements in eating, writing, and dressing.

Table 2 illustrates that in the ADD/Dyslexia group, significant improvement was seen, with kids achieving scores close to their normative grade levels and able to do tasks with reduced adult assistance. VADS outcomes showed improvement in short term memory.

5 Conclusion

Exploratory and goal-oriented learning requires feedforward and feedback that are cyclical and immediate. Patients with physical and neuro deficits who trained using such a modality, combining brain and muscle feedback, reported an ability to do tasks more independently, based on pre-selected goals.

Table 2 Pre-post outcome measures of Dyslexia/ADD group study

User	Age (months)	TOWRE-2 SWE		TOWRE-2 PDE		JCDHD		VADS	
		Week 0	Week 4	Week 0	Week 4	Week 0	Week 4	Week 0	Week 4
LDHR10	136	90	108	75	111	84	102	81	95
LDHR11	135	90	102	93	111	94	102	95	144
LDHR12	135	105	150	102	126	113	157	113	143
LDHR13	138	105	132	111	153	109	145	119	132
LDHR14	153	102	135	114	153	115	145	101	119
LDHR15	146	132	174	120	153	115	134	95	119
Mean	140.5	104	133.5	102.5	134.5	105	130.8	100.67	125.33
Std.	6.75	14.03	24.35	15.04	19.16	11.84	21.44	12.51	16.85

Acknowledgements The study was conducted with stroke patients from Wockhardt Hospitals, Mumbai (India), and children with Dyslexic Association of South Africa (DASA), Durban (South Africa). Synphne provided devices, training, and supervision. Hospital funded its own manpower and DASA manpower was sponsored by Synphne Pte. Ltd.

References

1. J.D. Velasquez, When robots weep: emotional memories and decision making, in *Proceedings of the Fifteenth National Conference on Artificial Intelligence (AAAI-98)* (MIT/AAAI Press, Madison, 1998)
2. J. Hawkins, S. Blakeslee, *On Intelligence* (Times Books, New York, 2004).
3. L. Smith, M. Gasser, The development of embodied cognition: six lessons from babies. *Artif. Life* **11**(12), 13–29 (2005)
4. G. Wulf, Self-controlled practice enhances motor learning: implications for physiotherapy. *Physiotherapy* **93**, 96–101 (2007)
5. J.T. Fairbrother, D.D. Laughlin, T.V. Nguyen, Self-controlled feedback facilitates motor learning in both high and low activity individuals. *Front. Psychol.* **3**, 323 (2012)
6. A.A.A. Timmermans, H.A.M. Seelen, R.D. Willmann, H. Kingma, Technology-assisted training of arm-hand skills in stroke: concepts on reacquisition of motor control and therapist guidelines for rehabilitation technology design. *J. NeuroEng. Rehabil.* **6**(1), 1–18 (2009)
7. S.J. Page, G.D. Fulk, P. Boyne, Clinically important differences for the upper-extremity Fugl-Meyer scale in people with minimal to moderate impairment due to chronic stroke. *Phys. Therapy* **92**(6), 791–798 (2012)
8. J.H. Van der Lee, V. De Groot, H. Beckerman, R.C. Wagenaar, G.J. Lankhorst, L.M. Bouter, The intra- and interrater reliability of the action research arm test: a practical test of upper extremity function in patients with stroke. *Arch. Phys. Med. Rehabil.* **82**(1), 14–19 (2001)

Ankle-Foot Orthoses in the Rehabilitation After Stroke: Results of a Randomized Controlled Trial



Corien D. M. Nikamp, Johan S. Rietman, Erik C. Prinsen,
Hermie J. Hermens, and Jaap H. Buurke

Abstract This paper provides an overview of the results of the EVOLUTIONS-trial, in which effects of providing ankle-foot orthoses on two different points in time in the rehabilitation after stroke were studied. Results showed functional improvements over time, while at the same time no changes in kinematics and muscle activity of the affected lower limb were found over a period of 26 weeks. Based on these results, compensation strategies of the unaffected lower limb are thought to play an important role in the rehabilitation after stroke.

1 Introduction

Walking function is often impaired after stroke. In order to improve walking, Ankle-Foot Orthoses (AFOs) are frequently prescribed. When looking into the available evidence of AFO-use after stroke, the majority of studies compared the effects of AFOs in short-term designs, in patients who were able to walk independently, who used AFOs already in daily life and were in the chronic state after stroke. These conditions do not match the conditions of stroke patients admitted in rehabilitation centers for which AFO-prescription are considered. As a result, there was insufficient evidence available to inform clinicians about whether or not to prescribe AFOs early or later after stroke, and about effects of long-term AFO-use. Therefore, the EVOLUTIONS-trial was conducted, in which the effects of providing AFOs on

This study was supported by grants from the Ministry of Health, Welfare and Sports (Innovatiecentrum) and Stichting Hulpfond het Roessingh, Enschede, The Netherlands.

The ankle-foot orthoses used in this study were provided by Basko Healthcare, Zaandam, The Netherlands. They were not involved in designing the study, data collection, data analysis or interpretation of data. In addition, they had not role in writing publications or the decision to submit articles for publication.

C. D. M. Nikamp (✉) · J. S. Rietman · E. C. Prinsen · H. J. Hermens · J. H. Buurke
Roessingh Research and Development, Enschede, The Netherlands
e-mail: c.nikamp@rrd.nl

University of Twente, Enschede, The Netherlands

© The Author(s), under exclusive license to Springer Nature Switzerland AG 2022
D. Torricelli et al. (eds.), *Converging Clinical and Engineering Research
on Neurorehabilitation IV*, Biosystems & Biorobotics 28,
https://doi.org/10.1007/978-3-030-70316-5_38

two different time points in the sub-acute rehabilitation post stroke were studied. Individual publications based on the results of this trial are already available and studied, amongst others, the effects on functional outcome measures [1], kinematics [2] and activity of the Tibialis Anterior (TA) muscle [3]. The aim of the current paper is to combine these results and state broad conclusions regarding the effect of AFO-provision on overall improvement after stroke.

2 Material and Methods

2.1 Study Design

We conducted a single center, randomized, controlled, parallel group study. The study was approved by the Medical Ethical Committee Twente and registered in the Dutch Trial register as NL1820. Subjects with and without independent walking ability were equally randomized into either AFO-provision at inclusion, study week 1 (early group), or AFO-provision eight weeks later, in study week 9 (delayed group).

2.2 Participants

Subjects were recruited from the Roessingh, Center for Rehabilitation in Enschede, The Netherlands. Inclusion criteria were: unilateral ischemic or hemorrhagic stroke leading to hemiparesis; minimal 18 years; maximal six weeks post-stroke; receiving inpatient rehabilitation care at inclusion; able to follow simple verbal instructions; indication for AFO-use determined by the treating rehabilitation physician and physiotherapist. Exclusion criteria were severe comprehensive aphasia, neglect or cardiac, pulmonary or orthopedic disorders that could interfere with gait.

2.3 Study Procedure

Longitudinal measurements were performed until 26 weeks after inclusion. Clinical tests related to balance, walking and activities of daily living were studied up to 17 weeks with biweekly intervals and a follow-up measurement at 26 weeks. 3D gait analyses measurements (using Vicon) including EMG-measurements were performed four times in the period of 26 weeks (in week 1, 9, 17 and 26). For more details and a full description of the study procedures, we would like to refer to the available papers [1–3].



Fig. 1 Three types of non-articulated AFOs used in the study

2.4 Intervention

Subjects were provided with one of three commonly used types of off-the-shelf, non-articulated, posterior leaf design, polyethylene or polypropylene AFOs. The types included flexible, semi-rigid or rigid designs (Basko Healthcare, Zaandam, The Netherlands), as shown in Fig. 1. Besides AFO-provision in week 1 (early group) or week 9 (delayed group), all subjects received usual care from experienced physiotherapists.

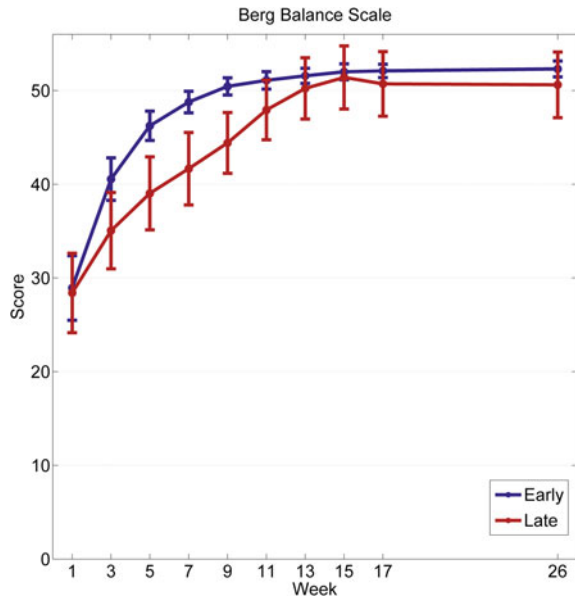
2.5 Outcome Measures

Clinical tests included walking speed (10 m walk test) and distance (6 min walk test), balance (Berg Balance Scale), functional mobility (Timed Up and Go Test, Stairs Test), independence of walking (Functional Ambulation Category) and activities of daily life (Rivermead Mobility Index and Barthel Index). 3D gait analysis included frontal and sagittal kinematics of the affected lower limb; spatiotemporal parameters and muscle activity patterns of amongst others the affected TA muscle.

2.6 Data Analysis

Independent group analysis were used to compare results after 26 weeks between the early and delayed group. Generalized Estimating Equation analyses and mixed model repeated measures analysis were performed to compare group by time interactions.

Fig. 2 Example of clinical test for the early (blue) and delayed (red) group. Mean (SE) score of the Berg Balance Scale is shown [1]



3 Results

Thirty-three subjects (16 early, 17 delayed) were included in the study of which six dropped out. Results of clinical tests showed that all subjects improved over time, see Fig. 2 for an example. The early group showed better outcomes on most tests in the first 11–13 weeks compared to the delayed group, but after 26 weeks no significant differences were found between both groups. Gait analysis showed that AFOs improved drop-foot during swing. Early or delayed AFO-provision did not influence pelvis, hip or knee kinematics during the 26 weeks. In addition, 26-weeks of AFO-use did not affect TA muscle activity and no differences with respect to TA muscle activity were found between both groups.

4 Discussion

We found no changes in kinematics and TA muscle activity of the affected lower limb over a period of 26 weeks after stroke. At the same time, subjects showed improvements on a functional level and early AFO-provision increased these improvements. This provokes discussion about how recovery after stroke is achieved. Behavioral restitution and compensation need to be distinguished in this discussion [4]. Behavioral restitution is defined as “return toward more normal patterns of motor control with the impaired effector” (for example the impaired ankle) and reflects the process

towards “true recovery”. Compensation is described as “a patient’s ability to accomplish a goal through substitution with a new approach, rather than using normal pre-stroke behavior.” This includes intact muscles of the affected limb, but also the unaffected limb to accomplish the goal.

We found functional improvements over time, measured with clinical scales. However, these scales do not differentiate behavioral restitution from compensation. In our study, EMG and kinematic outcome measures were obtained simultaneously. These outcome measures, together with kinetic measures, are currently considered as the best way to differentiate behavioral restitution from compensation. Kinematics of the affected leg, together with affected TA EMGs did not change over time, while subjects functionally improved. Based on these results, compensation appears to be an important factor in stroke rehabilitation. This highlights the need for further research of the contribution of the unaffected lower limb in the rehabilitation after stroke. Changes in unaffected lower limb kinematics and changes in spatiotemporal parameters need further study.

5 Conclusion

Early AFO-use is expected to result in higher functional levels earlier on in the rehabilitation, but does not lead to higher functional levels after 26 weeks. The functional improvements over time were found, without changes in affected lower limb kinematics and TA EMG. Based on these results, compensation mechanisms, including the contribution of the unaffected lower limb, are thought to be important in the rehabilitation after stroke. This highlights the need for further research into the role of the unaffected lower limb in the rehabilitation after stroke.

Acknowledgements We would like to thank patients and staff from Roessingh, Center for Rehabilitation and staff from Roessingh Rehabilitation Technology, Enschede, The Netherlands, for their participation and co-operation to the study.

References

1. C. Nikamp, J. Buurke, J. van der Palen, H. Hermens, J. Rietman, Six-month effects of early or delayed provision of an ankle-foot orthosis in patients with (sub)acute stroke: a randomized controlled trial. *Clin. Rehabil.* **31**, 1616–1624 (2017)
2. C. Nikamp, J. van der Palen, H. Hermens, J. Rietman, J. Buurke, The influence of early or delayed provision of ankle-foot orthoses on pelvis, hip, and knee kinematics in patients with sub-acute stroke: a randomized controlled trial. *Gait Posture* **63**, 260–267 (2018)
3. C. Nikamp, J. Buurke, L. Schaake, J. van der Palen, J. Rietman, H. Hermens, Effect of long-term use of ankle-foot orthoses on tibialis anterior muscle electromyography in patients with sub-acute stroke: a randomized controlled trial. *J. Rehabil. Med.* **51**, 11–17 (2019)

4. J. Bernhardt, K. Hayward, G. Kwakkel, N. Ward, S. Wolf, K. Borschmann et al., Agreed definitions and a shared vision for new standards in stroke recovery research: the stroke recovery and rehabilitation roundtable taskforce. *Neurorehabil. Neural. Repair* **31**, 793–799 (2017)

An Integrated Rehabilitation Platform Based on Action Observation Therapy, Mixed Reality and Wearable Technologies



Paolo Mosna, Stefano E. Lenzi, Stefano Lazzarini, Massimiliano Gobbo, Monica Angelini, Riccardo Buraschi, Stefano Negrini, Maddalena Fabbri Destro, Pietro Avanzini, Giacomo Rizzolatti, and Nicola F. Lopomo

Abstract This paper presents a novel approach to support rehabilitation employing Action Observation Therapy (AOT), mixed reality (MR) and wearable technologies to foster common rehabilitative methods in restoring motor function. Here, the platform was specifically designed to support the standard physical treatments in post-stroke patients during upper limb rehabilitation. The proposed platform integrates 3D stereo view of egocentric AOT stimuli, multi-level exergaming in MR and motion tracking. This solution represents a practical method for both in/outpatients and at-home rehabilitation programs. A feasibility study on sub-acute post-stroke patients was performed and preliminary findings suggested the effectiveness of this integrated approach.

P. Mosna (✉) · M. Gobbo · N. F. Lopomo
Università Degli Studi di Brescia, Brescia, Italy
e-mail: p.mosna@unibs.it

M. Gobbo
e-mail: massimiliano.gobbo@unibs.it

N. F. Lopomo
e-mail: nicola.lopomo@unibs.it

S. E. Lenzi · M. Angelini · M. F. Destro · P. Avanzini · G. Rizzolatti
Consiglio Nazionale Delle Ricerche, Parma, Italy
e-mail: s.lenzi002@unibs.it

M. Angelini
e-mail: monica.angelini@unibs.it

S. Lazzarini · R. Buraschi
IRCCS Fondazione Don Carlo Gnocchi ONLUS, Rovato, Italy

S. Negrini
University “La Statale”, Milan, Italy

IRCCS Istituto Ortopedico Galeazzi, Milan, Italy

S. Negrini
e-mail: stefano.negrini@unimi.it

1 Introduction

The actual contingencies due to the COVID-19 outbreak highlighted the needs of innovative treatments and therapies in both in- and out-patient contexts to support the continuity of care. The integration of mixed reality (MR) with wearable devices in coherent exergaming represents very promising solutions for the treatment of several neurological diseases [1]. Around 80% of people with stroke experience upper limb hemiplegia, and in 50% of these cases the motor dysfunction can stand for month or years [2]. Concerning neurorehabilitation, AOT represents a well-known approach able to stimulate the mirror neuron system (MNS) and to activate neural structure responsible for execution of the movement by observing others performing the same movements [3]. In order to obtain optimal results, AOT should be correctly administered to maximize the response of the MNS [4].

The main aim of this study was to design and develop a novel rehabilitation platform able to provide primary key indicators (PKIs) related to patient's performance assessed during the rehabilitation. The proposed solution seamlessly integrated different technologies to estimate several measurable PKIs. Adopted technologies overcome real world limitations, supporting AOT and the definition of structured, controlled and measurable procedure; in particular we introduced the use of: (1) stereoscopic 3D videos (3DVs) to support and provide a full immersive realistic experience during action observation phase, thus to maximize the possible response of the MNS, (2) MR to implement the rehabilitation exercises projecting interactive virtual objects in the real environment, (3) a low-cost optical device (OD) and a set of inertial sensors (IMUs) to track patient's motion, provide him/her with the ability to interact with the virtual objects, and estimate PKIs.

2 Materials and Methods

The designed application protocol is composed of 2 different phases: (1) Action observation phase (AOP) and (2) Execution phase (EP). During AOP, a 3D video acquired by means of a 180° stereoscopic camera (LucidVR, Lucid Creative) and containing the execution of a specific movement, is shown to the patient in egocentric by means of the VE. During EP the patient is required to execute herself/himself the very same movement exploiting a MR environment (Fig. 1). We strongly supported MR approach because it can provide mediated training that facilitate generalization and transference of knowledge from therapy to activities beyond rehabilitation [5]. Moreover, with MR the patients can see their own limbs, thus the embodiment is inherently natural. In this work the following exercises have been implemented: Reaching, Reaching and Grasping, Goalkeeper and Occupational Task. Further exercises can be easily added if required.

The platform was designed as an integration of various hardware and software technologies such as: Unity (3D game engine) and Microsoft .Net for the overall

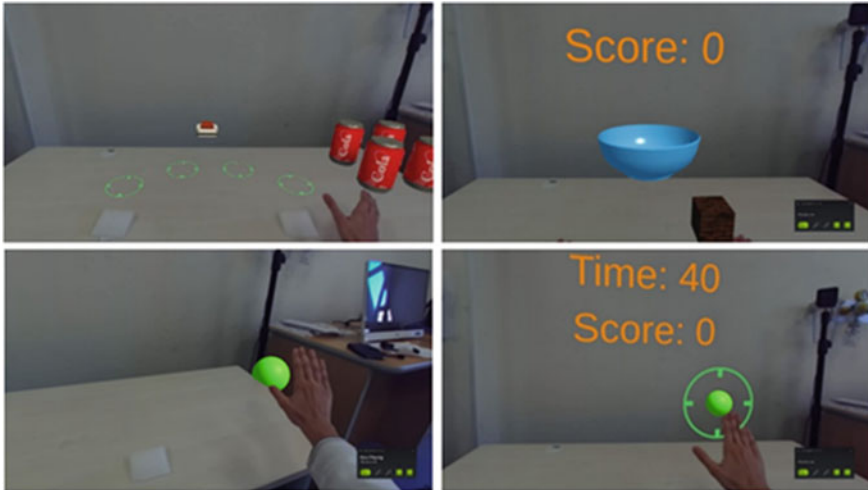


Fig. 1 Example of several tasks implemented in mixed reality

integration, Leap Motion as OD to track patient’s hands and finger movements, Zed Camera to support MR, HTC Vive VR headset to provide 3DVs and Cometa WaveTrack sensors as IMUs for the acquisition of upper limb motion data. The system can track hand and finger movements in 3D space, as well as the whole upper limb kinematics. Realtime data analysis here allowed to obtain a set of major PKIs (Table 1), which can be used to assess the rehabilitation program and adapt the exercises.

In addition to the upper limb kinematic data, temporal key events (TKEs) are also acquired, including: start of the hand motion, grasp begin, grasp end and target reached. TKEs are very important because they provide additional information on patient’s strategy while approaching the target. All the acquired data are stored in XML format files to be further analyzed. The system provides a management console (MC) used by the physician to setup the training phase for the patient. A configuration file is used to provide generic configuration to be applied to all the patients. MC allows to control therapy execution interacting with Unity using a bidirectional web-socket channel (Fig. 2).

Table 1 Primary key indicators

Hand max reaching velocity (HMRV)
% Cycle hand max velocity (CHMV%)
Mean spectral arc length (SPARC)
Mean reach path ratio (MRPR)
Tip max distance (TMD)
Mean interaction time (MIT)
Mean resolution time (MRT)

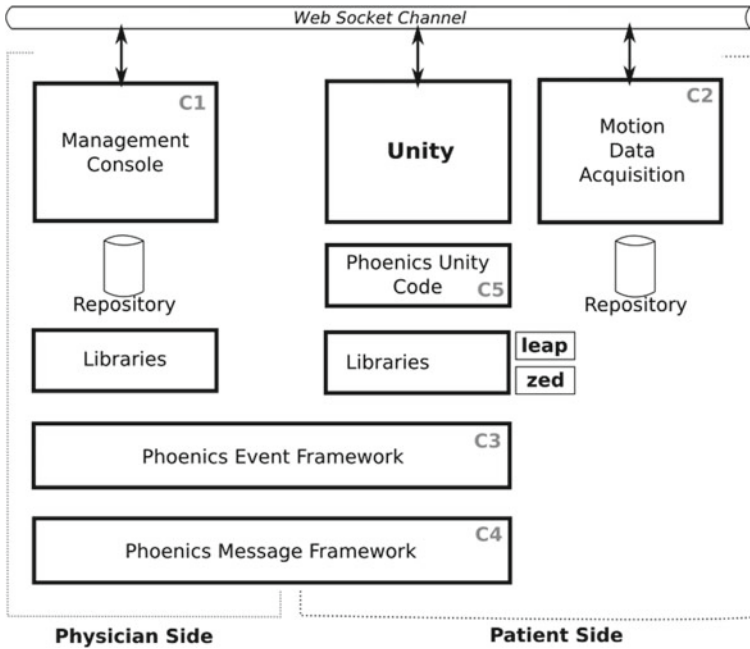


Fig. 2 Software architecture

A practical bi-directional event framework has been mounted on top of the web-socket channel allowing the physical separation between the patient’s side and the physician console. A first pilot study was realized in order to assess the overall system feasibility. The study was specifically realized on 2 sub-acute post-stroke patients with partially limited motor function and 2 healthy subjects. The study was approved by the local Ethical Committee (Prot. 09_13/02/19).

3 Results and Discussion

During the realization of the feasibility study no issues were reported (including motion sickness or critical system faults); furthermore, no fatigue insurgence was reported during all the training sessions. Concerning PKIs, an example of the progresses obtained during the sessions is reported in Fig. 3. The chart shows how S2 increased reaching velocity during the progress of the session, meanwhile the S1 maintain his performance. Now, the available data did not allow us to determine if the S2 improvement was specifically due to AOT, simple training through gaming or increased familiarity with the technology. However, a positive feedback from the on-field trial was related with the stability of the system, its usability and the good

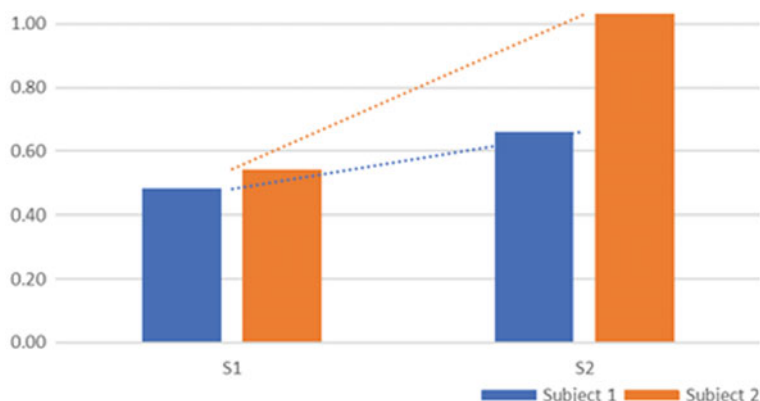


Fig. 3 Hand max reaching velocity with respect to the execution sessions

acceptance by the patients. The platform is currently under clinical validation at IRCCS Fondazione Don Gnocchi ONLUS “Spalenza” Center in Rovato (BS).

4 Conclusion

The proposed platform exploited the integration of different innovative technologies in the field of motor rehabilitation, demonstrating to be effective and well accepted by the patients and subjects involved in the study, highlighting the possibility to use quantitative PKIs and TKEs to assess and guide the overall rehabilitation program. Future works must dedicate to extends and select core PKIs, to improve the overall usability of the system and validate it through an extensive clinical trial.

Acknowledgements This study was fully funded through the call “Health & Wealth 2015”, Università degli Studi di Brescia, PHOENICS project.

References

1. A.-V. Nguyen et al., Virtual reality exergaming as adjunctive therapy in a sub-acute stroke rehabilitation setting: facilitators and barriers. *Disabil. Rehabil. Assist. Technol.* **14**(4), 317–324 (2019). <https://doi.org/10.1080/17483107.2018.1447608>
2. B. Zhang, et al., The effects of action observation training on improving upper limb motor functions in people with stroke: a systematic review and meta-analysis. *PLOS ONE* **14**(8), e0221166 (2019). <https://doi.org/10.1371/journal.pone.0221166>
3. M. Fabbri-Destro, G. Rizzolatti, Mirror neurons and mirror systems in monkeys and humans. *Physiology* **23**, 171–179 (2008). <https://doi.org/10.1152/physiol.00004.2008>

4. M. Angelini, M. Fabbri-Destro, N.F. Lopomo, M. Gobbo, G. Rizzolatti, P. Avanzini, Perspective-dependent reactivity of sensorimotor mu rhythm in alpha and beta ranges during action observation: an EEG study. *Sci. Rep.* **8**(1), 12429 (2018). <https://doi.org/10.1038/s41598-018-30912-w>
5. N. Lehrer, S. Attygalle, S.L. Wolf, T. Rikakis, Exploring the bases for a mixed reality stroke rehabilitation system, Part I: a unified approach for representing action, quantitative evaluation, and interactive feedback. *J. NeuroEng. Rehabil.* **8**(1), 51 (2011). <https://doi.org/10.1186/1743-0003-8-51>

A Novel Tool for Quantitative Assessment of Lower Limb Proprioception with Healthy Adults, Elderly, and Stroke Survivors



Asya Mikhaylov, Yogev Koren, Simona Bar-Haim, and Ilana Nisky

Abstract Stroke survivors and elderly often suffer from proprioceptive impairments that may contribute to disabilities in walking. Current clinical assessments of proprioception are often subjective and not accurate, and the treatment mainly focuses on the motor impairments. Here, we developed a novel tool for proprioception assessment of the lower-limb with a magnetic tracking system. We designed a protocol for assessing proprioception in both lower-limbs using position-matching and position-recall tests. We validated the tool by examining young adults, elderly and stroke survivors. By examining the Mean Absolute Error and Bias, significant differences were found between the elderly and the young adults in the position-matching tasks. This indicates that position-matching may be effective as a screening phase in identifying proprioceptive impairments of the lower limb.

1 Introduction

Stroke is a common cause of life-long impairment for the survivors. Many stroke survivors develop impairments such as distorted speech, motor skills and gait disturbances [1]. Some of those irregular patterns are a result of a damaged somatosensory

A. Mikhaylov · I. Nisky (✉)

Department of Biomedical Engineering, Ben-Gurion University of the Negev, Beer-Sheva, Israel
e-mail: nisky@bgu.ac.il

A. Mikhaylov

e-mail: asya@post.bgu.ac.il

A. Mikhaylov · Y. Koren · S. Bar-Haim · I. Nisky

Transitional Neurorehabilitation Lab, Adi Negev Nahalat Eran, Ofakim, Israel
e-mail: yogevk@post.bgu.ac.il

S. Bar-Haim

e-mail: adi-star@013.net

Y. Koren · S. Bar-Haim

Department of Physical Therapy, Ben-Gurion University of the Negev, Beer-Sheva, Israel

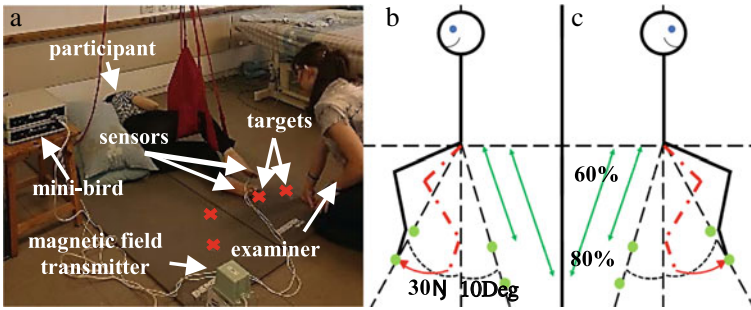


Fig. 1 **a** Setup with the test participant lying down on the side, **b** targets and body setup on the mattress when the participant is lying on the right lower-limb (black) and the left lower-limb is held by a sling (red), **c** targets and body setup on the mattress when the participant is lying on the left lower-limb and the right-lower limb is held by a sling

system [2, 3]. Another group that may suffer from similar impairments is the elderly, whose proprioception is evidently deteriorating with aging [4]. Proprioception is the sense of the state and motion of the limbs relative the body [3]. There are several ways to assess proprioception in the clinic, but most of these methods are highly subjective and inaccurate [2, 5]. To address these limitations, several studies aimed to develop sensorized and robotic methods for proprioception analysis in healthy and impaired individuals. Most of the research is focused on the upper limbs by using exoskeletons and sensor tracking devices [5–7]. In this work, we develop a novel tool for proprioception assessment of the lower-limb, and validate it by comparing two population groups: young adults and elderly. We also demonstrate the results of stroke survivors.

2 Materials and Methods

Eighteen young healthy adults, eight elderlies, and four stroke survivors participated in the evaluation. The protocol and consent form were approved by the Assaf Harofeh ethical committee.

During the evaluation the participant is lying down on a mattress, with one limb on the ground and the other limb held up by a sling, and with magnetic position sensors (Mini-Bird, Ascension Technologies) attached to their toes (Fig. 1a). The evaluation is based on a **position-matching** and a **position-recall** tasks with both the dominant (*D*) and non-dominant (*ND*) lower-limbs for the young adults and elderly, and the unaffected and affected lower-limbs for stroke survivors. **Position-matching**: The examiner places the toe of the target limb (bottom toe), and asks the participant to match the horizontal position of their test limb (upper toe) to the position of the target toe. To succeed in this task, the participant has to sense the position using *proprioception* of the target limb, *transmit* the information to the test

limb, and *execute* the matching with the test limb. We mark the condition in which the non-dominant limb is on the target and the dominant limb is the test as “*ND-D*”, and “*D-ND*” for the opposite. **Position-recall**: the participants’ bottom leg is not examined. Instead, the examiner holds the participants’ test (upper) toe above the target, asks the participant to memorize its position, and moves the limb away. The participants are then asked to move the toe (of the same limb) to the memorized target. To succeed in this task, one has to sense the position using *proprioception* of the test limb, *memorize* the position, and *execute* the matching with the test limb. The conditions are marked as “*D-D*” or “*ND-ND*”, for the dominant and non-dominant limbs, respectively. By comparing these conditions and tasks we hope to isolate the effects of proprioceptive, motor, transmission, and memory impairments.

Four targets are set on the mattress, and the position of the targets was adjusted for each participant to provide a comfortable and feasible workspace (Fig. 1b, c). Two targets were set at 30° in front of the central body line at 60 and 80% of the measured lower-limb length of the participant. The other two targets were set at 10° behind the central body line at similar distances (60 and 80%). Forty trials (ten for each target) were conducted in every condition.

We examined the Mean Absolute Error (MAE), the Bias, and the Mean Variable Error (MVE), as follows:

$$\text{MAE} = \frac{\sum_{i=1}^N \|x_{\text{match},i} - x_{\text{target},i}\|}{N}, \quad (1)$$

$$\text{Bias} = \|\bar{x}_{\text{target}} - \bar{x}_{\text{match}}\|, \quad (2)$$

$$\text{MVE} = \frac{\sum_{i=1}^N \|\bar{x}_{\text{match}} - x_{\text{match},i}\|}{N}, \quad (3)$$

where N is the number of the trials, and \bar{x} is the mean position in a 2D plane. For each of these metrics as a dependent variable separately, we fitted a 3-way ANOVA with repeated measures model. The fixed effects were the group type (young or elderly), the limb of the proprioceptive input (D or ND), the type of the task (matching or recall), and their interactions. The random effects were *participants* and *targets* (participants are *nested* within the group type). There were only four stroke survivors who took part of our study, and hence, we did not perform statistical analyses on their results. Nevertheless, their individual results are presented in Fig. 2b, c and d.

3 Results

An example of a young adult in ND-D condition is demonstrated in Fig. 2a: the different colors represent the four targets, the straight line represents the absolute

error of each trial, the triangles the mean target position and the diamonds the mean matching position of the target.

The results of the MAE and Bias (Fig. 2b, c) indicate that there is a significant difference between the elderly and the young adults (MAE: $\Delta = 23.7$ mm, $F_{1,24.91} = 5.74$, $p = 0.02$; Bias: $\Delta = 23.5$ mm, $F_{1,25.22} = 5.75$, $p = 0.02$). The interactions between group and task types are significant (MAE: $F_{1,361} = 8.88$, $p < 0.05$; Bias: $F_{1,361} = 10.96$, $p < 0.05$) and a distinctive difference was in the position-matching (MAE: $\Delta = 28.3$ mm, $t_{361} = 7.26$, $p < 0.05$; Bias: $\Delta = 29.9$ mm, $t_{361} = 6.79$, $p < 0.05$). The interactions between the group type, task type and input limb are significant as well (MAE: $F_{1,361} = 9.27$, $p < 0.05$; Bias: $F_{1,361} = 7.14$, $p < 0.05$), particularly in ND-D (MAE: $\Delta = 38.9$ mm, $t_{361} = 7.66$, $p < 0.05$; Bias: $\Delta = 39.6$ mm, $t_{361} = 6.91$, $p < 0.05$) indicating impairment in information transmission between the limbs rather than memory or motor problems. Interestingly, the MVE (Fig. 2d) results do not indicate significant differences between the groups. Importantly, the results within the elderly and the stroke survivors are highly variable compared to the young adults. This suggests that our tool can help identifying individuals with proprioceptive impairments within each group. We did not report effects that are close to the calibration error (10 mm) regardless of their statistical significance.

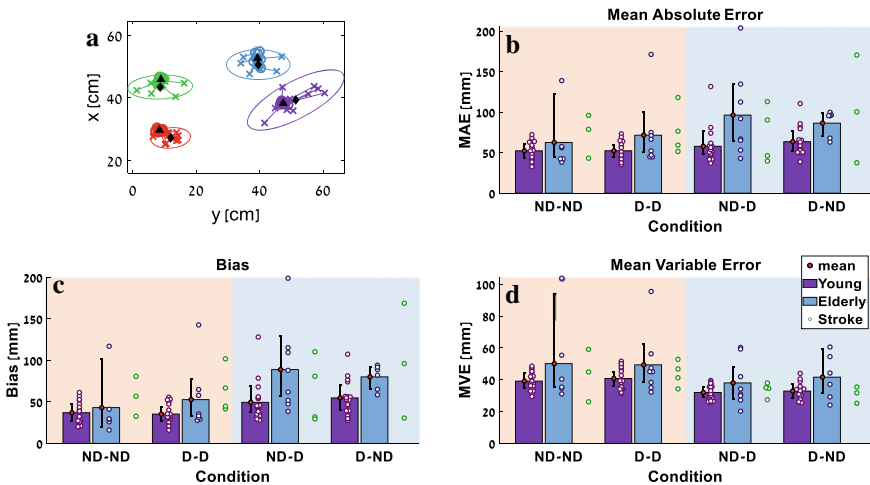


Fig. 2 a Example of a young adult in the ND-D condition; **b–d** The results of the three populations: young adults (purple), elderly (blue) and stroke survivors (green dots). The red dots represent the mean value in every condition. The black line represents 95% confidence interval of the mean of the collected data. The two conditions on the left are the position-recall tasks and the two conditions on the right are the position-matching tests: **b** MAE, **c** Bias, **d** MVE

4 Discussion

The difference between the young adults and the elderly is pronounced in the position-matching tasks, indicating that proprioceptive impairments may be identified by position-matching. However, to isolate the proprioceptive impairment from the motor impairment, the position-recall tasks must be used as well. We suggest to use the position-matching as screening, so only individuals with impaired position-matching results will be evaluated in position-recall, to examine if their results are affected by motor impairments.

5 Conclusions

Somatosensory impairments are often neglected in rehabilitation, partially due to the lack of objective assessment tools. We developed a novel tool for an objective lower-limb proprioceptive assessment combining position-matching and position-recall tests. The results of this evaluation may improve understanding of lower-limb impairments and improve treatment methods.

Acknowledgements This research is sponsored by the Israeli Ministry of Science and Technology (MOST) via the Israel-Italy Virtual Lab on Artificial Somatosensation for Humans and Humanoids. AM is supported by a scholarship from MOST and the Multidisciplinary scholarship of Ben-Gurion University of the Negev, Beer-Sheva, Israel. Special acknowledgement to Noy Goldhamer for assistance in data collection.

References

1. B.H. Dobkin, Rehabilitation after stroke. *N. Engl. J. Med.* **352**(16), 1677–1684 (2005)
2. G. Sayar and H. nüböl, “Assessing Proprioception,” *J. Neurobehav. Sci.*, p. 1, 2017.
3. J.C. Tuthill, E. Azim, Proprioception. *Curr. Biol.* **28**(5), R194–R203 (2018)
4. F. Ribeiro, J. Oliveira, Aging effects on joint proprioception: the role of physical activity in proprioception preservation. *Eur. Rev. Aging Phys. Act.* **4**(2), 71–76 (2007)
5. N. Leibowitz et al., Automated measurement of proprioception following stroke. *Disabil. Rehabil.* **30**(24), 1829–1836 (2008)
6. S.M. Sketch, A.J. Bastian, A.M. Okamura, Comparing proprioceptive acuity in the arm between joint space and task space. *IEEE Haptics Symp. HAPTICS* **2018**, 125–132 (2018)
7. S.P. Dukelow et al., Quantitative assessment of limb position sense following stroke. *Neurorehabil. Neural Repair* **24**(2), 178–187 (2010)

Accuracy of Single RGBD Camera-Based Upper-Limb Movement Tracking Using OpenPose



Timoth Dev, Reetajanetsureka, Samuelkamaleshkumar Selvaraj,
Henry Prakash Magimairaj, and Sivakumar Balasubramanian

Abstract In the context of upper-limb neurorehabilitation, kinematic tracking can be used to monitor and assess therapy, detect compensation, and provide objective feedback. In this paper, we integrated an RGBD (Red Green Blue Depth) camera with OpenPose for movement tracking. The objective of the current study was to evaluate the system's accuracy for tracking upper-limb activities-of-daily-living. After automatically removing occlusion through a simple velocity based method, the consolidated upper-limb joint angle error and wrist endpoint error with respect to a motion capture system was $6.7^\circ \pm 4.9^\circ$ and $2.6\text{ cm} \pm 1.8\text{ cm}$; the Spearman correlation coefficient was 0.76 and 0.87, respectively.

1 Introduction

Complex upper-limb movements involving interaction with objects are commonly employed in upper-limb neurorehabilitation, especially in occupational therapy. This form of training is often carried out only under intermittent supervision from a therapist, with little or no feedback to the patient and therapist about task performance, such as relative time spent performing tasks, range of joint movements, compensatory movements, etc. The exact content and intensity of training are also rarely quantified [1]. Some of these issues can be addressed through monitoring and quantification of movements performed during therapy. Computer vision-based systems would be ideal for such an application as they are compact, affordable, non-intrusive,

This work was supported by Anna University, DST-National Hub for Healthcare Instrumentation Development (NHHID).

T. Dev · S. Balasubramanian (✉)
BioRehab Group, Department of Bioengineering, Christian Medical College (CMC), Vellore,
India
e-mail: siva82kb@cmcvellore.ac.in

Reetajanetsureka · S. Selvaraj · H. P. Magimairaj
Department of Physical Medicine and Rehabilitation, CMC, Vellore, India

© The Author(s), under exclusive license to Springer Nature Switzerland AG 2022
D. Torricelli et al. (eds.), *Converging Clinical and Engineering Research
on Neurorehabilitation IV*, Biosystems & Biorobotics 28,
https://doi.org/10.1007/978-3-030-70316-5_41

and do not require any physical contact with the subject. Additionally, recent development in pose tracking algorithms [2] allows robust tracking of key-points on the human body for tracking movements.

In this paper, we present an RGBD camera (Microsoft Kinect v2) based system for tracking 3D endpoint and joint kinematics of the human upper-limb and trunk using the OpenPose algorithm [2]. We carried out a preliminary evaluation of the Kinect + OpenPose (KOP) system using a motion capture (MOCAP) system and implemented a simple algorithm for addressing self-occlusions while performing various tasks. To the best of the authors' knowledge, no work has been reported for tracking Activities of Daily Living (ADL) using Kinect + OpenPose.

2 Methods

KOP System Architecture: The Kinect is used as a sensor to record color (RGB) and depth data (XYZ) from the scene of interest 10Hz. The RGB data is fed to an OpenPose network to detect the body keypoint positions in pixel coordinates. The 2D pixel position of the keypoints are mapped to the 3D position with respect to the Kinect camera coordinate frame \mathcal{K} (Refer Fig. 2) by using the depth data. The 3D positions are then used to estimate joint angles of the shoulder, elbow, and trunk (Refer Fig. 1).

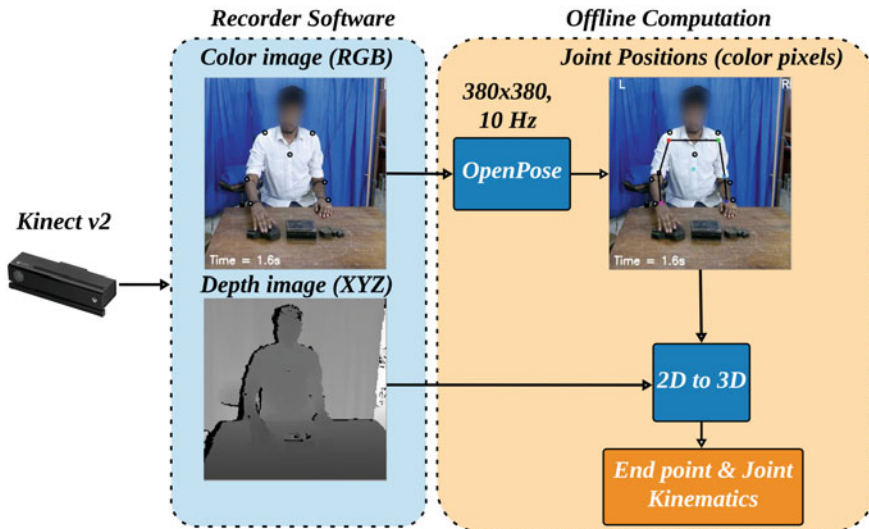


Fig. 1 Architecture of the Kinect + OpenPose system developed in the current study

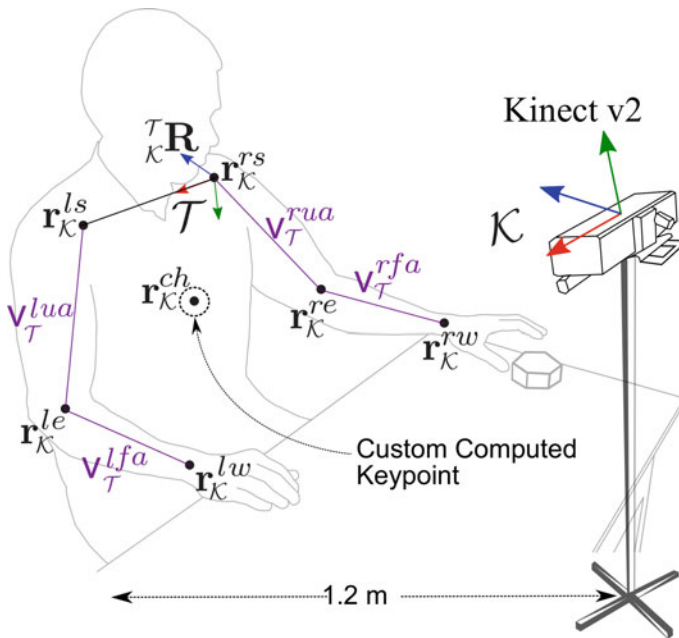


Fig. 2 Keypoints (black dots) used for kinematic analysis. \mathcal{K} and \mathcal{T} are the Kinect and Trunk reference frames. The vectors (violet color) between consecutive keypoints were used for shoulder and elbow angles calculation

Keypoints: The OpenPose keypoints of interest include: left and right wrists, elbows, and shoulders; an additional chest keypoint was computed. The positions of these keypoints with respect to the Kinect camera coordinate frame \mathcal{K} is given by $\mathbf{r}_{\mathcal{K}}^j = [x_j \ y_j \ z_j]^T$, where j corresponds to the different joints. The chest keypoint was computed as the 3D position of the point that is located 100 pixels below the mean of left and right shoulder locations in the color image.

Joint Angles: The trunk, shoulder, and elbow joint angles were estimated from the 3D positions of the different keypoints.

Trunk Angles: Three trunk angles were defined as the XYZ Euler angles parameterizing the orientation of the trunk reference frame \mathcal{T} at time t with respect to the same at $t = 0$. The trunk reference frame \mathcal{T} is defined as the one shown in Fig. 2, which requires the left and right shoulders, and the chest keypoint positions. The three Euler angles of the trunk correspond to the forward-backward lean, trunk twist angle, and left-right sideways lean angle.

Shoulder Angles: The left and right shoulder angles are estimated with respect to the trunk reference frame \mathcal{T} . The three shoulder angles are flexion/extension, abduction/adduction, and internal/external rotation angles. These three angles are computed by first computing the elbow and wrist positions with respect to the \mathcal{T} .

The angles computed for the left and right shoulders are similar, except for opposite signs for the abduction/adduction and internal/external angles to account for the mirror symmetry between the right and left arms.

Elbow Angle The elbow flexion/extension angles are calculated using the shoulder, elbow, and wrist positions.

Evaluation of the KOP System: The wrist endpoint position and joint angles were evaluated using an OptiTrack 8-camera, passive marker-based system on healthy human volunteers performing 10 different tasks related to ADL. The Kinect and the MOCAP data were recorded on the same computer, and the system time was used to synchronize these data streams. Nine healthy volunteers performed the following tasks: clean a surface, eat from a bowl, fold a cloth, pick up a cup, drink from a bottle, use a mobile phone, pick and place, comb hair, button a shirt, stack and unstack objects. Seven retro-reflective markers were placed close to the anatomical keypoints of interest (circled in black, Fig. 1). The marker data from the MOCAP system was recorded 100Hz. The KOP data was converted to the coordinate of the MOCAP system to compare with MOCAP. The KOP keypoints positions were filtered using a Savitsky-Golay filter (window length 0.3s; polynomial order- 1D).

Removing Short Interval Self-occlusions: The trunk keypoints (shoulder and chest) are prone to self-occlusion during arm movements by the upper-limb segments. These result in sharp jumps in the 3D position of the occluded keypoint for short-intervals. A simple velocity-threshold based algorithm was used to annotate and remove occluded data from further analysis automatically. This algorithm has two parameters: velocity threshold and time threshold. The RGB data from the 9 subjects performing the 10 tasks were manually annotated to find occluded data points, which was used as the ground truth for evaluating the performance of the algorithm for automatically annotating occlusions. The parameters for the proposed algorithm were determined by generating a Receiver Operating Characteristic (ROC) curve for different combinations of velocity and time threshold parameters. From the ROC curve, the optimal velocity and time thresholds to detect trunk occlusions were found to be 0.3 m/s and 1.1 s, respectively. These thresholds were then used to ignore the occluded 3D position data to evaluate the kinematic tracking of the Kinect + OpenPose (KOP) system.

3 Results

Summary of the KOP system evaluation with MOCAP is shown in Table 1, where the root mean square (RMS) error and Spearman Correlation Coefficient (CC) between the KOP system and MOCAP are presented before and after automatically removing occluded data segments. The KOP is able to track wrist position, the trunk and arm joint angles with reasonable accuracy. Removing occlusions further improves the accuracy of the system.

Table 1 KOP's wrist endpoint and joint angle accuracy

	Before occlusion removal		After occlusion removal	
	RMS \pm SD	CC	RMS \pm SD	CC
Wrist position (cm)	2.6 \pm 1.8	0.87	2.6 \pm 1.8	0.87
joint angle ($^{\circ}$)	10.7 \pm 7.1	0.75	6.7 \pm 4.9	0.76

4 Discussion and Conclusion

In this paper, we presented a preliminary evaluation of the Kinect + OpenPose (KOP) based system for tracking complex upper limb tasks. The KOP system with a simple occlusion removal algorithm provides reasonable accuracy for use in monitoring neurorehabilitation. These results are generally in agreement with two studies using the Kinect for tracking static poses. Huber et al. found an intraclass correlation coefficient of 0.76–0.98, and shoulder angle error of 2.5–24.2° [3]. Wilson et al. reported shoulder angle error of $\pm 10.5^{\circ}$, the CC is greater than 0.95 [5]. In the gait analysis literature, an error of $\pm 5^{\circ}$ is acceptable for gait analysis [4]. With further improvements in keypoint detection and occlusion removal algorithms, KOP or similar systems can be reliably used in occupational therapy.

References

1. H.M. Schambra et al., A taxonomy of functional upper extremity motion. *Front. Neurol.* **10**, (2019)
2. Z. Cao et al. OpenPose: realtime multi-person 2D pose estimation using part affinity fields. *arXiv preprint arXiv:1812.08008* (2018)
3. M.E. Huber et al., Validity and reliability of Kinect skeleton for measuring shoulder joint angles: a feasibility study. *Physiotherapy* **101**(4), 389–393 (2015)
4. J.L. McGinley et al., The reliability of three-dimensional kinematic gait measurements: a systematic review. *Gait Posture* **29**(3), 360–369 (2009)
5. J.D. Wilson et al., Can shoulder range of movement be measured accurately using the microsoft Kinect sensor plus medical interactive recovery assistant (MIRA) software? *J. Shoulder Elbow Surgery* **26**(12), e382–e389 (2017)

Designing a Music-Based Game for Training Pattern Recognition Control of a Myoelectric Prosthesis



D. Bessa, N. F. Rodrigues, E. Oliveira, J. Kolbenschlag, and C. Prahm

Abstract Access to early myoelectric training can be a crucial step in mastering prosthesis control. Controlling a prosthesis is a cognitively demanding task with high rejection rates. Serious games not only provide patients with an opportunity to train their myoelectric control, but also help maintain their engagement throughout the extensive rehabilitation process. This work proposes a novel serious game design to train machine learning based myoelectric control, implemented in the form of a music-based app. The prototype of the game was evaluated by seven able-bodied participants and three clinical professionals with regard to system usability and motivation. Results showed positive outcomes in motivation, and a need for specific system usability improvements.

1 Introduction

Arms and hands play a crucial part of our daily lives, they have an important role in performing tasks and communication. Therefore, the loss of an upper limb can greatly impact one's quality of life [1]. The main goal of using a prosthesis is to regain some functional capabilities and to perform bimanual tasks [2]. But for upper limb amputees to dexterously control prosthetic devices a long and repetitive rehabilitation process is required, the lack of motivation, extensive standard rehabilitation process and post traumatic depression can lead to high prosthesis rejection rates [3, 4].

D. Bessa (✉)

Department of Informatics, University of Minho, Braga, Portugal
e-mail: a75544@alunos.uminho.pt

N. F. Rodrigues · E. Oliveira

2Ai Polytechnique Institute of Cávado and Ave, Barcelos, Portugal
e-mail: eoliveira@ipca.pt

J. Kolbenschlag · C. Prahm

Department of Plastic and Reconstructive Surgery, Eberhard Karls University, BG Klinik, Tuebingen, Germany
e-mail: jkolbenschlag@bgu-tuebingen.de

Serious games were suggested to be as effective as standard rehabilitation, with the upside of higher patient engagement and motivation [5]. In the past decade, many serious games for myoelectric prosthesis training have been developed and tested, even though research is still limited in the effectiveness compared to traditional methods, because of their accessibility and engaging nature, serious games can support the rehabilitation process [6, 7].

2 Material and Methods

The game design was based on a popular commercial game named *Osu* [8], during which players need to interact with game objects while following the rhythm of a song. Similarly, our developed game focused on rhythm and subsequent muscle control, requiring precise and timed gestures based on the player's myoelectric (EMG) signals and dynamic arm movements.

The game used two different types of interactive objects: circles and sliders. The former required players to perform a gesture, such as a fist, on the circle's location. Sliders required the player to hold the gesture and move their arm to an indicated location. These objects aimed to mimic real life tasks by performing gestures while also moving. Each gesture had a corresponding fruit, and for players to score they needed to do the correct gesture, in the correct location at the correct time. Players received feedback on timing with game texts, and on gestures, a glowing light around the fruit appeared, as shown in Fig. 1.



Fig. 1 Screenshot of the game after an apple has been hit, a halo and a text appear as gesture and timing feedback

2.1 System

Unity game engine was used to implement the game, the Myo Armband, a consumer-grade EMG sensor armband developed by Thalmic Labs, equipped with eight surface EMG sensors and an inertial measurement unit, was used for gesture recognition and orientation. The armband can recognize four poses out of the box: fist, wave in, wave out, and finger spread, and custom profiles can be created and saved using the application Myo Connect, provided by Thalmic Labs.

2.2 Experimental Procedure

Seven able-bodied participants, two males and five females with an average age of 27 ± 4.28 (SD) as well as three clinical professionals, one male and two females with an average age of 48 ± 4.61 (SD) took part in this test.

The purpose of the study was explained to participants, as well as introduction to the game. The armband logo was placed on the radial side, and the armband diameter adjusted to the participants' arm. Using Myo Connect a custom profile was created for each participant, and participants got familiarized with the four gestures.

After the initial introduction and preparation, participants played for approximately 10 min, consisting of three levels with increasing difficulty, during the first level participants were guided on how to control and play the game. After the third level, they were instructed to answer the system usability scale (SUS), a modified intrinsic motivation inventory (IMI) questionnaire consisting of four subcategories (enjoyment, competence, effort, and pressure) and asked if they had any comments about the game.

3 Results

The usability results had high variation, the average of the SUS surveys was 64 ± 20.72 (SD), which means usability ranked below average. Usability was higher in the seven participants with an average of 69.64 ± 20.18 (SD) in comparison with the clinical professional average of 50.83 ± 18.43 (SD). The IMI enjoyment subclass was highly perceived by participants averaging 5.14 ± 1.09 (SD), effort measured 5.5 ± 0.71 (SD) equally highly perceived. Pressure averaged 3 ± 1.31 (SD), this result was considered positive, as pressure is a negative predictor of intrinsic motivation. Finally, the perceived competence averaged 3.4 ± 1.42 (SD). The IMI questionnaire results did not show significant differences between the professionals and participants.

The main problems that participants reported were the game control difficulty and lack of feedback. Five participants reported to have difficulties with cursor control

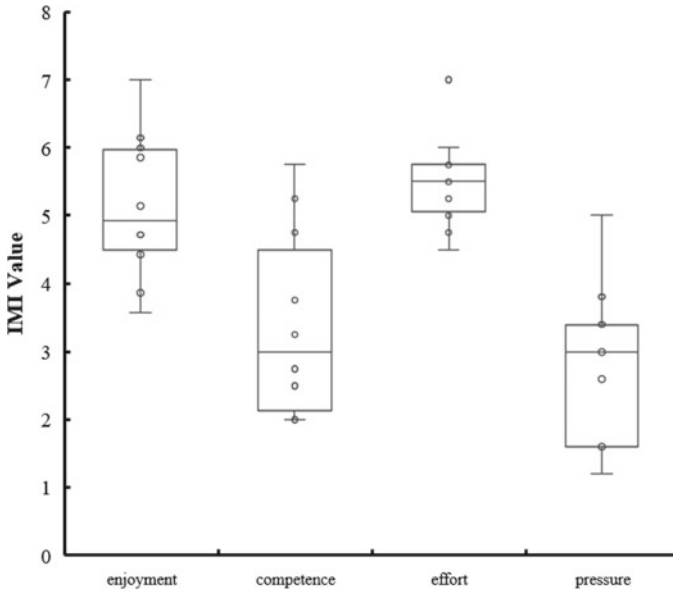


Fig. 2 Results from the IMI questionnaire by subclass average, using a 7-point Likert scale, with seven being “I strongly agree”

and gesture recognition and four participants felt the need for better positive feedback (Fig. 2).

4 Discussion

System usability and intrinsic motivation surveys have pointed out important problems to address in future game versions. Even though participants perceived the game as enjoyable overall, the system was too cumbersome to use in some instances, especially when performing gestures and moving the cursor.

Participants greatly improved after the initial level, even though they reported control problems and perceived competence below average, with an in-game introduction, focused on control and game mechanics or playing for a longer period of time could have improved participants perceived competence.

Positive feedback is one of the most important aspects of the game, and timed and correct feedback is required for transfer to prosthesis control [9]. Participants reported that they were unsure if they were doing the right gesture in some situations, to address this problem should be the main focus of future game versions.

Although enjoyment was above average, it could have been limited by the deficient control and gesture recognition. In [10], an increase in competence led to an increase

in enjoyment, meaning that improvements in visual feedback, gesture recognition, and control can potentially improve the system usability and enjoyment.

In the future, the Thalmic Labs Myo Connect application will not be used anymore to control the game, but instead we will use a different algorithm provided by a prosthetic company.

5 Conclusion

As the intervention consisted of just a short trial, there could be other problems that were not looked at, such as usability and motivation over time.

Overall, the system performed well, there were clear problems with usability and competence that can be addressed in future releases. Enjoyment, effort, and pressure seemed to indicate that participants felt motivated while playing the game. This study allowed to evaluate the design on usability and motivation, guiding future game development. The two main problems that were identified were the lack of feedback and difficulties in game control.

References

1. C. Castellini, R.M. Bongers, M. Nowak, C.K. Van Der Sluis, Upper-limb prosthetic myocontrol: two recommendations. *Front. Neurosci.* **9**(January), 496 (2016)
2. R.M. Bongers, P.J. Kyberd, H. Bouwsema, L.P.J. Kenney, D.H. Plettenburg, C.K. Van Der Sluis, Bernstein's levels of construction of movements applied to upper limb prosthetics. *J. Prosthet. Orthot.* **24**(2), 67–76 (2012)
3. E.A. Biddiss, T.O.M.T. Chau, Upper limb prosthesis use and abandonment: a survey of the last 25 years. *Prosthet. Orthot. Int.* **31**(September), 236–257 (2007)
4. C. Prahm, I. Vujaklija, Increasing motivation, effort and performance through game-based rehabilitation for upper limb myoelectric prosthesis control (2017)
5. B. Bonnechère, B. Jansen, L. Omelina, S. Van Sint, The use of commercial video games in rehabilitation: a systematic review. *Int. J. Rehabil. Res.* **39**, 277–290 (2016)
6. A. Tabor, S. Bateman, E. Scheme, D.R. Flatla, K. Gerling, Designing game-based myoelectric prosthesis training, pp. 1352–1363 (2017)
7. C. Prahm, MyoBeatz: using music and rhythm to improve prosthetic control in a mobile game for health, in *2019 IEEE 7th International Conference on Serious Games and Applications for Health* (2019), pp. 1–6
8. D. Herbert, Osu. 2007. Accessed July 2020. Available <https://osu.ppy.sh/>
9. H. Bouwsema, C.K. Van Der Sluis, R.M. Bongers, Effect of feedback during virtual training of grip force control with a myoelectric prosthesis. *PLoS ONE* **9**(5) (2014)
10. B.D. Winslow, M. Ruble, Z. Huber, Mobile, game-based training for myoelectric prosthesis control. *Front. Bioeng. Biotechnol.* **6**(July), 1–8 (2018)

Correlation Between EEG Band Power Parameters and Functional Scale in Stroke Patients



Marc Sebastián-Romagosa, Rupert Ortner, Josep Dinarès-Ferran,
and Christoph Guger

Abstract Stroke can cause severe motor and sensory impairments. Recent studies focus their attention to the Quantitative EEG (qEEG) searching for information in the brain signals that can help clinicians understating each patient's clinical state. In this study, we recorded 8 min of resting state EEG to 34 stroke patients in order to find some correlation between the brain signals and the functional motor state of the upper extremity. We used the Fugl-Meyer Assessment (FMA) for the functional assessment, and the Delta Alpha Ratio (DAR) and the Power Ratio Index (PRI) as features of the brain signals. The results showed that lower values of DAR and PRI are related with a better functionality in the upper extremity of the stroke patient. Future work must focus on exploring the relation of this parameters with other functional scales.

1 Introduction

Stroke is one of the most prevalent pathologies around the world and it can cause severe motor and sensory impairments that affect the daily activities of the survivors [1]. The hemiplegia is one of the most common consequences of the stroke and it is directly related with the injury in the brain.

M. Sebastián-Romagosa (✉) · R. Ortner · J. Dinarès-Ferran · C. Guger
g.tec medical engineering, Schiedlberg, Austria
e-mail: sebastian@gtec.at

R. Ortner
e-mail: ortner@gtec.at

J. Dinarès-Ferran
e-mail: dinares@gtec.at

C. Guger
e-mail: guger@gtec.at

Recent studies explored new methods to process and analyze brain signals acquired using noninvasive techniques with an easy setup like electroencephalography (EEG) [2–6]. Extracting features from the EEG using useful tools as Quantitative EEG (qEEG) can help clinicians understanding each patient’s clinical state. qEEG parameters have shown multiple correlations with different pathologies, making qEEG an essential tool for different clinical field. Some interesting parameters are the Delta Alpha Ratio (DAR) [7] and the Power Ratio Index (PRI) [8].

This study aims to find some correlation between the patients’ upper extremities functionality and their brain signals using the DAR and PRI parameters.

2 Methods

2.1 Participants

Thirty-four stroke patients were enrolled in the study (two of them were excluded) and their mean age was 65.3 years ($SD = 14.4$). Twenty-two of the patients were male (64.7%), and the other twelve were female (35.3%). Only seven of the patients were in subacute phase (20.6%) whereas the rest were in chronic phase (79.4%). The location of the stroke was in the right hemisphere in 23 patients and in the left hemisphere in 11 patients (32.4%).

2.2 Assessment

The Fugl-Meyer Assessment (FMA) is a widely used functionality scale for the motor assessment of patients with physical impairments after the stroke [9, 10]. The FMA for the upper extremity (FMAue) contains values between 0 and 66 points, where a score of 0 means no motor function in the upper extremity and 66 points reflects a normal functionality.

In this study the FMAue was used to assess the motor functionality for each patient.

2.3 EEG Acquisition

For the acquisition the patient wore an EEG cap with 16 active electrodes (g.SCARABEO, g.tec medical engineering GmbH, Austria) placed over the sensorimotor cortex according to the 10/10 international system: FC5, FC1, FCz, FC2, FC6, C5 C3, C1, Cz, C2, C4, C6, CP5, CP1, CP2, CP6. The Fpz electrode was connected

to the ground and a reference electrode was placed on the right earlobe. The EEG cap was connected to a biomedical amplifier (g.USBamp, g.tec medical engineering GmbH, Austria), which was connected to a computer for the EEG acquisition. For each patient we recorded 8 min of resting state with open eyes.

2.4 EEG Data Processing

Each EEG channel was divided in epochs of 4 s using a Hamming window with an overlapping of 2 s. To get the absolute power of a single channel for a specific band we applied a band pass filter and the Welch method among all epochs, and then we averaged all the frequency points obtained to get a single value for each channel. The final value of the absolute power of a specific band came from the average of the absolute power values for each electrode.

Frequency analysis of the EEG signals defines 5 main bands of interest: delta (1–4 Hz), theta (4–8 Hz), alpha (8–12 Hz), beta (12–30 Hz) and gamma (>30 Hz). This study focuses its interest in the relation between these power bands through its absolute power parameter.

The Delta Alpha Ratio (DAR) is defined as the ratio between the absolute power of the delta band and the absolute power of the alpha band. The Power Ratio Index (PRI) is defined as the sum of the absolute power of the delta and theta band divided by the sum of the absolute power of the alpha and beta band.

2.5 Statistical Analysis

The statistical analysis was performed using MATLAB 2017a. The statistical tests were chosen according to the sample size, the normality of the sample (Shapiro-Wilk Test) and the homogenous of the variance (Levene's Test).

3 Results

Table 1 shows the mean and standard deviation for the values of DAR, PRI and FMAue among all the patients. The scatter plot of DAR and FMAue (Fig. 1) shows that the upper extremity functionality is directly related with the DAR parameter (ρ)

Table 1 DAR, PRI and FMA statistical results

	DAR	PRI	FMAue
mean	5.02	3.50	26.06
SD	3.21	2.12	16.28

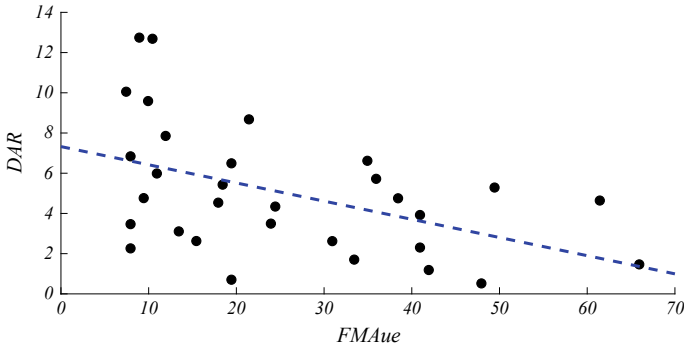


Fig. 1 Significant correlation between DAR and the FMAue scale

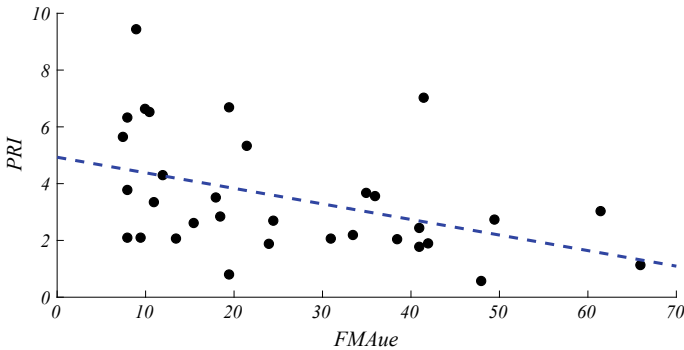


Fig. 2 Significant correlation between PRI and the FMAue scale

$= -0.462$, $P = 0.009$). In the same way, Fig. 2 shows that the PRI parameter has a significant correlation with the FMAue ($\rho = -0.452$, $P = 0.009$). Thus, lower values of the DAR and PRI parameters are related with a better functionality in the upper extremity of the stroke patient.

4 Discussion and Conclusion

DAR has been previously described as a useful tool to detect delayed cerebral ischemia [7] whereas PRI could be correlated with location of the injury [8]. Therefore, different studies have tried to use these parameters to correlate and predict motor functionality based on the EEG recordings [2, 11, 12].

In this study we found a strong correlation of DAR and PRI with the most used functional scale in the stroke patient assessment (FMA). Although, with the results of this study we cannot say that DAR and PRI alone can be used for diagnosis purposes,

but they might contribute to other neurological assessments and ongoing monitoring of brain damage and recovery for stroke patients.

This study showed that DAR and PRI could be useful in the assessment of the stroke patients. Future studies must focus on other qEEG parameters and find if they have some correlation with FMAue as well as with other functional scales used in the stroke assessment.

Acknowledgements This study has been supported by an EU funded H2020 Research and Innovation Staff Exchange 589 grant: PRO GAIT grant agreement number 778043. It also has been partially supported by the Ministry of Business and Knowledge of the Government of Catalonia (Industrial Doctorates Plan).

References

1. J. Kim, T. Thayabaranathan, G.A. Donnan, G. Howard, V.J. Howard, P.M. Rothwell et al., Global Stroke Statistics 2019. *Int. J. Stroke* **139**, 174749302090954 (2020). <https://doi.org/10.1177/1747493020909545>
2. J. Leon-Carrion, J.F. Martin-Rodriguez, J. Damas-Lopez, J.M. Barroso, y Martin, M.R. Dominguez-Morales, Delta-alpha ratio correlates with level of recovery after neurorehabilitation in patients with acquired brain injury. *Clin. Neurophysiol.* **120**(6), 1039–1045 (2009)
3. B. Foreman, J. Claassen, Quantitative EEG for the detection of brain ischemia. *Crit. Care* **16**(2), 216 (2012)
4. P.A.D.M. Kanda, R. Anghinah, M.T. Smidh, J.M. Silva, The clinical use of quantitative EEG in cognitive disorders. *Dement. Neuropsychol.* **3**(3), 195–203 (2009)
5. G. Rabiller, J.-W. He, Y. Nishijima, A. Wong, J. Liu, Perturbation of brain oscillations after ischemic stroke: a potential biomarker for post-stroke function and therapy. *Int. J. Mol. Sci.* **16**(10), 25605–25640 (2015)
6. J. Wu, R. Srinivasan, E. Burke Quinlan, A. Solodkin, S.L. Small, S.C. Cramer, Utility of EEG measures of brain function in patients with acute stroke. *J. Neurophysiol.* (2016)
7. J. Claassen et al., Quantitative continuous EEG for detecting delayed cerebral ischemia in patients with poor-grade subarachnoid hemorrhage. *Clin. Neurophysiol.* **115**(12), 2699–2710 (2004)
8. K. Nagata, C.E. Gross, G.W. Kindt, J.M. Geier, G.R. Adey, Topographic electroencephalographic study with power ratio index mapping in patients with malignant brain tumors. *Neurosurgery* **17**(4), 613–619 (1985)
9. D.J. Gladstone, C.J. Danells, S.E. Black, The Fugl-Meyer assessment of motor recovery after stroke: a critical review of its measurement properties. *Neurorehabil. Neural Repair* **16**, 232–240 (2002). <https://doi.org/10.1177/154596802401105171>
10. E.J. Woytowicz, J.C. Rietschel, R.N. Goodman, S.S. Conroy, J.D. Sorkin, J. Whitall et al., Determining levels of upper extremity movement impairment by applying a cluster analysis to the Fugl-Meyer assessment of the upper extremity in chronic stroke. *Arch. Phys. Med. Rehabil.* **98**, 456–462 (2017). <https://doi.org/10.1016/j.apmr.2016.06.023>
11. S.P. Finnigan, M. Walsh, S.E. Rose, J.B. Chalk, Quantitative EEG indices of sub-acute ischaemic stroke correlate with clinical outcomes. *Clin. Neurophysiol.* **118**, 2525–2532 (2007)
12. P. Trujillo et al., Quantitative EEG for predicting upper limb motor recovery in chronic stroke robot-assisted rehabilitation. *IEEE Trans. Neural Syst. Rehabil. Eng.* **25**(7), 1058–1067 (2017)

SS6: Simulation and Prediction of Human Motion

Adaptive Oscillators as Template for Modeling and Assisting Rhythmic Movements



Renaud Ronsse

Abstract This paper overviews our recent efforts for promoting adaptive oscillators as template for modeling and assisting rhythmic movements. Adaptive oscillators are dynamical systems that can be viewed as the simplest possible model of a neural Central Pattern Generator, augmented with learning dynamics. Therefore, if coupled to a human user producing a rhythmic movement, such an adaptive oscillator can be used to govern the behavior of an assistive robot providing different kinds of rhythmic movement support, with or without energy injection, and both for the upper- and the lower-limb.

1 Introduction

Rhythmic movements are repetitive actions executed along a periodic pattern. Some of them like breathing, chewing, or crawling are part of the essential repertoire for the survival of primitive species. Consequently, researchers established that they form a fundamental class of movements—or primitive—that is phylogenetically older than more complex activities like discrete reaching to a target [1]. Spinal neural circuitry plays a ubiquitous role in the execution of rhythmic movements. In particular, Central Pattern Generators (CPGs) are thought to be the source of rhythmicity in the production of muscular activation patterns governing locomotion movements in mammals [2]. Our recent work in bipedal locomotion modeling further showed how CPGs can be ideally combined with spinal reflexes for producing robust, versatile, and energy-efficient walking patterns [3].

In this contribution, we specifically focus on a tool that we extensively used in the recent past to model, predict, and assist human rhythmic movements, namely

This work was supported by the EU within the CYBERLEGSPlusPlus project (H2020-ICT-2016-1, Grant Agreement #731931), the Belgian F.R.S.-FNRS (Aspirant grant #16744574, FRIA grant F3/5/5-MCF/XH/FC-18101), and by the Foundation van Goethem Brichant.

R. Ronsse (✉)

Institute of Mechanics, Materials, and Civil Engineering, The Institute of Neuroscience, and Louvain Bionics, UCLouvain, Louvain-la-Neuve, Belgium
e-mail: renaud.ronsse@uclouvain.be

© The Author(s), under exclusive license to Springer Nature Switzerland AG 2022

271

D. Torricelli et al. (eds.), *Converging Clinical and Engineering Research on Neurorehabilitation IV*, Biosystems & Biorobotics 28,
https://doi.org/10.1007/978-3-030-70316-5_44

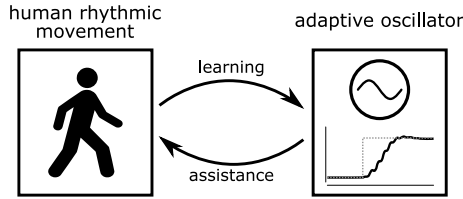


Fig. 1 General framework: an adaptive oscillator continuously learns the features of a rhythmic movements produced by a human, and in turns provides rhythmic assistance that is fine-tuned to the produced movement

adaptive oscillators (AOs). An AO can be viewed as a harmonic oscillator, i.e. the simplest model of a CPG, that is augmented with learning mechanisms in order to synchronize to an external signal. This general framework is pictured in Fig. 1. The rest of this paper overviews how we adapted it to representative scenarios of locomotion and upper-limb assistance.

2 Adaptive Oscillator

An AO is a dynamical system building upon a simple harmonic oscillator, i.e. $\dot{\phi} = \omega$, where ϕ and ω are the oscillator phase and frequency, respectively. More precisely, this oscillator is augmented with learning terms [4] storing in dedicated state variables the features (i.e. the phase ϕ_r , frequency ω_r , and amplitude α_r) of a quasi-rhythmic input signal, i.e. $x_r = \alpha_r \sin \phi_r$. Here, “quasi-rhythmic” should be understood in the sense that ω_r and α_r could be time-varying, yet at a slower timescale than the input frequency itself. The AO thus writes as:

$$\begin{aligned}\dot{\phi} &= \omega + v_\phi F / \alpha \cos \phi, \\ \dot{\omega} &= v_\omega F / \alpha \cos \phi, \\ \dot{\alpha} &= \eta F \sin \phi,\end{aligned}\tag{1}$$

where v_ϕ , v_ω and η are gains driving the learning timescales [5], and

$$F = x_r - \hat{x} = x_r - \alpha \sin \phi\tag{2}$$

is the error signal driving learning, i.e. the difference between the input signal and its estimate \hat{x} . The insert in the lower right corner of Fig. 1 captures a typical learning behavior of an AO when the input frequency is abruptly changing at a certain time (gray dotted line).

3 Locomotion Assistance

In its simplest form (1), an AO can thus be viewed as a state observer, estimating the features of a rhythmic input signal. If this signal is produced by a human user during locomotion—such as the hip angular pattern during walking—the AO could be used for instance to deliver a phase-dependent assistive torque to an exoskeleton [8] or even to a prosthesis replacing another missing joint [9]. Similarly, the same system could be used to predict the signal in the near future, via a time-shifted version of the estimator, i.e. $\hat{x}(t + \delta t) = \alpha \sin(\phi + \omega \delta t)$. This is the approach we followed in [10] in order to provide positive power assistance by attracting the user’s hips to their own predicted future trajectory through a compliant force field. In the same paper, we reported how AO could be used to provide torque assistance based on a dynamic model of the task and estimates of kinematic derivatives [5].

4 “Smoothing” Assistance

More recently, we tested AOs to provide specific assistance to patients with motor disorders, in particular regarding the execution of upper-limb rhythmic tasks. Indeed, stroke patients typically produce jerky reaching movements, and this has been observed in rhythmic tasks as well [11]. In [6], we developed an assist-as-needed control framework for stroke patients performing rhythmic movements. More precisely, an upper-limb assistive robot delivered a force that was directly proportional to the AO error signal F (2), see Fig. 2a. Therefore, if the patient was producing a perfectly harmonic movement—what we considered to be “perfectly smooth” in that

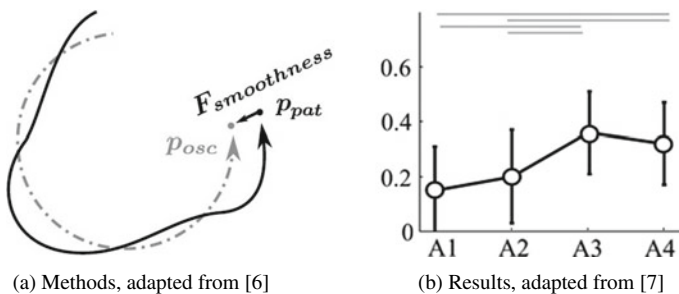


Fig. 2 Smoothing assistance framework. **a** When requested to produce an upper-limb movement (here, continuous drawing of a circle), a stroke patient typically produces a jerkier trajectory (here p_{pat}). The AO (1) continuously learns a smoother version of this movement p_{osc} . An assistive force proportional to their difference $F_{smoothness}$ is delivered in order to produce smoother movements. **b** Evolution over 4 assessment days (pre-treatment: A1, A2—post-treatment: A3 and A4) of 13 stroke patients during the execution of a typical rhythmic task in a metric capturing movement harmonicity. The error bars represent the 95% confidence intervals. The horizontal lines capture the assessment numbers being significantly different from each other

work— F converged to 0 and no assistance was provided; while the assistive field would encourage the movement to be smoother otherwise. Importantly, since the AO was continuously learning from the user's input signal, such assistance was providing no energy to the user on average, therefore encouraging active participation.

We conducted a longitudinal study with 13 post-stroke patients who received this robotic-based therapy during 12 sessions of 18-min spread over 1 month [7]. Their performance was assessed twice before the therapy (A1 and A2), once just after (A3) and once three months after the last session of the therapy, to assess the long-term retention of the intervention (A4). Figure 2b reports one of the main results of this study, namely the level of harmonicity of a typical self-produced rhythmic movement (i.e. while receiving no more assistance from the robot). In short, this index is bounded between 0 and 1, 1 corresponding to a pure harmonic movement. This figure shows that the therapy improved the patients' capacity to produce autonomous rhythmic movement with a better harmonicity, even months after the intervention ended. More intriguingly, we also reported some improvements in performing discrete movements, likely recruiting some transfer mechanisms which still have to be unveiled.

5 Conclusion

In this document, we overviewed our recent efforts in using adaptive oscillators for modeling and assisting rhythmic movements, both with the upper- and the lower-limb. We state that this mathematical tool is particularly suited to be used as a template for closed-loop interactions between a (disabled) user and an assistive robot. Since both parties continuously adapt to each other, the robotic assistance is suited to the current user's needs, while promoting his/her active participation to the task.

In future work, we will adapt the smoothing framework reported in Sect. 4 to the lower-limb, and test it with patients having specific gait disorders while using a wearable device. We will further continue our efforts in combining these AOs with task-specific assistive strategies, in order to support the user not only in level-ground walking but also in more energetically challenging tasks.

References

1. N. Hogan, D. Sternad, Dynamic primitives of motor behavior. *Biol. Cybern.* **106**, 727–739 (2012)
2. K. Minassian, U.S. Hofstoetter, F. Dzeladini, P.A. Guertin, A. Ijspeert, The human central pattern generator for locomotion: does it exist and contribute to walking? *Neuroscientist* **23**, 649–663 (2017)
3. N. Van der Noot, A.J. Ijspeert, R. Ronsse, Bio-inspired controller achieving forward speed modulation with a 3d bipedal walker. *Int. J. Rob. Res.* **37**, 168–196 (2018)

4. L. Righetti, J. Buchli, A.J. Ijspeert, Dynamic Hebbian learning in adaptive frequency oscillators. *Phys. D* **216**, 269–281 (2006)
5. R. Ronsse et al., Real-time estimate of velocity and acceleration of quasi-periodic signals using adaptive oscillators. *Rob. IEEE Trans.* **29**, 783–791 (2013)
6. P. Leconte, R. Ronsse, Performance-based robotic assistance during rhythmic arm exercises. *J. Neuroengineering Rehabil.* **13**, (2016)
7. P. Leconte, G. Stoquart, T. Lejeune, R. Ronsse, Rhythmic robotic training enhances motor skills of both rhythmic and discrete upper-limb movements after stroke: a longitudinal pilot study. *Int. J. Rehabil. Res.* **42**, 46–55 (2019)
8. V. Ruiz Garate, et al., Experimental validation of motor primitive-based control for leg exoskeletons during continuous multi-locomotion tasks. *Front. Neurobot.* **11** (2017)
9. Heins, S., et al., Compliant control of a transfemoral prosthesis by combining feed-forward and feedback, in 2020 8th IEEE RAS and EMBS International Conference on Biomedical Robotics and Biomechatronics (BioRob), to be published
10. R. Ronsse et al., Oscillator-based assistance of cyclical movements: model-based and model-free approaches. *Med. Biol. Eng. Comput.* **49**, 1173–1185 (2011)
11. M. Simkins, A. Burleigh Jacobs, J. Rosen, Rhythmic affects on stroke-induced joint synergies across a range of speeds. *Exp. Brain. Res.* **229**, 517–524 (2013)

Converting Biomechanical Models from OpenSim to MuJoCo



Aleksi Ikkala and Perttu Hämmäläinen

Abstract OpenSim is a widely used biomechanics simulator with several anatomically accurate human musculo-skeletal models. While OpenSim provides useful tools to analyse human movement, it is not fast enough to be routinely used for emerging research directions, e.g., learning and simulating motor control through deep neural networks and Reinforcement Learning (RL). We propose a framework for converting OpenSim models to MuJoCo, the de facto simulator in machine learning research, which itself lacks accurate musculo-skeletal human models. We show that with a few simple approximations of anatomical details, an OpenSim model can be automatically converted to a MuJoCo version that runs up to 600 times faster. We also demonstrate an approach to computationally optimize MuJoCo model parameters so that forward simulations of both simulators produce similar results.

1 Introduction

OpenSim [1, 2] is a physics simulator extensively used by biomechanics researchers. This community of researchers have also created many human and animal musculo-skeletal models, often based on cadaver studies. The unparalleled anatomical accuracy of various models have been validated in several papers (for instance [3, 4]).

Although OpenSim models excel in accuracy, the simulator lacks in speed: a forward simulation of a movement that lasts a few seconds can take minutes to run on a complex model comprised of tens of muscles and joints. Therefore, running OpenSim models on another physics simulator might provide enough speed-up to use these anatomically accurate models for e.g. machine learning or animation research.

MuJoCo is a fast and accurate simulator oft-used in machine learning research [5], which itself does not have biomechanical models that compare with the accuracy of

This work has been supported by Academy of Finland grant 299358.

A. Ikkala (✉) · P. Hämmäläinen
Computer Science Department, Aalto University, Espoo, Finland
e-mail: aleksi.ikkala@aalto.fi

© The Author(s), under exclusive license to Springer Nature Switzerland AG 2022
D. Torricelli et al. (eds.), *Converging Clinical and Engineering Research*
on *Neurorehabilitation IV*, Biosystems & Biorobotics 28,
https://doi.org/10.1007/978-3-030-70316-5_45

277

OpenSim models. Furthermore, the correspondence between OpenSim and MuJoCo model definitions, in terms of building blocks of the models and their configurations, is high enough to warrant attempts at creating an automatic model converter (see MuJoCo discussion forum for multiple threads on the subject). However, to the best of authors' knowledge, there are no MuJoCo converted models publicly available, nor is there a converter that works with reasonably complex OpenSim models. We present a new converter that is publicly available at <https://github.com/aikkala/O2MConverter> and is able to process complex OpenSim models.

2 Materials and Methods

In our experiments we used a complex OpenSim model comprised of a fixed torso and dynamic shoulder and arm [3]. The model has seven degrees of freedom, including shoulder rotation and elevation, elbow flexion, forearm rotation, and wrist flexion and deviation, but we locked wrist flexion and deviation to improve OpenSim simulation stability. The model is actuated by 50 muscles that cover all the remaining five degrees of freedom.

We used OpenSim 4.0 and MuJoCo 2.0 and their Python bindings to run the experiments, all on the same laptop equipped with an Intel i7-8850H processor and 32GB RAM.

2.1 Model Conversion

Converting OpenSim models to MuJoCo is relatively straightforward: both software use an XML based model definition, and the model parts—bodies, joints, musculo-tendon units—are largely equivalent. In fact, building an equivalent skeletal model in MuJoCo is only a matter of disassembling the bodies and joints of an OpenSim model and re-configuring them into a MuJoCo model.

However, there are some anatomical details that are difficult to model exactly in MuJoCo and must be approximated to some extent. For instance, in OpenSim forces acting on joints can be defined in a piecewise linear manner (called *CoordinateLimitForce*), which is cumbersome to model exactly in MuJoCo. OpenSim also offers more flexibility over the anatomical modelling of a musculo-tendon unit (MTU), and particularly problematic are OpenSim's dynamically moving MTU path points whose locations change as a function of a specified joint coordinate value (*MovingPathPoint* and *ConditionalPathPoint*). All these approximations cause inaccuracies in the converted model, which can be mitigated to some extent by optimizing the converted model's parameters.

2.2 Optimization

In order to optimize the converted model's parameters, we generated a 100 sets of muscle activations. These activations were modelled as slow frequency (1 Hz) sine waves with varying phases, sampled at a frequency 500 Hz. To increase OpenSim simulation stability, the muscle activation sets had a duration of 1 s, and only a third of muscles were active in a set.

These muscle activations were then used as controls in both OpenSim and MuJoCo forward dynamics simulations—with a simulation timestep of 2 milliseconds in both simulators—to generate trajectories. OpenSim's forward dynamics failed to run for 3 sets of muscle activations, and thus we used a subset of 78 trajectories for optimizing the parameters, and a subset of 19 trajectories to estimate joint errors before and after parameter optimization. The parameters that we optimized were: damping and joint limit softness for each non-locked degree of freedom, damping and stiffness for each tendon, and scale (roughly equivalent to strength) of each muscle (160 parameters in total).

The converted model's parameters were optimized with a Python implementation of CMA-ES [7, 8], a popular black-box optimization algorithm. We used squared difference of joint positions between OpenSim and MuJoCo forward simulations, summed over all seven degrees of freedom and all training trajectories, as the objective to be minimized. We also augmented the objective with a small cost term to discourage unrealistically high parameter values.

It is important to note that even smallest differences between the models can make their trajectories diverge significantly over time. To alleviate the divergence, we augmented the controls with corrective control signals. These corrective signals were optimized separately for each test set run by minimizing the sum of squared joint position differences, while simultaneously penalising for large corrective signal values using L2 loss. The corrective signals were sampled 10 Hz and modelled as cubic splines.

3 Results

To estimate the accuracy of the converted model, we compare the mean absolute errors for each joint over trajectories in the test set, before and after parameter optimization; see Fig. 1. See Fig. 2 for mean absolute difference between reference muscle activations and optimized muscle activations over test set runs.

A video example of OpenSim reference movement alongside with the converted model's replicated movements, with and without parameter and muscle activation optimization, is available at <https://youtu.be/Nz3R6-113IU>.

In addition to estimating accuracy of the converted model, we also compared the efficiency of both simulators by calculating average run time over all 97 forward simulations. One OpenSim simulation took 15.50 s on average, while a MuJoCo

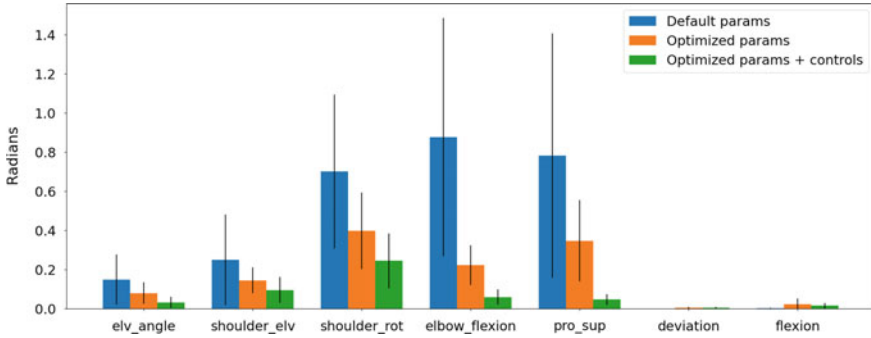


Fig. 1 Mean absolute error in radians for each joint over 19 test trajectories

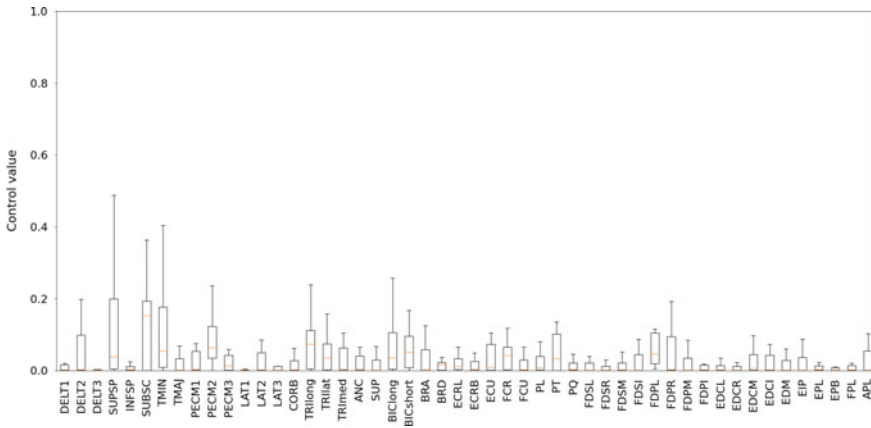


Fig. 2 A boxplot depicting mean absolute difference between reference and optimized muscle activations over 19 test trajectories (outliers not visualised). Muscle activations are in range [0, 1], making the maximum difference 1.0

simulation ran for 0.025 s on average, which makes MuJoCo roughly 600 times faster.

4 Discussion

Figures 1 and 2 indicate that divergence of forward simulation cannot be prevented simply by optimizing the converted model’s parameters. Fortunately, OpenSim and MuJoCo simulations can be made almost identical with only minor corrections to the muscle activations. This suggests that MuJoCo should be able to produce reasonably realistic results, e.g., in discovering muscle activation sequences through deep reinforcement learning (for example, see [9]).

Additionally, MuJoCo simulations are substantially faster, and the converted model does behave in a similar fashion to the OpenSim model even with only parameter optimization. This might be enough for some use cases, e.g. in animation and machine learning research.

Finally, it should be noted, that in addition to accuracy and speed, one should consider a third performance metric: stability. In order to ensure OpenSim simulations did not crash we had to lock wrist flexion and deviation, and find suitable starting positions for joints. Even then 3 out of the 100 OpenSim simulations crashed, whereas the MuJoCo model had no problems with wrist flexion and deviation or joint starting positions. This is a major advantage when using such complex biomechanical models for research that requires massive amounts of simulations, such as machine learning research.

References

1. S. Delp, F. Anderson, A. Arnold, P. Loan, A. Habib, C. John et al., OpenSim: open-source software to create and analyze dynamic simulations of movement. *IEEE Trans. Biomed. Eng.* **54**, 1940–1950 (2007)
2. A. Seth et al., OpenSim: simulating musculoskeletal dynamics and neuromuscular control to study human and animal movement, in *PLoS Computational Biology*, vol. 14, ed. by D. Schneidman (Public Library of Science, 2018), pp. e1006223
3. K. Saul et al., Benchmarking of dynamic simulation predictions in two software platforms using an upper limb musculoskeletal model. *Comput. Methods Biomech. Biomed. Eng.* **18**, Taylor and Francis Ltd, 2015, pp. 1445–1458
4. E. Arnold, S. Ward, R. Lieber, S. Delp, A model of the lower limb for analysis of human movement. *Ann. Biomed. Eng.* **38**, 269–279 (2010)
5. E. Todorov, T. Erez, Y. Tassa, MuJoCo: a physics engine for model-based control. *IEEE IROS* 5026–5033 (2012)
6. G. Brockman et al., OpenAI Gym (2016). [arXiv:1606.01540](https://arxiv.org/abs/1606.01540)
7. N. Hansen, S. Müller, P. Koumoutsakos, *Reducing the time complexity of the derandomized evolution strategy with covariance matrix adaptation (CMA-ES)*, in *Evolutionary Computation*, vol. 11 (MIT Press, Cambridge, MA, 2003), pp. 1–18
8. N. Hansen, Y. Akimoto, P. Baudis, CMA-ES/pycma on Github (2019)
9. S. Lee, M. Park, K. Lee, J. Lee, Scalable muscle-actuated human simulation and control, in *ACM Transactions on Graphics*, vol. 38, Association for Computing Machinery, New York, NY 2019, article 73

Quaternions-Based Normal Gait Kinematics Model



Juan C. Gonzalez-Islas, Omar A. Dominguez-Ramirez, Omar Lopez-Ortega, Ma. de los Angeles Alonso-Lavernia, and Felix A. Castro-Espinoza

Abstract For the human being, the gait is one of the most important way for locomotion. In this paper, we present a novel approach of forward kinematics of position using quaternions algebra to describe the lower limbs position during the gait cycle. Gait analysis was developed using an own quaternions-based numerical platform programmed on Matlab[®]. For this purpose, we use the joint database of the normal gait model available on OpenSim[®]. The normal gait pattern was studied in the sagittal, frontal and transverse planes (in anatomical joint space and gait space). The analyzed movements in this work were pelvis (rotation and tilt), hip and knee flexo-extensions, as well as ankle dorsiflexion and plantarflexion. We show high precision and flexibility in gait analysis using this method, which can be used for clinical diagnosis, sports medicine or biomechanical research.

1 Introduction

Biomechanical gait analysis is used as an assessment tool to evaluate kinetics and kinematics, which allows to determine normal and abnormal gait conditions. For clinical approaches, diseases such as: (i) cerebral palsy, (ii) arthritis, (iii) multiple

J. C. Gonzalez-Islas

Ph.D. Program of Computer Sciences, Autonomous University of Hidalgo State and researcher at Technological University of Tulancingo, Hidalgo, Mexico
e-mail: juan_gonzalez7024@uaeh.edu.mx

O. A. Dominguez-Ramirez (✉) · O. Lopez-Ortega · M. A. Alonso-Lavernia ·
F. A. Castro-Espinoza

Basic Sciences and Engineering Institute, Autonomous University of Hidalgo State, Hidalgo, Mexico
e-mail: omar@uaeh.edu.mx

O. Lopez-Ortega

e-mail: lopezo@uaeh.edu.mx

M. A. Alonso-Lavernia

e-mail: marial@uaeh.edu.mx

F. A. Castro-Espinoza

e-mail: fcastro@uaeh.edu.mx

© The Author(s), under exclusive license to Springer Nature Switzerland AG 2022

283

D. Torricelli et al. (eds.), *Converging Clinical and Engineering Research on Neurorehabilitation IV*, Biosystems & Biorobotics 28,
https://doi.org/10.1007/978-3-030-70316-5_46

sclerosis, (iv) Parkinson's disease, (v) stroke, among others [1], have been diagnosed through human gait analysis. There are several methods to develop this evaluation, the most common are based on qualitative analysis performed by the specialists [2]. However, the required precision to obtain reliable diagnoses in this sense, has encouraged the development of new approaches to instrument and model the human gait.

Commonly, quaternions formulated by Hamilton in 1843 [3], have been applied in rotations of rigid bodies in 3 and 4 dimensional euclidean space [4], in computer graphics [5] or in multicopter control [6]. In robotics, quaternions have been received especial attention to kinematics model, highlighting their advantages over the homogeneous transformation matrix (HTM) and the Denavit-Hartenberg (D-H) regarding computational cost, storage [7] and solution of singularity problems [8].

Although in [9] has been documented, better performance of quaternions over HTM and D-H to model the forward kinematics of an n-DoF robot arm, quaternions have not been used for kinematics modeling of the serial chain that represents the lower limbs during the human gait. In [10, 11], the quaternions-based 3D position of the frame of each independent body segment is obtained from gyroscope and accelerometer signals. However, these approaches require an extra calibration process to reduce the position estimation error derived from the use of inertial sensors. Also, in both works the anthropometry was not taken into account and the joint system is not considered as a serial chain.

In this work, an approach to model the forward kinematics of position of lower limbs during the human gait using quaternions algebra is presented. For this purpose, the joint lower limbs system is addressed as an open chain of 8 Degrees of Freedom (DoF), which unlike other works, considers in addition to the movements of the hip, knee and ankle, the rotation and inclination of the pelvis.

2 Materials and Methods

Forward kinematics of position of a rigid body is a vector function $\mathbf{F}_R(l_i, q)$ that relates the joint variables $q \in \mathbb{R}^{n \times 1}$ and the lengths of the i -th link l_i , with the cartesian coordinates $[x, y, z]^T \in \mathbb{R}^{3 \times 1}$. There are some well-known methods for this purpose such as geometric method, Denavit-Hartenberg (D-H) convention [12]. Nevertheless, these methods have been overcome by quaternions approaches [9].

A quaternion $Q = r + xi + yj + zk$ consists of a real part r and a pure part $v = xi + yj + zk$, which can be decomposed into $a + bu$, where $\mathbf{u} = \frac{x}{\|v\|}i + \frac{y}{\|v\|}j + \frac{z}{\|v\|}k$ is an imaginary unit three-vector [13]. A rotation over the angle q about an axis \mathbf{u} is represented by the unit quaternion $Q = \cos(\frac{q}{2}) + \mathbf{u} \sin(\frac{q}{2})$ [14]. Then, given a rotation represented by the unit quaternion Q , this can be applied to an arbitrary vector (pure quaternion) $\mathbf{v} \in \mathbb{R}^{3 \times 1}$ as $R(Q)\mathbf{v} = Q\mathbf{v}\bar{Q}$, where $\bar{Q} = \cos(\frac{q}{2}) - \mathbf{u} \sin(\frac{q}{2})$ is the conjugated rotation quaternion.

To model forward kinematics of position of the lower limbs during human gait using quaternions algebra, is proposed the human 8 DoF model shown in the Fig. 1.

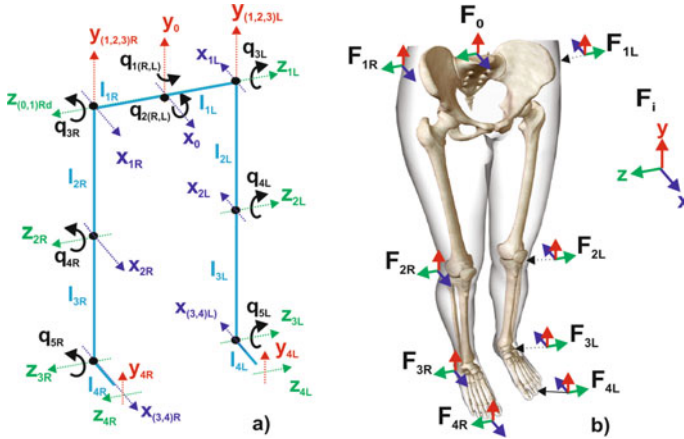


Fig. 1 **a** Kinematic chain representing the frames that define the movements of the lower limbs joints and **b** correspondences of frames in human body references

The model features the lower limbs as 7 rigid-body segments (1) pelvis, (2) right femur, (3) left femur, (4) right tibia, (5) left tibia, (6) right foot and (7) left foot. The relative motion of this segments is calculated by quaternions algebra. The anthropometry, which represents the length of the body-segments of the kinematic chain is adapted from [11] and the joint angles values are adopted from [15]. The pelvis, hip, knee and ankle joints, as well as, the big toe (end-effector), are modelled as a consecutive orthonormal frames, which is represented as a serial open chain during the swing phase.

For the modeling presented in this work, the base frame \mathbf{F}_0 placed in the pelvis is considered as absolute origin of the joint system, that is, the translation of this segment body is not considered. \mathbf{F}_0 is represented by quaternions as $\mathbf{F}_0 = [0, 0, 0, 0]$. Consecutively are defined the subsequent frames as: $\mathbf{F}_{1R} = [0, 0, 0, l_{1R}\mathbf{k}]$, $\mathbf{F}_{2R} = [0, 0, -l_{2R}\mathbf{j}, 0]$, $\mathbf{F}_{3R} = [0, 0, -l_{3R}\mathbf{j}, 0]$ and $\mathbf{F}_{4R} = [0, l_{4R}\mathbf{i}, 0, 0]$, which correspond to hip, knee, ankle and big toe of the right lower limb, respectively, where l_{1R} , l_{2R} , l_{3R} and l_{4R} are the links that represent the anthropometry of the pelvis, femur, tibia and foot of this extremity. Quaternions $Q_{1R} = \cos(\frac{q_{1R}}{2}) + \mathbf{u}_{1R} \sin(\frac{q_{1R}}{2})$, $Q_{2R} = \cos(\frac{q_{2R}}{2}) + \mathbf{u}_{2R} \sin(\frac{q_{2R}}{2})$, $Q_{3R} = \cos(\frac{q_{3R}}{2}) + \mathbf{u}_{3R} \sin(\frac{q_{3R}}{2})$, $Q_{4R} = \cos(\frac{q_{4R}}{2}) + \mathbf{u}_{4R} \sin(\frac{q_{4R}}{2})$ and $Q_{5R} = \cos(\frac{q_{5R}}{2}) + \mathbf{u}_{5R} \sin(\frac{q_{5R}}{2})$, are related to the movements of rotation and tilt of the pelvis, hip and knee flexion-extension, as well as ankle dorsiflexion and plantarflexion, where $\mathbf{u}_{1R} = [0, 0, \mathbf{j}, 0]$, $\mathbf{u}_{2R} = [0, \mathbf{i}, 0, 0]$, $\mathbf{u}_{3R} = \mathbf{u}_{4R} = \mathbf{u}_{5R} = [0, 0, 0, \mathbf{k}]$.

Similarly, for the left lower limb, $\mathbf{F}_{1L} = [0, 0, 0, l_{1L}\mathbf{k}]$, $\mathbf{F}_{2L} = [0, 0, -l_{2L}\mathbf{j}, 0]$, $\mathbf{F}_{3L} = [0, 0, -l_{3L}\mathbf{j}, 0]$ and $\mathbf{F}_{4L} = [0, l_{4L}\mathbf{i}, 0, 0]$ are defined to represent its hip, knee, ankle and big toe; while l_{1L} , l_{2L} , l_{3L} and l_{4L} represent pelvis, femur, tibia and foot, respectively. Quaternions $Q_{1L} = \cos(\frac{q_{1L}}{2}) + \mathbf{u}_{1L} \sin(\frac{q_{1L}}{2})$, $Q_{2L} = \cos(\frac{q_{2L}}{2}) + \mathbf{u}_{2L} \sin(\frac{q_{2L}}{2})$, $Q_{3L} = \cos(\frac{q_{3L}}{2}) + \mathbf{u}_{3L} \sin(\frac{q_{3L}}{2})$, $Q_{4L} = \cos(\frac{q_{4L}}{2}) + \mathbf{u}_{4L} \sin(\frac{q_{4L}}{2})$

and $Q_{5L} = \cos\left(\frac{q_{5L}}{2}\right) + \mathbf{u}_{5L} \sin\left(\frac{q_{5L}}{2}\right)$, are to the movements of rotation and tilt of the pelvis, hip and knee flexion-extension, as well as ankle dorsiflexion and plantarflexion, where $\mathbf{u}_{1L} = [0, 0, \mathbf{j}, 0]$, $\mathbf{u}_{2L} = [0, \mathbf{i}, 0, 0]$, $\mathbf{u}_{3L} = \mathbf{u}_{4L} = \mathbf{u}_{5L} = [0, 0, 0, \mathbf{k}]$.

Also, to develop the kinematic analysis in this work, the anatomical terms describing the relationships of the different parts of the body were based on the anatomical planes and the human model of Fig. 1: sagittal (XY), frontal (YZ) and transverse (XZ) and the directions: anterior (x axis), superior (y axis) and right (z axis) [1]. Then, given the serial kinematic chain shown in Fig. 1 and the joint angles, the cartesian positions in \mathbb{R}^3 for the 4 frames for both lower limbs are calculated using quaternions algebra. Recursively, for the frames \mathbf{F}_{4R} and \mathbf{F}_{4L} the cartesian positions are given by

$$\begin{aligned} F_{4R} = & Q_{1R} Q_{2R} \mathbf{F}_{1R} \overline{Q_{2R} Q_{1R}} \\ & + Q_{1R} Q_{2R} Q_{3R} \mathbf{F}_{2R} \overline{Q_{3R} Q_{2R} Q_{1R}} \\ & + Q_{1R} Q_{2R} Q_{3R} Q_{4R} \mathbf{F}_{3R} \overline{Q_{4R} Q_{3R} Q_{2R} Q_{1R}} \\ & + Q_{1R} Q_{2R} Q_{3R} Q_{4R} Q_{5R} \mathbf{F}_{4R} \overline{Q_{5R} Q_{4R} Q_{3R} Q_{2R} Q_{1R}} \end{aligned} \quad (1)$$

$$\begin{aligned} F_{4L} = & Q_{1L} Q_{2L} \mathbf{F}_{1L} \overline{Q_{2L} Q_{1L}} \\ & + Q_{1L} Q_{2L} Q_{3L} \mathbf{F}_{2L} \overline{Q_{3L} Q_{2L} Q_{1L}} \\ & + Q_{1L} Q_{2L} Q_{3L} Q_{4L} \mathbf{F}_{3L} \overline{Q_{4L} Q_{3L} Q_{2L} Q_{1L}} \\ & + Q_{1L} Q_{2L} Q_{3L} Q_{4L} Q_{5L} \mathbf{F}_{4L} \overline{Q_{5L} Q_{4L} Q_{3L} Q_{2L} Q_{1L}} \end{aligned} \quad (2)$$

3 Results

In this section, the most relevant results of this work are presented and described. One way to determine the biomechanical properties of gait is by evaluating the angles of rotation (transverse plane) and tilting (frontal plane) movements of the pelvis, flexion-extension of the hip and knee, as well as dorsiflexion and plantarflexion of the ankle (sagittal plane) of both lower limbs. In Fig. 2 are shown the joint angles values for each reference of the both lower limbs during a single cycle of a normal gait (gait pattern). Blue line corresponds to the right limb and the red to the left one. While, vertical black line indicates the final of the stance phase.

The joint angles measurement is very useful for gait analysis to evaluate the range of motion of the joints, which makes possible to diagnose some abnormalities in the joint lower limbs system and how these are related with some diseases. The modeling of the forward kinematics of position allows to relate the joint angles values with the cartesian coordinates of each reference in the workspace, allowing biomedical perception of gait in operational space. Then, evaluating the joint angles in (1) and (2) it is possible to calculate the vector function mapping to the cartesian coordinates in each reference as a function of the pelvis frame. In Figs. 3 and 4 can be seen the

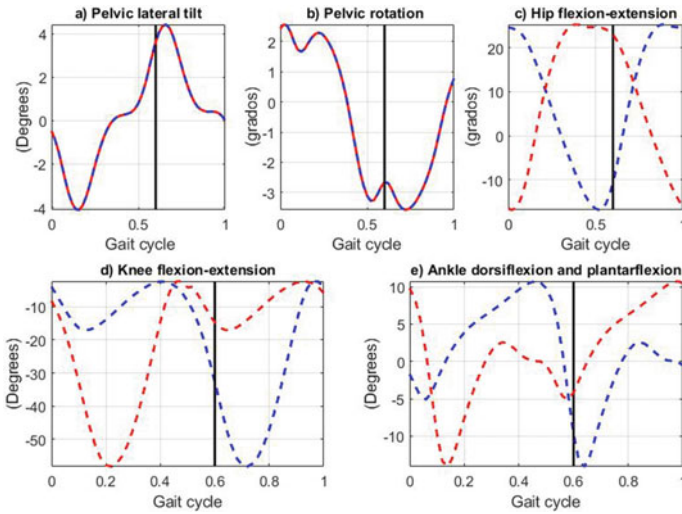


Fig. 2 Joint angles movements during on gait cycle. **a** Pelvic lateral tilt, **b** pelvic rotation, **c** hip flexion-extension, **d** knee flexion extension and **e** ankle dorsiflexion and plantarflexion

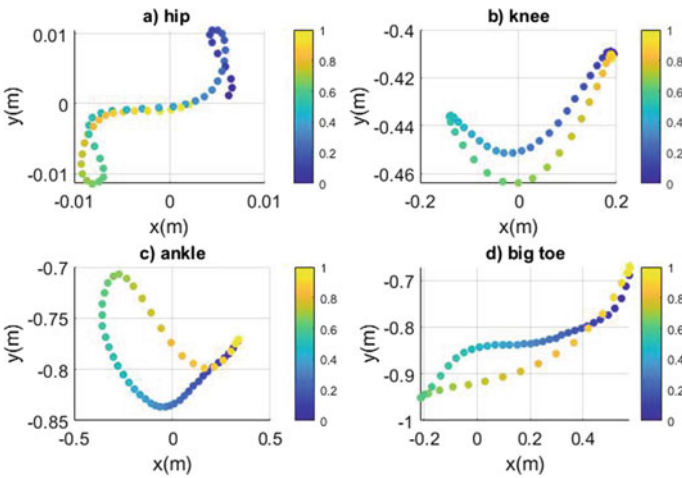


Fig. 3 Joint positions in sagittal plane during a one cycle of the normal gait for the right lower limb. **a** hip, **b** knee, **c** ankle and **d** big toe

positions of its joint references for both right and left lower limbs during one cycle of the normal gait. This visualization is related with movements of the flexion-extension of the hip and ankle, as well as, dorsiflexion y plantarflexion of the ankle. In all the following figures it is important to mention that the vertical color bar represents the evolution of the gait cycle, with zero (dark blue) being the beginning and 1 (light yellow) the end of the cycle.

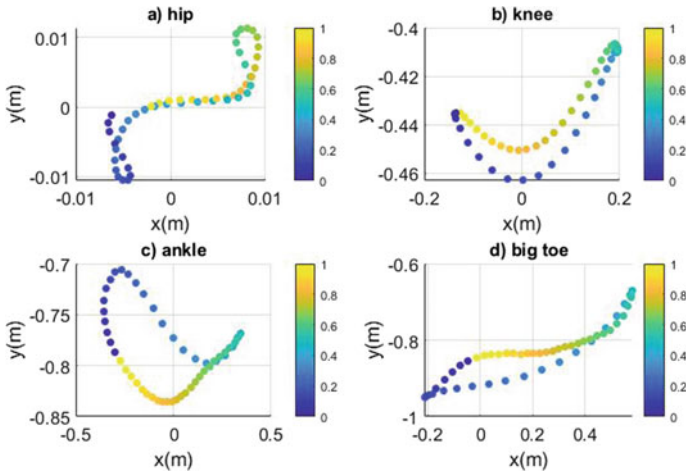


Fig. 4 Joint positions in sagittal plane during a one cycle of a normal gait for the left lower limb. **a** hip, **b** knee, **c** ankle and **d** big toe

There is a spatial synchronous correspondence between the position of each joint reference of the right lower limb with its corresponding one in the left limb during the evolution of the gait cycle. Therefore, the shape factor described by the joint positions is well defined. Generally, to evaluate the gait only the sagittal plane is used. However, the analysis in frontal and transverse planes provides very important information. For this reason, in order to analyze another perspective of the performance, in Figs. 5 and 6 are presented the positions of the joint references of the both right (above) and left (below) lower limbs, during a cycle of a normal gait in frontal and transverse planes, respectively.

The evaluation of the gait in frontal and transverse planes allows to observe particularities of performance that cannot be seen in the sagittal plane, for example, the rotation and lateral tilt of the hip. Similarly, it can be noted that in a normal gait, the movement pattern of both joints is synchronized and the shape factor is well determined, allowing the assessment of abnormalities inherent to diseases reflected in gait, which is sometimes not possible to perform in the joint space. Finally, to visualize a global perspective in the 3 anatomical planes of the evolution of a cycle of a normal gait, in Fig. 7 a visualization of 6 states of this evolution is presented.

4 Discussion

The analysis of the biomechanics of human gait has been established in the anatomical joint space, various works of characterization, analysis and design of technology for perception have been reported in the literature. Assuming a 28 DoF model as

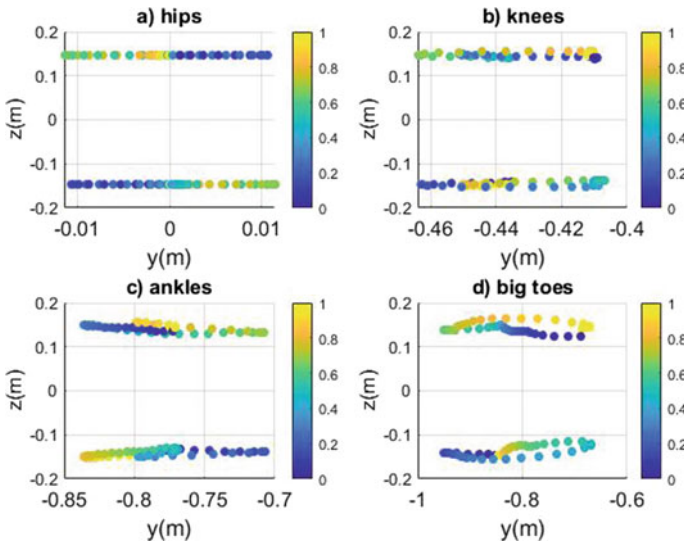


Fig. 5 Joint positions in frontal plane during a one cycle of a normal gait. **a** hip, **b** knee, **c** ankle and **d** big toe

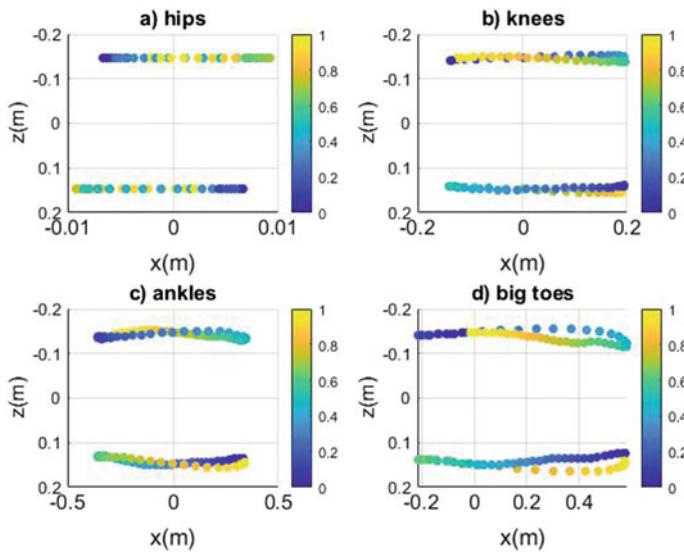


Fig. 6 Joint positions in transverse plane during a one cycle of a normal gait. **a** hip, **b** knee, **c** ankle and **d** big toe

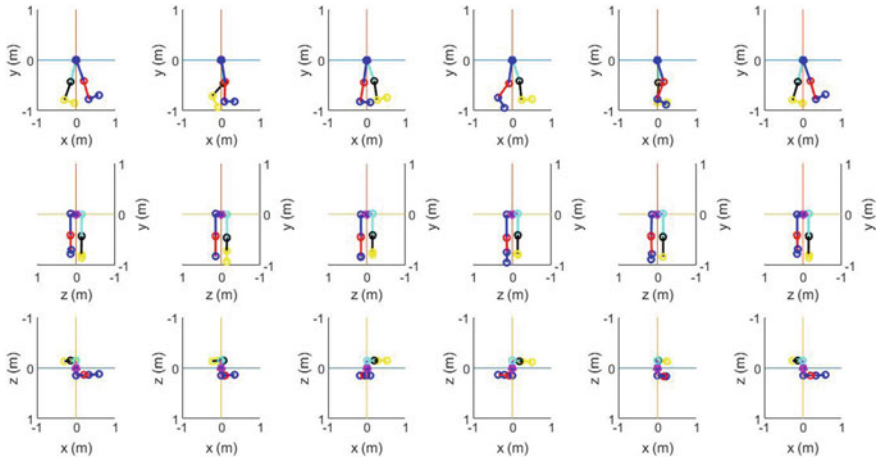


Fig. 7 View of 6 states of one cycle of the normal gait. Rows: first) sagittal plane, second) frontal plane and third) transverse plane

reported in [15]; It has implications for the complexity of both the technological platform required and the gait performance analysis. In this work, the use of a human biomechanical model in gait space (cartesian space) is proposed, using quaternion algebra, and that represents an alternative to identify performance in operational space.

With the evaluation of the numerical method proposed in a simple and systematic way, it is possible to establish a codependency analysis in the performance of the different body segments considered in this validation model at 8 DoF. The proposed method can be extended to chains with a greater number of degrees of freedom; however, those considered in this contribution are the minimum essential to establish a gait diagnosis. The performance in the anatomical planes showed in Figs. 3, 4, Figures 5, 6 and 7, allows to establish comparison criteria in the gait space, and even flexibly evaluate metrics in real time that would help the extraction of useful information in the analysis, diagnosis and clinical recommendation.

5 Conclusion

In this work, a novel quaternions-based method for mapping the joint variables to cartesian coordinates of the lower limbs during biped gait was presented. Validation in the use of our approach was developed for a normal gait pattern. The results allow to confirm that it is possible to replace the classic Denavit-Hartenberg and geometric methods to model forward kinematics of position when the kinematic chain is complex and the number of degrees of freedom increase. The gait performance analysis in the three anatomical planes in the operational space, make possible to

analyze precisely and rapidly to get a preliminary diagnosis, which is very important because the coexistence of the human with biomedical perception devices, generally they are established in the cartesian space. The method described allows to define future contributions, for example, compute of the inverse and differential kinematics, determination of the gait pattern from metrics in the operational space or design and control of humanoid robots for planning gait profiles.

References

1. M.W. Whittle, *Gait Analysis: An Introduction, in Linear Networks and Systems* (Butterworth-Heinemann, 2014)
2. S. Sharif Bidabadi, T. Tan, I. Murray and G. Lee, Tracking foot drop recovery following lumbar-spine surgery, applying multiclass gait classification using machine learning techniques. *Sensors*, **19**(11), 2542 (2019)
3. W.R. Hamilton, M. Vidyasagar, *Elements of Quaternions* (Green, and Company, Longmans, 1866)
4. J.P. Ward, *Quaternions and Cayley Numbers: Algebra and Applications*, vol. 403 (Springer Science and Business Media)
5. A. Vasilakis, I. Fudos, Skeleton-based rigid skinning for character animation, in *GRAPP*, pp. 302–308 (February, 2009)
6. S. Zhao, W. Dong, A. Jay, Farrell quaternion-based trajectory tracking control of vtol-uavs using command filtered backstepping, in *Proceedings of the American Control Conference (ACC)* (USA, Washington, DC, 2013)
7. E. Özgür, Y. Mezouar, Kinematic modeling and control of a robot arm using unit dual quaternions. *Robot. Autonomous Syst.* **77**, 66–73 (2016)
8. A. Cohen, M. Shoham, Application of hyper-dual numbers to rigid bodies equations of motion. *Mechan. Mach. Theo.* **111**, 76–84 (2017)
9. N.A. Aspragathos, J.K. Dimitros, A comparative study of three methods for robot kinematics. *IEEE Trans. Syst. Man, Cybernet.* **28**(2), 135–145 (1998)
10. A.M. Sabatini, Quaternion-based strap-down integration method for applications of inertial sensing to gait analysis. *Med. Biolog. Eng. Comput.* **43**(1), 94–101 (2005)
11. S. Tadano, R. Takeda, R. Miyagawa, Three dimensional gait analysis using wearable acceleration and gyro sensors based on quaternion calculations. *Sensors* **13**(7), 9321–9343 (2013)
12. M.W. Spong, M. Vidyasagar, *Robot Dynamics and Control* (Wiley, 2008), pp. 32–84
13. J.C. Hart, G.K. Francis, L.H. Kauffman, Visualizing quaternion rotation. *ACM Trans. Graph. (TOG)* **13**(3), 256–276 (1994)
14. K. Shoemake, Animating rotation with quaternion curves, in *Proceedings of the 12th Annual Conference on Computer Graphics and Interactive Techniques* (1985), pp. 245–254
15. A. Seth, J.L. Hicks, T.K. Uchida, A. Habib, C.L. Dembia, J.J. Dunne, C.F. Ong, M.S. DeMers, A. Rajagopal, M. Millard, S.R. Hamner, F.M. Arnold, J.R. Yong, S.K. Lakshmikanth, M.A. Sherman, S.L. Delp, OpenSim: Simulating musculoskeletal dynamics and neuromuscular control to study human and animal movement. *Plos Comput. Biol.* **14**(7), 94–101 (2018)

Estimation of Ground Reaction Forces from Lower Limb Joint Kinematics During Walking



Shui Kan Lam and I. Vujaklija

Abstract Ground reaction forces (GRF) and joint kinematics are critical parameters for gait analysis. The conventional approach to acquiring these data is to use force plates installed under the walkway and a stationary motion capture system. These instruments make real-world analysis difficult and incur high costs. One possible solution is to record kinematics with wearable sensors and to apply machine learning models to predict the GRF. However, a protocol that suits online applications and takes greater advantage of portable measurements has been underinvestigated. This study employed Extreme Gradient Boosting (XGBoost) to estimate within-subject three-dimensional (3D) GRF using five lower limb joint angles: hip flexion-extension, adduction-abduction and internal-external rotation, knee flexion-extension, and ankle plantar-dorsi flexion. These joint angles were computed from publicly available data, captured with a camera system (chosen as a benchmark), from six participants. For each subject, we used four-fold cross-validation to assess the estimator performance. The results showed that the model performed the best for anteroposterior direction, followed by vertical direction, then mediolateral direction, with median average R^2 values of 0.96, 0.90 and 0.64, respectively. This study demonstrated 3D GRF prediction based on kinematic features that could be obtained in an online manner. This simple protocol may improve the practicality of carrying out online analyses outside the laboratory with a small number of wearable sensors such as inertial measurement units.

1 Introduction

Ground reaction forces (GRF) and joint kinematics are crucial for understanding human locomotion. These observations can help monitor biomechanical loads and identify injury risks in sports. Furthermore, these parameters are used to derive the

S. K. Lam (✉) · I. Vujaklija
Bionic and Rehabilitation Engineering Group, Department of Electrical Engineering and Automation, Aalto University, Espoo, Finland
e-mail: wendy.lam@aalto.fi

internal joint and musculotendon variables, which are difficult to measure in vivo, for pathological studies and for the development of rehabilitation devices. These data are traditionally obtained with motion capture systems and force plates fixed along the walkway. These instruments are expensive, and their applications are limited to laboratory settings. This also constrains the number of consecutive gait cycles that can be analysed per walking trial. There have been attempts of using pressure insoles to address some of these issues [1]. Yet, the experiments are then limited to a certain type of footwear, which could affect the measured GRF [2]. With the emergence of wearable, cost-effective, lightweight inertial measurement units (IMUs), GRF could be predicted from the acquired kinematics with machine learning models. However, a protocol that (i) requires input features only from a small number of sensors to maintain a high overall equipment portability, and (ii) is suitable for real-time applications, has not been fully investigated.

In this study, we proposed to predict within-subject three-dimensional (3D) GRF based on five lower limb joint kinematics with a machine learning algorithm, Extreme Gradient Boosting (XGBoost) [3]. This ensemble tree-based learner has been employed in a variety of applications, and has a superior predictive performance when working with tabular data [4]. It should be noted that all the necessary input features for our model could be acquired in real time and the entire estimation could theoretically be executed in an online manner even though an offline investigation was performed in this study.

2 Methods

2.1 *Participants and Data Processing*

We employed a reference set of publicly available camera-based motion capture data from six healthy subjects (29.2 ± 12.7 years, 1.71 ± 0.09 m, 66.3 ± 8.0 kg) [5]. This set was chosen as a benchmark, as here we focused on system evaluation under optimal conditions. All participants had no limb surgery in the past two years of data collection. All of them performed at least four trials of ground-level walking at self-selected speed on walkway embedded with two force plates and they were instructed to walk normally. The marker trajectories and GRF for left stance were extracted from C3D files and subsequently stored with OpenSim-compatible format using MOTO-NMS toolbox [6]. A generic musculoskeletal model [7] was scaled to match the anthropometry of each participant in OpenSim [8] based on the marker locations. Joint kinematics of five degrees of freedom, namely hip flexion-extension, adduction-abduction and internal-external rotation, knee flexion-extension, and ankle plantar-dorsi flexion were computed via Inverse Kinematics tool from OpenSim [8]. The joint angles were then low-pass filtered at 6Hz with a second-order Butterworth filter.

2.2 Estimation Model and Data Analysis

XGBoost was applied to predict the intra-subject GRF in anteroposterior (AP), vertical (V) and mediolateral (ML) directions using the five pre-processed joint angles as input features. This algorithm iteratively minimizes the objective function consisting of the residuals of the learners and the regularization term which penalizes the overfitting behavior of the model,

$$\mathcal{L} = \sum_i l(\hat{y}_i, y_i) + \sum_k \Omega(f_k)$$

where l is the loss function of the model, \hat{y}_i and y_i are the estimated value and the true label for the i th sample respectively, and $\Omega(f_k)$ measures the model complexity of tree f_k [3]. For a trial dataset with m features, K learners are combined to make the final estimation,

$$\hat{y}_i = \sum_{k=1}^K f_k(x_i)$$

where $f_k \in \{f(x) = \omega_{q(x)}\} (q: \mathbb{R}^m \rightarrow T, \omega \in \mathbb{R}^T)$ is the tree's space, and q denotes the structure of each tree with T leaves and ω leaf weight [3].

The estimated GRF were then low-pass filtered at 15Hz using a second-order Butterworth filter. Coefficient of determination (R^2) values were calculated to evaluate the model performance. For each individual subject, the results from four trials were cross-validated. This strategy was used to tune the hyperparameters of the models and to assess the degree of within-subject generalization of the models. For each trial, one stance phase was analysed.

3 Results

The GRF estimates for each of the three directions from one trial and the distribution of average R^2 resulted from cross-validation across six subjects are shown in Fig. 1. The median values for AP, V and ML directions were 0.96, 0.90, and 0.64, respectively. The range and the interquartile range for AP, V and ML directions were (0.08, 0.13 and 0.29) and (0.02, 0.09 and 0.13), respectively. Both measures showed that the spreads for AP and V directions were small compared to that for ML direction. In other words, the degree of generalization of the models across subjects was relatively low for ML direction. This suggests that the features used in this study may not be representative enough for ML estimates. In overall, the estimator performed the best for AP direction despite the presence of one outlier, followed by V direction, then ML direction. The less accurate predictions for ML direction were also reported by other researchers [9].

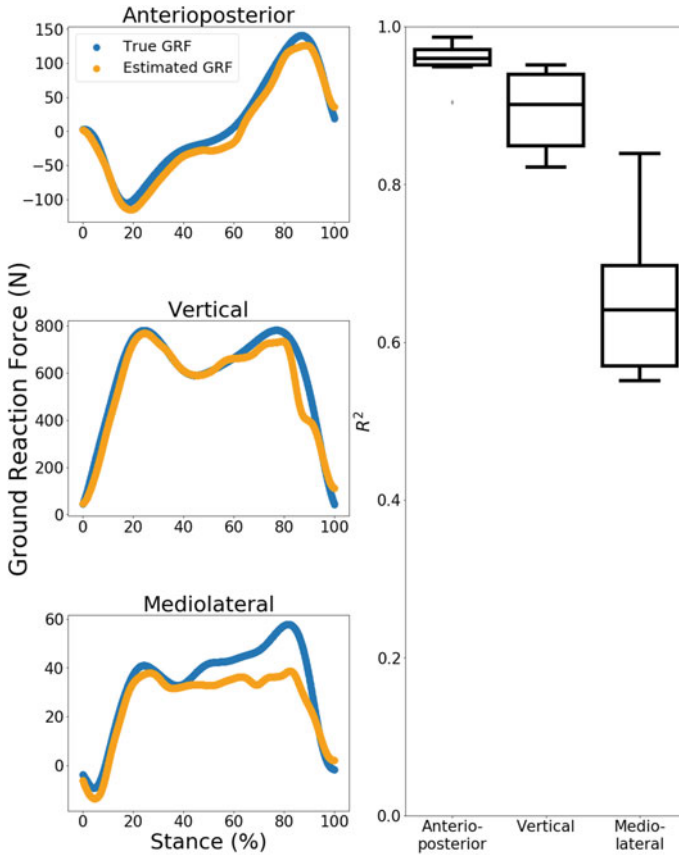


Fig. 1 Left panel illustrates the GRF estimation for one trial for AP (top), V (middle), and ML (bottom) directions. Right panel shows the distribution of average R^2 across six subjects for each of the three directions

4 Conclusion

This study predicted intra-subject 3D GRF across six healthy subjects based on five pre-computed lower limb joint angles using XGBoost. The results showed that the model estimates and the measured signals were highly correlated for both AP and V directions, and moderately correlated for ML direction. Future work on optimizing the inputs for ML predictions is planned. This protocol is characterized by its input features being real-time accessible with a small number of wearable sensors, for instance, IMUs. The proposed method may thus enhance the capabilities of translating online biomechanical analyses and the use of rehabilitation technologies to outside the laboratory.

References

1. A. Forner Cordero, H.J.F.M. Koopman, F.C.T. Van Der Helm, Use of pressure insoles to calculate the complete ground reaction forces. *J. Biomech.* **37**(9), 1427–1432 (2004)
2. J.P. Chen, M.J. Chung, C.Y. Wu, K.W. Cheng, M.J. Wang, Comparison of barefoot walking and shod walking between children with and without flat feet. *J. Am. Podiatr. Med. Assoc.* **105**(3), 218–225 (2015)
3. T. Chen, C. Guestrin, XGBoost: a scalable tree boosting system, in *Proceedings of the ACM SIGKDD International Conference on Knowledge Discovery and Data Mining*, 2016, pp. 785–794
4. S. Ramraj, N. Uzir, R. Sunil, S. Banerjee, Experimenting XGBoost algorithm for prediction and classification of different datasets. *Int. J. Control Theory Appl.* **9** (2016)
5. C. Schreiber, F. Moissenet, A multimodal dataset of human gait at different walking speeds established on injury-free adult participants. *Sci. data* **6**(1), 111 (2019)
6. A. Mantoan, C. Pizzolato, M. Sartori, Z. Sawacha, C. Cobelli, M. Reggiani, MOtoNMS: a MATLAB toolbox to process motion data for neuromusculoskeletal modeling and simulation. *Source Code Biol. Med.* **10**(1), 12 (2015)
7. S.R. Hamner, A. Seth, S.L. Delp, Muscle contributions to propulsion and support during running. *J. Biomech.* **43**(14), 2709–2716 (2010)
8. S.L. Delp et al., OpenSim: Open-source software to create and analyze dynamic simulations of movement. *IEEE Trans. Biomed. Eng.* **54**(11), 1940–1950 (2007)
9. G. Leporace, L.A. Batista, J. Nadal, Prediction of 3D ground reaction forces during gait based on accelerometer data. *Res. Biomed. Eng.* **34**(3), 211–216 (2018)

Effect of Muscle Modeling in the Efficiency and Accuracy of the Forward-Dynamics Simulation of Human Gait



Francisco Mouzo, Florian Michaud, Mario Lamas, Urbano Lugris, and Javier Cuadrado

Abstract This work compares the efficiency and accuracy of several muscle models, having in mind their future use in AI-based model-predictive controllers for gait simulation. The models are tested on the forward-dynamics simulation of a captured motion. Moreover, the effect of the number of modeled muscles on the efficiency is also studied. Results show that the Hill muscle model with rigid tendon is a good candidate for its use in the mentioned controllers, and that reducing the number of muscles strongly improves the computational efficiency.

1 Introduction

Simulation and prediction of human motion in general, and of gait in particular, is a topic of great interest for the robotics, biomechanics, multibody dynamics and computer graphics communities, as it can serve for anticipation of surgery outcome, orthotic-prosthetic design and customization, control of humanoid robots and virtual characters, etc. Two approaches have become popular to address this topic: optimal control and artificial intelligence (AI) based controllers. Although, depending on how they are stated, both may require the forward integration of the system dynamic equations or just the algebraic solution of the inverse problem, efficiency is always

F. Mouzo · F. Michaud · M. Lamas · U. Lugris · J. Cuadrado (✉)
Laboratory of Mechanical Engineering, University of La Coruña, Ferrol, Spain
e-mail: javier.cuadrado@udc.es

F. Mouzo
e-mail: francisco.mouzo@udc.es

F. Michaud
e-mail: florian.michaud@udc.es

M. Lamas
e-mail: m.lamasr@fuac.udc.es

U. Lugris
e-mail: urbano.lugris@udc.es

a concern [1]. In the specific case of AI-based controllers, which are often model-predictive controllers complemented with machine learning, efficiency is especially critical when controllers are expected to work and learn in real time [2]. This is why skeletal human models have been used so far in such controllers, as including the muscular component generally entails a notable increase in computational load. However, musculoskeletal models are supposed to improve the human likeness of the resulting motion.

The objective of this paper is to compare several muscle models to find out which is the trade-off they offer between efficiency and accuracy, having in mind their future use in AI-based controllers, which seek to maximize the human likeness at the minimum computational cost. For such purpose, the algorithm proposed in [2] has been taken as reference. Every time this algorithm needs to perform a function evaluation, it provides the trajectories of the joints (but not those of the base body) for a given time span, so that a forward-dynamics simulation must be run in which a controller tracks the input trajectories. To work on a similar scheme, the various muscle models were compared here within forward-dynamics simulations of a captured walking motion. A controller was in charge of tracking the captured joint trajectories while the measured ground reaction forces were applied to the feet, as made in [3] at skeletal level.

2 Material and Methods

A healthy adult female, 30 years old, 50 kg and 165 cm walked at her self-selected speed of 0.99 m/s on a walkway with two embedded force plates (AMTI, AccuGait, sampling at 100 Hz), while her motion was captured by 12 optical infrared cameras (Natural Point, OptiTrack FLEX 3, sampling at 100 Hz) that acquired the position of 37 reflective markers.

The human body was modeled as a 3D multibody system formed by 18 anatomical segments, considered as rigid bodies: two hindfeet, two forefeet, two shanks, two thighs, pelvis, torso, neck, head, two arms, two forearms, and two hands. The segments were linked by ideal spherical joints, thus defining a model with 57 degrees of freedom (DoF). Details about the treatment of the captured data and about the geometrical and inertial parameters can be found in [4]. At each leg, it was considered that the following 6 DoF were actuated by muscles: three rotations at the hip, flexion/extension at the knee, dorsi/plantarflexion and inversion/eversion at the ankle. The standard model included 43 muscles per leg (Fig. 1), while a simplified model was also developed with only 8 muscles per leg (the main muscle groups for the sagittal DoF). Muscle properties were obtained as explained in [5].

The forwards-dynamics simulation was carried out through a co-integration approach, already introduced in [6], and implemented in C++. The model was defined by a set of 57 independent coordinates. The equations of motion were derived with a semi-recursive formulation [7] and integrated in time through the implicit, single step, trapezoidal rule, in a Newton-Raphson scheme with a time step of 10 ms. At

Fig. 1 Graphical output of the forward-dynamics simulation of the captured motion. Case with 43 muscles at the right leg



each iteration, the generalized forces aimed at tracking the joint coordinates were obtained by a CTC-like approach for underactuated systems, and the muscular force-sharing problem was solved by optimization. Moreover, in the case of physiological modeling of muscles (see the paragraph below), limits for muscle forces were calculated only once per time step right after the initial prediction and, after convergence of the Newton-Raphson scheme, a root-solver was run to obtain the values of excitations and activations.

Four muscle models were compared. The full Hill model (H1) was chosen as the reference model (the equilibrium model in [8]), and two simplified versions were also considered: the Hill model without contraction dynamics (H2) (the rigid tendon model in [8]), and the Hill model without both activation and contraction dynamics (H3). The differential equation of the activation dynamics was not integrated in time, but a closed-form solution was used instead. The fourth model was non-physiological (NP), which implied the use of fixed limits (zero and the maximum isometric force) in the force-sharing problem.

Finally, the influence of the modeled number of muscles on the efficiency was also tested. Four cases were compared: 43 muscles at each leg (i.e. 86 muscles), 43 muscles at the right leg only, 8 muscles at each leg (i.e. 16 muscles), and 8 muscles at the right leg only.

3 Results

Table 1 shows the CPU-times required to run the 1.23-s simulation on a computer with processor Intel i7 6700K @ 4.00 GHz, for the different muscle modeling alternatives and numbers of muscles. As reference, the CPU-time required without muscles was 0.04 s.

And Table 2 gathers the aggregated RMS errors in excitations, activations and muscle forces incurred by each method, considering H1 as reference, in the case of 43 muscles at the right leg.

Additionally, Fig. 2 plots the histories of muscle forces obtained for rectus femoris with the four models, again in the case of 43 muscles at the right leg.

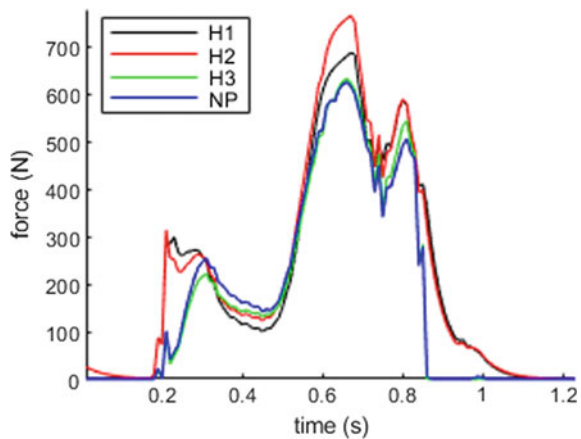
Table 1 Comparison of efficiency (s)

#muscles	H1	H2	H3	NP
86	1.42	0.22	0.21	0.20
43	0.69	0.13	0.12	0.11
16	0.22	0.08	0.07	0.06
8	0.13	0.07	0.06	0.05

Table 2 Comparison of accuracy

	H1	H2	H3	NP
Excit. ($\times 10^{-3}$)	–	8.40	31.9	–
Activ. ($\times 10^{-3}$)	–	6.14	23.3	–
Force (N)	–	3.12	11.8	12.8

Fig. 2 Histories of muscle forces at rectus femoris with the four methods compared, in the case of 43 muscles at the right leg



4 Discussion

Looking at the results of efficiency and accuracy, it can be concluded that the rigid tendon model (H2) offers a good balance between both aspects and, hence, it is a good candidate for the function evaluation of AI-based controllers simulating gait. Moreover, efficiency is notably improved when reducing the number of muscles.

Acknowledgements This work was funded by the Spanish MICIU under project PGC2018-095145-B-100, cofinanced by the EU through the EFRD program, and by the Galician Government under grant ED431C-2019/29.

References

1. M. Ezati, B. Ghannadi, J. McPhee, A review of simulation methods for human movement dynamics with emphasis on gait. *Multibody Syst. Dyn.* **47**(3), 265–292 (2019). <https://doi.org/10.1007/s11044-019-09685-1>
2. P. Hämmäläinen, S. Eriksson, E. Tanskanen, V. Kyrki, J. Lehtinen, Online motion synthesis using sequential Monte Carlo. *ACM Trans. Graph* **33**(4), art. 51 (2014)
3. F. Mouzo, U. Lugris, R. Pamies-Vila, J. Cuadrado, Skeletal-level control-based forward dynamic analysis of acquired healthy and assisted gait motion. *Multibody Syst. Dyn.* **44**(1), 1–29 (2018). <https://doi.org/10.1007/s11044-018-09634-4>
4. U. Lugris, J. Carlin, A. Luaces, J. Cuadrado, Gait analysis system for spinal cord injured subjects assisted by active orthoses and crutches. *J. Multi-Body Dyn.* **227**(4), 363–374 (2013)
5. F. Michaud, F. Mouzo, U. Lugris, J. Cuadrado, Energy expenditure estimation during crutch-orthosis-assisted gait of a spinal-cord-injured subject. *Front. Neurobot.* **13**, art. 55 (2019)
6. F. Michaud, U. Lugris, J. Cuadrado, A co-integration approach for the forward-dynamics based solution of the muscle recruitment problem, in *7^o Congresso Nacional de Biomecânica*. Guimarães, Portugal, Feb 2017
7. J. Cuadrado, D. Dopico, M. Gonzalez, M.A. Naya, A combined penalty and recursive real-time formulation for multibody dynamics. *J. Mech. Des.* **126**(4), 602–608 (2004)
8. M. Millard, T. Uchida, A. Seth, S. Delp, Flexing computational muscle: modeling and simulation of musculotendon dynamics. *J. Biomech. Eng.* **135**(2), 021004 (11 pages) (2013)

Sitting Posture Monitoring Device for People with Low Degree of Autonomy



Nerea Perez, Patrick Vermander, Elena Lara, Aitziber Mancisidor, and Itziar Cabanes

Abstract Sitting postural monitoring is essential to identify risky situations and avoid long-term muscle diseases. In this work, a low-cost sitting monitoring prototype is presented. It consists of 16 FSR pressure sensors located both in seat and backrest of a cushion. To evaluate the system several tests have been carried out, comparing the results with a commercial mat. The results show that the device allows to track efficiently postures reducing the cost in hardware and gaining flexibility for subsequent data storage and management.

1 Introduction

The adoption of a good sitting posture is especially relevant in people with limited mobility, since among the main effects of adopting an incorrect posture are falls, back, shoulder and neck pain, muscle tension and nervous problems, as sciatica among others [1]. Currently, given the impossibility that a health specialist looks after the patient for a long period of time, the monitoring and diagnosis of the postural state is developed through specific questionnaires to be filled out by patients. In an attempt to eliminate the subjective component of this questionnaires, in recent years, scientific interest in postural detection has increased.

Postural activity monitoring is essential to subsequently identify those risk situations that can cause long-term muscle problems, as well as to prevent possible dangerous situations and falls. In addition to wearable [2] and camera-based [3] sensors, pressure sensors stand out for this purpose as they are the least intrusive

N. Perez · P. Vermander · E. Lara · A. Mancisidor (✉) · I. Cabanes
Department of Automatic Control and System Engineering, Faculty of Engineering, University of the Basque Country UPV/EHU, Bilbao, Spain
e-mail: aitziber.mancisidor@ehu.eus

P. Vermander
e-mail: patrick.vermander@ehu.eus

I. Cabanes
e-mail: itziar.cabanes@ehu.eus

ones. Within this group, capacitive transduction sensors, in textile format [4] and resistive transduction sensors [5] can be distinguished. Commercial sensors of the latter type, in mesh form, are currently offered, such as the BPMS system from Tekscan Inc. [6] or the Seating Mat Dev Kit system from Sensing Tex [7]. However, they have an excessive amount of sensing elements which make them expensive and with a time of use limited (less than 4 h). In addition, as it is a closed solution, the data storage is limited, which makes it difficult to carry out a subsequent analysis and intelligent diagnosis of postural correction.

For this reason, in this paper we present the design and validation of a sitting posture monitoring system, with high durability and low cost, which in a future will serve to characterize people's physical activity patterns.

The rest of the article is structured as follows. In Sect. 2, the design of the system is described. In Sect. 3, different position trials and validation results are presented. Finally, the main ideas are summarized.

2 Sitting Posture Monitoring Device

With the aim of tracking sitting posture, several pressure sensors have been placed both the back and seat of a chair. The location of those is based on a preliminary study carried out with the Seating Mat Dev Kit from Sensing Tex [7], in which points where most pressure is exerted have been identified. In order to reduce the number of sensors but maintaining the quality of monitoring, the proposed design has 16 FSR sensors. These are distributed between the back and the seat as shown in Fig. 1.

The data acquisition has been done by a wireless microcontroller board (Arduino MEGA 2560) powered by a 6000 mA battery which provides more than 24 h of use. This structure allows to reduce the cost of a typical pressure mat in more than an 80%.

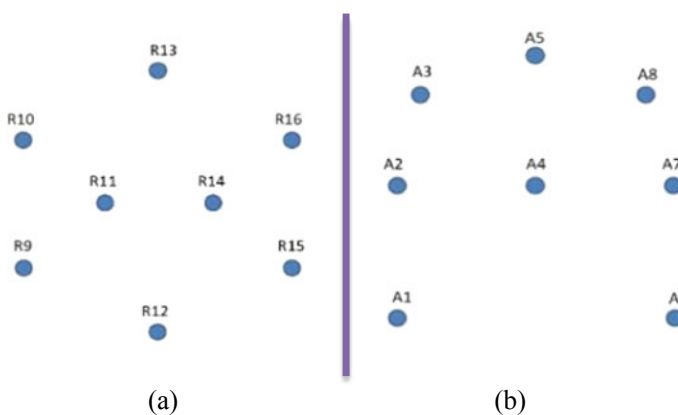


Fig. 1 The sensor distribution in the backrest (a) and seat (b)

In order to facilitate the use and visualization of data, a user-friendly interface has been developed to obtain the sensor readings, which shows in real time the pressure exerted on each sensor.

3 Experimental Validation and Results

Several experimental tests have been carried out to demonstrate the effectiveness of the proposed prototype. Twelve positions have been studied with healthy subjects, which are shown in Fig. 2 and are named in Table 1. Omitting posture 1 (correct sitting posture), the rest are situations or acts that occur in daily life of people with a low degree of autonomy. Among the different tests carried out, positions 2 and 6 will be shown in depth, as proof of the proper functioning of the device. In order to identify the pressure points in each sensor a variation of colour (from a dark blue to a yellow) and proportional size variation has been added.

The results from leaning to the right are shown in Fig. 3, starting from the correct posture, the back has been inclined about 15° from the vertical. In the upper graphs pressure measurements made by the proposed prototype are observed, whereas in the lower ones those made by the commercial mat. Similar measurements are observed in both devices. The position of the seat does not vary, but it can be seen how the

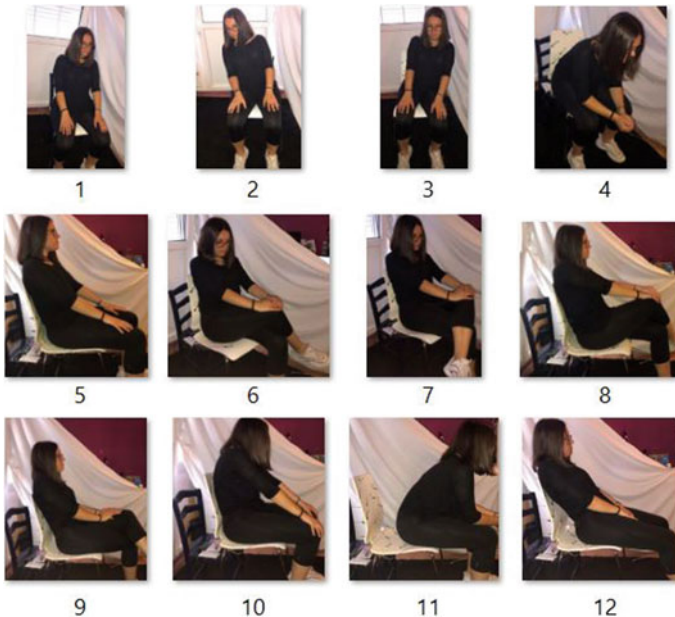


Fig. 2 Twelve positions that simulate situations or acts that occur in daily life of people with a low degree of autonomy

Table 1 Trial positions

N	Position	N	Position
1	Correct position	7	Left leg crossed over right
2	Leaning to the right	8	Right leg crossed and buttocks forward
3	Leaning to the left	9	Left leg crossed and buttocks forward
4	Leaning forward	10	Hypercifhosis
5	Leaning backward	11	Sitting on the edge of the chair
6	Right leg crossed over left	12	Sitting on the edge of the chair and leaning back

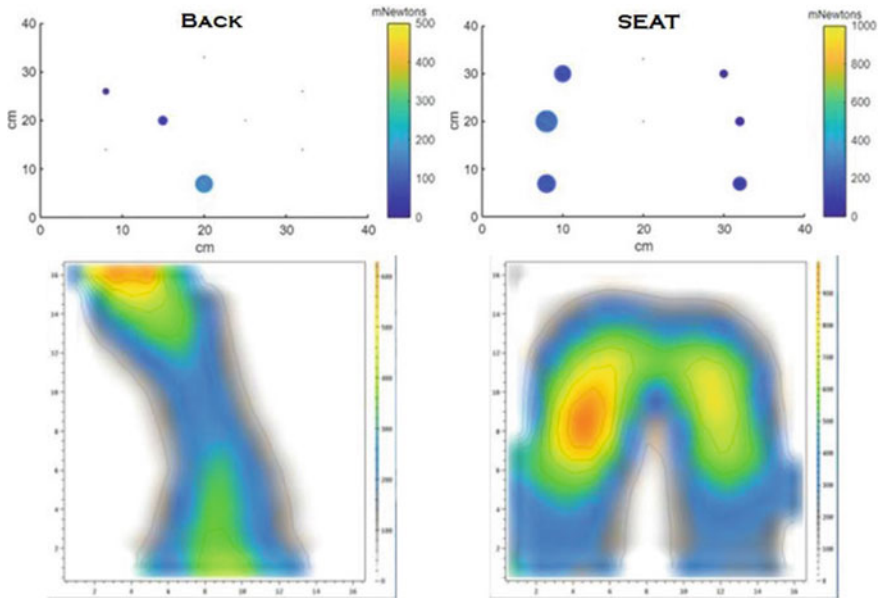


Fig. 3 Leaning to the right results, position 2

pressure exerted on the right side increases. On the backrest, the curvature according to the movement made can be observed.

The results from crossing the right leg over the left are shown in Fig. 4. Both, in the commercial reading and in the prototype, it is shown how the pressure on the left half of the seat increases while some of the pressure from the edge of the right corner is released.

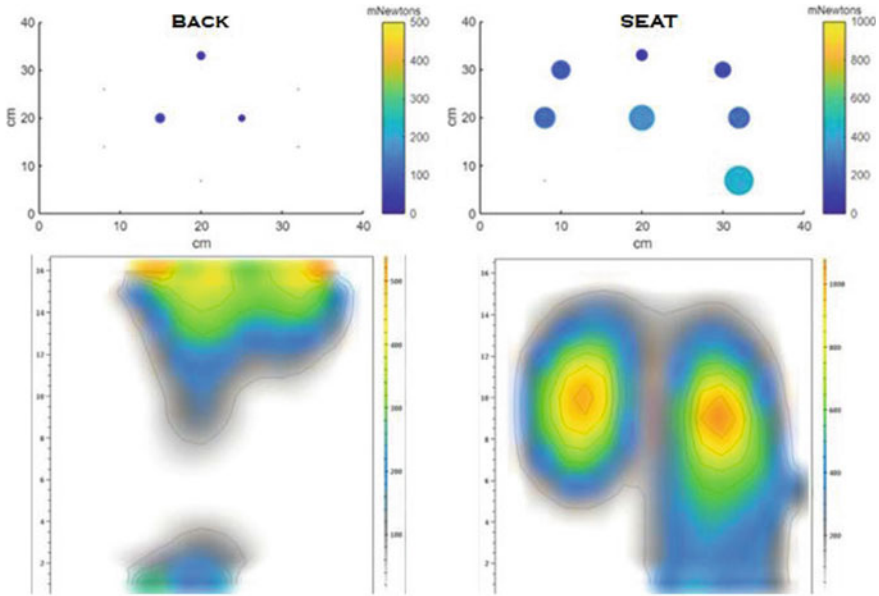


Fig. 4 Results of crossing the right leg over the left one, position 6

4 Conclusion

In this work, a low-cost and optimally designed sitting monitoring device has been developed. It is composed of 16 FSR pressure sensors located in the seat and backrest, which reduces costs significantly. Moreover, their location is optimal to monitor the most relevant parts of the seat and back. This device captures data continuously and it has a longer time of use compared to commercial ones. Furthermore, it has been validated with twelve different postures that tracked the human body efficiently.

This will allow supporting medical specialists and provide them with individualized patient information in an easy way, thanks to the graphical interface designed.

Acknowledgements This research was supported by the University of the Basque Country, project number GIU19/045 (GV/EJ IT1381-19).

References

1. W.J. Yi, O. Sarkar, S. Mathavan, J. Saniie, Wearable sensor data fusion for remote health assessment and fall detection, in *IEEE International Conference on Electro Information Technology*, 2014, pp. 303–307

2. A. Cristina, F. Geraldo, A.M. Kuasne, Prototype of wearable technology applied to the monitoring of the vertebral column. *Int. J. Online Biomed. Eng.* **16**(01), 34–50 (2020)
3. B. Liu, Y. Li, S. Zhang, X. Ye, Healthy human sitting posture estimation in RGB-D scenes using object context. *Multimed. Tools Appl.* **76**(8), 10721–10739 (2016). <https://doi.org/10.1007/s11042-015-3189-x>
4. M. Kim et al., Real-time sitting posture correction system based on highly durable and washable electronic textile pressure sensors. *Sens. Actuators, A* **269**, 394–400 (2018)
5. C. Ma, W. Li, R. Gravina, G. Fortino, Posture detection based on smart cushion for wheelchair users. *Sensors (Switzerland)* **17**(4), 6–18 (2017)
6. B. Arnrich, C. Setz, R. La Marca, G. Tröster, U. Ehlert, What does your chair know about your stress level? *IEEE Trans. Inf. Technol. Biomed.* **14**(2), 207–214 (2010)
7. Sensing Tex S.L. Sensing Mat Dev Kit. Available online: <https://sensingtex.com/product/seating-mat-dev-kit/>. Accessed 2020-07

Effects of Parkinson's Disease and a Secondary Cognitive Task on Standing Postural Stability



Vu Phan, Daniel S. Peterson, Sutton B. Richmond, and Hyunglae Lee

Abstract With recent successes in characterizing standing postural stability of people with neurological disorders, Time-to-Boundary (TTB) measures have potential to provide deeper insights into the impacts of Parkinson's disease (PD) and dual tasking on postural control. The TTB captures the critical relationship between the body sway and base of support, not incorporated into traditional stability measures. However, few studies have evaluated TTB in people with PD. The purpose of this study is to extend the existing work on how PD and a distracting cognitive task impacts standing postural stability. Different TTB measures were applied to data from fourteen PD and thirteen neurotypical adults (NA) subjects. Our results indicate that TTB measures are significantly worse in PD than NA subjects regardless of the existence of a secondary cognitive task. Further, medio-lateral TTB (but not anterior-posterior or 2-dimensional) was significantly negatively affected by the secondary cognitive task in both PD and NA groups.

1 Introduction

According to Marras et al. [1], the estimated number of people with Parkinson's disease (PwPD) in the US in 2020 is nearly 930,000. Importantly, compromised balance control is a major cause of chronic disability in PwPD. Preliminary studies have also shown that PwPD have abnormal body sway that links to falls [2]. Thus, studying the postural balance control of PwPD can improve our understanding of fall risks in this population.

V. Phan · H. Lee (✉)

School of Engineering of Matter, Transport and Energy, Arizona State University, Tempe, AZ, USA

e-mail: hyunglae.lee@asu.edu

D. S. Peterson

College of Health Solutions, Arizona State University, Tempe, AZ, USA

S. B. Richmond

Department of Applied Physiology and Kinesiology, University of Florida, Gainesville, FL, USA

© The Author(s), under exclusive license to Springer Nature Switzerland AG 2022

311

D. Torricelli et al. (eds.), *Converging Clinical and Engineering Research*

on *Neurorehabilitation IV*, Biosystems & Biorobotics 28,

https://doi.org/10.1007/978-3-030-70316-5_50

On a daily basis, completing postural and cognitive tasks at the same time is ubiquitous, and these two tasks together often worsen the performance on one or both tasks. This “dual-task interference” (DTI) suggests a partial overlap between neural structures contributing to control of postural and cognitive tasks. Such dual tasking is particularly difficult for PwPD and has been suggested to be related to falls in this population [3].

Given the influence of DTI and body sway on falls in PwPD, several studies have related effects of a secondary cognitive task on PwPD [4, 5]. However, reported results are somewhat inconsistent across different sway measures. This might be because the traditional measures used in those studies (e.g., sway velocity or total excursion) did not account for the relationship between body’s sway and its base of support (BOS) whereas this relationship is fundamental in balance control.

To cope with this limitation of the traditional measures, a relatively new multi-dimensional measure of postural control was developed, called Time-to-Boundary (TTB) [6]. Although this measure has been applied to characterize neurological disorders such as multiple sclerosis, only a few PD studies have utilized this measure. One study by van Wegen et al. demonstrated that PwPD have smaller medio-lateral (ML) TTB compared to neurotypical adults (NA) [6]. Another one by Workman et al. reported slight effect of a secondary cognitive task on anterior-posterior (AP) TTB in PwPD [5]. However, the effect of dual tasking on ML TTB has not been evaluated.

The purpose of this study is to further examine the effects of PD and a secondary cognitive task on the standing postural stability using different TTB measures. A better understanding of how those conditions impact postural control would provide a better predictor of fall risks in PwPD. Also, this understanding could contribute to the development of new therapeutic training or assistive devices to help prevent falls in PwPD.

2 Material and Methods

2.1 Subjects

Fourteen PD and thirteen NA subjects participated in this study. The mean age and standard deviation (in parenthesis) of PD and NA subjects are 72.61 (60.4) and 69.81 (7.55), respectively. The subjects were also free of any biomechanical injuries or neurological conditions other than PD impacting balance. The methods used in this study was approved by the Institutional Review Board of Arizona State University. Prior to the experiment, all subjects provided informed consent.

Table 1 Mean and standard deviations (in parentheses) of TTB measures

Measures		Single task	Dual task
2D TTB (s)	NA	13.22 (3.80)	12.78 (2.88)
	PD	9.78 (3.46)	9.76 (4.16)
AP TTB (s)	NA	17.88 (6.26)	17.65 (4.86)
	PD	13.79 (5.43)	13.94 (5.49)
ML TTB (s)	NA	71.80 (19.60)	63.22 (17.12)
	PD	53.40 (20.92)	45.16 (20.42)

2.2 Instrumentation

An instrumented treadmill system with two integrated force plates, a motion capture system, a headphone, and a microphone were utilized. The treadmill system (Motek-force Link, Amsterdam, Netherlands) was used to measure the center of pressure (COP) under separate foot of every subject, whereas the motion capture system (VICON, New York, USA) was used to capture the motion of markers placed on specific positions on subjects. Vicon Nexus 2.2 was used to synchronize the data from these two systems. Earbuds and a microphone were utilized to generate auditory stimulus and to capture the verbal response from the subjects (Table 1).

2.3 Protocol

The quiet stance experiment contained two tasks, namely single-task and dual-task. During standing, the subjects wore shoes and placed their feet on separate force platforms, with a heel-to-heel distance of 10 cm. In addition to standing, the subjects were required to complete an additional cognitive task in the dual-task trials. For the cognitive task, the auditory Stroop task was chosen because it was reported as an effective and reliable method for raising cognitive load in PD subjects [7]. The stimuli, which were words “high” and “low” with corresponding tones, were delivered to the subjects via the earbuds. Subjects were instructed to quickly and accurately name the tone of the stimulus, while ignoring the word. The microphone stuck on the skin near their voice-box captured responses.

At least two practice trials were given to ensure the subjects understood the cognitive task. After that, they performed two single-task trials, followed by two dual-task trials. Each trial lasts 50 s. Between trials, a short break was given to reduce fatigue.

2.4 Data Processing

Force plate and auditory (microphone) data were sampled at 2000 Hz. Force-plate data were filtered with a low-pass 4th order Butterworth filter with the cut-off frequency of 7 Hz. In addition, the motion capture data was acquired at the sampling rate of 200 Hz for all subjects.

To serve the calculation of TTB, the net COP was calculated for all subjects based on Winter et al. [8].

2.5 Time-To-Boundary (TTB)

The geometric boundary (i.e., the shape of the BOS) was obtained using the motion capture data recorded by markers at heels, toes, and ankles. Three TTB measures, namely 2D TTB, AP TTB, and ML TTB, were then calculated based on the method adopted from van Wegan et al. [6].

2.6 Statistical Analysis

Normality of the data was first checked by the Shapiro-Wilk tests, followed by a 2-way repeated ANOVA to assess the effects of PD and the cognitive task on the TTB measures. All statistical tests were conducted using the SPSS statistical package (IBM, NY) at a level of $p < 0.05$.

3 Results

Regarding the group effect (i.e., NA versus PD), statistical significance was obtained for 2D TTB ($p = 0.019$) and ML TTB ($p = 0.012$), but not AP TTB ($p = 0.062$). For the task effect (i.e., single- versus dual-task), only ML TTB ($p = 0.024$) was statistically significant. For both groups, we observed reduced ML TTB during dual-task trials, where the ML TTB was the worst in combined PD/dual tasking. No interaction effects were observed in any TTB measures ($ps > 0.167$).

4 Discussion

This study demonstrated that TTB measures of PD subjects are consistently worse than those of NA subjects regardless of the task conditions, suggesting that PwPD are more unstable during standing balance compared to their NA peers.

No strong impact of the secondary cognitive task in the AP TTB was also confirmed, which is consistent with the previous work on AP TTB by Workman and Thrasher [5].

However, contrary to the results in AP TTB, this study showed that the secondary cognitive task significantly deteriorates ML TTB. This could be due to the prioritization of postural control in the sagittal over frontal plane, making the subject more unstable in the ML direction. Interestingly, even though we utilized different measures compared to Bekkers et al. (total excursion & root-mean-square of COP trajectory) [4], we consistently conclude that an addition of a secondary cognitive task has more impact on stability in the ML than the AP direction in PwPD and NA.

5 Conclusion

This study demonstrates that PD has negative impacts on standing postural stability. Our results also suggest that ML TTB can be utilized as a sensitive measure to investigate the impact of the secondary cognitive task on standing postural stability. Future work is warranted to determine its relationship to falls in PwPD.

Acknowledgements This project was funded in part by the Arizona State University and Mayo Medical Center Pilot Seed Grant.

References

1. C. Marras et al., Prevalence of Parkinson's disease across North America. *npj Parkinson's Dis.* **4**, 21 (2018).
2. A. Ashburn et al., A community-dwelling sample of people with Parkinson's disease: characteristics of fallers and non-fallers. *Age Age.* **30**(1), 47–52 (2001)
3. S. Heinzl et al., Motor dual-tasking deficits predict falls in Parkinson's disease: a prospective study. *Parkinsonism Relat. Disord.* **26**, 73–77 (2016)
4. E.M.J. Bekkers et al., The impact of dual-tasking on postural stability in people with Parkinson's disease with and without freezing of gait. *Neurorehabil Neural Repair* **32**(2), 166–174 (2018)
5. C.D. Workman, T.A. Thrasher, The influence of dopaminergic medication on balance automaticity in Parkinson's disease. *Gait Posture* **70**, 98–103 (2019)
6. E.E. van Wegen et al., Stability boundaries and lateral postural control in parkinson's disease. *Mot. Control* **5**(3), 254–269 (2001)

7. M. Mancini et al., Postural sway as a marker of progression in Parkinson's disease: a pilot longitudinal study. *Gait Posture* **36**(3), 471–476 (2012)
8. D.A. Winter, Human balance and posture control during standing and walking. *Gait Posture* **3**(4), 193–214 (1995)

Gait Analysis for Normal and Crouch Gaits Applying No-Common Metrics in the Cartesian Space



Juan C. Gonzalez-Islas, Omar A. Dominguez-Ramirez, Omar Lopez-Ortega, Felix A. Castro-Espinoza, and Ma. de los Angeles Alonso-Lavernia

Abstract Gait analysis is a very important assessment tool to identify abnormalities in gait, which can be used to determine diseases such as cerebral palsy, spastic diplegia and quadriplegia. In this work, we proposed the use of no-common metrics based on area, RMS level and centroid to evaluate the lower limbs system during the gait cycle in the operational space. An evaluation and comparison of these metrics was performed for a normal (pattern), mild crouch and severe crouch gaits on the three anatomical planes. The obtained results allow us to determine the advantages and utilities of the metrics for clinical aims, useful to improve the diagnosis and treatment of the patients.

1 Introduction

Nowadays, gait has become a useful practical biometric for clinical diagnosis. The use of specific metrics to perform biomechanical gait analysis depends on the objective of interest. The most common gait metrics used are speed, cadence, and step length [1]; which have been associated with injury, frailty and influences of gender, height [2]

J. C. Gonzalez-Islas

Ph.D. Program of Computer Sciences of Autonomous University of Hidalgo State and researcher, Technological University of Tulancingo, Hidalgo, Mexico

O. A. Dominguez-Ramirez (✉) · O. Lopez-Ortega · F. A. Castro-Espinoza ·

M. A. Alonso-Lavernia

Basic Sciences and Engineering Institute of the Autonomous, University of Hidalgo State, Pachuca, Mexico

e-mail: omar@uaeh.edu.mx

O. Lopez-Ortega

e-mail: lopezo@uaeh.edu.mx

F. A. Castro-Espinoza

e-mail: fcastro@uaeh.edu.mx

M. A. Alonso-Lavernia

e-mail: marial@uaeh.edu.mx

and age during non-pathological gaits [3]. To assess the recovery following surgery for lumbar disk herniation, have used the metrics: daily step count, walking speed, step length and walking posture [4]. Another metrics such as: average duration of step swing and stance phase, pitch angle change and the average phase duration ratio were used to determine the fall risk in older patients [5].

The measurement of the area as a metric has been used in diverse areas such as flow topology [6] or acute nanoparticle toxicity in the lung [7]. While, with a different approach than this work has also been applied for automatic gender gait recognition based on silhouettes of a walking subjects [8]. The root-mean-square (RMS) level has been applied to determine the amount of energy over a time period in a signal and its applications focus on the electromagnetic context, however, in this work we show its usefulness in gait analysis. Regarding the centroid as a metric, it has been used to intelligently analyze soccer games [9] or for speech recognition [10]. In relation to the gait analysis, the measurement of the movement of the centroid of a subject in home environments has served to assess changes due to weighted vest therapy [11].

Crouch gait is a difficult movement abnormality among persons with cerebral palsy [12–14], as well as spastic diplegia and quadriplegia [15, 16], which is characterized by excessive flexion of the hips, knees and ankles during stance phase, on average more than 15° from normal gait. The biomechanical causes of this abnormal gait are often unclear, making it challenging to chose the most appropriate metrics to compare it with an unimpaired gait and determine the suitable treatment.

2 Materials and Methods

To calculate the gait metrics described in this work, previously quaternions algebra has been applied to model forward kinematics of position of the lower limbs during the gait [17]. For this end, the human model shown in Fig. 1 has been adopted as the kinematic chain that represents the skeletal system of the lower extremities. The 8 Degrees of Freedom (DoF) model is composed by 7 rigid-body segments, which are (1) pelvis, (2) right femur, (3) left femur, (4) right tibia, (5) left tibia, (6) right foot and (7) left foot. The antropometry and joint values were taken from [18] and [19], respectively.

The reference frames for the pelvis, hips, knees, ankles and toes are \mathbf{F}_0 , \mathbf{F}_1 , \mathbf{F}_2 , \mathbf{F}_3 , and \mathbf{F}_4 , respectively, where R and L subscripts are used to describe the right and left lower limbs accordingly. \mathbf{F}_0 is the base frame and in this work is considered in a absolute way, that is, the traslation of the pelvis is not taken into account. At the top left of the Fig. 1 is shown the frames configuration, which follows the right hand rule for the turning angles of the joints. The relative positions for each sample of the cycle using quaternions algebra [17] for the frames of the right lower limb are given by

$$\mathbf{F}_{1R} = Q_{2R} Q_{1R} \mathbf{F}_{1R} \overline{Q_{1R} Q_{2R}} \quad (1)$$

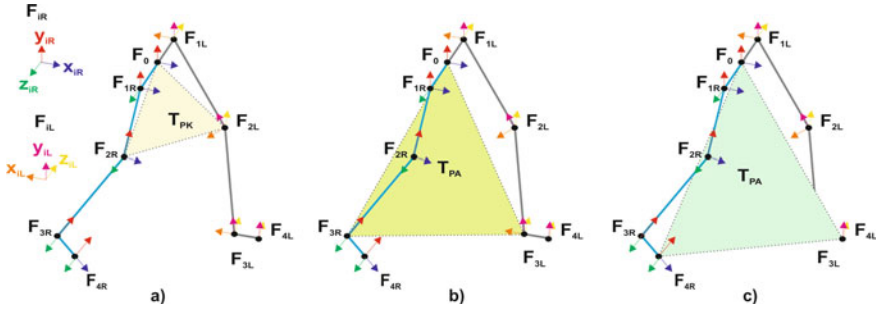


Fig. 1 Kinematic chain representing the frames that define the areas between pelvis and **a** knees, **b** ankles and **c** toes

$$\mathbf{F}_{2Rr} = \mathbf{F}_{1Rr} + Q_{3R} Q_{2R} Q_{1R} \mathbf{F}_{2R} \overline{Q_{1R} Q_{2R} Q_{3R}} \quad (2)$$

$$\mathbf{F}_{3Rr} = \mathbf{F}_{1Rr} + \mathbf{F}_{2Rr} + Q_{4R} Q_{3R} Q_{2R} Q_{1R} \mathbf{F}_{3R} \overline{Q_{1R} Q_{2R} Q_{3R} Q_{4R}} \quad (3)$$

$$\mathbf{F}_{4Rr} = \mathbf{F}_{1Rr} + \mathbf{F}_{2Rr} + \mathbf{F}_{3Rr} + Q_{5R} Q_{4R} Q_{3R} Q_{2R} Q_{1R} \mathbf{F}_{4R} \overline{Q_{1R} Q_{2R} Q_{3R} Q_{4R} Q_{5R}} \quad (4)$$

Similarly, for the frame references of the left lower limb

$$\mathbf{F}_{1Lr} = Q_{2L} Q_{1L} \mathbf{F}_{1L} \overline{Q_{1L} Q_{2L}} \quad (5)$$

$$\mathbf{F}_{2Lr} = \mathbf{F}_{1Lr} + Q_{3L} Q_{2L} Q_{1L} \mathbf{F}_{2L} \overline{Q_{1L} Q_{2L} Q_{3L}} \quad (6)$$

$$\mathbf{F}_{3Lr} = \mathbf{F}_{1Lr} + \mathbf{F}_{2Lr} + Q_{4R} Q_{3R} Q_{2L} Q_{1L} \mathbf{F}_{3L} \overline{Q_{1L} Q_{2L} Q_{3L} Q_{4L}} \quad (7)$$

$$\mathbf{F}_{4Lr} = \mathbf{F}_{1Lr} + \mathbf{F}_{2Lr} + \mathbf{F}_{3Lr} + Q_{5L} Q_{4L} Q_{3R} Q_{2L} Q_{1L} \mathbf{F}_{4L} \overline{Q_{1L} Q_{2L} Q_{3L} Q_{4L} Q_{5L}} \quad (8)$$

where Q_{1R} , Q_{2R} , Q_{3R} , Q_{4R} , Q_{5R} , Q_{1L} , Q_{2L} , Q_{3L} , Q_{4L} and Q_{5L} represent the quaternions regarding the movements of rotation and lateral tilt of the pelvis, flexion-extension of the hip and knee, as well as ankle dorsiflexion and plantarflexion for the right and left lower limbs, respectively. As a result, an N -dimensional vector with the cartesian coordinates for each reference is obtained, where N is the number of instrumented samples of the gait.

One of the metrics proposed in this work are based on the area of the triangles: $T_{PK} = \Delta \mathbf{F}_0 \mathbf{F}_{2R} \mathbf{F}_{2L}$ (Fig. 1a), $T_{PA} = \Delta \mathbf{F}_0 \mathbf{F}_{3R} \mathbf{F}_{3L}$ (Fig. 1b) and $T_{PT} = \Delta \mathbf{F}_0 \mathbf{F}_{4R} \mathbf{F}_{4L}$ (Fig. 1c), which are calculated using the cartesian coordinates of the respective frames during the gait cycle states as:

$$A_{pk} = \frac{1}{2} \left| F_{2R(x,y,z)} \times F_{2L(x,y,z)} \right| \quad (9)$$

$$A_{pa} = \frac{1}{2} \left| F_{3R(x,y,z)} \times F_{3L(x,y,z)} \right| \quad (10)$$

$$A_{pt} = \frac{1}{2} \left| F_{4R(x,y,z)} \times F_{4L(x,y,z)} \right| \quad (11)$$

To get a single value representing each area of the triangles for the overall cycle, the RMS level is computed. Furthermore, since this value does not depend on time but on the amplitude of the function, it can be applied for the analysis of areas. The RMS of the vector containing the area of each gait sample, in [20] is calculated as

$$A_{RMS} = \sqrt{\frac{1}{N} \sum_{n=1}^N |A_n|^2} \quad (12)$$

Another metric introduced to evaluate the performance of the lower limbs system during the gait is the calculation of the centroid of the triangles T_{PK} , T_{PA} and T_{PT} , as well as a global centroid. Using the averaging cartesian coordinates method, the centroid of the 3 vertices of the corresponding triangle is calculated. For $T_{PK} = \Delta \mathbf{F}_0 \mathbf{F}_{2R} \mathbf{F}_{2L}$ the cartesian coordinates of the centroid are given by $(\frac{F_{0x}+F_{2Rx}+F_{2Lx}}{3}, \frac{F_{0y}+F_{2Ry}+F_{2Ly}}{3}, \frac{F_{0z}+F_{2Rz}+F_{2Lz}}{3})$. In the same way the centroid coordinates for the T_{PA} and T_{PT} triangles are calculated.

Subsequently, the proposed metrics are evaluated during one cycle of each gait sample for normal, mild crouch and severe crouch gaits.

3 Results

As follows, in Fig. 2, areas between pelvis and the joint references are presented. In general, for the 3 triangles evaluated, the area for normal gait for each gait sample is greater than the areas in crouch gaits. For T_{PK} in a normal gait the maximum area $A_M = 0.092\text{m}^2$ occurs in the initial contact and the opposite initial contact events, in addition to presenting a characteristic form factor. In the same way, the maximum value $A_M = 0.092\text{m}^2$) for a mild crouch gait occurs at the same stage of the cycle, however, for a severe gait it is not. It is important to highlight that in a severe crouch gait for the triangle T_{PK} there is a lower value than in a normal gait, which is related

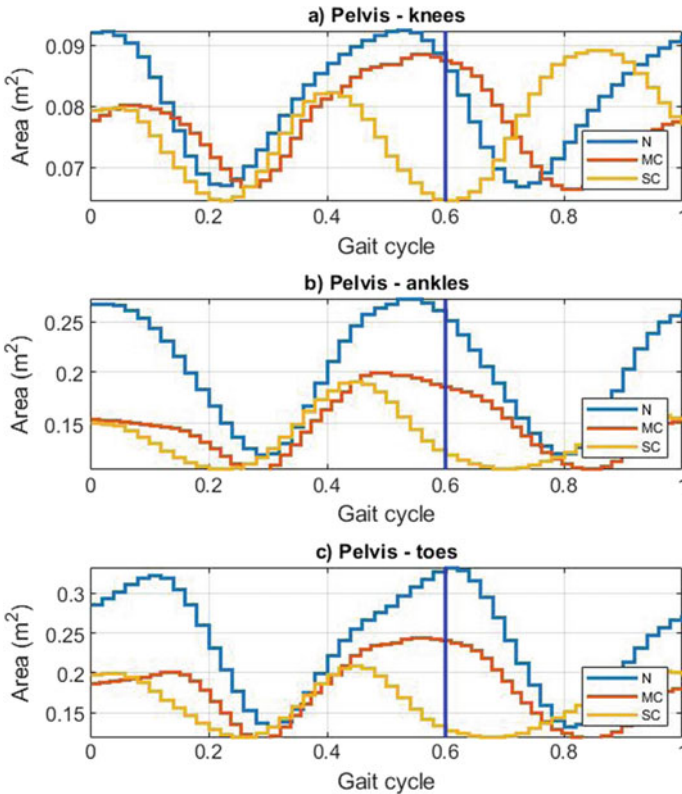


Fig. 2 Area between pelvis and both lower limbs references **a** knees, **b** ankles and **c** toes

to the reduction of the distance between the knees in heel rise and toe off events [19]. Regarding the areas of the T_{PA} and T_{PT} triangles, a similar behavior is shown, being evident the reduction of the area in each sampling of the gait cycle in more than 25%.

The centroid was another evaluation metric introduced in this work. Figures 3, 4 and 5 show sagittal, frontal and transverse planes views, respectively, of the global centroid for the 3 triangles of the 3 types of gait evaluated.

The three graphics regarding the analysis of the global centroid provide very important information, since it is possible to make a precise analysis of both the form factor of the movement pattern, as well as the maximum and minimum values of the global performance through the centroid in the gait space, which allows to differentiate between the three types of gait and thus determine abnormalities based on the normal gait pattern. In Table 1 the area RMS values, and global centroid coordinates for the triangles T_{PK} , T_{PA} and T_{PT} for the 3 gaits, as well as the coordinates of the global centroid are presented.

A minimum value for the RMS level of the mild and severe crouch gaits than the normal confirms a minimum range of movement and the excessive flexion of hip and

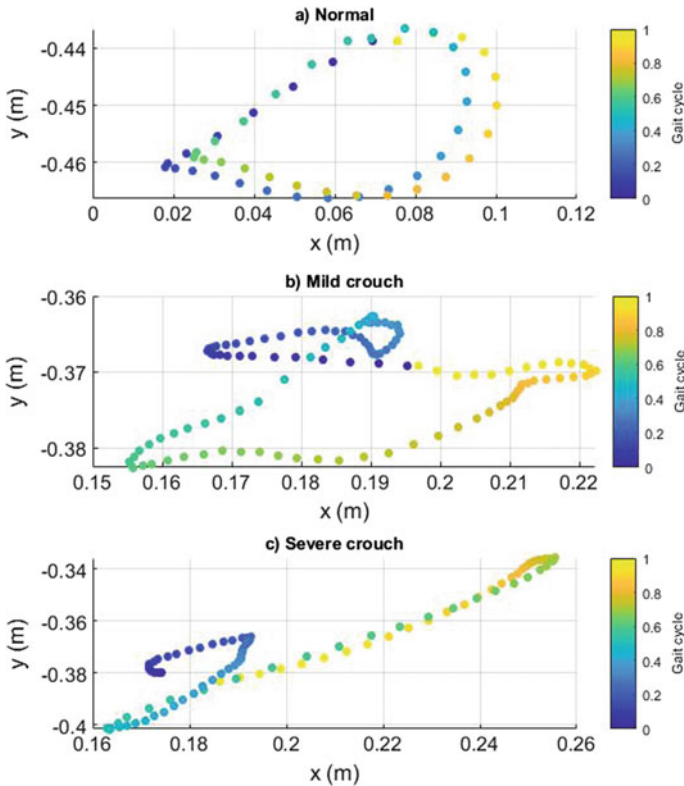


Fig. 3 Sagittal view for global centroids for human gaits: **a** normal, **b** mild crouch and **c** severe crouch

knee, as well as ankle dorsiflexion. While the average of the centroid of the triangles analyzed during the gait cycle confirms that they are lower than that of the abnormal gait pattern, considering in this work the framework of the pelvis in an absolute way.

4 Discussion

The proposed metrics enable the assessment of gait quality and determine gait abnormalities. Generally, a crouched gait is defined by excessive flexion of the hips and knees, as well as ankle dorsiflexion, which can be well determined by making an analysis in the joint space, however, since the coexistence of the human with biomedical perception devices is established in the cartesian space, the analysis of the areas of the triangles formed by the pelvis and joint references as result of the forward kinematics of position can be very useful to diagnose and treat a patient. Area is a measurement parameter that allows determining the degree of severity of the gait and

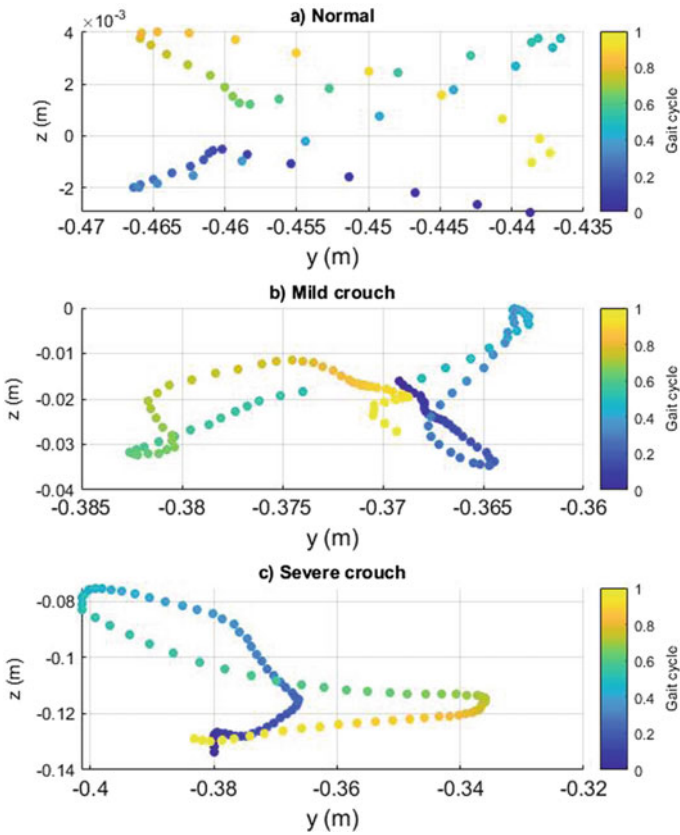


Fig. 4 Frontal view for global centroids for human gaits: **a** normal, **b** mild crouch and **c** severe crouch

it is directly related to the motion range of the joints. On the other hand, the centroid is generally associated with the location that represents the center of a group, in gait analysis for clinical settings, if we associate it relatively with the center of mass of a patient, the centroid provides information on the overall performance of the joint system during the gait cycle and the greater the instability of the centroid, the risk of falls can be determined. Although the RMS value has been used to determine the effective value of a periodic signal, since it does not depend on time but on amplitude, it is possible to use this parameter in the gait analysis and thus not mediate all values for each gait cycle sample. Furthermore, if we consider that a gait cycle is repeated periodically according to cadence, the RMS measurement can help in long term applications to determine gait anomalies inherent to fatigue, stress or injury.

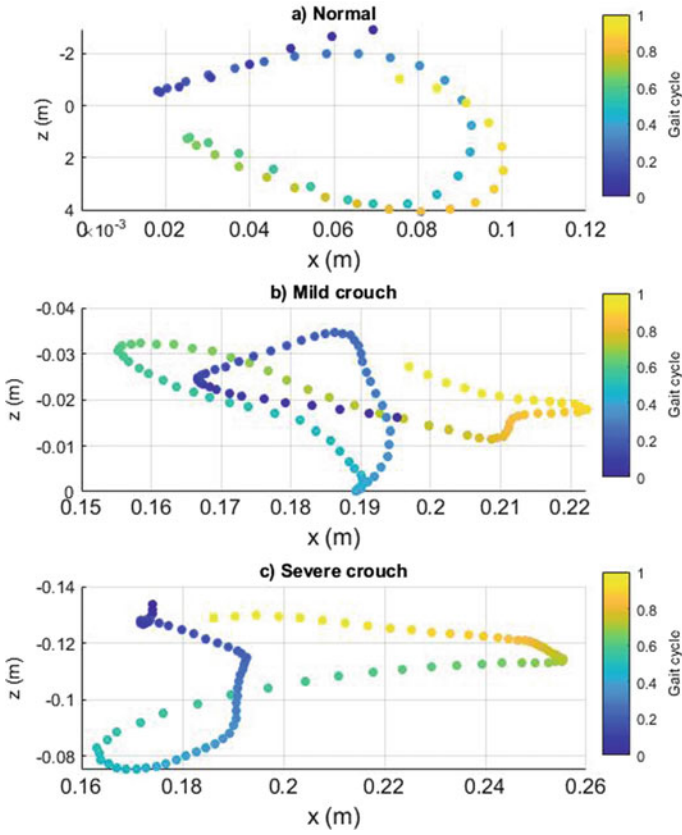


Fig. 5 Transverse global centroids for human gaits: **a** normal, **b** mild crouch and **c** severe crouch

Table 1 Centroid average of the triangles and area RMS values

$Triangle_{gait}$	$RMS (m^2)$	$Cent_{x,y,z} (m)$		
$T_{PK-Normal}$	0.0818	0.0409	-0.2883	0.0005
$T_{PK-Mild crouch}$	0.0773	0.1975	-0.2171	-0.0214
$T_{PK-Severe crouch}$	0.0764	0.1697	-0.2083	-0.0217
$T_{PA-Normal}$	0.2099	-0.0082	-0.5231	0.0001
$T_{PA-Mild crouch}$	0.1500	0.0986	-0.4452	-0.0101
$T_{PA-Severe crouch}$	0.1388	0.1511	-0.4619	-40.1063
$T_{PT-Normal}$	0.2483	0.1470	-0.5511	0.0019
$T_{PT-Mild crouch}$	0.1835	0.2654	-0.4498	-0.0281
$T_{PT-Severe crouch}$	0.1649	0.2879	-0.4368	-0.2032
$Global_{Normal}$		0.0599	-0.4542	0.0008
$Global_{Mild crouch}$		0.1872	-0.3707	-0.0199
$Global_{Severe crouch}$		0.2029	-0.369	-0.1104

5 Conclusion

In this work, the use of the no-common metrics such as area, RMS level and centroid for gait analysis have been presented. Which are used in a novel way to evaluate the global performance of the lower limbs during the gait cycle for a normal and crouch gaits in the operational space on the three anatomical planes. The obtained results are useful to determine the degree of progress or severity of a patient with the aim of improving the diagnosis or treatment used. The proposal described allows to determine future contributions. For example, calculation of the area between hip, knee and ankle or toes for each lower limb; the analysis of the RMS level in the joint space.

References

1. M.W. Whittle, *Gait Analysis: An Introduction* (Butterworth-Heinemann, Linear Networks and Systems, 2014)
2. R. Frimenko, C. Goodyear, D. Bruening, Interactions of sex and aging on spatiotemporal metrics in non-pathological gait: a descriptive meta-analysis. *Physiotherapy* 101(3), 266–272 (2015)
3. E. Stone, M. Skubic, M. Rantz, C. Abbott, S. Miller, Average in-home gait speed: investigation of a new metric for mobility and fall risk assessment of elders. *Gait & Posture* 41(1), 57–62 (2015)
4. F. Ghent, R.J. Mobbs, R.R. Mobbs, L. Sy, C. Beterridge, W.J. Choy, Assessment and post-intervention recovery following surgery for Lumbar Disc Herniation based on objective gait metrics from wearable devices using the Gait Posture index: GPI. *World Neurosurgery* (2020)
5. Z. Miodonska, P. Stepien, P. Badura, B. Choroba, J. Kawa, J. Derejczyk, E. Petka, Inertial data-based gait metrics correspondence to Tinetti Test and Berg Balance Scale assessments. *Biomed. Sig. Proc. Control* 44, 38–47 (2018)
6. W. De Leeuw, and R. Van Liere, Collapsing flow topology using area metrics, in *Proceedings Visualization '99*, (Cat. No. 99CB37067), IEEE, pp. 349–542
7. O. Schmid, T. Stoeger, Surface area is the biologically most effective dose metric for acute nanoparticle toxicity in the lung. *J. Aerosol Sci.* 99, 133–143 (2016)
8. J.P. Foster, M.S. Nixon, A. Prügel-Bennett, Automatic gait recognition using area-based metrics. *Pattern Recognition Lett.* 24(14), 2489–2497 (2003)
9. F. Clemente, M. Santos-Couceiro, F. Lourenço-Martins, R. Sousa, A. Figueiredo, Intelligent systems for analyzing soccer games: the weighted centroid. *Ingeniería e Investigación* 34(3), 70–75 (2014)
10. J. Wang, K. C. Wang, M. T. Law, F. Rudzicz, M. Brudno, Centroid-based deep metric learning for speaker recognition, in *ICASSP 2019-2019 IEEE International Conference on Acoustics, Speech and Signal Processing (ICASSP) IEEE.* (2019), pp. 3652–3656
11. R. Wallace, C. Abbott, C. Gibson-Horn, M. Rantz, M. Skubic, Metrics from in-home sensor data to assess gait change due to weighted vest therapy. *Smart Health* 3, 1–19 (2017)
12. J. Balzer, S. Schelldorfer, S. Bauer, M.L. van der Linden, Effects of simulated crouch gait on foot kinematics and kinetics in healthy children. *Gait & Posture*. 38(4), 619–624 (2013)
13. A.S. Arnold, F.C. Anderson, M.G. Pandy, S.L. Delp, Muscular contributions to hip and knee extension during the single limb stance phase of normal gait: a framework for investigating the causes of crouch gait. *J. Biomech.* 38(11), 2181–2189 (2005)
14. K.M. Steele, M.M. Schwartz, S.L. Delp, How much muscle strength is required to walk in a crouch gait? *J. Biomech.* 45(15), 2564–2569 (2012)

15. P. Kedem, D.M. Scher, Evaluation and management of crouch gait. *Current Opin. Pediatr.* **28**(1), 55–59 (2016)
16. J.M. Rodda, H.K. Graham, G.R. Nattrass, M. P. Galea, R. Baker R. Wolfe, Correction of severe crouch gait in patients with spastic diplegia with use of multilevel orthopaedic surgery. *JBJS.* **88**(12), 2653–2664 (2006)
17. J.C. González Islas, O.A. Domínguez-Ramírez, O. López Ortega, Biped gait analysis based on forward kinematics modeling using quaternions algebra. *Mexican J. Biomed. Eng.* **41**(3), 56–71 (2020). Retrieved from <http://rmib.mx/index.php/rmib/article/view/1080>
18. S. Tadano, R. Takeda, R. Miyagawa, Three dimensional gait analysis using wearable acceleration and gyro sensors based on quaternion calculations. *Sensors* **13**(7), 9321–9343 (2013)
19. A. Seth, J.L. Hicks, T.K. Uchida, A. Habib, C.L. Dembia, J.J. Dunne, C.F. Ong, M.S. DeMers, A. Rajagopal, M. Millard, S.R. Hamner, F.M. Arnold, J.R. Yong, S.K. Lakshmikanth, M.A. Sherman, S.L. Delp, OpenSim: simulating musculoskeletal dynamics and neuromuscular control to study human and animal movement. *Plos Comput. Bio.* **14**(7), 94–101 (2018)
20. N.G. Paulter, D.R. Larson, J.J. Blair, "The IEEE standard on transitions, pulses, and related waveforms," Std-181-2003. *IEEE Trans. Instrum. Measur.* **53**(4), 1209–1217 (2004)

Rapid Predictive Simulations to Study the Interaction Between Motor Control and Musculoskeletal Dynamics in Healthy and Pathological Human Movement



Friedl De Groote and Antoine Falisse

Abstract We recently proposed a framework for rapid predictive simulations of human movement and demonstrated its potential to dissociate the contributions of neural and musculoskeletal impairments to gait deficits in cerebral palsy. Here, we give an overview of the framework and its applications, and demonstrate how using a more complex foot model was important to improve the correspondence between simulated and measured knee and ankle mechanics in a healthy individual.

1 Introduction

Scientists have long tried to decipher the principles underlying bipedal locomotion with the aim of improving human gait performance and treatment of neuro-musculoskeletal disorders. A powerful approach to this problem is the use of physics-based predictive simulations that generate de novo movements based on a mathematical description of the neuro-musculoskeletal system without relying on experimental data. However, the high computational time of predictive simulations has limited model complexity. Although simulations based on models with limited complexity have greatly contributed to our understanding of the mechanics and energetics of human gait, they provide limited support for personalized clinical decision-making. For example, an orthopaedic surgeon planning a single event multi-level surgery in a patient with cerebral palsy cannot predict the effect of the surgery on the walking pattern of the patient using a 2D model since such surgeries typically include 3D corrections of bony geometries.

We recently developed a computationally efficient optimal control framework to predict human gaits based on complex 3D musculoskeletal models [1]. Human gaits are predicted by optimizing a performance criterion that describes the high-level goal of the motor task without relying on experimental motion data. The framework's computational efficiency results from combining direct collocation, implicit

F. De Groote (✉) · A. Falisse
Department of Movement Sciences, KU Leuven, Leuven, Belgium
e-mail: friedl.degroote@kuleuven.be

differential equations, and algorithmic differentiation. Our framework is more than 20 times faster than existing simulations with similarly complex models.

The low computation time allowed us to explore the effect of the performance criterion on the predicted kinematics. We found a human like walking gait when minimizing a weighted sum of metabolic energy rate, muscle activity, joint accelerations, and passive joint torques—all terms squared. The same criterion also predicted the walk-to-run transition and clinical gait deficiencies caused by muscle weakness and prosthesis use, suggesting that diverse healthy and pathological gaits can emerge from the same control strategy.

In a follow-up study, we performed a case study to demonstrate the potential of our simulation framework to dissociate the contributions of motor control and musculoskeletal deficits to gait impairments in cerebral palsy [2]. We modeled altered musculoskeletal geometry based on MRI images, altered muscle-tendon properties by personalizing Hill-type muscle-tendon parameters based on data collected during functional movements, simpler neuromuscular control by reducing the number of independent muscle synergies, and spasticity through delayed muscle activity feedback from muscle force and force rate. Our simulations revealed that, in the presence of aberrant musculoskeletal geometries, altered muscle-tendon properties rather than reduced neuromuscular control complexity and spasticity were the primary cause of the crouch gait pattern observed for this child. Hence, our simulations suggested that muscle-tendon properties should be the primary intervention target for this child. Indeed, the gait pattern of the child was more upright following muscle-tendon property and bone deformity corrections.

Although we have demonstrated the ability of our simulations to reproduce key features of healthy and pathological human locomotion, our simulated walking patterns deviated from walking patterns observed in healthy individuals in two ways. First, we failed to predict knee flexion during mid stance, resulting in lower knee extension torques and vasti activity than experimentally observed. Second, our simulations underestimated ankle plantarflexion at push-off although the ankle torque was in good agreement with experimental data.

Here, we demonstrate that a more complex foot model including toes and a metatarsophalangeal joint was important to obtain physiologically plausible knee and ankle mechanics during stance.

2 Material and Methods

We performed simulations using two musculoskeletal models that only differed in the number of degrees of freedom used to represent the foot. The first model was an OpenSim model with 29 degrees of freedom, 92 Hill-type muscles actuating the lower limbs and trunk, and eight torque actuators at the arms [3, 4]. The second model was derived from the first model by adding an additional degree of freedom to the foot. The metatarsophalangeal joint had stiffness and damping properties inspired

by experimental measures and was torque-actuated. We used Hunt-Crossley models to describe contact with the ground.

We formulated predictive simulations of gait as optimal control problems. We identified muscle excitations and gait cycle duration that minimized the cost function described above subject to constraints describing muscle and skeleton dynamics, imposing left–right symmetry and prescribing an average gait speed of 1.33 m/s. The resulting optimal control problems are typically challenging to solve because of the stiffness of the equations describing muscle and skeleton dynamics. Compared to other methods such as direct shooting, direct collocation reduces the sensitivity of the cost function to the optimization variables by reducing the time horizon of the integration. Applying direct collocation results in large sparse nonlinear programming problems (NLP). We improved the numerical conditioning of the NLP by using an implicit rather than explicit formulation of the muscle and skeleton dynamics. Additionally, we reduced computational time by applying algorithmic differentiation, rather than finite differences, to compute the derivatives required by the NLP solver.

Simulated kinematics, kinetics and muscle activities were evaluated against experimental data collected in one healthy adult. The subject walked overground at a self-selected speed of 1.33 ± 0.06 m/s. The musculoskeletal model was scaled to the subject’s anthropometry based on marker information from a standing calibration trial. Joint kinematics were calculated based on marker coordinates. Joint kinetics were calculated based on joint kinematics and ground reaction forces.

3 Results

The correspondence between measured and simulated kinematics, kinetics and muscle activations was markedly better when including the metatarsophalangeal joint in the model (Fig. 1). Hip kinematics and kinetics were similar for both models. Modeling the toes was important to predict knee flexion, knee extension torque and vasti activity during stance. Modeling the toes increased ankle plantarflexion during push-off although initiation of the plantarflexion movement occurred sooner than experimentally observed.

4 Discussion

It has been suggested that a walking movement with knee flexion during mid-stance requiring a knee extension torque and thus activity of the vasti muscles is energetically less efficient but improves stability against internal and external perturbations [5]. Here, we demonstrate that knee flexion during mid-stance is optimal even when not accounting for robustness against perturbations. The main terms in our cost function were metabolic rate and muscle activity, which are both related to gait efficiency.

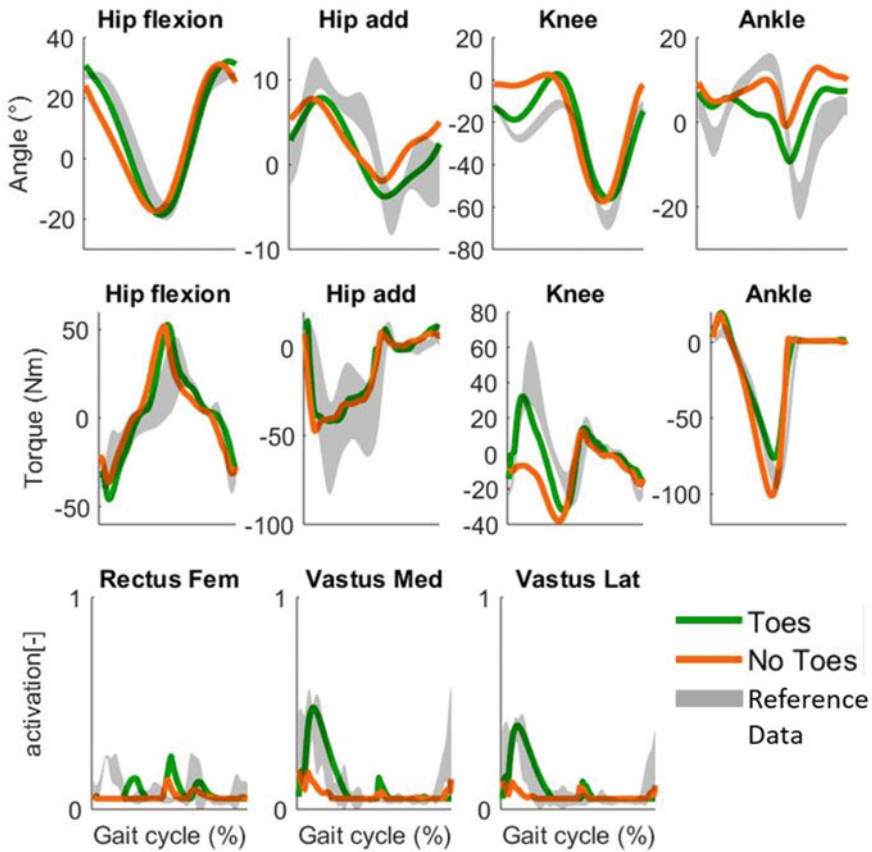


Fig. 1 Simulated and experimental gait kinematics, kinetics and muscle activities as a function of the gait cycle (heel contact to heel contact). Experimental data are shown as mean ± 2 standard deviations

Hence, if knee flexion is indeed needed for stability, stability and efficiency might not be conflicting requirements. We are currently extending our optimal control framework to a robust optimal control framework to study how robustness against perturbations shapes movement.

5 Conclusion

We expect that the ability to accurately and efficiently predict gait patterns based on complex musculoskeletal models will enable optimal design of treatments aiming to restore gait function in the future.

Acknowledgements This work was supported by the Research Foundation—Flanders (FWO) under research grant G079216N and by KU Leuven Internal Funding under research grant C24M/19/064.

References

1. A. Falisse, G. Serranoli, C.L. Dembia, J. Gillis, I. Jonkers, F. De Groote, Rapid predictive simulations with complex musculoskeletal models suggest that diverse healthy and pathological gaits can emerge from similar control strategies. *J. R. Soc. Interface* **16**, 20190402 (2019)
2. A. Falisse et al., Physics-based simulations to predict the differential effects of motor control and musculoskeletal deficits on gait dysfunction in cerebral palsy: a retrospective case study. *Front. Hum. Neurosci.* **14**, 40 (2020)
3. S.R. Hamner, A. Seth, S.L. Delp, Muscle contributions to propulsion and support during running. *J. Biomech.* **43**, 2709–2716 (2010)
4. A. Seth et al., OpenSim: simulating musculoskeletal dynamics and neuromuscular control to study human and animal movement. *PLOS Computat. Biol.* **14**, e1006223 (2018)
5. AD Koelewijn, E Dorschky, AJ van den Bogert, A metabolic energy expenditure model with a continuous first derivative and its application to predictive simulations of gait. *Comput. Methods Biomech. Biomed. Eng.* **21**, 521–531 (2018)

Sit-to-Stand Models of Older Adults Should Include Muscle Nonlinearities and Arms



Matthew Millard and Katja Mombaur

Abstract Standing from a chair is a demanding daily activity that many older adults find challenging because it requires large knee extension torques. Using a musculoskeletal model we first solve for the state trajectories that track the sit-to-stand movements of an older adult. Next, we solve for the state trajectories that predict a sit-to-stand movement by minimizing the sum of squared muscle activations. We use these simulation results to examine how well the predicted movements mimic the tracking solution and examine which of the nonlinear properties of muscle most affect the sit-to-stand movement.

1 Introduction

Many older adults struggle moving from sitting to standing (STS) safely and as a result more falls occur during STS transitions than during walking [1]. Existing simulation studies of STS show that a relatively complex model is required to simulate STS movements accurately. Norman-Gerum and McPhee illustrated that a compliant buttocks-chair model is required [2] due to the large deformations present during STS even among lean adults (3–6 cm). The simulations of Mombaur and Hoang [3] show that arms, which are typically excluded, can be used to ease the STS task. Bobbert et al. [4] included nine Hill-type muscles in their musculoskeletal model which they used to show that weakness and the avoidance of contact forces at the knee affects predicted motions. Only Norman-Gerum and Bobbert et al. compared their simulations to experimental data, and in both cases the data was recorded from fit younger adults.

Financial support from Carl Zeiss-Foundation is gratefully acknowledged.

M. Millard (✉)
ORB, ZITI, Heidelberg University, Heidelberg, Germany
e-mail: matthew.millard@ziti.uni-heidelberg.de

K. Mombaur
System Design Engineering, University of Waterloo, Waterloo, Canada
e-mail: katja.mombaur@uwaterloo.ca

© The Author(s), under exclusive license to Springer Nature Switzerland AG 2022
D. Torricelli et al. (eds.), *Converging Clinical and Engineering Research on Neurorehabilitation IV*, Biosystems & Biorobotics 28,
https://doi.org/10.1007/978-3-030-70316-5_53

In this work we investigate how the predicted motions of a musculoskeletal model compare to the STS data of an older adult (age 78) who is free of any impairment. To evaluate the accuracy of our simulations we compare a solution in which the model tracks the movements of the participant to a solution in which the model minimizes muscle activation squared. Under the common assumption that weakness is a dominant factor affecting sit-to-stand, we examine how the active-force-length and force-velocity multipliers of the knee extensors vary during STS to see which of these two characteristics is most limiting.

2 Methods

Motions and ground forces were recorded from an older adult female [5] (age 78, 1.58m tall, 58 kg) during STS transfers.¹ Using the participant's height and mass we scaled a 17-degree-of-freedom (DOF) rigid body model to the participant (Fig. 1a). The compliant circle-plane contact model of Norman-Gerum and McPhee [2] is used to model buttocks-seat interaction with static friction assumed. Foot-ground contact is modelled using kinematic constraints applied between a point located at the heel and toe of each foot (Fig. 1b).

Muscles are modelled as pairs of agonist-antagonist muscle-torque-generators (MTG) at each joint (Fig. 1b) [6]

$$\tau^M = \tau^{\text{ISO}}(a \mathbf{t}^A(\theta) \mathbf{t}^V(\dot{\theta}) + \mathbf{t}^{\text{PE}}(\theta)) \quad (1)$$

where τ^M is the torque developed by the MTG, τ^{ISO} is the max. isometric torque, a is the activation of the MTG, $\mathbf{t}^A(\theta)$ is the active torque-angle characteristic, $\mathbf{t}^V(\dot{\theta})$ is the torque-velocity characteristic, and $\mathbf{t}^{\text{PE}}(\theta)$ is the passive-torque angle characteristic. The strength and speed of the leg MTG's were taken directly from measurements made on senior females [7]. The strength and speed of the trunk was scaled using the strength ratio between a senior female and a young male at the hips (0.34) [7]. The strength of the arms was scaled using the ratio of elbow flexion strength measured by [8] to that of a young male [6] (0.47). First order activation dynamics were used but with a single time constant to ensure that the derivative is continuous to the second derivative.

To synthesize the movements of the model we use a direct multiple shooting method described by [9] and implemented in the software package MUSCOD-II developed by [10]. To reduce the numerical stiffness of the model we included the buttocks-seat model implicitly and used the constrained-inverse-dynamics method of Koch [11] to simulate the model. We use these methods to numerically solve for the state trajectory that tracks the recorded experimental \mathbf{q} and $\dot{\mathbf{q}}$ in the sense of least-squares (LSQ), and also to solve for the state trajectory that predicts motion by minimizing muscle activations squared (Min. a^2).

¹ Approved by the IRB of the medical faculty of Heidelberg University.

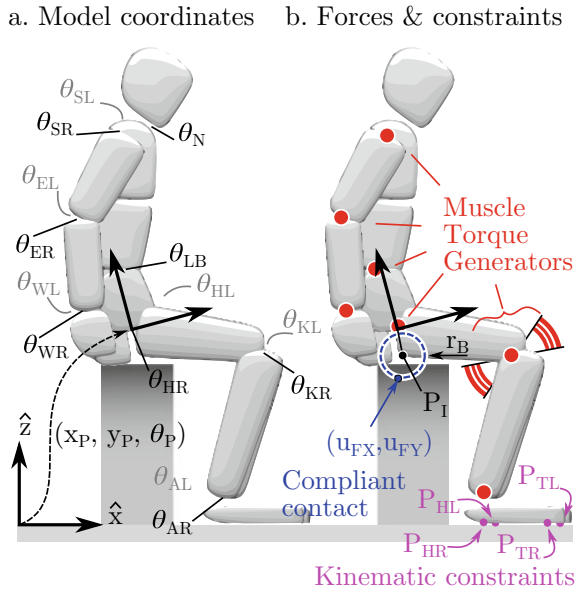


Fig. 1 The 17 DOF planar sit-to-stand model (a) has a floating base pelvis and revolute joints between body segments (a). The model is driven at the joints by pairs of agonist-antagonist MTGs [6], interacts with the chair through a compliant contact model (at point P_I), and with the ground through kinematic constraints at the heel (P_{HR}, P_{HL}) and toe (P_{TR}, P_{TL}) of each foot (b)

3 Results

The knee extensors are the most active muscles during STS in both the tracking and prediction solutions which is consistent with the literature [12]. While the $t^A(\theta)$ profiles have the same trends between the two solutions (Fig. 2a) the $t^V(\dot{\theta})$ profiles differ: the participant favors a knee velocity profile that is faster but less forceful than the prediction solution (Fig. 2b). At seat-off the values of $t^A(\theta)$ (0.85) and $t^V(\dot{\theta})$ (0.88) of the tracking solution are nearly identical. In contrast, the prediction solution favors a faster movement and so the value of $t^V(\dot{\theta})$ ends up being smaller (0.64), and therefore more limiting, than the value of $t^A(\theta)$ (0.85) at seat-off resulting in a shorter STS duration (1.8s vs. 2.2s).

Both the participant and movement prediction used the arms to dynamically assist the STS motion. That the participant actively used her arms, unbidden, is a strong argument for the inclusion of arms in STS models. It is also a strong argument that, when simulating an older adult, the results should be compared to experimental measurements taken from older adults: younger adults do not typically use their arms during STS. Although the use of the arms by both the tracking and the prediction solution is encouraging, there are clear differences between these solutions (Figs. 2 and 3).

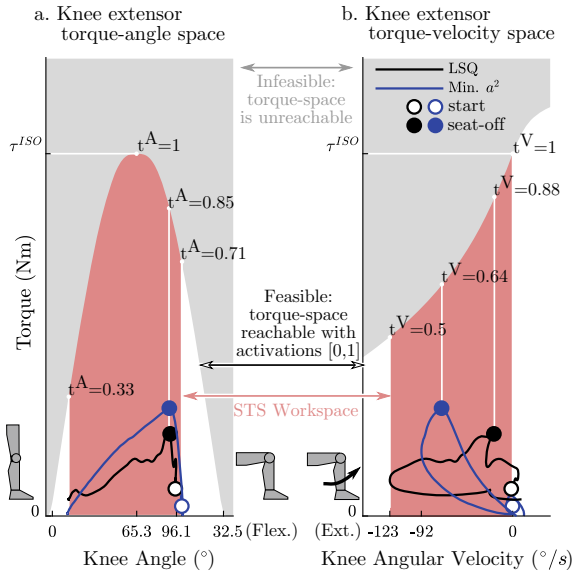
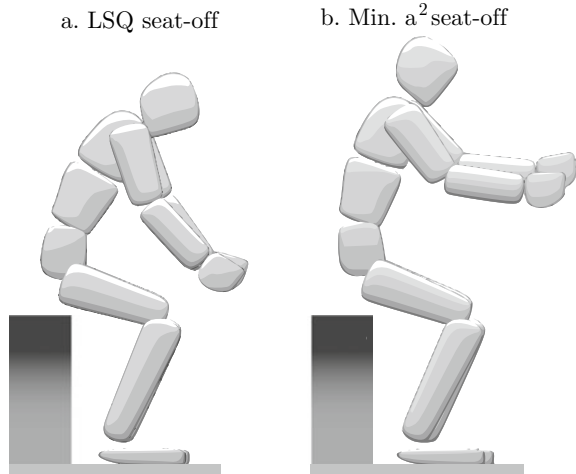


Fig. 2 The torque-angle profiles of the LSQ and Min. a^2 solutions (a) have similar profiles while the torque-velocity profiles (b) differ: the participant favors faster but less forceful movements. These profiles are pictured within the torque-angle space and torque-velocity space of the knee extensors

Fig. 3 The motion of the LSQ and Min. a^2 solutions differ most at seat-off where the Min. a^2 solution raises the arms higher than the participant



Unfortunately, we can only speculate about the reasons for the differences between the tracking and prediction solutions. The strength of the model likely differs from the participant because, even though the MTGs have been fitted to data measured from females over 65, the MTGs have not been fitted to this participant. Given accurately fitted muscles and enough STS trial data we could fit a cost function that would produce predictions that match the participant's average movements. However, trial-to-trial variability would remain unexplained. Hauer et al. [13] demonstrated that perhaps much of the observed variability can be attributed to attention: introducing a distraction-task during strength measurements produced reductions of 20%–50% in relative strength in older adults. While this does not make modeling and simulation any easier, the effect of distraction on the capacities of older adults seems too great to ignore.

4 CONCLUSION

Both arms and the nonlinear properties of muscle are important to include in STS models of older adults. Simulations of older adults should be compared to experimental data measured from older adults: younger adults are a poor approximation. Finally, the influence of distraction on the movement of older adults warrants further study.

References

1. T. Pozaic, U. Lindemann, A.K. Grebe, W. Stork, Sit-to-stand transition reveals acute fall risk in activities of daily living. *IEEE J. Transl. Eng. Health Med.* **4**, 1–1 (2016 Dec 1)
2. V. Norman-Gerum, J. McPhee, Constrained dynamic optimization of sit-to-stand motion driven by Bézier curves. *J. Biomech. Eng.* **140**(12) (2018 Dec 1)
3. K. Mombaur, K.L. Hoang, How to best support sit to stand transfers of geriatric patients: Motion optimization under external forces for the design of physical assistive devices. *J. Biomech.* **58**, 131–138 (2017 Jun 14)
4. M.F. Bobbert, D.A. Kistemaker, M.A. Vaz, M. Ackermann, Searching for strategies to reduce the mechanical demands of the sit-to-stand task with a muscle-actuated optimal control model. *Clin. Biomech.* **37**, 83–90 (2016 Aug 1)
5. L.H. Sloop, M. Millard, C. Werner, K. Mombaur, Slow but Steady: Similar Sit-to-Stand balance at Seat-Off in older vs. younger adults. *Front. Sports Act. Living* **2** (2020)
6. M. Millard, A.L. Emonds, M. Harant, K. Mombaur, A reduced muscle model and planar musculoskeletal model fit for the simulation of whole-body movements. *J. Biomech.* **89**, 11–20 (2019 May 24)
7. D.E. Anderson, M.L. Madigan, M.A. Nussbaum, Maximum voluntary joint torque as a function of joint angle and angular velocity: Model development and application to the lower limb. *J. Biomech.* **40**(14), 3105–13 (2007 Jan 1)
8. T. Rantanen, T. Parkkari, E. Heikkinen, Muscle strength according to level of physical exercise and educational background in middle-aged women in Finland. *Eur. J. Appl. Physiol. Occup. Physiol.* **65**(6), 507–512 (1992 Nov)

9. H.G. Bock, K.J. Plitt, A multiple shooting algorithm for direct solution of optimal control problems. *IFAC Proc.* Vol. **17**(2), 1603–1608 (1984 Jul 1)
10. D.B. Leineweber, A. Schäfer, H.G. Bock, J.P. Schlöder, An efficient multiple shooting based reduced SQP strategy for large-scale dynamic process optimization: Part II: Software aspects and applications. *Comput. Chem. Eng.* **27**(2):167–174 (2003 Feb 15)
11. K.H. Koch. PhD thesis, Ruprecht-Karls-Universität, 6, 2015
12. A.B. Schultz, N.B. Alexander, J.A. Ashton-Miller, Biomechanical analyses of rising from a chair. *J. Biomech.* **25**(12), 1383–1391 (1992 Dec 1)
13. K. Hauer, C. Marburger, P. Oster, Motor performance deteriorates with simultaneously performed cognitive tasks in geriatric patients. *Arch. Phys. Med. Rehabil.* **83**(2), 217–223 (2002 Feb 1)

Functional Analysis of Upper-Limb Movements in the Cartesian Domain



Marco Baracca, Paolo Bonifati, Ylenia Nisticò, Vincenzo Catrambone, Gaetano Valenza, A. Bicchi, Giuseppe Averta, and Matteo Bianchi

Abstract The characterization of human upper limb kinematics is fundamental not only in neuroscience and clinical practice, but also for the planning of human-like robot motions in rehabilitation and assistive robotics. One promising approach to endow anthropomorphic robotic manipulators with human motion characteristics is to directly embed human upper limb principal motion modes at joint level, which are computed through functional analysis, in the robot trajectory optimization. This planning method poses some challenges when the kinematics of the manipulator is different from the model used for human data acquisition. In a previous work, we proposed to tackle this issue by mapping human trajectories onto robotic systems relying on Cartesian impedance control. An alternative method could move from the application of the functional analysis to human upper limb kinematics, working directly in the Cartesian domain. In this work, we present the results of this characterization on the data from 33 healthy subjects during the execution of daily-living activities. We found statistical differences between the amount of variability explained by a given number of basis elements in different directions of the Cartesian space. This suggests that some directions of the space are associated with a more complex motion evolution with respect to others, opening interesting perspectives for robot planning, neuroscience and human motion control.

This work was partially supported by the EU H2020 project “SoftPro” (no. 688857) “SOPHIA” (no. 871237), by the European Research Council (ERC) under Grant 810346 (Natural BionicS), and by the Italian Ministry of Education and Research (MIUR) in the framework of the CrossLab project (Departments of Excellence). These authors equally contributed to this work.

M. Baracca · P. Bonifati · Y. Nisticò · V. Catrambone · G. Valenza · A. Bicchi · G. Averta (✉) · M. Bianchi

Centro di Ricerca “Enrico Piaggio”, Università di Pisa, Largo Lucio Lazzarino 1, 56126 Pisa, Italy

M. Baracca · P. Bonifati · Y. Nisticò · V. Catrambone · G. Valenza · G. Averta
Dipartimento di Ingegneria dell’Informazione, Università di Pisa, Largo Lucio Lazzarino 1, 56126 Pisa, Italy

A. Bicchi

Soft Robotics for Human Cooperation and Rehabilitation, Fondazione Istituto Italiano di Tecnologia, via Morego, 30, 16163 Genova, Italy

1 Introduction

The investigation of human upper limb kinematics is fundamental in different fields, which include neuroscience, clinical practice but also the generation of human like motions with anthropomorphic robots, with important implications also in rehabilitation and assistive robotics [1]. Indeed, human-likeness is an important step to ensure the safety and acceptability of the human-robot interaction. To study the temporal coordinated evolution of human movements, one interesting approach leverages on the application of functional analysis. In a nutshell, the idea is to move from a database of movements collected from humans and to identify a basis of time-series whose combination is able to reconstruct any arbitrary movement. One approach to do this is through functional Principal Component Analysis (fPCA) [2], which can be regarded as a functional extension of standard Principal Component Analysis (PCA). One of the benefits of this approach is that the basis of functions extracted from data is ordered following the amount of variance in the dataset that each function can explain (which is similar to what happens in static conditions with PCA).

More specifically, let us assume a database of movements described in a N -dimensional space: $x(t) : \mathbb{R} \rightarrow \mathbb{R}^N$ where $t \in [0, 1]$ is the normalized time. A generic upper limb motion $x(t)$ can then be decomposed in terms of the weighted sum of base elements $S_i(t)$, or functional Principal Components (fPCs): $x(t) \simeq \bar{x} + S_0(t) + \sum_{i=1}^{s_{\max}} \alpha_i \circ S_i(t)$, where $\alpha_i \in \mathbb{R}^N$ is a vector of weights, $S_i(t) \in \mathbb{R}^N$ is the i^{th} basis element or fPC and s_{\max} is the number of basis elements considered. The operator \circ is the Hadamard product, $\bar{x} \in \mathbb{R}^N$ is an average configuration extracted from data while $S_0 : \mathbb{R} \rightarrow \mathbb{R}^N$ is the average trajectory, aka *zero-order* fPC. The output of fPCA, which is calculated independently for each dimension of the space, is a basis of functions $\{S_1, \dots, S_{s_{\max}}\}$ that maximizes the explained variance of the movements in the collected dataset. Given a dataset with M elements collecting the trajectories recorded in a given dimension j , the first fPC $S_{j,1}(t)$ is the function that solves the following problem

$$\begin{aligned} \max_{S_{j,1}} \quad & \sum_{j=1}^N \left(\int S_{j,1}(t)x_j(t)dt \right)^2 \\ \text{subject to} \quad & \|S_{j,1}(t)\|_2^2 = \int_0^1 S_{j,1}^2(t)dt = 1 . \end{aligned} \tag{1}$$

Subsequent fPCs $S_{j,i}(t)$ are, again, the functions that solve Eq. 1 with an additional orthogonality condition imposed by $\int_0^1 S_{j,i}(t)S_p(t)dt = 0$, $\forall p \in \{1, \dots, i-1\}$. The core idea is that the output of this process is an ordered list of functions that are organised following the importance that each function has in reconstructing the whole dataset.

Note that this formalization of human trajectories is very compact and full of information, and can enable several practical implementations. For example, one can observe that the higher is the number of functional PCs required to reconstruct one

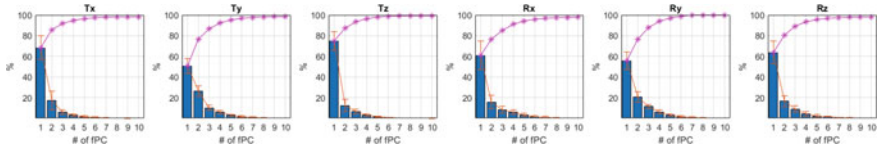


Fig. 1 Variance explained by the first 10 fPCS (blue bars, median and interquartile range) and its cumulative value (magenta line) for each DoF. The label T indicates translations, while label R indicates rotations. The subscript x refers to coronal axis, y to the transversal axis and, finally, z to the sagittal axis

specific movement, the more complex (or jerky) the motion is. This can have a direct impact for the evaluation of motion impairment, for example as a consequence of a stroke event [3], or to design incremental algorithms of human-like motion planning [1]. Indeed, a possible approach to the planning of robotic manipulators is to embed human upper limb principal motion modes at joint level, which are computed through functional analysis, in the robot trajectory optimization. This planning method poses some challenges when the kinematics of the manipulator is different from the model used for human data acquisition. In a previous work, we proposed to tackle this issue by mapping human trajectories onto robotic systems relying on Cartesian impedance control [4]. An alternative method could move from the application of the functional analysis to human upper limb kinematics, working directly in the Cartesian domain. In this work, we present the results of this characterization on the data from 33 healthy subjects during the execution of daily-living activities. We studied the stability of the fPCs in terms of shapes and importance across subjects and across different directions of the movements (intended as translation and orientation of the hand).

2 Functional PCs in Cartesian Domain

To study the fPCs in Cartesian domain we leveraged on data (collected in [2]) of 33 healthy participants (17 women, 26.6 y.o. on average, all right-handed) who were asked to perform a set of 30 activities of daily living, each repeated 3 times. Spatial movements of arm, forearm and hand were recorded through optical motion tracking (Phase Space®) using a redundant set of 20 markers fastened to the upper limb. An Extended Kalman Filter was then used to estimate the pose (in term of Cartesian position and orientation with respect to a reference system placed on the torso) of the hand in the 3D space during the whole motion execution. This procedure resulted in six independent DoFs describing the temporal evolution of hand pose during the task execution, three for the position in 3D space (X : upward; Y : rightward; Z : forward), and three for the relative orientation between the hand and the torso reference systems (Euler angles, ZYX parametrization). To enable temporal comparison between different trials, we performed Dynamic Time Warping, i.e. a procedure which maximises the covariation between different trials, ultimately resulting in syn-

chronized signals. More details can be found in [1]. Functional PCA was then used to identify - for each of the six DoFs defining the pose of the hand—the basis of functional components that approximate the variability of the recorded dataset (as in [1], we chose 15 5th order splines). As briefly mentioned in the previous section and extensively discussed in [1], the number of components that are necessary to explain a certain degree of variance in the data is related to the overall complexity of the movement. In other terms, if one DoF requires a higher number of independent components to explain the same amount of variance w.r.t. another, then we can argue that the first DoF is characterized by a more complex behavior. So far, to generate a generic motion using the fPCs, we used the same number of fPCS for all the DoFs of the model. This was justified by the fact that the planning was executed at the joint level. However, knowing in advance whether some DoFs require a lower number of components w.r.t. others may be exploited to simplify the planning problem in terms of number of coefficients to optimize. Furthermore, by working in the Cartesian domain, we could overcome the issue of mapping human functional modes onto robotic systems with dissimilar kinematics.

We observed that there are statistical significant differences between the complexity of the motion for different Cartesian DoFs. Indeed, as depicted in Fig. 1, although a very reduced number of independent fPCs can approximate with high accuracy the human movements in all the DoFs of the hand, which is in line with previous observations [2], there is a not-negligible difference in complexity across DoFs. Indeed, while for T_y the first fPC reaches the 50% of the total variance (50.33 ± 7.387), if we consider T_z , the variance explained by the first fPC is typically higher than 70% (74.85 ± 9.025). Because our data does not satisfy a condition of normality, to prove that differences across DoFs are statistically relevant we performed Wilcoxon rank sum test, which is a statistical non parametric test that can be applied on non-normal data. The comparison was performed for each DoF and for all the subjects, and the p value was then corrected with Bonferroni to compensate for multiple tests. Considering the translation DoFs, our analysis resulted in statistical difference between the variance explained by the first fPC ($p < 0.05$) in all the DoFs except between T_x and T_z . Regarding the rotational DoFs, instead, we observed statistical difference ($p < 0.05$) only between R_y and R_z , while no statistical difference is detectable between R_x and R_y and R_x and R_z . Statistical difference was observed between the variance explained by the second fPC ($p < 0.05$) for all the DoFs of the hand rotation/translation except for differences between R_x and R_z , which are not statistically relevant. Regarding the third fPC, statistical difference between the variance explained was observed between all the DoFs, unless T_x and T_z and R_x and R_z , while essentially no differences can be reported for higher order functional Principal Components (which account for a very limited amount of variability). To verify whether differences are detectable only in terms of “importance” of fPCs, or also the shape of the components is changed considering different directions (intended here in a general meaning of translations and rotations), we also verified the similarities between fPCs associated to different DoFs, calculated as dot product between vectors. We obtained very high similarities for fPC1, with a mean and std value equal to

0.91 ± 0.15 , while the higher order components show an increased variability, i.e. 0.58 ± 0.28 for fPC2 and 0.48 ± 0.27 for fPC3.

These results suggests that a different level of complexity characterizes the movement of the hand in the Cartesian domain. This open interesting questions for future research in neuroscience but also for the planning of human-like movements of companion robots or exoskeletons [1].

References

1. G. Averta, C. Della Santina, G. Valenza, A. Bicchi, and M. Bianchi, Exploiting upper-limb functional principal components for human-like motion generation of anthropomorphic robots. *J. NeuroEngineering Rehab.* **17**, 1–15 (2020)
2. G. Averta, C. Della Santina, E. Battaglia, F. Felici, M. Bianchi, A. Bicchi, Unveiling the principal modes of human upper limb movements through functional analysis. *Front. Robot. AI* **4**, 37 (2017)
3. A. Schwarz, G. Averta, J. M. Veerbeek, A. Luft, J.P. Held, G. Valenza, A. Bicchi, M. Bianchi, A functional analysis-based approach to quantify upper limb impairment level in chronic stroke patients: a pilot study, in *Engineering in Medicine and Biology Society, 2019. EMBC'19. 41th Annual International Conference of the IEEE. IEEE* (2019)
4. G. Averta, D. Caporale, C. Della Santina, A. Bicchi, M. Bianchi, A technical framework for human-like motion generation with autonomous anthropomorphic redundant manipulators, in *2020 IEEE International Conference On Robotics and Automation (ICRA)* (2020)

A Machine Learning Approach for Near-Fall Detection Based on Inertial and Force Data While Using a Conventional Rollator



Nuno Ferrete Ribeiro, Ana Pereira, Joana Figueiredo, José A. Afonso, and Cristina P. Santos

Abstract Falls are a major concern for society. They may result in death or in several injuries that require motor assistance, representing an economic burden. To overcome these problems, a diversity of fall prevention strategies implemented on assistive devices such as smart walkers, have been widely explored. This study presents a novel strategy by using exclusively information from wearable sensors to detect near-falls while the subject uses a conventional rollator. A comparative analysis was performed to identify the most suitable classifier and the most relevant subset of features for detecting near-fall events. Ten able-bodied subjects performed 240 trials and simulated 180 near-falls with the rollator. The Ensemble Learning with the first 51 ranked features by the mRMR presented the best performance results (Accuracy = 95.18%; Detection time before recovery = 1.48 ± 0.68 s). The results show that this strategy is suitable for use with conventional rollators, which are more used than smart walkers.

1 Introduction

WHEN smart walkers detect situations that may lead to a fall, they usually stop providing support to the user [1]. Current fall prevention strategies usually require

This work has been supported by the FCT—Fundação para a Ciência e Tecnologia—with the scholarship reference PD/BD/141515/2018, by the FEDER funds through the Programa Operacional Regional do Norte and national funds from FCT with the SmartOs project under Grant NORTE-01-0145-FEDER-030386, and under the national support to R&D units grant, through the reference project UIDB/04436/2020 and UIDP/04436/2020.

N. F. Ribeiro (✉) · A. Pereira · J. Figueiredo · J. A. Afonso · C. P. Santos
Center for MicroEletroMechanical Systems (CMEMS), University of Minho, 4800-058
Guimarães, Portugal
e-mail: nuno.fribeiro@dei.uminho.pt

© The Author(s), under exclusive license to Springer Nature Switzerland AG 2022
D. Torricelli et al. (eds.), *Converging Clinical and Engineering Research*
on *Neurorehabilitation IV*, Biosystems & Birobotics 28,
https://doi.org/10.1007/978-3-030-70316-5_55

345

information from non-wearable sensors placed on the walker, e.g. laser range finders (LRF) [2], stereo cameras [3], force/torque sensors [2], and depth cameras [4]. Smart walkers are less used than conventional rollators. However, the number of near-fall detection strategies for conventional rollators is lower. To the best knowledge of the authors, there is yet no near-fall detection strategy completely independent from the rollator and based only on an Inertial Measurement Unit (IMU) placed at the user's lower trunk and Force Sensitive Resistors (FSRs) in the feet. These sensors have already been studied as mentioned in [5] but without the support of any conventional rollator. This study aims therefore to implement the abovementioned strategy. A comparative analysis was performed to understand which is the most suitable machine learning classifier for near-fall detection, as well as the subset of most representative features. This will allow to understand what information is really important for this classification problem towards the minimal sensor setup and computational load for real-time application.

2 Methods

2.1 System Overview and Experimental Protocol

The proposed system (Fig. 1) comprises an IMU located near to L5 lumbar vertebra and S1 sacral vertebra where the Center of Mass (CoM) is usually considered; shoes equipped with four FSRs to detect foot contacts with the ground; and Arduino for sensor data acquisition at 100Hz. Trunk's acceleration and angular velocity were measured on three directions: Anteroposterior (AP), Vertical (V) and Mediolateral (ML). The experiments involved 10 able-bodied subjects (5 females and 5 males) with a mean age of 25.00 ± 1.61 years old, a mean height of 1.69 ± 0.11 m and a mean weight of 66.50 ± 11.32 kg. All participants provided written and informed consent, respecting the ethical conduct defined by the University of Minho Ethics Committee. Participants were asked to walk with the support of a rollator for 4 different activities at 2 different gait speeds (comfortable and slow): walk forward for 10 m; and walk forward and simulate near-falls to the right, left and forward. Each simulation was performed after an audible sound randomly applied by the assessor. Participants performed three trials per condition.

2.2 Data Processing and Machine-Learning Approach

We performed the following procedures after data collection: (i) data processing using a 1st order lowpass filter (exponential smoothing) with 0.5 as the smoothing factor and a cut-off 10Hz [6]; (ii) feature calculation which resulted in a data set with a total of 169 features (Table 1); (iii) feature normalization by subject's

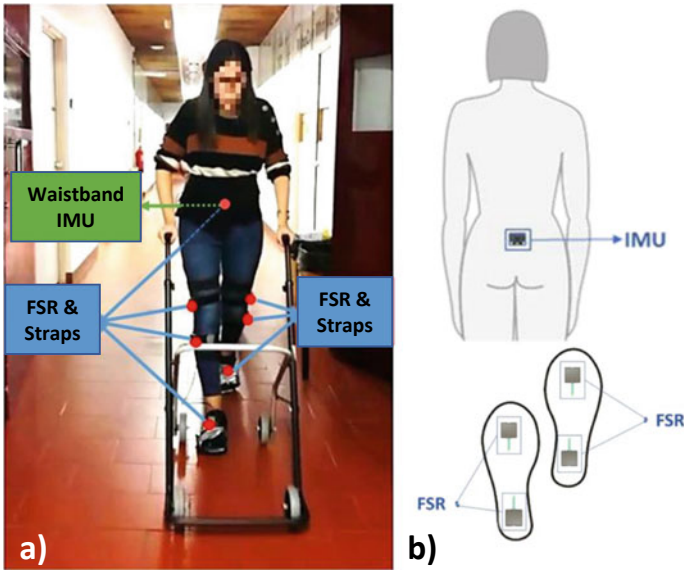


Fig. 1 System description: **a** Waistband IMU and rollator; **b** Wearable sensors location (IMU—back lower trunk; FSR—heel and toe)

height and min-max scaling [0;1]; (iv) feature selection by using two methods—Minimum-Redundancy Maximum-Relevancy (mRMR) and Relief-F - and adapting Principal Component Analysis (PCA); (v) data labelling where near-falls only were considered after the last valid and regular step before the near-fall simulation; and (vi) splitting data by using the hold-out method (70% and 30% for training and test, respectively). Subsequently, we implemented a 5-fold cross-validation (CV) with 10 repetitions using only training data to: (i) select the best subset of features respecting the rankings; and (ii) compare machine learning classifiers (Discriminant Analysis, K-Nearest Neighbors—KNN, Ensemble Learning, Decision Tree—DT, and Support Vector Machine) using only the subset of features found previously. From these procedures, we identified the most accurate machine learning classifier for near-fall detection and conducted a hyperparameter optimization. Lastly, we implemented a post-processing method that uses the current and past classifier outputs to eliminate misclassifications.

3 Results and Discussion

A total of 180 simulated near-falls using a conventional rollator were analyzed for near-fall detection. Based on 5-fold CV results, the best performances were achieved with KNN, Ensemble Learning and DT with features ranked by mRMR and Relief-

Table 1 Feature Table (51 features ranked by mRMR in bold)

Feature description
Acceleration - Acc (V, ML , AP), Angular velocity - Gyr (V, ML , AP)
4 FSR signals: toe right , heel right, toe left, heel left
Sum Vector Magnitude (SumVM) of Acc and Gyr*
Skewness, Kurtosis, Minimum , Maximum (AP), Mean , Variance, Standard deviation of Acc - (V, ML, AP)
Skewness, Kurtosis, Minimum , Maximum (ML), Mean (ML), Variance, Standard deviation of Gyr - (V, ML, AP)
Skewness, Kurtosis, Minimum , Maximum (Gyr), Mean , Variance, Standard deviation of SumVM of Acc and Gyr
Correlation between axes - Acc and Gyr - (V-ML, V-AP, ML-AP)
Acc after high-pass filter (AP , ML , V)**
SumVM of Acc raw data*, Dynamic Sum Vector*, Vertical Acc*, Total Angular Change , Resultant Angular Acc**, Activity Signal Magnitude Area (ASMA)**, Signal Magnitude Area (SMA)
Peak-to-peak values (PPV), Root Mean Square (RMS) (AP), Ratio Index (RI), RI of PPV of Acc - (V, ML, AP)
PPV, RMS (V, AP), RI, RI of PPV of Gyr - (V, ML, AP)
PPV, RMS, RI, RI of PPV of SumVM of Acc and Gyr
Quaternions**, Roll**, Pitch**, Yaw** and Absolute vertical Acc*
SumVM of resultant angle change*, Maximum resultant angular acceleration, Sum of Flutation Frequency, SumVM of Resultant of Average Acc* , SumVM of Resultant of Standard Deviation*
Resultant angle change** , Flutation Frequency, Resultant of Average Acc** (AP , ML), Resultant of Standard Deviation** (AP , ML), Gravity Component*, Velocity (AP , V), Displacement (AP , V), Cumulative horizontal sway length , Mean sway velocity (ML , V), Displacement Range - (AP, ML, V)
Slope**, Fast Change Vector, SumVM of horizontal plane*, EMA** , Rotational Angle using Acc**, Z-score* , Magnitude of Angular Displacement*, Acc and Gyr Resultant of Delta Changes**, Cumulative horizontal displacement

* - features that require only the current sample from initial data; ** - features that require only the current and the previous sample from initial data; Excepting features 1–10, the remaining features require a time-window of 5 samples (current sample and the 4 previous ones)

F. However, the KNN stands out with the following performance and with the first 59 ranked features by Relief-F: Accuracy= 99.93%, Sensitivity (SENS)= 99.71%, Specificity (SPEC)= 99.97%, Precision (PREC)= 99.81%, F1-score= 99.76% and Matthews correlation coefficient (MCC)= 99.71%. The following classifiers appear below with an accuracy higher than 99%: KNN (60 features - mRMR), Ensemble Learning (60 features—Relief-F), Ensemble Learning (51 features—mRMR) and DT (20 features - Relief-F). The classifiers were further tested with unseen data. The Ensemble Learning achieved the best performance using the first 51 features ranked by the mRMR (Table 1): Accuracy= 95.18%, SENS= 71.63%, SPEC= 99.33%, PREC= 94.96%, F1-score= 81.66% and MCC= 79.99%). The hyperparam-

ter optimization outcomes are: (i) Ensemble Aggregation Method - Bag; (ii) Learning Cycles - 498; (iii) Minimum Leaf Size - 1; and (iv) No Learn Rate. Although accuracy and specificity values are high, the sensitivity value is low. Thus, we implemented a post-processing method based on a time window that contains the current and past classifier outputs to increase this value. A window size of 22 samples was obtained with training data. When using test data, a near-fall was detected on average 0.71 ± 0.48 s after the start and 1.48 ± 0.68 s before the recovery, being able to detect all 56 near-falls. The number of misclassified normal walking samples decreased 98%. Although more detailed, our results are in line with the scientific literature [1–4].

4 Conclusion

We presented the Ensemble Learning with the first 51 features ranked by the mRMR from wearable data as an effective strategy for near-fall detection when walking with conventional walkers, advancing the state-of-the-art strategies that are focused on smart walkers less usually used by end-users. The proposed strategy is accurate (higher than 95%) for a considerable sample of healthy subjects and detection times indicate a detection closer to the beginning of the near-fall than to the recovery stage. Future work focus on (i) investigate the best IMU location and computational load of the proposed strategy; (ii) use data from older adults to obtain results more related to end-users; and (iii) use this information in a closed-loop system capable of actuating in high fall risk situations preventing the fall.

References

1. A. Pereira, N. F. Ribeiro, C.P. Santos, A survey of fall prevention systems implemented on smart walkers *, in *2019 IEEE 6th Portuguese Meeting on Bioengineering (ENBENG)*, pp. 1–4 (2019)
2. W. Xu, J. Huang, L. Cheng, A novel coordinated motion fusion-based walking-aid robot system. *Sensors* **18**(9) (2018)
3. S. Taghvaei, Y. Hirata, K. Kosuge, Vision-based human state estimation to control an intelligent passive walker, in *2010 IEEE/SICE International Symposium on System Integration*, pp. 146–151 (2010)
4. S. Taghvaei, K. Kosuge, Image-based fall detection and classification of a user with a walking support system. *Front. Mech. Eng.* **13**(3), 427–441 (2018)
5. I. Pang, Y. Okubo, D. Sturnieks, S.R. Lord, M.A. Brodie, *Detection of Near Falls Using Wearable Devices: A Systematic Review* (2019)
6. J. Figueiredo, P. Félix, L. Costa, J.C. Moreno, C.P. Santos, Gait event detection in controlled and real-life situations: repeated measures from healthy subjects. *IEEE Trans. Neural Syst. Rehab. Eng.* **26**, 1945–1956 (2018)

Clustering of Data that Quantify the Degree of Impairment of the Upper Limb in Patients with Alterations of the Central Nervous System



Anaya-Campos L., Quiñones-Uriostegui I., Quijano Y., and Bueyes-Roiz V.

Abstract Previous studies have sought to improve the way of classifying upper limb motor involvement in patients with alterations or pathologies in the central nervous system, so it has become of great importance to find an objective way of measuring and classifying the degree of ability to move. This work compares two classification methods to be able to group the SSULF scale into five classes to have a better assessment and degree of upper limb motor functionality in patients diagnosed with spinal cord injury or vascular brain event.

1 Introduction

This article contains the comparison between K-Means and C-Means clustering methods using a cloud of clinical data from patients of the Luis Guillermo Ibarra Ibarra National Institute of Rehabilitation obtained for functional evaluation of the upper limb in patients with pathologies in the nervous system. Such as spinal cord injury (BF) and vascular brain events (CVD).

These data were obtained by carrying out the Sorting Block Box (*SBB*) protocol within the institute, which consists of specific activities for filling and emptying the board. The *SBB* together with an inertial IMU sensor assess the patient's motor ability and after processing this data obtained from the board together with that of the IMU in specialized software, a smoothness of movement value is given for its interpretation for medical assessment [3][4].

With studies of smoothness of movement, new smoothness quantification metrics were introduced and compared among them to see which one obtained a better smoothness result. Smoothness of movement is shown as an effective, reliable and adequate measure to evaluate the upper limb, as well as smooth and coordinated

A.-C. L. · Q.-U. I. · Q. Y. · B.-R. V. (✉)

Movement Analysis Laboratory, National Institute of Rehabilitation, Mexico City, Mexico

© The Author(s), under exclusive license to Springer Nature Switzerland AG 2022

351

D. Torricelli et al. (eds.), *Converging Clinical and Engineering Research on Neurorehabilitation IV*, Biosystems & Biorobotics 28,

https://doi.org/10.1007/978-3-030-70316-5_56

Fig. 1 Measurement protocol with the SBB[1]



movements are an indication of healthy human motor control and learning [1]. These studies on the smoothness of movements, concluded in the realization of a new smoothness metric called Spectral Arc Length Metric (*SALM*) defined as the arc length of the amplitude and the frequency normalized Fourier magnitude spectrum of the speed profile, considering a movement with a velocity profile $v(t)$:

$$n_{sal} = - \int_0^{\omega_c} \sqrt{\left(\frac{1}{\omega_c}\right)^2 + \left(\frac{dV(\omega)}{d\omega}\right)^2} * d\omega \quad (1)$$

$$V(\omega) = \frac{V(\omega)}{V(0)} \quad (2)$$

where in the equation, $\omega_c = 20 \text{ Hz}$, is the frequency band that covers normal and abnormal human movements and $V(\omega)$ is the Fourier magnitude spectrum of $v(t)$.

Taking into account that this *SALM* metric uses kinematic data such as speed, it serves to detect the differences between motor control skills, learning and recovery, among all the metrics under investigation it is the chosen candidate to use in the experimental data of this work [1–3].

The Smoothness Scale for Upper Limb Function (*SSULF*) are the categories obtained from the analysis of previous *SALM* results that were used as scores for the proposed new scale [3][4].

2 Methods

After the experimentation process, the data obtained from a total of 2688 SBB repeats, the results obtained from the *SALM* of the control group and the diagnosed patients were used to construct a validation for extreme groups using two different methods

Fig. 2 Result of the quantification of a task using the SALM metric

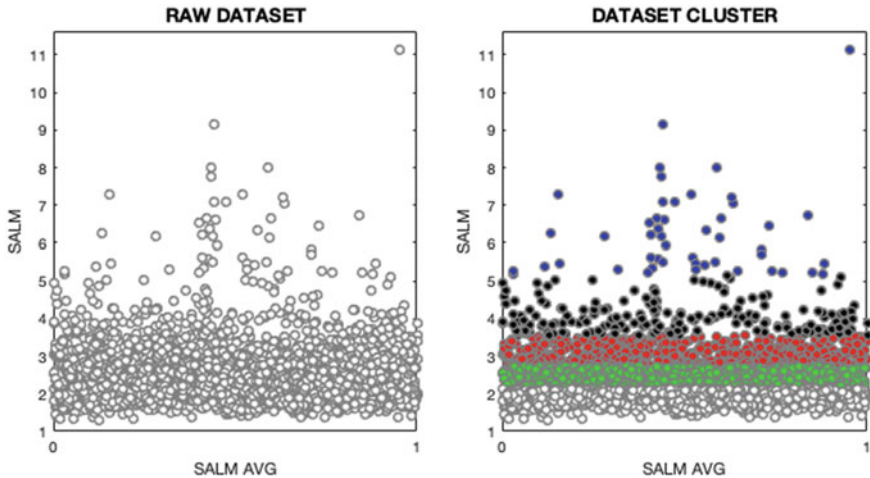
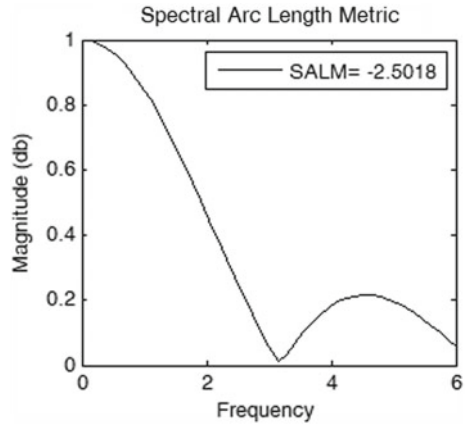


Fig. 3 The scatter diagram shows the distribution of the data of all the 16 different subtasks from Sorting Block Box with the use of Shimmer IMU in the comparison of SALM vs SALM average

(K-means and Fuzzy C-means) of clustering using the same data to compare and determine which one best classifies the data.

Now, compared to the two methods proposed in this study, the following table was created to compare the results obtained with the different grouping methods. You can see the difference between the limits of each class for the new SSULF metric proposed in this study. We can see that the Fuzzy C-means method is the one that has the classes with the limits less separated than the other techniques, so we can assume that the classification is better for our purpose (Table 1).

Table 1 Results of the 2 methods of clustering

No.	limits	SSULF				
		1	2	3	4	5
(1)	MIN	0	2.20	3.15	4.72	7.63
	MAX	2.19	3.14	4.71	7.62	max
(2)	MIN	0	2.11	2.96	4.38	7.03
	MAX	2.10	2.95	4.37	7.02	max

1. K-Means, 2. Fuzzy C-Means

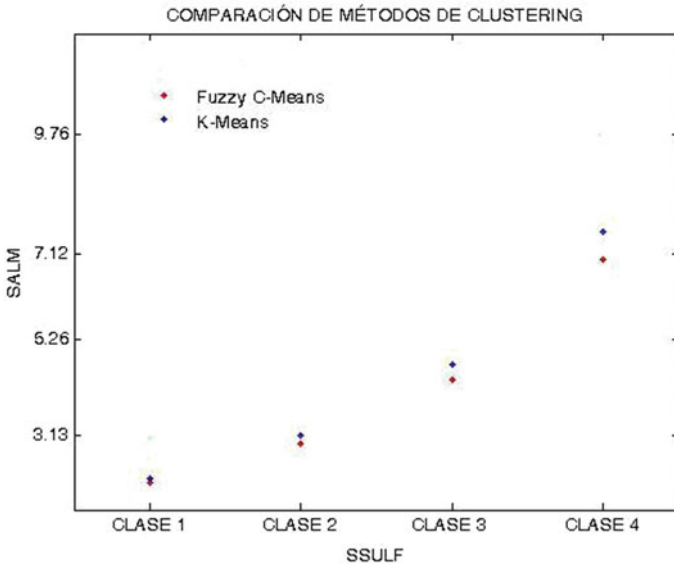


Fig. 4 Graphical comparison of the two clustering methods

3 Discussion

There are several applications where decision making and exploratory pattern analysis must be performed on large data sets. Studies of fuzzy or neuro-diffuse clustering, weighted arithmetic average, unweighted arithmetic average, room method, neural network methods are proposed, knowing that clustering is a subjective process; the same set of data elements often needs to be partitioned differently for different applications. This subjectivity makes the grouping process difficult.

4 Conclusion

As a conclusion of this analysis, we can determine that with the data obtained and the classification made with the two methods, we decided that the classification made by The Fuzzy K-means method is more consistent because it has a greater sensitivity when separating the classes, that is, the classes are less separated from each other in their values, which makes them have a greater capacity when determining if a data is of one kind or another.

As this study is not definitive, since there are more and different grouping methods, future work could cover these doubts and clarify which method could achieve a better classification of the data presented, although with the approach made with these methods they give a sample of that they do work and classify as expected.

References

1. Y. Quijano et al., Upper Limb Functional Assessment of Children with Cerebral Palsy Using a Sorting Box, in *En prensa 36 Annual International IEEE EMBS Conference 2014*
2. Y. Quijano-Gonzalez, A. Melendez-Calderon, E. Burdet, J.E. Chong-Quero, D. Villanueva-Ayala, J.C. Perez-Moreno, Upper limb functional assessment of children with cerebral palsy using a sorting box, in *Engineering in Medicine and Biology Society (EMBC)*, pp. 2330, 2333 (2014)
3. Y. Quijano González, Quiñones Urióstegui Ivett, J.E. Chong-Quero, A. Alessi Montero, P. Ula-cia Flores, A. León Garmendia, IMU placement in the assessment of the upper limb using smoothness metrics, in *2016 GCMAS Annual Conference*
4. L. Anaya, Y. Quijano, I. Quiñones, A. Alessi, V. Bueyes, E. Chong, Segmentación de Tareas en el Dispositivo Sorting Block Bock, para la Valoración Funcional del Miembro Superior de Niños con Parálisis Cerebral, in *Memorias del XXXIX Congreso Nacional de Ingeniería Biomedica* (2016)
5. F. McNeill, E. Thro, *Fuzzy Logic, a practical approach.* (1st Ed.) (Academic Press Ltd, Cambridge Mass, 1994), p. 21
6. J. Mordeson, S. Premchand, *Fuzzy Mathematics.* (Studies in Fuzziness and soft computing No. 20) (Physica-Verlag, Heidelberg, New York, 2001)
7. J.A. Hartigan, M.A. Wong, A k-means clustering algorithm, *AppStat* (28), 100–108 (1979) ((DOI Link BibRef 7900)
8. S.Z. Selim, M.A. Ismail, K-Means-Type Algorithms: A Generalized Convergence Theorem and Characterization of Local Optimality. *PAMI*(6) **1**, 81–87. See also Fuzzy C-Means: Optimality of solutions and effective termination of the algorithm (1984)
9. A. Navarro, C.R. Allen, Adaptive classifier based on K-means clustering and dynamic programing. *OptEng* **1**

Artificial Neural Networks to Quantify Motor Skills in Children with Cerebral Hemiparesis



L. Anaya-Campos, I. Quiñones-Uriostegui, Y. Quijano, and V. Bueyes-Roiz

Abstract Previous studies have sought to improve the way of classifying upper limb motor involvement in patients with alterations or pathologies in the central nervous system, so it has become of great importance to find an objective way of measuring and classifying the degree of movement capacity. This work uses the artificial neural network method to quantify the motor skills at five levels of the SSULF scale proposed to have a better assessment of the degree of upper limb motor functionality in patients diagnosed with cerebral hemiparesis.

1 Introduction

Cerebral Palsy (CP) is a group of permanent pre, post, and perinatal disorders of development, motion, and posture due to non-progressive changes that occur during brain development, as a result of injuries to the Central Nervous System [1].

The Sorting Block Box consists of a board with holes in different geometric shapes (box, triangle, circle, rectangle) and 4 pieces of wood that must be placed in their respective spaces; said board has various sensors inside that detect the force of the movement and whether or not the piece is in place, in addition to this, the information is being transferred by a data acquisition card, to a computer [4]. After completing a part filling or emptying task, a program developed in LabVIEW (National Instruments, USA), generates two data files with the information collected from the various sensors involved, to be analyzed later. In addition to the SBB, an inertial IMU sensor is placed on the back of the hand in order to quantify the trajectories [5] (Fig. 1).

Each trajectory delimits a sub-movement [3], that is, a sub-movement is to take the orange piece with the right hand and place it in its hole and another sub-movement is the action is to press the green button indicating the end of the movement; that's called a filling task. The next submovement would be to take the orange piece from the hole and return it to its original place and then press the green button indicating the end of the movement; This is called the emptying task. Taking this into account,

L. Anaya-Campos (✉) · I. Quiñones-Uriostegui · Y. Quijano · V. Bueyes-Roiz
Movement Analysis Laboratory, National Institute of Rehabilitation, Mexico City, Mexico

© The Author(s), under exclusive license to Springer Nature Switzerland AG 2022
D. Torricelli et al. (eds.), *Converging Clinical and Engineering Research*
on *Neurorehabilitation IV*, Biosystems & Biorobotics 28,
https://doi.org/10.1007/978-3-030-70316-5_57

357

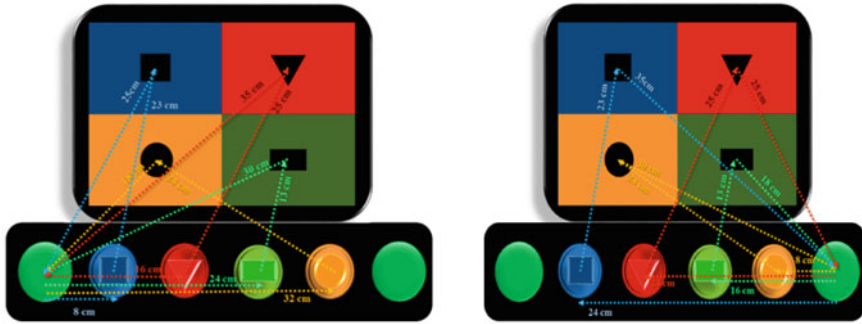


Fig. 1 Sorting Block Box board. The distances (cm) of the ideal trajectories traveled by the left arm (left) and the right arm (right) are shown

being 4 pieces with 4 movements and each movement with 2 sub-movements, it gives us a total of 16 sub-movements to analyze. The use of three metrics will give us the measurement results of the children. These metrics were determined by reading bibliographies and previous studies carried out as smoothness of movement metrics [2, 3, 5].

The Spectral Arc Length Metric is defined as the size of the Fourier spectrum curve of the velocity profile of a motion:

$$n_{sal} = - \int_0^{\omega_c} \sqrt{\left(\frac{1}{\omega_c}\right)^2 + \left(\frac{dV(\omega)}{d\omega}\right)^2} * d\omega \tag{1}$$

$$V(\omega) = \frac{V(\omega)}{V(0)} \tag{2}$$

where in the equation, $\omega_c = 20$ Hz, is the frequency band that covers normal and abnormal human movements and $V(\omega)$ is the Fourier magnitude spectrum of $v(t)$.

The Peaks Metric is the number of local maxima in the speed profile of a movement:

$$n_{pm} \triangleq -\#\{v_{m\acute{a}xima}\} \tag{3}$$

$$v_{m\acute{a}xima} \triangleq \left\{ v(t) : \frac{dv}{dt} = 0 \ \& \ \frac{d^2v}{dt^2} < 0 \right\} \tag{4}$$

The Log Dimensionless Jerk Metric is the negative log of the Jerk (third derivative of position with respect to time) total normalized to the square:

$$n_{ldj} \triangleq -\ln \left(\frac{(t_2 - t_1)^3}{v_{peak}^2} \int_{t_1}^{t_2} \left| \frac{d^2v}{dt^2} \right|^2 dt \right) \tag{5}$$

$$v_{peak} \triangleq \max_{t \in [t_1, t_2]} v(t) \tag{6}$$

2 Methods

After the experimentation process, the data obtained from a total of 2784 evaluations with the SBB, the results obtained from the three metrics of the control group and the diagnosed patients were used to construct a validation for extreme groups using the K-method. means of grouping.

Using the *K* – means grouping method, we obtained the results shown bellow with a total of 5 clusters for the SSULF classification the parameter limits of each SSULF class of the SALM metric:

$$SSULF_{SALM} = \begin{cases} 1. 0 \leq SALM \leq 2.2123 \\ 2. 2.2123 < SALM \leq 3.2256 \\ 3. 3.3356 < SALM \leq 5.1387 \\ 4. 5.1387 < SALM \leq 9.0882 \\ 5. 9.0882 < SALM \end{cases} \tag{7}$$

$$SSULF_{PM} = \begin{cases} 1. 0 \leq PM \leq 35.1 \\ 2. 35.1 < PM \leq 135.85 \\ 3. 135.85 < PM \leq 292.5 \\ 4. 292.5 < PM \leq 451.75 \\ 5. 451.75 < PM \end{cases} \tag{8}$$

$$SSULF_{LDJM} = \begin{cases} 1. 0 \leq LDJM \leq 27.95 \\ 2. 27.95 < LDJM \leq 105.3 \\ 3. 105.3 < LDJM \leq 247.65 \\ 4. 247.65 < LDJM \leq 451.75 \\ 5. 451.75 < LDJM \end{cases} \tag{9}$$

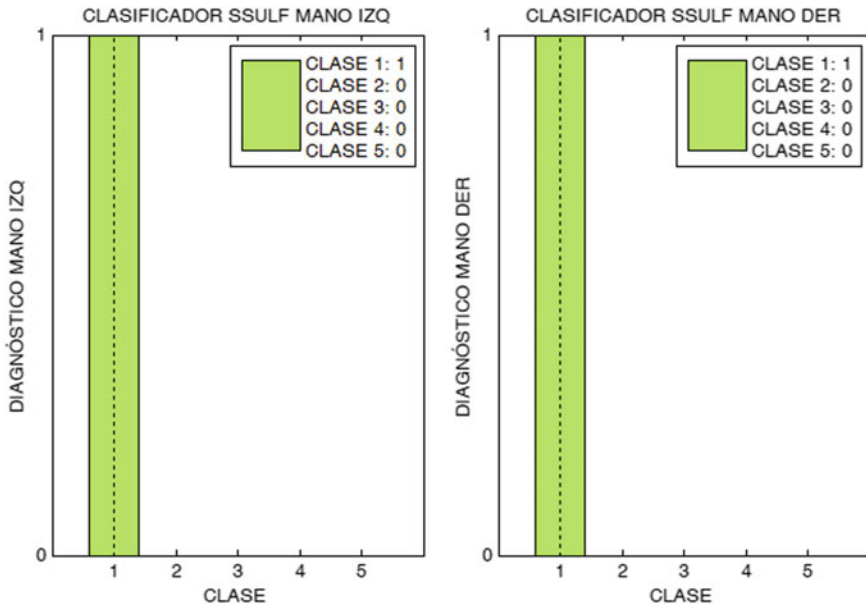


Fig. 2 Final assessment with the SSULF scale using as a basis the classification by artificial neural networks with 16 inputs and 3 hidden layers with 8-10-12 neurons per layer

3 Results

Using these limit values for each SSULF metric, neural networks of different values in hidden layers were trained to train to identify the SSULF value of each assessment. Now with the trained neural network, the value of the 16 subtasks per attempt is entered and the network returns the classification, in this case the level of assessment in which the subject falls, from the SSULF scale, as can be seen in the Fig. 2.

4 Discussion

The segmented analysis presented focuses primarily on functional assessment of the upper limb with the help of the SBB. In this study, the use of this device as a method of taking information about the movement of subjects diagnosed with cerebral palsy and their understanding. The movements of the filling and emptying actions of the SBB board could be assessed through three smoothness metrics (SALM, PM, LDJM). These metrics were found to be effective in assessing functionality between healthy subjects and subjects diagnosed with hemiparesis. The three metrics were able to demonstrate the differences between an affected and unaffected upper limb of the same individual.

5 Conclusion

However, there were variations between magnitudes recorded on the PM scale that showed differences in the values obtained due to the time it took for the subjects to finish the movement. On the other hand, the SALM and LDJM metrics tend to show less abrupt changes no matter how long it takes the subject to perform each action. The use of softness metrics has been shown to be an effective indicator of upper limb movement by showing the differences between an affected limb and an unaffected limb denoting differences between trajectory changes, limb spatial position and trunk, as well as flexion and shoulder extension. Likewise, softness is an indicator of the motor control and spatial-temporal coordination of the subject that leads to an even deeper analysis than that presented in this document. This subsequent analysis due to the omitted variables is proposed later in the future work.

References

1. Salud Secretaría de, SEMAR, and SEDENA: Resumen de Evidencias y Recomendaciones, evaluación diagnóstica del niño con parálisis cerebral en el tercer nivel de atención (2009)
2. Anaya, L., Quijano, Y., Quiñones, I., Alessi, A., Bueyes, V., Chong, E.: Segmentación de Tareas en el Dispositivo Sorting Block Bock, para la Valoración Funcional del Miembro Superior de Niños con Parálisis Cerebral, Memorias del XXXIX Congreso Nacional de Ingeniería Biomédica (2016)
3. Quijano, Y., et al.: Upper Limb Functional Assessment of Children with Cerebral Palsy Using a Sorting Box. En prensa 36 Annual International IEEE EMBS Conference 2014
4. S. Balasubramanian, A. Melendez-Calderon, A. Roby-Brami, E. Burdet, On the analysis of movement smoothness. *J NeuroEngineering Rehabil BioMed Central* **12**(1), 112 (2015)
5. Anaya, L., Quijano, Y., Quiñones, I., Alessi, A., Bueyes, V., Chong, E., Segmentación de Tareas en el Dispositivo Sorting Block Bock, para la Valoración Funcional del Miembro Superior de Niños con Parálisis Cerebral, Memorias del XXXIX Congreso Nacional de Ingeniería Biomédica (2016)

Analysis of a Predictive Forward Simulator of Human Gaits



T. Bonis, N. Pronost, and S. Bouakaz

Abstract Although predictive forward gait simulators have existed for a little while, only few sensitivity studies have been proposed. We present a study analysing precision, accuracy, stability and sensitivity of such simulator. We studied a gait simulator based on the trajectory mimicking method proposed by Lee et al. [1]. We assessed the effect of motion variation on the resulting gait simulation using the sensitivity analysis method proposed by Saltelli et al. [2]. Our method supports the use of this simulator for prediction.

1 Introduction

In recent years, predictive gait simulators met some successful applications. Lee et al. [1] showed that muscle contraction patterns and post-operation gaits can be predicted. Falisse et al. [3] can predict transitions between walking and running, the effects of some muscles weaknesses, and the effects of wearing an orthosis. To our knowledge, only Falisse et al. [3] studied the sensitivity of their framework, and only to foot shape variation. We propose a method to analyze the sensitivity of such simulator to many parameters. We illustrate our method on a simulator proposed by Lee et al. [1].

The simulator proposed by Lee et al. trains a neural network (NN) to produce stable walking simulations using target position for proportional-derivative (PD) controllers (trajectory mimicking) and a second NN computes muscle activations (muscle coordination). This preliminary study focuses on the effect of wearing a knee brace without modeling muscles. Without loss of generality, it allows us to

This research is supported by the ANR agency under grant number ANR-16-CE92-0042. The authors would like to acknowledge the Labor für Biomechanik und Biomaterialien at the Medizinische Hochschule Hannover for their collaboration.

T. Bonis (✉) · N. Pronost · S. Bouakaz
Université de Lyon, Université Claude Bernard Lyon 1, CNRS LIRIS Lab, Lyon 69622, France
e-mail: thomas.bonis@univ-lyon1.fr

simplify the model and the framework by removing the muscle coordination part which makes the framework faster and allows us to perform a large number of simulations for our sensitivity study.

2 Materials and Methods

After training our controller to replicate a reference gait motion, a quasi-random low-discrepancy sequence is used to generate sets of motions variations for the forward simulator. Measures are performed on the resulting simulations in order to analyze the predictive capability of the simulator. Input variations and measures are detailed in Sect. 2.2.

2.1 Model and Simulation

The model used in our simulator is based on the full body *gait2392* OpenSim model [4] where arms and muscles have been removed for computational performances.

The reference motion has been obtained through a common pipeline : motion capture with Plug-In Gait marker-set then scaling and inverse kinematics using OpenSim. The stability of the simulator have been improved by smoothing every joint angle trajectory with a two-10Hz Butterworth filter, then the angular trajectories have been cyclified. The resulting motion is used to train the trajectory mimicking controller with a reward function based on the tracking of the angular trajectories, the end-effector positions and the cost of transportation.

2.2 Inputs and Measures

For each trained NN, many simulations are done thanks to input variations.

Inputs. The variation over $\phi \in [0, 1]$, the normalized starting time in the gait cycle, is used to avoid ill-conditioned simulations. Two inputs have been chosen to simulate the effect of wearing a knee-brace: the limitation of the range of motion of the right knee (*RK*) and the distortion of the reference angular trajectory of the right knee. The distortion is made using variations of the four extremum control points (*D1*, *D2*, *D3*, *D4*) of the spline approximating the right knee trajectory.

Measures. We chose commonly used measures in biomechanical studies [5] and introduced additional measures that are relevant to our case study (see Table 2). We used spatio-temporal measures but also mean, minimum and maximum of angular trajectories during various phases of the gait cycle. We do not compare directly joint trajectories in order to get more quantitative outcomes. For each simulation the measures have been automatically computed.

2.3 Analysis

In this work, we use the data from one healthy subject (M, 26). The gait with the best ‘cycle’ was studied.

Precision. First, we tested the precision of the training as the learning process is stochastic. 18 training sessions were done and we measured P^i for each measure as:

$$P^i = \sigma(\overline{M_{simu}^i(\phi)})_{NN_j} \text{ with } 0 < j < 17$$

where $\overline{M_{simu}^i(\phi)}$ is the mean of each measure i over the variation of the normalized starting time ϕ in the gait cycle.

Accuracy. In order to assess the accuracy of the simulator, we computed A^i for each measure, for a selected NN:

$$A^i = |M_{ref}^i - \overline{M_{simu}^i(\phi)}|$$

where the M_{ref}^i is the value measured on the reference motion.

We ran simulations for 80.000 sets of input values. These sets were generated using a Sobol sequence of 6 inputs with 10.000 samples. The sequence and the number of samples have been chosen to be optimal to compute the sensibility indices according to Saltelli et al. [2]. The measures from these simulations are used for sensitivity and stability analysis.

Stability. In the stability analysis, for each input, we searched for the upper and lower limits allowing 10 successfull gait cycles.

Sensibility. The main effect index (S_{main}) was used as the sensitivity index. There are various ways to compute this index and we used the one introduced by Saltelli et al. [2]. It can be viewed intuitively as the expected variance that would be left if all parameters but parameter k could be fixed and normalized by the global variance. We computed those values for an increasing number of samples to determine if they converge towards stable values.

3 Results

Table 1 presents the results for the stability analysis and Table 2 presents the results for precision, accuracy and sensitivity. For the sensitivity, N means that for 9.000 to 10.000 samples the value of S_{main} is less than 1. If for 9.000 to 10.000 samples the value of S_{main} is greater than 1, the rank is displayed. U is used otherwise.

We observe 23° of ankle range of motion during a cycle. Also a precision of 12° for the minimum ankle DF in SW is an important variation. Likewise, double support is usually less than 10%, so 5% of accuracy is rough. Sensitivity results may

Table 1 Stability study: upper and lower limits for each parameter

Parameter	Lower limit	Upper limit
<i>RK</i>	53.5°	120°
<i>D1</i>	-60°	0°
<i>D2</i>	0°	38°
<i>D3</i>	-15°	12.9°
<i>D4</i>	0°	36.5°

Table 2 Column P is the precision, A is the accuracy, and the last 4 columns are for sensitivity ordering. When two values are given, the first one refers to the left side and second one to the right side

Measures	<i>P</i>	<i>A</i>	D1	D2	D3	D4
Walking velocity $m.s^{-1}$	0.04	0.03	9	N	N	N
Stride length <i>m</i>	0.04	0.04	N	N	N	N
Cadence $step.min^{-1}$	0.06	0.03	N	N	N	N
Stance (ST) time %	0.02 0.021	3.0 4.0	N N	N N	N N	N N
Double support %	0.02	5.0	U	U	U	U
Time to peak knee <i>F s</i>	0.04 0.05	0.02 0.01	1 10	3 N	3 N	6 11
Mean pelvis tilt	1.2	2.2	N	5	2	5
Max hip F in swing (SW)	3.0 3.4	6.7 9.0	N N	N N	N N	N N
Mean hip F in ST	2.2 2.0	2.5 0.48	U N	N N	6 N	3 N
Hip flexion (F) at initial contact (IC)	4.0 3.9	7.9 8.1	3 N	1 N	7 N	1 N
Max hip abduction in SW	2.3 2.7	2.0 0.12	6 4	N 6	N U	7 2
Max knee F in SW	2.3 3.3	3.5 3.0	7 5	4 7	9 4	N 4
Min knee F in SW	3.7 3.4	4.6 6.3	N N	N N	N N	N N
Max knee F in SS	4.5 2.8	8.0 12	N N	N N	N N	N N
Min knee F in SS	2.9 3.1	3.3 6.1	11 N	N 2	1 N	N 9
Max ankle dorsiflexion (DF) in ST	2.4 2.9	4.7 5.5	N N	N N	N N	N N
Min ankle DF in ST	3.7 4.2	12 14	12 N	N N	N N	N N
Max ankle DF in SW	2.2 2.7	3.0 3.3	2 N	N N	8 N	10 N
Min ankle DF in SW	4.1 4.7	12 14	8 N	N N	5 N	8 N

be interpret as follows: the relation between inputs variations and measures are not straight. For example, the distortion D1 modify the maximum right knee flexion in swing phase on the reference motion and this value is not the one with the highest main effect index for D1 variation.

The sensitivity experiment shows that the maximum right knee flexion in swing phase is not the most influenced measure during variation of D1, so the relation between parametres and measures are not straight forward.

4 Discussion and Conclusion

As outlined above, this work is a preliminary study of a forward gait simulator where precision and accuracy of the training, stability and sensitivity of the simulation are observed regarding input variations. Precision and accuracy successfully highlight some weaknesses of the simulator. Furthermore, stability confirms that the framework is suitable for predictive simulation. As suspected, the relationship between the inputs and the measurements is complex. We expect that further researches will highlight similar relations between inputs and measurements in clinical studies.

References

1. S. Lee, M. Park, K. Lee, J. Lee, Scalable muscle-actuated human simulation and control. *ACM Trans. Graph.* **38**(4) (2019)
2. A. Saltelli, P. Annoni, I. Azzini, F. Campolongo, M. Ratto, S. Tarantola, Variance based sensitivity analysis of model output. Design and estimator for the total sensitivity index. *Comput. Phys. Commun.* **181**(2), 259–270 (2010)
3. A. Falisse, G. Serrancolí, C.L. Dembia, J. Gillis, I. Jonkers, F. De Groote, Rapid predictive simulations with complex musculoskeletal models suggest that diverse healthy and pathological human gaits can emerge from similar control strategies. *J. Royal Soc. Interface* **16**(157), 20190402 (2019)
4. S.L. Delp, F.C. Anderson, A.S. Arnold, P. Loan, A. Habib, C.T. John, E. Guendelman, D.G. Thelen, OpenSim: open-source software to create and analyze dynamic simulations of movement. *IEEE Trans. Biomed. Eng.* (2007)
5. M. Roberts, D. Mongeon, F. Prince, Biomechanical parameters for gait analysis: a systematic review of healthy human gait. *Phys. Therapy Rehab.* **4**(1), 6 (2017)

SS7: Development of Novel Neural Interfaces to Improve Neurorehabilitation

Effects of Decomposition Parameters and Estimator Type on Pseudo-online Motor Unit Based Wrist Joint Angle Prediction



Dennis Yeung , Francesco Negro , and I. Vujaklija 

Abstract The decomposition of HD-EMG into motor unit (MU) discharge timings permit a detailed window into the motoneuronal manifestation of motor intent. Recently, the feasibility of MU-driven wrist joint angle estimation was preliminarily demonstrated although the influences of certain parameter selections have yet to be fully investigated. Here, a decomposition algorithm was used to predict wrist joint kinematics over three DoFs in a pseudo-online manner. Three separate estimator types were tested and the effects of two key parameters on their prediction accuracies were studied: the decomposition extension factor and process window length. Pre-recorded EMG from four able-bodied subjects was decomposed in a simulated real-time manner as to permit parameter scanning, with the tested estimators being linear regression (LR), linear discriminant analysis (LDA), and LDA with LR for proportionality control (LDA-LR). Results showed the best performing combination of parameters were an extension factor of 8 with window length of 50 ms which allowed the LDA-LR estimator to yield an average R^2 value of 0.86 ± 0.05 . Under the most computationally demanding set of parameters, the median processing time of the algorithm on a desktop computer was 47 ms which was within the update rate of the proposed system. Such results also indicate that parameters optimal for online control applications deviate from those ideal for offline physiological studies.

D. Yeung (✉) · I. Vujaklija
Bionic and Rehabilitation Engineering Group, Department of Electrical Engineering and Automation, Aalto University, Espoo, Finland
e-mail: dennis.yeung@aalto.fi

F. Negro
Department of Clinical and Experimental Sciences, University of Brescia, Brescia, Italy

1 Introduction

Motor unit (MU) discharge timings constitute the encoding for muscle activation and various techniques to extract such information via decomposition of electromyography recordings (EMG) have been proposed [1, 2]. Recently, Kapelner et al. demonstrated that the prediction of wrist kinematics can be improved using neural features extracted from high-density EMG measurements [3], however such decomposition was performed in an offline manner. Indeed, traditional decomposition methods have high computation overheads that restrict their application to mainly offline studies, though efforts have been made to address this issue [4]. In particular, Barsakcioglu & Farina proposed a system capable of extracting activity from five MUs in the forearm for real-time control of a hand prosthesis with on/off control of 4 device functions [5].

In this study, a similar approach for online decomposition was implemented for the continuous estimation of wrist kinematics. The estimation was done in pseudo-real time as the extraction of neural information was processed in a windowed manner to simulate a real-time application. We compared the performance of three estimators: linear regression (LR), linear discriminate analysis (LDA) with cumulative spike counts used for proportionality control, and LDA with class-specific LR for proportionality (LDA-LR). LR acts as a simple regressor, LDA is a well-established myocontrol classifier, whereas LDA-LR aims to combine the intrinsic proportional capabilities of LR and the clear motion distinction of LDA. The effects of the decomposition extension factor (R) and the window length (WL) across the three estimators were also analyzed by scanning a range of settings. R influences the quantity of sources that are identified while WL affects system responsiveness with both parameters contributing to process computation overhead.

2 Methods

2.1 *Experiment Setup and Protocol*

Four healthy right-handed males, aged 28–33, participated in the study approved by local ethical board of Aalto University. They all provided written informed consent. HD-EMG was recorded from each subject's dominant side with three 8×8 electrode matrices spaced evenly around the bulk of the forearm, sampled at 2048 Hz by a benchtop bioamplifier (OT Bioelettronica, IT). Wrist joint angles were recorded by three wireless Inertial Measurement Units (IMUs) (Xsens Technologies B.V, NL) attached to the posterior sides of the upper-arm, lower forearm and hand.

Subjects performed three repetitions of six wrist motor tasks following trapezoidal activation profiles with 2 s up/down ramps and 10 s plateaus: flexion/extension (DoF1+/DoF1–), radial/ulnar deviation (DoF2+/DoF2–) and pronation/supination (DoF3+/DoF3–) with the data being segmented into three folds of train/test sets. A

framework developed by Negro et al. [6] was employed for batch decomposition of the train set EMG and the resultant decomposed spike count (DSC) features were used to train the estimators. The online decomposition algorithm was then used to extract DSC features from the test set for kinematics estimation. To simulate a real-time application, test set data was processed in windows which advanced in steps of 50 ms. For WL values beyond 50 ms, this resulted in overlaps of 50–450 ms between consecutive windows.

2.2 Pseudo-online Decomposition and Estimation

The proposed online algorithm alleviates the computational requirements of blind source extraction by relying on properties obtained from prior decomposition of the training set. From the batch method, underlying sources of the EMG were identified through the optimization of a set of separation vectors:

$$\mathbf{S}(t) = \mathbf{B}^T \underline{\underline{\mathbf{W}}} \underline{\underline{\mathbf{X}}}(t) \quad (1)$$

where $\mathbf{S}(t)$ is the set of sources, \mathbf{B} , the bank of matched filters, $\underline{\underline{\mathbf{W}}}$, the whitening matrix and $\underline{\underline{\mathbf{X}}}$, the extended zero-meaned EMG. Here, \mathbf{B} and $\underline{\underline{\mathbf{W}}}$ matrices for each motor task were first obtained from their respective training sets via the batch method. These were then applied by the online algorithm to extract source signals from the test data. Peaks detected in these source signals were then accepted as spikes if they fell within their respective cluster limits from the original decomposition of the train set.

3 Results

The number of MUs extracted from each motor task, averaged across all subjects, is shown in Fig. 1. As R was increased, the number of identified MUs also increased although this trend levelled off beyond R = 9. Estimation with LDA-LR performed the best overall with the highest R² value of 0.86 ± 0.05 from R = 8 and WL = 50 ms. For LR, the best value was 0.83 ± 0.6 from R = 9 and WL = 150 ms while, for LDA, this was 0.81 ± 0.06 from R = 8 and WL = 50 ms. It can be seen from Fig. 2 that the parameters R and WL affected each estimator type differently. While a significant improvement was seen in all estimators by increasing R from 1 to 3, less improvement was seen from further increase of R. This may be that the additional MUs obtained with higher R values offer minimal extra information towards the joint kinematics state for this set of simple motor tasks. This also suggests that, for proportional myocontrol applications, lower R values may be used than those recommended for physiological studies [6].

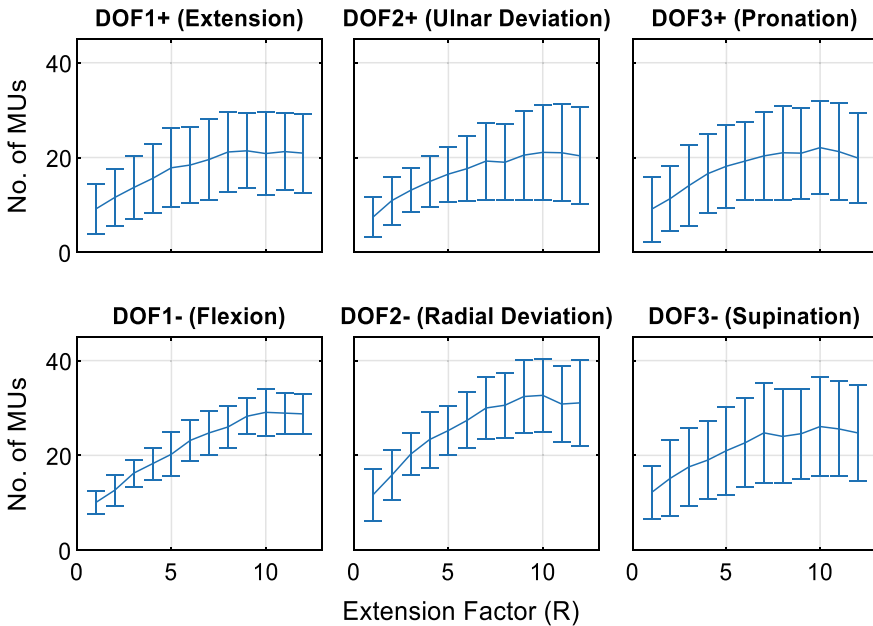


Fig. 1 Average number of MUs extracted from each motor task across all subjects

WL had little effect on LR performance as large values may only contribute to the smoothness of the estimations. LDA performed poorly with larger WLs which indicates higher misclassification rates as larger spans of time were used to calculate DSC. This trend was also repeated for LDA-LR which improved on the naïve method for proportionality estimation used by LDA. As such LDA-LR, yielded higher and more consistent goodness-of-fit values.

The processing time of the online algorithm performed on a PC (Intel Xeon 3.60 GHz 32 GB RAM & MATLAB 2019a, Mathworks, USA) at the highest loads ($R = 13$, $WL = 500$ ms) was measured and a median time of 47 ms was obtained which was below the estimation update rate. It should be noted however, that further focus on code optimization would lead to even shorter process times.

4 Conclusion

This work analyzed the effects of two key parameters for online decomposition of EMG on the estimation accuracy of wrist joint angles. While a higher decomposition extension factor led to the extraction of more MUs, the contribution of additional sources to estimation accuracy diminishes. Similarly, larger values of window length did not yield the optimal performance. The results therefore indicate that a less

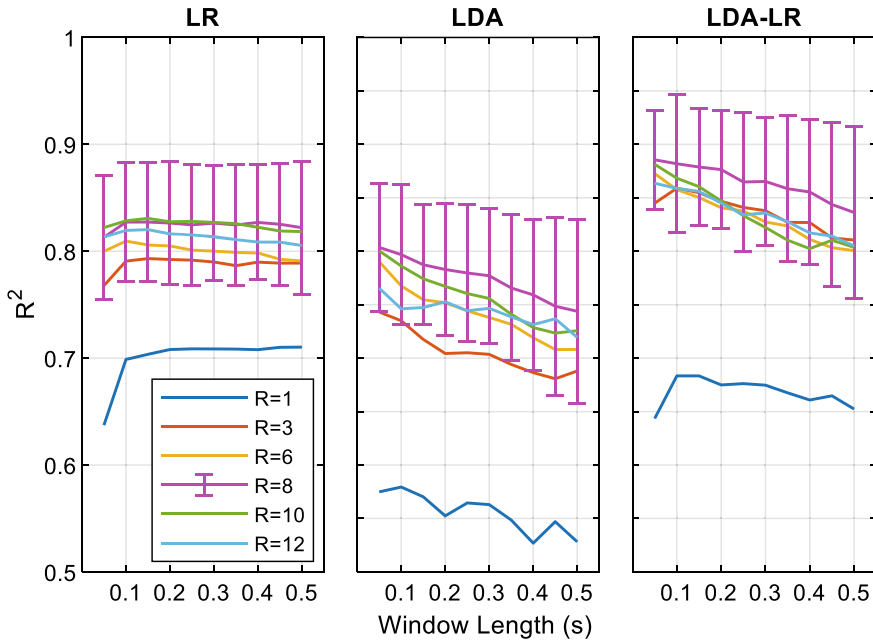


Fig. 2 Effects of R and WL on the estimation accuracies of the LR, LDA and LDA-LR estimators

computationally demanding set of online decomposition parameters may be used in the case of neural data-driven control applications.

References

1. A. Holobar, D. Farina, Blind source identification from the multichannel surface electromyogram. *Physiol. Meas.* **35**(7), R143–R165 (2014)
2. D. Farina et al., Man/machine interface based on the discharge timings of spinal motor neurons after targeted muscle reinnervation. *Nat. Biomed. Eng.* **1**, 25 (2017)
3. T. Kapelner et al., Predicting wrist kinematics from motor unit discharge timings for the control of active prostheses. *J. Neuroeng. Rehabil.* **16**(1), 47 (2019)
4. V. Glaser, A. Holobar, D. Zazula, Real-time motor unit identification from high-density surface EMG. *IEEE Trans. Neural Syst. Rehabil. Eng.* **21**(6), 949–958 (2013)
5. D.Y. Barsakcioglu, D. Farina, A real-time surface EMG decomposition system for non-invasive human-machine interfaces, in *IEEE Biomedical Circuits and Systems Conference (BioCAS) 2018*, pp. 1–4
6. F. Negro, S. Muceli, A.M. Castronovo, A. Holobar, D. Farina, Multi-channel intramuscular and surface EMG decomposition by convolutive blind source separation. *J. Neural Eng.* **13**(2), 026027 (2016)

Highly Intuitive 3-DOF Simultaneous and Proportional Myocontrol of Wrist and Hand



Markus Nowak, I. Vujaklija, Claudio Castellini, and Dario Farina

Abstract While simultaneous and proportional activation of multiple degrees of freedom (DOFs) is supported by novel prosthetic hands, there are still no commercial controllers to appropriately enable it. Here, we test a ridge regression based myocontrol method in two real-time scenarios: 13 subjects with an extended high-density EMG electrode set (192 channels) and 4 subjects with a reduced set of electrodes (16 channels). In each scenario, the algorithm was trained on 3 repetitions of single DOF motions (rest, wrist flexion/extension and rotation, and hand closing) and then subjects were asked to reach 24 on-screen goals consisting of one-DOF, two-DOF, and three-DOF targets. The results showed that participants were able to reach all types of targets and that their one-DOF success rate remained high despite the simultaneous control of multiple DoFs ($95.9 \pm 5.7\%$). Moreover, the performance did not significantly change when reducing the number of electrodes ($97.6 \pm 4.5\%$ for 16 channels).

The study was partially funded by the DFG project *Tact_Hand* (CA-1389/1-1) and the ERC Synergy project *NaturalBionicS*.

M. Nowak (✉) · C. Castellini
German Aerospace Center (DLR), Institute of Robotics and Mechatronics, Wessling, Germany
e-mail: markus.nowak@dlr.de

C. Castellini
e-mail: claudio.castellini@dlr.de

I. Vujaklija
Department of Electrical Engineering and Automation, Aalto University, Espoo, Finland
e-mail: ivan.vujaklija@aalto.fi

D. Farina
Department of Bioengineering, Imperial College London, London, UK
e-mail: d.farina@imperial.ac.uk

© The Author(s), under exclusive license to Springer Nature Switzerland AG 2022
D. Torricelli et al. (eds.), *Converging Clinical and Engineering Research on Neurorehabilitation IV*, Biosystems & Biorobotics 28,
https://doi.org/10.1007/978-3-030-70316-5_60

1 Introduction

Multi-articulate prosthetic hands have been commercially available for over a decade. Even though they feature multiple motorized degrees of freedom (DOFs), the most commonly provided control interface is a switching paradigm leaving users to progressively cycle through preset functions [1]. Recently, advanced prosthetic systems have been controlled with pattern recognition algorithms [2, 3] capable of directly distinguishing individual gestures by classifying electromyographic (EMG) activity of user's residual muscles. While this is an important advance, the lack of simultaneous functions makes it still far from meeting the expectations of natural control.

Enabling simultaneous control over multiple DOFs was attempted by extending the pattern recognition approaches to facilitate simultaneous classes [4]. While feasible, this approach remained bound to laboratory conditions. To overcome the inherent discrete nature of classifiers, a focus has been put on regression approaches which aim to establish a continuous mapping between the observed EMGs and the functional domain of prosthetic joints [5]. However, even after demonstrating that a high number of DOFs can be concurrently controlled in this way in robotic systems using high-density EMG (HD-EMG) [6], the most recent home-tested prosthetic systems are still bound to only two DOFs [7].

Here, we propose a regression-based approach which follows the recommendations on being highly intuitive and requiring minimal calibration [8] to deliver 3-DOF simultaneous and proportional control over the wrist and hand (wrist flexion/extension, wrist pronation/supination, and hand closing and rest). The approach was evaluated in real-time and its robustness was examined by progressive channel reduction.

2 Materials and Methods

2.1 Control Strategy

We acquired 192 monopolar EMG signals with three 8-by-8 ELSCH064NM3 sensor matrices (*EMG-USB2+* amplifier, OTBioelettronica, Italy), which were placed around the circumference of the forearm. A moving average (MAV) filter was applied to the rectified signal to extract the envelope and a ridge regression (RR) machine learning (ML) method was applied to the EMG envelopes.¹

¹ The EMG was gathered at 2048 Hz and treated with a 5th order Butterworth bandpass-filter (20–500 Hz). Features were calculated from the rectified, low-pass filtered signal (2nd order Butterworth at 2 Hz cut-off), and averaged across a window of 100 samples with a 3/4 overlap. The regularization parameter in RR was kept at 1.0.

2.2 Experiment Description

To investigate the combined capability of user and ML method we recruited 13 able-bodied participants (age 27.5 ± 3). The study was approved by the local ethics committee of Imperial College of London and all participants have given their written consents before participation.

The EMG sensor matrices were placed around the participant's forearm covering the entire circumference. Reference electrodes were placed at the wrist, and subjects were seated comfortably in front of a PC screen (Fig. 1).

The subjects performed three repetitions of the aforementioned actions of the wrist and hand at a comfortable level for 2s. These $3 \times 6 = 18$ recordings of the MAV of all available channels were used for training the RR algorithm. Thereafter they performed 24 randomly presented goal reaching tasks (12 one-DOF, 8 two-DOF and 4 three-DOF goals, equally distributed with respect to the origin). These tasks accounted for different levels of activation, e.g. 30% of wrist flexion combined with 80% of wrist pronation and 0% hand closure in a two-DOF goal. The subject had 20s to attempt and reach each goal (15% of the normalised work space), and stay within it for 0.3 s.

Of the 13 subjects, four completed an additional round of the same 24 tasks, but with a reduced number of EMG sensors—16 of the original 192 sensors were used for training the ML method. The reduced set featured eight electrode pairs (along the muscle fibre direction) evenly distributed around the widest circumference of the forearm. We did not aim at targeting specific muscle groups.

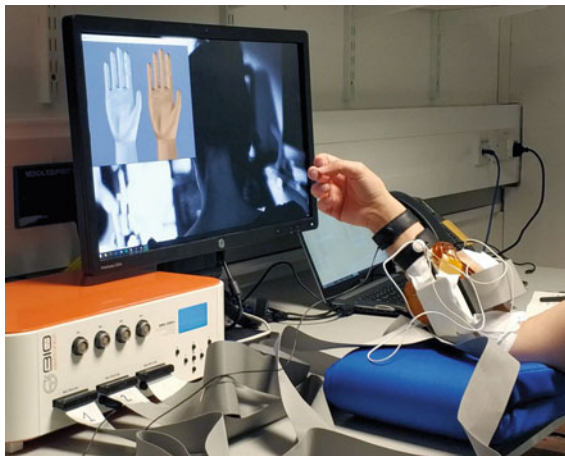


Fig. 1 Experimental setup with *EMG-USB2+* amplifier, PC screen with prediction and target stimulus, and participant equipped with three 8×8 sensor matrices

2.3 Statistical Evaluation

For evaluation purposes we compared the performance of all 192 versus the reduced 16 sensors. Also, we have considered the difference when dealing with one-DOF, two-DOF and three-DOF goals. Therefore, we calculated the success rate (SR) per subject across these categories and performed a statistical analysis with the two factors *Sensor Number* [full, reduced] and *TargetDOFs* [1–3]. We used a two-way repeated-measures ANOVA with $\alpha = 0.05$. Significant interactions were followed up by a pair-wise comparison with Bonferroni correction.

3 Results

Figure 2 summarizes the results of the user study in terms of SR per category as well as the results of the statistical analysis. The factor *TargetDOF* was highly significant with $F(2, 6) = 30.66, p < 10^{-3}$, while the factor *Sensor Number* showed no significant influence on the outcome measure with $F(1, 3) = 0.00, p = 1.00$. The

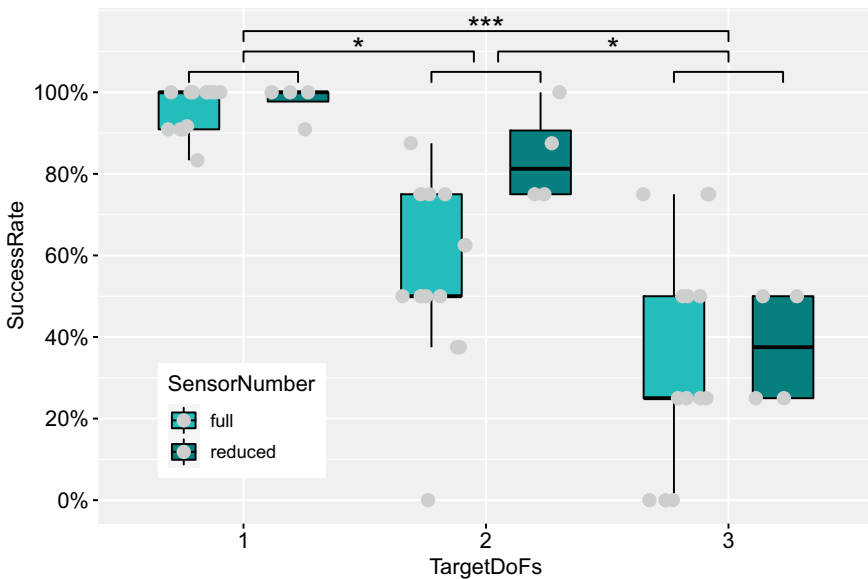


Fig. 2 Box plot with SR of all subjects, superimposed by a dot plot of the individual subject results. Brackets with asterisks represent significant difference, brackets without asterisks represent grouping

interaction term showed no significance either with $F(2, 6) = 2.51$, $p = 0.16$.² A post-hoc of the significant factor *TargetDOF* revealed that each level is significantly different from another with $p \in [0.018, 0.00027]$.

4 Discussion

Results show that although the participants have trained the algorithm *only* with single actions, they were capable of real-time command of two-DOF and even three-DOF combined actions. To the best of our knowledge this is the first time that such a level of control is achieved using intuitive control inputs. Although there was a significant performance degradation when facing more difficult tasks (i.e. two-/three-DOF), this did not impact one-DOF control.

Another remarkable finding is the fact that the channel reduction did not have a significant influence on the performance. A slight, yet not significant, improvement was observed when decreasing the number of EMG channels, which might potentially originate from an increase in signal-to-noise ratio for the reduced set.

5 Conclusion

Here we demonstrated for the first time a successful real-time myocontrol over 3-DOFs in a concurrent and proportional fashion with natural inputs and minimal user and machine training. We achieved this by relying on a simple ML method trained on only individual DOF data, yet the system remained intuitive enough to allow users to achieve simultaneous control by eliciting EMGs of concurrent DOFs. In future, we intend to test this approach with amputee subjects and physical prosthetic systems.

References

1. I. Vujaklija, D. Farina, O.C. Aszmann, New developments in prosthetic arm systems. *Orthopedic Res. Rev.* **8**, 31 (2016)
2. Complete Control Handbook, *Coapt LLC* (Chicago IL, 2018)
3. Ottobock, Technology for people 4.0: Ottobock at OTWorld 2018. <https://www.ottobock.com/en/newsroom/news/technology-for-people-4-0-ottobock-at-otworld-2018.html> (2018) (Online Accessed: 25 May 2020)
4. M. Ortiz-Catalan, B. Håkansson, R. Brånemark, Real-time and simultaneous control of artificial limbs based on pattern recognition algorithms. *IEEE Trans. Neural Syst. Rehab. Eng.* **22**(4), 756–764 (2014)

² Sphericity and normality of the residuals were tested with Mauchly's test and with Shapiro-Wilk test, respectively. Furthermore, since repeated measures ANOVA cannot deal with missing data, we additionally performed a multi-level linear analysis, which confirmed the findings.

5. I. Vujaklija, Novel control strategies for upper limb prosthetics, in *International Conference on NeuroRehabilitation* (Springer, Heidelberg, 2018), pp. 171–174
6. M. Ison, I. Vujaklija, B. Whitsell, D. Farina, P. Artemiadis, Simultaneous myoelectric control of a robot arm using muscle synergy-inspired inputs from high-density electrode grids,” in *2015 IEEE International Conference on Robotics and Automation (ICRA)* (2015), pp. 6469–6474
7. J.M. Hahne, M.A. Schweisfurth, M. Koppe, D. Farina, Simultaneous control of multiple functions of bionic hand prostheses: performance and robustness in end users. *Sci. Robot.* **3**(19), eaat3630 (2018)
8. C. Castellini, R.M. Bongers, M. Nowak, C.K. van der Sluis, Upper-limb prosthetic myocontrol: two recommendations. *Front. Neurosci.* **9**, 496 (2016)

A Portable P300-Based Brain–Computer Interface as an Alternative Communication Device



Víctor Martínez-Cagigal, Eduardo Santamaría-Vázquez,
and Roberto Hornero

Abstract Motor and cognitive disabilities may lead to communication difficulties, exacerbated by the intelligibility of speech and gesture. In this context, brain–computer interfaces (BCIs) can be viewed as novel augmentative and alternative communication technologies to assist these people. Despite the extensive research in BCIs during the last decades, portability of most of the studies is still a handicap. In this preliminary work, we present a truly portable P300-based BCI system as an aid for communication in cerebral palsy patients. Our system, that integrates more than 2.000 pictograms to select from, can be installed in any Android device and uses a cloud server to process the electroencephalographic signals of the users. A pilot testing was made with 12 healthy subjects, reaching a mean accuracy of 90%, assuring its viability and suggesting further testing with target users in the near future.

This work has received funding from projects ‘DPI2017-84280-R’ of ‘Ministerio de Ciencia, Innovación y Universidades—Agencia Estatal de Investigación’ and ‘European Regional Development Fund’ (FEDER), and ‘0378_AD_EEGWA_2P’ (Cooperation Programme Interreg V-A Spain-Portugal POCTEP 2014–2020) of the European Commission and FEDER; as well as from the CIBER-BBN through ‘Instituto de Salud Carlos III’. V. M.-C. and E. S.-V. were in receipt of PIF grants from the University of Valladolid and the ‘Consejería de Educación de la JCyL’, respectively.

V. Martínez-Cagigal (✉) · E. Santamaría-Vázquez · R. Hornero
Biomedical Engineering Group, University of Valladolid, Valladolid, Spain
e-mail: victor.martinez@gib.tel.uva.es

E. Santamaría-Vázquez
e-mail: eduardo.santamaria@gib.tel.uva.es

R. Hornero
e-mail: robhor@tel.uva.es

Centro de Investigación Biomédica en Red¹ in Bioingeniería, Biomaterials and Nanomedicine (CIBER-BBN), Zaragoza, Spain

1 Introduction

Brain–Computer Interface (BCI) systems allow users to control applications or external devices using their own brain signals. In particular, P300-based BCIs make use of unexpected visual stimuli through the *oddball* paradigm to identify users' intentions and translate them into application commands [1]. Due to this ability, P300-based BCIs emerged as novel technologies that could assist motor-disabled people and improve their quality of life [2]. Assistive BCIs may be used as augmentative and alternative communication (AAC) devices by those whose ability to communicate is restricted [2]. During the last decades, many P300-based BCIs were developed to spell words under different paradigms and devices. However, very few of them provided portable BCIs to be used on a daily basis by the severely disabled [3].

In this work, we present a pilot study of a truly portable P300-based BCI to meet the daily communication needs of children that suffer cerebral palsy (CP). CP is considered the most common movement disorder in children, reflecting abnormal brain development that leads to spasticity, dyskinesia and ataxia [4]. Since there is no cure, people with CP require long-term care and therapies. Particularly, children with CP usually present communication difficulties in form of intelligibility of speech and gesture caused by motor and cognitive impairments [4]. Thus, AAC are essential to bridge the communication gap and avoid developmental delays.

The objective of this study is to design and develop an Android-based P300-BCI to provide a new way to communicate for children with CP. In this preliminary work, the application was pilot tested by 12 control subjects. A proper evaluation with CP users is planned in the near future.

2 Subjects and Methods

A total of 12 healthy subjects (HS) participated in the study (mean age: 27 ± 3.41 years, 10 males, 2 females). All of them gave their informed consent to participate.

As shown in Fig. 1(a), the structure of the developed application lies on three main entities: (1) the user, whose electroencephalographic (EEG) signals are monitored; (2) the portable device, which receives the signals and displays the visual stimuli; and (3) the cloud processing server, which processes the data and returns the selected commands, providing a visual feedback.

2.1 Signal Acquisition

In order to prioritize the portability of the BCI system, the EEG acquisition equipment was wireless and sent the signal to the final device via Bluetooth. We used a *g.Nautilus*

cap (*g.Tec*, Austria) with 8 active channels placed on Fz, Cz, Pz, P3, P4, PO7, PO8, and Oz; using AFz as a ground and the ear lobe as the reference. The equipment had a sampling frequency 250Hz and the signals were pre-processed using band-pass filter (1–30Hz) and common average reference (CAR) [3].

2.2 Mobile Application, Signal Processing and Pilot Testing

The application, developed for Android devices, include the following functionalities:

- (1) Signal visualization. The *app* incorporates a button in the top-right corner to visualize the EEG signal in real-time in any moment, as shown in Fig. 1b.
- (2) Create matrix. Users are able to create and edit an unlimited number of *oddball* matrices from a database of more than 2.000 different images. These pictograms represent common concepts, actions and requests used by CP patients on their daily basis (Fig. 1c, d).
- (3) Offline training. This mode allows users to record trials for creating a model afterward. Stimuli are presented in a row-col paradigm (RCP) fashion, intended to elicit P300 evoked potentials whenever the target’s row or column are highlighted [1] (Fig. 1e).
- (4) Model training. Once enough training trials are recorded, the *app* allows sending them to the Python-based cloud processing server. The cloud extracts each stimulus epoch using a 0–800 ms window (z-scored baseline from –200–0 ms) decimated to 20 Hz [3]. Then, a step-wise linear discriminant analysis (SWLDA) model is trained to detect whether the epoch belongs to a target or not [3]. Finally, the model is sent back to the device, which stores it (Fig. 1f).
- (5) Online spelling. In this mode, the SWLDA model of each user is used to spell words. After each trial, data are sent to the cloud to classify the target command,

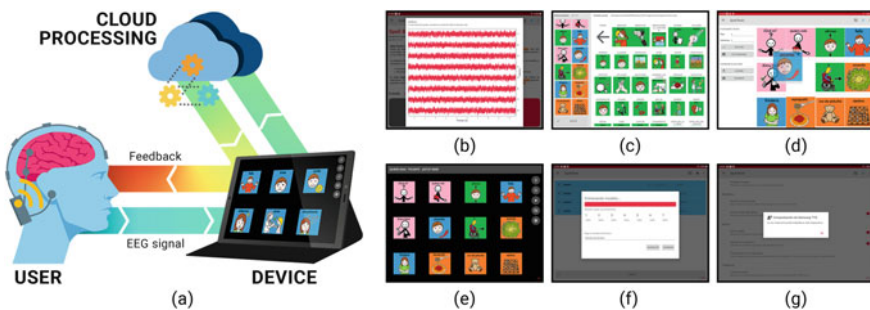


Fig. 1 a Structure of the portable P300-based BCI, composed by three main entities: user, device, and cloud processing. Snapshots of the application: **b** real-time signal viewer, **c** pictograms database, **d** matrix creation, **e** RCP matrix, **f** SWLDA model training, **g** configuration screen

Table 1 Pilot testing results

Subject	Age	Sex	N_s	Accuracy	Duration	OCM
H01	26	M	5	88%	2:50	8.82
H02	26	M	6	92%	2:54	8.62
H03	30	M	10	75%	3:10	7.89
H04	34	F	6	88%	2:54	8.62
H05	26	M	8	100%	3:02	8.24
H06	25	M	10	80%	3:10	7.89
H07	26	M	6	92%	2:54	8.62
H08	33	M	7	96%	2:58	8.43
H09	24	F	5	92%	2:50	8.82
H10	24	M	7	92%	2:58	8.43
H11	25	M	6	88%	2:54	8.62
H12	25	M	8	100%	3:02	8.24
Mean	27	-	7	90%	2:58	8.44
SD	3	-	1	7%	0:06	0.32

M: male, F: female, N_s : number of sequences, SD: standard deviation, OCM: output characters per minute. Duration specified in min:sec format

which is then returned to the device through a blocking socket. Once received, the *app* highlights it and a virtual voice reads out loud its description (Fig. 1e).

- (6) Configuration. The *app* also allows users to configure all signal processing details (e.g., window length, filters), as well as aspects of the RCP (e.g., number of sequences, timings, latency monitoring, number of row/columns) (Fig. 1g).

As a preliminary work, the portable BCI was tested by 12 HS that were asked for spelling a total of 25 trials. SWLDA training was performed with 12 offline trials, returning the model and the optimal number of sequences per each user prior to the assessment.

3 Results

Results of the pilot assessment are summarized in Table 1, including demographic characteristics of each subject, their optimal number of sequences, online accuracy, task duration and output characters per minute (OCM) [3].

4 Discussion and Conclusion

As shown, an average accuracy of $90\% \pm 7\%$ was achieved, which assures the efficacy of the proposed system. It is also noteworthy that the mean number of sequences

was 7 ± 1 , leading to a selection of an average of 8.44 ± 0.32 characters per minute. Although they are expected to decay in an online assessment with target users, these results suggest that the proposed system is suitable for providing an effective communication aid for the severely disabled. Moreover, it was demonstrated that the BCI application, together with the cloud processing server, were able to process the trials in real-time, resulting completely unnoticed by the user.

Despite these positive results, further improvements could be made. It could be studied whether it is possible to execute the processing pipeline in the device, avoiding the requirement of an Internet connection and the cloud server. An online assessment with CP patients should be performed to guarantee the viability of our proposal in real environments.

References

1. J. Wolpaw, E.W. Wolpaw, *Brain-Computer Interfaces: Principles and Practice*. OUP USA (2012)
2. M.J. Vansteensel, B. Jarosiewicz, Brain-computer interfaces for communication. *Handb. Clin. Neurol.* (Elsevier) **168**, 67–85 (2020)
3. V. Martínez-Cagigal, E. Santamaría-Vázquez, J. Gomez-Pilar, R. Hornero, Towards an accessible use of smartphone-based social networks through brain-computer interfaces. *Expert Syst. Appl.* **120**, 155–166 (2019)
4. NINDS, Cerebral Palsy: Hope Through Research, National Institutes of Health (NIH), Bethesda (Maryland), Tech. Rep. (2013)

On the Crosstalk in Motor Unit Spike Train Identification from High-Density Surface Electromyograms



Matjaž Divjak, Lukas G. Wiedemann, Andrew J. McDaid, and A. Holobar

Abstract We analyzed the problem of motor unit (MU) crosstalk in the spike trains that are identified from high-density surface electromyograms (HDsEMG). We used advanced volume conductor model to simulate five muscles with 500 MUs distributed in the 60×30 mm elliptical muscle cross-section. HDsEMG signals were generated during 20 s long isometric muscle contractions at 10%, 30%, 50% and 70% of the maximum excitation. Noiseless and noisy HDsEMG signals were recorded by an array of 10×9 electrodes and decomposed by the Convolution Kernel Compensation (CKC) method to yield estimated MU spike trains (MUSTs). Results show that $70.4 \pm 26.1\%$ of MUSTs exhibit crosstalk from other MUs, but with relatively low spike amplitudes. Across all the simulated contraction and noise levels, the crosstalk in the identified MUSTs came mostly from nearby MUs (average distance from the dominant MU with the largest spikes in MUST <3.5 mm) and relatively small MUs (average number of MU fibers <150).

1 Introduction

The use of high-density surface electromyogram (HDsEMG) decomposition into contributions of individual motor units (MUs) is increasing, as it enables noninvasive investigation of muscle control strategies [6]. Different blind source separation (BSS) techniques have been proposed for HDsEMG decomposition [1, 5] proving the feasibility of noninvasive MU identification in several skeletal muscles [2]. Different quality measures of MU identification, such as Pulse-to-Noise Ratio (PNR) [7] have also been proposed, quantifying the energy ratio between the spikes of the dominant MU and the noise in the identified spike trains. But to the best of our knowledge, the

M. Divjak · A. Holobar (✉)

Faculty of Electrical Engineering and Computer Science, University of Maribor, Maribor, Slovenia
e-mail: ales.holobar@um.si

L. G. Wiedemann · A. J. McDaid

Department of Mechanical Engineering, The University of Auckland, Auckland, New Zealand

crosstalk from MUs in the spike trains identified by BSS approaches has never been systematically analyzed.

In this study we used synthetic HDsEMG signals to quantify the number of MU spike trains (MUSTs) that include crosstalk from nearby MUs as well as investigate the properties of MUs whose spikes are merged into the identified MUST. Moreover, we analyzed the impact of additive noise and different muscle contraction levels on the MU crosstalk in MUSTs, which were identified by the previously established Convolution Kernel Compensation (CKC) decomposition technique [5].

2 Methods

2.1 Synthetic HDsEMG

HDsEMG signals were generated by convolving the MU action potentials (MUAPs) calculated by advanced volume conductor model [3] with MU firing patterns calculated by the model in [4]. Five muscles with different MU distribution were simulated, with 60×30 mm elliptical muscle cross-section, 500 MUs per muscle and 130 mm long fibers. The MU size was distributed exponentially (from 24 to 2408 fibers) with many small MUs and progressively fewer large MUs. Multilayer cylindrical volume conductor model [3] comprised 20, 30, 4 and 1 mm thick bone, muscle, fat and skin layers. MU conduction velocity was normally distributed with mean value of 4.0 ± 0.3 m/s. MUs started firing at 8 Hz and increased their firing rate linearly up to 35 Hz with simulated muscle excitation. For each simulated muscle, 20 s long isometric constant force contractions at 10%, 30%, 50% and 70% of maximum excitation level were simulated, resulting in 262, 388, 446 and 484 active MUs per recorded HDsEMG signal. HDsEMG signals were acquired at 2048 samples/s by an array of 10×9 circular electrodes with diameter of 1 mm and interelectrode distance of 5 mm. Additive noise with Signal-to-Noise Ratio (SNR) of ∞ , 20 and 10 dB was added to the generated HDsEMG signals.

2.2 MUST Identification from HDsEMG

For each simulated contraction and noise level, MUSTs were identified from HDsEMG by the CKC technique [5], without any manual editing. Only MUSTs with PNR >28 dB were kept for further analysis [7].

To analyze the MU crosstalk, all the spikes surpassing the 2.5% of the maximum spike height in each estimated MUST were compared against the simulated MU firings and all the MUs contributing at least 30% of their firings were identified (identification tolerance of ± 0.5 ms). Among them, the MU contributing the highest spikes was classified as the *dominant* MU in the MUST. Afterwards, the distances of

the *nondominant* (merged) MUs to the dominant MU were calculated by measuring the distances between the centroids of simulated MU territories. In addition, the sizes of nondominant MUs were calculated by counting the number of their fibers. These MU sizes and distances were compared to the sizes and distances of all the MUs that were identified by CKC but did not contribute to the crosstalk in the MUST (we will refer to these MUs as *unmerged* MUs). As in the case of merged MUs, the properties of unmerged MUs were also calculated for each identified MUST.

Non-parametric Kruskal-Wallis test was used for statistical analysis. In the case of significant effect, Bonferroni correction was applied with significance level set to $P < 0.05$.

3 Results

On average, 41 ± 5.1 , 20.4 ± 1.1 , 14 ± 3.1 and 13.2 ± 3 MUSTs were identified by CKC from noiseless HDsEMG signals at 10%, 30%, 50% and 70% excitation level, respectively. At SNR of 20 dB, these figures decreased to 13.4 ± 1.5 , 7 ± 3.4 , 1.8 ± 0.8 and 2.2 ± 0.8 MUSTs per contraction. When accumulated across all the excitation levels, 40.2%, 85.2% and 85.7% of MUSTs exhibited crosstalk from other MUs at SNR of ∞ , 20 and 10 dB, respectively. However, only 4.3%, 0.8% and 0.0% of MUSTs exhibited crosstalk with spike heights larger than 30% of the maximum spike in the identified MUST. The distribution of MU sizes and distances to the dominant MU are depicted in Figs. 1 and 2.

Merged MUs had significantly smaller size and distances to the dominant MU than unmerged MUs, regardless of the simulated noise and excitation level (Figs. 1

Fig. 1 The distribution of sizes and distances of unmerged MUs and nondominant merged MUs to the dominant MU in MUSTs in the case of noiseless HDsEMG signals. Results are accumulated across all the contraction levels and all the muscles

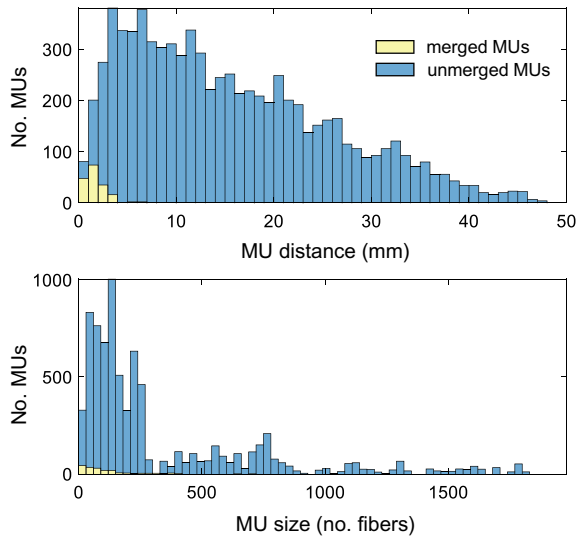
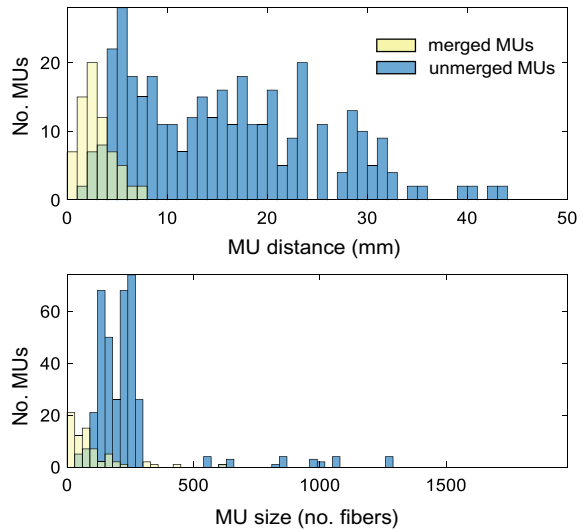


Fig. 2 The distribution of sizes and distances of unmerged MUs and nondominant merged MUs to the dominant MU in MUSTs in the case of 10 dB noise. Results are accumulated across all the contraction levels and all the muscles



and 2). When accumulated across all excitation levels, the average distance of merged MUs to the dominant MU increased significantly with the noise level (2.0 ± 2.3 mm at ∞ dB, 2.6 ± 1.6 mm at 20 dB and 2.9 ± 1.7 mm at 10 dB). There were no significant differences between the distances of merged MUs at different excitation levels when accumulated across all noise levels. The merged MUs had less than 150 fibers on average.

4 Conclusion

The results of this study show that on average $70.4 \pm 26.1\%$ of MUSTs identified by CKC exhibit crosstalk from MUs that are relatively close to the dominant MU in the MUST (average distance <3.5 mm). Crosstalk is more common in small MUs than in large MUs (Figs. 1 and 2). The percentage of MUSTs with crosstalk decreases significantly with the threshold used for spike segmentation. In this study, on average only $1.7 \pm 2.3\%$ of MUSTs exhibited MU crosstalk with the spike amplitudes larger than 30% of the highest identified spike. This suggests that, in given simulated conditions, the identification of the dominant MU in the MUST is not significantly jeopardized by the crosstalk from other MUs. Evaluation of MU crosstalk in experimental conditions is required and currently still missing.

Acknowledgements This study was supported by the Slovenian Research Agency (projects J2-1731 and L7-9421 and Programme funding P2-0041) and by the Marsden Fund managed by the Royal Society of New Zealand (grant number: 3706165).

References

1. M. Chen, P. Zhou, A novel framework based on FastICA for high density surface EMG decomposition. *IEEE Trans. Neural Syst. Rehabil. Eng.* **24**(1), 117–127 (2016)
2. A. Del Vecchio, A. Holobar, D. Falla, F. Felici, R.M. Enoka, D. Farina, Tutorial: analysis of motor unit discharge characteristics from high-density surface EMG signals. *J. Electromyogr. Kinesiol.* **53** (2020)
3. D. Farina, L. Mesin, S. Martina, R. Merletti, A surface EMG generation model with multilayer cylindrical description of the volume conductor. *IEEE Trans. Biomed. Eng.* **51**(3), 415–426 (2004)
4. A.J. Fuglevand, D.A. Winter, A.E. Patla, Models of recruitment and rate coding organization in motor-unit pools. *J. Neurophysiol.* **70**(6), 2470–2488 (1993)
5. A. Holobar, D. Zazula, Multichannel blind source separation using convolution Kernel compensation. *IEEE Trans. Signal Process.* **55**(9), 4487–4496 (2007)
6. A. Holobar, D. Farina, Blind source identification from the multichannel surface electromyogram. *Physiol. Meas.* **35**(7), R143–R165 (2014)
7. A. Holobar, M.A. Minetto, D. Farina, Accurate identification of motor unit discharge patterns from high-density surface EMG and validation with a novel signal-based performance metric. *J. Neural Eng.* **11**(1), 016008 (2014)

Altered Motor Unit Territories After Intramuscular Botulinum Toxin Injection in Spastic Biceps Brachii Muscle



Sourav Chandra, A. Holobar, Babak Afsharipour, William Zev Rymer, and Nina L. Suresh

Abstract Intramuscular botulinum toxin (BT) injections are used to alleviate the spasticity effects in chronic stroke survivors. The toxin injection works by means of chemodenervation of muscle fibers from their respective motor neuron (MN). Thus it most likely affects the territories of active motor units (MU) although the uniformity and territorial range is unreported and thereby unknown. Here, we have demonstrated the BT effect on motor unit territory area (MUTA) using a novel noninvasive high-density surface electromyography (HDsEMG) decomposition based detection and quantification method. The HDsEMG recordings were performed during isometric voluntary contractions about the elbow joint. We were able to analyze the effect of BT on MUTA of individual MUs with different MU recruitment thresholds in the biceps brachii (BB) muscle. We report on data from two stroke survivors before and after two weeks of their BT injection. Our results show that after the BT injection reduction of the MUTA was more prominent in larger MUs compared to the smaller MUs.

1 Introduction

Focal spasticity with hypertonia and hyperreflexia in chronic stroke survivors is often mediated locally by BT which induces cholinergic blockade of the neuromuscular junction (NMJ) limiting the transmission between the muscle fiber and the motor axon [1]. BT is administered as intramuscular injection to the spastic muscle that results in complete or in part deactivation of the motor unit (MU), potentially causing

S. Chandra (✉) · W. Z. Rymer · N. L. Suresh
Northwestern University and Shirley Ryan Ability Lab, Chicago, USA
e-mail: sourav.chandra@northwestern.edu

A. Holobar
University of Maribor, Maribor, Slovenia

B. Afsharipour
University of Alberta, Edmonton, Canada

a change in active MU territory. As a result, a significant reduction of voluntary contraction capacity is evident after the BT injection [2]. MU territory has been used as an indicator of paresis in earlier studies based on invasive recordings [3] and can be an objective estimate of any neuromuscular disease [4]. To our knowledge, the effects of BT on motor unit territory are yet unreported and unknown. BT induced denervation of the fibers are participant to exposure of the NMJ to the toxin, however, there is limited literature differentiating the action of the BT on different MU sizes, as well, the uniformity of the effect on a single MU and across the MU pool of a given muscle is unknown. Here, we have used a novel noninvasive HDsEMG decomposition based method to identify the MU territory as seen in the surface of the BT injected biceps brachii muscle during an isometric voluntary contraction. We have found that the correlation between the size of the MU and the respective active motor unit territory area (MUTA) changes after the BT injection. We also report on a 15% reduction of the MUTAs for the larger MUs.

2 Methods

2.1 *Experimental Setup*

The HDsEMG signals were recorded from biceps brachii (BB) muscle of two chronic stroke survivors, during a voluntary isometric, non-fatiguing elbow flexion under kinematic constraints. Visual feedback of a trapezoidal force trajectory was provided to the participants. All the contraction trials were based on their respective Maximal Voluntary Contraction (MVC). Multiple experimental trials were performed at contraction level of 50% of the MVC at each session.

The participants were seated with 120° elbow flexion, 10° shoulder flexion, 45° shoulder abduction, and 45° forearm pronation. The forearm was cast and secured in a custom-built fixture centered at the wrist. The fixture was equipped with a six degrees-of-freedom load cell (FT4007 from ATI, NC, USA) to record maximum voluntary forces generated at the wrist during elbow flexion. The forces and HDsEMG signals were synchronized and recorded simultaneously.

2.2 *Participant Details*

We report on recordings from the stroke-affected arms of hemispheric stroke survivors who present with focal spasticity and for whom intramuscular (biceps brachii) BT is part of their clinical care plan. The experimental protocols were approved by the Institutional Review Board of the Northwestern University and the participants signed the informed consent before commencement of the study

Table 1 Details of the participants, stroke since (years), BT injected side, Modified Ashworth scores (MAS) and Fugl-Meyer scores (FMS)

SubID (sex/age)	Y Pst stroke	Inj. side	MAS		FMS	
			Pre	Post	Pre	Post
B1(M/60)	7	R	2	2	19	21
B2(F/40)	10	L	2	1	19	22

sessions. Two participants were studied before and after their BT injections. Details of the participants are summarized in Table 1.

2.3 HDsEMG Setup

A 128-channel HDsEMG surface electrode grid in a 16×8 (Inter Electrode Distance (IED) = 8.5 mm, electrode diameter 3 mm) arrangement and amplifier (TMSi. Inc.) were used to record monopolar (MP) HDsEMG data at a sampling rate of 2 kHz. The length and width of the HDsEMG grid were approximately 14 cm and 7.5 cm, sufficient to cover the skin surface above the impaired BB muscle. To preserve the consistency of electrode placement across the recording sessions, the boundaries of the grid electrode from bony references (such as acromion, cubital fossa, medial and lateral epicondyles of the humerus) were recorded and maintained during data collection sessions.

2.4 Decomposition of the HDsEMG

By using Convolution Kernel Compensation (CKC) method [5] The grid recordings during the 50% contraction level were off-line decomposed into contributions of individual MUs. After the decomposition, the results were manually edited where the unreliably identified MU spike trains (Pulse-to-Noise Ratio > 25 dB [5]) were rejected for further analysis.

2.5 Estimation of Topological Properties of the MU Territory

After the MU firings have been identified, spike-triggered averaging was used to estimate the Motor Unit Action Potential (MUAP) shape at each double differential HDsEMG channel [6]. The peak to peak amplitude (PPA) of MUAP was then calculated at each channel. The grid channels with MUAP PPA exceeding the 10% of the largest MUAP PPA per MU were identified and a convex hull [7] was fitted to

those channels. The area of the contiguous region indicated by the convex hull was designated as MUTA and was estimated for each identified MU. The MUTAs of all the MUs detected during the two 50% MVC trials per participant were selected for further analysis.

The channel exhibiting the largest MUAP PPA value was selected as the center of the MUTA. Afterwards, all the PPAs were normalized with the largest PPA among all the detected MUs per participant. A regression fit was performed on the normalized PPAs and the respective MUTAs before and after the BT injection.

3 Results

3.1 MUTA Before and After BT Injection

Figure 1 shows an example of the detected MUTAs before and after the BT injection in B2 participant. Figure 2 shows the MUTAs across the different sizes of detected MUs before and after the BT injection.

For both the investigated participants, we have found MUs with larger MUAP PPAs having larger MUTAs. The correlation coefficient among the MUAP PPAs and MUTAs was positive (0.7, 0.8) before and negative (-0.2, -0.4) after the BT injection. Both the participants showed more than 15% reduction of MUTA after the BT injection among the larger (10% of the largest) MUs (Fig. 2). During these trials both the participants also demonstrated a reduction of contraction force by >60%.

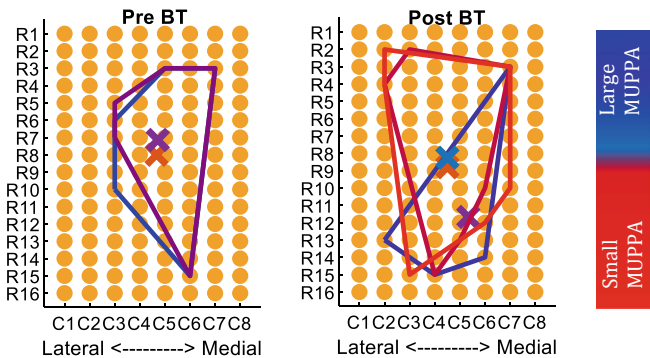


Fig. 1 MUTAs before (pre BT) and after (post BT) injection in B2 participant. The MUTA boundaries are marked with blue (for larger MUAPs) and red lines (for smaller MUAPs) across the rows (R) and the columns (C). The centroids are shown with × marks

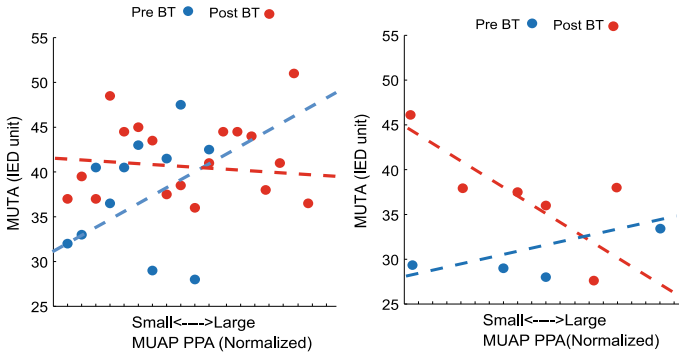


Fig. 2 Covariation of MUAP PPAs and MUTAs before and after the BT injection for B1 (left panel) and B2 participant (right panel)

4 Discussion

In this work, we have introduced a novel noninvasive HDsEMG based method for quantification of the individual MU territories as detected on the surface of the skin above the investigated muscle. We have used this method to find out the effect of BT injection on the MUTAs for different sizes of MUs in the affected BB muscle of hemispheric stroke survivors. Our result suggests that the MUTAs of the relatively large MUs get reduced more than the smaller MUs after the BT injection. The contraction force was also reduced after the injection. At this current stage, the proposed detection method is limited to the estimation of the MUTA at the surface of the skin and requires decomposition of HDsEMG signals into contributions from individual MUs. In future this method can potentially enhance exiting functional assessments for BT treatment of spasticity.

Acknowledgements This study was supported by the Slovenian Research Agency (projects BI-US/18-19-037, J2-7357, J2-1731 and Programme funding P2-0041) and by the National Institute on Disability, Independent Living, and Rehabilitation Research (NIDILRR).

References

1. S. Ozcakir, K. Sivrioglu, Botulinum toxin in poststroke spasticity. *Clin. Med. Res.* **5**(2), 132–138 (2007)
2. S. Chandra, B. Afsharipour, W.Z. Rymer, N.L. Suresh, Precise quantification of the time course of voluntary activation capacity following Botulinum toxin injections in the biceps brachii muscles of chronic stroke survivors. *J. Neuroeng. Rehabil.* **17**(1), 2020
3. F. Erminio, F. Buchthal, P. Rosenfalck, Motor unit territory and muscle fiber concentration in paresis due to peripheral nerve injury and anterior horn cell involvement. *Neurology* **9**(10), 657 LP – 657, (1959)

4. S. Bodine-Fowler, A. Garfinkel, R.R. Roy, V.R. Edgerton, Spatial distribution of muscle fibers within the territory of a motor unit. *Muscle Nerve* **13**(12), 1133–1145 (1990)
5. A. Holobar, M.A. Minetto, D. Farina, Accurate identification of motor unit discharge patterns from high-density surface EMG and validation with a novel signal-based performance metric. *J. Neural Eng.* **11**(1), 016008 (2014)
6. X. Hu, W.Z. Rymer, N.L. Suresh, Assessment of validity of a high-yield surface electromyogram decomposition. *J. Neuroeng. Rehabil.* **10**(1), 99 (2013)
7. C.B. Barber, D.P. Dobkin, H. Huhdanpaa, The Quickhull Algorithm for Convex Hulls. *ACM Trans. Math. Softw.* **22**(4), 469–483 (1996)

Motor Unit Tracking Across Low Contraction Levels of Biceps Brachii Muscle



A. Frančič and A. Holobar

Abstract We tested the feasibility of motor unit (MU) identification by MU filters, that are estimated from high-density surface electromyograms (HDEMGs) of the biceps brachii muscle, recorded at four different contraction levels, namely at 5, 10, 15 and 20% of maximum voluntary contraction (MVC). We used the Convolution Kernel Compensation (CKC) method to blindly estimate the MU filters at each individual contraction level (MU filter calibration phase) and applied these filters to HDEMG signals recorded at other contraction levels in the same muscle (MU filter application phase). At 5, 10, 15 and 20% MVC contractions MU filters estimated by CKC identified 4.1 ± 1.6 , 4.3 ± 1.2 , 5.9 ± 1.9 and 6.4 ± 0.9 MUs, respectively. The number of identified MU spike trains decreased significantly when we applied the identified MU filters to lower-than-calibration contraction levels. A similar decrease in the number of identified MUs was observed when applying MU filters to higher-than-calibration contractions. These results suggest that MU tracking across different contractions levels of biceps brachii muscle is not trivial.

1 Introduction

Decomposition of high-density surface electromyograms (HDEMGs) into contributions of individual motor units (MUs) enables noninvasive analysis of relatively large populations of MUs in the investigated muscle [2, 5]. Several approaches to blind identification of MU firings have been proposed [1, 7, 9]. Building on the blind-source-separation (BSS) framework, these approaches search for a weighted linear

This study was supported by the Slovenian Research Agency (projects J2-1731 and L7-9421 and Programme funding P2-0041).

A. Frančič (✉) · A. Holobar
System Software Laboratory, Institute of Computer Science, Faculty of Electrical Engineering and Computer Science, University of Maribor, 2000 Maribor, Slovenia
e-mail: aljaz.francic@um.si

A. Holobar
e-mail: ales.holobar@um.si

spatio-temporal combination of HDEMG channels that yields the estimation of an individual MU spike train. The weights in this linear combination are called a MU filter.

In non-fatiguing isometric contractions the MU action potentials (MUAPs) stay relatively stable [8]. Therefore, once estimated, the MU filter can be applied to newly acquired recordings of muscle contractions (providing that the position of recording electrodes does not change), identifying the firing pattern of the corresponding MU in newly acquired HDEMGs. For this purpose, the MU filters are first estimated on a 10 to 20 s long HDEMGs (frequently called MU filter calibration phase) and, afterwards, applied to new HDEMGs (application phase). Contraction levels can differ in calibration and application phase, but efficiency of such MU tracking across different contraction levels of different muscles is currently less reported and largely unknown. In this study, we investigated this efficiency in low contraction levels of biceps brachii muscle of healthy young males.

2 Methods

We used a 12×5 surface electrode array to record 20 second long HDEMG signals from the biceps brachii (BB) muscle of 8 males, aged 27 ± 4 , during isometric contraction at 5, 10, 15 and 20% of maximum voluntary contraction (MVC). Visual feedback on force was provided to the subjects.

We applied the Convolution Kernel Compensation (CKC) method [7] to estimate the MU filters in all of the HDEMG recordings (calibration phase). This yielded several MU filters per each HDEMG recordings constituting one filter bank per each tested person and per each tested contraction level. Each estimated filter bank was then applied to HDEMGs recorded at other contraction levels in the same person, yielding the corresponding MU spike trains (MU filter application phase). We then calculated the number of identified MUs and pulse-to-noise ratios (PNR) [6] for each calibration-application pair of HDEMG signals. A motor unit was classified as unidentified/not active, whenever a MU filter identified a spike train with PNR below 25 dB or when median MU discharge rate (MDR) was below 8 Hz.

For each calibration phase, we used Kruskal-Wallis test with significance level set to $p = 0.05$ to mutually compare the decomposition results of different application phases.

3 Results

The average number of MU filters, identified by the CKC method at different contraction levels (calibration phase) is reported in the diagonal elements of Table 1. The non-diagonal elements report the number of MUs that were also successfully

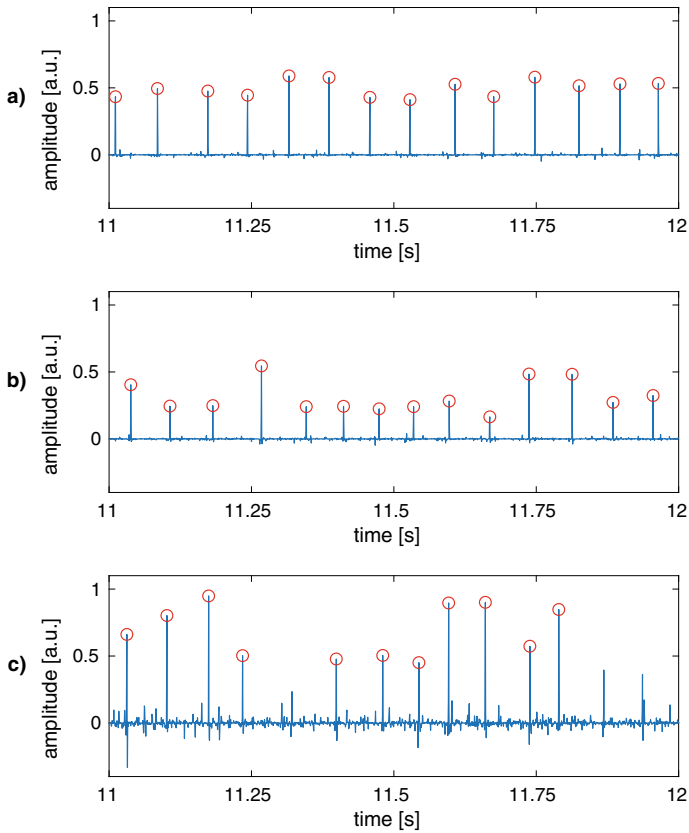


Fig. 1 Representative examples of identified MU spike trains (blue lines) and MU firings (red circles). For clarity reasons only 1 second long epochs are depicted. Panel (a) depicts a MU spike train estimated by a MU filter, calibrated on and applied to EMGs of 10% MVC. In this case, PNR was 39.7 dB and MDR was 14.3 Hz. Panel (b) depicts a MU spike train, estimated by the same MU filter as in Panel (a), but applied to 15% MVC EMGs. PNR was 32.6 dB and MDR was 15.2 Hz. Panel (c) depicts a MU spike train, estimated by the same MU filter, applied to 20% MVC EMGs. Missed MU firings are evident. PNR was 27.3 dB and MDR was 14.4 Hz

tracked in other contraction levels by applying the MU filters from calibration phase to other contraction levels.

Figure 1 depicts examples of identified motor unit spike trains. Pulse-to-Noise Ratio (mean \pm SD) of identified MU spike trains is reported in Table 2.

Table 1 Number of identified MUs (mean \pm SD)

		Application (% MVC)			
		5	10	15	20
Calibration (% MVC)	5	4.1 \pm 1.6 ^{bcd}	0.1 \pm 0.4	0.1 \pm 0.4	0.1 \pm 0.4
	10	0.3 \pm 0.7 ^b	4.3 \pm 1.2 ^d	1.8 \pm 1.5	0.9 \pm 0.8
	15	0.5 \pm 0.9 ^c	2 \pm 1.5	5.9 \pm 1.9 ^d	1.5 \pm 1.1
	20	0.5 \pm 1.1 ^d	1.4 \pm 1.4 ^d	2.6 \pm 1.7	6.4 \pm 0.9

^b Significantly different from results of application at 10 % MVC

^c Significantly different from results of application at 15 % MVC

^d Significantly different from results of application at 20 % MVC

Table 2 Pulse-to-Noise Ratio (PNR, mean \pm SD)

		Application (% MVC)			
		5	10	15	20
Calibration (% MVC)	5	35.4 \pm 1.6	25.8 \pm 0	25.1 \pm 0	26.6 \pm 0
	10	25.8 \pm 0	32.1 \pm 2.3 ^d	28.5 \pm 2	28.1 \pm 1.1
	15	26.8 \pm 0.8 ^c	29.4 \pm 2.7	32.9 \pm 2 ^d	27.3 \pm 1.3
	20	27.2 \pm 0.7	28.2 \pm 1.8 ^d	28.8 \pm 2	32.4 \pm 2.4

4 Discussion and Conclusion

MU filters, estimated by CKC from EMG recordings at 5, 10, 15 and 20% MVC identified 4.1 ± 1.6 , 4.3 ± 1.2 , 5.9 ± 1.9 and 6.4 ± 0.9 MUs, respectively (Table 1). When applied to higher-than-calibration contraction levels (upper diagonal elements of Table 1), MU filters identified relatively low number of MUs. When calibrated on 10% MVC signals and applied to 15% MVC signals, the MU filters identified 1.8 ± 1.5 MUs. When calibrated on 15% MVC signals and applied to 20% MVC signals, the MU filters identified 1.5 ± 1.1 MUs. These results suggest that tracking of the low-threshold MUs at higher contraction levels of biceps brachii is not trivial.

When MU filters were applied to lower-than-calibration contraction levels (lower diagonal elements in Table 1), the number of identified MUs also decreased. This is partially expected as not all the MUs, identified at higher contraction levels were active at lower contraction levels. However, some MU filters were transferable from 15 to 10% MVC and from 20 to 15% MVC (Table 1) as there was no significant difference in the number of identified MUs (Table 1) and PNR (Table 2) when compared to the calibration phase.

Mean PNR (Table 2) decreased in higher-than-calibration application conditions (upper diagonal elements of Table 2) and also in lower-than-calibration application conditions (lower diagonal elements of Table 2). Some of the differences were significant.

These results can at least partially be explained by the Henneman's size principle [4] and the fact that the MUs with smaller MUAPs are more difficult to identify than

MUs with larger MUAPs [2, 5]. Overall, at low contraction levels of biceps brachii, such as the ones investigated in this study, limited MU filter transfer is possible. Therefore, when transferring MU filters, we must carefully evaluate the quality of the generated MU spike trains. Metrics, such as PNR and MDR can help us reject and ignore the identified motor units that might not have been accurately estimated.

In summary, we demonstrated that the MU filter reuse in biceps brachii muscle across different low contraction levels is possible, but is relatively inefficient, especially when compared to the results of similar studies on the tibialis anterior muscle [3]. Even a small increase of contraction level by 5% can significantly increase the level of cross-talk from other MUs and hinder the MU identification from HDEMG signals. The quality of MU tracking must, therefore, be strictly controlled and assessed for each individual MU.

References

1. M. Chen, P. Zhou, A novel framework based on fastica for high density surface emg decomposition. *IEEE Trans. Neural Syst. Rehab. Eng.* **24**(1), 117–127 (2015)
2. D. Farina, A. Holobar, Characterization of human motor units from surface emg decomposition. *Proc. IEEE* **104**(2), 353–373 (2016)
3. A. Francic, A. Holobar, Motor unit tracking across different contraction levels in high-density surface electromyograms of tibialis anterior muscle, in *ISEK 2020 Congress* (2020)
4. E. Henneman, Relation between size of neurons and their susceptibility to discharge. *Science* **126**(3287), 1345–1347 (1957)
5. A. Holobar, D. Farina, Blind source identification from the multichannel surface electromyogram. *Physiological Measurement* **35**(7), R143 (2014)
6. A. Holobar, M.A. Minetto, D. Farina, Accurate identification of motor unit discharge patterns from high-density surface emg and validation with a novel signal-based performance metric. *J. Neural Eng.* **11**(1), 016008 (2014)
7. A. Holobar, D. Zazula, Multichannel blind source separation using convolution kernel compensation. *IEEE Trans. Signal Process.* **55**(9), 4487–4496 (2007)
8. R. Merletti, D. Farina, *Surface Electromyography: Physiology, Engineering, and Applications* (Wiley, New York, 2016)
9. F. Negro, S. Muceli, A.M. Castronovo, A. Holobar, D. Farina, Multi-channel intramuscular and surface emg decomposition by convolutive blind source separation. *J. Neural Eng.* **13**(2), 026027 (2016)

Preventing Cognitive Decline in Elderly Population Through Neurofeedback Training: A Pilot Study



Eduardo Santamaría-Vázquez, Víctor Martínez-Cagigal, Daniel Rodríguez, Jaime Finat, and Roberto Hornero

Abstract Neurofeedback training (NFT) allows to self-regulate neural activity, having application on a wide range of disorders to improve cognitive functions. This work was aimed at designing, developing and testing a novel NFT platform to prevent cognitive decline due to normal ageing in elderly population. A closed-loop brain-computer interface based on electroencephalography (EEG) was implemented to measure brain activity in real time. The system is highly configurable and it includes engaging games and applications for visual feedback. In order to evaluate the efficacy of the platform, we performed experiments with 9 healthy subjects over 65 years. General cognitive functions and basal EEG activity were assessed before and after the experiments. Data analysis showed improvements in cognitive performance associated to physiological changes in the EEG. In spite of the promising results, this study has to be extended to extract further conclusions.

This work has received funding from projects ‘DPI2017-84280’ of ‘Ministerio de Ciencia, Innovación y Universidades - Agencia Estatal de Investigación’ and ‘European Regional Development Fund’ (FEDER) and from the CIBER-BBN through ‘Instituto de Salud Carlos III’. E. S.V. and V. M.C. were in receipt of PIF grants from the University of Valladolid and the ‘Consejería de Educación de la Junta de Castilla y León’, respectively.

E. Santamaría-Vázquez (✉) · V. Martínez-Cagigal · R. Hornero
Biomedical Engineering Group, University of Valladolid, Valladolid, Spain
e-mail: eduardo.santamaria@gib.tel.uva.es

V. Martínez-Cagigal
e-mail: victor.martinez@gib.tel.uva.es

R. Hornero
e-mail: robhor@tel.uva.es

Centro de Investigación Biomédica en Red¹ in Bioengineering, Biomaterials and Nanomedicine (CIBER-BBN), Zaragoza, Spain

D. Rodríguez · J. Finat
ASPAYM-Castilla y León Foundation, Research Centre for Physical Disabilities, Valladolid, Spain
e-mail: danielrodriguez@aspaymcyll.org

J. Finat
e-mail: jaimefinat@aspaymcyll.org

1 Introduction

The increase in life expectancy and the low birth rate that can be observed in many parts of the world pose critical challenges. According to the World Population Ageing 2019 report from United Nations [1], 1 in 6 people in the world will be over the age of 65 by 2050. This situation is accentuated in developed regions, where the percentage of people aged 65 years or over will be 22.1% by 2030, leading to social, economic and health difficulties that will put entire systems on edge [1]. In this context, efforts to mitigate pressure over health care systems are of crucial importance. Cognitive decline associated to normal ageing has been recognized as one of the most important risk factors in this population. However, efforts to find protective treatments and therapies to mitigate cognitive decline have not been fully successful yet.

Neurofeedback training (NFT) allows to self-regulate brain activity through real-time feedback of neural activation parameters, usually obtained from the electroencephalography (EEG). NFT has emerged in recent years as a promising methodology to correct pathological states and behaviours such as attention deficit hyperactivity disorder, anxiety or depression, and even to improve recovery expectancies after suffering brain damage provoked by stroke or trauma [2]. Furthermore, NFT has also been proposed as a cognitive enhancement tool for healthy subjects [2]. This study is focused on investigating the use of NFT to prevent cognitive decline in the elderly. Previous attempts showed promising results, but more studies are needed to extract definitive conclusions [3]. This preliminary work was aimed at designing, developing and testing a novel NFT platform to enhance the general cognitive state in order to prevent the decline associated with normal ageing. To evaluate the efficacy of the platform, we performed a pilot study with 9 subjects aged 65 or over.

2 Materials and Methods

See Fig. 1.

2.1 NFT Platform

Our novel platform implements a closed-loop brain-computer interface (BCI) that analyses the subject's EEG and offers visual feedback in real time. The platform is highly configurable and implements a wide range of signal processing methods, allowing to design custom NFT protocols. Based on previous evidence, 4 training tasks were designed to enhance the general cognitive performance. The first three tasks were focused on memory, attentional control and conceptual activity executive functions, whereas the fourth task was intended to increase the overall cognitive performance. For the memory task, the alpha (8–13 Hz) band was stimulated in the

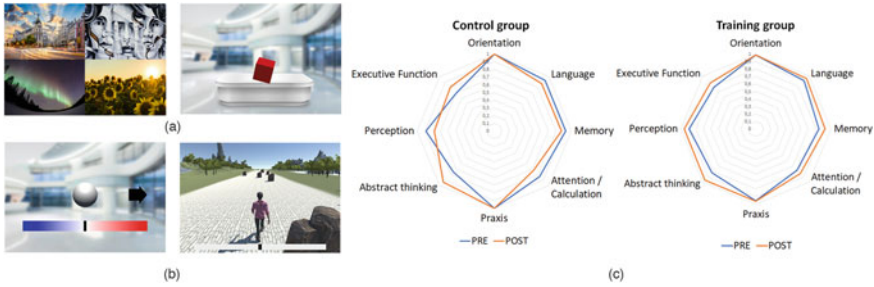


Fig. 1 Screenshots of the NFT platform and results of the cognitive function assessment. **a** Visual feedback with one degree of freedom for tasks 1–3. **b** Visual feedback with two degrees of freedom for SMR training in task 4. **c** Normalized scores of the Cambridge Cognitive Examination Revised (CAMCOG-R) for both groups of participants

frontal area of the cortex (electrodes Fz, F3 and F4) [4]. In the attentional control task, alpha and beta (13–30 Hz) bands were stimulated in the central region of the cortex (electrodes Cz, C3 and C4). Previous studies showed that this area regulates attention and concentration, and they could be enhanced through NFT [5]. For the conceptual activity task, the user had to stimulate alpha band in the parietal region of the cortex (electrodes Pz, P3, P4) [6]. In the previous 3 tasks, the parameter used to offer feedback was the relative power estimated by means of the power spectral density (PSD) normalized by a baseline recording. Therefore, the feedback applications have 1 degree of freedom (i.e., increase/decrease of the power), being positive feedback associated with an increase of the power. Noteworthy, the user had to find his own strategy to achieve this goal through mental imagery [2]. Feedback applications of these tasks are shown in Fig. 1a. For the fourth task, the user had to modulate his activity in the two cerebral hemispheres independently using motor imagery to produce contralateral synchronization/desynchronization events in the sensorimotor cortex in alpha and beta bands. These signals are known as sensorimotor rhythms (SMR), and had been widely used in BCI. In this case, we used 2 motor imagery classes (i.e., right/left hands), which allows to control applications with two degrees of freedom. For the visual feedback, two applications of different difficulties were designed (see Fig. 1b). Previous studies showed that SMR training could enhance the general cognitive state [3].

2.2 Experiment

A total of 9 healthy subjects (mean age 70 ± 4.5 years, 7 males) participated in this pilot study. Subjects were randomly divided into two groups: 7 were assigned to the training group (TG) and 2 to the control group (CG). Noteworthy, we had an initial population of 10 subjects per group, but only 9 finished the tests due to the COVID-19 situation. Subjects assigned to the TG performed a total of 6 NFT sessions of 2 h

with the platform, whereas the CG did not take any training. For both groups, the Cambridge Cognitive Examination Revised (CAMCOG-R), applied by a qualified neuropsychologist, was used to assess the cognitive functions before and after the intervention. Additionally, in order to study physiological changes, 5 min of EEG in basal state (eyes closed) were recorded before and after the intervention for the TG. EEG signals were acquired with a g.USBamp (g.Tec, Austria) using 11 electrodes placed on Fz, F3, F4, Cz, C3, C4, Pz, P3, P4, T7 y T8 and a sampling rate 256 Hz.

3 Results and Discussion

Results of the neuropsychological assessment are depicted in Fig. 1c. As can be seen, the TG increased its overall cognitive performance after the intervention, improving in 6 out of 8 categories (i.e., executive function, perception, abstract thinking, attention/calculation, memory and language). Moreover, the CG did not show the same tendency, improving in executive function and abstract thinking but reaching lower scores in the rest of categories. Additionally, the spectral analysis of the basal EEG recordings showed that the relative power in theta band decreased after the intervention for the TG (p -value = 0.018; Wilcoxon Signed Rank Test). No significant changes were found in the other bands. In this regard, cognitive decline has been associated with increased powers in theta band [7]. Thus, cognitive improvements are associated with significant changes in theta band for the TG.

4 Conclusion

This study presents a novel and preliminary NFT platform for cognitive training in elderly population. The developed platform includes attractive visual feedback applications and signal processing methods to design custom NFT protocols. Moreover, we performed a pilot study with 9 subjects. Results showed that the designed protocol increased the overall cognitive performance in the TG after 6 sessions of training. In spite of the promising results, this study has to be extended with more subjects in the TG and CG to extract further conclusions.

References

1. United Nations, World Population Ageing 2019. Tech. Rep. (2019)
2. S. Enriquez-Geppert, R.J. Huster, C.S. Herrmann, EEG-neurofeedback as a tool to modulate cognition and behavior: a review tutorial. *Front. Human Neurosci.* **11**(February), 1–19 (2017)
3. J. Gomez-Pilar, R. Corralejo, L.F. Nicolas-Alonso, D. Álvarez, R. Hornero, Neurofeedback training with a motor imagery-based BCI: neurocognitive improvements and EEG changes in the elderly. *Med. Biol. Eng. Comput.* **54**(11), 1655–1666 (2016)

4. J.J. Hsueh, T.S. Chen, J.J. Chen, F.Z. Shaw, Neurofeedback training of EEG alpha rhythm enhances episodic and working memory. *Human Brain Mapping* **37**(7), 2662–2675 (2016)
5. D. Vernon, T. Egner, N. Cooper, T. Compton, C. Neilands, A. Sheri, J. Gruzelier, The effect of training distinct neurofeedback protocols on aspects of cognitive performance. *Int. J. Psychophysiol.* **47**(1), 75–85 (2003)
6. B. Zoefel, R.J. Huster, C.S. Herrmann, Neurofeedback training of the upper alpha frequency band in EEG improves cognitive performance. *NeuroImage* **54**(2), 1427–1431 (2011)
7. M. Grunwald, A. Hensel, H. Wolf, T. Weiss, H.J. Gertz, Does the hippocampal atrophy correlate with the cortical theta power in elderly subjects with a range of cognitive impairment? *J. Clin. Neurophysiol.* **24**(1), 22–26 (2007)

Wearable Sensor for Multi-wavelength Near-Infrared Spectroscopy of Skin Hemodynamics Along with Underlying Muscle Electromyography



Radhika Mujumdar, Mancheung Cheung, Shweta Pramod Kadam, and Anirban Dutta

Abstract Intermittent claudication in peripheral arterial disease (PAD) may be monitored with near-infrared spectroscopy (NIRS) of an exercising muscle and skin; however, skin NIRS data in conjunction with electromyography (EMG) of muscle activation has not been investigated. This paper presents the development of a wearable skin NIRS sensor to determine the changes in the blood oxygenation and blood volume of the skin tissue overlying the calf muscle in response to underlying muscle EMG activation during exercise. Skin NIRS sensor was based on the optode sensor configuration found using Monte Carlo-based simulations with a skin tissue model, that was compared with a state-of-the-art device frequency-domain NIRS system. A proof of concept experiment on a healthy volunteer showed promising results with future applications in monitoring critical limb ischemia in PAD during calf muscle exercise.

1 Introduction

Peripheral arterial disease (PAD) occurs due to partial or complete obstruction of ≥ 1 peripheral arteries [1]. More than 200 million people have PAD worldwide, where intermittent claudication is indicative of exercise-induced ischemic leg pain. Intermittent claudication also manifests in the skin perfusion [2] that has not been investigated well. Recent studies are investigating the role of exercise for these patients. In this single-subject study, we investigate the skin perfusion changes using near-infrared spectroscopy (NIRS) during muscle activation measured with electromyography (EMG). For this investigation, we developed a continuous wave multi-wavelength NIRS sensor for skin than can be used during exercise to monitor revascularization procedures based on skin blood flow changes [3]. The more advanced stage is known as critical limb ischemia (CLI) when patients can have leg pain at rest. This paper presents the design of wearable, portable multi-wavelength NIRS-EMG sensor was

R. Mujumdar · M. Cheung · S. P. Kadam · A. Dutta (✉)
The State University of New York at Buffalo, Buffalo, NY, USA
e-mail: anirband@buffalo.edu

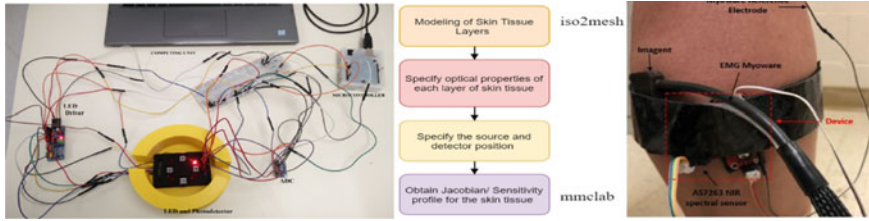


Fig. 1 Left panel: bench testing setup. Middle panel: block diagram to obtain sensitivity profiles from simulations. Right panel: our wearable sensor and FD-NIRS (Imagent™) sensor placement on the calf muscle

based on the principle of Beer-Lambert law to detect the variations in oxygenated (HbO) and deoxygenated (HHb) hemoglobin (also, mitochondrial Cytochrome c Oxidase) [4] in the skin tissue in relation to the muscle contractions. Muscle contractions, e.g., during calf raise exercise in patients with PAD, can stimulate mitochondrial respiration that can be monitored using a wearable multi-wavelength skin NIRS-EMG sensor after our single-subject evaluation in this study.

2 Methods

2.1 Wearable Multi-wavelength Skin NIRS-EMG Sensor

A wearable continuous wave (CW) multi-distance NIRS (mwNIRS) sensor is shown in the left panel of Fig. 1 that can separate the hemodynamics in the skin and the muscle tissue based on the sensitivity profile found from Monte Carlo (MC) simulation—middle panel of Fig. 1. Our proof of concept, single-subject study, was performed with a multi-wavelength source (S)—detector (D) distance of 4 mm that was found suitable for skin NIRS. The wearable device also captured the EMG signal from the underlying lateral gastrocnemius (calf) muscle. The device consists of an Arduino Uno microcontroller (Arduino LLC, Italy) for signal acquisition, Myoware EMG sensor (Advancer Technologies LLC, USA), and AS7263 NIR Spectral Sensor (SparkFun Electronics, USA). The right panel of Fig. 1 shows the device placed alongside the frequency domain (FD) NIRS (Imagent™, ISS, USA) that measured calf muscle hemodynamics.

2.2 Simulation to Establish Skin NIRS

NIRS method relies on a number of factors, including incident intensity and wavelength of photons, absorption coefficient, scattering coefficient, the refractive index

of the tissue, optical path length and thickness of the tissue, and the source-detector distance (SD) [5–8]. A simulation-based on the MC model [9] was carried out to visualize the photon trajectory, from a virtual source of photons, through the calf tissues, i.e., skin, fat, and muscle. The model for skin mwNIRS sensor was implemented using the MMCLAB (2017 edition). A 3-layer model representing the muscle, fat, and the skin tissues of thickness 30 mm, 10.6 mm [7], and 1.6 mm [6] respectively was modeled based on prior works. For the FD-NIRS muscle sensor, a set of simulations were carried out for two wavelengths, i.e., 690 and 830 nm, at varying SD distances, i.e., 15, 20, 25, and 30 mm. The gold standard FD-NIRS (Imagent™, ISS, USA) data provided us the measurement of the muscle hemodynamics that was related to the skin hemodynamics (oxyhemoglobin: HbO, deoxyhemoglobin: HHb, total hemoglobin: THb = HbO + HHb) in this single-subject study. An isotropic photon source with an intensity of 10^6 incident photons was considered with simulation parameters, i.e., the refractive index (n), absorption coefficient (μ_a), reduced scatter coefficient (μ_s), and scattering anisotropy (g), for the three tissues taken from prior works [7, 8]. Figure 2a, b show the ‘banana’ shaped photon trajectory at 690 nm with SD of 15 mm and 30 mm, respectively. The high fluence rate of the photons is depicted by the red color tones and the low fluence rate with the blue shades. There was more scattering at the lower wavelengths, 680 and 690 nm. It can also be seen that the photons penetrated deeper (with higher fluence rate) into the muscle tissue with greater (>30 mm) SD, while their trajectory mostly remained within the skin tissue for a lesser SD [10]. With the SD fixed for skin at 4 mm, the MC simulation was carried for five different wavelengths, i.e., 680, 730, 760, 810, and 860 nm, and their corresponding μ_a , μ_s , n , and g [7]. Figure 2c shows the simulation results for 760 nm. In this study, four wavelengths were selected for a robust fit of the modified Beer-Lambert law to HbO and HHb concentration changes.

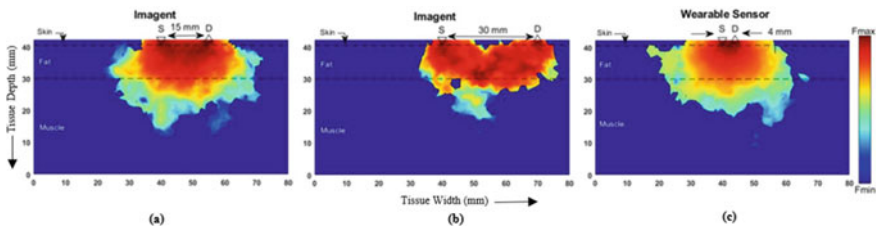


Fig. 2 Photon trajectory and the variance in fluence rate within the three (skin, fat, muscle) tissue layers corresponding to the varying SD obtained using MC simulation; **a** FD-NIRS Imagent™, SD = 15 mm, **b** FD-NIRS Imagent™, SD = 30 mm and **c** our wearable sensor, SD = 4 mm

2.3 Experiments

A healthy subject (age: 25 years) volunteered for this case study. The experiment consisted of two sets of repetitions of calf raises at a frequency of 10 and 30 beats per minute (BPM). CW mwNIRS-EMG and FD-NIRS were used, Fig. 1.

2.4 Signal Processing

HbO and HHb concentrations in the skin blood were calculated using the Modified Beer-Lambert's equation with robust linear least squares regression using four (730, 760, 810, and 860 nm) wavelengths. The data from mwNIRS-EMG sensor was analyzed in MATLAB R2018a.

3 Results

The left panel of Fig. 3 shows the plots of changes in HHb, HbO, and THb (blood volume) concentration in response to the muscle activation (rising curve) and deactivation (falling curve) as indicated by the voltage plot from the linear envelope of the EMG. The right panel shows the FD-NIRS sensor data that showed a delay in the THb changes (green box) following muscle activation (yellow box).

4 Conclusion

The changes in the skin and muscle blood volume (THb) showed a relationship with the underlying muscle EMG activity. Recently, Mancheung showed [11] changes in the muscle NIRS THb with muscle contraction rate (BPM) where a decrease in the first peak of blood vessel's end velocity was related to an increase in viscosity and a decrease in pulsatile frequency—Fig. 4. Muscle NIRS provided important information, especially delay between THb and EMG, that can be separated from skin THb using a multi-distance sensor.

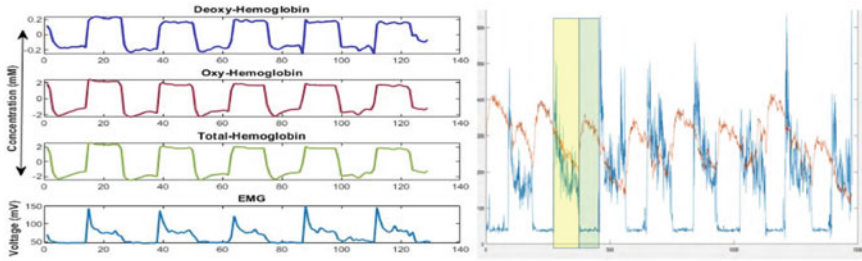


Fig. 3 Left panel: changes in HHb, HbO, THb with respect to muscle in ‘On’ (activation), and ‘Off’ (inactivation) states. Right panel: FD-NIRS sensor data that shows a delay in THb (in orange) following EMG (in blue)

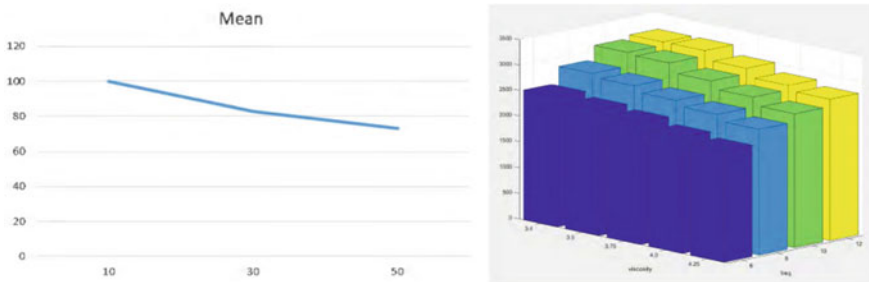


Fig. 4 Left panel: normalized FD-NIRS THb changes (Y-axis 100% at 10 BPM) with the muscle contraction rate (X-axis BPM). Right panel: simulation results of the first peak of blood vessel’s end velocity for blood viscosity (viscosity: 3.4, 3.5, 3.75, 4.0, 4.25) N*s/m² and pulsatile frequency (freq: 12, 10, 8, 6) Hz. Which is relevant in human ageing (Ref. [11])

Acknowledgements Funded by the Community for Global Health Equity (CGHE) Seed Funding, University at Buffalo, USA and SIAGNOS LLC, USA.

References

1. M.H. Criqui, V. Aboyans, Epidemiology of peripheral artery disease. *Circ. Res.* **116**(9), 1509–1526 (2015)
2. D.L. Sontheimer, Peripheral vascular disease: diagnosis and treatment. *Am. Fam. Physician* **73**(11), 1971–1976 (2006)
3. G.H. Simmons, B.J. Wong, L.A. Holowatz, W. Larry Kenney. Changes in the control of skin blood flow with exercise training: where do cutaneous vascular adaptations fit in? *Exp. Physiol.* **96**(9), 822–828 (2011)
4. M. Rak et al., Mitochondrial cytochrome c oxidase deficiency. *Clin. Sci.* **130**(6), 393–407 (2016)
5. A.N. Bashkatov, E.A. Genina, V.V. Tuchin, Optical properties of skin, subcutaneous, and muscle tissues: a review. *J. Innov. Opt. Health Sci.* **4**(01), 9–38 (2011)

6. D.-S. Ho, E.-H. Kim, I.-D. Hwang, K.-S. Shin, O. Jung-Taek, B.-M. Kim, Optical skin-fat thickness measurement using miniaturized chip LEDs: a preliminary human study. *J. Opt. Soc. Korea* **13**(3), 304–309 (2009)
7. S.L. Jacques, Optical properties of biological tissues: a review. *Phys. Med. Biol.* **58**(11), (2013): R37
8. T. Lister, P.A. Wright, P.H. Chappell, Optical properties of human skin. *J. Biomed. Opt.* **17**(9), 090901 (2012)
9. S. Chatterjee, J.P. Phillips, P.A. Kyriacou, Differential pathlength factor estimation for brain-like tissue from a single-layer Monte Carlo model, in *2015 37th Annual International Conference of the IEEE Engineering in Medicine and Biology Society (EMBC)*, pp. 3279–3282. IEEE, 2015.
10. C. Ash, M. Dubec, K. Donne, T. Bashford, Effect of wavelength and beam width on penetration in light-tissue interaction using computational methods. *Lasers Med. Sci.* **32**(8), 1909–1918 (2017). <https://doi.org/10.1007/s10103-017-2317-4>
11. M. Cheung, Hemodynamics due to calf muscle activity–biophysical modeling and experiments using frequency domain near infrared spectroscopy in healthy humans. MS thesis. <https://ubir.buffalo.edu/xmlui/handle/10477/78042?show=full>

**SS8: “One Size Does Not Fit All”: New
Approaches for a Patient-Tailored
Rehabilitation Process**

Closed-Loop Acquisition of Training Data Improves Myocontrol of a Prosthetic Hand



Donato Brusamento, Andrea Gigli, Roberto Meattini, Claudio Melchiorri, and Claudio Castellini

Abstract Modern myocontrol of prosthetic upper limbs employs pattern recognition models to map the muscular activity of the residual limb onto control commands for the prosthesis. The quality of pattern-recognition-based myocontrol, and that of the resulting user experience, depend on the quality of the data used to build the model. Surprisingly, the prosthetic community has so far given marginal attention to this aspect, especially as far as the involvement of the user in the data acquisition process is concerned. This work shows that closed-loop data acquisition strategies using a feedback-aided approach outperform the standard open-loop acquisition by helping users detect areas of the input space that need more training data. The experiment was conducted in realistic settings, involving one prosthetic hand and tasks inspired by activities of daily living.

1 Introduction

Pattern-recognition techniques allow controlling poliarticulated prostheses using non-invasive measurements of the muscular activity, such as surface electromyography (sEMG). This is done by training a myocontrol model from a set of muscular activations labelled with the corresponding hand postures. Despite producing models with considerable predictive capabilities, the performance of these approaches depends on how well the training data reflect the actual testing conditions.

Among other factors, changes in the limb position introduce variability in the recorded muscular activity and hinder myocontrol performance. Solutions to this

This work was partially supported by the DFG project Deep-Hand, CA1389/1-2.

D. Brusamento (✉) · A. Gigli · C. Castellini
Intitute of Robotics and Mechatronics, German Aerospace Center, Munich, Germany
e-mail: donato.brusamento@dlr.de

R. Meattini · C. Melchiorri
DEI—Department of Electrical, Electronic and Information Engineering,
University of Bologna, Bologna, Italy

© The Author(s), under exclusive license to Springer Nature Switzerland AG 2022
D. Torricelli et al. (eds.), *Converging Clinical and Engineering Research*
on *Neurorehabilitation IV*, Biosystems & Birobotics 28,
https://doi.org/10.1007/978-3-030-70316-5_67

problem involve acquiring training data for the desired hand posture in multiple areas of the reachable space, i.e., in multiple arm configurations [1]. A possibility is to move the arm during the data acquisition to reduce the amount of time and the physical effort required to cover the reachable space [2].

The efficiency of dynamic training data acquisition relates to the arm trajectory that the subject must follow. The trajectory should enforce arm configurations in which the myocontrol model's predictions tend to be less precise. Identifying those critical arm configurations before the experiment seems unfeasible because they depend on the subject's characteristics and the performed hand gesture. In this regard, standard open-loop data acquisition, which is based on predefined movement routines, may fail to reinforce the model where needed. We argue that it is possible to identify model weak points during the data acquisition, by monitoring the instantaneous prediction error generated by the stream of training samples.

For this reason, we propose a closed-loop dynamic data acquisition paradigm in which critical arm configurations are identified in real-time and signalled to the subject with acoustic feedback, leading subjects to enforce movements in critical arm configurations. Here we compare the myocontrol models obtained from one open-loop and two closed-loop dynamic acquisition procedures. All the procedures build myocontrol models incrementally and online. One closed loop scheme also exploits a sample selection criterion to reduce the number of model updates performed.

2 Methods

2.1 Data Acquisition

Simultaneous and proportional myocontrol of a prosthetic hand was implemented with an instance of incremental Ridge Regression with Random Fourier Features [3]. The model was trained online during the data acquisition with a stream of 8-channel sEMG samples labelled with normalized velocity commands for the prosthesis fingers.

The acquisition procedure focused on three hand gestures, namely a power grasp, a resting hand, and a pointing index. Each of the proposed acquisition procedures took 45 s for each hand gesture, 135 s in total. The resulting regression model was capable of predicting graded velocity commands, despite being trained on a discrete set of hand gestures.

2.1.1 Open-Loop Dynamic Data Acquisition (OL-DA)

was based on the dynamic data acquisition procedure presented in [2]. Subjects performed the target hand gestures while moving their arm in a helical trajectory spanning the reachable space. The movement proceeded with constant speed from the waist level to the head with the palm oriented downward, and in the opposite direction

with the palm upward. The movement was repeated twice uninterruptedly. All the recorded training samples were used to build the myocontrol model in real-time.

2.1.2 Closed-Loop Dynamic Data Acquisition (CL-DA)

combined OL-DA with an acoustic feedback signal dependent on the prediction error obtained for the incoming training samples. Subjects were instructed to perform the same trajectory as in OL-DA, reducing the arm speed anytime the feedback volume increased. They were not required to complete two entire cycles of the helical trajectory in the given 45 s. The prediction error for a labelled training pair $\{\mathbf{x}, \mathbf{y}\}$ was $e_p = |\mathbf{y} - \hat{\mathbf{y}}|^2$, with $\hat{\mathbf{y}}$ being the model's prediction for the sample \mathbf{x} . The acoustic feedback was related quadratically to the prediction error so to emphasize significant model inaccuracies. The feedback's intensity varied from 0 (silent) to the maximum volume of the control laptop's speakers.

2.1.3 Closed-Loop Dynamic Data Acquisition with Sample Selection (CLSS-DA)

was formally equivalent to CL-DA but included a criterion to discard redundant training samples in real-time. All the training samples were used to generate the feedback signal, but only those which returned a prediction error $e_p > \theta$ were used to update the model. θ was set to 5% of the highest possible prediction error, corresponding to predicting a power grasp instead of a resting hand gesture.

2.2 *Experimental Evaluation*

The effectiveness of the acquisition protocols was assessed by engaging 12 non-disabled subjects (20 – 32 years old) in a series of realistic manipulation tasks using a commercially available prosthetic hand. A Thalmic Labs' Myo armband provided 200Hz 8-channel sEMG measurement of the forearm activity. An Össur's i-LIMB revolution prosthetic hand was attached to a standard wrist/hand orthotic splint, Fig. 1. A control laptop collected, rectified, and low-pass filtered the sEMG, and used it to train the myocontrol model.

The tasks included serving food and water, sweeping and tidying up (completing a pegboard), and dialling phone numbers. The task sequence was repeated three times for each acquisition protocol. Two repetitions allowed subjects to familiarize themselves with the system, while the third was used to measure myocontrol performance based on the tasks' completion times. Each subject tested all the acquisition protocols in random order, to counterbalance learning effects.

Fig. 1 The experiment setup included a Myo armband for sEMG, an i-LIMB revolution prosthetic hand, a computer, and several household objects



The performances of different protocols were compared using a Friedman test followed by post-hoc Wilcoxon signed-rank tests with Holm-Bonferroni adjustment of the p-value. The significance level was set to $\alpha = 0.05$.

3 Results

Figure 2 shows the duration of the third repetition of the task sequence. The model produced by CL-DA allowed the subjects to complete the tasks significantly faster than that provided by OL-DA (average task sequence duration of 163 s versus 206 s, $W = 6$, Holm-Bonferroni adjusted $\hat{p} = 0.029$). The average performance of CLSS-DA (168 s) was equivalent to CL-DA and better than OL-DA, but this result was not supported by statistical evidence.

Although each acquisition protocol collected an equivalent amount of training data (about 29000 samples), CLSS-DA trained the model only using about 25% of it.

4 Discussion

We compared one standard open-loop data acquisition procedure, used to reduce the influence of the limb position on myocontrol, to two novel closed-loop acquisition

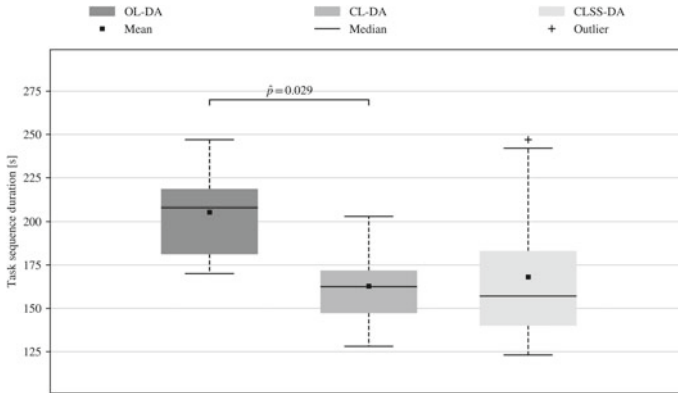


Fig. 2 Subjects completed the task sequence significantly faster in the CL-DA condition compared to the OL-DA condition. The performance of CLSS-DA did not differ significantly from those of the other acquisition strategies

protocols. During closed-loop data acquisition, information about the model's accuracy was fed back to the subjects using an acoustic signal, a design choice easily integrable in daily routines for myocontrol training and recalibration. The feedback signal ultimately guided subjects to enforce training signals that strengthened the model. One of the closed-loop procedures also implemented a selection criterion to discard unnecessary input samples.

Our experiment showed that closed-loop acquisition improved myocontrol performance in challenging manipulation tasks for non-disabled subjects. The sample selection criterion could reduce the computational load of the training phase, but should be carefully tuned not to hinder the model's performance. Furthermore, the presented approach heavily relies on the user's capacity to maintain the correct gesture during training, which could be more challenging in amputees due to a reduced proprioceptive awareness: this topic will be further investigated.

References

1. E. Scheme, K. Biron, K. Englehart, *Improving myoelectric pattern recognition positional robustness using advanced training protocols* (33rd Annu. Int. Conf. of the IEEE Engineering in Medicine and Biology Society, Boston, 2011), pp. 4828–4831
2. A. Gigli, A. Gijssberts, C. Castellini, The merits of dynamic data acquisition for realistic myocontrol. *Front. Bioeng. Biotechnol.* **8**, 361 (2020)
3. A. Gijssberts et al., Stable myoelectric control of a hand prosthesis using non-linear incremental learning. *Front. Neurobotics* **8**, 8 (2014)

Allied Rehabilitation Using Web-Based Caregiver MEDIated Exercises for STROKE: The ARMED4STROKE Trial Design



Corien D. M. Nikamp, Gert Kwakkel, Erik C. Prinsen, Rinske H. M. Nijland, Marijn Mulder, Erwin E. H. van Wegen, Hermie J. Hermens, and Jaap H. Buurke

Abstract This paper describes the design of the Armed4Stroke program. Patients after stroke and their caregivers are included as a couple. The caregiver is trained as a co-therapist by a physiotherapist experienced in providing caregiver-mediated exercises (CME) to support and motivate the patient. The program consists of 8 weeks of gait and gait-related exercises, complementary to regular rehabilitation therapy. The couple will receive a tailor-made exercise program, which is adapted to the patients' abilities and goals and is progressive in nature. The program is supported by videos with exercise instructions, which are accessible using a web-based tele-rehabilitation system. It is hypothesized that CME, supported with tele-rehabilitation is able to promote daily mobility and to reduce anxiety and depression in patients after stroke and their caregivers.

C. D. M. Nikamp (✉) · E. C. Prinsen · H. J. Hermens · J. H. Buurke
Roessingh Research and Development, Enschede, The Netherlands
e-mail: c.nikamp@rrd.nl

University of Twente, Enschede, The Netherlands

G. Kwakkel · R. H. M. Nijland · M. Mulder
Amsterdam Rehabilitation Research Centre, Reade, Amsterdam, The Netherlands

G. Kwakkel · M. Mulder
Department of Rehabilitation Medicine, Amsterdam Neuroscience and Amsterdam Movement Sciences, Amsterdam UMC, VUmc, Amsterdam, The Netherlands

E. E. H. van Wegen
Department of Rehabilitation Medicine, Amsterdam Movement Sciences, Amsterdam UMC, VUmc Amsterdam, Amsterdam, The Netherlands

1 Introduction

Recovery of walking ability is an important goal for patients post stroke. Stroke rehabilitation is typically front loaded, with resources mainly focused on inpatient care, where professionals support patients in their exercises. After inpatient treatment, support often tapers off and the majority of stroke survivors become physically inactive, whereas poor activity levels correlate with physical and psychological outcomes and quality of life. Consequently, stroke survivors and their caregivers experience the transition from inpatient care to the community as a significant hurdle.

Two key elements can be used to augment the level of exercise, even after inpatient care is finished: (1) Caregiver Mediated Exercise (CME); and (2) extension of rehabilitation to the patients' own home. CME is an approach in which caregivers are actively involved in the rehabilitation program after stroke. During CME, the patient performs exercises with an informal caregiver, under supervision of a trained physiotherapist. The couple will receive an exercise program adapted to patients' abilities and goals. A proof-of-concept trial showed that CME, combined with e-Health technology was feasible, safe and effective in reducing anxiety of patients and depression of caregivers [1]. The patient and caregiver may experience a smoother transition to the home situation and the involvement of the caregiver did not increase caregiving burden [2]. Hence, CME is a promising paradigm to improve outcomes on psychological measures. In addition, the caregiver could support and motivate the patient to continuing exercises at home, when professional support from inpatient rehabilitation tapers off. (2) The caregiver is instructed and trained as a "co-therapist" to maintain their support in the home situation. To support the couple, there are regular face-to-face sessions in which the exercise program will be adapted according to the progress of the patient and to (adjusted) abilities and goals. The program is supported by videos of the exercise, which are built in a web based tele-rehabilitation system. The combination of face-to-face supported CME with tele-rehabilitation aims to promote self-generated physical activity and to increase motivation. The CME and tele-rehabilitation components are included in the Allied Rehabilitation using caregiver MEDiated exercises for Stroke (Armed4Stroke) program, which already starts during the subacute phase post stroke. Compared to the previous proof-of-concept trial, there is an increased focus on rehabilitation in the home situation and the number of videos in the online tele-rehabilitation system suitable for performance at home is substantially increased.

This paper describes the design of the trial that aims to assess the added value of the Armed4Stroke program: (1) to improve the level of daily mobility at home; (2) on length of inpatient stay, activities of daily living and psychosocial measures.

2 Material and Methods

2.1 Study Design

The study has a single, observer-blinded randomized controlled trial design. Patients are randomly allocated to either 8 weeks of Armed4Stroke program in addition to usual inpatient or outpatient care (i.e. experimental group), or to 8 weeks of usual care alone (i.e. control group). The study is registered in the Dutch trial register as NL7422 and approved by the Medical Ethics Review Committee of the VU University Medical Centre, Amsterdam, The Netherlands.

2.2 Participants

Seventy-two stroke patients and their caregiver are recruited in multiple centers in the Netherlands, during their inpatient and/or outpatient stay. The caregiver can be any person close to the patient (like partner, family member or neighbor). Inclusion criteria for the patient are: <3 months after stroke; ≥ 18 years of age; written informed consent; able to understand the Dutch language; knowing and able to appoint a caregiver who wants to participate in the program (with a max. of 2 caregivers); living independently before the stroke; living at home or planned to be discharged home; being able to follow instructions; sufficiently motivated for CME. Inclusion criteria for the caregiver are: ≥ 18 years of age; written informed consent; able to understand the Dutch language; sufficiently motivated for CME; medically stable and physically able to perform the exercises together with the patient. Serious comorbidity that interferes with participation is exclusion criterion for both patient and caregiver.

2.3 Study Procedure

Prior to the study, all involved physiotherapists received training in applying the Armed4Stroke program. The measurements are performed by a trained assessor who is blinded to treatment allocation. Adverse and serious adverse events are monitored.

2.4 Intervention

The Armed4Stroke program consists of 8 weeks of complementary exercise therapy done with a caregiver, supported by tele-rehabilitation, next to the usual therapy. The goals and progress of the patient are leading in setting the complementary exercise therapy. The tailor-made program contains task-specific exercises focusing on gait

and gait related activities and is progressive in nature from basic (transfer) activities to high level gait exercises. The program is supported by videos of exercises, which are accessible using the web-based tele-rehabilitation system. The couple is asked to do exercises minimally 5 times per week for 30 min. During inpatient stay, couples are advised to perform the exercises during the weekend, when patients are mostly inactive. During the 8-week program, at least 4 face-to-face sessions with the physical therapist are planned to adapt the exercise program according to the progress of the patient. Participants in the control group will receive usual care according to the clinical guidelines of the Royal Dutch Society of Physical Therapy [3].

2.5 Outcome Measures

Outcome measures are assessed at baseline (T0), following the 8-week intervention or control period (T1), and 6 months after randomization (T2). The primary outcome is the self-reported mobility domain of the Stroke Impact Scale 3.0. This is a disease-specific questionnaire that evaluates self-reported health status in eight domains [4]. Secondary outcomes for patients are: walking ability (10m walking speed and 6 min walking distance), balance (Berg Balance Scale) and lower limb strength (Motricity Index), assessed using clinical tests. In addition, the amount of daily activity during one week is measured using MOX-activity sensors, and length of inpatient stay are recorded in participating rehabilitation settings for included stroke patients. Furthermore, scales like Rivermead Mobility Index and Nottingham Extended ADL, assessing self-reported mobility, activity of daily living, and functional outcome are used. Caregiving strain is assessed in caregivers. Patients and caregivers are assessed on quality of life, self-efficacy, family functioning, fatigue, anxiety and depression and the preparedness for the transition from in/outpatient setting to the home.

2.6 Data Analysis

Baseline values will be calculated and between-group differences will be studied to determine whether groups are comparable at baseline using the appropriate statistical tests. The primary and secondary outcomes will be compared between the intervention and control group at the different time points (T0, T1, T2) using multilevel regression analysis.

3 Results

Currently, 8 subjects (4 M/4 F, age 54–78 years, 35–91 days after stroke) are included in the study that started in two rehabilitation centers. The first subjects are about to start T2 assessment. Additional rehabilitation centers are joining the study to further increase inclusion rates.

4 Discussion

The current trial is an extension of the previously conducted proof-of-concept trial that showed that CME combined with tele-rehabilitation was feasible and safe, and effective in improving psychological outcomes [1]. Since the amount of exercises available in the tele-rehabilitation system is extended, the current trial also aims to improve outcomes on a functional level.

5 Conclusion

Results of the trial are expected to confirm that CME, supported with tele-rehabilitation are able to promote daily mobility and activities of daily living, decrease length of inpatient stay, and to reduce anxiety and depression in patients after stroke and reduce caregivers' burden.

Acknowledgments This study was funded by the ZonMW/Wetenschappelijk College Fysiotherapie (WCF), grant nr 858001102. We would like to thank E. Kret for contributing to performing the study measurements.

References

1. J. Vloothuis, M. Mulder, R. Nijland, Q. Goedhart, M. Konijnenbelt, H. Mulder et al., Caregiver-mediated exercises with e-health support for early supported discharge after stroke (CARE4STROKE): a randomized controlled trial. *PloS One* **14**(4), e0214241 (2019)
2. J. Vloothuis, M. Depla, C. Hertogh, G. Kwakkel, E. van Wegen, Experiences of patients with stroke and their caregivers with caregiver-mediated exercises during the CARE4STROKE trial. *Disabil Rehabil* **42**(5), 698–704 (2020)
3. J. Veerbeek, E. van Wegen, R. van Peppen, P. van der Wees, E. Hendriks, M. Rietberg et al., What is the evidence for physical therapy poststroke? A systematic review and meta-analysis. *PloS One* **9**(2), e87987 (2014)
4. P. Duncan, R. Bode, S. Min Lai, S. Perera, Rasch analysis of a new stroke-specific outcome scale: the stroke impact scale. *Arch. Phys. Med. Rehabil.* **84**(7), 950–963 (2003)

Augmented Reality for Rehabilitation Tuning and Assessment



M. Pezzera, E. Chitti, and N. A. Borghese

Abstract A therapist relies on his/her experience and knowledge to define the most suitable rehabilitation program for the patient and tune it on the actual patient status. Here we propose a non-intrusive method, based on AR, which allows to provide therapists, in real-time, while the patient is exercising, quantitative information extracted from the ongoing session and the previous ones, which can help them to make more informed decisions related to the current rehabilitation session. This is expected to improve the overall effectiveness of rehabilitation.

1 Introduction

In physical rehabilitation, much of the decision-making process on the rehabilitation program is carried out by therapists upon a qualitative analysis. These, on the basis of their past experience and their visual judgment of patient motion, tune the rehabilitation program to the current condition of the patient [1]. Although the advantages of this qualitative approach in rehabilitation are well known [2, 3], the integration of quantitative data can provide therapists with more objective information on which to base their decisions [3, 4].

In this work, we have explored how the use of Augmented Reality (AR) can support therapists during the rehabilitation sessions: showing metrics derived from the past rehabilitation exercises as well as from the current ones could allow them to make more informed decisions.

M. Pezzera (✉) · E. Chitti · N. A. Borghese
Department of Computer Science, Università degli studi di Milano, Milan, Italy
e-mail: manuel.pezzera@unimi.it

E. Chitti
e-mail: eleonora.chitti@unimi.it

N. A. Borghese
e-mail: alberto.borghese@unimi.it

2 Methodology

Without a lack of generality, we will consider postural rehabilitation. In this domain, a core set of exercises has been identified [5] along with a suitable evaluation metrics to describe the patient's performance along specific rehabilitation dimensions: range of motion, speed, accuracy, stability, and force [6]. These metrics also evaluate safety during the exercise: deviations from ideal posture should be computed and corrected to avoid maladaptation [7, 8].

In traditional rehabilitation, the therapist observes the patient, advises him/her and, if required, modifies the difficulty of the current exercise and/or changes the exercise mix. For instance, in the *Weight Shift Lateral* exercise, in which the patient has to shift his/her body laterally standing on the feet, the therapist may notice that the patient is becoming unstable during movement and may decide to reduce the required range of shift. Quantification of the amount of instability can help in making a decision, especially if it can be compared with the degree of instability in the previous rehabilitation sessions. The therapist may decide that the patient is experiencing a transient worsening of his/her condition or the instability is in line with that of previous days. In the latter case, the therapist may decide to insist with the same difficulty level.

To this aim, we have developed an instrument that provides such quantitative information to the therapist, while the patient is performing the exercises, superimposed to the natural view of the patient, exploiting the AR paradigm. We have called such instrument MIRARTS (MIXed Reality Adaptive Rehabilitation Therapist Station).

It integrates the data provided by trackers of the patient motion with an AR device. In particular, we have used the Nintendo Wii Balance Board to acquire the center of pressure (COP), the Microsoft Kinect to track the body skeleton, and Microsoft Hololens as an AR device; the latter can show virtual objects superimposed on the real scene.

For each exercise, we have defined, with the help of the therapists, a set of key graphs that provide a clear picture of what the patient is doing. Each exercise is associated with a different number and type of graphs, which show the representative metrics for that exercise. Two of the graphs that are always shown, are the time course of the COP along the anteroposterior and the lateral axis, that are linked to postural control [9]. Additional graphs represent specific features associated with the different exercises. For instance, in leg lift exercises, in which the patient has to lift one leg at a time alternatively, the height reached by the feet is a representative metric for assessing the range of motion.

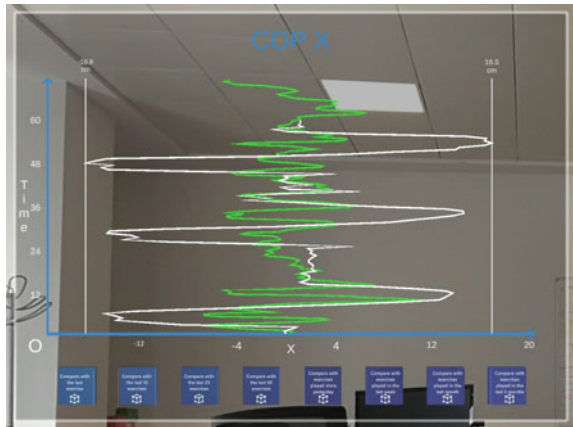
A particular metric is aimed to ensure patient safety: deviations of the orientation and position of body segments that may provoke maladaptation, fatigue, and stress can be detected [7].

The deviation from a healthy posture during exercising is mapped on a value inside a given range that is shown over time. This is an important element as it provides direct information on the quality of movement.

Fig. 1 View of what the therapist sees through Hololens. Around the patient, metrics describing his/her performance are shown. On the left side, it is possible to see the progress of COP over time, while on the right, summary metrics and monitoring parameters can be found



Fig. 2 Comparison of the current execution with the past trend. The trend of the COP along the horizontal axis is shown here, representing the range of motion reached by the patient in the current exercise (white line), compared to the range of motion reached in an exercise in a previous session (green line)



Besides graphs, numerical values of the different metrics can be reported to the therapist. All this information can be reproduced on the sides of the patient, as shown in Fig. 1.

All the graphs can be compared, in real-time, with past performance in the same type of exercises. In this way, the therapist can control the progress of the patient over time. For instance, the plot in Fig. 2 shows the range of motion achieved in the current exercise (white line), compared with that achieved in a previous session (green line).

3 Discussion

Through AR, therapists are supplied with a set of graphs and metrics, distributed in the lateral space surrounding the patient, allowing the therapist to view both the

patient while performing the exercise and all the information that can support the evaluation.

To allow the best reading and interpretation of the graphs, they are dynamically oriented towards the therapist, to maximize readability and not to force him/her to move to read them. The graphs are visualized around the patient that is supposed to stand at 1 m from the therapist.

Automatic font size adjustment can also be implemented to improve the readability of the information shown.

Although in this version, the number of graphs is fixed and previously identified with the help of therapists, the system has been developed to guarantee flexibility, allowing easy addition of new metrics or modification of existing ones according to the therapist's needs and preferences.

MIRARTS has also been integrated with our exer-games platform [6], allowing to modify the difficulty of the exer-games at run-time, helping the therapist to obtain an exercise configuration more suitable to the patient. In fact, deciding on the basis of the real-time analysis of the movement and on its comparison with previous analogous movements can make the decision more effective for the rehabilitation program.

These decisions are usually made by evaluating the patient's condition at a specific moment, having the possibility to evaluate the patient's trend in the last days or weeks can further help clinicians.

A similar quantitative evaluation is already carried out during routine follow-up visits, when the patient undergoes quantitative tests aimed to assess his/her rehabilitation state (e.g., [10]), and on the outcome of this visit, rehabilitation treatment is tuned.

However, these tests are long and complex, and cannot be performed frequently. We aim here to provide the therapist with all the data acquired on the field that could be used to do this tuning, reducing the need for follow-up visits.

Currently, it has not yet been possible to test MIRARTS with patients to test its effectiveness.

4 Conclusion

In this article, we have shown how, using AR, metrics that evaluate the exercise of patients can be shown in real-time to the therapist, who can make more informed decisions on how to tune rehabilitation exercises, making rehabilitation most effective.

References

1. D.G. Tate, The state of rehabilitation research: art or science? *Arch. Phys. Med. Rehabil.*, pp. 160–166 (2006)
2. P. Ochieng, An analysis of the strengths and limitation of qualitative and quantitative research paradigms. *Prob. Educ. 21st Century* **13**, 13 (2009)
3. S. VanderKaay, S.E. Moll, R.E. Gewurtz, P. Jindal, A. Loyola-Sanchez, T.L. Packham, C.Y. Lim, Qualitative research in rehabilitation science: opportunities, challenges, and future directions. *Disabil. Rehabil.* **40**(6), 705–713 (2018).
4. J. Hearn, J. Lawler, G. Dowswell, Qualitative evaluations, combined methods and key challenges: general lessons from the qualitative evaluation of community intervention in stroke rehabilitation. *Evaluation* **9**(1), 30–54 (2003)
5. M.B. Rietberg, D. Brooks, B.M. Uitdehaag, G. Kwakkel, Exercise therapy for multiple sclerosis. *Cochrane Database Syst. Rev.* **1** (2005).
6. N.A. Borghese, M. Pezzera, R. Mainetti, J. Essenziale, R. Cazzaniga, B. Reggiori, S. Mercurio, P. Confalonieri, A cloud-based platform for effective supervision of autonomous home rehabilitation through exer-games, in *2018 IEEE 6th International Conference on Serious Games and Applications for Health (SeGAH)*, pp. 1–6, 2018.
7. M. Pirovano, E. Surer, R. Mainetti, L. Pier Luca, N. A. Borghese, Exergaming and rehabilitation: a methodology for the design of effective and safe therapeutic exergames. *Entertainment Comput.* **14**, 55–65 (2016)
8. L. Prosperini, D. Fortuna, C. Giannì, L. Leonardi, M. R. Marchetti, C. Pozzilli, Home-based balance training using the Wii balance board: a randomized, crossover pilot study in multiple sclerosis. *Neurorehabilitation and Neural Repair* **27**(6), 516–525 (2013)
9. R.M. Palmieri, C.D. Ingersoll, M.B. Stone, B.A. Krause, Center-of-pressure parameters used in the assessment of postural control. *J. Sport Rehabil.* **11**(1), 51–66 (2002)
10. C. Fjeldstad, G. Pardo, C. Frederiksen, D. Bembem, M. Bembem, Assessment of postural balance in multiple sclerosis. *Int. J. MS Care* **11**(1), 1–5 (2009)

Towards the Use of Neuromusculoskeletal Modeling in Clinical Practice: A Feasibility Study in Parkinson Disease Patients



M. Romanato, D. Volpe, A. Guiotto, F. Spolaor, M. Sartori, and Z. Sawacha

Abstract Electromyography (EMG)-driven neuromusculo-skeletal models (NMSM) are currently used to estimate joint moments and muscle forces during dynamic movements considering subject-specific neural-excitation patterns provided by the EMG data. However, these models are rarely adopted in routine clinical applications. This is partly due to limitations in obtaining realistic maxima voluntary contractions (MVC) in pathological subjects for calibration purposes and in the number of required experimental EMG signals that are difficult to be assessed in neurological conditions (e.g. Parkinson's Disease (PD)). This study aims at verifying the feasibility of introducing EMG-driven NMSM for planning rehabilitation treatments in PD. Thus, a minimal experimental setup compatible with clinics requirements is proposed herein. Four different NMSM were implemented with two different EMG normalization methods and with two different set of experimental EMGs for the muscletendon unit mapping. Results seems promising as no statistically significant differences between the full model and the proposed reduced model were observed.

M. Romanato (✉) · A. Guiotto · F. Spolaor · Z. Sawacha (✉)
Department of Information Engineering, University of Padua, Padua, Italy
e-mail: romanato@dei.unipd.it

Z. Sawacha
e-mail: zimi.sawacha@dei.unipd.it

D. Volpe
Fresco Parkinson Center, Villa Margherita, S.Stefano, Vicenza, Italy

M. Sartori
Department of Biomechanical Engineering, University of Twente, Enschede, The Netherlands

1 Introduction

EMG-driven NMSM can provide important information about the unique anatomical, neurological and functional characteristics of the subjects through the computation of human internal variables, such as muscle activations, muscle forces, and joint moments, from an individual neural signal. These can be used to identify the target of the rehabilitation program or to predict outcomes of different treatments, based on patient-specific characteristics. Despite the potential of adopting these techniques, these models are rarely introduced in clinical practice mainly due to the difficulty of validating the results of muscle forces and the experimental setup and acquisition protocol might result complex and long. Indeed, as it is fundamental to consider restriction due to subjects' physical capacities, people with movement impairments as PD patients, might not bear neither the large numbers of sensors attached to the body, neither the additional trials to perform MVC needed for model calibration purposes.

For this purpose, we proposed in a previous study [1] a minimally invasive setup (reduced) with 4 EMG channels, calibrated through normalized EMG signals with respect of the walking trials (WTNr), to analyze the differences in muscle forces and activations between a healthy cohort and Parkinson's disease patients. The aim of the present study is to compare the results obtained by WTNr model on a healthy cohort with the ones obtained by three different implementation of the model in order to detect the impact of various setup on the estimated variables: an MVC trial normalization full setup (MVCTNf) model [2], an MVC trial normalization reduced setup (MVCTNr) model and a WTN full setup (WTNf) model. In order to verify the impact of different NMSM on clinical decision making, results of the current study were compared with the WTNr applied to a cohort of PD subjects [1].

2 Material and Methods

2.1 Participants and Data Collection

Three healthy subjects (age = 60 ± 1 years, BMI = 27.4 ± 4.7 kg/m²) and 10 PD subjects (age = 66.9 ± 12.8 years, BMI = 27.4 ± 3.6 kg/m²) have been enrolled for the study. A six cameras stereophotogrammetric system (60Hz, BTS), synchronized with two force plates (960Hz, Bertec) and a 16-channel EMG system (1000Hz, BTS) were used to acquire the data. Two different EMG set up were adopted respectively for the healthy (WTNf), and the pathological ones (WTNr): right limb gluteus maximus and medius, tensor fasciae latae, adductor longus, sartorius, semitendinosus, biceps and rectus femoris, vastus medialis and lateralis, peroneus longus, gastrocnemius medialis and lateralis, soleus and tibialis anterior (WTNf); right and left biceps and rectus femoris, gastrocnemius lateralis, tibialis anterior (WTNr) (Table 1).

Table 1 Mapped musculotendon units

Musculotendon unit	Experimental EMG Full setup	Experimental EMG Reduced setup
rectfem	Rectus Femoris	Rectus Femoris
vasmed	Vastus Medialis	Rectus Femoris
vaslat	Vastus Lateralis	Rectus Femoris
vasmed	(Vastus Lateralis + Vastus Medialis)/2	Rectus Femoris
bifemlh	Biceps Femoris	Biceps Femoris
bifemsh	Biceps Femoris	Biceps Femoris
semiten	Semitendinosus	Biceps Femoris
semimem	Semitendinosus	Biceps Femoris
latgas	Gastrocnemius Lateralis	Gastrocnemius Lateralis
medgas	Gastrocnemius Medialis	Gastrocnemius Lateralis
sol	Soleus	Gastrocnemius Lateralis
tibant	Tibialis Anterior	Tibialis Anterior

Musculotendon units and the mapping experimental EMG for both full and reduced setups

2.2 Data Processing

Six right foot strikes were selected when the foot was naturally landing on the force plates. Data were processed through MOtoNMS [3], OpenSim and CEINMS [4]. Two different methods were adopted to normalize the healthy subjects EMG signals: the WTN and the MVCTN; while only the WTN was applied on the PD subjects' dataset. In the WTN, the peak amplitude of each EMG linear envelope was computed across all the subject's trials. The MVCTN method consists instead in calculating the maximum EMG value from the MVC acquisition [5]. A generic musculoskeletal model (gait2392 [6]) was used to linearly scale each subjects' geometry in OpenSim. Inverse kinematics, inverse dynamics and muscle analysis tools were used to obtain joint angles and moments, musculotendon moments and moment arms. CEINMS was adopted as toolbox to estimate the muscle activations and forces that best matched the experimental EMGs and joint moments. The implementation of the full setup reflected the one described in [2], while in the reduced setup, only 4 EMG channels were mapped to a total of 12 musculotendon units (Table 1). Two degrees of freedom (ankle plantar-dorsi flexion and knee flexion-extension) were analyzed separately. For each subject 3 dynamic trials were used for the calibration. Then, CEINMS was used to predict the knee and ankle moments, muscle forces and activations with a hybrid EMG-informed model [2].

3 Results

Models accuracy in tracking experimental muscle excitations and moments is reported in Fig. 1. All models accurately represented the estimates of muscle excitations and joint moments. Although WTNr model produced the highest root mean square error (RMSE), statistically significant differences were detected only within the bifemlh activation of the MVCTNf. Both the coefficient of determination (R^2) and the envelope peak position did not show any remarkable difference across the models. Concerning the tracking of the experimental moments significant differences were detected in the swing phase and load acceptance, yet a good model prediction is shown at RMSE and R^2 level. Comparison between healthy and PD subjects showed statically significant differences on muscle forces and joint moments.

4 Discussion

We proposed an EMG-driven NMSM with a minimal experimental setup coupled with a clinically feasible EMG normalization method, and compared with models of enhanced complexity. Statistically significant differences between the four models were not revealed, suggesting that the WTNr might be a valuable tool in muscle force estimation in clinics environment, consistent both at EMG and dynamic levels. Results seem promising in adopting the proposed model in rehabilitation treatment assessment for neuromuscular disorders as PD.

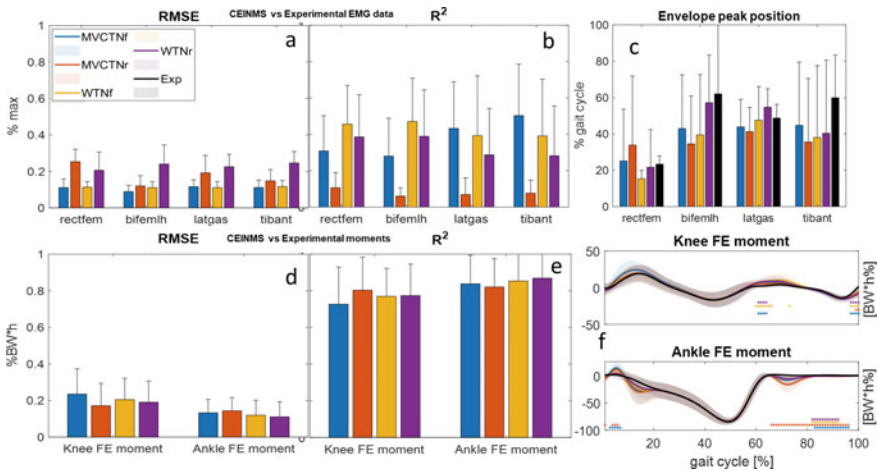


Fig. 1 Comparison between CEINMS models muscle excitations and joint moments versus corresponding experimental data (i.e., EMG envelopes, external joint moments): RMSE (a and d), R^2 (b and e), envelope peak position (c) and joint moment bands (f). Stars indicate statistically significant differences, oneway ANOVA ($P < 0.05$).

5 Conclusion

Even though the loss of information associated with the reduced set up should not be neglected, the current study showed the potential of adopting the quantitative assessment of the forces generated by an activated muscle in the clinical assessment of neurological patients. Further studies are needed to confirm this preliminary results.


Acknowledgements The work was supported by the Fresco Parkinson Institute Italia Onlus.

References

1. M. Romanato, D. Volpe, M. Sartori, Z. Sawacha, *Muscle forces and activations in Parkinson's disease: a model-based approach*, Proceedings GNB 2020, to be published.
2. M. Sartori, D. Farina, D.G. Lloyd, Hybrid neuromusculoskeletal modeling to best track joint moments using a balance between muscle excitations derived from electromyograms and optimization. *J. Biomech* **47**, 3613–3621 (2014)
3. A. Mantoan, C. Pizzolato, M. Sartori, Z. Sawacha, C. Cobelli, M. Reggiani, *MOtoNMS: A MATLAB toolbox to process motion data for neuromusculoskeletal modeling and simulation*, Source Code Biol, 2015, Med. 12:10.
4. C. Pizzolato, D.G. Lloyd, M. Sartori, E. Ceseracciu, T.F. Besier, M. Reggiani, CEINMS: A toolbox to investigate the influence of different neural control solutions on the prediction of muscle excitation and joint moments during dynamic motor tasks. *J. Biomech.* **48**, 3929–3936 (2015)
5. A. Mantoan, *Towards the application of multi-DOFEMG-driven musculoskeletal modeling in clinical practice: methodological aspects*. 2015. PhD thesis. <https://paduaresearch.cab.unipd.it/7976/>
6. S.L. Delp, J.P. Loan, M.G. Hoy, F.E. Zajac, E.L. Topp, J.M. Rosen, An interactive graphics-based model of the lower extremity to study orthopaedic surgical procedures. *IEEE Trans. Biomed. Eng.* **37**, 757–767 (1990)

The Effect of Visual, Auditory, Tactile and Cognitive Feedback in Motor Skill Training: A Pilot Study Based on VR Gaming



F. Alnajjar , Qi An, Mohit Saravanan, Khaled Khalil, Munkhjargal Gochoo, and S. Shimoda

Abstract In this study, we investigated the effects of various feedback systems in motor skill training. Twelve young healthy adults were recruited to play a game in a virtual reality (VR) environment. During the interaction with the VR game, various feedback and guidance, including visual, auditory, tactile and cognitive, were presented to the participants throughout different sessions. We monitored the influence of these feedbacks and guidance on the gaining speed of the motor skills of the participants. Initial results reveal that combining visual and tactile feedback achieved a remarkable superiority in recruiting a particular motor skill compared to other feedback methods. The results of this study can be used to guide designing proper feedback systems for speed motor skill training and/or rehabilitation.

1 Introduction

Stroke is a leading cause of long-term motor disability [1, 2]. It influences the post-stroke patient's status of independence and the quality of their life [3]. When voluntarily moving their limbs, stroke survivors, involuntarily, experience abnormal muscle patterns. This abnormality causes limited range of arm motion and/or weak muscle strength on the hand [4]. In the conventional rehabilitation, physiotherapists mainly target to discourage these abnormal muscle patterns at the early stage of

F. Alnajjar (✉) · M. Gochoo
College of Information Technology, UAE University, 15551 Abu-Dhabi, UAE
e-mail: fady.alnajjar@uaeu.ac.ae

Q. An
Graduate School of Engineering, The University of Tokyo, Tokyo, Japan

M. Saravanan · K. Khalil
University of Toronto, Toronto, Canada

F. Alnajjar · S. Shimoda
Intelligent Behavior Control Unit, Center of Brain Science (CBS), CBS-TOYOTA Collaboration Center (BTCC), RIKEN, Nagoya, Japan
e-mail: shingo.shimoda@riken.jp

the rehabilitation by proposing manually a feedback/guidance to redirect the correct movement of the patient limbs [5].

Technological advancements in wearable rehabilitation robots and gaming are promising an advanced rehabilitation era [4, 6]. Such advancements aim to enhance, in particular, the level of home-based stroke rehabilitation systems. One of the main challenges to achieve effective and motivational home rehabilitation is by providing a quick, accurate, informative, and easy-to-understand guidance/feedback to the patient during the therapy. Proper feedback/guidance can engage better the patients during the home rehabilitation sessions and influence strongly on their motor recovery.

In this paper, we have investigated the effect of different feedback systems in healthy adults while performing a VR gaming using upper limb movements. We examined which of these systems able to provide adequate feedback capable to speed up the recruitment of a particular muscle patterns.

2 Methods

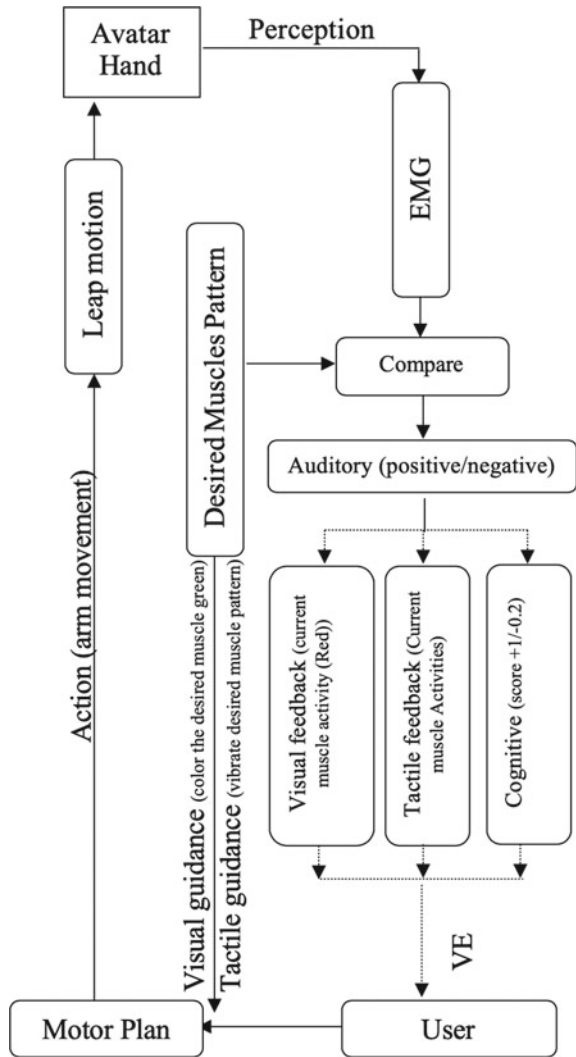
2.1 Participants

Twelve volunteered young healthy male adults participated in this study, mean age (SD) was 20.6 (0.7) years old. All participants were right-handed, and no one had experienced any motor disability or fine motor problems. We assigned equally all the participants to six different groups (Group A–F). We used one of the groups (group A) to build the “desired” muscles patterns for five different movements (wrist-flexion,—extension, and—ulnar-deviation, elbow flexion, and—extension). The associated muscles to these movements were the Extensor Carpi Radialis, Flexor Carpi Ulnaris, Extensor Digitorum, Palmaris Longus, Biceps Brachii, and the Triceps Brachii. Participants were requested to perform the movement with their non-dominant arm only. The remaining groups were requested to take part in the training sessions, which uses the guidance/feedback system, Fig. 1.

2.2 Procedure

To guide and assess the participants’ movements, a virtual environment (VE) was used to build the VR system. A leap motion was mounted on the Oculus Rift headset to capture the user’s hand motion. Low-Poly 3D hand model was used to represent the user hand in the VE (sketchfab.com). Muscles on the hand were represented using a customized muscle model. By the VE, participants can go through the various tasks, review the tasks’ instructions, monitor their scores, and review the guidance and

Fig. 1 A scheme represents the whole scenario of the developed feedback/guidance system: (1) The user reviews the guidance then perform the arm movement. (2) EMG data is recorded and compared to the desired muscle-pattern/movement. (3) A feedback is given to the user. The process is repeated until the desired muscle-pattern/movement is achieved



feedback. The system also allows the operator to monitor, in real-time, the training development of the participants.

2.3 Guidance and Feedback

During the training sessions, we asked the participants (Groups B–F) to sit and move the left arm freely following the guidance on the VR. The condition was to always start from the same initial position (a virtual marker were set) and perform one movement

at a time. A complete movement was considered every two seconds starting from the time the participant moved his arm. The guidance/feedback presented as follows:

- *Auditory feedback*: This group gets no guidance before their arm movement. However, positive or negative auditory feedbacks are given to the participants immediately after each complete movement.
- *Visual guidance/feedback*: Before the participant start each movement, a visual guide highlights in “Green” the muscles that the participant needs to activate to achieve the desired movement. Immediately after each movement, the incorrectly activated muscles will be highlighted in “Red”, and the correctly activated muscles will be highlighted in “blinking green”.
- *Tactile guidance/feedback*: An Arduino-based vibrator was placed on the desired muscles to guide the participant’s movement.
- *Cognitive feedback*: A scoring system was developed to report a feedback to the participants after each of their arm movement. A (+1)/(-1) was given every time the participant activates the a desired/undesired muscles, respectively.

3 Results and Discussion

We instructed the participants from each group to follow the guidance and the feedback given to them by the VR system, and to keep trying various movements until they reached the desired movement. All the groups successfully completed the assigned tasks.

Figure 2 illustrates the number of trials required by each group to successfully reach the desired muscle patterns. From the figure, it is obvious that movements that involve more than one muscle activity, takes longer to be accomplished than the one with simple movement. Results show that the auditory and cognitive training require the larger number of trials to reach the desired movement, followed by the tactile feedback and then the visual feedback. The model, which merge the visual and the tactile feedback required fewer trials.

To collect the participant feedback about the experiment each participant was interviewed after the training session. Participants who experienced the tactile feedback alone reported at some point, the vibrators cues were confusing and difficult to interpret. Participants who experienced the merged model reported that they felt comfortable and more guided when the vibrators and visual feedback cues were given together. All the participants have reported that having the auditory feedback in addition to other feedbacks was helpful.

4 Conclusion

This pilot study explores multimodal guidance and feedback and their impact on the speed of employing a certain movement through activation or inhibition of a specific

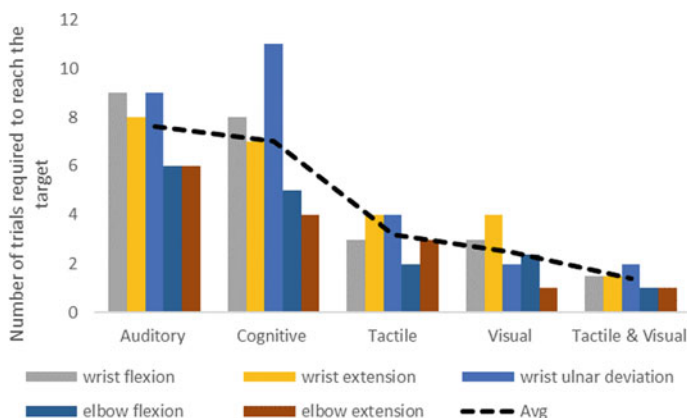


Fig. 2 Number of trials required by each group to reach the desired muscle pattern. Each bar in the figure is an average of the results of two participants

muscle pattern. Five muscles-patterns/movement, represented by six muscles, were used to assess the participants' actions during the training in the VR system. Results reveal that a model that merges both visual and tactile guidance and feedback appears to be useful as a motor training tool compared to the other sets of feedbacks. Although this study has been conducted on healthy individuals not on post-stroke patients, we have showed in previous study that there is a similarity underlying the neuromuscular strategies for both adaptation in healthy individuals, and the recovery of motor function after stroke [4]. The main limitation of this study is the small number of participants, which did not allow do proper randomization. Future work will, therefore, focus on increasing the sample size and overcome some other limitations. Investigating the feasibility of using muscle synergies for designing the feedback is also planned for future direction [7].

References

1. J. Adamson et al., Is stroke the most common cause of disability? *J. Stroke Cerebrovasc. Dis.* **13**(4), 171–177 (2004)
2. C. Sarti et al., International trends in mortality from stroke, 1968–1994. *Stroke* **31**(7), 1588–1601 (2000)
3. R.A. States et al., Overground physical therapy gait training for chronic stroke patients with mobility deficits. *Stroke* **40**(11) (2009)
4. F. Alnajjar et al., Motor control system for adaptation of healthy individuals and recovery of poststroke patients: a case study on muscle synergies. *Neural Plast.* **2019**, 1–3 (2019)
5. Alsinglawi et al., A framework for home-based stroke rehabilitation using interactive games and augmented reality feedback. *Biosyst. Biorobot.* 252–255 (2018).
6. P. Tamayo-Serrano et al., Gamified in-home rehabilitation for stroke survivors: analytical review. *Int. J. Serious Game.* **5**(1) (2018)
7. F. Alnajjar et al., Sensory synergy as environmental input integration. *Front. Neurosci.* **8** (2015)

Comparison of Wearable Sensor Based Algorithms for Upper Limb Activity Detection



Tanya Subash, Ann David, Varadhan SKM, and Sivakumar Balasubramanian

Abstract Upper limb activity detection using wearable sensors is useful for continuous monitoring in rehabilitation. In this study, we analysed four popular algorithms that compute real world amount of arm use using wrist triaxial accelerometry or inertial measurement units, and compared them to “actual” arm-use identified from videos by two independent assessors. It was found that the accelerometry-based methods are sensitive to arm movements, but are poor at distinguishing functional and non-functional movements. Use of arm orientation information makes the arm-use estimation robust to overestimation due to several non-functional movements, while losing some sensitivity to functional movements. A merger of principles from these two methods might result in a more accurate approach for arm-use detection.

1 Introduction

Accurate tracking of arm movements helps to (i) identify the translation of rehabilitation effects to a natural setting, (ii) give real-time feedback to patients regarding their arm movements, and (iii) provide early detection of unwanted compensatory strategies like overuse of unaffected arm. Using triaxial accelerometry for estimation of the amount of *functional* use lends particular value to the field of neurorehabilitation. This is because, ADLs (Activities of Daily Living) are densely punctuated by non-functional movements, more so for recovering patients. Thus, activity estimations that encompass both functional and non-functional movements tend to overestimate a patient’s actual use of the affected limb in daily life.

The authors Tanya Subash and Ann David contributed equally.

T. Subash · A. David · S. Balasubramanian (✉)
Department of Bioengineering, CMC, Vellore, India
e-mail: siva82kb@cmcvellore.ac.in

A. David · V. SKM
Department of Applied Mechanics, IIT, Madras, India

© The Author(s), under exclusive license to Springer Nature Switzerland AG 2022
D. Torricelli et al. (eds.), *Converging Clinical and Engineering Research on Neurorehabilitation IV*, Biosystems & Biorobotics 28,
https://doi.org/10.1007/978-3-030-70316-5_72

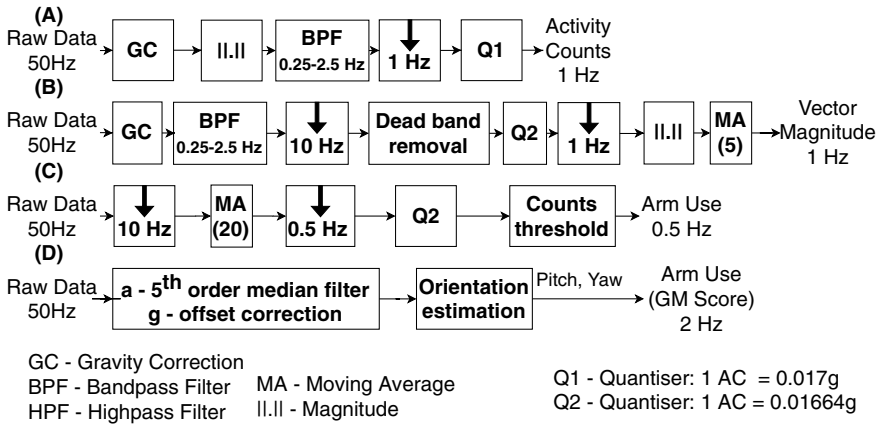


Fig. 1 Flowchart to describe the algorithms analysed. **a** Activity Counts; **b** Vector Magnitude; **c** Threshold Filter; **d** Gross Movement

Previous works [1–4] posit methods of processing inertial measurement unit (IMU) data to compute amount of functional use. This work attempts to evaluate the validity of these methods to accurately quantify functional activity by reducing their outputs to binary signals that indicate use and non-use, and comparing them to annotated videos.

2 Methods

2.1 Experiment

A wrist-worn watch-like device called IMU Watch was used in this study to record arm movements. An IMU Watch consists of a SEN-14001 board (Sparkfun Inc.) with a SAMD21 microprocessor and 9-DOF IMU (MPU9250, InvenSense-TDK Co). It records real-time triaxial linear acceleration and angular velocity 50 Hz.

Ten right-handed healthy individuals participated in the study. The inclusion criteria were (i) no prior history of upper limb (UL) movement problems due to neurological conditions; (ii) no current difficulty in UL movements; and (iii) age between 20 and 70 years. The study was approved by the institutional review board of Christian Medical College (CMC) Vellore (IRB Min. No. 12321 dated 30.10.2019). After providing informed consent, participants performed 15 functional tasks (e.g. eating from a bowl, opening a door) while wearing an IMU watch on each arm. The experiment was videotaped and then annotated by two independent assessors to indicate presence of functional activity (like reaching for, manipulating or transferring objects) of the left and right arms (Fig. 1).

2.2 Data Processing

The raw data from the watches were first re-sampled 50Hz using zero-order hold interpolation to account for any missing data. The following four different algorithms were analysed,

2.2.1 Activity Counts (AC) [1]

The accelerometer data was gravity corrected (Mahony algorithm [5]) and its magnitude was computed and bandpass filtered between 0.25 Hz and 2.5 Hz (17-th order Chebyshev II). A 1s long moving average filter was applied on the data and downsampled 1 Hz. This 1 Hz signal was quantized into ACs, where $1AC = 0.017g$. *Laterality* was computed as the difference between the ACs of the affected and non-affected arms divided by their sum. Here, 'affected' and 'non-affected' arm refer to the non-dominant and dominant arm, respectively. Thresholds were applied on *laterality* time series to obtain periods of 'resting' (both counts equal to 0), 'unimanual movement of the affected side' ($laterality < -0.95$), 'unimanual movement of the non-affected side' ($laterality > 0.95$), and 'bimanual movement' ($-0.95 \leq laterality \leq 0.95$).

2.2.2 Vector Magnitude (VM) [2]

Bailey et al. uses ACs given by ActiLife 6 proprietary software (ActiGraph, Pensacola) [2]. In this study, we followed the method as in [6] to generate ACs except for using Madgwick algorithm [7] for gravity compensation. Gravity corrected accelerometer data is bandpass filtered between 0.25Hz and 2.5Hz (10-th order Butterworth), down sampled 10Hz, and rectified. A deadband filter was applied to remove values below $\pm 0.068g$ [6]. This data was downsampled 1 Hz by taking the sum and expressed as ACs such that $1AC = 0.01664g$. Bailey et al. applied a moving average filter with window size 5 to compute the vector magnitude of triaxial AC. They define uni-manual activity when VM is zero for either of the arms. A zero threshold filter was used to generate the final binary signal to detect presence or absence of arm movement.

2.2.3 Threshold Filter (TF) [3]

Uswatte et al. used data from two uni-axial accelerometers to measure functional activity in each arm [3]. The acceleration from the corresponding axes (x and z), resampled 10Hz, were used in this analysis. Activity counts were generated such that $1AC = 0.01664g$. Functional activity was recorded whenever the ACs from the 2 axes crossed a threshold of 2. It is possible that the acceleration was corrected

for gravity, but in the interest of faithful reproduction this data transformation was restricted to the steps indicated in the paper.

2.2.4 Gross Movement (GM) Score [4]

The yaw and pitch of the forearm in an earth-fixed reference frame are estimated using Madgwick algorithm [7]. GM is computed as 1 (indicating presence of functional movement) for every 2 s window if the total change in yaw and pitch is more than 30° and the absolute pitch of forearm is less than 30° .

3 Results

The summary of the validation analysis is shown in Table 1. The key difference between the algorithms is found in their false positive and negative rates. GM algorithm has a higher false negative rate and a lower false positive rate than the other AC-based algorithms. The accuracy of detection in tabletop tasks of GM is lower than the rest due to the strict angular threshold defined for the algorithm [8]. However, among the non-tabletop tasks, the accuracy is highest for the GM algorithm at 76.35% along with a Gwet's agreement of 0.5506. The other algorithms tend to overestimate the presence of functional activity due to non-functional arm swing during ambulation. Thus, they fare poorly with accuracy between 25 and 35% and Gwet's agreement between -0.25 and -0.45

Table 1 Results from task-wise validation of the algorithms against video annotations

	False Positive (%)	False Negative (%)	Accuracy (%)	Gwet's AC1
Tabletop Tasks				
<i>AC</i>	21.69 (32.04)	6.42 (15.24)	71.88 (33.32)	0.4966 (0.6561)
<i>VM</i>	10.73 (17.58)	9.32 (19.42)	79.95 (24.37)	0.6598 (0.4610)
<i>TF</i>	24.40 (34.51)	0.10 (0.80)	75.50 (34.47)	0.5641 (0.6802)
<i>GM</i>	3.52 (7.02)	28.94 (33.02)	67.53 (32.23)	0.4171 (0.6401)
Non-tabletop Tasks				
<i>AC</i>	67.17 (46.60)	6.53 (20.89)	26.31 (41.57)	-0.4551 (0.8516)
<i>VM</i>	65.90 (46.08)	0.00 (0.00)	34.10 (46.08)	-0.2869 (0.9231)
<i>TF</i>	67.41 (46.28)	0.00 (0.00)	32.59 (46.28)	-0.3419 (0.9334)
<i>GM</i>	0.09 (0.98)	23.56 (37.69)	76.35 (37.65)	0.5506 (0.7394)

4 Discussion

The algorithms proposed by de Lucena et al., Bailey et al., and Uswatte et al. rely heavily on the amount of acceleration to detect arm-use. While this approach fares reasonably well for tasks performed on a tabletop, it tends to overestimate activity during ambulation. On the other hand, the GM algorithm employs a ‘functional range’ to measure arm use, which makes it highly robust to arm swing during ambulation at the expense of reduced sensitivity for finer movements that dominate everyday tabletop tasks like writing and typing.

Non-functional movements were predominantly absent for the tabletop tasks in the current experiment, which could explain the fairly uniform scores obtained across the algorithms. Therefore, there may be a decline in performance in a natural setting, not limited to the AC-based algorithms as non-functional movements such as gesticulation fall squarely in the ‘functional range’ defined by GM.

5 Conclusion

The current study presented the first direct comparison of the different arm-use measurement algorithms using wearable sensors proposed in the literature. Most AC-based algorithms have good sensitivity, but poor specificity. The GM algorithm attains good specificity at the expense of slight loss of sensitivity. Future work must investigate appropriate modifications to the GM algorithm and the use of machine learning approaches to improve the status quo in functional activity detection.

Acknowledgements We thank Heena Subash and Samuel Elias for data collection.

References

1. D.S. de Lucena, et al., Wearable sensing for rehabilitation after stroke: Bimanual jerk asymmetry encodes unique information about the variability of upper extremity recovery, in *2017 International Conference on Rehabilitation Robotics (ICORR)*, pp. 1603–1608 (IEEE, 2017)
2. R.R. Bailey, An accelerometry-based methodology for assessment of real-world bilateral upper extremity activity. *PloS one* **9**(7), e103135 (2014)
3. G. Uswatte et al., Ambulatory monitoring of arm movement using accelerometry: an objective measure of upper-extremity rehabilitation in persons with chronic stroke. *Arch. Phys. Med. Rehab.* **86**(7), 1498–1501 (2005)
4. K. Leuenberger et al., A method to qualitatively assess arm use in stroke survivors in the home environment. *Med. Biol. Eng. Comput.* **55**(1), 141–150 (2017)
5. R. Mahony et al., Nonlinear complementary filters on the special orthogonal group. *IEEE Trans. Automatic Control* **53**(5), 1203–1218 (2008)
6. J.C. Brønd et al., Generating ActiGraph counts from raw acceleration recorded by an alternative monitor. *Med. Sci. Sports Exerc.* **49**(11), 2351–2360 (2017)

7. S.O.H. Madgwick, et al., Estimation of IMU and MARG orientation using a gradient descent algorithm, in *2011 IEEE International Conference on Rehabilitation Robotics*, Zurich, pp. 1–7 (2011)
8. A. David, et al., Quantification of the relative arm-use in patients with hemiparesis using inertial measurement units. medRxiv (2020)

Targeted Muscle Training with a Hybrid Body-Machine Interface



Dalia De Santis and Ferdinando A. Mussa-Ivaldi

Abstract Studies have shown that motor recovery after neurological injuries is dependent on functional reorganization. In particular, engaging muscles in skilled activities triggers a process of remodeling that could lead to improving functional outcomes. Here, we propose a novel approach for engaging targeted muscles into skilled activities while operating assistive interfaces based on wearable sensors. To enforce contribution of specific muscles to the control output of a movement-based assistive interface, we introduced a signal dependent on muscle activation as replacement of a highly correlated signal dependent on limb kinematics, as measured by a set of inertial sensors. The latter were weighted against the EMG contribution and sent as input to a linear map projecting kinematic signals onto a 2D screen. Modulation of the weighting factor allows switching from a kinematic only (assistive) to a hybrid (rehabilitative) mode by increasing or decreasing EMG contribution to the operation of the interface.

1 Introduction

Loss of independence after neurological injuries is commonly resulting from the inability to voluntarily control muscle activation to the degree required for completing functional activities without assistance. Generally, assistive devices employ interfaces that bridge the input still available to their users (e.g. movement of unaffected limbs, the activity of certain muscles) and the output of a device as means to bypass the disability [1–3]. Learning to skillfully operate these devices triggers a process of neural adaptation, and leads to the gradual consolidation of specific coordination strategies [4].

D. De Santis (✉)

Fondazione istituto italiano di tecnologia, Genoa, Italy
e-mail: dalia.desantis@iit.it

D. De Santis · F. A. Mussa-Ivaldi

Northwestern University and the Shirley Ryan AbilityLab, Chicago, IL, USA
e-mail: sandro@northwestern.edu

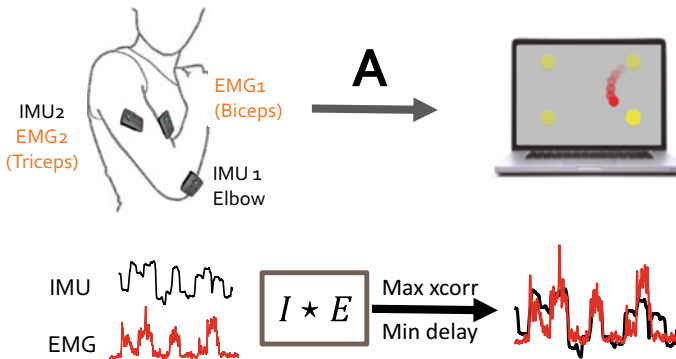


Fig. 1 Experimental setup and rationale for computing the hybrid map starting from a kinematic map that transforms body motions into motion of the cursor

To this end, it has been proposed that assistive interfaces could be used at the same time as means to retrain motor functions. This is the case for body-machine interfaces (BoMIs) that allow their users to perform skillful tasks via artificially re-mapping available movements into a suitable control space [5]. Interfaces based on movement have, however, the major drawback of not allowing selective involvement of only certain muscles in the operation. Accordingly, only the overall effect of coordinated muscle activations can be controlled and observed. Myoelectric interfaces, on the other side, directly map the activity of a selected group of muscles into control inputs for the device, but suffer from recording instabilities, are sensitive to electrode placement and inject more uncertainty in the control due to the lower signal-to noise ratio [6].

Here, we propose a hybrid interface design for exploiting the advantages of movement-based interfaces while also allowing for a direct and selective contribution of muscles in the control. In particular, we tested the ability of the interface to increase triceps, but not biceps, activation with practice. The EMG activity of biceps and triceps muscles is initially recorded during operation of the interface in movement-mode. The observed activation is then remapped onto the movement inputs such that causality between limb kinematics and muscle activity is maximized. We introduced a weighting coefficient to adjust the contribution of movement and muscle signals over time and allow intuitively switching from an assistive mode (movement-based) to a training mode (hybrid).

2 Material and Methods

2.1 Hybrid Interface Design

In a typical body-machine interface, the interface map is a linear transformation between the input space of body movement signals – generated by inertial measurement units (IMU) – to the output space of the device, for instance the coordinates of a 2D cursor. To include muscle activity in the design map, we started from the assumption that specific patterns of muscle activity are observed while individuals control the BoMI, and that these patterns consolidate with time [7]. Moreover, since muscle activity and joint movement are biomechanically coupled, we hypothesized that it is possible to observe specific patterns of movement-muscle coordination during interface use that are specific to the interface map. Hence, our approach was not aiming at modifying the interface map, but rather modifying the input to the map so that it accounts for both movement and EMG contribution to the output. For doing so, we identified the movement that exhibited the highest correlation and minimal delay relative to a targeted muscle activity as the desired coordination element (Fig. 1).

We then constructed an IMU-equivalent signal from the target EMG envelope imposing an equivalence between the z-scores of the two signals as follows:

$$IMU_e = -c \cdot (g \cdot EMG - \mu_E) \frac{\sigma_I}{\sigma_E} + \mu_I, \tag{1}$$

where μ_E, σ_E and μ_I, σ_I are, respectively, the estimated mean and standard deviation of the EMG envelope and the IMU orientation recorded at baseline, and $c = \{-1; 1\}$ accounts for the sign of the cross-correlation. The parameter g is used to modulate

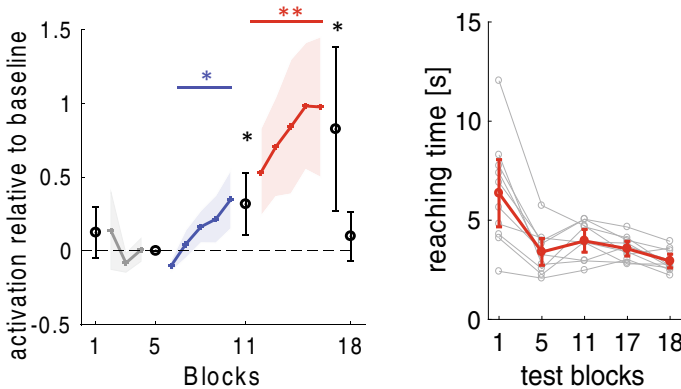


Fig. 2 Left: effect of input hybridization on triceps activation during baseline (gray), α modulation (blue), and g -modulation (red). Test blocks are in black. Right: reaching time in the test blocks for each subject (gray lines) and on average (red line). 1 block = 20 trials. * $p < 0.05$, ** $p < 0.01$

the effective amplitude of the muscle activation during training so as to induce a muscle to contract more ($g < 1$) or less ($g > 1$) than baseline. The hybrid input to the interface is then computed as linear combination of the original and reconstructed IMU signal weighted by a coefficient $0 \leq \alpha \leq 1$ controlling the amount of EMG contribution to the interface ($\alpha = 0$ is the baseline condition), as in Eq. 2:

$$\text{IMU}_{\text{hybrid}} = (1 - \alpha) \cdot \text{IMU} + \alpha \cdot \text{IMU}_e, \quad (2)$$

2.2 Experimental Protocol

Ten unimpaired volunteers practiced a reaching task with the BoMI using their dominant arm and forearm for one session of about 1 h. Biceps and triceps muscle activities as well as arm and forearm movements were recorded using three IMU/EMG sensors (Delsys™ Trigno), placed as in Fig. 1. Pitch and Roll angles of two sensors (IMU1 and IMU2) were used as movement input to the interface. The BoMI map was calibrated for each participant extracting the first two principal components of movement variance during 30 s of random arm motions. The Roll and Pitch of each sensor were then mapped by the BoMI to obtain the x, y position of a cursor displayed on a screen. Participants had to control the cursor to reach targets appearing at random positions on the screen in three conditions: (i) baseline, using only IMU inputs; (ii) α modulation, with α increasing every 20 trials by 0.25, (iii) g modulation, with $\alpha = 1$ and the gain decreasing every 20 trials. Before and after each condition a reaching test to 4 targets (20 trials) as in Fig. 1 was used to evaluate the control performance across conditions. The practice started and ended with a test in the reference condition of $\alpha = 0$. The target muscle was the Triceps brachii.

3 Results

All participants learned to perform the reaching task across conditions (Fig. 2—left). As shown in Fig. 2—right, the time to reach a target during the test significantly decreased with practice and was minimally affected by the change in control condition. Triceps activity increased significantly compared to baseline with $\alpha > 0.25$ and further increased with $g < 1$ (t-test block vs baseline). In contrast, the activity of the biceps did not significantly change with training (result not shown). The triceps activity modulation was not retained when returning to baseline.

4 Discussion and Conclusions

We propose a novel approach for engaging targeted muscles into skilled activities while operating assistive interfaces based on wearable sensors. A recent work explored the advantages of integrating EMG and kinematics for controlling body-machine interfaces [6]. The authors suggest that the parameters of a non-linear regression could be tuned to modulate muscle contributions to the control. Here, we implemented an intuitive way to provide targeted muscle training that exploits (i) the stability and ease of control of a kinematic interface and (ii) the natural biomechanical causality between muscle activation and movement. The proposed approach can be easily extended to multiple muscles, for instance to include antagonist muscles to help regulating co-activation. The upper bound to the number of muscles that can be included is provided by the natural motor redundancy as encoded by the BoMI map. Furthermore, we speculate that the proposed hybrid interface could be used to compare the effect of intuitive versus Non-intuitive EMG-kinematics mapping to study abstract learning in human-machine interfaces [8].

Acknowledgements Research supported by NIDRR grant H133E120010 and NICHD grant 1R01HD072080. Results incorporated in this manuscript have received funding from the European Union's Horizon 2020 research and innovation program under the Marie Skłodowska-Curie, REBoT, G.A. No 750464.

References

1. F. Abdollahi et al., Body-machine interface enables people with cervical spinal cord injury to control devices with available body movements: proof of concept. *Neurorehabil. Neural Repair* **31**(5), 487–493 (2017)
2. L. Schmalfuß et al., Steer by ear: myoelectric auricular control of powered wheelchairs for individuals with spinal cord injury. *Restor. Neurol. Neurosci.* **34**(1), 79–95 (2015)
3. C.L. Fall et al., Wireless sEMG-based body-machine interface for assistive technology devices. *IEEE J. Biomed. Heal. Inf.* **21**(4), 967–977 (2017)
4. M. Ison, P. Artemiadis, Proportional myoelectric control of robots: muscle synergy development drives performance enhancement, retainment, and generalization. *IEEE Trans. Robot.* **31**(2), 259–268 (2015)
5. C. Pierella et al., Remapping residual coordination for controlling assistive devices and recovering motor functions. *Neuropsychologia* **79**(Pt B), 364–376 (2015)
6. F. Rizzoglio, C. Pierella, D. De Santis, F.A. Mussa-Ivaldi, M. Casadio, A hybrid body-machine interface integrating signals from muscles and motions. *J. Neural Eng.* (2020)
7. C. Pierella et al., Changes in neuromuscular activity during motor training with a body-machine interface after spinal cord injury, in *IEEE International Conference on Rehabilitation Robotics*, 2017, vol. 2017, pp. 1100–1105
8. M. Dyson, S. Dupan, H. Jones, K. Nazarpour, Learning, Generalization, and Scalability of Abstract Myoelectric Control. *IEEE Trans. Neural Syst. Rehabil. Eng.*, p. 1, (2020)

Towards Objective Assessment of Upper Limb Spasticity by Means of Collaborative Robots



Edwin Daniel Oña, Ana Casanova, Anaëlle Gordillo, Carlos Balaguer, and Alberto Jardón

Abstract At present, rehabilitation robotics field has stressed on developing systems for enhancing the rehabilitation cycle, considering primarily the intervention stage of the process. However, the assessment of functional problems is essential to define optimal rehabilitation treatments. This paper presents a robot-based strategy for the evaluation of a disabling motor problem like spasticity. Focusing on the upper extremity, we use a collaborative robot for the limb mobilisation and, in this way, evaluate the resistance to move that is related to the spasticity level. As a result, an objective rating of spasticity is obtained.

1 Introduction

Spasticity is a muscle control disorder characterised by the increment of muscle tone with exaggerated stretch reflexes, as one component of the upper motor neuron syndrome [1]. The quantification of this disorder is hard and complex due to the complex nature of motor control and heterogeneity of consequences. In this sense, robotics can play a significant role in improving this manual procedure [2].

Several studies have been conducted to explore the use of robot-based approaches to reduce spasticity [3]. One example is the REHAROB system that employs two industrial robotic arms to move the user's arm aiming to reduce the spasticity level by passive exercises [4]. Similar approaches are used for the case of the lower extremity [5]. Hence, robot-based mobilisation offers various advantages regarding traditional manually-performed techniques.

Work funded by the Spanish Ministry of Economy and Competitiveness via the ROBOESPAS project (DPI2017-87562-C2-1-R), and by the RoboCity2030-DIH-CM Madrid Robotics Digital Innovation Hub (S2018/NMT-4331), which is funded by the Programas de Actividades I+D Comunidad de Madrid and cofunded by the Structural Funds of the EU.

E. D. Oña (✉) · A. Casanova · A. Gordillo · C. Balaguer · A. Jardón
RoboticsLab, Universidad Carlos III de Madrid, Madrid, Spain
e-mail: eona@ing.uc3m.es

© The Author(s), under exclusive license to Springer Nature Switzerland AG 2022
D. Torricelli et al. (eds.), *Converging Clinical and Engineering Research on Neurorehabilitation IV*, Biosystems & Biorobotics 28,
https://doi.org/10.1007/978-3-030-70316-5_74

However, other studies have focused on measuring the degree of spasticity using robotics. A system based on the KINARM exoskeleton is presented in [6] for quantitative assessment of post-stroke elbow spasticity. Other system uses a Fanuc 6 Degree of Freedom (DOF) robotic arm to manipulate the individual’s limb through passive elbow flexion/extension in the sagittal plane [7]. A different strategy is proposed in [8] by using a body sensor network (BSN) for detecting motion and inferring the spasticity level.

This latter is another key issue in spasticity management, the analysing of data acquired. Robotic systems allow for gathering reliable data about the user’s performance; however, a better usage of this data is needed. Thus, some efforts have been made on scoring the degree of spasticity using the data acquired from sensors and muscle activity [9].

This paper presents ongoing research towards developing a framework based on a collaborative robot for the assessment of UL spasticity. The strategy aims to measure the velocity-dependent resistance of the elbow when the robot moves the patient’s arm, giving an objective spasticity descriptor.

2 Materials and Methods

The proposed strategy comprises three blocks: robot-aided limb mobilisation, modelling of arm behaviour and rating the acquired data from robot and muscles. Figure 1 depicts the framework for elbow assessment. For the administration, the user must be seated facing the robot and the arm movement is performed in a sagittal plane.

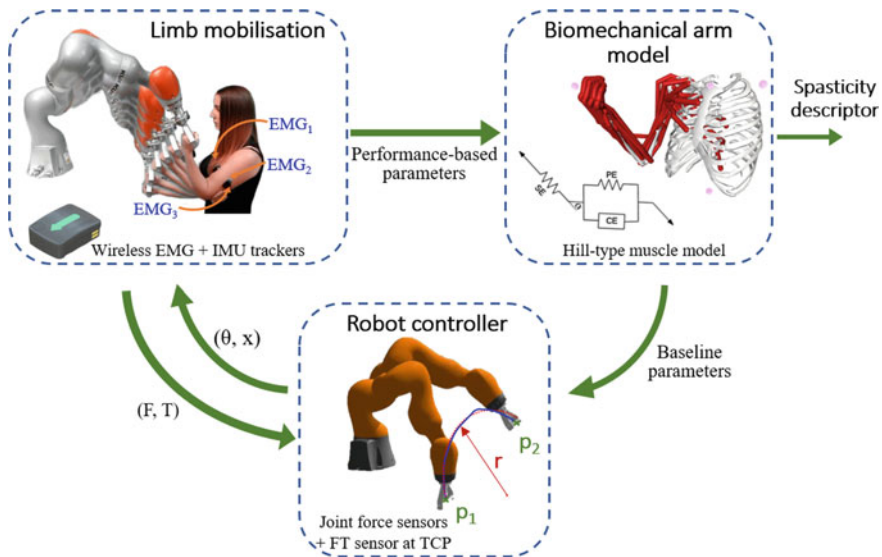


Fig. 1 Robot-based strategy for the assessment of UL spasticity

2.1 Robot-Aided Mobilisation

Robot-aided limb mobilisation is performed in two stages: (1) tailoring and (2) replication. The tailoring phase aims to fit the trajectory of the robot to the physical characteristics of the patient's arm. For that purpose, the patient must hold the robot tip with the hand, move the arm from 0° to the maximum range of motion. This preliminary trajectory is tuned by the robot controller in order to smooth the path. Note that for this stage the robot is executing a gravity compensation mode which restricts the allowed robot movement to a certain plane so the patient can move the robot easily.

Then, in the replication phase, the robot automatically performs the captured and fitted and mirrored trajectory. In the previous stage just flexion is recorded, but in this stage flexo-extension is reproduced. The patient must hold the robot's tip while relaxing all the arm muscles to allow the robot to move the patient's arm. During this phase, three wireless electromyography (EMG) sensors are attached to the patient's arm. The chosen EMG devices are the Trigno Avanti sensors manufactured by DELSYS, which also provide inertial information, allowing us to estimate their orientation. The sensors are located at the biceps brachii, triceps lateral head and triceps long head, which are some of the muscles involved in this movement.

The mobilisation is performed several times at different speed rates. The measurements from robot joint sensors, force-torque sensor on the robot's tip and EMG sensors are gathered for further analysis.

2.2 Modelling of Arm Behaviour

Proper modelling of arm behaviour is crucial to obtain accurate spasticity descriptors as it allows to get an insight of the muscles characteristics while the patient's arm is mobilised. The biomechanical model, developed using OpenSim modelling software, includes the muscles involved in the flexo-extension movement of the elbow. Two Hill based muscle models have been considered: Thelen and Millard. They have been modified to include the spastic behaviour, which may be represented using the following equation:

$$U(t + t_d) = \begin{cases} G \cdot v(t) + u(t + t_d) & v(t) > T \\ u(t + t_d) & v(t) \leq T \end{cases} \quad (1)$$

where U is the whole muscle activation including the spasticity factor, u is the muscle activation, t_d is delay, G is spastic gain, v is the contraction speed of fibers, and T is the threshold beyond which spasticity appears.

Equation 1 may be used in two different cases. On one side given some known muscle activations $U(t)$ and fiber velocities $v(t)$, an estimation of the spastic gain G may be inferred. On the other side, given some known fiber velocities $v(t)$ and the patient corresponding spastic gain G , the simulated muscle activations are obtained. This will be useful to check the validity of our model.

3 Results

At this research stage, a comparison between simulated and real arm behaviour is conducted. For this aim, sensor information coming from the robot (path and force sensing at the tip) and Trigno sensors (orientations) is fed into the biomechanical model to simulate the flexo-extension movement. Figure 2 presents a comparison between simulated and experimental muscular activations for a healthy user ($G = 0$) in flexo-extension elbow motion. Despite the differences, the biomechanical model provides a valid estimation of the muscle response. This fact suggests that spastic gain estimation using this model may be reliable.

4 Discussion and Conclusions

This paper proposes that using a collaborative robotic arm is a feasible approach to objectively assess elbow spasticity. The proposed system uses a single LBR IIWA 14 R820 robot manufactured by KUKA. The use of this robot involves various pros and cons during the evaluation process.

On the one hand, unlike related works that use industrial robotic arms [4, 7], the use of a collaborative robot ensures the patient's safeguarding by default. Besides,

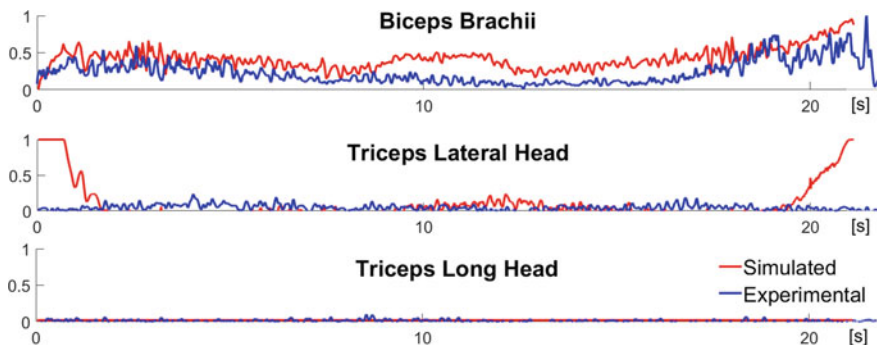


Fig. 2 Comparison between the simulated muscular activations for flexo-extension elbow movement ($G = 0$) and experimental ones

it is an easily releasable setup due to the fact that limb mobilisation is performed through only one contact point (hand-held). Secondly, neither the robotic arm nor the wireless EMG sensors restrict the range of elbow movement. Consequently, the evaluation of the elbow functionality throughout its entire range of motion (0° – 140°) is achieved.

On the other hand, a drawback of not restricting the trunk movements could derive in performing compensatory movements. In this sense, the inertial information provided by the wireless EMG sensors can help to detect such compensatory events. Thus, the arm motion can be reconstructed and further analysed.

Finally, while the proposed strategy seems promising, it is necessary to pilot the system in order to detect the effects of compensatory movements and build a reference model of arm behaviour. The integration of different performance-based data into the biomechanical arm model could provide a high-resolution spasticity descriptor, and reduce the inter-operator variability.

References

1. J.W. Lance, The control of muscle tone, reflexes, and movement: Robert wartenbeg lecture. *Neurology* **30**(12), 1303–1303 (1980)
2. E.D. Oña Simbaña, P. Sánchez-Herrera Baeza, A. Jardón Huete, C. Balaguer, Review of automated systems for upper limbs functional assessment in neurorehabilitation. *IEEE Access* **7**, 32352–32367 (2019)
3. R. de-la Torre, E.D. Oña, C. Balaguer, A. Jardón, Robot-aided systems for improving the assessment of upper limb spasticity: a systematic review. *Sensors* **20**(18), 5251 (2020)
4. A. Toth, G. Fazekas, G. Arz, M. Jurak, M. Horvath, Passive robotic movement therapy of the spastic hemiparetic arm with reharob: report of the first clinical test and the follow-up system improvement, in *9th International Conference on Rehabilitation Robotics, ICORR 2005*, pp. 127–130 (IEEE, 2005)
5. D. Shakti, L. Mathew, N. Kumar, C. Kataria, Effectiveness of robo-assisted lower limb rehabilitation for spastic patients: a systematic review. *Biosens. Bioelectronics* **117**, 403–415 (2018)
6. A. Centen, C.R. Lowrey, S.H. Scott, T.-T. Yeh, G. Mochizuki, Kaps (kinematic assessment of passive stretch): a tool to assess elbow flexor and extensor spasticity after stroke using a robotic exoskeleton. *J. Neuroengineering Rehab.* **14**(1), 59 (2017)
7. N. Seth, D. Johnson, G.W. Taylor, O.B. Allen, H.A. Abdullah, Robotic pilot study for analysing spasticity: clinical data versus healthy controls. *J. Neuroengineering Rehab.* **12**(1), 109 (2015)
8. B.J. Misgeld, M. Lüken, D. Heitzmann, S.I. Wolf, S. Leonhardt, Body-sensor-network-based spasticity detection. *IEEE J. Biomed. Health Informatics* **20**(3), 748–755 (2015)
9. B. Hu, X. Zhang, J. Mu, M. Wu, Y. Wang, Spasticity assessment based on the hilbert-huang transform marginal spectrum entropy and the root mean square of surface electromyography signals: a preliminary study. *Biomed. Eng. Online* **17**(1), 1–20 (2018)

Source Localization of Simulated Electroencephalogram of Virtual Epileptic Patient to Investigate Clinically Feasible Montages



Zoe Herrick, Ping Li, and Anirban Dutta

Abstract Electroencephalogram (EEG) source localization is used to estimate regions of ictal onset in epilepsy patients with temporal lobe epilepsy. Localization of EEG data struggles to achieve high spatial resolution, especially in deep brain regions, and is difficult to validate. In this paper we generate simulated EEG data using a spatiotemporally realistic generative brain network model (BNM) based on patient structural and functional data, created with The Virtual Brain (TVB) platform, to qualitatively assess head model approaches, distributed source inverse methods and clinically feasible electrode montages. We find that sLORETA is highly sensitive to head model errors, where dSPM is robust and wMNE displays some sensitivity. Additionally, increased electrode density over regions of interest provides a clinically feasible means to improve localization accuracy of a sparse montage. Finally, TVB platform can be utilized to model patient anatomy and physiology where resultant simulated EEG can be source localized for personalized neurological care.

1 Introduction

Focal epilepsy, characterized by seizures which originate in one region of the brain, accounts for 60% of the ~2.3 million adults and more than 450,000 adolescents who live with epilepsy in the US alone [1]. Of those with focal epilepsy, 60% have temporal lobe epilepsy (TLE), which is subdivided into two major categories. Neocortical or lateral TLE involves outer regions of the temporal lobe. Mesial TLE originates in medial structures such as the hippocampus and comprises 80% of those with TLE [2]. Determining seizure onset location in these cases is difficult due to depth within the brain. Invasive stereoelectroencephalography (sEEG) depth electrodes are often used for a more precise estimate. Proximity to regions vital for language

Z. Herrick · P. Li · A. Dutta (✉)
University at Buffalo SUNY, Buffalo, USA
e-mail: anirband@buffalo.edu

Z. Herrick
e-mail: zoeherri@buffalo.edu

processing and memory makes accurate identification of the onset region imperative for a successful post-surgical outcome. The National Institute of Neurological Disorders and Stroke (NINDS) has targeted some research toward developing methods for accurately mapping relevant areas of the brain in preoperative planning. They do so with the use of imaging tech in an effort to minimize language deficits that can occur. Research has shown that high density EEG localization is capable of achieving high accuracy, however this is often not feasible in clinical settings due to the expense of equipment. This paper qualitatively assesses head model approaches, distributed source inverse methods and clinically feasible electrode montages through the lens of spatiotemporally realistic simulated EEG data produced by a generative BNM.

2 Methods

2.1 *The Virtual Brain*

TVB is openly available and simulates brain activity with a generative BNM. Brain regions, or nodes, are heterogeneously modeled as discrete neural mass models with a connectivity matrix modeled after patient white matter tracts governing strength and time delay of network connections [3]. The Epileptor model [4] was chosen to govern all nodes with variable epileptogenicity, x_0 , assigned to each node. Three model configurations were created, identical except for the x_0 parameter, and named according to their network role; Epileptogenic zones, Propagation zones, and Other Nodes were assigned x_0 values -1.6 , -1.8 , and -2.4 respectively. Increased negativity indicates stability with bifurcation of stable and epileptogenic behavior marked by critical value $x_{0c} = -2.04$. The amygdala, hippocampal cortex, and parahippocampal cortex in the right hemisphere (radiological convention in MNI atlas space) were assigned as Epileptogenic zones where the model could autonomously generate seizures. Propagation zones were the right ventral temporal cortex and superior temporal cortex, where seizure activity could spread but not originate. All other nodes were assigned as such and thus modeled as healthy tissue unaffected by epileptic activity. Simulated brain activity was mapped to 63 simulated EEG electrodes on the model scalp surface with a forward model to produce EEG data.

2.2 *Brainstorm*

Brainstorm ICBM 152_2019 anatomy template was selected as the protocol default anatomy for all subjects. Using the OpenMEEG software [5], BEM surfaces were generated via the Brainstorm approach, not Field Trip, for computational efficiency and warped using the simulated electrode locations. For each of three head models,

one surface and two volume, five montages were applied ranging from sparse 10–20 to the full montage of 63 electrodes. Assuming unconstrained sources, weighted minimum norm (wMNE), dynamic statistical parametric mapping (dSPM), and standardized low resolution electromagnetic tomography (sLORETA) inverse methods were applied to each head model as kernels to optimize hard drive space and computation time. A custom color bar scale was applied for each inverse method due to their distinct mathematical approaches producing varied units. Scales had a minimum value of 0 and maximum value of 0.15, $2.00\text{e}+9$, and 7.00 for wMNE, dSPM, and sLORETA respectively.

3 Results

Of the 3 short seizures simulated, the first was selected for analysis after clinical assessment deemed it most realistic. TVB simulation data revealed seizure onset was in the right hippocampus (radiological convention in MNI atlas space). dSPM (Fig. 1a) failed to lateralize, producing bitemporal localization but displayed no mis-localization of the medial source on lateral surfaces. Activation was near ground truth, falling superiorly and posteriorly to the hippocampi. wMNE (Fig. 1b) mis-localized heavily to the lateral cortex surface. Strongest activation was seen on the anterior left temporal lobe (neurological convention), roughly superficial to the appropriate medial region in the expected hemisphere. sLORETA activation (Fig. 1c) was highly disperse and trended from the ventral temporal region towards the parietal lobe, correlating strongly with the region of greatest head model warping. Results were split across hemispheres but estimated activation was greater on the left with strongest activation on the inferior ventral left temporal lobe.

Montage impact is best observed in sLORETA results (Fig. 2) by the parietal shift. A similar trend is observed in activation strength of dSPM results, which represents model confidence. The temporal montage (Fig. 2c), comprised of the sparse 10–20 montage and 5 additional electrodes at each temporal lobe, displayed localization results comparable to those achieved with the full montage (Fig. 2a). Application of one additional electrode in each temporal region (Fig. 2d) marginally improved localization beyond the 10–20 montage results (Fig. 2e). Selectively increasing density in temporal ROIs (Fig. 2c) significantly improved localization results of the sparse montage while an increase in general density (Fig. 2b) beyond the temporal montage did not show significant improvement, supporting selectively dense sparse montages.

4 Conclusion

Simulated epileptic EEG data generated in TVB can be used to assess distributed source localization methods on a spatiotemporal scale. Assessment of localization

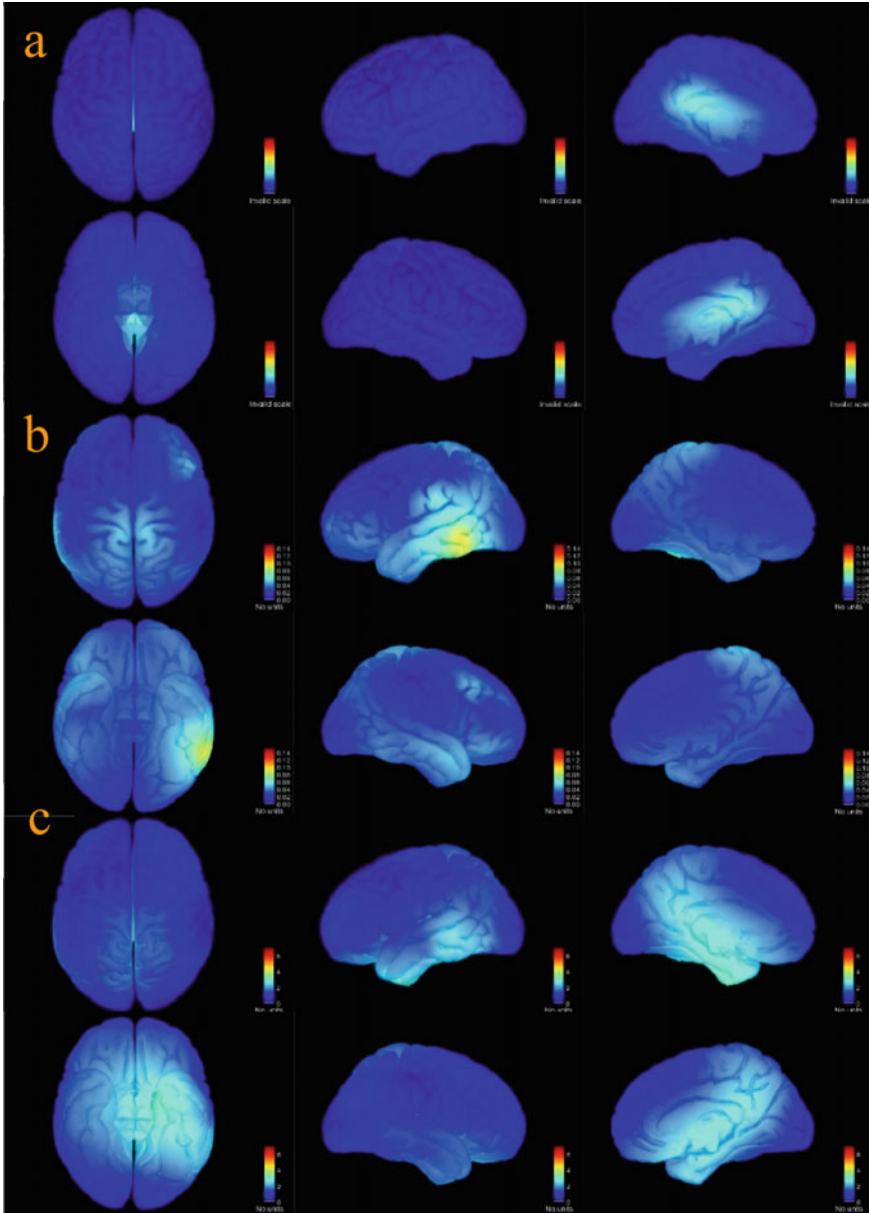


Fig. 1 Comparison of localization estimations of distributed source inverse methods at seizure 1 onset on surface head model. For dSPM (a), wMNE (b) and sLORETA (c), 6 images display various cortical surfaces. Moving right from upper left, images depict top, left lateral, left medial, bottom, right lateral and right medial views. In top and bottom cases, anterior points up. Red indicates strongest activation on each color scale

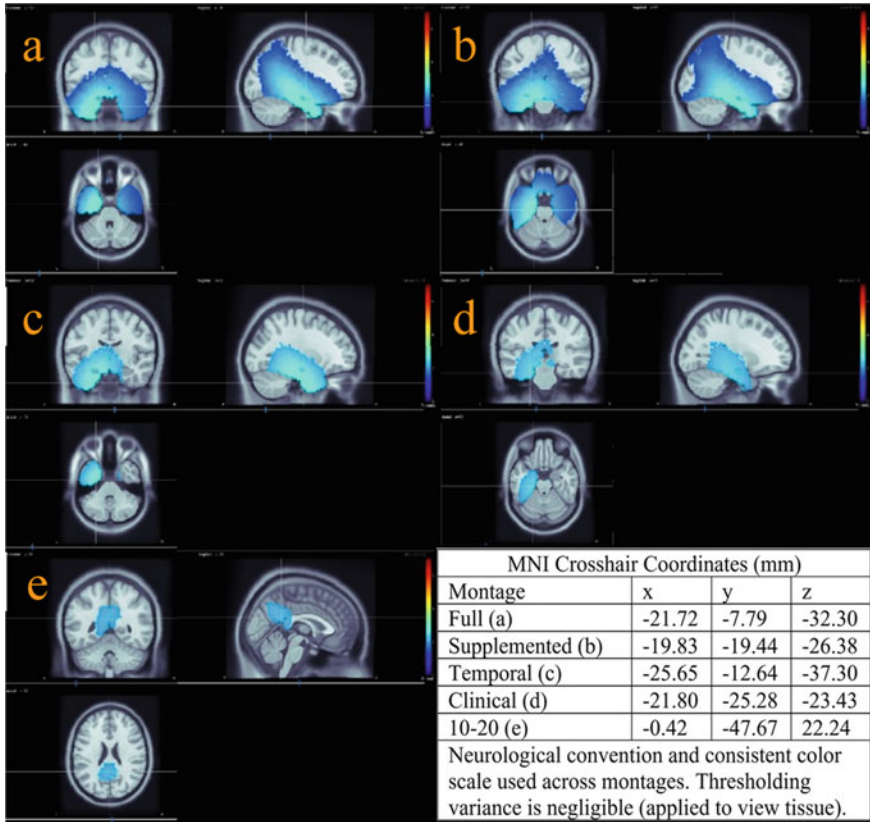


Fig. 2 Comparison of sLORETA localization results on adaptive grid volume head model across 5 montages. Table of crosshair locations denotes montages. As montage sparsity increases, estimated activation shifts into the parietal lobe and decreases in strength. Color bar scale is consistent across montages. Thresholding varies only for visualization of underlying tissue. Location and intensity of highest color bar value region is the focus

results achieved with this data elucidates the potential for clinically feasible selectively dense montages to optimize localization in a clinical setting. Personalized neurological care for TLE patients is possible with this approach. A bottleneck exists in generation of the simulated data but can be overcome with an individual trained in TVB collaborating with clinicians.

Acknowledgment Sponsor and financial support acknowledgments are placed in the unnumbered footnote on the first page.

References

1. O. o. C. a. P. L. NINDS, *Epilepsy: Hope Through Research*. NIH. <https://www.ninds.nih.gov/Disorders/Patient-Caregiver-Education/Hope-Through-Research/Epilepsies-and-Seizures-Hope-Through>. Accessed 7/1/2020
2. H. Klein, C. Joshi, *Temporal Lobe Epilepsy (TLE)*. Epilepsy Foundation of America. <https://www.epilepsy.com/learn/types-epilepsy-syndromes/temporal-lobe-epilepsy-aka-tle>. Accessed 7/1/2020
3. V.K. Jirsa et al., The virtual epileptic patient: individualized whole-brain models of epilepsy spread. *Neuroimage* **145**, 377–388 (2017). <https://doi.org/10.1016/j.neuroimage.2016.04.049>
4. V.K. Jirsa, W.C. Stacey, P.P. Quilichini, A.I. Ivanov, C. Bernard, On the nature of seizure dynamics, (in eng). *Brain* **137**(Pt 8), 2210–2230 (2014). <https://doi.org/10.1093/brain/awu133>
5. A. Gramfort, T. Papadopoulo, E. Olivi, M. Clerc, OpenMEEG: opensource software for quasistatic bioelectromagnetics. *BioMed. Eng. OnLine* **9**(1), 45. 2010/09/06 2010. <https://doi.org/10.1186/1475-925X-9-45>

An Open-Source, Wheelchair Accessible and Immersive Driving Simulator for Training People with Spinal Cord Injury



Filippo Gandolfi, A. Bellitto, Angelo Basteris, A. Canessa, A. Massone, Serena Ricci, and M. Casadio

Abstract Independence is one of the greatest achievements for people with Spinal Cord Injury (SCI). Indeed, mobility represents a big challenge that needs to be addressed, also considering that road accidents are frequently the cause of SCI. Immersive Virtual Reality (VR) combined with a driving simulator may provide a realistic experience, helping users to relearn driving and overcome the traumatic event. The aim of this project was to implement a wheelchair accessible, immersive driving simulator for the training and assessment of SCI people. Here we present a proof of concept of an open-source, VR compatible, driving simulator. The system combines a VR headset with an adaptive driving controller and a VR scenario. Starting from CARLA, an open simulator for autonomous driving, we created driving scenarios designed to fit the needs of SCI rehabilitation. Also, we defined future developments required to create a device usable for the assessment of cognitive and motor abilities.

F.G. and A.Be. equally contributed to this work, This work was supported by the “Spinal Cord Italian Laboratory” (S.C.I.L.) of the Unità Spinale Unipolare, Santa Corona Hospital of Pietra Ligure (SV, Italy) and the “Centro di Simulazione e Formazione Avanzata” (SimAv) of the University of Genova (GE, Italy).

F. Gandolfi (✉) · A. Bellitto (✉) · A. Canessa · S. Ricci · M. Casadio
DIBRIS, University of Genova, Genova (GE), Italy
e-mail: filippo.gandolfi95@gmail.com

A. Bellitto
e-mail: amy.bellitto@edu.unige.it

F. Gandolfi · A. Bellitto · A. Canessa · A. Massone · S. Ricci · M. Casadio
S.C.I.L., Unità Spinale Unipolare, Santa Corona Hospital, Pietra Ligure (SV), Italy

A. Basteris
Health Informatics and Technology, University of Southern Denmark, Odense, Denmark

© The Author(s), under exclusive license to Springer Nature Switzerland AG 2022
D. Torricelli et al. (eds.), *Converging Clinical and Engineering Research*
on *Neurorehabilitation IV*, Biosystems & Birobotics 28,
https://doi.org/10.1007/978-3-030-70316-5_76

1 Introduction

Regain the ability to drive is a priority for people recovering from a Spinal Cord Injury (SCI) [1]. Without a mean of transportation, common areas of life, such as reintegration into society and employment, are highly affected. Currently, standard tools provided to help patients re-learn driving are driving simulators. Though these devices offer a mean to practice driving in a safe and controlled environment, often simulators do not provide fully realistic driving experiences, are not immediately and freely accessible to patients and do not offer the possibility to investigate the re-learning and rehabilitation process that occurs during practice. Currently available simulators, indeed, either provide a realistic and immersive driving experience specifically designed for gaming or advanced mechanical research [2] and thus are not adapted to the needs of motor impaired individuals or are designed to test the ability of driving of the user in terms of reactions and applied forces and do not offer the opportunity to practice in a realistic driving environment [3].

Here we present a new open-source driving simulator designed to combine these features into a single device. Specifically, we developed a system for the training and assessment of the driving ability of people with SCI based on the integration of virtual reality technology (VR) and adaptive driving equipment.

2 Objectives

The goal of the project was to address the limits of the currently available simulators by designing and developing a wheelchair accessible, easy to use and immersive driving simulator, specifically designed for people with SCI.

The features of the simulator were selected in collaboration with the physicians and physiotherapists of the Santa Corona Hospital (Pietra Ligure, SV, Italy) and can be summarized as follow:

- Provide an immersive and realistic driving experience.
- Guarantee a safe and controlled training platform to allow people with SCI to relearn driving, and fully comprehend how the motor alteration induced by the injury has affected their ability to drive.
- Investigate the learning process that occurs during practice.
- Provide physicians with an objective motor and cognitive assessment of the individual's ability to drive.
- Be easily accessible to wheelchair users in an autonomous way.
- Provide a controller platform for the psychological recovery of people injured in road accidents, to overcome the traumatic event.
- Offer a generic and customizable interface to allow the use of different types of adapted driving controllers.

3 Solution

The driving simulator consists of two subsystems: hardware, comprised of a driving controller and a VR headset, and software, which includes virtual driving scenarios.

3.1 Hardware

The hardware system is composed of two main parts: the driving controller and the VR headset (Fig. 1). The latter, comprises of an HTC Vive (HTC Corporation, TWN and Valve Corporation, WA, USA), a head-mounted display (HDM) that provides an immersive 3D vision of the driving scenario, and a Leap Motion Controller (Ultraleap, CA, USA), specifically designed to track the user’s hands in real time. The Leap Motion is attached to the HMD and captures information about the hands to create a virtual representation of the hands that can interact with the objects present in the setup and represented in the VR (Fig. 2).

The driving controller is a 4-axis joystick, similar to the joystick car systems usually adopted by people with SCI. However, we have developed the system so that it can be used with different types of adapted driving devices such as a steering wheel provided with a spinner knob or/and a common push/pull brake and accelerator hand control.

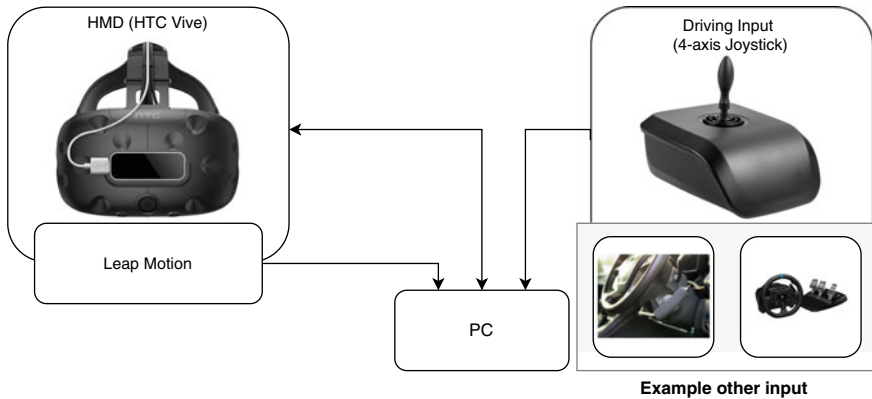


Fig. 1 Hardware diagram: signals from HMD the controllers are managed by the input interface BP. Sources paravan.com; ergomobility.co.uk; logitech.com



Fig. 2 Driver's view via VR headset

3.2 Software

The software system includes an interface, to acquire and translate the input signals of the driving controller into driving commands for a virtual vehicle, and several driving virtual scenarios in which the user is able to drive the vehicle, which contains a virtual replica of the adapted control device that moves exactly as in reality, while experiencing real-life driving scenarios, such as pedestrians crossing the road or a traffic jam. The virtual driving scenarios (Fig. 2) were developed using an adapted version of CARLA, an open-source simulator for autonomous driving research, developed by Intel Labs, Toyota Research Institute and Computer Vision Center, Barcelona [4]. The platform supports python nodes that allow the integration of different sensors and scenarios in the environment. The environment is built with C++ libraries, while the 3D simulation is powered by Unreal Engine (Epic Games, NC, USA), a real-time game engine supporting Blueprint (BP) visual scripting system. BP allows programmers to use gameplay elements to create the virtual experience. Briefly, CARLA provides most of the objects to create maps, spawn vehicles and pedestrians, assign routes and autopilot to IA vehicles. Also, it offers C++ libraries to manage the vehicle, estimating its properties and behavior, such as position, acceleration and traffic violations. Moreover, CARLA offers a set of default python nodes to generate new simulation scenarios (like an unpredicted pedestrian crossing the road), change the weather settings and lights conditions and spawn a self-selected number of cars in the scene.

As our goal was to develop a driving simulator, we had to implement a first-person VR driving mode, allowing users to see the street from a driver's perspective. This implementation was possible thanks to the open-source nature of the software and its modularity. We implemented the first-person view by adding a new VR camera in the driver's seat (Fig. 2); also, we improved the vehicle interior by adding both the steering wheel and the adapted driving controller. Exactly as in real life, we were able to set the movement of the steering wheel and adapted driving controller, so that

they moved according to the signals input received from the hardware components (i.e. the real driving controller), via BP. To increase the realism of the scenario we also introduced a sound effect module that reproduces car and ambient sounds.

4 Conclusion

In this work, we propose an open-source first-person view driving simulator aimed at promoting the return to driving of people with SCI. The system presented is based on the integration of an adapted open-source simulator for autonomous driving with a VR system and customized driving controllers. Our system responds to the initial requests made by the physicians, physiotherapists and people with SCI who have previously experienced the return to driving process.

We are developing a graphical user interface (GUI) that will allow SCI-users to practice driving freely and easily and offer physiotherapists the ability to select and customize the driving rehabilitation treatment by setting the virtual driving map, the level of difficulty and other environmental conditions. We plan to integrate the hardware with sensors to examine both the interaction between the user and the driving controller, such as the pressure of the hands on the controller, and the user itself, such as the posture.

Summing, this project started with the idea of supporting SCI patients during their physical, mental and emotional recovery in the rehab center by specifically focusing on helping them regain transport independence. Indeed, the literature and the brainstorming with the medical team and professionals in the field of mobility highlighted the need to provide an effective tool to help SCI people to return driving and the simulator presented in this work is our solution to this issue. In the future, the system will be easily translated and adapted to support the driving rehabilitation of individuals with other types of motor disorders.

Acknowledgements We thank the municipality and the local office of Loano (Savona, Italy), Amelotti Maria Giuliana, Berto Luca and Gimelli Alessandro for their support.

References

1. C.A. Unsworth, A. Bakera, Driver rehabilitation: a systematic review of the types and effectiveness of interventions used by occupational therapists to improve on-road fitness-to-drive, in *Accident Analysis and Prevention*, pp. 106–114 (2014)
2. Q. Hussain, W.K.M. Alhajyaseen, A. Pirdavani, N. Reinolsmann, K. Brijs, T. Brijs, Speed perception and actual speed in a driving simulator and real-world: a validation study, in *Transportation Research Part F*, pp. 637–650 (2019)
3. J. Rodseth, E.P. Washabaugh, A. Al Haddad, P. Kartje, D.G. Tate, C. Krishnan, A novel low-cost solution for driving assessment in individuals with and without disabilities, in *Applied Ergonomics*, pp. 335–344 (2017)
4. A. Dosovitskiy, G. Ros, F. Codevilla, A. Lopez, V. Koltun, CARLA: an open urban driving simulator, in *Proceedings of the 1st Annual Conference on Robot Learning*, pp. 1–16 (2017)

SS9: Joint Stiffness: The Sleeping Giant of Neuromechanics

A Powered Ankle Foot Orthosis Based on Shaft Twisted String Actuation to Assist Persons with Foot-Drop: A Feasibility Study



Pedrin Denoth, Pascal Geitner, Lukas Krähenbühl, Konrad S. Stadler, and Eveline S. Graf

Abstract In recent years various powered ankle foot orthoses (PAFO) have been developed to assist disabled persons during walking. Different actuation technologies have previously been used, each with their individual challenges (e.g. high weight). As a new actuation technique, we used shaft twisted string actuation (STSA). We tested the effect of the STSA-PAFO on the gait of five participants with a diagnosed foot-drop. For all participants the ankle dorsiflexion has increased at initial contact and during swing phase with the PAFO compared to no orthosis. Compared to the prescribed AFO, two participants showed an increase in total ROM during swing-phase with the STSA-PAFO. Further, the peak plantarflexion has increased in three participants at push-off with the STSA-PAFO. During user testing in laboratory setting the STSA-PAFO showed good function and is a promising approach for further development.

1 Introduction

Foot-drop is a common gait disability. It is characterized through an inability to dorsiflex (DF) the foot [1]. A person with foot-drop is unable to clear the foot properly during the swing phase of walking [1]. A standard treatment for foot-drop are ankle foot orthoses (AFOs). In recent years, powered AFOs (PAFO) have been developed to ensure a more dynamic gait and improve gait patterns of disabled persons [2]. Up to date, most PAFOs are still in an early stage of development and facing different problems. The biggest challenges in the development of PAFOs are the requirement of

P. Denoth (✉) · E. S. Graf

Zurich University of Applied Science, School of Health Professions, Institute of Physiotherapy, Winterthur, Switzerland

E. S. Graf

e-mail: eveline.graf@zhaw.ch

P. Geitner · L. Krähenbühl · K. S. Stadler

Zurich University of Applied Science, School of Engineering, Institute of Mechatronic Systems, Winterthur, Switzerland

light weight, small size, high efficiency and low noise [3]. To fulfil these requirements, a promising actuation technology is twisted string actuation (TSA) [4]. The principle of TSA is to twist strings with a relatively low torque which leads to a contraction of the strings and a high linear force [4]. TSA helps to reduce the weight and complexity by not needing a transmission element and can be operated with small high-speed motors [5]. However, the friction of the strings is highly influencing the acting torque [6]. To reduce the friction and increase the speed of linear contraction, we layered the strings on a steel shaft rather than on themselves. We named the principle shaft twisted string actuation (STSA). The STSA was used in the development of a new PAFO prototype (Fig. 1) [7]. The goal of this study is to evaluate the effect of the STSA-PAFO on walking biomechanics of people with a diagnosed foot-drop as well as usability.

2 Methods

2.1 PAFO

The STSA-System is mounted on a shinpad connected to the shoe with two strings. To enable foot-clearance (DF) during swing phase, the strings get twisted around the shaft and the shoe gets pulled toward the motor (Fig. 1). The actuation of the motor (maxon, 120 W) is based on the detection of certain gait events with pressure sensitive sensors. To process the information and control the motor we used a processor board with a Texas Instrument processor (TI F28377s). The electronic and power supply was attached to a backpack (tethered design) [7].

2.2 Subjects and Clinical Evaluation

Five persons with foot-drop (age 34–58) were included after providing informed consent. The drop-feet were caused by a range of neurological disorders like stroke and iSCI. All participants were able to walk independently (FAC-Score 5) but were allowed to use crutches/canes when needed.

A marker based VICON Motion System was used to record kinematic data (240 Hz). A cluster marker approach was used to determine joint angles [8]. For testing the user-friendliness of the PAFO, the participants rated the PAFO with the system usability scale (SUS). Further, they rated their perceived exertion and pressure (NRS 0–10). The researchers completed a narrative report about predefined points e.g. the battery runtime.

Each participant walked with three conditions on an even surface, in a defined order: without AFO, with the STSA-PAFO and with their own prescribed AFO.

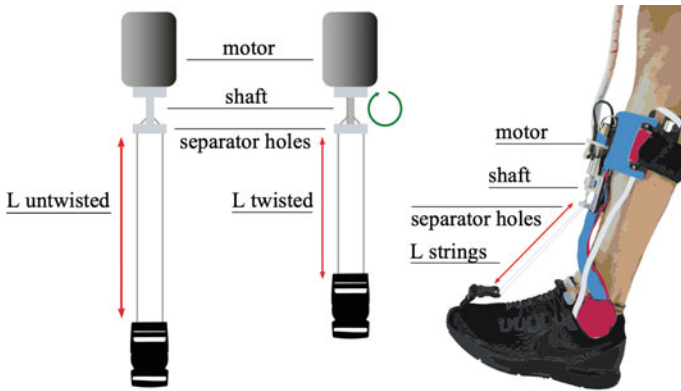


Fig. 1. Illustration of the principle and the design of the STSA-PAFO.

Two participants walked with two different STSA motor torques, after feeling uncomfortable with the first setting of the PAFO (Fig. 2a, b).

3 Results

For all participants the ankle DF has increased at initial contact and during swing phase with the STSA-PAFO compared to no orthosis. Compared to the prescribed AFO the total ROM during swing phase has increased for participants 02 (+24.07°) and 03 (+8.5°) with the STSA-PAFO. For participants 04 (+0.8°) and 05 (+1°) the changes were small. Participant 01 did not have a prescribed orthosis. A higher peak plantarflexion at push-off can be seen with the STSA-PAFO in participants 02, 03 and 05 (Fig. 2a–e).

At initial contact, smaller knee flexion was noticed with the prescribed AFO and the STSA-PAFO compared to no orthosis for two participants. Only slight changes in hip kinematic occurred.

The SUS scores of the participants were ranging from 60 to 85 points. Perceived pressure and exertion were 4 in maximum, but mainly 0–2.

The investigator report showed a good function in the laboratory. Two short (<5min) shut down but no severe event occurred and the battery charging was sufficient.

4 Discussion

The main goal of all (P)AFOs for patients with foot-drop is to assist the foot during swing phase and initial contact [9]. The increase of the ankle DF at initial contact and

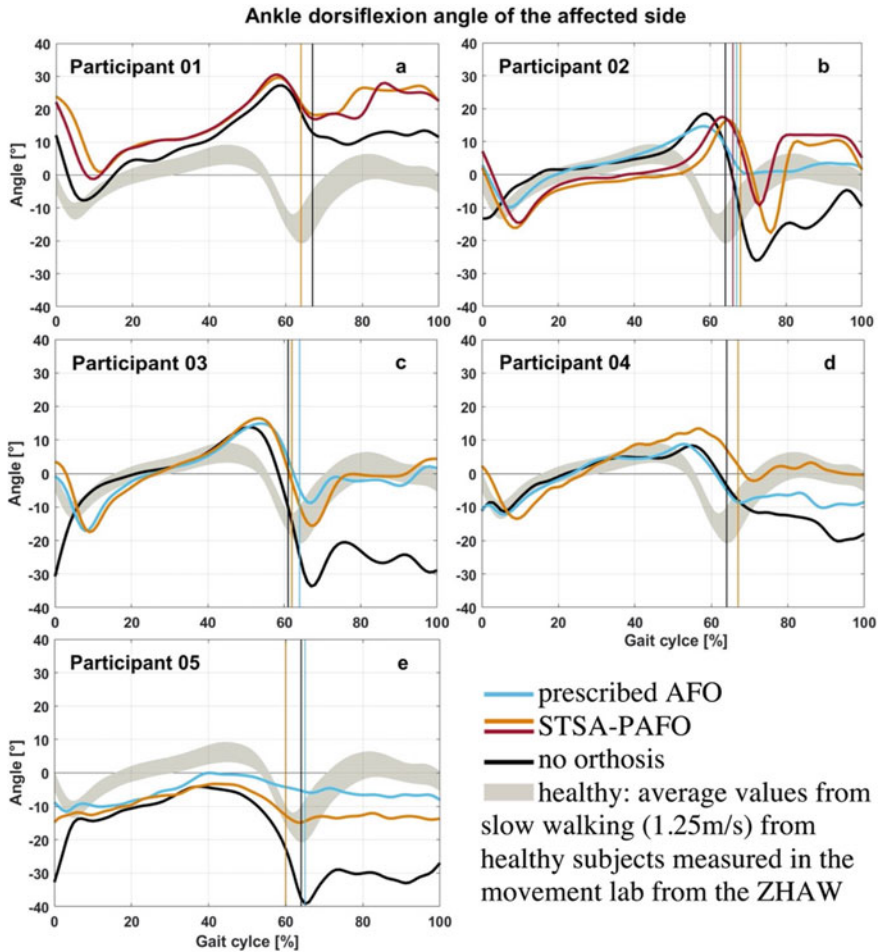




Fig. 2 a–e Ankle dorsiflexion angle for all participants. Note, participants who walked with different STSA-PAFO settings were listed as  STSA-PAFO¹ and  STSA-PAFO². The vertical line indicates the start of the swing phase.

during swing phase when walking with the STSA-PAFO compared to no orthosis shows that the STSA-PAFO works as intended. These findings are comparable to previous work with other PAFOs [9].

Compared to the prescribed AFO, the plantarflexion angles at push-off converged towards the average values measured from healthy subject while walking with the STSA-PAFO in participants 02, 03 and 05. Furthermore, the total ROM during swing phase from participants 02 and 03 converged towards the average values, what indicat that at least for some patients with foot-drop, a STSA-PAFO may be a benefit.

The SUS scores of 4 participants were similar, ranging from 77.5 to 85 points, which indicates acceptable usability [10]. The value 60 from participant 02 can be

interpreted as “not passable” usability [10]. For the early development stage we assess the overall rating of the usability as good.

The idea of the STSA was to reduce the friction between the strings. After the test procedure, the strings still showed high abrasion. We assumed that the main reason was the friction between the strings and the steel in the separator holes (Fig. 1). In further development, the design of the shaft and the separator holes need to be optimized.

Most PAFOS were tested at healthy subjects [2] or give only few information about mean or peak values and no movement diagrams are shown [11]. Our work provides detailed information about movement patterns of people with foot-drop and their reaction to a PAFO.

5 Conclusions

This feasibility study showed that STSA can be used for PAFOs, at least in a laboratory. The PAFO improved the DF values at initial contact in all participants and the ROM of the ankle joint during swing phase in two participants.

References

1. J. Graham, Foot drop: Explaining the causes, characteristics and treatment. *Br. J. Neurosci. Nurs.* **6**, 168–177 (2010)
2. M. Moltedo, et al., Powered ankle-foot orthoses: the effects of the assistance on healthy and impaired users while walking. *J. NeuroEng. Rehabil.* **15** (2018)
3. K.A. Shorter et al., Technologies for powered ankle-foot orthotic systems: possibilities and challenges. *IEEE/ASME Trans. Mechatron.* **18**, 337–347 (2013)
4. D. Popov, I. Gaponov, J. Ryu, A preliminary study on a twisted strings-based elbow exoskeleton, in *2013 World Haptics Conference (WHC)*. Daejeon (IEEE; 2013) [cited 2019 Aug 15], pp. 479–84
5. G. Palli, S. Pirozzi, Optical force sensor for the DEXMART hand twisted string actuation system. *Sens. Transducers* **148**, 6 (2013)
6. R. Müller, M. Hessinger, HF. Schlaak, PP. Pott, Modelling and characterisation of twisted string actuation for usage in active knee orthoses. *IFAC-PapersOnLine* **48**, 207–212 (2015)
7. P. Geitner, L. Krähenbühl, Exoskeleton to prevent foot-drop. ZHAW (2019). <https://doi.org/10.21256/ZHAW-20040>
8. R. List, T. Gülay, M. Stoop, S. Lorenzetti, Kinematics of the trunk and the lower extremities during restricted and unrestricted squats. *J. Strength Conditioning Res.* **27**, 1529–1538 (2013)
9. L.F. Yeung, et al., Design of an exoskeleton ankle robot for robot-assisted gait training of stroke patients, in *2017 International Conference on Rehabilitation Robotics (ICORR)* (IEEE, London), pp. 211–215
10. A. Bangor, P.T. Kortum, J.T. Mille, An empirical evaluation of the system usability scale. *Int. J. Human-Comput. Interact.* **24**, 574–594 (2008)
11. A. Pourghasem et al., The effect of a powered ankle foot orthosis on walking in a stroke subject: a case study. *J. Phys. Ther. Sci.* **28**, 3236–3240 (2016)

Towards a Myoelectric Prosthetic Wrist with Rigid and Compliant Behaviour



P. Capsi-Morales, C. Piazza, G. Grioli, A. Bicchi, and M. G. Catalano

Abstract The simple kinematics of commercial prosthetic wrists limits the individuals in performing a wide range of tasks and restore natural motor functions. We propose a functional prosthesis that improves grasping capabilities through the addition of a simple yet useful 3 DoF myoelectric wrist joint with compliant and rigid properties. Its locking capability enables the adjustment of hand configuration in pre-grasping phases and separates the hand motion from the wrist motion. The proposed wrist, combined with a prosthetic hand, was tested with 8 able-bodied subjects and 1 subject with limb loss. It was compared to a common commercial rotational wrist and to subjects' natural wrist. Results evidence the feasibility of the prototype, improved performance capabilities, and the subjects' first impression about the proposed system. Finally, a prosthesis user tested and compared systems during Activities of Daily Living (ADL).

1 Introduction

The human-machine interface and the mechanical features of robotic devices could limit the performance and development of arms prostheses. The lack of compact and reliable actuators and the difficulties to mimic human prehension capabilities result

*This research has received funding from the European Union's Horizon 2020 Research, ERC programme under the Grant Agreement No.810346 (Natural Bionics). The content of this publication is the sole responsibility of the authors. The European Commission or its services cannot be held responsible for any use that may be made of the information it contains.

P. Capsi-Morales · G. Grioli · A. Bicchi · M. G. Catalano
Istituto Italiano di Tecnologia, Via Morego 30, 16163 Genova, Italy

P. Capsi-Morales (✉) · C. Piazza · A. Bicchi
Centro "E. Piaggio" and Dipartimento di Ingegneria dell'Informazione, University of Pisa, Largo Lucio Lazzarino 1, 56127 Pisa, Italy

C. Piazza
Department of Computer Science, Technical University of Munich (TUM), Boltzmannstr. 3, 85748 Garching, Germany

© The Author(s), under exclusive license to Springer Nature Switzerland AG 2022
D. Torricelli et al. (eds.), *Converging Clinical and Engineering Research on Neurorehabilitation IV*, Biosystems & Biorobotics 28,
https://doi.org/10.1007/978-3-030-70316-5_78

in a reduced set of practicable movements [1]. Prosthesis users are often forced to alter their strategy and perform unnatural compensatory movements to increase their range of motion [2], to apply larger forces on objects and to obtain acceptable levels of smoothness, accuracy and energy efficiency [3]. Compensatory movements increase the discomfort, often resulting in residual limb pain or overuse syndromes [4].

In [5], the authors demonstrate that a single DOF hand with wrist flex/extension allows functions comparable to a highly performing poly-articulated hand without wrist. Moreover, [6] suggests that an adaptive wrist with both compliant and rigid behaviours could benefit the user by alternating between its adaptative capacity for the approach, and stability once the object is grasped.

This work presents a preliminary design of an innovative and compact 3 DOFs prosthetic wrist. The wrist can switch behaviour between two states: compliant and rigid, through the actuation of one motor. Taking advantage from the environment, this prototype enables the setting up of the prosthetic hand orientation during the pre-grasping phase, and the adjustment of its stiffness through sEMG signals. We hypothesize that this design could reduce compensatory movements and facilitate the reach of objects while promoting stability in the transport and holding phases. We study the proposed system and compare it with the most common active wrist - a prono/supination rotator - using time-based metrics and biomechanical measures from 8 able-bodied subjects. Furthermore, one prosthesis user provides a qualitative evaluation during the performance of ADL (see the prototype implemented in a user's socket in Table 1).

2 Materials and Methods

We propose a prosthetic wrist based on a spherical joint that can be friction-locked through the actuation of one motor. Moreover, a compliant stage provides adaptable behaviour when the joint is unlocked. 8 able-bodied subjects evaluated the system functionality versus one of the most common active wrist on the market (a prono/supination joint). Both robotic wrists were connected to the same under-actuated prosthetic hand, called SoftHand Pro (SHP) [7]. The whole system was controlled by two EMG channels, as common sockets for transradial amputees embed. In this case, they correspond to the FDS and EDC muscles. The selection of the actuator to command between the wrist and the hand is based on the velocity of the user's muscle activations through a Finite State Machine and a timer. A fast activation commands the wrist, while a slower activation commands the hand closure. Once wrist control is elicited, while the friction-lockable wrist requires an impulse to lock the joint, the rotational wrist requires continuous muscle activation to select the prono/supination angle. The experimental protocol is based on functional movements related to reaching, grasping and transport. It consists in the grasping and moving action of 3 different objects from 3 shelves at different heights. An Xsens was used to gather subjects' motion and to analyse their body posture. Finally, a survey was

conducted after each wrist type experiment about systems usability and satisfaction. Furthermore, one prosthesis user performed purpose-oriented movements inspired by ADL with the 3 systems, focusing on the reaching phase. While the control system for unimpaired users was their left natural wrist, the prosthesis user used her unimpaired arm (right) during the experiments.

3 Results

Xsens provides the angles between upper subject's body segments. We select 5 different angles to evaluate the level of compensation when executing a task. Moreover, we analyse the time required to perform a task successfully and the frequency of wrists control elicitation usage. All experiments were video recorded to evaluate which DOFs are more used, and depending on which parameter (object or height).

The percentage of active usage and time execution for all able-bodied subjects are presented in Fig. 1. A larger frequency of activation implies a larger desired use of the robotic device. A shorter time implies a faster execution of the task, which is related to an easier use. Figure 1c shows results from the time execution when both prosthetic wrists are actively used. Moreover, an example of a qualitative comparison for the prosthesis user is shown in Table 1.

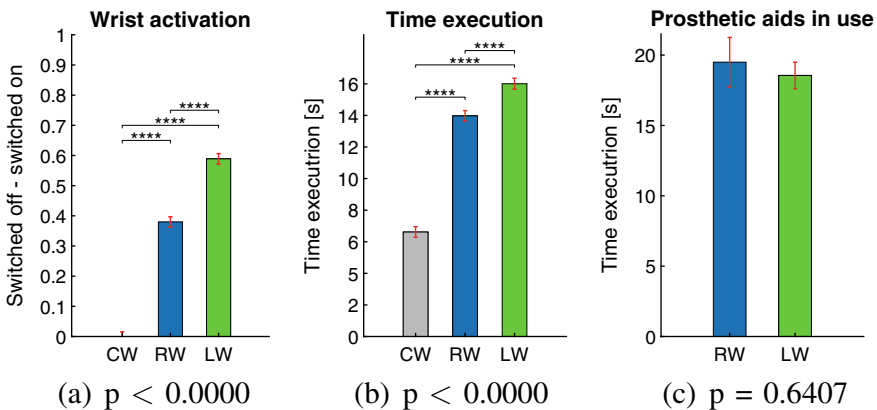
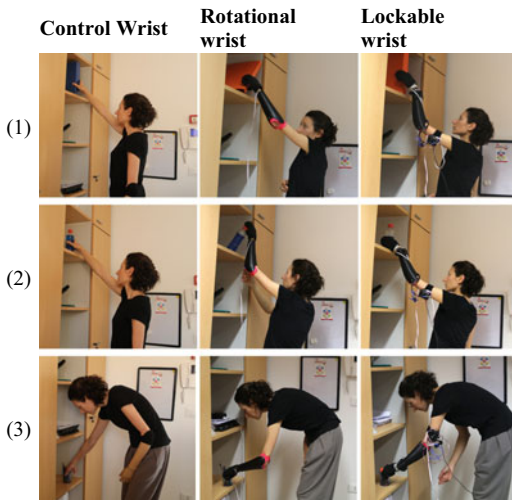


Fig. 1 Frequency of activation (a) and time execution (b) for able-bodied subjects ($n = 8$). Panel (c) shows the time execution when the prosthetic wrists (RW - rotational wrist, LW - lockable wrist) has been voluntarily used for the execution of a task. CW refers to the control wrist. The p-values from a N-way ANOVA test are detailed in their caption. Tukey-kramer test significance is detailed with asterisks in the upper part of each graph with **** for $p \leq 0.0001$. The estimated means for each wrist of study are presented with a bar plot and the red errorbar refers to their standard error

Table 1 ADL: Grasping object from extreme height conditions

4 Discussion

Results from functional tasks proved a significantly larger frequency of active usage of the lockable wrist compared to the rotational wrist. Moreover, although Fig. 1b shows that the lockable wrist is 2 s slower in performance than the rotational, the fact that users voluntarily activate the lockable wrist in 20% more of the occasions could be affecting to the total execution time. Indeed, looking at Fig. 1c, where both robotic aids are voluntarily used, we realize that the lockable wrist use did not compromise the time execution of the overall prosthesis, increasing only the prosthetic arm functionality. Furthermore, users appear to show preference and acceptance of the proposed system, which will be evaluated through surveys results.

Regarding the completion of ADL, Table 1 shows that with the lockable wrist, the user not only presents a more natural body posture, but also a safer grasp is observed in extreme cases, where the stability of the object can be compromised when using the rotational wrist. Overall, ADL results of the lockable wrist suggest a decrease in the time to complete the task (usually related to cognitive load), an increase in intuitiveness and a softer interaction.

5 Conclusions

Results prove the interest of able-bodied subjects in active use of the proposed system. Experiments with the prosthesis user suggest enlarged capabilities to adapt to different requirements. Although a preliminary evaluation of Xsens data seems

to favour the proposed system in presenting a more natural body posture, further analysis of compensatory movements is needed. Future work points towards a more compact and light design with a larger range of motion, and the study of a variable stiffness system, that will allow the user to control the joint level of rigidity with a more intuitive control strategy.

Acknowledgements The authors warmly thank Mattia Poggiani and Andrea Di Basco for their help in the experimental validation and the manufacturing of the system, respectively.

References

1. M. Controzzi, C. Cipriani, M.C. Carrozza, Design of artificial hands: a review, in *The Human Hand as an Inspiration for Robot Hand Development* (Springer, 2014), pp. 219–246
2. Ø. Stavadahl, Optimal wrist prosthesis kinematics: three-dimensional rotation statistics and parameter estimation, Ph.D. dissertation, Institutt for teknisk kybernetikk (2002)
3. E. Todorov, Optimality principles in sensorimotor control. *Nature Neurosci.* **7**(9), 907 (2004)
4. K. Østlie, R.J. Franklin, O.H. Skjeldal, A. Skrondal, P. Magnus, Musculoskeletal pain and overuse syndromes in adult acquired major upper-limb amputees. *Arch. Phys. Med. Rehab.* **92**(12), 1967–1973 (2011)
5. F. Montagnani, M. Controzzi, C. Cipriani, Is it finger or wrist dexterity that is missing in current hand prostheses? *IEEE Trans. Neural Syst. Rehab. Eng.* **23**(4), 600–609 (2015)
6. P.J. Kyberd, The influence of passive wrist joints on the functionality of prosthetic hands. *Prosthetics Orthotics Int.* **36**(1), 33–38 (2012)
7. S.B. Godfrey, K.D. Zhao, A. Theuer, M.G. Catalano, M. Bianchi, R. Breighner, D. Bhaskaran, R. Lennon, G. Grioli, M. Santello et al., The soft-hand pro: functional evaluation of a novel, flexible, and robust myoelectric prosthesis. *PloS One* **13**(10), e0205653 (2018)

Identification of Time-Varying Ankle Joint Impedance During Periodic Torque Experiments Using Kernel-Based Regression



Gaia Cavallo, Christopher P. Cop, M. Sartori, Alfred C. Schouten, and John Lataire

Abstract Joint impedance is a common way of representing human joint dynamics. Since ankle joint impedance varies within the gait cycle, time-varying system identification techniques can be used to estimate it. Commonly, time-varying system identification techniques assume repeatably of joint impedance over cyclic motions, without taking into consideration the inherent variability of human behavior. In this paper, a method that assumes smooth, cyclic joint impedance, yet allows for cycle-to-cycle variability, is proposed. The method was tested on isometric, cyclic experimental data from the ankle under conditions with a time variation comparable to the expected one during the gait cycle. The estimated model could describe the data with high accuracy (VAF of 94.96%) and retrieve realistic inertia, damping and stiffness parameters. The results provide motivation to further apply the method on experiments under dynamic conditions and to employ the proposed method as a tool for investigating the human joint dynamics during cyclic movements.

1 Introduction

The dynamical behavior of a human joint can be described by joint impedance. Joint impedance characterizes how much resistance a joint opposes to an angular perturbation. During locomotion, the joint impedance of the lower limbs' joints is

This work was financially supported by the Research Foundation Flanders (FWO-Vlaanderen, Ph.D. fellowship nr 1182019N), by the Flemish Government (Methusalem Fund METH1) and by ERC Starting Grant INTERACT (803035).

G. Cavallo (✉) · J. Lataire
ELEC Department, Vrije Universiteit Brussel, Brussels, Belgium
e-mail: gaia.cavallo@vub.be

C. P. Cop · M. Sartori · A. C. Schouten
Department of Biomechanical Engineering, University of Twente, Enschede, The Netherlands

A. C. Schouten
Department of Biomechanical Engineering, Delft University of Technology,
Delft, The Netherlands

© The Author(s), under exclusive license to Springer Nature Switzerland AG 2022
D. Torricelli et al. (eds.), *Converging Clinical and Engineering Research*
on *Neurorehabilitation IV*, Biosystems & Biorobotics 28,
https://doi.org/10.1007/978-3-030-70316-5_79

regulated over time by the neuromuscular system. For example, the joint impedance of the ankle is low during the swing phase, and increases during the stance phase to allow for the generation of a net torque for push-off [1]. Knowing how the ankle joint impedance is regulated during locomotion provides important information to design biomimetic wearable devices that can reproduce the function of a healthy ankle joint [1].

Joint impedance can be estimated using system identification techniques, starting from the measurements of an angular perturbation applied to the joint and the resulting joint torque. Since joint impedance changes within the gait cycle, time-varying system identification techniques are required. In literature, system identification techniques that assume repeatably of the joint impedance over cyclic motions have been proposed [2]. This assumption is not in accordance with the inherent variability of human behavior and therefore the identification techniques might lead to biased estimates when applied to human data.

In this article, a kernel-based regression (KBR) method is proposed. A smooth, cyclic behavior of the joint impedance is assumed, yet a cycle-to-cycle variability is allowed. The method is applied to the analysis of isometric experimental data, in which the ankle torque tracks a periodic trajectory, designed to induce a time variation of joint impedance comparable to the expected one during the gait cycle.

2 Method

2.1 Experiment

The experimental data were acquired from one healthy subject. Prior to the experiment, the subject gave written informed consent. The protocol was approved by the ethics board of the University of Twente. The right foot of the subject was attached to the Achilles Rehabilitation Device (MOOG, Nieuw-Vennep, The Netherlands). The apparatus is a one degree of freedom ankle manipulator which can apply angular perturbations to the ankle joint in the sagittal plane [3]. The foot of the subject was firmly attached to the footplate of the manipulator, such that the angle of the manipulator corresponded to the angle of the ankle joint. The angle of the manipulator was controlled. The angular displacement was designed as a 90 s multisine signal (sum of sinusoidal waves) with RMS amplitude 0.015 rad, random phase and excitation frequencies from 0.6 to 20 Hz.

The device measured both the angular displacement and the torque applied by the subject with a sampling frequency of 2048 Hz. The subject was instructed to change the ankle torque to track a predefined desired trajectory, shown in black in Fig. 1a. The desired torque trajectory was periodic within the frequency range of normal human walking and the amplitude was adjusted to be comfortable for the subject and limit muscular fatigue. The subject received visual feedback on the desired torque trajectory and on a low-passed representation the exerted ankle torque. Three trials

were measured, each composed of 45 cycles of the torque trajectory. The signals are considered positive in the dorsiflexion direction.

2.2 System Identification

It is assumed that the measured torque $\tau_m(t)$ is the superposition of voluntary torque $\tau_{\text{ext}}(t)$, i.e. the desired trajectory and uncorrelated with the perturbations, and perturbation-induced torque $\tau_{\text{E}}(t)$, which can be described by an inertia-spring-damper model:

$$\begin{aligned}\tau_m(t) &= \tau_{\text{ext}}(t) + \tau_{\text{E}}(t) \\ &= \tau_{\text{ext}}(t) + I\ddot{\phi}_m(t) + B(t)\dot{\phi}_m(t) + K(t)\phi_m(t)\end{aligned}\quad (1)$$

where $\phi_m(t)$, $\dot{\phi}_m(t)$ and $\ddot{\phi}_m(t)$ are the angular position and its first- and second-order derivatives, respectively, I is the constant (time-invariant) inertia, and $B(t)$ and $K(t)$ the time-varying damping and stiffness. $B(t)$, $K(t)$ and $\tau_{\text{ext}}(t)$ are considered Gaussian processes, whose statistical properties are characterized by a covariance function, called the kernel function. A locally periodic kernel function is selected, which imposes that the variations of the parameters are smooth and have a periodicity of 2 s, with a cycle-to-cycle variability of 20% [5]. The unknown inertia, stiffness, damping and external torque $\hat{\tau}_{\text{ext}}(t)$ are retrieved simultaneously by means of KBR [4, 5], considering the angular position as input and the measured torque as output. The estimate of the measured torque $\hat{\tau}_m(t)$ is consequently computed. The identification is performed in the frequency domain, at bins up to 20 Hz. The accuracy of the estimate is expressed in terms of the variance accounted for (VAF) [5] between $\tau_m(t) - \hat{\tau}_{\text{ext}}(t)$ and $\hat{\tau}_m(t) - \hat{\tau}_{\text{ext}}(t)$.

3 Results

The measured torque is plotted in Fig. 1b, where the abscissa was normalized to represent the measurements with respect to the cycle percentage. The measurements for 15 randomly selected cycles are shown. The estimated external torque $\hat{\tau}_{\text{ext}}(t)$ component is represented in Fig. 1a, where each colored line represents the estimate for one cycle. The estimate resembles the desired torque trajectory and the resulting VAF is of 94.96%. The estimated damping and stiffness are represented in Fig. 1c, d, respectively. For each cycle, the estimated stiffness has a peak value in correspondence to the maximum plantarflexion (around 45% of the cycle), whilst the estimated damping has a peak around 50% of the cycle. The inertia estimate is 0.019 Nms²/rad.

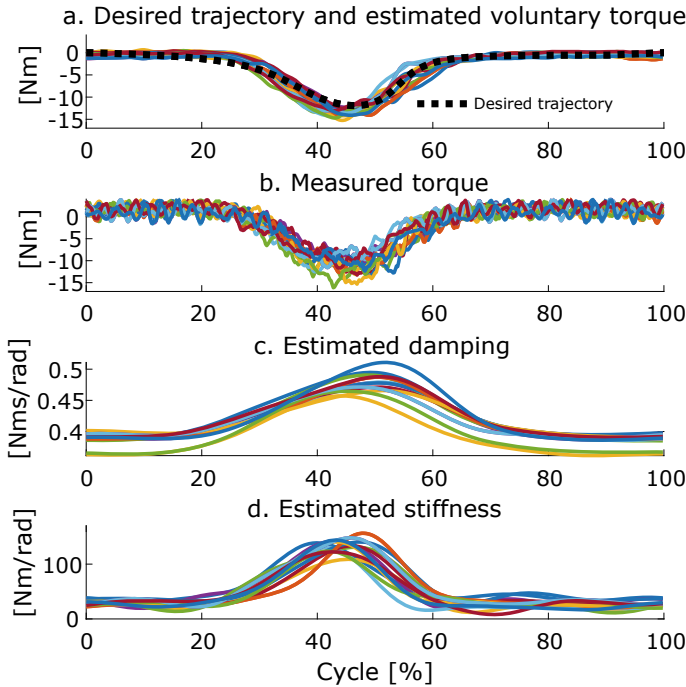


Fig. 1 **a** Desired torque trajectory (dotted black line) and estimated voluntary torque. **b** Measured torque. **c, d** Estimated damping and stiffness. For all the plots, the abscissa is normalized to represent the quantities with respect to the percentage of the cycle (length 2 s), and the quantities are represented for 15 randomly selected cycles of the torque trajectory

4 Discussion

4.1 Estimated parameters

The variability of the subject behavior is observable in Fig. 1b, in which there are cycle-to-cycle differences in the maximum amplitude of the measured torque and the timing of the amplitude peaks. The estimated damping and stiffness parameters present a plausible time-varying behavior in accordance with the measured torque, with peak values in correspondence to the maximum plantarflexion torque for each cycle. The estimated stiffness resembles the estimate obtained in [6]. Future work should be done to provide a physiological interpretation of the parameters, potentially comparing the results with physiological-based models [3].

Accordingly to the experimental conditions, the inertia was set time-invariant. However, the identification method can deal with time-varying inertia.

4.2 Experimental Condition

With the given experimental condition, we wanted to test the proposed identification method on human experiments with a time variation comparable to the expected one during the gait cycle. The high VAF supports the validity of the estimated model. Furthermore, the estimator was previously validated on a simulation study with a comparable time variation [5].

The experiment was performed during isometric conditions, where the time variation of the joint impedance was an artifact of the experimental task. However, the good performance of the method on the presented data provides motivation to continue testing the method on more realistic experimental conditions. Future work should include adjusting the method to be applicable to closed-loop conditions, in order to identify joint impedance during experiments under dynamic conditions, and provide a human-inspired guideline for the design of actuated wearable devices [1].

References

1. H. Dallali, L. Knop et al., Estimating the multivariable human ankle impedance in dorsi-plantarflexion and inversion-eversion directions using EMG signals and artificial neural networks. *Int. J. Intell. Robot Appl.* **1**(1), 19–31 (2017)
2. J.B. MacNeil, R.E. Kearney, I.W. Hunter, Identification of time-varying biological systems from ensemble data (joint dynamics application). *IEEE Trans. Biomed. Eng.* **39**(12), 1213–1225 (1992)
3. C.P. Cop, G. Durandau, et al., Model-based estimation of ankle joint stiffness during dynamic tasks : a validation-based approach (2019), pp. 4104–4107
4. J. Lataire, R. Pintelon et al., Continuous-time linear time-varying system identification with a frequency-domain kernel-based estimator. *IET Control Theory Appl.* **11**(4), 457–465 (2017)
5. G. Cavallo, A.C. Schouten, J. Lataire, Locally periodic kernel-based regression to identify time-varying ankle impedance during locomotion: a simulation study, in *42nd Annual International Conference of the IEEE EMBS (EMBC)*, Montreal, QC, Canada (2020), pp. 4835–4838
6. D.L. Guarin, R.E. Kearney, Identification of intrinsic and reflex ankle stiffness during imposed walking movements with constant muscle activation. **44**(6) (2000)

Robotic Approach to Characterize Ankle Stiffness in Multiple Sclerosis Patients During Standing and Walking



Varun Nalam, Ermytrude Adjei, Joshua Russell, Megan C. Eikenberry, Dean Wingerchuk, and Hyunglae Lee

Abstract This paper presents a pilot study evaluating the effectiveness of a new robotic approach to characterize altered ankle stiffness in multiple sclerosis (MS) population during standing and walking. The approach utilizing a dual-axis robotic platform could accurately quantify ankle stiffness of the pilot MS patient, with reliability as high as that observed in unimpaired individuals. Further, investigation of the quantified ankle stiffness together with sensor measurements of ankle muscle activation and ankle torque enabled understanding of the mechanisms contributing to ankle stiffness modulation. For the pilot MS subject, muscle contracture, weakness, and reduced range of motion were identified as potential contributors to the modulation of ankle stiffness during standing and walking. Upon successful validation of a future study on a larger group of MS patients, this robotic approach is expected to help clinicians better understand a patient's altered ankle mechanics, identify the underlying neuromuscular deficiencies, and prescribe patient-specific rehabilitation exercises.

1 Introduction

Compromised balance during standing and walking is a major consequence of chronic disability in multiple sclerosis (MS) patients [1]. Notably, most MS patients have significant ankle impairments such as weakness, contractures and spasticity [2,

Research supported by ASU/Mayo Clinic Seed Grant.

V. Nalam · E. Adjei · J. Russell · H. Lee (✉)

Fulton Schools of Engineering and Neuromuscular Control and Human Robotics Laboratory,
Arizona State University, Temp, AZ, USA

e-mail: hyunglae.lee@asu.edu

M. C. Eikenberry

Department of Physical Therapy, Northwestern University, Downers Grove, IL, USA

D. Wingerchuk

Department of Neurology, Mayo Clinic Arizona, Scottsdale, AZ, USA

3], which may lead to impairment in lower extremity function. While there has been much effort to characterize altered ankle mechanics following MS, most of the characterizations were limited to subjective clinical examinations during non-functional (e.g., seated) tasks [4]. Little is known about how MS alters ankle mechanics during standing and walking. In this study, we presented a novel robotic approach to characterize ankle mechanics, ran a pilot study with one MS patient, and evaluated its reliability. In particular, we quantified ankle stiffness since it is known to play a dominant role in standing balance and locomotion.

2 Material and Methods

To quantify ankle stiffness during standing balance and walking, we used a dual-axis robotic platform, which can apply kinematic perturbations to the ankle in the sagittal and frontal planes and measure the corresponding ankle torques. The platform was fully validated to accurately quantify 2-dimensional (2D) human ankle stiffness during various postural balance and locomotion tasks [5].

In addition to the robotic platform, a dual-axis goniometer, an electromyography (EMG) system, a visual feedback display, and a safety harness, were used. The goniometer was attached to the foot-shank complex to measure 2D ankle kinematics in the sagittal and frontal planes. To monitor muscle activity throughout the experiment, surface EMG sensors were attached to the belly of four major ankle muscles: tibialis anterior (TA), soleus (SL), medial gastrocnemius (MG), and peroneus longus (PL). Prior to experiments, maximum voluntary contraction (MVC) of each muscle was measured. The visual feedback display, showing center of pressure (COP) of the foot and weight distribution between legs, was used in the standing experiment to aid maintenance of consistent standing posture.

One subject (Age: 67, height: 162.6 cm, weight: 88.6 kg), diagnosed with relapsing remitting MS 4 years prior to the study, participated in the pilot study consisting of standing and walking experiments. The subject was a community ambulator (comfortable walking speed: 0.94 m/s) and exhibited slight spasticity in plantarflexors (Modified Ashworth Scale: 1+). The participant gave informed consent prior to participation and the study was approved by ASU Institutional Review Board (STUDY00008706).

In the standing experiment, the subject was instructed to maintain a consistent upright standing posture (Fig. 1a). Once the target posture was maintained for a randomized time interval of 0.5–2 s, a ramp-and-hold perturbation (amplitude: 3°, duration: 100 ms) was applied to the ankle. In the walking experiment, the subject was instructed to walk on the elevated walkway at a self-selected cadence rate which was ensured by metronome-based audio feedback (Fig. 1b). The same perturbation was applied at 50% of the stance phase. Thirty perturbations were applied in sets of 10 trials in the sagittal and frontal planes for the standing experiment and only in the sagittal plane for the walking experiment.

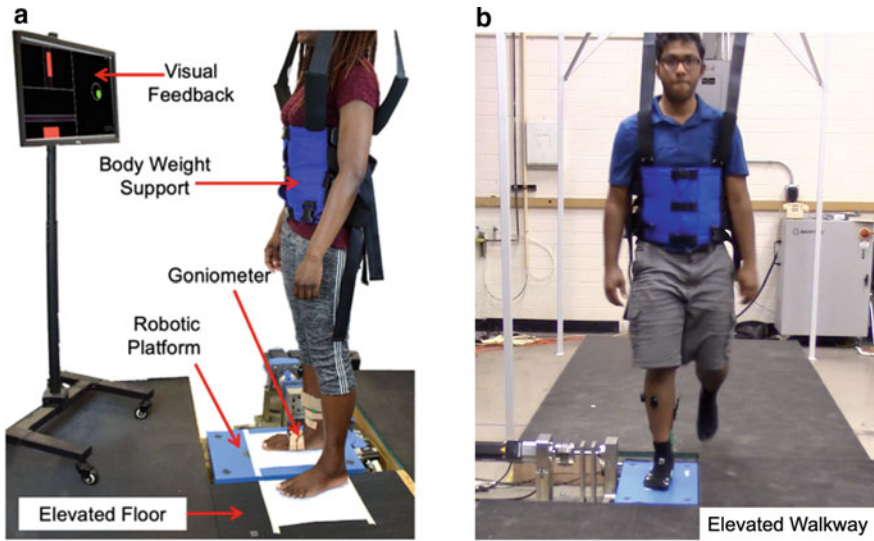


Fig. 1 The experimental setup for **a** standing and **b** walking experiments

Ankle kinematics and ankle torque data were filtered using a 2nd order Butterworth low-pass filter with a cut-off frequency of 20 Hz. In calculating ankle torques, torques due to platform dynamics were first quantified under no loading and subtracted from the measured torques.

Ankle stiffness was quantified by fitting a 2nd order model, consisting of stiffness, damping, and inertia, to the measured ankle kinematics and torques over the perturbation window. To verify the reliability of quantification, the percentage variance accounted for (%VAF) between the measured ankle torque and the estimated ankle torque from the best fit model was calculated. Further, EMG amplitude and COP data were averaged over 25 ms prior to the onset of perturbation. Of note, COP displacement is highly correlated with ankle torque and thus it is an indirect measure of ankle torque [6].

Results of the pilot MS subject were compared with results of 10 young unimpaired individuals (controls) reported in our previous study [6].

3 Results

The high %VAF (greater than 98.7% in all experiments) confirmed the reliability of the robotic approach to accurately quantify ankle stiffness in the tested MS patient (Table 1).

In the standing experiment, ankle stiffness in the sagittal plane (270.3 Nm/rad) was almost twice that of controls (143.3 (standard deviation: 41.4) Nm/rad). Ankle

Table 1 Comparison of ankle stiffness, EMG amplitude, and COP between the pilot MS subject and unimpaired individuals

		Stiffness (Nm/rad)	%VAF	TA (% MVC)	PL (% MVC)	SL (% MVC)	MG (% MVC)	COP (cm)
Standing sagittal	MS subject	270.3	99.8	2.8	13.6	13.9	12.1	-0.31
	Unimpaired	143.3	99.0	3.0	5.4	8.1	6.0	-0.02
Standing frontal	MS subject	82.8	98.7	2.8	9.7	9.9	12.6	0.59
	Unimpaired	29.2	96.1	2.8	4.8	7.4	5.9	0.01
Walking 50% stance	MS subject	284.4	99.4	7.6	35.7	49.2	43.2	3.5
	Unimpaired	319.4	99.1	4.9	20.2	14.5	37.4	8.6

stiffness in the frontal plane (82.8 Nm/rad) was also substantially higher than that of controls (29.2 (10.1) Nm/rad). However, this significant difference cannot be explained by differences in the muscle activation or COP.

In the walking experiment, ankle stiffness of the MS subject (284.4 Nm/rad) was comparable to that of controls (319.4 (82.1) Nm/rad). It is important to note that activation of plantarflexors of the MS subject was much higher than that of controls, in particular SL (49.2 vs. 14.5 (7.4) %MVC). However, even with high muscle activation, COP (i.e., ankle torque) of the MS subject (3.5 cm) was significantly lower than that of controls (8.6 (2.8) cm).

4 Discussion and Conclusion

This pilot study confirmed that the robotic approach, which integrates the dual-axis robotic platform and the system identification method, can accurately characterize altered ankle stiffness following MS. The reliability of the robotic characterization for the pilot MS patient, quantified by %VAF, was as high as that observed in unimpaired individuals. To the best of our knowledge, this is the first ever study to directly quantify the MS patient's ankle stiffness during standing and walking.

In this study, the pilot MS subject exhibited significantly higher ankle stiffness in both the sagittal and frontal planes during quiet standing, which cannot be fully explained by the increase in muscle activation and COP levels compared to those in unimpaired controls. This result may be due to stiffened passive tissue and/or muscle contracture due to MS.

During walking, even with high muscle activation in plantarflexors, ankle torque was significantly lower than that observed in unimpaired walking, evidenced by significantly low COP displacement. It can be inferred that plantarflexor activation was not properly transferred to ankle torque generation in the stance phase of walking, possibly due to muscle weakness and a reduced range of motion of the ankle. Low expected ankle stiffness due to low ankle torque generation was offset by high ankle

stiffness observed in the standing task, resulting in the overall ankle stiffness of this subject being comparable to that of controls during walking.

While results of this pilot study suggest the potential of the presented robotic approach to quantify altered ankle mechanics and to understand neuromuscular mechanisms contributing to the alteration, a future validation study on a larger group of MS patients is necessary to fully validate the presented robotic approach. Upon successful validation, this robotic approach will help clinicians better identify the nature of a patient's particular neuromuscular deficiencies and allow them to prescribe patient-specific rehabilitation exercises.

References

1. S.H. Corporaal, H. Gensicke, J. Kuhle, L. Kappos, J.H. Allum, O. Yaldizli, Balance control in multiple sclerosis: correlations of trunk sway during stance and gait tests with disease severity. *Gait Posture* **37**(1), 55–60 (2013)
2. P.D. Hoang, S.C. Gandevia, R.D. Herbert, Prevalence of joint contractures and muscle weakness in people with multiple sclerosis. *Disabil. Rehabil.* **36**(19), 1588–1593 (2014)
3. M.P. Barnes, R.M. Kent, J.K. Semlyen, K.M. McMullen, Spasticity in multiple sclerosis. *Neurorehabil. Neural Repair* **17**(1), 66–70 (2003)
4. T. Sinkjaer, E. Toft, K. Larsen, S. Andreassen, H.J. Hansen, Nonreflex and reflex mediated ankle joint stiffness in multiple-sclerosis patients with spasticity. *Muscle Nerve* **16**(1), 69–76 (1993)
5. V. Nalam, H. Lee, Development of a two-axis robotic platform for the characterization of two-dimensional ankle mechanics. *IEEE/ASME Trans. Mechatron.* (2019)
6. V. Nalam, *Characterization of 2D Human Ankle Stiffness during Postural Balance and Walking for Robot-Aided Ankle Rehabilitation*. PhD, Mechanical Engineering, Arizona State University, PhD Thesis, 2020

A Muscle Model Incorporating Fiber Architecture Features for the Estimation of Joint Stiffness During Dynamic Movement



Christopher P. Cop, Alfred C. Schouten, Bart F. J. M. Koopman,
and M. Sartori

Abstract Quantifying human joint stiffness *in vivo* during movement remains challenging. Well established stiffness estimation methods include system identification and the notion of quasi-stiffness, with experimental and conceptual limitations, respectively. Joint stiffness computation via biomechanical models is an emerging solution to overcome such limitations. However, these models make assumptions that hamper their generalization across muscle architectures. Here we present a stiffness formulation that considers the muscle's pennation angle, and its comparison to a simpler formulation that does not. Model-based stiffness estimates are evaluated against joint-perturbation-based system identification. Results on muscles with different pennation angle show that our formulation seamlessly adjusts the muscle-tendon units' stiffness depending on their architecture. At the joint level, our new model improved the stiffness estimations. Our study's relevance is the creation and validation of a modeling formulation that does not require joint perturbation. This will enable better estimations and understanding of stiffness properties and human movement.

1 Introduction

JOINT stiffness is a biomechanical property that dictates how human limbs interact with the environment. The mechanisms the neuromuscular system uses to modulate it and to provide stability in response to perturbations are not understood yet. Hence, over the last decades there has been a growing interest to quantify human *in vivo* joint stiffness.

This work has been funded by ERC Starting Grant INTERACT (803035).

C. P. Cop (✉) · A. C. Schouten · B. F. J. M. Koopman · M. Sartori
Department of Biomechanical Engineering, University of Twente, Twente, The Netherlands
e-mail: c.p.cop@utwente.nl

A. C. Schouten
Department of Biomechanical Engineering, Delft University of Technology,
Delft, The Netherlands

© The Author(s), under exclusive license to Springer Nature Switzerland AG 2022
D. Torricelli et al. (eds.), *Converging Clinical and Engineering Research
on Neurorehabilitation IV*, Biosystems & Biorobotics 28,
https://doi.org/10.1007/978-3-030-70316-5_81

507

Joint stiffness has been mostly studied via system identification (Sys. Id.) techniques or using a surrogate concept, i.e. quasi-stiffness. Despite their numerous advantages, both methodologies entail major limitations. On the one hand, Sys. Id. requires an experimental setup in which the joint is externally perturbed. This makes it an undesirable method to study natural movements. On the other hand, quasi-stiffness does not solely represent the position-dependent component of joint impedance, i.e. joint stiffness, as quasi-stiffness also includes velocity- and activation-dependent components.

To overcome these limitations, we propose a stiffness formulation based on biomechanical modeling to estimate joint stiffness in static and dynamic tasks [1]. The idea is to compute joint stiffness by estimating and projecting the stiffness of its constituting elements. However, assumptions and simplifications are often required to model such elements, e.g. the muscle's pennation angle is not considered in the stiffness computation.

In this work we present a joint stiffness model formulation that considers the pennation angle of the modeled muscle-tendon units (MTUs). Moreover, we show the effect of including the pennation angle in the computation of MTU stiffness in muscles with different pennation angle. Lastly, we compare the performance of our new formulation to a simpler model that does not take the pennation angle into account in the stiffness computation. Remarkably, model-based stiffness estimates are directly compared to perturbation-based time-varying system identification values derived from the same subjects and motor tasks. This provides a thorough validation means for our proposed methodology.

2 Methods

2.1 Data Collection

Data from five healthy young subjects (age: 24.2 ± 1.0 years; height: 1.78 ± 0.06 m; weight: 70.0 ± 5.4 kg) were used in this study. Ethical approval was granted by the Ethics Committee of the University of Twente and the participants gave written informed consent.

The subjects' right foot was attached to an admittance controlled dynamometer. The ankle's angle and torque were measured in dynamic movement trials in which the subject tracked a sinusoidal plantar-dorsi flexion angle target (amplitude: 0.15 rad, frequency: 0.6 Hz). Position perturbations, with an amplitude of 0.03 rad and a switching time of 0.15 s, were applied to the ankle in a pseudo-random manner. Electromyography (EMG) signals from five lower leg muscles were acquired: soleus, gastrocnemius lateralis/medialis, peroneus, and tibialis anterior. More details in [2].

2.2 Joint Stiffness Models

The EMG-driven musculoskeletal model shown in [1] was adapted to compute the subject's right ankle stiffness. First, a generic model was calibrated to obtain subject-specific MTU parameters. Then, the ankle joint stiffness (K^J) was computed from the stiffness of its constituting MTUs:

$$K^J = \sum_{i=1}^{\#mtu} (K_i^{mtu} \cdot r_i^2 - \frac{\partial r_i}{\partial \theta^A} \cdot F_i) \quad (1)$$

where F_i , r_i and K_i^{mtu} represent the force, moment arm and stiffness, respectively, of the i th MTU spanning the plantar-dorsi flexion degree of freedom of the ankle, and θ^A is the ankle angle in the saggital plane.

MTU stiffness, K^{mtu} , equals the tendon stiffness, K^t , in series with the equivalent muscle fiber stiffness along the tendon's line of action, K_{eq}^m , i.e. $K^{mtu} = (K^{t^{-1}} + K_{eq}^{m^{-1}})^{-1}$

Based on the work presented in [3], the equivalent stiffness of a muscle along the tendon's line of action is:

$$\begin{aligned} K_{eq}^m &= \frac{dF_{eq}^m}{dl_{eq}^m} = \frac{d}{dl_{eq}^m} (F^m \cos \alpha) = \frac{d}{dl_{eq}^m} \left(F^m \frac{l_{eq}^m}{l^m} \right) = \dots \\ &\dots = \frac{dF^m}{dl^m} \cos^2 \alpha + \frac{F^m}{l^m} \sin^2 \alpha \end{aligned} \quad (2)$$

where F_{eq}^m and l_{eq}^m are the force and length, respectively, of the muscle fiber along the direction of the tendon's line of action, F^m and l^m are the force and length, respectively, of the muscle fiber along its axis, and α represents the muscle fiber's pennation angle. All aforementioned parameters are estimated by the EMG-driven musculoskeletal model.

Two different models were used in this study: the model described in (1) and (2) that takes the pennation angle into account, i.e. model A, and a simpler model, as presented in [1], that does not account for pennation angle in the stiffness computation and thus considers $K_{eq}^m = \frac{dF^m}{dl^m}$, i.e. model B.

2.3 Data Analysis

Reference joint stiffness values were obtained using a closed-loop ensemble-based time-varying Sys. Id. method extensively described in [4].

At the MTU level, we quantified the difference in magnitude between models A and B by computing their root mean squared error normalized by the maximum

stiffness value (nRMSE) for two MTUs with different pennation angle at optimal fiber length: the tibialis anterior ($\alpha \approx 5^\circ$), and the soleus ($\alpha \approx 25^\circ$).

At the joint level, the results obtained with models A and B were compared to the reference, both in magnitude and in shape, using the root mean squared error (RMSE) and the coefficient of determination (R^2), respectively.

3 Results

We show stiffness estimations at the MTU level for a single subject (Fig. 1a), and at the joint level for the average across all five subjects (Fig. 1b).

At the MTU level, the nRMSEs for the soleus and the tibialis anterior were 0.03 and 0.004, respectively (Fig. 1a).

At the joint level, the stiffness estimations of models A and B were compared to the reference (Fig. 1b). For the average across all five subjects, the R^2 and RMSE values were 0.56 and 3.48 N·m/rad, respectively, for model A, and 0.47 and 4.68 N·m/rad, respectively, for model B.

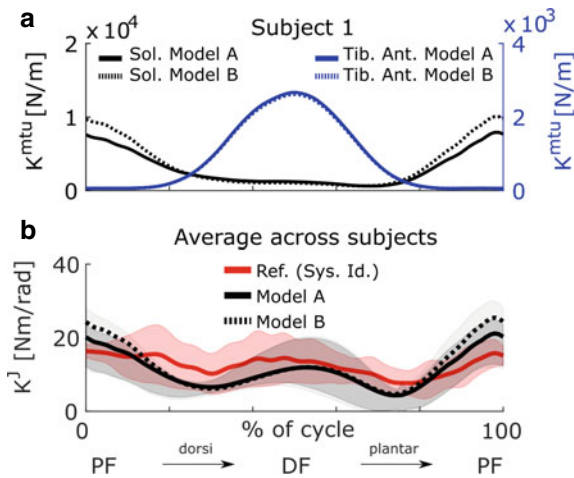


Fig. 1 **a** MTU stiffness of the soleus (black) and the tibialis anterior (blue) muscles computed by models A (solid lines) and B (dotted lines). Note that this plot has two axes of ordinates: one corresponding to the soleus (left) and one corresponding to the tibialis anterior (right). **b** Joint stiffness estimates averaged across all five subjects of model A (solid line), model B (dotted line), and the reference stiffness estimate obtained via system identification (red). The shaded area corresponds to the standard deviation

4 Discussion

To the best of our knowledge this work shows, for the first time, a joint stiffness model that considers pennation angle (i.e. model A) and is directly validated against Sys. Id..

We demonstrate that our proposed joint stiffness formulation can capture multiple muscle architectures simultaneously (Fig. 1a), and seamlessly adjust the equivalent muscle fiber stiffness according to time-varying changing pennation angle (2).

Figure 1b shows how model A improved joint stiffness estimation compared to model B. Interestingly, in the proximity of the dorsiflexion peak of the task (around 50% of the cycle), models A and B compute a similar joint stiffness profile, because most of the dorsiflexion stiffness comes from the tibialis anterior, i.e. a muscle with small α (2).

The largest discrepancy of models A and B is found around the task's plantarflexion peak (around 0 and 100% of the cycle), because the calf muscles, which are usually pennated, contribute to the joint's plantarflexion stiffness (2).

Our results indicate that including the pennation angle in the joint stiffness computation enables better estimations within the plantar-dorsi flexion cycle. This may have implications for the estimation of stiffness during more advanced motor tasks involving complex interplay between pennated and fusiform muscles, e.g. locomotion, stair climbing, etc.

5 Conclusion

Here we presented the first results of an EMG-driven joint stiffness model that takes pennation angle into account and is directly validated. Despite their preliminary nature, our results seem to indicate that including more information on muscle architecture has an impact on joint stiffness estimation and generalization. This will bring us one step further in the understanding of movement neuromechanics.

References

1. M. Sartori, M. Maculan, C. Pizzolato, M. Reggiani, D. Farina, Modeling and simulating the neuromuscular mechanisms regulating ankle and knee joint stiffness during human locomotion. *J. Neurophys.* **114**(4), 2509–2527 (2015)
2. C.P. Cop, Model-based estimation of ankle joint stiffness during dynamic tasks: a validation-based approach, in *41st Annual International Conference of the IEEE Engineering in Medicine and Biology Society (EMBC)*, vol. 2019, Berlin, Germany (2019), pp. 4104–4107
3. T. Jenkins, M. Bryant, Pennate actuators: force, contraction and stiffness. *Bioinspiration Biomim.* **15**(4), 046005 (2020)
4. Moya-Esteban A, Estimation of time-varying ankle joint stiffness under dynamic conditions via system identification techniques, in *41st Annual International Conference of the IEEE Engineering in Medicine and Biology Society (EMBC)*, vol. 2019, Berlin, Germany (2019), pp. 2119–2122

Quantifying Joint Stiffness During Movement: A Quantitative Comparison of Time-Varying System Identification Methods



Mark van de Ruit, Winfred Mugge, and Alfred C. Schouten

Abstract Careful control of joint impedance, or dynamic joint stiffness, is crucial for successful performance of movement. Time-varying system identification (TV-SysID) enables quantification of joint impedance during movement. Several TV-SysID methods exist, but have never been systematically compared. Here, we simulate time-varying joint behavior and propose three performance metrics that enable to quantify and compare TV-SysID methods. Time-varying joint stiffness is simulated using a square wave and subsequently estimated with three TV-SysID methods: the ensemble, short data segment, and basis impulse response function method. These methods were compared based on (1) bias with respect to the simulated joint stiffness, (2) random error across 100 simulation trials, and (3) maximum adaptation speed in joint stiffness that can be captured. This approach revealed that each TV-SysID method has its own unique properties. The simulation method and performance metrics pave the way for developing a framework to quantify the strengths and weaknesses of TV-SysID algorithms for estimating joint impedance.

1 Introduction

Joint impedance is a dynamical property of our neuromuscular system that describes the relationship between joint displacement and restoring torque. Joint impedance

This work is part of the talent programme VENI with project number 17351, which is financed by the Dutch Research Council (NWO).

M. van de Ruit (✉) · W. Mugge · A. C. Schouten
Laboratory for Neuromechanics & Motor Control, Department of Biomechanical Engineering,
Delft University of Technology, 2628CD Delft, The Netherlands
e-mail: m.l.vanderuit-1@tudelft.nl

W. Mugge
e-mail: w.mugge@tudelft.nl

A. C. Schouten
e-mail: a.c.schouten@tudelft.nl

is determined by the inertial, viscous, and elastic properties of a joint [1]. Improper control of joint impedance during movement has been associated with movement disorders such as seen after stroke or in people with Parkinson’s Disease [2, 3]. Knowledge on joint impedance is not only important for better understanding of impairments of motor control, but is also crucial for providing intuitive exoskeletons, development of active biomimetic prosthetics and design of haptic robots that ecologically interact with humans. The challenge is to accurately identify joint impedance during movement.

Human joint impedance, specifically joint damping and joint stiffness, have been demonstrated to change with joint torque, joint angle, and muscle activation level, thereby varying tremendously throughout a movement [4, 5]. Time-varying system identification (TV-SysID) enables the identification of changing joint properties over time. Thirty years of research have seen development of various TV-SysID methods that are specifically suited for application to data recorded from human joints [e.g. 6–8]. TV-SysID algorithms hugely differ with respect to a priori assumptions, amount of data required and speed of time-varying behavior that can be captured. Yet, we lack means to systematically compare performance of TV-SysID methods and quantify their key properties. Here, we use a simulation of time-varying joint behavior and three quantification metrics to construct a framework for systematic comparison of TV-SysID methods for the identification of joint impedance.

2 Methods

2.1 Simulation Study

Time-varying joint stiffness was simulated using a model of human joint dynamics. A simple time-varying 2nd-order mass-spring-damper model $H_{joint}(s)$ can describe the dynamics of a joint when only small rotations are applied:

$$H_{joint}(s, t) = I(t)s^2 + b(t)s + k(t) \quad (1)$$

in which s is the Laplace variable and equals $j2\pi f$ (f represents the frequency). $H_{joint}(s, t)$ represents the intrinsic joint dynamics where I is the limb inertia, b the joint viscosity and k the joint stiffness.

An anti-causal open-loop model was implemented in MATLAB 2019b—Simulink 9.7 (The MathWorks, Inc., Natick, Massachusetts, United States) as:

$$y(t) = H_{joint}(s, t)u(t) + v(t) \quad (2)$$

where $u(t)$ is the angular input perturbation signal, $y(t)$ the measured output torque and $v(t)$ is the measurement noise (Fig. 1). Measurement noise $v(t)$ was added as

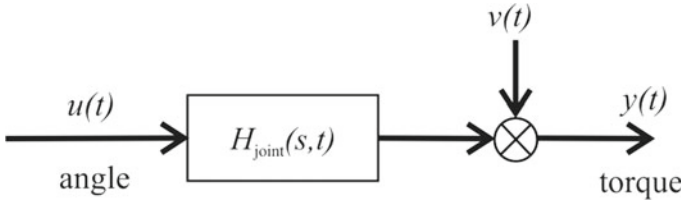


Fig. 1 The simulation model used with $H_{joint}(s,t)$ representing the time-varying joint dynamics, $u(t)$ the angular perturbation input signal, $y(t)$ the measured output torque and $v(t)$ the measurement noise

a 40 Hz low-pass filtered (4th-order Butterworth) normally distributed noise and scaled such to achieve a signal-to-noise ratio (SNR) of 10 dB.

The limb inertia (I) and joint viscosity (b) in the model were taken as 0.02 kgm^2 and 2.2 Nms/rad respectively, to represent the human ankle joint, and considered time-invariant. Joint stiffness (k) was considered time-varying, following a 0.5 Hz square wave, transitioning between 50 and 150 Nm/rad.

The model's perturbation input $u(t)$ was a 5 Hz low-pass filtered (2nd-order Butterworth) noise signal.

Each simulation trial lasted 150 s and was repeated 100 times with a new random input and noise realization ($f_s = 1000 \text{ Hz}$).

2.2 Data Analysis

The data from the simulations were analyzed using three TV-SysID methods:

- Ensemble Impulse Response Function (eIRF) [6]: Assumes time-invariant system dynamics at each time point across the realizations, i.e., the ensemble. Therefore, uses time-invariant system identification at each time point to construct a time-varying impulse response function (TV-IRF).
- Short Data Segments (SDS) [8]: Extension of eIRF in which local time-invariant dynamics is not only assumed across realizations but also across a short time window, resulting in the need for less data.
- Basis impulse response function (bIRF) [7]: Extension of eIRF where the TV-IRFs are approximated by a linear combination of cubic B-splines basis functions. This method assumes system parameters to vary smoothly with time.

Three metrics were used to assess the quality of the estimate of time-varying joint stiffness. First, the bias error describes the estimation error with respect to the simulated simulation joint stiffness:

$$e_B = \sqrt{\frac{\Delta t}{T} \sum_{i=1}^{T/\Delta t} \left(\widehat{K}_i(i\Delta t) - K_i(i\Delta t) \right)^2}, \tag{3}$$

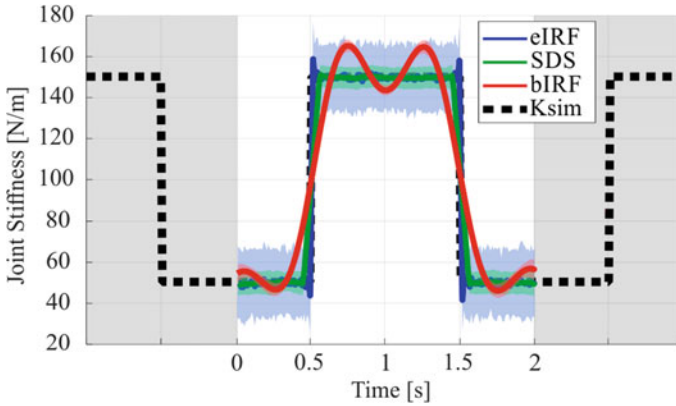


Fig. 2 Simulated and estimated joint stiffness. Data was segmented in 2 s periods and aligned before estimation by the eIRF, SDS and bIRF TV-SysID methods (mean $\pm 2 * S.D.$ of 100 trials—solid line and shaded area). The simulated time-varying joint stiffness (Ksim—dashed line) is added for reference

where $K(t)$ the simulated stiffness and $\widehat{K}(t)$ the mean estimated stiffness across all simulated trials. Second, the random error quantifies the variance of the estimate across simulation trials (noise sensitivity):

$$e_R = \sqrt{\frac{\Delta t}{S \Delta T} \sum_{i=1}^{T/\Delta t} \sum_{s=1}^S \left(\widehat{K}_i(i \Delta t, s) - \widehat{K}_i(i \Delta t) \right)^2}, \tag{4}$$

where $\widehat{K}(t, s)$ is the stiffness estimated at timepoint t for simulation trial s . Third, the slope, quantified by taking the maximum of the numerical derivative of estimated joint stiffness, provides a measure of the maximum speed in adaptation that can be captured.

3 Results

Figure 2 shows the estimated joint stiffness using all three TV-SysID methods. Bias error, random error and slope associated with these estimates of joint stiffness are summarized in Fig. 3. eIRF accurately captures simulated joint stiffness including the instantaneous change but does so with high variance. In contrast, SDS and bIRF provide an estimate with lower variance, but greater bias and flatter transition slopes.

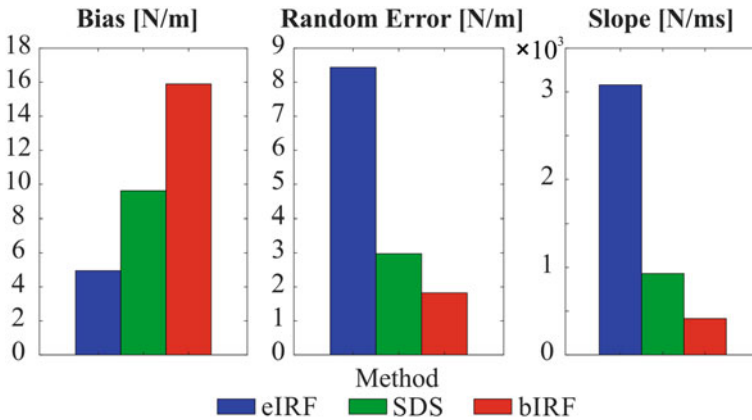


Fig. 3 Estimation performance for the eIRF, SDS and bIRF method

4 Conclusion

The results demonstrate the unique properties for each TV-SysID method. The presented simulation method and performance metrics enable researchers to systematically investigate the strengths and weaknesses of their newly developed algorithms or make a justified choice which TV-SysID method to use depending on their application. Further work will have to elucidate the effect of e.g. including time-varying joint damping, different noise types, different SNRs and different amounts of data, but also demonstrate the methods applicability on experimental data. Our work will be used to develop a framework for comparison of TV-SysID methods for the identification of human joint impedance.

References

1. R.E. Kearney, I.W. Hunter, System identification of human joint dynamics. *Crit. Rev. Biomed. Eng.* **18**, 55–87 (1990)
2. C.G. Meskers et al., Muscle weakness and lack of reflex gain adaptation predominate during post-stroke posture control of the wrist. *J. Neuroeng. Rehabil.* **6**, 29 (2009)
3. R. Xia, M. Radovic, A.J. Threlkeld, Z. Mao, Z., System identification and modeling approach to characterizing rigidity in Parkinson’s disease: neural and non-neural contributions, in *4th International Conference on Bioinformatics and Biomedical Engineering* (2010)
4. I.W. Hunter, R.E. Kearney, Dynamics of human ankle stiffness: variation with mean ankle torque. *J. Biomech.* **15**, 747–752 (1982)
5. M.M. Mirbagheri, H. Barbeau, R.E. Kearney, Intrinsic and reflex contributions to human ankle stiffness: variation with activation level and position. *Exp. Brain Res.* **135**, 423–436 (2000)
6. J.B. MacNeil, R.E. Kearney, I.W. Hunter, Identification of time-varying biological systems from ensemble data. *IEEE Trans. Biomed. Eng.* **39**, 1213–1225 (1992)
7. D.L. Guarin, R.E. Kearney, Estimation of time-varying, intrinsic and reflex dynamic joint stiffness during movement. *Appl. Ankle Joint Front Comput. Neurosci.* **11**, 51 (2017)

8. D. Ludvig, E.J. Perreault, System identification of physiological systems using short data segments. *IEEE Trans. Biomed. Eng.* **59**, 3541–3549 (2012)

Inhibition of Knee Sensory Receptors Alters Quadriceps Muscle Coordination in the Rat



Cristiano Alessandro and Matthew C Tresch

Abstract Internal joint structures such as ligaments are rich with sensory receptors. How the central nervous system (CNS) uses the information provided by these receptors to modify motor commands or guide rehabilitation is still poorly understood. Here, we provide evidence that the sensory afferents originating from the receptors within the knee capsule affect the coordination of the quadriceps muscles in the rat. This result suggests the existence of control loops driven by these receptors. Lesions to internal joint structures should therefore not solely be considered as musculoskeletal injuries, but more broadly as neuromuscular injuries.

1 Introduction

Damage to internal joint structures, such as ligament ruptures and meniscal tears, are often considered pure musculoskeletal injuries. Typical treatments for these conditions aim at restoring joint biomechanics and muscle strength by surgical reconstruction and rehabilitation. However, internal joint structures are not only mechanical stabilizers; they also provide the central nervous system (CNS) with useful information about the movements of the limbs and the state of the joints (e.g. signaling

Research supported by NIH, Grant Number NS086973 (MCT).

C. Alessandro (✉) · M. C. Tresch
Northwestern University, Chicago, IL, USA
e-mail: cristiano.alessandro@unimib.it

M. C. Tresch
e-mail: m-tresch@northwestern.edu

C. Alessandro
University of Milano-Bicocca, Milan, Italy

University of Pavia, Pavia, Italy

M. C. Tresch
Shirley Ryan AbilityLab, Chicago, IL, USA

potentially aberrant joint loading) thanks to the many sensory receptors within their tissues [1]. From this perspective, lesions to the musculoskeletal system might be considered more broadly as neuromuscular injuries.

While the existence of sensory receptors within joint structures is well-known, how joint sensory afferents are used by the CNS to generate motor commands is still unclear [2]. One possibility is that joint afferents are involved in control loops that influence muscle activity on a fast time scale. We evaluate this hypothesis here by comparing quadriceps muscle activity in rats during locomotion before and after injection of lidocaine (a local anesthetic) into the knee capsule. This injection will temporarily inhibit knee joint receptors; hence, acute changes of muscle activity following this manipulation would suggest the existence of fast control loops driven by these receptors. We characterize changes both in the activity of individual muscles and in the coordinated activity of pairs of muscles, assessing potential neuromechanical couplings mediated by joint sensory afferents. We compare the effect of lidocaine to that of a sham injection that does not affect joint sensory afferents.

2 Materials and Methods

We performed experiments on adult female Sprague Dawley rats ($n = 12$). All procedures were approved by the Animal Care Committee of Northwestern University.

2.1 *Experimental Protocol*

Bipolar electromyographic (EMG) electrodes were implanted in quadriceps muscles (vastus medialis, VM; vastus lateralis, VL; vastus intermedius, VI; rectus femoris, RF) as previously described [3]. EMG signals were recorded during at least 2 min of treadmill locomotion at 15 m/min, before (baseline) and 20 min after injection of 0.05 ml of lidocaine into the knee capsule. On a different day, the same experiment was repeated with a sham injection for control; i.e. a needle was inserted into the knee capsule without injecting any anesthetic. This sham controls for any effects due to the injection procedures or to the time for re-testing locomotor behavior. Differently from the lidocaine injection, this sham control does not stretch the tissues due to the absence of fluid injected into the knee capsule. However, the local anesthesia from lidocaine should suppress any neural activity caused by this distension. The order of these experiments was randomized. We verified in acute experiments (not shown) that the lidocaine injection silences joint sensory afferents without affecting muscle function.

2.2 Data Analyses

Rectified EMGs were segmented into separate time-normalized strides, and binned to obtain the EMG envelopes. To estimate the activation intensity of each muscle, the EMG envelopes were integrated across the stance phase of locomotion for each stride. To assess the influence of joint sensory afferents on the activity of individual muscles, we compared the stride-averaged activation intensity of each muscle before and after injection of lidocaine. To evaluate the role of joint sensory afferents in muscle coordination, we calculated the Pearson correlation between the activation intensities of each pair of muscles as a measure of muscle covariation [3], and compared the correlation coefficients obtained before and after the injection.

2.3 Statistics

Muscle intensities were log-transformed, and correlation coefficients were Fisher-transformed to obtain symmetric distributions. We fit Linear Mixed Effect Models to the stride-averaged intensities of each muscle, and to the correlation coefficients of each muscle-pair, using time-to-injection (before, after), injection type (lidocaine, sham) and their interactions as fixed effects, and animal identifier as random effect. Bonferroni-corrected post-hoc tests were used to compare the independent variables obtained before and after injection, for both lidocaine and sham.

3 Results

Figure 1a depicts the group-averaged EMG envelopes of the quadriceps muscles across the gait cycle, before and after lidocaine injection. The activation intensity

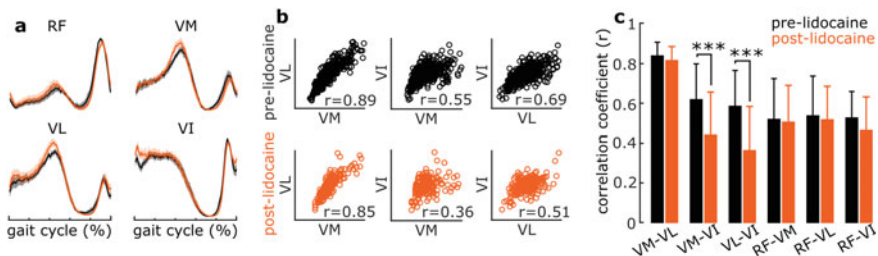


Fig. 1 **a** EMG envelopes of the quadriceps muscles along the gait cycle, before (black) and after (orange) injection of lidocaine (mean±standard error across animals, $N = 12$). **b** Covariation of the vasti muscles activation intensities for a representative animal (each circle represents a stride), and corresponding correlation coefficients (r). **c** Correlation coefficients of each pair of quadriceps muscles (mean ± standard deviations across animals, $N = 12$). *** $p < 0.001$

of all muscles did not change significantly ($p_{\text{time-to-injection}} > 0.05$) after injection of lidocaine or sham (interaction between time-to-injection and injection type: $p > 0.05$).

The scatter plots in Fig. 1b illustrate the co-variation of the vasti muscle activation intensities across strides for a representative animal, along with the associated correlation coefficients. Figure 1c illustrates the correlation coefficients for each muscle pair averaged across all animals. We found a significant decrease of VM-VI and VL-VI correlations after lidocaine (post-hoc: $p < 0.001$), but not after sham injection (post-hoc: $p > 0.05$; not shown). The correlations between the activation intensities of the other muscle-pairs did not change significantly ($p_{\text{time-to-injection}} > 0.05$) after injection of lidocaine or sham (interaction between time-to-injection and injection type: $p > 0.05$).

4 Conclusions and Discussion

We analyzed the role of knee sensory afferents in quadriceps muscle activity and coordination in rats. Inhibiting the sensory receptors within the knee capsule did not affect individual muscle activity but it significantly reduced VM-VI and VL-VI correlations, suggesting that knee sensory afferents mediate control loops amongst these muscles.

Previous experiments demonstrated the existence of reflex loops between knee ligament receptors and the hamstring muscles [4]. Similarly, our results suggest that sensory receptors within the knee capsule drive the coordination amongst the vasti muscles. In future studies we will identify the joint structures that encapsulate these receptors, evaluate the influence of tendon sensory afferents potentially affected by the lidocaine injections in these experiments, and assess whether these results are driven by spinal reflexes.

Our results suggest that damage to structures within the knee should be considered as neuromuscular injuries. Lesions that compromise knee joint receptors will affect the coordination between the vasti muscles, potentially contributing to long-term disabilities like osteoarthritis [5]. Rehabilitation should therefore restore healthy muscle coordination, and not only muscle strength.

The functional role of the mechanisms identified here is still unclear in the context of current motor control theories [6]. Additional work will address whether these mechanisms facilitate task performance [7, 8], reduce stresses and strains within the joints [9, 10] or both.

References

1. H. Çabuk, F.K. Çabuk, Mechanoreceptors of the ligaments and tendons around the knee. *Clin. Anat.* **29**(6), 789–795 (2016)

2. P. Sjolander, H. Johansson, M. Djupsjobacka, Spinal and supraspinal effects of activity in ligament afferents. *J. Electromyogr. Kinesiol.* **12**(3), 167–176 (2002)
3. C. Alessandro et al., Coordination amongst quadriceps muscles suggests neural regulation of internal joint stresses, not simplification of task performance. *Proc. Natl. Acad. Sci. USA* **117**(14), 8135–8142 (2020)
4. M. Solomonow, Sensory-Motor control of ligaments and associated neuromuscular disorders. *J. Electromyogr. Kinesiol.* **16**(6), 549–557 (2006)
5. C. Nagelli et al., Does anterior cruciate ligament innervation matter for joint function and development of osteoarthritis? *J. Knee Surg.* **30**(4), 364–371 (2017)
6. C. Alessandro, N. Beckers, P. Goebel, F. Resquin, J. González, R. Osu, Motor control and learning theories, in *Emerging Therapies in Neurorehabilitation II*. ed. by J.L. Pons, R. Raya, J. González (Springer, Cham, 2016), pp. 225–250. https://doi.org/10.1007/978-3-319-24901-8_9
7. C. Alessandro, J.P. Carbajal, A. d'Avella, Synthesis and adaptation of effective motor synergies for the solution of reaching tasks, in *From Animals to Animats 12*. ed. by T. Ziemke, C. Balkenius, J. Hallam (Springer, Heidelberg, 2012), pp. 33–43. https://doi.org/10.1007/978-3-642-33093-3_4
8. C. Alessandro, F. Nori, Identification of synergies by optimization of trajectory tracking tasks, in *BioRob 2012* (Rome, 2012), pp. 924–930
9. C. Alessandro, B. Rellinger, F. Barroso, M. Tresch, Adaptation after vastus lateralis denervation in rats demonstrates neural regulation of joint stresses and strains. *Elife* **7**, e38215 (2018)
10. F. Barroso, C. Alessandro, M. Tresch, Adaptation of muscle activation after patellar loading demonstrates neural control of joint variables. *Sci. Rep.* **9**, 20370 (2019)

A Transparent Lower Limb Perturbator to Investigate Joint Impedance During Gait



Ronald C. van 't Veld, S. S. Fricke, Ander Vallinas Prieto, Arvid Q. L. Keemink, Alfred C. Schouten, H. van der Kooij, and E. H. F. van Asseldonk

Abstract Joint impedance plays an important role in postural control and movement. However, current experimental knowledge on lower limb impedance during gait is limited to the ankle joint. We designed the LOwer limb PERTurbator (LOPER) aimed to assess knee and hip joint impedance during gait. The LOPER applies force perturbations with a 39 Hz bandwidth, tested on a free-hanging leg. In minimal impedance mode, peak interaction forces during walking are low (<5 N). Also, this mode has a negligible effect on the gait pattern, as it is smaller than the within-subject variability during normal walking. In short, the LOPER is a transparent device able to elicit a clear response at both hip and knee joints to investigate lower limb dynamics. A second motor added to the LOPER could improve isolation of the perturbation contribution to knee and hip dynamics. People with neurological disorders can benefit from knowledge of joint impedance during gait through improved biomimetic devices and clinical decision making.

1 Introduction

Joint impedance, especially its stiffness component, plays an important role in postural control and movement. For example, humans adapt ankle, knee and hip joint impedance during walking to enable a successful gait pattern and interaction with their environment. Joint impedance determines the mechanical resistance to external

This work was supported by the Netherlands Organisation for Scientific Research (NWO), domain Applied and Engineering Sciences under project numbers 12850 (AWARD) and 14903 (Reflexioning).

R. C. van 't Veld (✉) · S. S. Fricke · A. V. Prieto · A. Q. L. Keemink · A. C. Schouten · H. van der Kooij · E. H. F. van Asseldonk
Department of Biomechanical Engineering, University of Twente, Enschede, The Netherlands
e-mail: r.c.vantveld@utwente.nl

A. C. Schouten · H. van der Kooij
Department of Biomechanical Engineering, Delft University of Technology,
Delft, The Netherlands

© The Author(s), under exclusive license to Springer Nature Switzerland AG 2022
D. Torricelli et al. (eds.), *Converging Clinical and Engineering Research on Neurorehabilitation IV*, Biosystems & Biorobotics 28,
https://doi.org/10.1007/978-3-030-70316-5_84

perturbations and can be estimated by measuring the joint's response to perturbations. Several neurological disorders, e.g. spinal cord injury, affect joint impedance and people's ability to modulate it [1]. Knowledge of lower limb joint impedance during gait could be used to support people with these neurological disorders through the development of better biomimetic devices and improved clinical decision making [2, 3]. However, current experimental knowledge on lower limb impedance during walking is limited to the ankle joint [2, 4].

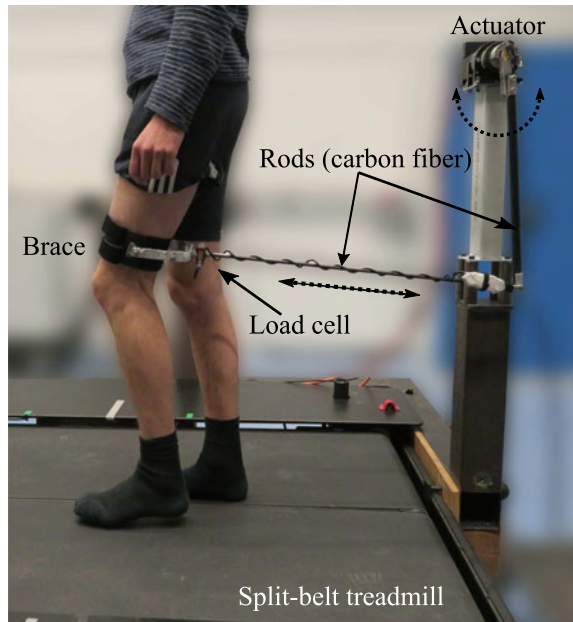
Experimental joint impedance estimation during gait requires a device able to apply perturbations without affecting gait when no perturbations are applied, i.e. a transparent device. Multiple devices have been developed to determine knee or ankle impedance during walking, e.g. [5, 6]. Unfortunately, to our knowledge, no device currently complies with the following requirements: (1) assess knee and hip joint impedance during gait; and (2) have a negligible effect on the unperturbed gait pattern. This study presents the LOWER limb PERTurbator (LOPER), aimed to comply with these two requirements, and evaluates its transparency during gait.

2 Material and Methods

The LOPER consists of a motor, two carbon fiber rods, a load cell, an aluminium frame and a brace, which is connected to the left upper leg via Velcro straps, see Fig. 1. To minimize the additional load on the user, the motor (SMH60, Parker, USA) is bolted on a grounded, steel structure. The angular motor motion is translated into a linear motion via the two carbon fiber rods and a ball joint linkage. To minimize interaction forces, first the load cell (FUTEK FSH00086, USA) measuring interaction force at 1000 Hz is implemented close to the human limb. Second, the LOPER is controlled using an admittance control law with low virtual impedance. To prevent human-robot interaction instability due to this low virtual impedance, indirect PI force control with inner-loop velocity control was implemented [7].

Five people (1 female, 26.4 ± 1.3 yr, height 1.71 ± 0.09 m, weight 68.4 ± 11.5 kg) participated in the evaluation study. The University of Twente EWI/ET ethics committee approved the study and all participants provided written informed consent. First, the force bandwidth was tested on a single participant in a standing posture on a free-hanging left leg. Second, participants walked 3×4 min. on a split-belt treadmill (custom Y-Mill, Forcelink, The Netherlands) to assess the minimal impedance mode and ability to apply perturbations. In order, participants walked: (1) without the LOPER; (2) with the LOPER in minimal impedance mode (unperturbed); (3) with pulse-shaped force perturbations (width 100 ms, amplitude 40 N) applied 50 ms after toe-off. These perturbations were applied randomly after every 3–5 strides during the swing phase of the left leg. A motion capture system (Qualysis AB, Sweden) recorded marker positions on anatomical landmarks at 128 Hz and these were used

Fig. 1 Overview of the LOPER (Lower limb PERTurbator). The rotary actuator is placed on a steel support frame. The rotational actuator motion is converted to a linear motion through the carbon-fiber rods with a ball joint linkage. The motion is transferred into the human leg through an aluminum frame with brace connected to the user. The load cell measuring interaction forces is placed between the aluminum frame and carbon-fiber rod



to compute knee and hip joint angles (OpenSim4.0, gait 2392 model). Ensemble averages over strides were used to compute outcome measures: root mean square (RMS) of interaction force, maximal absolute interaction force, RMS error (RMSE) between joint angles of trials with and without device and intra subject variability (ISV_{ave}) [8].

3 Results

We designed and evaluated the LOPER, which can apply force perturbations to the left upper leg, see Fig. 2. First, a 39 Hz force bandwidth was found when tested on a free-hanging leg. This bandwidth is higher than the 10 Hz bandwidth required based on knee and hip joint dynamics during postural tasks [9]. Second, maximum absolute interaction force across-subjects (4.63 ± 0.79 N) and RMS interaction forces (2.00 ± 0.20 N) were lower than, respectively, 20 and 10 N required to obtain negligible effects on a gait pattern [8]. Third, the average RMSEs for hip and knee angle between the trial without the device and the minimal impedance trial were 0.030 ± 0.010 rad and 0.052 ± 0.026 rad respectively. Both RMSEs were lower than the ISV_{ave} (0.047 and 0.086 rad) for walking without the device, again confirming the negligible effect that the device, in minimal impedance mode, had on the gait pattern.

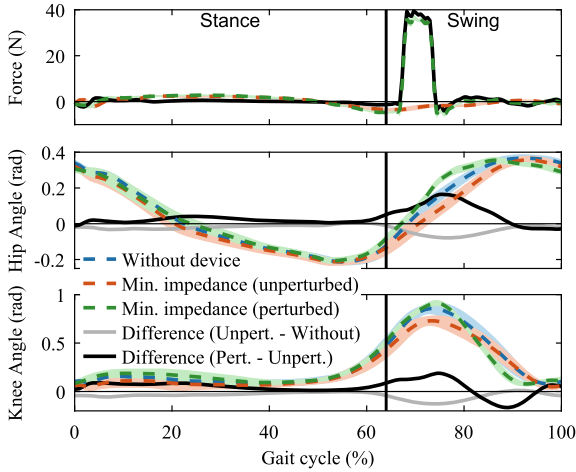


Fig. 2 Interaction forces (top) and hip (middle) and knee (bottom) joint angles for left leg of representative participant during walking. The lines show averages across strides without device, unperturbed strides with device and perturbed strides with device, as well as the differences between these conditions. The shaded areas show the standard deviation across strides. The positive axes show force in forward direction and a flexion angle. Start (0%) of gait cycle is at left heel strike

4 Discussion and Conclusions

This study presents the LOWER limb PERTurbator (LOPER), aimed to experimentally assess knee and hip joint impedance during gait. The LOPER applies force perturbations with a 39 Hz bandwidth, when tested on a free-hanging leg. In minimal impedance mode, peak interaction forces during walking are low (<5 N) and the effect on the gait pattern is smaller than within-subject variability during normal walking. The largest differences between the trials with and without the device were found during the beginning/mid swing, likely due to the larger interaction forces observed, see Fig. 2. These larger interaction forces can be attributed to the virtual mass and high accelerations at this portion of the gait cycle.

Moreover, perturbations affect both knee and hip joint simultaneously, see Fig. 2, which makes it difficult to analyze the dynamics of a single joint. This simultaneous excitation is due to the placement of the motor on a grounded structure to minimize the additional load on the user. As result, the angular motor motion is translated into a linear motion and the motor thus applies a force, not a torque, to the lower limb. Future work may therefore include the use of a biomechanical model to analyze the experimental data or the use of a second motor to apply perturbations to both lower and upper leg simultaneously. Furthermore, we chose to only apply perturbations during the swing phase. Ultimately, we will use the device to investigate knee and hip joint impedance during the entire gait cycle. In short, the LOPER is a transparent device able to elicit a clear response at both hip and knee joints to investigate lower limb dynamics.

References

1. V. Dietz, T. Sinkjær, Spastic movement disorder: impaired reflex function and altered muscle mechanics. *Lancet Neurol.* **6**(8), 725–733 (2007)
2. E.J. Rouse, L.J. Hargrove, E.J. Perreault, T.A. Kuiken, Estimation of human ankle impedance during the stance phase of walking. *IEEE Trans. Neural Syst. Rehab. Eng.* **22**(4), 870–878 (2014)
3. S. Maggioni, A. Melendez-Calderon, E.H.F. van Asseldonk, V. Klamroth-Marganska, L. Lünenburger, R. Riener, H. van der Kooij, Robot-aided assessment of lower extremity functions: a review. *J. Neuroeng. Rehabil.* **13**(1), 1–25 (2016)
4. H. Lee, N. Hogan, Time-varying ankle mechanical impedance during human locomotion. *IEEE Trans. Neural Syst. Rehab. Eng.* **23**(5), 755–764 (2015)
5. E.J. Rouse, L.J. Hargrove, E.J. Perreault, M.A. Peshkin, T. Kuiken, Development of a mechatronic platform and validation of methods for estimating ankle stiffness during the stance phase of walking. *J. Biomech. Eng.* **135**(8), 1–8 (2013)
6. M.R. Tucker, C. Shirota, O. Lambercy, J.S. Sulzer, R. Gassert, Design and characterization of an exoskeleton for perturbing the knee during gait. *IEEE Trans. Biomed. Eng.* **64**(10), 2331–2343 (2017)
7. A.Q.L. Keemink, H. van der Kooij, A.H.A. Stienen, Admittance control for physical human-robot interaction. *Int. J. Robot. Res.* **37**(11), 1421–1444 (2018)
8. J.H. Meuleman, E.H.F. van Asseldonk, H. van der Kooij, The effect of directional inertias added to pelvis and ankle on gait. *J. Neuroeng. Rehabil.* **10**(40), 1–12 (2013)
9. B. Koopman, E.H.F. van Asseldonk, H. van der Kooij, Estimation of human hip and knee multi-joint dynamics using the LOPES gait trainer. *IEEE Trans. Robot.* **32**(4), 920–932 (2016)

Apparent Stiffness and Damping as a Metric for Fall Risk



Jordan Smith, Robert Felmlee, Jozsef Laczko, Mary Crowe,
Scott Steinbrink, and Davide Piovesan

Abstract Currently, the only mechanisms in place to help people stand up require the assistance of care staff and a strong upper body. We hypothesize that there is a valid mathematical model to predict the optimal lower limb stiffness and damping to predict the risk of falling. These found values can be used to create an adjustable device that can help people stand more easily on their own.

1 Introduction

Injuries due to falling are a common problem in the elderly population [1]. As of right now, there are few means to prevent this from happening. The current study aims to develop tests that can be used to predict fall risk. Currently, a popular test that

J. Smith · R. Felmlee · S. Steinbrink · D. Piovesan
Gannon University, Erie, PA, USA
e-mail: smith341@gannon.edu

R. Felmlee
e-mail: felmlee001@gannon.edu

S. Steinbrink
e-mail: steinbri001@gannon.edu

D. Piovesan
e-mail: piovesan001@gannon.edu

J. Laczko (✉)
Wigner Research Centre for Physics, Budapest, Hungary
e-mail: laczko.jozsef@wigner.hu

University of Pécs, Pécs, Hungary

Department of Physiology, Feinberg School of Medicine, Northwestern University, Chicago, IL,
USA

M. Crowe
Lake Erie College of Osteopathic Medicine, Erie, PA, USA
e-mail: mcrowe01241@med.lecom.edu

is used is the sit to stand test [2, 3]. This test includes the subjects standing up from a seated position, then walking ten steps and turning around and returning to where they first stood up. This test is timed, and the time is used to predict how likely they are to fall when standing up. A different way to predict if someone is at risk of falling would be to use a sit to stand test to characterize and give value to specific physical properties of each person. If the human body is modeled as a simplified second-order system as suggested by the Reference Configuration (RC) theory [4], a simulation can be created to represent the motion of sitting to standing. Data collected from sit to standing trials can be used to find a set of lumped parameters characterizing the physical and physiological behavior of each participant. Assuming the system to be second-order and neuro-mechanical in nature, the apparent damping and spring coefficients can be used to determine how likely each subject is to fall. Furthermore, depending on the personalized coefficients, it is possible to quantify the amount of assistance that a potential assistive device could be adjusted to so help that person specifically. The results that will be presented will be on the average range of damping and spring coefficients in healthy subjects, so to determine a normative database.

2 Methods

2.1 *Experimental Setup*

Two AMTI AccuGait portable force platforms are used in this experiment. The software that accompanies the forceplates is the AMTI NetForce. Each forceplate must be calibrated for each subject. It first required to be zeroed, and then the subject must stand still on the forceplate in order for the proprietary algorithm to detect the subject's true weight and thus optimize the resolution of the measurement. Once the weight of the subject is taken, then the forceplate is calibrated and ready for testing. Position of the subject was measured using a Codamotion System (Charnwood Dynamics), and EMG signal was recorded for 8 major muscles of each leg. Schematic of the experiment is shown in Fig. 1. While data was acquired for completeness, in this work only the signal from the force platform was used.

2.2 *Testing*

Six subjects were tested during sit-to stand transition. Seated on an adjustable chair without armrests, with the feet on the ground, the shanks at 90° to the thighs, and the thighs at -90° with respect to the torso, the subjects had to stand up on top of the forceplates.

Subjects were forbidden to use their arm to aid the transition and were asked to cross them in front of the chest. Each subject performed 30 trials (Fig. 2a, b). The

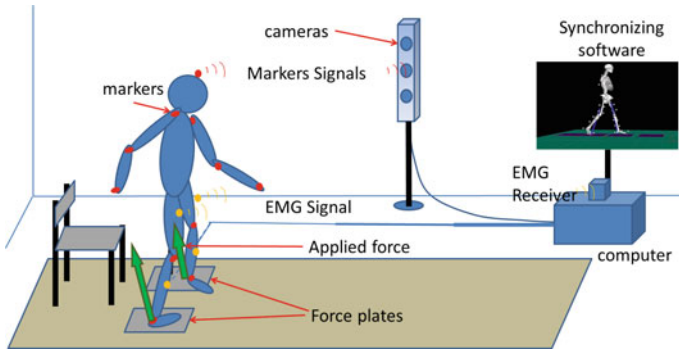


Fig. 1 Instrumental set-up

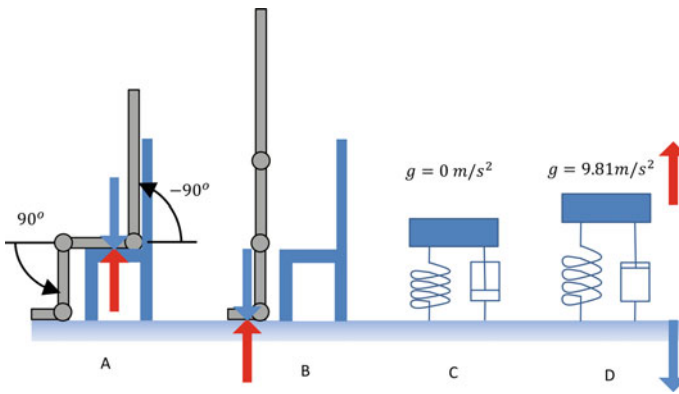


Fig. 2 Schematics of experiment and model **A** subject seated with reaction force on the chair. **B** Subject standing with reaction force completely on feet. **C** Model representing the subject according to RC theory. **D** Application of a virtual step in gravity and reaction force by the apparent second-order components

performance of each trial was timed and was required to be less than 3.5 s. This time is very close to the self paced time to stand up for most unimpaired individuals and allows to capture the evolution of the ground reaction force as the subject stabilizes. During the data post-processing each subject force data was synchronized using a cross-correlation function.

2.3 Mechanical Model

The feet of a person in the seating position apply minimal force to the ground, as the weight of the subject is counteracted by the chair (Fig. 2a). As the person stands up, the reaction force at the feet increases and stabilizes after a period of time to

counteract the full weight of the person (Fig. 2b). We can model the reaction force at the feet on the ground, as a second-order model, constituted by a spring (K), damping (B) and mass (M), reacting to a step in gravity (Fig. 2c, d). The model also includes a delay (d), that takes into account the reaction time of the subject, representative of the conglomeration of neurological signal transmission and cognitive instruction process time.

$$M\ddot{x}(t) + B\dot{x}(t) + Kx(t) = F(t - d) \quad (1)$$

Equation 1 represents the mechanical model where $x(t)$ is the position of the subject center of mass (located about at the navel) along the vertical axis with respect to the knees. We know the mass (M) to be approximately, the mass of the person minus the mass of feet and shanks. Apparent stiffness (K), damping (B), and delay (d) are unknown but can be estimated using an optimization algorithm that fits the force output of the model to the force time-profile recorded for each subject via the force platforms. We used a standard Nonlinear least-squares solver, in combination with a Monte-Carlo method, where the initial value of the optimization was randomized to avoid relative minima.

3 Results

Average ground reaction force during a sit-to-stand motion over time are presented in Fig. 3 for a representative subject.

Figure 4 depicts the fitting of a model on a single trial. We found experimentally that there is a specific range in which the damping and spring coefficient lie. This range for the damping in healthy subjects is from 150 to 300 Ns/m. The range for the spring coefficient in healthy subjects is from 7 to 15 N/m.

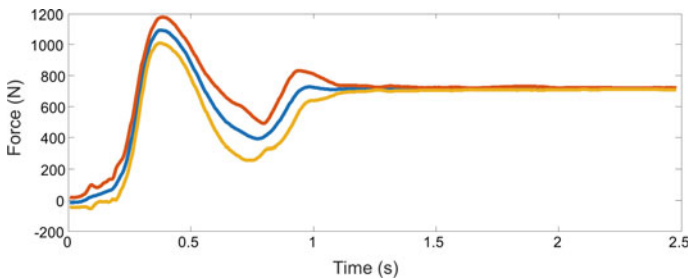


Fig. 3 Average ground reaction force during a sit-to-stand motion over time for 30 Trials (blue), and standard deviations (red and yellow) for a representative subject

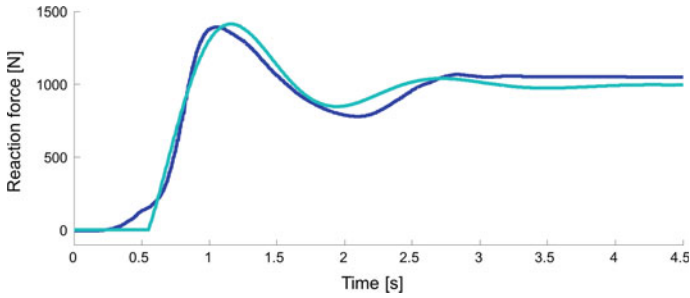


Fig. 4 Reaction force of a representative subject (dark blue) compared to fitted output of the model (light blue)

4 Conclusion

The number of subjects in this study is small, and the method has not been applied to unimpaired individuals, yet. On the other hand, the method is simple and based on well-known physical first principles so as to clearly identify biophysical parameters that play a crucial role in the stability of a biomechanical system. We posit that if a subject exhibits damping or stiffness coefficients outside these ranges, they are potentially at risk for falling. For example, if the spring coefficient is too low, it suggests that a subject cannot generate enough force in order to stand up all of the way, since the displacement of the center of mass from sitting to standing is constrained by his/her size. If the damping coefficient is too low or too high, the subject may not be able to stabilize after standing up, thus keeping them off balance and potentially contributing to a fall. Furthermore, the effect of delays in the control loop is known to be a factor in the instability of mechanical systems. The method proposed here, although simplistic, can provide a figure of merit of the neuro-mechanical delays responsible for balance instabilities.

If a subject is found to be at risk of falling, devices might be tailored to their specific needs and thus help them to stand more safely. To assist with a low spring coefficient, a device with springs parallel with the person could be used to help pull them up. If the damping coefficient is too low, a spring device that helps slow their forward and upward momentum could be used to help them avoid a fall once they are up [5].

References

1. H. Hosseini, N. Hosseini, Epidemiology and prevention of fall injuries among the elderly. *Hosp. Top.* **86**, 15–20 (2008)
2. A.J. Campbell, M.J. Borrie, G.F. Spears, Risk factors for falls in a community-based prospective study of people 70 years and older. *J. Gerontol.* **44**, M112–M117 (1989)

3. M.C. Nevitt, S.R. Cummings, S. Kidd, D. Black, Risk factors for recurrent nonsyncopal falls: a prospective study. *JAMA* **261**, 2663–2668 (1989)
4. V. Abolins, C. Cuadra, J. Ricotta, M.L. Latash, What do people match when they try to match force? Analysis at the level of hypothetical control variables. *Exp. Brain Res.* 2020
5. M. Yagiela, R.W. Johnson, A. Schmitz, S. Steinbrink, D. Piovesan, Dynamic analysis and design of an innovative sit-to-stand gait trainer. *J. Eng. Sci. Med. Diagnost. Therapy* **3** (2020)

**SS10: Neural Correlates
of Cognitive-Motor Robotic
Neurorehabilitation**

Feature Consistency Criterion for Motor Imagery-Based Neuromodulation



Carlos A. Stefano Filho, J. Ignacio Serrano, Romis Attux,
Gabriela Castellano, M. Dolores del Castillo, and Eduardo Rocon

Abstract Motor imagery (MI) has been increasingly studied for neurorehabilitation purposes. However, issues such as large intra- and inter-subject variability still limit its practical, and more clinical, applications. Seeking appropriate features for MI-neuromodulation training is thus a crucial step. This work presents a protocol that selects features related to the MI mental patterns maximizing consistency (i.e., minimizing variability) across two recordings in different days. We apply our methodology to 3 healthy adults and 3 children with cerebral palsy, illustrating its feasibility for MI training protocols.

1 Introduction

MOTOR imagery (MI), the mental rehearsal of a movement task without its overt execution, encompasses a wide field of applications ranging from motor performance training to brain-computer interfaces (BCIs) [1], particularly presenting increasing interest in neurorehabilitation [2].

In the electroencephalography (EEG) signal, MI induces event-related desynchronizations (ERDs; i.e., a motor-associated power decrease in relation to baseline) on

This work was supported by: FAPESP (São Paulo Research Foundation) grants #2019/18409-9 and #2013/07559-3; CNPq (Brazilian's National Council for Scientific and Technological Development) grant #308811/2019-4; Programas de Actividades I+D en la Comunidad de Madrid and Structural Funds of the EU (S2018/NMT-4331); Ministry of Economy and Competitiveness (DPI2015-68664-C4-1-R).

C. A. Stefano Filho (✉) · R. Attux · G. Castellano
Neurophysics Group, Signal Processing for Communications,
University of Campinas, Campinas, Brazil

C. A. Stefano Filho
Brazilian Institute for Neuroscience and Neurotechnology (BRAINN), Campinas, Brazil

C. A. Stefano Filho · J. Ignacio Serrano · M. Dolores del Castillo · E. Rocon
Center for Automation and Robotics (CAR), Spanish National Research Council (CSIC),
Madrid, Spain

© The Author(s), under exclusive license to Springer Nature Switzerland AG 2022
D. Torricelli et al. (eds.), *Converging Clinical and Engineering Research*
on *Neurorehabilitation IV*, Biosystems & Biorobotics 28,
https://doi.org/10.1007/978-3-030-70316-5_86

the contralateral motor cortex in the μ (8–13 Hz) and β (13–30 Hz) frequency ranges [3]. Although this knowledge could base many applications, MI still remains mainly outside clinical environments, as subjects usually experience difficulties performing this type of task [4]. Additionally, most MI-based systems usually lack robustness [5], which is critical to properly understand the quantities being measured and manipulated during MI-based neuromodulation. This is especially true for chronic patients whose residual function is the target of such therapies.

Furthermore, MI mental patterns suffer from large inter- and intra-subject variability [6]. Although transfer learning attempts have been proposed to cope with this issue, they might be ineffective if subjects display unlike non-stationarities [6]. Hence, in this work, we propose a strategy to identify consistent features between two data recordings acquired at distinct days. Our methodology should enable investigating intra- and inter-subject variability without model-bound assumptions. To illustrate it under an MI-based neuromodulation scenario, we applied our approach to both healthy and neurologically damaged subjects.

2 Materials and methods

2.1 Data Acquisition and Pre-processing

Data from three healthy adults (all right-handed; aged 25, 28 and 29 years old) were acquired with the OpenBCI Cyton Board (8 channels), at 250 Hz. Moreover, data from three children with cerebral palsy (aged 11, 13 and 15 years old) following Single-Event Multilevel Surgery and presenting no cognitive deficits were acquired with the 31-channels ActiCap EEG cap and the BrainVision amplifier (BrainProducts GmbH, Germany), also at 250 Hz. Two data recordings at different days were available for each subject: the time gap for the children was of 5 days whereas, for the healthy subjects, this time was of either 1 (subjects S01 and S03) or 5 days (subject S02). The acquisition interface, a virtual environment designed in Unity, was displayed in a computer screen for the healthy subjects and on virtual reality glasses (Oculus Rift) for the children, which were sitting on a reclining pallet at a 50° inclination.

The interface led the participants' first person avatar through pre-defined paths at constant pace with a series of obstacles. At obstacles encounters, the walking stopped and subjects were instructed to relax (baseline period; 4 s). Next, participants should imagine the walking resuming (MI period; 4 s). The obstacle would then disappear and the avatar would resume walking. A total of 22 and 19 obstacles were placed for the children and healthy participants, respectively.

Data preprocessing included a common average reference filter for common artifacts removal and high-pass filtering with a 2 Hz stop-band frequency, 3 Hz pass-band frequency, pass-band ripple of 0.5 and 65 dB stop-band attenuation. Each trial (encompassing the baseline and MI periods) was divided into smaller one-second windows for data analyses.

2.2 ERD Computation

ERDs were investigated through the signal's power variations (ΔP , computed through Welch's transform) between the MI (T) and baseline (B) periods, for bands θ —4 to 7 Hz; α_1 —7 to 10 Hz; α_2 —10 to 13 Hz; β_1 —13 to 18 Hz; β_2 —18 to 25 Hz; and β_3 —25 to 30 Hz. For each electrode e , one-second window k , and frequency bin f_i within these bands, then:

$$\Delta P_{f_i, e, k} = \frac{P_T(f_i, e, k) - \langle P_B(f_i, e) \rangle}{\langle P_B(f_i, e) \rangle}. \quad (1)$$

In (1), the quantity $\langle P_B(f_i, e) \rangle$ represents the averaged baseline power spectrum previous to the current task windows under consideration. The power at each band, $\Delta P_{f_i, e, k}$, was taken as the sum of $\Delta P_{f_i, e, k}$ across the bins within that band. Following the methodology introduced in [7], an ERD was only accounted as such if it exceeded a threshold $\sigma_{f, e}$, established through the signals' band power fluctuation, through its variation coefficient at baseline blocks. To assess whether this criterion was met, we set, for each window k :

$$x_k(f, e) = \begin{cases} 1, & \text{if } |\Delta P_{f, e, k}| > \sigma_{f, e} \\ 0, & \text{otherwise} \end{cases}. \quad (2)$$

The ERD occurrence (EO) is given by averaging $x_k(f, e)$ over k . EO values fall within [0, 1], indicating how often the expected ERD response was found for each (f, e) pair.

2.3 Consistency Criterion

To define the optimum (f, e) pairs, we designed a consistency index— $C(f, e)$ —that should be maximized considering both data recordings (superscripts) for each subject:

$$C(f, e) = \frac{EO_{f, e}^{(1)} + EO_{f, e}^{(2)}}{\max[EO^{(r)}] + |EO_{f, e}^{(1)} - EO_{f, e}^{(2)}|}. \quad (3)$$

In (3), $\max[EO^{(r)}]$ refers to the maximum $EO_{f, e}$ between the two recordings for a given subject. Hence, $C(f, e)$ concomitantly favors the smallest EO differences across data recordings and the largest EO values.

3 Results and Discussion

Figure 1 displays plots of $C(f, e)$ for the healthy (a) and the children (b) participants. The brighter the tone, the higher the corresponding $C(f, e)$.

These results illustrate that: (1) each participant displays specific frequency bands and/or electrodes for which the consistency criterion is maximized; and (2) the most consistent (f, e) pairs for EO are not necessarily restricted to the primary sensorimotor cortex: for example, the (α_1, Fz) and (β_3, Pz) pairs for S01 and P01, respectively. The high consistency estimated in these situations is actually in accordance with more recent studies that highlight involvement of frontal and parietal areas in MI (e.g., [2, 7, 8]). In fact, since MI also involves cognitive processes, it would be expected that its underlying neural correlates would imply areas not necessarily restricted to the pri-

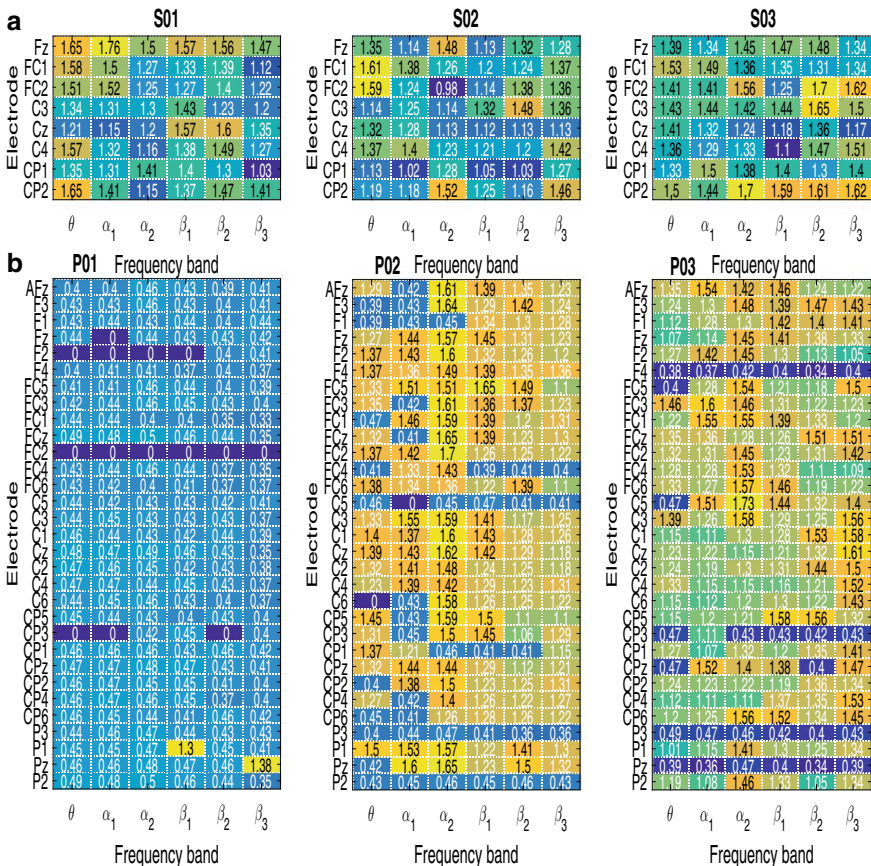


Fig. 1 $C(f, e)$ plots for participants in the healthy (a) and children (b) groups. The color contrasts provide intra-subject comparisons

mary sensorimotor cortex. Nevertheless, when activity was also highlighted in more traditionally used electrodes for this type of study, such as the C-labeled sensors, our methodology straightforwardly enables to verify the most suitable frequency bands that maximize consistency for EO and, thus, account for spectral variability as well (e.g., α_2 for P02, and β_3 for P03).

4 Conclusion

The proposed methodology partially reflected the traditionally expected response over the primary sensorimotor cortex, and underlined the possible involvement of frontal and parietal areas in the MI response. Its applicability is straightforward and can be easily replicated for MI-training feature selection, as long as at least two recording sessions are available. Finally, it directly highlights subjects' individualities, consequently providing an immediate manner for establishing optimum individual features for training protocols under the consistency criterion. A priori neurophysiological knowledge can also be employed to further screen the highest consistent values according to the desired application (e.g., by restraining candidate features to specific cortical locations or spectral ranges). Future studies may seek whether $C(f, e)$ correlates to the MI capability or to the severity of motor deficits (specially observing results for P01, Fig. 1b).

References

1. N. Padfield, J. Zabalza, H. Zhao, V. Masero, J. Ren, EEG-based brain-computer interfaces using motor-imagery: techniques and challenges. *Sensors* **19**(6), 1423 (2019)
2. Y. Tong et al., Motor imagery-based rehabilitation: potential neural correlates and clinical application for functional recovery of motor deficits after stroke. *Aging Disease* **8**(3), 364–371 (2017)
3. G. Pfurtscheller, C. Brunner, A. Schlogl, F.H.L. da Silva, Mu rhythm (de)synchronization and EEG single-trial classification of different motor imagery tasks. *NeuroImage* **31**, 153–159 (2006)
4. J.W. Choi, S. Jo, Effective motor imagery training with visual feedback for non-invasive brain computer interface, in *6th International Conference on Brain and Computer interface (BCI), GangWon* (2018) pp. 1–4
5. F. Lotte, F. Larue, C. Mühl, Flaws in current human training protocols for spontaneous Brain-Computer Interfaces: lessons learned from instructional design. *Front. Hum. Neurosci.* **7**, 568 (2013)
6. S. Saha, M. Baumert, Intra- and inter-subject variability in EEG-based sensorimotor brain computer interface: a review. *Front. Comput. Neurosci.* **13** Article 87 (2020)
7. C. A. Stefano Filho, et al., On the (in)efficacy of motor imagery training without feedback and event-related desynchronizations considerations'. *Biomed. Phys. Eng. Express* **6**, 035030 (2020)
8. S. Pilgramm et al., Motor imagery of hand actions: Decoding the content of motor imagery from brain activity in frontal and parietal motor areas. *Hum. Brain Mapping* **37**(1), 81–93 (2016)

Real-Time Access to Attention and Attention-Based Brain-Machine Interfaces



C. Gaillard, C. De Sousa, J. Amengual, and S. Ben Hamed

Abstract We demonstrate real-time high spatial and temporal resolution access to attention, a high-level cognitive function, from both multi-unit neuronal activity and local field potentials. We show that this prefrontal attention spotlight is rhythmic at multiple time scales, its location being predictive of behavior. Last, when using this attentional tracking as a neurofeedback signal, behavioral performance is improved. These results enhance the range of applications of cognitive BMIs.

1 Introduction

Brain-machine interfaces (BMIs) using motor cortical activity to drive external effectors like a robotic arm have proven their great assistive potential. Indeed, tetraplegic patients can control neuroprostheses and recover some degree of autonomy thanks to the direct access to their motor cortical information [1]. An emerging parallel effort is now directed to BMIs controlled by endogenous cognitive activity, or cognitive BMIs. While more challenging, this approach opens up new dimensions for both assistive (e.g. tracking attention in locked-in patients) and rehabilitative (e.g. reversing attentional deficits in neglect patients [2]) technologies [3]. In this context, explicit access

S. B. H was supported by ERC Brain3.0 #681978, ANR-11-BSV4-0011 and ANR-14-ASTR-0011-01, LABEX CORTEX (ANR-11-LABX-0042, ANR-11-IDEX-0007) fundings.

C. Gaillard · C. De Sousa · J. Amengual · S. Ben Hamed (✉)
Institut Des Sciences Cognitives Marc Jeannerod, CNRS—Université de Lyon, Lyon, France
e-mail: benhamed@isc.cnrs.fr

C. Gaillard
e-mail: corentin.gaillard@isc.cnrs.fr

C. De Sousa
e-mail: carine.desousa@isc.cnrs.fr

J. Amengual
e-mail: julian.amengual@isc.cnrs.fr

to higher cortical cognitive functions, such as covert attention, with the same informational precision as achieved for motor signals remains a challenge. This is due to several specific factors. Indeed, attention information, is known only to the subject. As a result, it can solely be inferred transiently by an observer from the subject's overt behavior or report. In addition, recent behavioral evidence suggests that attention is extremely dynamic in both space and time. Thus, accessing this function in real-time poses specific computational challenges. Here, we demonstrate, for the first time, real time access to spatial attention with high temporal and spatial resolution, *independently from eye position*. Indeed, while previous studies report 2 hemifield or 4 quadrant classification of attention position [4], we achieve (x, y) continuous decoding of attentional spotlight position and validate this decoding through behavioral correlation [5–7]. This allows us to describe novel core properties of spatial attention and report enhanced attention using attention-based neurofeedback.

2 Material and Methods

2.1 *Monkey Training and Neuronal Recordings*

Two male rhesus monkeys (*Macaca mulatta*) were trained on a spatial cued target detection task. Specifically, 4 Gy square landmarks (LMs) were displayed, all throughout the trial, at the four corners of a $20^\circ \times 20^\circ$ hypothetical square centered onto the fixation cross. After a variable delay from fixation onset (700–1200 ms), a small green square was presented (350 ms), close to the fixation cross, in the direction of one of the LM. Monkeys were rewarded for detecting a subtle change in luminosity of this cued LM (target) as fast as possible. To make sure monkeys oriented their attention to the cued LM, the uncued LMs could occasionally change luminosity. Monkeys had to ignore these distractors. They had to maintain fixation all throughout the task. Monkeys were implanted to allow for neuronal recordings from the prefrontal cortex (frontal eye field, FEF, bilaterally), a cortical region at the source of spatial attention signals. Neuronal recordings were performed using two 24-contact recording probes inserted daily, collecting both spiking activity and local field potentials. All procedures were approved in compliance with the Directive 2010/63/UE (#C2EA42-13-02-0401-01). Detailed procedures can be found elsewhere [5].

2.2 *Neuronal Decoding*

A regularized linear decoder was used to associate, on correct trials, the neuronal activity estimated on the 48 recording channels on a given interval in the cue to target interval (averaged onto either 150 or 50 ms for higher temporal resolution) and the

cued location. The decoder was trained on a random set of 70% of the correct trials at a specific time in the cue to target interval, then tested on the 30% remaining at all time after cue presentation. The output of the classifier was read as a continuous (x , y) estimate of attention location or as a class output, corresponding to one of the 4 possible visual quadrants attention can be cued to. Best prediction was achieved on activities right before target onset.

3 Results

3.1 *Real-Time Access to Spatial Attention from Prefrontal Spikes and Local Field Potentials Predicts Behavior*

We demonstrated direct two dimensional real-time access to where monkeys were covertly paying attention, using machine-learning decoding methods applied to their ongoing prefrontal cortical activity [6]. Decoded attention was highly predictive of overt behavior in a cued target-detection task. Indeed, monkeys had a higher probability of detecting a visual stimulus as the distance between decoded attention and stimulus location decreased. This was true whether the visual stimulus was presented at the cued target location or at another distractor location. In error trials, in which the animals failed to detect the cued target stimulus, both the locations of attention and visual cue were misencoded.

This real-time access to attention was achieved both from multi-unit neuronal activity (MUA) and local field potentials (LFPs) [6], an intracortical proxy to sEEG or ECoG signals. Specifically, the locus of spatial attention was reliably decoded from all frequency bands, though low- and high-gamma band yielded highest decoding accuracies. In all frequency bands, decoded spatial attention information was predictive of behavioral performance, as described for MUAs (Fig. 1).

3.2 *Dynamic Attention Explores Space at an Alpha Rhythm*

Recent behavioral evidence suggests that attention samples space rhythmically. Increasing the temporal resolution of our real-time access to the attentional spotlight, by averaging individual neuronal recordings on 50 ms windows, we showed that attention, rather than being statically anchored at a given location, moves around in space and continuously explores space at a 7–12 Hz rhythm [7]. Sensory encoding and behavioral reports were increased at a specific optimal phase with respect to this rhythm. We propose that this prefrontal neuronal rhythm reflects an alpha-clocked sampling of visual input in the absence of eye movements. These attentional explorations are highly flexible. How they spatially unfold depends both on within-trial and across-task contingencies.

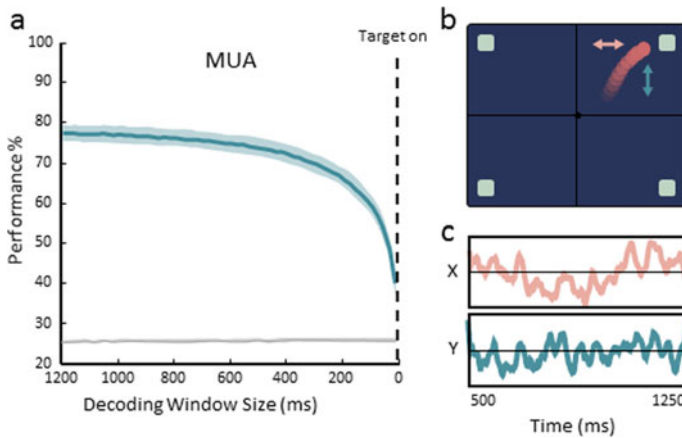


Fig. 1 Prefrontal (FEF) neuronal activity allows efficient access to and tracking of attentional spotlight. **a** Attention position classification performance as a function of FEF MUA pre-target time window used to train a classifier (gray: 95% C.I. \pm s.e., blue: mean \pm s.e.). **b** Representation of the dynamic attentional spotlight on a screen during a determined pre-target time interval (pink: decoded X; blue: decoded Y components). **c** Displacement of attentional spotlight during the cue to target interval (500–1250 post cue), along the x (pink) and in y (blue) dimensions for one exemplar trial

3.3 *Attentional Information Fluctuates at a Very Slow Rhythm of 4–6 Cycles Per Hour*

Oscillations in brain activity are described as a major feature supporting attentional processes. However, this rhythmic mechanism is always described at the sub-second time scale, in specific theta and alpha frequency ranges. In contrast, the description of slower oscillatory mechanisms at the minute to hour time scales is missing. We described that the decoded spatial attention information oscillates every 10–15 min [8]. In these cycles, prefrontal attentional content alternates between distinct states of rich and low attention information. These oscillations are both described in the LFP and MUA signals. Importantly, these oscillations in the decoded attentional information content account for variations in overt behavioral performance. We thus demonstrate that both overt performance and prefrontal cortex attentional mechanisms are rhythmic at multiple time-scales ranging from the fast alpha scale to a much lower 10–15 min scale. This result participates to a new multiscale and dynamic model of attentional processes, the understanding of which is critical to develop and optimize attention interventions including attention driven cognitive BMIs.

3.4 Attention-Based Neurofeedback Modulates Behavior

We have decoded the spatial locus of attention from prefrontal neuronal activities in real time while monkeys were engaged in a cued target detection task and we have indicated to the monkey, with a sound of variable pitch how precisely they were orienting their attention to the cued location. The higher the orienting accuracy, the higher the pitch, the higher the final reward. Relative to the pre-neurofeedback condition, after the neurofeedback intervention, subjects engaged in the task longer, produced less conservative responses and had increased accuracies at their baseline preferred location.

4 Conclusion

Overall, we thus demonstrate that real-time access to cognitive functions, such as attention, with a high informational (here high spatial and temporal) resolution is not only achievable but also provides a better description of the neuronal correlates of the function of interest and enhances the range of applications of cognitive BMIs.

References

1. J.E. O'Doherty et al., Active tactile exploration using a brain-machine-brain interface. *Nature* **479**(7372), 228–231 (2011)
2. E. Astrand, C. Wardak, S. Ben Hamed, Selective visual attention to drive cognitive brain-machine interfaces: from concepts to neurofeedback and rehabilitation applications. *Front. Syst. Neurosci.* **8**, 144 (2014)
3. T. Ros, A. Michela, A. Bellman, P. Vuadens, A. Saj, P. Vuilleumier, Increased alpha-rhythm dynamic range promotes recovery from visuospatial neglect: a neurofeedback study. *Neural Plast.* **2017**, 7407241 (2017)
4. S. Tremblay, G. Doucet, F. Pieper, A. Sachs, J. Martinez-Trujillo, Single-trial decoding of visual attention from local field potentials in the primate lateral prefrontal cortex is frequency-dependent. *J. Neurosci.* **35**, 9038–9049 (2015)
5. E. Astrand, C. Wardak, P. Baraduc, S. Ben Hamed, Direct two-dimensional access to the spatial location of covert attention in macaque prefrontal cortex. *Curr Biol.* **26**(13), 1699–1704 (2016)
6. C. De Sousa Ferreira, C. Gaillard, S. Ben Hadj Hassen, F. Di Bello, S. Ben Hamed, Behavioral validation of novel high resolution attention decoding method from multi units & local field potentials. *Neuroimage* **231**, 117853 (2021)
7. C. Gaillard, S. Ben Hadj Hassen, F. Di Bello, Y. Bihan-Poudec, R. VanRullen, S. Ben Hamed, Prefrontal attentional saccades explore space rhythmically. *Nat. Commun.* **11**(1), 925
8. C. Gaillard, C. De Sousa Ferreira, S. Ben Hadj Hassen, F. Di Bello, S. Ben Hamed, *Very Slow (Minutes) Attentional Rhythms in the Prefrontal Cortex Submitted*

Explicitness of Task Instructions Supports Motor Learning and Modulates Engagement of Attentional Brain Networks



Joaquin Penalver-Andres, Karin A. Buetler, Thomas König, René M. Müri, and Laura Marchal-Crespo

Abstract Motor learning is a complex cognitive and motor process underlying neurorehabilitation. Cognitive (e.g., attentional) engagement is important for motor learning, especially early in the learning process. In this study, we investigated if task instructions enforcing the underlying task rule of a virtual sailing task modulate attentional engagement and motor learning. Our results suggest that enforcing the rule of a motor task using explicit knowledge or visual cues enhances motor learning compared with no enforcement of task rules. Further, training with visual cues may support early visuo-attentional engagement.

1 Introduction

Motor learning is a complex cognitive and motor process leading to behavioral and neural changes (i.e., brain plasticity) underlying neurorehabilitation. Fitts proposed three delimited phases of motor learning: the *cognitive*, *associative*, and *autonomous* phase [1]. In the earlier cognitive and associative phases—where task rules are discovered and appropriate sequences of actions determined and refined—attentional engagement is essential for motor learning, e.g., to focus on relevant stimuli (selective visual attention) and to generate selective and controlled responses (executive attention).

J. Penalver-Andres (✉) · K. A. Buetler · L. Marchal-Crespo
Motor Learning and Neurorehabilitation Laboratory, University of Bern, Bern, Switzerland
e-mail: joaquin.penalverdeandres@artorg.unibe.ch

T. König
Translational Research Center, University Hospital of Psychiatry and Psychotherapy, University of Bern, Bern, Switzerland

R. M. Müri
Department of Neurology, University Neurorehabilitation, University Hospital Bern (Inselspital), University of Bern, Bern, Switzerland

L. Marchal-Crespo
Department of Cognitive Robotics, Delft University of Technology, Delft, The Netherlands

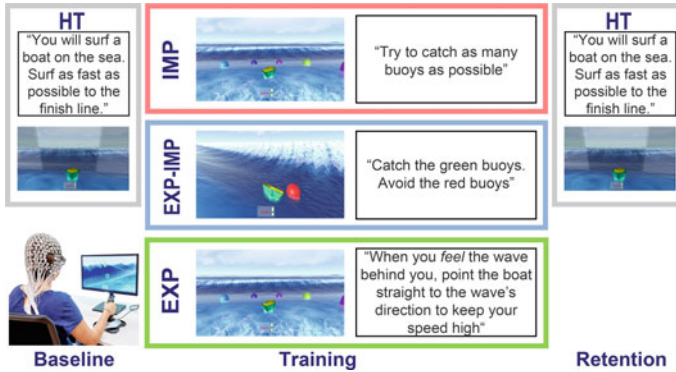


Fig. 1 Experimental protocol and task instruction types used

In line with this, studies have shown that enforcing task rules during training—e.g., using visual cues and/or explicit knowledge—is associated with increased automaticity of movements, enhanced goal-action coupling [2], and inhibition of self-related (internal) distractors [3, 4]. However, to date, less is known about the effect of enforcing task rules on the attentional engagement during motor learning.

Yet, a better understanding of the influence of task rule enforcement on attentional engagement during motor learning may help to design more efficient training paradigms, namely for neurorehabilitation. For example, explicit knowledge about the task rule could be provided during training, depending on the attentional deficits after stroke, to optimally support motor recovery.

Therefore, the goal of this study was to investigate the influence of different task instructions types that vary in the degree of explicitness of the task rules during training on motor learning and attentional brain networks (i.e., reflected in alpha-band cortical activity [3, 5]) using electroencephalography (EEG).

2 Methods

2.1 Experimental Setup and Participants

Thirty-six healthy naïve volunteers (41.67% women; $\mu_{\text{age}} = 27.9$ years, $\sigma_{\text{age}} = 6.64$ years; gender and age balanced across groups, $p > 0.05$) performed a virtual sailing game developed in Unity (*Unity Technologies, USA*) using a Logitech joystick (*Logitech, Switzerland*) (see Fig. 1). The height and position of the chin rest, chair, joystick, and computer screen were controlled across participants and adapted accordingly for left-handers. Participants' neural activity was recorded using a 256-channel Hydrogel cap and EGI Net Amps amplifier (*Electric Geodesics, USA*). EEG data and Unity PC were synchronized via a parallel port.

2.2 Virtual Sailing Task and Instructions

The task of the participants was to sail a boat on a wavy sea in a virtual environment using the joystick (i.e., *Horizon Task, HT*). Wave height, frequency, and direction were controlled across participants. The boat would tilt forward and accelerate if two conditions were met: (1) a wave as high as the boat height reached the back part of the boat (i.e., *sailable wave onset*); and (2) the participant aligned the front of the boat perpendicular to the wave rim (i.e., the *underlying task rule*). The goal was to sail 36 sailable waves as fast as possible to a finish line. Participants performed the HT task at baseline and retention (Fig. 1).

Participants were randomly assigned to one of three training groups that used three different *task instruction types* (Fig. 1):

- (1) *Implicit Task Instruction (IMP)*: Single floating buoys appeared at random locations over an imaginary semi-circumference of radius 25 m.u. (*maritime units*) spanning from -90° to 90° relative to the advancing direction of the wave, centred 40 m.u. ahead of the boat in the wave direction. Participants were instructed to “*Try to catch as many buoys as possible*”. Thus, participants were disclosed no explicit information about the underlying task rule; they were just compelled to explore it.
- (2) *Explicit Task Instruction (EXP)*: Buoys were placed as in IMP. Participants were instructed: “*When you feel the wave behind you, point the boat straight to the wave direction to keep your speed high*”. Thus, the underlying task rule to succeed was disclosed.
- (3) *Explicit-Implicit Task Instruction (EXP-IMP)*: Visual cues, i.e., green “Go” buoys and red “No-Go” buoys, were placed ahead at 10 m.u. distance on the perpendicular to the wave rim. Participants were explicitly instructed to “*catch the green buoys*” and to “*avoid the red buoys*” to experience *catching* and *missing* a wave, respectively.

2.3 Data Collection and Analysis

The distance sailed towards the finish line during the wave propulsion time (i.e., [+150 ms, 3.44 s] from sailable wave onset) was computed. The distance improvement (Retention-Baseline) for *hit* waves (i.e., that resulted in a sustained speed increase) was used to assess participants’ ability to sail longer distances on waves as an effect of Task Instruction Type (tested using Kruskal-Wallis and corrected Mann-Whitney tests, $\alpha < 0.05$).

EEG data were pre-processed (i.e., artefact channel removal, 0.1–40 Hz band-pass filtering, and eye-artefact correction) using the Automagic toolbox for EEGLab, resulting in the inclusion of a total of 186 electrodes in the analysis. Temporal-Spectral Evolution (*TSE*) [6] of the alpha-band (7–15 Hz) signal reflecting alpha

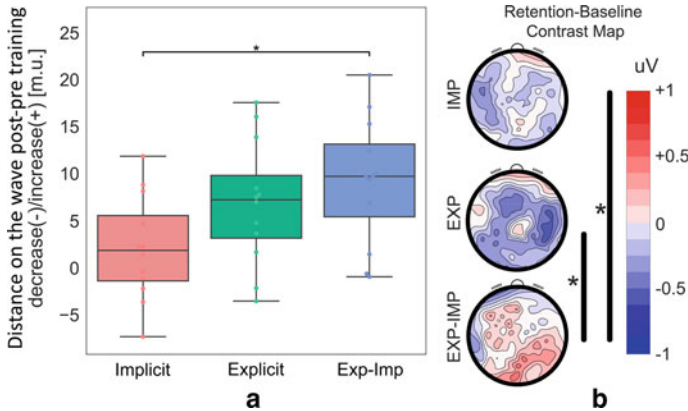


Fig. 2 Behavioral (a) and electrophysiological (b) results. Scalp maps (b) depict retention-baseline contrast map changes of alpha wave strength in micro-volts for each task instruction type. $^*(p < 0.05)$

wave strength was extracted for the time window $[-1 \text{ s}, +1 \text{ s}]$ from sailable wave onset across all electrodes and averaged per participant, Trial Type (*Hit/Missed* wave), and Phase (*Baseline/Retention*) using EEGLab. Contrast maps were computed as the TSE difference between trial types, characterizing the learning of the HT as the *neural-attentional distance* between hit and missed waves. To test if alpha TSE in the contrast maps is modulated across Task Instruction Type and Phase, a mixed-measures topographic ANOVA was performed (TANOVA, [7]). Alpha TSE in time intervals showing significant interactions was compared via corrected post-hoc pairwise comparisons between Task Instruction Type and baseline-normalized (i.e., Retention-Baseline) contrast maps (t-maps, [7], Fig. 2b).

3 Results

3.1 Enforcing Task Rule Supports Motor Learning

Task Instruction Type had a significant effect on the distance sailed ($p = 0.03$, Fig. 2a): Participants in the EXP-IMP ($p = 0.02$) group improved more than participants in IMP group. The improvement marginally differed between the EXP and IMP groups ($p = 0.09$).

3.2 Visual Cueing Supports Attentional Engagement

Alpha TSE difference in the contrast maps -50 to 350 ms relative to sailable wave onset evolved significantly differently depending on the Task Instruction Type (TANOVA, Task Instruction Type \times Phase, $p = 0.007$). Group EXP-IMP showed more occipital and frontal alpha wave strength after training than the EXP group ($p = 0.006$, Fig. 2b) and a trend for more parieto-occipital alpha wave strength than the IMP group ($p = 0.07$, Fig. 2b). Participants in EXP and IMP groups only showed a statistical trend for a significant difference ($p = 0.12$; IMP > EXP, Fig. 2b).

4 Conclusion

Our findings suggest superior motor learning linked to training with explicit knowledge about the task rules (EXP) and with visual cues enforcing these rules (EXP-IMP) compared with training without any enforcement of the task rules (IMP). Our neurophysiological results show that training with visual cues (EXP-IMP) enhanced alpha wave strength over parieto-occipital and frontal areas compared with the other task instruction types. Since it is generally acknowledged that alpha wave strength is linked with cortical inhibition [5], our finding on an enhanced alpha wave strength in EXP-IMP versus EXP and IMP may reflect a lower engagement of attentional brain networks after training with visual cues. Even though participants in the EXP and EXP-IMP groups improved their motor performance, training with visual cues (EXP-IMP) may be associated with cognitive facilitation, namely a lower engagement of selective visual (occipital) and executive (frontal) attentional brain networks after training [3–6]. Our results suggest that training parameters such as task instructions indeed modulate the attentional engagement during motor learning and may be an important factor to consider in neurorehabilitation. Studies with larger samples may further explore the effect of training parameters on cognitive processes during motor learning.

Acknowledgments This work was partially supported by the Swiss National Science Foundation through the grant PP00P2163800 and NCCR Robotics.

References

1. P. Fitts, *Human Performance* (Brooks/Cole Pub., 1967)
2. W.K. Lam, et al., Analogy versus explicit learning of a modified basketball shooting task: Performance and kinematic outcomes. *J. Sports Sci.* (2009)
3. L. Payne et al., Attention-modulated Alpha-band oscillations protect against intrusion of irrelevant information. *J. Cogn. Neurosci.* (2013)
4. J. Samaha, et al., Effects of meaningfulness on perception: Alpha-band oscillations carry perceptual expectations and influence early visual responses. *Sci. Rep.* (2018)

5. W. Klimesch, Alpha-band oscillations, attention, and controlled access to stored information. *Trends Cogn. Sci.* (2012)
6. G. Thut, et al., α -Band electroencephalographic activity over occipital cortex indexes visuospatial attention bias and predicts visual target detection. *J. Neurosci.* (2006)
7. M. Habermann, et al., A student's guide to randomization statistics for multichannel event-related potentials using Ragu. *Front. Neurosci.* (2018)

Agency and Responsibility While Controlling Movement Through Brain-Computer Interfaces for Neurorehabilitation



Maria V. Sanchez-Vives, Mel Slater, and Birgit Nierula

Abstract Brain-computer interfacing (BCI) that reads brain activity and generates commands to control the movements of the body—real, virtual, prosthetic or robotic—can be used as a means for neurorehabilitation. BCI can be used to carry out motor actions which, being lost through the real body, bypass it and use other effectors. However, do BCI-generated body movements result in feelings of agency? Our findings highlight the advantages of motor-imagery-based BCI protocols over steady-state visual-evoked potentials for their use in controlling surrogate bodies. BCI paradigms that use the activation of sensorimotor areas (motor imagery) induce greater agency and sense of responsibility, resulting in a more effective user-experience for neurorehabilitation.

Funded by Commission for Universities and Research of the Department of Business and Knowledge of the Generalitat de Catalunya—AGAUR—(2017 SGR 1296), Neurovirtual Group and partially funded by AGAUR—(IU16-011508). Partially funded by Fundació Mutua Madrileña under grant AP171552019. MS is supported by ERC MoTIVE grant #742989.

M. V. Sanchez-Vives (✉)
ICREA, Barcelona, Spain
e-mail: msanche3@clinic.cat

M. V. Sanchez-Vives · B. Nierula
Systems Neuroscience Group, IDIBAPS, Barcelona, Spain

M. Slater (✉)
Event Lab, Faculty of Psychology, University of Barcelona, Barcelona, Spain
e-mail: melslater@ub.edu

B. Nierula (✉)
Max Planck Research Group Pain Perception, Max Planck Institute for Human Cognitive and Brain Sciences, Leipzig, Germany
e-mail: nierula@cbs.mpg.de

1 Introduction

Neurorehabilitation is the rehabilitation of neural circuits, such that the neural processing carried out by these circuits and their functional outputs are recovered. The recovery of motor function lost after neural lesions (e.g., stroke, traumatic brain injury) is a primary objective of neurorehabilitation. There are various approaches inducing recovery of the damaged neural circuits, which may include direct action on the nervous tissue by means of stimulation. However, a common approach is to act on the body, with the objective of modifying sensorimotor activity to stimulate the corresponding sensorimotor neural circuits. When doing this, we act as if the body is an interface to the brain, and by acting on the body (moving, stimulating), we also influence brain circuits. Another strategy is to induce activity in neural circuits and, by means of brain-computer interfaces (BCI), record this activity and use it to control the body, thus providing feedback (visual, motor, proprioceptive, tactile) that closes the loop and contributes to neuroplasticity and recovery.

However, is it necessary that this body that moves be the real body? Over a decade of intense research in the field of embodiment confirms that the brain identifies virtual bodies as its own, provided that sensorimotor afferences are congruent [1–4]. Virtual body ownership not only impacts brain activity, but also has cognitive and behavioural consequences. In particular, we have demonstrated that ownership of a virtual body can be induced and that the consequences of this ownership range from influencing pain threshold [5, 6], to inducing brain error signals as a consequence of incorrect movements of the virtual body [7] or to influencing racial bias depending on the skin tone of the virtual body [8, 9].

Since the “embodiment” of a virtual body and its actions have such a large impact, controlling the movements of a virtual body can be a useful paradigm for rehabilitation. In our study [10] we described how a patient can use a head-mounted display and enter a rehabilitation centre in immersive virtual reality, where he/she owns a body, and this body goes through rehabilitation and realistically interacts with the therapist. Body ownership and correct feedback (visual, tactile, force) can trick the brain into the illusion that the actual movements are being carried out. However, the control of the movements of the virtual body can be achieved by different means, most commonly by tracking the real body that translates into virtual body control. Another possibility is the use of BCI.

1.1 *Brain-Computer Interface: Paradigms*

A BCI records, decodes and translates the neurophysiological signal corresponding to brain activity into electric signals [11, 12] that are used to control devices, robots, computers, or, as in this case, the movements of a virtual body [13–15].

There are different paradigms that can be used for BCI. One is based on steady-state visually evoked potentials (SSVEP) [12]. SSVEP-based BCI protocols exploit

visual stimuli that flicker at a specific frequency. When centred in the fovea, such stimuli produce oscillations at the stimulation frequency over the visual cortex that the BCI algorithm can detect with relatively high accuracy.

Sensorimotor rhythm (SMR)-based BCI protocols rely on changes in alpha-and/or beta-oscillations over somatosensory areas and use motor imagery to produce changes in the SMR. These changes can be seen in a decrease in band power relative to baseline [11] and have been observed in the alpha and/or beta-band during motor planning, imagination, execution, and observation of a movement [16, 17]. SMR-based BCI protocols utilize the somatotopic layout of the sensorimotor cortex, such that the BCI algorithm can distinguish whether the participant was imagining a foot, hand or lip movement.

1.2 Agency and Responsibility

Agency is the attribution of an action to the self and has important relevance in our everyday lives. It implies the capability to perform and control an action that is in accordance with objectives. It involves the subjective experience of being in control of one's actions [18]. This experience occurs when there is an association between the voluntary command and its outcome. Responsibility also has a close connection to agency [18], since when a subject has agency over an action that has an effect, the subject should feel responsible for this effect. The question that guides the issue being analysed here is: *Do we feel agency and responsibility over actions controlled by means of BCI?*

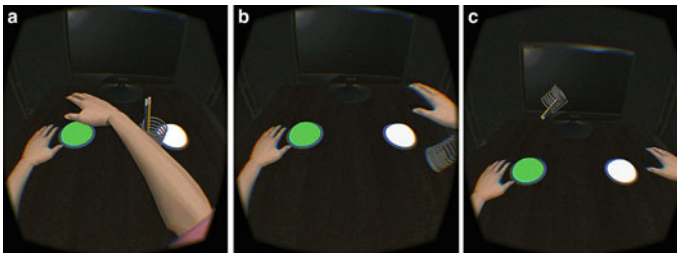


Fig. 1 “Embodied” virtual body controlled by BCI. In four random trials of one experimental condition an object fell off the table. In three of those trials the virtual body knocked the object off the table (**a**, **b**) and in one trial the object fell off the table by itself (**c**). Participants were asked to rate the degree of perceived responsibility for this outcome directly after the trial [14]

1.3 Agency Over Virtual Bodies

The illusion of ownership of a virtual body [1, 2] has consequences at different levels (physiological, behavioural, cognitive). One such consequence is that high levels of body ownership engender an illusion of agency over the movements and actions carried out by the virtual body [19], a strategy that can be used for neurorehabilitation. Ownership and agency over an embodied robotic body has been found to be associated with guilt over an action that the robot carried out independently of the subject, indicating a strong identification with the actions of the surrogate body. As well as ownership being induced by the correspondence between actual and surrogate body movements, it can also be induced through a BCI [13].

1.4 Agency and Responsibility Over BCI-Controlled-Movements

After inducing embodiment of a virtual body in [14], subjects saw their ‘owned’ virtual arm performing a task (Fig. 1) either by means of control of the movement through motor imagery (SMR) or control of the movement through activation of visual areas (SSVEP) [14, 15]. Both conditions were carried out using BCI and both shared the intention and the resulting action. BCI-control of movements engendered a sense of agency, which was strongest for motor imagery. Interestingly, only motor imagery-BCI induced responsibility. Furthermore, increased activity of sensorimotor areas correlated with levels of agency and responsibility. BCI-performance, however, could not explain the results as participants performed better in SSVEP than in motor imagery BCI.

2 Conclusion

The embodiment of a virtual body can be achieved through congruent sensorimotor inputs. The control of a virtual body by means of BCI can be used to induce neuroplasticity and neurorehabilitation. However, not all BCI paradigms are as effective in inducing agency and responsibility over motor actions. Paradigms involving activity in sensorimotor areas are more effective as measured with the subjective experience of agency over the virtual movement, with practical and ethical implications. Activation of the sensorimotor cortex for BCI during embodiment may also have a higher impact on neuroplasticity, although this requires further investigation.

References

1. M. Slater, D. Pérez Marcos, H. Ehrsson, M.V. Sanchez-Vives, Towards a digital body: the virtual arm illusion. *Front. Hum. Neurosci.* **2**, 6 (2008)
2. M. Slater, D. Pérez Marcos, H. Ehrsson, M.V. Sanchez-Vives, Inducing illusory ownership of a virtual body. *Front. Neurosci.* **3**, 29 (2009)
3. M.V. Sanchez-Vives, B. Spanlang, A. Frisoli, M. Bergamasco, M. Slater, Virtual hand illusion induced by visuomotor correlations. *PLoS ONE* **5**(4), e10381 (2010)
4. O. Blanke, Multisensory brain mechanisms of bodily self-consciousness. *Nat. Rev. Neurosci.* **13**(8), 556–571 (2012)
5. B. Nierula, M. Martini, M. Matamala-Gomez, M. Slater, M.V. Sanchez-Vives, Seeing an embodied virtual hand is analgesic contingent on colocation. *J. Pain* **18**(6), 645–655 (2017)
6. M. Matamala-Gomez, B. Nierula, T. Donegan, M. Slater, M.V. Sanchez-Vives, *J. Clin. Med.* **9**(2), 291 (2020)
7. G. Padrao, M. Gonzalez-Franco, M.V. Sanchez-Vives, M. Slater, A. Rodriguez-Fornells, *Neuroimage* **124**, 147–156 (2016)
8. T.C. Peck, S. Seinfeld, S.M. Aglioti, M. Slater, *Conscious Cogn.* **22**, 779–787 (2013)
9. L. Maister, M. Slater, M.V. Sanchez-Vives, M. Tsakiris, *TICS* **19**(1), 6–12 (2015)
10. D. Perez-Marcos, et al., A fully immersive set-up for remote interaction and neurorehabilitation based on virtual body ownership. *Front. Neurol.* **3**, 110 (2012)
11. G. Pfurtscheller, F.L. Da Silva, Event-related EEG/MEG synchronization and desynchronization: basic principles. *Clin. Neurophysiol.* **110**(11), 1842–1857 (1999)
12. J.R. Wolpaw, N. Birbaumer, D.J. McFarland, G. Pfurtscheller, T.M. Vaughan, Brain–computer interfaces for communication and control. *Clin. Neurophysiol.* **113**(6), 767–791 (2002)
13. D. Perez-Marcos, M. Slater, M.V. Sanchez-Vives, Inducing a virtual hand ownership illusion through a brain–computer interface. *NeuroReport* **20**(6), 589–594 (2009)
14. B. Nierula, B. Spanlang, M. Martini, M. Borrell, V.V. Nikulin, M.V. Sanchez-Vives, Agency and responsibility over virtual movements controlled through different paradigms of brain–computer interface. *J. Physiol.* (2019). <https://doi.org/10.1113/JP278167>
15. B. Nierula, M.V. Sanchez-Vives, Can BCI paradigms induce feelings of agency and responsibility over movements? in *Brain-Computer Interface Research* (Springer, Cham), pp. 103–114
16. C. Neuper, M. Wörtz, G. Pfurtscheller, ERD/ERS patterns reflecting sensorimotor activation and deactivation. *Prog. Brain Res.* **159**, 211–222 (2006)
17. V.V. Nikulin, F.U. Hohlefeld, A.M. Jacobs, G. Curio, Quasi-movements: a novel motor–cognitive phenomenon. *Neuropsychologia* **46**(2), 727–742 (2008)
18. P. Haggard, Sense of agency in the human brain. *Nat. Rev. Neurosci.* **18**(4), 196 (2017)
19. D. Banakou, M. Slater, Body ownership causes illusory self-attribution of speaking and influences subsequent real speaking. *Proc. Natl. Acad. Sci.* **111**(49), 17678–17683 (2014)

Adaptation to Virtual Surgeries Across Multiple Practice Sessions



Daniele Borzelli, Sergio Gurgone, Maura Mezzetti, Paolo De Pasquale, Denise J. Berger, Demetrio Milardi, Giuseppe Acri, and Andrea D'Avella

Abstract Myoelectric control of an isometric reaching task in a virtual environment allows to investigate motor adaptation after simulating a perturbation of the muscle pulling directions (virtual surgeries). Such perturbations can be compatible or incompatible with the muscle synergies involved in the generation of multidirectional forces. A recombination of the synergies can generate forces in all directions after a compatible surgery but require new synergies after an incompatible surgery. Previous work demonstrated that, in a single experimental session, subjects adapted only to a compatible perturbation. In this study, we investigated whether extended practice leads to adaptation also after an incompatible perturbation. After three daily sessions, participants who practiced the incompatible surgery improved their performance, achieving a similar performance to that of those who practiced the compatible surgery. These results suggest that extended practice with incompatible virtual surgeries allows learning how to skillfully use novel muscle patterns.

D. Borzelli (✉) · S. Gurgone · P. De Pasquale · D. Milardi · G. Acri · A. D'Avella
Department of Biomedical and Dental Sciences and Morphofunctional Imaging, University of Messina, Messina, Italy
e-mail: dborzelli@unime.it

D. Borzelli · P. De Pasquale · A. D'Avella
Laboratory of Neuromotor Physiology, IRCCS Fondazione Santa Lucia, Rome, Italy

M. Mezzetti
Department of Economics and Finance, University of Rome "Tor Vergata", Rome, Italy

D. J. Berger
Department of Systems Medicine, Centre of Space Bio-Medicine, University of Rome "Tor Vergata", Rome, Italy

1 Introduction

MYOELECTRIC control of a virtual end-effector during the exertion of submaximal isometric forces has been used to investigate how the CNS adapts to simulated perturbations of the muscle pulling forces and to provide direct support to muscle synergies [1]. These perturbations (virtual surgeries) were designed such that participants, in order to move the end-effector in all target directions, had to either recombine the existing set of muscle synergies (compatible surgeries), or to use novel muscle patterns (incompatible surgeries). As predicted by a neural organization of muscle synergies, assuming that learning of new synergies is a slower adaptive process than recombining existing synergies, after a single-session of practice, performance (i.e. the fraction of trials in which the participant reached the target) increased after a compatible surgery whereas it did not significantly increase after an incompatible surgery. However, we hypothesize that more time available for practice would lead to learning of new synergies and, thus, to adaptation also after an incompatible perturbation. Therefore, in this study, we tested this prediction by asking participants to practice the virtual surgeries for three daily sessions.

2 Material and Methods

2.1 Subjects

Eighteen right-handed subjects (mean age \pm std: 27.2 ± 6.5) participated in the experiments after giving written informed consent. All procedures were conducted in conformance with the Declaration of Helsinki and were approved by the Ethical Review Board of IRCCS Neurolesi ‘Bonino Pulejo’ (Fig. 1).

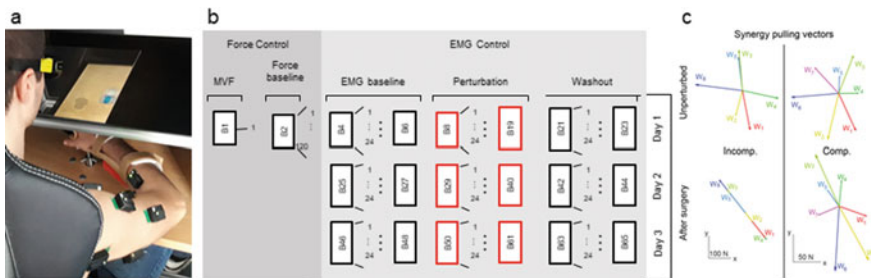


Fig. 1 **a** Experimental apparatus. **b** Sequence of blocks performed during the three sessions and analyzed in this study. **c** Example of synergy pulling vectors before (top) and after (bottom) an incompatible (left) and a compatible (right) surgery

2.2 Setup

Participants sat in a chair with car belts immobilized the torso and shoulders and had their hand and forearm fixed in an orthosis rigidly connected with a 6-axis force and torque transducer (Fig. 1a). They viewed stereoscopically, through shutter glasses, a scene with a spherical cursor and spherical targets above a desktop displayed by a 3D monitor and reflected on a mirror occluding the real desktop. The cursor displacement from a central rest position corresponding to the position of the palm was proportional to the force either exerted (force control blocks) or estimated from EMG (EMG control blocks) in real-time. Bipolar wireless surface EMG electrodes collected the activity of 15 shoulder and elbow muscles.

2.3 Protocol

The experiment consisted of 3 daily sessions (see Fig. 1b). After two initial force control blocks, required to estimate maximum voluntary force (MVF), EMG-to-force mapping, muscle synergy matrix, and perturbation matrix, participants performed an isometric reaching task using EMG control. In each daily session participants then performed a sequence of 21 blocks, each composed of 24 trials, in which they were asked to move the virtual cursor accurately and quickly from the rest position to a target, in one of eight horizontal directions. In 18 blocks feedback from the three-dimensional position of the cursor was available: 3 unperturbed EMG baseline blocks, 12 perturbed blocks, 3 unperturbed washout blocks. The remaining blocks in which the cursor position was not displayed were not analyzed.

2.4 EMG-To-Force Mapping, Synergy and Perturbation Matrices

The EMG-to-force matrix was calculated from the regression of the EMG data on each end-point force component. The muscle synergy matrix was identified by non-negative matrix factorization from the EMG data. The number of synergies was selected as the minimum number that explained at least 90% of the data variation collected during the force baseline block.

Virtual surgeries (see Fig. 1c), which simulated a rearrangement of the tendon positioning on the shoulder-elbow system, were performed by altering the EMG-to-force mapping as a rotation in muscle space [1]. Participants were randomly assigned to one of two groups: ten practiced the incompatible surgery (one of which was excluded because of poor EMG-to-force mapping reconstruction) and eight practiced the compatible surgery.

The EMG-to-force mapping, the synergy matrix, and the perturbation matrix were calculated with data collected during the force baseline. Such matrices were consistent across the three experimental sessions [2].

2.5 Statistics

Generalized linear mixed models were used to assess the relationship between the trial success variable (1 if the participant reached the target, 0 otherwise) and both random (participant) and fixed (type of surgery, session number, perturbed block number, and target) effects during each trial. P-values were obtained by likelihood ratio tests of the full model with the type of surgery effect against the model without it.

3 Results

Participants were able to control the cursor and reach the target in $76.8\% \pm 9.9\%$ of the trials during EMG baseline blocks. The R^2 of the reconstruction of the tri-dimensional force, collected during the EMG baseline blocks was 0.84 ± 0.05 . Consistently with previous studies [3], 6.1 ± 0.8 (mean \pm std over subjects) synergies explained 0.81 ± 0.06 of the variability of the EMG pattern collected during the EMG baseline blocks.

On average performance improved over the three sessions with both types of perturbations (Fig. 2). The effect of the type of surgery on trial success in all three sessions was significant ($p = 0.021$), indicating an overall difference in the performance of participants who practiced the incompatible or the compatible perturbations. Notably, the standard deviation across subjects of the performance as a function of block number (Fig. 2, *shaded areas*) was large, suggesting remarkable individual differences in learning ability.

When considering each session separately, the effect of the type of surgery was significant in the first ($p = 0.013$, in line with [1]), and second ($p = 0.002$) sessions, but not in the third session ($p = 0.190$), suggesting that a long enough exposure to the incompatible surgery allows participants to achieve a performance similar to the one achieved by those who practiced the compatible surgery.

4 Conclusion

In this study, participants were given three daily sessions to practice an isometric force reaching task, in the presence of a virtual perturbation of the mapping between

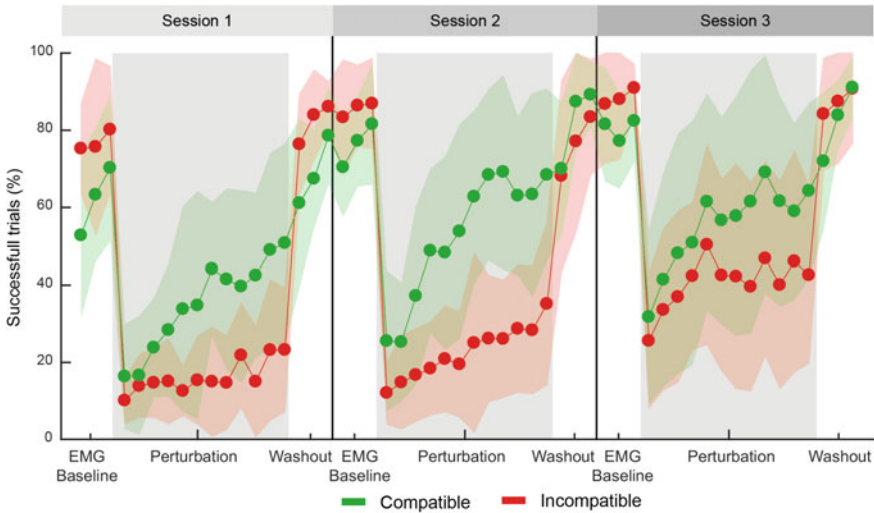


Fig. 2 Percentage of successful trials for each block (mean \pm std across subjects). Force control blocks are not displayed

EMG and force, either compatible or incompatible with muscle synergies. As a significant difference in the performance with the two types of surgeries was observed during the first and second sessions but not during the third one, this result supports the hypothesis that with enough practice it is possible to learn new muscle synergies, i.e. to generate novel muscle coordination patterns necessary to perform a goal-oriented task with a novel mapping. It also indicates that the adaptive process involved in the compensation of incompatible surgeries (learning new synergies) is slower than the process involved in the compensation of compatible surgeries (recombining existing synergies) but effective in improving performance already after three sessions. Analyses will further characterize these processes by investigating savings and retention, feedback and feedforward control, and implicit and explicit learning strategies. Finally, as both adapting to an incompatible perturbation and learning a new motor skill require novel muscle coordination patterns, investigating neuroplasticity after extended practice with virtual surgeries may provide novel insights on the underlying neural mechanisms. Training with myoelectric control in a virtual environment might also be useful in neurorehabilitation.

Acknowledgments This work was supported by the Italian University Ministry (PRIN grant 2015HFWRYY).

References

1. D.J. Berger, R. Gentner, T. Edmunds, D.K. Pai, A. D'Avella, Differences in adaptation rates after virtual surgeries provide direct evidence for modularity. *J. Neurosci.* **33**(30), 12384–12394 (2013)
2. D. Borzelli, S. Gurgone, P. De Pasquale, D. J. Berger, & A. d'Avella, Consistency of myoelectric control across multiple sessions, in *Biosystems and Biorobotics*, vol. 21 (2019), pp. 1166–1170
3. D. Borzelli, D.J. Berger, D.K. Pai, A. D'Avella, Effort minimization and synergistic muscle recruitment for three-dimensional force generation. *Front. Comput. Neurosci.* **7**, 186 (2013)

Brain-Computer Interface-Based Neurorehabilitation: From the Lab to the Users' Home



C. Escolano, E. López-Larraz, J. Mínguez, and L. Montesano

Abstract Most of the research in brain-computer interfaces (BCIs) to date is conducted using stationary electroencephalogram (EEG) equipment with high density recordings, and performed in controlled laboratory settings. Moving BCI-based neurorehabilitation or motor substitution applications from the laboratory to home settings will improve accessibility to these therapies while allowing a more intensive data collection to foster the scientific progress. One of the barriers for this is the EEG technology itself. We developed a new dry EEG system within the More-Grasp H2020 EU project to allow BCI home use for spinal cord injury patients. This paper describes the EEG activity measured with this new EEG system under well known experimental protocols such as resting-state, visual evoked potentials, and self-initiated reach-and-grasp movements.

1 Introduction

One of the aims of brain-computer interfaces (BCIs) is to improve the quality of life of people with difficulties to perform daily life activities, such as communication or mobility. Control of neuroprosthetics is one of the most studied BCI applications, as it can be used for neurorehabilitation and motor substitution for people suffering motor impairments due to a spinal cord injury (SCI) or stroke. The basic idea is

C. Escolano, J. Mínguez, E. López-Larraz and L. Montesano are with Bitbrain.

C. Escolano (✉) · E. López-Larraz · J. Mínguez · L. Montesano
Bitbrain, Zaragoza, Spain
e-mail: carlos.escolano@bitbrain.es

E. López-Larraz
e-mail: eduardo.lopez@bitbrain.es

J. Mínguez
e-mail: javierminguez@bitbrain.es

L. Montesano
e-mail: luis.montesano@bitbrain.es

© The Author(s), under exclusive license to Springer Nature Switzerland AG 2022
D. Torricelli et al. (eds.), *Converging Clinical and Engineering Research on Neurorehabilitation IV*, Biosystems & Biorobotics 28,
https://doi.org/10.1007/978-3-030-70316-5_91

that the modulation of brain activity can be used to control external devices that compensate the lost function [1] or facilitate functional recovery through their use [2].

Most of this research is done using stationary electroencephalogram (EEG) equipment with high density recordings in controlled laboratory settings (e.g., electromagnetically isolated rooms). These conditions, however, need to be reconsidered when transitioning to more ecological settings (such as the home of the users), which brings other factors such as usability and user acceptance. Indeed, this is not just a barrier for the transfer of results to real life. It also hinders the scientific progress since the amount of data and evidence that can be collected, analyzed and shared is limited to those that can be collected in research centers, which are usually expensive and difficult to scale up.

Bringing the technology to the end users' home will be a game changer for this type of applications: it will allow to reach more people that will potentially use the system for longer periods of time, with the potential to boost the results and the impact in their lives. This is, however, not an easy endeavour. Designing BCIs for home-use requires considering several usability factors to favor a frequent use (even daily), such as short set up times, easy to handle mobile devices, and gel-less electrodes that do not require to wash the hair and apply heavy hygienic afterwards. Notwithstanding, the signal quality needs to be in a similar range that the research-grade counterparts.

This study presents a new dry-EEG system developed within the MoreGrasp H2020 EU project [3], following a user-centered design methodology to be used for motor substitution and rehabilitation of SCI survivors at home. The main characteristics of the system are: (1) dry-EEG sensors that do not require any conductive substance and improve usability; (2) layout over the sensorimotor cortex; and (3) comfortable headset that can be set up in a few minutes without technical support. As mentioned, it is essential to provide reliable EEG signals with sufficient quality for the intended motor BCI applications. This paper reports the results of the wearable dry-EEG device (Hero, Bitbrain, Spain) used to record spontaneous activity, visual evoked potentials, and EEG-correlates of reach-and-grasp movements.

2 Methods

We conducted two separate experiments to cover the most typical EEG patterns used in BCI applications (right-handed able-bodied participants). The first one recorded resting state EEG and visual evoked potentials ($n = 16$, 20–35 age range); the second one, EEG correlates of self-initiated reach-and-grasp actions ($n = 15$, 15–30 age range).

The two experiments were conducted in Bitbrain (Fig. 1) using the wireless dry-EEG device (Hero, Bitbrain, Spain). The system has 11 sensors located over the sensorimotor cortex (FC3, FCZ, FC4, C3, C1, CZ, C2, C4, CP3, CPZ, and CP4) with the ground and reference sensors in the left earlobe, and a sampling rate of



Fig. 1 Wireless dry-EEG device during the execution of the reach-and-grasp actions

256 Hz. The software employed for stimulus presentation and data collection was a multimodal BCI programming platform (BCI Development Platform, Bitbrain).

1. *Resting state EEG*: EEG was recorded in resting state conditions (eyes closed and eyes open, 3 min each).
2. *Visual oddball P300 task*: The task consisted of two blocks, where each block had 30 target and 90 non-target stimuli (1/4 target probability). A red (target) or blue (non-target) dot was displayed on the screen during 250 ms. The inter-stimulus interval was random in the [1.25–1.75] s range. Total time for each block was 3.5 min.
3. *Self-initiated reach-and-grasp actions*: Participants were instructed to perform reach-and-grasp actions with their right hand towards two objects: a glass (palmar grasp) and a spoon within a jar (lateral grasp). We asked them to focus their gaze on the object to grasp for at least 2 s before starting the movement. A total of 80 trials per condition were recorded, distributed in four runs (20 trials each). The location of the objects were switched between runs.

3 Results

3.1 Resting State EEG

EEG data from resting state conditions were transformed to the frequency domain using a short-term FFT transform. Figure 2a shows the group-level power spectra in both eyes closed and open conditions for the CPz sensor (mean and standard error of the mean), which shows the typical alpha-blocking phenomenon reported in literature.

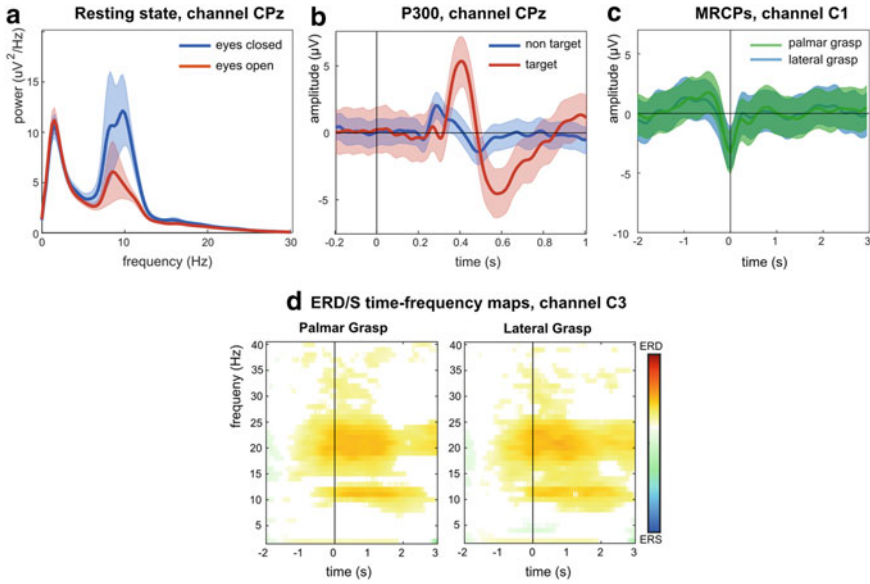


Fig. 2 EEG correlates for the dry-EEG device in **a** resting state conditions, **b** a visual evoked P300 paradigm, and **c–d** a motor task involving reach-and-grasp actions (MRCPs and ERD/S time-frequency maps)

3.2 Visual Oddball P300 Task

EEG data from the P300 task was bandpass filtered in the [1–10] Hz range. Data was epoched using a [−0.2 1] s time window relative to stimulus onset. For each condition (target, non-target) the average across trials was computed, and the 95% confidence interval of a bootstrap procedure (1000 permutations) using the mean as the statistic. Figure 2b shows the group-level visual-evoked potential for the CPz sensor. There is a clear difference between target and non-target conditions, depicting a visual P300 waveform in agreement with literature in this domain [5].

3.3 Self-initiated Reach-and-Grasp Actions

We analyzed low-frequency movement-related cortical potentials (MRCPs) and event-related (de)synchronization (ERD/S) time-frequency maps. For the MRCPs, a low-pass filter with a cut-off frequency of 3 Hz was applied. Then, EEG data was epoched into trials with a [−2 3] s time window relative to the movement onset. We determined a 95% confidence interval for each condition using non-parametric *t*-percentile bootstrap statistics and computed the grand-average across participants. Regarding the ERD/S time-frequency maps, we applied a [1–60] Hz bandpass filter

and computed the ERD/S for each frequency bin (range [2–40] Hz, 1 Hz resolution) using a reference interval of $[-2 -1]$ s with respect to the movement onset. To obtain grand-average ERD/S maps, we computed the average and confidence intervals (non-parametric t -percentile bootstrap statistics, $\alpha = 0.05$), and the non-significant time-frequency points are not shown in the maps.

Figure 2c–d shows the group-level MRCPs and ERD/S time-frequency maps in contralateral sensors. A negative deflection can be observed in the MRCPs waveform at movement onset that starts around 0.5 s before the movement onset. Desynchronization patterns can be observed in the time-frequency ERD/S maps, with larger values in alpha (8–12) Hz and beta (15–25) Hz frequency bands. For a detailed comparison with other type of electrodes see [4], which also shows that, using the same number and location of sensors, the decoding performance is not statistically different from widely spread and standard EEG research systems.

4 Conclusion

EEG systems are the cornerstone for the effective introduction of BCIs in real-world applications outside the lab, as well as for the effective adoption in user-centered fields. In recent years, there have been strong R&D efforts in developing new EEG technologies with enhanced usability and comfort, without sacrificing reliability and accuracy. This paper briefly described how one of these new dry-EEG devices was able to reliably measure the most typical brain patterns used for BCIs in practical scenarios.

Acknowledgements We thank Andreas Schwarz and Gernot Müller-Putz for their support with the MRCP and ERD analysis.

References

1. J. Millán, d. R., et al., Combining brain-computer interfaces and assistive technologies: state-of-the-art and challenges. *Front. Neurosci.* **4**, 161 (2010)
2. E. López-Larraz et al., Brain-machine interfaces for rehabilitation in stroke: a review. *Neuro Rehabil.* **43**, 77–97 (2018)
3. Müller-Putz, G. R., et al., Applying intuitive EEG-controlled grasp neuroprostheses in individuals with spinal cord injury: preliminary results from the MoreGrasp clinical feasibility study, in *41st Annual International Conference on IEEE EMBS (EMBC)* (2019), pp. 5949–5955
4. A. Schwarz et al., Analyzing and decoding natural reach-and-grasp actions using gel, water and dry EEG systems. *Front. Neurosci.* **14**, 849 (2020)
5. R. Fazel-Rezai et al., P300 brain computer interface: current challenges and emerging trends. *Front. Neuroeng.* **5**, 14 (2012)
6. E. López-Larraz et al., Continuous decoding of movement intention of upper limb self-initiated analytic movements from pre-movement EEG correlates. *J. Neuroeng. Rehabil.* **11**, 153 (2014)

Healing the Virtualizing Brain Using Virtual Reality: How Goal-Oriented, Embodied, Immersive VR Training Works



Paul F. M. J. Verschure

Abstract This paper analyzes the question what the principles are behind the success of the Rehabilitation Gaming System in the treatment of functional deficits post stroke. The hypothesis is that by projecting the recovering brain in a virtual task space adhering to basic ecological parameters such as embodiment, the forward models underlying voluntary action are optimally driven to functionally reorganize. This virtualization hypothesis is further linked to the Distributed Adaptive Control theory of mind and brain and specific results obtained with intracranial epilepsy patients and the detailed study of motor control.

1 Stroke and the Rehabilitation Gaming System

Stroke is the leading burden of disease for neurological disorders accounting for about 5% of global disability adjusted life years [1]. It is predicted that by 2025, 1.5 million European people will suffer a stroke annually. In addition to primary effects, these patients face additional poor outcomes including re-hospitalisation (33%), recurrent events (7–13%), dementia (7–23%) mild cognitive disorder (35–47%), depression (30–50%), and fatigue (35–92%) [2]. This rapid growth in the number of patients needing care and rehabilitation requires an urgent response that is both scientifically grounded and scalable. We have realized such a solution called the Rehabilitation Gaming System (RGS) which combines theoretical neuroscience grounded, Virtual Reality based, and AI enhanced intervention protocols (Fig. 1). The core concept behind RGS is that the recovering brain is to establish new pathways to organize voluntary goal-oriented action which has to couple the different layers of control. In other words, rehabilitation starts with the modulation of goal setting and stimulation of the forward models that guide voluntary action. This is in contrast to the standard approach of neurorehabilitation which strongly focuses on

P. F. M. J. Verschure (✉)

Institute of Bioengineering for Catalunya, Barcelona Institute of Science and Technology, Catalan Institute of Advanced Studies, Barcelona, Spain

URL: <https://specs-lab.com>



Fig. 1 The RGS setup illustrating its different components and underlying hypotheses

peripheral manipulation and repetitive movement as for instance captured in occupational therapy and constraint induced movement therapy. However, both of these well-established methods have also become under some scrutiny due to a lack of impact [3]. In comparison, RGS has shown impact in a range of domains including: motor, affective, cognitive [4] and language [5] and over a broad range of chronicity [6]. RGS has shown that only the passive observation of its VR training protocols leads to strong activation of fronto-parietal cortical networks [7]. More surprisingly it was demonstrated using a guided transcranial magnetic stimulation protocol that in chronic stroke patients who train with RGS, also the innervation of distal hand muscles, i.e. the abductor pollicis brevis, improves as a function of training, even when the associated hand functions are not explicitly targeted in the training protocol beyond the imagining and animation of grasp movements [8]. Another illustration of the benefits of RGS rehabilitation is that the intention compatible augmentation of actions in a virtual environment leads to rapid restoration of symmetry in hand use lost due to acquired non-use [9]. Hence, these observations raise the fundamental question why the engagement in task oriented, embodied training is effective? All these RGS examples share an important feature: the training protocols modulate the internal models underlying action, rather than forcing or driving explicit execution and repetition. I will further investigate this hypothesis.

2 Distributed Adaptive Control and Virtualization

RGS is based on the Distributed Adaptive Control theory of mind and brain which proposes that the brain is a multi-layered control architecture from the predefined

reactive control loops of the brain stem to immediate adaptive shaping of action by the cerebellum and the learned cognitive control provided by forebrain systems such as the neocortex, hippocampus and basal ganglia [10]. Moving up this hierarchy means that control strategies switch from predefined fast feedback loops to memory dependent forward models at varying spatio-temporal scales. This shift can be characterized as an incremental virtualization of the task space and the self that operates in it [11]. In other words, instead of operating directly on actual sensory signals, the forebrain operates on internal models of what these signals represent. We have found a dramatic illustration of this virtualization process in the recordings of human pharmaco-resistant epilepsy patients who were asked to perform a memory recall task [12]. Using reinstatement analysis, we were able to show that item specific neural responses showed a distinct time warping between encoding and recall in the hippocampus, the latter appearing much earlier after stimulus onset as compared to their occurrence during encoding. This shows that the analog event of the stimulus onset is not dominating the neuronal response in the hippocampal-cortical system, but rather the internal representations it has formed.

We have also found evidence for a forward model dependent virtualization in motor learning. The dominant model of motor control relies on the notion of an, so called, inverse model that by learning from errors acquires corrective responses that replace reflexive feedback control [13]. However, these models have difficulties in realistic task environments where an agent encounters an unpredictable and variable world because they replace feedback by feedforward control creating a brittleness to exceptions. In contrast, adaptive motor control can also be obtained by relying on a cascade of purely forward sensory predictions that drive feedback control via, so called, counterfactual errors [14]. In other words, primitive and fast brain control systems are driven into action via top-down virtual error control signals that are shaped through learning to drive feedback control in an anticipatory manner. Surprisingly this concept explains a number of physiological results that thus far appeared elusive in particular with respect to the significant recurrent coupling between the adaptive motor control circuits of the cerebellum and the forward models of the frontal cortex [15].

3 Conclusions

In conclusion, the RGS system has shown that projecting a recovering brain into a virtual task space with a distinct embodiment, ecological validity and goal setting is effective. This has led to the prediction that neurorehabilitation should target the internal models that drive goal-oriented action rather than explicitly controlling movement. A detailed exploration of this notion has shown that it can be interpreted as a manifestation of the virtualization that occurs when frontal memory dependent brain processes engage with action control. Stroke patients that survive most frequently display lesions in the neocortex and white matter tracts [16]. Given the virtualization hypothesis, this implies that deficits will be largely dependent on the disruption of

the internal models of perception, cognition and action control rather than the direct control of the skeletal-muscle system. RGS induces the significant impact that has been reported in all domains of stroke symptomatology by virtue of modulating and driving the cortical systems underlying voluntary action.

Acknowledgments Supported by the European Commission via the ERC project cRGS and EIT Health project RGS@Home.

References

1. J.J. Sejvar, Global burden of neurological disease: what's in a name?. *Lancet Neurol* **16**(11), 858–859 (2017)
2. Y. Béjot, et al., Epidemiology of stroke in Europe and trends for the 21st century. *La Presse Médicale* **45**(12), e391–e398 (2016)
3. G. Kwakkel, et al., Effects of unilateral upper limb training in two distinct prognostic groups early after stroke the EXPLICIT-stroke randomized clinical trial. *Neurorehabil. Neural Repair* 1545968315624784 (2016)
4. M. Maier, et al., Depression modulates attentional processing after stroke, in *International Conference on NeuroRehabilitation* (Springer, Berlin, 2018), pp. 702–706
5. K. Grechuta et al., Augmented sensorimotor dyadic therapy boosts recovery in patients with nonfluent aphasia: a randomised controlled trial. *Stroke* **50**(5), 1270–1274 (2019)
6. B. B. Rubio, et al.: A critical time window for recovery extends beyond one-year post-stroke. *J. Neurophysiol.*
7. Prochnow, D. et al. (2013) 'A functional magnetic resonance imaging study of visuomotor processing in a virtual reality-based paradigm: Rehabilitation Gaming System.', *The European journal of neuroscience*, *37*(9), pp. 1441–7. doi: <https://doi.org/10.1111/ejn.12157>.
8. B. R. Ballester, et al., Domiciliary VR-based therapy for functional recovery and cortical reorganization: randomized controlled trial in participants at the chronic stage post stroke. *JMIR Serious Games* **5**(3) (2017)
9. B. R. Ballester, et al., The visual amplification of goal-oriented movements counteracts acquired non-use in hemiparetic stroke patients. *J. NeuroEng. Rehabil.* **12**(1) (2015). <https://doi.org/10.1186/s12984-015-0039-z>
10. P. F. M. J. Verschure, C. M. A. Pennartz, G. Pezzulo, The why, what, where, when and how of goal-directed choice: neuronal and computational principles. *Philos.Trans. R. Soc. Lond B. Biol.Sci.* **369**, 20130483 (2014). <https://doi.org/10.1098/rstb.2013.0483>
11. P. F. M. J. Verschure, Synthetic consciousness: the distributed adaptive control perspective. *Philos. Trans. R. Soc. London Ser. B Biol. Sci.* **371**(1701), 263–275 (2016). <https://doi.org/10.1098/rstb.2015.0448>
12. D. Pacheco Estefan, et al., Coordinated representational reinstatement in the human hippocampus and lateral temporal cortex during episodic memory retrieval. *Nat. Commun.* **10**(1), 2255 (2019)
13. M. Kawato, K. Furukawa, R. Suzuki, A hierarchical neural-network model for control and learning of voluntary movement. *Biol. Cybern.* **57**(3), 169–185. <https://doi.org/10.1007/BF00364149>
14. G. Maffei, et al. The perceptual shaping of anticipatory actions. *Proc. R. Soci. B: Biol. Sci.* **284**(1869). <https://doi.org/10.1098/rspb.2017.1780>
15. M.M. Ten Brinke, H.-J. Boele, C.I. De Zeeuw, Conditioned climbing fiber responses in cerebellar cortex and nuclei. *Neurosci. Lett.* **688**, 26–36 (2019)
16. M. Corbetta, et al., Common behavioral clusters and subcortical anatomy in stroke. *Neuron* **85**(5), 927–941 (2015). <https://doi.org/10.1016/j.neuron.2015.02.027>

The Application of Sensory Error Manipulations to Motor Rehabilitation and Diagnostics After Brain Damage



Ballester R. Belén and Verschure F. M. J. Paul

Abstract The recovery of motor function after suffering a brain injury is still poorly understood. There are complex interactions between motor learning and motor recovery principles, which guide neural reorganization and allow the reacquisition and restitution of goal-oriented motor patterns (Maier et al. in *Front. Syst. Neurosci.* 13:74 (2019) [1]). This paper, reviews several studies and applications for rehabilitation and impairment assessment. Were we capitalize on the interaction between motor learning and motor recovery principles and investigate the manipulation of visuomotor feedback for the delivery of optimal neurorehabilitation and diagnostics for motor deficits after stroke and cannabis addiction.

1 The Reduction in the Magnitude of Sensory Errors Promotes the Use of the Affected Arm in Stroke Patients

1.1 Evidence from an Observational Study

Twenty hemiparetic stroke patients underwent a test with reduced visual error feedback while performing a bimanual reaching movement task in a non-immersive Virtual Reality (VR) setup (Fig. 1) [2]. We found that in patients experiencing visual amplification of goal-oriented reaching movements in VR, the probability of spontaneously using the paretic limb increased significantly ($p < 0.01$, Wilcoxon signed-rank test). This effect was attenuated during the washout phase but remained significantly different from baseline ($p = 0.04$, Wilcoxon signed-rank test). Interestingly, a sequential analysis revealed that the selection of the paretic limb was strongly biased

B. R. Belén · V. F. M. J. Paul
SPECS Lab, Institute for Bioengineering of Catalonia (IBEC), The Barcelona Institute of Science and Technology, Barcelona, Spain

V. F. M. J. Paul (✉)
Institució Catalana de La Recerca I Estudis Avançats, Barcelona, Spain
e-mail: paul.verschure@specs-lab.com

by the performance outcome (success or failure) experienced during the previous trial ($p < 0.05$, repeated-measures ANOVA). We could not detect a comparable sensitivity to failure when using the non-paretic limb.

1.2 Evidence from Longitudinal Randomized Controlled Trial

In a double-blind, controlled clinical trial we examined the long-term effects of exposing individuals with hemiparesis to diminished error feedback during the execution of goal-oriented movements [3]. Twenty-three hemiparetic stroke patients were recruited and were assigned to an experimental or a control group. Both groups underwent 6 weeks of therapy using the Rehabilitation Gaming System [4], 5 days a week, for 30 min a day. The experimental group experienced augmented goal-oriented movements of the virtual representation of the paretic limb (RIMT). Our results showed that after six weeks of daily training with RIMT, chronic stroke patients experienced superior gains at 6 weeks after the intervention has ended in comparison to Occupational Therapy ($F(1, 16) = 5.85$, $p < 0.05$, $r = 0.52$). This finding was supported by a significant increase in the paretic arm use during training ($p = 0.02$, Wilcoxon Signed-rank). Patients in the CG, who did not experience the visual amplification of goal-oriented reaching movements in VR, did not show any significant improvements in arm use ($p > 0.05$, Wilcoxon Signed-rank).

2 Low Variable Error Feedback Facilitates Implicit Adaptation

Several human and animal studies suggest that motor adaptation is strongly driven by the history of visual errors [5]. A better understanding of the mechanisms supporting motor adaptation could provide guidelines for the optimal design of effective rehabilitation protocols that capitalize on error feedback manipulation. In this context, we have used the task described earlier to explore the effects of building a history of errors. For this, we conducted an experiment in which 18 subjects with no neurological damage used a chair-mounted arm support to perform planar reaching movements towards a target while learning to compensate for visuomotor rotations [6]. Subjects performed 450 reaches grouped into 3 blocks assigned to conditions M+, NM, and M-. During M+, visual directional errors were reduced, therefore increasing the probability of exposure to small error magnitudes. In the M- condition, visual directional errors were enlarged, thus exposing the subject to larger and more variable errors. In the NM condition, we did not manipulate the feedback. Group 2 experienced these conditions in reversed order. We observed that when frequently exposed to small visual errors (M+), subjects increased their adaptation rates ($p < 0.01$,

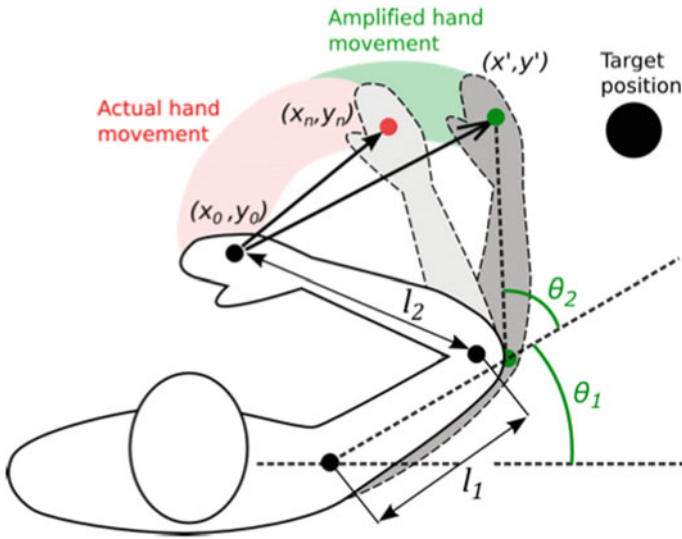


Fig. 1 Amplification of goal-oriented reaching movements in VR. The trajectory of the movement executed (red shadow) is amplified both in extent and accuracy (green shadow) towards the target position, deriving from the start position (X_0, Y_0) and current position (X_n, Y_n) of the actual movement. The movement amplification vector is a weighted combination of two terms: an accuracy amplification vector and an extent amplification vector. The ratio between the executed range and the distance to the target systematically determines the contribution of each of these two components and will cancel the amount of amplification of the movement extent when the patient exceeds in the distance the desired movement. However, if the direction of the executed movement matches the target direction, this ratio will approach 0, thus decreasing the amount of accuracy amplification. Figure adapted from Ballester et al. [2]

Wilcoxon signed-rank) (Fig. 2a). This effect remained significant during the first half of the NM block ($p < 0.05$, Wilcoxon signed-rank) when there was no manipulation of the visual feedback (Fig. 2b). These observations support the hypothesis that the motor system may have access to a history of errors and exposure to a distribution of visual motor errors with low variability and centered around task-relevant error values accelerates motor adaptation.

3 Implicit Motor Adaptation is Impaired in Chronic Cannabis Users

Functional cerebellar alterations are frequently studied with visuomotor rotation (VMR) paradigms. In this context, Subjects are exposed to sequences of visual prediction errors caused by an imposed mismatch between the performed motor action and its outcome. It has been shown that Individuals with cerebellar structural damage show impaired adaptation performance [8]. Further, individuals with no

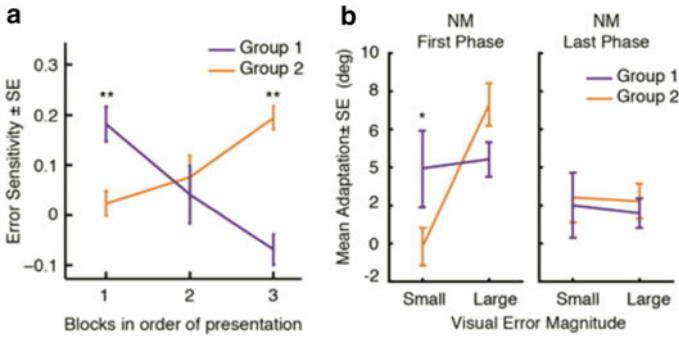


Fig. 2 **a** Mean error sensitivity [5] for all subjects through blocks, in order of presentation for Group 1 (first exposed to low variable small errors) and Group 2 (firstly exposed to highly variable errors). **b** Mean adaptation by group during the first and the second half of the NM block for small errors (12 ± 6) and large errors (24 ± 6). Figure adapted from Ballester et al. [6]

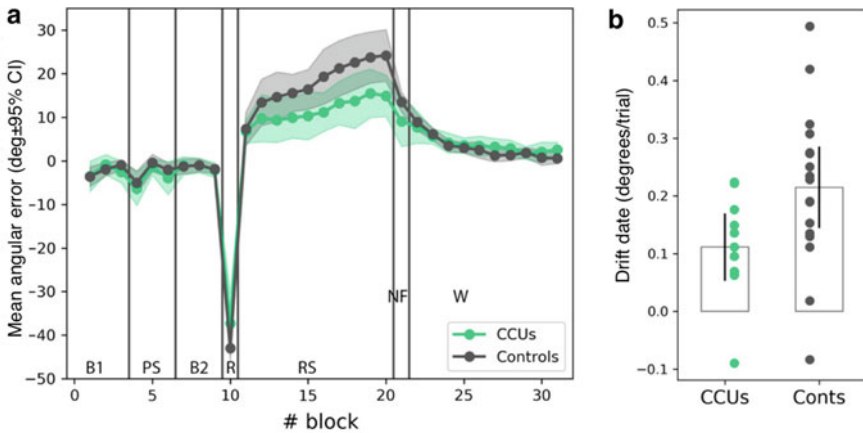


Fig. 3 Motor adaptation in chronic cannabis users (CCUs) and control participants (Conts). **a** Evolution of the directional error across the different phases of the experiment. Notice the increasing adaptation values accumulating differently for both groups during the visuomotor rotation phase (RS). **b** Average adaptation rates in the visuomotor rotation phase (RS). Error bars indicate the 95% confidence intervals. Figure from Herreros et al. [7]

specific structural brain abnormalities may also show an impaired implicit adaptation behaviour in implicit adaptation tasks, probably related to misdiagnosed cerebellar functional deficits [9]. For instance, in the case of cannabis addicts, the cerebellum may be highly affected by prolonged exposure to cannabis, due to its high density in endocannabinoid receptors. To explore this hypothesis, we recruited 18 chronic cannabis users and 18 age-matched controls. Cannabis users were diagnosed with severe cannabis use disorder (≥ 6 criteria), and 75% were marijuana smokers. In these subjects we have observed an impaired implicit motor adaptation in cannabis users

(drift rate: $19.3+/-6.8^\circ$ versus $27.4+/-11.6^\circ$; $t(26) = -2.1$, $p = 0.048$, Cohen's $d = -0.8$, 95% CI = $(-1.7, -0.15)$ (Fig. 3). These results emphasize the potential of visuomotor rotation tasks for clinical diagnosis and assessment.

4 Conclusion

In this brief review, we have highlighted three experimental paradigms based on the manipulation of error feedback. These paradigms are tested with stroke and cannabis user via an interactive Virtual Reality setup, and have clinical relevance. We show that the benefits of reducing visual error feedback during the execution of goal-oriented movements are two-fold: (1) it promotes de spontaneous use of the affected arm in stroke patients with hemiparesis, and (2) it boosts implicit motor adaptation. Finally, in the cannabis addiction domain, we show the potential of visuomotor rotation paradigms as a clinical tool for the diagnosis and assessment of undiagnosed cerebellar alterations. Future studies should explore the reliability of this paradigm as a potential tool for assessing recovery, as well as diagnosing cerebellar alterations in other addiction-induced conditions, such as alcohol use disorders.

Acknowledgments This study was supported by the European Commission (EC), the European Research Council under grant agreement 341196 (CDAC), EC H2020 project socSMCs (H2020EU.1.2.2. 641321), and by the RGS@home, EIT Health project 19277. EIT Health is supported by EIT, a body of the European Union.

References

1. M. Maier, B.R. Ballester, P.F. Verschure, Principles of neurorehabilitation after stroke based on motor learning and brain plasticity mechanisms. *Front. Syst. Neurosci.* **13**, 74 (2019)
2. B.R. Ballester et al., The visual amplification of goal-oriented movements counteracts acquired non-use in hemiparetic stroke patients. *J. Neuroeng. Rehabil.* **12**(1), 50 (2015)
3. B.R. Ballester, M. Maier, R.M.S.S. Mozo, V. Castañeda, A. Duff, P.F. Verschure, Counteracting learned non-use in chronic stroke patients with reinforcement-induced movement therapy. *J. Neuroeng. Rehabil.* **13**(1), 74 (2016)
4. M. S. Cameirão, S. B. I Badia, E. D. Oller, P. F. Verschure, Neurorehabilitation using the virtual reality based rehabilitation gaming system: methodology, design, psychometrics, usability and validation. *J. Neuroeng. Rehabil.* **7**(1), 48 (2010)
5. D.J. Herzfeld, P.A. Vaswani, M.K. Marko, R. Shadmehr, A memory of errors in sensorimotor learning. *Science* **345**(6202), 1349–1353 (2014)
6. B.R. Ballester, L.S. Oliva, A. Duff, P. Verschure, Accelerating motor adaptation by virtual reality based modulation of error memories, in *2015 IEEE International Conference on Rehabilitation Robotics (ICORR)* (IEEE, 2015), pp. 623–629
7. I. Herreros, L. Miquel, C. Blithikioti, L. Nuño, B. Rubio Balleste, K. Grechuta, P. Verschure, et al., Motor adaptation impairment in chronic cannabis users assessed by a visuomotor rotation task. *J. Clin. Med.* **8**(7), 1049 (2019)
8. M.J. Weiner, M. Hallett, H.H. Funkenstein, Adaptation to lateral displacement of vision in patients with lesions of the central nervous system. *Neurology* **33**(6), 766 (1983)

9. C. Blithikioti, L. Miquel, A. Batalla, B. Rubio, G. Maffei, I. Herreros, M. Balcells-Oliveró, et al., Cerebellar alterations in cannabis users: a systematic review. *Addict. Biol.* **24**(6), 1121–1137 (2019)

SS11: Advances and Challenges on Artificial Sensory Feedback Techniques in Manipulation and Locomotion

Investigation of Vibrotactile Transducers for a Bone Conduction Sensory Feedback System



Raphael M. Mayer, Siyuan Chen, Zhuo Li, Alireza Mohammadi, Ying Tan, Gursel Alici, Peter Choong, and Denny Oetomo

Abstract Bone conduction as sensory feedback interface has shown promising properties in upper limb prostheses. Longitudinal studies are essential for the enhancement of sensory feedback in upper limb prostheses and require a deployable (compact size and low cost) wearable system. This paper compares three low cost transducers to one of the current state of the art transducers utilized in audiology. The force output and total harmonic distortion of all transducers are compared. One transducer, whilst being small in size and costing a fraction of other available transducers, showed good performance.

1 Introduction

Effective and practical sensory feedback within prosthetic applications is a desired goal that has been investigated over the past decade and has shown promising results for effective closed-loop control of grasping [1]. Recent studies have investigated vibrotactile feedback on the bone as a sensory feedback interface due to its advantageous properties (e.g. larger bandwidth and having no static force dependency) [2–5], yet longitudinal studies of such an interface have yet to be conducted.

This project is funded by the Valma Angliss Trust and the University of Melbourne.

R. M. Mayer (✉) · S. Chen · Z. Li · A. Mohammadi · Y. Tan · D. Oetomo
Human Robotics Laboratory, Department of Mechanical Engineering, The University of Melbourne, Melbourne, VIC, Australia
e-mail: r.mayer@student.unimelb.edu.au

P. Choong
Department of Surgery, St Vincent's Hospital, The University of Melbourne, Melbourne, VIC, Australia

G. Alici
School of MMMB, University of Wollongong, Wollongong, NSW, Australia

G. Alici · P. Choong · D. Oetomo
ARC Centre of Excellence for Electromaterials Science, Wollongong, NSW, Australia

© The Author(s), under exclusive license to Springer Nature Switzerland AG 2022
D. Torricelli et al. (eds.), *Converging Clinical and Engineering Research on Neurorehabilitation IV*, Biosystems & Biorobotics 28,
https://doi.org/10.1007/978-3-030-70316-5_94

A recent review [1] summarized that previously published longitudinal studies of sensory feedback have: (1) performed repeated testing over few days/weeks, yet a consistent use throughout the day over weeks has only been shown in [6]; (2) investigated impact of training/adaption due to sensory feedback [7], which showed increased performance over an 8-day period [8]; (3) shown benefits in the learning of prosthetic use for grasp force manipulation via EMG [9]. The impact of long term sensory feedback on the performance of grasping and object manipulation has yet to be determined. In order to conduct further longitudinal studies by the authors, utilizing bone conduction, a wearable system which can be integrated into the current prosthetic of the user in a practical manner is necessary.

A sensory feedback system includes three main components: (1) Sensory Input: sensors deployed onto the prosthetic hand; (2) Micro-Controller: computational unit; (3) Sensory Feedback Interface: stimulation unit to generate sensory feedback. In this paper, we focus on the third component to investigate the performance of different transducers in providing sensory feedback via bone conduction.

This paper compares three low cost transducers to the current gold standard in audiology for bone conduction (B81—Radioear) [10]. There are two important measures for transducers used in sensory feedback: force output and total harmonic distortion. The frequency dependent force output needs to surpass the frequency dependent perception threshold to provide feedback [4] to the user. The total harmonic distortion needs to be within limits to not cause misperception between different frequencies [3].

2 Methods

The force output F_{out} and total harmonic distortion THD are measured in the following for four different transducers and the manufacturer specifications given in Table 1.

2.1 Test Setup

A personal computer **PC** (Intel Core i7-8, 16GB RAM, Windows 10™) is connected to a frequency generator **FG** (USB-6343, National Instruments) and an amplifier **A** (A4017, Redback Inc., Australia). The vibrotactile transducers **VT** are mounted onto the Artificial Mastoid **AM** (4930, Brüel & Kjære, Denmark) with a static force of $F_s = 5.4$ N to evaluate the frequency dependent force output F_{out} and the total harmonic distortion **THD** using the Sound Level Meter **SLM** (2250, Brüel & Kjære, Denmark).

Table 1 Manufacturer specifications for the 3 transducers compared to the gold standard B81: Dimension (L × W × D), output force (F_{out}), total harmonic distortion (THD), minimum frequency (F_0) and resistance (R).

Type	L × W × D (mm)	F_{out} (dB re.1 μ N)	THD (%)	F_0 (Hz)	R (Ω)
B81 (Radioear, USA)	31.7 × 18.2 × 16	119*	1.1*	100	12.5*
BC-10 (Ortofon, Denmark)	13.5x29.5x18	118*	1.5*	–	15*
RC-BC10 (Recon, HK)	18.5 × 18.5 × 7.5	86*	5*	240 ±20%	8*
RC-BC51 (Recon, HK)	d = 16.6 × 5.3	84** ±3	5***	220 ±20%	8* ±15%

*at 1V_{rms} and 1kHz; **mean force at [500, 2k, 4k, 10k]Hz; at 2.53V from 0.01m; ***at 1W/1m and 1kHz

2.2 Performance Measure

The frequency dependent force output $F_{out}(f)$ is calculated from the output voltage $V_{out}(f)$ measured via SLM from the AM output: $F_{out}(f) = V_{out}(f)/S(f)$, where $S(f)$ is the frequency dependent mastoid sensitivity. THD is calculated from the measured power spectral density (1/3-octave). Measures have been obtained for $f \in [100, 200, 400, 750, 1500, 3000, 6000]$ Hz at an amplitude of $a = 1$ V_{rms}. For each transducer three samples are tested.

3 Results

Figure 1 shows the B81 achieves the highest force output (gold standard). $F_{out_{mean}}$ and $F_{out_{1kHz}}$ are shown in Table 2.

Figure 1b shows the THD of BC-10 is similar to B81 above 300 Hz, below 300 Hz the BC-10 has a higher THD. The THD results of RC-BC10 are similar to the B81 whilst the obtained results for the RC-BC51 show the highest overall THD. The higher THDs compared to the manufacturer specifications are likely due to the utilization of the setup in the laboratory instead of an audiology booth.

4 Discussion

The obtained F_{out} for B81 and BC-10 is higher than the necessary perception threshold [4]. BC-10 shows a 11.4 dB lower mean force output compared to the B81. The RC-BC10 and RC-BC51 achieved 27.7dB and 52.3dB lower force outputs respec-

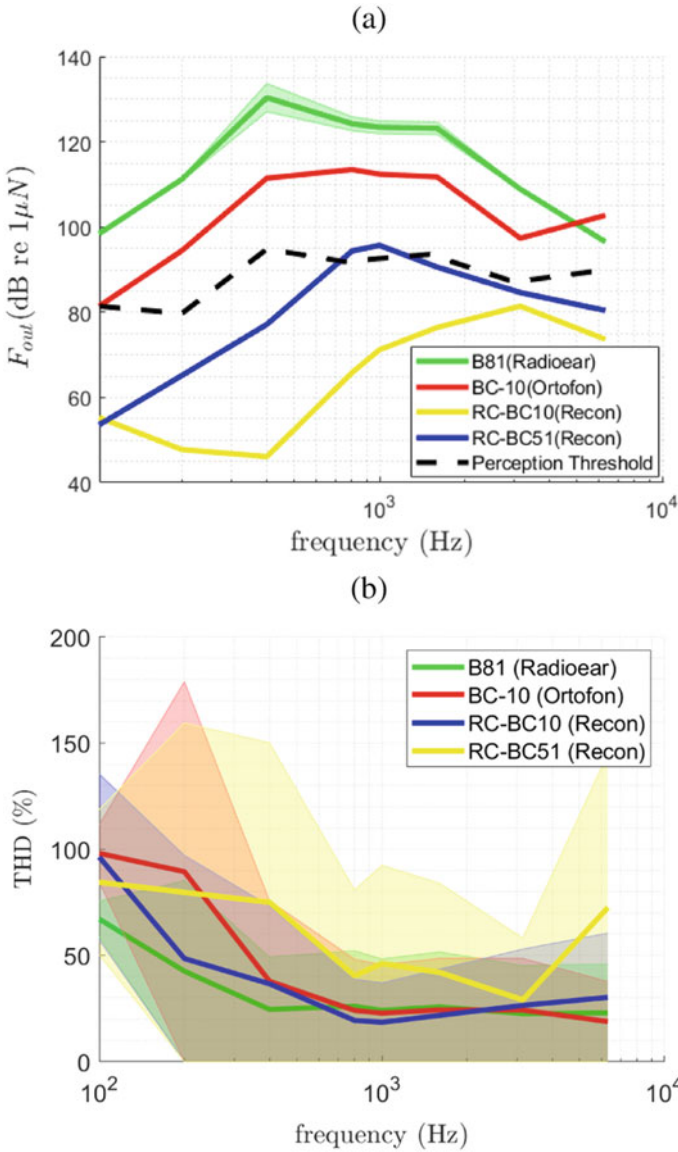


Fig. 1 The performance of the 4 transducers: **a** force output F_{out} ; **b** total harmonic distortion THD. Mean is shown as solid line and one standard deviation as shaded area. The plotted perception threshold is from [4]

Table 2 Comparison of force output F_{out} and THD

Type	$F_{out_{1kHz}}$ (dB)	$F_{out_{mean}}$ (dB)	THD_{1kHz} (%)	THD_{mean} (%)
B81	123.4	114.5	24.2	32
BC-10	112.4	103.1	22.8	42.5
RC-BC10	95.7	80.1	18.6	37.3
RC-BC51	71.2	64.7	46.2	58.7

tively, compared to the B81 and are therefore not achieving the necessary perception threshold. The achieved THD of the BC-10 is similar to that of the B81 (above 300 Hz). The RC-BC10 achieves a similar THD, whilst the RC-BC51 achieves a higher THD compared to the B81. F_0 of the BC-10 is not given but it shows good performance for the obtained THD and F_{out} . For RC-BC10 and RC-BC51 F_0 is higher than the reported lowest perceivable limit in bone conduction (100 Hz), limiting the possible bandwidth.

5 Conclusion

The BC-10 achieves slightly less force output and a similar THD at a fraction of the costs of the B81 (100AUD while B81 costs 735AUD). It is smaller in size making it easier to integrate and surpasses the necessary perception threshold. The BC-10 is suitable as a vibrotactile transducer in applications of bone conduction as sensory feedback.

References

1. B. Stephens-Fripp, G. Alici, R. Mutlu, A review of non-invasive sensory feedback methods for transradial prosthetic hands. *IEEE Access* **6**, 6878–6899 (2018)
2. R.M. Mayer, A. Mohammadi, Y. Tan, G. Alici, P. Choong, D. Oetomo, Psychometric evaluation of multi-point tactile stimulation via bone conduction, in *8th International Conference on Biomedical Robotics & Biomechanics (BIOROB2020)*, New York, NY (2020)
3. R.M. Mayer, R. Garcia-Rosas, A. Mohammadi, Y. Tan, G. Alici, P. Choong, D. Oetomo, Tactile feedback in closed-loop control of myoelectric hand grasping: conveying information of multiple sensors simultaneously via a single feedback channel. *Front. Neurosci.* **14**(348), 4 (2020)
4. R.M. Mayer, A. Mohammadi, G. Alici, P. Choong, D. Oetomo, Bone conduction as sensory feedback interface: a preliminary study, *41st Proceedings of Annual Conference of the IEEE Engineering in Medical and Biology*, (2019), pp. 5322–5325
5. F. Clemente, B. Håkansson, C. Cipriani, J. Wessberg, K. Kulbacka-Ortiz, R. Brånemark, K.-J. Fredén Jansson, M. Ortiz-Catalan, Touch and hearing mediate osseoperception, *Scientific Reports*, vol. 7 (2017)

6. F. Clemente, M. D'Alonzo, M. Controzzi, B.B. Edin, C. Cipriani, Non-invasive, temporally discrete feedback of object contact and release improves grasp control of closed-loop myoelectric transradial prostheses. *IEEE Trans. Neural Syst. Rehabil. Eng.* **24**(12), 1314–1322
7. G. Chai, D. Zhang, X. Zhu, Developing non-somatotopic phantom finger sensation to comparable levels of somatotopic sensation through user training with electro-tactile stimulation. *IEEE Trans. Neural Syst. Rehabil. Eng.* **25**(5), 469–480 (2017)
8. C.E. Stepp, Q. An, Y. Matsuoka, Repeated training with augmentative vibrotactile feedback increases object manipulation performance. *PLoS ONE* **7**(2) (2012)
9. M. Štrbac, M. Isaković, M. Belić, I. Popović, I. Simanić, D. Farina, T. Keller, S. Došen, Short-and long-term learning of feedforward control of a myoelectric prosthesis with sensory feedback by amputees. *IEEE Trans. Neural Syst. Rehabil. Eng.* **25**(11), 2133–2145 (2017)
10. K.J.F. Jansson, B. Håkansson, L. Johannsen, T. Tengstrand, Electro-acoustic performance of the new bone vibrator Radioear B81: A comparison with the conventional Radioear B71. *Int. J. Audiol.* **54**(5), 334–340 (2015)

Multi-frequency Stimulation: Spatial Differentiation of Bone-Conducted Tactile Stimulation on the Elbow Bony Landmarks



Raphael M. Mayer, Alireza Mohammadi, Ying Tan, Gursel Alici, Peter Choong, and Denny Oetomo

Abstract Sensory feedback in upper limb prostheses is a highly desirable feature and bone conduction as one of the feedback methods has shown promising characteristics. Multiple feedback information is required simultaneously for effective grasping and manipulation and has been recently studied in conjunction with bone conduction. The user's ability to identify the stimulation in the case of simultaneous stimulation of the same frequency on multiple sites via bone conduction has shown a low performance. However, simultaneous stimulation on multiple sites using different frequencies per site has not been studied yet. In this paper, the psychometric evaluation of multiple frequencies on the multiple physiological bony landmarks on the elbow is investigated. The proposed approach is evaluated on a human-subject experiment with ten able-bodied subjects. The vibrotactile transducers are placed on the bony landmarks of the elbow and the identification rate of the number of active stimulation points determined. The outcomes show an increased identification rate for one and three simultaneous stimulation sites.

This project is funded by the Valma Angliss Trust and the University of Melbourne.

R. M. Mayer (✉) · A. Mohammadi · Y. Tan · D. Oetomo
Department of Mechanical Engineering, The University of Melbourne, Melbourne, VIC, Australia
e-mail: r.mayer@student.unimelb.edu.au

P. Choong
Department of Surgery, St Vincent's Hospital, The University of Melbourne, Melbourne, VIC, Australia

G. Alici
School of MMB, University of Wollongong, Wollongong, NSW, Australia

G. Alici · P. Choong · D. Oetomo
ARC Centre of Excellence for Electromaterials Science, Wollongong, NSW, Australia

© The Author(s), under exclusive license to Springer Nature Switzerland AG 2022
D. Torricelli et al. (eds.), *Converging Clinical and Engineering Research on Neurorehabilitation IV*, Biosystems & Biorobotics 28,
https://doi.org/10.1007/978-3-030-70316-5_95

1 Introduction

Supplying sensory feedback via non-invasive interfaces has been studied and developed in the past decade [1, 2]. Recent studies have investigated the use of vibrotactile stimulation on the bone as a sensory feedback interface due to its advantageous properties of a larger bandwidth and showing no static force dependency [3–5].

The use of multiple bone conduction stimulation sites simultaneously was studied in [3]. This is required to provide multiple feedback information simultaneously during prosthetic grasping [6, 7] and to increase the overall bandwidth for the feedback information to the human user.

In the exercise of human user identifying which of the bony sites is being stimulated, vibrotactile stimulation through bone conduction showed a high performance when stimulated one site at a time, with frequency below 750 Hz [3]. However, a low performance was reported when the multiple sites were stimulated simultaneously [3]. It must be noted that in that study, all sites were stimulated with the same frequency and amplitude. The objective of this paper is to investigate the efficacy of the interface, in other words, the ability of the subjects in discriminating simultaneous stimulation on multiple sites, when each site is stimulated with a different frequency.

The following hypothesis is therefore investigated.

Utilizing different stimulation frequencies will increase the detection rate of multiple simultaneous stimulation sites.

To this end, the experiments determine the capability of human subjects in identifying the number of simultaneously activated stimulation sites when each of them is stimulated with a different frequency. The experiment is carried out similar as in [3], to further investigate the human ability to discriminate simultaneously applied bone-conducted vibrotactile stimulation using similar frequencies versus different frequencies on multiple stimulation sites.

2 Methods

The experiment was conducted with 10 able-bodied subjects (1 female, 9 male; age 28.3 ± 4.3 years). The subjects read the plain language statement and signed the consent form approved by the Ethics Committee of the University of Melbourne (Ethics Id 1852875.1).

2.1 Setup

A personal computer **PC** (Intel Core i7-8, 16GB RAM, Windows 10™) is connected to a frequency generator **FG** (USB-6343, National Instruments) and an amplifier **A** (A4017, Redback Inc., Australia) and three vibrotactile transducers **VT** (B81,

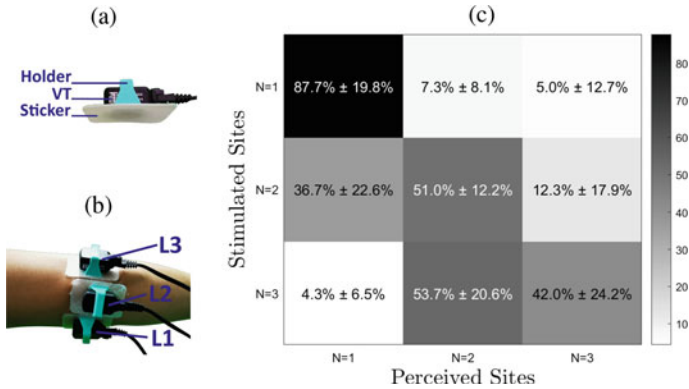


Fig. 1 The **a** transducers are fixed to the **b** bony landmarks (Pictures from [3]), and the **c** NPIR confusion matrix of the detected number of stimulation sites is obtained

RadioEar Corporation). VT’s are mounted on the bony landmarks of the dominant hand (medical grade double-sided tape; strapping tape): epicondylus medialis (L_1), ulnar olecranon (L_2) and epicondylus lateralis (L_3), see Fig. 1. A custom MATLAB® GUI guides the user through the experiment and controls the stimulation parameters.

2.2 Protocol and Performance Measure

Subjects are asked whether one, two or three stimulation sites are active simultaneously. Each stimulation site L_1 – L_3 is stimulated with a different frequency $f_{L_1} = 100$ Hz, $f_{L_2} = 400$ Hz, $f_{L_3} = 750$ Hz at amplitude $a = 0.57$ V. The number of active sites are one, two (all permutations) or three and each repeated 10 times, resulting in a total of 90 stimulations presented in a randomized order to the user. The *N-Point Identification Rate (NPIR)* is the success rate that a subject correctly identifies the number of active stimulation sites [3]. A non-parametric statistic analysis, a Friedman test [8] is applied followed by a post-hoc analysis via Wilcoxon signed rank test [9] and to interpret the magnitude of difference the effect size calculated via Cohen’s d value using a pooled standard deviation [10]. The comparison to previous results is shown as mean difference.

3 Results

The mean *NPIR* of the ten different subjects and standard deviation are shown in Fig. 1c as the diagonal elements and the misclassification rate as the off-diagonal entries.

Table 1 The p values of the post-hoc Wilcoxon signed rank. Significance level is $p < 0.05$

	N = 1 versus 2	N = 1 versus 3	N = 2 versus 3
p -value	0.007	0.012	0.208
Cohen's d	2.23	2.07	0.47

Table 2 Comparison of the mean NPIR with different frequencies obtained in this study to the mean NPIR with stimulated with the same frequency. The mean NPIR is given as well as the standard deviation calculated for six subjects in [3] and ten subjects in this study

	N = 1	N = 2	N = 3
NPIR _{mean} from [3]	76.3 ± 7.9%	53.7 ± 10.8%	28.9 ± 13.5%
NPIR _{mean}	87.7 ± 19.8%	51.0 ± 12.2%	42.0 ± 24.2%
Mean difference	+11.4%	-2.7%	+13.1%

A Friedman test indicates a statistically significant difference in performance $p = 0.004$ (significance level $p < 0.05$) for the NPIR achieved for the three different numbers of active stimulation sites.

A post-hoc test, shown in Table 1 indicates statistically significant difference in performance for 1 versus 2 and 1 versus 3 sites, yet no statistical significant difference between 2 and 3 stimulation sites.

The comparison of the mean NPIR stimulation results of this study (different frequencies) with previous study (same frequency) at different locations is shown in Table 2.

4 Discussion

Stimulation on a single site significantly outperforms two and three sites, which is a large effect size (according to Cohen's $d > 0.8$), see Table 1. No significant difference was found between two and three sites. Relatively small misclassification rates are obtained for one stimulation site (row $N = 1$ in Figure 1) whereas higher rates were found between two and three stimulated and perceived sites. Two stimulation sites are misclassified as one site, whilst three stimulation sites are misclassified as two sites, indicating that the highest errors occur at $N = 2, 3$ simultaneous stimulation sites, being perceived as $N - 1$ sites. This coincides with subjects reporting that turning on L_2/L_3 (higher frequencies) simultaneously with L_1 (lowest frequency) suppresses the sensation of the lower frequency on L_1 and therefore is difficult to perceive.

A comparison to the results obtained in [3], where all sites were stimulated with the same frequency, shows an improvement of 11.4 and 13.1% for $N = 1$ and $N = 3$, respectively, although a small reduction of 2.7% was observed for $N = 2$, see Table 2.

5 Conclusion

The obtained results show an increased NPIR when different simultaneous stimulation frequencies are applied to different sites. Subjects are able to differentiate between different stimulation's easier when they are separated in frequency domain. This is observed in the cases of one and three sites compared to previous reported results [3] where the same frequencies were applied to each site. The presented study investigated three static frequencies with a large interval in between them, smaller intervals might be possible. Future studies should investigate the minimum distance between the frequency applied on different stimulation sites necessary to improve the NPIR as well as a systematic way of choosing the frequency for each stimulation site.

References

1. B. Stephens-Fripp, G. Alici, R. Mutlu, A review of non-invasive sensory feedback methods for transradial prosthetic hands. *IEEE Access* **6**, 6878–6899 (2018)
2. J.W. Sensinger, S. Dosen, A review of sensory feedback in upper-limb prostheses from the perspective of human motor control. *Front. Neurosci.* **14**, 345 (2020)
3. R.M. Mayer, A. Mohammadi, Y. Tan, G. Alici, P. Choong, D. Oetomo, Psychometric evaluation of multi-point tactile stimulation via bone conduction, in *8th International Conference on Biomedical Robotics & Biomechanics (BIOROB2020)*, New York, NY (2020)
4. R.M. Mayer, R. Garcia-Rosas, A. Mohammadi, Y. Tan, G. Alici, P. Choong, D. Oetomo, Tactile feedback in closed-loop control of myoelectric hand grasping: conveying information of multiple sensors simultaneously via a single feedback channel. *Front. Neurosci.* **14**(348), 4 (2020)
5. R.M. Mayer, A. Mohammadi, G. Alici, P. Choong, D. Oetomo, Bone conduction as sensory feedback interface: a preliminary study, *41st Proceedings of Annual Conference on IEEE Engineering in Medicine and Biology* (2019), pp. 5322–5325
6. G. Westling, R. Johansson, Factors influencing the force control during precision grip. *Exp. Brain Res.* **53**, 277–284 (1984)
7. R. Johansson, G. Westling, Signals in tactile afferents from the fingers eliciting adaptive motor responses during precision grip. *Exp. Brain Res.*, **66**, 141–154 (1987)
8. W. Daniel, *Applied Nonparametric Statistics*, 2nd edn. (1990)
9. F. Wilcoxon, Individual comparisons by ranking methods. *Biometrics Bull.*, **1**(6), 80–83 (1945)
10. J. Cohen, The earth is round ($p < 0.05$). *Am. Psychol.* **49**(12), 997–1003 (1994)

A User-Centered Approach to Artificial Sensory Substitution for Blind People Assistance



Federica Barontini, Gemma Carolina Bettelani, Barbara Leporini, Giuseppe Averta, and Matteo Bianchi

Abstract Artificial sensory substitution plays a crucial role in different domains, including prosthetics, rehabilitation and assistive technologies. The sense of touch has historically represented the ideal candidate to convey information on the external environment, both contact-related and visual, when the natural action-perception loop is broken or not available. This is particularly true for blind people assistance, in which touch elicitation has been used to make content perceivable (e.g. Braille text or graphical reproduction), or to deliver informative cues for navigation. However, despite the significant technological advancements for what concerns both devices for touch-mediated access to alphanumeric stimuli, and technology-enabled haptic navigation supports, the majority of the proposed solutions has met with scarce acceptance in end users community. Main reason for this, in our opinion, is the poor involvement of the blind people in the design process. In this work, we report on a user-centric approach that we successfully applied for haptics-enabled systems for blind people assistance, whose engineering and validation have received significant inputs from the visually-impaired people. We also present an application of our approach to the design of a single-cell refreshable Braille device and to the devel-

This work was partially supported by the EU H2020 project “SOPHIA” (no. 871237), and by the Italian Ministry of Education and Research (MIUR) in the framework of the CrossLab project (Departments of Excellence), and in the framework of PRIN 2017 with the project “TIGHT: Tactile InteGration for Humans and arTificial systems”, grant number 2017SB48FP. Federica Barontini and Gemma Carolina Bettlani are equally contributed to this work.

F. Barontini (✉) · G. C. Bettelani · G. Averta · M. Bianchi
Centro di Ricerca “Enrico Piaggio”, Università di Pisa, Largo Lucio Lazzarino 1, 56126 Pisa, Italy
e-mail: matteo.bianchi@unipi.it

F. Barontini · G. C. Bettelani · M. Bianchi
Dipartimento di Ingegneria dell’Informazione, University of Pisa, Via G. Caruso 16,
56122 Pisa, Italy

F. Barontini
Fondazione Istituto Italiano di Tecnologia, via Morego 30, 16163 Genova, Italy

B. Leporini
Istituto di Scienza e Tecnologie dell’Informazione (ISTI) “A. Faedo”, Area della Ricerca del CNR di Pisa, Via G. Moruzzi, 1, 56124 Pisa, Italy

© The Author(s), under exclusive license to Springer Nature Switzerland AG 2022

599

D. Torricelli et al. (eds.), *Converging Clinical and Engineering Research on Neurorehabilitation IV*, Biosystems & Biorobotics 28,
https://doi.org/10.1007/978-3-030-70316-5_96

opment of a wearable haptic system for indoor navigation. After a summary of our previous results, we critically discuss next avenues and propose novel solutions for touch-mediated delivery of information for navigation, whose implementation has been totally driven by the feedback collected from real end-users.

1 Introduction

According to Rita and Kercel [1], “*Persons who become blind do not lose the capacity to see*”. This sentence well explains the concept of *Sensory Substitution* for blind people assistance, i.e. the possibility to deliver information commonly acquired through vision, relying on another channel, usually touch. Vision and touch are, indeed, highly intertwined for perception generation, synergistically working toward a multi-sensory representation [2]. In [3], it was also reported that a supramodal representation of objects exists in the ventral extrastriate pathway of sighted and congenitally blind individuals. Furthermore, the usage of the haptics channel to deliver vision-related information is preferable to the auditory one—which is usually augmented in blind people, whose elicitation could disturb posture and equilibrium control and severely affect social interactions [4]. For these reasons, a lot of effort has been devoted to develop haptic interfaces that mainly target navigation assistance—Electronic Travel Aids (ETAs)—which can surrogate spatial information on position and obstacle location and deliver it to the users via tactile sensory substitution [5]; and the accessibility of textual content through touch-related elicitation, commonly through refreshable Braille devices—whose raised dots change dynamically, enabling the representation of different texts with the same device [6]. Despite the significant technological advancements, the majority of these solutions have met with scarce acceptance in end users, due to the lack of intuitiveness and comfort of usage or because of the high costs. Main cause for this, in our opinion, can be ascribed to a non-perfect work-flow design: blind people have been minimally involved in the design and the validation phases of these prototypes. We propose a user-centered approach for the development of haptic interfaces for sensory substitution, presenting a single-cell refreshable Braille device *Readable* [7], and a wearable haptics-based navigation system for indoor guidance [4], see Fig. 1. We report on the developmental phases and novel solutions for navigation information touch-mediated delivery, which have been identified moving from the feedback collected from real end-users.

2 Readable Device

In [7], we presented *Readable* (see Fig. 1a), a new electromagnetic refreshable single Braille cell. The system allows for the independent control of six dots and a spacing between the contact points comparable with the standard Braille coding. For more

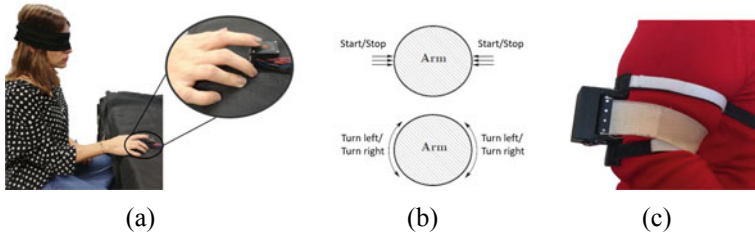


Fig. 1 A participant “reading” through the *Readable* device (a) presented in [7]; Working modes of the wearable haptic device for the delivery of navigation cues in the system reported in [4] (b) and overview of the interface worn on the subject’s arm (c)

details please refer to [7]. The prototype was tested with eight blind people, who were expert Braille code readers. The evaluation phase was of paramount importance not only to show the capabilities of our system to correctly reproduce alphanumeric stimuli (no statistical differences in the recognition of the coded stimuli when the subjects used the *Readable* with respect to the interaction with traditional paper letters), but also to open to new application scenarios where our device could offer real benefits to real end-users, in every-day life. Indeed, blind participants (2 female, 56 ± 20 y.o) evaluated the interface as intuitive, cost-aware, useful and well-accepted and identified the following areas where the usage of the *Readable* would be preferable with respect to the complete multi-cell Braille display or audio feedback: displaying the status of the household appliances; displaying the current floor of an elevator; integration in a cordless phone for a first call notification; showing the temperature measured via the thermometer; showing the light status on/off. This information will guide our future developments and a more in depth analysis of the applicability of *Readable* in every-day life, also for navigation applications.

3 Wearable Haptics for Indoor Navigation

In [4], we presented an indoor navigation system, which was composed of a RGB-D camera (to acquire the visual information on the environment and the obstacles), a processing unit - laptop (which used such information to implement obstacle avoidance strategies) and finally a wearable haptic interfaces (to deliver tangential stimuli to guide the user in an unknown environment). The development of the system was entirely driven by the requirements and the feedback provided by blind people. More details can be found in [4]. For the reasons above, the first step of our work was to interview four blind people to identify which features and functionalities a navigation system should ideally have. For the sake of space, we report only the main features related to the ideal interface, whose aim should be to intuitively and effectively deliver the navigation information to the user: (1) *Haptic Information* Tactile stimulation was preferable to the auditory cues, as also reported in [5]. (2) *Simplicity and intuitive-*

ness of the delivered navigation commands Clear and unequivocal instructions were evaluated as crucial for important communications. For instance, a clear and single strong pressure to indicate a change of direction (instead of constant stimulation) or obstacle detection are preferable. (3) *Wearable and hands-free system* The arm was considered as a good body location for haptic communication. We translated these requirements under a design point of view in the CUFF device (see Fig. 1b, c), a wearable haptic interface that consists of a belt attached to two motors that can rotate counterclockwise from a reference position (i.e. “turn left” information), clockwise (“turn right”), or squeeze the users’ arm (single strong squeezing corresponding to “stop” command; two light squeezing stimuli corresponding to “go” instruction). The results of the experiments with blind people showed that our system could be an effective support during indoor navigation with the white cane, and a viable tool for training blind people to the usage of travel aids. However, after the delivery of turn right/left commands, the CUFF motors returned to the reference position. This sometimes caused a misleading perception in users. Furthermore, the sliding stimulus for implementing a turning command was always constant and set to the maximum; this enabled a more clear stimulus detection, but did not allow to graduate the information delivery based on the presence of obstacles. For these reasons, after the work presented in [4], we decided to integrate vibrotactile information in the CUFF, to help to disambiguate these types of stimuli and provide a gradient in the stimulus delivery (to communicate a more or less intense turning action, and/or the location of the obstacles). The first step was the engineering of an elastic bend—see Fig. 2, with six cylindrical vibrating motors [8], positioned at a distance of 3.5 mm between each other [9]. The motors, powered with 3 V provided by the USB connection with the laptop, can vibrate at a frequency of 250 Hz [10].

We asked four naive sighted, blindfolded volunteers (30.4 ± 3.2 , 2 Female) to understand which was the amplitude of the stimulus (based on the number of the motors that were vibrating) and in which direction (left or right) they were vibrating. The different randomized stimuli (15 rep. for each modality) were the following, both starting from the right and the left of Fig. 2b; (1) small stimulus amplitude (vibration of the first two motors); (2) mid stimulus amplitude (vibration of the first four motors); (3) large stimulus amplitude (vibration of all motors). We found that

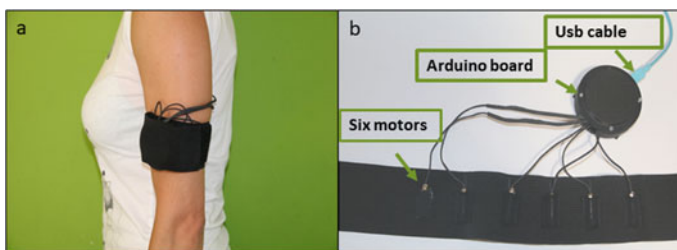


Fig. 2 On the left: the device worn by a participant. On the right: the six motors glued in the inner part of the bend

only one participant gave a wrong answer for the stimulus “*starting from right: mid stimulus amplitude*”. These results are encouraging, and push us to pursue the integration of the vibrotactile belt in the CUFF and its testing with blind users.

References

1. P.B. y Rita, S.W. Kercel, Sensory substitution and the human–machine interface. *Trends Cognit. Sci.* **7**(12), 541–546 (2003). <http://www.sciencedirect.com/science/article/pii/S1364661303002900>
2. S. Lacey, C. Campbell, K. Sathian, Vision and touch: multiple or multisensory representations of objects? *Perception* **36**(10), 1513–1521 (2007)
3. E. Ricciardi, M.L. Furey, M. I. Gobbini, M. Guazzelli, J.V. Haxby, P. Pietrini, Tactile processing of different object categories involves extrastriate visual cortical areas in the human brain, in *EuroHaptics 2004* (2004)
4. F. Barontini, M.G. Catalano, L. Pallottino, B. Leporini, M. Bianchi, Integrating wearable haptics and obstacle avoidance for the visually impaired in indoor navigation: A user-centered approach. *IEEE Trans. Haptics* **1**–1 (2020)
5. D. Dakopoulos, N.G. Bourbakis, Wearable obstacle avoidance electronic travel aids for blind: a survey. *IEEE Trans. Syst. Man Cybern. Part C (Appl. Rev.)* **40**(1), 25–35 (2010)
6. D. Leonardis, L. Claudio, A. Frisoli, A survey on innovative refreshable braille display technologies, in *International Conference on Applied Human Factors and Ergonomics* (Springer, 2017), pp. 488–498
7. G.C. Bettelani, G. Averta, M.G. Catalano, B. Leporini, M. Bianchi, Design and validation of the readable device: a single-cell electromagnetic refreshable braille display. *IEEE Trans. Haptics* **13**(1), 239–245 (2020)
8. Available <https://microdcmotors.com/product/smt-smd-smallest-vibration-motor-nfp-rf2323/>
9. S. Schätzle, T. Hulin, C. Preusche, G. Hirzinger, Evaluation of vibrotactile feedback to the human arm, in *Proceedings of EuroHaptics*. Citeseer (2006), pp. 557–560
10. R.W. Cholewiak, A.A. Collins, Sensory and physiological bases of touch. *The Psychology of Touch* (1991), pp. 23–60

Post-stroke Voluntary Movements Improve When Combined with Vibration-Induced Illusion of Movement



Francesca Ferrari, Courtney E. Shell, Zachary C. Thumser,
Francesco Clemente, Ela B. Plow, Christian Cipriani, and Paul D. Marasco

Abstract Improving upper limb motor recovery is a major goal of stroke rehabilitation. However, after rehabilitation, stroke patients often still experience difficulty completing motor tasks. Sensory feedback can be impaired by stroke damage, and inadequate feedback and integration with motor control may prevent these patients from achieving smooth motor coordination. Here, we tested the effects of augmenting natural movement proprioception with vibration-induced illusions of movement during a reaching task. When participants reached for a target with the affected

F. Ferrari · F. Clemente · C. Cipriani
The BioRobotics Institute, Scuola Superiore Sant'Anna, Pisa, Italy

Department of Excellence in Robotics & A.I., Scuola Superiore Sant'Anna, Pisa, Italy

F. Ferrari
e-mail: fra.ferrari@santannapisa.it

F. Clemente
e-mail: f.clemente@santannapisa.it

C. Cipriani
e-mail: ch.cipriani@santannapisa.it

C. E. Shell · Z. C. Thumser · P. D. Marasco (✉)
Laboratory for Bionic Integration, Department of Biomedical Engineering, Cleveland Clinic
Lerner Research Institute, Cleveland, OH, USA
e-mail: marascp2@ccf.org

C. E. Shell
e-mail: courtney.shell@stdavids.com

Z. C. Thumser
e-mail: thumsez@ccf.org

C. E. Shell · P. D. Marasco
Advanced Platform Technology Center, Louis Stokes Cleveland VA Medical Center, Cleveland,
OH, USA

C. E. Shell
Neuroscience Institute, Office of Research, St. David's HealthCare, Austin, TX, USA

Z. C. Thumser
Research Service, Louis Stokes Cleveland VA Medical Center, Cleveland, OH, USA

© The Author(s), under exclusive license to Springer Nature Switzerland AG 2022

D. Torricelli et al. (eds.), *Converging Clinical and Engineering Research on Neurorehabilitation IV*, Biosystems & Biorobotics 28,
https://doi.org/10.1007/978-3-030-70316-5_97

arm (stroke patients) or dominant arm (able-bodied participants), 90 Hz vibration on either the biceps brachii or triceps brachii induced the illusion of movement. Participants also completed control trials where sham (25 Hz) or no vibration were applied. Fitts' Law and kinematic analyses revealed that vibration-induced movement illusions delivered to the primary agonist muscle involved in active movement improved stroke patients' reaching motions. Incorporating this technique in rehabilitation could promote functional motor recovery.

1 Introduction

STROKE is a leading cause of long-term disability [1]. Several rehabilitation therapies, using approaches such as electrostimulation, repetitive task training and robot-mediated therapies, have been used to recover motor performance after stroke [2]. However, 78% of patients still exhibit persistent motor impairments [3]. Somatosensory deficits also occur after stroke in about 11–85% of patients [4]. Despite this high incidence, therapies specifically designed to restore sensory inputs are rarely employed in rehabilitation following stroke [5]. If proprioception is completely absent, movements are slow, clumsy, poorly coordinated and inadequately adapted to complex tasks [6].

In this study, we investigate whether augmenting native proprioceptive feedback improves motor task performance with the affected arm in stroke patients. The augmented proprioceptive feedback was delivered using vibration-induced movement illusions (i.e., kinaesthetic feedback, KF), generally perceived as the joint movement associated with elongation of the vibrated muscle [7]. Participants, stroke patients and able-bodied, were instructed to perform a reaching task while either

Table 1 Experimental conditions. The order of the experimental conditions was randomized for each participant. Each condition was repeated three times and included reaches to 9 different targets

Experimental condition	Vibration frequency (Hz)	Stimulated muscle
NO VIB	0	None
TRI 90	90	Triceps Brachii
BI 90	25	Biceps Brachii
TRI 25	90	Triceps Brachii
BI 25	25	Biceps Brachii

E. B. Plow

Department of Biomedical Engineering, Cleveland Clinic Lerner Research Institute, Cleveland, OH, USA

e-mail: plowe2@ccf.org

Cleveland Clinic Lerner College of Medicine, Case Western Reserve University, Cleveland, OH, USA

an agonist and antagonist muscle received vibration to evaluate how augmenting feedback affects movement.

2 Material and Methods

Twelve able-bodied (8 female, 29 ± 8.7 years old, age range 19–48 years) and 6 stroke patients (1 female, 3 left-side affected, 4 ischemic, 57 ± 11.4 years old, age range 33–66 years) completed the study. Each participant sat in an adjustable chair in front of a touch screen laid flat on a table (Cintiq 27QHD, Wacom Co., Ltd., Kazo, Japan). Participants were instructed to perform a reaching task from a fixed starting position at the bottom of the screen to a target of random size and position (target width 2, 3, or 6 cm and distance from the starting position equal to 20, 40, or 80% of the participant's maximum reach). An opaque vertical panel was arranged in the middle of the touch screen, hiding from view the arm that performed the reaching task. Target and start bars extended across both halves of the screen so that they remained visible (Fig. 1).

A wearable vibration factor (custom-made, HDT Global, Solon, OH, United States) was placed on the stimulated muscle over the point at which the participant reported sensations of movement about the elbow or forearm movement. To assess the effects of KF on movement, five different experimental conditions were repeated three times (Table 1). In each condition, only one muscle was stimulated, biceps brachii or triceps brachii, using a specific vibration frequency (illusion-inducing (90 Hz), sham (25 Hz), and no vibration). In all cases, vibration was applied only during elbow extension. Marker clusters were placed on the forearm and upper arm while a single marker was placed on the elbow and either the index or middle finger so that a motion capture system (Optitrack V120: Trio, Natural Point, Inc., Corvallis, OR, United States) could track the upper limb movements (Fig. 1).

A kinematic analysis of arm movements was performed using custom-written MATLAB analysis code (R2011a, Mathworks, Natick, MA, United States). Fitts' Law, which characterizes the relationship between movement time and accuracy [8], was also used to quantify motor performance.

Kinematic measurements (trajectory smoothness and directness, elbow angle extension, velocity and time to peak) and Fitts' Law parameters (time to reach, index of difficulty, traveled distance) describing movements during the different experimental conditions were compared by fitting linear mixed models to each individual measure. Models included fixed effects for vibration condition (5 levels), target distance (3 levels), and an interaction effect for vibration condition * target distance. Fitts' Law throughput was compared using one-way repeated measures ANOVA.

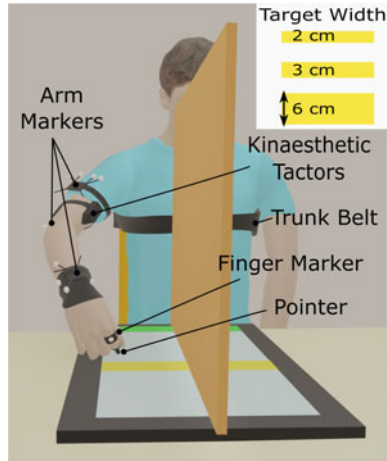


Fig. 1 Experimental setup. Participants were instructed to touch the start button (green) then, as fast and precisely as possible, reach to touch the target button (yellow). A vertical panel blocked view of arm activity. A trunk belt and wrist brace limited extraneous movements. Markers on the arm and hand were used to track upper limb kinematics. Kinaesthetic factors provided vibration to the biceps brachii or triceps brachii when dictated by the experimental condition

3 Results

While able-bodied participants were largely unresponsive to vibration, 90 Hz illusory KF injected into the actively contracting (agonist) triceps muscle increased movement smoothness (Fig. 2a), elbow extension (Fig. 2b) and movement directness in stroke patients. Conversely, injecting 90 Hz illusory KF into the passively-stretched (antagonist) biceps during reaching negatively impacted those same parameters. The Fitts' Law analyses reflected similar effects, with a trend towards increased throughput with 90 Hz triceps vibration and decreased throughput with 90 Hz biceps vibration, driven by changes in distance reached and, for the biceps, increased movement time.

4 Discussion

Illusory KF providing augmented proprioceptive feedback to the agonist muscle in a voluntary movement improved performance in stroke patients. Interestingly, while able-bodied participants showed few significant changes in motor performance under different vibration conditions, slight trends similar to significant changes observed in stroke patients were present. The sensory system weights and integrates information from multiple sources [9]. Able-bodied participants likely weighted their intact and fully functioning sensory feedback higher than the illusions induced by vibration, which diminished the effects of the feedback augmentation. Stroke patients, with

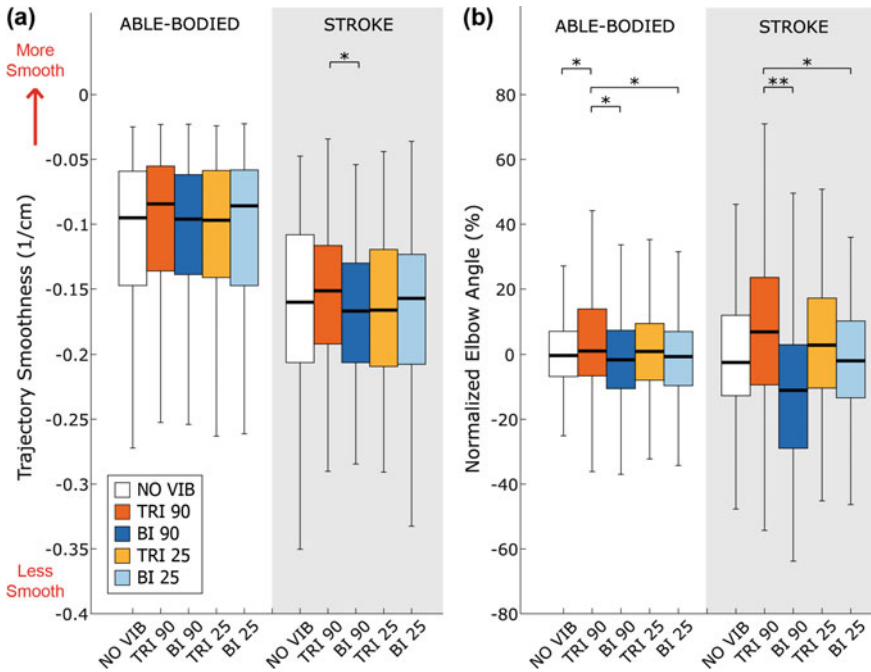


Fig. 2 (a) Trajectory smoothness and (b) normalized elbow angle. For both graphs, medians and interquartile ranges with whiskers encompassing the range of non-outlier values for able-bodied participants' (left) and stroke patients' (right) responses to no (white), 90 Hz vibration on the triceps (orange) and biceps (dark blue), and 25 Hz vibration on the triceps (yellow) and biceps (light blue) are shown (* $p < 0.05$, ** $p < 0.001$)

impaired and limited native sensory feedback, were more influenced by the illusions induced by vibration. Future work will evaluate whether extended exposure to therapies integrating KF will promote long-lasting motor recovery. Moreover, fMRI will identify areas of the brain influenced by KF.

5 Conclusion

Stroke patients moved to a target in a reaching task more smoothly and directly, with greater elbow extension, when they received illusion-inducing vibration to the agonist muscle. Therapies including such augmented proprioceptive feedback could promote better motor recovery.

Acknowledgements Work by F. F., F. C., and C. C. was funded by the European Research Council under the MYKI project (ERC-2015-StG, Grant no. 679820).

References

1. E.B. Plow, D.A. Cunningham, N. Varnerin, A. Machado, Rethinking stimulation of the brain in stroke rehabilitation: Why higher motor areas might be better alternatives for patients with greater impairments. *Neuroscientist* **21**(3), 225–240 (2015)
2. P. Langhorne, F. Coupar, A. Pollock, Motor recovery after stroke: a systematic review. *Lancet Neurol.* **8**(8), 741–754 (2009)
3. K.A. Potter-Baker et al., A game of hide and seek: Is it possible to recruit more patients for NIBS studies in stroke? *J. Neurol. Sci.* **358**(1–2), 472–474 (2015)
4. S. Meyer et al., Somatosensory impairments in the upper limb poststroke: Distribution and association with motor function and visuospatial neglect. *Neurorehabil. Neural Repair* **30**(8), 731–742 (2016)
5. N. Bolognini, C. Russo, D.J. Edwards, The sensory side of post-stroke motor rehabilitation. *Restor. Neurol. Neurosci.* **34**(4), 571–586 (2016)
6. J. Gordon, M.F. Ghilardi, C. Ghez, Impairments of reaching movements in patients without proprioception. I. Spatial Errors. *J. Neurophysiol.* **73**(1), 347–360 (1995)
7. J.P. Roll, J.P. Vedel, Kinaesthetic role of muscle afferents in man, studied by tendon vibration and microneurography. *Exp. Brain Res.* **47**, 177–190 (1982)
8. R.W. Soukoreff, I.S. MacKenzie, Towards a standard for pointing device evaluation, perspectives on 27 years of Fitts' law research in HCI. *Int. J. Hum. Comput. Stud.* **61**(6), 751–789 (2004)
9. J. Diedrichsen, R. Shadmehr, R.B. Ivry, The coordination of movement: optimal feedback control and beyond. *Trends Cogn. Sci.* **14**(1), 31–39 (2010)

Effects of Non-in Situ Vibrations on Hand Sensations: A Pilot Study



Anke Fischer, Leonardo Cappello, Leonard F. Engels,
and Christian Cipriani

Abstract The use of hand prostheses implies manipulating objects without tactile information. Although prosthetic users might benefit from supplementary sensory feedback, its advantages might be hindered by unreliable feedforward control of the prosthetic devices. The ideal tool to study supplementary sensory feedback with healthy participants is the sensory deprived human hand. In this work, we propose the use of a technique to reduce tactile sensation of the fingertips without the need for local anesthesia, based on the application of a continuous vibrational stimulus to the wrist. We quantitatively investigated its effects with established clinical tests, and we obtained encouraging yet preliminary results. The extent of this sensory reduction should be explored in further experiments with larger pools of participants.

1 Introduction

To evaluate supplementary sensory feedback techniques for prosthetics, any confounding factors and constraints that might mask the potential benefits of the feedback should be removed. The weight of the prosthesis, its limited dexterity, and the difficulty in controlling it are examples of these factors. Therefore, the ideal

A. Fischer
Institute for Information Processing Technologies (ITIV), Karlsruhe Institute of Technology,
Karlsruhe, Germany
e-mail: anke.fischer@student.kit.edu

L. Cappello (✉) · L. F. Engels · C. Cipriani
The BioRobotics Institute, Scuola Superiore Sant'Anna, Pisa, Italy
e-mail: leonardo.cappello@santannapisa.it

Department of Excellence in Robotics and AI, Scuola Superiore Sant'Anna, Pisa, Italy

L. F. Engels
e-mail: leonard.engels@santannapisa.it

C. Cipriani
e-mail: christian.cipriani@santannapisa.it

feed-forward tool is undoubtedly the sensory-deprived human hand [1]. However, local anesthesia is not seamless to apply outside of a clinical environment to block sensory receptors and may carry some risk, especially for extended investigations [2]. Alternative ways to tackle this problem consist of physically separating the user from the manipulated object, i.e., employing augmented reality or remote robotic arms [3]. These systems too are not ideal, since they can be difficult to control, may lead to fatigue due to the weight of the control interfaces, and the accuracy of the motion tracking systems might be detrimental to the performances. In this work, we propose a novel noninvasive approach based on intense vibrations to attenuate the sensation of the hand. This approach leverages the sensory adaptation mechanism of the mechanoreceptors of the hand [4, 5]: when intense vibrations are applied, the mechanoreceptors tend to adapt to the stimulus, making the hand less sensitive to other mechanical events such as pressure or vibrations [6, 7].

2 Materials and Methods

2.1 Participants

We recruited 23 healthy participants (age range: 23–41), each of them was enrolled in up to three experimental groups in order to have three groups populated with 10 participants each. The participants who were enrolled in more than one group underwent the procedure only once per day to avoid aftereffects. The study was conducted according to the Declaration of Helsinki and was approved by the Ethical Committee of Scuola Superiore Sant'Anna (approval number 2/2017). All subjects gave written informed consent before participating in the study.

2.2 Experimental Set-up and Procedure

To assess the effects of sensory attenuation due to vibrations, we employed three clinical tests widely used to assess perception in upper and lower extremities. They are: (i) the Semmes-Weinstein monofilament (MF) test, which allows to estimate skin sensitivity to pressure; (ii) the two-point discrimination (TPD) test, which allows to measure the spatial acuity of the skin area examined; and (iii) the vibration sensation (VS) test, which is commonly used to measure the sensitivity to vibration [8]. In the MF test, we selected six different locations of the hand and we tapped each with three different filaments, respectively of 0.02 g, 0.04 g and 0.07 g (Tactile Monofilaments, Baseline®). The participants were asked to report whether they perceived the contact with the filament, and we counted the number of unperceived taps. For the TPD test, we employed a common caliper to assess the minimum perceivable distance of two separate contact points on the index fingertip pad. In this test, the participants

Fig. 1 The experimental set-up. A vibrational motor applied a prolonged vibration to the wrist. In this figure, the actuator for the VS test is shown, applied to the index finger



were asked to report whether they perceived the contact as two distinct points or only one. Finally, the VS test involved the use of a piezoelectric actuator (PC4QR, Thorlabs) to apply a vibration to the index fingertip pad with an initial amplitude of $3.13 \mu\text{m}$ (easily perceivable by all the participants) and a frequency of 59 kHz (i.e., the resonance frequency of the actuator). The initial amplitude of the vibration was gradually reduced over a time of 90 s to zero or until the participants signalled that they could not perceive the vibration anymore.

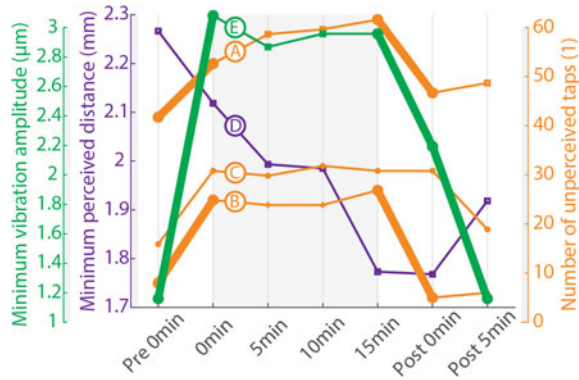
Our experiment consisted of a baseline assessment with the three clinical tests (MF, TPD, VS) prior the beginning of the stimulation, followed by a prolonged application of vibratory stimulus for 15 min (amplitude of 0.25 mm, frequency of 110 Hz, verified to be safe for the participants [9]) by means of an electrodynamic actuator (Mini shaker 4810, Brüel & Kjaer) applied to the volar surface of the wrist with a custom support structure (Fig. 1). Depending on the experimental group, each participant underwent only one of the three clinical tests according to the experimental group, which was administered at the beginning of the stimulation and after 5, 10, and 15 min. Subsequently, the stimulation was interrupted, and the participant underwent other two assessments: one immediately after the termination of the stimulus, and the last one after 5 min.

The experimental data were recorded for subsequent offline analysis. Statistical analysis was performed to capture significant differences in the data. We tested normality with Shapiro Wilk test, and since the data were not normally distributed, used the Friedman test, followed by Bonferroni-corrected Wilcoxon tests.

3 Results

The results of the MF test and the VS test showed significantly reduced sensitivity after the application of the vibration, while the outcomes of the TPD test were

Fig. 2 Experimental results: in orange, the MF test (lines A, B, and C respectively for the 0.02 g, 0.04 g and 0.07 g filaments); in purple, the TPD test (line D); and in green, the VS test (line E). Thick lines represent significant differences between measurements. The grey area represents the application of the vibrational stimulus



not significantly affected (Fig. 2). In particular, significant changes can be noticed immediately after switching the stimulus on and off.

Notably, some participants reported the sensation of kinesthetic illusion during the application of the stimulus [10].

4 Discussion

With the proposed stimulation method, we demonstrated that it is possible to significantly reduce tactile sensitivity, except for spatial resolution, without the need for local anesthesia. Nevertheless, a larger pool of participants should be tested to draw significant conclusions on its effectiveness. We cannot conclude whether this reduction is comparable to the use of gloves or to topic anesthesia due to the lack of quantitative outcomes in the literature. For example, the studies of Bensmaia et al. and Hollins et al. [6, 7] focused on qualitative outcomes of reducing sensations, rather than on quantitative measurements.

To improve system usability, a smaller actuator can be employed, such as a tactor (e.g., C-2, Engineering Acoustics Inc.). Finally, particular attention should be paid to containing the kinesthetic illusion effect, possibly caused by the activation of muscle spindles by the vibration [10]. Applying the stimulation in frequency ranges different from those that elicit this effect could prevent this side effect.

Acknowledgments This work was partially funded by the European Commission under the DeTOP project (EIT-ICT-24-2015, GA #687905) and partially by INAIL (the Italian national workers' compensation) under the CECA2020 project. The work of C.C. was partially funded by the European Research Council under the MYKI project (ERC-2015-StG, Grant no. 679820).

References

1. L. Engels, L. Cappello, C. Cipriani, Digital extensions with bi-axial fingertip sensors for supplementary tactile feedback studies, in *7th IEEE International Conference on Biomedical Robotics and Biomechatronics*, 1199–1204 (2018)
2. R.S. Johansson, G. Westling, Roles of glabrous skin receptors and sensorimotor memory in automatic control of precision grip when lifting rougher or more slippery objects. *Exp. Brain Res.* **56**, 550–564 (1984)
3. A.W. Shehata, L.F. Engels, M. Controzzi, C. Cipriani, E.J. Scheme, J.W. Sensinger, Improving internal model strength and performance of prosthetic hands using augmented feedback. *J. NeuroEng. Rehabil.* **15**, 70 (2018)
4. E.R. Kandel, J.H. Schwartz, T.M. Jessell, S.A. Siegelbaum, A.J. Hudspeth, *Principles of Neural Science* (McGraw-Hill Companies, 2013)
5. S. O'Mara, M.J. Rowe, R.P. Tarvin, Neural mechanisms in vibrotactile adaptation. *J. Neurophysiol.* **59**, 2 (1988)
6. M. Hollins, A.K. Goble, B.L. Whitsel, M. Tommerdahl, Time course and action spectrum of vibrotactile adaptation. *Somatosens Mot. Res.* **2**(7), 205–221 (1990)
7. S.J. Bensmaia, Y.Y. Leung, K.O. Johnson, Vibratory adaptation of cutaneous mechanoreceptive afferents. *J. Neurophysiol.* **94**(5), 3023–3036 (2005)
8. A. Boulton et al., Comprehensive foot examination and risk assessment: a report of the task force of the foot care interest group of the American Diabetes Association, with endorsement by the American Association of Clinical Endocrinologists. *Diabetes Care* **31**(8), 1679–1685 (2008)
9. C.M. Nelson, P.F. Brereton, The European vibration directive. *Ind. Health* **43**, 472–479 (2005)
10. F. Ferrari, F. Clemente, C. Cipriani, The preload force affects the perception threshold of muscle vibration-induced movement illusions. *Exp. Brain Res.* **237**(1), 111–120 (2018). <https://doi.org/10.1007/s00221-018-5402-4>

HaptiTrack: A Novel Device for the Evaluation of Tactile Sensitivity in Active and in Passive Tasks



Simone Ciotti, Matteo Bianchi, Davide Doria, Francesco Lacquaniti, and Alessandro Moscatelli

Abstract Several neurological, metabolic and psychological conditions may lead to tactile dysfunctions. Quantitative Sensation Tests (QST) are currently available for the assessment of tactile sensitivity, including light touch testing, monofilament tests, and vibration-based tests. However, standard QSTs display a high intra- and inter-individual variability. To this end, we developed new interface that generates 2D motion of a contact plate, provides hand and finger tracking, and measures contact force and torque. Due to these multiple features, the device can be a powerful tool for the evaluation of touch in both, active and passive tasks.

1 Introduction

The sense of touch allows us to perceive the mechanical properties of the objects through the contact with the skin [1]. Several neurological, metabolic and psychological conditions may lead to tactile dysfunctions, such as paresthesia (abnormal sensation such as tingling or tickling) and hypoesthesia (reduced tactile sensitivity) [2]. Quantitative Sensation Tests (QST) are currently available for the assessment of tactile dysfunction, including light touch testing, monofilament tests, and vibration-based tests. However, standard QSTs display a high intra- and inter-individual variability. In a preliminary study (currently ongoing) we developed a novel protocol to evaluate tactile sensitivity in type 1 diabetes mellitus by using a custom-made haptic interface delivering passive stimuli, i.e. with the hand stationary. Recent studies highlighted the importance of touch in motor control [3]. Therefore, it may be impor-

S. Ciotti (✉) · F. Lacquaniti · A. Moscatelli

Department of Systems Medicine and Center of Space Biomedicine, University of Rome Tor Vergata, Rome, Italy

Laboratory of Neuromotor Physiology, IRCCS Fondazione Santa Lucia, Rome, Italy

M. Bianchi · D. Doria

Reasearch Center “E. Piaggio” University of Pisa, 56126 Pisa, Italy

Department of Information Engineering, University of Pisa, 56122 Pisa, Italy

© The Author(s), under exclusive license to Springer Nature Switzerland AG 2022

D. Torricelli et al. (eds.), *Converging Clinical and Engineering Research*

on *Neurorehabilitation IV*, Biosystems & Biorobotics 28,

https://doi.org/10.1007/978-3-030-70316-5_99

tant to evaluate touch also in active task (e.g., surface exploration and reaching). To this end, we developed new interface that generates 2D motion of a contact plate, provides hand and finger tracking, and measures contact force and torque. Due to these multiple features, the device can be a powerful tool for the evaluation of touch in both, active and passive tasks. The novel haptic interface, the *HaptiTrack* device, will be used for the evaluation of tactile sensitivity diabetes mellitus in future work.

2 Material and Methods

2.1 Hardware Description

The HaptiTrack device is shown in Fig. 1. The device is similar to a pantograph with two orthogonal axes mounted on top of each other for the displacement of the contact surface on a horizontal plane. Each axis consist of a compact single-axis actuator (MISUMI LX3005CP-MX-B1-N-600-FA2), endowed with a precision grade ball screw. The device is endowed with two proximity sensors that switch off the power-supply in case the device position would exceed the allowed range. Each of the two axis is driven by Maxon motor (DCX26L GB KL 24V with planetary gearhead GPX26 C 3.9:1). A control board (SoftHand Board v1.0 by qrobotics) combined with a 16-bit resolution encoder are used to control the angular position and speed of each motor. Each ball screw is connected to the motor by a rubber-type shaft coupling (Nabeya Bi-tech XGS-25CS-6-6), ensuring high damping capacity. The device is equipped with a sensorized surface with a 3D printed textured plate on top ($100 \times 100 \times 3$ mm). Four damping components (TAICA Gel Bush A-1) placed



Fig. 1 The HaptiTrack device fixed inside a safety cage with mounted OptiTrack Flex13 cameras in each corner

between the contact surface and the movable axis reduce high-frequency vibrations generated by the motors. A 6-axis force/torque sensor (ATI Mini45) is placed below the contact plate. Sensing range and resolution are suitable for force/torque measuring within the typical human range [4]. OptiTrack system is used to track the fingertip of the user. Four OptiTrack Flex13 cameras are firmly attached to the metal frame of the device. A rigid body made of a 3D-printed thimble with 4 passive markers (3 mm of diameter) ensured a reliable tracking.

2.2 Control Algorithm

We tested the capacity of the device to update the position of the plate to follow the finger movement of a participant. A single participant moved her fingertip back and forth on the contact plate (1D motion). The position of the contact surface was updated every 2 ms, according to Eq. 1:

$$\bar{\mathbf{x}}_{new} = \bar{\mathbf{x}}_{old} + \gamma(\bar{\mathbf{X}}_{new} - \bar{\mathbf{X}}_{old}) \quad (1)$$

where $\bar{\mathbf{x}}_{new}$ and $\bar{\mathbf{x}}_{old}$ are the x and y position of the contact surface in the previous and in the current step, $\bar{\mathbf{X}}_{new}$ and $\bar{\mathbf{X}}_{old}$ are the current and the previous position of the fingertip measured from the OptiTrack, and γ is the position gain between the user's finger and the contact surface. In different trials, we set the values of gain γ to one of the following values: ± 1 , ± 0.8 , ± 0.5 , ± 0.4 , 0.0 . At the beginning of each trial, the initial position of the contact surface was always set to zero. As a contact was detected, $\bar{\mathbf{X}}_{new}$ and $\bar{\mathbf{X}}_{old}$ were initialized at the current finger position. If the measured force module was < 0.1 N the contact surface position was not updated.

We used a custom-made software written in C++ and libraries Eigen, Boost, and OptiTrack NatNet to control the apparatus and for the synchronization of the OptiTrack, the ATI Mini45, and the motor encoders.

3 Results

3.1 Vibrations

The vibration along the three axes were recorded with an accelerometer attached to the contact plate and measured at the two motion speed of 20 and 100 mm/s (Fig. 2a). The peak vibrations along the y axis is likely due to the change in motion direction of the plate at the end of each swept.

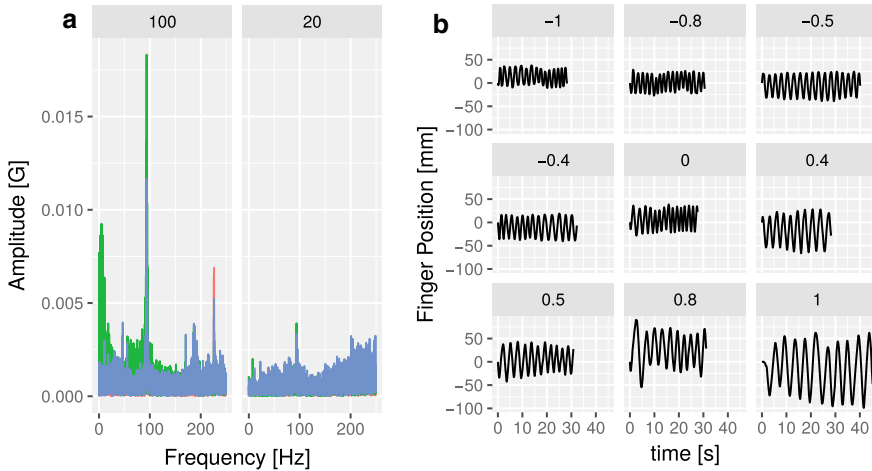


Fig. 2 **a** Measured vibration along the three axes (x , y , z) for a sinusoid movement along the y axis at two target speed and for the maximum movement width (stroke). **b** The back and forth movement of the fingertip (one participant)

3.2 Pursuit Gain

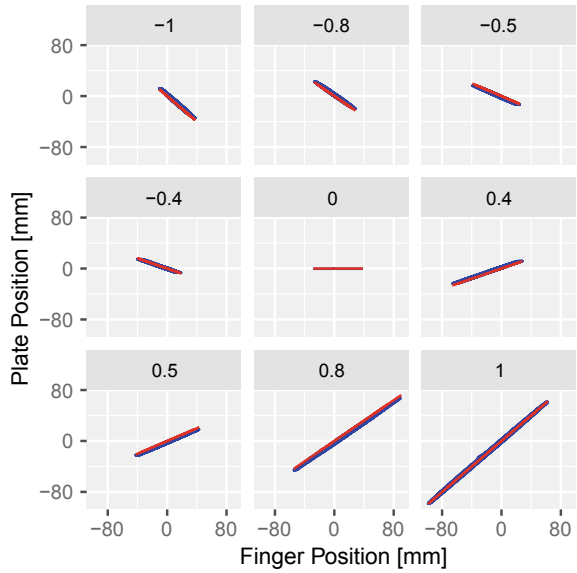
Figure 2b illustrates the back-and-forth displacement of the participant's fingertip. The amplitude of movement was larger for positive gains, where the plate was following. Instead, this was restricted to half of the plate's width for $\gamma = -1$.

By changing the value of γ , it was possible to disentangle tactile and hand motion. If $\gamma = 0$ the contact surface was stationary, if $\gamma = 1$ the contact surface follows the user's finger on the y -axis (zero tactile motion), and if $\gamma = -1$ the y -axis is in counterphase respect to the user's finger movement direction. We compared the actual and the target position of the plate for different finger movements and values of gain. As illustrated in Figure 3 the actual position of the plate closely matches the target position (we removed a small offset between the two due to the inertia of the apparatus). The correlation between the target and the actual value of plate position was 0.99 ($p < 0.001$).

4 Discussion

Here, we presented a novel haptic device for the study of tactile motion in active and passive tasks. In the preliminary evaluation, the device was able to produce the requested displacement to pursue the finger movement. In future work, this device will be used in behavioral experiment in healthy volunteers and people affected by neurological diseases for the evaluation of tactile sensitivity.

Fig. 3 Finger and Plate position for different values of gain, γ . The label above each panel is the value of gain. Target and actual values are represented in red and blue, respectively



Acknowledgements This work was partially supported by the Italian Ministry of Health (Ricerca Corrente, IRCCS Fondazione Santa Lucia) and Italian Ministry of University and Research (PRIN 2017SB48FP).

References

1. E.P. Gardner, K.O. Johnson, “Touch”, in ed. by E.R. Kandel, J. Schwartz, T. Jessel, S.A. Siegelbaum, A.J. Hudspeth, *Principles of Neural Science*, 5th edn (McGraw-Hill, New York, 2013), Chap. 23, pp. 451–471
2. A.H. Ropper, M.A. Samuels, J. Klein, *Adams and Victor’s Principles of Neurology*, 11th edn. (McGraw-Hill Education, 2019)
3. A. Moscatelli, M. Bianchi, S. Ciotti, G.C. Bettelani, C.V. Parise, F. Lacquaniti, A. Bicchi, Touch as an auxiliary proprioceptive cue for movement control. *Sci. Adv.* **5**(6), eaaw3121 (2019)
4. B. Delhaye, V. Hayward, P. Lefevre, J.-L. Thonnard, Texture-induced vibrations in the forearm during tactile exploration. *Front. Behav. Neurosci.* **6**(July), 37 (2012)

A Parallel Actuated Haptic Device for De-localized Tactile Feedback in Prosthetics



Daniele Leonardis, Leonardo Cappello, Christian Cipriani,
and Antonio Frisoli

Abstract This work presents a parallel actuated haptic device designed for delivering de-localized tactile feedback in prosthetics. Its peculiar design seeks to improve balance between static and slow output forces, such as grip force, and wide bandwidth tactile signals, such as vibrations, textures and fast contact transients. To this aim the device implements two actuators coupled in parallel with different mechanical transmissions. A cantilever mechanism obtains a compact arrangement of the moving parts and improves wearability of the device. We present results of the preliminary tests of the device using a force sensor: they show the enhanced capabilities of the device in modulation of the output force from static to high frequency components.

Keywords Tactile feedback · Haptics · Prosthetics · Parallel actuator · Twisted string

1 Introduction

Tactile feedback is a fundamental sensory pathway in manipulation: it is constantly integrated with other senses, such as proprioception, vision and auditory signals, to provide a rich set of information which are critical in accomplishing fine manipulation tasks.

In the field of haptics, a variety of different wearable devices have been developed to artificially render specific tactile features [1] directly at the level of fingertips. Conversely in the field of prosthetics, the problem is how to provide similar cues, acquired by prosthetic hand's sensor, to the user. A viable solution is to apply supplementary tactile feedback to more proximal segments of the body with respect to the amputation (e.g., the forearm, the chest, etc.), in a de-localized fashion. Vibro-tactile

D. Leonardis (✉) · A. Frisoli
PERCRO Laboratory, TeCIP Institute of Scuola Superiore Sant'Anna, Pisa, Italy
e-mail: d.leonardis@santannapisa.it

L. Cappello · C. Cipriani
Biorobotics Institute of Scuola Superiore Sant'Anna, Pisa, Italy

© The Author(s), under exclusive license to Springer Nature Switzerland AG 2022
D. Torricelli et al. (eds.), *Converging Clinical and Engineering Research on Neurorehabilitation IV*, Biosystems & Biorobotics 28,
https://doi.org/10.1007/978-3-030-70316-5_100

feedback has been used to this purpose as source of discrete events (DESC), resulting very effective in improving grasping performance of the user [2, 3]. Going beyond the rendering of discrete tactile events, a richer and informative tactile feedback can be achieved by modulating the force signal provided by the haptic actuator on the user’s skin [4]. Rendering of grasping force modulation, contact transients, vibrations of the grasped object and even textures [5] could be experimented also for de-localized tactile feedback.

Wearable haptic devices designed for modulating the contact force of a plate in contact with the user’s skin have been developed with various size and features. A common design problem is to find a convenient trade-off between size, maximum force and output bandwidth of the device.

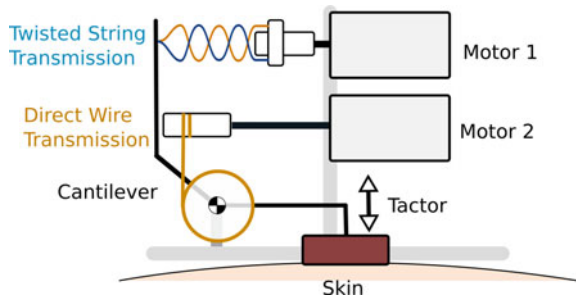
Direct electromagnetic actuators (i.e. voice coils) allow for wide bandwidth haptic rendering [6], with the drawback of a limited maximum output force compared to actuator’s mass. Small actuators provided with mechanical reduction can be used to amplify the output force [7], yet at the cost of reduced output bandwidth and lower quality of the haptic feedback in terms of noise.

In this work we explore a novel approach to obtain a compact and wearable haptic device with both good performances in maximum static force rendering and wide modulation bandwidth: we use two actuators coupled in parallel by different wire transmissions: a direct drive transmission, to obtain wide bandwidth frequency response, and a twisted string transmission [8], to amplify static and low-dynamics

Fig. 1 Prototype of the developed parallel actuated haptic device (held in a hand for size comparison)



Fig. 2 Scheme of the parallel actuation mechanism implemented in the haptic device



force components. A cantilever mechanism allows for a low-friction, compact device design.

2 Methods

2.1 *The Parallel Actuated Haptic Device*

The developed haptic device (Fig. 1) implements two identical DC motors (Minebea type FF-050-SH) arranged in parallel in a compact mechanism (dimensions are $36 \times 24 \times 16$ mm, total mass 38 g). A cantilever mechanism connects the body of the device with an output moving plate placed below the mechanism, in contact with the user's skin. Two different mechanical transmissions were implemented, as shown in Fig. 2: a direct drive transmission connecting the output pulley of the first motor to the cantilever mechanism of the moving plate. The direct wire transmission is highly efficient and obtains wide output bandwidth, although with low reduction rate and thus limited output force. The second actuator implements a twisted string transmission, obtaining a mechanical reduction with higher output force at the cost of limited bandwidth. Importantly, the typology of the implemented transmissions was selected avoiding those introducing noise and vibration in the rendered signals (i.e. gear reduction).

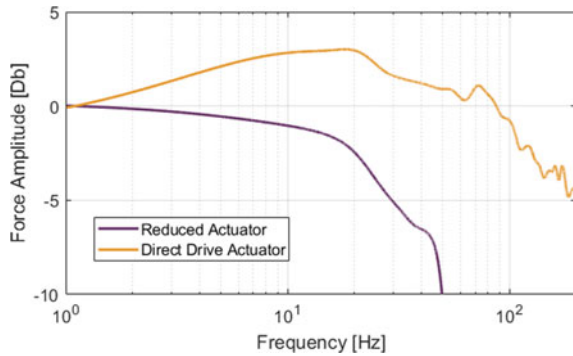
2.2 *Experimental Setup*

In this work we present a preliminary test of the parallel haptic device at the bench, aimed at measuring its effective force modulation capabilities. We used a miniaturized force sensor (Optoforce 10N, tri-axial force sensor, resolution 1 mN) fixed on a support in contact with the moving plate of the device. Then, we connected the two DC actuators of the device to a DRV8835 h-bridge. The h-bridge was driven by a Teensy 3.6 microcontroller board. We explored the frequency response of the device by separately driving the two actuators with a chirp voltage reference signal. The signal had an amplitude of 2.5 V (offset 2.5 V).

3 Results

Figure 3 shows the frequency response of the two actuators. Curves are expressed in Db and normalized with respect to the static gain (measured at the lowest stimulation frequency of 1 Hz). It highlights the expected behavior of the system: the twisted string actuator, capable of higher output force in static and low dynamics condition,

Fig. 3 Frequency response of the two actuators with different transmission and reduction



presents a limited frequency bandwidth (20 Hz cutoff) which can be effectively compensated by the direct drive actuator (150 Hz cutoff). Maximum measured force at the contact plate was 2.3 N for the twisted actuator, and 0.44 N for the direct-drive actuator. Additional experiments will be targeted to optimize the different reduction ratio of the actuators, taking into account the spectral energy distribution of tactile signals in typical manipulation tasks.

4 Conclusion

This work presented a compact wearable haptic device designed for application in prosthetics and tactile feedback in general. The novel approach uses coupled parallel actuators, in order to improve bandwidth and maximum output force in the haptic rendering. The obtained frequency distribution between the coupled actuators particularly fits haptic rendering, where high amplitude, slow force components (i.e. grasping force) are coupled with fast transients and high frequency tactile signals (i.e. vibrations, textures). The proposed device will be leveraged to deliver rich tactile feedback to prosthetic users, in the attempt of improving their manipulation performances, and ultimately their quality of life.

Acknowledgements This work was developed within project TELOS (funded by Regione Toscana, Italy, Bando Ricerca Salute 2018).

References

1. C. Pacchierotti, S. Sinclair, M. Solazzi, A. Frisoli, V. Hayward, D. Prattichizzo, Wearable haptic systems for the fingertip and the hand: taxonomy, review, and perspectives. *IEEE Trans. Haptics* **10**(4), 580–600 (2017)

2. C. Cipriani, J.L. Segil, F. Clemente, B. Edin, Humans can integrate feedback of discrete events in their sensorimotor control of a robotic hand. *Exp. Brain Res.* **232**(11), 3421–3429 (2014). <https://doi.org/10.1007/s00221-014-4024-8>
3. F. Clemente, M. D’Alonzo, M. Controzzi, B.B. Edin, C. Cipriani, Non-invasive, temporally discrete feedback of object contact and release improves grasp control of closed-loop myoelectric transradial prostheses. *IEEE Trans. Neural Syst. Rehabil. Eng.* **24**(12), 1314–1322 (2015)
4. L. Cappello, W. Alghilan, M. Gabardi, D. Leonardis, M. Barsotti, A. Frisoli, C. Cipriani, Continuous supplementary tactile feedback can be applied (and then removed) to enhance precision manipulation. *J. Neuro Eng. Rehabil.* (2020)
5. M. Wiertlewski, J. Lozada, V. Hayward, The spatial spectrum of tangential skin displacement can encode tactual texture. *IEEE Trans. Rob.* **27**(3), 461–472 (2011)
6. M. Gabardi, M. Solazzi, D. Leonardis, A. Frisoli, A new wearable fingertip haptic interface for the rendering of virtual shapes and surface features, in *2016 IEEE Haptics Symposium (HAPTICS)*. (IEEE, 2016), pp. 140–146
7. D. Leonardis, M. Solazzi, I. Bortone, A. Frisoli, A 3-RSR haptic wearable device for rendering fingertip contact forces. *IEEE Trans. Haptics* **10**(3), 305–316 (2016)
8. S.H. Jeong, K.S. Kim, A 2-speed small transmission mechanism based on twisted string actuation and a dog clutch. *IEEE Rob. Autom. Lett.* **3**(3), 1338–1345 (2018)

A Compact Soft Exoskeleton for Haptic Feedback in Rehabilitation and for Hand Closing Assistance



Tommaso Bagneschi, Daniele Leonardis, Domenico Chiaradia,
and Antonio Frisoli

Abstract In this work we present a novel soft exoskeleton providing active support of the hand closing: it implements a particular design of the tendon routing and of the actuator arrangement with the purpose of a compact and more comfortable system. Differently than other soft hand exoskeletons, the whole actuating system is embedded at the hand dorsum, resulting in shorter tendon routing, more comfortable pulling force distribution, and more practical use of the device. An additional feature of the proposed design is the increased adaptability to different hand sizes, thanks to the modular design of the soft polymer rings. Envisaged applications of the soft exoskeleton are in neurorehabilitation, to provide haptic feedback coupled to motor intention of the user, and for assistance in hand grasping.

1 Introduction

To convey haptic feedback or motor assistance at the level of the hand is a challenging objective for robotic device design, due to the complexity of the hand kinematics, limited available workspace, and high forces involved. Many hand exoskeleton that have been developed are based on rigid kinematics with links and joints positioned in series, aligned to the bones and joints of the fingers [1]. Other solutions show adaptive capabilities by including user's fingers in the parallel kinematic of the system [2]. Recently soft exoskeletons have been developed to overcome the limits of rigid robots: actuated gloves for assistance and rehabilitation that assist the movement of the fingers through the traction of cables, which mimic the functioning of the biological tendons [3–5]. The number and placement of the cables can vary from one cable per finger to help flexion and an elastic for extension [6], up to four cables per finger that mimic the geometry of the four major finger muscle–tendon units

This research was supported by the GRASP project, funded by italian MIUR.

T. Bagneschi · D. Leonardis (✉) · D. Chiaradia · A. Frisoli
Scuola Superiore Sant'Anna, Percro Laboratory, San Giuliano Terme, Italy
e-mail: d.leonardis@santannapisa.it

© The Author(s), under exclusive license to Springer Nature Switzerland AG 2022
D. Torricelli et al. (eds.), *Converging Clinical and Engineering Research
on Neurorehabilitation IV*, Biosystems & Birobotics 28,
https://doi.org/10.1007/978-3-030-70316-5_101

[7]. A critical point of soft exoskeleton devices is the tendon routing and its fixing points to the device itself and in turn to the user's hand. Distribution of the exerted pulling forces can greatly vary effectiveness of the actuation and comfort of the device. In this work we propose a novel design of the tendon routing and of the actuator placement that obtains shorter tendon routing, a more compact device with the actuator embedded at the hand dorsum, and a more stable fixing on the user's hand when tendons are pulled.

2 Methods

The main structure of the soft exoskeleton consists of a laterally open leather glove, supporting bolted and sewed soft-polymer (Thermoplastic Polyurethane) parts. Finger units consist of a series of TPU rings and of a thimble. The number of rings can be varied to better fit phalanges of different sizes. The open ring approach, with two parallel tendons per finger has been chosen [8] due to its improved stability and comfort in wearing.

The actuator (LewanSoul LX-16A Servo) consists of a gear reduced DC motor with embedded drive electronics and position sensor. It is positioned directly at the hand dorsum in order to make the exoskeleton compact, thus leaving the wrist free (Fig. 1). The cables are laterally folded around the palm and actuated by a small radius pulley connected to the servomotor shaft. In this preliminary prototype, the extension is passive by means of elastic elements placed on the finger dorsum (black

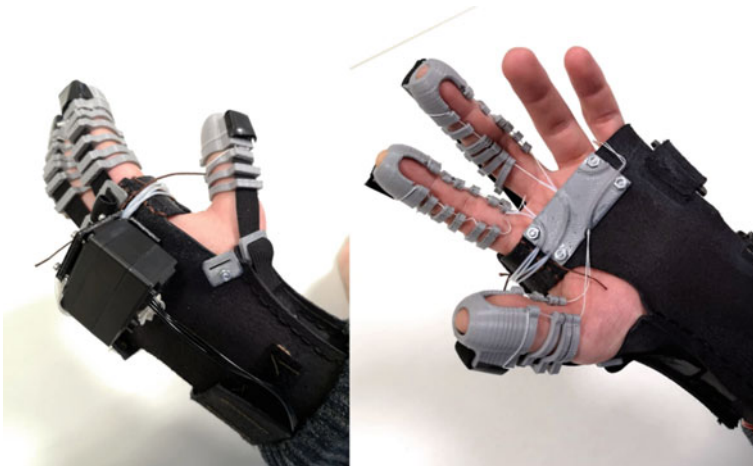


Fig. 1 Preliminary prototype of the compact soft exoskeleton. Actuator and tendon transmission are arranged around palm and hand dorsum, with no remote mechanical parts

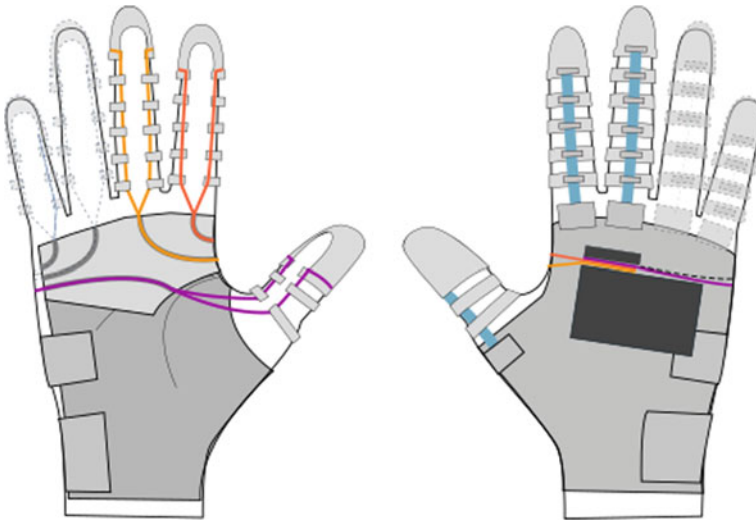


Fig. 2 Scheme of the tendon routing and actuator arrangement obtaining a compact actuated hand exoskeleton with no remote parts

elastic ribbon shown in figures) and fixed to the thimbles with adjustable buckles. The total mass of the prototype was 173 g. The dimensions of the actuator module (hand dorsum) was $45.7 \times 30.4 \times 40.6$ mm.

2.1 Preliminary Experimental Results

To estimate the grasping pressure for the exoskeleton-assisted hand a pressure sensorized plastic bottle was used (Bosch BMP280 pressure sensor). The bottle was filled with water to increase its stiffness. A healthy subject was enrolled for this preliminary study. The subject wore the exoskeleton which was adjusted to the size of his hand. A voltage reference was applied to the motor to obtain a closing and opening sequence. The stall output torque at 2.5V corresponds to 19 N pulling force applied to the tendon transmission. In Fig. 3a, the measured pressure averaged over ten repetitions is shown. The same experiment was repeated with a rigid plastic handle including a force sensor (Futek LSB200) to measure a grasping force for comparison. Results of the force measurement are shown in Fig. 3b. Fig. 3 show the measured pressure as a function of the output shaft position.

3 Discussion and Conclusions

Figure 3a shows a short time during which no pressure is applied, while the extended hand must come into contact with the surface of the bottle, and an interval of time during which with a positive voltage a gradual increase in pressure up to a peak is observed. Immediately afterwards with the inversion of voltage the hand relaxes and the pressure drops. Figure 4 highlights the compliance introduced in the system by the soft parts, by the fixing interface of the exoskeleton to the hand, and by soft tissues of the hand itself. Compliance of the system can be modeled with a quadratic model, obtained performing a quadratic regression to fit the measured data.

Regarding functionality of the prototype, the developed compact device design resulted capable of mobilizing the passive hand with considerable maximum grasping force (12.8 N). The modular ring system was easily adaptable to the finger joints, and the open structure with parallel tendons resulted in a simple donning of the finger modules. It also allows to relax pulling and tightening forces when the grasping

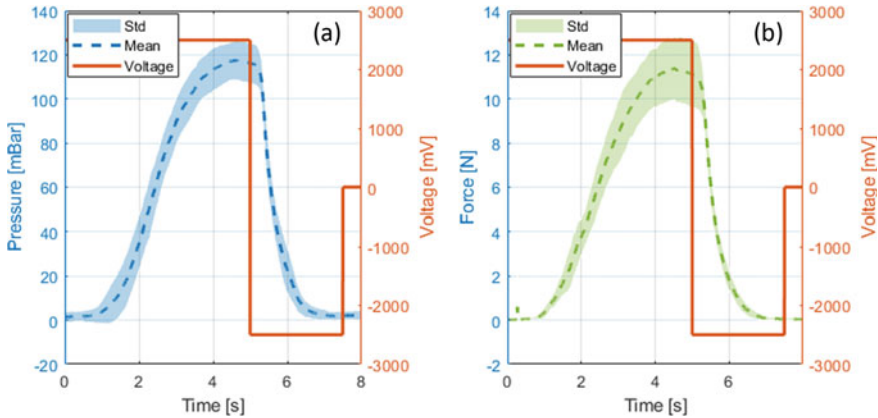


Fig. 3 Measured grasping pressure and grasping force with passive user, averaged over ten trials. Orange line represents the voltage reference applied to the servomotor

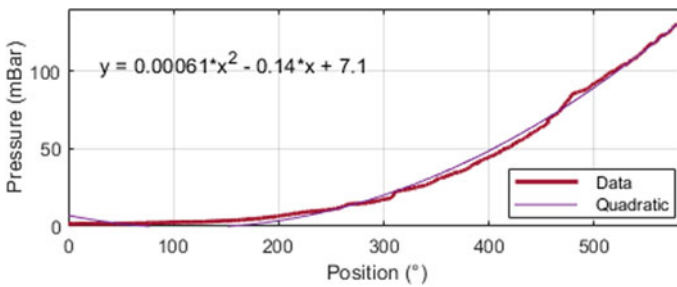


Fig. 4 Measured grasping pressure as a function of position in degrees (solid line) and quadratic model fit to the measured data (dotted line)

assistance is released. Importantly, the developed tendon routing folded around the user's palm permits to apply relatively high pulling forces with a stable wearability of the device on the user hand.

For this prototype tested on passive hands, elastic elements for finger extension were sufficient, although barely capable of recovering the passive fingers to full extension. Increasing the preload of the elastic bands had negative effects on user's comfort. Therefore, the passive hand opening method appears suitable on patients with flaccid hand only. Another critical aspect to improve is the thickness of the palm plate supporting the tendon routing. We fabricated it in soft TPU polymer, however, thickness of the assembly has to be further reduced to improve grasping capabilities. One last problem to examine is the thumb. Having a different articulation from the remaining fingers, a special support (i.e. with a compliant semi-rigid structure) has to be developed for supporting its correct movement in opposition to the other fingers. Rings, thimble and buckles have been produced with an FDM printer in TPU to make these parts adaptable to the patient.

Overall, functionality of the prototype is promising. Its main advantages in terms of compactness and adaptability to different hands make the device suitable for hand mobilization in neurorehabilitation settings, where haptic feedback congruent with motor intention is already a crucial objective. At a later stage of development, the device can be considered to provide hand grasping assistance in real everyday tasks.

References

1. T.T. Worsnopp, M.A. Peshkin, J.E. Colgate, D.G. Kamper. An actuated finger exoskeleton for hand rehabilitation following stroke, in *2007 IEEE 10th international conference on rehabilitation robotics* (IEEE, 2007), pp. 896–901
2. M. Sarac, D. Leonardis, M. Gabardi, M. Solazzi, A. Frisoli, Bilateral rehabilitation of hand grasping with an underactuated hand exoskeleton, in *International Conference on NeuroRehabilitation* (Springer, 2018), pp. 205–209
3. M. Xiloyannis, L. Galli, D. Chiaradia, A. Frisoli, F. Braghin, L. Masia, A soft tendon-driven robotic glove: Preliminary evaluation, in *International Conference on NeuroRehabilitation* (Springer, 2018), pp. 329–333
4. B.B. Kang, H. Lee, H. In, U. Jeong, J. Chung, K.-J. Cho, Development of a polymer-based tendon-driven wearable robotic hand, in *2016 IEEE International Conference on Robotics and Automation (ICRA)* (IEEE, 2016), pp. 3750–3755
5. A. Dwivedi, L. Gerez, W. Hasan, C. Yang, M. Liarokapis, A soft exoglove equipped with a wearable muscle-machine interface based on forcemyography and electromyography. *IEEE Robot. Autom. Lett.* **4**(4), 3240–3246 (2019)
6. L. Gerez, A. Dwivedi, M. Liarokapis, A hybrid, soft exoskeleton glove equipped with a telescopic extra thumb and abduction capabilities
7. S.W. Lee, K.A. Landers, H. Park, Development of a biomimetic hand extendon device (biomhed) for restoration of functional hand movement post-stroke. *IEEE Trans. Neural Syst. Rehabil. Eng.* **22**(4), 886–898 (2014)
8. B.B. Kang, H. Choi, H. Lee, K.-J. Cho, Exo-glove poly II: a polymer-based soft wearable robot for the hand with a tendon-driven actuation system. *Soft Robot.* **6**(2), 214–227 (2019)

Human Neuromarkers of Tactile Perception: State of the Art in Methods and Findings



Gianna Adalia Cannestro, Moaed A. Abd, Erik D. Engeberg,
and Emmanuelle Tognoli

Abstract Tactile perception is a multifaceted sense with complicated convergent/divergent peripheral pathways. Its neuromarkers remain poorly understood, due to the sense's inherent complexity and the confounding factor of intricate motor, cognitive and affective correlates. This gap hinders research evaluating interventions to restore touch in artificial hands. We inventorize state-of-the-art and recent innovations in control systems with soft and hard robotics that are poised to unlock more targeted non-invasive stimulations. We review neuromarkers observed for pressure, vibration, brushing, texture discrimination, pain, heat and cold, complemented with the covariates from movement, attention, working memory, multisensory and sensorimotor integration or competition (audition, vision) and affect. We analyze neural oscillations during sensory and (peripheral and central) electro-magnetic stimulation. This review matures a framework of reverse prediction, in which non-invasive observation of neural activity robustly and unobtrusively quantifies tactile perception.

Keywords Haptics · Afferent pathway · Somatosensation · Artificial sensory feedback · Robotic hand · Non-invasive · Tactile perception

1 Introduction

Several research groups, including our own, are working toward the development of artificial hands that restore the sense of touch, in an effort to facilitate dexterity and

This work was supported by the National Institute of Health (NIH) [R01, EB 025819] and FAU's Brain Institute.

G. A. Cannestro (✉) · E. D. Engeberg · E. Tognoli (✉)
Center for Complex Systems and Brain Sciences, Florida Atlantic University, Boca Raton, USA
e-mail: gcannestro2015@fau.edu

E. Tognoli
e-mail: etognoli@fau.edu

M. A. Abd · E. D. Engeberg
Ocean and Mechanical Engineering, Florida Atlantic University, Boca Raton, USA

© The Author(s), under exclusive license to Springer Nature Switzerland AG 2022
D. Torricelli et al. (eds.), *Converging Clinical and Engineering Research on Neurorehabilitation IV*, Biosystems & Biorobotics 28,
https://doi.org/10.1007/978-3-030-70316-5_102

fluidity of daily manual actions for amputees and limb absent users of prosthetic arms, and to support remote manual control in teleoperation. The development of technologies to restore afferent pathways calls for tools to monitor tactile perception continuously, unobtrusively, and non-invasively. A preferred site to achieve this monitoring lies with the brain: it is the destination of afferent tactile signals, with slightly better spatial separation of somatosensory and motor activities than what is achievable noninvasively in the peripheral nervous system, where both afferent (sensory) and efferent (motor) pathways are blended in shared nerves. To monitor tactile perception unobtrusively via non-invasive recording of brain activity (e.g. electro- and magneto-encephalography, EEG and MEG [1]), it is necessary to understand which neurophysiological activities correlate with qualitative and quantitative variations of tactile sensations. The non-invasive neuroscience of touch, however, remains less well understood than other senses, for a plurality of reasons. First, instrumentation to stimulate the various tactile experiences with temporal, spatial and functional precision remains a work-in-progress. Second, the sense of touch possesses a large and diverse array of receptors working synergistically. Those receptors' complicated convergent and divergent connectivity to the brain compounds the usual difficulties with teasing apart perception from its cognitive, behavioral, and environmental modulators. And finally, naming of electrophysiological activities confuses syntheses (viz. Identical names to activities from distinct brain networks, and distinct names for activities that pertain together). In the following presentation, we aim to accomplish four goals: (1) review technological developments supporting the disentanglement of tactile perception's multiple facets, leading to breakthrough neurophysiological studies; (2) identify neuromarkers of somatosensation and (3) their cognitive, affective, motor and environmental covariates; and (4) list bottlenecks to resolve in order to establish robust neuromarkers of tactile perception.

2 Technology Review: Tactile Stimulation Paradigms

A variety of techniques has been used to apply tactile stimulations and quantify associated brain responses. Studies span the simplest approaches (e.g. brush strokes applied onto a subject's arm) into engineered control systems that leverage mechanical, thermal, optical, acoustic, or electrical stimulations to improve temporal, spatial and functional precision. All sites along the pathways from sensory receptor to brain have been targeted: stimuli applied to the skin to recruit tactile receptors; electrical or ultrasonic stimulation applied to afferent nerves to induce peripheral activities mimicking the response to natural stimuli (directly or with co-optation of muscles); electrical or magnetic stimulations directly aimed at somatosensory brain areas to confirm elicitation of tactile experiences.

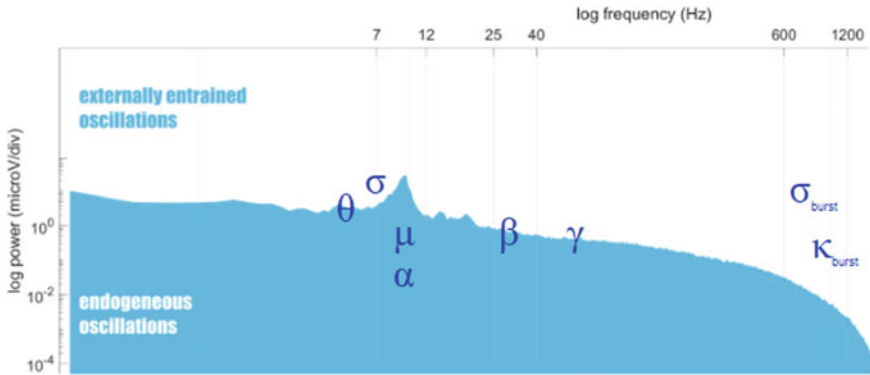


Fig. 1 Overview of EEG/MEG neuromarkers examined in this work

3 Neuromarkers of Somatosensation

With the aforementioned tools, considerable evidence implicates 6 oscillatory activities of the brain in somatosensation (Fig. 1). Mu (also called Rolandic alpha, a 8–12 Hz activity over somatosensory/motor cortex) and Beta (13–30 Hz, a slightly more anterior activity toward motor cortex and putatively involved in sensorimotor integration) undergo suppression and rebound during and after somatosensory stimulation and the direct electrical stimulation of peripheral nerve. Their sources were tied to somatosensory cortices, and reciprocally, stimulation of somatosensory areas with Mu frequencies elicited tactile percept [2]. Prestimulus Mu also modulated perception of faint tactile stimuli [3]. Theta (4–7 Hz, fronto-central) and Gamma (30–100 Hz, central regions of the brain) increased during somatosensory events [4, 5], and electrical stimulation of the somatosensory cortex at Gamma frequency elicited tactile sensations [2]. Finally, transient ultra-fast activities, Sigma (450–750 Hz) and Kappa bursts (850–1200 Hz), were discovered with Median Nerve Stimulation and seemed specific of afferent tactile information [6, 7], though few studies aid their functional understanding due to the great technical challenge of their recording.

4 Cognitive, Behavioral, Affective and Environmental Covariates

To reverse inferences and unobtrusively monitor the quality of artificially-restored somatosensory feedback with neuromarkers, a solid understanding of somatosensory covariates is needed. Beta and Theta activities were modulated by affective contexts and pain [4, 8]. Attention modulated the dynamics of Mu and Beta [3, 9]. Increased Gamma activity in the somatosensory cortex was also tied to attention

[9]. Lastly, a tremendous overlap exists between somatosensory and motor functions that intimately co-evolved. Movement modulates most of the same activities as somatosensation, namely Mu (and its variant Sigma), Beta, Theta and Gamma [10]. Current theoretical models suggest that Gamma might be related to spatial attention, sensory gating and inhibition, whereas theta has been proposed for sensorimotor integration, novelty and change detection.

5 Discussion

We asked if the neuroscience of touch had achieved maturity to quantitatively assess somatosensory experience from non-invasive monitoring of the brain. The answer to this question is not yet. There are six candidate neuromarkers of tactile perception, but four of them are confounded with other mental activities as well as environmental modulation [11]. The other two [6, 7], albeit challenging to record, bear some promise but will need increased vetting of their modulators. We also raised the functional heterogeneity of Beta (an endogenous rhythm of sensorimotor cortex possibly distinct from entrained rhythm with vibrotactile stimulation). It would further be desirable to disentangle the different facets of somatosensory experience with respect to specialized receptors pathways, (e.g., high frequency vibration signaling a slipping object or sustained modulation of pressure signaling force control). Except for Beta entrainment, the current literature on oscillations does not offer unambiguous specificity of its oscillations with respect to different facets of somatosensation (the timing of evoked potentials might help, since receptor types are wired with sharply distinct conduction velocities, but this lies beyond the scope of the present work). Insight into specific receptor pathways will require new well-integrated electrophysiological studies generalizing the approach undertaken in [4], complemented with better stimulation devices leveraging progress in soft and hard robotics [12]. Those advances in tactile neuroscience, combined with the application of bidirectional prosthetics, will open the path to much-needed neuro-rehabilitation studies comparing behavioral and neurophysiological characteristics of somatosensation in traumatic or congenital amputees and limb-intact populations using haptically-augmented prosthetic hands.

References

1. N. Naseer, H. Ayaz, F. Dehais, Portable and wearable brain technologies for neuroenhancement and neurorehabilitation. *BioMed Res. Int.* (2018)
2. M. Feurra, W. Paulus, V. Walsh, R. Kanai, Frequency specific modulation of human somatosensory cortex. *Front. Psychol.* **2**, 13 (2011)
3. S. Haegens et al., Thalamocortical rhythms during a vibrotactile detection task. *Proc. Natl. Acad. Sci.* **111**, E1797–E1805 (2014)
4. G. Michail, C. Dresel, V. Witkovský, A. Stankewitz, E. Schulz, Neuronal oscillations in various frequency bands differ between pain and touch. *Front. Hum. Neurosci.* **10**, 182 (2016)

5. C. Nangini, B. Ross, F. Tam, S.J. Graham, Magnetoencephalographic study of vibrotactile evoked transient and steady-state responses in human somatosensory cortex. *Neuroimage* **33**, 252–262 (2006)
6. G. Curio et al., Localization of evoked neuromagnetic 600 Hz activity in the cerebral somatosensory system. *Electroencephalography Clin. Neurophysiol.* **91**, 483–487 (1994)
7. T. Fedele, H.J. Scheer, M. Burghoff, G. Curio, R. Körber, Ultra-low-noise EEG/MEG systems enable bimodal non-invasive detection of spike-like human somatosensory evoked responses at 1 kHz. *Physiol. Measure.* **36**, 357 (2015)
8. H. Singh et al., The brain's response to pleasant touch: an EEG investigation of tactile caressing. *Front. Hum. Neurosci.* **8**, 893 (2014)
9. B.M. Adhikari, K. Sathian, C.M. Epstein, B. Lamichhane, M. Dhamala, Oscillatory activity in neocortical networks during tactile discrimination near the limit of spatial acuity. *Neuroimage* **91**, 300–310 (2014)
10. W.A. MacKay, Wheels of motion: oscillatory potentials in motor cortex, in *Motor Cortex in Voluntary Movements: A Distributed System for Distributed Functions*, 1st edn., ed. by A. Riehle, E. Vaadia (CRC Press, New York, 2005), pp. 181–211
11. C. Sitges, X. Bornas, J. Llabrés, M. Noguera, P. Montoya, Linear and nonlinear analyses of EEG dynamics during non-painful somatosensory processing in chronic pain patients. *Int. J. Psychophysiol.* **77**, 176–183 (2010)
12. M.A. Abd, M. Bornstein, E. Tognoli, E.D. Engeberg, Armband with soft robotic actuators and vibrotactile stimulators for bimodal haptic feedback from a dexterous artificial hand, in *2018 IEEE/ASME International Conference on Advanced Intelligent Mechatronics (AIM)* (2018), pp. 13–20

SS12: Human-Machine Interface for Real-Time Wearable Robots Control

Wearable Neurofeedback Training for Boosting Attention Regulation at the Wheel



Davide Crivelli, Laura Angioletti, and Michela Balconi

Abstract We tested the effects of a three-week neurofeedback (NF) empowerment protocol on drivers' cognitive performance by looking at both behavioural and electrophysiological (Event-Related Potentials, ERPs) markers of attention regulation skills. Results highlighted higher task-related ERP marking attention orientation and cognitive control processes (the N2 ERP component) in the experimental group receiving NF training compared to control subjects. Present findings suggest that intensive NF-based training might be a valuable way to improve drivers focused and sustained attention mechanisms, with practical implications for the development of proactive prevention protocols for driving performance.

Keywords Wearable devices · Neurofeedback · Distracted driving · Attention Regulation · Neurocognitive Empowerment · Proactive prevention

1 Introduction

In past years, most of solutions proposed to cope with the highly-relevant issue of distracted driving have focused on the development of driving monitoring and assistance systems (DMAS)—i.e. non-invasive technological aids installed on the vehicle able to collect data on driving performance and provide feedbacks on the alteration of driver's states such as drowsiness and distraction [1]. As an alternative to such forms of reactive prevention measures, a proactive prevention approach would

Authors kindly thank Cattolica Assicurazioni Group as project partner.

D. Crivelli · L. Angioletti · M. Balconi (✉)

International Research Center for Cognitive Applied Neuroscience (IrcCAN), Faculty of Psychology, Catholic University of the Sacred Heart, Milan, Italy
e-mail: michela.balconi@unicatt.it

D. Crivelli
e-mail: davide.crivelli@unicatt.it

L. Angioletti
e-mail: laura.angioletti1@unicatt.it

© The Author(s), under exclusive license to Springer Nature Switzerland AG 2022
D. Torricelli et al. (eds.), *Converging Clinical and Engineering Research on Neurorehabilitation IV*, Biosystems & Biorobotics 28,
https://doi.org/10.1007/978-3-030-70316-5_103

focus on reducing the impact of human factors on distracted driving by working on the driver itself via empowerment and optimization of attention regulation, stress management, and self-regulation skills.

A recent series of applied studies showed that supporting mental training programs with neurocognitive empowerment methods, such as wearable neurofeedback (NF) devices, can enhance neurocognitive empowerment effects in terms of regulation of attention resources and adaptive stress coping both in experimental settings and in real-life contexts [2–4], such as at the workplace [5] or in sports [6].

2 Material and Methods

2.1 Sample

Fifty adults (38 females; $M_{\text{age}} = 22.96$, $SD_{\text{age}} = 2.48$) without clinically relevant signs of stress or anxiety were included in the study and randomly divided into an experimental (EXP) and an active control (CNT) group. The study was approved by the competent Ethics Committee and followed the principles of the Declaration of Helsinki.

2.2 Study Design and Training Procedure

The study design included pre-/post-training assessment phases applied to the experimental/control groups, to investigate training effects on drivers' attention performance, distractibility, and ERP markers of cognitive control.

EXP participants completed a combined NF and mental training protocol, in which they had to perform breathing-awareness practices with the support of a wearable NF device—i.e. the LowDown Focus glasses (Smith Optics Inc., Clearfield, UT). CNT participants were, instead, asked to perform breathing practices without the support of the NF device. Therefore, their training could not benefit from external feedbacks on their mindset and its modulations.

Both EXP and CNT interventions lasted 21 days and included daily sessions of practice (gradually incremented duration: from 10 min a day to 20 min a day).

2.3 Pre-/Post-training Assessment

Assessment of higher attention and interference control skills were tested via a challenging computerized Stroop like task (Stim2 software, Compumedics Neuroscan, Charlotte, NC) during EEG acquisition. For task description see [7].

2.4 EEG Recording and Reduction

Central electrophysiological responses were collected and amplified via a 16-channel V-Amps system (Brain Products GmbH, Gilching, Germany). The electrode montage included a vertical EOG derivation and 15 sintered Ag/AgCl sensors referenced to linked earlobes and placed according the 10–10 International System—F7, F3, Fz, F4, F8, T7, C3, Cz, C4, T8, P3, Pz, P4, O1, and O2. Impedance values were reduced below 5 k Ω and checked during data collection. EOG and EEG data were sampled at 1000 Hz, using a bandpass (0.01–250 Hz) and a notch (50 Hz) input filter.

EEG data were then processed offline via Vision Analyzer2 software (Brain Products GmbH, Gilching, Germany). Firstly, EEG signals were filtered offline using specific IIR bandpass filters (0.1–30 Hz bandpass filter, 24 db/octave). They were then corrected by using a semi-automated ICA-based artefact detection and correction algorithm. Following visual inspection of EEG tracks and manual rejection of residual movement, muscle or ocular artefacts (rejection rate: <8%), they were segmented based on experimental conditions and related markers.

Task-related EEG activity collected during the Stroop like task was segmented from 200 ms before to 800 ms after Congruent versus Incongruent stimuli onset. Event-related waveforms were then baseline-corrected, and artefact-free epochs were averaged to enhance systematic electrophysiological responses to the experimental conditions. A preliminary morphological analysis of individual average waveforms highlighted the presence of a potentially relevant modulation of the N2 component. Peak amplitude and latency data for such component have finally been extracted thanks to a semi-automated weighted peak detection algorithm.

2.5 Data Analysis

Performance and electrophysiological data collected pre-/post-training in EXP and CNT groups were compared via independent-samples t-tests (PASW Statistics 18, SPSS Inc., Quarry Bay, HK). False Discovery Rate was controlled by applying the Benjamini-Hochberg procedure. Threshold for statistical significance was set to $\alpha = 0.05$. Equality of variances between groups was checked by Levene's test, so to verify the assumption of homoscedasticity and to accordingly compute subsequent inferential tests. As a measure of between-group effect size, we have computed Cohen's d values [8].

3 Results

As for the analysis of performance data, comparison of post-training behavioural measures at the Stroop task (response times and accuracy) did not highlight statistically significant differences between the groups (all $p > 0.05$).

As for electrophysiological data, we applied focused between-group statistical comparison to the N2 latency and peak amplitude data collected at left, midline, and right frontal (F3, Fz, F4), central (C3, Cz, C4), and parietal (P3, Pz, P4) electrode sites. Between-group comparisons of post-training peak amplitude data for the N2 component in response to congruent stimuli highlighted a statistically significant difference between EXP and CNT, with higher N2 amplitude in the former with respect to the latter at Fz electrode site ($t(48) = 2.106$, $p = 0.040$, $d = 0.632$; $M_{EXP} = -8.42$, $SD_{EXP} = 5.90$; $M_{CNT} = -5.27$, $SD_{CNT} = 3.85$). No significant effects were found for N2 latency data (all $p > 0.05$).

4 Discussion and Conclusions

After NF training, EXP drivers showed ampler N2 ERP components than CNT in response to target stimuli of the computerized Stroop task. Such improved ERP marker—in agreement with the nature of the eliciting task, localization of the ERP, and its functional role [9]—suggests that the EXP group displayed heightened activation of prefrontal attention and cognitive control mechanisms with respect to CNT participants, which could act as a facilitating factor for effective and safe driving especially in case of complex situations connoted by perceptual and sensory interferences. The fact that training effect reflected into ERP markers but did not significantly affect behavioural performance at the Stroop task might be justified by postulating either that training effects was beginning to consolidate but needed more time to fully express or that the width of empowerment effects was limited by ceiling effect. While those alternative interpretations are worth further investigation, previous evidence tip the scale in favour of the former.

Present findings suggest that an intensive neurofeedback-based training might represent a potentially-valuable mean to improve not only drivers' self-regulation and stress management skills, but also their focused and sustained attention regulation mechanisms, with practical implications for the development of proactive prevention protocols for distracted driving. Indeed, interventions aimed at reducing the impact of human factors such as distractibility and attention fatigue both in everyday and professional drivers hold a remarkable potential for containing social-economical costs of road accidents.

Yet, we acknowledge that present empirical observations would benefit from replication with different and larger samples of drivers (e.g. haulage professionals or coach drivers), so to increase their generalizability. Moreover, future research would benefit

from correlating behavioural and neurophysiological measures with real-life driving performance so to properly test their predictive potential.

References

1. M.Q. Khan, S. Lee, A comprehensive survey of driving monitoring and assistance systems. *Sensors* **19**, 2574 (2019)
2. M. Balconi, G. Fronza, D. Crivelli, Effects of technology-mediated mindfulness practice on stress: psychophysiological and self-report measures. *Stress* **22**, 200–209 (2019)
3. M. Balconi, G. Fronza, I. Venturella, D. Crivelli, Conscious, pre-conscious and unconscious mechanisms in emotional behaviour. Some applications to the mindfulness approach with wearable devices. *Appl. Sci.* **7**, 1280 (2017)
4. D. Crivelli, G. Fronza, I. Venturella, M. Balconi, Supporting mindfulness practices with brain-sensing devices. Cognitive and electrophysiological evidence. *Mindfulness* **10**, 301–311 (2019)
5. D. Crivelli, G. Fronza, I. Venturella, M. Balconi, Stress and neurocognitive efficiency in managerial contexts: a study on technology-mediated mindfulness practice. *Int. J. Workplace Health Manag.* **12**, 42–56 (2019)
6. D. Crivelli, G. Fronza, M. Balconi, Neurocognitive enhancement effects of combined mindfulness–neurofeedback training in sport. *Neuroscience* **412**, 83–93 (2019)
7. M. Balconi, D. Crivelli, L. Angioletti, Efficacy of a neurofeedback training on attention and driving performance: physiological and behavioral measures. *Front. Neurosci.* **13**, 996 (2019)
8. J. Cohen, *Statistical Power Analysis for the Behavioral Sciences* (Lawrence Erlbaum Associates, Hillsdale, NJ, 1988).
9. J.R. Folstein, C. Van Petten, Influence of cognitive control and mismatch on the N2 component of the ERP: a review. *Psychophysiology* **45**, 152–170 (2008)

Wearable Neurotechnologies for Neurocognitive Empowerment in Applied Contexts



Davide Crivelli, Giulia Fronda, Laura Angioletti, Claudia Spinosa, and Michela Balconi

Abstract Recently, the use of wearable devices and neurotechnologies for well-being and neurocognitive empowerment has increased, allowing users to achieve better awareness and control of their mindset and mood states. We present an overview of main results from a research line on the effectiveness of an intensive training protocol supported by wearable neurofeedback devices in the field of neurocognitive empowerment and stress management. Specifically, the potential of such neurotechnology-supported training was tested by collecting behavioural, psychometric, neuropsychological, and physiological outcomes and comparing experimental and active control groups. The protocol was tested in different experimental and applied contexts—including sports, workplace, and healthy aging. Based on the multi-level assessment of training outcomes, results highlighted the effectiveness of using intensive neurotechnology-mediated protocols to enhance focusing and attention regulation skills and to reduce anxiety/stress levels while increasing mental vigour, hinting at the potential of such new technologies for neurocognitive empowerment.

Keywords Wearable devices · Neurocognitive empowerment · Neurofeedback · Stress management · Peak performance · Self-regulation · Self-awareness

D. Crivelli · G. Fronda · L. Angioletti · C. Spinosa · M. Balconi (✉)
International Research Center for Cognitive Applied Neuroscience (IrcCAN), Faculty of Psychology, Catholic University of the Sacred Heart, Milan, Italy
e-mail: michela.balconi@unicatt.it

D. Crivelli
e-mail: davide.crivelli@unicatt.it

G. Fronda
e-mail: giulia.fronda@unicatt.it

L. Angioletti
e-mail: laura.angioletti1@unicatt.it

C. Spinosa
e-mail: claudia.spinosa@unicatt.it

1 Introduction

Recent years have been connoted by a clear increase of the availability and use of brain-sensing devices designed to foster health awareness, improve subjective well-being, and promote cognitive empowerment [1, 2]. Wearable devices that non-invasively and easily track users' neural and physiological activity may help users to become aware and to consciously process information on implicit markers of their body states [3]. Namely, by applying the principle of operating conditioning and promoting implicit learning, those devices allow individuals to gain active control of their cortical activity and foster cognitive plasticity and empowerment, with positive effects on their emotion and attention regulation skills [1].

The interest in practical implications of such neurotechnologies has now moved from clinical settings to different applied research contexts, such as stress management, sports, and workplace [4–6]. In particular, technological progresses lead to the miniaturization and increase of usability of neurofeedback systems—i.e. hardware-software systems that allow users to train and improve their awareness of mindsets and to implicitly learn to control their neural correlates by visualizing in real-time the modulation of their brain signals [7].

In this paper, we report an overview of main outcomes of a research line on possible effects of a neurotechnology-supported mental training protocol, which combined mindfulness-based practices aimed at improving cognitive control and emotional regulation with wearable devices designed to foster and ease such form of mental training.

2 Materials and Methods

2.1 *Sample*

A total of 100 participants were enrolled in the various studies included in the research line. Studies focused on different age ranges (from 20 to 75 years old) and application settings (higher education, sports, workplace, healthy aging). All enrolled participants had no history of psychiatric or neurological diseases, cognitive deficits, clinically relevant level of stress, nor reported significant stressful life events during the last six months before recruitment. All experimental procedures and techniques followed the principles of the Declaration of Helsinki and were reviewed and approved by the competent Ethics Committee. Each participant signed a written informed consent to take part in the project.

2.2 Procedure

The experimental design used in each study commonly included three phases: pre-intervention assessment phase, intervention phase, and post-intervention assessment phase. Participants were divided into experimental and active control groups. For the experimental groups, daily sessions of mindfulness-based practices were supported by the use of a wearable device, consisting in a head-band or a pair of glasses with an in-built wearable neurofeedback system connected to a dedicated smartphone app designed to support mental training practices. Differently, for the active control groups, daily sessions were based on breathing techniques not supported by the wearable devices. The intervention phase lasted for 14-to-28 daily sessions. During such phase, participants practiced with an incremental time commitment—namely, from 10 to 20 min a day.

During the assessment phases, three main orders of outcome measures were collected: psychometric, neuropsychological, and psychophysiological. Psychometric measures focused on mood states, perceived stress, and anxiety levels, including the Perceived Stress Scale (PSS), the State-Trait Anxiety Inventory (STAI), Geriatric Depression Scale (GDS), and the Profile of Mood States inventory (POMS). Neuropsychological measures focused on executive control skills, attention regulation, and focusing, including even computerized cognitive tests such as a challenging version of a Stroop-like task and standardized reaction times batteries. Finally, psychophysiological measurements focused on electrophysiological and autonomic markers of cognitive efficiency and regulation of the stress response at rest and during exposure to stressors, including both frequency-domain and time-domain EEG measures (metrics based on alpha and beta EEG oscillations and event-related potentials, ERPs, related to the orientation of attention resources—i.e. the N2 deflection) and heart rate variability (HRV) measure. For further information on the assessment procedures and experimental design, please refer to Balconi et al. [4] and Crivelli et al. [8].

Besides peculiar differences in data analysis across different studies (specifications can be found in [1, 4–6, 8]), the data analysis pipeline included: scoring and quantification of psychometric, neuropsychological, and psychophysiological measures; inferential statistics (t-test and/or ANOVA models); and computation of effect size to estimate the strength and robustness of observed training-related differences.

3 Results

As reported by Balconi and colleagues [3, 8], a four-week neurotechnology-supported protocol was able to induce, in samples of mildly-stressed young adults, a statistically significant improvement of attention performance, as measured by reduced response times at challenging computerized tasks tapping on inhibition

control and attention regulation (i.e. Stroop-like task and standardized reaction times battery). Notably, such behavioural outcomes were mirrored even by electrophysiological measures. Namely, resting-state correlates of relaxation and EEG reactivity indices as well as task-related event-related markers of attention orientation (i.e. the frontal N2 ERP) were positively modulated by the intensive training. Again, the wearable neurofeedback protocol also proved to be able to induce a statistically significant reduction of perceived stress and anxiety, reduced mental fatigue, and increased mental vigour [1, 4], as measures by psychometric tests standardized on the reference population (PSS, STAI, and POMS). Such reported changes in mood and psychological factors were also associated with a remarkable improvement of autonomic markers of vagal tone—i.e. HRV—both at rest and during exposure to stressors.

Relevantly, even latest studies that focused on elderly users, sportspeople, and top-level professionals exposed to work-related stressors highlighted a comparable set of outcomes, with additional and specific improvements concerning: reduced subclinical depression signs as well as reduced frontal alpha asymmetry in the aging sample; greater behavioural and EEG/ERP markers of neurocognitive efficiency, improved cardiovascular responses to stress, and reduced perceived anger in the professionals sample [6]; early training effects over both performance and electrophysiological markers of focusing and attention regulation, and a general reduction of stress and anxiety levels in a sample of sportspeople [5].

4 Discussion and Conclusions

The present overview reports outcome data on the effectiveness of combining neurotechnologies with traditional intervention methods for the empowerment of cognitive-affective skills. Indeed, current results concerning cognitive performance at computerized tasks, subjective levels of stress/anxiety and mood states, and improved physiological markers of neurocognitive efficiency and stress regulation suggest that supporting mental training with wearable neurofeedback devices can be useful to further optimize cognitive processes (such as focusing and executive control) across the lifespan and in different application contexts. According to recent accounts on the role of cognitive control and neurovisceral integration processes, training with the support of devices providing feedbacks on endogenous bodily reactions would help practicers learn to self-regulate their cortical activity, achieve an increased state of neurocognitive efficiency, and develop better self-regulation skills. We suggest that such outcomes might be fostered by training cognitive control mechanisms, strengthening prefrontal regulatory system exerting control on autonomic activity, and better information-exchange in the frontal-parietal network that mediates the processes of vigilance, attention, and monitoring [1, 9]. Although present findings already outline a quite robust background on effectiveness of the contribution of wearable devices to make traditional empowerment protocols more efficient, further studies and novel technological advancement are still needed to further extend available

observations and define new perspectives in the flourishing field of neurotechnologies for self-enhancement.

References

1. M. Balconi, G. Fronda, I. Venturella, D. Crivelli, Conscious, pre-conscious and unconscious mechanisms in emotional behaviour. Some applications to the mindfulness approach with wearable devices. *Appl. Sci.* **7**, 1280 (2017)
2. M. Chan, D. Esteve, J.Y. Fourniols, C. Escriba, E. Campo, Smart wearable systems: current status and future challenges. *Artif. Intel. Med.* **56**, 137–156 (2012)
3. M. Balconi, D. Crivelli, Wearable devices for self-enhancement and improvement of plasticity: effects on neurocognitive efficiency, in *Quantifying and Processing Biomedical and Behavioral Signals*. ed. by A. Esposito, M. Faundez-Zanuy, F.C. Morabito, E. Pasero (Springer, Cham, 2019), pp. 11–22
4. M. Balconi, G. Fronda, D. Crivelli, Effects of technology-mediated mindfulness practice on stress: psychophysiological and self-report measures. *Stress* **22**, 200–209 (2019)
5. D. Crivelli, G. Fronda, M. Balconi, Neurocognitive enhancement effects of combined mindfulness–neurofeedback training in sport. *Neuroscience* **412**, 83–93 (2019)
6. D. Crivelli, G. Fronda, I. Venturella, M. Balconi, Stress and neurocognitive efficiency in managerial contexts. *Int. J. Workplace Health Manag.* **12**, 42–56 (2019)
7. T. Budzynski, H. Budzynski, J.R. Evans, A. Abarbanel, *Introduction to Quantitative EEG and Neurofeedback. Advanced Theory and Applications* (Academic Press, New York, 2009)
8. D. Crivelli, G. Fronda, I. Venturella, M. Balconi, Supporting mindfulness practices with brain-sensing devices. Cognitive and electrophysiological evidences. *Mindfulness* **10**, 301–311 (2019)
9. Y.-Y. Tang, B. Bruya, Mechanisms of mind-body interaction and optimal performance. *Front. Psychol.* **8**, 647 (2017)

Simultaneous and Proportional Myocontrol of a Hand Exoskeleton for Spinal Muscular Atrophy: A Preliminary Evaluation



Marco Ricciardi, Alberto Topini, Nicola Secciani, Alessandro Ridolfi, and Claudio Castellini

Abstract Spinal Muscular Atrophy (SMA) is a neuromuscular disease characterized by the degeneration of the α -motor neurons in the spinal cord, resulting in progressive proximal muscle weakness and paralysis. It is the second most common fatal autosomal recessive disorder after cystic fibrosis in the world. In the context of assistive robotics for SMA, in this work the authors have preliminarily assessed the feasibility of using low-cost electromyography pattern recognition and simultaneous/proportional myocontrol to enforce smooth, intuitive control of an assistive hand exoskeleton system. A target achievement control test has involved ten healthy subjects. Synthetic noise has been added to their surface ElectroMyoGraphic (sEMG) signals in order to reach a signal-to-noise ratio similar to that of sEMG signals gathered from a SMA patient. The results indicate that, even neglecting any learning effect, an SMA patient could reach an average success rate of up to 82% through the proposed approach.

1 Introduction

Spinal Muscular Atrophy (SMA) is a severe neuromuscular disease characterized by the degeneration of α -motor neurons in the spinal cord, resulting in a progressive proximal muscle weakness and paralysis [1]. Although there currently is no treatment

This work was partially supported by the German Research Society project Deep-Hand (DFG Sachbeihilfe CA-1389/1-2). The authors would like to thank Annette Hagengruber and Jörn Vogel of the DLR for useful insights and for making available to us sEMG signals recorded from a SMA patient.

M. Ricciardi · A. Topini (✉) · N. Secciani · A. Ridolfi
Department of Industrial Engineering (DIEF), University of Florence, Via di Santa Marta 3,
Florence 50139, Italy
e-mail: alberto.topini@unifi.it

C. Castellini
Institute of Robotics and Mechatronics, DLR—German Aerospace Center, 82234 Wessling,
Germany

for SMA, much can be done in the context of Assistive Robotics to assist the patient's loss of motor functions. In particular, given the type of SMA and its stage, the patient can still be able to produce significant voluntary muscular activity. Indeed, as long as the patient can produce reasonably distinct and repeatable sEMG signal patterns, Machine Learning (ML) can be used to control an assistive device. Given the nature of the interaction between the devices and their users, it is desirable to let the patient take full, proportional, smooth and intuitive control [2].

Two different ML approaches [3, 4] are currently being tested by the authors to assess the control experience on an assistive Hand Exoskeleton System (HES) [5]. In this work, the feasibility of applying simultaneous, proportional and incremental myocontrol to the device has been evaluated through a Target Achievement Control (TAC) test [6], simulated by means of a Blender model of the HES. At this point of the experimentation, the HES has no other purpose than to visually familiarize the user with the final system.

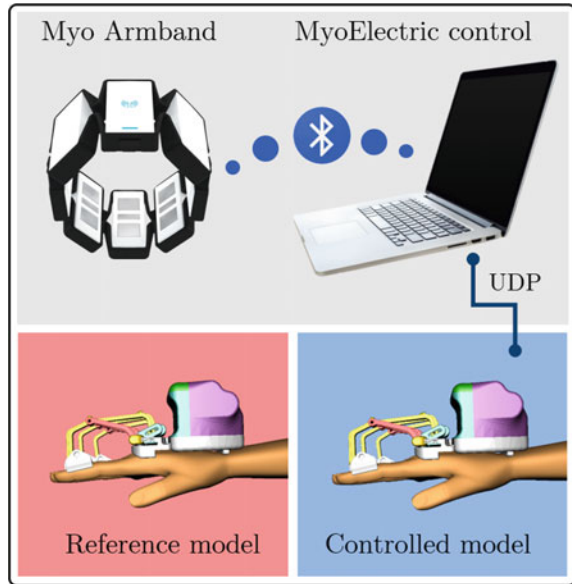
2 Materials and Methods

In this study, ten healthy participants (aged between 24 and 61 years)—voluntarily enrolled—have been asked to control a virtual avatar of the exoskeleton using their own voluntary muscle activity, recorded in real-time using a Myo armband. Synthetic noise (Gaussian noise with variable variance) has been added to the sEMG signals in order to progressively reach the Signal-to-Noise Ratio (SNR) that characterized those collected from SMA patients. It is worth noting that, although there are no specific references in the literature, this approach has been considered sufficiently reliable since SMA is known to weaken the muscle activity (thus lowering the SNR) without altering neuromuscular patterns. The target SNR (SNR4 = 15.97) has been identified through previous recordings from a patient affected by SMA type II, and other three different SNR levels have been defined (SNR3 = 52.80; SNR2 = 125.11; SNR1 = 211.82); where a higher SNR corresponds to a better signal.

2.1 *Experimental Setup*

As can be seen from Fig. 1, the experimental setup relies on the wearing of the Myo armband that transmits the sEMG signal, by means of Bluetooth communication, to a laptop running the intent detection system. The sEMG signal is acquired, processed and labeled by a custom software suite written in the C# and Python languages. Finally, the HES configuration, reference and prediction, are provided to two distinct Blender digital twins through a User Datagram Protocol (UDP) message-based system.

Fig. 1 The exploited experimental setup. On the gray background the employed hardware, while below the virtual models of the HES



2.2 Experimental Protocol

The test participants have been asked to wear the Myo armband in a preliminary stage of the experiment as well as to avoid sensor doffing or displacements; as a matter of fact, this procedure aprioristically reduces the presence of undesired effects, such as electrode shifts, and allows for coherent results over the whole experimental campaign. The procedural architecture comprises of two primary hierarchical stages: firstly, during the so-called “training phase”, the myoelectric control develops and learns a regression model that deals with the prediction of the hand configurations starting from the sEMG signals; subsequently, the TAC test evaluates the performance of the learned model to generalize over several, distinct tasks. For what concerns the data acquisition and training process, the subjects, after having received a comprehensive description of the routines, carry out three different hand gestures (complete closure, complete extension, and resting) in a double-repetition sequence. The whole procedure exploits a straightforward Graphical User Interface (GUI) which, by guiding the test contributors, unifies the test architecture over the whole set of participants.

Conversely, the TAC test has been structured so as to achieve four actions (complete closure, semi-closure, semi-extension, complete extension) alongside four incremental SNR levels, for a total of sixteen different combinations. The participants have been then asked to fulfill five unordered repetitions of each of the aforementioned combinations: the whole test was hence composed of series of 80 tasks.

As far as the specific protocol is concerned, the participants have been requested to reproduce and hold for 1.5 s the hand configuration displayed by the “reference

model” within a maximum time interval of 20 s. Since the predicted hand motion is also shown by the “controlled model”, matching the positions of the two virtual avatars emerges as the actual aim for the user during the test.

3 Results

The above-described procedure has been quantitatively evaluated by means of two major metrics: the Success Rate (SR), defined as the percentage of correctly performed tasks with respect to the total number of achievable tasks, and the Time to Complete the Task (TCT), which outlines the time required to successfully fulfill a task. As illustrated in Fig. 2, the SR average value decreases, within a range 82–96%, as the noise level rises; additionally, the TCT outcomes do confirm this performance-worsening pattern (Table 1) by highlighting larger TCT for noisier sEMG signals.

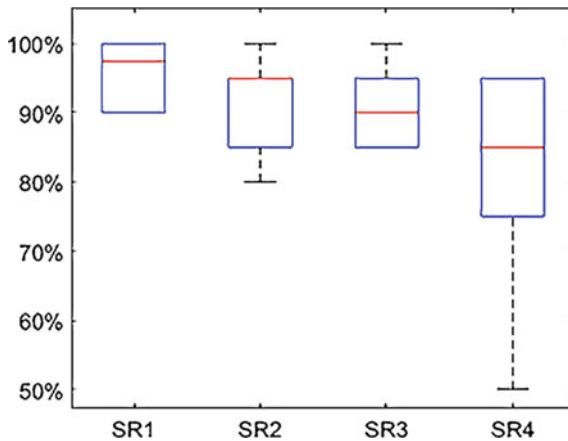


Fig. 2 Boxplot reporting the success rate for SNR level. The numerical index of the SR on the x-axis indicates the corresponding SNR level

Table 1 TCT over decreasing SNR levels

SNR level	TCT [s]
<i>SNR1</i>	4.217 ± 1.535
<i>SNR2</i>	4.414 ± 1.924
<i>SNR3</i>	5.597 ± 2.256
<i>SNR4</i>	5.614 ± 2.367

4 Discussion and Conclusions

On average, our participants have reached a TAC test SR ranging from 82 to 96%, depending on the SNR level. An SR of 82% corresponds to the lowest SNR, which was akin to that found on the signals generated by the reference SMA patient. With all due caution, this could possibly indicate that a patient of a similar type and stage of SMA could achieve similar results, using the same myocontrol system while controlling the HES. Notice, moreover, that the tests were quite short (about 20 min per participant), so no learning effect whatsoever has been observable either in their SRs or in their TCTs. It seems reasonable to claim that, if a patient were allowed to wear and control the exoskeleton for a longer time and across multiple sessions, he/she would display a definite learning curve, thereby further improving the results. Finally it is important to notice that, even if the model training has been performed over just three different gestures, the regression algorithm allows for the continuous discrimination of all the intermediate positions.

References

1. A. D'Amico, E. Mercuri, F.D. Tiziano, E. Bertini, Spinal muscular atrophy. *Orphanet J. Rare Dis.* **6**(1), 1–10 (2011)
2. P. Beckerle, C. Castellini, B. Lenggenhager, Robotic interfaces for cognitive psychology and embodiment research: a research roadmap. *Wiley Interdisc. Rev. Cognit. Sci.* **10**(2), e1486 (2019)
3. N. Secciani, M. Bianchi, A. Ridolfi, F. Vannetti, B. Allotta, Assessment of a hand exoskeleton control strategy based on user's intentions classification starting from surface EMG signals, in *International Symposium on Wearable Robotics* (2019), pp. 440–444
4. I. Strazzulla, M. Nowak, M. Controzzi, C. Cipriani, C. Castellini, Online bimanual manipulation using surface electromyography and incremental learning. *IEEE Trans. Neural Syst. Rehabil. Eng.* **25**(3), 227–234 (2016)
5. N. Secciani, M. Bianchi, A. Ridolfi, F. Vannetti Yary Volpe, L. Governi, M. Bianchini, B. Allotta, Tailor-made hand exoskeletons at the university of florence: from kinematics to mechatronic design **7**(2), 22 (2019)
6. A.M. Simon, L.J. Hargrove, B.A. Lock, T.A. Kuiken, The target achievement control test: evaluating real-time myoelectric pattern recognition control of a multifunctional upper-limb prosthesis. *J. Rehabil. Res. Dev.* **48**(6), 619 (2011)

Study of the ERD Induced by Different Motor Tasks Through Non-invasive EEG Analysis to Improve Stroke Rehabilitation Outcomes



S. Ezquerro, A. Bertomeu-Motos, J. Barios, J. M. Catalan, J. Diez, and N. Garcia-Aracil

Abstract Several studies have shown that active, passive and imagery motor activities in healthy participants produce similar changes in the cortical activity over sensorimotor areas (SM). In this study, 26 stroke patients were recruited. They performed three different motor activities, according to the literature, with the paretic hand: active hand movement, passive hand movement with an exoskeleton and motor imagery. The results shown an ERD phenomenon over contralesional SM in two of the three tasks, being negligible in the motor imagery. These results suggest that rehabilitation based on passive hand mobilization could improve the recovery outcomes in patient with no active hand movements.

1 Introduction

It is well known that stroke produces changes in motor cortex activation during the execution of movements. These changes during active or passive movements and motor imagery have been widely investigated [1].

On the other hand, brain activation related with movement execution is associated with event-related changes in EEG spectrum. EEG oscillatory between 10 and 20 Hz over sensorimotor areas (SM) decrease the power in motor tasks, this phenomenon is known as event-related desynchronization (ERD) [2].

Studies with EEG-fMRI showed that active movement implies changes in the activity of the central areas [3]. In addition, the ERD in the beta band is shown in several studies during induced motor movement in healthy volunteers [4]. Finally, the ERD in motor imagery tasks are described in foot or tongue imagery movements in healthy volunteers [5, 6]. However, it is unclear the ERD phenomenon during motor imagery related to hand movements [7].

S. Ezquerro (✉) · A. Bertomeu-Motos · J. Barios · J. M. Catalan · J. Diez · N. Garcia-Aracil
Biomedical Neuroengineering Research Group, Miguel Hernandez University, Elche, Spain
e-mail: sezquerro@umh.es

© The Author(s), under exclusive license to Springer Nature Switzerland AG 2022
D. Torricelli et al. (eds.), *Converging Clinical and Engineering Research
on Neurorehabilitation IV*, Biosystems & Birobotics 28,
https://doi.org/10.1007/978-3-030-70316-5_106

661

The aim of our research is to study the differences between three similar tasks, based on previous studies, passive hand movement, produced by a hand exoskeleton, active hand movement and motor imagery in chronic stroke patients.

2 Materials and Methods

2.1 Participants

Twenty six stroke patients participated in this study. They had an unique stroke episode with unilateral motor affectation, that had to be severe after two weeks of the episode. The protocol was approved by ethics committee of the Miguel Hernandez University of Elche, Spain. All participants gave written informed consent before the session.

2.2 Setup

The participants sat in a silent room with a table and a computer screen. The setup was formed by a modular hand exoskeleton, developed at the Miguel Hernandez University [8], used to perform the passive hand movements. The commercial EEG amplifier, from BrainVision[®], was used to acquire the EEG signals configured to record 24 electrodes placed according to 10/20 International System. Finally, for the EEG recordings, the BCI2000, a freely distributed software for multipurpose standard BCI platform [9], was used.

2.3 Description of the Task

Participants were instructed in three different activities presented in the same order. First, PASSIVE task, the hand exoskeleton closed and opened the hand simulating grasp movements. In the second activity, ACTIVE task, the participants performed continuous grasp movements. Finally, IMAGINE task, where the participants imagined the grasping movements. All the activities were performed with the paretic hand. Each activity had two different cues, one regarding with the current activity, and the other was a RELAX cue, where the participants had to relax.

3 Results

The results were obtained after the EEG post-processing analysis, using in-house scripts and EEGLAB toolbox, and excluding the noisy portions of the EEG signal from paroxysmal and muscular artifacts.

Figure 1 shows the topographical analysis of all the patients, between 800 and 1500 ms from the onset, regarding the current movement task (A), and regarding the RELAX task (B). In Fig. 1a, the PASSIVE task, an ERD dipole is lateralized over the contralesional SM area, and not over the ipsilesional SM area. Regarding the ACTIVE task, the power decrease dipole is distributed over central and lateral areas, with a hyperactivation with respect to the RELAX task. Finally, IMAGINE task did not present any ERD dipole at any SM areas.

On the other hand, Fig. 1b did not show any ERD dipole, as was expected, due to the stroke patient were instructed to not imagine or move the hand, and to stay in a state of relaxation.

Figure 2 shows the sensorimotor activity during the three activities in beta band and it is presented in both hemispheres (C3 and C4) during the hand movement tasks. Ipsilesional hemisphere (C3) results show a similar power decrease in PASSIVE and ACTIVE tasks. However, the ERD in the IMAGINE task is lower than in the other two tasks, as was expected from the results presented in Fig. 1a. However, no significant differences were found in terms of ERD power between the three groups, Kruskal-

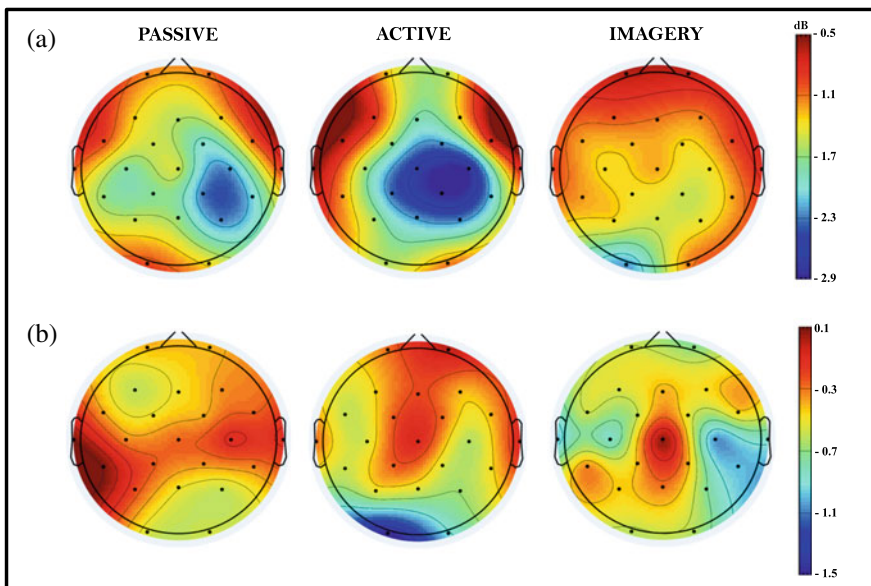


Fig. 1 Figure represents the topographic scalp of stroke patients in the three different tasks. It is presented in the beta band (16–22 Hz), between 800 and 1500 ms from the onset of the task

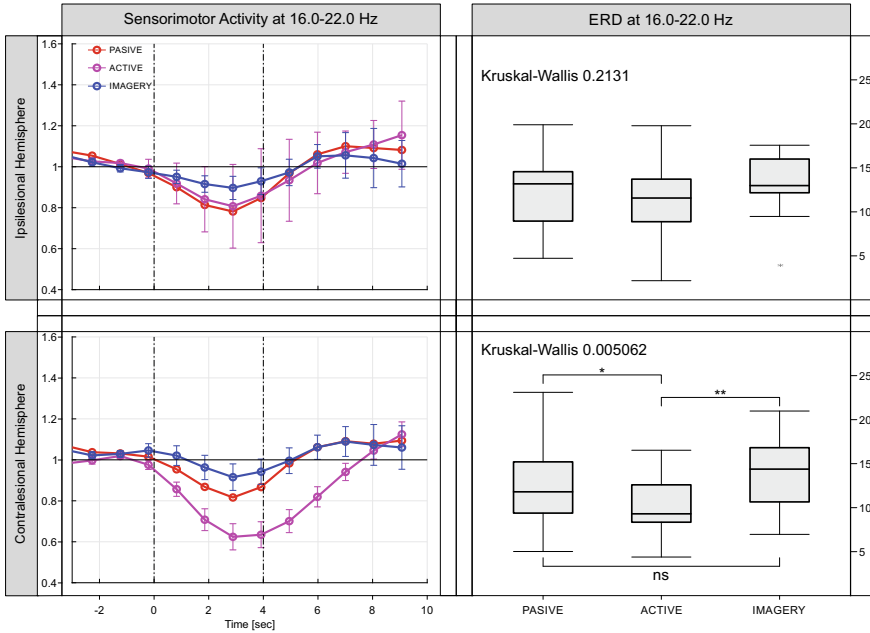


Fig. 2 Sensorimotor activity in beta band (16–22 Hz) when the participants performed the three tasks (*left*). Boxplot with statistical analysis between the three tasks regarding the ERD power (*right*)

Wallis test with a p -value = 0.2131. On the other hand, the sensorimotor activity in the contralesional hemisphere (C4) between the three tasks presents statistical differences regarding the ERD power, Kruskal-Wallis with p -value = 0.005062. It is observed that the ERD power in the ACTIVE task is higher than in the PASSIVE task, but remains negligible in the IMAGINE task.

4 Discussion

The presented study evaluates, using non-invasive EEG, the ERD activation in beta band during three motor tasks using the paretic hand. The results shows, regarding the topographical analysis, that the lesional SM area did not produce an ERD dipole in any task, despite the bilateral dipole that is shown in healthy subjects [10]. However, this dipole is unilateral over the healthy SM area, but it is only presented in the proprioceptive tasks, ACTIVE and PASSIVE, and not in the IMAGINE tasks.

On the other hand, if we observe the sensorimotor activity at beta band, a decrease of the EEG power, related to the ERD, is shown in the lesional SM area, very similar in ACTIVE and PASSIVE tasks, and negligible in IMAGINE task. This result suggest that a better recovery outcomes in the injured SM area could be obtained using a passive

mobilization of the affected hand for those patients who cannot move the hand. However, the healthy SM area shows a hyperactivation, regarding the ERD power, in the ACTIVE task, as was observed in previous studies, compared with the PASSIVE and IMAGINE task.

5 Conclusion

Motor impairment after stroke is one of the goals of the rehabilitation where different tasks and techniques are employed during this process. After our study, the results obtained suggest that passive hand movement using an exoskeleton induce similar cortical activation over the lesional hemisphere than active hand movement. Furthermore, this passive movement also produced ERD over contralesional hemisphere since motor imagery the ERD is negligible. In conclusion, motor rehabilitation based in passive movements, for stroke patients, could increase the recovery outcomes for those with severe motor disabilities.

References

1. A. Feydy, R. Carlier, A. Roby-Brami, B. Bussel, F. Cazalis, L. Pierot, Y. Burnod, M. Maier, Longitudinal study of motor recovery after stroke: recruitment and focusing of brain activation. *Stroke* **33**(6), 1610–1617 (2002)
2. G. Pfurtscheller, A. Berghold, Patterns of cortical activation during planning of voluntary movement. *Electroencephalogr. Clin. Neurophysiol.* **72**(3), 250–258 (1989)
3. S.F. Storti, E. Formaggio, A. Beltramello, A. Fiaschi, P. Manganotti, Wavelet analysis as a tool for investigating movement-related cortical oscillations in EEG-FMRI coregistration. *Brain Topogr.* **23**(1), 46–57 (2010)
4. G. Tacchino, M. Gandolla, S. Coelli, R. Barbieri, A. Pedrocchi, A.M. Bianchi, EEG analysis during active and assisted repetitive movements: evidence for differences in neural engagement. *IEEE Trans. Neural Syst. Rehabil. Eng.* **25**(6), 761–771 (2016)
5. G. Pfurtscheller, C. Neuper, C. Brunner, F.L. Da Silva, Beta rebound after different types of motor imagery in man. *Neurosci. Lett.* **378**(3), 156–159 (2005)
6. A. Spiegler, B. Graimann, G. Pfurtscheller, Phase coupling between different motor areas during tongue-movement imagery. *Neurosci. Lett.* **369**(1), 50–54 (2004)
7. C. Neuper, R. Scherer, M. Reiner, G. Pfurtscheller, Imagery of motor actions: differential effects of kinesthetic and visual-motor mode of imagery in single-trial eeg. *Cognit. Brain Res.* **25**(3), 668–677 (2005)
8. J.A. Diez, A. Blanco, J.M. Catalan, F.J. Badesa, L.D. Lledo, N. Garcia-Aracil, Hand exoskeleton for rehabilitation therapies with integrated optical force sensor. *Adv. Mech. Eng.* **10**(2), 1687814017753881 (2018)
9. G. Schalk, D.J. McFarland, T. Hinterberger, N. Birbaumer, J.R. Wolpaw, Bci2000: a general-purpose brain-computer interface (BCI) system. *IEEE Trans. Biomed. Eng.* **51**(6), 1034–1043 (2004)
10. G. Pfurtscheller, C. Brunner, A. Schlögl, F.L. Da Silva, Mu rhythm (de) synchronization and EEG single-trial classification of different motor imagery tasks. *Neuroimage* **31**(1), 153–159 (2006)

Real-Time Cycling Cadence Estimation Using an Inertial Sensor for Gamified Pedaling Therapy



Ana Rojo, Rafael Raya, and J. C. Moreno

Abstract In an increasingly aging population, impaired motor control and loss of balance and lower limb muscle strength are triggering an increased risk of falls and hip fractures. With the intention of preventing them, are enforced intervention programs based on pedaling exercises to improve physical conditioning of the elderly. To achieve physical results adherence to cycling exercises must be promoted. For this reason, providing a compact and portable sensing solution to record pedaling parameters and offer visual real-time feedback would become very valuable. Therefore, obtaining pedaling information from the rotation measurements of an inertial sensor placed on the thigh, requires firstly the recognition of flexion/extension angle. Then, different processing steps are performed on the data consisting of a Kalman filter for smooth estimation of the angles, a peak detection consisting of the sliding window application and symmetry threshold of the angle curve. Finally, the performance of the cadence estimation method corroborates the suitability of its usage in cycling training feedback.

Keywords Inertial sensors · Motion tracking · Pedaling · Rehabilitation · Therapy · Lower limb · Videogames · Serious games

Funding for Industrial Doctorates of Autonomous Community of Madrid (IND2019/TIC17090).

Real-time Cycling Cadence Estimation using an Inertial Sensor for Gamified Pedaling Therapy.

A. Rojo (✉)

Neural Rehabilitation Group of the Spanish National Research Council, Werium Assistive Solutions S.L., Universidad San Pablo CEU, Madrid, Spain

e-mail: ana.rojo@weriumsolutions.com

R. Raya

Werium Assistive Solutions S.L., Universidad San Pablo CEU, Madrid, Spain

e-mail: rafael.raya@weriumsolutions.com

J. C. Moreno

Neural Rehabilitation Group of the Spanish National Research Council, Madrid, Spain

e-mail: jc.moreno@csic.es

1 Introduction

Functional impairment of the lower limb is one of the most common consequences of the ageing process [1]. New training interventions based on pedaling activity have been developed to promote the improvement of functional gait in elders. Recent studies reported that cycling training has positive effects on muscle strength, bone density, spasticity, cardiopulmonary function and many other physiological and psychological benefits in stroke patients [2]. All the factors are directly related to improvement of functional abilities in postural control and gait.

Providing patient feedback has been shown to enhance patient cortical activity, functional performance, muscle control and fatigue [3, 4]. Among the possible modalities of extrinsic biofeedback adopted for stroke patients, visual input is the most widely used [5]. Visual feedback during cycling could improve neuromuscular control and the overall training performance [6], which is generally based on cadence and load.

The generation of cycling training home-based exercises requires the employment of user-friendly and low-cost pedaling systems that perform the estimation of pedaling cadence. Wireless inertial sensors are small, lightweight, and do not interfere with the execution of movements during measurements [7, 8]. Therefore, in order to generate fusion-sensor algorithms to measure cycling movement, the state-of-the-art methodologies focused in two different strategies: (1) estimation of segment orientation and 3D joint angles using sets of inertial measurement unit based [9]. (2) Cycling pose estimation with force and inertial sensors [10].

This paper proposes a cadence estimation strategy based on inertial sensor-based knee joint kinematics analysis during cycling. Thanks to this approach, cycling performance parameters correlated with the cadence could be obtained to provide extrinsic feedback to patient.

2 Methods

2.1 *Cycling Analysis*

We determined that the cadence estimation algorithm should be based on the detection of cycle initiation phase. The biomechanical model of the pedal crank for each cycle has two peaks at 90° and 270° and two dead spots. Although the angles of the gear crank are unknown, each pedaling phase sets a rigid transformation between body segments involved in pedaling movement.

Usually, the problem with providing a three-dimensional kinematics measurement based on IMUs in cycling is that false kinematic measurements due to the gyroscope drifting caused by data integration and the magnetic interference arising from proximity to pedals and handlebars. This problem is tackled by taking few approaches. The first, by performing calibration procedures for the calculation of the relative

orientation between IMU frames and body segment frames, which relationship is assumed to be invariant.

The second one, mounting the sensor on the thigh instead of foot or pedal. Aligning the axes of a fixed mounted IMU with the anatomical directions enables to assess the body segment orientation. Then, the calculation of the Euler angles from the rotation matrix returns the orientation of the thigh decomposed in the 3 axes:

$$\begin{aligned}\theta_z &= a \sin(-r_{01}); \textit{knee-joint tilt angle} \\ \theta_x &= a \tan 2(r_{21}, r_{11}); \textit{knee-joint rotation angle} \\ \theta_y &= a \tan 2(r_{02}, r_{00}); \textit{knee-joint flexion/extension angle}\end{aligned}$$

Within this segment frame reference, the estimation of the flexion/extension angle of the knee-joint corresponds to Y-rotation of Euler angles.

2.2 *Knee-Joint Angle Processing*

The wireless inertial sensor used for data transmission has a sampling frequency of 50 Hz. Consequently, the calculated angles are released as discreet data. Therefore, in order to draw the movement curve described by the pedaling we must estimate an interpolation between these data. To this end, we seek to obtain this angle curve estimation by applying Kalman filter to angles, regarding the cycling motion could be described by sinusoidal function.

Next step addresses cycling phase detection, here formulated as an issue to peak detection of the oscillation. The peak detection step consists of data section into 80 ms sliding window with 60 ms overlap. For each sectioned data, a symmetry axis value threshold is applied to classify the data into maxima or minima, and among the maxima a search is made for the higher value for that segment. To avoid peak detection failures due to baseline changes, the symmetry axis threshold is adjusted from the average of the amplitude values of the last 1000 ms with a 20 ms refresh rate.

2.3 *Cycling Cadence Estimation*

Each cycle detection time is buffered when user is pedaling. As a result, parameters of interest can be extracted from the pedaling dynamics. The pedaling cadence is obtained based on the time deltas and the distance traveled, it is calculated from the estimation of the cadence estimation and taking a standard wheel radius.

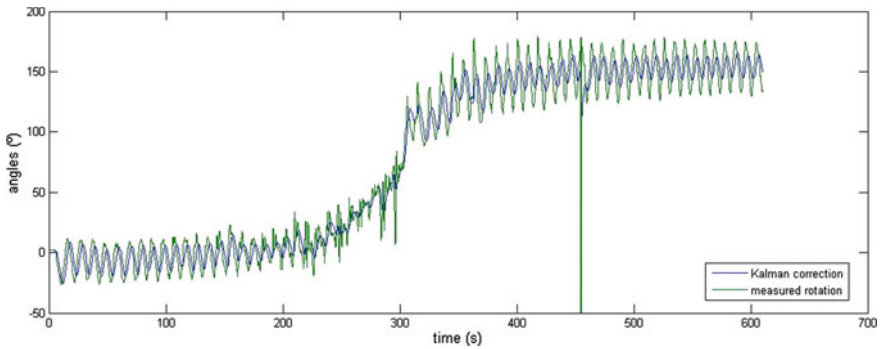


Fig. 1 Sample data collected during a test cycling using an IMU. Cycle-peak detection measured right knee flexion/extension angles and Kalman estimation are plotted in blue and green, respectively

3 Results

In this way, to provide extrinsic real-time feedback on the pedaling cadence, collected data from cycle peak detections, measured angles and Kalman estimated angles have been plotted to check on cadence estimation algorithm performance. The dataset highlighted in Fig. 1 shows sample data from the test.

4 Discussion

A single IMU is easily configurable to any static bicycle system, without hindering cycling motion. The conjunction of the use of these inertial sensors with motion parameters estimation algorithms can lead to an improvement in the assessment and practice of exercise. Therefore, the proposed estimation method can facilitate the collection of cycling cadence parameter, regardless of differences between users and bicycle equipment.

The main differential contribution of this system lies in the generation of a method of precise estimation of the pedaling dynamics from a single sensor placed on the thigh. This solution frees the user from the use of special pedaling equipment, such as electronic goniometry systems, does not use cables and is easily implanted on the user. In addition, detection of pedaling not based on analysis of the pedal axle allows studies of each limb independently, as would be required in trials with patients with partial injuries.

The obtained method provides consistent, reliable and real-time detection with a maximum delay of 5 ms. In a further step, it allows the estimation of other kinematic parameters such as instantaneous speed or distance ridden. In this direction, future work will employ the system to develop pedaling virtual reality platform with extrinsic feedback to promote adherence to home-based exercise.

Acknowledgements The financial support for the industrial doctorates of Autonomous Community of Madrid (IND2019/TIC17090) towards this research is hereby acknowledge.

References

1. O. Lazoura, P.J. Papadaki, E. Antoniadou, N. Groumas, A. Papadimitriou, P. Thriskos, et al., Skeletal and body composition changes in hemiplegic patients. *J. Clin. Densitom* **13**, 175–180 (2010)
2. C. Peng, S. Chen, C. Lai, C. Chen, Review: clinical benefits of functional electrical stimulation cycling exercise for subjects with central neurological impairments **31**(1), 1–11 (2011)
3. S. Ferrante, E. Ambrosini, P. Ravelli et al., A biofeedback cycling training to improve locomotion: a case series study based on gait pattern classification of 153 stroke patients. *J. Neuroeng Rehabil* **8**, 47 (2011)
4. H.-C. Yang, C.-L. Lee, R. Lin, et al., Effect of biofeedback cycling training on functional recovery and walking ability of lower extremity in patients with stroke. *Kaohsiung J. Med. Sci.* **30**(1), 3542 (2014)
5. S. Ebrahim, Costeffectiveness of stroke prevention. *Br. Med. Bull.* **56**(2), 557–570 (2000)
6. S.I. Lin, C.C. Lo, P.Y. Lin, J.J. Chen, Biomechanical assessments of the effect of visual feedback on cycling for patients with stroke. *J. Electromyogr. Kinesiol.* **22**, 582–588 (2012)
7. R. Mazzocchio, S. Meunier, S. Ferrante, F. Molteni, L.G. Cohen, Cycling, a tool for locomotor recovery after motor lesions. *Neuro Rehabil.* **23**, 67–80 (2008)
8. V. Camomilla, E. Bergamini, S. Fantozzi, G. Vannozzi, Trends supporting the in-field use of wearable inertial sensors for sport performance evaluation: a systematic review. *Sensors* **18**, 873 (2018). <https://doi.org/10.3390/s18030873>
9. S. Cain, *Measurement of Bicycle and Rider Kinematics During Real-World Cycling Using Wireless Array of Inertial Sensors* (2016). <https://doi.org/10.6084/M.FIGSHARE.3851883>
10. Y. Zhang, K. Chen, J. Yi, Rider trunk and bicycle pose estimation with fusion of force/inertial sensors. *IEEE Trans. Biomed. Eng.* **60**(9), 2541–2551 (2013). <https://doi.org/10.1109/TBME.2013.2260339>

Development of an Interface for the Control of Robotic Exoskeletons Based on Stroke Rehabilitation Techniques



P. Barría, R. Aguilar, D. Unquen, A. Moris, A. Andrade, A. Biskupovic, and J. M. Azorín

Abstract This work presents the development and implementation of an interface to control a robotic exoskeleton for gait rehabilitation in patients with stroke through exercises based on conventional neuro-rehabilitation therapies. Movement patterns of each exercise were acquired using an optoelectronic ten-camera system in a group of subjects without pathology. An interface for robotic control was developed in the LABVIEW environment that allows kinematics of each exercise to be reproduced in a robotic exoskeleton. The interface allows us to control: the assistance percentage, movement patterns, movement speed, number of repetitions, and resting time. The software presents plot panels for each joint that shows programmed kinematic and executed curves in real-time as a feedback tool for therapist. Finally, the kinematic data is stored in a directory with the patient's name and session date for post-analysis.

This study was sponsored and financially supported by Innovation and Competitiveness Fund 2017 of the Regional Government of Magallanes and Chilean Antarctica, Punta Arenas, Chile.

P. Barría (✉) · D. Unquen · A. Moris · A. Andrade
Research Unit, Rehabilitation Center Club de Leones Cruz del Sur, Punta Arenas, Chile
e-mail: pbarria@rehabilitamos.org

A. Moris
e-mail: laboratorios@rehabilitamos.org

P. Barría · J. M. Azorín
BMIIlab at Universidad Miguel Hernandez de Elche, Elche, Spain
e-mail: jm.azorin@umh.es

R. Aguilar
Department of Electrical Engineering, University of Magallanes, Punta Arenas, Chile
e-mail: rolando.aguilar@umag.cl

A. Biskupovic
Department of Electrical Engineering, Pontifical Catholic University of Chile, Santiago, Chile
e-mail: aebiskupovic@uc.cl

© The Author(s), under exclusive license to Springer Nature Switzerland AG 2022
D. Torricelli et al. (eds.), *Converging Clinical and Engineering Research on Neurorehabilitation IV*, Biosystems & Birobotics 28,
https://doi.org/10.1007/978-3-030-70316-5_108

1 Introduction

Stroke is one of the leading causes of morbidity and mortality in adults in the developed world and the leading cause of disability in all industrialized countries [1]. Hemiplegia is one of the most common deficiencies after stroke, causing a significant reduction in gait performance [2]. Gait recovery is an important goal in the stroke rehabilitation program. Currently, available treatment methods include classical gait rehabilitation techniques, functional electrical stimulation, robotic devices, and brain-computer interfaces. Technology-based rehabilitation techniques such as robotic devices need more research to demonstrate their suitability for gait training [3]. The objective of the present research was to develop an interface to control a motorized exoskeleton of the lower extremities focused on the gait rehabilitation of people with stroke based on movement sequences used in classical therapies.

2 Materials and Methods

2.1 Subjects

The study included 3 volunteers without pathologies from Punta Arenas, Chile, who were evaluated in the movement analysis laboratory in the Rehabilitation Center “Club de Leones Cruz del Sur” using photogrammetry during May 2019. All participants signed informed consent.

2.2 Motion Sequences Acquisition

Instrumented motion analysis was developed using a VICON ten-camera optoelectronic system (VICON Oxford Metrics, Oxford, UK). The data acquisition procedure was developed using the conventional dynamic VICON NEXUS 2.9 pipeline by the laboratory operator, according to the Plug-in-Gait biomechanical model [4]. For data acquisition, passive reflective markers were fixed to the subjects’ skin with adhesive tape on the anatomical reference structures of each leg. All the kinematic data was collected with a sampling rate 120Hz. Subjects were evaluated while executing neurodevelopmental-based rehabilitation sequences, which were selected by a Certified IBITA Bobath Concept Therapist. Table 1 describes movement sequences selected for the study. In each evaluation session, 10 repetitions of each exercise were recorded at a self-determined speed. The kinematic data was processed and filtered with a 4th order, zero-delay, Butterworth low-pass filter 6 Hz and subsequently exported in c3d format for implementation in the exoskeleton control interface.

Table 1 Exercises acquired by photogrammetry

Movement	Description
Step without discharge	Placing the foot on a stair without weight discharge
Step with discharge	Placing the foot on a stair with weight discharge
Pre-gait	Stance and swing alternating movement
Sit-to-stand	Changing position from sitting to standing position
Stand-to-sit	Changing position from standing to sitting position
Normal gait	Symmetric gait at self-determined speed

The first exercise (step on the stepper without weight discharge) involves lifting one leg to place the foot on a stepper without weight discharge in a standing position. The second exercise (placing one foot on the stepper with weight discharge) consists on performing the same movement as the previous exercise, but this time with weight discharge. The third exercise (pre-gait) starts with a standing position with parallel feet, followed by the movement of one foot forward, which then is moved backwards before returning to the baseline, mimicking a normal walking sequence. The fourth exercise (sit-to-stand transfer) consists of changing position from sitting in a chair to a standing position. The fifth exercise (stand-to-sit transfer) consists of changing position from a standing position to a sitting position in a chair. The last exercise involves walking in a normal movement pattern on a treadmill.

2.3 Robotic Rehabilitation Platform

A rehabilitation platform consisting of software, a robotic lower-limb exoskeleton (H3, Technaid, Spain), and an anti-gravitational support harness (Fig. 1) was implemented. A control software for the devices was developed, allowing selective movement of the joints and recording data from each rehabilitation session. The software executes in the exoskeleton a set of normal movement profiles extracted from people without pathology, which are adapted to the conditions of each patient by customizing different control variables (minimum and maximum angles, degrees of mobility, percentage of joint assistance).

The exoskeleton helps the movement of the lower extremities through electric motors aligned with the articular axes of the users [5]. It also detects the movements performed by the patient (hip, knee, and ankle flexors and extensors) through sensors in the articular axes and force sensors located in the sole of the exoskeleton and allows to control the range of motion with robotic assistance in each motor. The support of the electric motor in the joints can be gradually adjusted according to the



Fig. 1 Robotic gait training platform. The figure shows the “step with discharge” exercise with weight support and exoskeleton in stroke patients

movement and remaining functions of the patient’s lower extremities muscles. As a consequence of the independent movement assistance of each joint, it is possible to synchronize the devices with the voluntary movement of the patients, and in this way, an individualized and adjustable locomotion training was designed for the bilateral hip, knee, and ankle flexors and extensors.

3 Results and Discussion

3.1 Results

The exoskeleton-control interface allows customization of movement sequences (Table 1) for rehabilitation, importing joint kinematic information from lower extremities generated from the photogrammetry system. Figure 2 shows the graphical interface of the application, with the kinematic curves of the hip, knee, and ankle joints of the sagittal plane for the normal gait movement sequence displayed in the LabView software which are sent to the exoskeleton via CAN bus.

3.2 Discussion

The developed interface allows controlling all the variables of the robotic device, allowing adjustments to be made in each joint to customize therapy for each patient, a feature that not all commercial robotic platforms have. This feature could be used

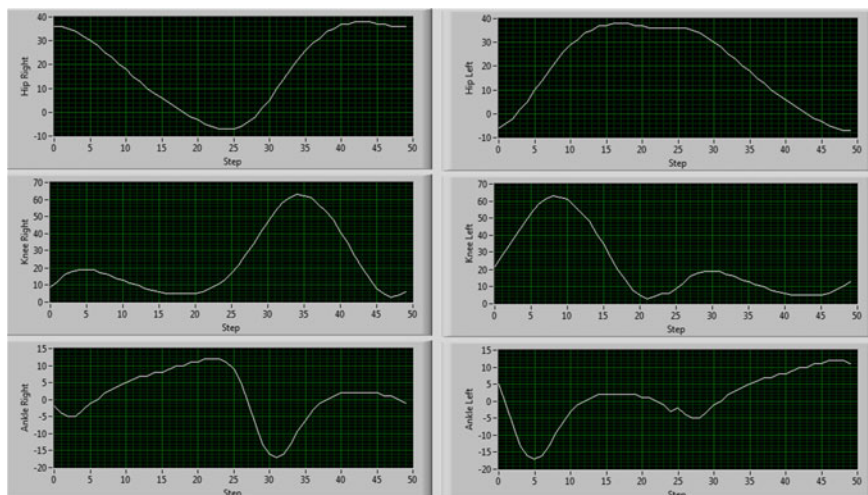


Fig. 2 Kinematics of normal gait imported through the graphical interface for exoskeleton control

for improving the design of clinical trials for gait rehabilitation post-stroke [6]. Additionally, the system can incorporate new movement patterns, being compatible with one of the main movement analysis systems in the area of biomechanics.

4 Conclusion

This work presented a control interface for exoskeletons of lower extremities, which incorporates the classic techniques used in gait rehabilitation after stroke. The usefulness of photogrammetric systems for the personalized design of therapies with robotic devices was demonstrated, which can be used to complement the rehabilitation process of stroke and other health conditions.

References

1. G. B. of Disease Collaborators et al., Global, regional, and national burden of neurological disorders, 1990–2016: a systematic analysis for the global burden of disease study 2016 (2019)
2. S.J. Olney, C. Richards, Hemiparetic gait following stroke. Part I: characteristics. *Gait Posture* **4**(2), 136–148 (1996)
3. J.-M. Belda-Lois, S. Mena-del Horno, I. Bermejo-Bosch, J.C. Moreno, J.L. Pons, D. Farina, M. Iosa, M. Molinari, F. Tamburella, A. Ramos, et al., Rehabilitation of gait after stroke: a review towards a top-down approach. *J. Neuroeng. Rehabil.* **8**(1), 66 (2011)
4. R.B. Davis, S. Ounpuu, D. Tyburski, J.R. Gage, A gait analysis data collection and reduction technique (1991)

5. M. Bortole, A. Venkatakrishnan, F. Zhu, J.C. Moreno, G.E. Francisco, J.L. Pons, J.L. Contreras-Vidal, The h2 robotic exoskeleton for gait rehabilitation after stroke: early findings from a clinical study. *J. Neuroeng. Rehabil.* **12**(1), 54 (2015)
6. D.R. Louie, J.J. Eng, Powered robotic exoskeletons in post-stroke rehabilitation of gait: a scoping review. *J. Neuroeng. Rehabil.* **13**(1), 53 (2016)

KNN Learning Techniques for Proportional Myocontrol in Prosthetics



Tim Sziburis, Markus Nowak, and Davide Brunelli

Abstract This work has been conducted in the context of pattern-recognition-based control for electromyographic prostheses. It presents a k-nearest neighbour (kNN) classification technique for gesture recognition, extended by a proportionality scheme. The methods proposed are practically implemented and validated. Datasets are captured by means of a state-of-the-art 8-channel electromyography (EMG) arm-band positioned on the forearm. Based on this data, the influence of kNN's parameters is analyzed in pilot experiments. Moreover, the effect of proportionality scaling and rest thresholding schemes is investigated. A randomized, double-blind user study is conducted to compare the implemented method with the state-of-research algorithm Ridge Regression with Random Fourier Features (RR-RFF) for different levels of gesture exertion. The results from these experiments show a statistically significant improvement in favour of the kNN-based algorithm.

1 Motivation and Related Work

The kNN learning scheme has been applied for myoelectric control of prosthetic devices several times [1–4]. So far, kNN was utilized for sole classification as an intention detection method based on EMG signals. In preliminary experiments, kNN showed promising results in gesture detection referring to success rate (SR) as well as generalizability. It is considered as robust (i.e., against electrode shift [5] and sampling frequency variation [6]). Further benefits are the algorithm's incrementality

T. Sziburis (✉) · M. Nowak
German Aerospace Center (DLR), Robotics and Mechatronics Center (RMC),
Münchner Str. 20, 82234 Weßling, Germany
e-mail: tim.sziburis@cern.ch

T. Sziburis
High Precision Alignment Technologies Section, CERN, 1211 Geneva 23, Switzerland

D. Brunelli
Department of Industrial Engineering, DII, University of Trento, 38123 Trento, Italy

© The Author(s), under exclusive license to Springer Nature Switzerland AG 2022
D. Torricelli et al. (eds.), *Converging Clinical and Engineering Research*
on *Neurorehabilitation IV*, Biosystems & Biorobotics 28,
https://doi.org/10.1007/978-3-030-70316-5_109

and low level of implementation complexity. As kNN is an instance-based machine learning algorithm, training of an explicit model is not necessary.

Since proportionality is a key feature in myocontrol, regression algorithms gain more popularity [7, 8]; moreover several attempts were made to combine classification concepts with proportional scaling in EMG-based intention detection: LDA [9, 10], neural networks [11, 12] and common spatial patterns [13] have been used to control the velocity based on the signal intensity. To the authors' knowledge, kNN was not adapted as a proportional scheme so far. In this study, we developed such a scheme investigating several modalities to include proportionality.

2 Conceptual Approach

It is assumed that the intensity of an exerted gesture is approximately proportional to the amplitude of the signal (mean of all channels of the 8-channel EMG signal). We intend to use this property for proportional scaling of gestures classified by kNN. The rectified sensor reading is divided into a normalized signal and the signal strength (normalization factor), while the former is used for gesture prediction, and the latter for scaling under the assumption of linear correlation of signal strength and proportional intent for the particular gesture. The rest gesture is treated independently. The mean magnitude of the rest samples gathered during training (t_0) is taken as baseline for rest. If the threshold $t = g \cdot t_0$ (gain g) is exceeded, a gesture is not classified as rest anymore. An increase in t reduces unwanted activations.

However, a higher level of t requires the user to exert higher forces to activate a gesture and therefore also leads to a lower resolution of proportionality. There is a trade-off between suppressing unwanted activations and providing a high level of resolution (maintaining the maximum). We therefore introduce a divisor d which scales the proportionality function offset $m_0 = \frac{t}{d}$; but not the threshold for rest t itself. Different configurations are tested in pilot tests.

3 Control Method Adaptation

The training process comprises: (1) capturing training data, (2) calculating class magnitude means for proportionality scaling, (3) normalization of this data, (4) block-wise cross-validation for obtaining the optimal k in terms of accuracy.

The prediction process is structured as follows: (1) rest thresholding, (2) normalization of new sample, (3) calculating k nearest neighbours of the new sample, (4) applying distance weighting on the k selected neighbouring samples, (5) executing kNN classification by majority voting, and (6) signal magnitude analysis and scaling the prediction proportionally.

For the preparation of the user study, we conducted a two-step method adaptation (analyzing seven actions: rest, power grasp, point, wrist flexion/extension, prona-

tion/supination). First, we performed offline cross-validation to determine the most suited kNN parameters (k , distance metric and weighting factor). This was followed by a single-subject pilot to evaluate different ways of introducing proportionality.

3.1 Cross-Validation

The accuracy of kNN with varying parameter sets in block-wise cross-validation was determined in an offline study on different datasets from a single subject. In the case of low k (k relative to the total numbers of training samples until 5–10%), neither the metric nor the weighting was of high importance as long as applying a Minkowski-based distance, yielding 98–100% correct classifications. Results were consistently worse with Mahalanobis distance. For higher k s the Euclidean norm turned out to be the best choice, together with a weighting of $\frac{1}{d^2}$. This configuration is chosen in the subsequent sections, with $k = 1$.

3.2 Pilot Tests on One Subject

Rest thresholding (introduction of t) increased the SR for non-overlapping classes, as misclassifications with rest could be reduced. Maxima were achieved for $g = 2.5$.

For by trend overlapping classes applying a divisor d enabled low-intensity gestures to be more easily exerted and increased the performance. Together with normalization, higher d s guaranteed that the necessary force effort to exert a full gesture does not noticeably exceed the particular training magnitudes. The originally discovered problem that with a higher d low-intensity gestures got less reachable was effaced with normalization. Averaged over all datasets, the maximum SR ($93 \pm 6\%$) was achieved for $d = 5$.

3.3 User Study

A user study with 12 subjects was conducted for evaluating the suitability in practical scenarios (using $t = 2.5 \cdot t_0$ and $d = 5$). After signing consent forms, the participants sat in front of a screen in a standardized pose. For the training process they followed a visual stimulus, performing a repetitive series of actions, comprising the four gestures power grasp, point, wrist flexion/extension. In the prediction/test phase they were asked to follow the stimulus again, viewing a visual feedback. The goals were not only at full activation (as during training), but at levels of 33 and 67% as well. They were also randomized between subjects. We compared the performance in terms of SR for kNN with a regression algorithm, namely RR-RFF [8], followed up by a statistical analysis using a one-way ANOVA on SR.

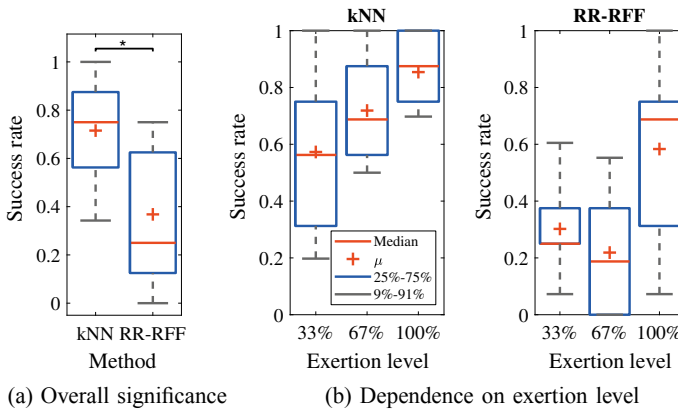


Fig. 1 User study SR results, comparing kNN and RR-RFF

4 Results

ANOVA (level of significance 5%) reveals a stochastic significant difference in favor of kNN compared to RR-RFF, see Fig. 1a. The achieved SRs for different intensity levels of gesture exertion in Fig. 1b shows no level where RR-RFF would have outperformed kNN in median or mean of SR.

RR-RFF seems to perform well only on the intensity level it was trained with. At lower levels the performance drops drastically. This drop is less severe for kNN, where it is potentially due to training on full intensity level, and a high rest threshold causing movements with low signal amplitudes being classified as rest. The effect might be curtailed by user-specific parameter adjustments, and a learning process with subjects getting used to the algorithm's specific behaviour.

5 Conclusions and Outlook

This paper evaluated the extension of kNN classification by proportionality scaling for intent detection by using a state-of-the-art 8-channel myocontrol armband. kNN can be a means towards better generalization capabilities to improve user satisfaction in prosthetics. In comparison to state-of-the-art RR-RFF, the algorithm does not involve complex numeric operations, particularly during training, and has few parameters to be tuned. An appropriate parameterization was validated in a user study. Besides higher SR, the overall result of kNN showed a lower standard deviation than in RR-RFF, which leads to the assumption that kNN performs more stable and robust with less nondeterminism in the algorithm's behaviour. Other classification techniques may also benefit from the presented proportionality scheme. In contrast to kNN, RR-RFF allows the simultaneous detection of mixed gestures, though. The

low complexity of kNN can be of high importance for embedded system implementations. In this context, special attention must be paid to the prediction phase of standard kNN where each sample has to be related to each single other sample. This will be treated in further work.

References

1. C. Cipriani, et al., Online myoelectric control of a dexterous hand prosthesis by transradial amputees. *IEEE Trans. Neural Syst. Rehabil. Eng.* **19**(3), 260–270 (2011) <https://doi.org/10.1109/TNSRE.2011.2108667>
2. R.N. Khushaba, A. Al-Timemy, A. Al-Ani, A. Al-Jumaily, Myoelectric feature extraction using temporal-spatial descriptors for multifunction prosthetic hand control, in *38th Conference Proceedings IEEE Engineering Medical Biology Society* (2016), pp. 1696–1699 <https://doi.org/10.1109/EMBC.2016.7591042>
3. P. Geethanjali, Comparative study of pca in classification of multichannel EMG signals. *APESM* **38**(2), 331–343 (2015) <https://doi.org/10.1007/s13246-015-0343-8>
4. R.M.G. Tello, et al., Towards semg classification based on Bayesian and k-nn to control a prosthetic hand, in *ISSNIP BRC* (2013) <https://doi.org/10.1109/BRC.2013.6487520>
5. Q.X. Li, et al., Improving robustness against electrode shift of semg based hand gesture recognition using online semi-supervised learning, in *2016 International Conference Machine Learning Cybernetics*, vol. 1 (2016), pp. 344–349 <https://doi.org/10.1109/ICMLC.2016.7860925>
6. H. Chen, et al., Exploring the relation between EMG sampling frequency and hand motion recognition accuracy, in *IEEE International Conference System Man Cybernet (SMC)* (2017), pp. 1139–1144 <https://doi.org/10.1109/SMC.2017.8122765>
7. A. Ameri, E.N. Kamavuako, E.J. Scheme, K.B. Englehart, P.A. Parker, Support vector regression for improved real-time, simultaneous myoelectric control. *IEEE Trans. Neural Syst. Rehabil. Eng.* **22**(6), 1198–1209 (2014)
8. A. Gijssberts, et al., Stable myoelectric control of a hand prosthesis using non-linear incremental learning. *Front. Neurobot.* **8** (2014) <https://doi.org/10.3389/fnbot.2014.00008>
9. S. Lobov, N. Krilova, I. Kastalskiy, V. Kazantsev, V. Makarov, A human-computer interface based on electromyography command-proportional control, in *Proceedings of Neurotechnix, vol. 1* (2016), pp. 57–64 <https://doi.org/10.5220/0006033300570064>
10. B. Hudgins, P.Parker, R.N. Scott, A new strategy for multifunction myoelectric control. *IEEE Trans. Biomed. Eng.* **40**(1), 82–94 (1993) <https://doi.org/10.1109/10.204774>
11. E. Scheme et al., Motion normalized proportional control for improved pattern recognition-based myoelectric control. *IEEE Trans. Neural Syst. Rehabil. Eng.* **22**(1), 149–157 (2014)
12. A.M. Simon, K. Stern, L.J. Hargrove, A comparison of proportional control methods for pattern recognition control, in *Conference Proceedings IEEE Engineering Medical Biology Society* (2011), pp. 3354–3357
13. S. Amsuess, P. Goebel, B. Graimann, D. Farina, A multi-class proportional myocontrol algorithm for upper limb prosthesis control: validation in real-life scenarios on amputees. *IEEE Trans. Neural Syst. Rehabil. Eng.* **23**(5), 827–836 (2015)

Controlling an Assistive Robotic Manipulator via a Non-linear Body-Machine Interface



Marco Giordano, Fabio Rizzoglio, G. Ballardini,
Ferdinando A. Mussa-Ivaldi, and M. Casadio

Abstract Controlling an assistive robotic manipulator can play a crucial role in improving lives of individuals with motor impairments. Here, we propose the use of state-of-the-art machine learning techniques for dimensionality reduction—non-linear autoencoder (AE) networks—within a Body-Machine Interface (BoMI) framework for controlling a 4D virtual manipulator. Compared to their linear counterparts, non-linear AEs allow retaining more of the original variance and spreading it more uniformly along the latent dimensions. This advantage has the potential to facilitate an effective control of devices with multiple degrees of freedom (DoFs). We tested the approach on a cohort of unimpaired participants practicing a reaching task in 3D space. As a result, all participants were able to reach a high level of control skills after training with the interface. Such findings highlight the potential of BoMIs based on non-linear AEs as a control platform for assistive manipulators.

Keyword Autoencoders · Robot manipulator · Body Machine interface

This work was supported by the Marie Curie Integration [Grant FP7- PEOPLE-2012-CIG-334201], the Ministry of Science and Technology, Israel (Joint Israel-Italy lab in Biorobotics Artificial somatosensorial for humans and humanoids), the National Science Foundation [Grant 1632259, Grant 1823889], the NIDILRR [Grant 90REGE0005-01] and the NICHD [Grant 5R01HD072080]

MG and FR contributed equally to this work.

M. Giordano · F. Rizzoglio (✉) · G. Ballardini · M. Casadio
University of Genoa, Genoa, Italy
e-mail: fabio.rizzoglio@edu.unige.it

G. Ballardini
e-mail: gjulia.ballardini@edu.unige.it

M. Casadio
e-mail: maura.casadio@unige.it

F. Rizzoglio · F. A. Mussa-Ivaldi
Shirley Ryan Ability Lab, Northwestern University, Chicago, IL, USA
e-mail: sandro@northwestern.edu

1 Introduction

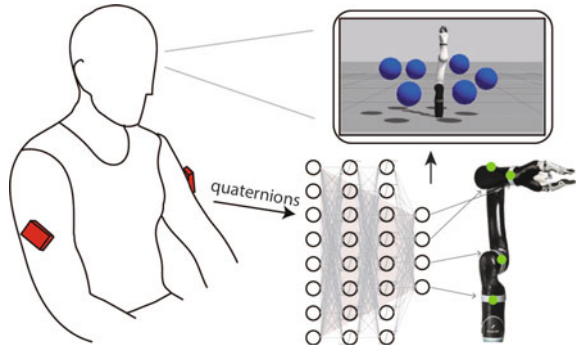
Individuals with severe motor impairments, such as after a spinal cord injury, lack the ability to independently perform activities of daily living. Common activities, including grooming and object manipulation, could be facilitated through the use of assistive devices, such as robotic manipulators. The intrinsic limit in the use of devices with many degrees of freedom (DoFs), is that their kinematic complexity might place a high cognitive burden on the users. Here, we propose an approach based on the framework of Body-Machine Interfaces (BoMIs) [1]. BoMIs capture residual movements and map them into commands that can empower individuals with motor impairments to control assistive devices [2, 3]. To do so, BoMIs typically rely on a linear dimensionality reduction technique—Principal Component Analysis (PCA) [4]. PCA identifies a lower dimensional, linear latent space by maximizing the covariance of the input signals. Despite its widespread use in BoMIs, PCA might not be suited for controlling devices with a large number of DoFs, as the variance explained by its latent dimensions significantly drops after the first couple of them. Here, we propose the use of autoencoder (AE) networks [5] to overcome this difficulty. AEs are artificial neural networks that compress data into a latent *code* via non-linear dimensionality reduction. Not only non-linear AEs are able to estimate the dimensionality of their input more parsimoniously than PCA [6], but their structure can also be customized to obtain a variance that is more uniformly distributed across its latent dimensions. This study serves as a first proof-of-concept for the use of an AE-based BoMI for controlling a robotic manipulator.

2 Methods

For this preliminary study, we recruited four unimpaired participants (age 25.8 ± 2.2 , 3 females). They signed a consent form approved by the institutional review board (n. registro CE DIBRIS: 009/2020). We recorded their upper body movements with two Inertial Measurement Unit (IMU) sensors (BNO055 Sensors, *Bosch, Gerlingen-Schillerhöhe, Germany*) placed bilaterally on participants' arms.

We used an AE to map the 8D body movements—quaternions from the IMUs—into angular movements of the joints of a 4D virtual robotic manipulator. The map for controlling the manipulator was the same for all participants and was obtained after a calibration procedure. In this phase, a subject (age 25, male) that did not participate in the following study was asked to freely move his arms for 60 s. The kinematic data recorded in this phase were used to train an AE with four codes via a validation procedure that aimed at choosing the AE structure with (i) maximum variance explained and (ii) a variance uniformly distributed across the codes. Then, we set the encoder sub-network of such AE in the BoMI scheme (see Fig. 1) to convert the 8D kinematic-vector into a 4D signal for controlling the joints of a

Fig. 1 Setup of the experiment. Quaternions from two IMUs (red boxes) were mapped via the AE encoder to the four joints (green dots) of the virtual MICO. The participant received visual feedback on a PC monitor



virtual manipulator. The manipulator was designed in Gazebo [7] and resembled the MICO robotic arm (*Kinova Robotics, Canada*).

We mapped the first code of the AE to control the movements of the wrist angle of the manipulator—the most distal joint—and proceeding in order toward the base so that the fourth code mapped the robot’s base-joint angle, as illustrated in Fig. 1. Each code was re-scaled to fit the maximum extension of each joint angle (360° for the base-joint angle, 180° for the others).

The protocol consisted of a 3D center-out reaching task. We collected data from participants as they practiced with the interface over two non-consecutive days. Participants were asked to reach six targets placed uniformly along a circle, at different heights, with the end-effector of the robot. A total of 144 targets were presented. The position of the robot—based at the center of the workspace—and targets were displayed on a computer monitor. A trial was considered successful if the target remained between the fingers of the gripper of the manipulator for 500 ms. Repeated measures ANOVA was used to test the effect of training time.

3 Results

Figure 2a shows the time participants took to reach the targets after leaving the central position. Figure 2b shows an index of straightness of movements, defined as the path length of the end effector divided by nominal distance. After the first day of training, participants were able to move the robot faster ($p < 0.001$) and the end effector straighter, ($p < 0.001$) towards the targets. In the second day of training, participants were able to retain performances acquired during day 1 and their learning curve converged towards a stable level by the end of the session.

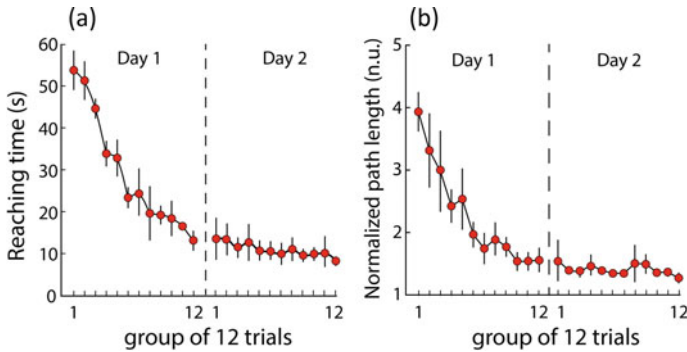


Fig. 2 Reaching time (Panel A) and normalized path length of the robot end effector (Panel B) throughout various epochs of training. Mean and standard deviation across participants are shown every 12 trials. Day 1 and day 2 performance are divided by a horizontal dashed line

4 Discussion

Controlling a device with multiple DoFs is a challenging task. Whereas a *discrete* control would allow users to control an n -dimensional device with a one-dimensional interface by manually switching between n modes, continuous control is a more natural and effective operation that can be obtained by sharing the computational burden between human and computer [3]. However, as pointed out in a recent study by Javaremi and Argall, “there is no one-size-fits-all method for control sharing as each person is unique in their desired control preference” [8]. In this sense, our approach based solely on the use of BoMI stands out, as it allows direct and continuous operation by the user. Moreover, the unsupervised nature of the BoMI allows for adaptability of the interface—via the calibration procedure—to its users’ residual movements, which is of primary importance in the presence of motor impairments. Additionally, we believe that this instance of BoMI, based on non-linear AEs, overcomes the limitations that would be encountered using PCA. AEs are less constrained than PCA, as they can capture non-linear features embedded in the input signal, while concurrently distributing the original variance more uniformly into their codes. Therefore, they establish as a platform that is better suited for the control of devices with multiple DoFs. This first proof of concept demonstrates that naïve unimpaired users can learn to efficiently operate the manipulator. They were able to significantly decrease the time to reach targets and increase the straightness of the trajectories made with the robot end effector within a single session of training. Interestingly, performance levels were retained at the beginning of day 2, even if the two sessions were performed during non-consecutive days. Also, the two-day sessions highlight convergence towards a stable level of performance. We consider these findings as supportive of a future implementation of our interface as assistive tool for people with motor impairments.

5 Conclusion

We presented a method based on the use of a non-linear autoencoder for controlling assistive robot manipulators with multiple degrees of freedom. This first proof of concept successfully proved the feasibility of the approach and set the basis for future tests on a population with motor impairments.

References

1. M. Casadio, R. Ranganathan, F.A. Mussa-Ivaldi, The body-machine interface: a new perspective on an old theme. *J. Mot. Behav.* **44**(6), 419–433 (2012). <https://doi.org/10.1080/00222895.2012.700968>
2. E.B. Thorp et al., Upper body-based power wheelchair control interface for individuals with tetraplegia. *IEEE Trans. Neural Syst. Rehabil. Eng.* **24**(2), 249–260 (2016). <https://doi.org/10.1109/TNSRE.2015.2439240>
3. S. Jain, A. Farshchiansadegh, A. Broad, F. Abdollahi, F. Mussa-Ivaldi, B. Argall, Assistive robotic manipulation through shared autonomy and a Body-Machine Interface. *IEEE Int. Conf. Rehabil. Robot.* **2015**, 526–531, (2015). <https://doi.org/10.1109/ICORR.2015.7281253>
4. A. Farshchiansadegh, et al., A body machine interface based on inertial sensors, in *2014 36th Annual International Conference on IEEE Engineering in Medical and Biology Society EMBC 2014* (2014), pp. 6120–6124. <https://doi.org/10.1109/EMBC.2014.6945026>
5. M.A. Kramer, Nonlinear principal component analysis using autoassociative neural networks. *AIChE J.* **37**(2), 233–243 (1991). <https://doi.org/10.1002/aic.690370209>
6. A.A. Portnova-fahreva, F. Rizzoglio, I. Nisky, M. Casadio, Linear and non-linear techniques on full hand kinematics. *Front. Bioeng. Biotechnol.* **8**, 1–8 (2020). <https://doi.org/10.3389/fbioe.2020.00429>
7. N. Koenig, A. Howard, Design and use paradigms for gazebo, an open-source multi-robot simulator, in *2004 IEEE/RSJ International Conference on Intelligent Robots and Systems (IROS)(IEEE Cat. No. 04CH37566)*, vol. 3 (2004), pp. 2149–2154
8. M.N. Javaremi, B.D. Argall, *Characterization of Assistive Robot Arm Teleoperation: A Preliminary Study to Inform Shared Control*. arXiv Prepr. arXiv2008.00109 (2020)

Offline Repeatability Correlates with Real-Time Performance of Pattern Recognition Controllers



Yuni Teh and Levi J. Hargrove

Abstract Previous studies have shown that offline classification accuracy does not always correlate with real-time performance. However, the relationships between real-time performance and other offline measures, such as feature space metrics, are not clearly understood. We evaluated controller performance in intact limb (ITL) and amputee (AMP) subjects using online and offline tests in four limb positions and with three limb loads. We quantified the Pearson correlation coefficients between three offline metrics (offline accuracy, repeatability index, separability index) and four real-time metrics (completion rate, remaining time, movement efficacy, stopping efficacy). Our results showed that repeatability index had the strongest correlations with all real-time metrics (ITL: $r \geq 0.91$, AMP: $r \geq 0.68$). This suggests that pattern recognition control algorithms and training protocols should aim to optimize repeatability as opposed to accuracy or separability.

This work was supported by the National Institutes of Health NIH R01HD094861 and the Congressionally Directed Medical Research Program W81XWH-17-1-0332.

Y. Teh (✉) · L. J. Hargrove
Shirley Ryan AbilityLab, Regenstein Center for Bionic Medicine,
Northwestern University, Chicago, IL 60611, USA
e-mail: yuni@u.northwestern.edu

L. J. Hargrove
e-mail: l-hargrove@northwestern.edu

Y. Teh
Department of Biomedical Engineering, Northwestern University, Chicago, IL 60611, USA

L. J. Hargrove
Department of Physical Medicine and Rehabilitation,
Northwestern University, Chicago, IL 60611, USA

© The Author(s), under exclusive license to Springer Nature Switzerland AG 2022
D. Torricelli et al. (eds.), *Converging Clinical and Engineering Research
on Neurorehabilitation IV*, Biosystems & Biorobotics 28,
https://doi.org/10.1007/978-3-030-70316-5_111

691

1 Introduction

Although online testing is the most realistic way to evaluate prosthesis controllers, it can be time consuming and fatiguing. Thus, experimenters often initially rely on offline analyses to assess new algorithms. For pattern recognition (PR) controllers, classification accuracy is the most commonly reported offline metric even though it does not always correlate with real-time performance [1, 2].

However, PR controllers can also be characterized by offline feature space metrics, such as the repeatability index (RI) and separability index (SI) [3]. It is unclear whether these metrics can relate to real-time performance more accurately. To our knowledge, only one study has quantified the relationship between feature space and online metrics [4]. However, the experiment did not include amputee subjects and had limited test conditions.

In this study, we quantified the correlations between three offline (two feature space) and four online metrics in subjects with intact limbs (ITL) and subjects with below-elbow amputations (AMP). To increase the variance of data collected, tests were conducted in different limb positions and with different limb loads. We compared the correlation coefficients of each offline metric to determine which was the best estimate of real-time performance.

2 Methods

This experiment was approved by Northwestern University's Institutional Review Board. Fourteen ITL subjects and five AMP subjects participated after giving informed consent. Each subject used EMG signals from their right forearm or residual limb to use linear discriminant analysis controllers trained with four time domain-features (mean absolute value, waveform length, zero crossings, and slope sign changes) and six autoregressive coefficients. Offline and online tests were completed in four limb positions (Fig. 1) and with three external limb loads (0g, 400g, 600g).

2.1 Classifier Training Protocols

All ITL subjects and two AMP subjects trained 3 degrees of freedom (hand open/close, wrist pronation/supination, wrist flexion/extension). The remaining three AMP subjects did not train wrist flexion due to time constraints and lack of PR control experience. There were two training protocols:

1. Static Subjects held their arm in P1 while performing contractions. The limb was not loaded in this condition.
2. Dynamic Subjects moved their arm around in their workspace while performing contractions. A 400g load was attached to the limb.

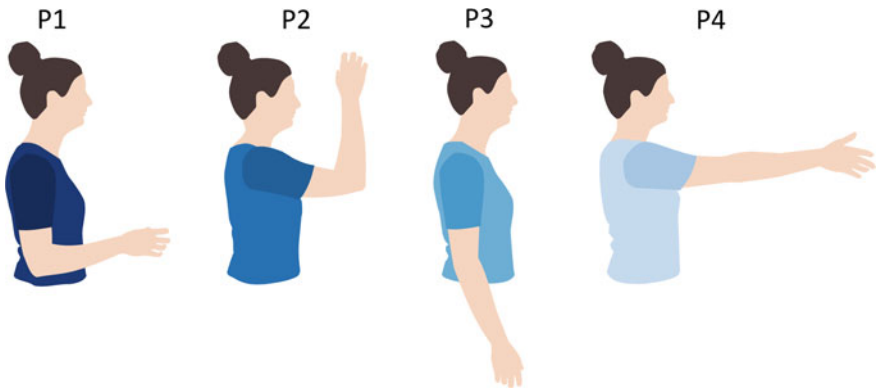


Fig. 1 Limb positions used during data collection

2.2 *Offline Data Collection*

To collect offline testing data, subjects held each trained movement in each limb position and with each load for 2.5 s. No feedback about their contractions was provided. We calculated three offline metrics for each test condition:

1. Offline Accuracy (OA) The percentage of correct predictions in each class, averaged across all classes.
2. Repeatability Index (RI) The modified Mahalanobis distance between training and testing distributions of the same class, averaged across all classes. In this paper, we inverted the sign of this metric, such that a more positive number represents better repeatability within classes.
3. Separability Index (SI) The shortest interclass modified Mahalanobis distance between training and testing datasets, averaged across all classes. A larger SI denotes better separability between classes.

2.3 *Online Target Acquisition Control (TAC) Tests*

Subjects completed 3D TAC tests in a virtual reality environment, as described in [5]. We calculated four metrics: completion rate (CR), remaining time (RT), movement efficacy (ME), stopping efficacy (SE) as defined in [5]. Remaining time is the inverse of completion time; a larger RT means that the trial was completed faster.

2.4 Correlation Analysis

We calculated the Pearson correlation coefficient (r) between each offline and online metric. All metrics were chosen such that larger positive correlations were more desirable. To determine significant differences between the strength of these correlations, we compared their 95% confidence intervals (CI).

3 Results

For ITL subjects (Fig. 2), RI had the strongest positive correlations ($r \geq 0.91$) with all real-time metrics, followed by OA ($r \geq 0.45$). All RI and OA correlations were statistically significant. In contrast, all SI correlations were negative and only one (SE) was statistically significant. The confidence intervals showed that the correlation coefficients were significantly more positive for RI than for OA and SI.

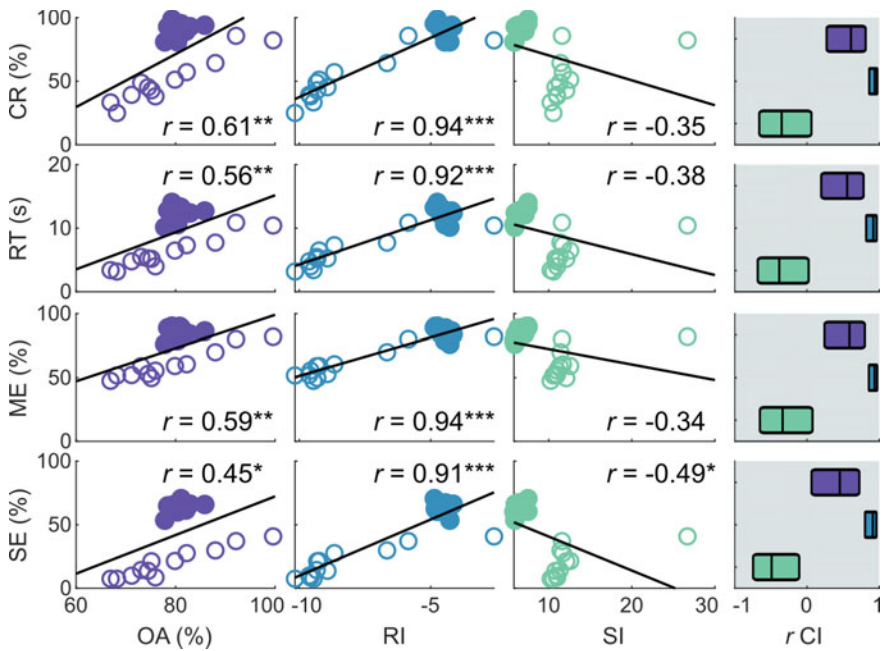


Fig. 2 Intact limb subject results. Hollow and filled circles represent trials using static and dynamic training, respectively. *: $p < 0.05$, **: $p < 0.01$, ***: $p < 0.001$

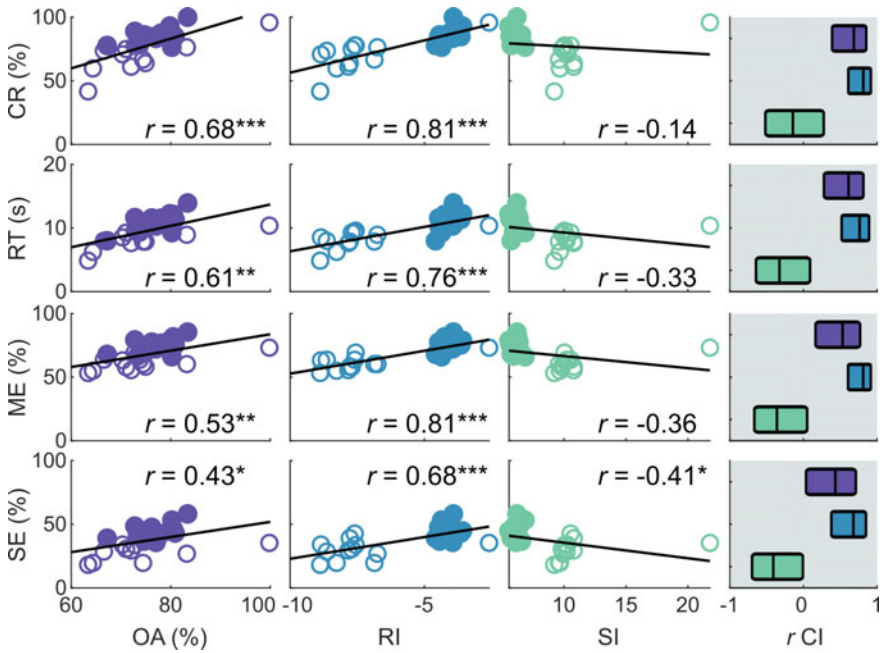


Fig. 3 Amputee subject results. Hollow and filled circles represent trials using static and dynamic training, respectively. *: $p < 0.05$, **: $p < 0.01$, ***: $p < 0.001$

For AMP subjects (Fig. 3), RI also strongly correlated ($r \geq 0.68$) with real-time metrics. This was not significantly different from OA ($r \geq 0.43$). All SI correlations were negative and only the correlation with SE was statistically significant. Both RI and OA correlations were significantly different from SI correlations.

4 Discussion

Previous publications showed an inconsistent relationship between offline accuracy and real-time metrics, leading researchers to discount the use of offline accuracy to infer actual performance. We investigated how other offline metrics correlated with real-time metrics and showed that repeatability, or the distance between training and testing sets, has a stronger correlation with real-time metrics compared to offline accuracy and separability.

Our results suggest that real-time performance is more dependent on how consistent the contractions are rather than how distinct they are. In fact, the correlations between SI and real-time metrics were negative because dynamic training improved online control despite reducing separability. Thus, future development of controllers could err on the side of increasing repeatability at the potential expense of separability or accuracy and still improve performance.

5 Conclusion

In this study, we quantified and compared the extent to which offline accuracy, repeatability, and separability correlated with online performance metrics. Our results showed that repeatability had the strongest correlations, suggesting that it is a better measure for inferring real-time performance.

References

1. L. Hargrove, Y. Losier, B. Lock, K. Englehart, B. Hudgins, A real-time pattern recognition based myoelectric control usability study implemented in a virtual environment, in *Proceedings of International Conference IEEE Engineering Medicine and Biological Society* (2007), pp. 4842–4845
2. M. Ortiz-Catalan, F. Rouhani, R. Brånemark, B. Håkansson, Offline accuracy: a potentially misleading metric in myoelectric pattern recognition for prosthetic control, in *Proceedings International Conference IEEE Engineering Medicine and Biology Society* (2015), pp. 1140–1143
3. N.E. Bunderson, T.A. Kuiken, Quantification of feature space changes with experience during electromyogram pattern recognition control. *IEEE Trans. Neural Syst. Rehabil. Eng.* **20**(3), 239–246 (2012)
4. M.B. Kristoffersen, A.W. Franzke, C.K. van der Sluis, A. Murgia, R.M. Bongers, The effect of feedback during training sessions on learning pattern-recognition-based prosthesis control. *IEEE Trans. Neural Syst. Rehabil. Eng.* **27**(10), 2087–2096 (2019)
5. Y. Teh, L.J. Hargrove, Understanding limb position and external load effects on real-time pattern recognition control in amputees. *IEEE Trans. Neural Syst. Rehabil. Eng.* **28**(7), 1605–1613 (2020)

Understanding Human-Prosthesis Interaction via Reinforcement Learning-Based Echo Control: A Case Study



Ruofan Wu, Minhan Li, Jennie Si, and He (Helen) Huang

Abstract This case study aimed to understand human-prosthesis interaction while the impedance control of a robotic prosthesis was tuned in order to echo the knee kinematics on the intact joint. Echo control derives from a common belief that if the prosthesis joint mechanics meet those of the intact joint, more symmetrical and normal gait should be reached in the prosthesis user. In this study, our previous developed reinforcement learning (RL) control was used to tune impedance of a power knee prosthesis in walking to achieve echo control. It was tested on one able-bodied human subject walking with the robotic knee. The results showed that the prosthesis control parameter tuning was coupled with changes in intact knee mechanics. Nevertheless, regardless such neuromechanic coupling between the two lower limbs, RL was robust to tune prosthesis control and meet the intact knee kinematics. Finally, the RL echo control enabled us to examine gait symmetry. Additional research efforts are still needed to identify the influence of echo control of prosthetic knee on gait tempospatial symmetry.

1 Introduction

Powered lower limb prosthesis provides great promise for amputees to restore basic activities in daily life. However, the performance of transfemoral amputees using these powered devices have not shown consistent improvement [1, 2]. This may be

This work was supported in part by National Science Foundation #1563454, #1563921, #1808752 and #1808898.

R. Wu · J. Si (✉)
School of Electrical, Computer, and Energy Engineering,
Arizona State University, Tempe, AZ 85281, USA
e-mail: si@asu.edu

M. Li · H. (Helen) Huang (✉)
NCSU/UNC Department of Biomedical Engineering,
NC State University, Raleigh, NC 27695-7115, USA
e-mail: hhuang11@ncsu.edu

University of North Carolina at Chapel Hill, Chapel Hill, NC 27599, USA

© The Author(s), under exclusive license to Springer Nature Switzerland AG 2022
D. Torricelli et al. (eds.), *Converging Clinical and Engineering Research on Neurorehabilitation IV*, Biosystems & Biorobotics 28,
https://doi.org/10.1007/978-3-030-70316-5_112

due to a lack of cohesion between the human and the computer controlled prosthesis. Unfortunately, little is known about how the human and the prosthesis interact even though the prosthesis can be physically attached to its human user to enable walking. It has long been hypothesized that mirroring the intact knee kinematic joint trajectory by the prosthetic knee can improve gait symmetry. Yet, controlling the prosthetic knee to mimic or echo the intact knee has not been achieved to enable the test of this hypothesis.

Echo control ideas have long existed for decades. Grimes et al. developed an echo control scheme for the stance phase of a gait cycle to track a modified trajectory from the sound limb [3]. Joshi et al. developed a control strategy based on echoing the stride duration of the intact side [4]. However, both approaches of echo control only manipulated a fraction of a gait cycle. Few results have been reported in recent years.

Previously, we have successfully tested a new class of control approaches, namely reinforcement learning (RL) control, to automatically tune the impedance parameters to enable level ground walking [5–7]. A key characteristic of the RL control is its ability to directly learn a parameter tuning policy during the interaction between the human user and the prosthesis. Even though our previous RL control designs were for the prosthetic knee to meet a prescribed knee profile, it is expected to be able to learn a new control policy for the prosthetic knee to echo the intact knee. It is also expected to provide an opportunity to study the human-prosthesis interaction and symmetry during the entire control tuning process.

Therefore, the goal of this study is to study human-prosthesis interaction while achieving echo control by using our previously developed RL-based prosthesis tuning method. Specifically we were interested in understanding (1) whether human and prosthesis knee can co-adapt to achieve echoed motion, and (2) whether echoed motion can improve gait temporal symmetry. The results will contribute important knowledge in human-prosthesis interaction and inform future control of robotic prosthesis for optimal gait performance of individuals with lower limb amputations.

2 Methods

In this study, we deployed a previously developed reinforcement learning controller [5], which acted as a supplementary impedance parameter tuner for the powered knee prosthesis control in order to echo the features of intact side knee kinematics. As previously reported, the reinforcement learning controller was implemented within the well-established finite state machine and impedance control (FSM-IC) framework. The intact side knee kinematics was obtained through measurements of the knee angle by a goniometer provided by Biometrics Ltd. [8]. The features such as peak angle and phase duration were extracted from both limbs as inputs to the RL controller. The RL enabled parameter tuning process involved two types of updates: the impedance values were updated based on measured knee angle and angular velocity given a control policy for the FSM-IC; whereas the control policy was updated by the policy iteration algorithm developed in [5]. Policy evaluation and

policy improvement were alternately performed until meeting tuning performance conditions.

With IRB approval, we recruited one able-bodied subject to perform a level ground treadmill walking task at the speed of 0.6 m/s. We measured bilateral knee kinematics and stance time symmetry during the prosthesis tuning procedure. The procedure terminated when the differences of knee kinematics between two limbs was smaller than a predefined threshold.

3 Results and Discussions

Figure 1 shows the changes of knee profiles of the intact side and the prosthesis side during the prosthesis tuning iterations. The gait trajectories were averaged over a batch of 15 policy updates. Significant adaptation of both knee trajectories were observed as prosthetic knee parameters updated and the two knee profiles move into each other. It indicated the preservation of neuromechanic coupling between lower limbs even though one side of the limb was replaced by a robotic device.

Through RL-based prosthesis control tuning, the peak error reduced from 10° to 0° in the Stance Flexion Phase, from 7° to 0.2° for the Stance Extension Phase, and from 21° to 0° for the swing extension phase. For the swing flexion phase, the peak error remained same in the desired bound. This result implied that RL was robust to tune the prosthesis control to meet the desired gait pattern, even though the desired kinematics features changed. More interestingly, both biological knee and robotic knee could essential co-adapt with each other to achieve similar trajectory.

The symmetry index was calculated by the difference of two limbs, divided by the sum of them. Figure 2 shows the stance time symmetry index at the beginning and the end of the tuning process, which was 0.23 and 0.20, respectively. But such slight improvement should not be considered statistically significant yet as we only tested a single subject. However, it is apparent that the echo control of knee motion cannot achieve complete gait symmetry. This is not surprising since the mechanics of the prosthesis (which lacks a powered ankle) are different from those of a biological limb. Putting all these together, under the current experimental condition, our results indicated that using echo control to restore gait temporal symmetry may be questionable even though the common perception expects to see improved gait temporal symmetry based on echoed motion between the two limbs. Further study involving more individuals with lower limb amputations are needed to provide statistically significant test results on temporal symmetry under echo control.

4 Conclusion

In this case study, we investigated human-prosthesis interaction when the prosthesis knee control was tuned by RL to match the kinematics of intact knee. Inter-limb

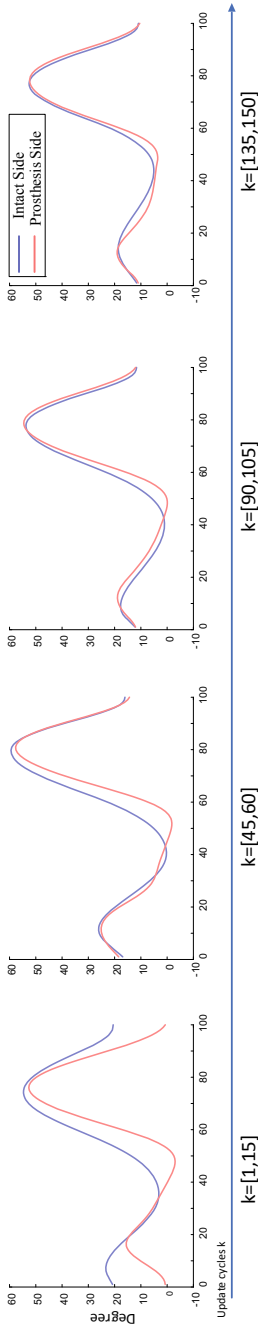
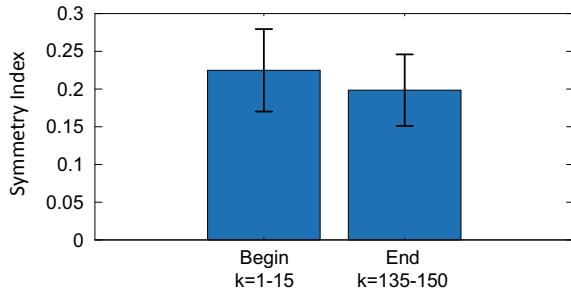


Fig. 1 Knee profiles of both intact side and prosthesis side from the beginning period, in-between period and the end period of a complete learning update session

Fig. 2 Comparison of stance time symmetry between the beginning (first 15 samples, $k = 1-15$) and the end period (last 15 samples, $k = 135-150$) of a complete learning update session. The bars represent the mean SI with the lines indicate the standard deviation



coupling was observed. That is to say, when prosthesis mechanics changed, the intact limb also modified the movement pattern. Our designed RL-based prosthesis tuning was robust and can co-adapt to the changing targeted knee profile from the intact knee and essentially accomplished echo control. Furthermore, achieving knee motion symmetry did not significantly improve the gait temporal symmetry, which was different from the common perception. Additional research is still needed to validate our observation in this case study.

References

1. V. Creyelman, I. Knippels, P. Janssen, E. Biesbrouck, K. Lechler, L. Peeraer, Assessment of transfemoral amputees using a passive microprocessor-controlled knee versus an active powered microprocessor-controlled knee for level walking. *Biomed. Eng. Online* **15**(3), 142 (2016)
2. B.J. Hafner, R.L. Askew, Physical performance and self-report outcomes associated with use of passive, adaptive, and active prosthetic knees in persons with unilateral, transfemoral amputation: Randomized crossover trial. *J. Rehabil. Res. & Dev.* **52**(6) (2015)
3. D. Grimes, W. Flowers, Multi-mode above-knee prosthesis controller, in *Control Aspects of Prosthetics and Orthotics* (Elsevier 1983), pp. 43–53
4. D. Joshi, R. Singh, R. Ribeiro, S. Srivastava, U. Singh, S. Anand, Development of echo control strategy for AK prosthesis: An embedded system approach, in *2010 International Conference on Systems in Medicine and Biology* (IEEE 2010), pp. 143–147
5. M. Li, X. Gao, Y. Wen, J. Si, H.H. Huang, Offline policy iteration based reinforcement learning controller for online robotic knee prosthesis parameter tuning, in *2019 International Conference on Robotics and Automation, ICRA 2019* (Institute of Electrical and Electronics Engineers Inc., 2019), pp. 2831–2837
6. Y. Wen, J. Si, X. Gao, S. Huang, H. Huang, S. Member, A new powered lower limb prosthesis control. *IEEE Trans. Neural Netw. Learn. Syst.* **28**(9), 2215–2220 (2017)
7. X. Gao, Y. Wen, M. Li, J. Si, H.H. Huang, Robotic knee parameter tuning using approximate policy iteration, in *International Conference on Cognitive Systems and Signal Processing* (Springer, 2018), pp. 554–563
8. Biometrics Ltd., Twin-axis electrogoniometers (goniometer) for joint movement analysis. [Online]. Available: <http://www.biometricsltd.com/goniometer.htm>

**SS13: Novel Developments of Non-Invasive
Brain and Peripheral Stimulation
in Neurorehabilitation**

Comparison of Configuration Postures for a Foot Drop Multi-field FES Device



Aitor Martín, Cristina Rodríguez-de-Pablo, Haritz Zabaleta, Eukene Imatz-Ojanguren, and Thierry Keller

Abstract Functional electrical stimulation (FES) is a popular technique to treat foot drop, a common gait impairment caused by inadequate dorsiflexion of the ankle. Multi-field surface electrodes provide easier and faster electrode donning and doffing and higher selectivity of stimulation, solving the problems of traditional FES devices. It also allows an automatic configuration of the device. This pilot study analyses the effectivity of different postures for the automatic configuration of the Fesia Walk system, a commercial multifield technology-based FES device. 5 healthy subjects participated in the study, and 5 configurations were held at 3 body postures within 5 days. The analysis focused on the ability of the system to classify the movements (dorsiflexion, plantarflexion, eversion and inversion) of the ankle in the 3 configuration postures. Results show that sitting on top of a table with both knees extended and ankle and foot hanging freely is the most appropriate posture for configuration as it only presents limitations to generate inversion.

Keywords Functional electrical stimulation · FES · Multi-field electrode · Postures · Foot drop

This work has been supported in part by FIK.

A. Martín (✉) · C. Rodríguez-de-Pablo · H. Zabaleta
Fesia Technology, Donostia-San Sebastián, Spain
e-mail: amartin@fesia.net

C. Rodríguez-de-Pablo
e-mail: crodriguez@fesia.net

H. Zabaleta
e-mail: hzabaleta@fesia.net

E. Imatz-Ojanguren · T. Keller
Tecnalia, Derio, Spain
e-mail: eukene.imatz@tecnalia.com

T. Keller
e-mail: thierry.keller@tecnalia.com

1 Introduction

Neurologic patients often show “foot drop”, a common gait impairment caused by inadequate dorsal flexion [1]. Considering that it results in the inability to perform meaningful daily life activities, promoting motor recovery is essential [2].

Functional electrical stimulation (FES) consists of artificially stimulating motor nerves to elicit muscle contractions and thus, restore motor function. It is one of the options for treating foot drop by stimulating the common peroneal nerve to generate the dorsiflexion [2, 3].

The correct placement and configuration of FES devices based on conventional electrodes is a manual process, which can be time-consuming or limited in term of movement selectivity. However, the use of multi-field surface electrodes, which comprise several small stimulation fields, can solve these problems, providing easier and faster electrode donning and doffing and higher selectivity of stimulation. In addition, the inclusion of inertial sensors in this type of multi-field FES devices bring the possibility of performing an automatic motor-point search [4].

In this pilot study we present an analysis that compares the automatic configuration effectivity for different postures and repeated configurations using a commercial multi-field technology-based FES device.

2 Material and Methods

2.1 Material

For this study, the Fesia Walk system (Fesia Technology, Donostia-San Sebastián, Spain) (Fig. 1) was used. Fesia Walk is a multi-field FES system for foot drop compensation, which consists of a stimulator, a garment, a multi-field electrode, a wireless inertial sensor and a software application. It delivers a train of biphasic pulses of different widths and amplitudes in an asynchronous manner.

During the automatic configuration, the 16 electrode fields are activated individually at different amplitudes, and the sensor, placed on the foot, measures the resulting foot movements. The resulting movements are then assigned by a classification algorithm to one of the 4 movement groups: dorsiflexion, plantarflexion, eversion or inversion and the fields that produce optimally these movements are selected [5].

2.2 Experimental Protocol

This pilot study was held with 5 healthy subjects (age 30.4 ± 4.9). All the participants signed an informed consent.



Fig. 1 Fesialink walk (Fesia Technology, Donostia-San Sebastián, Spain)

Three configuration postures were studied during 5 days: posture 1, sitting on top of a stretcher with knee at 90° and foot hanging freely; posture 2, sitting on top of a stretcher with knee extended and ankle and foot hanging freely; and posture 3, sitting in a chair with both knees extended and crossing the legs with the affected ankle on top of the healthy ankle.

5 configuration iterations were carried out daily for each of the configuration postures with the following resting times between them: no rest, 1 min of passive rest, 2 min of active rest (moving/walking), 5 min of active rest (moving/walking). Then, a minimum of 10 min of rest between postures was ensured.

The stimulation waveform was biphasic compensated. Parameters were set to frequency 25 Hz and pulse width 250 μ s. The amplitude was set for each day and posture at 10 mA above motor threshold or above motor threshold at subject's tolerance. The motor threshold was defined as the minimum amplitude at which foot movement was visually appreciated. Anodes were fixed and set as B&C in Fig. 1.

2.3 Analysis

The analysis focused on the fields selected by the classification algorithm as optimal for performing each of the four movements. The aim was to find differences in terms of selected fields between different postures.

3 Results

In Fig. 2 we can see the fields selected by the classification algorithm for each movement and posture. Each subplot includes the results from configurations carried out during different days and with different subjects (100 configurations).

When configuration was carried out in posture 1, in most of the cases, no fields were found for generating plantarflexion (83%), inversion (62%) or, less frequently, eversion (31%). Regarding posture 2, it failed to find fields that generated an inversion (40%). Finally, during posture 3, the configuration failed to find fields that generated plantarflexion (33%), eversion (34%), and in a lower extent, inversion (12%). It is important to note that all the postures seemed to be good for detecting dorsiflexion.

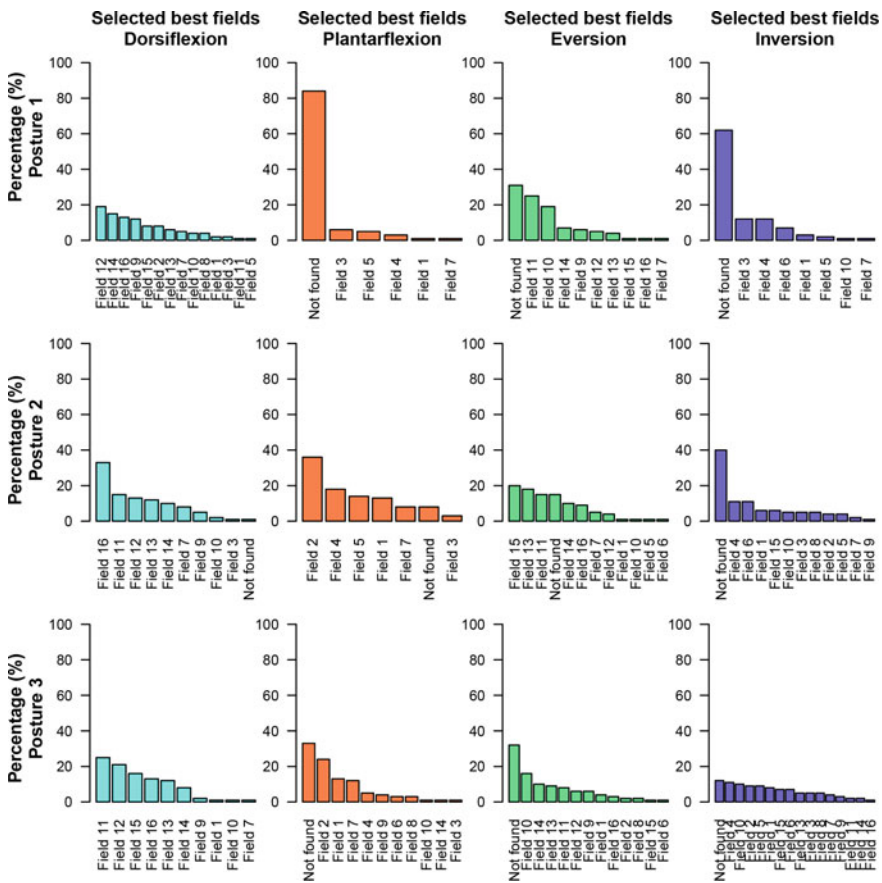


Fig. 2 Fields selected for each movement and each posture

4 Discussion

The aim of the study was to determine the optimal posture for the automatic configuration of the FES system.

If we analyze the effect of the different postures, we can see that in posture 1 it was difficult to detect plantarflexion, inversion and eversion; whereas in posture 2 problems were only found for detecting inversion; and in posture 3 both eversion and plantarflexion detection failed frequently. This fact could be due to the constraints of the postures themselves, as in posture 1 the ankle was in a plantarflexion position due to gravity, and in posture 3 the affected ankle was resting on top of the non-affected limb, which could limit its range of movement.

For foot drop application, the most important movement is the dorsiflexion, which was properly detected during configurations held in all postures and all subjects. The second most important movement is the plantarflexion, which supports the take-off phase. And finally, among eversion and inversion, it is usually more important to achieve an eversion, because most hemiplegic patients have the ankle joint in an inverted position, which is important to compensate during swing phase to reduce the falling risk caused by tripping over the non-affected foot [6].

5 Conclusions

We conclude that posture 2, where patients are sitting on top of a stretcher with the knee extended and the foot hanging freely, is the most appropriate posture for the automatic configuration as it only presented limitations detecting inversion. Although the study was carried out with healthy people, these results can be extrapolated to patients with neurological pathology, since it has been studied a characteristic that does not vary if there is a neurological disorder. Further research with people with neurological disorders is necessary to confirm these conclusions.

References

1. J. Perry, J. Burnfield, *Gait Analysis: Normal and Pathological Function*, 2nd edn. (SLACK Incorporated, New Jersey, 2010).
2. O.A. Howlett, N.A. Lannin, L. Ada, C. McKinstry, Functional electrical stimulation improves activity after stroke: a systematic review with meta-analysis. *Arch. Phys. Med. Rehabil.* **96**, 934–943 (2015)
3. T. Street, C. Singleton, Five-year follow-up of a longitudinal cohort study of the effectiveness of functional electrical stimulation for people with multiple sclerosis. *Int. J. MS. Care.* **20**, 224–230 (2018)
4. E. Imatz-Ojanguren, G. Sánchez-Márquez, J.R. Asiain-Aristu, J. Cueto-Mendo, E. Jaunarena-Goicoechea, H. Zabaleta, et al., A foot drop compensation device based on surface multi-field

- functional electrical stimulation-usability study in a clinical environment. *J. Rehabil. Assist. Technol. Eng.* **6** (2019)
5. J. Malešević, S.D. Dujović, A.M. Savić, L. Konstantinović, A. Vidaković, G. Bijelić et al., A decision support system for electrode shaping in multi-pad FES foot drop coorection. *J. Neuroeng. Rehabil.* **14**, 1–4 (2017)
 6. D. Hyndman, A. Ashburn, E. Stack, Fall events among people with stroke living in the community: circumstances of falls and characteristics of fallers. *Arch. Phys. Med. Rehabil.* **83**, 165–170 (2002)

Pathways of Hemodynamic Response During Anodal Transcranial Direct Current Stimulation: A Computational Approach



Yashika Arora, Anirban Dutta, and Shubhajit Roy Chowdhury

Abstract Transcranial direct current stimulation (tDCS) has been a popular way of modulating brain activity in a non-invasive manner and has shown to affect neural plasticity and cerebrovascular response in humans. It is important to analyze how transcranial direct current stimulation-generated electric fields can induce effects on hemodynamic response. The paper presents a computational model to evaluate vessel volume response under anodal transcranial direct current stimulation. The study considers a basic system of neurovascular unit (NVU) consisting of the vascular smooth muscle, perivascular space, synaptic space and, astrocyte glial cell. The paper analyzes the effect of tDCS on neurovascular dynamics considering near-infrared spectroscopy (NIRS) data. The proposed model based on neurovascular dynamics tracked vascular response elicited through neuronal activity via various signaling pathways during anodal tDCS. The results suggest that the stimulation can perturb the vessel response via both neuronal and non-neuronal pathways.

Keywords Hemodynamic response · Near-Infrared spectroscopy · Neurovascular unit · Transcranial direct current stimulation

The work is funded by Indian Institute of Technology Mandi, Science and Engineering Research Board (SERB), a statutory body of the Department of Science and Technology, Government of India and, Ministry of Electronics and Information Technology (MeitY), Government of India.

Y. Arora (✉) · S. R. Chowdhury

School of Computing and Electrical Engineering, Indian Institute of Technology Mandi, Suran, India

e-mail: yashika_arora@students.iitmandi.ac.in

S. R. Chowdhury

e-mail: src@iitmandi.ac.in

A. Dutta

Department of Biomedical Engineering, University at Buffalo SUNY, Buffalo, NY, USA

e-mail: anirband@buffalo.edu

1 Introduction

Transcranial direct current stimulation (tDCS) is known to produce neuromodulatory effects through generation of induced electric field (EF) in the cortex through the application of weak direct current using scalp electrodes [1]. It is evident from various studies that tDCS influences the neural activity and vascular changes. Experimental studies have shown that tDCS tend to modulate neuronal activity through modulation of cortical neurotransmitters during tDCS [2, 3]. Furthermore, there is evidence of studies on cerebral blood flow (CBF) modulation through tDCS [4].

The exact mechanisms of signaling pathways in humans causing modulation of cortical excitability and cerebrovascular response are not clear. Evidences point to signaling pathway from neurons mediated via glia cells in which neuronal activity elicits a local change in cerebral blood flow (CBF) through the phenomenon of neurovascular coupling (NVC) [5]. At the cellular level, the neurovascular coupling leads to the notion of neurovascular unit (NVU) which is an integrated system of neurons, astrocytes, and vascular cells that facilitate brain homeostasis [6]. Other than neurons, recent in-vitro studies have demonstrated the influence of tDCS on non-neuronal targets like: axons, dendrites, astrocytes and vascular cells [7]. The study presents a physiologically constrained computational model to evaluate vessel volume response to tDCS considering NVU dynamics.

2 Methods

2.1 Hemodynamic Responses During tDCS

Using near-infrared spectroscopic (NIRS) technique, a proxy measure of cerebral blood flow is obtained by measuring oxy- and deoxy hemoglobin concentrations. It is a popular technique of measuring hemodynamic changes during tDCS stimulation in humans. From our previous study in healthy volunteers, it has been observed that there was inter-subject variability in NIRS data during tDCS stimulation [8]. The normalized values of total-hemoglobin for three healthy volunteers during tDCS stimulation are shown in Fig. 1. The tDCS input was a trapezoidal wave of 2 mA current for 10 min with ramp up and ramp down period of 30 s [8].

2.2 Proposed Model

In this work, a model based on compartments of neurovascular unit is proposed to evaluate the pathways of hemodynamic response during tDCS. The block diagram of the model is given in Fig. 2. The NVU model presented by Witthoft and Karni-

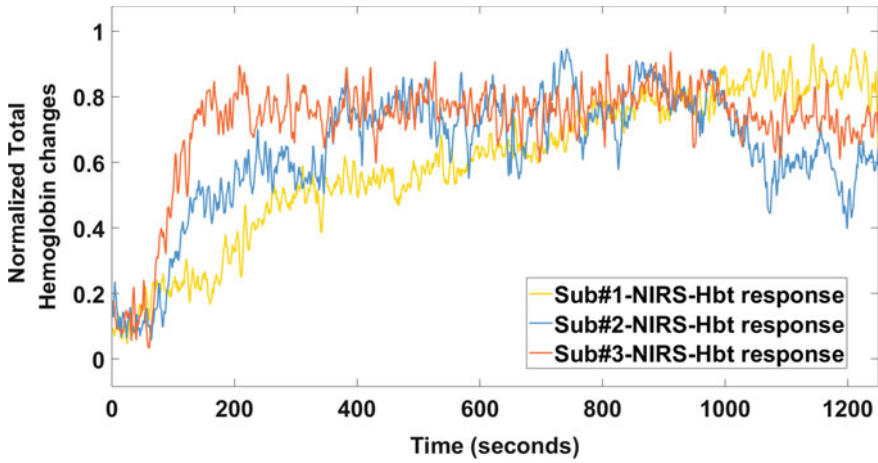


Fig. 1 Normalized total hemoglobin changes during tDCS [8]

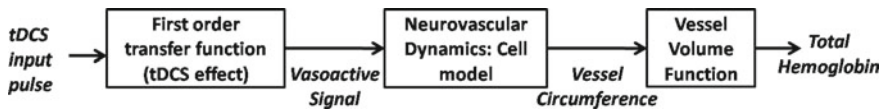


Fig. 2 Block diagram of the proposed model

adakis [9] has been used for analyzing the neurovascular compartment dynamics. The equations governing the pathway from synaptic potassium to vessel circumference has been used for the implementation in MATLAB-Simulink environment. The cell model had 4 compartments: synaptic space, astrocytic space, perivascular space and smooth muscle cell (SMC).

The first order transfer function models the effect of tDCS on vasoactive signal in various compartments of NVU. The vessel volume function assumes the lumped response of vessel circumference and was considered as normalized response for the model. For analyzing the role of tDCS on vessel response, four cases were considered. First, synaptic potassium driven pathway was considered which assumes effect of tDCS on synaptic potassium and equations were solved. Similarly, the model was solved considering the effect of tDCS on astrocytic membrane potential, perivascular potassium and membrane potential of smooth muscle cell.

Additional current term corresponding to tDCS (I_T) has been assumed which is a function of applied tDCS pulse for the astrocytic membrane potential (V_k) [9]. For third pathway, additional potassium concentration in perivascular space corresponding to tDCS ($[K^+]_r$) has been assumed which is a function of applied tDCS pulse. For fourth pathway, additional voltage gated current channel (I_{KV}) that gets affected by tDCS is taken in consideration for equation for SMC's membrane potential (V_m) [9].

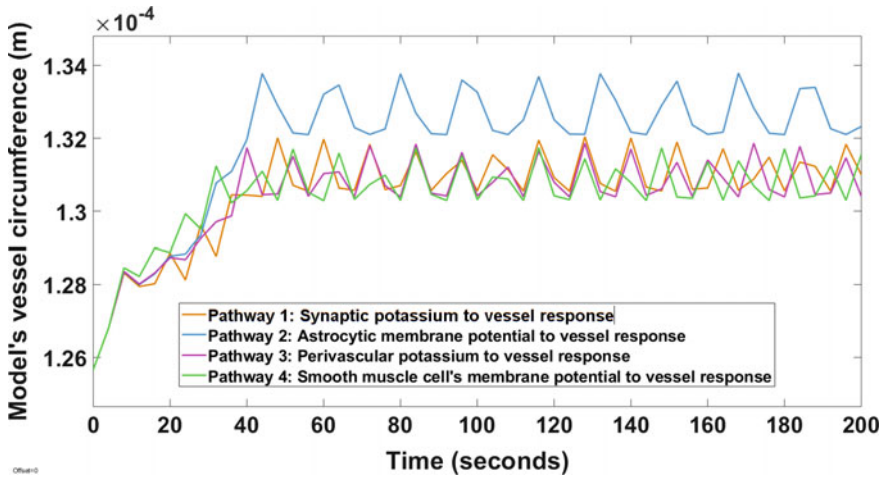


Fig. 3 Vessel response driven through synaptic, astrocytic, perivascular and smooth muscle cell pathways

3 Results

The vessel circumference obtained by solving the model with various pathways considering an input of tDCS wave as trapezoidal wave starting at 5 s (30 s ramp-up and ramp down period) is given in Fig. 3.

4 Discussion

The simulated results in Fig. 3 show the vessel response driven through different compartments of NVU. The response time of the pathways varies with respect to input pulse and first order filter function parameters. The response time (time when steady state oscillations are reached) for different pathways extracted from the plots is given in Table 1. The response time can be an important metric to investigate

Table 1 Response time for different pathways

Pathway	Response time (s)
1. Synaptic potassium to vessel response	48
2. Astrocytic membrane potential to vessel response	44
3. Perivascular potassium to vessel response	41
4. SMC's membrane potential to vessel response	39

the NVU pathways related to the cerebrovascular reactivity to tDCS in health and disease [10]. Due to the complexity of the NVU system, computational modeling informed animal studies will be necessary. This can also establish the safety of tDCS in cerebrovascular diseases which is relevant due to a longer initial dip [11].

5 Conclusion

This study presented a physiologically constrained model to assess various pathways contributing to hemodynamic response considering the influence of anodal tDCS on various cell components of NVU. To the best of our knowledge, this study is the first one to analyze the effects of tDCS at cellular level considering the compartmental dynamics of neurovascular unit. This would further help in analyzing the vascular basis of the brain functions affected by tDCS.

References

1. M.A. Nitsche, W. Paulus, Excitability changes induced in the human motor cortex by weak transcranial direct current stimulation. *J. Physiol.* **527**(3), 633–639 (2000)
2. C.J. Stagg et al., Polarity-sensitive modulation of cortical neurotransmitters by transcranial stimulation. *J. Neurosci.* **29**(16), 5202–5206 (2009)
3. A. Hone-Blanchet, R.A. Edden, S. Fecteau, Online effects of transcranial direct current stimulation in real time on human prefrontal and striatal metabolites. *Biol. Psychiat.* **80**(6), 432–438 (2016)
4. X. Zheng, D.C. Alsop, G. Schlaug, Effects of transcranial direct current stimulation (tDCS) on human regional cerebral blood flow. *Neuroimage* **58**(1), 26–33; H. Poor, *An Introduction to Signal Detection and Estimation*, chap. 4 (Springer, New York, 1985)
5. C. Huneau, H. Benali, H. Chabriat, Investigating human neurovascular coupling using functional neuroimaging: a critical review of dynamic models. *Front. Neurosci.* **9**, 467 (2015)
6. B.V. Zlokovic, Neurodegeneration and the neurovascular unit. *Nat. Med.* **16**(12), 1370 (2010)
7. M. Bikson, W. Paulus, Z. Esmaeilpour, G. Kronberg, M.A. Nitsche, Mechanisms of acute and after effects of transcranial direct current stimulation, in *Practical Guide to Transcranial Direct Current Stimulation* (Springer, Berlin, 2019), pp. 81–113
8. M. Sood et al., NIRS-EEG joint imaging during transcranial direct current stimulation: online parameter estimation with an autoregressive model. *J. Neurosci. Methods* **274**, 71–80 (2016)
9. A. Witthoft, G.E. Karniadakis, A bidirectional model for communication in the neurovascular unit. *J. Theor. Biol.* **311**, 80–93 (2012)
10. U. Jindal, M. Sood, A. Dutta, S.R. Chowdhury, Development of point of care testing device for neurovascular coupling from simultaneous recording of EEG and NIRS during anodal transcranial direct current stimulation. *IEEE J. Trans. Eng. Health Med.* **3**, 1–2 (2015)
11. A. Dutta, A. Jacob, S.R. Chowdhury, A. Das, M.A. Nitsche, EEG-NIRS based assessment of neurovascular coupling during anodal transcranial direct current stimulation—a stroke case series. *J. Med. Syst.* **39**(4), 36 (2015)

Effect of Transcutaneous High-Frequency Alternating Current Over Handgrip Muscle Strength



D. Serrano-Muñoz, J. Gómez-Soriano, D. Martín-Caro, R. López-Peco, J. Taylor, and J. Avendaño-Coy

Abstract High frequency alternating current (HFAC) stimulation has been shown to produce a peripheral nerve conduction block. Currently, all the studies applying HFAC stimulation in clinical studies have employed frequencies below 20 kHz. The main aim of this study was to investigate the neuromodulatory effect of transcutaneous HFAC applied at higher than 20 kHz on maximal handgrip strength (MHS). A randomized, crossover, double-blinded, placebo-controlled trial was conducted in eight healthy volunteers. Transcutaneous stimulation at 30–40–50 kHz and sham stimulation were applied over the ulnar and median nerves for 20 min. MHS was registered prior to, during, immediately after, and 10 min following stimulation. The 30 and 40 kHz HFAC stimulation reduced MHS during the stimulation when compared to baseline, suggesting a partial block of nerve activity. These results open potential development of this non-invasive stimulation technique as a therapy in subjects with motor nerve hyperactivity.

Keywords High-frequency alternating current · Neuromodulation · Handgrip strength · Transcutaneous electric stimulation · Motor nerve block

1 Introduction

In recent years, there have been numerous animal experimentation studies that have investigated the effect of alternating currents using a unmodulated frequency greater

Funding for DSM was provided by the European Regional Development Fund (2019/7375).

D. Serrano-Muñoz (✉) · J. Gómez-Soriano · D. Martín-Caro · R. López-Peco · J. Avendaño-Coy
Toledo Physiotherapy Research Group (GIFTO), Facultad de Fisioterapia Y Enfermería de
Toledo, Universidad de Castilla-La Mancha, Ciudad Real, Spain
e-mail: diego.serrano@uclm.es

J. Taylor

Sensorimotor Function Group At the Hospital Nacional de Paraplégicos, Toledo, Spain

Harris Manchester College, University of Oxford, Oxford, UK

than 1 kHz, on rapid reversible peripheral nerve block without causing damage to the nerve [1].

In humans, there is evidence that unmodulated alternating current applied transcutaneously over the peripheral nervous system up to 20 kHz produces a partial block of the nerve fibers, since it produces a decrease in the grip force [2]. Currently, all clinical studies applying HFAC stimulation [3–6], using either invasive or transcutaneous techniques, have employed frequencies below 20 kHz. However, a study performed by Ackerman et al. [7] in non-human primates has shown that the most effective stimulation frequency to perform a nerve block was in the range of 20–40 kHz.

The purpose of this study was to determine the effect on maximal handgrip strength (MHS) of a non-invasive HFAC stimulus applied at 30, 40 and 50 kHz to the ulnar and median nerves in healthy subjects, compared to sham stimulation.

2 Material and Methods

A randomized, crossover, double-blinded, placebo-controlled trial was conducted in 8 healthy volunteers after signing the informed consent form approved by the Local Ethics Committee.

All interventions were applied for 20 min. Surface electrodes (6 cm × 4 cm, Enraf-Nonius, Netherlands), were placed on the anterior face of the dominant forearm, over the ulnar and median nerves. Participants received four interventions (30–40–50 kHz and sham stimulation), and the order of these interventions was randomized using a web page tool (www.randomizer.org). An electrical stimulator device delivered a biphasic square unmodulated electrical current, at a frequency of 30, 40 and 50 kHz. Intensity was determined by the subjective perception of a “strong but comfortable tingling” sensation reported by the subject, and it was adjusted every two minutes to avoid habituation.

The sham stimulation session was applied using the same stimulation device and electrodes but increasing the intensity during the first 30 s and then decreasing it to zero. A minimal washout period of 24 h was observed. Handgrip strength was measured with a dynamometer (Grip Strength Dynamometer, Tokyo). Three repetitions were registered, and the mean value calculated as the average of the MHS. MHS was measured before, during, immediately after, and 10 min after the end of intervention. The setup is illustrated in Fig. 1.

Statistical analysis was performed with software (SPSS Statistics version 24.0). Two-way repeated ANOVA (time and intervention factors) was performed with a Bonferroni post-hoc test. Values of $p < 0.05$ were considered significant.

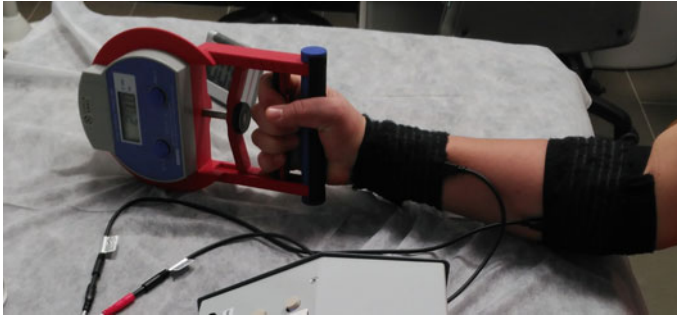
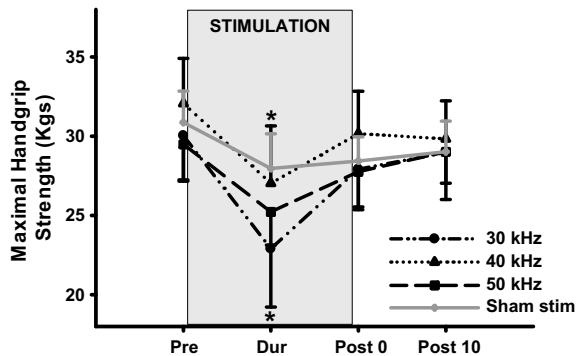


Fig. 1 HFAC electrode placement and handgrip dynamometry assessment

3 Results

Eight subjects (6 females, 75%) with a mean age of 22.5 years (SD 2.5) completed the study. The final current intensity for 50 kHz intervention was 236.1 mA, SD 56.2, for the 40 kHz intervention (207.8 mA, SD 39.9) and for the 30 kHz intervention (159.8 mA, SD 53.4). Stimulation was well tolerated by all subjects and no adverse events related to HFAC stimulation were observed. No differences were reported for MHS between groups before the assigned interventions. Significant differences in the “time” factor ($F = 12.04$; $p = 0.001$) were detected. Specifically, HFAC applied at 30kHz significantly decreased MHS at 15 min during the intervention (22.9 kg, SEM 2.99 $p = 0.001$) when compared to baseline (30.1 kg, SEM 2.5). HFAC applied at 40 kHz, also decreased MHS at 15 min (27.0 kg, SEM 2.99 $p = 0.03$) when compared to baseline (32.1 kg, SEM 2.5). Neither sham stimulation nor 50 kHz HFAC changed MHS. Between-group comparisons did not show any statistical differences. See Fig. 2.

Fig. 2 Effect of high frequency alternating current stimulation on maximal handgrip strength. Sham stimulation (grey), 30 kHz (circle), 40 kHz (triangle), and 50 kHz (square). Data are represented as mean and standard error. * Indicates significant difference when compared to baseline (Pre, $p < 0.05$)



4 Discussion

This is the first study that has applied transcutaneous HFAC at frequencies higher than 20 kHz over the human peripheral nerve with a decrease in MSH with frequencies of 30 and 40 kHz. These results suggest that 30 and 40 kHz HFAC stimulation could evoke a partial nerve conduction block, which has been previously demonstrated using 10 and 20 kHz stimulus [2, 8, 9]. However, stimulation at 50 kHz did not show any effect. Due to the limited number of recruited subjects it is difficult to know if a possible effect of 50 kHz stimulation was not detected because of a type II error. Future studies with a more adequate sample size should highlight the optimal stimulation frequency required to perform the most effective nerve block.

This study also showed that the functional effects of the stimulation were reverted immediately after the end of the stimulation, which supports previous preclinical and clinical studies [10]. These findings could have relevant clinical applications to reduce specific motor activity during stimulation. Furthermore, none of the participants reported adverse effects when HFAC was applied, suggesting that the transcutaneous HFAC stimulation protocol was safe. Temporary nerve block mediated by transcutaneous HFAC could be applied to reduce aberrant nerve activity that leads to specific symptoms of spasticity such as hypertonia, spasms, tremors and chronic pain, although the optimal stimulation frequency remains unknown. HFAC stimulation could have a great potential as a therapeutic tool to treat pathologies characterized by a hyperactivity of the nervous system.

5 Conclusion

Transcutaneous high frequency alternating current stimulation applied at a frequency of 30 and 40 kHz, over the ulnar and median nerves in healthy volunteers reduces muscle handgrip strength during stimulation. HFAC has potential for clinical applications, such as the treatment of spasms, hypertonia or tremors, where a selective stimulation protocol could be effective in partially blocking motor nerve fibers.

Acknowledgements We are grateful for the cooperation of the students of the physiotherapy degree with this project.

References

1. N. Bhadra, K.L. Kilgore, High-frequency electrical conduction block of mammalian peripheral motor nerve. *Muscle Nerve* **32**(6), 782–790 (2005)
2. D. Serrano-Munoz et al., 20-kHz alternating current stimulation: effects on motor and somatosensory thresholds. *J. Neuroeng. Rehabil.* **17**(1), 22 (2020)

3. J. Avendaño-Coy et al., Effect of unmodulated 5-kHz alternating currents versus transcutaneous electrical nerve stimulation on mechanical and thermal pain, tactile threshold, and peripheral nerve conduction: a double-blind, placebo-controlled crossover trial. *Arch. Phys. Med. Rehabil.* **98**(5), 888–895 (2017)
4. M. Camilleri, et al., Selection of electrical algorithms to treat obesity with intermittent vagal block using an implantable medical device. *Surg. Obes. Relat. Dis.* **5**(2), 224–229; discussion 229–230 (2009)
5. M.G. Sarr et al., The EMPOWER study: randomized, prospective, double-blind, multicenter trial of vagal blockade to induce weight loss in morbid obesity. *Obes. Surg.* **22**(11), 1771–1782 (2012)
6. A. Soin, N.S. Shah, Z.-P. Fang, High-frequency electrical nerve block for postamputation pain: a pilot study. *Neuromodulation* **18**(3), 197–205 (2015)
7. D.M. Ackermann et al., Electrical conduction block in large nerves: high-frequency current delivery in the nonhuman primate. *Muscle Nerve* **43**(6), 897–899 (2011)
8. D. Serrano-Munoz et al., Effect of high-frequency alternating current transcutaneous stimulation over muscle strength: a controlled pilot study. *J. Neuroeng. Rehabil.* **15**(1), 103 (2018)
9. Y. Kim, H.J. Cho, H.S. Park, Technical development of transcutaneous electrical nerve inhibition using medium-frequency alternating current. *J. Neuroeng. Rehabil.* **15**(1), 80 (2018)
10. D.M. Ackermann et al., Conduction block of peripheral nerve using high-frequency alternating currents delivered through an intrafascicular electrode. *Muscle Nerve* **41**(1), 117–119 (2010)

A Music Therapy Serious Game with Dynamic Difficulty Adjustment for Stimulating Short-Term Memory



María A. Gutiérrez, Juan J. Rosero, Diego E. Guzmán, and Carlos F. Rengifo

Abstract This paper presents a serious game, called Music Therapy Brain Training (MTBT), intended for stimulating short-term memory. Its main contribution is an algorithm for dynamic difficulty adjustment (DDA) that adapts the challenge to the user's ability to avoid anxiety and boredom. The app was tested on 15 healthy people without medical records of cognitive decline, and on a 76-years-old woman in an early stage of Alzheimer's disease. Nine of the 15 healthy participants and the woman increased their performance session by session, and for the others the data were inconclusive. In addition, for 12 of the healthy participants and the Alzheimer's patient, the level of difficulty established by the DDA, and the user's ability, showed a strong positive linear correlation. This fact, together with self-reported user experience lead us to conclude that DDA kept these 15 participants in Csikszentmihalyi's flow state.

1 Introduction

Serious games are apps that aims at teaching or learning. They provide motivating environments to players, who learn through their mistakes and constant feedback [1]. These type of games are gaining increasing acceptance because of their simplicity and because most people prefer to learn by playing [1]. Although serious games are widely used for education, there are other important areas such as military, research, and health in which these have been successfully used [2].

M. A. Gutiérrez (✉) · J. J. Rosero · D. E. Guzmán · C. F. Rengifo
Universidad del Cauca, Popayán, Colombia
e-mail: mariafe@unicauca.edu.co

J. J. Rosero
e-mail: juanjos@unicauca.edu.co

D. E. Guzmán
e-mail: diegoguzman@unicauca.edu.co

C. F. Rengifo
e-mail: caferen@unicauca.edu.co

© The Author(s), under exclusive license to Springer Nature Switzerland AG 2022
D. Torricelli et al. (eds.), *Converging Clinical and Engineering Research on Neurorehabilitation IV*, Biosystems & Birobotics 28,
https://doi.org/10.1007/978-3-030-70316-5_116

Mobile apps lead to different health benefits, which is why their usage has been constantly growing in recent years. It is also hoped that, in the near future, such technology will lower the cost of health care [3] by using apps to monitor health status, support rehabilitation, encourage healthy habit and promote illness self-management and recovery [4]. Despite the above, statistics indicate that only 35% of current mobile health applications are targeted at disease management and treatment, and within this subset, only 29% care for mental health [5] (Autism, Anxiety, Depression, Alzheimer's, etc.).

In relation to mental health, short-term memory loss is one of the cognitive disorders that affects much of the world's population. Epidemiological data for short-term memory loss are directly related to the different conditions that induce memory impairment [6]. For example, with regard to neurodegenerative diseases, it is estimated that there are about 50 million people in the world who have dementia and that about 10 million new cases are reported each year [7]. In Latin America, dementia in the adult population over the age of 65 was 11% [8].

A deteriorated short-term memory causes isolation, inability to remember when they last fed, and difficulty recognizing their loved ones [9]. In addition, these people show problems with the temporal memorization and reproduction of newly acquired verbal, visual, and spatial information [10].

The rate at which short-term memory impairment increases can be reduced by conventional cognitive rehabilitation [11], which, despite offering favorable results, is exhausting for the patient in the long term [12]. Through music, cognitive rehabilitation can be carried out, as it reduces behavioral problems caused mainly by stress [13]. However, music therapy taught by therapists can be expensive [3]; therefore, it is necessary to propose more affordable options [14].

1.1 Related Work

Information and communication technologies have enabled rehabilitation alternatives for short-term memory loss [15]. These alternatives use serious games to improve cognitive abilities such as memory, attention, and visuo-spatial dexterity [12, 16–18]. In this regard, applications, such as *MyDailyRoutine*, can schedule the user daily tasks in which an avatar must move through different spaces of a house and then perform a sequence of steps in the correct order, such as preparing coffee or washing clothes. The physiotherapists who participated in this research concluded that this serious game has great potential for cognitive rehabilitation of older adults [12].

Lumosity is an application that assesses two important aspects related to short-term memory loss, the visual-spatial part and the ability to remember previously seen elements [16]. Authors of [16] concluded that serious games are more accessible, usable, and challenging for people with short-term memory loss, if such games: (i) are related to the daily life of patients through the use of real images or music, (ii) provide auditory instructions in the native language of the user, and (iii) generate motivating messages when scores are low. Samarasinghe et al. [16] and Vallejo et al.

[17] highlight that there are serious and recreational games for cognitive stimulation, but they do not focus on short-term memory loss.

Navarro et al. [19] presents an application for cognitive stimulation based on fuzzy logic rules, where the therapists redefine, evaluate and adjust the rules that govern the difficulty of the game according to patient's response. The results on patients indicated that the system adapts therapy plans in response to changes in the memory deterioration in an effective manner [19].

Dynamic difficulty adjustment (DDA) make games more enjoyable modifying parameters, scenarios or behaviors [20]. To this end, DDA adapts the game to players abilities to provide a constant challenge. An example of DDA is BACH, a piano learning interface that adjusts challenge according to the brain state of the pianists. As their workload falls below a threshold, the difficulty is automatically increased since it is assumed that the pianist have mastered the material and can handle more cognitive information. Yuksel et al. [21] concludes that the apprentices significantly increased their precision and speed in comparison with the control group; furthermore, the users expressed having learned better with BACH and being satisfied with the times and the dynamic level changes.

In this work, we describe an app named Music Therapy Brain Training (MTBT) for short-term memory stimulation through music therapy. MTBT uses a DDA whose objective is to avoid anxiety and boredom. The first occurs when the user's ability is below the challenge of the game, and the second in the opposite case.

2 Materials and Methods

2.1 Populations

Our study involved three populations. The first comprised by 59 people (30.01 ± 16.56) who used the app one time to assess the difficulty of the questions based on the number of incorrect answers. The second population consisted of 15 people (35.28 ± 11.42) without medical records of cognitive impairment (Memory Alteration Test > 35), who played MTBT twice a day during eight days. The last population was a woman 76 years old in an initial stage of Alzheimer disease, who used the app three times a day during 16 days.

2.2 Software Description

MTBT comprises the 4 modules presented in Fig. 1.

1. *APK MTBT* is a mobile application developed in Android Studio under Java language. *APK MTBT* must be installed on a device with Android 5.1 (LOLLIPOP or higher) whose API level must be equal to or higher than 21. To design MTBT,

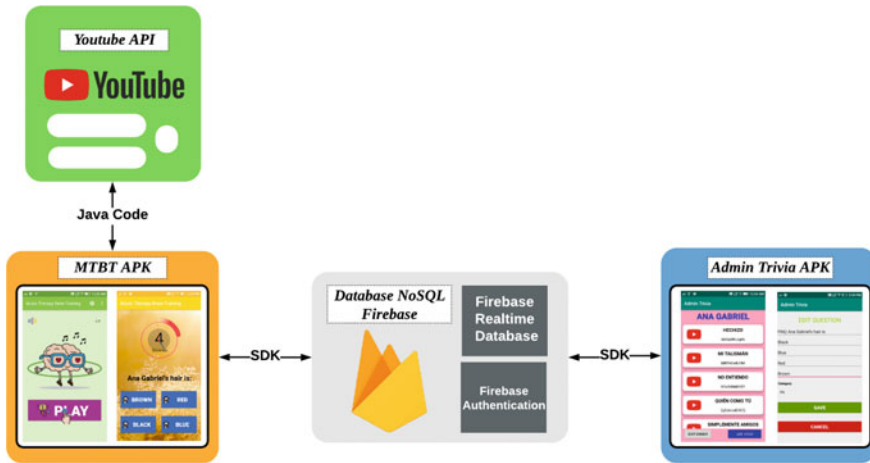


Fig. 1 Interaction between the YouTube API, the MTBT user's interface, firebase and admin Trivia

we followed the guidelines presented in [16], which states that a serious game aimed at people over 60 years should make use of: real images or music, written or auditory instructions, and motivating messages when scores are low.

2. *Firebase module* stores musical genres, singers, songs, and a set of questions and answers related to music videos, personal data of the user and the scores obtained in each therapeutic rehabilitation session, a NoSQL Firebase database known as Firebase Real time Database was selected. Firebase enables user registration and authentication through Firebase Authentication, and additionally saves data to the cloud.
3. *Apk Admin Trivia* was developed in Java. Its purpose is to communicate Apk MTBT with the Firebase module, to create, read, update and delete (CRUD) elements of the database.
4. *Youtube API* is a library for Android whose purpose is to control the user's interaction with the selected music video. In this development, this API was used to create an interface in which the selected video can only be stopped or played, but not forwarded or rolled back. Additionally, the API was used to always view the video in full screen mode to prevent the user from being distracted by other apps.

2.3 The Game

MTBT uses the YouTube API module to play, for one minute, a video of the singer chosen by the user. The video can be paused and played; however, as previously mentioned, it cannot be moved forward or backward. The user answers 12 questions about

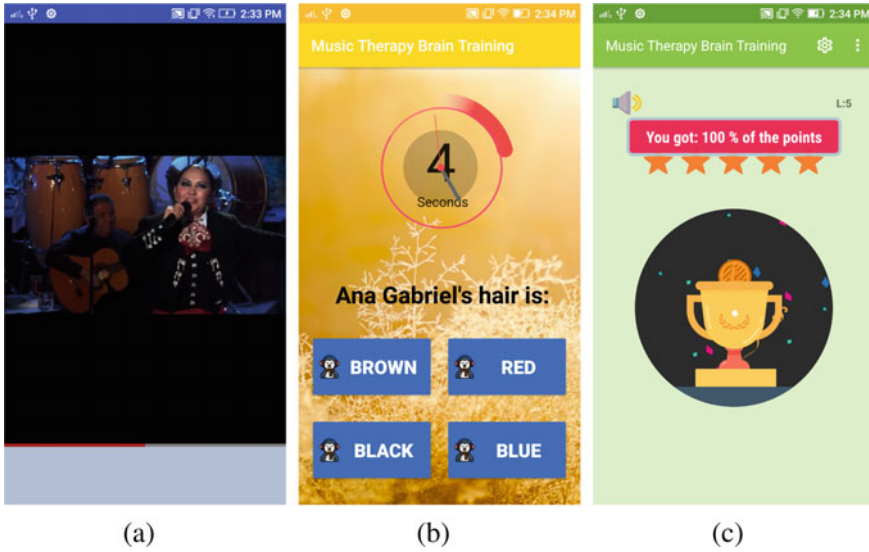


Fig. 2 User interfaces for: **a** video reproduction, **b** questions, **c** score display

the video. These questions are classified into four categories [22]: physical appearance of the singer (PA), details of the video (VD), colors and accessories (CA), and the lyrics of the song (SL). These categories allow the brain to use different functions for intermediate level information processing [23, 24]. In MTBT, the user is instructed to change the video every four days, because repetition leads to acoustic coding, which improves the storage of information [25]. According to [26], the compressibility in the information, that is, the encoding in a more compact representation, simplifies the memorization and increases the amount of information retained in the short-term memory (Fig. 2).

2.4 Dynamic Difficulty Adjustment Algorithm

The DDA was parameterized using the scores and average time to answer a question. This data was collected from a population of 59 people who used the app one time. The scores were used to assess the difficulty of each of the four categories of questions previously mentioned. The resulting categories from the easiest to the hardest were SL, VD, CA and PA. The easiest questions were assigned to the lowest levels, and the number of questions from one level to the next was increased by two. The resulting distribution of questions per level are presented in Table 1. The required score to pass a level is defined as $1 \times n_{SL} + 2 \times n_{VD} + 3 \times n_{CA} + 4 \times n_{PA}$, where n_{SL} , n_{VD} , n_{CA} , and n_{PA} are the number of questions of a given level that belong to the categories SL, VD, CA, and PA, respectively.

Table 1 Number of questions and score for each game level

Level	Questions per category				Score
	n_{SL}	n_{VD}	n_{CA}	n_{PA}	
1	2	0	0	0	2
2	1	2	1	0	8
3	2	2	1	1	13
4	3	2	2	1	17
5	3	3	2	2	23
6	3	3	3	4	30

Table 2 Maximal time to answer the questions of each level

Level	n_i	t_i	$n_i \times t_i$
1	2	15.606	31.212
2	4	7.550	30.200
3	6	6.578	39.468
4	8	5.869	46.952
5	10	5.463	54.630
6	12	4.613	55.356

The average time to answer a question, obtained by the 59 participants were ranked from lowest to highest and stored in an array. Positions 10, 20, 30, 40, 50, and 59 of the array defined the parameters $t_6, t_5, t_4, t_3, t_2,$ and t_1 , respectively. $n_i \times t_i$ defines the maximal time to answer the questions of the level i , where n_i is the number of questions of the level i (Table 2).

The DDA includes two reward system to avoid frustration: *More Time* and *Bonus*. The first is activated when the player has remained in the same level for two consecutive sessions. In such a case, the time allotted to answer a question is that of the previous level. *Bonus* applies only when *More Time* is active and the user has increased his score, but this new score is not enough to pass the current level. In this scenario, if the user correctly answers an additional question, he is promoted to the next level.

3 Results and Discussion

3.1 Performance Versus Time

The user's scores obtained each day were averaged and then linear regression was applied. For the second and third populations, linear regression was made using 8

Table 3 Users' performance

User	Pearson	p-value
1	0.689	0.029
2	0.635	0.045
3	0.815	0.007
4	0.852	0.004
5	0.433	0.142
6	0.874	0.002
7	0.761	0.014
8	0.346	0.201
9	0.398	0.164
10	0.353	0.196
11	0.741	0.018
12	0.811	0.007
13	0.151	0.361
14	-0.010	0.510
15	0.567	0.072
Alz.	0.897	< 0.001

and 16 days respectively. Columns two and three of Table 3 present the Pearson's coefficients (right tail test) and the corresponding *p*-values. Participants 1, 2, 3, 4, 6, 7, 11, 12, and Alzheimer exhibited positive correlation with *p*-values lower than 0.05, indicating that their performance increased session by session. For the other users no statistical evidence of correlation between user's performance and the number of training sessions was found.

Figure 3 shows that median scores (horizontal red line), of the 15 healthy participants, increased during the first four days. In day five, however, all the median score decreased because the singer appearing on the videos changed. As a consequence, the users required to store and retrieve new information from their memories to answer the questions. The interquartile ranges (height of the blue boxes) decreased with time, which indicates that training tends to equal the performance of the players.

Figure 4 indicates that the score of the Alzheimer's woman increased linearly with time. For this participant, the Pearson's correlation coefficient was 0.897 (*p* < 0.001).

3.2 Flow State Assessment

To assess the balance between game's challenge and user's ability, a new linear regression was made, this time involving the difficulty level and the inverse of the average time employed to answer the questions of a given session – the shorter

Fig. 3 Score versus day for the healthy participants

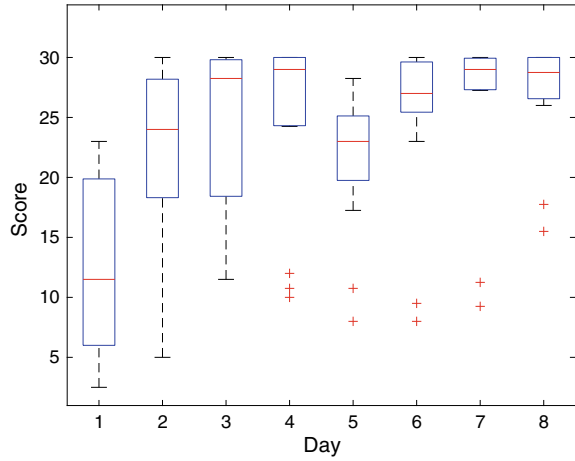
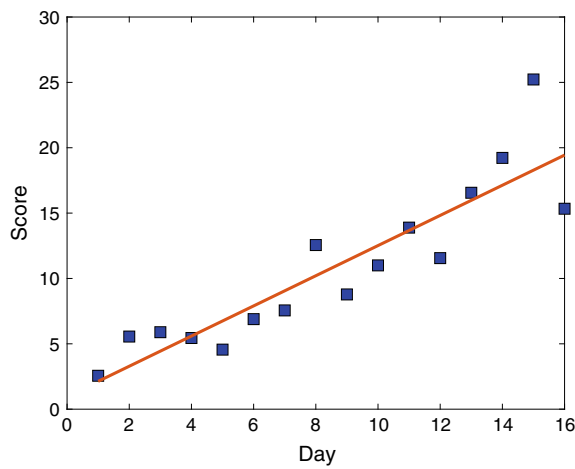


Fig. 4 Score versus day for the participant with Alzheimer



this average time the greater the ability. The columns two and three of the Table 4 present the Pearson’s coefficients and the corresponding p -values. All participants, except the 4, 14, and 15 presented positive correlations with $p < 0.05$, which suggest the proposed DDA increased difficulty level in proportion to user’s ability. Column four presents user’s self-perception of gaming experience on the scale: high anxiety (HA), moderate anxiety (MA), little anxiety (LA), comfort (C), little boredom (LB), moderate boredom (MB), and high boredom (HB). According to the flow theory of Csikszentmihalyi [27], the linearity between challenge and ability for users 1, 2, 3, 5 to 13, and Alzheimer, and their gaming experience, suggest that the DDA kept them in the flow state [28].

Table 4 Users' performance

User	Pearson	<i>p</i> -value	Experience
1	0.893	0.001	C
2	0.976	< 0.001	C
3	0.876	0.002	C
4	0.409	0.157	C
5	0.973	< 0.001	C
6	0.880	0.002	LA
7	0.817	0.007	C
8	0.891	0.001	C
9	0.799	0.009	C
10	0.765	0.013	C
11	0.797	0.009	HB
12	0.755	0.015	C
13	0.882	0.002	LA
14	0.618	0.051	C
15	0.480	0.114	C
Alz.	0.981	< 0.001	C

Fig. 5 Score versus performance for the participant with Alzheimer

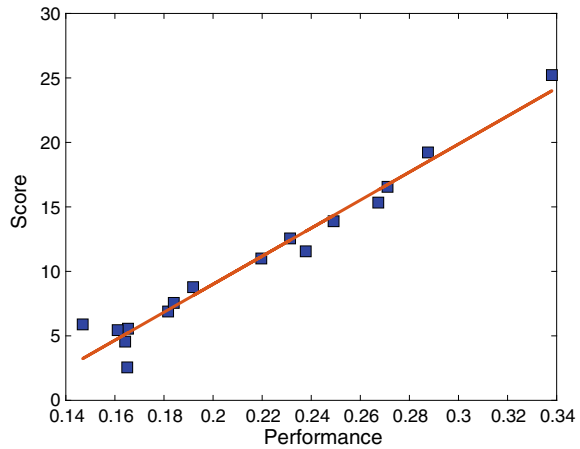


Figure 5 indicates a linear relationship between score and performance of the Alzheimer's woman. For this participant, the Pearson's correlation coefficient was 0.981 ($p < 0.001$).

Table 3 shows that participants 1 to 7, 11, 12 and Alzheimer increased their score as the number of sessions increased. The excellent results obtained by the participant with Alzheimer's were mainly due to the fact that she strictly followed the training schedule, which resulted in a greater ability to remember; supporting the theory

of [29]. The author of [29] states that in order to achieve efficient memorization, it is advisable to repeatedly review the information to be remembered at an established time. Participants 9, 10, and 13 declare that they did not follow the rule to change the video every four days, and they decided to change the video every day. This explains their poor performance, given that the questions and answers for each video were different. Additionally, users 8 and 14 expressed that external factors prevented them from concentrating while using MTBT, and consequently, their performance did not increase significantly from one session to another. Participant 15 presented a modest correlation (0.567) with a p -value equal to 0.072, which is small but greater than the threshold of 0.05.

In addition to the performance analysis described in the above paragraph, we analyzed the relationship between score and the inverse of the average time required to answer a question. Table 4 shows that the proposed DDA led 12 of 15 participants to a linear relationship between score and ability, and furthermore, most of these participants expressed that they did not experience anxiety or boredom. We highlight that for the Alzheimer participant, in addition to her self-reported comfortable experience with TMBT, her caregiver mentioned that at the end of the different sessions, she expressed happiness and satisfaction when evoking the rhythm and lyrics of the song.

4 Conclusion

Despite the fact that only one participant with cognitive impairment participated in the present study, we concluded that music therapy through mobile applications could be a viable option for short-term memory therapy. A key factor in developing these type of applications is to include a DDA. This is because by preventing anxiety and boredom, the chances of maintaining patient adherence to therapy are increased. In subsequent works, we plan to increase the population with impaired short-term memory and, especially, to evaluate, through standardized tests, the effect of the proposed music therapy approach.

References

1. C.R. Tejada, D.A.G. Peña, P.A.O. Valencia, Estado del arte de los juegos serios sobre plataforma móvil android para el aprendizaje del modelado de software. *Ingeniería solidaria* **13**(23), 138–150 (2017)
2. S. Cruz-Lara, B. Fernández Manjón, C. Vaz De Carvalho, Enfoques Innovadores en Juegos Serios, *IEEE VAEP RITA* **1**(1), pp. 19–21 (2013). [Online]. Available: <https://hal.inria.fr/hal-00820350>
3. A. Gulliver, G. Pike, M. Banfield, A.R. Morse, N. Katruss, M. Pescud, M. McMaster, H. Valerius, S. West, Evaluation of the music engagement program for people with Alzheimer's disease and dementia: study protocol for a pilot trial. *Contemp. Clin. Trials Commun.* **15**, 100419 (2019)

4. L. Ramey, C. Osborne, D. Kasitinon, S. Juengst, Apps and mobile health technology in rehabilitation: the good, the bad, and the unknown. *Phys. Med. Rehabil. Clinics* **30**(2), 485–497 (2019)
5. M. Aitken, Patient adoption of mhealth: use, evidence and remaining barriers to mainstream acceptance. IMS institute of health informatics. Retrieved 17 July 2016 (2015)
6. M. Cascella, Y. Al Khalili, Short term memory impairment, 2019. [Online]. Available: <http://europepmc.org/books/NBK545136>
7. D.B. Martínez, M.G. Soldevilla, A.P. Santiago, J.T. Martínez, Enfermedad de alzheimer. *Med.-Programa de Formación Médica Continuada Acreditado* **12**(74), 4338–4346 (2019)
8. C.Z. Sánchez, M.O.C. Sanabria, M.Z. Sánchez, P.A.C. López, M.S. Sanabria, S.H. Hernández, K.V. Vanegas, A.U. Valera, Prevalencia de demencia en adultos mayores de américa latina: revisión sistemática. *Rev. Esp. Geriatr. Gerontol.* **54**(6), 346–355 (2019)
9. P. Adolfsson, H. Lindstedt, I. Pettersson, L.N. Hermansson, G. Janeslätt, Perception of the influence of environmental factors in the use of electronic planning devices in adults with cognitive disabilities. *Disabil. Rehabil. Assist. Technol.* **11**(6), 493–500 (2016)
10. S. Majerus, M. Van der Linden, Memory disorders in children. *Handb. Clin. Neurol.* **111**, 251–255 (2013)
11. R. Matilla-Mora, R.M. Martínez-Piédrola, J.F. Huete et al., Eficacia de la terapia ocupacional y otras terapias no farmacológicas en el deterioro cognitivo y la enfermedad de alzheimer. *Rev. Esp. Geriatr. Gerontol.* **51**(6), 349–356 (2016)
12. R. Baranyi, R. Perndorfer, N. Lederer, B. Scholz, T. Grechenig, Mydailyroutine-a serious game to support people suffering from a cerebral dysfunction, in *2016 IEEE International Conference on Serious Games and Applications for Health (SeGAH)* (IEEE, 2016), pp. 1–6
13. M.G. Gallego, J.G. García, Music therapy and Alzheimer’s disease: cognitive, psychological, and behavioural effects. *Neurología (English Edition)* **32**(5), 300–308 (2017)
14. W.C. Ung, F. Meriaudeau, T.B. Tang, Optimizing mental workload by functional near-infrared spectroscopy based dynamic difficulty adjustment, in *40th Annual International Conference of the IEEE Engineering in Medicine and Biology Society (EMBC)* (IEEE 2018)
15. N. Abolhassani, B. Santos-Eggimann, A. Chiolero, V. Santschi, Y. Henchoz, Readiness to accept health information and communication technologies: a population-based survey of community-dwelling older adults. *Int. J. Med. Inf.* **130**, 103950 (2019)
16. H. Samarasinghe, W. Weerasooriya, G. Weerasinghe, Y. Ekanayaka, R. Rajapakse, D. Wijesinghe, Serious games design considerations for people with alzheimer’s disease in developing nations, in *2017 IEEE 5th International Conference on Serious Games and Applications for Health (SeGAH)* (IEEE, 2017), pp. 1–5
17. V. Vallejo, P. Wyss, A. Chesham, A.V. Mitache, R.M. Müri, U.P. Mosimann, T. Nef, Evaluation of a new serious game based multitasking assessment tool for cognition and activities of daily living: Comparison with a real cooking task. *Comput. Hum. Behav.* **70**, 500–506 (2017)
18. P. Robert, A. König, H. Amieva, S. Andrieu, F. Bremond, R. Bullock, M. Ceccaldi, B. Dubois, S. Gauthier, P.-A. Kenigsberg et al., Recommendations for the use of serious games in people with Alzheimer’s disease, related disorders and frailty. *Front. Aging Neurosci.* **6**, 54 (2014)
19. J. Navarro, F. Doctor, V. Zamudio, R. Iqbal, A.K. Sangaiyah, C. Lino, Fuzzy adaptive cognitive stimulation therapy generation for Alzheimer’s sufferers: towards a pervasive dementia care monitoring platform. *Futur. Gener. Comput. Syst.* **88**, 479–490 (2018)
20. M.P. Silva, V. do Nascimento Silva, L. Chaimowicz, Dynamic difficulty adjustment on moba games. *Entertain. Comput.* **18**, 103–123 (2017)
21. B.F. Yuksel, K.B. Oleson, L. Harrison, E.M. Peck, D. Afergan, R. Chang, R.J. Jacob, Learn piano with Bach: an adaptive learning interface that adjusts task difficulty based on brain state, in *Proceedings of the 2016 Chi Conference on Human Factors in Computing Systems* (2016), pp. 5372–5384
22. M.P. I.G. Carrillo, M.d. J.J. González, J.J. Fradera, N.E.M. Pérez, J.A.G. Soto, Intervención de musicoterapia en la memoria de corto plazo del adulto mayor sin deterioro cognitivo. *Revista de Investigación Científica en Psicología* (2019)
23. M. Kundera, *La memoria humana* (Banco Central de Venezuela, Caracas, 2010)

24. B. Ibarrola, *Aprendizaje emocionante: neurociencia para el aula*. Ediciones SM España, vol. 5 (2014)
25. M. Jáuregui, E. Razumiejczyk, Memoria y aprendizaje: una revisión de los aportes cognitivos. *Psicología y psicopedagogía* **26**, 20–44 (2011)
26. M. Chekaf, N. Cowan, F. Mathy, Chunk formation in immediate memory and how it relates to data compression. *Cognition* **155**, 96–107 (2016)
27. M. Csikszentmihalyi, *Flow: The Psychology of Optimal Experience* (Harper Perennial Modern Classics, 1990)
28. J. Chen, Flow in games (and everything else). *Commun. ACM* **50**, 31–34 (2007). [Online]. Available: <http://doi.org/10.1145/1232743.1232769>
29. B. Tabibian, U. Upadhyay, A. De, A. Zarezade, B. Schölkopf, M. Gomez-Rodriguez, Enhancing human learning via spaced repetition optimization. *Proc. Natl. Acad. Sci.* **116**(10), 3988–3993 (2019)

Feasibility of Transcutaneous Spinal Cord Stimulation Combined with Robotic-Assisted Gait Training (Lokomat) for Gait Rehabilitation of an Incomplete Spinal Cord Injury Subject



N. Comino-Suárez, J. Gómez-Soriano, D. Serrano-Muñoz, A. Megía-García, A. J. del Ama, A. Gil-Agudo, and J. C. Moreno

Abstract The aim of this study was to analyze the feasibility and safety of transcutaneous spinal cord stimulation (tSCS), applied over T11–T12 vertebral level combined with robotic-assisted gait training in a volunteer with incomplete spinal cord injury (SCI). We performed 20 sessions, with 30 min in Lokomat, which first 20 min tSCS was applied. The outcomes measured were the lower extremity motor score (LEMS), modified Ashworth scale (MAS), the lower limbs strength by a hand

This project (Motor rehabilitation of spinal cord injury by combined application of robotic exoskeleton, spinal cord stimulation and cortical modulation–RECODE-) has been granted by Ministerio de Economía, Industria y Competitividad in the EXPLORA 2017 program. Grant number: DPI2017-91117-EXP.

N. Comino-Suárez (✉) · J. C. Moreno
Neural Rehabilitation Group of the Spanish National Research Council, Madrid, Spain
e-mail: natalia.comino@cajal.csic.es

J. C. Moreno
e-mail: jc.moreno@csic.es

A. Megía-García · A. Gil-Agudo
Biomechanics and Technical Aids Department, National Hospital for Spinal Cord Injury, Toledo, Spain
e-mail: amegiag@externas.sescam.jccm.es

A. Gil-Agudo
e-mail: amgila@sescam.jccm.es

J. Gómez-Soriano · D. Serrano-Muñoz
Physiotherapy Research Group From Toledo, University of Castilla-La Mancha, Toledo, Spain
e-mail: julio.Soriano@uclm.es

D. Serrano-Muñoz
e-mail: diego.serrano@uclm.es

A. J. del Ama
University Rey Juan Carlos, Madrid, Spain
e-mail: antonio.delama@urjc.es

dynamometer, functional outcomes using 10 m walk test (10MWT), timed up and go test (TUG), Walking index of spinal cord injury (WISCI-II), the spinal cord independence measure (SCIM-III) and pain perceived during treatment. The assessment was done at baseline, after and follow-up at 4 weeks post-treatment. The preliminary results support that the tSCS combined with Lokomat seems to be a safety therapy and there was not a relationship between the level of stimulation intensity and pain perceived.

Keywords Neuromodulation · Spinal cord injury · Robotics · tSCS · Gait

1 Introduction

Spinal cord injury (SCI) often results in complete or partial paralysis, having a profound physical, psychological and socioeconomic impact on the affected person's life [1]. Robot-assisted gait training has emerged as a promising therapy for improving walking ability, balance and motor function in neurological patients. The mechanism of this approach is due to the execution of repetitive and task-specific training able to generate appropriate afferent input, activating the central pattern generators (CPG) in the lumbosacral spinal cord and inducing plastic changes [2]. An additional non-invasive approach for the stimulation of spinal locomotor circuits is the transcutaneous spinal cord stimulation (tSCS), which applied below the level of lesion in SCI patients allows the activation of rhythmic, flexo-extension movements in the paralyzed lower limbs [3]. The aim of the present study was to analyze the feasibility and safety of a program of 20 sessions of 30 Hz tSCS combined with Lokomat in an individual with incomplete SCI.

2 Material and Methods

2.1 *Subject and Clinical Data*

The participant was a 56 year-old man (from the National Hospital for Spinal Cord Injury, Toledo, Spain) who suffered a postsurgical, incomplete SCI two months before the enrollment. The level of injury was T10 and classified as grade D on the American Spinal Injury Association Impairment Scale (AIS). The subject was a clinically stable adult, without concomitant pathologies, metallic implant or electronic devices in the area of stimulation. A mild grade of spasticity (grade 1 on MAS) and inability to stand or walk with or without technical aids (WISCI-II level was 0 and SCIM-III score was 67 points). The study was approved by the local ethics committee and met the requirements of the Helsinki declaration. The subject signed the written informed consent form to participate in the experiment.

2.2 Intervention

The patient received twenty sessions, 5 sessions per week, of 30 min with Lokomat (Hocoma AG, Volketswil, Switzerland) and 20 min of tSCS was applied at the beginning of each session. During Lokomat training, the patient was fitted with a harness and was unloaded by 50% of his body weight. The parameters were adjusted according to the physical characteristics of the patient. The training speed varied between 1 and 2 km/h, being slow at the beginning of session and progressively increased while maintaining gait quality. tSCS was delivered using self-adhesive electrodes (ValuTrode, Axelgaard Manufacturing Co, LTD, Fallbrook, USA), the anode electrode (9 cm × 5 cm) was placed over the T11–T12 intervertebral space and two interconnected reference electrodes (9 cm × 5 cm) were placed symmetrically at both sides of the umbilicus. A biphasic square current was applied using an electro-stimulator (DS8R, Digitimer, UK) with a frequency of 30 Hz and a pulse duration of 1 ms. The electrode placement and current parameters has been used in previous studies [3, 4]. For the stimulation intensity, we used the maximum intensity tolerated by the patient.

2.3 Outcome Measures

Two blinded therapists performed the assessment before, after and a follow-up at 4 weeks post-intervention. As primary outcome, the LEMS was obtained by a trained doctor. As secondary outcomes, the spasticity using MAS, gait function with 10MWT, TUG, WISCI-II scale, grade of disability with SCIM-III, and level of perceived pain during the intervention was measured after each session using the visual analogue scale (VAS). The strength in the lower limbs was calculated by the average of three maximal voluntary isometric contractions of quadriceps (Q) and tibialis anterior (TA) with a hand dynamometer (Micro fet 2TM).

3 Results

The patient completed the twenty-programmed sessions. The intensity of the tSCS intervention varied over sessions, with a range of 13–35 mA. The pain perceived during the program was 2.16 ± 1.29 points (mean \pm standard deviation) in VAS. The correlation between the intensity of current applied and perceived pain during the intervention was analyzed (Pearson' r) with no significant results (-0.21 $p = 0,374$) (see Fig. 1).

All functional outcomes compared with baseline results experienced improvements post-treatment and at follow-up at 4 weeks (see Tables 1 and 2).

Fig. 1 Bar and line chart. Relationship between patient level of pain (left axis) and the intensity (mA) applied during therapy (right axis)

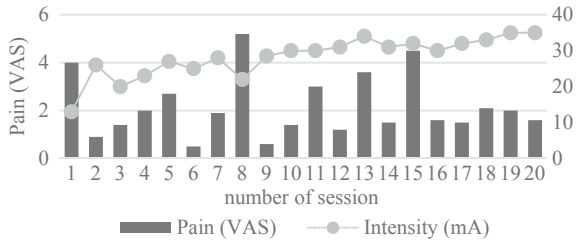


Table 1 Clinical outcomes

Outcome	Baseline	Post-treatment	Follow-up
LEMS (total)	24	30	34
10MWT (s)	NA	31	22
TUG (s)	NA	38	30
WISCI-II	0	8	16
SCIM-III	67	69	78
MAS (left)	1	1	1
MAS (right)	1	1	1

Note Lower extremity motor score (LEMS), 10 m walk test (10MWT), seconds (s), Not available (NA), Timed up and go test (TUG), Walking index of spinal cord injury (WISCI-II), Spinal cord independence measure version III (SCIM-III), Modified Ashworth scale (MAS)

Table 2 Lower limbs muscle strength (kilograms)

Muscle	Baseline	Post-treatment	Follow-up
Q (left)	29.93	42	56.63
Q (right)	16.07	24.40	27.6
TA (left)	20.17	29.30	29.73
TA (right)	0	0	0

Note Quadriceps (Q), tibialis anterior (TA)

Regarding adverse effects, the patient reported more discomfort, itching and reddens skin in the area of spinal electrode in six of twenty sessions (6th–8th, 11th, 12th and 19th sessions).

4 Discussion

tSCS limitations are the uncomfortable side effects described as pain, paresthasias or motor contraction in the area of stimulation. The results obtained in this incomplete

SCI subject suggest that the application of 30 Hz of tSCS seems to be safety, generating slight discomfort or pain, which is not associated with higher or lower levels of current intensities. The present results showed positive effects in clinical outcomes assessed. After the intervention, the strength in the lower limbs was increased 10 points in the total LEMS score. The patient was able to walk using a walker, reducing 9 s the time in 10MWT and 8 s in TUG. As well as in the functional independence, with an increase of 16 points in WISCI-II and 11 points in SCIM-III. However, compared with the results obtained in the study of Hofstoetter et al. 2014 [5] no change was found in the grade of spasticity in this subject. Despite the positive effects on clinical outcomes, functional improvements cannot being attributed to the tSCS as an adjunct to the robotic therapy. Further studies counting with a control group and larger subject population are required to analyze the effectiveness of this therapy.

5 Conclusion

tSCS is a new therapy with minimal side effects, which combined with robotic-assisted therapy, has a great potential for recovery of motor function and walking ability after SCI.

References

1. A. Domingo, T. Lam, Reliability and validity of using the Lokomat to assess lower limb joint position sense in people with incomplete spinal cord injury. *J. Neuroeng. Rehabil.* **11**, 167 (2014)
2. M. Hubli, V. Dietz, The physiological basis of neurorehabilitation–locomotor training after spinal cord injury. *J. Neuroeng. Rehabil.* **10**, 5 (2013)
3. U.S. Hofstoetter, M. Krenn, S.M. Danner, C. Hofer, H. Kern, W.B. McKay, et al., Augmentation of voluntary locomotor activity by transcutaneous spinal cord stimulation in motor-incomplete spinal cord-injured individuals. *Artif. Organs.* **39**(10), E176–E186. Available from: <https://doi.org/10.1111/aor.12615>
4. K. Minassian, U.S. Hofstoetter, S.M. Danner, W. Mayr, J.A. Bruce, W.B. McKay et al., Spinal rhythm generation by step-induced feedback and transcutaneous posterior root stimulation in complete spinal cord-injured individuals. *Neurorehabil. Neural Repair.* **30**(3), 233–243 (2016)
5. U.S. Hofstoetter, W.B. McKay, K.E. Tansey, W. Mayr, H. Kern, K. Minassian, Modification of spasticity by transcutaneous spinal cord stimulation in individuals with incomplete spinal cord injury. *J. Spinal Cord Med.* [Internet] **37**(2), 202–211. Available from: <https://pubmed.ncbi.nlm.nih.gov/24090290>

On Spatial Whitening of High-Density Surface Electromyograms in Compound Muscle Action Potential Decomposition by Differential Evolution



Matej Kramberger and A. Holobar

Abstract We propose a differential evolution based decomposition of Compound Muscle Action Potential (CMAP), recorded by high-density surface electromyograms (HDEMG) and test it on spatially whitened and non-whitened synthetic HDEMG signals. We simulated three different levels of muscle stimulation with 136, 168 and 200 activated motor units (MUs), five different levels of MU synchronization and two different noise levels. We show that spatial whitening of HDEMG improves the decomposition of CMAP but in low MU synchronization levels only. In noiseless signals and 10% MU synchronization the number of identified MUs increased from 3.4 ± 2.3 to 10.8 ± 2.8 MUs, from 5.8 ± 2.3 to 12.0 ± 0.0 MUs and from 5.8 ± 0.8 to 12.4 ± 1.7 MUs when spatial whitening was applied to HDEMG signals with 136, 168 and 200 active MUs. At 20% MU synchronization, the number of identified MUs increased from 7.6 ± 2.9 to 12.2 ± 3.6 MUs, from 10.2 ± 2.8 to 12.6 ± 3.8 MUs and from 8.6 ± 3.0 to 14.4 ± 3.3 MUs. Similar results were observed for signals with SNR of 20 dB.

1 Introduction

In the last two decades, motor unit (MU) firing identification from high-density surface electromyograms (HDEMG) has gained considerable research interest [3, 7]. However, this MU identification was mainly limited to isometric voluntary muscle contractions where MU fire asynchronously. Therefore, Independent Component Analysis (ICA) approaches were used to decompose HDEMG into contributions of individual MUs [7].

This work was supported by the Slovenian Research Agency (projects J2-1731 and L7-9421 and Programme funding P2-0041).

M. Kramberger (✉) · A. Holobar
System Software Laboratory, Faculty of Electrical Engineering and Computer Science,
Institute of Computer Science, University of Maribor, Maribor 2000, Slovenia
e-mail: matej.kramberger@um.si

© The Author(s), under exclusive license to Springer Nature Switzerland AG 2022
D. Torricelli et al. (eds.), *Converging Clinical and Engineering Research*
on *Neurorehabilitation IV*, Biosystems & Birobotics 28,
https://doi.org/10.1007/978-3-030-70316-5_118

741

In this study, we propose an alternative approach towards CMAP decomposition that is based on improved differential evolution (DE) algorithm [2]. This method requires a priory knowledge of MU action potential (MUAP) shapes and uses them to decompose CMAP into contributions of different MUs. The required MUAP shapes can be estimated from voluntary contractions by previously introduced ICA algorithms [8]. We test the CMAP decomposition on spatially whitened and non-whitened synthetic HDEMG signals, as spatial whitening has been demonstrated to facilitate MU firing identification in voluntary contractions [8].

2 CMAPs Simulation

We used volume conductor model in [4] to simulate skeletal muscle with 130 mm long fibers, distributed in elliptical cross-section of 30×15 mm, with the average fiber density of 20 fibres/mm² [1]. In total, 200 MUs were simulated, with many small and exponentially fewer large MUs [6]. The number of fibers per MU ranged from 24 for the smallest MU to 2408 for the largest MU. The skin and the subcutaneous fat layer were 1 mm and 4 mm thick, respectively.

The simulated array of 10×9 circular surface electrodes with 1 mm diameter and interelectrode distance of 5 mm was centered above the innervation zone. Three different stimulation levels were simulated, resulting in 136, 168 and all 200 MUs activated per stimulus. Sampling frequency was set to 2048 samples/s and MU firings were normally distributed around the stimulus time with the standard deviation set to 13, 7, 3, 1 and 0 ms, resulting in 10, 20, 40, 80 and 100% synchronization of MU firings. Five different simulation runs were conducted, each having randomly distributed MUs within the simulated muscle tissue. Generated CMAPs with different synchronization of MUs are exemplified in Fig. 1.

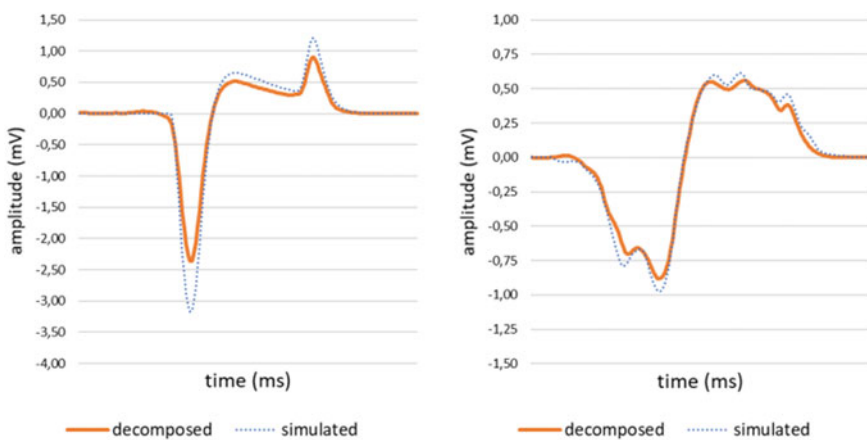


Fig. 1 Decomposed and simulated CMAP with 168 active MUs on non-whitened HDEMG channel (1, 4) for 100% (left) and 40% (right) MU synchronization

3 The Proposed Method

CMAP decomposition was based on an improved version of jDERpo algorithm [2], modified by changing the data representation, mutation and crossover operators to binary form [5]. The population individual was represented as a sequence of binary genes where each gene comprised ten bits, with the first two bits encoding MU inclusion and the remaining eight bits encoding MU firing time within the CMAP. In the fitness function, binary gene sequence was converted to decimal form and estimated CMAP was composed from selected MUAPs at selected positions. Estimated CMAP was then compared against the measured one by using Normalized Root Mean Square Error (NRMSE) estimator.

In order to speed up the CMAP decomposition, the NRMSE value was computed on 16 HDEMG channels positioned on the crossings of the 1st, 4th, 7th and 10th row with the 1st, 3th, 7th and 9th column. Control parameters of the jDERpo algorithm [2] were set to: population size $NP = 100$, initial crossover rate $CR = 0.4$, initial scale factor $F = 0.05$, $\tau_1 = 0.1$, $\tau_2 = 0.1$, $F_{upp} = 1.0$, $CR_{upp} = 1.0$, $p = 0.4$ and the number of generations $G = 3500$. The population was randomly initialized for all MUs inclusions and firing times.

We have pre-processed all simulated CMAPs and MUAPs by spatial whitening [7]. For this purpose, the HDEMG signals were extended by adding 9 delayed repetitions of each HDEMG channel and whitened. MU firing identification tolerance was set to 1 ms.

4 Results

When averaged across all the simulation runs and MU synchronization levels in noiseless signals, 19.9 ± 15.5 MUs, 19.5 ± 14.3 MUs and 19.0 ± 12.9 MUs were accurately identified from CMAPs with 136, 168 and 200 active MUs, respectively. With 20 dB Gaussian noise, the method identified 19.8 ± 13.4 MUs, 19.1 ± 14.1 MUs and 19.4 ± 13.8 MUs. The number of identified MU firings increased with MU synchronization (Figs. 2, 3 and 4).

Spatial whitening [7, 8] has improved decomposition of CMAPs but on low MU synchronization levels only. At MU synchronization level greater than 40%, decomposition with spatial whitening proved to be less successful than the decomposition of the non-whitened HDEMG signals (Figs. 2, 3 and 4).

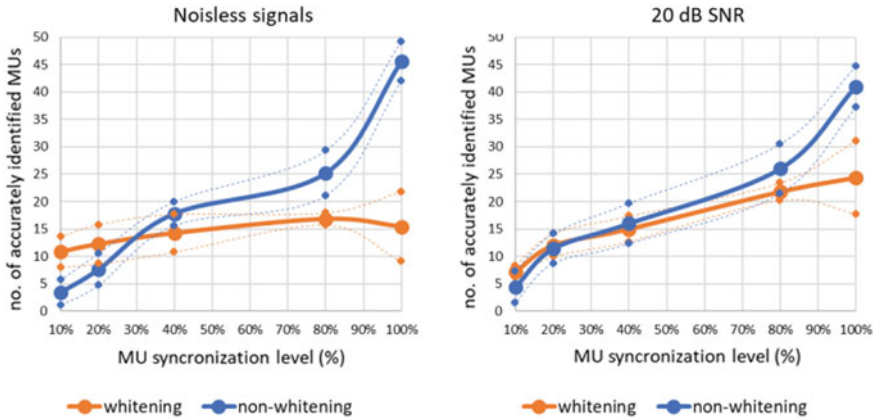


Fig. 2 Number of accurately identified MU firings, averaged across all the simulation runs with 136 active MUs

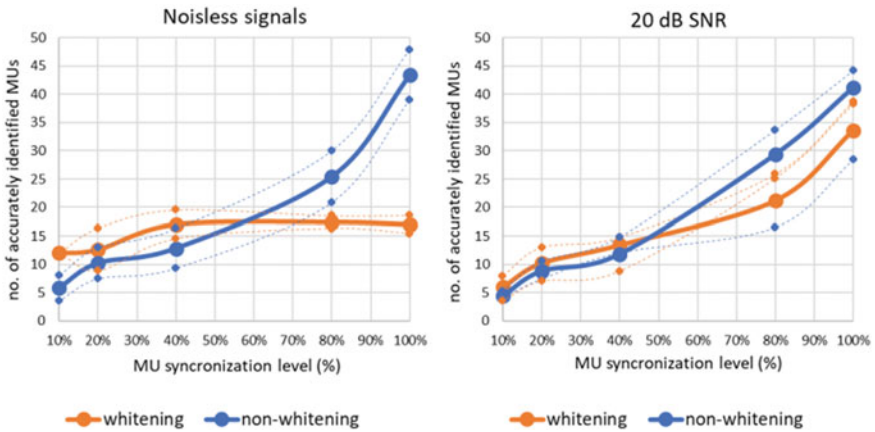


Fig. 3 Number of accurately identified MU firings averaged across all the simulation runs with 168 active MUs

5 Conclusion

We demonstrated the efficiency of the modified jDERpo algorithm [2, 5] for CMAP decomposition at different MU synchronization levels and different numbers of active MUs. We also showed that spatial whitening of HDEMG improves CMAP decomposition on low MU synchronization levels.

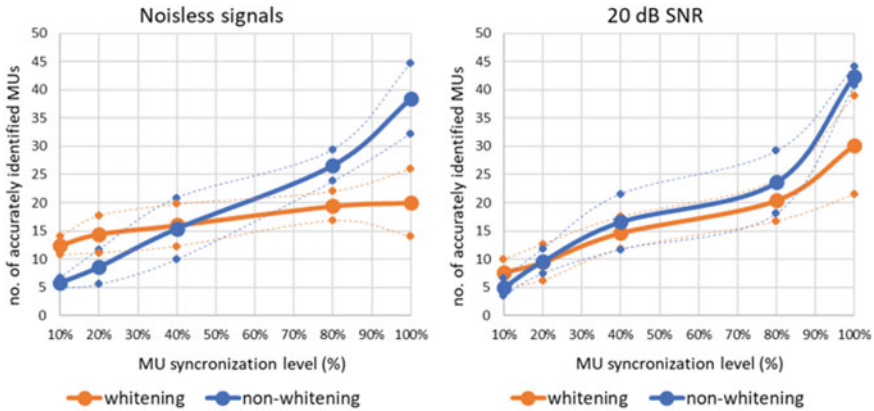


Fig. 4 Number of accurately identified MU firings averaged across all the simulation runs with 200 active MUs

The proposed algorithm was tested on synthetic CMAPs only, where all of the MU firing times and all the MUAPs are known. Before using this CMAP decomposition in experimental conditions, we should first estimate MUAPs of MUs, active in the investigated muscle. This can be performed by using the pre-existing decomposition methods, such as [7, 8]. However, it remains to be tested how much the errors in MUAP estimation affect the proposed CMAP decomposition in experimental conditions.

References

1. J.B. Armstrong, P.K. Rose, S. Vanner, G.J. Bakker, F.J. Richmond, Compartmentalization of motor units in the cat neck muscle, biventer cervicis. *J. Neurophysiol.* **60**(1), 30–45 (1988). PMID: 3404221
2. J. Brest, A. Zamuda, I. Fister, B. Boskovic, Some improvements of the self-adaptive JDE algorithm. In *2014 IEEE Symposium on Differential Evolution (SDE) (2014)*, pages 1–8
3. D. Farina, A. Holobar, Characterization of human motor units from surface EMG decomposition. *Proc. IEEE* **104**(2), 353–373 (2016)
4. D. Farina, L. Mesin, S. Martina, R. Merletti, A surface EMG generation model with multilayer cylindrical description of the volume conductor. *IEEE Trans. Biomed. Eng.* **51**(3), 415–426 (2004)
5. T. Gong, A.L. Tuson, Differential evolution for binary encoding, in *Soft Computing in Industrial Applications* ed. by A. Saad, K. Dahal, M. Sarfraz, R. Roy (Berlin, Heidelberg. Springer Berlin Heidelberg, 2007), pp. 251–262
6. E. Henneman, Relation between size of neurons and their susceptibility to discharge. *Science* **126**(3287), 1345–1347 (1957)
7. A. Holobar, D. Farina, Blind source identification from the multichannel surface electromyogram. *Physiol. Meas.* **35**(7), R143–R165 (2014)
8. A. Holobar, D. Zazula, Multichannel blind source separation using convolution Kernel compensation. *IEEE Trans. Sig. Process.* **55**(9), 4487–4496 (2007)

A Phenomenon of Self-support Exercise in Severe Stroke Patients



F. Alnajjar, S. Shimoda, and Alistair A. Vogan

Abstract Unilateral arm paralysis is a common outcome of stroke and can have a devastating impact on its victims. In this study, we attempt to determine the impact of recruiting a post-stroke patient's contralesional nervous system with the aim to reactivate the ipsilesional neural circuits and, ultimately, stimulate functional motor recovery. We establish such a phenomenon to be possible when a patient utilizes a non-paretic arm to support the movement/training of the paretic arm. In 10 subacute severe post-stroke patients, it was observed that a self-support exercise (SSE)—defined here as the self-guided biomechanical support provided by a non-paretic arm—unexpectedly triggered muscle activities in the supported paretic arm similar in intensity to the healthy activities of the non-paretic limb. Additionally, bilateral normalization of neural activation in the sensorimotor cortex between the stroke-affected and unaffected hemispheres during SSE was discovered during brain imaging. This strongly suggests the facilitation of interhemispheric communication in post-stroke motor recovery. We propose this finding may lead to a new era of available rehabilitation techniques.

Keywords Post-stroke rehabilitation · Muscle synergy · Biological control system · Muscles · Brain activities

This work was funded by Toyota Motor Corporation, Aichi, Japan.

F. Alnajjar (✉)

College of Information Technology, UAE University, 15551 Abu-Dhabi, UAE

e-mail: fady.alnajjar@uaeu.ac.ae

A. A. Vogan

University College, UAE University, Abu-Dhabi, UAE

F. Alnajjar · S. Shimoda

Intelligent Behavior Control Unit, Center of Brain Science (CBS), CBS-TOYOTA Collaboration

Center (BTCC), RIKEN, 2271-130, Nagoya 463-0003, Aichi, Japan

e-mail: shingo.shimoda@riken.jp

© The Author(s), under exclusive license to Springer Nature Switzerland AG 2022

747

D. Torricelli et al. (eds.), *Converging Clinical and Engineering Research*

on *Neurorehabilitation IV*, Biosystems & Biorobotics 28,

https://doi.org/10.1007/978-3-030-70316-5_119

1 Introduction

Stroke is the leading cause of long-term disability worldwide. Approximately two-thirds of all stroke survivors require immediate rehabilitation for the hoped-for recovery of lost motor function [1]. Unfortunately, conventional rehabilitation techniques are limited and can pose a financial burden for both patients and their families in the long run. Because of this, the development of novel rehabilitation strategies that not only promote rapid and complete motor function recovery but also a better understanding of the mechanisms of recovery for neural circuits are needed.

Traditional stroke rehabilitation strategies have mainly focused on paretic limb rehabilitation interventions [2, 3], non-paretic limb interventions [4], or bilateral training [5]. However, few studies have investigated how the use of a patient's unaffected neural circuits in the healthy cortical hemisphere affect the impaired limb in terms of functional rehabilitation of the bilateral cortical sensorimotor network.

In this study, we investigated the muscle/brain activities of the stroke survivors when they utilized the non-paretic arm to support the move of the paretic arm. In addition, we discussed the significance of our findings for the design of a biologically-based stroke rehabilitation system.

2 Methods

2.1 Study and Task Design

This study aimed to highlight the immediate effect of SSE on severe stroke survivors. Ten subacute severe post-stroke patients participated (mean age 62 ± 7).

During this study, patients were directed to perform elbow exercise tasks under four scenarios: (1) *single paretic arm exercise* (moving the paretic arm only), (2) *bimanual exercise* (moving both the paretic and non-paretic arms with no direct contact), (3) *externally support exercise* (moving the paretic arm with the support of a therapist), and (4) *the SSE* (moving the paretic arm with the support of the non-paretic arm of the patient). These scenarios were performed in three randomized sets, with each set consisting of ten trials per exercise.

2.2 Measuring Muscle and Brain Activities

Electromyography (EMG) was used to measure the activity in both the paretic and non-paretic arms of four major muscles associated with the movements of these four scenarios. The muscles recorded were the pectoralis-major (PMM), biceps-brachii (BM), brachioradialis (BRM), and anterior deltoid (AD).

A continuous wave functional near-infrared spectroscopy (fNIRS) system (OMM-3000; Shimadzu Corp.) was used to monitor brain hemodynamic changes in stroke patients. Changes in oxyhemoglobin, deoxyhemoglobin, and total hemoglobin levels as a function of light absorbance and path length were calculated in 48 channels. We used a fixed task cycle (resting-state, task-state, and resting-state) of 20 s for each motion type. Each task cycle contained 10 trials, and each cycle was performed four times. To reduce the possibility of creating processing artifacts, the sequence of motion types was randomized. The final evaluation was determined by the load average of the four cycles.

Utilizing fNIRS, we investigated the contralateral and ipsilateral hemodynamic response of the primary sensorimotor cortex M1/S1 during the performance of the four scenarios and calculated the Laterality Index (LI). LI is a measure to compare the neural activity between hemispheres. It can quantify left and right hemispheric contributions and connectivity depending on conditions [6]. *LI* values range between +1 and -1, where all activation has occurred in the ipsilesional/contralesional hemisphere, respectively. *Zero* indicates that balanced activation has occurred across hemispheres. A balance in hemispheric activation occurs naturally in a healthy individual when performing a bimanual task [6].

3 Results

3.1 *Muscles Activities in the Paretic Arm*

To determine the immediate effect of SSE, metrics were gathered from the major muscles of the arms of stroke-paretic and non-paretic individuals using EMG while these individuals performed elbow flexion exercises following the four mentioned scenarios. These metrics indicated that patients performing the SSE—but *not* the other three types of motions—possessed remarkable muscle activations in the paretic arm (see Fig. 1 for an example of the BM muscle.) Self-support exercise (SSE) appeared to be unique among physiotherapeutic strategies due to the significant EMG activations observed exclusively during their execution.

3.2 *Sensorimotor Interhemispheric Connectivity*

While executing the four scenarios, we measured the sensorimotor cortical activity using fNIRS. Patients performing single, bimanual and externally supported exercises had weak ipsilesional sensorimotor cortex activity compared with the contralesional sensorimotor cortex, Fig. 1a. In contrast, when performing the SSE, ipsilesional sensorimotor cortex activity was (significantly) increased to a level comparable to that of the contralesional sensorimotor cortex, Fig. 1b. The value of *LI*, therefore,

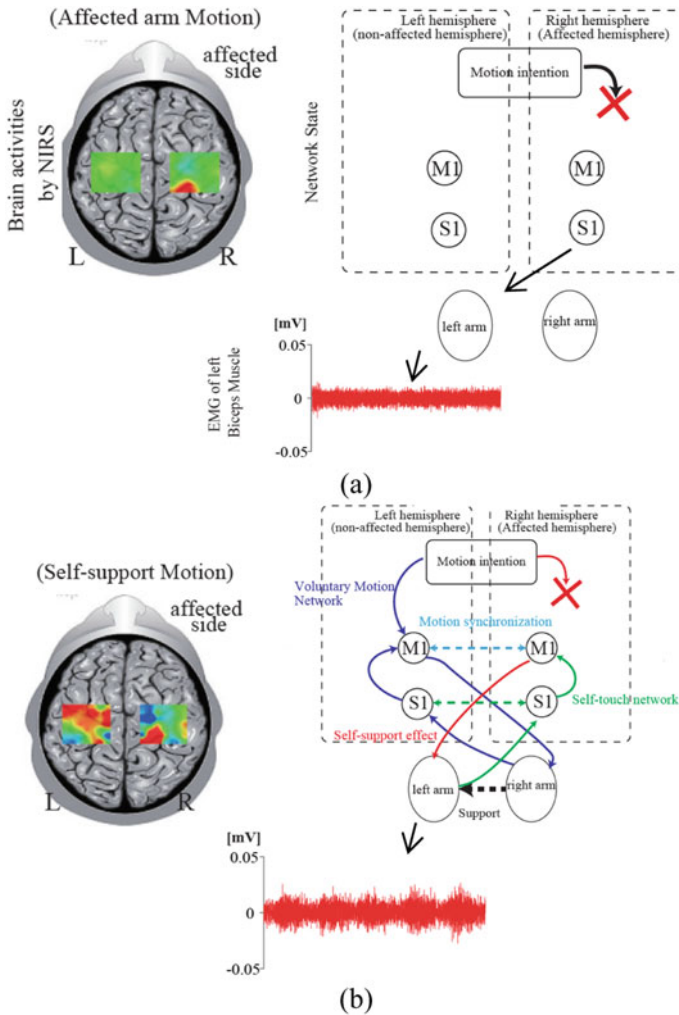


Fig. 1 Visualization of fNIRS and EMG of a patient with severe impairment during the elbow flexion task. **a** Single paretic arm exercise. **b** Self-support exercise. No brain activities were observed in the single paretic arm exercise in the affected hemisphere, resulting in no muscle activity. (*Note* during these exercises patients attempted to move their paretic limb.) During the self-supported exercise, the affected hemisphere was better activated, generating levels comparable to the intact hemisphere

was relatively large in all motion scenarios ($LI > 0.5$), with the exception of the SSE ($LI < 0.25$). A large LI value indicates an imbalance of brain activity on the affected side, relative to the unaffected side. Conversely, a small LI value indicates sensorimotor cortex activity in both hemispheres is relatively equal. From our previous study

in the age-matched healthy individuals, both bimanual and SSE showed LI values closer to 0 [6], suggesting both hemispheres are activated equally in the healthy case.

Due to the concordant increase in EMG signals and the comparable activity levels reached in the right and left hemispheres (see Fig. 1), it appears SSE activates dormant cortical neural circuits for self-repair.

4 Conclusion

In this paper, we have reported our observations on the phenomenon of Self-Support Exercise (SSE). In particular, we have shown that SSE can trigger an immediate and unexpected upsurge of EMG-identified muscle activity in the paretic arm. Our findings suggest that when guided by appropriate contralesional circuits, SSE facilitates the crucial development in connectivity of damaged neural pathways.

We hypothesize that with proper biofeedback the concurrent activation of self-support-driven neural circuits can be coupled with top-down engagement of motor intention signals from higher executive areas, (i.e., closing the loop), to restore the function of sensorimotor pathways and lead to functional motor recovery.

The paradigm of self-support may be generalizable beyond arm movement and could, in fact, extend to other stroke-related areas, such as gait rehabilitation. It is possible that SSE may facilitate the restoration of local neural circuits in the impaired leg through the guidance or ‘supervision’ of the healthy leg, and this may, in turn, produce the development of rudimentary walking patterns. We are presently envisioning an application of this scenario for future research.

References

1. C. Ellis, et al., Racial/ethnic differences in poststroke rehabilitation outcomes. *Stroke Res. Treat.* (2014)
2. J.D. Schaechter et al., Motor recovery and cortical reorganization after constraint-induced movement therapy in stroke patients. *Neurorehabil. Neural Rep.* **16**(4), 326–338 (2002)
3. F. Alnajjar, et al., Motor control system for adaptation of healthy individuals and recovery of post stroke patients: a case study on muscle synergies. *Neural Plastic.* **13** (2019)
4. L. Oujamaa et al., Rehabilitation of arm function after stroke. Literature review. *Ann. Phys. Rehabil. Med.* **52**(3), 269–293 (2009)
5. A. Wolf et al., Efficacy and task structure of bimanual training post stroke: a systematic review. *Top Stro. Rehabil.* **21**(3), 181–196 (2014)
6. F. Alnajjar et al., Self-support biofeedback training for recovery from motor impairment after stroke. *IEEE Access* **8**, 72138–72157 (2020)

Human Brain Organoid Platform for Neuroengineering Optical Theranostics in Neonatal Sepsis



Sneha S. Karanth, Radhika Mujumdar, Jagdish P. Sahoo, Abhijit Das, Michal K. Stachowiak, and Anirban Dutta

Abstract Early-onset neonatal sepsis can increase the risk of hypoxic-ischemic encephalopathy (HIE) that can worsen the patient's prognosis. We investigated neurometabolic coupling (NMC) in five full-term neonates with HIE and sepsis that was found lower than the other five with HIE only. We hypothesized that transcranial photobiomodulation might upregulate cerebral oxygen metabolism, which may restore NMC. We developed a human brain organoid platform to evaluate the effects of photobiomodulation around 810 nm on the Cytochrome-C Oxidase (CCO) activity and electrophysiology. We found that 10 min of photobiomodulation increased CCO activity, pH, and temperature while decreased the spectral exponent in 1–40 Hz from electrophysiology data. For future work, it is postulated that photobiomodulation at ~810 nm may ameliorate metabolic acidosis and dysfunctional NMC in neonatal sepsis, thereby reducing the risk of HIE transition.

1 Introduction

NEONATAL sepsis due to systemic infection in the newborn is the most common cause of neonatal mortality in India that is highest in the world [1]. The development of mitochondrial dysfunction and ineffective oxygen utilization is indicated in sepsis [2]. Here, the measurement of oxygen extraction fraction requires measurements

Funded by the Community for Global Health Equity Seed Funding, University at Buffalo (SUNY Buffalo), USA; SIAGNOS LLC, Department of Biotechnology (DBT), Government of India, the Bill and Melinda Gates Foundation and IKP Knowledge Park, India.

S. S. Karanth · R. Mujumdar · M. K. Stachowiak · A. Dutta (✉)
SUNY Buffalo, Buffalo, USA
e-mail: anirband@buffalo.edu

J. P. Sahoo
Institute of Medical Sciences and Sum Hospital, Bhubaneswar, India

A. Das
NHS Walton Centre, Liverpool, UK

of cerebral blood flow; however, the mitochondrial dysfunction may be detected using inexpensive near-infrared spectroscopy. Specifically, studies have indicated abnormalities in the function of complex IV (cytochrome oxidase), the final electron acceptor in the electron transport chain that can be monitored in sepsis using non-invasive broadband near-infrared spectroscopy (bbNIRS) [3]. Sepsis is also one of the main risk factors for the development of hypoxic-ischemic encephalopathy (HIE). Therefore, bbNIRS can be combined with electroencephalography (EEG) to detect seizures and the state of the neurovascular coupling (NVC) [4] for HIE diagnostics in neonatal sepsis. Recently, transcranial photobiomodulation has been shown to locally upregulate cerebral oxygen metabolism [5]; however, its photothermal effects [6] can be detrimental in HIE [7]. Here, ‘phase zero’ brain organoid model-based studies can provide a fundamental understanding [8] of such theranostics [9].

2 Methods

2.1 Mini-Brain Computer Interface (mBCI)

Three-month-old cerebral organoids were generated using healthy control cell lines following previously established protocol [10]. A 32-channel tetrode (eight polyimide-coated nickel-chrome tetrode wire of diameter $\sim 50 \mu\text{m}$ arranged in a circular grid of $\sim 2 \text{ mm}$ diameter) microdrive [11] was interfaced with Intan RHD2132 amplifier (Intan Technologies, USA) for recording with the Open Ephys data acquisition system for sampling at 30 kSamples/sec each. Broadband Vis-NIR spectroscopy was performed with SILVER-Nova spectrometer (Stellarnet, U.S.A.) over the 190–1110 nm wavelength range with 200 μm slit for high sensitivity using SL1 high stability Tungsten Halogen light (350–2500 nm) source (Stellarnet, U.S.A.), and R600-8-VisNIR Reflectance Probe (Stellarnet, U.S.A.). SpectraWiz spectrometer software (Stellarnet, U.S.A.) recorded the Broadband Vis-NIR spectroscopy data in conjunction with Open Ephys GUI for the electrophysiological recordings [8].

2.2 Calibration of Cytochrome-C Oxidase Activity

We calibrated the Broadband Vis-NIR spectroscopy system (490–900 nm) using a colorimetric assay kit (CYTOCOX1, Sigma-Aldrich, USA) for the determination of CCO activity in the standard 2 ml sample at various concentrations as well as in the buffer solution. Partial least square (PLS) processing of the Vis-NIR spectra was investigated to develop a multivariate regression model for the determination of the CCO activity in the organoid model. We then determined the PLS loadings on the Vis-NIR spectra to identify the four best wavelengths in NIR for a multi-wavelength CCO sensor.

2.3 *Vis-NIR Spectroscopy with Electrophysiology During Photobiomodulation*

We recorded spontaneous neuronal activity (LFP) for a total of 10 min from 32-channel tetrode along with Vis-NIR spectroscopy when the organoid was illuminated at 20 mW/cm² with 810 nm based on our prior work [6]. pH and temperature changes from baseline (pH 7) after 10 min of photobiomodulation was also measured. A three-step fitting procedure [8] discarded oscillatory peaks in LFP prior to estimating the background slope of power spectral density.

2.4 *Neonatal Study on HIE With and Without Sepsis*

Full-term neonates (>36 weeks of gestation) at Sarnat Grade II, five with and five without sepsis, were selected from our clinical trial (trial registration: CTRI/2020/02/023190) at the Institute of Medical Sciences and Sum Hospital, Bhubaneswar, India. EEG electrodes were placed at the standard F3/P3-F4/P4 along with the overlapping multi-wavelength (~780 nm, ~810 nm, ~820 nm, ~840 nm) NIRS (mwNIRS) to assess neurovascular (NVC) and neurometabolic (NMC) coupling. This montage was selected to cover the brain area representative of the global watershed region. Amplitude-integrated EEG (aEEG) was computed, and wavelet coherence analysis was performed with the tissue oxygen index (NVC) and CCO changes (NMC). mwNIRS used a low-power 5 mW LED that could be increased up to 25 mW for local photobiomodulation in the neonates.

3 Results

Multivariate regression modeling using partial least square regression (PLSR) provided an R-squared goodness-of-fit of 0.99 for the PLSR model. Four NIR wavelengths (~780 nm, ~810 nm, ~820 nm, ~840 nm) with the best PLSR loading and available in LED chips were selected for mwNIRS. In the healthy brain organoid, 10 min of photobiomodulation (~810 nm) changed the pH from 7 to 9, and the temperature increased by ~0.6 °C (Fig. 1). Also, the spectral exponent in 1–40 Hz frequency band decreased from -0.8 ± 0.2 to -1.2 ± 0.5 while the CCO activity increased from 53 ± 2 to 68 ± 5 nM. The NVC (<0.001 Hz) in neonates was comparable across HIE and HIE + sepsis conditions; however, NMC was found to be lower in HIE + sepsis than the HIE group (Table 1).

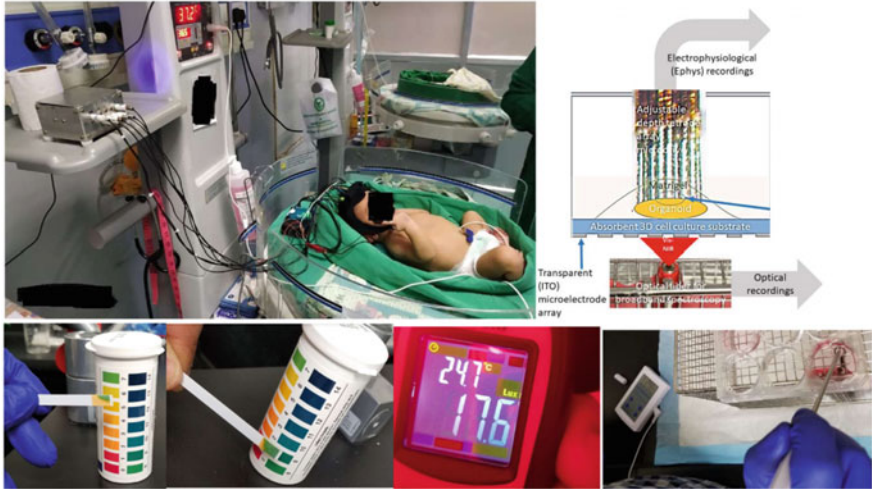


Fig. 1. Top left shows EEG-mwNIRS monitoring in the neonatal intensive care unit. The top right shows the brain organoid platform [8]. The bottom panel shows pH change, illuminance, and temperature from left to right.

Table 1. Neonatal study

Full-term neonates	NVC (mean ± standard deviation)	NMC (mean ± standard deviation)
HIE (<i>N</i> = 5)	0.52 ± 0.27	0.41 ± 0.18
HIE + Sepsis (<i>N</i> = 5)	0.45 ± 0.36	0.22 ± 0.15

4 Conclusion

Our brain organoid platform showed an increase in CCO activity, pH, and temperature while a decrease in the spectral exponent in 1–40 Hz due to 10 min of photobiomodulation at ~810 nm. Also, NMC (<0.001 Hz) was found lower in the HIE + sepsis condition that needs further investigation.

Acknowledgements E. K. Stachowiak, M. Liput, J. Augustyniak for organoid study.

References

1. S. Murthy, M. A. Godinho, V. Guddattu, L.E.S. Lewis, N.S. Nair, Risk factors of neonatal sepsis in India: a systematic review and meta-analysis. *PLoS One* **14**(4) (2019). <https://doi.org/10.1371/journal.pone.0215683>

2. R.J. Levy, C.S. Deutschman, Cytochrome c oxidase dysfunction in sepsis. *Crit. Care Med.* **35**(9 Suppl), S468–S475 (2007). <https://doi.org/10.1097/01.ccm.0000278604.93569.27>
3. M. Banaji et al., Modelling of mitochondrial oxygen consumption and NIRS detection of cytochrome oxidase redox state. *Adv. Exp. Med. Biol.* **662**, 285–291 (2010). https://doi.org/10.1007/978-1-4419-1241-1_41
4. Y. Das, H. Liu, F. Tian, S. Kota, R. Zhang, L.F. Chalak, Rigor of neurovascular coupling (NVC) assessment in newborns using different amplitude EEG algorithms. *Sci. Rep.* **10**(1) (2020). Article No. 1. <https://doi.org/10.1038/s41598-020-66227-y>
5. X. Wang et al., Transcranial photobiomodulation with 1064 nm laser modulates brain electroencephalogram rhythms. *NPH* **6**(2), (2019). <https://doi.org/10.1117/1.nph.6.2.025013>
6. M. Bhattacharya, A. Dutta, Computational modeling of the photon transport, tissue heating, and Cytochrome C oxidase absorption during transcranial near-infrared stimulation. *Brain Sci.* **9**(8), 179 (2019). <https://doi.org/10.3390/brainsci9080179>
7. A. Laptook et al., Elevated temperature after hypoxic-ischemic encephalopathy: a risk factor for adverse outcome. *Pediatrics* **122**(3), 491–499 (2008). <https://doi.org/10.1542/peds.2007-1673>
8. A. Dutta et al., ‘Phase Zero’ clinical study platform combining broadband Vis/near-infrared spectroscopy and electrophysiology to study human brain organoid models of neurodevelopmental disorders. *bioRxiv*, p. 2020.06.09.143313 (2020). <https://doi.org/10.1101/2020.06.09.143313>
9. A. Dutta, A. Das, D. Kondziella, M.K. Stachowiak, Bioenergy crisis in coronavirus diseases? *Brain Sci.* **10**(5) (2020). Art. No. 5 <https://doi.org/10.3390/brainsci10050277>
10. E.K. Stachowiak et al., Cerebral organoids reveal early cortical maldevelopment in schizophrenia—computational anatomy and genomics, role of FGFR1. *Transl. Psychiatry* **7** (2017). <https://doi.org/10.1038/s41398-017-0054-x>
11. J. Voigts, J.H. Siegle, D.L. Pritchett, C.I. Moore, The flexDrive: an ultra-light implant for optical control and highly parallel chronic recording of neuronal ensembles in freely moving mice. *Front. Syst. Neurosci.* **7** (2013). <https://doi.org/10.3389/fnsys.2013.00008>

Grey-Box Model-Based Analysis of the Effects of Anodal Transcranial Direct Current Stimulation on the Reaction Time in Healthy Human



Namrata Sridhar Kadambi, Shilpa Ramanarayanan, Filip Stefanovic, and Anirban Dutta

Abstract Transcranial direct current stimulation (tDCS) can modulate corticomuscular coherence and reaction time of the targeted muscle during a single-muscle ballistic myoelectric control where anodal tDCS of the primary motor cortex (M1) leg representation decreased the reaction time while the cerebellar tDCS (ctDCS) increased the same. In this study, we present corticomuscular coherence changes due to anodal leg M1 tDCS and ctDCS. We also present a grey-box model that explained the tDCS effects on the reaction time in healthy humans where tDCS effects were captured by a Boltzmann function.

Keywords Transcranial direct current stimulation · Myoelectric control · Corticomuscular coherence · Grey-box model · Cerebellum

1 Introduction

Transcranial direct current stimulation (tDCS) has been shown to modulate brain connectivity that may play a facilitatory role in the brain-computer interfaces (BCIs) [1]. Our prior work showed that the neuromodulatory effects on the reaction time of anodal tDCS at the primary motor cortex (M1) could be explained by a Simplified Spinal-Like Controller (SSL) model [2]. Specifically, the corticomuscular

University at Buffalo SUNY, Alexander von Humboldt Foundation, and the Campus France (PROCOPE Mobility Grants) supported this work.

N. S. Kadambi · S. Ramanarayanan · F. Stefanovic · A. Dutta (✉)
University at Buffalo SUNY, Buffalo, USA
e-mail: anirband@buffalo.edu

N. S. Kadambi
e-mail: namratas@buffalo.edu

S. Ramanarayanan
e-mail: sramanar@buffalo.edu

F. Stefanovic
e-mail: filipste@buffalo.edu

coherence (CMC), modulated by anodal tDCS of the leg representations in the M1 (leg M1), was found to be related to the reaction time. Our prior work also found that leg M1 anodal tDCS decreased the reaction time while anodal cerebellar tDCS (ctDCS) increased the same when compared to sham tDCS [3]; however, the grey-box model was not investigated. Therefore, we investigate the effects of anodal ctDCS by augmenting the SSLC model [2].

2 Methods

2.1 Corticomuscular Coherence and Reaction Time

Eleven healthy right-leg dominant male volunteers (age: 24–36 years) provided informed consent for this study. All the experiments were approved by the local ethics committee of the University Medicine Goettingen, Germany. The visuomotor task consisted of four states, focus, relax, ready, and activation of the right tibialis anterior (TA) muscle as quickly as possible in response to a visual cue when the TARGET jumped to a randomized value between 40 and 80% of maximum voluntary contraction (MVC). For each volunteer, the visuomotor task consisted of 15 trials before and after tDCS intervention (details in Dutta et al. [3])—see left panel of Fig. 1. Electroencephalogram (EEG) and electromyogram (EMG) data from the muscle activation part was analyzed for corticomuscular coherence (CMC)—details in Kha et al. [4]. Briefly, EMG was amplified and band-pass filtered (anti-aliasing, frequency band = 10–500 Hz) before being sampled at 2000 Hz by a 12-bit data acquisition system (NI USB-6009, National Instruments, USA). Eyes-open resting-state EEG was recorded at 500 Hz from the central site Cz (10–20 montage) as well as the nearby electrodes F3, F4, P3, P4 (international 10–20 system) before (pre-tDCS) and after (post-tDCS) anodal ctDCS. Morlet wavelet coherence plots between EMG and EEG signals from bilateral TA muscles and Cz (10–20 EEG system) were obtained using Grinsted’s toolbox [5]—details in Kha et al. [4].

2.2 Computational Modification of SSLC Model

The human neuromuscular system was simulated using a grey-box simplified spinal-like topology that included cortical areas—cerebellum (CB), basal ganglia (BG), collicular maps (SC)—as well as signal conduction delays (δ), interneurons (IN), Renshaw cells (RC), motoneurons (Mn) and non-linear muscle models [2, 4]—see right panel of Fig. 1. Visual feedback includes data from subject recorded CURSOR and TARGET positions and is used by the SC to calculate an error signal that is projected downstream. The INs act as summation blocks that integrated signals from cortical and spinal areas such as the RC. The RC provided efferent copies of motor

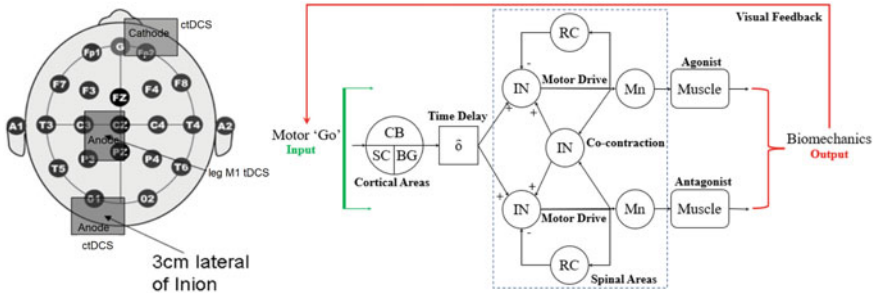


Fig. 1 The left panel shows the ctDCS montage (from [3]). The right panel shows the SSLC for an antagonist muscle pair

activation back to the spinal-level circuits, while muscles included proprioceptive mechanisms that define muscle stretch length and stretch rate to the circuit. The INs then modulate the motor signal into a resultant muscle activation ranging from 0 to 1. The Mn innervate Virtual Muscles (VM) that generate force output to drive the system biomechanics and neuromuscular response.

The cortico-cerebellar-spinal (CCS) pathway is represented by a Boltzmann function:

$$S = \frac{a}{1 + e^{-b(x-c)} + z} \tag{1}$$

where a encodes the height of the sigmoid function, b represents the slope of the function, c determines the point of the deflection of the curve, and z sets the scale of the curve. Each parameter (a , b , c , and z) is sequentially increased during the visuomotor task while the remaining parameters are held at pre-determined constants. By modifying these variables, we can emulate changes to the CCS based on the recruitment curve [4, 6] found using Transcranial Magnetic Stimulation (TMS) that describes the input-output properties [2]. In this study, we performed an exploratory analysis by varying the parameters of the sigmoid to observe the causal changes.

3 Results

Cross wavelet transform plots before and after anodal tDCS are shown in Fig. 2. The root mean square (RMS) of the wavelet coherence in the EEG beta band (12–30 Hz) was computed to find the CMC delay and peak before and after anodal tDCS, as illustrated in Fig. 2 for pre-tDCS. One-way ANOVA test on the normalized change in the CMC delay, i.e., (post-pre)/(post + pre), showed a significant ($p < 0.05$) effect of the anodal tDCS montages (leg M1, cerebellum). Also, leg M1 tDCS had a significant ($p < 0.05$) effect on the normalized change in the CMC peak. Post hoc analysis confirmed that the CMC delay was decreased by leg M1 tDCS for the right

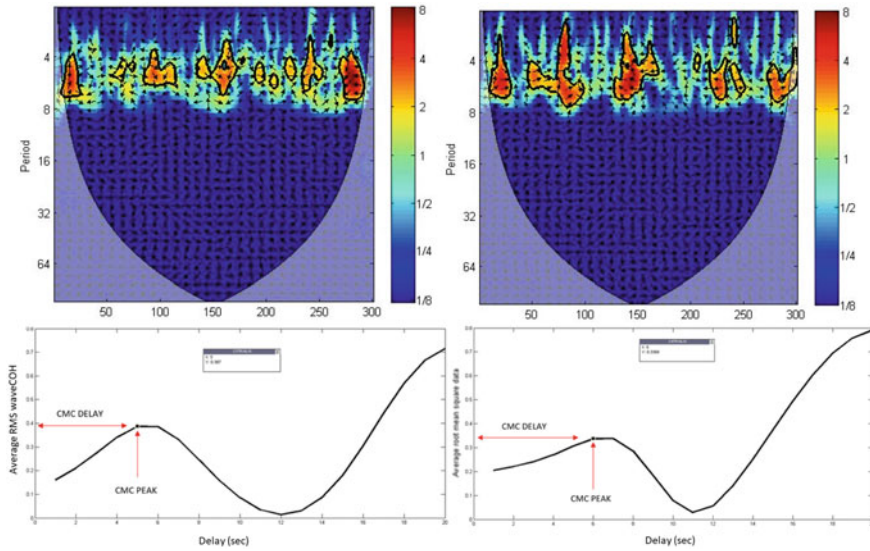


Fig. 2 Top panel: Example of the Cross wavelet transform (CWT). Top left: CWT plot for Cz EEG and right TA muscle pre-tDCS. Top right: CWT plot for Cz EEG and right TA muscle post-tDCS. The X-axis is the time axis in seconds (max. 300 s). Bottom panel: Example of the root mean square (RMS) of the wavelet coherence (waveCOH). Bottom left: RMS waveCOH (12-30Hz) for Cz EEG and right TA muscle pre-tDCS. Bottom right: RMS waveCOH (12-30Hz) for Cz EEG and right TA muscle post-tDCS. The x-axis in seconds (max. 20 s)

leg (that performed visuomotor task) while ctDCS increased the same. CMC peak was increased by the leg M1 tDCS for the right leg. Here, tDCS effects on the CMC peak and delay showed modulation of the CCS pathway.

Figure 3 shows the rise times to peak muscle force generation (y-axis) by the controller with respect to the specific Boltzmann parameters a , b , c , and z , respectively. In addition, plots are overlaid based on different muscle lengths shown in different colors. We observed that the response time showed a Gaussian type curve for the majority of muscle length positions and that the response time varies between 110.4 and 244.4 ms. Although parameters ‘ b ’ and ‘ c ’ (Fig. 3b, c, respectively) follow a similar trend as shown, for ‘ a ’ the curve exhibits a greater slope—Fig. 3a. Whereas, ‘ z ’ presents a more gradual slope than ‘ a ’ (see Fig. 3d). These graphs indicate that the response time of the modulated CCS system exhibited a mixed response depending on the muscle length and that shorter muscle lengths provide faster response times when compared to longer muscle lengths.

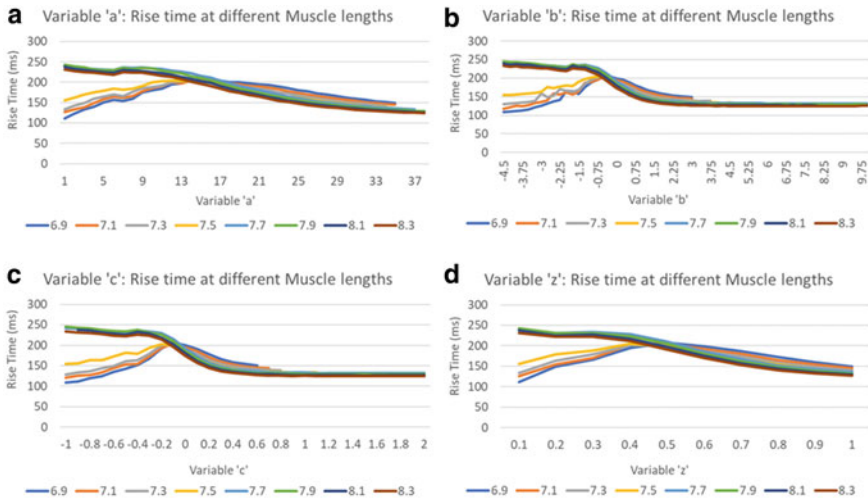


Fig. 3 The plot of Boltzmann parameters and their corresponding response time. **a** Boltzmann parameter ‘a’, **b** Boltzmann parameter ‘b’, **c** Boltzmann parameter ‘c’, **d** Boltzmann parameter ‘z’

4 Conclusion

The Boltzmann function is a good representation of the recruitment curve [2], that can be found using TMS, and can capture modulation of excitability alterations by leg M1 tDCS and ctDCS [4, 6]. Therefore, grey-box modeling using Boltzmann function as a representation of the state of the CCS pathway can provide a relationship between the neurophysiological aspects of the behavioral results. Such an approach can provide further insights into the tDCS effects in health and disease, including post-stroke spasticity.

References

1. B.S. Baxter, B.J. Edelman, A. Sohrabpour, B. He, Anodal transcranial direct current stimulation increases bilateral directed brain connectivity during motor-imagery based brain-computer interface control. *Front Neurosci*, **11** (2017). <https://doi.org/10.3389/fnins.2017.00691>
2. F. Stefanovic, H.L. Galiana, A simplified spinal-like controller facilitates muscle synergies and robust reaching motions. *IEEE Trans. Neural Syst. Rehabil. Eng.* **22**(1), 77–87 (2014). <https://doi.org/10.1109/TNSRE.2013.2274284>
3. A. Dutta, W. Paulus, M.A. Nitsche, Facilitating myoelectric-control with transcranial direct current stimulation: a preliminary study in healthy humans. *J. Neuroeng. Rehabil.* **11**, 13 (2014). <https://doi.org/10.1186/1743-0003-11-13>
4. V. Kha, A.S. Foerster, S. Bennett, M.A. Nitsche, F. Stefanovic, A. Dutta, Systems analysis of human visuo-myoelectric control facilitated by anodal transcranial direct current stimulation in healthy humans. *Front. Neurosci.* **12**, 278 (2018). <https://doi.org/10.3389/fnins.2018.00278>

5. "Cross Wavelet and Wavelet Coherence Toolbox," *Wavelet coherence*. <https://grinsted.github.io/wavelet-coherence/> (accessed July 27, 2020)
6. G. Batsikadze, et al., Effects of cerebellar transcranial direct current stimulation on cerebellar-brain inhibition in humans: a systematic evaluation, in *Brain Stimulation: Basic, Translational, and Clinical Research in Neuromodulation* (2019). <https://doi.org/10.1016/j.brs.2019.04.010>

Different Stimuli Configuration in Paired Associative Stimulation Protocol: A Pilot Study



A. San Agustín, José L. Pons, A. Oliviero, and J. C. Moreno

Abstract Paired Associative Stimulation (PAS) application is a neuromodulation strategy for the promotion of plastic changes and motor rehabilitation. Different stimuli configuration has been applied following a PAS protocol, although using same technical parameters. In this pilot study, we compared three different PAS conditions with a control group. Movement task involved PAS resulted to be less specific although induced excitability potentiation to adjacent muscles. A further methodological research in favour of plastic mechanism understanding and optimization of PAS application will be developed.

1 Introduction

PAS paradigm is a neuromodulation methodology based on two nervous stimuli synchronized in time to converge in the same cortical localization. Its repetitive application triggers excitability enhancement and plastic changes on the targeted cortical localization [1].

In the beginning, PAS was conducted pairing a single TMS pulse with low frequency peripheral nervous stimulation (PNS) in motor cortex. PNS was applied in median nerve 25 ms before TMS pulse was administer in the contralateral primary motor cortex (M1), in order to both activations meet (**PNS + TMS**) [2].

A. San Agustín (✉)

School of Medicine, Universidad Autónoma de Madrid (UAM), Madrid, Spain

e-mail: asanagustin@cajal.csic.es

A. San Agustín · J. C. Moreno

Neural Rehabilitation Group of the Spanish National Research Council, Madrid, Spain

J. L. Pons

Legs & Walking AbilityLab, Shirley Ryan AbilityLab, Chicago, IL, USA

A. Oliviero

FENNSI Group of National Hospital of Paraplegics, Toledo, Spain

PAS paradigm has been proved to be effective with other stimuli configuration [3]. Electrical nerve stimulation in common peroneal nerve combined with a voluntary dorsiflexion exercise task (**PNS + Task**) likewise modulated neural excitability, produced long-lasting facilitatory effects and enhanced sensorimotor reorganization [4]. On the other hand, TMS pulse over M1 50 ms before contralateral voluntary thumb abduction movement produced changes in motor behavior and enhanced the corticospinal excitability (**TMS + Task**) [5, 6]. However, the extent of effectiveness of each PAS variation, regarding an approach that encompasses all configurations, is unknown due to the differences in the studies' parameters, which does not allow the comparison between them.

The goal of the present pilot study is to measure the changes in excitability derived from different PAS conditions (**PNS + TMS**, **PNS + Task** and **TMS + Task**) with the same methodology parameters (same motor pathway, pair repetitions and assessment protocol) to compare the different stimuli combination effects.

2 Material and Methods

2.1 *Experimental Conditions and Procedures*

This study is structured in three assessment times and one experimental phase (**TMS + PNS**, **PNS + Task**, **TMS + Task** or **Task Control**).

The assessment phases are conducted before (**PRE**), immediately after (**POST**) and 30 min after (**POST30**) the experimental phase. During **PRE** assessment times, TMS was applied in the scalp above motor cortex that elicits a higher Motor Evoked Potential (**MEP**) in contralateral Abductor Pollicis Brevis (**APB**) muscle (**APB hot-spot**). Then, 20 single pulses were applied at an intensity that elicited 1 mV of **MEP**. The TMS localization was non-invasively marked in subject's scalp for further placement. During **POST** and **POST30** assessment times, the previous intensity was set to trigger 20 TMS single pulses at the same scalp localization.

Regarding the experimental phases, each subject (ages 28 ± 7 , 2 female, 2 male) experienced a different PAS configuration, however, they shared the same stimulated nervous pathway (**APB** motor pathway), same PAS repetitions in the application (200 pairs) and same nervous excitability assessment (20 Motor Evoked Potentials (**MEP**) at 1 mV of rMT as explained above).

Firstly, in **TMS + PNS** configuration, the synchronized stimulation maintain an ISI of 5 s (0.2 Hz), TMS was placed at **APB hot-spot** and set in 1 mV intensity, PNS was placed in the median nerve and set in three times the perceptual threshold intensity and 0.2 ms of duration. The time synchronization between the stimuli corresponded to the application of PNS 25 ms before TMS. In **PNS + Task** group, a simple reaction time (**RT**) task was performed (explanation below) paired with a PNS pulse that was applied with the same parameters as the PNS of the first condition. The individual **RT** was measured before the experimental phase in order to synchronize

it with PNS at the same time. In **TMS + Task** group, the RT task was performed paired with TMS single pulse in APB hot-spot. TMS was applied 25 ms before the previously measured mean RT. Finally, the control group's (**Task group**) subject performed the simple RT task 200 times without any stimulation, in order to show in comparison the effectiveness of PAS methodology not derived from the execution of the movement itself.

2.2 Simple Reaction Time Task

The task goal was to click the right button of the mouse with the dominant thumb finger as fast as possible when the cue (a white cross) appeared on the screen (grey background). A black dot was shown on the screen during randomly 5–8 s while the subject was preparing for the cross visualization.

2.3 Transcranial Magnetic Stimulation (TMS)

TMS was applied using a figure-of-eight double 70 mm remote control coil and a single pulse, monophasic stimulator (Magstim 200² stimulator). Every TMS pulse was applied in a posterior to anterior current direction.

2.4 Electromyography (EMG) Recordings

We recorded the MEPs generated by TMS on APB, Abductor Digiti Minimi (ADM), First Dorsal Interosseous (FDI), Flexor Carpi Radialis (FLX) and Extensor Carpi Radialis (EXT) muscles of the dominant hand and arm during assessment phases. The reference and the ground electrodes were placed on the dominant hand wrist. EMG data were collected using g.USBamp biosignal amplifier (g.tec) and digitized at a rate of 2400 Hz. An electrical notch filter was used at 50 Hz and raw EMG data was stored for offline analysis.

2.5 Data Analysis

Our goal was to compare the different PAS approaches and their effectivity to enhance nervous system excitability. Thus, we divided POST and POST30 times separately with their correspondent PRE time, in order to compare this proportion between the groups. We analyzed MEP amplitudes with Student T test for repeated measures.

3 Results

We compared MEP's amplitude across different PAS configurations in order to assess excitability changes of the cortico-spinal pathway derived from different stimuli (Fig. 1).

We will describe the T test comparison regarding APB and ADM results between configurations. In APB, in POST time, PNS + TMS (Mean = 2.08 SE = .27) was significantly enhanced compared to TMS + T (Mean = .84 SE = .28, $t(19) = 3,708$, $p = .008$). In POST30 time PNS + TMS (Mean = 5.26 SE = .59) was significantly enhanced compared to each other configurations (PNS + T: Mean = 1.68 SE = .59, $t(19) = 3,015$, $p = .007$; TMS + T: Mean = 1.29 SE = 0.28, $t(19) = 3,551$, $p = .002$; T: Mean = .94 SE = .59, $t(19) = 3,719$, $p = .001$).

In ADM muscle, at POST and POST30 times PNS + T (POST: Mean = 1.87 SE = .16; POST30: Mean = 1.66 SE = .15) and TMS + T (POST: Mean = 2.04 SE = .16; POST30: Mean = 2.05 SE.15) were significantly potentiated compared to TMS + PNS (POST: Mean = .94 SE = .16, $t(19) = -3.708$, $p = .000$ and $t(19) = 5.842$, $p = .000$; POST30: Mean = .80 SE = .15, $t(19) = -3.492$, $p = .002$ and $t(19) = 4.296$, $p = .000$) and T (POST: Mean = .91 SE = .16, $t(19) = -4.879$, $p = .000$ and $t(19) = 4.312$, $p = .000$; POST30: Mean = .77 SE = .15, $t(19) = -6.896$, $p = .000$ and $t(19) = 6.058$, $p = .000$ respectively).

4 Conclusion and Discussion

The results herein presented pointed that the configuration of PAS which does not imply a motor task (TMS + PNS), is likely more specific in affecting the stimulated motor pathway and, on the contrary, PAS therapies activating the cortex by a movement task (PNS + T and TMS + T), showed to reach the potentiation to an adjacent muscle, likely due to APB fatigue. We demonstrated the study feasibility to compare different PAS configurations and future work will evaluate the efficacy of this experimental approach.

The methodological research in PAS are of great importance to help us in the development of optimal use of these techniques, supporting a better PAS therapy application in the patients' rehabilitation.

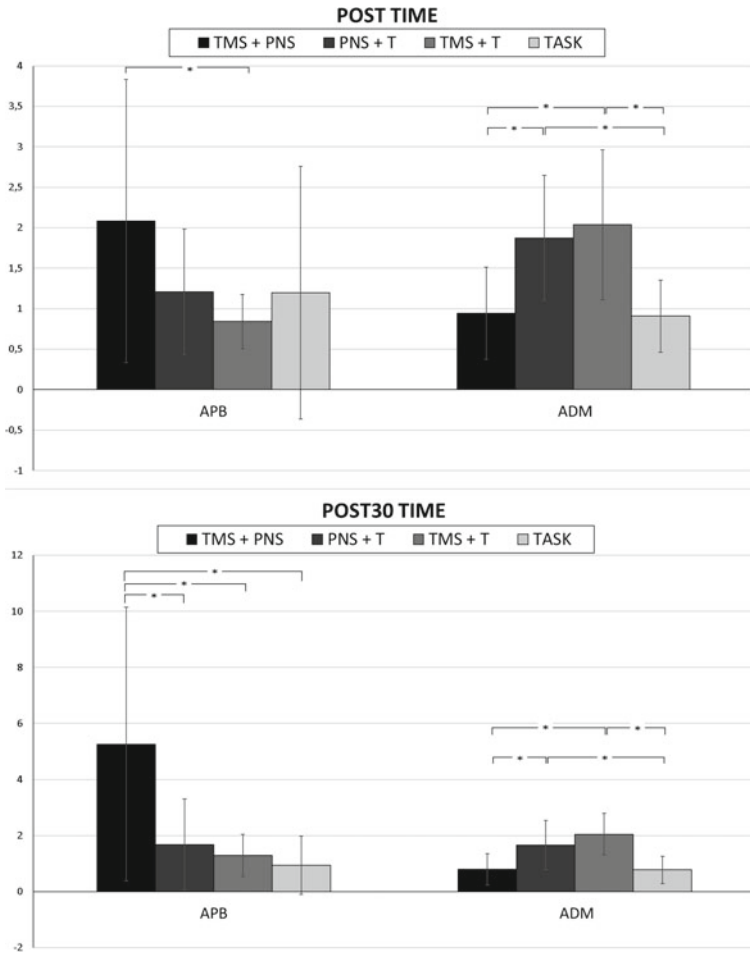


Fig. 1 The mean \pm SD of MEPs for APB and ADM muscles normalized to Pre 1 mV intensity in different experimental PAS configurations

References

1. J. Classen, A. Wolters, K. Stefan, M. Wycislo, F. Sandbrink, A. Schmidt, E. Kunesch, in *Paired Associative Stimulation*. In Supplements to Clinical neurophysiology, vol. 57 (Elsevier), pp. 563–569
2. K. Stefan, E. Kunesch, R. Benecke, L.G. Cohen, J. Classen, Mechanisms of enhancement of human motor cortex excitability induced by interventional paired associative stimulation. *J. Physiol.* **543**(2), 699–708 (2002)
3. R.G. Carson, N.C. Kennedy, Modulation of human corticospinal excitability by paired associative stimulation. *Front. Hum. Neurosci.* **7**, 823 (2013)

4. S. Khaslavskaja, T. Sinkjaer, Motor cortex excitability following repetitive electrical stimulation of the common peroneal nerve depends on the voluntary drive. *Exp. Brain Res.* **162**(4), 497–502 (2005)
5. M.N. Thabit, Y. Ueki, S. Koganemaru, G. Fawi, H. Fukuyama, T. Mima, Movement-related cortical stimulation can induce human motor plasticity. *J. Neurosci.* **30**(34), 11529–11536 (2010)
6. A. San Agustín, G. Asín-Prieto, J.L. Pons, Fatigue compensating muscle excitability enhancement by transcranial magnetic stimulation: A case report, in *International Conference on NeuroRehabilitation* (pp. 839–843). Springer, Cham (2018, October)

Intensity Dependent Long-Term Potentiation and Inhibition in Paired Associated Stimulation by Transcranial Magnetic Stimulation: A Pilot Study



A. San Agustín, D. Crevillén, A. Oliviero, José L. Pons, and J. C. Moreno

Abstract The Paired Associated Stimulation (PAS) protocol has been probed to successfully induce motor cortico-spinal plasticity. However, there is not an official consensus for the optimal Transcranial Magnetic Stimulation (TMS) intensity in PAS applications. The aim of this pilot study is to research the implication of intensity factor during the plasticity induction by PAS in later excitability assessment through each measurable intensity (90, 100, 110, 120 and 130% of the rMT). The results point to a conditioning of the intensity on the Motor Evoked Potentials (MEPs) towards a polarized outcome between high and low frequencies. Regardless, a complete research would be necessary to determine the impact extent of the PAS intensity factor.

1 Introduction

OUR knowledge about synaptic plasticity has greatly progressed during the last decades. The Hebb's postulation regarding the correlation of the synaptic modification with the activity performed [1], together with the process of long-term potentiation (LTP) and long-term depression (LTD) [2], have become some of the main cornerstones in the neural plasticity field.

The work of Stefan et al. was a step forward to induce synaptic plasticity in the human primary motor cortex (M1) by PAS of the M1 with transcranial magnetic

A. S. Agustín (✉) · D. Crevillén · J. C. Moreno
Neural Rehabilitation Group of the Spanish National Research Council, Madrid, Spain
e-mail: asanagustin@cajal.csic.es

A. S. Agustín
School of Medicine, Universidad Autónoma de Madrid (UAM), Madrid, Spain

A. Oliviero
FENNSI Group, National Hospital of Paraplegics, Toledo, Spain

J. . L. Pons
Legs & Walking AbilityLab, Shirley Ryan AbilityLab, Chicago, IL, USA

stimulation (TMS) and contralateral low frequency peripheral nerve stimulation [3]. In this line, Thabit et al. proved the induction of LTP based on the synchronization of voluntary thumb abduction and TMS at the **120% of the rMT** in M1 [4]. However, not every PAS application is set in the same intensity induction, neither the same intensity is applied to assess excitability changes before and after the plasticity induction (for short PAS protocol review see [5]).

In order to determine the impact of the intensity applied in the excitability modulation **during the PAS**, in the present study we paired a voluntary abduction of the thumb with contralateral M1 TMS at two different intensities: 110 and 130% of rMT and we assessed the MEP induced at 90, 100, 110, 120 and 130% of the rMT to compare the differences between the two subjects.

2 Materials and Methods

2.1 Subjects

Experiments were performed on 2 healthy female volunteers aged 22 years, none of them presenting a history of neurological disorders neither being under any kind of drug treatment. The protocol was approved by the Ethics Committee of Consejo Superior de Investigaciones Científicas (CSIC), and both subjects gave written informed consent before the experimental procedures.

2.2 EMG Recordings

During the experiments, surface electromyogram (EMG) of Abductor Pollicis Brevis (APB) and Abductor Digiti Minimi (ADM) muscles of the dominant hand were recorded. The EMG signals were amplified, bandpass filtered (5–2000 Hz) and digitized at 10 kHz during the performance of the task for the posterior analysis.

2.3 TMS

TMS was applied using a figure-of-eight coil connected to a Magstim 2000 stimulator (Magstim Company). The optimal motor point for eliciting MEP for APB muscle (hot-spot) was established and the optimal position was marked on the scalp to ensure identical placement of the coil throughout all the experimental procedures.

2.4 *MEP Measurements*

The rMT for the APB muscle was defined as the lowest stimulus intensity required for eliciting a MEP with peak to peak range of ± 50 mV in 5 of 10 trials. For evaluating the changes in the corticospinal excitability, we applied 2 times 5 pulses of an intensity range from 90 to 130% of the rMT randomly ordered. The cortical excitability was obtained by measuring the amplitude of the MEPs at each intensity value.

2.5 *Simple Reaction Time (RT) Task*

The task consisted in a grey background with a simple visual clue (a black dot) that when changed to a white cross, the subjects had to click as fast as possible. The cue refresh rate was randomly set for each trial between 5 and 8 s.

2.6 *Experimental Procedure*

The experimental structure is based on three MEP assessment times: before (PRE), immediately after (POST) and 30 min after (POST30) PAS intervention, and two PAS intervention times of 60 trials each.

Before PRE assessment, the individual RMT was determined and mean RT of the simple RT task was measured by 30 evaluation trials. PAS protocol was applied combining TMS in contralateral M1 25 ms before the individual mean RT while the subject was performing the task.

2.7 *Data Analysis*

We analyzed the MEP amplitudes with a Student T test for repeated measures. There were two PAS types in this study, one per subject: the one applied at 110% and the other at 130% of rMT.

3 *Results*

The Student test for average comparison for repeated measures revealed that, concerning Time pairwise comparison (Fig. 1) in the **110% PAS type**, comparing with PRE time (APB-90%: Mean = 30.10 SE = 9.25; 100%: Mean = 97.26 SE = 19.76; 110%: Mean = 507.38 SE = 94.74), MEP amplitude was significantly higher

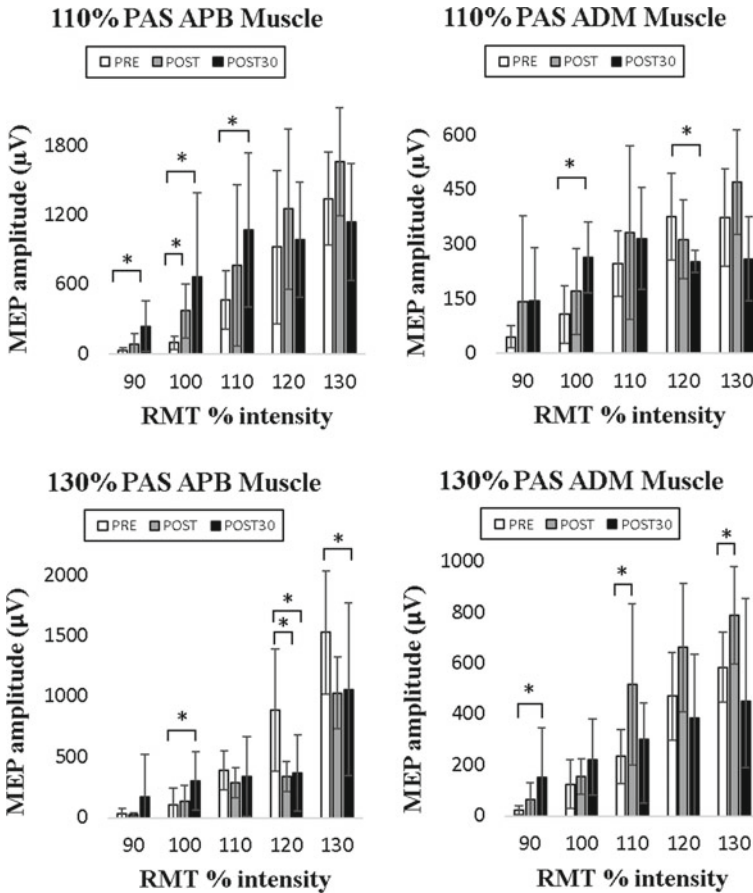


Fig. 1 The mean \pm SD of MEPs for APB and ADM muscles at 90, 100, 110, 120 and 130% of rMT for *110 PAS type* and *130 PAS type* in different experimental phases: PRE, POST and POST30

in APB, in POST time at 100% (Mean = 374.32 SE = 77.99, $p = 0.011$) and in POST30 time at 90% (Mean = 241.56 SE = 76.48, $p = 0.030$), 100% (Mean = 667.34 SE = 243.389, $p = 0.039$) and 110% (Mean = 1110.97 SE = 249.60, $p = 0.033$) of rMT.

Concerning ADM, the MEP amplitude compared with PRE (100%: Mean = 107.28 SE = 26.59; 120% Mean = 375.68 SE = 42.22), was significantly higher in POST30 time at 100% (Mean = 296.14 SE = 48.09, $p = 0.001$) of rMT and significantly lower in POST30 time at 120% (Mean = 253.24 SE = 10.45, $p = 0.012$).

In *130% PAS type*, the MEP amplitude in APB muscle compared to PRE time (100%: Mean = 116.69 SE = 47.61, 120%: Mean = 886.51 SE = 159.41; 130%: Mean = 1530.49 SE = 160.45) was significantly lower in POST time, at 120% (Mean = 338.62 SE = 39.45; $p = 0.005$) and 130% (Mean = 1029.36 SE = 93.62; $p =$

0.001) of rMT. In POST30 time, the MEP amplitude significantly increased at 100% (Mean = 303.36 SE = 76.75; $p = 0.009$) and decreased at 120% (Mean = 371.03 SE = 104.99; $p = 0.010$).

Regarding ADM muscle, compared to PRE time (90% Mean = 23.77 SE = 6.10, 110% Mean = 234.16 SE = 33.56, 130% Mean = 585.47 SE = 43.37) there is a MEP amplitude increment in POST time (110% Mean = 517.29 SE = 100.19, $p = 0.038$ and 130% Mean = 789.36 SE = 61.00, $p = 0.017$) and in POST30 time (90% Mean = 152.64 SE = 50.24, $p = 0.035$).

4 Discussion

The results of the **110% PAS** presented a significant increase at low intensities for the APB. This outcome appears to indicate that the PAS protocol at a low intensity increases the cortical excitability of the main muscle involved in the task at lower intensities.

Simultaneously, the data for the **130% PAS** showed a significant decrease for the APB muscle at higher intensities. However, it triggered a generalized increase in ADM muscle.

5 Conclusion

Our study likely indicates that the intensity factor is potentially a crucial variable in PAS neuromodulation outcome. However, it is not possible yet to describe its influence in the process of neural plasticity. For that purpose, it will be necessary to expand the sample, besides the performance of other complementary tests to better define such mechanisms.

We demonstrated the study feasibility to research the PAS protocol technique in relation to applied intensity factor and future studies will evaluate the efficacy of this experimental approach.

Acknowledgment This work was supported by the Neuro Rehabilitation Group (NRG) from the Cajal Institute of the Spanish National Research Council, Madrid, Spain.

References

1. D.O. Hebb, *The Organization of Behavior: A Neuropsychological Theory* (Wiley; Chapman & Hall, 1949)

2. T.V. Bliss, T. Lømo, Long-lasting potentiation of synaptic transmission in the dentate area of the anaesthetized rabbit following stimulation of the perforant path. *J. Physiol.* **232**(2), 331–356 (1973)
3. K. Stefan, E. Kunesch, L.G. Cohen, R. Benecke, J. Classen, Induction of plasticity in the human motor cortex by paired associative stimulation. *Brain* **123**(3), 572–584 (2000)
4. M.N. Thabit, Y. Ueki, S. Koganemaru, G. Fawi, H. Fukuyama, T. Mima, Movement-related cortical stimulation can induce human motor plasticity. *J. Neurosci.* **30**(34), 11529–11536 (2010)
5. A. San Agustín, J.L. Pons, Paired associative stimulation protocols with transcranial magnetic stimulation for motor cortex potentiation. In *School And Symposium On Advanced Neurorehabilitation (SSNR2018)* (p. 44)

Bilateral and Multi-joint Surface Electrical Stimulation for Tremor Reduction. An Essential Tremor Pilot Study



Alejandro Pascual-Valdunciel, Beatriz Adán-Barrientos, Alejandra García-Álvarez, Miguel González-Sánchez, Javier Ricardo Pérez-Sánchez, J. C. Moreno, Francisco Grandas, Filipe O. Barroso, and José L. Pons

Abstract Pathological tremor can be a disabling condition that affects millions of people worldwide. Tremor reduction strategies based on peripheral electrical stimulation of afferent pathways are a promising alternative minimizing the adverse effects of traditional solutions, although a better understanding of the targeted mechanisms is required. Here, we performed a pilot study with two stimulation strategies based on bilateral and multi-joint stimulation below motor threshold, which were tested in two patients with Essential Tremor.

1 Introduction

Essential Tremor (ET), which is one of main disorders leading to pathological tremor and the most prevalent movement disorder in the world, may hamper the execution

This work was funded by the EU programme (EXTEND—Bidirectional Hyper-Connected Neural System) under grant agreement No 779982.

A. Pascual-Valdunciel · J. C. Moreno · F. O. Barroso (✉)
Cajal Institute, CSIC, Madrid, Spain
e-mail: filipe.barroso@cajal.csic.es

A. Pascual-Valdunciel
E.T.S. Ingenieros de Telecomunicación, Universidad Politécnica de Madrid, Madrid, Spain

B. Adán-Barrientos
Carlos III University of Madrid, Madrid, Spain

A. García-Álvarez
University San Pablo CEU, Madrid, Spain

M. González-Sánchez · J. R. Pérez-Sánchez · F. Grandas
Servicio de Neurología, Hospital General Universitario Gregorio Marañón, Madrid, Spain

J. L. Pons
Legs & Walking AbilityLab, Shirley Ryan AbilityLab, Chicago, IL, USA

of activities of daily living [1]. A large population of ET patients does not benefit from medication, deep brain stimulation (DBS), or neurosurgery, which are among the main tremor treatments [1]. In the last years, electrical stimulation of afferent pathways has been explored as promising line to modulate tremor with minimal adverse effects [2]. However, results so far have been variable across patients and the underlying mechanisms are still poorly understood [2]. Electrical stimulation of Ia afferent pathways has been proved to modulate inhibition of muscular activity through the reciprocal inhibition pathway [3] and this approach has already been applied to reduce tremor in ET patients through the out-of-phase stimulation of wrist flexor and extensor muscles [4]. Most of studies using electrical stimulation of afferent pathways only targeted wrist tremor, although tremor is known to mechanically propagate from proximal to distal joints [5]. Additionally, tremor might manifest bilaterally. Consequently, other neural circuitries converging into the contralateral side are not considered when applying electrical stimulation to target only one upper limb. Here, we propose and test in two ET patients two novel stimulation approaches: bilateral stimulation of both upper limbs, and combined stimulation of flexor and extensor muscles of wrist and elbow. On one hand, bilateral stimulation seeks to counterbalance the possible excitation and inhibition mechanisms activated in the contralateral limb through crossed reflexes. On the other hand, multi-joint electrical stimulation aims to activate homonymous projections between agonists to elicit inhibition mechanisms in the antagonist tremorigenic muscles.

2 Material and Methods

2.1 Patients

Two ET patients (female aged 73, male aged 62) were recruited from Hospital Universitario Gregorio Marañón (Madrid, Spain). All procedures were conducted in accordance with the Declaration of Helsinki and approved by the hospital ethical committee.

2.2 Experimental Procedure

For the bilateral stimulation experiment, surface electromyography (sEMG) electrodes were placed over the muscle belly of Flexor Carpi Radialis (FCR) and Extensor Carpi Radialis (ECR) of both arms, and stimulation electrodes were placed over radial and medial nerves at the arm level of both sides [3]. For the multi-joint stimulation experiment, both sEMG and stimulation electrodes were placed over the muscle belly of FCR, ECR, biceps brachii (BB) and triceps brachii (TB) of the arm in which tremor was more predominant. Seven Inertial Measurement Sensors (IMUs) (Technaid S.L.,

Spain) were placed on both sides of the upper limb to objectively quantify tremor kinematics. An embedded control unit including a voltage-based electrical stimulator and an EMG amplifier (OT Bioelettronica, Italy) was used to acquire the sEMG signals at 1,000 kHz and to operate the control algorithm driving the stimulation.

A neurologist assessed the tremor condition of each patient, who was sat on a chair during the experimental session. After instrumenting the patient with the IMUs and the electrodes, stimulation parameters were calibrated. Pulse width and stimulation frequency was set to 400 μ s and 100 Hz, respectively. Stimulation amplitude was calibrated for each muscle above sensation threshold and below motor threshold (maximum current was 5 mA).

The experimental session consisted on ten stimulation trials in which the subjects were asked to hold their arms outstretched and pronated for 60 s. Each trial was divided in two 30 s windows in which the stimulation system was turned ON or OFF randomly. During the bilateral stimulation experiment, three stimulation conditions were tested during the ON windows: (1a) Bilateral stimulation of both arms; (1b) Stimulation of the dominant tremorigenic arm; (1c) Stimulation of the non-dominant tremorigenic arm. During the multi-joint stimulation experiment, three conditions were tested: (2a) Combined stimulation of both wrist and elbow flexors and extensors; (2b) Stimulation of elbow flexors and extensors; (2c) Stimulation of wrist flexors and extensors.

Selective and adaptive timely stimulation (SATS) strategy was applied during the ON windows in alternating 1s recording and 2s stimulation windows (see Pascual-Valdunciel et al. [6]). Patients were able to rest the time needed between trials.

2.3 Data and Statistical Analysis

Raw quaternions recorded with the IMUs were transformed to joint angles and filtered in the tremor band (3–9 Hz) [4]. Then, the power spectral density was computed and integrated to compute the tremor power. A tremor score was created to normalize data from each joint accordingly to Eq. (1) [6].

$$Tremorscore = 0.5 + 0.5 \times \frac{(systemOFF - systemON)}{\max(systemOFF; systemON)} \quad (1)$$

Tremor score equal to 0.5 represents no change in tremor amplitude between the OFF and ON windows, while 1 represents 100% tremor reduction, or 0 represents 100% tremor aggravation. In order to compare the phase difference between the two arms, the filtered angles were segmented in tremor cycles and the phase difference was computed considering the nearest peaks between the two signals.

Since this contribution describes a pilot study, descriptive statistics were used to analyze the data from the two patients.

3 Results

Both patients completed the experiments without any adverse effects. Figure 1a represents the tremor scores for the bilateral stimulation experiment. Bilateral stimulation reduced wrist flexion-extension tremor in both tremorgenic predominant arm (0.58 ± 0.22) and non-tremorgenic predominant arm (0.54 ± 0.36) in 4 out of 6 trials. The single stimulation of the non-predominant tremorgenic arm or the predominant tremorgenic arm reduced tremor in the ipsilateral stimulated wrists in all the performed trials. The effect was quite variable on the contralateral side (tremor increased in half of the trials and decreased in the other half of the trials). Main tremor frequencies in the predominant and non-predominant tremorgenic arm were 5.3 and 5.8 Hz, respectively. Tremor was out-of-phase between both wrists (tremor phase shifted $>70^\circ$) 67.7% of the time.

Figure 1b represents the tremor scores for the multi-joint tremor reduction experiment. Single stimulation of BB and TB and single stimulation of FCR and ECR did not achieved tremor reduction neither in the elbow nor the wrist. Combined stimulation of flexor and extensor muscles of both wrist and elbow reduced tremor in both wrist (0.60 ± 17) and elbow joints (0.56 ± 30).

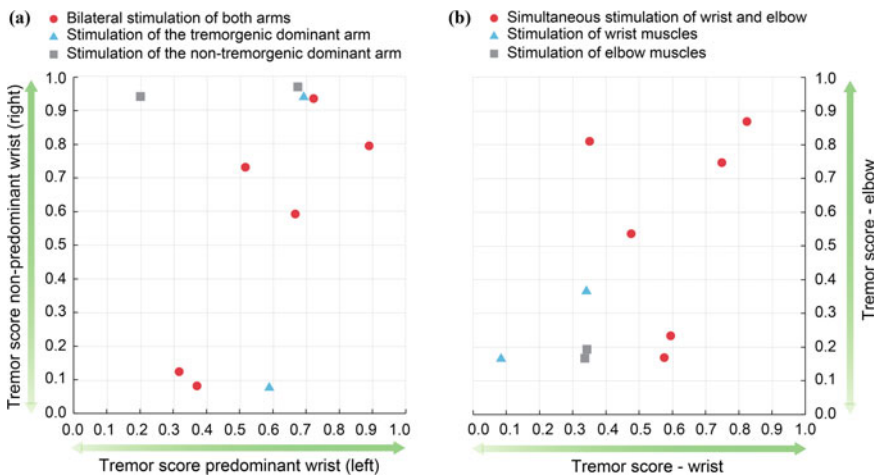


Fig. 1 Tremor scores between the 30 s OFF period and 30 s ON period for each stimulation condition. **a** Bilateral stimulation experiment. **b** Multi-joint stimulation experiment.

4 Discussion

This contribution presents two tremor reduction approaches based on the stimulation of afferent pathways drawing from the shortcomings of previous studies. The variability in the tremor reduction results here presented may be explained through the concomitant variability to case studies and the capability of the stimulator, limited to 5 V power. The prevailing phase shift between both sides and the bilateral tremor reduction scores reported suggest that the stimulation of both affected limbs and the exploration of other spinal circuitries rather than reciprocal inhibition should be considered to refine tremor reduction strategies. Moreover, the stimulation of multiple muscles controlling the elbow alongside the wrist relies on the need of addressing the different sources of mechanical tremor, proved to propagate from proximal to distal joints and vice versa. Forthcoming works should be steered towards testing these approaches in larger ET populations.

References

1. V. Shanker, Essential tremor: diagnosis and management. *BMJ*, 14485 (2019)
2. F.O. Barroso, A. Pascual-Valdunciel, J.L. Pons, in *Review on Tremor Suppression Using Afferent Electrical Stimulation*, ed. by L. Masia, S. Micera, M. Akay, J. Pons. *Converging Clinical and Engineering Research on Neurorehabilitation III*. ICNR 2018. *Biosystems & Biorobotics* (Springer, Cham, 2018), pp. 1092–1096
3. A. Pascual-Valdunciel, F.O. Barroso, S. Muceli, J. Taylor, D. Farina, J.L. Pons, Modulation of reciprocal inhibition at the wrist as a neurophysiological correlate of tremor suppression: a pilot healthy subject study, pp. 6267–6272 (2019)
4. S. Dosen et al., Online tremor suppression using electromyography and low-level electrical stimulation. *IEEE Trans. Neural Syst. Rehabil. Eng.* **23**(3), 385–395 (2015)
5. T.H. Corie, S.K. Charles, Simulated tremor propagation in the upper limb: from muscle activity to joint displacement. *J. Biomech. Eng.* **141**(8) (2019)
6. A. Pascual Valdunciel et al., Intramuscular stimulation of muscle afferents attains prolonged tremor reduction in essential tremor patients. *IEEE Trans. Biomed. Eng.* 1–9 (2020)

**SS14: Protocols and Software
for the Standardization of sEMG
Processing and Analysis for Muscle
Synergy Extraction**

Feasibility Assessment of Muscle Force Estimation Using the Myo Armband During Arm Curl Training



Maialen Zelaia Amilibia, Gabriel Hadjadje, Camilo Cortés,
A. de los Reyes-Guzmán, A. Gil-Agudo, and Álvaro Bertelsen

Abstract As the life expectancy is increasing, the preservation of the autonomy and quality of life of the elderly is becoming a critical socio-economic issue. To prevent conditions such as the frailty, new devices that help the elderly to exercise safely are being investigated (e.g. robotic-based systems). Within such a framework, this work explores the use of inexpensive and easy to use electromyographs (i.e. Myo armband) for the rough estimation of muscle forces from training sessions captures of the arm curl with various loads, such that this information can be used later for the monitoring of the subject physical condition. To assess the quality of the estimations based on the Myo armband, we compared them to those obtained from a professional electromyograph. Preliminary results suggest that the obtained estimations are reasonable for the intended use.

1 Introduction

Frailty is an age-related decline state of nutrition, cognitive, emotional and physical capability, leading to serious impairments or death. As predictions say that in year 2050, 20% of the population will be composed of elders [1], the prevention and treatment of frailty is critical. Early detection and treatment of the frailty based on exercise routines that improve the force, resistance, and equilibrium are key factors to accomplish these goals.

Partial financing obtained from the Basque Government through the Elkartek KK-2017/00085 grant for project Falco.

M. Zelaia Amilibia · G. Hadjadje · C. Cortés (✉) · Á. Bertelsen
Digital Health & Biomedical Technologies, Vicomtech Foundation,
Basque Research and Technology Alliance (BRTA), Gipuzkoa, Spain
e-mail: ccortes@vicomtech.org

Biodonostia Health Research Institute, Donostia-San Sebastián, Spain

A. de los Reyes-Guzmán · A. Gil-Agudo
Biomechanics and Technical Aids Department, National Hospital for Spinal Cord Injury,
Toledo, Spain

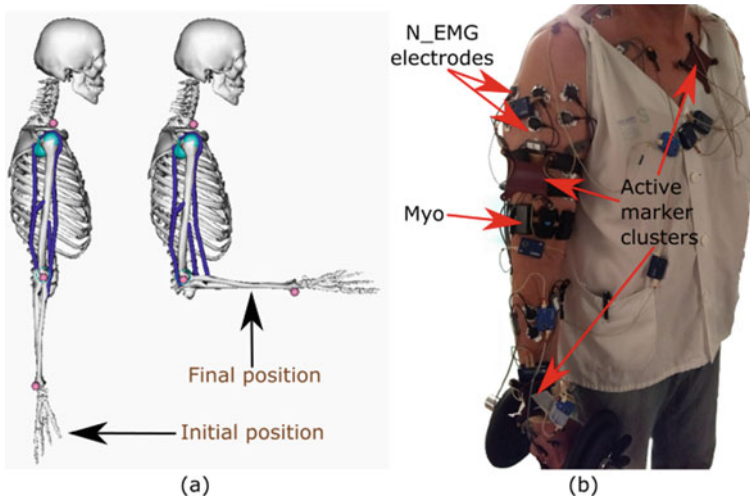


Fig. 1 Data collection: **a** initial and final position of the arm curl movement and **b** motion and EMG recording setup

New devices are being investigated to provide the elderly with safer ways to exercise, such as robotic-based systems that monitor the subject movement to avoid compensatory movements and regulate the load to avoid injuries. Finding ways to use the data captured from the training sessions with those systems to track the subjects evolution also needs to be researched.

This work explores the use of a low-cost electromyograph (Myo armband) to estimate the biceps and triceps muscle forces during the arm curl training (Fig. 1a), which is a relevant exercise in clinical tests for frailty [2, 3]. In this way, we expect to obtain rough force estimations that could be part of an objective metric set that helps therapists to assess and plan the interventions.

Although the Myo armband has been used for clinical applications such as prostheses control [4, 5] or arm fatigue detection [6], to the best of our knowledge, the assessment of the muscle force estimations in the mentioned scenario has not been conducted.

2 Materials and Methods

2.1 Data Collection

Two healthy subjects executed: (a) 5 trials of the arm curl movement with 4 load conditions (no load, low, medium, and high loads), (b) one elbow extension and (c) one elbow flexion with maximum load. The definition of the load levels depended

on the subject physical capability, using dumbbells with weights ranging from 1 to 7 kg. Kinematics were captured using a Codamotion system (200 Hz) with 28 active markers placed on the shoulders, trunk, arm, forearm, and hand. The complete movement protocol was recorded twice per subject with: (a) the surface EMG recording system (Noraxon, Scottsdale, Arizona, USA) (N_EMG) 1500 Hz (16-bit sampling resolution) with one channel per muscle (following SENIAM protocol) and (b) the Myo 200 Hz (8-bit sampling resolution), with its 8-channels around the upper arm (4th channel centered around the biceps).

2.2 Data Processing

A personalized musculoskeletal (MS) upper limb model was created for each subject using the recorded markers. Next, inverse kinematics and dynamics were estimated and a muscle analysis was executed to obtain muscle lengths and muscle moment arms (applied on the elbow joint) for each of the recordings (all of them using OpenSim).

Both N_EMG and MYO armband electromyography (EMG) signals were filtered to obtain their envelopes and then normalized based on the highest activation value recorded among each subject trials. N_EMG recordings were already synchronized with the motion captures. Myo armband recordings were synchronized with the motion by correlating its angular signals in the antero-posterior plane with the shoulder flexion obtained from the inverse kinematics.

2.3 Force Estimation

In order to estimate muscle forces that were consistent with the EMG and the inverse dynamics, we used the Calibrated EMG-Informed NMS Modelling Toolbox (CEINMS) [7], which estimates adjusted muscle excitations that resemble the recorded EMG envelopes while producing muscle forces that generate net moments at a joint close to the estimated joint moment obtained from the inverse dynamics.

CEINMS requires definition of a mapping between the EMG envelopes and the musculo-tendon units (MTU) of the MS model. In the case of the Myo armband, a manual weighted mapping of its EMG channels was made to feed the Biceps long (BLong), Biceps Short (BShort), Triceps short (TShort), and Triceps long (Tlong) MTUs. In the case of the N_EMG signals, the biceps channel was assigned to feed BShort and BLong MTUs, and the triceps channel to feed the TShort and Tlong MTUs.

CEINMS requires a calibration of the MTU parameters of the model. We used the no load, medium and maximum load trials for this. The low and high load trials were used for the validation of the models by computing an error function that assesses the difference between the muscle excitations and joint moments estimated by CEINMS and the experimentally measured ones.

Table 1 Relative error [%] between the muscle force estimations obtained from the N_EMG and Myo armband recordings

Trial	TLong	TLat	BLong	BShort
S1 low	63.92	87.65	2.54	33.28
S1 high	59.63	59.07	33.59	29.83
S2 low	35.56	12.52	53.57	26.47
S2 high	37.30	37.88	10.83	6.49
Mean	49.10	49.28	25.13	24.02

3 Results

Table 1 shows the relative errors between the mean force estimations for each MTU obtained from the N_EMG and Myo armband derived signals. In general, it can be observed that the estimation errors are lower for the muscles that contribute the most to the arm curl: BLong and Bshort.

4 Discussion

The results suggest that, in spite of the large differences in the quality of the acquisition of EMG signals (e.g. sampling rates, bit sampling resolutions, etc.) between the EMG recording devices, the Myo armband data can be post-processed effectively to obtain coarse muscle force estimations (mean relative error $\approx 25\%$ for the main contributing muscles). We believe that such accuracy is enough to conduct follow-ups of the subject force generation capability with a very simple setup for EMG recording. Notice that this work focuses on the differences in the estimations obtained from the EMG systems but does not address the accuracy of the force magnitudes, which would require to record reaction forces on the floor and a study of the MS model residual forces. In addition to this, other limitations that need to be addressed to generate stronger evidence on this research question are: (a) involve more subjects (including pre-frail and frail subjects) in the study, (b) evaluate the long-term validity of the subjects MTU parameters and the necessity of recalibration, and (c) take into account the effect of muscle fatigue in the estimations.

5 Conclusion

This work presented a preliminary assessment of the feasibility to use the Myo armband EMG recordings to estimate the biceps and triceps muscle forces during the arm curl exercise with various load conditions. The force estimations were compared

to those obtained from a professional EMG recording device. The results suggested that coarse force estimations can be obtained from the Myo armband for the follow-up of the force generation capability of a subject. Although more evidence needs to be generated in future studies to corroborate this, devices like the Myo armband seem promising and attractive due to their low-cost and ease of use for patient monitoring.

References

1. G.P. Duarte, J.L.F. Santos, M.L. Lebrão, Duarte, Relationship of falls among the elderly and frailty components. *Revista Brasileira de Epidemiologia* **21**, e180017 (2019)
2. D. Simonetti, L. Zollo, E. Papaleo, G. Carpino, E. Guglielmelli, Multimodal adaptive interfaces for 3D robot-mediated upper limb neuro-rehabilitation: an overview of bio-cooperative systems. *Robot. Auton. Syst.* **85**, 62–72 (2016)
3. H. Arrieta, C. Rezola-Pardo, I. Zarrazuquin, I. Echeverria, J.J. Yanguas, M. Iturburu, S.M. Gil, A. Rodriguez-Larrad, J. Irazusta, J. A multicomponent exercise program improves physical function in long-term nursing home residents: a randomized controlled trial. *Exp. Gerontol.* **103**, 94–100 (2018)
4. G.A.M. de Souza, M.G.N.M. da Silva, A.E.F. da Gama, Upper limb muscle activation: an EMG analysis using Myo® armband, in *XXVI Brazilian Congress on Biomedical Engineering* (Springer, Singapore, 2019)
5. N.Y. Sattar et al., Real-time EMG signal processing with implementation of PID control for upper-limb prosthesis, in *IEEE/ASME International Conference on Advanced Intelligent Mechatronics (AIM)* (IEEE, 2019)
6. M. Montoya, O. Henao, J. Muñoz, Muscle fatigue detection through wearable sensors: a comparative study using the MYO armband, in *Proceedings of the XVIII International Conference on Human Computer Interaction* (2017)
7. C. Pizzolato et al., CEINMS: a toolbox to investigate the influence of different neural control solutions on the prediction of muscle excitation and joint moments during dynamic motor tasks. *J. Biomech.* **48**(14), 3929–3936 (2015)
8. V. Serrau et al., Muscle activation of the elbow flexor and extensor muscles during self-resistance exercises: comparison of unilateral maximal contraction and bilateral self-resistance. *J. Strength Condition. Res.* **26**(9), 2468–2477 (2012)

The Influence of Harmonics Filtering for Weak EMG Analysis



R. Aydın, F. Alnajjar, M. Sonoo, A. Costa Garcia, K. Takatsune, and S. Shimoda

Abstract Cerebral palsy is a neurological disorder which caused by a brain injury or developmental malfunction of the brain. Cerebral palsy may cause many adverse results such as movement and postural stability problems. One of the medical conditions that may occur with such problems is scoliosis. There are few treatment options, one of the common methods is the use of a back brace. The patients can be more active when they wear the brace. The purpose of our research is to clarify the difference between the conditions with and without brace focusing on the difference of surface electromyography (s-EMG) activities. In many cases, however, s-EMG signal is too weak to analyse in typical way. In this paper, we discuss the filtering method of the weak s-EMG signals. We use a notch filter whose cut-off frequencies are determined by fast Fourier transform of the raw signals. We show that the filter does not make strong influence for the features of s-EMG signals to be able to discuss the differences between the conditions which are with and without wearing a back brace.

1 Introduction

Cerebral palsy is a neurodevelopmental disorder that is prevalent amongst children and adolescents and it caused by a brain injury or brain malfunctioning during its development. Cerebral plays mainly effects movement and posture [1]. One of the major problems regarding movement and the posture that had been affected is scoliosis. Scoliosis manifests itself as sidewise incurvation of the spine. Depending on the

We would like to thank TOYOTA Motor Co. LTD for their sponsorship.

R. Aydın · M. Sonoo · A. Costa Garcia · S. Shimoda (✉)
Intelligent Behavior Control Unit, RIKEN Center for Brain Science (CBS), Wako, Japan
e-mail: shingo.shimoda@riken.jp

F. Alnajjar
College of Information Technology (CIT), UAE University, Al Ain, UAE

K. Takatsune
Department of Intelligent Science and Technology, Kyoto University, Kyoto, Japan

age at which the progression has started and the extent of the impairment, the condition may vary. There are few treatment options medications, therapies and surgery. Moreover, the use of a rigid back brace has been favoured in the literature for such patient populations. A considerable amount of studies have presented evidence for effectiveness of brace on scoliosis patients. There are studies in which the findings demonstrated that the prevalence of the surgery might have decreased by the brace usage [2], especially when combined with physical treatment [3]. The improvement in the pulmonary function [4] and the prevention of the increase in the curvature rate have been found as well [5]. However, such researches have the disadvantage of studying weak EMG signals. s-EMG signal may be very weak or at low level when the movement ability is limited. Especially in such patients muscle weakness and contraction generally lead such problem with s-EMG recording. Therefore, filtering is very essential and crucial step before any further classification or analysis steps. The notch filter is a very common tool to filter data from power line noise.

In this pilot study, the main goal was to see the effectiveness of the notch filtering with 3 cut-off points on s-EMG data that is taken from a patient whose s-EMG data contains very low information and high noise which is difficult to use and to observe if there any differences in EMG frequency spectrums of the signal in a patient with scoliosis condition with and without a back brace. We use notch filters which cut-off frequencies are determined by fast Fourier transform of the raw signals.

2 Material and Methods

2.1 s-EMG Recordings

Lab made s-EMG sensors mainly used over frontal and back lower abdominal muscles. The back muscles were recorded with 16-channels whereas front abdominal muscles were recorded with 20-channels EMG. Sampling rate was set to 2000 Hz.

2.2 Study Protocol

The study had carried out in an hospital with therapist and medical professionals. Patient asked to perform some daily life tasks such as eating, drinking, standing up and walking with and without a brace brace. Firstly, patient followed guidelines of medical professional then only s-EMG sensors placed and recording started. Recordings were taken while she performed tasks until otherwise instructed. After tasks completed with only s-EMG sensors, patient stopped and had a brace on and s-EMG sensors. Then the patient performed same tasks (Fig. 1).



Fig. 1 The left image displays patient while wearing only s-EMG whereas the right image demonstrates when the patient wearing s- EMG and brace

2.3 Data Filtering

s-EMG data has been collected and simply filtered with a notch filtering. Three cut off points at 60, 120, and 240 Hz. This step had completed to correct the harmonics of the power line noise in the data. The filtering of the data has proven to be acceptable for this dataset well and the main investigation of the current study has been successfully employed and showed good results (Fig. 2).

As it can be observed from the images that the noise has been successfully unmasked from the data without changing the data characteristics. Therefore, the filtering has been proven to be acceptable for this data type. Filtering in the frequency domain has shown the same level of the effectiveness which can be observed from the below image (Fig. 3).

3 Results

The main goal of this paper has been achieved by showing the effectiveness of the applied filter with 4 cut-off points on raw s-EMG signals. The data was filtered out from the power line noise and its harmonics without interfering the actual data characteristics. Therefore, we can confidently declare our filter as an acceptable filter for such raw s-EMG signals.

In addition to results of our main goal with filtering, we observed some behavioural changes with regard to patient performance while s-EMG and brace were on. The preliminary results from the pilot study have shown positive effects of wearing a back brace on a scoliosis patient. The results are divided into two main categories as observational behavioural results and the EMG analysis of the recorded muscle signals. The results from the observational bodily and behavioural changes have shown that the posture after wearing the back brace has been improved and especially contralateral hand moved more freely compared to the non- brace condition

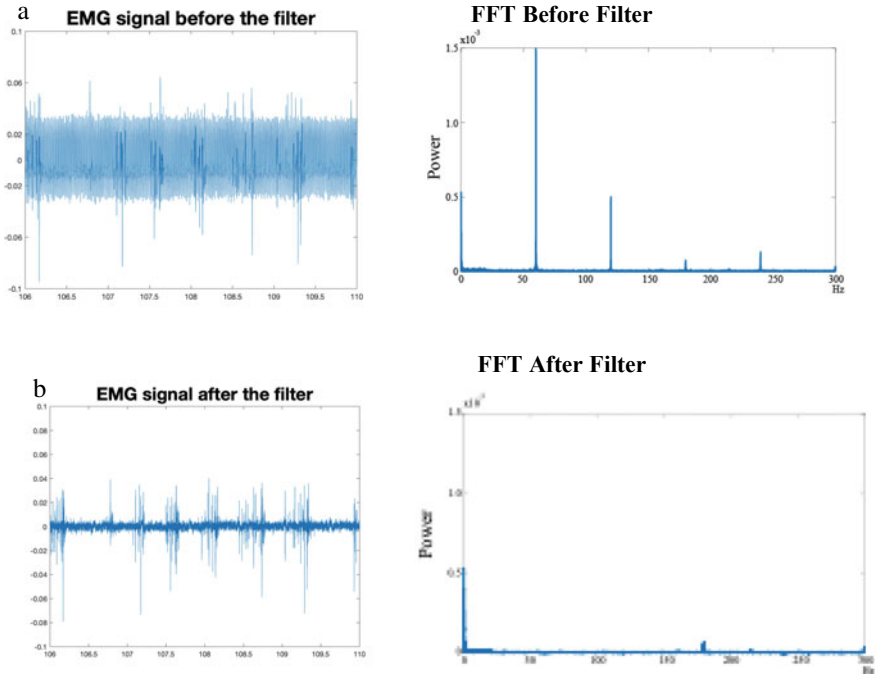


Fig. 2 a The left image displays the raw EMG signal and the right image represents its FFT result before filtering in which the harmonics manifested by peaks at 60, 120, and 240 Hz. b The left image shows the same EMG signal after the filter applied while the right image demonstrates the FFT results of the EMG data after filter

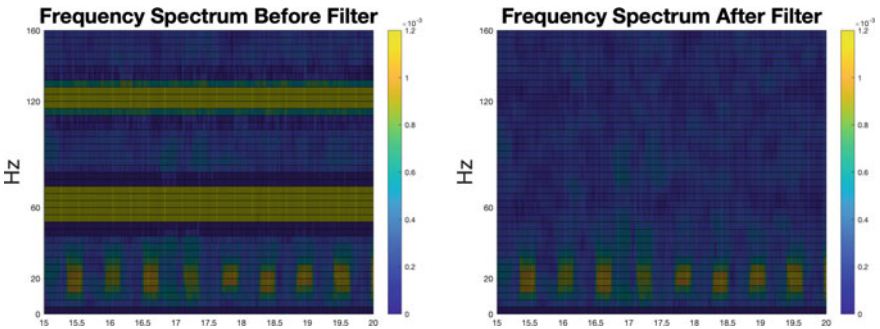


Fig. 3 The left image shows the EMG frequency spectrum before the filter is applied to the data while the right image shows the EMG frequency spectrum of the same data after the filter is applied

under the same daily tasks. The position of the body parts such as shoulders and arm seems to be more natural with the brace use. By natural positioning we refer this from subjects' behavior of keep shoulder more upright and keeping the arm contralateral arm closer to the trunk. Also, these mechanical bodily changes have been observed by medical professionals. Moreover, keeping standing up motion and walking were possible only with the brace wearing condition which clearly shows effectiveness of the brace. Further results also can be interpreted as a change in the neural pathway and the results from the s-EMG have suggested evidence for the viability of median frequency method to measure muscle fibre types which are very important to screen the progression of the curve and the correct classification of the diagnosis subsequently to its treatment.

4 Conclusion

In this paper, we have discussed the influence of harmonics filtering for weak EMG signal analysis. The nature of the EMG signals are different from other bio-signals such as EEG. EMG signals, in general, are very clear and harmonic noise does not pose a big problem in many cases. When the motions are small like the patients with movement difficulties, however, the measured EMG signals will be too weak to analyze with the conventional approach.

The current paper has examined the signal analysis for weak EMG data which contained harmonic noise. We have shown that the combination of notch filtering and frequency domain analysis can clarify the EMG signal to detect the feature of muscle activities embedded in the raw-EMG signals.

Acknowledgment This pilot study was supported by RIKEN Research Institute and Toyota Motor Co. LTD to whom we would like to thank for their supports.

References

1. C. Sankar, N. Mundkur, Cerebral palsy-definition, classification, etiology and early diagnosis. *Indian J. Pediatr.* **72**, 865–868 (2005)
2. M.A. Asher, D.C. Burton, Adolescent idiopathic scoliosis: natural history and long term treatment effects. *Scoliosis* **1**(1), 2 (2006)
3. K. Pehrsson, S. Larsson, A. Oden, A. Nachemson, Long-term follow-up of patients with untreated scoliosis. A study of mortality, causes of death, and symptoms. *Spine* **17**(9), 1091–1096 (1992)
4. H.R. Weiss, G. Weiss, H.J. Schaar, Incidence of surgery in conservatively treated patients with scoliosis. *Pediatr. Rehabil.* **6**(2), 111–118 (2003)
5. S.L. Weinstein, L.A. Dolan, J.G. Wright, M.B. Dobbs, Effects of bracing in adolescents with idiopathic scoliosis. *N. Engl. J. Med.* **369**(16), 1512–1521 (2013)

Online Continuous Detection of Time-Varying Muscle Synergies



Simone Ranaldi, Claudio Castellini, Andrea D'Avella, and Silvia Conforto

Abstract Muscle synergies have been widely used as a compact description of the neuromuscular motor control strategies. The online detection of synergistic activations might therefore improve the feasibility of sEMG-based control algorithms. In this study, a simple online detector of time-varying muscle synergies activation timings is proposed, and its performance is evaluated in a simulated online scenario on a small sample of experimental signals.

1 Introduction

The surface electromyography signal (sEMG) has been widely used to characterize the neural strategies underlying human motor control. The direct relationship between sEMG signals and neuromuscular control strategies has been often taken as a motivation to exploit those signals for improve the control of prostheses or virtual reality avatars [1]. Moreover, it is well known that the human musculoskeletal system has a redundant nature and that different muscles must be coordinated to achieve a variety of biomechanical functions. Thus, a physiologically inspired dimensionality reduction technique may significantly improve the outcomes of any real-time decision algorithm using the sEMG signal.

The coordination of different muscles is typically represented under the muscle synergy model; regardless of the physiological interpretation and mathematical

S. Ranaldi (✉) · S. Conforto
Department of Engineering, University of Roma Tre, Rome, Italy
e-mail: simone.ranaldi@uniroma3.it

C. Castellini
Institute for Robotics and Mechatronics, DLR—German Aerospace Center, Weßling, Germany

A. D'Avella
Laboratory of Neuromotor Physiology, IRCCS Fondazione Santa Lucia, Rome, Italy

Department of Biomedical and Dental Sciences and Morphofunctional Imaging, University of Messina, Messina, Italy

implementation, the general feature of this model is that different muscles are acting in a patterned or grouped manner, i.e. as a *synergy*, to generate complex movements. Among the different muscle synergy models, the time-varying model is the one that describes muscle coordination in the most compact way [2]. Moreover, the combination of spatial and temporal information in the same synergy makes this description the most suitable for investigating the sEMG signal in a windowed way, potentially improving reliability of any sEMG-based decision algorithm. While the online processing of muscle synergies has been shown to be relatively straightforward when a synchronous model is exploited [3], the real-time detection of the time-varying synergistic structure is more complex and requires the optimization of different processing blocks.

In this work, a simple, projection-based method to identify the activation of time-varying synergies starting from a pre-existent dictionary is presented and tested, with focus on its implications for online sEMG processing.

2 Methods

2.1 Time-Varying Muscle Synergies

The time-varying synergy model describes the coordination of several different muscles as the combination of the activity of a set of patterned muscle activations. In this description, a muscle synergy or motor module is defined as the potentially asynchronous activation, within a fixed time frame, of different muscles [2]. Considering this, any complex muscle activation pattern can be generated by the linear combination of a small number of synergies, optimally scaled in amplitude and shifted in time.

In the model of the time varying muscle synergy, each motor module is represented by a $N_m \times L$ matrix, where N_m is the number of muscles and L is the length of the synergies. If the muscle coordination is well represented by N_s synergies, the sEMG envelope during a biomechanical event is then described by N_s matrices determining the dictionary of synergies and two vectors of length N_s , C and τ , indicating the scaling and timing coefficients.

2.2 Experimental Protocol

The online synergy detector has been tested on upper limb reaching data coming from three subjects among those enrolled in [2]. All the details on the experimental protocol can be found in the referenced study. For this work, the kinematics of the movement was used only as a reference for the segmentation of the electromyographic

signal. The sEMG envelopes, originally recorded at 1 kHz, have been down sampled at 100 Hz.

2.3 Data Analysis

The tonic component of the sEMG amplitude was estimated and removed from the signal, and time-varying synergies were then extracted following the same procedure adopted in [2]. To be coherent with the previous results on the same data, 5 synergies were extracted from all the subjects and the length of each module has been set to 500 ms. The R^2 value coming from the synergy approximation has been evaluated, and the W matrices were used as a dictionary for the online detector.

2.4 Online Detector

The online detector works by projecting the first 200 ms of each synergy on the sEMG envelopes. At each time sample, all the synergies are projected onto the multi-muscle signal and the synergy with the greatest projection value after normalization is selected as a candidate for being active. The scalar product for that synergy is then evaluated for the subsequent windows until its maximum is reached; the beginning sample of this window is then fixed as the onset of the synergy and the scaling coefficient is set to the corresponding scalar product value. The synergy profile is then scaled by the amplitude coefficient and subtracted from the corresponding samples of the sEMG signal, similarly to what is done in the extraction algorithm [2]; moreover, when a synergy is found to be active it undergoes a refractory period for its entire duration. If at any time instant a different synergy has a higher scalar product with respect to the current candidate, that synergy is selected as the new candidate without defining any activation of the previous one; this criterion has been inserted to ensure that no spurious activations can be detected when no synergy is present, given that in presence of zero activity the projection values are randomly fluctuating.

The quality of the online detection has been quantified by using the estimated C and τ to reconstruct the original data and comparing the R^2 coming from this approximation to the one found with the original synergy extraction algorithm. Moreover, the errors in the identification of the C and τ values have been computed as an additional metric.

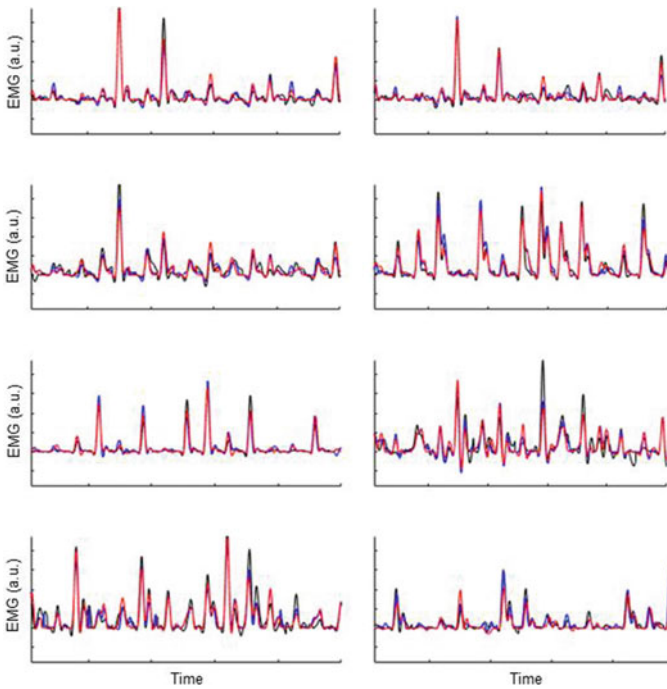


Fig. 1 An example of the reconstruction of the original data (black) coming from the synergy extraction (blue) and from the online detector (red)

3 Results

In order to ensure the validity of the results regardless of convergence to local minima, all the synergy estimation and subsequent projections have been replicated 30 times. R^2 values coming from the original synergy extraction algorithm have been found to be 0.80 ± 0.01 , while for the reconstructed data the quality of the reconstruction drops to 0.77 ± 0.02 . On average, the online detector has an error of 5% of the original value for the amplitude coefficients and of 15 ms on the timing instants. From Fig. 1 an example of the comparison between the original data and the two reconstruction is shown on randomly selected subset of muscles for a 10 s time interval.

4 Discussion

The presented results show that it is, in general, possible to build an algorithm for the online detection of the onset of the time-varying synergy from a multi-muscle sEMG recording. The small drop between the quality of the reconstruction from the optimization algorithm for synergy extraction and the one from the projection

algorithm suggests that the performance of this kind of detector depends strongly on the quality of the synergy dictionary, that must be built on a subject-specific basis before the application of the controller. In this sense, future studies will have to investigate whether the dictionary built upon a relatively small portion of the time series is able to describe longer sequences of activations. In an ideal stationary model, if the calibration signal spans the entire movement space the synergy matrices are a complete basis for the sEMG space; however, several factors might affect the signal, potentially requiring a re-calibration of the dictionary. Among those factors, the co-adaptation mechanisms between the user and the controlled device might play a significant role and must be accurately characterized in a real life scenario.

A potential limitation of this online detector is the impossibility to account for activation of variable length; while in the literature some attempts to identify muscle synergies with a dynamic time warping approach have been proposed [4], the solution to the problem requires complex and computationally expensive algorithm that will detrimentally affect the real-time performance of the detector.

5 Conclusions

In this study, a projection algorithm for the online identification of time-varying synergies has been proposed. The results have shown that, if the synergy dictionary is well defined, it is possible to identify the onsets and the amplitude coefficients of the time-varying synergy starting from a window smaller than the length of the synergy itself. While some optimization procedures might be needed for a real-world implementation of this method, the results are promising in the framework of using these modular motor control concepts in myoelectric control algorithms.

References

1. C. Castellini, R.M. Bongers, M. Nowak, C.K. van der Sluis, Upper-limb prosthetic myocontrol: two recommendations. *Front. Neurosci.* **9** (2016)
2. A. d'Avella, A. Portone, L. Fernandez, F. Lacquaniti, Control of fast-reaching movements by muscle synergy combinations. *J. Neurosci.* **26**(30), 7791–7810 (2006)
3. F. Lunardini, C. Casellato, A. d'Avella, T.D. Sanger, A. Pedrocchi, Robustness and reliability of synergy-based myocontrol of a multiple degree of freedom robotic arm. *IEEE Trans. Neural Syst. Rehabil. Eng.* **24**(9), 940–950 (2016)
4. F.M. Ramos, A. d'Avella, M. Hayashibe. Identification of time-varying and time-scalable synergies from continuous electromyographic patterns. *IEEE Robot. Autom. Lett.* **4**(3), 3053–3058 (2019)

Approximate Credibility Intervals for Independent Component Analysis



Olivier Thill and Luca Citi

Abstract Independent component analysis (ICA) is often used to retrieve the activation patterns of motor units (MUs) from electromyographic (EMG) data. This chapter uses a Bayesian approach to look at the uncertainties around the ICA results. This is done both in regards to the amount of training data provided and in regard to how the certainty differs for each MU source recovered by ICA.

1 The Electromyographic Inverse Problem

1.1 Problem Description

Raw electromyographic data \mathbf{X} as recorded by an array of electrodes on the skin surface is a mixture of the electric potentials \mathbf{Y} caused by the activations of the motor units (MUs) within the muscle. Each of the n rows in \mathbf{Y} is a trace of a MU activation pattern which will be referred to as a source in the following. Assuming a simple linear generative model and additive noise, the relationship between \mathbf{X} and \mathbf{Y} can be written as:

$$\mathbf{X} = \mathbf{M}\mathbf{Y} + \mathbf{N} \quad (1)$$

where \mathbf{N} represents noise due to the recording process but also to the presence of any background physiological signals beyond those of interest; \mathbf{M} is the unknown mixing matrix linking \mathbf{Y} to \mathbf{X} . In the noiseless mixture approximation, this can be restated as:

$$\mathbf{Y} = \mathbf{W}\mathbf{X} \quad (2)$$

This work was supported by the European Commission under the DeTOP project (LEIT-ICT-24-2015, GA #687905).

O. Thill · L. Citi (✉)

School of Computer Science and Electronic Engineering, University of Essex, Colchester, UK
e-mail: lciti@essex.ac.uk

where \mathbf{W} , called the un-mixing matrix, is the inverse of \mathbf{M} . For a complete overview of the general problem see [1].

1.2 Aims

This chapter presents a method to measure the uncertainties of each signal in estimates of \mathbf{Y} . These measurements could be of use to quantify the quality of the algorithm used to derive the estimates given \mathbf{X} or as input to a feature selection algorithm.

This work uses EMG data solely as example, the method presented here ought to be applicable in a straightforward manner to any inverse problem as defined in (1) and (2) such as when dealing with electroencephalogram (EEG) data but also for datasets outside the brain computer interface domain.

2 Methods

2.1 Parameter Inference

Our algorithm starts by finding estimates $\hat{\mathbf{W}}$ and $\hat{\mathbf{Y}}$ of the un-mixing matrix and of the sources using the reloaded fast ICA algorithm [2] in the noiseless case corresponding to (2).

The estimate $\hat{\mathbf{W}}$ of the un-mixing matrix can be interpreted as the maximum-a-posteriori (MAP) solution of the likelihood formulation of the ICA:

$$\mathcal{L}(\mathbf{W}|\mathbf{X}) = \prod_i \prod_t (1 - \tanh(\mathbf{W}[i, :] \mathbf{X}[:, t])^2) \|\mathbf{W}\| \quad (3)$$

where t is an index for the samples in time and i indexes rows of \mathbf{W} which themselves produce the i th source in \mathbf{Y} .

Then, under the assumption of a flat prior, the Laplace approximation [3] around the MAP $\hat{\mathbf{W}}$ was derived for each row of \mathbf{W} . Let the matrix $\hat{\mathbf{H}}_i$ be the Hessian of the log-likelihood with respect to row i of \mathbf{W} , then the posterior of \mathbf{W} can be expressed as follows:

$$\hat{\Sigma}_i = (-\hat{\mathbf{H}}_i)^{-1}, \quad (4)$$

$$\mathbf{W}[i, :] | \mathbf{X} \sim \mathcal{N}(\hat{\mathbf{W}}[i, :], \hat{\Sigma}_i).$$

2.2 Posterior Predictive Distribution

Given new EMG data $\tilde{\mathbf{X}}$ assumed to be generated by some unknown sources $\tilde{\mathbf{Y}}$ through the same mixing process that generated \mathbf{X} (i.e. with an un-mixing matrix distributed according to (4)), the posterior predictive distribution of $\tilde{\mathbf{Y}}$ can be calculated as follows:

$$\tilde{\mathbf{Y}}[i, t] | \mathbf{X}, \tilde{\mathbf{X}} \sim \mathcal{N}(\hat{\mathbf{W}}[i, :] \tilde{\mathbf{X}}[:, t], \tilde{\mathbf{X}}[:, t]' \hat{\Sigma}_i \tilde{\mathbf{X}}[:, t]). \quad (5)$$

In particular the mean and standard deviation of the i th source at sample t of the test signal $\tilde{\mathbf{Y}}$ can be found as:

$$\begin{aligned} \mu_{it} &= \hat{\mathbf{W}}[i, :] \tilde{\mathbf{X}}[:, t] \\ \sigma_{it} &= \sqrt{\tilde{\mathbf{X}}[:, t]' \hat{\Sigma}_i \tilde{\mathbf{X}}[:, t]} \end{aligned} \quad (6)$$

A normalised score which can be understood as a signal to noise ratio of the posterior predictive distribution is calculated for each source in $\tilde{\mathbf{Y}}$:

$$\text{SNR}_i = \frac{\sum_t \mu_{it}^2}{\sum_t \sigma_{it}^2}. \quad (7)$$

This SNR is calculated as the ratio of the total power of the mean (interpreted as an approximation of the true signal) and the total power of the deviations from that signal.

3 Experimental Setup

3.1 The SEEDS Datasets

Our method was tested on the datasets described in [4], which is a collection of EMG recordings. The data were downsampled from 2048 to 256 Hz using a digital filter.

3.2 Preprocessing

There are often periods of inactivity at the beginning and end of each recording. Thus, from each recording only the continuous blocks of 1280 samples (5 s) with the highest mean absolute magnitude were taken. Each block was visually inspected to ascertain that the selection was not caused by artefacts.

Each block was split into a training and a test set. As the effect of different training set sizes is of interest, the experiment was rerun for each block with a number of different training set sizes.

The different sizes for a training set were: 256, 385, 512, 640, 768, 896, 1024. The training data was always the centremost while the test set was composed on the data remaining before and after the training data.

4 Results

A visual representation of the $\tilde{\mathbf{Y}}$ s corresponding to (6) is shown in Fig. 1. Note how a larger training set (red lines) leads to a smaller uncertainty in the estimation of the sources corresponding to the test set. Figures 2 and 3 show the signal to noise ratios as a function of the rank of the source, ordered either as returned by reloaded fast ICA or by the signal to noise ratio itself.

The experiment has been run over multiple recordings and the results from each run were qualitatively similar across all of them to the small subset shown in this section.

4.1 SNR Given Training Size

As expected, the signal to noise ratio shown in Figs. 2 and 3 degrades steadily as the training size decreases. This is because shorter training sets lead to larger uncertainties in the estimation of \mathbf{W} (i.e. larger Σ_i) which translates into larger uncertainties in the reconstructed $\tilde{\mathbf{Y}}$ s.

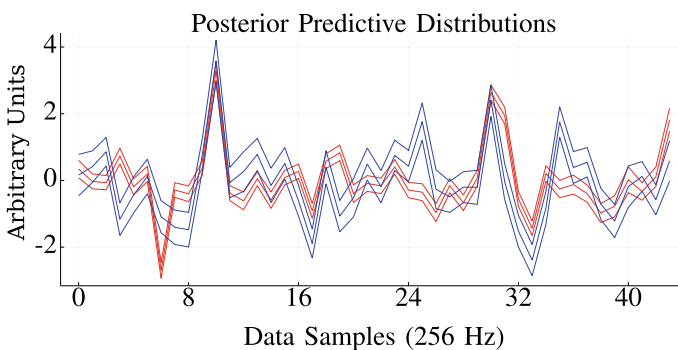


Fig. 1 Two example $\tilde{\mathbf{Y}}$ traces of, most likely, the same source. Shown is the mean and the mean \pm the standard deviation over time for each trace. The red trace was obtained from a model trained with 1024 data samples and the blue trace from one trained with 256 data samples

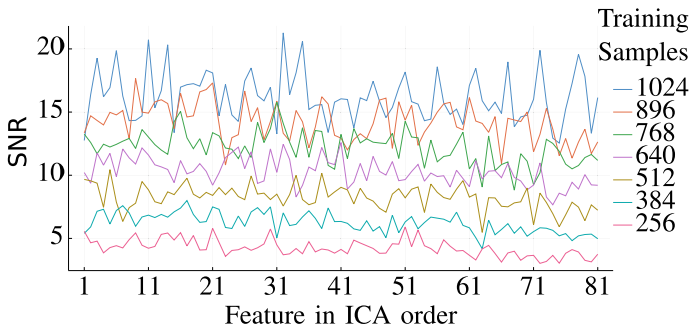


Fig. 2 Signal to noise ratio calculated over the test data ordered according to ICA source rank

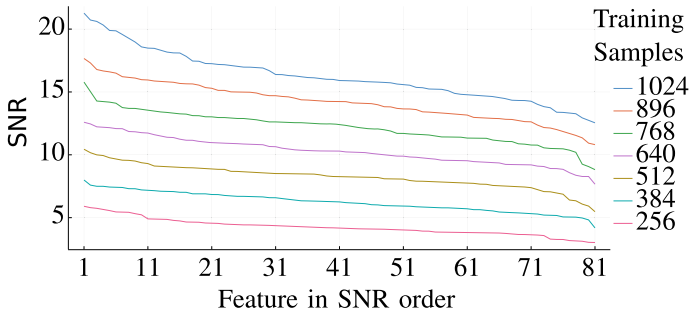


Fig. 3 Signal to noise ratio calculated over the test data ordered according to decreasing SNR

4.2 SNR Given Source Rank

The reloaded fast ICA algorithms returns the unmixed features in order of best to worst according to its own heuristic, see [2]. As can be seen from Fig. 2 this heuristic gives a similar ordering than ordering by SNR would give. However visual inspection of the actual predictive posterior traces of the sources (\tilde{Y}) reveals SNR to be a far better predictor as most of the strong negative peaks found in Fig. 2, correspond to “noise” sources and not to unmixed motor unit action potential signals while the other sources are actual unmixed signals.

For comparison Fig. 3 shows how SNR changes with the sources ordered from highest to lowest SNR. Here the dip towards the end corresponds to “noise” sources.

5 Conclusion

The results show that the signal to noise ratio can give insight on the quality of unmixed signals. One possible use case might be feature selection since “noise”

channels showed, in the data sets explored, visible different SNR than other sources reconstructed by the same un-mixing matrix. Further research could look into using the benefits of using an informative prior rather than the flat prior used so far.

References

1. R. Merletti, D. Farina (eds.), *Surface Electromyography?: Physiology, Engineering, and Applications* (Wiley, New York, 2016)
2. K. Nordhausen, P. Ilmonen, et al., Deflation-based FastICA reloaded, in *19th European Signal Processing Conference* (2011), pp. 1854–1858
3. A. Gelman, J.B. Carlin et al., *Bayesian Data Analysis* (Chapman and Hall/CRC, London, 1995)
4. A. Matran-Fernandez, I.J. Rodríguez Martínez, et al., SEEDS, simultaneous recordings of high-density EMG and angle joint angles during multiple hand movements. *Sci. Data* **6**(1), 186 (2019)

Muscle Tension Analysis in Stroke Patient Sit-to-Stand Motion by Joint Torque-Based Normalization



Ruoxi Wang, Qi An, Ningjia Yang, Hiroki Kogami, Kazunori Yoshida, Hiroyuki Hamada, S. Shimoda, Hiroshi Yamasaki, M. Sonoo, F. Alnajjar, Noriaki Hattori, Kouji Takahashi, Takanori Fujii, Hironori Otomune, Ichiro Miyai, Atsushi Yamashita, and Hajime Asama

Abstract Patients with stroke exhibit distinct muscle activation features in sit-to-stand motion due to motor deficiency. Muscle activation amplitude is an important feature but has not been clarified due to the lack of a valid normalization method to enable intra-subject comparisons. This study, focusing on the paretic side, examines the change in muscle tension manifested in activation amplitude for a patient with stroke in serial measurements by a novel method based on joint torques. We constructed a musculoskeletal model, calculated joint torques by inverse dynamics, and solved muscle activation by forward dynamics simulation. Results showed that tibialis anterior, gastrocnemius, vastus lateralis, rectus abdominis, and erector spinae muscles on the paretic side showed significant improvement in generating maximum muscle tension after a rehabilitation training for 120 days.

1 Introduction

The global population is aging rapidly, accompanied by a steep increase in the prevalence of stroke disease [1]. Today, stroke is a leading cause of disability and death. Patients with stroke suffer motor deficiency in sit-to-stand (STS) motion. For instance, they are prone to falling, which is a common cause of hospitalization [2]. STS is thus a rehabilitation focus for training to improve stroke patients' indepen-

R. Wang · H. Kogami · K. Yoshida · H. Hamada · A. Yamashita · H. Asama
Department of Precision Engineering, The University of Tokyo, Tokyo, Japan

Q. An (✉)
Department of Information Science and Electrical Engineering,
Kyushu University, Fukuoka, Japan
e-mail: anqi@ait.kyushu-u.ac.jp

N. Yang · S. Shimoda · H. Yamasaki · M. Sonoo · F. Alnajjar
RIKEN Brain Science Institute, Aichi, Japan

N. Hattori · K. Takahashi · T. Fujii · H. Otomune · I. Miyai
Morinomiya Hospital, Osaka, Japan

dence and life qualities. To facilitate diagnoses and develop effective rehabilitation strategies, it is essential to understand the mechanism in STS in which patients suffer substantially.

Patients suffering stroke show distinct muscle activation temporal features in STS [2]. Besides muscle activation time, activation amplitude is also an important feature for interpreting the contribution of muscle strength in motions and evaluating motor performance [3]. However, activation amplitude features, especially amplitude changes in rehabilitation, remain unclear due to the lack of a feasible normalization method for stroke subjects.

Both muscle activation time and amplitude measured by surface electromyography (sEMG) on different days during rehabilitation may differ. sEMG normalization is necessary for comparing activation amplitudes due to different human skin conditions and slight inconsistencies in manual placements of sEMG sensors on different days, even if it is with the same subject. If changes in activation amplitude could be clarified for patients in stroke rehabilitation, it would unveil how patients' muscle tension improvements reflect motor recovery, thus suggesting effective training strategies. Therefore, this study, first focused on the paretic side, aims to clarify muscle tension improvements manifested in muscle activation amplitude increases in stroke rehabilitation by normalizing muscle activation based on joint torques, considering that activated muscle forces generate joint torques. Both muscle activities and joint torques were thus examined in this study.

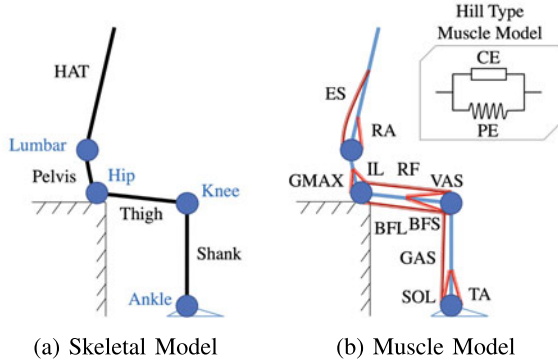
2 Methods

2.1 Musculoskeletal Model

A skeletal model with segments of shank, thigh, pelvis, and HAT (head, arm, and trunk) is constructed to calculate joint torque \mathbf{T}_{jnt} at the ankle, knee, hip, and lumbar joints from body kinematics [4], as in Fig. 1a. \mathbf{T}_{jnt} is solved given joint angles, segment inertia, viscous resistance forces, gravitational forces, and non-linear forces, by inverse dynamics.

A muscle model in Fig. 1b is constructed for forward dynamics simulation to map joint torque τ_k at the ankle, knee, hip, and lumbar joints to motion [4]. Eleven muscles are considered: tibialis anterior (TA), soleus (SOL), gastrocnemius (GAS), rectus femoris (RF), vastus lateralis (VAS), biceps femoris long head (BFL), biceps femoris short head (BFS), gluteus maximus (GMAX), rectus abdominis (RA), erector spinae (ES), and iliopsoas (IL). τ_k is generated by muscle forces F_i exerted at muscle moment arms r_{ki} , as in (1). Hill Type muscle model is applied to calculate F_i , which equals the sum of actively generated tension F_i^{CE} by the contractile element (CE) and passively generated tension by the parallel element (PE) [5]. F_i^{CE} is calculated from (2), where f_{fl} and f_{fv} indicate muscle force-length and force-velocity relationships, respectively;

Fig. 1 Musculoskeletal model. **a** Skeletal model for joint torques calculation by inverse dynamics. **b** Hill Type muscle model for forward dynamics simulation



F_i^{\max} is maximum muscle contraction force; \hat{m}_i is the normalized muscle activation amplitude. The passively generated tension presents when a muscle extends beyond its optimal length.

Due to muscle redundancy induced by bi-articular muscles, the normalized muscle activation amplitude \hat{m}_i in (2) is solved by optimization. Under the constraint that τ_k in (1) equals \mathbf{T}_{jnt} obtained from body kinematics, \mathbf{T}_{jnt} is thereupon decomposed to the desired muscle activation \hat{m}_i by minimizing the error between simulated \hat{m}_i and measured muscle activation m_i , as in (3), to let the model generate a motion resembling the motion performed.

$$\tau_k = \sum_{k=1}^4 \sum_{i=1}^{11} r_{ki} F_i, \tag{1}$$

$$F_i^{\text{CE}} = f_{\text{fl}} f_{\text{fv}} F_i^{\max} \hat{m}_i, \tag{2}$$

$$Z = \sum_{i=1}^{11} \frac{1}{2} \|\hat{m}_i - m_i\|^2. \tag{3}$$

2.2 Measurement Experiment

Measurement experiments were conducted with one patient with stroke for serial assessments of motor recovery using the proposed models. The participant is male, 56 years old, and sustains motor impairment on his left side due to putaminal hemorrhage. Four measurements (on day 25, 95, 116, 144 after stroke onset) were done when the patient was receiving rehabilitation training in the hospital. The patient was invited to repeat 10 trials of sit-to-stand without external assistance at a self-paced speed.

Body kinematics, feet and hip reaction forces, and muscle activities were recorded 100 Hz, 2000 Hz, and 2000 Hz, respectively, using optical motion capture system

(Motion Analysis Corp.), force plates (TechGihan Corp.), and Wireless sEMG sensors (Cometa Corp.). sEMG sensors were placed at the same muscles considered in the musculoskeletal model (in Fig. 1b), except for iliopsoas (IL) since IL is an inner hip joint flexion muscle that cannot be measured with sEMG. Each muscle is either uniaxial or bi-articular and contributes to STS by flexing or extending the ankle, knee, hip, and lumbar joints. Measured muscle activation (m_i) signals were band-pass filtered with a zero-lag fourth-order Butterworth filter of 40–400 Hz and rectified with a fourth-order low-pass Butterworth filter 4 Hz. The reaction force data was low-pass filtered 20 Hz. Each STS trial, consisting of 1 s before and 2 s after the seat-off moment, was extracted from the whole process for data synchronization.

Informed consent was obtained from the patient. Experiments were approved by the Morinomiya Hospital, Japan.

3 Results and Discussion

Maximum muscle tension and peak joint torque generation of the paretic side between the first (day 25) and last (day 144) measurements were examined by paired t-tests [6]. The patient's TA, GAS, VAS, RA, and ES muscles showed significant increases ($P < 0.05$) in maximum muscle tension and activation amplitude. Since stroke patients with no or low-amplitude activation in their TA muscles were prone to falling [2], the significant increases in activating the TA muscle may explain why our patient became less likely to fall as he recovered. Additionally, significant increases in maximum joint torque generation were found at the knee and lumbar joints, whereas the hip joint showed a significant decrease in torque generation. It may suggest that the patient relied less on the hip joint and adopted a different strategy in activating muscles associated with the hip joint to stand up as motor abilities recovered.

4 Conclusion

This study compared and clarified muscle tension improvements reflected in motor recovery of the paretic side for a patient in serial measurements during stroke rehabilitation, using the proposed joint torque-based normalization method. Our results may assist in suggesting effective rehabilitation strategies for stroke survivors. For future work, we aim to explore a better optimization algorithm to minimize errors and consider more stroke and healthy subjects to better understand patients' motor recovery processes.

Acknowledgements This work was supported by JSPS KAKENHI Grant Number 19H05729, 19K22799 and 18H01405.

References

1. GBD 2016 Disease and Injury Incidence and Prevalence Collaborators, Global, regional, and national incidence, prevalence, and years lived with disability for 328 diseases and injuries for 195 countries, 1990–2016: a systematic analysis for the global burden of disease study 2016. *Lancet* **390**(10100), 1211–1259 (2017)
2. P.T. Cheng, C.L. Chen, C.M. Wang, W.H. Hong, Leg muscle activation patterns of sit-to-stand movement in stroke patients. *Am. J. Phys. Med. Rehabil.* **83**(1), 10–16 (2004)
3. V.R. Edgerton, S.L. Wolf, D.J. Levendowski, R.R. Roy, Theoretical basis for patterning EMG amplitudes to assess muscle dysfunction. *Med. Sci. Sports Exerc.* **28**(6), 744–751 (1996)
4. Q. An et al., Analysis of muscle synergy contribution on human standing-up motion using a neuro-musculoskeletal model, in *IEEE International Conference on Robotics and Automation (ICRA)* (2015), pp. 5885–5890
5. F.E. Zajac, Muscle and tendon: properties, models, scaling, and application to biomechanics and motor control. *Crit. Rev. Biomed. Eng.* **17**(4), 359–411 (1989)
6. G. Spyropoulos, T. Tsatalas, D.E. Tsapoulos, V. Sideris, G. Giakas, Biomechanics of sit-to-stand transition after muscle damage. *Gait Posture* **38**(1), 62–67 (2013)

SS15: Technologies for Daily Robotic Assistance and Rehabilitation

An Embedded Implementation of EMG-Driven Control for Assisted Bilateral Therapy



A. Císnal, V. Moreno-SanJuan, D. Sierra, J. P. Turiel, and J. C. Fraile

Abstract The RobHand (Robot for Hand Rehabilitation) platform supports EMG-driven assisted bilateral therapy enabling active-assistive training. The robotic rehabilitation platform incorporates a custom-made EMG embedded solution for real-time gesture recognition whose output is used in the exoskeleton bio-cooperative controller. The recorded EMG signals are processed creating two biofeedback paths (a force source and a visual one) to help the user in developing awareness of and confidence in voluntary control of the system while performing rehabilitation tasks.

1 Introduction

The availability of robotic rehabilitation systems has enabled patients to perform bilateral assisted training, which follows the same principles of the traditional mirror therapy; the only difference is that the illusion provided by the mirror is replaced by the real motion of the paretic limb because of the assistance of the robot. Mirror therapy has been widely used for many years because of its usefulness in motor recovery [1, 2]. In the past years, bilateral assisted therapy, which is based on replicating the reference motion that produces the healthy hand in the exoskeleton attached to the impaired hand, has achieved wide dissemination [3–5].

A real-time embedded implementation of EMG-driven control for RobHand (Robot for Hand Rehabilitation), a robotic rehabilitation system that supports bilateral assisted training for hand rehabilitation is presented.

Electromyography (EMG) enables the detection of the muscular activity and therefore, the user intention of movement and gesture recognition. EMG-driven control

This work has been partly funded by a grant from the Spanish Centro para el Desarrollo Tecnológico Industrial (CDTI) under project ROBHAND-IDI 2017 0263 with funds from Fondo Europeo de Desarrollo Regional (FEDER).

A. Císnal (✉) · V. Moreno-SanJuan · D. Sierra · J. P. Turiel · J. C. Fraile
Institute of Advanced Production Technologies (ITAP), University of Valladolid, Valladolid, Spain
e-mail: císnal@ieee.org

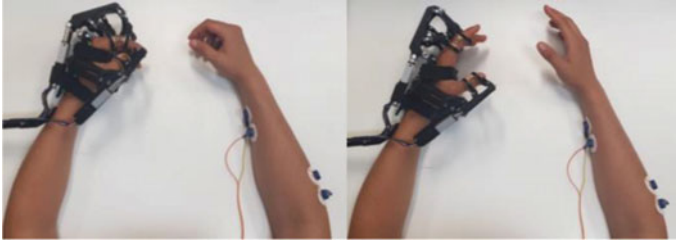


Fig. 1 A user performing an EMG-driven bilateral assisted therapy with RobHand robotic platform

enables the user to train in an active-assistive way, which has been found more effective on motor skills improvement than the passive control. However, the number of embedded implementations of EMG are relatively limited [6–9]. The RobHand platform incorporates an embedded solution for real-time EMG-based hand gesture recognition for the exoskeleton control. It also incorporates an innovative EMG-based visual biofeedback environment, which shows the recorded normalized EMG signals value on a graphic interface using dynamic size bars.

2 Materials and Methods

2.1 Robotic Hand Module

The RobHand exoskeleton is based on a 4-bar linkage underactuated mechanism that assists the hand on performing grasping and releasing movements. It has 5-finger independent modules, each one is powered by a linear motor and has one active and one passive rotation DoF for flexion and extension of the MCP and PIP joint angles, respectively (Fig. 1).

2.2 Electronic System

The resulting electrical activity (raw EMG signals) can be acquired by surface electrodes and appropriate conditioning circuitry. A custom-made application-specific integrated circuit is designed to acquire and perform the analog conditioning of the sEMG signals and to transmit them to a real-time microcontroller. The MCU performs the digital treatment of the signals to calculate the input of the EMG-driven control (based on no-pattern recognition algorithm) and apply the appropriate control signals to the actuators to move the hand exoskeleton according to the user's intention.

The real-time MCU used is the TMS320F28069M (Texas Instruments), which is based on the Harvard architecture and has a 32-bit CPU and a clock speed up to

90 MHz. A custom 2-channel electromyographic data acquisition ASIC, characterized by a 24-bit resolution differential channels and 112 DB of dynamic range (DR) has been designed and developed. Each channel consists of an instrument amplifier followed by a RC low-pass filter (150 Hz cut-off frequency) and is designed to compensate the differential input offset. Analog electromyographic signals are converted to digital signals using an integrated ADC Front End.

2.3 EMG-Driven Assisted Bilateral Training

For detection of hand opening and closing movements, two pairs of surface electrodes (Lessa—AB Medica Group, with a contact area of 30×30 mm) are placed on the skin surface of the belly of the target muscles (Extensor Digitorum and Flexor Digitorum Superficialis) with a center distance of 3 cm, while the reference electrode is attached to the skin surface of the olecranon.

The signals, recorded by the custom-made EMG acquisition system with a sampling frequency of 200 Hz, are filtered to remove the offset and eliminate electromagnetics interferences. The filtered signals are rectified by calculating their envelopes using the Hilbert transform in the time domain. Then, the signals are down-sampled with a 15-points FIR decimation and applied to a 20-points Parks-McClellan low-pass FIR filter (linear minimum-phase, low-pass filter) for producing a smother representation. The resulting rectified signals have a period of 75 ms and are normalized with respect to the previous measured MVC values of the patient. The normalized signals are used as the input of the bio-cooperative controller to detect the user's intention.

The control is based on a threshold-algorithm and it allows to recognize the actual pose of the hand, only considering three predefined poses (rest, open and close hand), and to replicate that pose on the exoskeleton (Fig. 2).

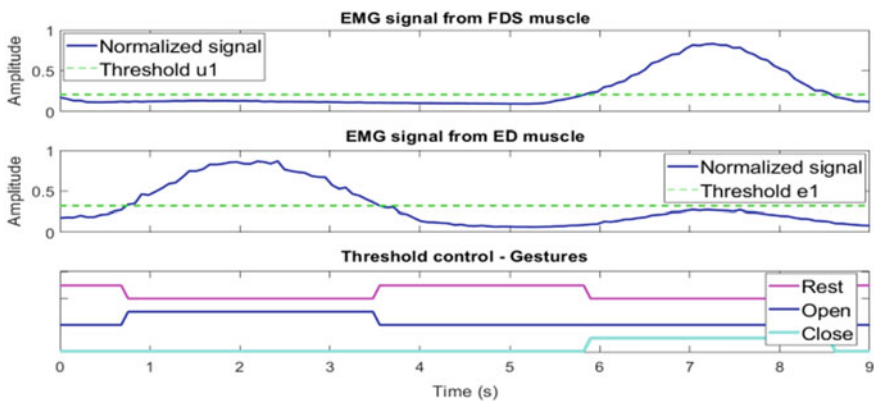


Fig. 2 Threshold based EMG-driven control for gesture detection

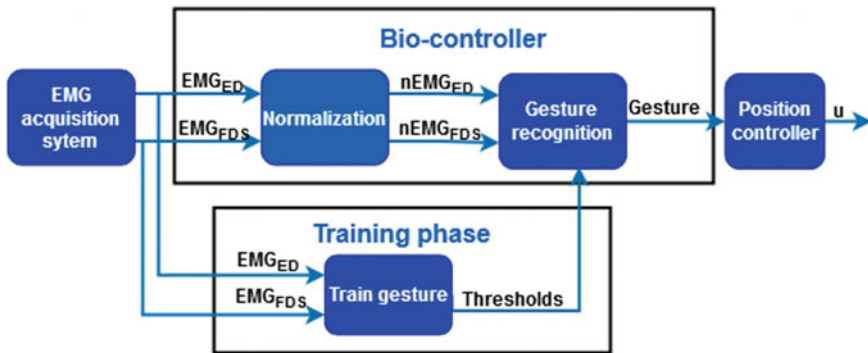


Fig. 3 Control loop for threshold based EMG-driven control

A calibration procedure should be done before starting a new training session to determine the necessary thresholds for the EMG-driven control and the MVC, which is necessary for normalizing the EMG signals. The thresholds are the maximum limit value corresponding to the muscular deactivation: μ_1 for Flexor Digitorum Superficialis (FDS) muscle and ε_1 for Extensor Digitorum (ED) muscle. The gesture recognition module progresses the normalized signals to verify the condition of the state transitions each 75 ms to determine the three predefined conditions and to move the actuators according the recognized gesture (Fig. 3).

3 Results and Discussion

Bilateral assisted therapy encourages the active participation of the patients even if the patients can not move the paretic hand independently, which specially takes a great importance at early stages of rehabilitation.

Clinical trials have been conducted with six chronic stroke patients with the collaboration of the “Hospital Clínico Universitario de Valladolid”. Preliminary results have indicated that the EMG-driven bilateral assisted therapy based on virtual environments provides more motivation in comparison with previous trials conducted with RobHand using passive training paradigms. Patients claims to feel they have an active role in the rehabilitation and a challenging goal, encouraging to continue rehabilitation.

Future studies should be carried out to indicate whether the EMG-based visual biofeedback leads to improvements in rehabilitation outcomes.

4 Conclusion

A robotic rehabilitation platform for performing bilateral assisted training is presented. The robotic platform incorporates an embedded solution for real-time EMG-based hand gesture recognition: a device capable of recording EMG signals in real-time in combination with the high performance of the TMS320F28069M MCU used for on-board processing.

RobHand implements a biofeedback, which involves measuring the sEMG signals of the forearm and revealing them to the human in real-time to raise awareness of or to control those events. The sEMG is simultaneously used as visual feedback and as a force feedback source.

References

1. N. Hajjalizade et al., The effect of task-based mirror therapy on upper limb functions and activities of daily living in patients with chronic cerebrovascular accident: a randomized control trial. *J. Basic Clin. Pathophysiol.* **1**(1), 1–2 (2016)
2. H. Thieme, J. Mehrholz, M. Pohl, J. Behrens, C. Dohle, Mirror therapy for improving motor function after stroke (Review). *Cochrane Database Syst. Rev.* **3** (2012)
3. S. Ueki et al., Development of a hand-assist robot with multi-degrees-of-freedom for rehabilitation therapy. *IEEE/ASME Trans. Mechatro.* **17**(1), 136–146 (2012)
4. D. Leonardis et al., An EMG-controlled robotic hand exoskeleton for bilateral rehabilitation. *IEEE Trans. Haptic* **8**(2), 140–151 (2015)
5. H. Wu et al., in Virtual reality based robotic therapy for stroke rehabilitation: an initial study, 2011 IEEE Int. Conf. Mechatronics Autom. ICMA 2011 (2011), pp. 1196–1200
6. S. Benatti et al., A versatile embedded platform for EMG acquisition and gesture recognition. *IEEE Trans. Biomed. Circuits Syst.* **9**(5), 620–630 (2015)
7. S. Benatti et al., in EMG-based hand gesture recognition with flexible analog front end, 2014 IEEE Biomed. Circuits Syst. Conf. BioCAS—Proc. (2014), pp. 57–60
8. F. Tenore, R.S. Armiger et al., in An embedded controller for a 7-degree of freedom prosthetic arm, 2008 30th Annu. Int. Conf. IEEE Eng. Med. Biol. Soc. (2008), pp. 185–188
9. J. Liu, F. Zhang, H.H. Huang, in An open and configurable embedded system for EMG pattern recognition implementation for artificial arms, 2014 36th Annu. Int. Conf. IEEE Eng. Med. Biol. Soc. EMBC (2014), pp. 4095–4098

MERLIN: Upper-Limb Rehabilitation Robot System for Home Environment



Ainara Garzo, Javier Arcas-Ruiz-Ruano, Iñigo Dorronsoro,
Gabriel Gaminde, Je Hyung Jung, Javier Téllez, and Thierry Keller

Abstract ArmAssist is a cost-effective robotic system for post-stroke upper-limb rehabilitation. The system incorporates the ArmAssist Assessment platform based on serious games that enables fast, quantitative and automatic evaluation of the arm functions. The aim of the MERLIN European project is to bring this system to the patients' homes to personalize the therapy with reduced supervision while increasing the number of movement repetitions to improve the effectiveness. To this end, the ArmAssist system developed by TECNALIA, has been integrated with GMV's Antari Home Care platform, to customize and supervise the training remotely. Additionally, several technical improvements have been done to enhance the usability and functionality of the system according to the patients and therapists' feedback. In this paper, the technical progress of the MERLIN system is presented.

1 Introduction

It is estimated that the 75% of people who suffered a stroke have remaining upper limb deficits [1] and no more than the 20% of them recover the complete functional mobility in the first 6 months [2]. Several studies showed that intense and task-oriented rehabilitation improves functional outcomes [3]. However, increasing the intensity of rehabilitation is difficult due to the high number of affected people and the limited healthcare resources.

Research supported by FIK and has received funding from EIT Health. EIT Health is supported by the European Institute of Innovation and Technology (EIT), a body of the European Union receives support from the European Union's Horizon 2020 Research and innovation programme.

A. Garzo (✉) · J. Arcas-Ruiz-Ruano · I. Dorronsoro · G. Gaminde · J. H. Jung · T. Keller
Neurorehabilitation Area within the Health Division of TECNALIA, Basque Research and
Technology Alliance (BRTA), San Sebastian, Spain
e-mail: ainara.garzo@tecnalia.com

J. Téllez
Digital Health Division of GMV, Madrid, Spain
e-mail: jtellez@gmv.com

In the last decades, robot-based systems have been considered a solution to increase the number of movement repetitions at reduced costs. Safe and intensive rehabilitation exercises can be done thanks to the precision of movements that the robots could provide [4]. Moreover, game-based telerehabilitation combined with robotic systems have created a motivating environment [5] and can increase the quality and quantity of the therapy due to an enjoyable environment [6].

2 Background

The ArmAssist (AA) system is a modular solution that combines a portable robotic device and a software platform based on serious games for upper-limb rehabilitation. The AA can measure the patient's active arm movements in terms of parameters such as position, orientation, forearm angle and arm support/lifting or vertical force. Prono-supination and grasping movements are also trained and measured [7]. Games have been designed with the aim of training the different movements that could be carried-out with the device.

Previous studies showed that the use of AA in clinical setting was well accepted by therapists and patients, and makes the therapy more enjoyable and motivating thus engage patients carrying out the therapy voluntarily [8, 9]. Further, improvements in the motor function of the patients after using the AA have been demonstrated [10].

Some robotic products can be found in the market for arm rehabilitation for clinic set-up use as Armeo Power by Hocoma, InMotion Arm/Hand by Bionik or Amadeo by Tyromotion. For home use Pablo by Tyromotion, Rapael by Neofect, or Armeo Spring by Hocoma can be found. However, AA is more affordable and provides more functionalities comparing to the cheapest solutions.

This paper presents the technical progress of the MERLIN project where the AA has been adapted to be used by patients at home to provide daily, intensive, patient tailored and motivating rehabilitation [11].

3 Methods

A multidisciplinary team including neuroengineers, physiotherapists and experts in medical devices participated in a co-design workshop with the aim of defining the MERLIN system requirements to bring it to patients' homes. These requirements are shown in Table 1.

Table 1 Requirements

System component	Requirement
Hardware	Cover springs, make smooth edges, etc. to protect the patient hand
Hardware	Look for a solution to make the system portable: mat, computer, transport
Software	Clear written and auditive instructions to the patient
Software	Include an asynchronous communication between patients and therapists using written messages
Software	Therapy evolution information must be available for therapists and patients
Software	Patients need to receive the therapy scheduling daily
Software	The therapy assessment and results must be stored in a safe and secure database
Software	Therapists need tools for designing and customizing the patients' therapy easily. The information to be defined must be: affected limb, game level and duration, component to train (grasp, prono-supination, lifting, etc.), and days to repeat the game
Software	Patient privacy and safety must be guaranteed anytime

4 Results

According to the defined requirements a new set-up was designed, including a flexible mat that can be rolled-up and easily stored when not being used, and a portable suitcase for the system transport. The software has been adapted to work on a tablet instead of an All-in-One PCs with the aim of making a portable system. In addition, pre-series of an industrialized version of the AA including the mechanical proposed improvements were manufactured. Figure 1 shows the previous version of the AA (a) used in clinical settings and (b) the new design for home use.

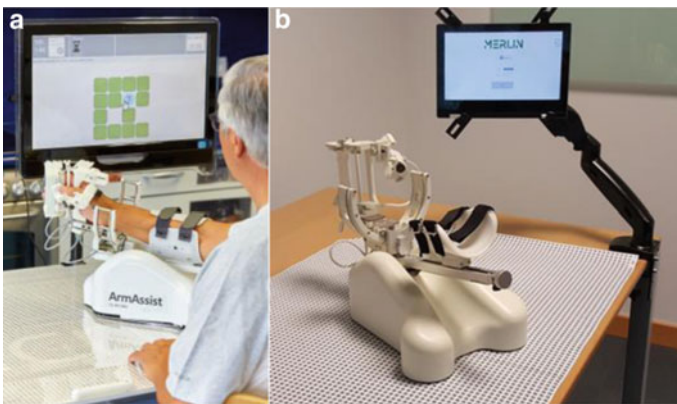


Fig. 1 a ArmAssist system in clinical setting and b MERLIN system adapted for home set-up

The Antari Home Care platform [12], was integrated with the original rehabilitation AA platform to provide to clinicians an efficient way to design the therapy and personalize it (set of games, frequency, scheduling). The integration of both platforms allows therapists to visually monitor the performance and evolution of the patient and adapt the therapy plan according to it.

Voice and written instructions were also included in the software to guide patients through the tasks to be performed in each game. The messages were made available in Spanish, English and Dutch, as the clinical evaluation has been done in Spain and the Netherlands. The patients have the option of cancelling the voice messages to avoid disturbances. A messaging system between clinicians and patients was also added, as well as authentication system for any user. Additionally, a section to monitor patients' evolution was developed for therapists and patients. In case that patients are willing to train more than the planned therapy, a free zone could be activated by the therapist where the patients can select their preferred games.

5 Conclusions

The MERLIN system has been designed to bring robotic assisted rehabilitation to patients' homes with the objective of allowing the patients to improve the effectiveness on the therapy increasing the intensity and duration of the training. The AA has been redesigned and improved for home setting in terms of hardware and software. The enhanced AA system has been positively evaluated by the patients and therapists in two different studies organized in Spain and the Netherlands using the evaluation procedure of similar studies [13]. Currently, the outcomes of the studies have been being analyzed quantitatively in terms of usability and effectiveness and the process will be finished after publication process.

Acknowledgment Special thanks to C. Rodriguez-de-Pablo, J. Perry, A. Beloso, D. Valencia, H. Zabaleta and B. Garcia-Mendizabal for their contributions to the system development and to MERLIN project partners for their participation on the co-design workshop. Authors would like to thank QJ Rehab for providing enhanced industrialized version of AA.

References

1. N.S. Ward, K. Kelly, F. Brander, The future of stroke rehabilitation—upper limb recovery. *Adv. Clin. Neurosci. Rehabil.* **15**(4), 6–8 (2015)
2. G. Kwakkel, B.J. Kollen, J.V. Van der Grond, A.J.H. Prevo, Probability of regaining dexterity in the flaccid upper limb: impact of severity of paresis and time since onset in acute stroke. *Stroke* **34**(9), 2181–2186 (2003). <https://doi.org/10.1161/01.STR.0000087172.16305.CD>
3. C. J. Winstein et al., Guidelines for Adult Stroke Rehabilitation and Recovery: A Guideline for Healthcare Professionals from the American Heart Association/American Stroke Association, vol. 47(6) (2016)

4. C. O'Neill et al., Inflation soft wearable robot for reducing therapist fatigue during upper extremity rehabilitation in severe stroke. *IEEE Robot. Autom. Lett.* **5**(3), 3899–3906 (2020). <https://doi.org/10.1109/LRA.2020.2982861>
5. M.D. Popović, M.D. Kostić, S.Z. Rodić, L.M. Konstantinović, Feedback-mediated upper extremities exercise: increasing patient motivation in poststroke rehabilitation. *Biomed. Res. Int.* **2014**, 11 (2014). <https://doi.org/10.1155/2014/520374>
6. C. Rodríguez-de-Pablo et al., Post-stroke Robotic Upper-Limb Telerehabilitation Using Serious Games to Increase Patient Motivation: First Results from ArmAssist System Clinical Trial, in *Advances in Neurotechnology, Electronics and Informatics*, ed. by A.R. Londral, P. Encarnação. BB, vol. 12 (Springer, Cham, 2016), pp. 63–78. https://doi.org/10.1007/978-3-319-26242-0_5
7. J.C. Perry, H. Zabaleta, A. Belloso, C. Rodríguez-De-Pablo, F.I. Cavallaro, T. Keller, in *ArmAssist: development of a functional prototype for at-home telerehabilitation of post-stroke arm impairment*, Proc. IEEE RAS EMBS Int. Conf. Biomed. Robot. Biomechatronics (2012), pp. 1561–1566. doi: <https://doi.org/10.1109/BioRob.2012.6290858>
8. J. Perry, C. Rodríguez de Pablo, S. Balasubramanian, F. Cavallaro, A. Belloso, T. Keller, Assessment and training in home-based telerehabilitation of arm mobility impairment. *J. Access. Des. All JACCES* **3**(2), 45–75 (2013)
9. C. Rodríguez-de-Pablo, A. Savić, T. Keller, in *Game-Based Assessment in Upper-Limb Post-stroke Telerehabilitation*, *Converging Clinical and Engineering Research on Neurorehabilitation II* (2017), pp. 413–417
10. T.J.D. Tomić et al., ArmAssist robotic system versus matched conventional therapy for post-stroke upper limb rehabilitation: a randomized clinical trial. *Biomed. Res. Int.* **2017** (2017). <https://doi.org/10.1155/2017/7659893>.
11. C. Rodríguez-De-Pablo, S.G. Rozevink, F. Mayordomo, J. Téllez, S. Kocić, T. Keller, in *MERLIN : Homecare Arm Rehabilitation*, INRS2019. International Neurorehabilitation Symposium (2019)
12. GMV, 'Antari Home Care'. [Online]. Available: www.gmv.com
13. S.M. Nijenhuis et al., Feasibility study into self-administered training at home using an arm and hand device with motivational gaming environment in chronic stroke. *J. Neuroeng. Rehabil.* **12**, 89–101 (2015). <https://doi.org/10.1186/s12984-015-0080-y>

A Wearable Sensorised Thimble for Assessment and Rehabilitation of Grasping



P. Maiolino, L. Ottoveggio, E. Montalesi, S. Denei, F. Mastrogiovanni, M. Casadio, and G. Cannata

Abstract This paper presents the design and preliminary evaluation of a wearable sensorised thimble based on CySkin Technology. It can be used to monitor grasping pressures and contact area during assessment and rehabilitation of people with deficits in the neural control of movements and/or neurological diseases. The design of the wearable thimble has been thought to minimally constrain the hand movement and to provide seven distributed pressure measurements. A preliminary evaluation experiment using three wearable thimbles to grasp an object with different weight is also presented.

Keywords Wearable glove · Tactile sensing · Grasping

1 Introduction

People with neurological diseases or injury such as multiple sclerosis and stroke, are required to perform physical therapy to improve hand function through repetitive task practice rehabilitation [1]. A device which can provide information about grasping pressure and contact area has the potential to increase the benefits of rehabilitative therapy by informing the therapist which can monitor patient's progress and drive his/her task practice. Such a system could also be used with healthy patients to understand human grasp for the design of robotic hands and prostheses. This paper presents the design and preliminary experimental assessment of a wearable tactile sensor fingertips which provide distributed pressure measurements. The design is based on CySkin technology [2] and has been thought to minimally constrain the hand movement and to provide a comfortable fit to preserve cutaneous feedback of patients. Tactile sensors' responses has been calibrated with respect to the applied

P. Maiolino (✉)
ORI, University of Oxford, Oxford, UK
e-mail: perla.maiolino@eng.ox.ac.uk

L. Ottoveggio · E. Montalesi · S. Denei · F. Mastrogiovanni · M. Casadio · G. Cannata
DIBRIS, University of Genoa, Genoa, Italy

© The Author(s), under exclusive license to Springer Nature Switzerland AG 2022
D. Torricelli et al. (eds.), *Converging Clinical and Engineering Research on Neurorehabilitation IV*, Biosystems & Biorobotics 28,
https://doi.org/10.1007/978-3-030-70316-5_132

pressure. To assess the validity of the design a preliminary experiments involving the grasping and holding of a bottle with different weight is presented.

2 Reference Technology

CySkin [2] is a large-area capacitive pressure sensor that consists in interconnected FPCB triangular modules hosting each 11 capacitive transducers (i.e. taxels) that can be conformed to 3-dimensional (3D) shape. A *CySkin* basic module can be cut to easily fit to the different shapes of the surfaces to be covered. It hosts a Capacitance to Digital Converter (AD7147 from Analog Devices) and a micro controller (ST Microelectronics) for the data acquisition, synchronization and transmission. The micro controller acquires tactile information with a sample time of 50 ms. An Intelligent Hub Board (IHB) performs a preliminary processing of the tactile data and send them to a PC through the CAN bus.

3 Manufacturing Procedures

The manufacturing of the sensorised thimble has required the following procedure. First of all, a supporting shell has been designed and 3D printed to host the *CySkin* sensor. The shell's size (Fig. 2a) has been designed to easily fit in an average hand's fingertip and to have two holes to accommodate for the *Cyskin* sensor electronics and the wires connection. Three taxels of a *CySkin* triangular module have been cut to adapt to the supporting shell area, reducing the number of taxels to seven. Because of the small curvature radius of the shell, the integration of the sensor has required a vacuum system to help the sensor FPCB to conform perfectly to the shell's external surface. Figure 2b shows the integrated sensor. To allow for the best fit and comfortable feeling for the user and to avoid for the finger to be exposed to the sensor electronics, a plastic shell to be integrated in the inner side of the wearable thimble has been manufactured by mechanically thermoforming PET-G material; an elastic band has been glued to hold in place the thimble on the user's finger (Fig. 2c). The sensor requires a ground plane to be able to detect contact from not conductive objects. This has been made embedding a conductive Lycra® in a thermoplastic elastomer (TPE) that has been shaped with mechanical thermoforming. The elastomeric substrate is highly deformable and present an elastic behaviour. These features provide a good adaptability and grip to the contact surface of manipulated objects. A conductive Lycra strip has been made pass through a specifically designed hole in the shell in order to solder it with the ground wire of the sensor and allow for noise shielding. Figure 2d shows two views of the wearable thimble. The same procedure has been repeated to obtain three different thimbles which are shown on the user's hand in Fig. 1.



Fig. 1 The wearable sensorised thimble for grasping rehabilitation. Three prototypes for thumb, index and middle finger have been manufactured

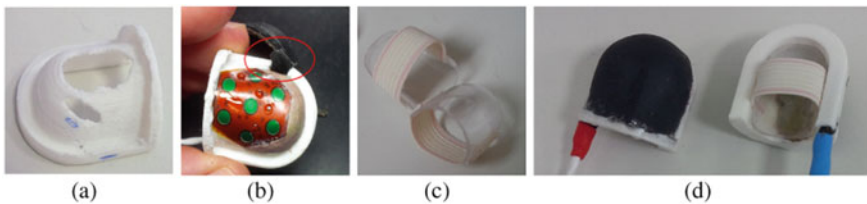


Fig. 2 **a** The 3D printed support shell with the holes for hosting the sensor electronics. **b** The Cyskin tactile sensor module integrated on the support shell surface; in the red circle is highlighted the conductive Lycra strip. **c** The inner lid with the elastic band. **d** Two finished prototypes of the thimble; it is possible to see the top side which shows the ground plane embedded in the soft elastomer and the bottom side

4 Experiments

4.1 Validation

A preliminary assessment has been performed to evaluate the performance of the system during grasping task. In particular an experimental methodology has been defined to evaluate if the system is able to measure pressure values consistently with human grasping [3] and if the sensor measurements could allow to evaluate the ability of the subject to adapt grip force to object weight [4]. To evaluate these aspects two glass bottles, one full of sand and the other empty, were chosen to perform a gripping and lifting task. The subject wore thimbles on thumb, index and middle fingers. The task consisted in reaching and holding the bottle for one second, lifting the bottle and placing it back on the table. The task has been repeated several times. After at least nine repetitions and randomly in different experiments, the bottle was changed with the other of different weight, without subject's knowledge. For each subject the

procedure was repeated two times: first beginning with the light bottle and then with the heaviest one. The experiment was performed with ten subjects. The data of each sensor was calibrated in pressure and force.

4.2 Results

Figure 3a shows the taxels' responses of the thumb during the experiment performed by subject 1 where, after the ninth lift, the heaviest bottle is substituted by the lightest one. It is possible to notice that during the ninth lift task the user quickly adapt the applied pressure to the light bottle weight. Figure 3b shows the taxels' responses of the index finger for subject 1 during the opposite experiment (i.e. from light to heavy). Here the subject adapts the applied pressure over repetition for the light bottle until the heavy bottle is lifted and the applied pressure increase again. Finally Fig. 3c

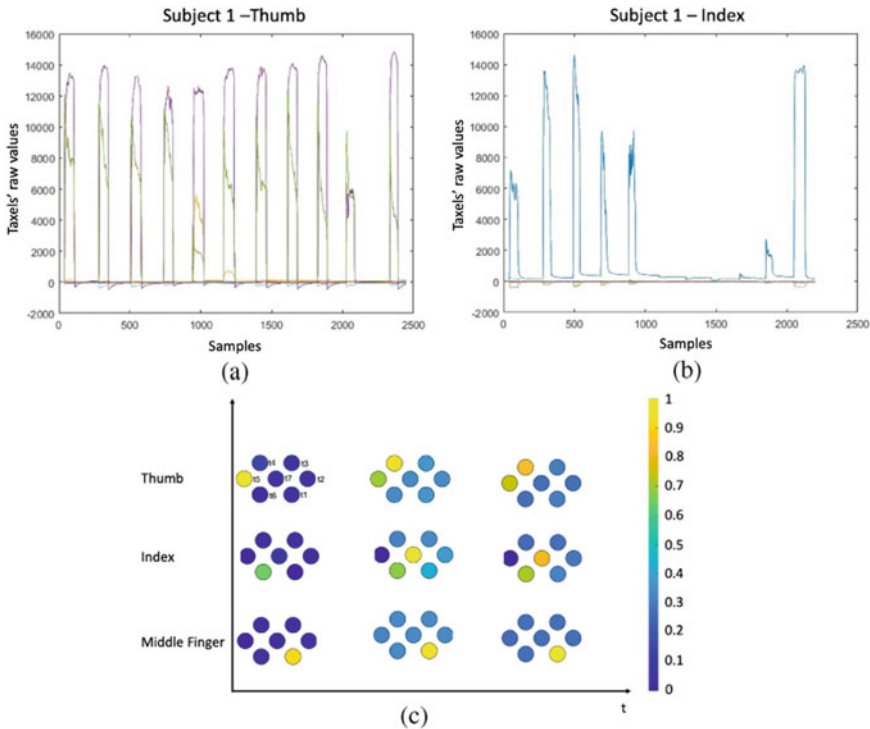


Fig. 3 **a** taxels' output for the thumb of subject 1 during heavy-light lifting task. **b** taxels' output for the index finger of subject 1 during light-heavy lifting task. **c** Contact area. The activation level for each taxel is reported while grasping the bottle in three different instant. The taxels are shown as they are placed in the FPCB, but the orientation of the FPCB on the finger can be different. Taxel ids are also shown

shows the contact area of three fingertips during three different instants of the lifting task. It is possible to notice how the activation level of the taxels change over time.

The maximum values in taxels' output converted in force registered during the experiments have been 10.38 N, 5.23 N and 2.44 N for the thumb, index and middle finger respectively.

5 Conclusion

The design and manufacturing of a sensorised thimble for assessment and rehabilitation of grasping has been presented. Experiments have been performed to evaluate the performance of the system in the application conditions. Results supported the suitability of the designed system for grasping rehabilitation tasks.

Acknowledgements The research leading to these results received funding from the EC within the Horizon 2020 Framework (CHIST-ERA, 2014–2020), project InDex and by Ministry of Science and Technology, Israel for Joint Israel-Italy Lab in Biorobotics Artificial Somatosensation for Humans and Humanoids.

References

1. C.D. Takahashi, L. Der-Yeghiaian, V. Le, R.R. Motiwala, S.C. Cramer, Robot-based hand motor therapy after stroke. *Brain* **131**(2), 425–437 (2008)
2. <https://www.cyskin.com/>
3. J. Hermsdrfer, Analysis of grip forces during object manipulation, in *Sensorimotor Control of Grasping, Physiology and Pathophysiology* (Cambridge University Press, 2009), pp. 3–19
4. R.S. Johansson, Sensory control of dexterous manipulation in humans, in *Hand and Brain: The Neurophysiology and Psychology of Hand Movements* (Academic Press, San Diego, USA, 1996), pp. 381–414

Isometric Force Pillow: Using Air Pressure to Quantify Involuntary Finger Flexion in the Presence of Hypertonia



Caitlyn E. Seim, Chuzhang Han, Alexis J. Lowber, Claire Brooks, Marie Payne, Maarten G. Lansberg, Kara E. Flavin, Julius P. A. Dewald, and Allison M. Okamura

Abstract Survivors of central nervous system injury commonly present with spastic hypertonia. The affected muscles are hyperexcitable and can display involuntary static muscle tone and an exaggerated stretch reflex. These symptoms affect posture and disrupt activities of daily living. Symptoms are typically measured using subjective manual tests such as the Modified Ashworth Scale; however, more quantitative measures are necessary to evaluate potential treatments. The hands are one of the most common targets for intervention, but few investigators attempt to quantify symptoms of spastic hypertonia affecting the fingers. We present the isometric force pillow (IFP) to quantify involuntary grip force. This lightweight, computerized tool provides a holistic measure of finger flexion force and can be used in various orientations for clinical testing and to measure the impact of assistive devices.

Keywords Hypertonia · Spasticity · Tool · Measurement · Quantify · Stroke

C. E. Seim (✉) · C. Han · C. Brooks · A. M. Okamura
Department of Mechanical Engineering, Stanford University, Stanford, USA
e-mail: cseim@stanford.edu

A. J. Lowber
Department of Computer Science, Stanford University, Stanford, USA

M. Payne
Department of Civil Engineering, Stanford University, Stanford, USA

M. G. Lansberg · K. E. Flavin
Department of Neurology, Stanford University, Stanford, USA

J. P. A. Dewald
Department of Physical Therapy and Human Movement Sciences, Northwestern University, Evanston, USA

1 Background

Survivors of central nervous system injury often present with spastic hypertonia (involuntary muscle tone and spasticity). Abnormal supraspinal drive post-injury leads to motoneuron hyperexcitability [1], resulting in involuntary muscle contractions that can impact posture and limit range of motion. During passive movement, the limb can show an exaggerated stretch reflex as a function of movement velocity (spasticity). At rest, the limb is commonly bent or flexed from static muscle tone (hypertonia). When the upper limb is affected, symptoms may cause pain and prevent activities of daily living such as hand washing and dressing.

A variety of treatment options are used clinically, including splints, pharmaceuticals, and surgical interventions. More treatments are also in development, such as therapeutic stimulation and robotic devices. The quantification of symptoms is both clinically and scientifically relevant. However, most therapists and investigators still rely on manual ratings that can be highly subjective [2–5]. The most common measure, the Modified Ashworth Scale (MAS), is known to be subjective and have poor intra- and inter-rater variability [6]. Other measures like the Modified Tardieu Scale (MTS) have also been shown to have high variability [7].

Some tools have been developed to quantitatively assess symptoms, but much of this work focuses on the limb's response to imposed movement. The affected muscle is stretched at constant velocities by a therapist or machine while joint angle is recorded using robotic devices [5], fiber optic tools [3], or marker tracking. Simultaneously, stiffness is measured through EMG [3, 8], torque sensors [4, 5, 7], or load cells [8]. Although such tools that move the limb can provide data on spasticity, imposed movement is relatively uncommon in daily life. Since the limb is often at rest, measurement of static symptoms (such as contorted posture or involuntary muscle torque) could provide useful data. Few existing tools measure static symptoms of hypertonia. Germanotta et al. used a large robotic device [4], and Stienen et al. created a 2-DoF hinge for the wrist and MCP joints [9].

Most work on quantifying spastic hypertonia also focuses on the elbow, knee, or ankle joints [3, 5, 7, 8]; yet the hands are one of the most common areas for intervention [10]. Hand function is key to performing many tasks of self sufficiency, and unchecked hypertonia in the hands can lead to secondary problems [11]. Thus, measuring the level of spastic hypertonia on the hands is particularly important. However, the fingers are particularly difficult to analyze due to their many degrees of freedom. Actuating each finger or all the phalanges together is challenging due to different phalanx bone lengths. The fingers can also be difficult to secure to a device in the presence of hypertonia. Here we present the isometric force pillow (IFP): a lightweight, handheld tool designed to provide a holistic, quantitative measure of involuntary hand flexion due to spastic hypertonia.

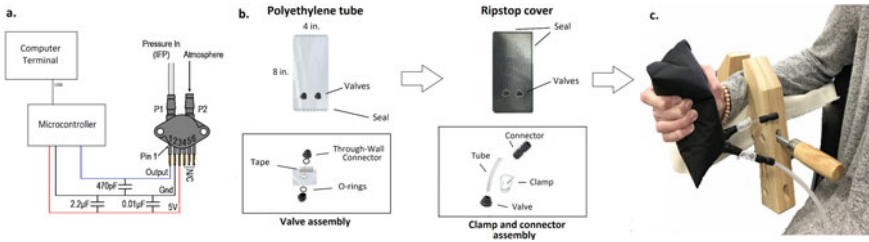


Fig. 1 a Schematic of the IFP electronics. b Assembly of the IFP. c The isometric force pillow used in a gravity-neutral position. The tube leads to the pressure sensor of 1a. The other valve is clamped after initial inflation using a hand vacuum pump

2 Design

The objective was to develop a tool to measure symptoms of spastic hypertonia in the hands, in order to provide quantitative data when studying treatment efficacy. Spastic hypertonia often causes the finger flexors to contract, so measuring flexion force is an accepted strategy [4, 9, 12].

The tool was intended to be low-cost and compact in order to promote perceived ease of use. Preliminary prototypes used a hinge-like design that measured finger flexion using a load cell—aiming to expand the Wrist Finger Torque Sensor [9] into a stand-alone design with a focus on the fingers. When the preliminary prototypes were tested on stroke survivors with upper-limb hypertonia, the fingers were difficult to secure even using straps. Like other tools [4, 5, 8, 9] the hinge had to be mounted on a rigid surface. If the individual’s elbow or wrist was contracted, their hand could not reach the tool. Those with moderate to severe spastic hypertonia could not use the prototypes. This design was also only capable of measuring force at the MCP joints.

The hinge design was replaced with a graspable cushion (Fig. 1c), the isometric force pillow (IFP). The IFP has an ergonomic form similar to some orthotic devices for hypertonia, such as the Hand Contracture Carrot Orthosis (AliMed, Inc.). The IFP uses air pressure to measure finger flexion force; which provides a holistic measure of contraction at multiple joints. This self-contained method of measuring force does not require attachment to a rigid mount and thus allows the unit to be free-moving; it is capable of being used both in the gravity-neutral position and in other orientations. The IFP is tethered only by a flexible tube.

2.1 Mechanical Design

The cushion is 8 in. in length by 4 in. in diameter when not inflated. These dimensions allow fingers of various lengths to be extended when grasping the device, without

allowing the thumb and fingertips to touch. Air pressure in the IFP is maintained to provide an accurate differential pressure measurement. An airtight seal is created in an 8-step process (Fig. 1b).

4-mil heavy duty polyethylene tubing cut at a length of 8 in. forms the inner layer of the cushion. Two air-tight valves are assembled using through-wall connectors (5779K677, McMaster-Carr). Holes of 1/4" diameter are cut in the polyethylene tubing and double-sided VHB acrylic tape (S-10123, Uline) is applied surrounding each hole. 1/4" rubber O-rings are placed on both the inside and the outside of the polyethylene tubing, and the through-wall connectors are twisted shut. After the valves are in place, a tabletop impulse sealer (H-163, Uline) seals the polyethylene tubing.

A sheet of silicone-coated ripstop nylon (FRCS, Seattle Fabrics Inc.) is cut to wrap over the polyethylene tubing and is sealed on by the tabletop impulse sealer. The nylon material adds friction to prevent slippage while the IFP is in use. It also prevents the polyethylene tubing from stretching during inflation and squeezing, and prevents bursting. Four inches of 1/4" soft plastic tubing attaches to each valve and a mini tubing clamp (59199, U.S. Plastic Corp.) is added so each valve could be sealed. One of these tubes attaches to a pressure sensor using a straight tube connector (5779K14, McMaster-Carr). The other tube is used to inflate the cushion via a hand vacuum pump (MV8255, Mityvac). After inflation, the pump is disconnected and the tube is clamped.

2.2 *Electronics and Software*

A 50 kPa differential pressure sensor (MPX5050-DP, NXP Semiconductors) measures pressure within the IFP and can detect small changes in grip (<0.5 PSI). One port (P1) on the sensor connects to the IFP valve via soft tubing. The other port (P2) is exposed to atmospheric pressure. The power, ground, and output voltage pins on the sensor connect to a microcontroller (Arduino Duemilanove) using a 3-wire ribbon cable. The circuit board houses a power supply decoupling and output filtering circuit (Fig. 1a).

A custom script converts the analog voltage from the sensor into gauge pressure readings 10Hz. The sensor readings are calibrated by subtracting a constant offset. The offset was empirically measured with both sensor P1 and P2 exposed to atmospheric pressure. The calibrated pressure values are smoothed using a moving average filter with a sample size of 10. The pressure reading is then displayed on a computer terminal for clinicians or investigators.

3 Discussion

The IFP tool provides a holistic, quantitative measure of involuntary grip due to spastic hypertonia. The majority of other tools that aim to quantify symptoms of spastic hypertonia impose movement on the limb, which provides data primarily on spasticity. In contrast, the IFP measures static flexion force from the fingers. Since static flexion leads to many secondary problems in spastic hypertonia, our tool provides valuable data that might also indicate problems such as difficulty to access and clean the palm and the progression of contractures. The tool could also be used to evaluate involuntary grip when using assistive devices or pharmacological interventions to relieve hypertonia.

Circumstantial factors must always be controlled when measuring muscle tone and spasticity. Arm position is one such factor [1] and measurement using the IFP in a standardized, gravity-neutral position is optimal. Those with difficulty achieving a standardized arm position due to severe hypertonia can get repeated measures using the IFP to provide intrasubject trends. Most prior work relies on mounted hardware that is not accessible to some patients [4, 5]. For other patients it can be necessary to repeatedly stretch the affected limb to fit into these tools, and these stretches impact the validity of measures by temporarily reducing hypertonia [13].

Acknowledgements This research was supported, in part, by the Stanford Wu Tsai Neurosciences Institute Neuroscience: Translate Program and the Eunice Kennedy Shriver National Institute of Child Health and Human Development of the National Institutes of Health (NIH) under Award Number F32HD100104.

References

1. J.G. McPherson, L.M. McPherson, C.K. Thompson, M.D. Ellis, C.J. Heckman, J. Dewald, Altered neuromodulatory drive may contribute to exaggerated tonic vibration reflexes in chronic hemiparetic stroke. *Front. Hum. Neurosci.* **12**, 131 (2018)
2. P. Caliendo, C. Celletti, L. Padua, I. Minciotti, G. Russo, G. Granata, G. La Torre, E. Granieri, F. Camerota, Focal muscle vibration in the treatment of upper limb spasticity: a pilot randomized controlled trial in patients with chronic stroke. *Arch. Phys. Med. Rehabil.* **93**(9), 1656–1661 (2012)
3. C.A. McGibbon, A. Sexton, M. Jones, C. O’Connell, Elbow spasticity during passive stretch-reflex: clinical evaluation using a wearable sensor system. *J. Neuroeng. Rehabil.* **10**(1), 61 (2013)
4. M. Germanotta, V. Gower, D. Papadopoulou, A. Cruciani, C. Pecchioli, R. Mosca, G. Speranza, C. Falsini, F. Cecchi, F. Vannetti, Reliability, validity and discriminant ability of a robotic device for finger training in patients with subacute stroke. *J. Neuroeng. Rehabil.* **17**(1), 1–10 (2020)
5. N. Seth, D. Johnson, G.W. Taylor, O.B. Allen, H.A. Abdullah, Robotic pilot study for analysing spasticity: clinical data versus healthy controls. *J. Neuroeng. Rehabil.* **12**(1), 109 (2015)
6. W.K.L. Yam, M.S.M. Leung, Interrater reliability of modified ashworth scale and modified tardieu scale in children with spastic cerebral palsy. *J. Child Neurol.* **21**(12), 1031–1035 (2006)
7. A. Centen, C.R. Lowrey, S.H. Scott, T.-T. Yeh, G. Mochizuki, KAPS (kinematic assessment of passive stretch): a tool to assess elbow flexor and extensor spasticity after stroke using a robotic exoskeleton. *J. Neuroeng. Rehabil.* **14**(1), 59 (2017)

8. A.A. Alhusaini, C.M. Dean, J. Crosbie, R.B. Shepherd, J. Lewis, Evaluation of spasticity in children with cerebral palsy using ashworth and tardieu scales compared with laboratory measures. *J. Child Neurol.* **25**(10), 1242–1247 (2010)
9. A.H.A. Stienen, T.S. Moulton, L.C. Miller, J.P.A. Dewald, Wrist and finger torque sensor for the quantification of upper limb motor impairments following brain injury, in *IEEE International Conference on Rehabilitation Robotics* (2011), pp. 1–5
10. Y. Ren, H.-S. Park, L.-Q. Zhang, Developing a whole-arm exoskeleton robot with hand opening and closing mechanism for upper limb stroke rehabilitation, in *IEEE International Conference on Rehabilitation Robotics* (2009), pp. 761–765
11. I. Heijnen, R. Franken, B. Bevaart, J. Meijer, Long-term outcome of superficialis-to-profundus tendon transfer in patients with clenched fist due to spastic hemiplegia. *Disabil. Rehabil.* **30**(9), 675–678 (2008)
12. Y. Lan, J. Yao, J.P. Dewald, The impact of shoulder abduction loading on volitional hand opening and grasping in chronic hemiparetic stroke. *Neurorehabil. Neural Rep.* **31**(6), 521–529 (2017)
13. B.D. Schmit, J.P. Dewald, W.Z. Rymer, Stretch reflex adaptation in elbow flexors during repeated passive movements in unilateral brain-injured patients. *Arch. Phys. Med. Rehabil.* **81**(3), 269–278 (2000)

Feasibility of Using Visual Cues for Evoking Self-induced Perturbations for Assessing Dynamic Balance During Walking



Andrej Olenšek, Matjaž Zadavec, and Zlatko Matjačić

Abstract In this paper we explore the feasibility of using visual cues for evoking self-induced perturbations for assessing dynamic balance during walking. We upgraded BAR-TM with a floor projection system that projects on the walking surface of instrumented treadmill target points the user should step on. The proposed method was tested in a healthy subject. Subject's response to self-induced perturbations was evaluated in terms of center of mass (CoM), center of pressure (CoP) and ground reaction force (GRF). Results show that extent of required movement re-planning and execution depends greatly on the required repositioning of the foot placement away from pre-planned foot placement of stationary gait. Accordingly, subject developed specific response strategies to cope with different types of perturbations.

1 Introduction

Ability to deliver appropriate dynamic balancing response after being subjected to unexpected unstable or fall threatening event is one of the key elements of safe and stable walking. This ability may be to a large extent impaired in case of central nervous system injuries or diseases where patients often have to cope with different levels of impaired motor control that in turn constrain development of suitable reactive balancing mechanisms during walking in such situations. Even after completing rehabilitation it is not uncommon for patients to display certain degree of reduced balance function. To tackle this problem mechanisms have been developed in recent years that in a fall-safe manner impose well controlled gait perturbations on the patients in an attempt to engage them into re-learning suitable dynamic balance as

This research was partially supported by the Slovenian Research Agency under research project J2–8172, research program number P2–0228 and by the European Union's Horizon 2020 research and innovation programme under grant agreement number 779963 (project EUROBENCH – subproject BeStable).

A. Olenšek (✉) · M. Zadavec · Z. Matjačić
University Rehabilitation Institute Republic of Slovenia, Ljubljana, Slovenia
e-mail: andrej.olensek@mail.ir-rs.si

© The Author(s), under exclusive license to Springer Nature Switzerland AG 2022
D. Torricelli et al. (eds.), *Converging Clinical and Engineering Research on Neurorehabilitation IV*, Biosystems & Birobotics 28,
https://doi.org/10.1007/978-3-030-70316-5_134

well as for assessing their balance responses. These devices exhibit considerable diversity when considering in what way they implement perturbation modalities. In some devices gait perturbations take the form of a slip [1] or a trip [2], other incorporate moving walking surface [3], waist pulls or pushes [4]. While these state of the art devices are highly capable in the specific task they are designed for, they are also very diverse in their design, complex and expensive and they exhibit different visco-elastic properties that influence dynamic properties of the systems. For this reason consensus across the field will be difficult to achieve and the proliferation of such technology in healthcare delayed.

In the present study we would like to explore the possibility whether adequate reactive responses can be evoked also if instead of being subjected to external mechanical perturbations the subject is evoked to self-induce changes in stable gait by means of well-timed visual cues.

2 Methods

2.1 *Design of System for Delivering Visual Cues*

A floor projection system was integrated with Balance Assessment Robot [4] that in intervals projects on the walking surface of instrumented treadmill target points the user should step on. The positions of target points on walking surface are determined as the average landing points for the left and right leg in five steps during stationary gait displaced in forward and/or in mediolateral direction. Visual target points are presented to the user only during the perturbation period. The onset of perturbation period either coincides with foot strike or can be delayed to mid stance or terminal stance and the end is determined with predefined length of perturbation interval. If self-induced perturbation is to start during right stance the target is presented for left leg and vice versa. The proposed method of self-induced perturbation was tested in one healthy subject.

2.2 *Data Collection and Analysis*

The experimental session started with a short accommodation period that lasted approximately five minutes and where the subject was able to get acquainted with the experimental conditions. The session continued with a period of unperturbed walking followed by a perturbation period when the subject was presented with series of visual targets on the walking surface that were displaced with respect to average landing points in five previous steps in medial or lateral direction, forward direction and diagonal directions (combinations of forward and medial or lateral direction). Perturbations were triggered either at the time of left or right foot strike.

The subject was instructed to step on the visual targets upon being projected on walking surface and afterwards to return to the center of instrumented treadmill. To ensure subject would regain stability and restore stationary gait perturbations were triggered in intervals of no less than six seconds. The sequence of visual targets was randomly selected prior to the beginning of the experiment.

CoP, CoM and GRF were obtained for unperturbed walking and for at least seven repetitions of each perturbation. Recorded data were then segmented into strides where left stride was considered to be the period between two consecutive left foot strikes and right stride was considered to be the period between two consecutive foot strikes of the right leg. Data were then averaged across strides to obtain subject's response to self-induced perturbations.

3 Results

Figure 1 shows average CoM, GRF and CoP during unperturbed and perturbed walking. Preliminary results showed that after target point was presented to the user CoP and CoM positions were appropriately modulated according to the positions of visual targets. When self-induced perturbations were evoked in forward-lateral direction we observe that CoM and CoP mediolateral and anteroposterior positions increased considerably with respect to unperturbed walking to account for new point of contact according to the visual target. To oppose excessive mediolateral movement of CoM mediolateral GRF increased in the opposite direction as the movement of the CoM. Though not so pronounced similar mechanism was present in anteroposterior direction where anteroposterior GRF increased with respect to unperturbed walking

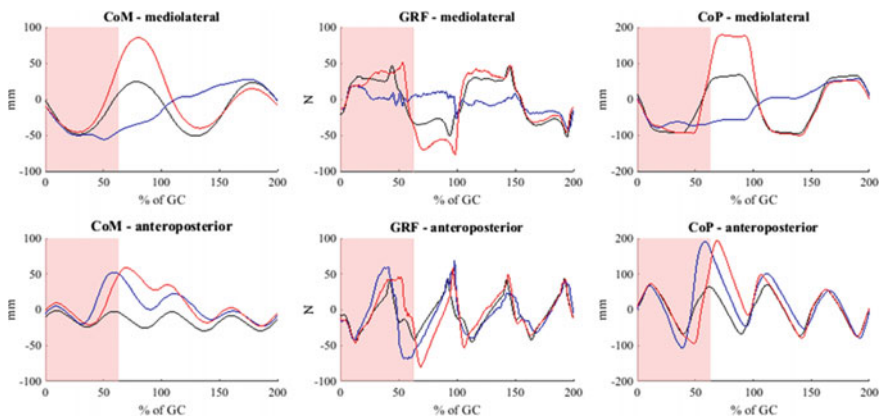


Fig. 1 Preliminary results: average CoM, GRF, CoP in mediolateral and anteroposterior directions during unperturbed walking (solid black line), after perturbation in forward-lateral direction (solid red line) and after perturbation in forward-medial direction (solid blue line). All perturbations were triggered at the time of left foot strike. Perturbation interval is marked by red solid area

to oppose excessive anteroposterior CoM movement. In the case of perturbation in forward-lateral direction the subject was able to restore stationary gait already the following step.

When self-induced perturbations were evoked in forward-medial direction we observe that subject's response span over two gait cycles. First, CoM and CoP mediolateral and anteroposterior positions decreased considerably with respect to unperturbed walking to account for new point of contact according to the visual target—according to CoP the subject placed the right foot approximately in front of the left foot. In the following stride the subject again adjusted foot placement as well as CoM and CoP – according to CoP by crossing left leg over the right leg before settling again in stationary gait.

4 Conclusion

Unlike mechanical perturbations where one opposes external mechanical impulse to regain balance, balance instability in self-induced perturbations originates from unexpected movement re-planning and subsequent execution that is required upon being presented with unexpected movement task via visual cues. The extent of movement re-planning and execution depends greatly on the required repositioning of the foot placement away from pre-planned foot placement of stationary gait. Preliminary results suggest that the proposed method of using visual cues as a source of self-induced perturbations may be feasible alternative to mechanical perturbations, however further studies are needed to determine optimal parameters.

References

1. C. O'Connell, A. Chambers, A. Mahboobin, R. Cham, Effects of slip severity on muscle activation of the trailing leg during an unexpected slip. *J. Electromyogr. Kinesiol.* **28**, 61–66 (2016)
2. B. Sharafi, G. Hoffmann, A.Q. Tan, Y.Y. Dhaher, Evidence of impaired neuromuscular responses in the support leg to a destabilizing swing phase perturbation in hemiparetic gait. *Exp. Brain Res.* **234**(12), 3497–3508 (2016). <https://doi.org/10.1007/s00221-016-4743-0>
3. K.A. Inkol, A.H. Huntley, L.A. Vallis, Repeated exposure to forward support-surface perturbation during overground walking alters upper-body kinematics and step parameters. *J. Mot. Behav.* **51**, 318–330 (2018)
4. A. Olenšek, M. Zadavec, Z. Matjačić, A novel robot for imposing perturbations during overground walking: mechanism, control and normative stepping responses. *J. Neuroeng. Rehabil.* **13**, 1–9 (2016)

Development of Impact Absorber Mechanism for Wearable Exoskeleton Using Shape Memory Alloy Spring



Hyunho Kim, Hyerim Jeon, Yongho Jeong, and Yeongjin Kim

Abstract When a person who has difficulty in moving or the elderly person come from a higher level to a lower level such as stairs, where the height difference is large, they experience a big falling impact on their bodies. This study represents an impact absorber module for an exoskeleton in rehabilitation patients. The module could enhance the durability of the exoskeleton and the safety of the user, especially in extreme environments. Our wearable impact absorber module consists of a light-weight metal body and a shape memory alloy (SMA) spring. We have confirmed that the impact absorption module, which is dropped from a certain height, increased the contact time between the ground and the module, and reduced the maximum contact force.

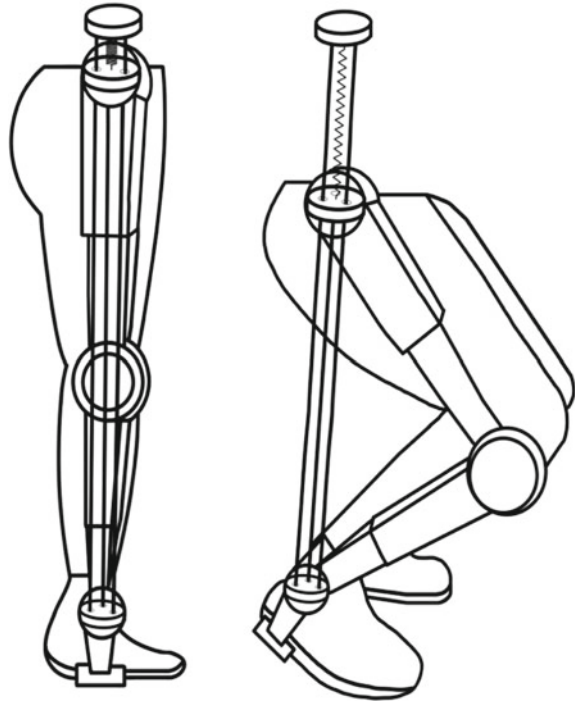
1 Introduction

Wearable exoskeletons are known to help locomotion, protect the body, and reduce muscle fatigue for rehabilitation of the elderly patients [1]. User safety is one of the important for these people. In particular, when moving in a stair, the user in the exoskeleton could encounter a falling impact on the waist and ankles. To reduce the falling impact, motor [2], hydraulic and pneumatic cylinders [3, 4] were previously used. However, these methods increased the weight of the exoskeleton. Therefore, the miniaturization and lightening of the impact absorber module for the exoskeleton are essential.

Shape memory Alloy (SMA) spring is a metal that is restored to its original shape when heat is applied above a certain temperature. It also has been actively used as an actuator in various fields such as surgical robots [5] due to its high energy density and suitability for light-weighting and miniaturizing. We have enhanced the human suitability of exoskeleton through the ease of reuse and miniaturization of SMA springs. In this study, we proposed a SMA spring based wearable impact absorption

H. Kim · H. Jeon · Y. Jeong · Y. Kim (✉)
Incheon National University, Incheon 22012, Republic of Korea
e-mail: Ykim@inu.ac.kr

Fig. 1 Schematic representation of the concept of impact absorber module



module. When the user wearing the impact absorption module falls from a high level to a low level, a SMA spring in a damping structure can increase the contact time between the ground and the user. Thus, due to law of the momentum conservation, the maximum impact force can be reduced. The used SMA springs can be easily reused by restoring its original shape of the SMA springs through heating current. We dropped the impact absorption module from a certain height to measure the impulse and impact time by using force sensors and drop speed by using a high-speed camera.

2 Experimental Setup

2.1 Impact Absorber Module

The proposed impact absorber module (See Figs. 1 and 2a) in the experiment was 384 g, consisting of an upper disk, a bottom disk with weights (200 g), three rods, and a SMA spring with 0.7 mm diameter, 5 mm diameter, and the number of coils of 21. To evaluate the impact absorbing performance of the module, we made a rigid body with the identical mass and shape with the module and compared both falling impulse of the module falling and the rigid body falling.

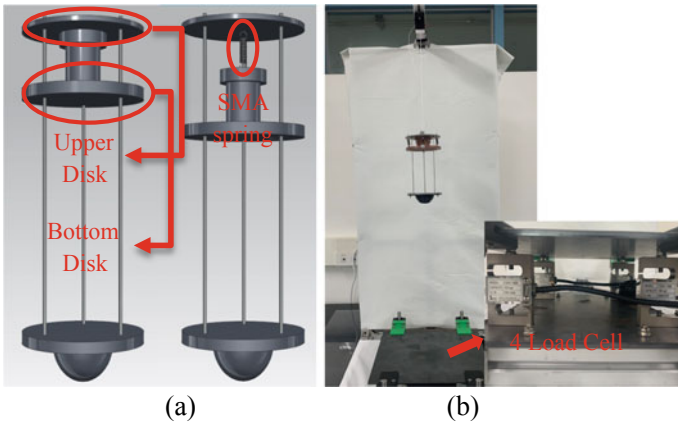


Fig. 2 **a**Rigid body and impact absorber module. **b** Experimental setup

2.2 Drop Test

As shown in Fig. 2b, when the rigid body or the absorber module is dropped from a height of 0.5 m through a gripper, the contact forces are measured by using four load cells and are collected (100,000 Hz) through USB-6343 (USA, National Instruments). In addition, we measured the displacement per frame through the high-speed camera (Sweden, Qualisys) to find out the actual drop speed, and compare that with the theoretical speed. After the experiment, we applied heating currents to the impact absorption module to restore the shape of the SMA spring and cooled for about 10 min.

3 Result

Figure 3 shows the mean force-time graph measured in the load cell when the rigid body and impact absorber collide with the ground ($n = 5$). While the rigid body collision appeared to have one peak, the impact absorber collision showed two relatively small peaks. The reason for these results is that, in the case of the rigid body, there was only a single collision. However, in the case of the impact absorber, there were the primary collision due to the upper disk and the secondary collision due to the bottom disk. We checked these phenomena with a high-speed camera as shown in Fig. 4. The maximum impact force applied to the load cells is reduced by approximately 61% from 828.2 N to 324.4 N. Next, we compared the collision time of both cases through the high-speed camera. The rigid body case showed a crash time of 4.19 ms, and in the impact absorber case, an upper disk showed a crash time of 3.15 ms and a bottom disk showed a crash time of 31.82 ms, respectively.

According to the law of impulse and momentum, (1) shows that the amount of impulse can be calculated from the drop height and mass of an object.

$$I = F \Delta t = \Delta(mv) \left(v = \sqrt{2gh} \right) \quad (1)$$

According to (1), longer collision time leads to a decrease in the maximum impact force. Thus, the SMA spring-based module indicated a significant reduction in the impact force.

4 Discussion

For the miniaturization and lightening of exoskeleton, SMA springs were used for an impact absorber module. Several drop testing confirmed that the device increased collision time at certain heights and weights, and reduced the maximum impact force by 61%. The total weight of the module is about 131 g and this means that this module is light weighted and has high impact absorption capability.

We will quantify impact absorption capacity according to various parameters such as weight based on human and spring stiffness. This process will expand the system of the impact absorber to make it more suitable for the human body. Thus this module can be used for impact absorption in various areas, including military, industrial, as well as in medical applications.

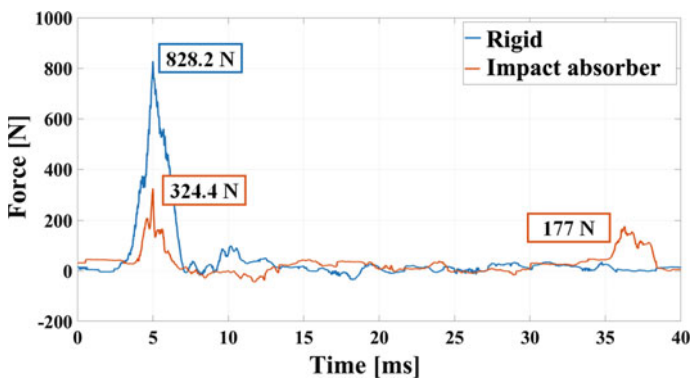


Fig. 3 Experimental results of drop impact

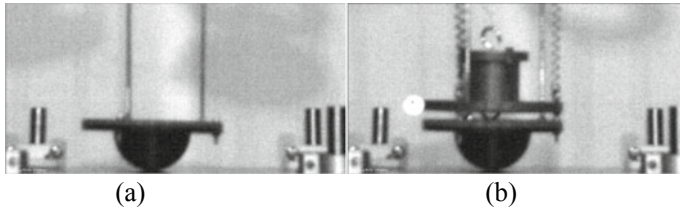


Fig. 4 **a** Rigid body at impact moment. **b** Impact absorber at impact moment

Acknowledgment This research was supported by Basic Science Research Program through the National Research Foundation of Korea(NRF) funded by the Ministry of Science, ICT & Future Planning(2019R1C1C1007091).

This research was supported by Korea Electric Power Corporation. (Grant number: R19XO01–27).

References

1. M. Grimmer, R. Riener, C.J. Walsh, A. Seyfarth, Mobility related physical and functional losses due to aging and disease—a motivation for lower limb exoskeletons. *J. Neuroeng. Rehabil.* **16**(1), 2 (2019)
2. Y. Li et al., Design and preliminary validation of a lower limb exoskeleton with compact and modular actuation. *IEEE Access* **8**, 66338–66352 (2020)
3. Y. Yang, X. Dong, X. Liu, D. Huang, Robust repetitive learning-based trajectory tracking control for a leg exoskeleton driven by hybrid hydraulic system. *IEEE Access* **8**, 27705–27714 (2020)
4. E.U. Heo, S.J. Kim, J. Kim, Backdrivable and fully-portable pneumatic back support exoskeleton for lifting assistance. *IEEE Robot. Autom. Lett.* **5**(2), 2047–2053 (2020)
5. M. Ho, Y. Kim, S.S. Cheng, R. Gullapalli, J.P. Desai, Design, development, and evaluation of an MRI-guided SMA spring-actuated neurosurgical robot. *The International journal of robotics research* **34**(8), 1147–1163 (2015)

A Robot-Aided Rehabilitation Platform for Occupational Therapy with Real Objects



C. Tamantini, M. Lapresa, F. Cordella, F. Scotto di Luzio, C. Lauretti, and L. Zollo

Abstract Robot-aided rehabilitation enables to assist the patient in executing task-oriented exercises and typically takes advantage of virtual environments in which motor tasks are performed. However, this approach introduces a mismatch between the visual and the proprioceptive stimuli the patient perceives. The use of real tools to perform rehabilitation tasks could overcome this drawback. Nevertheless, several issues arise, such as the estimation of the pose of the real objects in the workspace and the planning of the trajectories the robot has to execute to guide the patient's limb to reach the objects. In this paper, a robot-aided upper-limb rehabilitation system able to recognize the objects the patient has to interact with, by means of an RGB-D camera, and to dynamically plan the robot trajectories is proposed. The computational burden and the performance of the proposed system, and in particular of the Pose Estimation Pipeline and of the robot Motion Planner, are evaluated. The obtained results in terms of pose estimation and reaching errors pave the way to the application of the proposed system in a real rehabilitation scenario.

Keywords Robot-aided rehabilitation · Vision-based pose estimation · Dynamical movement primitives

1 Introduction

Robot-aided rehabilitation platforms have been developed in the last decades to guide the patient's affected limb in executing controlled and assisted movements with a task-oriented approach [1]. It is particularly useful in occupational therapy contexts.

Robot-aided rehabilitation is often supported by virtual reality: the interaction of the patient with virtual objects promotes his/her involvement during the therapy. Despite the widespread use of virtual environments, a misalignment between visual

C. Tamantini (✉) · M. Lapresa · F. Cordella · F. Scotto di Luzio · C. Lauretti · L. Zollo
Research Unit of Advanced Robotics and Human-Centred Technologies, Università Campus
Bio-Medico di Roma, Rome, Italy
e-mail: c.tamantini@unicampus.it

© The Author(s), under exclusive license to Springer Nature Switzerland AG 2022
D. Torricelli et al. (eds.), *Converging Clinical and Engineering Research*
on *Neurorehabilitation IV*, Biosystems & Biorobotics 28,
https://doi.org/10.1007/978-3-030-70316-5_136

851

and proprioceptive stimuli can be found. In fact, the haptic feedback that a robotic system can return to the patient may mismatch what happens in the virtual environment [2]. To overcome this drawback, real tools can be used during the exercises to guarantee the involvement of the subjects and avoid the sensory misalignment.

The desired motion of the robot in guiding the patient's arm (i.e. in reaching the objects to be manipulated) should guarantee a human limb motion as natural as possible to re-educate the patient to move. The Motion Planner module plans the movements to be executed. The trajectories that are currently adopted in robot-aided rehabilitation are mainly analytical displacements, modeled according to the minimum-jerk theory [3]. However, tasks such as complex Activities of Daily Living (ADLs) cannot be modeled with these methods. Learning from demonstration techniques, based on non-linear second-order dynamic systems, also known as Dynamic Movement Primitives (DMPs) [4], enable to plan complex and generalizable trajectories (with respect to different target positions to be reached) taking as a reference movements previously recorded on healthy subjects [5].

Currently, only a few rehabilitation robotic systems exploit real tools during the therapy [6]. The main drawback is the high computational burden the integration of real objects in the rehabilitation session requires. In fact, it implies the adoption of (i) object recognition and pose estimation algorithms, (ii) robot motion planners to help patients in reaching the recognized objects. The literature algorithms used to segment, recognize and estimate the object pose in an unstructured environment, and to plan robot trajectories, have a high computational burden [6], therefore limiting their use in online applications such as robot-aided rehabilitation.

This paper aims at proposing an intelligent robot-aided upper-limb rehabilitation system able to recognize, with a low computational burden, the objects the subject has to interact with and to online generate, with a DMP-based Motion Planner, the Cartesian trajectories for a rehabilitation robot performing occupational therapy tasks.

2 Materials and Methods

The overall architecture of the proposed system is reported in Fig. 1.

It is composed of: (i) a pose estimation pipeline based on an RGB-D camera to estimate the pose of the objects in the rehabilitation scenario, (ii) a DMP-based Motion Planner, based on the equations presented in [4], to compute the trajectories the end-effector of the robot has to perform to reach the recognized objects.

The vision system used in this work is the Kinect v2, whose spatial resolution in the xy plane is 0.003 and 0.01 m along the z axis. This RGB-D camera acquires images and PointClouds at 30 Hz under Robot Operating System (ROS) framework. The PointCloud retrieved from the scene is elaborated to estimate the position and the orientation of the objects in the workspace. They have to be single-coloured objects to be correctly recognised by the proposed pipeline. In particular, the pipeline implemented by using the PCL library [7] to segment the object of interest from the scene

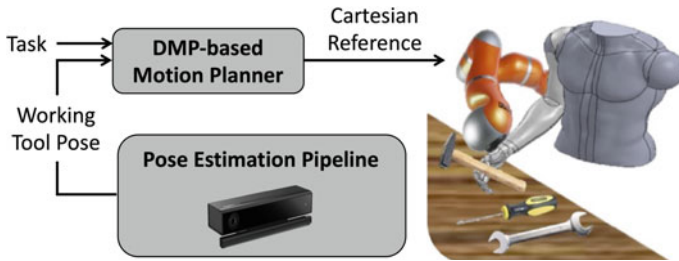


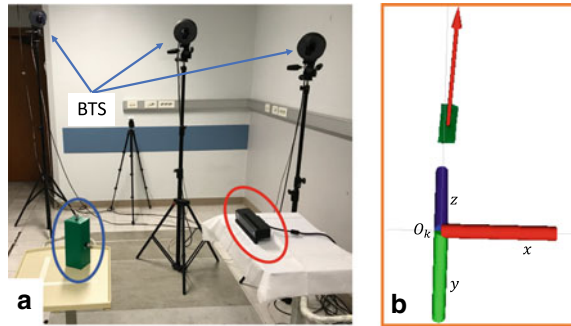
Fig. 1 Block scheme of the proposed approach

and estimate its pose, is composed of the sequential steps: (i) *Pass Through*: points that are lying outside the workspace are removed; (ii) *Extract Indices*: points that have a different color than that of the tool are removed; (iii) *Radius Outlier Removal*: isolated points are removed; (iv) *Moment of Inertia Estimation*: the position of the centroid and the covariance matrix of the input PointCloud are computed. The eigenvectors extracted from the obtained covariance matrix represent the main components of the PointCloud in descending order. The \vec{x} axis explains the maximum variance of the PointCloud describing the orientation of the objects to be reached.

The performance of the implemented pipeline is compared with the one obtained by a motion capture system (i.e. BTS Smart-DX). It is composed of eight optoelectronic cameras recording the 3D positions of retroreflective markers at a frame rate of 60 Hz with an accuracy ≤ 0.2 mm. Two objects, i.e. a box and a hammer, are positioned in the scene and a synchronized acquisition of the two vision systems is performed. In order to retrieve the reference frame of the analyzed objects (with the origin coincident with the object centroid) with the optoelectronic system, three retroreflective markers are placed on the objects orthogonal surfaces. The experimental setup used to validate the proposed pipeline is shown in Fig. 2A. The experimental protocol consists in moving the two objects in six different positions and orientations from a known starting pose. This way, the perfect knowledge of the relative position of the two vision systems is not necessary. The errors in estimating the displacement of the objects with respect to the initial configuration are evaluated. To quantify the overall execution speed, the frequency of the pose estimation is measured.

The pose of the objects retrieved from the RGB-D camera is given as input to the DMP-based Motion Planner. Reaching trajectories, obtained from a previous work [5], are used as demonstration to compute DMP Cartesian references. The error made by the DMP-based Motion Planner in reaching the object position from a fixed starting position $p_0 = [0, 0, 0]^T$ m is used as performance index to evaluate its accuracy.

Fig. 2 **a** Setup for the validation of the pose estimation pipeline. The BTS optoelectronic system, the Kinect v2 (circled in red) and the object to be recognized (circled in blue) are shown. **b** Pose estimation pipeline outputs: segmented object and its estimated pose



3 Results and Discussions

The objects segmentation and the pose estimated by the proposed pipeline are shown in Fig. 2b. The object position errors obtained with the pose estimation algorithm are 0.75 ± 0.14 cm and 1.38 ± 1.04 cm for the box and the hammer, respectively. The highest orientation error is obtained for the box (i.e. 0.11 ± 0.09 rad) when more than one face of the object is visible. In these cases, the first eigenvector of the covariance matrix is not aligned with the object largest dimension. It is important to outline that the magnitude of the error depends on the amount of points belonging to the surfaces orthogonal to the one descriptive of the orientation. Therefore, the slender shape of the hammer enables to estimate its pose with a lower orientation errors (0.03 ± 0.01 rad). The frequency of the pose estimation is 25.54 ± 0.66 Hz. Being the acquisition frequency of the Kinect v2 30Hz, we can conclude that the proposed pipeline is able to effectively identify the pose of objects with a limited computational burden. Other approaches proposed in the literature showed higher drops in the pose estimation frequency (4 Hz).

The mean and standard deviation of the reaching error obtained with the DMP-based Motion Planner is 9.1 ± 2.6 mm, which is acceptable for the proposed application.

4 Conclusions

In this work, a robot-aided rehabilitation system capable of recognizing the pose of the objects and planning Cartesian trajectories is proposed. The Pose Estimation Pipeline and the DMP-based Motion Planner tested show promising results, therefore enabling the application of the system in a real rehabilitation scenario. The computational burden is low enough to allow a rapid and accurate estimation of the pose of the tools. The error in estimating the object pose is compatible with the spatial resolution of the adopted sensor. To ameliorate the orientation estimation, future work will be devoted to implement a filter capable of segmenting the largest visible surface of the

body. The DMP-based Motion Planner proves its capability to generate Cartesian reference trajectories with a small residual error. Different tasks according to the detected tool could also be implemented to extend the system capabilities.

Acknowledgements This work was supported partly by Campus Bio-Medico University of Rome with the SAFE-MOVER project, partly by the Italian Institute for Labour Accidents (INAIL) with the PPR AS 1/3 (CUP: E57B16000160005) and partly by the SENSE-RISC project (CUP: B56C18004200005).

References

1. P. Maciejasz, A survey on robotic devices for upper limb rehabilitation. *J. Neuroeng. Rehabil.* (2014)
2. J. Crosbie et al., Virtual reality in stroke rehabilitation: still more virtual than real. *Disabil. Rehabil.* (2007)
3. T. Flash et al., The coordination of arm movements: an experimentally confirmed mathematical model. *J. Neurosci.* (1985)
4. A.J. Ijspeert et al., Dynamical movement primitives: learning attractor models for motor behaviors. *Neural Comput.* **25**(2), 328–373 (2013)
5. C. Lauretti et al., Learning by demonstration for motion planning of upper-limb exoskeletons. *Front. Neurorobot.* **12**, 5 (2018)
6. C. Loconsole et al., A new kinect-based guidance mode for upper limb robot-aided neurorehabilitation, in *2012 IEEE/RSJ International Conference on Intelligent Robots and Systems (IROS)* (IEEE, 2012), pp. 1037–1042
7. R.B. Rusu et. al., 3d is here: point cloud library (pcl), in *2011 IEEE International Conference on Robotics and Automation* (2011)

Effects of an Overground Robotic Based Gait Training Intervention on Parameters Provided by a Smart-Tip: An Exploratory Study in People with Multiple Sclerosis



L. Santisteban, E. Otxoa, A. Zubizarreta, and A. Rodriguez-Larrad

Abstract Multiple Sclerosis is a progressive disease of the central nervous system, which frequently affects gait. We have developed an instrumented smart-tip that provides objective information of the movement and forces exerted on the assistive device during gait assessment. This study presents encouraging preliminary results of an overground exoskeleton based gait training intervention on parameters collected by the smart-tip, Results indicate that the data provided by the smart-tip might be more sensitive to changes in gait performance than usual assessment tests do.

1 Introduction

MULTIPLE SCLEROSIS (MS) is an inflammatory demyelinating chronic disease. One of the most common and disabling motor disorders affecting people living with MS (pwMS) is gait impairment [1, 2]. Accumulating evidence supports the feasibility and effectiveness of exoskeleton-assisted training for improving gait ability in pwMS, despite the neurodegenerative nature of the disease [3].

There are several tests validated for assessing gait ability in the clinical setting, such as the 10-m walking test (10MWT) or the Timed Up and Go test (TUG). Both

Sponsor and financial support, acknowledgment.

This project has a MINECO founding of the Spanish government DPI2017–82694-R (AEI/FEDER,UE).

We would like to acknowledge ADEMBI and all the participants for their time and disposal to participate in the study.

L. Santisteban (✉) · E. Otxoa · A. Zubizarreta · A. Rodriguez-Larrad (✉)
University of the Basque Country, UPV-EHU, Leioa, Spain
e-mail: leire.santisteban@ehu.eus

A. Rodriguez-Larrad
e-mail: ana.rodriguez@ehu.eus

A. Zubizarreta
e-mail: asier.zubizarreta@ehu.eus

can be performed with an assistive device (AD) for walking, as usually needed by pwMS with moderate to severe gait impairment (e.g. crutch or cane). However, data on how the AD is used is not usually collected, despite it could be a source of complementary information to detect subtle changes in gait ability.

With this idea in mind, we have developed a smart-tip that could be adapted to any AD. [4]. This smart-tip is an evolution of a previous version, which reduces the weight and integrates in the tip casing a 9 degrees-of-freedom Inertial Measurement Unit (Mti by XSens), a piezoelectric force sensor (C9C by HBM) and a barometer (BMP280 by Bosch), which allows quantifying 3D orientation and speed, exerted force and relative altitude, respectively.

The objective of the present work is to evaluate the effects of an overground robotic based gait training intervention on the parameters provided by the smart-tip. We sought to test the hypothesis that the smart-tip provided parameters can give sensitive information to changes that could be useful while determining interventions efficacy in pwMS.

2 Material and Methods

2.1 Trial Design and Participants

This study presents the results of an overground exoskeleton based gait training intervention performed by the control group after a randomized control trial, which was carried out in ADEMBI (Asociación de Esclerosis Múltiple de Bizkaia, Bilbao, Spain) between April and July 2019 [5]. Thus, this is a single-group intervention study. The inclusion criteria were as follows: (a) aged ≥ 18 years, (b) diagnosis of MS according to McDonald criteria, (c) moderate to severe gait impairments defined by an Expanded Disability Status Scale (EDSS) score ranging from 4.5 to 7, and (d) the need for one or two AD for walking outdoors. Data from the participants are summarized in Table 1. Ethics Committee of Clinical Research of Euskadi (CEIm) (Code PS2018017); Protocol registration Code (ACTRN12619000014156).

2.2 Intervention

The intervention consisted on 3 months of individualized and progressive gait training assisted by an overground robotic exoskeleton (Ekso™, Ekso Bionics, USA). Twice weekly sessions were individually supervised by experienced physical therapists properly trained and certified in Ekso™ driving. The sessions included two modalities of exoskeleton use: (1) *PreGait*: to exercise static balance and weight shifts at the beginning of each session; and (2) *ProStepPlus*: to train gait, with steps triggered by the user's lateral weight shift. The duration of the training sessions progressively

Table 1 Participant characteristics (n = 7)

<i>Age (years)</i>		48.1 (12.8)
<i>Gender (Female)</i>		3 (42.8%)
<i>MS type</i>	Remittent recurrent	2 (28.5%)
	Primary progressive	3 (42.8%)
	Secondary progressive	2 (28.5%)
<i>Years since diagnosis</i>		9.2 (6.4)
<i>Expanded disability status scale</i>		5.9 (0.8)
<i>Assistive device</i>		Stick: 4 (57.1%) Crutch: 3 (42.8%)

Data are reported in mean (standard deviation) or number (%)

increased as participants showed greater tolerance aiming to reach a maximum of 40 min of gait training by the end of the 3-month period.

2.3 Outcome Measures

Assessments were performed before and after the intervention by blinded researchers. The primary outcome measure was 10MWT at the participants’ own habitual pace. The gait speed in performing the test was measured by photoelectric cells (Polifemo, Microgate, Italy). The smart-tip was adapted to each participant’s AD while performing the 10MWT for registering: number of steps, Mean Force (MeF), and Maximal Force (MF), i.e., axial load applied by the patient in the AD. The latter were calculated by considering each gait cycle. The relative motion of the AD with respect to the body has been calculated, through the lateromedial and anteroposterior angles, this is, the lateral angle of the AD with respect to the advance plane of the patient, and the angle with respect to the vertical, respectively. From these measurements the maximum values are calculated: MLA for the lateromedial angle and MAPA for the anteroposterior angle. The secondary outcomes included the Timed Up and Go test (TUG) [6], and the Short Physical Performance Battery test (SPPB) [7].

Table 2 Exoskeleton training intervention effects

	PRE	POST	p
<i>10MWT</i>			
Gait speed (m/s)	0.7 (0.2)	0.7 (0.2)	0.39
Number of steps (n)	8.3 (3.5)	6.8 (1.8)	0.06
MeF (Nw)	7.4 (4.7)	6.4 (5.2)	0.09
MF (Nw)	12.2 (5.3)	9.0 (6.3)	0.04*
MLA (Degrees)	4.8 (5)	4.0 (5.1)	0.04*
MAPA (Degrees)	27.9 (4.7)	30.3 (3.3)	0.01*
<i>TUG (sc)</i>	20.3 (8)	19.9 (8.7)	0.11
<i>SPPB (score)</i>	6.4 (2.5)	7.9 (2.11)	0.88

PRE: Data at baseline; POST: data after the intervention; 10MWT: 10 Minute Walking Test; MeF: Mean force; MF: Maximal force; MLA: Maximal lateral angle; MAPA: Maximal antero posterior angle; TUG: Timed up and go; SPPB: Short performance physical battery

Data are reported in mean (standard deviation)

*p < 0.05 Wilcoxon test

Bold represents the values that are statistically significant

3 Results

4 Discussion

As can be seen in Table 2 taking into account information provided by clinical scales (10MWT, TUG, SPPB), changes between baseline and after robot based gait intervention assessments, there is a tendency to improvement after the intervention but changes are not statistically significant. Although there are some technological devices that provide fine assessment of gait capacities, they don't take into account the AD use and its implication in gait improvement [8]. Nevertheless, taking into account the data provided by the smart-tip, we find statistically significant differences in some parameters: force applied in the AD is reduced, the lateral angle is reduced and the anteroposterior angle is increased, meaning that the intervention was effective for improving gait performance of the participants. As we enounced in our hypothesis, assessment with this new tool might provide sensitive information to changes in gait performance.

5 Conclusion

The main result of this work is that the smart-tip might objectively detect changes in gait performance that are not identified with habitual clinical scales. Parameters like

anteroposterior angle, lateral angle and force applied in the AD could be useful for gait assessment in MS clinical context.

References

1. J. Howard, Epidemiology of multiple sclerosis. *Neurol. Clin.* **34**(4), 919–939 (2016)
2. C. Heesen, J. Bohm, C. Reich, J. Kasper, M. Goebel, S.M. Gold, Patient perception of bodily functions in multiple sclerosis: Gait and visual function are the most valuable. *Mult. Scler.* **14**(7), 988–991 (2008)
3. B. Amatya, F. Khan, M. Galea, Rehabilitation for people with multiple sclerosis: an overview of Cochrane Reviews. *Cochrane Database Syst. Rev.* Jan 14;1:CD012732 (2019)
4. A. Brull, A. Zubizarreta, I. Cabanes, A. Rodriguez-Larrad, Sensorized tip for monitoring people with multiple sclerosis that require assistive devices for walking. *Sensors (Basel)* **20**(15), 4329 (2020)
5. R. Berriozabalgoitia, B. Sanz, A.B. Fraile-Bermudez, E. Otxoa, I. Yeregui, I. Bidaurrezaga-Letona et al., An overground robotic gait training program for people with multiple sclerosis: a protocol for a randomized clinical trial. *Front Med (Lausanne)* **9**(7), 238 (2020)
6. Y. Nilsagard, C. Lundholm, L.G. Gunnarsson, E. Dcnison, Clinical relevance using timed walk tests and “timed up and go” testing in persons with multiple sclerosis. *Physiother. Res. Int.* **12**(2), 105–114 (2007)
7. R.W. Motl, Y.C. Learmonth, T.R. Wojcicki, J. Fanning, E.A. Hubbard, D. Kinnett-Hopkins et al., Preliminary validation of the short physical performance battery in older adults with multiple sclerosis: secondary data analysis. *BMC Geriatr.* **15**, 157, 015-0156-3 (2015)
8. Y. Moon, R.S. McGinnis, K. Seagers, R.W. Motl, N. Sheth, J.A. Wright Jr, R. Ghaffari, J.J. Sosnoff, Monitoring gait in multiple sclerosis with novel wearable motion sensors. *PLoS ONE* (2017)

Simultaneous Control of Natural and Extra Degrees-of-Freedom by Isometric Force and EMG Null Space Activation



Sergio Gurgone, Daniele Borzelli, Paolo De Pasquale, Denise J. Berger, Tommaso Lisini Baldi, Nicole D'Aurizio, Domenico Prattichizzo, and Andrea D'Avella

Abstract Myoelectric signals allow to control prostheses and exoskeletons intuitively and effectively by estimating movement intention from the activation of multiple muscles. However, not all muscle activation patterns generate movements, because of the redundancy of the musculoskeletal system. Therefore, such “*null space*” activations could be used to control extra degrees-of-freedom while simultaneously performing a task. Here, we tested the feasibility of this approach by instructing participants to match the position and orientation of an ellipsoidal target by displacing and rotating an ellipsoidal cursor through the generation of isometric force and electromyographic null space activation. Participants were able to perform the task and their performance improved with practice. However, there was a large variability across participants in their ability to hold the cursor within the target. These

This work was supported by the Italian University Ministry (PRIN2015 HFWRY, PRIN2017 TIGHT).

S. Gurgone (✉)

Department of Mathematical and Informatics Sciences, Physical Sciences and Earth Sciences, University of Messina, Messina, Italy
e-mail: sgurgone@unime.it

D. Borzelli · P. De Pasquale · A. D'Avella

Department of Biomedical and Dental Sciences and Morphofunctional Imaging, University of Messina, Messina, Italy
e-mail: adavella@unime.it; a.davella@hsantalucia.it

D. J. Berger

Centre of Space Bio-Medicine, Department of Systems Medicine, University of Rome Tor Vergata, Rome, Italy

D. Borzelli · P. De Pasquale · D. J. Berger · A. D'Avella

Laboratory of Neuromotor Physiology, IRCCS Fondazione Santa Lucia, Rome, Italy

T. Lisini Baldi · N. D'Aurizio · D. Prattichizzo

Department of Information Engineering and Mathematics, University of Siena, Siena, Italy

D. Prattichizzo

Istituto Italiano Di Tecnologia (IIT), Genoa, Italy

results support the feasibility of null space control and suggest that task difficulty must be optimized according to the individual control ability.

1 Introduction

MYOELECTIC CONTROL, i.e. the control of a device using electromyographic (EMG) signals, is both a powerful tool to investigate basic principles of motor control [1] and a promising approach for the control of prostheses [2] and exoskeletons [3]. Indeed, it is possible to detect which movement an individual intends to perform from EMG signal from many different muscles, using a data-driven linear [1] or non-linear [4] mapping between these signals and the forces or kinematics, or a musculoskeletal model [5].

Due to the redundancy of the musculoskeletal system, i.e. the presence of a higher number of muscles than the endpoint degrees of freedom (DoFs), many muscle patterns are not mapped onto movements or force generation, but instead lie in the EMG “null space”. This space includes, for example, the co-contraction of two antagonistic muscles, which counterbalance the effect of each other. EMG null space has been used to control the impedance of robotic devices [6], but no studies to date have looked into the possibility of using null space to directly control extra degrees of freedom while simultaneously performing natural movements, thus augmenting human motor abilities.

To assess the feasibility of this approach, we designed an experiment in which we tested the performances of human subjects during an isometric force task in which they had to control simultaneously also an extra degree of freedom through null space activation in arm and/or shoulder muscles.

2 Material and Methods

2.1 Subjects

Eight naïve right-handed subjects (mean \pm SD age: 27.5 ± 7.8 , age range 20–45, 2 females and 6 males) participated in the experiments after giving written informed consent. All procedures were conducted in conformance with the Declaration of Helsinki and were approved by the Ethical Review Board of IRCCS Neurolesi ‘Bonino Pulejo’.

2.2 Setup

Participants sat on a gaming chair with the right hand inserted in an orthosis connected to a force transducer, with arm and forearm forming a 90° angle. Car belts immobilized torso and shoulders. They wore 3D shutter glasses and viewed stereoscopically a virtual scene displayed on a monitor through a horizontal mirror occluding the hand. Real-time feedback of the exerted force was given as the displacement of a virtual cursor, simulated, through an adaptive filter [1], as a mass-spring-damper system with critical damping, accelerated by the applied force. Surface EMG activity was recorded, using bipolar surface electrodes (Delsys Trigno Wireless), from 15 muscles acting on the shoulder and elbow: brachioradialis; biceps brachii long and short heads; pectoralis major; anterior, middle and posterior deltoid; triceps brachii lateral and long heads; infraspinatus; teres major; latissimus dorsi; lower, middle and upper trapezius.

2.3 Protocol

The experiment was divided into 17 blocks. In the first block, participants were asked to exert maximum voluntary force (MVF) along one direction on the horizontal plane (anterior), to normalize target distance in the successive blocks. In the second block (force control, FC), participants were asked to move a virtual spherical cursor into a spherical target in one of 20 spatial directions (distance 15 or 25% of MVF), and to stay inside it (holding phase) for 0.5 s, with 4 s of time limit. EMG and force data collected were used to calculate the EMG signal normalization, and to estimate by regression the EMG-to-force matrix H , such that $F = Hm$, where F is the force vector and m the EMG activation vector. The null space of H , i.e. the set of vectors n that map into the null vector ($Hn = 0$) was calculated as an orthonormal matrix N (using the MATLAB function *null*). In the third block (null space estimation, NSE), the participant had to hold the cursor inside a target placed in the origin, for 1 s, while an oscillation perturbing the motion of the cursor. To reduce it, the subjects had to increase their null space activation and were instructed to stiffen their right arm and shoulder [7]. EMG data collected in this block were used to calculate the principal components of N to be used to control the extra DoF. The fourth block was a FC block with 8 equally spaced planar targets (3 reps.) at 20% of MVF with an ellipsoidal cursor and targets. In the following 12 blocks (null space control, NSC), participants had also to rotate the cursor around the medio-lateral axis by null space activation and stay inside the targets for 1 s. All the targets had the same orientation of 60° (20% of the maximum null space activation in the NSE block). A FC block with the ellipsoidal target was performed at the end.

2.4 Control of the Extra DoF

The EMG data collected in the NSE block allowed the estimation of the null space dimensions from the N matrix used by each participant through principal component analysis (PCA). A number of components explaining 80% of the total variation of the EMG data was selected to control the extra DoF in the NSC blocks, using a sigmoidal function of the projection norm of EMG activation in these components.

3 Results

Participants were able to control the cursor and reach the target in $92 \pm 6\%$ (mean \pm STD) of the trials during the first FC block and to stay in the targets for the required time in $63 \pm 19\%$ of the selected trials. In the two FC block before and after the NSC blocks results were similar, with $88 \pm 25\%$ and $95 \pm 12\%$ respectively for reaching, and $67 \pm 31\%$ and $77 \pm 24\%$ for holding. The R^2 for the reconstruction of the 3D force in the three blocks was 0.76 ± 0.11 , 0.78 ± 0.13 and 0.67 ± 0.23 , respectively. Throughout the NSC blocks, participants improved their ability to control simultaneously the cursor position (natural DoF) using force and orientation (extra DoF) using null space activation, with progressively straighter trajectories (Fig. 1). A generalized liner mixed model (GLMM), with block and target variables as fixed effects and subject as random effect, showed a significant increase in the mean fraction of trials in which the target was successfully reached as a function of block ($p < 0.001$, slope 0.05), with a maximum value of $92 \pm 9\%$ (Fig. 2). Although a GLMM applied to the fraction of trials in which the cursor was successfully held in the target showed similar results for the effect of block ($p < 0.001$, slope 0.04), individual performances

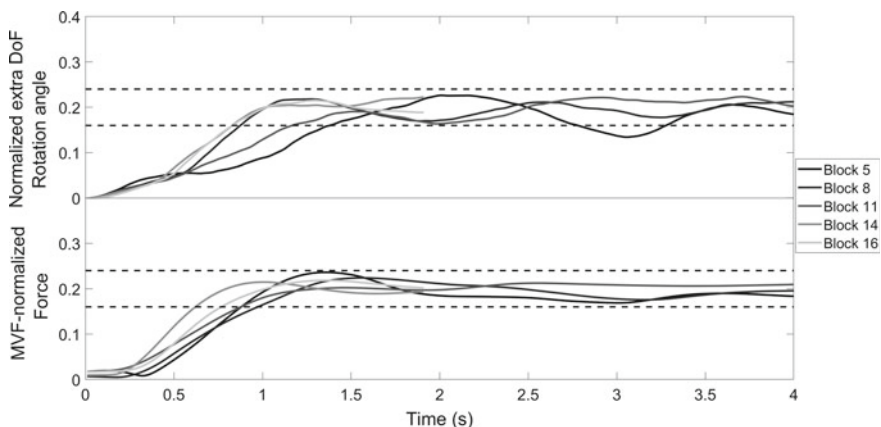


Fig. 1 Examples of activation of the magnitude of the force vector and of the extra DoF, normalized to their maximum values, for different blocks. Dashed lines represent target tolerance

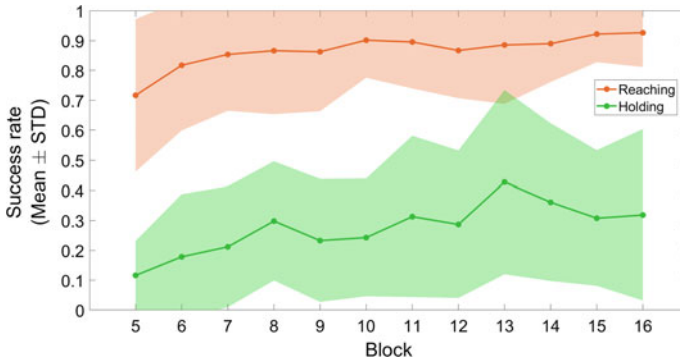


Fig. 2 Mean success rate across participants and targets in each block for reaching and for holding. Shaded areas represent standard deviation

were highly variable and on average rather low (highest value across blocks: $43 \pm 30\%$) (Fig. 2).

4 Discussion and Conclusions

With this work, we demonstrated the feasibility of using EMG null space activation to control an extra DoF while performing simultaneously an isometric force-control task. We found that it is possible to control the position and orientation of an ellipsoidal cursor to match different target position and orientations using both force and null space control. However, we also observed high variability among subjects for what concern holding performance. Future work will investigate individual abilities and how to optimize a null space control interface according to those.

References

1. D.J. Berger, R. Gentner, T. Edmunds, D.K. Pai, A. d'Avella, Differences in adaptation rates after virtual surgeries provide direct evidence for modularity. *J. Neurosci.* **33**(30), 12384–12394 (2013)
2. D. Farina, S. Amsuss, Reflections on the present and future of upper limb prostheses. *Expert Rev. Med. Devices* **13**, 321–324 (2016)
3. E. Ambrosini et al., A myocontrolled neuroprosthesis integrated with a passive exoskeleton to support upper limb activities. *J. Electromyogr. Kinesiol.* **24**(2), 307–317 (2014)
4. I. Vujaklija et al., Online mapping of EMG signals into kinematics by autoencoding. *J NeuroEng. Rehabil.* **15**(21) (2018)
5. N. Lotti et al., Adaptive model-based myoelectric control for a soft wearable arm exosuit: a new generation of wearable robot control. *IEEE Robot. Autom. Mag.* **27**(1), 43–53 (2020)

6. A. Ajoudani, N.G. Tsagarakis, A. Bicchi, in Tele-impedance: towards transferring human impedance regulation skills to robots, *2012 IEEE International Conference on Robotics and Automation* (Saint Paul, MN, 2012), pp. 382–388
7. D. Borzelli, B. Cesqui, D.J. Berger, E. Burdet, A. D'Avella, Muscle patterns underlying voluntary modulation of co-contraction. *PLoS ONE* **13**(10), e0205911 (2018)

Preliminary Clinical Evaluation of the X-Limb Hand: A 3D Printed Soft Robotic Hand Prosthesis



Alireza Mohammadi, Jim Lavranos, Ying Tan, Peter Choong,
and Denny Oetomo

Abstract This paper presents the initial clinical assessment of the X-Limb hand, a 3D printed myoelectric hand prosthesis with fully soft/compliant structure. The design also takes into account the practical requirements including light-weight, multi-grasping capability, ease of manufacture and intrinsic actuation. The X-Limb hand is tested with one person with unilateral congenital below-the-elbow deficiency who never used any type of hand prosthesis. He performed two prosthetic functionality benchmark measures: Jebsen-Taylor Hand Function Test (JHFT) and Box and Block (BB) test. The results of the X-Limb hand are compared with the DEKA arm (the most advanced upper-limb prosthesis) and SoftHand Pro (a clinically assessed flexible myoelectric hand) using the z -score method as there was only one subject in our study. The results showed comparative performance of the subject using the X-Limb hand to the performance of the DEKA Arm and SoftHand Pro in other two studies. The promising performance of the first time prosthetic hand user demonstrates the capability of the X-Limb hand in performing wide range of tasks and shows its potential to significantly reduce the difficulty in learning to operate a myoelectric hand prosthesis.

Keywords Prosthetic hand · Soft robotics · Myoelectric hand prosthesis · 3D printing

A. Mohammadi (✉) · Y. Tan · D. Oetomo
Human Robotic Lab, Mechanical Engineering Department, The University of Melbourne,
Parkville, VIC 3010, Australia
e-mail: alirezam@unimelb.edu.au

D. Oetomo
e-mail: doetomo@unimelb.edu.au

J. Lavranos
Caulfield Hospital, Caulfield, VIC 3162, Australia

P. Choong
Department of Surgery, University of Melbourne at St. Vincent's Hospital,
Fitzroy, VIC 3065, Australia
e-mail: pchoong@unimelb.edu.au

© The Author(s), under exclusive license to Springer Nature Switzerland AG 2022
D. Torricelli et al. (eds.), *Converging Clinical and Engineering Research
on Neurorehabilitation IV*, Biosystems & Biorobotics 28,
https://doi.org/10.1007/978-3-030-70316-5_139

1 Introduction

Soft robotics is an emerging field which has shown great potential in addressing issues with current hand prostheses, i.e., non-compliant structure, heavy weight and complex system. The inherent material compliance in the soft robotic systems provides safer, cheaper, and simpler mechanisms (and consequently simpler control structures) compared to the traditional rigid robotic systems [1].

Current soft hand prostheses such as Hannes Hand [2], SoftHand Pro [3] and RBO Hand 2 [4] are not satisfying the practicality requirements including the weight (less than human biological hand), ease of manufacturing and personalisation. In [5], we addressed the practical requirements in the X-Limb hand with the consideration of the trade-off between practicality and performance and demonstrated its capability in performing grasping tasks required for activities of daily living (ADLs). The X-Limb had a weight of 253 g, three grasps types (with capability of individual finger movement), power-grip force of 21.5 N and hand closing speed of 1.3 s.

X-Limb represents a simplified solution to the prosthetic hand design not only in the physical design but also in the interface to its functionality. More specifically, the design focuses only on two main grasps (pinch and power), produced with the synergy of fingers. This allows a very basic simple operation of the hand while retaining the ability to perform the required tasks of the benchmark tests in this paper.

Although the functionality of the X-Limb has been tested on different grasping tasks, it has not been tested on any individual with upper-limb amputation yet. Therefore, the objective of this study is to evaluate the performance of one subject with unilateral transradial limb difference who is fitted with the X-Limb hand and compare the performance results with two state-of-the-art myoelectric hand prostheses.

2 Method

The experiments were conducted with one subject (male, 22-years-old) with congenital transradial (below-the-elbow) limb deficiency in the left side (non-dominant side) who never used any types of hand prosthesis. The subject read the plain language statement and signed the consent form approved by the Ethics Committee of the University of Melbourne (Ethics ID 1852363.1).

A custom prosthetic socket build for the participant using 3D scanning of his residual and 3D printing with the same flexible material of the X-Limb hand and then secured on the residual limb by an adjustable elbow strap. A single EMG electrode is used for flexion and extension of the X-Limb. In order to reduce the complexity of the experiment for the naive subject, a single tactile button on the X-Limb arm is used to switch between grasp types. Other forms of switching can be used. The experimental results in [6] demonstrated that first time subjects were more effective in performing the task of selecting the right grasp using the buttons than through the attempt of producing the right EMG signals (as seen in some commercial devices).

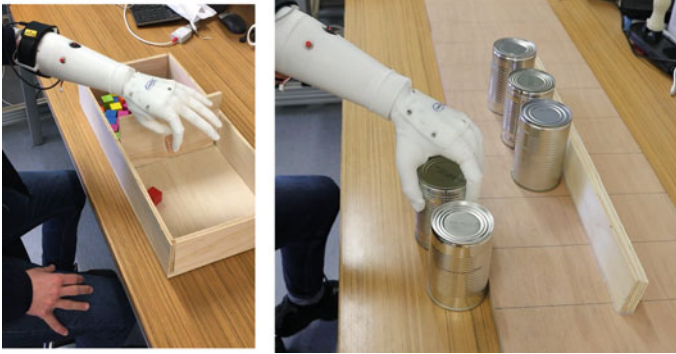


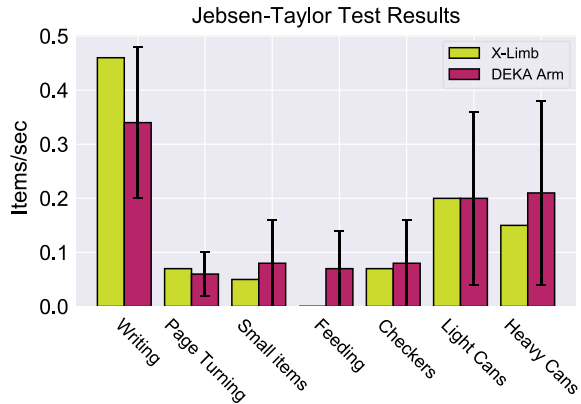
Fig. 1 Participant performing prosthetic hand assessment tasks: Box and Block test (left) and carrying heavy cans as one of the tasks of the Jebsen-Taylor Hand Function Test (right)

Two grasp types are used in the experiments: pinch and power. In power grasp, the thumb will move from the natural open hand position towards the center of the palm in coordination with other fingers. When the thumb is in adduction position, the actuation of the index finger will produce the pinch grasp [5]. The participant received one hour of training to use EMG signals for opening and closing of the X-Limb hand in two grasp types.

As shown in Fig. 1, two prosthetic functionality benchmark tests are used: (1) The Box and Blocks (BB) test (number of 1-in. blocks moved from one side of a box to another in 60s) to measure the gross manual dexterity and speed. The results are compared with SoftHand Pro [3]; (2) Jebsen-Taylor Hand Function Test (JHFT) which is a measure of dexterity and simulated ADLs. The modified version used in this study which caps maximum time for each task at 120s and scores the number of items completed per second. The results are compared with DEKA Arm [7].

In order to compare the performance of one subject with results of the group of participants in the other studies, we exploit the z -score test [8]. The z -score measures how many standard deviations above or below the mean a data point is and defined as $z\text{-score} = (x - \mu) / \sigma$ where x is the single data point (the score of one subject in our study), μ and σ are the mean and standard deviation of the group (the performance of the group of the participants in using SoftHand Pro and DEKA Arm as reported in [3, 7]). Then, in order to know how well the subject performed compared to the participants in the other groups, we use the z -table (standard normal distribution table). The table determines the percentage of the groups participants who obtained higher and lower scores than single subject.

Fig. 2 Jebsen-Taylor hand function test results and comparison with the results of DEKA arm. Higher values show better performance (performing task quicker)



3 Results and Discussion

The average of three trials of the subject using X-Limb in performing BB test is 8 blocks in one minute. The reported results of 9 participants in [3] using the SoftHand Pro after 6–8 h of training showed the mean and standard deviation of $\mu = 9.5$ and $\sigma = 4$, respectively. Therefore, the z -score = -0.38 shows that the X-Limb hand user performed better than 34% of the SoftHand Pro users.

The results of the subject in performing JHFT tasks and the reported results of 23 participants in [7] using DEKA Arm at the end of the initial training sessions are shown in Fig. 2. The subject performed the tasks once and then we recorded the scores. The z -scores of X-Limb hand user for the 7 tasks of the JHFT (writing, page turning, small items, feeding, checkers, light cans, heavy cans) in comparison to DEKA Arm users are (0.85, 0.25, -0.37 , -1 , -0.12 , 0, -0.35) which shows that the performance of the X-Limb hand user is better than (80%, 60%, 35%, 15%, 45%, 50%, 36%) of the DEKA Arm users, respectively. Excluding the feeding task, the performance of the X-Limb hand user was comparable to the DEKA Arm users. In the feeding task, due to small size of the teaspoon, the X-Limb was not able to grasp it.

4 Conclusions

The results of this study demonstrated the capability of a first time myoelectric hand user in using the X-Limb hand and showed comparable results to the state-of-the-art myoelectric hand prostheses. The future work will focus on testing the X-Limb hand with more subjects including children (using the paediatric version of the X-Limb [9]) and providing bone conduction vibrotactile feedback [10].

Acknowledgements This project is funded by the Valma Angliss Trust and The University of Melbourne.

References

1. D. Rus, M.T. Tolley, Design, fabrication and control of soft robots. *Nature* **521**(7553), 467 (2015)
2. M. Laffranchi, et al., The Hannes hand prosthesis replicates the key biological properties of the human hand. *Sci. Robot.* **5**(46) (2020)
3. S.B. Godfrey et al., The Softhand pro: functional evaluation of a novel, flexible, and robust myoelectric prosthesis. *PLoS ONE* **13**(10), e0205653 (2018)
4. R. Deimel, O. Brock, A novel type of compliant and underactuated robotic hand for dexterous grasping. *Int. J. Robot. Res.* **35**(1–3), 161–185 (2016)
5. A. Mohammadi, J. Lavranos, H. Zhou, R. Mutlu, G. Alici, Y. Tan, P. Choong, D. Oetomo, A practical 3d-printed soft robotic prosthetic hand with multi-articulating capabilities. *PLoS ONE* **15**(5), e0232766 (2020)
6. A. Mohammadi, J. Lavranos, R. Howe, P. Choong, D. Oetomo, Grasp specific and user friendly interface design for myoelectric hand prostheses, in *International Conference on Rehabilitation Robotics (ICORR)* (2017), pp. 1621–1626
7. L.J. Resnik, M.L. Borgia, F. Acluche, J.M. Cancio, G. Latlief, N. Sasson, How do the outcomes of the DEKA arm compare to conventional prostheses? *PLoS ONE* **13**(1), e0191326 (2018)
8. R.H. Mycroft, D.C. Mitchell, J. Kay, An evaluation of statistical procedures for comparing an individual's performance with that of a group of controls. *Cogn. Neuropsychol.* **19**(4), 291–299 (2002)
9. A. Mohammadi, J. Lavranos, Y. Tan, P. Choong, D. Oetomo, A paediatric 3d-printed soft robotic hand prosthesis for children with upper limb loss, in *IEEE EMBC* (2020), pp. 3310–3313
10. R.M. Mayer, R. Garcia-Rosas, A. Mohammadi, Y. Tan, G. Alici, P. Choong, D. Oetomo, Tactile feedback in closed-loop control of myoelectric hand grasping: conveying information of multiple sensors simultaneously via a single feedback channel. *Front. Neurosci.* **14**, 348 (2020)

Surface EMG Based Guidance Force Feedback System for Muscle-Specific Upper Limb Training in Stroke Patients



Sojung Lee and Suncheol Kwon

Abstract A system for surface EMG (SEMG)-based guidance force control training is presented, which can be utilized to treat stroke patients. The four muscles to be trained to realize reaching movements in a horizontal plane were selected based on the four directions considered. When the stroke patient uses specific muscles, the robot enables feedback to induce the use of specific muscles. This is realized by generating a SEMG-based guidance force in the direction perpendicular to the reference trajectory. The feedback from the robot helps the patients reach the vicinity of the reference trajectory. When the muscles were not measured, the robot guidance force was not provided for specific muscle training.

1 Introduction

Upper extremity rehabilitation training using a robot helps in high-intensity repetitive training, and it is possible to quantitatively acquire kinematic information to understand the exercise recovery process. This training is effective for restoring upper limb function because it is possible to acquire motor skills based on feedback through visual or force control rather than repetition of simple movement [1].

However, there are limitations to the current upper limb rehabilitation robots. The control algorithm of current upper limb robotic rehabilitation is based on the kinematic (accuracy, speed, and smoothness) data of the robot endpoint (e.g., hand

This study was supported by the Research Programs (NRCTR-IN20004) of the Korea National Rehabilitation Center, Ministry of Health and Welfare, Republic of Korea.

S. Lee · S. Kwon (✉)

Rehabilitative and Assistive Technology Department, National Rehabilitation Research Institute, National Rehabilitation Center, Seoul, Korea

e-mail: suncheolkwon@korea.kr

S. Lee

e-mail: choamsa@korea.kr

position). This cannot induce to train specific muscles against abnormal movements such as the trunk compensation pattern [2].

SEMG can verify the use of specific muscles and attempt to generate movements and has the advantage of confirming the movement control recovery process [3]. There are several studies that investigate the possibility of classifying movement patterns through SEMG signals to trigger or assist in upper limb movements [2, 3], to detect abnormal movements through SEMG signals during robot training [5, 6] and to make to correct the movements by providing visual feedback on muscle activation patterns [7].

Therefore, in this study, we propose the upper limb robotic rehabilitation system adapted SEMG-based guidance force feedback. The SEMG signal was applied to the force controller of the three-degree-of-freedom multi-joint commercial robot. When the stroke patient intends to use specific muscles, the robot enables feedback to induce the use of specific muscles by generating a SEMG-based guidance force in the direction perpendicular to the reference trajectory.

2 Methods

2.1 The Control System

The system was implemented using Proficio robot (Barrett Technology, LLC., Newton, MA), and Trigno Avanti (Delsys, Inc., Boston, MA), wireless EMG acquisition system. EMG signals were collected using the NI DAQ board (NI PCI-6221) such that the SEMG and the robot assistance force in synchronization at high speed. Using the real-time control library provided by Barrett technology, the SEMG signals used to control the interaction force (Fig. 1). The SEMG signals were processed a sampling rate of 1 kHz and were smoothed using the moving average window filter.

2.2 Experimental Environments

Two experimental environments were designed. The aim was to realize movement (14 cm) of the robotic arm in the four directions (right, left, backward, and forward, 90° from the starting center point each) in a horizontal plane in both these environments.

In experiment 1, the stroke patients were provided with guidance force, which was proportional to trajectory error. If there is a difference between the desired path and the position of the robot handle, guidance force proportional to the difference is provided. In experiment 2, the stroke patients were provided with guidance force, which was

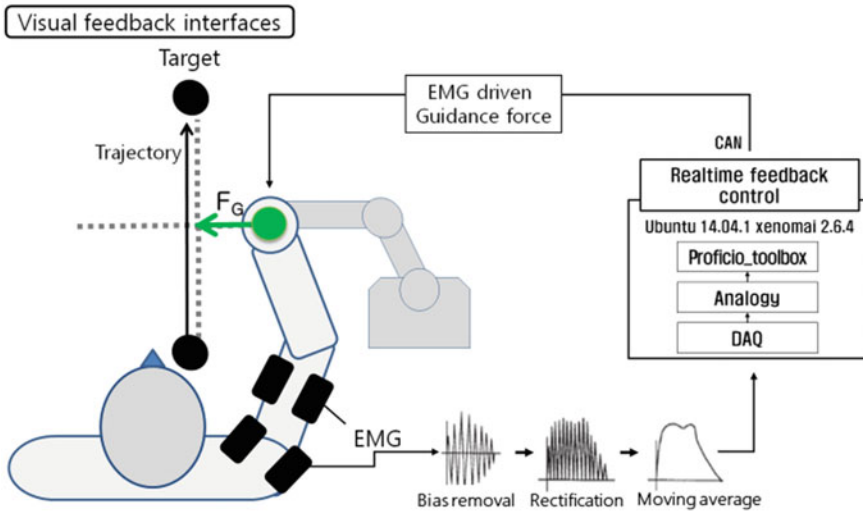


Fig. 1 The experimental setup

Table 1 Target position and matched reference muscles

Target position	Reference muscles
Forward	Triceps brachii long head (TR)
Right	Deltoid posterior (DP)
Backward	Biceps brachii (BI)
Left	Pectoralis major clavicularis part (PM)

proportional to pre-selected muscle’s SEMG signal. The muscles (measured for non-disabled persons) were selected for each direction based on previous studies [2, 3] (Table 1).

Before training, isometric muscle testing was performed for the 4-way task, and the SEMG signal was simultaneously measured to calculate the guidance gain between the SEMG signal and the muscle strength. During training, if a muscle is activated while attempting to correct the trajectory away from the reference trajectory, an guidance force proportional to the EMG signal in the perpendicular direction of the reference trajectory is provided. In contrast, if SEMG signals that match the reaching direction are not measured, then the guidance force is not provided. The visual and auditory feedback is provided to verify the training process of the participants.

3 Results

SEMG based guidance force feedback system was developed as follows (Fig. 2). A

Fig. 2 The experimental setup



total of 4 targets in the forward, right, backward, and left direction along with the position of the end-effector were displayed on the screen.

The guidance force in the perpendicular direction of reference trajectory for experiment 1 is as follows (1).

$$F_G = K_p e + K_d \frac{de}{dt} \quad (e = Pos_{desired} - Pos_{current}) \quad (1)$$

In previous studies, the virtual spring constant, $K_p = 200$ and damping constant, $K_D = 10$ were selected.

The guidance force for experiment 2 is expressed in (2). For example, in the forward direction, if the major intention to modify the trajectory to the left is observed through the EMG signal, the stroke patient receives the guidance force as follows (2).

$$F_G = K \cdot EMG_{PM} \quad (2)$$

The coefficient matrix K was calculated by performing individual isometric muscle tests in each of the four directions, before the experiment (3).

$$\begin{bmatrix} F_x \\ F_y \end{bmatrix} = \begin{bmatrix} K_{xTR} & K_{xDP} & K_{xBI} & K_{xPM} \\ K_{yTR} & K_{yDP} & K_{yBI} & K_{yPM} \end{bmatrix} \begin{bmatrix} EMG_{TR} \\ EMG_{DP} \\ EMG_{BI} \\ EMG_{PM} \end{bmatrix} \quad (3)$$

The results of experiments 1 and 2 represented that different guidance forces were provided by reflecting the spring, damper constant, and SEMG signal characteristics.

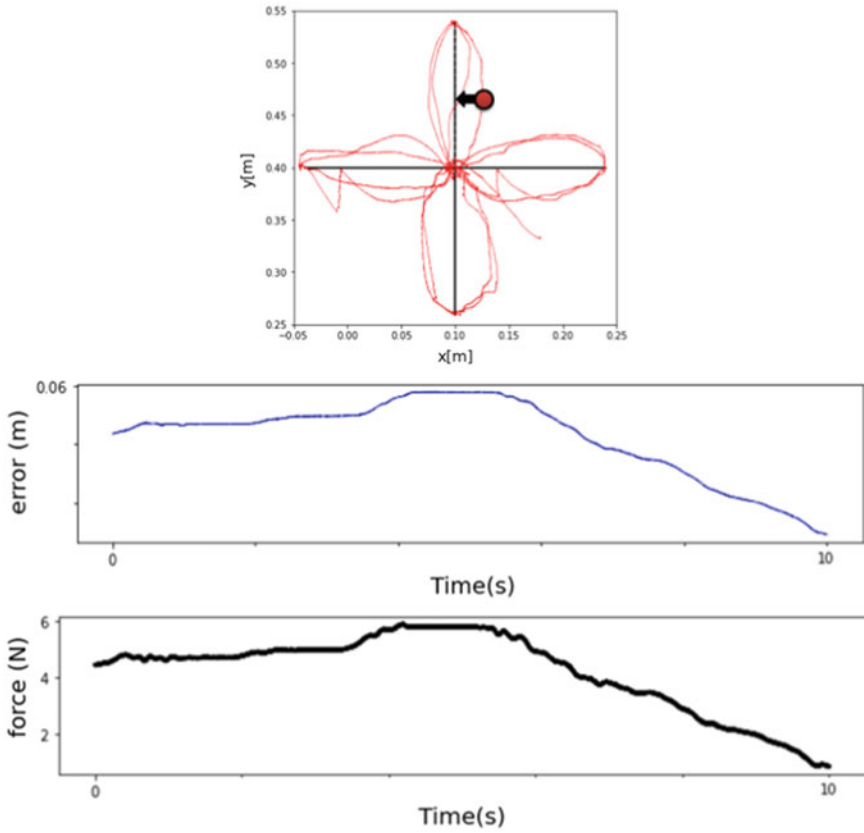


Fig. 3 Experiment 1: Intention to modify the trajectory (Red point: The point where user want to modify the trajectory, Black arrow: Movement direction), Trajectory error (m) and Guidance force (N)

4 Conclusion

A system that can provide stroke patients with guidance force feedback to induce specific muscles using SEMG was introduced. The force proportional to the SEMG was provided to guide the reference trajectory and was compared with compliant guidance force using the virtual spring-damper components. We plan to study the feasibility and clinical effects of the proposed system in stroke survivors.

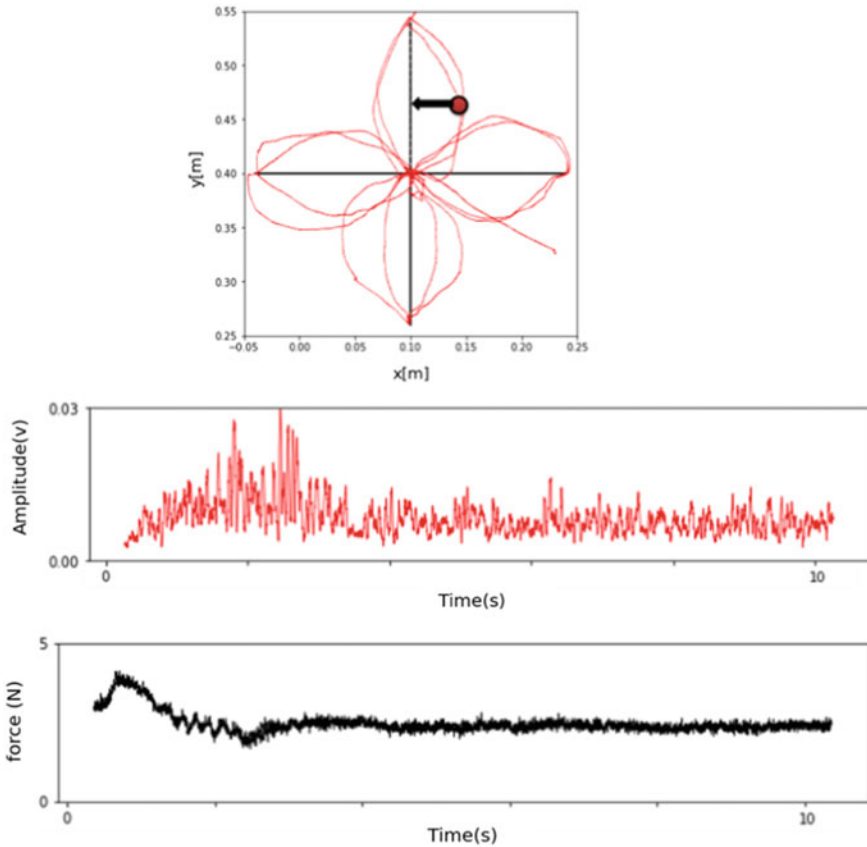


Fig. 4 Experiment 2: Intention to modify the trajectory (Red point: The point where user want to modify the trajectory, Black arrow: Movement direction), Pectoralis major muscle EMG modulation (V) and Guidance force (N)

References

1. J. Kim, S.-W. Park, Y. Lee, H. Seo, Clinical outcomes of robot-assisted arm rehabilitation in stroke patients. *Brain Neurorehabil.* **8**(1), 46 (2015)
2. J.P.A. Dewald, V. Sheshadri, M.L. Dawson, R.F. Beer, Upper-limb discoordination in hemiparetic stroke: implications for neurorehabilitation. *Top. Stroke Rehabil.* **8**(1), 1–12 (2001)
3. L. Dipietro, M. Ferraro, J.J. Palazzolo, H.I. Krebs, B.T. Volpe, N. Hogan, Customized interactive robotic treatment for stroke: EMG-triggered therapy. *IEEE Trans. Neural Syst. Rehabil. Eng.* **13**(3), 325–334 (2005)
4. B. Cesqui, P. Tropea, S. Micera, H. Krebs, EMG-based pattern recognition approach in post stroke robot-aided rehabilitation: a feasibility study. *J. NeuroEng. Rehabil.* **10**(1), 75 (2013)
5. X. Hu, K.Y. Tong, R. Song, V.S. Tsang, P.O. Leung, L. Li, Variation of muscle coactivation patterns in chronic stroke during robot-assisted elbow training. *Arch. Phys. Med. Rehabil.* **88**(8), 1022–1029 (2007)

6. P.A. Dewald, V. Sheshadri, M.L. Dawson, R.F. Beer, Upper-limb discoordination in Hemiparetic stroke: implications for neurorehabilitation. *Top. Stroke Rehabil.* **8**(1), 1–12 (2001)
7. J. Luo et al., Characterization of the coordination of agonist and antagonist muscles among stroke patients, healthy late middle-aged and young controls using a myoelectric-controlled interface. *J. Neural Eng.* **15**(5), (2018)

Hybrid Actuation Mechanism for an Ultra Low-Cost Transhumeral Prosthesis: Preliminary Study



T. Reboli, S. Meloni, G. Ballardini, G. Carlini, M. Casadio, F. Sante, M. Serafica, G. Vigo, and L. Schiatti

Abstract In this work, we present a novel hybrid approach to the actuation of an ultra low-cost upper limb prosthesis. An open-source mechanical design has been developed allowing the control of two degrees of freedom: opening-closing of the hand and flexion-extension of the elbow. The hand actuation mechanism has been designed in order to be easily convertible from electrically powered to body powered, thanks to the addition of a spring and a cable. In the study, we describe the mechanical design of both degrees of actuation and the hybrid solution, as well as the control schema and the preliminary tests for electromechanical characterization of the hand module.

Keywords Ultra low-cost prostheses · Hybrid actuation · Upper limb amputation

1 Introduction

The need of developing ultra low-cost prostheses arises from the consideration that access to public healthcare, and specifically prosthetic care, is not equally distributed

T. Reboli and S. Meloni are equal contribution.

T. Reboli

Department of Mechanical, Energy, Management and Transportation Engineering (DIME),
Polytechnic School University of Genoa, Genoa, Italy
e-mail: tommaso.reboli@edu.unige.it

S. Meloni · G. Ballardini · G. Carlini · M. Casadio · F. Sante
Department of Computer Science, Bioengineering, Robotics and Systems Engineering (DIBRIS),
University of Genoa, Genoa, Italy

M. Serafica · G. Vigo
Time for Peace-Genova Onlus, Genoa, Italy

L. Schiatti (✉)
Unit for Visually Impaired People (U-VIP), Istituto Italiano di Tecnologia, Genoa, Italy
e-mail: Lucia.Schiatti@iit.it

© The Author(s), under exclusive license to Springer Nature Switzerland AG 2022
D. Torricelli et al. (eds.), *Converging Clinical and Engineering Research*
on *Neurorehabilitation IV*, Biosystems & Biorobotics 28,
https://doi.org/10.1007/978-3-030-70316-5_141

883

over the world. In particular, WHO estimates that 80% of people with amputations reside in Lower-Middle Income Countries (LMICs), and only 3% of them have access to rehabilitative care [1, 2]. This is mainly due to the unaffordable cost of commercially available prostheses, especially for what concern upper limbs, given the major technological complexity that is required to restore an arm/hand functionality. Indeed, the commercial cost of a functional prosthetic hand can range between \$4000–\$10,000 and \$25,000–\$75,000 for a body-powered and an externally powered actuation, respectively [3]. To be accessible by amputees in LMICs, and therefore have an impact on their working capabilities and economical condition, such cost should be kept below \$1000–\$500. All existing low-cost upper limb prostheses are developed for amputations below the elbow, despite the fact that 25% of amputations are above the elbow [3], and that the need of restoring an arm's functionality is higher in the latter scenario, especially in resource-constrained and rural settings. A body powered actuation, i.e. driven by cables controlled by body movements, is the main choice when targeting LMICs [4]. It allows an equipment- and electronic-free design, resulting in a more durable and easily maintainable product. At the same time, externally powered solutions present several advantages, such as light weight, higher usability for weak subjects, and easier control of multiple Degrees of Freedom (DOFs). A hybrid approach could be especially useful in resource-constrained countries, to guarantee the use of the hand in different conditions. However, there is a lack of such solutions for the ultra low-cost prostheses. In this work, we present a novel design of a transhumeral prosthesis allowing the control of two degrees of freedom, i.e. hand opening/closing and elbow flexion/extension, and a hybrid actuation of the hand, either body or externally powered.

2 Prosthesis Design and Characterization

2.1 Mechanical Design

Related literature suggests that, besides providing the amputee with increased functionality, prostheses suitable to be used in LMICs have to be affordable, easy to repair and maintain at a low cost, robust and durable [5]. Accordingly, specific requirements for components and mechanical performance were defined, including: hand length 18–19 cm, forearm length 24–25 cm, overall weight limit 1.8 kg, total materials and components cost limit \$200 (including actuators), hand hold strength 100 N, maximum hand closing time 5 s, maximum liftable load 20 N. Mechanical design, including component assemblies creation and dynamic analysis, was conducted with the CAD software CREO by PTC. The design process was divided in two main parts: (1) externally powered design for hand and elbow actuation, and (2) body powered design for hand actuation. In order to contain the weight of the device, most of the components were realized in aluminium.

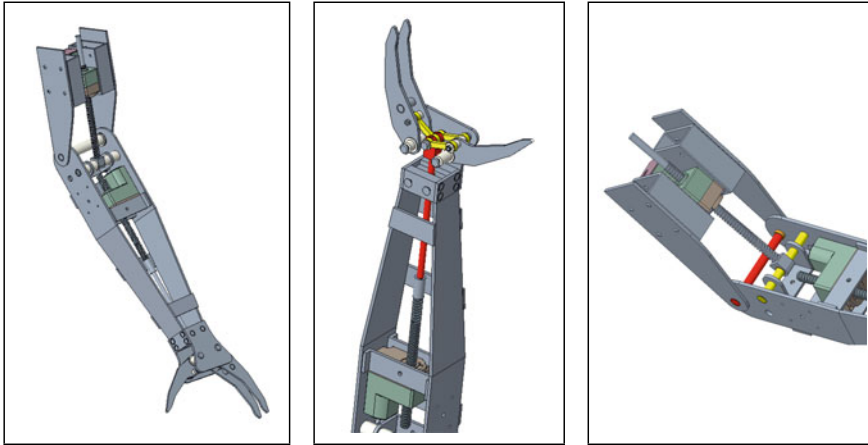


Fig. 1 Mechanical design of the 2 degrees of actuation of the electrically powered prosthesis (left): hand (center) and elbow (right)

For what concerns the externally powered design, dedicated kinematics were designed for both the hand and the elbow, in order to let each degree of freedom be moved by a linear actuator (Fig. 1, left). The hand is actuated by pulling the red pin (Fig. 1, center), which, through a system of connecting rods, let the fingers move from an open to a closed condition. Different dynamic analyses have been performed to evaluate the pull force to be applied to the pin to produce 100 N of hold strength. Such information allowed selecting a suitable linear actuator equipped with a screw reduction (model DABX 270 C). This kind of actuator allows reaching and maintaining a position with no need to continuously absorb power, thus minimizing energy consumption and increasing the autonomy. The same actuator was used to drive the elbow mechanism (Fig. 1, right), and pins were consequently displaced allowing to reach a maximum liftable load of 2 kg.

The design process aimed at using the same mechanical structure to actuate the hand with both body and external energy. By replacing the red pin shown in Fig. 1 (center) with a spring-based connection pin, it is possible to move the fingers by pulling a cable activated by a patient's specific body movements. As shown in Fig. 2, based on the spring and cable placement, two options for body-powered hand actuation were implemented: respectively default closed (left) and default open (right) modes.¹

¹ Both mechanical and electronic CAD projects are available open source at: <https://timeforpeacegenova.wordpress.com/materiale-open-source/>.

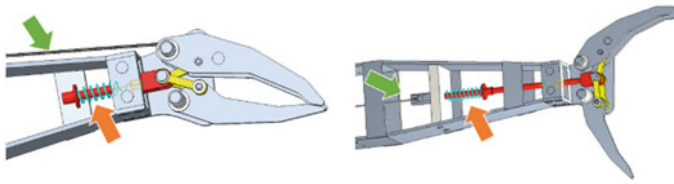


Fig. 2 Mechanical design of the hybrid (electrically/body powered) actuation of the hand: default closed (left) and open (right) solutions

2.2 Motor Control

The externally powered prosthesis is actuated by two motors (hand, elbow). Each motor is driven by a PWM signal generated by a microcontroller (ATmega328P), which regulates the motor speed. Direction of rotation (and each DOF's movement) is controlled by an H-bridge (driver LMD18201). The logical scheme of the electronic circuit driving the actuator is shown in Fig. 3. When the current is below a preset threshold, the microcontroller reads the control signal (myoelectric or from other source) and it controls the motor speed (incremented at each cycle for forward and reverse signals). Otherwise motor brake is activated.

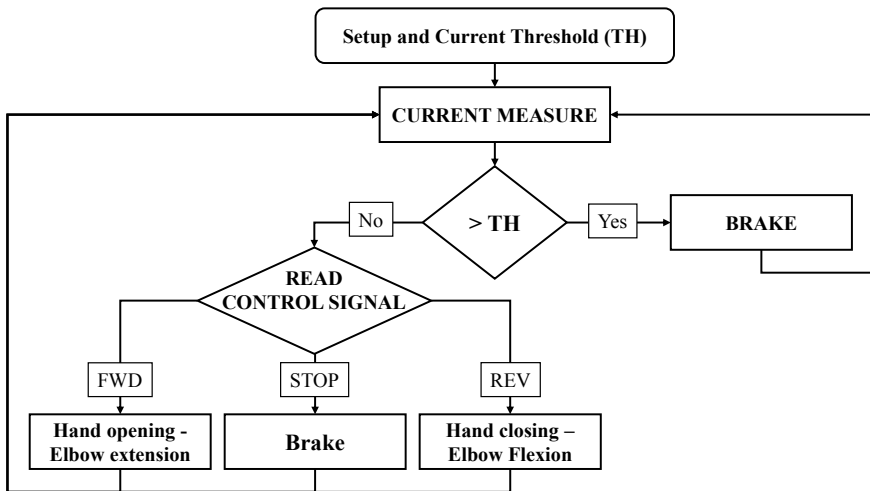


Fig. 3 Motor control logical scheme

Table 1 Electromechanical characterization and outcomes

Test type	Outcome
Current-force	Linear relationship between absorbed current (I) and motor's push/pull force (F): $F \simeq 540 * (I - I_0) N$ with $I \leq 1A$
Circuit delay	Max 10 ms between STOP command and BRAKE signal activation
Motor delay	Max 50 ms between STOP command and motor brake in the worst case scenario, resulting in a maximum fingers' displacement of 2.11 mm

2.3 Electromechanical Characterization

A preliminary characterization of the actuator has been performed, in order to evaluate: (1) the proper functioning of current sensor, (2) the correlation among absorbed power and actuator's pull strength, (3) the circuit delay in answering to commands, and (4) the delay between the control signal and the physical actuator's stop. Main outcomes (from tests 2–4) are summarized in Table 1. Preliminary tests showed that the time between the brake signal and the motor physical stop is around 50 ms, which corresponds to 2 mm of fingers' total extra run. This is definitely acceptable, first because tests have been performed with no load (worst case scenario), and second because with an external rubber glove this extra-space will determine a desirable increasing grip on the object.

3 Conclusion

In this work we presented a novel open-source design for a transhumeral prosthesis targeting developing countries. The overall cost of components (including actuators and electronics) is below \$200, and the prosthesis satisfies mechanical and weight ($\simeq 1.7$ kg) requirements to guarantee usability and robustness. We introduced a hybrid approach to the hand mechanism's actuation, which could provide a viable compromise among the performance advantages and the usability disadvantages of adopting sophisticated solutions, such as myoelectric prostheses, in resource-constrained settings. Future work will include: (1) the realization of an outer covering (glove), which will introduce additional loads to the actuator; (2) the evaluation of a less powerful (and therefore cheaper and more compact) actuator; and (3) the experimental evaluation of the complete prototype with amputees, to test the prosthesis' effectiveness in real-world scenarios.

References

1. World Health Organization et al., *World Report on Disability 2011* (World Health Organization, 2011)
2. C.S. Harkins, A. McGarry, A. Buis, Provision of prosthetic and orthotic services in low-income countries: a review of the literature. *Prosthet. Orthot. Int.* **37**(5), 353–361 (2013)
3. J.T. Kate, G. Smit, P. Breedveld, 3D-printed upper limb prostheses: a review. *Disabil. Rehabil. Assist. Technol.* **12**(3), 300–314 (2017)
4. B. Phillips, G. Zingalis, S. Ritter, K. Mehta, A review of current upper-limb prostheses for resource constrained settings, in *IEEE Global Humanitarian Technology Conference (GHTC)* (IEEE, 2015), pp. 52–58
5. A.J. Ikeda, A.M. Grabowski, A. Lindsley, E. Sadeghi-Demneh, K.D. Reisinger, A scoping literature review of the provision of orthoses and prostheses in resource-limited environments 2000–2010. Part two: research and outcomes. *Prosthet. Orthot. Int.* **38**(5), 342–362 (2014)

SS16: Neuromechanical Biomarkers in Robot-Assisted Motor Rehabilitation

Empirical Evidence Connecting the Neural Mechanism Behind Motor Coordination and Force Generation on Healthy Humans



Álvaro Costa-García, A. Úbeda, E. Iáñez, and S. Shimoda

Abstract This work describes a methodology to estimate changes of muscle synergies contribution to motion under different task constraints. For that purpose, the temporal and spatial patterns of muscle synergies are correlated among consecutive repetitions of periodic cycling under different levels of pedal rotation resistance. Results show higher influence of muscle synergies for an increasing resistance level which suggests that the neural mechanism behind motor force generation are closely related to the potentiation of basic motor primitives rather than other mechanisms of motor control like reflexes and tacit adaptations. Moreover, the indices extracted from the spatial and temporal patterns of muscle synergies showed potential as future biomarkers of human motor performance.

1 Introduction

The study of human movement presents many challenges associated to the complexity of the neural mechanisms in charge of controlling the musculoskeletal system. Human brains are the result of millions of years of evolution. During this process, earlier nervous systems were developing integrative solutions for the process of larger amounts of multimodal information which was convenient for survival. This trend towards the compartmentalization of function led to the appearance of different neural mechanisms like the existence of 2 neural pathways to process visual information,

Á. Costa-García (✉) · S. Shimoda

Intelligent Behaviour Control Unit (RIKEN), CBS-TOYOTA Collaboration Center, Nagoya Science Park Research and Development Center, 2271-130, Anagahora, Shimoshidami, Moriyama-ku, Nagoya, Aichi 463-0003, Japan
e-mail: acosta@brain.riken.jp

A. Úbeda

Human Robotics Group, University of Alicante, Alicante, Spain

E. Iáñez

Brain Machine Interface Systems Lab, Edificio Innova, Parque Científico UMH, Miguel Hernández University (UMH), Avinguda de la Universitat s/n, 03202 Elche, Alicante, Spain

reflexes and muscle synergies among others which are continuously competing for the control of the musculoskeletal system [1, 2]. Among these neural mechanisms, the definition of muscle synergies has been proved as an efficient theory to explain how the brain reduces the level of complexity of the motion by the creation of motor primitives encoded in the spinal cord [3, 4]. The methodologies behind muscle synergies computation are based on mathematical approaches that find common temporal patterns of activation across the electromyography (EMG) of the set of muscles contributing to the motion [5]. However, even in periodic motions performed by healthy humans, the patterns extracted cannot be used to fully reconstruct the original EMG data. Usually the reconstruction represents between 80 and 95% of the original data being this value quite variable depending on many factors (task conditions, subject variabilities, etc.). These are expected results because although muscle synergies play an important role on motor control, it is not the only process behind it. In this work we propose a novel approach to evaluate the amount of contribution of muscle synergies to motion under different task constrains. The methodology was inspired from the concept of muscle synergy similarity index proposed by [6] where the spatial patterns of synergies extracted from left and right body sides were correlated to study body asymmetries. In this work we will correlate both temporal and spatial patterns of consecutive repetitions of a periodic motion under different task constrains in order to estimate changes in the level of contribution of muscle synergies. This methodology will be useful not only for the study of motor control but also as biomarkers to quantify muscle synergy stability and their influence on a given movement [7].

2 Materials and Methods

2.1 *Experimental Set-Up*

The experimental environment consists on a static bike which pedal can be switched between different resistance levels. An inertial measurement unit (IMU) was located on the axis of the pedal to measure angular rotation. The information recorded from the IMU was used to create real time feedback about the angular speed. This information was provided through a visual interface showing a marker in a screen which positions increases and decrease linearly with the angular speed. During the experiment 4 muscle from subject's dominant leg were measured with bipolar electrodes located on Vastus Lateralis (VL), Bicep Femoralis (BF), Medial Gastrocnemius (MG) and Tibial Anterior (TA) with a sampling frequency 1500Hz.

2.2 *Experimental Protocol*

Five right handed subjects (2 males and 3 females) with ages 21.1 ± 0.5 years old participated in the experiment. They were requested to perform three cycling sessions. Each session was composed of four trials of 30s in which the subject was pedaling at a constant speed under 4 different resistance conditions (no resistance +3 increasing resistance levels). Resistance levels were randomized on every session to avoid experimental bias.

2.3 *Signal Processing*

EMG Signals were high pass filtered 10Hz rectified and low pass filtered 10Hz prior to synergy computation. Individual repetitions were segmented according to the algorithm described in [8] which uses the periodic activation of each muscle to obtain a robust segmentation points that maintain the spatial and temporal information from signals. From each repetition 2 synergies were extracted using the Non Negative Matrix Factorization [9].

2.4 *Synergy Stability Indices*

The correlation coefficients of both temporal and spatial patterns extracted from muscle synergies were computed across all individual muscle activation within each resistance condition (low, medium and high). This provided 2 indices to evaluate temporal and spatial stability with ranges between -1 and 1 (being 1 the representation of perfect correlation).

3 **Results**

Figure 1a shows a bidirectional representation of both indices (spatial correlation in the X -axis and temporal correlation in the Y -axis) for each resistance condition while Fig. 1b, c show a boxplot representation of each index. A Wilcoxon sum-rank test with a confidence interval of 95% was conducted to compare among resistance levels. A Bonferroni–Holmes correction for multiple comparisons was applied to the confidence interval and significant pairs were marked with an asterisk.

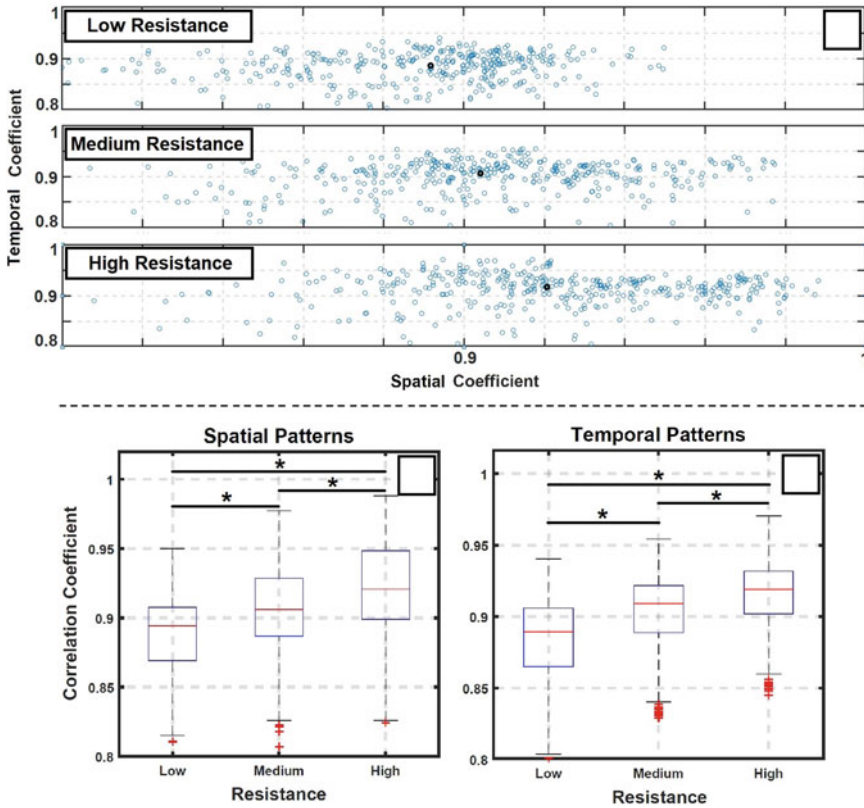


Fig. 1 Temporal and spatial correlation coefficients. **a** Graphs showing the bidimensional representation of spatial (Y-axis) and temporal (X-axis) correlation coefficients for all subjects and trials on each level of resistance. Black dots represent the median values of each distribution. **b** Boxplot representation of spatial coefficients for each resistance level. **b**, **c** Boxplot representation of temporal coefficients for each resistance level. Asterisks mark significant differences of each pair of data sets after a Wilcoxon sun-rank test with a confidence interval of 95% and a Bonferroni-Holms correction for multiple comparisons

4 Discussion

Both spatial and temporal correlation coefficients show significant differences for every pair of resistance conditions (Fig. 1b, c). This fact combined with the increase of the median values on both indices for an increasing resistance level (black dots on Fig. 1a) presents clear evidences connecting the neural mechanisms in charge of force generation with the increase of motor primitives stability. These results suggest that the neural primitives in charge of muscle recruitment and coordination also play an important role in the tuning of force on healthy subjects. In a previous work it was found that, for stroke patients, this two mechanism are decoupled [10]. If on

healthy subject muscle force and muscle coordination commands travel through the same pathways, the decoupling on these factors observed on stroke patients should be originated at a higher neural levels.

5 Conclusion

This work shows evidences of a close relationship between the neural mechanisms of muscle coordination and force generation on healthy subjects. Therefore, the decoupling between these two mechanisms observed in stroke patients should be originated in higher-level brain processes in charge of sending both types of information through the same neural pathways. Moreover, the indices developed in this work are a powerful tool as biomarkers representing the stability of muscle synergies and therefore their overall influence in the control of motion for a given task.

Acknowledgements This work was partially founded from National Japanese Kakenhi Grant system and from Novel Metrics for the Evaluation of Motor Function Using Advanced Electromyographic Techniques Project Reference: GV/2019/025.

References

1. O. Hikosaka, K. Nakamura, K. Sakai, H. Nakahara, Central mechanisms of motor skill learning. *Curr. Opin. Neurobiol.* **12**(2), 217–222 (2002)
2. E. Morsella, The mechanisms of human action: introduction and background, in *Oxford Handbook of Human Action* (2009), pp. 1–32
3. A. d'Avella, E. Bizzi, Shared and specific muscle synergies in natural motor behaviors. *Proc. Natl. Acad. Sci.* **102**(8), 3076–3081 (2005)
4. E. Bizzi, V.C. Cheung, The neural origin of muscle synergies. *Front. Comput. Neurosci.* **7**, 51 (2013)
5. M.C. Tresch, V.C. Cheung, A. d'Avella, Matrix factorization algorithms for the identification of muscle synergies: evaluation on simulated and experimental data sets. *J. Neurophys.* **95**(4), 2199–2212 (2006)
6. F. Alnajjar, K.-I. Ozaki, M. Itkonen, H. Yamasaki, M. Tanimoto, I. Ueda, M. Kamiya, M. Tournier, C. Nagai, A.C. Garcia et al., Self-support biofeedback training for recovery from motor impairment after stroke. *IEEE Access* **8**, 72138–72157 (2020)
7. V.C. Cheung, L. Piron, M. Agostini, S. Silvoni, A. Turolla, E. Bizzi, Stability of muscle synergies for voluntary actions after cortical stroke in humans. *Proc. Natl. Acad. Sci.* **106**(46), 19563–19568 (2009)
8. Á. Costa-García, E. Iáñez, M. Sonoo, S. Okajima, H. Yamasaki, S. Ueda, S. Shimoda, Segmentation and averaging of SEMG muscle activations prior to synergy extraction. *IEEE Robot. Autom. Lett.* **5**(2), 3106–3112 (2020)
9. M.S. Shourijeh, T.E. Flaxman, D.L. Benoit, An approach for improving repeatability and reliability of non-negative matrix factorization for muscle synergy analysis. *J. Electromyogr. Kinesiol.* **26**, 36–43 (2016)
10. Á. Costa-García, K.-I. Ozaki, H. Yamasaki, M. Itkonen, F. Alnajjar, S. Okajima, M. Tanimoto, I. Kondo, S. Shimoda, Model for prompt and effective classification of motion recovery after stroke considering muscle strength and coordination factors. *J. Neuroeng. Rehabil.* **16**(1), 1–11 (2019)

Synergistic Parameters of Motor Adaptation in Variable Resistance Cycling Activities



A. M. Pertusa, I. Vujaklija, R. M. Sánchez-Pérez, E. Iáñez, A. Costa, and A. Úbeda

Abstract Muscle synergies are a promising assessment tool in motor rehabilitation. In this study, we propose a basic experimental framework with minimum instrumentation and experiment duration for the evaluation of muscle synergies that can be easily translated to clinical application. To that end, we analyze synergistic parameters in cycling activities under different force constraints by modifying the resistance level of a stationary bike. Results suggest that the contribution of specific motor primitives changes with resistance as a result of motor adaptation to greater physical effort. In addition, we observe changes in the contribution of the different muscular groups, particularly the muscles of the posterior chain. These are interesting findings that are likely to be altered in patients with pathological motor conditions and thus can potentially serve as clinical biomarkers.

Keywords Electromyography · Muscle synergies · Cycling · Rehabilitation

A. M. Pertusa · A. Úbeda (✉)

Human Robotics Group, University of Alicante, Alicante, Spain
e-mail: andres.ubeda@ua.es

I. Vujaklija

Department of Electrical Engineering and Automation, University of Aalto, Espoo, Finland
e-mail: ivan.vujaklija@aalto.fi

R. M. Sánchez-Pérez

Neurology Unit, General Hospital of Alicante, Alicante, Spain

E. Iáñez

Brain-Machine Interface Systems Lab, Miguel Hernández University, Elche, Spain
e-mail: elianez@umh.es

A. Costa

Intelligent Behavior Control Unit, RIKEN Institute, Nagoya, Japan
e-mail: acosta@brain.riken.jp

© The Author(s), under exclusive license to Springer Nature Switzerland AG 2022
D. Torricelli et al. (eds.), *Converging Clinical and Engineering Research on Neurorehabilitation IV*, Biosystems & Biorobotics 28,
https://doi.org/10.1007/978-3-030-70316-5_143

1 Introduction

Repetitive motor primitives have been related to the activation of different muscular groups during the performance of specific tasks. This suggests that the Central Nervous System (CNS) divides muscular activation in simple modules to command more complex tasks [1]. These modules are called muscle synergies. This approach is particularly visible in motor activities that require periodical contractions of different muscle groups such as walking or cycling [2]. The application of muscle synergies in the assessment of motor rehabilitation can be well characterized through the estimation of motor primitives [1, 3]. In this study, we have evaluated muscle synergies during cycling activities as cycling provides an ideal constrained scenario where muscle synergies can be accurately computed while changing specific parameters such as velocity, torque or cycling style. The analysis of muscle synergies in cycling under different biomechanical constraints has been evaluated previously [4], but its clinical application remains laboursome and is limited to a few studies [2]. This preliminary study aims at establishing a set of synergistic parameters of motor adaptation in a very simple protocol with minimum instrumentation and experiment duration. To obtain the potential set of biomarkers different force conditions are evaluated on a group of able-bodied participants by modifying the resistance level of a stationary bike. The main goal is to design an experimental framework that can be successfully translated to the clinical evaluation of pathological motor adaptation of stroke patients.

2 Materials and Methods

2.1 *Experimental Design*

Ten subjects (5 female and 5 male, aged 21.9 ± 0.4 years) participated in the experiments. Experiments took place at University of Alicante. Informed consent following the Declaration of Helsinki was signed by all participants. Subjects sat on a stationary bike with a knee angle of 145° under a maximum possible extension. Electromyographic (EMG) data was measured from four bipolar electrodes (Noraxon MiniDTS) placed on four different muscles of the dominant leg. The selected muscles were Vastus Lateralis (VLAT), Biceps Femoris (BF), Tibialis Anterior (TA) and Gastrocnemius Medialis (GAM). Kinematic information of the pedal stroke was measured with an inertial sensor placed at the axis of the pedals. Subjects were shown a graphical interface indicating the linear speed with a moving red dot that could be freely controlled in the vertical direction by increasing or decreasing speed. Subjects were asked to maintain a speed of 20 km/h on each trial across 5 different resistance levels: 1-No resistance, 2-Very low, 3-Low, 4-Medium, 5-High. These levels were selected from the levels provided by the bike (up to 8). The experiment was divided into

two phases: warm up and cycling. For the warm up phase, level 1 was selected and subjects performed three 30-s trials at the fixed speed with resting periods of 5 s in between and a preparation period of 10 s right before each trial (135 s in total). For the cycling phase, three 30-s trials per level were performed (from levels 2 to 5). Levels were randomized using the same timing protocol as in the warm up phase (540 s in total). The total time of the experiment was around 15 min.

2.2 Muscle Synergies Analysis

EMG data was segmented and averaged using the method described in [5]. After applying this process, the non-negative matrix factorization (NMF) method was used to extract the non-negative coefficient matrix (C) and the weight matrix (W) for each resistance level and subject. Three synergies were extracted for each condition (average Variance Accounted For (VAF) of 96.5%, with a threshold VAF of 95%). Two parameters were evaluated in relation to the increase of resistance level: the relative proportion of each synergy (in percentage) and the changes in behavior of the muscles (weight values). Paired tests across different resistance levels were computed for each of the parameters (Mann–Whitney U test).

3 Results

Results showed a sequential activation of the TA and the VLAT followed by the co-activation of the GAM and the BF. Figure 1 shows the change in weight values with the increase of resistance level. Synergy 1 remains stable, although VLAT slightly increases its activation ($p < 0.05$). A similar behavior can be observed for synergy 2, with a greater increase of VLAT activity ($p < 0.05$). More significant changes appear in synergy 3, where there is a clear exchange in the activity between GAM and BF with a rather significant increase in the weight of BF ($p < 0.001$) and a similar significant decrease in the weight of GAM ($p < 0.001$). Figure 2 shows the average contribution of each synergy for each different resistance level. The first synergy is stable and stays in a range between 21 and 26% with no significant differences between levels ($p > 0.05$). However, synergies 2 and 3 change in proportion with a significant increase of the contribution of synergy 2 from 35.01 to 47.70% ($p < 0.01$) and a significant decrease of the contribution of synergy 3 from 38.68 to 29.93% ($p < 0.05$).

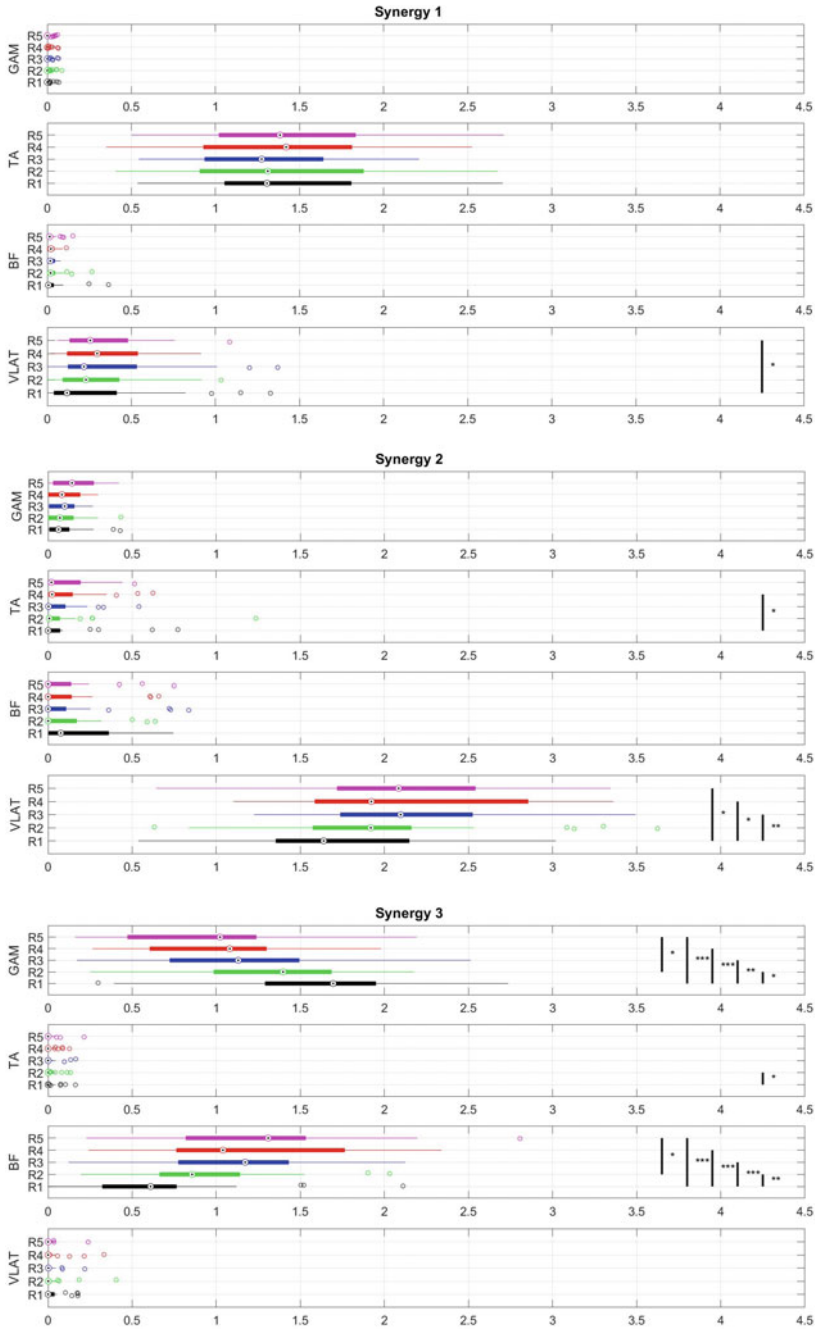


Fig. 1 Weight values of the contribution of the three different extracted synergies (circles represent outliers). Each graph shows the effects of the increase of resistance level for a distribution across subjects (significant differences: * $p < 0.05$, ** $p < 0.01$, *** $p < 0.001$)

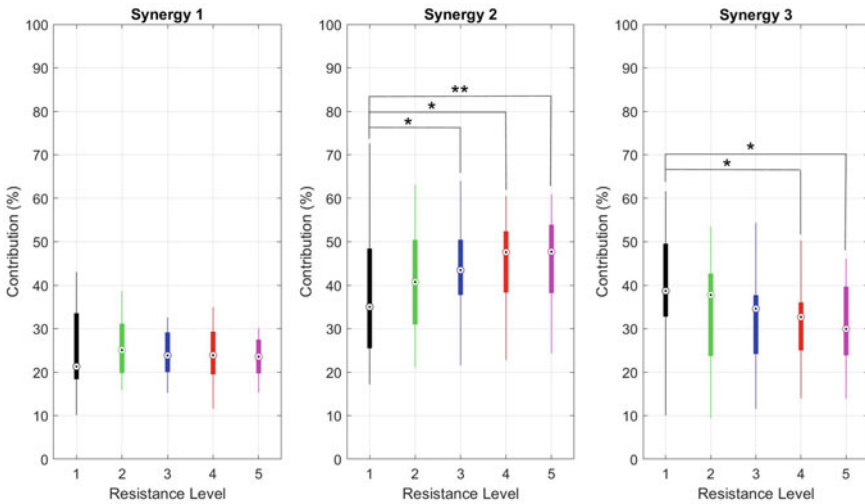


Fig. 2 Evolution of synergies contribution with the increase of resistance level (significant differences: * $p < 0.05$, ** $p < 0.01$)

4 Discussion and Conclusion

Changes in muscle weights imply that for higher resistance levels, subjects readapt the recruitment of muscles of the posterior chain and increase the effort of BF muscle while decreasing activity on the GAM. An increase in the contribution of VLAT muscle is also observed together with a decrease in the combined contribution of GAM and BF. This is an interesting behavior that should be compared with pathological motor adaptation, for instance, in stroke patients, as very little analysis has been done on the behavior of muscle synergies and stroke during cycling activities. This study is limited by the small number of muscles measured as additional muscles could have influence in the synergies computation. However, the experimental framework presented in this study provides a good starting point to a successful clinical application to extract motor recovery biomarkers.

Acknowledgements This work has been supported by Conselleria d’Educació, Cultura i Esport, Generalitat Valenciana, Spain, through project GV/2019/025.

References

1. R.E. Singh, K. Iqbal, G. White, T.E. Hutchinson, A systematic review on muscle synergies: from building blocks to a neurorehabilitation tool. *Appl. Bionic. Biomech.* 3615368 (2018)
2. F.O. Barroso, D. Torricelli, E. Bravo-Esteban, J. Taylor, J. Gómez-Soriano, C. Santos, J.C. Moreno, J.L. Pons, Muscle synergies in cycling after incomplete spinal cord injury: correlation with clinical measures of motor function and spasticity. *Front. Hum. Neurosci.* **9** (2016)

3. S.A. Safavynia, G. Torres-Oviedo, L.H. Ting, Muscle synergies: implications for clinical evaluation and rehabilitation of movement. *Top Spinal Cord Inj. Rehabil.* **17**(1), 16–24 (2011)
4. M. Zych, I. Rankin, D. Holland, G. Severini, Temporal and spatial asymmetries during stationary cause different feedforward and feedback modifications in the muscular control of the lower limbs. *J. Neurophys.* **121**, 163–176 (2019)
5. A. Costa-García, E. Iáñez, M. Sonoo, S. Okajima, H. Yamasaki, S. Ueda, S. Shimoda, Segmentation and averaging of sEMG muscle activations prior to synergy extraction. *IEEE Robot. Autom. Lett.* **5**(2), 3106–3112 (2020)

Muscle Synergies as a Tool to Unveil Specific Features in the Muscle Patterns After Cerebellar Damage



Denise J. Berger, Marcella Masciullo, M. Molinari, Francesco Lacquaniti, and Andrea D'Avella

Abstract We have recently provided evidence that cerebellar damage affects the spatiotemporal but not the spatial organization of the muscle patterns, suggesting that the cerebellum plays a key role in shaping their spatiotemporal organization. Here we show that the reconstruction of muscle patterns using spatiotemporal muscle synergies from healthy subjects unveils specific features in the muscle patterns of individuals with cerebellar ataxia. These results suggest a prediction power of time-varying muscle synergies that may provide novel markers of disease state after cerebellar damage. Understanding the changes in the modular organization of the motor system after neurological lesions is highly relevant for upper limb rehabilitation. Identification of an “abnormal” EMG feature in cerebellar disorders may have important clinical applications, because it may lead to the development of novel

This work was supported by Italian Ministry of Health Grant RF-2011-02347869, Italian Ministry of Education, University and Research Grants PRIN 2015HFWRYY and PRIN 2017CBF8NJ_005, the Italian Ministry of Health (Ricerca corrente, IRCCS Fondazione Santa Lucia), and Italian Space Agency Grants I/006/06/0 and 2019-11-U.0.

D. J. Berger (✉) · F. Lacquaniti
Department of Systems Medicine, Centre of Space Bio-medicine, University of Rome Tor Vergata, 00133 Rome, Italy
e-mail: d.berger@hsantalucia.it

M. Masciullo
SPInal REhabilitation Lab (SPIRE), IRCCS Fondazione Santa Lucia, Via Ardeatina 306, 00179 Rome, Italy

D. J. Berger · M. Molinari
Neuro-Robot Rehabilitation Laboratory, IRCCS Fondazione S. Lucia, via Ardeatina 306, 00179 Rome, Italy

F. Lacquaniti · A. D'Avella
Laboratory of Neuromotor Physiology, Fondazione Santa Lucia, 00179 Rome, Italy
e-mail: a.davella@hsantalucia.it

A. D'Avella
Department of Biomedical and Dental Sciences, Morphofunctional Imaging, University of Messina, 98124 Messina, Italy

objective and quantitative indicators of motor impairment directly related to the specific pathophysiology.

1 Introduction

The role of the cerebellum in determining the spatiotemporal characteristics of the muscle activation patterns subserving goal-directed movements is still largely unknown. We have recently shown that, while spatial (SP or time-invariant) muscle synergies extracted from healthy subjects (HS) can reconstruct muscle activity of cerebellar ataxia (CA) subjects, spatiotemporal (ST, or time-varying) muscle synergies fail in accurately reproducing their muscle patterns [1, 2]. We thereby provided evidence that cerebellar damage affects the spatiotemporal but not the spatial organization of the muscle patterns, suggesting that the cerebellum plays a key role in shaping their spatiotemporal organization.

Here, we go a step further, in that we aim at characterizing specific changes in the muscle patterns of CA subjects using SP and ST muscle synergies extracted from HS. Characterizing the changes in the muscle patterns in subjects with cerebellar impairment, may have a significant impact on our understanding of the neural control of movement, on testing the hypothesis of a modular human motor system, and on the development of novel methodologies in neuro-rehabilitation.

2 Materials and Methods

2.1 *Experimental Setup and Protocol*

The experimental apparatus, (described in detail in [1, 3]) consisted of one central sphere, indicating the start location, eight peripheral spheres, positioned on a circle at 30 cm from the start on a vertical plane at approximately 45° from each other and indicating target locations. Start and target spheres could be illuminated from inside by a LED. Subjects sat in front of the structure in a wheel chair. Subjects pointed with the index finger to the illuminated sphere and moved the finger from the central start location to one of the eight possible peripheral targets. CA subjects were instructed to move as fast as possible to the target. The trials performed by HS were selected for the analysis such that their kinematic features matched each individual CA subject [1].

2.2 Data Collection and Analysis

We collected kinematic and electromyographic (EMG) data from four healthy subjects, and three degenerative cerebellar patients (with molecular diagnosis of Spinocerebellar ataxia type 2, SCA2). The position of the finger was recorded using an optical motion capture system (8 Optitrak Flex-13 cameras, Natural Point Inc., Corvallis, OR, USA). EMG activity from 13 arm and shoulder muscles (brachioradialis; biceps brachii short (BicShort) and long head, anterior, middle, and posterior deltoid; infraspinatus; lower and middle (TrapMid) trapezius; triceps brachii, long, medial (TricMed), and lateral head; pectoralis major) were recorded using a wireless EMG system (Trigno, Delsys Inc., Natick, MA, USA). Kinematic and EMG data were digitally low-pass filtered (15-Hz cutoff for kinematic data, 10-Hz cutoff for EMG data after rectification). We extracted SP synergies from the averaged, phasic, normalized muscle patterns from all HS using NMF [4] and ST synergies from the averaged, phasic, amplitude-normalized muscle patterns from all HS using an iterative time-varying synergy identification algorithms [5]. We then used these identified muscle synergies for the HSs to reconstruct the muscle patterns of CA and HS and assessed the reconstruction quality of the two.

3 Results

To illustrate how muscle synergies may provide specific markers of cerebellar damage, we investigated whether ST synergies from healthy control subjects produce different reconstructions of muscle activities of CA, or whether they consistently isolate the very same abnormal feature of their EMG data. Figure 1 illustrates three examples of CA muscle waveforms for one direction (up) reconstructed using ST synergies from four different control subjects (BicShort, TricMed, and TrapMid muscles, Fig. 1a–c, respectively). In the first example (Fig. 1a), we observed two peaks in the CA EMG waveform. Using ST synergies from controls, the second peak is consistently underestimated for all reconstructions (Fig. 1a, leftmost column). However, using SP synergies (Fig. 1a, bottom), the second peak is well reconstructed by the muscle synergies. The mean reconstruction R^2 values for that muscle are 0.21 and 0.81, respectively. Importantly, ST synergies from HS muscle data reliably reconstructed EMG waveforms belonging to other subjects (Fig. 1, columns 2–5, mean $R^2 = 0.62$).

In the second example, the reconstruction of the activity of TricMed muscle with ST synergies consistently showed the suppression of both peaks with respect to the controls (Fig. 1b). Using SP synergies the first peak is also overestimated but the reconstruction of the second peak is accurately reconstructed. In the third example (Fig. 1c), ST synergies consistently estimated a delay in the onset of the TrapMid muscle activity, a bimodal activity and a higher activation at the beginning. These

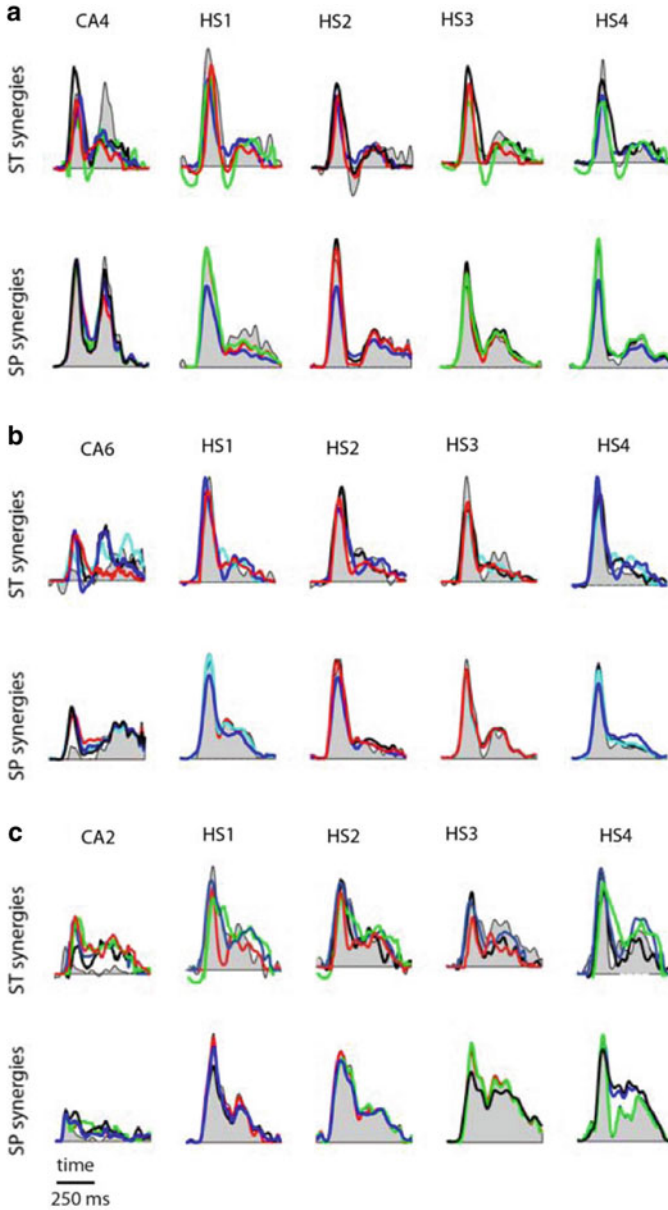


Fig. 1 a–c EMG reconstruction for EMG data for upward direction using ST (top) and SP synergies (bottom). The left column shows the EMG data (grey area) of three different CA patient (CA4, 6, 2) for three different muscles (a: BicShort; b: TricMed, and c: TrapMid) with four EMG reconstructions (colored lines; HS1: green, HS2 black, HS3: blue, and HS4 red) using synergies from four control subjects (HS1–4). Column two to five show the corresponding EMG data (grey area) of the 4 different control subjects (HS1–4) with the three EMG reconstructions (colored lines) using synergies from the other three control subjects, respectively

features are accurately captured by SP muscle synergies from HS (Fig. 1c, leftmost column, bottom).

To summarize, muscle patterns of CA subjects show specific features in the spatiotemporal activity pattern which deviate from the muscle activity patterns from HS. These features in the muscle patterns are unveiled by ST muscle synergies extracted from HS.

4 Conclusion

We have shown how the reconstructions of muscle patterns using ST muscle synergies from HS unveils specific features in the muscle patterns of CA subjects, which deviate consistently from the control activity, and thereby indicate a prediction power of ST synergies that may provide novel biomarkers of specific functional impairments associated with cerebellar damage. Such novel biomarkers may allow for an objective and reliable assessment of the efficacy of therapeutic interventions, including robot-assisted motor rehabilitation therapies targeting the specific dysfunctional muscle pattern features identified with muscle synergy analyses. An interesting avenue for future research would be to determine characteristic features in the muscle patterns of a large population of patients with cerebellar ataxias and other neurological lesions, to cluster these features across the different patient populations, and to correlate the cluster to the specific lesion.

References

1. D. Berger, M. Masciullo, M. Molinari, F. Lacquaniti, A. d'Avella, Does the cerebellum shape the spatiotemporal organization of muscle patterns? Insights from subjects with cerebellar ataxias. *J. Neurophysiol.* **123**(5), 1691–1710 (2020)
2. D. Berger, F. Ferrari, A. Esposito, M. Masciullo, M. Molinari, F. Lacquaniti, A. d'Avella, Changes in muscle synergy organization after neurological lesions. *Biosyst. Biorobot.* **15**, 939–943 (2017)
3. A. d'Avella, A. Portone, L. Fernandez, F. Lacquaniti, Control of fast-reaching movements by muscle synergy combinations. *J. Neurosci.* **26**(30), 7791–7810 (2006)
4. D.D. Lee, H.S. Seung, Learning the parts of objects by non-negative matrix factorization. *Nature* **401**(6755), 788–791 (1999)
5. A. d'Avella, E. Bizzi, Shared and specific muscle synergies in natural motor behaviors. *Proc. Natl. Acad. Sci. USA* **102**(8), 3076–3081 (2005)

On Repeatability of MU Fatiguing in Low-Level Sustained Isometric Contractions of Tibialis Anterior Muscle



Giovanni Corvini, A. Holobar, and J. C. Moreno

Abstract The objective of this study was to investigate the repeatability of Motor Units (MUs) fatiguing profiles during repetitive low-level isometric contractions of the Tibialis Anterior muscle. This feature could be used in a wearable robot for lower limb rehabilitation. We focused on the analysis of MU firing rates and the Motor Unit Action Potential (MUAP) shapes. We successfully tracked several MUs across different contraction repetitions to see the changes in their properties. We evaluated the presence of muscle fatigue and found that the mean MU firing rates decrease while the MUAP shapes do not change across the epochs and contractions. Results suggest that the global EMG descriptor (Mean Frequency) changes are mainly caused by changes in MU firing rate and recruitment patterns and not due to the changes in the MUAPs shape.

Keywords MNF · Firing rate · MUAP shape · Fatigue · HDsEMG

1 Introduction

A Motor Unit (MU) consists of an alpha motor neuron and all muscle fibers it innervates [1]. Nowadays, the assessment of MU properties is possible via the High-Density surface Electromyography (HDsEMG). The latter supports an insight into the central nervous system (CNS) and could be used to clarify the relationships between

This study was supported by the Slovenian Research Agency (J2-1731, L7-9421 and Programme funding P2-0041) and by the Fundació La Marató de TV3 (Programme funding 192138).

G. Corvini (✉) · J. C. Moreno
Neural Rehabilitation Group of the Spanish National Research Council, Madrid, Spain
e-mail: gio.corvini@gmail.com

J. C. Moreno
e-mail: jc.moreno@csic.es

A. Holobar
Faculty of Electrical Engineering and Computer Science, University of Maribor, Maribor, Slovenia
e-mail: ales.holobar@um.si

central motor control strategies and muscle fatigue [2]. Although different techniques have been developed to assess muscle fatigue, both in time and frequency domain, their main limitation was related to the unfeasibility of reliably assessing neuromuscular changes in presence of fatigue. Thanks to the HDsEMG electrodes and innovative decomposition techniques [3], it is possible to investigate the behaviour of neuromuscular system in response to fatigue on the level of individual MUs. A recent review provides a comprehensive view of the studies that focus on myoelectric manifestation of fatigue with the multi-channel approach [4] but, to our knowledge, the repeatability of MU fatiguing profiles has still not been fully investigated. In this study we started to address this issue by studying the relationship between global HDsEMG metrics and MU physiological properties (e.g. shape of Motor Unit Action Potential (MUAP) and MU firing rates) during low-level fatiguing isometric contractions of the Tibialis Anterior (TA) muscle.

2 Material and Methods

2.1 Participants

Two healthy men [mean (\pm SD), age: 26 (\pm 1) yr, height: 180 (\pm 3) cm, body mass: 74 (\pm 3) kg] participated to the experiment. They were asked to avoid fatiguing activities the day before the HDsEMG recordings.

2.2 Experimental Protocol

Participants were comfortably seated on a chair with the foot of their dominant leg placed under a fixed structure, to which a force sensor was attached. They were asked to perform a dorsiflexion and they were provided with a visual feedback based on the exerted force. First, they performed three 5 s long Maximum Voluntary Contractions (MVC) in which we recorded and averaged the maximum force value of each subject. Then, they completed four consecutive sessions of the experiment. Each session consisted of 120 s long constant isometric submaximal voluntary contraction at nearly 25% of their maximum force. Each participant was provided with five minutes of rest before each session during the experiment.

2.3 Data Acquisition and Signal Processing

Following SENIAM recommendations [5], monopolar HDsEMG was recorded from the TA muscle during its isometric contraction at approximately 25% of its maximum

force. Signals were sampled at a frequency of 2000 Hz with a two-dimensional electrode grid (SESSANTAQUATTRO, OTBIOelettronica, Italy), comprising 13×5 electrodes (diameter of 3 mm and inter-electrode distance of 8 mm).

Data processing has been done offline. Signals were filtered with a bandpass filter at 10 and 500 Hz, and with a notch filter at 50 Hz to remove the Power-Line Interference (PLI). First, Mean Frequency (MNF) and Root Mean Square (RMS) values were computed to identify the presence of muscle fatigue. These measures have been calculated from the differential HDsEMG signals with a nonoverlapping sliding time window of 200 ms [6]. A Correlation Coefficient (CC) was computed between each pair of channels and the triplet with the highest CC was selected for the result analysis. Individual MUs were identified by decomposing the signals with the Convolution Kernel Compensation (CKC) method [3]. The decomposition results have been manually inspected and cleaned: all the MUs with the mean firing rate less than 5 Hz or greater than 30 Hz were removed since they are extremely rare during submaximal contraction. Moreover, the Pulse-to-Noise Ratio (PNR) metric was used to evaluate the accuracy of the result: the threshold was set to 30 dB, corresponding to the sensitivity of MU firing identification greater than 90% [7]. For the statistical analysis, 120 s long signals have been split in four 30 s long non-overlapping epochs. We utilized the Shapiro-Wilk test for normality and the paired t-test to compare MNF among epochs. The non-parametric Wilcoxon signed rank test was used to compare mean firing rates among epochs. Only the MUs active in all the epochs have been considered for the statistical analysis.

3 Results

Shapiro-Wilk test indicated normality of the MNF data ($p > 0.05$) and a non-normality of the MU firing rate data ($p < 0.05$) for both subjects. Mean MNF, computed as average of the four contractions for each epoch, showed a substantial decrease between the first and the third epoch in the first subject (3.08 Hz, $p < 0.05$) and between the first and the second, the first and the third, and the first and the last epoch in the second subject (4.61, 6.61 and 8.68 Hz, respectively, $p < 0.01$). However, RMS value of HDsEMG did not change significantly. We successfully identified (and tracked among contractions) 32 MUs in both subjects. MU firing rates decreased by nearly 2 Hz from the beginning to the end of each contraction (Fig. 1), while increased by nearly 2 Hz among contractions for each single epoch. For both subjects, the Wilcoxon signed rank test showed a statistically significant difference (* $p < 0.05$ and ** $p < 0.01$) between each pair of epochs in each contraction.

Finally, we studied the spatial distribution of the MUAPs and we found that MUAP shapes remained stable among the epochs and among the contractions, as exemplified in Fig. 2.

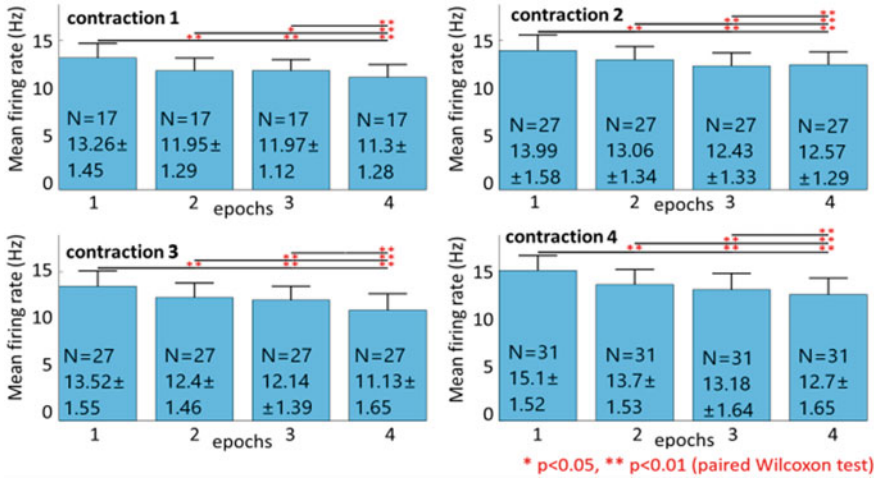


Fig. 1 The mean MU firing rate (\pm standard deviation) computed in four 30 s long epochs for each contraction in the second subject. “N” is the number of all MUs that were active during the entire contraction. Similar results were observed also in the first subject; Wilcoxon signed rank test, * $p < 0.05$ and ** $p < 0.01$

4 Discussion

Fatigue was identified through the significant decrease of MNF variable and confirmed by the decrease in the mean MU firing rates. Moreover, in the last contraction we noticed a greater number of active MUs, suggesting that additional MUs were recruited to maintain the same level of contraction. We did not see evident changes in the MUAP shapes neither among epochs nor among contractions (Fig. 2). Even the RMS of HDsEMG did not change significantly. Therefore, we assumed that the observed changes in global MNF were only affected by the MU firing rates and the MU recruitment, and not by the shape of the MUAPs. Further investigations are required to explore these observations.

5 Conclusion

Our results showed that during isometric submaximal fatiguing contractions of TA muscle there was a decrease in the MU firing rates but the shapes of the MUAPs did not change. This suggests that the decrease in MNF is likely dependent on MU firing changes only and thus identify the presence of central fatigue rather than peripheral fatigue, which is used to mainly be represented by changes in MUAP shapes. Nevertheless, fatigue mechanisms have not been fully understood yet and need to be investigated. Finally, the decrease among epochs of MU firing rates, as well

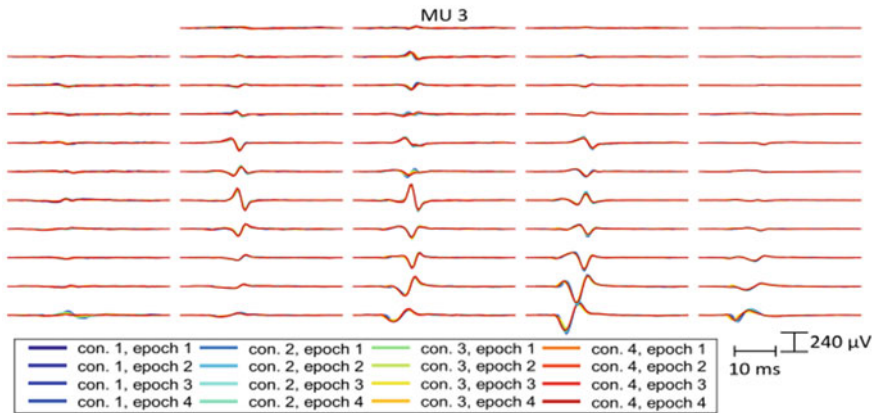


Fig. 2 Spatial distribution of the MUAP and changes of MUAP shape of a representative MU. Different colors indicate different epochs of all four contractions. MUAP shape did not change significantly across the epochs and contractions. Similar consistency of MUAP shapes was observed in other identified MUs

as the increase among contractions due to additional MUs recruitment, confirmed that MU fatiguing patterns are relatively repeatable across different sessions. However, the main limitation of this study is the number of subjects; hence, further studies are required to validate these results.

References

1. R. Merletti, D. Farina, R.M. Enoka: *Surface Electromyography, Physiology, Engineering and Applications* (Wiley, Hoboken, 2016)
2. C.J. De Luca, Z. Erim, Common drive of motor units in regulation of muscle force. *Trend Neurosci.* **17**, 299–305 (1994)
3. A. Holobar, D. Farina, M. Gazzoni, R. Merletti, D. Zazula, Estimating motor unit discharge patterns from high-density surface electromyogram. *Clin. Neurophys.* **120**, 551–562 (2009)
4. M. Gazzoni, A. Botter, T. Vieira, Surface EMG and muscle fatigue: multi-channel approaches to the study of myoelectric manifestations of muscle fatigue. *Physiol. Measur.* **38**(5), R27–R60 (2017)
5. H.J. et al., *European Recommendations for Surface Electromyography: Results of the SENIAM Project* (1999)
6. F.D. Farfán, J.C. Politti, C.J. Felice, Evaluation of EMG processing techniques using information theory. *BioMed. Eng. Online* **9**, 72 (2010)
7. A. Holobar, M.A. Minetto, D. Farina, Accurate identification of motor unit discharge patterns from high-density surface EMG and validation with a novel signal-based performance metric. *J. Neural Eng.* **11**(1), 016008 (2014)

Kinematic Features Analysis from Active and Active-Assistive Upper Arm Robotic Rehabilitation



Donghwan Hwang, Joon-Ho Shin, and Suncheol Kwon

Abstract The relationship between clinical assessments and the patient's motor characteristics can be an important part of knowing the patient's rehabilitation progress. In this study, we investigate the relationship between the clinical assessment and kinematic features of upper arm movements in stroke patients. We evaluated the Fugl-Meyer Assessment score (FMA score) and calculated the kinematic features by observing the patients who were performing reaching tasks. Multiple-linear-regression analysis was performed to investigate the correlation between the FMA score and the kinematic features. Different kinematic features of active and active-assistive robotic rehabilitation were found to correlate with the FMA score.

1 Introduction

Clinical evaluation method for assessing sensorimotor impairment in stroke patients typically involve the Fugl-Meyer score [1]. The relationship between the clinical assessments and the patient's motor characteristics remains not fully understood and is currently difficult to explain statistically [2, 3]. Studies on the relationship between the kinematic features of a patient's movements and clinical scales may qualitatively improve assessments of patients' upper arms after a stroke.

The purpose of this study was to evaluate the relationship between the clinical assessment and the kinematic features. Stroke patients were divided into two groups, active and active-assistive robotic rehabilitation. And they performed upper arms

This work was in part supported by the National Rehabilitation Center, Ministry of Health and Welfare, Republic of Korea, under grant NRCTR-IN19004.

D. Hwang · S. Kwon (✉)

Department of Rehabilitation and Assistive Technology, National Rehabilitation Center, Seoul, Republic of Korea

J.-H. Shin

Department of Neurorehabilitation, National Rehabilitation Center, Seoul, Republic of Korea

© The Author(s), under exclusive license to Springer Nature Switzerland AG 2022

915

D. Torricelli et al. (eds.), *Converging Clinical and Engineering Research*

on *Neurorehabilitation IV*, Biosystems & Birobotics 28,

https://doi.org/10.1007/978-3-030-70316-5_146

rehabilitation. We analyzed the kinematic features of the patient's reaching task in the rehabilitation process.

2 Method

This study was approved by National Rehabilitation Center, Republic of Korea (approval no. NRC-2017-01-007).

In this single-blind randomized controlled trial, 6 patients with cerebral infarction and 9 patients with cerebral hemorrhage participated in 20 sessions, of 30 min each, of upper arm robotic intervention (5 days per week for, 4 weeks).

Rehabilitation interventions were provided using Armeo®Spring (Hocoma, Switzerland) for active robotic rehabilitation and Armeo®Power (Hocoma, Switzerland) for active-assistive robotic rehabilitation as shown in Fig. 1.

Clinical and kinematic assessments of upper arm function were performed 0 (baseline), 14, and 28 days after the start of the rehabilitation.

We evaluated the FMA score to conduct the clinical assessment. And we evaluated the kinematic features through 3D trajectory of the reaching task. The patients performed reaching tasks directed toward three targets (as shown in Fig. 4), which were located in the lateral, middle, and medial directions(as shown in Fig. 2) at a distance of 75% of the patient's arm length. The reaching tasks was in the following order: (1) Start point (on the table), (2) Lateral target, (3) Start point, (4) Middle target, (5) Start point, (7) Medial target, and (8) Start point.

During the task, the three-dimensional trajectory of the index fingertip was tracked using a magnetic tracking system (trakSTAR, Ascension Technology Corp, USA, as shown in Fig. 3). The evaluation is carried out with only patient's own voluntary power without the help of robotic devices as shown in Fig. 4.



Fig. 1 Upper Arm robotic rehabilitation devices

Fig. 2 Reaching targets

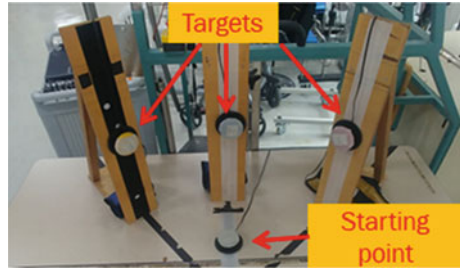


Fig. 3 Magnetic tracking system (trakSTAR)



Fig. 4 Reaching task with trakSTAR for calculating the kinematic features



We calculated the kinematic features using four different characteristics: Hand path ratio [4] to evaluate movement efficiency, Target error [4] to evaluate movement accuracy, Mean arrest period ratio [5] to evaluate movement smoothness and Time to velocity peak [6] to evaluate movement control strategy from the measured trajectories.

Multiple-linear-regression analysis was then performed to investigate the correlation between the FMA score and the kinematic features.

Table 1 Multiple linear regression result of kinematic features

	Selected features	R^2	P -value
Active robotic rehabilitation	Hand path ratio Target error Mean arrest period ratio	0.532	0.000
Active-assistive robotic rehabilitation	Target error Mean arrest period ratio Time to velocity peak	0.490	0.000

3 Results

In the case of active robotic rehabilitation, Hand path ratio, Target error, and Mean arrest period ratio were selected ($R^2 = 0.532, p < 0.01$). In the case of active-assistive robotic rehabilitation, Target error, Mean arrest period ratio, and Time to velocity peak were selected through multiple-linear-regression analysis ($R^2 = 0.490, p < 0.01$) (Table 1).

The results indicate that the Hand path ratio, which represents movement efficiency, of the active robotic rehabilitation correlates with the FMA score, and the Time to velocity peak, which represents movement control strategy, of the active-assistive robotic rehabilitation correlates with the FMA score.

4 Conclusion

This study analyzed the kinematic features of the upper arm movements of post-stroke patients. The results indicate that the kinematic features of active and active-assistive robotic rehabilitation correlate with the FMA score. In the case of active robotic rehabilitation, Hand path ratio, which represents movement efficiency, correlates with the FMA score. In the case of active-assistive robotic rehabilitation, Time to velocity peak, which represents movement control strategy, correlates with the FMA score.

In order to evaluate the statistical significance of rehabilitation intervention, it is necessary not only to measure kinematic features during the evaluating, but also to measure kinematic features during the training. And the number of participants may be insufficient to draw a conclusion. Therefore, future studies with kinematic features taken during the training and a large study population are needed. We are also going to plan to analyze the relationship between robotic rehabilitation and motor function using other clinical assessments such as the Wolf Motor Function Test.

References

1. A.R. Fugl-Meyer, L. Jääskö, I. Leyman, S. Olsson, S. Steglind, The post-stroke hemiplegic patient. 1. A method for evaluation of physical performance. *Scandinavian J. Rehabil. Med.* **7**(1), 13 (1975)
2. J.D. Riley et al., Anatomy of stroke injury predicts gains from therapy. *Stroke* **42**(2), 421–426 (2011)
3. C. Stinear, Prediction of recovery of motor function after stroke. *Lancet Neurol.* **9**(12), 1228–1232 (2010)
4. C.E. Lang et al., Deficits in grasp versus reach during acute hemiparesis. *Exp. Brain Res.* **166**(1), 126–136 (2005)
5. E. Vergaro, M. Casadio, V. Squeri, P. Giannoni, P. Morasso, V. Sanguineti, Self-adaptive robot training of stroke survivors for continuous tracking movements. *J. Neuroeng. Rehabil.* **7**(1), 1–12 (2010)
6. P.R. Culmer, M.C. Levesley, M. Mon-Williams, J.H. Williams, A new tool for assessing human movement: the kinematic assessment tool. *J. Neurosci. Methods* **184**(1), 184–192 (2009)

SS17: AITADIS Session

Subscription Video on Demand (SVOD) Platform Accessibility Verification Method



Gema López-Sanchez and Francisco Utray

Abstract How can you measure the percentage of sensory accessibility in the new Subscription Video on Demand (SVOD) platforms? This investigation aims to answer this research question. For this, a qualitative methodology model based on a content analysis of 37 variables is presented, which have been written based on the Spanish technical regulations *UNE 153010 of May 2012 of the Subtitling for deaf people and people with hearing disabilities* and *UNE 153020 of January 2005 of the Audio description for people with visual disabilities*. This method is applicable for cinema, series and short films presented at SVOD and is limited to the accessibility of subtitling for deaf people (CC) and the audio description for blind people.

1 Introduction

People with sensory disabilities show great interest in the new SVOD (Subscription Video on Demand) platforms [1], such as Netflix, HBO, Movistar Plus or Amazon Prime Video, among others [1]. From a commercial point of view, the audience that offer sensory disabilities can be understood as a niche market and companies that offer adapted products and services obtain a competitive advantage as a result [2]. On the other hand, the normalization of audiovisual accessibility is an indispensable requirement for the construction of inclusive societies that guarantee social welfare.

The objective of this work is to present a useful, efficient and reliable methodology for measuring the percentage of accessibility in subtitling and audio description of audiovisual products on SVOD platforms.

G. López-Sanchez
Centro Español del Subtitulado y la Audiodescripción (CESyA), Leganés, Spain
e-mail: gelopezs@inf.uc3m.es

F. Utray (✉)
Universidad Carlos III de Madrid, Getafe, Spain
e-mail: futrayer@hum.uc3m.es

Table 1 Criteria for determining the code variables for content analysis

General criteria (categorical)	SVOD analyzed (V1)	
	Type of product analyzed and own production (V2)	
	Genre (V3)	
	Position in the suggestion list grill (V4)	
	Language available for audio (V5)	
	Language available for subtitling (V6)	
	Language available for audio description (V7)	
	Sing language option (V8)	
Adaptation of the quality of the subtitling to the 2012 AENOR standard	Visual aspects	Position of the subtitles (V9)
		Position of the sound effects (V10)
		Number of text lines (V11)
		Staticity of text lines (V12)
		Different text lines by characters (V13)
		Minimum character size (V14)
		Typography (V15)
		Color contrast between characters and box (V16)
		Temporal aspects: exposure speed of subtitling and synchronism (V17)
		Separation of subtitles and their background (V18)
	Identification of characters	Chosen technique for character identification (V19)
		Maintaining the color assigned to each character (V20)
		Color difference (V21)
		Use of labels (V22)
		Use of hyphen in dialogues (V23)
	Sound effects, contextual information and music	Sound effects subtitling (V24)
		Use of sound effects (V25)
		Contextual information subtitling (V26)
		Contextual information presentation (V27)
		Music subtitling (V28)

(continued)

Table 1 (continued)

		Presentation of music subtitling (V29)
	Editorial criteria	Text division and character limit (V30)
		Grammatical and spelling criteria (V31)
	Voice-over	There is voice-over (V32)
		Voice-over presentation (V33)
		Distinction between voice-over and character voice (V34)
Adaptation of the quality of the audio description to the AENOR standard of 2005	Locution (V35)	
	Audio description script (V36)	
	Audio (V37)	

2 State of the Art

The legal system, and also common sense, recognize the right of participation of people with disabilities in social life. Gone is the time when a person with a disability was considered 'less valid' and their social marginalization was 'justified' for it.

The concern of public institutions for the accessibility and non-discriminatory representation of people with disabilities in the media is a fact that is reflected in the number of style guides and manuals published in this regard, such as those promoted by the Spanish Center of Documentation on Disability (CEDD) of the Royal Board on Disability [3].

Likewise, there is greater awareness on the part of television producers about accessibility services, since the data offered by the Spanish Center for Subtitling and Audio Description (CESyA) show an evolution of these services. According to its latest report, it has gone from 50% to 75% of subtitled programming. Since the current General Audiovisual Law was imposed, the number of annual audio-described hours has increased from 154 to 8,738, and from 88 to 3657 h in the case of programming with sign language [4].

Several authors have already analyzed the parameters of accessibility to media such as Digital Terrestrial Television (DTT) [5], online platforms [6] or the historical heritage itself, including museums, theaters and centers [7]. However, the academic literature on the accessibility of SVODs is not yet abundant.

3 SVOD Accessibility Verification Method

3.1 Code

In order to carry out the content analysis, a table of indicators with 37 variables has been drawn up that contains the criteria established by the AENOR standards for Accessibility: *UNE 153010 of May 2012 of the Subtitling for deaf people and people with hearing disabilities* [8] and *UNE 153020 of January 2005 of the Audio description for people with visual disabilities* [9]. The following table has been designed regarding both UNE regulations. The code has been based on the following qualitative criteria:

3.2 Requirements

To avoid the ‘filter bubbles’ of the SVOD algorithm, which conditions the content that the platform offers the users based on their previous searches to show them similar content [10]; it is recommended to create a new account in the SVOD that you want to analyze, prior to applying the methodology. This makes it possible to observe the platform ‘without bias’ beyond the positioning of audiovisual products set by the SVOD itself.

The selection criteria for the products to be analyzed will be determined by the need to obtain a heterogeneous, random and representative sample. In the case of search by section and genre, the first product shown by each SVOD in the genre lists must be analyzed. The films will be analyzed in their entirety, while in the serial programs—programs and series—the first episode of the first season will be chosen as the representative episode. Because series and films are generally the best-ranked product in the suggestion lists, non-random selections will be made to add other products—such as documentaries or shows—to the sample in order to increase their heterogeneity.

All subtitles and audio descriptions shall be analyzed in the same language.

References

1. B.G. Nieto, Interview conducted on February 24, 2020
2. K. Ellis, Netflix closed captions offer an accessible model for the streaming video industry, but what about audio description? *Commun. Polit. Cult.* **47**(3), 4 (2015). ISSN: 1836-0645. <https://search.informit.com.au/documentSummary;dn=113665255090751;res=IELHSS>
3. P. Hernández, E. Peñas, Guía de estilo sobre discapacidad para profesionales de la comunicación, in *Real Patronato sobre Discapacidad* (España, Madrid, 2019)

4. CESyA. *Los servicios de accesibilidad a la TDT en 2019: más subtítulos, más LSE y menos audiodescripción* (España, Madrid, 2019). <https://www.cesya.es/drupal7/accesibilidadTDT2019>
5. U.D. Francisco, *Accesibilidad a la TDT en España para personas con discapacidad sensorial (2005–2007)*, in *Real Patronato Sobre Discapacidad* (España, Madrid, 2009). <https://e-archivo.uc3m.es/handle/10016/6630>
6. C. Egea García, *Contenido Web accesible*. Revista DIM: Didáctica, Innovación Y Multimedia. *Revista DIM: Didáctica, Innovación y Multimedia* (España, Madrid, 2007, Ch. 9).
7. B. Consuegra Cano, *El acceso al patrimonio histórico de las personas ciegas y deficientes visuales* (ONCE, Madrid, 2002)
8. AENOR, *Audiodescripción para personas con discapacidad visual. Requisitos para la audiodescripción y elaboración de audioguías*, in *UNE 153020* (Asociación Española de Normalización y Certificación (AENOR), Madrid, España, 2005)
9. AENOR, *Subtitulado para personas sordas y personas con discapacidad auditiva. Subtitulado a través del teletexto*, in *UNE 153010* (Asociación Española de Normalización y Certificación (AENOR), Madrid, España, 2012)
10. K. Pikkat, *The Reinforcing Loop: An Exploration of Filter Bubbles in Social Platforms* (iSChannel, 2018, Ch. 13), p. 30

Application of Capabilities of Upper Extremity Questionnaire During a Robotic Therapy Based on Armeo[®] Spring Exoskeleton



V. Lozano-Berrio, A. de los Reyes-Guzmán, M. Alcobendas-Maestro, B. Polonio-López, and A. Gil-Agudo

Abstract The robotic technology has been increasingly used for assessing and treating upper extremity motor deficits. The aim of this study was to determine the effects the robotic device Armeo[®] Spring and conventional rehabilitation in the perception for tetraplegic spinal cord injured patients about the difficulties or limitations in function of their upper limbs. A total of 13 patients with subacute cervical SCI were recruited, age between 16 and 75 years, received an treatment based on 40 sessions with the exoskeleton Armeo[®] Spring as a complement to the conventional therapy. All the patients were evaluated with The Capabilities of Upper Extremity questionnaire (CUE) in two different situations, at baseline and at ending all the experimental sessions. As conclusion, the findings demonstrate that robotic-assisted training combined with the conventional rehabilitation in tetraplegic SCI patients, improves the perception about the function of their upper limbs.

This research has served as support to request the research project Rehab Hand (Plataforma de bajo coste para rehabilitación del miembro superior basado en Realidad Virtual, ref. DPI2016-77167-R). Funded by grant from the Spanish Ministry of Economy and Competitiveness and cofunded from FEDER, National Plan for Scientific and Technological Research and Innovation.

V. Lozano-Berrio (✉) · A. de los Reyes-Guzmán
Biomechanics and Technical Aids Department, Hospital Nacional de Paraplégicos, Toledo, Spain
e-mail: vlozanob@sescam.jccm.es

A. de los Reyes-Guzmán
e-mail: adlos@sescam.jccm.es

M. Alcobendas-Maestro · A. Gil-Agudo
Rehabilitation Department, Hospital Nacional de Paraplégicos, Toledo, Spain
e-mail: malcobendas@sescam.jccm.es

A. Gil-Agudo
e-mail: amgila@sescam.jccm.es

B. Polonio-López
Faculty of Health Sciences, University of Castilla-La Mancha, Ciudad Real, Spain
e-mail: begona.polonio@uclm.es

1 Introduction

Spinal Cord injury (SCI) is one the most devastating injuries that causes lifelong disability. Individuals affected of cervical SCI, experience partial or complete loss of arm and hand function. It's necessary to promote the recovery of upper extremity (UE) movements and improving functions of upper limbs, through intense, repetitive, and rhythmic activities [1, 2].

The robotic technology has been increasingly used for assessing and treating UE motor deficits. These devices combine benefits of repetitive task oriented training, greater intensity of practice, and less dependence on therapist assistance. One commercial robotic device is Armeo[®]Spring. It is a rehabilitative exoskeleton intended for patients who have lost function of their UE. This device, based on weight compensation, allow the patient to train specific exercises in order to increase muscle strength and range of motion in different joints, with the overall goal of improving motor function, through virtual gaming in a three dimensional workspace [2, 3].

To know the effectiveness and effect of the robot-assisted upper limb rehabilitation is needed the use of the different clinical and functional scales, before and after a treatment program to identify motor and functional recovery [4].

The aim of this study was to determine the effects the robotic device Armeo[®]Spring and conventional rehabilitation in the perception for tetraplegic SCI patients about the difficulties or limitations in function of their upper limbs.

2 Methods

2.1 Participants

A total of 13 patients with subacute cervical SCI were recruited from the inpatient population at Hospital Nacional de Paraplégicos. The inclusion criteria were: to suffer a cervical SCI with a motor level between C4 and C8 with a classification in the ASIA Impairment Scale A-D, evaluated by clinical staff [5]; traumatic or non-progressive medical etiology; less than 6 months of injury evolution (subacute); age between 16 and 75 years; to have reached the seated posture and be informed and consent to participate in the study. The exclusion criteria were: to suffer unstable orthopaedic injuries such as unconsolidated fractures or with unstable osteosynthesis systems in upper limbs; skin lesions and/or pressure ulcers in the exoskeleton placement area; having joint stiffness and/or severe spasticity; bronchopneumopathy and/or severe heart disease that will require monitoring during exercise; visual problems and/or cognitive impairment, and do not sign the corresponding informed consent.

Fig. 1 Patient with Armeo[®] Spring device



2.2 Experimental Setup

Patients receive an UE treatment based on the exoskeleton Armeo Spring (Hocoma AG, Switzerland) as a complement to the conventional therapy. Patients were scheduled for five 30 min sessions per week for 8 weeks to complete a total of 40 sessions with the exoskeleton.

All the patients were evaluated by a set of clinical scales in two different situations: at baseline and at ending all the experimental sessions. Specifically, the Capabilities of Upper Extremity Questionnaire (CUE) [6] is applied in the present study (Fig. 1).

2.3 Capabilities of Upper Extremity Questionnaire

The CUE instrument is a questionnaire of 32-items developed to evaluate the difficulty in performing determined tasks with the UE regarding patients' perception. It was designed to measure UE functional limitations in patients with cervical SCI. Responses to each item are given on a 7 points scale representing self-perceived difficulty in performing the task, with 1 representing "unable to perform" and 7 "can perform without difficulty". So, the minimum total score is 32 and the maximum 224 [6].

The following variables were used for expressing the results: CUE score in relation to the right arm; CUE score in relation to the left arm; CUE score in bilateral actions; total CUE score and the total score expressed as a percentage in function of the normality as in (1).

$$Normality (\%) = \frac{Totalscore - 32}{192} \times 100 \quad (1)$$

Table 1 Results about the capabilities upper extremity questionnaire in pre and post conditions

Variables	Sci Patients (<i>n</i> = 13)	
	Pre	Post
Right arm	49.00 (31.50) ^b	62.00 (29.50) ^b
Left arm	63.00 (57.50) ^a	71.00 (45.50) ^a
Both arms	5.00 (8.00)	8.00 (8.50)
Total score	120.00 (72.50) ^b	153.00 (75.50) ^b
Normality (%)	45.83 (37.76) ^b	63.02 (39.32) ^b

^a(*p* < 0.05); ^b(*p* < 0.01)

2.4 Data Analysis

A non parametric statistical method, the Wilcoxon test, was applied to find possible differences between both, the pre condition (at baseline) and post condition (at ending the study).

For all the variables analyzed, the results were expressed as the median and the interquartile range.

3 Results

The results in relation to the scores within the CUE questionnaire were shown in Table 1. For each variable, the pre and post conditions were compared. For all the variables analyzed, the results in post condition were greater than those at baseline.

Therefore, significant statistically differences were found between the scores for the right arm, the left arm, the total score and the total score expressed as percentage. Concretely, the CUE score for the left arm was greater at ending the study (71.00(45.50)) than at baseline (63.00 (57.50)) (*p* < 0.05). This difference was higher for the right arm: 62.00(29.50) at ending vs. 49.00(31.50) at baseline (*p* < 0.01). These differences were reflected in the CUE total score and in the score expressed as percentage relative to the normality (the total CUE score 224-points). So, in the result as a percentage at ending the study the score was 63.02(39.32)% versus 45.83(37.76)% at baseline (*p* < 0.01).

4 Discussion

The goal of this study was determine the effects the robotic device Armeo®Spring and conventional rehabilitation in the perception for cervical SCI about the difficulties or limitations in function of the UE. The main study result has demonstrated that robotic-assisted training combined with the conventional rehabilitation in SCI

patients, improved the perception about the function and use of their UE. However, further research must be to apply this methodology in a control group, with the aim of analyzing the effectiveness of robotic therapy in cervical SCI patients.

5 Conclusion

Further research is necessary to analyze the relationship between CUE and UE functional recovery of the cervical SCI patients improving the present study with the addition of a control group.

References

1. N. Yozbatiran, G.E. Francisco, Robot-assisted therapy for the upper limb after cervical spinal cord injury. *Phys. Med. Rehabil. Clin.* **30**(2), 367–384 (2019)
2. B.E. Perry, E.K. Evans, D.S. Stokic, Weight compensation characteristics of Armeo® Spring exoskeleton: implications for clinical practice and research. *J. Neuroeng. Rehabil.* **14**(1), 1–10 (2017)
3. A.Y. Sánchez, A.C. Gómez, Efectividad del dispositivo Armeo® en la rehabilitación del miembro superior en pacientes que han sufrido un ictus. Revisión de la bibliografía. *Revista de Neurología*, **70**(3), 93–102 (2020)
4. E.W.A. Cacho, R. de Oliveira, R.L. Ortolan, R. Varoto, A. Cliquet, Upper limb assessment in tetraplegia: clinical, functional and kinematic correlations. *Int. J. Rehabil. Res.* **34**(1), 65–72 (2011)
5. S. Kirshblum, W. Waring, Updates for the international standards for neurological classification of spinal cord injury. *Phys. Med. Rehabil. Clin.* **25**(3), 505–517 (2014)
6. R.J. Marino, J.A. Shea, M.G. Stineman, The capabilities of upper extremity instrument: reliability and validity of a measure of functional limitation in tetraplegia. *Arch. Phys. Med. Rehabil.* **79**(12), 1512–1521 (1998)

Safety, Feasibility and Acceptance with HANK Ambulatory Robotic Exoskeleton in Incomplete Spinal Cord Injury Patients



A. Megía-García, A. J. del-Ama, V. Lozano-Berrio, I. Sinovas-Alonso, N. Comino-Suárez, and A. Gil-Agudo

Abstract Recovery of walking ability has been established as a priority objective by spinal cord injury subjects (SCI). In the present contribution we showed results about safety, feasibility and acceptance of an ambulatory exoskeleton gait training program. The sample was eight subjects with subacute incomplete SCI (7 AIS C and one AIS D, T2-L3). Participants carried out a mean of 17.1 sessions (SD 2.1) of 20 min approximately. There were no serious adverse events and no falls during the study. Participants rated 1.8 (1) cm pain, 3.8 (1.7) cm fatigue and 3.6 (SD 2) cm discomfort in VAS (0–10 cm). The 75% of participants consider HANK exoskeleton as secure, ease for using, durability and effectiveness to achieve the therapeutics goals. Results providing evidence for safety and feasibility of HANK for gait training in patients with subacute SCI.

This work was partially supported Institute of Health Carlos III (Spain) and co-funded by FEDER (PI15/01437) and by the Spanish Ministerio de Ciencia, Innovación y Universidades, under the Programa Estatal de Investigación, Desarrollo e Innovación Orientada a los Retos de la Sociedad (Ref.: RTI2018-097290-B-C31).

A. Megía-García (✉) · V. Lozano-Berrio · I. Sinovas-Alonso · A. Gil-Agudo
Biomechanics and Technical Aids Department, Hospital Nacional de Paraplégicos, Toledo, Spain
e-mail: amegiag@externas.sescam.jccm.es

V. Lozano-Berrio
e-mail: vlozanob@sescam.jccm.es

I. Sinovas-Alonso
e-mail: msinovas@sescam.jccm.es

A. Gil-Agudo
e-mail: amgila@sescam.jccm.es

A. J. del-Ama
Electronic Technology Area, Universidad Rey Juan Carlos, Móstoles, Spain
e-mail: antonio.delama@urjc.es

N. Comino-Suárez
Neural Rehabilitation Group, Cajal Institute, Consejo Superior de Investigaciones Científicas, Madrid, Spain
e-mail: natalia.comino@cajal.csic.es

1 Introduction

Spinal cord injury (SCI) has a strong impact on the individual and society. A recent review estimates a worldwide incidence of between 13 and 220 cases per million inhabitants, with an average age of 44.2 years in Europe, the main cause being traumatic (falls, road accidents and sports accidents) [1].

Recovery of walking ability has been established as a priority objective by patients and clinical staff [1, 2] but the loss of this ability is associated with the appearance of secondary disorders, such as bone demineralization, muscle atrophy or urinary tract infections [2].

In recent years we have witnessed an increase in the appearance of robotic therapies in walking rehabilitation, due to both technological progress and an advance in the knowledge that these devices may have on the neuroplasticity [3]. These devices allow multiple step repetitions while having full weight bearing on the body thus, being task-specific of gait rehabilitation [4]. Therefore, the patient practices normal walking patterns in safe environments. In the present contribution we showed results about safety, feasibility and acceptance of a gait training program with exoskeleton HANK in spinal cord injury subjects.

2 Methods

2.1 HANK Exoskeleton

HANK exoskeleton (Gogo Mobility, Traña-Matiena, Bizkaia) (as shown in Fig. 1) is

Fig. 1 HANK ambulatory exoskeleton



a revised version of a previously published exoskeleton (Exo-H2) [5], whose clinical applicability was previously studied in patients with stroke and incomplete SCI. The mechanical structure has been optimized to provide a lighter and more rigid solution. Likewise, the ankle, knee and hip actuators have been redesigned to deliver higher power output with a more compact design. Left and right structures are connected via a flexible arm that allows bending in the coronal planes to allow for adaptation to different pelvis width while showing high stiffness in the sagittal and frontal planes.

The therapist's interface is implemented in an Android tablet, which connects via Bluetooth with HANK main controller. Here the therapist can select different operation modes: rising, standing, sitting down, left/right step, continuous walking. Joint trajectories corresponding to a normative walking pattern are stored at the HANK controller. In this work the guidance force was set at 100% for all participants.

2.2 Participants

The sample was eight subjects with incomplete SCI (7 AIS C and one AIS D) recruited at the National Hospital for Paraplegics (Toledo, Spain). Five were males and 3 females, with a mean age of 41.7 years old (SD 13.5) and a mean of range of time since injury of 5.6 months (SD 1.1). The level of injury was between T3-L2 and the etiology was traumatic (5 participants) ischemic (2 participants) and neoplastic (One participant). The present study was approved by the local Toledo Ethical Committee (Ref. No. 39; 07/02/2017)

2.3 Gait Exoskeleton Training

Each session consisting on 20 min for dressing on and off the exoskeleton, 20 min for walking training, 10 min to rest and 5 min to register assessment variables (pain, fatigue, discomfort, and adverse event). Walking was indoors in the physical therapy room. Guidance force was set to 100% for all joints. External support (walker or crutches and physical external) was always used, but were modified according to the functional status, preferences, and ability of the participants.

2.4 Outcomes Variables

Subjects who carried out the treatment with HANK gave us an idea of the feasibility and acceptance. After each training session a Visual Analogue Scale (VAS; 0–10 cm) was recorded to register pain, fatigue and comfort perceived during each session by asking the question: “what was your perceived pain/exertion/comfort for the whole session on a scale from 0 to 10 cm? Moreover, at the end of program, satisfaction of

Table 1 QUEST

Items	Participant’s answer (%)				
	Not at all	Not very	More or less	Quite satisfied	Very satisfied
Satisfaction with ATD	0	0	50	25	25
Dimensions	0	0	50	25	25
Weight	0	12.5	37.5	50	0
Easy adjust	0	25	0	62.5	12.5
Safe/secure	0	0	25	37.5	37.5
Durability	0	0	25	50	25
Use simplicity	0	0	25	12.5	62.5
Comfort	0	12.5	50	12.5	25
Effectiveness	0	0	25	12.5	62.5

participants was evaluated through the Quebec User Evaluation of Satisfaction with Assistive Technology (QUEST).

3 Results

There were no serious adverse events and no falls during the study. Two participants suffered mild skin erythema at the tibia contact zone during the first session related to the strap. It was solved adding padding to the specific zones and disappeared within one day. Also, mild muscle neck and shoulder pain after training session was reported in 3 patients, probably related to the walking aids.

With respect to pain fatigue and comfort, participants rated 1.8 (SD 1) cm pain, 3.8 (SD1.7) cm fatigue and 3.6 (SD 2) cm discomfort in VAS (0–10 cm).

The satisfaction of participants with the assistance technology device (ATD) are represented in Table 1.

4 Discussion

This a prospective study with HANK exoskeleton for gait training in a sample of patients with subacute incomplete SCI. The intervention has showed be feasible and secure. No patients withdrew out the study due to intervention with HANK. Moreover, serious adverse effects and no falls were found. Few cases with skin issues in contact areas were found in our sample similar to that reported previously with Ekso and Rewalk exoskeletons [6, 7]. Self-perceived pain during the sessions was rated low in VAS scale. Fatigue and discomfort were somewhat higher but still less than 5 cm. The most of participants (6/8) consider HANK exoskeleton as secure, ease for using and effectiveness to achieve the therapeutics goals (QUEST = quite

satisfied/very satisfied). However, regarding to comfort and dimensions the 50% of participants showed low grade of satisfaction (QUEST = more or less/not very satisfied).

5 Conclusion

This article presented the results of a prospective study of a walking treatment with the HANK, a lower limb robotic ambulatory exoskeleton for gait rehabilitation. Results obtained providing evidence for safety, feasibility and acceptance of HANK for gait training in patients with subacute SCI. The most of participants considered HANK exoskeleton as secure, ease for using and effectiveness to achieve the therapeutics goals. Clinical trials are necessary to analyze the effectiveness of gait robotic training to improve functional gait variables.

References

1. Y. Kang et al., "Epidemiology of worldwide spinal cord injury: a literature review. *神经修复* **6**(1), 1–9 (2018)
2. P.L. Ditunno, M. Patrick, M. Stineman, J.F. Ditunno, Who wants to walk? Preferences for recovery after SCI: a longitudinal and cross-sectional study. *Spinal Cord* **46**(7), 500–506 (2008)
3. A. Esquenazi, A. Packel, Robotic-assisted gait training and restoration. *American Journal of Physical Medicine & Rehabilitation* **91**(11), S217–S231 (2012)
4. L.E. Miller, A.K. Zimmermann, W.G. Herbert, Clinical effectiveness and safety of powered exoskeleton-assisted walking in patients with spinal cord injury: systematic review with meta-analysis. *Med. Devices (Auckland, NZ)* **9**, 455 (2016)
5. A. Gil-Agudo et al., Robot therapy with the H2 exoskeleton for gait rehabilitation in patients with incomplete spinal cord injury. *A Clin. Exp. Rehabil.* **54**(2), 87 (2020)
6. A. Esquenazi, M. Talaty, A. Packel, M. Saulino, The ReWalk powered exoskeleton to restore ambulatory function to individuals with thoracic-level motor-complete spinal cord injury. *Am. J. Phys. Med. Rehabil.* **91**(11), 911–921 (2012)
7. C.B. Baunsgaard et al., Gait training after spinal cord injury: safety, feasibility and gait function following 8 weeks of training with the exoskeletons from Ekso Bionics. *Spinal Cord* **56**(2), 106 (2018)

Towards Functional Description of Gait Impairments After Neurological Diseases for the Development of Personalized Robotic and Neuroprosthetic Wearable Systems for Walking Assistance



I. Sinovas-Alonso, A. Gil-Agudo, N. Comino-Suárez, A. Megía-García, N. Murillo-Licea, E. Opisso-Salleras, J. Vidal-Samsó, and A. J. del-Ama

Abstract Recovering walking ability is one of the main goals of patients having suffered a stroke or a spinal cord lesion. Lower extremity robotic exoskeletons and neuroprosthesis are intended to compensate walking deficits or to provide gait training following lower limb paralysis. Prior to the design of exoskeletons and neuroprosthesis, the designers have to be informed with an application scenario in

This project (Personalized Robotic and Neuroprosthetic Modular Wearable Systems for Assistance of Impaired Walking–TAILOR-) has been granted by Ministerio de Ciencia, Innovación y Universidades in the Programa Estatal de I+D+i Orientada a los Retos de la Sociedad. Grant number: RTI2018-097290-B-C31.

I. Sinovas-Alonso (✉) · A. Gil-Agudo · A. Megía-García
Biomechanics and Technical Aids Department, Hospital Nacional de Paraplégicos, Toledo, Spain
e-mail: msinovas@sescam.jccm.es

A. Gil-Agudo
e-mail: amgila@sescam.jccm.es

A. Megía-García
e-mail: amegiag@externas.sescam.jccm.es

N. Comino-Suárez
Neural Rehabilitation Group, Instituto Cajal, Consejo Superior de Investigaciones Científicas (CSIC), Madrid, Spain
e-mail: natalia.comino@cajal.csic.es

N. Murillo-Licea · E. Opisso-Salleras · J. Vidal-Samsó
Institut Guttmann, Barcelona, Spain
e-mail: nmurillo@guttmann.com

E. Opisso-Salleras
e-mail: eopisso@guttmann.com

J. Vidal-Samsó
e-mail: jvidal@guttmann.com

A. J. del-Ama
Universidad Rey Juan Carlos, Madrid, Spain
e-mail: antonio.delama@urjc.es

which how the device is going to assist walking is described. To date, the scenarios have been described as pathology-dependent (i.e. full assistance for complete paraplegia). However, most pathologies lead to similar functional impairments. One of the TAILOR project objectives is to understand the common functional features shared by the most prevalent pathologies, providing a single, common description of functional requirements to drive the design of lower limb robotic exoskeletons and neuroprosthesis. In this work we present three common scenarios for walking assistance for stroke and Spinal Cord Injury.

1 Introduction

Ambulation ability is frequently affected in people with neurological impairment, such as Spinal Cord Injury (SCI) [1] or after having suffered a stroke [2], becoming one of the main rehabilitation’s goals in these patients [3, 4]. Lower extremity (LE) robotic exoskeletons are emerging technologies that assist gait training in people with LE paralysis [1–5]. Compared to previously existing locomotor training paradigms, exoskeletons may improve user independence, as well as cardiovascular health, energy expenditure, body composition, gait parameters, level of physical activity and quality of life [6]. To date, exoskeletons are applied to a range of pathologies and functional abilities, forcing the user to adapt to the exoskeleton features: four to six actuated degrees of freedom in the saggital plane, and restriction of the remaining ones. TAILOR project aims at developing modular and customizable exoskeletons (wearable robots—WR) and neuroprosthesis (NP) that can be adapted to the functional status of the user, regardless of pathology that originated the disability.

Our hypothesis was that a common functional description can be found amongst SCI and stroke, the two pathologies in which TAILOR project is focusing on. The objective of this work is to describe the process and result of the functional requirement analysis towards a purely functional description.

Table 1 Common functional requirements and gait scenarios

	Scenario B		Scenario C	
	SCI	Stroke	SCI	Stroke
Impairment level	AIS C/D	Hemiplegia	CES	Hemiparesia
Spasticity	Yes	Yes	No	Yes
Trunk control	Yes	Yes	Yes	Yes
Involved joints	Hip, knee, ankle	Knee, ankle	Variable	Ankle
WISCI II	4–13	–	>13	–
FAC	–	1–2	–	≥3

2 Materials and Methods

Five meetings (video conferencing and in-person meetings) were carried out between the Biomechanics and Technical Aids Department of the Hospital Nacional de Paraplégicos and the Institut Guttmann during the period from August 2019 to January 2020. A team of long-time experts in the rehabilitation treatment and the use of LE robotic exoskeletons and NP after stroke and SCI, composed by two physicians, four physical therapist and two engineers, exchanged their professional experiences with the aim of defining different functional scenarios which will be common for the gait of these patients neurologically impaired.

3 Results

As a result of the meetings, three scenarios were identified related to the common functional requirements after SCI (paraplegia in first motor neuron injuries and *cauda equina* syndrome—CES) and stroke (hemiplegic or hemiparetic patients), from the greatest impairment scenario (A) to the lowest one (C). In between these two scenarios, a third scenario was defined—medium impairment scenario (B)—in order to provide an intermediate definition of functional needs of the users.

Scenario A, unlike scenarios B and C, is the one that only targets users with paraplegia (AIS—American Spinal Injury Association Impairment Scale—A or B), who have not voluntary control of LE and absence or partial trunk control, depending on the level of lesion. These users may feature muscle spasticity and have a score <4 in the Walking Index for Spinal Cord Injury (WISCI) II.

Scenarios B and C are described in Table 1.

Common inclusion and exclusion clinical criteria were identified for all the scenarios. Inclusion criteria were detailed as it follows: (1) patients aged from 16 to 70 years old; (2) height of 160-200 cm; (3) weight lower than 100 kg; (4) no neurological or orthopedic involvement in upper limbs; (5) able to stand or to walk with technical aids; (6) healthy bone density; (7) skeleton must not suffer from any fractures or instability; (8) good physical conditioning allowing the treatment; (9) to be able to understand and sign written informed consent. Exclusion criteria were defined as it follows: (1) history of severe neurological injuries other than SCI or stroke; (2) severe concurrent medical diseases; (3) pressure injuries; (4) heterotopic ossification or significant contractures that impair joint mobility; (5) significant leg length discrepancies; (6) psychiatric or cognitive situations that may interfere with proper operation of the device; (7) pregnancy; (8) patients incapable of holding crutches or a walker; (9) score ≥ 3 in the Modified Ashworth Scale.

4 Discussion

Based on the functional requirements of each scenario, the technical requirements of TAILOR devices were different with the aim of personalizing the user's functional needs.

4.1 Greater Impairment Scenario: Functional Compensation of Walking

TAILOR devices should provide functional compensation to LE while providing trunk and pelvis stability. Given the nature of the lesion, the muscles below the level of lesion may be responsive to functional electrical stimulation (FES). Thus, this scenario foresees the application of NP. However, depending on the time elapsed since the injury, the muscles may have suffered from atrophy, being the NP not effective in some cases.

4.2 Medium Impairment Scenario: Moderate Walking Assistance

In this scenario, the LE muscles (below the neurological level of injury, in the case of SCI) can be neurologically preserved and therefore be responsive to FES, being the NP the main assistive system for this scenario, having the possibility of incorporating a reduced power WR in combination with the NP if necessary to support the action of the NP.

Given that users of scenarios A and B may be NP users, some other exclusion clinical criteria must be identified: (1) electrical current intolerance; (2) body electronic dispositive implant; (3) skin injury in the area of stimulation; (4) active cancer disease.

4.3 Low Impairment Scenario: Slight Walking Assistance

Depending on the nature of the lesion, it is expected a very variable impact on hip extensors and knee flexors (present in CES, mainly), as well as ankle extensor and flexor muscles (which we assume to be present in both, CES and hemiparesia). In CES users, muscles below the level of lesion may not be neurologically preserved and, consequently, will not be responsive to FES. As a result, in this scenario the use of NP is not foreseen, having only the possibility of incorporating a low power WR,

given that in hemiparetic users only a foot drop brace is conceived to assist ankle joint.

5 Conclusion

Since gait recovery is the main and common objective in people who suffered a stroke or a spinal cord lesion, LE robotic exoskeletons and neuroprosthesis should be conceived from a functional standpoint regardless of the pathology, what means that are the user's needs which should determine the functional requirements that will drive the design of these gait training devices.

References

1. E. Swinnen, S. Duerinck, J.P. Baeyens, R. Meeusen, E. Kerckhofs, Effectiveness of robot-assisted gait training in persons with spinal cord injury: a systematic review. *J. Rehabil. Med.* **42**(6), 520–526 (2010)
2. L.R. Sheffler, J. Chae, Hemiparetic Gait. *Phys. Med. Rehabil. Clin. N. Am.* **26**(4), 611–23 (2015)
3. B.T. Neville, D. Murray, K.B. Rosen, C.A. Bryson, J.-P. Collins, A.A. Guccione, Effects of performance-based training on gait and balance in individuals with incomplete spinal cord injury. *Arch. Phys. Med. Rehabil.* **100**(10), 1888–1893 (2019)
4. Y.R. Mao, W.L. Lo, Q. Lin, L. Li, X. Xiao, P. Raghavan, et al., The effect of body weight support treadmill training on gait recovery, proximal lower limb motor pattern, and balance in patients with subacute stroke. *BioMed. Res. Int.* 175719 (2015)
5. K. Lo, M. Stephenson, C. Lockwood, Effectiveness of robotic assisted rehabilitation for mobility and functional ability in adult stroke patients: a systematic review. *JBI Database Syst. Rev. Implement Rep.* **15**(12), 3049–3091 (2017)
6. A.S. Gorgey, Robotic exoskeletons: The current pros and cons. *World J. Orthop.* **18**, **9**(9), 112–119 (2018)

Implementation of an Exoskeleton for Neuromuscular Hand Rehabilitation



B. Troncoso, P. Alberti, P. Maldonado-Cárdenas, E. Peña, and P. Barría

Abstract This article shows the design, development, implementation, and control software associated with a hand exoskeleton capable of assisting in basic actions, such as opening and closing. Robotic architectures, geometric and kinematic analysis are reviewed, obtaining a proprietary design based on the biometrics of Chilean individuals. The exoskeleton meets basic clinical requirements, allowing work with ranges of movement in each finger with no pressure points in the skin or discomfort with use, being capable of adjusting to the thumb and adapting to any hand. The software created for training and rehabilitation, both for the therapist and the end-user, contains control of patient records, therapies, and a graphic interface that allows for personalized routines to be configured after calibration. The software allows rehabilitation specialists to be able to use the exoskeleton, after receiving a brief safety and basic function introduction, and thus be able to perform robotic therapies in any health center.

Keywords Exoskeleton · Rehabilitation · Software control · Rehabilitation-techniques

B. Troncoso (✉) · P. Alberti · P. Maldonado-Cárdenas · E. Peña
Departamento de Ingeniería en Computación, Universidad de Magallanes, Punta Arenas, Chile
e-mail: btroncos@umag.cl

P. Alberti
e-mail: pedro.alberti@umag.cl

P. Maldonado-Cárdenas
e-mail: patricia.maldonado@umag.cl

E. Peña
e-mail: eduardo.pena@umag.cl

P. Barría
Research Unit, Rehabilitation Center Club de Leones Cruz del Sur, Punta Arenas, Chile
e-mail: pbarria@rehabilitamos.org

BMIlab, Universidad Miguel Hernandez de Elche, Elche, Spain

© The Author(s), under exclusive license to Springer Nature Switzerland AG 2022
D. Torricelli et al. (eds.), *Converging Clinical and Engineering Research on Neurorehabilitation IV*, Biosystems & Biorobotics 28,
https://doi.org/10.1007/978-3-030-70316-5_151

1 Introduction

Exoskeleton-type rehabilitation robots have redefined current rehabilitation techniques. These robots have the attribute of having their joints aligned with those of the user in such a way that many times it can resemble an armor that both protects and allows for movement of the joints. In general, these robots require a more complex design and an adaptation mechanism for the user. Today there is already evidence of the validity of these robotic systems, conclusions that indicate that the obtained measures not only have a concurrent validity against conventional clinical scales but also have the possibility of providing more useful evaluations in severe hemiparetic patients when compared to conventional clinical scales.

2 Materials and Methods

For the implementation of this class of robotic device it was necessary to carry out an exhaustive review of the devices already implemented, all the materials and technologies necessary for its construction, such as 3D printing, servo motors and the control mechanism, which consists of a control and management software for both patients and therapies.

2.1 Analysis and Mechanical Design of the Exoskeleton

After a general geometric and kinematic analysis of the behavior of the human hand [1], it was necessary to determine the length of each finger of every hand, considering our national reality. We decided on a more generic approach, allowing the design to be adapted on a larger scale for a larger or smaller hand if necessary. This approach consists [2] of taking the average lengths of each finger of the left hand of the biometric study¹ and determining a proportion with respect to the length of a finger. For this case, the middle finger (Table 1) was used as the reference finger.

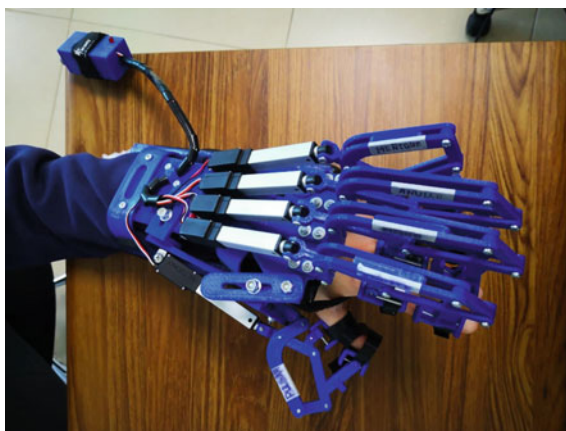
The following step was selecting an already designed exoskeleton [3–6], to act as a starting point to begin implementing the first prototypes, and determining what would be the main characteristics on which our final design should focus.

At a mechanical level, some of the factors to consider were: the complexity of the design, different ranges of extension and flexion, adaptability, and flexibility of the system to the hand of the patient, strength, and integrity of the device, among others. Regarding the necessary control to manipulate the exoskeleton, we considered the following: Type of activation system, the flexibility of the software, interfaces, etc.

¹ For the purposes of this project, the average measurements of the Chilean man's left hand were used, due to the higher incidence of people with left hemiparesis at the Club de Leones Rehabilitation Corporation Cruz del Sur, where the clinical tests of the device will be carried.

Table 1 Average sized of each finger and applied scale

Finger	Thumb	Index	Middle	Ring	Little
Average length (mm)	72.4	104.5	114.6	108.9	88.4
Applied scale in respect to middle finger (%)	63.17	91.18	100	95.02	77.13

Fig. 1 Top view of the final design of the exoskeleton

Each finger was printed, implementing the scales in Table 1. The phalanges of each finger are held using thin Velcro straps (Fig. 1). The thumb has four pieces with a rail system, which allows a significant adjustment range to adapt to the different conditions of each patient.

2.2 Control Software

The entire mechanical system is governed by the software created for the control system (Fig. 1). Special emphasis was placed on the therapy-related interface, which is in charge of controlling the servo motors. For this purpose, specialized boards, protocols, and specialized software packages were used, which are also open-source.

3 Results and Discussion

3.1 Results

The final exoskeleton has an approximate weight of 700 g. The alignment and movement do not require greater effort on any part of the fingers during the movement.

This is due to the flexibility and design of the parts related to the middle phalanx, which are adaptable to the plane of the phalanx, even when some system mismatch occurs.

Regarding the ranges of movement, the index, middle, ring, and little fingers achieved flexion angles of the metacarpophalangeal joint that were very close to 90° , while in the interphalangeal joint angles close to 45° were achieved. In the case of the thumb, a maximum 50° angle was achieved in the metacarpophalangeal joint, and an extension close to the maximum was achieved for the interphalangeal joint, with an approximate 45° as minimum flexion.

The software fulfills its main functionality of allowing full control of the device, even being able to control each finger individually and define work routines. It can also store patient records and their respective sessions. It also has enough indications and visual support that the user can intuitively navigate through it.

Regarding the portability of the exoskeleton and all its associated electronic devices, a modular presentation was achieved: the exoskeleton, 2 m connection cable, multiplatform software, possibility of connection to local power supplies.

3.2 Discussion

This project has many possibilities for future improvement due to it involving two major challenges: first, *The Mechanical System*, with the possibility of incorporating new technologies as alternatives for exoskeleton activation, such as motion sensors or control using *EMG*; and the second, *the Designed Software*, which could incorporate a potentiometer to determine the effort exerted by the servo-motor, allowing control of the stress registers and thus allowing for determining the degree of improvement of the patient.

Finally, it should be noted that the decision was made to implement the left hand. This implies that the reproduction of a second exoskeleton for the right hand should be immediate and less costly in the design phase.

4 Conclusion

This paper has shown the first version of the design and implementation of a fully functional exoskeleton, accompanied by a control software that meets all the safety, usability, and control requirements necessary for the development of clinical studies focused on hand rehabilitation.

After a geometric and kinematic analysis, with which it was possible to understand what the general joint movements of the hands are, it was determined which exoskeleton amongst those reviewed was a more convenient reference in terms of design. The preconceived idea was to select the one with the least possible design complexity, but considering if it has an acceptable range of motion. The use of

ergonomics was key to specifying the measurements, and that it had a size similar to the anatomy of an average Chilean hand. The thumb was quite a challenge. The mounting of the thumb with adjustable bars allows great flexibility for adapting to a position that accommodates the patient and is apparently a fairly relevant added value when compared to other exoskeletons in the referenced literature.

Finally, the portability gives the professional a great advantage when it comes to placing the entire system for the session in a comfortable and orderly manner.

Acknowledgements This study was sponsored and financially supported by Departamento de Ingeniería en Computación at Universidad de Magallanes, Punta Arenas, Chile and Rehabilitation Center Club de Leones Cruz del Sur, Punta Arenas Chile.

References

1. I.P. Romero, M. Aarón, Análisis cinemático e implementación de una mano robótica servo-articulada aplicable como prótesis (2011)
2. O. Binvignat, A. Almagiá, P.A. Lizana, E. Lizana, Aspectos Biometricos de la Mano de Individuos Chilenos. *Int. J. Morphol.* **30**, 599–606 (2012)
3. A. Cissal, V. Lobo, V. Moreno, J.C. Fraile, R. Alonso, J.P. Turiel, Robhand, un exoesqueleto de mano para la rehabilitación neuromotora aplicando terapias activas y pasivas, in *Actas de las XXXIX Jornadas de Automática* (Badajoz, 2018)
4. L. Belloso, J. Ángel, Diseño mecánico y primer prototipo de un robot de rehabilitación de mano (2017)
5. M. Sarac, M. Solazzi, M. Otaduy, A. Frisoli, Rendering strategies for underactuated hand exoskeletons. *IEEE Robot. Autom. Lett.* **PP**, 1 (2018)
6. C.N. Schabowsky, S.B. Godfrey, R.J. Holley, P.S. Lum, Development and pilot testing of HEX-ORR: hand exoskeleton rehabilitation robot. *J. Neuroeng. Rehabil.* **7**(1), 36 (2010)

Design and Implementation of a “Wireless-Hand” Mechatronic Prototype for the Control of a Robotic Hand



E. Peña, P. Alberti, S. Bustamante, P. Maldonado-Cárdenas, and P. Barría

Abstract The technological transfer between the areas of computer engineering and health have allowed collaborative work and effective support between both areas. This is how the development of robotics in the present can aid in repetitive activities or activities that present a lesser degree of direct intervention with the patient in certain therapies. This paper presents the design, creation, and programming of a “Wireless-Hand” mechatronic prototype that allows for remote control of a robotic hand. For this, a glove with flex sensors and micro-controlled circuits was designed, which connects wirelessly with the robotic hand, allowing communication and control over it. For the connection to be optimal in terms of data transfer and connectivity, three types of technologies are compared: Zigbee, Bluetooth, and WiFi.

Keywords Robotic hand · Wireless transmission · Flex sensors · Bluetooth · WiFi

1 Introduction

The Computer Engineering department of the University of Magallanes, in conjunction with the Rehabilitation Center Club de Leones Cruz del Sur, both from Punta Arenas, Chile, are collaborating on various projects to aid in the rehabilitation of

E. Peña (✉) · P. Alberti · S. Bustamante · P. Maldonado-Cárdenas
Departamento de Ingeniería en Computación, Universidad de Magallanes, Punta Arenas, Chile
e-mail: eduardo.pena@umag.cl

P. Alberti
e-mail: pedro.alberti@umag.cl

S. Bustamante
e-mail: sebbusta@umag.cl

P. Maldonado-Cárdenas
e-mail: patricia.maldonado@umag.cl

P. Barría
Research Unit, Rehabilitation Center Club de Leones Cruz del Sur, Punta Arenas, Chile
e-mail: pbarria@rehabilitamos.org

© The Author(s), under exclusive license to Springer Nature Switzerland AG 2022
D. Torricelli et al. (eds.), *Converging Clinical and Engineering Research on Neurorehabilitation IV*, Biosystems & Biorobotics 28,
https://doi.org/10.1007/978-3-030-70316-5_152

people with disabilities. For this purpose, transdisciplinary works that promote the transfer of knowledge between the areas of engineering and health are carried out.

This paper presents the design, implementation and programming of a mechatronic control device that allows a robotic hand to be managed wirelessly through the movement of a human hand.

The prototype developed with this project will be used to study the human-machine interaction in people with disabilities and limited hand mobility, to evaluate the potential of the device to assist the activities of daily life that involve the manipulation of objects and tools.

The characteristics are: facility to manipulate and degree of freedom, which allows to capture the movements of one hand to repeat it (reflect them) in the robotic hand, in a remote way, and at a distance longer than a meter, maintaining the accuracy of its movements. Flex sensors are used to establish a connection to an arduino board and three types of technologies to ensure the wireless signal. These systems are mounted in a glove, that is modified to integrate the electronic part that is needed for the flex sensors. The robotic arm used was printed in the The University of Magallanes Department of Computer Engineering, using the french design INMOOV [1]. After that, we proceed to evaluate three types of technologies applied, comparing response times, temperature and scope, resulting in the Zigbee technology the best for the present design.

2 “Wireless-Hand” Design

2.1 Objectives

Through the “Wireless-Hand” we want to reproduce hand opening and closing movements in a robotic hand. For this purpose, both wireless and mechatronic technology will be used for its design and control.

2.2 Technology Used

To promote the autonomy of the Wireless-Hand, three types of technologies will be used: Zigbee [2], Bluetooth [3] y WiFi [4, 5]. An arduino card called Lilypad 328 will be used, through these five flex sensors will be connected 4, 5” [6] that are able to determinate the movements (flexions) of the fingers (Fig. 1a).

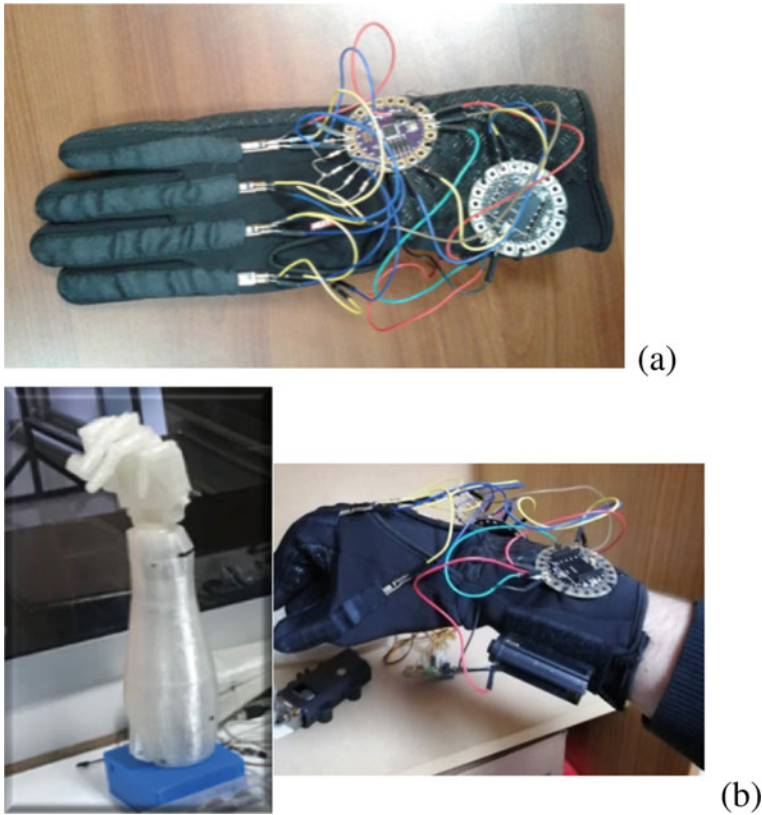


Fig. 1 Working “Wireless-Hand” prototype

2.3 Tests and Results

The tests developed in the laboratory consisted of the execution of hand movements by a healthy volunteer under a controlled environment with the mechatronic device, evaluating the response of the wirelessly connected robotic arm (Fig. 1b). Exchanging wireless technologies, varying distances, and forcing it to work in environments with electronic noise and temperature, which the device could encounter under normal conditions. The motion response of the robotic device and its latency were analyzed.

The three technologies used were compared under the laboratory tests Zigbee-Bluetooth-WiFi met the objective of moving the robotic arm wirelessly at a distance between 1 and 4 m without obstacles and operating at ambient temperature, even reaching 10 m without problems. Tables 1 and 2 show the main characteristics of these wireless devices quantitatively and qualitatively, which led us to select the one which showed the best performance for our project.

Table 1 Quantitative comparison table

Device	Zigbee	Bluetooth	WiFi
Temperature (°C)	26.1	24.5	24.3
Response time (s)	53.8ms	53.7 ms	53.4 ms
Dissipated energy (J)	196.02	297	475
Frequency (GHz)	2.4	2.4–2.48	2.4
Maximum reach (m)	60	10	~30
Transfer speed (bps)	250 Kbs	1 Kbps	11/54/300Mbps
Supply voltage (V)	2.1–3.6	3.3	3.3–3.6
Consumption (sleep mode) (A)	1 uA	1 uA	20 uA
Consumption (reception) (A)	33–45 mA	~50 mA	80–225 mA
Transmission consumption (A)	28–31 mA	~50 mA	80–225 mA
Device value (US\$)	9.7	10.7	31.7

Table 2 Qualitative comparison table

	Zigbee	Bluetooth	WiFi
Ease of hardware configuration	YES	YES	YES
Ease of codification	YES	YES	NO
Ease of incorporation into “Wireless-hand” device	YES	YES	YES

The three technologies respond to the requirement to replicate the movements of a human hand in a robotic model.

At the moment of the selection, it is important to consider the distance between the glove and the robotic arm, cost of the technology, programming accessibility, maintenance, and above all the final user comfort. The temperature emitted by the different devices is what led us to choose Zigbee as the right one for emitting less heat radiation after 25 min (see Fig. 2).

3 Conclusions and Future Works

In the selection of the most suitable Wireless device for the characteristics of this project both qualitative and quantitative elements were considered. The selected device was Zigbee, due to the fact that the communication interface between hardware and software is easy to work with, which allows potential when creating applications.

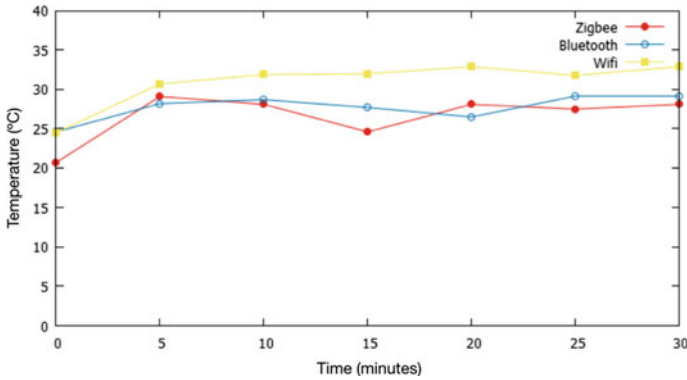


Fig. 2 Comparison of temperature of the wireless devices

Currently, Zigbee support is the most accessible, it works with small ranges of electric charge, and can work at distances greater than two meters without exceeding 70m. The monetary cost of the base card is below 10US\$, which makes it a highly profitable and reproducible application.

By integrating the wireless devices combined with an Arduino platform, the mechatronic device designed for the “wireless-hand”, it is possible to obtain a prototype that allows for the wireless movement of a robotic hand.

The above implies that the potential of applying the “wireless-hand” in the different areas, especially health, could be improved and even expanded, considering that the cost is insignificant when compared to the benefit it would provide.

Among the future works that are taken into account are:

- Testing the device on “beta-tester” patients who are undergoing rehabilitation therapies to collect feedback and optimize the “Wireless-Hand” prototype
- Integrating the full movement of the arm and forearm, adding position and inertial sensors to the “Wireless-Hand”
- The capacity to receive, through the wireless glove, signals from the robotic arm related to the pressure exerted on an object and its position.
- Control in an even more specific way the movements of the fingers, adding additional material to the “Wireless-Hand” and reacting to the touch of the electromechanical arm with pressure sensors.

Acknowledgements This study was sponsored and financially supported by Departamento de Ingeniería en Computación at Universidad de Magallanes, Punta Arenas, Chile and Rehabilitation Center Club de Leones Cruz del Sur, Punta Arenas Chile.

References

1. Planos bajo InMoov Robot licensed under CC BY-NC (2014). <http://inmoov.fr/>
2. E. Crespo, Aprendiendo Arduino, ZigBee/Xbee (2016). <https://aprendiendoarduino.wordpress.com/>
3. I.-S. Manual-Técnico, Bluetooth to Serial Port Module HC-05 (2018). http://biblioteca.geekfactory.mx/bluetooth_bee_pro/datasheet_hc-05.pdf
4. S. Latorre-Díaz, Blog Seba Electronic Labs (2016). <http://sebalabs.blogspot.com/2016/09/arduino-16-wifibee-esp8266-sin-libreria.html>
5. N. Santos, ESP8266 WiFi Bee: connecting to an access point with AT commands (2017). <https://techtutorialsx.com/2017/05/18/esp8266-wifi-bee-connecting-to-an-access-point-with-at-commands/>
6. Rambal, Sensor Flex 2.2'' (2019). <https://rambal.com/presion-peso-nivel-flex/250-sensor-flex.html>

Analysis of Frequency Bands and Channels Configuration for Detecting Intention of Change Direction Through EEG



V. Quiles, L. Ferrero, E. Iáñez, M. Ortiz, and J. M. Azorín

Abstract The design of solid interfaces based on the patterns of brain activity that underlie human decision-making are a field of interest in creating interfaces that allow recover the pathway between the brain and the muscular system to be rectified. In this work, a Brain Machine Interface is presented to detect the user's intention through the differentiation of the EEG signals into two classes according to their temporal and frequency characteristics, comparing different electrodes configurations. The better band for all the configuration seems to be Theta (4–7 Hz) from a centralize sensorimotor area, which obtained 69 and 70% accuracy results for two subjects.

This research has been carried out in the framework of the project Walk-Controlling lower-limb exoskeletons by means of brain-machine interfaces to assist people with walking disabilities (RTI2018-096677-B-I00), funded by the Spanish Ministry of Science and Innovation, the Spanish State Agency of Research, and the European Union through the European Regional Development Fund.

V. Quiles (✉) · L. Ferrero · E. Iáñez · M. Ortiz · J. M. Azorín
Brain–Machine Interface System Laboratory, Miguel Hernández University of Elche, Miguel Hernández University of Elche, Elche, Spain
e-mail: vquiles@umh.es

L. Ferrero
e-mail: lferrero@umh.es

E. Iáñez
e-mail: elianez@umh.es

M. Ortiz
e-mail: mortiz@umh.es

J. M. Azorín
e-mail: jm.azorin@umh.es

1 Introduction

Brain Machine Interfaces (BMIs) allow to create a natural path between brain activity and motor activity. This fact has great possibilities in the rehabilitation field and the assistance. In the rehabilitation field this technology finds a perfect window for therapies in cerebrovascular accident patients, allowing to provide a neural feedback. In the assistance field, Spinal Cord Injury patients without cerebral neural circuits damaged could easily create a path between cerebral signal recording by EEG and an assistive device, like an exoskeleton [1].

The design of the BMI ranges from the analysis of the EEG signal, the creation of a model of brain activity and the codification of commands to the assistive devices. The signal is preprocessed with a variety of protocols described in the bibliography depending on the activity of interest [2]. In the analysis fields, cerebral activity is associated to temporal and frequency features in the EEG, like: Movement Related Cortical Potential [3], Event Related Desynchronization (ERD) [4] or Steady State Visually Evoked Potential [5]. The most relevant features selected are classified following a strategy (discrete classification, continuous regression and Hybrid and indirect approaches) for create control commands patterns depending on the cerebral state and close the loop control.

In this work the common brain activity while walking has been differentiated against a transient state associate with the intention of turning instants before subject choices perform the action.

2 Material and methods

2.1 Subjects

As a preliminary test, two healthy subjects, with ages 27 (female) and 26 (male) years old participated in the study. Subjects had not known diseases and approved voluntary his/her participation in the study by giving his/her informed consent according the Helsinki declaration approved by the Ethics Committee of the Responsible Research Office of Miguel Hernández University of Elche (Spain).

2.2 Brain-Machine Interface (BMI)

The subject was equipped with the non-invasive 32 electrode EEG system actiCHamp (Brain Products GmbH, Germany). Signals were transmitted wirelessly by a Move transmitter to the actiCHamp. The actiCap with 27 electrodes following a 10–10 distribution were selected for recording EEG activity (F3, FZ, FC1, FCZ, C1, CZ, CP1, CPZ, FC5, FC3, C5, C3, CP5, CP3, P3, PZ, F4, FC2, FC4, FC6, C2, C4, CP2,

Table 1 Results for both subjects for the different features and electrodes configurations

	Hjorth+ Freq. (Hz)	Subject 1			Subject 2		
		Total (%)	Walk (%)	Turn (%)	Total (%)	Walk (%)	Turn (%)
Both sides (5 electrodes) FC1, FC2, C3, Cz, C4	4-7	69 ± 9	63 ± 21	76 ± 14	70 ± 7	68 ± 15	72 ± 22
	8-14	66 ± 15	50 ± 20	82 ± 17	67 ± 10	61 ± 19	73 ± 23
	15-22	64 ± 13	46 ± 22	81 ± 18	66 ± 10	61 ± 18	72 ± 24
	23-30	62 ± 13	45 ± 19	79 ± 17	66 ± 10	61 ± 18	72 ± 24
Right side (6 electrodes) Fz, FC2, FC6, Cz, C2, C4	4-7	69 ± 13	63 ± 21	75 ± 16	65 ± 14	68 ± 26	61 ± 16
	8-14	68 ± 14	55 ± 21	81 ± 16	64 ± 14	69 ± 20	58 ± 16
	15-22	62 ± 12	53 ± 19	71 ± 13	61 ± 13	64 ± 20	58 ± 18
	23-30	63 ± 15	55 ± 13	71 ± 22	60 ± 12	64 ± 20	57 ± 17
Left side (6 electrodes) Fz, FC1, FC5, Cz, C1, C3	4-7	63 ± 11	55 ± 22	70 ± 16	60 ± 11	66 ± 18	55 ± 19
	8-14	65 ± 11	52 ± 26	80 ± 20	59 ± 13	58 ± 19	60 ± 19
	15-22	60 ± 11	48 ± 20	73 ± 19	57 ± 14	57 ± 20	57 ± 20
	23-30	62 ± 13	48 ± 22	76 ± 21	56 ± 14	57 ± 23	56 ± 18
Average for each frequency range	4-7	67 ± 3	60 ± 5	73 ± 3	65 ± 5	67 ± 1	63 ± 9
	8-14	66 ± 2	52 ± 3	80 ± 3	63 ± 4	63 ± 6	64 ± 8
	15-22	62 ± 2	49 ± 4	80 ± 5	61 ± 5	60 ± 3	62 ± 8
	23-30	62 ± 1	49 ± 5	80 ± 5	61 ± 5	61 ± 4	61 ± 8

Average is shown at the end. Best results are shown in grey color

CP4, C6, CP6, P4). Ref is placed in right ear lobe and ground in the frontal region. Other 4 electrodes were placed to record EOG activity in bipolar configuration (HR, HL, VU, VD). Signals are registered at 500 Hz and a Notch filter is applied at 50 Hz by hardware.

An inertial measurement unit (IMU) (Tech MCS V3, Technaid, Spain) placed on lumbar was registered at 50 Hz. This way, it is possible to detect the moment in which subjects performs the physical turn.

2.3 Experimental Procedure

Subjects performed 10 trials with 8 repetitions of a motor turning intention. Subjects remain stand and relaxed for 15 s. Then, subjects start walking straight and after more than 10 s, at their own will, they perform a turn around 45 degrees in the desired direction (right or left).

2.4 Analysis

First, data from the IMU is analyzed to select the turn moment of the user and properly label EEG data. The signal is smoothed with a gaussian filtered with factor 30. Then, the algorithm computes the maximum difference between the consecutive inflexion points, calculated of the matrix rotation signal XZ that must fulfil next premise.

$$f''(xi) = 0 \text{ AND } f'''(xi) \neq 0 \tag{1}$$

An adaptative artifact removal algorithm H^∞ [6] has been applied using the first 15 s of every trial to converge. The parameters regarding the sample frequency were:

$\gamma = 1.15$, $q = 1e - 10$, $p_0 = 0.5$. Then, EEG signals are analyzed in windows of 0.5 s. A state variable band-pass filter (0.1–30 Hz) and a Laplacian filter are applied to every window.

Finally, two classes of 1.75 s are selected. The *Turn* class is selected from -1.85 to -0.1 s regarding the moment of turn labeled through the IMU analysis. *Walk* class is selected from -8 to -6.25 s.

2.5 Features and Electrodes Selection for Classification

Temporal and frequency features are extracted for every class window. For frequency features, an autoregressive estimation potential method in different ranges has been obtained: theta (4–7 Hz), alpha (8–14 Hz), low beta (15–22 Hz) and high beta (23–30 Hz). Each of these features have been combined with temporal Hjorth parameters, a usual indicator of statistics properties (normalized slope descriptors) of the signal in the time domain: activity, mobility and complexity. Three electrodes combinations have been analyzed focus on motor and somatosensory areas (left side, right side, and both).

Linear Support Vector Machine classifier has been used to obtain accuracy percentages of a cross validation. Percentages of individual classes are also obtained for analyzing balance of the results.

3 Results and Discussion

The average success in class detection and standard deviation have been obtained for the *Walk* class, the *Turn* class and the Total (success at correctly detecting each class), for the different electrode configurations representing the left/right/central motor area in different bands.

The right electrode configuration showed better results than the left electrode configuration in the first two bands of the frequency features (Table 1). Possibly due to brain patterns that differentiate between left and right turn. The best results in this setup were in the theta band in the same way as in Both sides setup and alpha band was the second best. Respect to the centralize electrodes configuration were obtained the best and most balanced results for the theta band in both subjects 69 ± 9 (%) and 70 ± 7 (%), which showed the highest Total results and the lowest standard deviation. Despite, the accuracy results were not completely balanced for the two classes, the *Turn* class showed more accurate results. The best configuration was the same for both subjects, since Subject 2 obtained more balanced results between the two classes.

4 Conclusion

The built interface could be a promising interface for real time applying some standardization and fashion to consolidate these good results to control the intention of turn using the theta band of motor area. Furthermore, this paradigm intends to be integrated with other control protocols to fully control an exoskeleton.

This preliminary study will be tested on more subjects and an online analysis will be performed.

References

1. J.D.R. Millán et al., Combining brain-computer interfaces and assistive technologies: State-of-the-art and challenges. *Front. Neurosci.* **4** (2010)
2. J.L.C.V. Yongtian He, D. Eguren, J.M. Azorín, R.G. Grossman, T.P. Luu, Brain-machine interfaces for controlling lower-limb powered robotic systems. *J. Neural Eng.* **15**(2), 021004 (2018)
3. J.-H. Jeong, N.-S. Kwak, M.-H. Lee, S.-W. Lee, Decoding of walking intention under lower limb exoskeleton environment using MRCP feature, in *7th Graz Brain-Computer Interface Conference*, pp. 7–9 (2017)
4. K. Lee, D. Liu, L. Perroud, R. Chavarriaga, J. del Millán, A brain-controlled exoskeleton with cascaded event-related desynchronization classifiers. *Rob. Auton. Syst.* **90**, 15–23 (2017)
5. N.-S. Kwak, K.-R. Müller, S.-W. Lee, A convolutional neural network for steady state visual evoked potential classification under ambulatory environment. *PLoS ONE* **12**(2), e0172578 (2017)
6. A. Kilicarslan, R.G. Grossman, J.L. Contreras-Vidal, A robust adaptive denoising framework for real-time artifact removal in scalp EEG measurements. *J. Neural Eng.* **13**(2) (2016)

Gait Analysis as an Objective Tool Previous to Botulinum Toxin Injection in Spinal Cord Injured Patients: A Case Study



C. Redondo-Galán, S. Ceruelo-Abajo, I. Sinovas-Alonso,
A. de los Reyes-Guzmán, J. Madrid-Sánchez, and A. Gil-Agudo

Abstract Spasticity is one of the consequences after Spinal Cord Injury (SCI). Sometimes this cannot be controlled with the use of oral antispasmodics and it is necessary to infiltrate botulinum toxin. Photogrammetry technique is a useful tool to objectively determine the motor sequelae and facilitate therapeutic decisions. The aim of the present study is to present the results of the gait analysis related to a case study. Through photogrammetry, the range of motion (ROM) of the hip, knee and ankle joints (kinematics), the muscular activity and the kinetics were analyzed, providing objective information about the decision in view of the possible infiltration of botulinum toxin.

1 Introduction

Spasticity is a motor disorder occurring in many neurological conditions including Spinal Cord Injuries [1].

In spinal spasticity, which is usually generalized, botulinum toxin is useful as an adjuvant therapy in specific situations [2]. OnabotulinumtoxinA has demonstrated significant benefit in adult focal spasticity [3]. Gait analysis is a well-established tool for the quantitative assessment of gait disturbances providing functional diagnosis,

C. Redondo-Galán (✉) · S. Ceruelo-Abajo · J. Madrid-Sánchez · A. Gil-Agudo
Neural Rehabilitation Group, Hospital Nacional de Paraplégicos, Toledo, Spain

S. Ceruelo-Abajo
e-mail: sceruelo@sescam.jccm.es

A. Gil-Agudo
e-mail: amgila@sescam.jccm.es

I. Sinovas-Alonso · A. de los Reyes-Guzmán
Biomechanics and Technical Aids Department, Hospital Nacional de Paraplégicos, Toledo, Spain
e-mail: msinovas@sescam.jccm.es

A. de los Reyes-Guzmán
e-mail: adlos@sescam.jccm.es

assessment for treatment planning, and monitoring of disease progress [4]. Initially gait analysis was introduced to clinical practice to improve the management of children with cerebral palsy [5]. However, there is good evidence to extend its use to patients with various upper motor neuron diseases [4].

2 Methods

2.1 Case Study

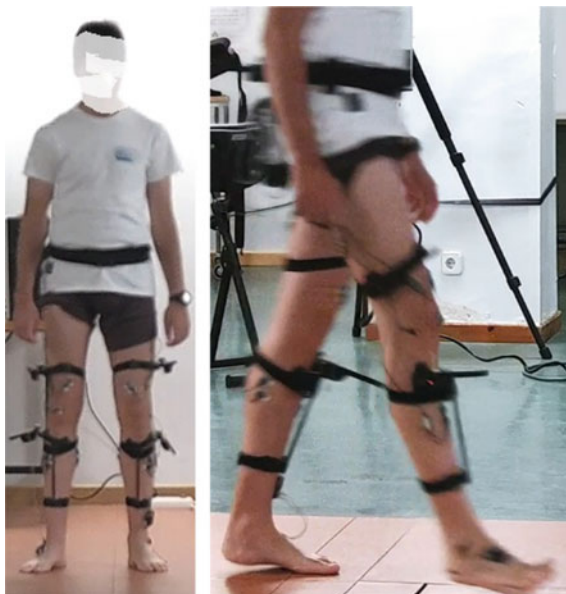
Descriptive and experimental study of a case: 15-years-old male with T5 AIS (ASIA Impairment Scale) D Spinal Cord Injury [6] secondary to fibrillary medullary astrocytoma, presenting focal spasticity in the right lower limb treated with oral Baclofen, without clinical improvement. WISCI II (Walking Index for Spinal Cord Injury): 12 [7] with AFO (Ankle-Foot Orthosis).

We proposed to use Gait Analysis (Fig. 1) as a tool to evaluate the patient's functional status previous to botulinum toxin injection.

2.2 Gait Biomechanical Analysis

The biomechanical study of gait was carried out by means of the photogrammetry system Codamotion (Charnwood Dynamics, Ltd, UK). Twenty two active markers were located on the lower limbs and pelvis following the model previously described by other authors [8]. The markers were positioned on the anatomical references described in previous work to analyze the joint displacement of the hip, knee and ankle during gait cycles [9]: sacrum, anterior superior iliac spines (ASIS), posterior superior iliac spines (PSIS), lateral surface of the thigh (anterior and posterior femur markers), lateral femoral condyles, lateral surface of the leg (anterior and posterior tibia markers), lateral malleolus, calcaneus (posterior lateral heel), and 5th metatarsal head. Moreover, synchronized with Codamotion the surface electromyographic activity of four muscles for each lower limb (upper leg: semitendinosus and vastus medialis; lower leg: tibialis anterior and gastrocnemius medialis) was registered by means of Noraxon. SENIAM recommendations for the skin preparation and MG surface sensor location were followed [10]. The patient was informed not to change his walking gait with self-selected speed and the average of five complete cycles was saved. The patient signed the Informed Consent.

Fig. 1 Gait biomechanical analysis



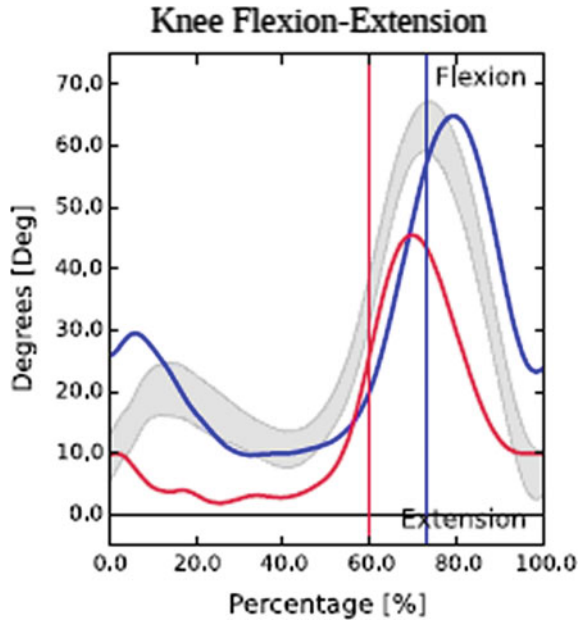
2.3 Data Processing and Variables Analyzed

Once the acquisition was completed, the results were analyzed using the biomechanical model of both lower limbs scaled to the anthropometric measurements (height, weight, ankle and knee width, pelvis width and depth) of the patient. Regarding the kinematics of the lower limbs, the maximum and minimum values of the stance and swing phases, the time of the cycle in which appear (expressed in % of the gait cycle), the joint amplitude (difference between the maximum and minimum value of the complete cycle) as well as the following events: initial contact and toe off, are calculated. Data collection was carried out on all joints, hip, knee and ankle, calculating the joint displacement, their extensor moment and power, and the ground forces. Likewise, the spatial-temporal parameters of gait were analyzed: speed (m/s), cycle duration (s), cycle length (cm), time step (s), cadence (steps/min), duration of the stance and swing phases (expressed in % of gait cycle duration). In relation to the surface electromyography (sEMG), the muscle activation patterns of all the muscles analyzed were calculated.

3 Results

After the previous analysis, the most relevant findings were:

Fig. 2 Knee joint flexo-extension



- Right knee: in the swing phase the range of flexion is decreased and there is no flexion in the loading response phase (Fig. 2).
- Right ankle: initial contact with equine foot, and plantar flexion increased in swing phase (Fig. 3).

Related to the sEMG result, activation of the right gastrocnemius in the final phase of the oscillation could be seen (Fig. 4).

As a result of the findings, it was recommended to inject botulinum toxin in the right gastrocnemius. Eco-guided control injection was performed after signing the Informed Consent.

4 Discussion

Gait Analysis is a tool that can be used previous to botulinum toxin infiltration in patients with spasticity following Spinal Cord Injury.

Oral treatments are sometimes not effective for spasticity and it's necessary to inject botulinum toxin.

Having objective and exact tools such as gait analysis facilitates decisions on local application of the toxin. It requires availability of the technique and multidisciplinary support.

Fig. 3 Ankle joint dorsi-plantar flexion

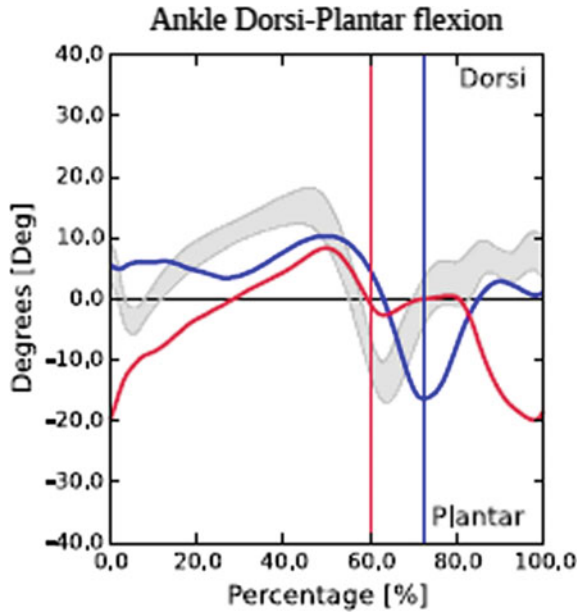
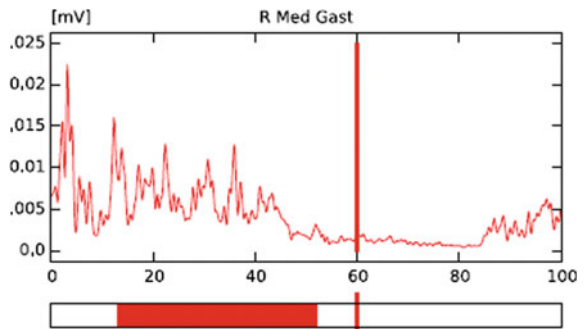


Fig. 4 EMG parameters



5 Conclusion

The Gait Analysis allows us to evaluate time-space parameters such as: speed, step length, step width, cycle/minute frequency, cadence...

It is an objective tool for making therapeutic decisions such as botulinum toxin injection.

References

1. D. Dressler et al., Defining spasticity: A new approach considering current movement disorders terminology and botulinum toxin therapy. *J. Neurol.* **265**(4), 856–862 (2018). <https://doi.org/10.1007/s00415-018-8759-1>
2. M. Alcobendas-Maestro, R. Palazón-García, E. Vargas-Baquero, A. Esclarín-Ruz, Clinical practice guidelines for the treatment of spinal spasticity with botulinum toxin. *Rehabilitation* **49**, 38–44 (2015)
3. L. Nalysnyk, S. Papapetropoulos, P. Rotella, OnabotulinumtoxinA muscle injection patterns in adult spasticity: a systematic literature review. *BMC Neurol.* 113–118 (2013)
4. R. Baker, A. Esquenazi, M.G. Benedetti, Gait analysis: clinical facts. *Eur. J. Phys. Rehabil. Med.* **52**(4), 560–574 (2016)
5. M. Domagalska, A. Szopa, M. Svczewska, The relationship between clinical measurements and gait analysis data in children with cerebral palsy. *Gait Posture* **38**(4), 1038–1043 (2013)
6. ASIA and ISCoS International Standards Committee, The 2019 revision of the international standards for neurological classification of spinal cord injury (ISNCSCI)—What’s new? *Spinal Cord.* **57**(10), 815–817 (2019)
7. P.L. Dittuno, J.F. Dittuno, Walking index for spinal cord injury (WISCI II): scale revision. *Spinal Cord.* **39**(12), 654–656 (2001)
8. M.P. Kadaba, Repeatability of kinematic, kinetic, and electromyographic data in normal adult gait. *J. Orthop. Res.* **7**(6), 849–860 (1989)
9. A. Gil-Agudo, A. De la Peña-González, A. Del Ama-Espinosa, E. Pérez-Rizo, Comparative biomechanical gait analysis of patients with central cord syndrome walking with one crutch and two crutches. *Clin. Biomech.* **24**(7), 551–557 (2009)
10. J. Hermens, B. Frerikx, C. Disselhorst-Klug, G. Raub, Development of recommendations for SEMG sensors and sensor placement procedures. *J. Electromyogr. Kinesiol.* **10**(5), 361–374 (2000)

Ewe: A Computational Tool to Assist People in Emergencies



Luz Ariel and Fechine Joseana

Abstract Currently, there are a variety of wearable devices dedicated to emergency monitoring. However, these solutions are still restricted to the highest strata of society, making it a great challenge for the government to allow access to technologies for a large part of the population. In this sense, a research now provides a computational tool (emergency bracelet), of low cost, that helps these social minorities in the scope of health.

1 Introduction

The advances in technology have a positive impact on man's life, such as wearables, which can be added to the user's body and assist in a variety of applications, such as monitoring the user's physiological and sensory functions. Currently, there are a variety of companies offering wearable devices for emergency monitoring, such as Lincare [1] and Iris Senior [2].

However, these solutions are still restricted to the highest strata of society, corroborating with [3] when he affirms that the inclusion of Information and Communication Technologies (TICS) is a great challenge of the public power, in allowing access to the great part population to the benefits of new technologies.

In the literature, there are already initiatives, such as the WatchAlert [4] and the tool proposed by Vanzella [5]. The first proposes the use of a wearable, with Android Wear connected to a smartphone, to send the emergency request, the second, in turn, presents a bracelet equipped with an Esp8266 card, which requests help by sending the information to a server via through the Wi-Fi connection.

In this context, it is of paramount importance to develop low-cost solutions that meet the most disadvantaged strata of society in the health area. Given the above,

L. Ariel (✉) · F. Joseana
Federal University of Campina Grande, Campina Grande, Brazil
e-mail: ariel.luz@ccc.ufcg.edu.br

F. Joseana
e-mail: joseana@computacao.ufcg.edu.br

Table 1 Tool comparison

Features	Ewe	Iris senior	Lincare	Vanzella tool	Watch-alert
Wi-Fi network				✓	
Bluetooth network		✓	✓		✓
GSM network	✓				
GPS support	✓	✓			
Fall detection	✓	✓	✓	✓	✓
Audible alert	✓				
Display	✓		✓		✓

this work proposes the development of Ewe, a computational tool that aims to give autonomy, freedom and inclusion to these people.

2 Proposed Solution

The proposed solution arose from the need to improve the Genuino Rescue tool, developed by [6].

Genuino Rescue consists of a bracelet with an Arduino connected to a smartphone via a Bluetooth connection, responsible for sending an emergency SMS message to the user’s family members, as well as triggering the Mobile Emergency Service (SAMU) to help victim.

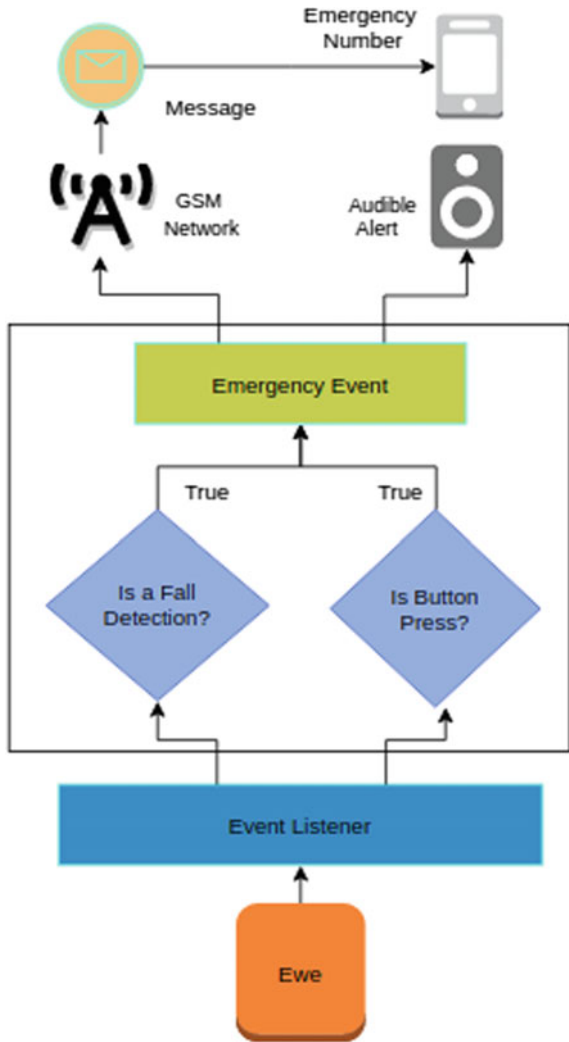
Unlike Genuino Rescue and related works presented, in which there is a dependence on the smartphone to perform the tasks, attributing an additional cost for the solution to work, or the need for a Wi-Fi connection to send the information, Ewe intends to be an independent tool.

The Ewe offers previously required functions of the cell phone (Table 1), such as support for the GSM chip, which allows use in environments without an internet connection, added to new features such as the integration of an OLED display for viewing information about the operation and audible alert as a complement to emergency notification.

3 Partial Results

Initially, the architecture of the proposed solution was elaborated (Fig. 1), followed by the simulation of the construction of the device (Fig. 2). Subsequently, the prototype was built on a breadboard and the following components were used: Esp32 board—DevKitC, GSM Sim800L module, MCU-6050 accelerometer, GPS NEO6MV2, push button and a battery, as showing in the 3D model of the circuit (Fig. 3).

Fig. 1 Ewe solution architecture



In the current state, the prototype has the following functions: (i) collision detection by the user; (ii) the user's location; (iii) sending SMS to an emergency number; (iv) visualization of information related to the functioning of the prototype and (v) audible alert.

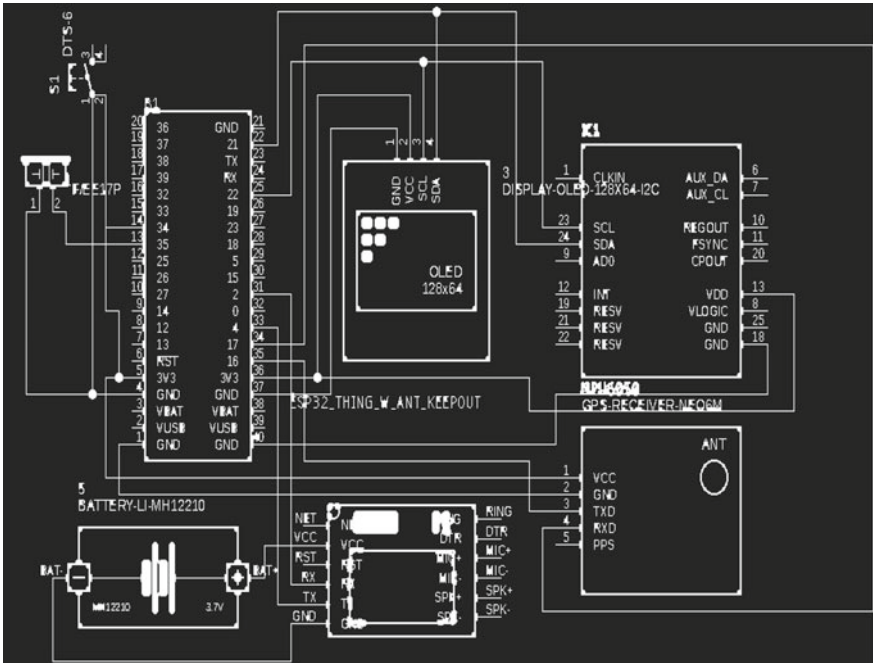


Fig. 2 Circuit diagram with Ewe components

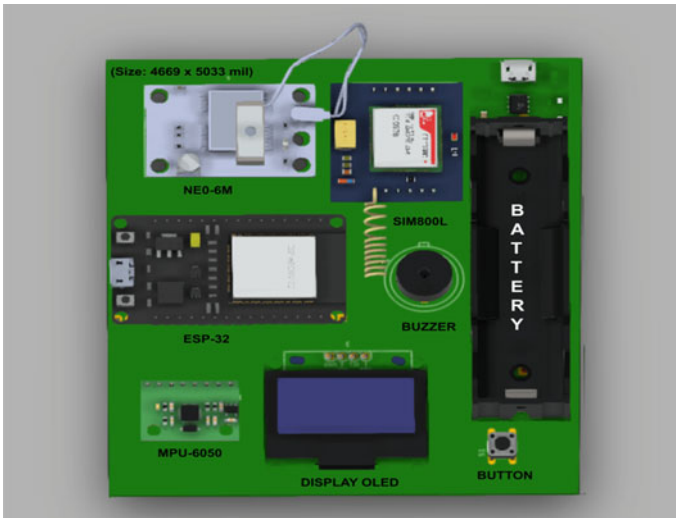


Fig. 3 3D modeling of Ewe on a printed circuit (PCB)

4 Conclusion

This work presents a proposal for a computational tool to help people in emergencies. The current phase consisted in the construction of the prototype in breadboard and the integration with the components, which made it possible to test the performance of critical sensors for the tool, namely, acceleration and location.

The results obtained are already close to expectations, showing the viability of the sensors for the application. As future work, we intend to improve the accuracy of the accelerometer collision detection, initiate the miniaturization of the prototype for the modeled printed circuit and perform tests with the target audience, in order to improve the prototype for future construction and validation of the device.

References

1. Lincare, *Lincare* (2019). Available at: <https://lincare.com.br>. Accessed 15 Aug 2019
2. Digital, W., *Monitoramento E Teleassistência 24H De Emergência Para Idosos* (2020). Equipamentos para monitoramento de idosos. Available at: <https://www.irissenior.com.br/>. Accessed 15 Aug 2020
3. Comitê Gestor da Internet no Brasil (CGIB), *Pesquisa sobre o uso das tecnologias de informação e comunicação no Brasil – Tic Centros Públicos de Acesso 2013*. São Paulo (2014)
4. R. Almeida, A. Macedo, Í. Araújo, P. Aguilar, Andrade, R.: WatchAlert: Uma evolução do aplicativo fAlert para detecção de quedas em smartwatches, in *Anais Estendidos do XXII Simpósio Brasileiro de Sistemas Multimídia e Web* (SBC, Porto Alegre), pp. 124–127
5. A. Vanzella, *Sistema de queda e monitoramento da frequência cardíaca utilizando ESP8266 e Protocolo MQTT*, 2018. Dissertação (Mestrado em Engenharia Elétrica e Computação). (Universidade Estadual do Oeste do Paraná, Foz do Iguaçu, 2018) 97 f
6. A. Luz, D. Ferreira, E. Taveiros, H. Cabral, *Genuino Rescue: Uma Ferramenta de Auxílio ao Serviço de Atendimento Móvel de Urgência*. Workshop de eXperimentos em Tecnologia Bahia-Alagoas (2017)